Modelling the Environmental Transfer of Tritium and Carbon-14 to Biota and Man

Report of the Tritium and Carbon-14 Working Group of EMRAS Theme 1

Environmental Modelling for RAdiation Safety (EMRAS) Programme

FOREWORD

Environmental assessment models are used for evaluating the radiological impact of actual and potential releases of radionuclides to the environment. They are essential tools for use in the regulatory control of routine discharges to the environment and also in planning measures to be taken in the event of accidental releases; they are also used for predicting the impact of releases which may occur far into the future, for example, from underground radioactive waste repositories. It is important to check, to the extent possible, the reliability of the predictions of such models by comparison with measured values in the environment or by comparing with the predictions of other models.

The International Atomic Energy Agency (IAEA) has been organizing programmes of international model testing since the 1980s. The programmes have contributed to a general improvement in models, in transfer data and in the capabilities of modellers in Member States. The documents published by the IAEA on this subject in the last two decades demonstrate the comprehensive nature of the programmes and record the associated advances which have been made.

From 2003 to 2007, the IAEA organised a programme titled “Environmental Modelling for RAdiation Safety” (EMRAS). The programme comprised three themes:

Theme 1: Radioactive Release Assessment

- Working Group 1: Revision of IAEA Technical Report Series No. 364 “Handbook of parameter values for the prediction of radionuclide transfer in temperate environments (TRS-364) working group;
- Working Group 2: Modelling of tritium and carbon-14 transfer to biota and man working group;
- Working Group 3: the Chernobyl I-131 release: model validation and assessment of the countermeasure effectiveness working group;
- Working Group 4: Model validation for radionuclide transport in the aquatic system “Watershed-River” and in estuaries working group.

Theme 2: Remediation of Sites with Radioactive Residues

- Working Group 1: Modelling of naturally occurring radioactive materials (NORM) releases and the remediation benefits for sites contaminated by extractive industries (U/Th mining and milling, oil and gas industry, phosphate industry, etc.) working group;
- Working Group 2: Remediation assessment for urban areas contaminated with dispersed radionuclides working group.

Theme 3: Protection of the Environment

- Working Group 1: Model validation for biota dose assessment working group.

This report describes the work of the Tritium and Carbon-14 Working Group under Theme 1. The IAEA wishes to acknowledge the contribution of the Working Group Leader, P. Davis of Canada, and the Scenario Leaders (listed in Table 1.2) to the preparation of this report. The IAEA Scientific Secretary for this publication was initially M. Balonov and subsequently V. Berkovskyy both of the Division of Radiation, Transport and Waste Safety.

CONTENTS

SUMMARY

Hydrogen and carbon are biologically-regulated, essential elements that are highly mobile in the environment and the human body. As isotopes of these elements, tritium and ^{14}C enter freely into water (in the case of tritium), plants, animals and humans. This complex behaviour means that there are substantial uncertainties in the predictions of models that calculate the transfer of tritium and ^{14}C through the environment. The EMRAS Tritium/C14 Working Group (WG) was set up to establish the confidence that can be placed in the predictions of such models, to recommend improved modelling approaches, and to encourage experimental work leading to the development of data sets for model testing. The activities of the WG focused on the assessment of models for organically bound tritium (OBT) formation and translocation in plants and animals, the area where model uncertainties are largest. Environmental ^{14}C models were also addressed because the dynamics of carbon and OBT are similar.

The goals of the WG were achieved primarily through nine test scenarios in which model predictions were compared with observations obtained in laboratory or field studies. Seven of the scenarios involved tritium, covering terrestrial and aquatic ecosystems and steady-state and dynamic conditions. The remaining two scenarios concerned ^{14}C, one addressing steady-state concentrations in plants and the other time-dependent concentrations in animals. The WG also considered one model intercomparison exercise involving the calculation of doses following a hypothetical, short-term release of tritium to the atmosphere in a farming area. Finally, the WG discussed the nature of OBT and proposed a definition to promote common understanding and usage within the international tritium community.

The models used by the various participants varied in complexity from simple specific activity approaches to dynamic compartment models and process-oriented models, in which the various transfer processes were simulated explicitly. The predictions varied by a factor of about 2 for scenarios involving continuous releases and a factor of 10 or more for short-term releases. In general, the simple and complex models performed equally well for chronic releases, but complex models were required to reproduce the observations for short-term releases. For most scenarios, the predictions tended to bracket the observations, suggesting that, in an average sense, the models reflect a good conceptual understanding of the environmental transport of tritium and ^{14}C. In some scenarios, part of the difference between predictions and observations could be attributed to the uncertainty in the observations as well as in the predictions.

Uncertainty estimates were requested as part of each scenario, and most participants submitted results for the steady-state exercises. For endpoints involving tritiated water (HTO) and ^{14}C, these were roughly consistent with a 95% confidence interval (97.5^{th} percentile divided by the 2.5^{th} percentile) of a factor 3 to 4. The uncertainties in the OBT concentrations were slightly higher. Few of the participants in the dynamic scenarios determined their uncertainties. However, the scatter in the predictions and the differences between predictions and observations suggest that the 95% confidence intervals on HTO and ^{14}C concentrations were about a factor of 10 or more. The confidence intervals were generally smaller for OBT than for HTO, reflecting the fact that, for the dynamic scenarios, HTO varies rapidly over time whereas OBT integrates.

The uncertainty in the predictions of environmental tritium and ^{14}C models can be reduced by:

- ensuring that the air concentrations used to drive the models are of high quality and match the resolution and averaging requirements of the scenario. Performance was better for models that were driven by air concentrations averaged over the OBT or ^{14}C residence time in the compartment of interest;
- incorporating as much site-specific information as possible on land use, local soil properties and predominant plant cultivars and animal breeds;
- implementing realistic growth curves for the plant cultivars of interest;
- basing all sub-models on the physical approaches available for the disciplines in question. For example, knowledge from the agricultural sciences should be used to improve models for crop growth, photosynthesis and translocation;
- recognizing and accounting for any unusual conditions (water stress, an uncommon cultivar or breed) in the model application.

Further work in the following areas would help to improve tritium and ^{14}C dose assessments:

- testing and improving models for the following processes: plant uptake of HTO at night and when it is raining; OBT formation in plants at night; translocation of OBT to fruit and roots; isotopic discrimination; tritium behaviour in soils following deposition from the atmosphere; and tritium behaviour in winter;
- modifying the steady-state models for chronic releases to account for the fact that fluctuations in release rates and meteorological conditions result in a state of quasi-equilibrium in the environment, rather than the complete equilibrium assumed by the models;
- developing a standard conceptual model for accidental tritium releases;
- investigating and understanding the large OBT/HTO ratios that have been observed in soils, plants and fish under conditions that are ostensibly at equilibrium.

The ten scenarios developed by the Tritium/C14 WG provide a valuable source of test data for validating environmental tritium and ^{14}C models.

CHAPTER 1. INTRODUCTION

1.1. Background

The EMRAS (Environmental Modelling for Radiation Safety) Programme was established by the International Atomic Energy Agency (IAEA) with the aim of improving models of radionuclide transfer through the environment, thereby enhancing the capability of Member States to assess the consequences of radioactive releases and optimize radiation protection of humans and the environment. The programme included a working group on "Modelling of Tritium and Carbon-14 Transfer to Biota and Man" (hereafter referred to as the Tritium/C14 WG). Participants in the WG are listed in the section entitled Contributors to Drafting and Review, given at the end of the report. Working groups involving tritium and ^{14}C were also included in the previous international model testing programmes BIOMOVS II (Biosphere Model Validation Study – Phase II [1, 2]) and BIOMASS (Biosphere Modelling and Assessment [3]). The "Special Radionuclides" Working Group of BIOMOVS II considered a number of scenarios including organically bound tritium formation in plants exposed to elevated tritium concentrations in air at night; the emission of tritium to the atmosphere from contaminated soils and wetlands; and the fate of a short-term release of ^{14}C to a small lake. The Tritium Working Group of BIOMASS tested models of the environmental transport of tritium in the vicinity of long-term atmospheric and sub-surface sources. EMRAS continued the work of these previous programmes, focusing on areas where uncertainties remained highest in the predictive capabilities of the models.

Although tritium and ^{14}C are low-energy beta emitters, they are of interest because they are isotopes of hydrogen and carbon, biologically-regulated, essential elements that are highly mobile in the environment and the human body. Tritium and ^{14}C enter freely into the same chemical compounds as hydrogen and carbon, including water (in the case of tritium), plants (through photosynthesis) and animals and humans (through various metabolic processes). This behaviour, plus the fact that tritium and ^{14}C transfer responds rapidly to changes in meteorological and plant conditions, means that the environmental modelling of tritium and ^{14}C is complicated, and must be carried out using methods different from the partitioning and accumulation concepts used for other radionuclides. The uncertainty in the model predictions is large, particularly for accidental releases, and there is a need for improved models that provide more reliable dose assessments. This need is particularly urgent given the expected renaissance in nuclear energy and the ongoing development of fusion reactors.

The activities of the EMRAS Tritium/C14 WG focused on the assessment of models for organically bound tritium (OBT) formation and translocation in plants and animals, the area where model uncertainties are largest. The WG necessarily considered models for tritiated water (HTO) as well, since an understanding of environmental HTO is needed before OBT can be modelled with any confidence. Environmental ^{14}C models were also addressed because the dynamics of carbon and OBT are similar. The overall objectives of the WG were to establish the confidence in the predictions of environmental tritium and ^{14}C models, to recommend improved modelling approaches and parameter values, to identify knowledge gaps, and to encourage experimental work leading to the development of data sets for model testing.

This document is the final report of the EMRAS Tritium/C14 WG. The present overview chapter addresses the scope of WG activities, provides a definition of organically bound tritium, briefly summarizes the results of the ten scenarios considered by the WG, and lists the

overall conclusions drawn from the study. The detailed final reports of the scenarios are contained in Chapters 2–11.

1.2. Scope of work

The goals of the Tritium/C14 WG were achieved primarily through nine test scenarios in which model predictions were compared with observations obtained in laboratory or field studies. A given scenario included information on the source term (the release rate of tritium or ^{14}C to air or water, or concentrations during exposure), and parameter values describing the environment through which the radionuclides passed (meteorological conditions, plant and animal properties, ingestion rates and so on, as applicable). Given this information, participants were asked to calculate tritium or ^{14}C concentrations in specific environmental compartments at specific times for comparison with observations. The results were discussed at bi-annual meetings with the aim of:

(1) explaining differences in the predictions in terms of differences in the conceptual models, modelling approaches or parameter values used by the various modellers;
(2) identifying the models that best reproduced the observations; and
(3) identifying knowledge gaps.

In general, the observations were not revealed until after the WG members had submitted their predictions, which resulted in a blind test of the models.

The nine test scenarios considered by the Tritium/C14 WG are listed in Tables 1.1 and 1.2. Seven of these involved tritium, covering terrestrial and aquatic ecosystems and steady-state and dynamic conditions. The remaining two scenarios concerned ^{14}C, one addressing steady-state concentrations in plants and the other time-dependent concentrations in animals. Five of the scenarios were based on data contributed by participants and two involved data from the literature. In the remaining two cases (the mussel uptake and depuration scenarios), new experimental work was undertaken by one participating organization to provide data that were otherwise not available on time-dependent OBT formation in aquatic animals.

The Tritium/C14 WG considered one further scenario, which involved the calculation of doses following a hypothetical, short-term release of tritium to the atmosphere in a farming area. Since suitable test data were unavailable, this scenario was carried out as a model intercomparison exercise. It was approached in the same way as the model-data exercises except that all the information in the scenario description was hypothetical, and no conclusions could be drawn regarding the model that performed best. But the scenario proved useful for individual participants, and provided guidance in setting derived intervention levels (the tritium concentration in agricultural crops above which interdiction is desirable to avert a given dose from all exposure pathways).

The Tritium/C14 WG was also active in two additional areas:

— in proposing a definition for OBT (see Section 1.3); and
— in proposing models and parameter values for tritium and ^{14}C for the revision of TRS 364 (see elsewhere on this CD).

Table 1.1. Scenarios considered by the Tritium/C14 WG.

Radio-nuclide	Scenario	Type of exposure	Endpoints
Tritium	Perch Lake	Chronic	Steady-state tritium concentrations in an aquatic ecosystem chronically contaminated with HTO
	Pickering	Chronic	Steady-state tritium concentrations in an agricultural ecosystem chronically contaminated with HTO
	Pine Tree	Chronic	Steady-state tritium concentrations in groundwater and pine trees chronically exposed to HTO in air
	Soybean	Acute	Time-dependent tritium concentrations in soybeans acutely exposed to HTO in air
	Pig	Dynamic	Time-dependent tritium concentrations in pigs subject to a contaminated diet
	Mussel uptake	Dynamic	Time-dependent tritium concentrations in mussels exposed to an abrupt increase in ambient tritium levels
	Mussel depuration	Dynamic	Time-dependent tritium concentrations in mussels exposed to an abrupt decrease in ambient tritium levels
	Hypothetical	Acute	Time-dependent concentrations and doses following an acute atmospheric tritium release over farmland
^{14}C	Rice	Chronic	Steady-state ^{14}C concentrations in rice growing near a continuous atmospheric source of ^{14}C
	Potato	Acute	Time-dependent ^{14}C concentrations in potatoes acutely exposed to ^{14}C in air

Table 1.2. Leaders and participants in the scenarios.

Scenario	Leader	Number of participants	Participating countries
Perch Lake	P. Davis, AECL Canada	8	France, Germany, Japan (2), Lithuania, Romania, Russia, UK,
Pickering	P. Davis, AECL Canada	8	France, Germany, Japan, Lithuania, Romania, UK (2), USA
Pine tree	Y. Inoue, NIRS Japan	5	France, Japan (2), Romania, USA
Soybean	H. Lee, KAERI Korea	12	Canada, France (2), Germany, Japan (2), Korea, Romania, Russia, UK (2), USA
Pig	D. Galeriu, IFIN-HH Romania	6	Canada, France, Japan, Romania, UK, US
Mussel uptake	T. Yankovich, AECL Canada	5	France, Germany, Japan (2), Romania
Mussel depuration	T. Yankovich, AECL Canada	4	France, Germany, Japan, Romania
Hypothetical	P. Guetat / L. Patryl, CEA, France	8	Canada, France, Germany, India, Japan (2), Korea, Romania
Rice	J. Koarashi, JAEA Japan	5	Canada, France, Japan (2), Romania
Potato	A. Melintescu, IFIN-HH, Romania	4	France, Japan, Romania, UK

1.3. Definition of OBT

Throughout the EMRAS Programme, the Tritium/C14 WG discussed the nature of OBT, and worked to develop a definition to promote common usage and understanding of the term within the tritium community. Much of the discussion centred on the place of buried tritium in the definition. Buried tritium is tritium in exchangeable positions in large molecules that is not removed when the dried sample is washed with tritium free water. It therefore appears as fixed OBT in traditional analytical procedures, although it behaves as exchangeable OBT in the body. If buried tritium exists in significant amounts, it could mean that the dose coefficient for OBT is too large.

The final OBT definition agreed upon by the WG is short, but is accompanied by a number of notes:

Definition: OBT is carbon-bound and buried tritium formed in living systems through natural environmental or biological processes from HTO (or HT via HTO). Other types of organic tritium (e.g. tritiated methane, tritiated pump oil, radiochemicals and so on) should be called tritiated organics, which can exist in any chemical or physical form.

Notes:

(1) Buried tritium is tritium that occupies exchangeable positions in large biomolecules in dry matter but that is not removed by rinsing with tritium-free water. Buried tritium therefore contributes to the OBT concentration in the traditional experimental determination of OBT. It is analogous to buried hydrogen in biochemistry.

(2) OBT should not include tritium bound to sulphur, nitrogen or oxygen (exchangeable OBT) that can be removed by washing with tritium-free water. This fraction depends strongly on the HTO concentration in effect at the time of sampling and can exchange with water vapour during analysis. Inclusion of the exchangeable fraction would lead to measurements that are highly variable and difficult to interpret.

(3) From an analytical perspective, OBT is the activity in dry biomatter that is not exchangeable with water. In measuring OBT concentrations, exchangeable OBT should first be removed by moderately drying the sample without decomposing the organic molecules, washing the residue repeatedly with tritium free water and then drying the material again. The OBT concentration can then be determined as the tritium activity in the dry sample. This is generally done by combusting the sample and determining the activity in the combustion water by liquid scintillation counting, or by analysing the sample by He-3 mass spectrometry. There are no generally accepted standard techniques for measuring OBT and the methods used should be documented when reporting results.

(4) In the washing process, exchangeable tritium nuclei are removed and replaced by hydrogen nuclei, but exchangeable hydrogen nuclei are simply replaced by other hydrogen nuclei. Thus measurements of OBT do not reflect the specific activity of the non-exchangeable hydrogen. This specific activity can be estimated by dividing the measured concentration by the fraction of hydrogen nuclei in the dry sample that are non-exchangeable. For example, this fraction has been empirically determined to be 0.78 for leaf tissues, but different values may apply for other plant or animal materials. Care must be taken in comparing model predictions and experimental data that the same quantity (OBT concentration or specific activity of non-exchangeable hydrogen nuclei) is being considered.

(5) OBT concentrations should be reported in units of Bq/L of combustion water. This is the fundamental unit that can be converted, if necessary, to the specific activity of the non-exchangeable hydrogen nuclei. Use of Bq/L makes it easy to compare concentrations in different media and to determine whether specific activity is depleted, preserved or enriched when tritium is transferred from one compartment to another.

(6) OBT refers to organic tritium formed from HTO by natural processes in living organisms, or in materials such as soils or lake sediments that are derived from living material. Put another way, OBT is that organic tritium found in a normal diet that imparts a dose consistent with the ICRP ingestion dose coefficient for OBT. All other types of organic tritium, no matter how they form or how they appear in the environment, should be called tritiated organics and assigned their own dose coefficient for purposes of dose calculation.

This definition recognizes the possibility that buried tritium may make up part of what is commonly measured as OBT using current analytical techniques, and is consistent with existing OBT dose coefficients.

Due to the concern over buried tritium, two organizations participating in the WG carried out experiments to determine whether buried tritium makes up a significant fraction of what is traditionally measured as OBT. The results were contradictory, with one experiment [4, 5] suggesting that the fraction is 50% or more and the other [6] that the fraction is at most 5–10%. In the face of this discrepancy, it was decided that the question must remain open pending new experimental data.

1.4. Results of individual Scenarios

A brief description of each Tritium/C14 WG scenario is given below, including a discussion of the models used to generate the predictions and the conclusions reached in each case. More detailed results are available in the final EMRAS reports for each scenario, which follow in Chapters 2–11, and which are posted on the EMRAS website (http://www-ns.iaea.org/projects/emras/emras-tritium-wg.htm).

1.4.1. Perch Lake Scenario

The Perch Lake scenario was based on data collected in Perch Lake, a small, shallow freshwater lake located within the borders of AECL's Chalk River Laboratories. The lake contains elevated levels of tritium due to long-term discharge from nearby waste management areas. Tritium concentrations were measured in samples of air, lake water, sediments, aquatic plants (algae, bladderworts, hornworts and cattails) and animals (clams, bullheads and pike) collected at three locations in the lake in 2003 May, July and October. Given the measured HTO concentrations in water, sediments and air, participants in the scenario were asked to calculate:

(1) HTO and non-exchangeable OBT concentrations in algae, worts and cattails for the May sampling period at the three sampling sites.
(2) HTO and non-exchangeable OBT concentrations in clams, bullheads and pike for each of the three sampling periods.
(3) Non-exchangeable OBT concentrations in sediments for the May sampling time at the three sampling sites.

Eight participants submitted results for this scenario. All but one assumed the HTO concentration in a given plant or animal was equal to the water concentration to which it was exposed. The OBT concentration in a given endpoint was generally based on the corresponding HTO concentration, with some allowance made for isotopic discrimination in the case of plants and metabolic processes in the case of animals. In contrast, two participants used dynamic models to estimate OBT concentrations in algae and all animals, and a third modeler took a similar approach for fish. In each case, these models took account of the growth rate of the animal, ingestion and excretion rates and internal metabolic/catabolic processes to describe the incorporation of OBT in the animal and the conversion between OBT and HTO. The participants showed considerable variability in their approach to modeling sediments, in one case setting the OBT concentration equal to the mean of the predicted plant and animal OBT concentrations and in another assuming the sediment OBT concentration was in equilibrium with the OBT concentration in the organic matter of decomposing terrestrial vegetation that found its way into the lake.

The predictions of a given model for HTO concentrations in plants and animals typically lay within 30% of the corresponding observation. The models were unbiased with respect to HTO concentrations in plants but tended to be conservative for HTO concentrations in animals. The good performance of the models for these endpoints was due to the assumption (supported by the observations) that the HTO concentration in a given plant or animal was equal to the water compartment to which it was exposed. The small differences between the predictions and observations arose primarily from the fact that it was not always easy to identify this compartment. In particular, the data suggest that the submerged parts of cattails were in equilibrium with sediment water rather than lake water, and that clams and bullheads were in equilibrium with bottom water rather than sediment water. A second reason for the differences between predictions and observations lay in the way in which the models treated spatial averaging, particularly for fish. The best prediction of HTO concentration in bullheads was obtained by averaging the bottom waters over the entire lake, including near-shore and offshore zones. Similarly, the best prediction of HTO concentration in pike occurred by averaging over the water column as well as over the entire lake.

The models typically predicted OBT concentrations within a factor of two of the observations. They tended to be conservative for OBT concentrations in plants but to underestimate OBT concentrations in animals. The mispredictions were caused largely by inappropriate choices for the discrimination and metabolic factors used to calculate OBT concentrations from the HTO concentrations. In addition, apart from the dynamic models, none of the participants considered any sort of time-averaging when calculating OBT concentrations. In contrast, the observed concentrations correlated better with the time-averaged HTO concentrations than with point measurements.

1.4.2. Pickering Scenario

The Pickering scenario was based on environmental tritium measurements made in the vicinity of Pickering Nuclear Generating Station (PNGS) in July and September 2002. HTO concentrations were measured in air, precipitation, soil, drinking water, plants (including the crops that make up the diet of the local farm animals) and products derived from the animals themselves; OBT concentrations were measured in the plant and animal samples. The samples were taken at two dairy farms (DF8 and DF11), a hobby farm (F27) and a small garden plot (P2), all of which were located to the northeast of PNGS at distances between 1 and 10 km. The dairy farms yielded samples of pasture grasses, a variety of grains, milk and meat, whereas F27 produced mainly fruit, garden vegetables, chickens and eggs. A limited number

of plants were grown at P2 for research purposes and raspberry leaves and grass were sampled. Estimates of the total food intake by the cows were available from the farmers. The chickens raised at F27 were essentially free-range and their food intake was not regulated or monitored. The amount of drinking water ingested by the cows and chickens was not known. Given the information on diets and the measured HTO concentrations in air, precipitation and drinking water, participants in the scenario were asked to calculate:

(1) HTO and non-exchangeable OBT concentrations in the sampled plants and animal products for each site and sampling period.
(2) HTO concentrations in the top 5 cm soil layer for each site and sampling period.

The modeling approaches taken by the eight participants in this scenario varied widely. Three participants used dynamic compartment models formulated in terms of a series of coupled first-order differential equations. Rate constants for the transfers between compartments were derived from consideration of the hydrogen inventories of the compartments and the hydrogen fluxes between them. Predictions for the Pickering scenario, which is an equilibrium situation, were obtained from the steady-state solution to the equations. The models used by the other participants were based for the most part on simple analytical equations that described transfers between most compartments using empirically-based bulk parameters. The air concentrations used to drive the models were averaged over different time periods, with some participants employing the average over the May to September period and others using averages over the month prior to sampling.

All models but one performed well for HTO in soil, predicting concentrations that agreed with each other and with the observations when uncertainties were taken into account. In contrast, all of the models significantly overestimated the OBT concentrations in plants, by an average factor of 1.9 at the dairy farms and 3.4 at F27. This appears to be due in part to overprediction of the concentration of HTO in the plant leaves, where OBT is formed by photosynthesis. For most models, the ratio of HTO concentration in plant leaves to HTO concentration in air moisture was substantially larger than the value of 0.68 that has been observed in other studies. Additionally, the models appear to underestimate the effect of isotopic discrimination in OBT formation. Most of the predicted OBT/HTO ratios for the plant leaves were larger than the value of 0.7 observed elsewhere. Finally, the air concentrations given in the scenario description, which had a large associated uncertainty, may have been too high.

Most of the models predicted HTO concentrations in calf flesh that were in good agreement with the observations. This may be due in large part to the fact that drinking water concentrations, which play a major role in determining tritium body burdens, were provided in the scenario description. Model performance was not as good for OBT, which was overestimated in most cases. The models did not do as well for eggs and chickens as for milk and calf flesh, partly because the concentrations in chicken feed were overestimated to a greater extent than in cow feed and partly because the ingestion rates of feed and drinking water were not known for the chickens.

Generally speaking, the level of agreement between predictions and observations was about the same for the numerical models as for the analytical models, although the numerical models tended to be responsible for all of the very high predictions.

1.4.3. Pine Tree Scenario

The Pine Tree scenario was based on data collected near an industrial site in Japan where tritium is released continuously to the atmosphere from four closely grouped stacks with heights ranging from 30 to 90 m. Monthly measurements of tritium concentrations in rain, groundwater and pine trees were instituted in 1981 at three sites (P3, MS2 and G4) within 2 km of the stacks. Monthly measurements of HTO concentrations in air, rain and pine needles were made at a fourth site (MP7) starting in 1984.

Modelers were provided with estimates of the infiltration rate of water into the unsaturated soil layer, the vertical pore water velocity in the unsaturated layer and the mean horizontal flow rate in the aquifer, consistent with a simplified conceptual model of the geology and groundwater flow at the site. Soil characteristics, meteorological data and atmospheric tritium discharge rates from four stacks were also provided. Given this information, the modelers were requested to calculate the following endpoints:

(1) Monthly tritium concentrations in air moisture and precipitation, and HTO and OBT concentrations in pine needles from 1982 to 1986 at sampling site P3.
(2) Yearly HTO concentrations in air moisture, precipitation and pine needles and OBT concentrations in pine needles and tree rings at MS2 for the period 1984 to 1987.
(3) Monthly tritium concentrations in well water at G4 from 1984 to 1987.

Most participants used a Gaussian plume model to calculate atmospheric dispersion and tritium concentrations in air and precipitation. The models differed in a number of respects, including the way in which plume rise was treated, the wind speed used in the calculations, the horizontal and vertical dispersion parameters, and the way in which dry deposition and re-emission of HTO from the ground surface was modeled. Most participants calculated wet deposition and concentrations in rain using a washout coefficient, but the values of the coefficient varied among the models. One participant used a random walk model rather than a Gaussian plume model to do the dispersion calculations.

All modelers estimated the HTO concentration in pine needles using the equation of Murphy [7], which explicitly accounts for the contribution of air moisture and soil water to the tritium content of the needle. However, the participants made different assumptions regarding the relative contributions of the two sources. The modelers calculated OBT concentrations in pine needles by multiplying the HTO concentration by an isotopic discrimination factor that varied from 0.6 to 0.8. The OBT concentrations in the tree rings were calculated by multiplying the needle OBT concentrations by a factor I_D that varied from 0.5 to 1.0, which was assumed to describe isotope effects in the metabolic process of translocating OBT from needles to rings.

Two participants used a simple compartment model to calculate tritium concentrations in groundwater based on the travel time from the surface to the aquifer and the turnover rate of water in the aquifer. The remaining participants used sophisticated dispersion models that utilized all of the hydrological information given in the scenario description. However, each modeler interpreted this information differently, so that the assumptions and parameter values used in the calculations differed substantially from modeler to modeler.

All of the models underestimated the observed air moisture concentrations by factors ranging from 1.2 to 5 on average. It is possible that the observed concentrations were relatively high because the airborne plume was subject to prolonged periods in which it was trapped beneath the internal boundary layer that forms at the site when the wind blows onshore during the day,

a process that was not treated in the models. The predictions underestimated HTO and OBT concentrations in pine needles to the same extent as in air, indicating that the models of air-to-plant transfer and OBT formation are satisfactory. The model predictions bracketed the observations for concentrations in rain and in tree ring OBT, which suggests that the values used for the washout coefficient and the I_D parameter were too high. In fact, the data indicate that $I_D \sim 0.5$.

The sophisticated dispersion models were able to predict the time evolution of tritium concentration in groundwater to within a factor of two if proper assumptions and parameter values were applied. The simple compartment models predicted equally well if key parameters such as the turnover rate of water in the aquifer could be estimated. The differences between predictions and observations proved to depend not as much on differences in the models themselves as on the assumptions and parameter values used in their application.

1.4.4. Soybean Scenario

The Soybean scenario was based on experiments in which soybean plants were exposed to elevated HTO concentrations in air for one hour periods in a glove box. A total of six experiments (SB1 to SB6) were carried out at six stages in the growth of the plants. The soybeans used in experiments SB1 and SB4 were sampled several times between exposure and harvest to measure the HTO concentrations of each plant part as a function of time. The other plants were sampled and analyzed twice for their OBT content, at the end of the exposure and at harvest. The surface soil of the pots was covered by vinyl paper during the exposures to prevent tritium from depositing to the soil. Following exposure, the plants were removed from the glove box and placed outdoors.

Information on biomass growth rates, tritium concentrations in air in the glove box during the exposure, background tritium concentrations and meteorological conditions were given as part of the scenario. Modelers were asked to predict:

(1) HTO concentrations in the free water of the plant body (leaves and stems) and pods (shells and seeds) in the SB1 and SB4 experiments at the times the plants were sampled.
(2) Non-exchangeable OBT concentrations in the plant body and pods at harvest for each of the six experiments.

Twelve participants submitted calculations for the soybean scenario, each using a detailed, process-oriented model to make the predictions. In each model, the uptake of HTO by the leaves during the exposure itself was simulated as a gradient transfer process. OBT was assumed to be created by photosynthesis, with tritium being incorporated into new organic material in proportion to the HTO concentration in the leaves. The models also accounted for the transfer of tritium to other parts of the plant, which occurred by exchange in the case of HTO and translocation in the case of OBT. This was generally modeled as an instantaneous equilibrium with different partitioning factors for shells and seeds or with a single factor for the pods as a whole. Once the exposure stopped, the models simulated the loss of tritium from the plants. Some models adopted a single loss rate from all parts of the plant whereas others allowed a rapid rate from the leaves and a slower rate from the pods. All of the models simulated the continued formation of OBT at concentrations that reflected the residual levels of HTO in the leaves. Some models accounted for the reverse transfer from OBT to HTO, which was redistributed throughout the plant. All of these processes depend critically on the growth stage of the plant, which controls the initial rate of uptake by the leaves, the rate of

OBT formation and routes of translocation, and the amount of new plant material formed after the exposure that can dilute the tritium concentrations. Most modelers calculated the growth rates based on CO_2 assimilation since there was considerable variability in the data given in the scenario description.

The observed HTO concentrations in the plant body dropped off quickly with time, by two to three orders of magnitude in the first 24 hours after the exposure. All of the predictions lay above the observed data in the first hour post exposure, but by less than an order of magnitude in most cases. The uptake of HTO by the plants may have been limited by high temperatures in the glove box, which were not taken into account in the models. The predictions diverged significantly after one hour, ranging over five orders of magnitude. Some models overestimated the observations and some underestimated, by more than three orders of magnitude in some cases. The models showed similar discrepancies in predicting HTO concentrations in the pods.

The HTO concentrations in all parts of the plants at harvest were about two orders of magnitude higher than background levels of HTO in air, indicating that there were residual effects of the exposure up to two months later. This observation was reproduced by those models that simulated the slow conversion of OBT to HTO in the plant, indicating that the breakdown of OBT is likely responsible for the relatively high HTO concentrations at harvest.

The observed OBT concentration in the pods at harvest increased for experiments SB1 through SB4 as the time between exposure and harvest decreased, and then dropped off for experiments SB5 and SB6. The low values for the first two experiments, which were carried out before or just after flowering, reflect the fact that HTO concentrations in the plant had dropped off substantially by the time the pods started to form, so that the OBT produced and translocated to the pods had a correspondingly low concentration. Experiments SB3, SB4 and SB5 took place when the pods were actively growing. Dry matter produced during and shortly after the exposure would have incorporated high levels of tritium. OBT concentrations in the pods dropped off in SB6 as little new dry matter was able to form in the short time available between exposure and harvest, and any OBT translocated to the pods was diluted in the relatively large amount of uncontaminated dry matter already present. The predictions of some models captured this variation well while others remained almost constant or increased slightly from experiment to experiment. The predictions tended to bracket the observations but ranged over more than a factor of 100. A few models underestimated the OBT concentrations in the pods by up to five orders of magnitude for experiments SB1 through SB3. The leaf HTO concentrations in these models dropped off very quickly with time after the exposure and new dry matter was essentially uncontaminated with tritium by the time the pods had begun to form.

1.4.5. Pig Scenario

The Pig scenario was based on unpublished data from an experiment in which a pregnant sow was fed OBT-contaminated feed for 84 days before delivery. The genotype and initial mass of the sow were known, as were the composition and OBT concentration of its diet, but no information was available on intake rates as a function of time or urine production. The total tritium concentration in urine and the OBT concentration in the dry matter of the faeces were measured over the study period. In addition, the sow was slaughtered immediately after delivery and the HTO and OBT concentrations were measured in various organs.

The modelers were asked to predict the following quantities:

(1) The concentration of total tritium in urine and faeces as a function of time during the study.
(2) The HTO and OBT concentrations in muscle, heart, lungs, jejunem, ileum, liver, colon, kidney, brain and blood at the time of delivery.

The models used in the scenario varied in complexity. The two simplest consisted of compartment models that assumed all OBT in the diet entered a single organic compartment. The rate at which OBT was transferred from this compartment to body HTO was determined by considering the digestibility of the food. Concentrations in the various organs were derived from concentration in muscle using a correction factor based upon the fat and protein contents of the organ, the turnover rates of fat and protein, and the hydrogen contents of fat, protein and carbohydrate. In a further two models, the OBT intake was partitioned between body water and two organic compartments with different turnover rates. However, the initial partitioning of the OBT among these compartments, and the loss rates from the compartments, differed substantially between the models.

The last two participants in the scenario used process-oriented models to obtain their results. One model was based on the assumption that OBT turnover rates in organs can be assessed using the rates for net maintenance energy turnover. This model has six organic compartments and distinguishes between organs with respect to their transfer rates. The dry matter intake is partitioned into metabolisable and excreted fractions, which are associated with non-exchangeable and exchangeable OBT respectively. The final model in the scenario assumed that the tritium in the feed was in the form of HTO rather than OBT, since the model does not treat OBT in animals. The dynamics of total tritium in urine were calculated as a gradient transfer process driven by the difference between the HTO concentration in the intake and in body water.

Some models overpredicted the total tritium in urine and some underpredicted, but all results were within a factor 10 of the observations, and most were within a factor of 3. The overestimates were due to the fact that most OBT intakes were distributed too quickly to body water, with an excretion rate that was too high for a pig. In contrast, the underpredictions were explained by a low excretion rate and the assumption that all input OBT appears in the organic compartment. The water intake rates given in the scenario description may have been underestimated and this may also have influenced the model results.

All of the models predicted OBT concentrations in faeces that were within a factor of 7 of the observations, but none was able to reproduce the observed dynamics. Underestimates arose in those models that did not take into account the fact that contamination in faeces is related to the contamination of undigested feed, which was observed to be four times higher than the average contamination in the diet.

The predictions of all but one of the models for the HTO concentration in organs at slaughter were within a factor of 2 of the observations; in the exceptional case, the observations were underestimated by a factor 5. Similar results were obtained for OBT concentrations in organs, where only one set of predictions differed from the observations by more than a factor of two. Generally speaking, the simpler models performed as well as the more complex models in this scenario.

1.4.6. Mussel Uptake Scenario

The Mussel Uptake scenario was based on data collected at Chalk River Laboratories (CRL) of AECL. Freshwater Barnes mussels (*Elliptio complanata*) were transplanted from an area in the Ottawa River with background tritium concentrations to Perch Lake, a small Canadian Shield lake on CRL property that has historically received measurable inputs of tritium from up-gradient waste management areas. Some mussels were exposed to tritium in water only and others to tritium in water and sediments. Following transplantation, the mussels were sampled on an expanding time step over the course of an 86 day period. The HTO and OBT concentrations were measured in the soft tissue of each mussel sample to follow the build-up of tritium in the animals over time. Participants in the scenario were asked to predict these concentrations given the background levels in the mussels at the time of transplantation, the HTO concentration in the lake water to which they were exposed, the HTO and OBT concentrations in the nearby sediments and in the plankton in the lake, the water temperature, and the mussel fresh weights, shell dimensions and water contents.

The participants in this scenario used dynamic compartment models for their calculations, with transfers between compartments based on published rates of tritium uptake and loss by aquatic animals. In each model, the mussels were assumed to assimilate HTO from the water column, plankton and sediments (for those mussels exposed to sediments); plankton and sediments were the sources of OBT. Food intake rates depended upon the rate of water filtration by the mussels and the concentration of plankton in the water. The models differed with respect to the number of compartments, the values adopted for the rate constants, the growth rates of the mussels and the effect of water temperature on the growth, and the characteristics of the mussels themselves.

The experimental data showed that the HTO concentration in the mussels quickly reached steady state with the concentration in lake water. All models reproduced this result, but overestimated the time required to achieve equilibrium by intervals ranging from one hour to a few days. This deficiency can be simply corrected by increasing the rate at which HTO is transferred from water to the mussels. All models also underpredicted the OBT concentration in the mussels one hour after transplantation, but overpredicted the rate of OBT formation over the next 24 hours. In addition, the subsequent dynamics were not well modelled, although all of the participants predicted OBT concentrations that were within a factor of three of the observation at the end of the study period. Four of the five models overpredicted this concentration, perhaps because they did not take into account the loss of OBT by female mussels during egg production and release. With one exception, the models all predicted similar mussel concentrations for the two exposure scenarios (water only and water plus sediments), in agreement with the observations.

1.4.7. Mussel Depuration Scenario

The Mussel Depuration scenario was similar in all respects to that for the uptake phase except that the mussels were exposed to an abrupt decrease in their ambient tritium levels, rather than an increase. Mussels that had spent all their lives in Perch Lake and were therefore in equilibrium with environmental tritium concentrations of around 5000 Bq/L, were transplanted to a control site with a background activity of 50 Bq/L. Following transplantation, HTO and OBT measurements were taken hourly for the first two hours and then at longer time intervals for the duration of the study, which lasted for 117 days. The same supporting information was made available as for the uptake phase, and the endpoints of the scenario were the same.

The models used for the uptake scenario were also used for the depuration phase, although two modelers made modifications based on their earlier results. One added an additional compartment representing stomach contents to account for OBT associated with food that had not yet been digested. The second revised the transfer parameters in the model based on a calibration of model predictions against observations from the uptake scenario.

The experimental data showed that the HTO concentration in the mussels dropped off quickly following transplantation, reaching steady state with the concentration in lake water within two hours. All models predicted equilibrium with lake water but most over-estimated the time required to do so, by two hours to one day. For the first 12 days following transplantation, all models reproduced the observed OBT dynamics well but underpredicted the OBT concentrations by a factor of 2 to 3. After 12 days, predictions of two of the models (including the one with calibrated transfer parameters) converged on the observations. The other two (including the model with the additional stomach compartment) continued to overestimate the rate of loss from the mussels and underpredicted the OBT concentrations by a factor of 20 at the end of the study period.

1.4.8. Scenarios Based on Hypothetical Releases

The aim of this study was to estimate the consequences of an acute atmospheric release of tritium, and to use the results to provide information that would be helpful to decision makers in managing an accident, taking into account the meteorological conditions in effect at the time of the release. Since no dataset was available that covered this situation, the calculations were made for hypothetical conditions. Ten grams of tritium (as either HTO or HT) were assumed to be released from an isolated 20 m stack over a 1 hour period at the end of June, when crops were coming up in the field. Three different meteorological cases were considered: fine weather in daytime (Case 1); rainy conditions during the day (Case 2); and clear conditions at night (Case 3). The scenario description included information on crop yields, crop water contents, time between release and harvest, and food intake rates by members of the public.

Modelers were asked to make the following predictions for HT and HTO releases for Cases 1–3:

(1) Time-integrated HTO concentrations in air at downwind distances of 1, 3, 10 and 30 km.
(2) Total doses after one year from all exposure pathways (ingestion, inhalation and skin absorption) at downwind distances of 1, 3, 10 and 30 km.
(3) A breakdown of the total dose by exposure pathway at a downwind distance of 1 km.
(4) The contribution of HTO and OBT in the air and soil pathways to the total dose at a downwind distance of 1 km.

Most participants calculated air concentrations using a Gaussian plume model with constant wind direction during the release but most adopted different lateral and vertical dispersion parameters. In most cases, dry deposition was modelled using a deposition velocity that was either calculated or defined, and wet deposition was estimated using a washout coefficient, but the values of the deposition parameters varied from model to model. Plume depletion due to wet and dry deposition was included in most models. Air concentrations due to re-emission from plants and soil were calculated by three of the eight participants. The weather conditions in effect after the release were specified differently by each modeller, which resulted in different predictions of wet deposition, root uptake and re-emission from soil.

The models used to calculate the transfer of HTO from air to plants, and the formation of OBT in the plants, were similar to those described above for the Soybean scenario. The models used in the Hypothetical scenario additionally treated the uptake of tritium from soil. Two general approaches were taken to estimating HTO concentrations in soil, one based on the solution of the advection-diffusion equation and the other based on simple water balance considerations. The root uptake of tritium by plants was estimated from the transpiration flux or through the assumption of specific activity equilibrium between soil water and plant water.

The models used to calculate tritium concentrations in animal products were similar to those described above for the Pig scenario. All participants calculated doses in a similar manner by multiplying the rates of tritium intake by a dose conversion factor, although the modellers made different assumptions regarding the number and timing of harvests for each crop.

The air concentrations calculated by the various participants ranged over a factor of 10 at all downwind distances in Case 1 and at short distances for Cases 2 and 3. The variability increased to a factor of 100 at longer distances in Cases 2 and 3. The differences were due primarily to the different lateral and vertical dispersion parameters adopted by the different modelers and, for Case 2, to the different assumptions made about washout.

The predicted total dose averaged over all models for HTO releases increased from 2 mSv for Case 1 to 17 mSv for Case 2 to 26 mSv for Case 3. There was substantial variability about these values, ranging from a factor 15 at all downwind distances for Case 1 to a factor of 10^4 at 30 km for Case 2. For all cases, the variability was driven in part by the variability in the predicted air concentrations and in part by differences in the way the participants modeled tritium transfer through the food chain. The extreme variability at large downwind distances in Case 2 was due to the different ways in which washout was modeled. The total doses predicted for the HT release were only a few percent of the HTO doses and showed similar variability.

For all cases, the models identified the ingestion of cereals and green vegetables as the largest contributors to total dose, followed by ingestion of animal products and inhalation. Larger ingestion doses were received from the air pathways than the soil pathways, and from OBT as opposed to HTO.

The model predictions suggest that a dose of 5 mSv will be saved if garden crops are interdicted when the HTO concentration exceeds 10^7 Bq kg^{-1} fresh weight in leafy vegetables in the first day after the accident. This derived intervention level drops to 10^6 Bq kg^{-1} in the second day. These values are independent of the weather conditions at the time of release.

1.4.9. Rice Scenario

The Rice scenario was based on 10 years of monitoring data collected around the Tokai reprocessing plant (TRP) in Tokai-mura, Japan. Carbon-14 is released continuously to the atmosphere in the form of $^{14}CO_2$ from three 90 m stacks on the TRP site. Monthly-averaged $^{14}CO_2$ air samples were collected at three monitoring stations within 4 km of the site, and at two remote background stations. Rice grain samples were collected in late September (the normal harvest time for rice) at two sites within 2 km of the TRP and at a background site 12 km distant.

The scenario description included information on weekly ^{14}C release rates, physical characteristics of the stacks, hourly meteorological data observed at stack height, annual

background levels of ^{14}C in Japan, the management schedule of a paddy field in Tokai-mura and the growth of rice plants. From this information, participants were asked to calculate:

(1) Monthly mean ^{14}C concentrations in air at four monitoring stations from May to October (i.e. the rice growing season) for 1992 to 1997.
(2) Carbon-14 concentrations in rice grains collected at three monitoring sites for 1992 to 2001.

Four of the five modelers in this scenario employed the sector-averaged Gaussian plume model to calculate $^{14}CO_2$ concentrations in air, with the fifth using a straight-line Gaussian model. Despite the similarity in structure, the models differed significantly in the way they treated plume rise, vertical dispersion and plume depletion due to dry deposition, as well as in the values they adopted for the surface roughness length, and in the meteorological data they used. None of the models accounted for wet deposition or re-emission from soil and plants to the air.

The approaches to modeling the uptake of ^{14}C in rice plants varied widely. Two participants set the rice concentration equal to the average air concentration (on a Bq/gC basis), on the assumption of specific activity equilibrium between plant and air. However, different averaging times were adopted in the two models. Two other participants employed dynamic multi-compartment models, simulating the incorporation of ^{14}C into new dry matter during plant growth, and translocation of the photosynthetic assimilate from the vegetative parts of the plant to the grain. These models differed in the number of compartments they employed and the values of their parameters. The final participant used a process-oriented model describing the incorporation of ^{14}C into rice grain. The model was based on a logistic growth function for the plant dry matter, and the development of the plant depended on the air temperature above a specific temperature.

Despite the difference in approaches to calculating plume rise, vertical dispersion and plume depletion in the Gaussian models used by the participants, the various predictions of atmospheric $^{14}CO_2$ concentrations agreed with each other and with the observations when uncertainties were taken into account. Thus, different formulations of the simple Gaussian model can provide acceptable accuracy, even in the calculation of air concentrations at locations close to the source. No one model produced consistently superior predictions over all sites and times.

The predicted ^{14}C concentrations in rice also agreed with the observations despite differences in the way the dynamic models treated the translocation of photosynthates, formed in the plant body before flowering, to the grain. The performance of the simple specific activity models was as good as that of the dynamic models, although the same is unlikely to be true for an acute release.

The time over which the air concentrations are averaged is a key factor in applying the specific activity (SA) model. Of the two SA models in the Rice scenario, one averaged over August and September, on the assumption that the relevant air concentrations were those in effect during the period of grain formation. On the other hand, the second averaged over the period May to October, on the assumption that the ^{14}C content of the grain depended in part on the concentration fixed in the vegetative parts of the plant before grain formation and subsequently translocated to the grain. Averaging over the grain formation period resulted in better predictions, indicating that translocation makes a minor contribution to the total ^{14}C content of the grain.

1.4.10. Potato Scenario

The Potato Scenario was based on experiments in which potato tubers were exposed to $^{14}CO_2$ in a wind tunnel for approximately 10 hour periods at six different stages of plant growth (P1–P6). Thirty pots containing three plants each were placed in the wind tunnel for each experiment. Following fumigation, samples were taken immediately to measure the initial amount of ^{14}C fixed by the crop, and the plants were then moved outside to a garden. Subsequent samples were taken at intervals that varied in number and frequency according to the age of the crop at fumigation. ^{14}C air concentrations, air temperatures and photosynthetically active radiation were measured in the tunnel during each experiment. The average dry weights and dry weight fractions of the roots, leaves, stems and tubers were measured at every sampling time in all experiments.From this information, the modelers were asked to calculate the following endpoints:

(1) The ^{14}C concentration in the leaves at each sampling time for each experiment.
(2) The ^{14}C concentration in the tubers at the final sampling time for each experiment.

All of the models participating in the Potato scenario were dynamic compartment models. All assumed that ^{14}C is incorporated into plants as a result of photosynthetic carbon assimilation and that translocation occurs between leaves, where photosynthesis takes place, and storage organs. The total growth rate of the plant was assumed to correspond to the net photosynthetic carbon assimilation rate, which was a function of leaf biomass, photosynthetically active radiation and leaf area index, among other parameters. The allocation of assimilates to different parts of the plant depended on the growth stage. The models exhibited differences with respect to objective (realistic vs. conservative), number of compartments, the way in which the photosynthesis model was formulated and the values of the required parameters.

For experiments P1 to P3, model predictions of ^{14}C concentrations in leaves bracketed the observations, but individual results often differed from the measurements by an order of magnitude. For experiments P4 to P6, a number of models did not predict any ^{14}C in the leaves, although significant amounts were always observed. This was explained by an improper choice in these models for the partition fractions of new photosynthates to the various plant parts. Those models that did predict a finite amount of ^{14}C in the leaves tended to overestimate the concentrations for experiments P4 and P5.

The predictions were poor for experiment P6, which involved plants at a late stage of growth. Most models adopted a high photosynthetic rate for this case based on the time between seeding and exposure. However, a much lower rate would have been more appropriate given that the plants were seeded much later in the year than normal. The late seeding and early and sudden onset of senescence may have contributed to the poor predictions in general, since the models were developed on the basis of a more normal plant growth scenario. All of the models overestimated the leaf concentration for the last sampling point in each experiment, when the plants were close to senescence. The models ignored translocation from leaves to tubers at this late stage of growth.

One model consistently overestimated leaf concentrations because it used a maximum value for the photosynthetic rate, rather than a rate that varied depending on light levels and air temperature. The overestimates produced by another model could be reduced by a factor three by driving the models with an air concentration that was a weighted average based on photosynthetic rate, rather than a straightforward arithmetic average.

Most models overestimated the ^{14}C concentrations in the tubers, but on the whole the predictions lay within a factor of 10 of the observations. This is better agreement than was obtained for the leaves, suggesting that compensatory errors are at play, at least for models that over predict the leaf concentrations.

The simpler models were found to be adequate for predicting the initial incorporation of ^{14}C into the leaves, but more complex models performed better in simulating the ^{14}C dynamics and the translocation rates to various parts of the plant.

1.5. Discussion and conclusions

1.5.1. Key achievements of the Tritium/C14 WG

The EMRAS Tritium/C14 WG tested environmental tritium and ^{14}C models in scenarios that covered terrestrial and aquatic ecosystems, steady-state and dynamic conditions, and acute and chronic releases. This has resulted in improved understanding of the processes and factors affecting the reliability of these models, and has helped to define the level of confidence that can be placed in them. Because of the many differences in the models used by the various participants, it was often difficult to isolate the key reasons for the differences in their predictions. Nevertheless, it was usually possible to identify the modelling approaches that led to the best predictions for a specific scenario. In general, the simple specific activity models performed as well as the more complex dynamic models for chronic releases, but complex models were required to reproduce the observations for short-term releases.

Participation in the WG has helped to maintain the capability of modellers in Member States to assess the impact of tritium and ^{14}C releases to the environment. In many cases, participants modified their models during the course of the programme to reflect approaches or information that came to light during discussions at WG meetings. The modified models invariably performed better than the originals.

The scenarios developed by the WG provide a valuable source of test data for validating environmental tritium and ^{14}C models. In most cases, the test data already existed but were organized and qualified for use by the scenario leaders. In the case of the mussel uptake and depuration scenarios, new experimental work was undertaken to provide suitable data in an area where they were previously lacking. The debate over the nature and definition of organically bound tritium also led to new experiments to investigate the existence and magnitude of buried tritium. In all cases, the analysis of the experimental data that was required to put them in a form suitable for model testing led to increased understanding of tritium and ^{14}C transport in the environment.

Results from the hypothetical scenarios provided a rational way to derive intervention levels for tritium (the tritium concentration in agricultural crops above which interdiction is desirable to avert a given dose from all exposure pathways). The model predictions suggest that a dose of 5 mSv will be saved if garden crops are interdicted when the HTO concentration exceeds 10^7 Bq kg^{-1} fresh weight in leafy vegetables in the first day after the accident. This level drops to 10^6 Bq kg^{-1} in the second day. These values are independent of the weather conditions at the time of release.

1.5.2. Model performance

The models used by the various participants in a given scenario were conceptually similar, in the sense that each included the key processes that control environmental tritium and ^{14}C

transfer (uptake by plants, fixation in organic compounds, transfer to animals through ingestion, and so on). However, the models differed substantially in the way the processes were implemented. The simpler models were based on specific activity concepts, with concentrations in a given compartment determined by the specific activities in the hydrogen or carbon pools that contributed tritium or ^{14}C to the compartment. The more complex approaches were formulated in terms of dynamic compartment models or process-oriented models, in which the various transfer processes were simulated explicitly. Even here, the models differed in the number of compartments considered, the required parameters and their values, the growth curves adopted for plants and animals, the plant cultivars and animal breeds assumed, and so on.

The differences in the models led to variability in the predictions of about a factor of 2 for scenarios involving continuous releases, and a factor of 10 or more for short-term releases. In the former case, performance was better for models that were driven by air concentrations averaged over the OBT or ^{14}C residence time in the compartment of interest (one or two months prior to sampling in the case of OBT concentrations in plants and animals; the period of grain formation in the case of ^{14}C concentrations in rice). The dynamics of OBT and ^{14}C concentrations were generally poorly reproduced in scenarios involving short-term releases. The observed concentrations at harvest depended on the growth stage of the plant at the time of exposure, and performance was best for models with realistic growth curves. For most scenarios, the predictions tended to bracket the observations, suggesting that, in an average sense, the models reflect a good conceptual understanding of the environmental transport of tritium and ^{14}C. In some scenarios, part of the difference between predictions and observations could be attributed to the uncertainty in the observations as well as in the predictions.

Participants in each of the scenarios were asked to supply uncertainty estimates with their predictions. However, not all did so and those that did carried out their analyses in different ways, and obtained different results. The methods used included expert judgment, perturbation analysis, numerical Monte Carlo analysis, and analysis of variations in the observations. The magnitude of the estimated uncertainties depended on the endpoint in question and, for dynamic scenarios, on the time after exposure.

Most participants estimated the uncertainty in their predictions for the steady-state scenarios (Perch Lake, Pickering, Pine Tree and Rice). For the HTO and ^{14}C endpoints, these were roughly consistent with a 95% confidence interval (97.5^{th} percentile divided by the 2.5^{th} percentile) of a factor 3 to 4. In general, the modellers estimated slightly higher uncertainties for OBT concentrations than for HTO, which is reasonable given that the uncertainties in OBT include those for HTO plus additional ones specific to OBT itself.

Few of the participants in the dynamic scenarios (Soybean, Mussel Uptake, Mussel Depuration, Pig, Hypothetical and Potato) assessed their uncertainties, and those estimates that were supplied varied widely. Thus, no definitive conclusions can be drawn regarding the uncertainties in the model predictions. However, rough estimates can be obtained from an overall assessment of the scatter in the predictions and the differences between predictions and observations. These suggest that the 95% confidence intervals on HTO and ^{14}C concentrations were about a factor of 10 shortly after exposure. These intervals stayed roughly constant over time for the Mussel, Pig and Potato scenarios, but increased to a factor of 100 or more at later times in the Soybean scenario and at greater distances in the Hypothetical scenario. The confidence intervals were generally smaller for OBT than for

HTO, reflecting the fact that, for the dynamic scenarios, HTO varies rapidly over time whereas OBT integrates.

The uncertainties in the models can be reduced by:

- ensuring that the air concentrations used to drive the models are of high quality and match the resolution and averaging requirements of the scenario;
- incorporating as much site-specific information as possible on land use, local soil properties and predominant crop cultivars and animal breeds, together with realistic assumptions concerning the habits of the maximally exposed individual;
- basing all sub-models on the physical approaches available for the disciplines in question. For example, knowledge from the agricultural sciences should be used to improve models for crop growth, photosynthesis, translocation and so on. Recent progress in understanding environmental carbon and hydrogen cycling should also be considered;
- recognizing and accounting for any unusual experimental conditions (water stress, an uncommon cultivar or breed) in the model application;
- using suitable spatial and temporal averaging in the models. Predicted OBT concentrations in plants and animals should be based on air concentrations averaged over the month or two prior to sampling. Predicted ^{14}C concentrations in grain should be based on air concentrations averaged over the period of grain formation;
- using realistic plant and animal growth models in the calculations;
- incorporating changing meteorological and environmental conditions into the models in a dynamic way.

Overall, the variation in the predictions of the participating models was about the same in EMRAS as it was in the previous model testing programmes BIOMASS and BIOMOVS II. This is partly because model performance is scenario specific, so that a model that did well in a BIOMASS scenario may not necessarily do well in an EMRAS scenario. Moreover, different modellers participated in the different programmes, bringing with them different models, so that the process of model improvement started anew with each programme. Thus the fact that the variability in predictions has remained static over time does not suggest that model performance has not improved. Improvements are readily apparent in individual models applied to specific scenarios.

1.5.3. Recommendations for future work

Further work in the following areas would help to improve tritium and ^{14}C dose assessments:

- testing and improving models of atmospheric dispersion; plant uptake of HTO at night and when it is raining; OBT formation in plants at night; translocation of OBT to fruit and roots; isotopic discrimination; tritium behaviour in soils following deposition, including deposition of HT and conversion to HTO; tritium behaviour in winter, including washout by snow, dry deposition to snow and the fate of tritium in the snow pack; and transformation and losses in cooking;
- modifying the steady-state models for chronic releases to account for the fact that fluctuations in release rates and meteorological conditions result in a state of quasi-equilibrium in the environment, rather than the complete equilibrium assumed by the models;
- developing a standard conceptual model for accidental tritium releases;

— carrying out rigorous uncertainty analyses of the dynamic models to better quantify the uncertainties in their predictions for a variety of scenarios;
— investigating and understanding the large OBT/HTO ratios that have been observed in soils, plants and fish under conditions that are ostensibly at equilibrium;
— extending tritium dosimetry to address infants and pregnant women.

CHAPTER 2. THE PERCH LAKE SCENARIO

2.1. Scenario description

This scenario is based on data collected in Perch Lake, a small, shallow freshwater lake located within the borders of AECL's Chalk River Laboratories in northeastern Ontario (Figure 2.1). The lake contains elevated levels of tritium due to long-term discharge from nearby waste management areas. The tritium forms a well-defined subsurface plume that discharges into the lake through sediments and a stream (Inlet 2 in Figure 2.1). Inlet 1 shows slightly elevated levels of tritium but Inlets 3, 4 and 5 are all uncontaminated.

Tritium concentrations were measured in samples of air, lake water, sediments, aquatic plants (algae, bladderworts, hornworts and cattails) and animals (clams, bullheads and pike) collected in the summer and fall of 2003. Bladderwort and hornwort (hereafter referred to collectively as worts) are both unrooted plants that are completely submerged and obtain their nutrients from the water. These two species were composited for analysis. The cattails are rooted in the top 5–10 cm of the sediments, from which they draw their nutrients. They extend above the water into the air, and the submerged and emergent parts were analysed separately. Bullheads are omnivorous, benthic fish and pike are larger piscivores. Both types of fish likely move throughout the lake, eating other fish and invertebrates. The fish samples were divided into three parts (flesh, head and internal organs), each of which was analyzed separately.

The air, water, sediment and plant samples were taken primarily from three locations: at S1, located near Inlet 1; at S2 near Inlet 2; and at S3 near Inlet 3 (Figure 2.1). A few samples were also taken at S4 near Inlet 4 and near the outlet of the lake. Some water samples were collected from the surface of the lake and others at depth near the bottom. Most of the plant and sediment samples were collected from shore at the edge of the lake. Some of the water samples were also taken close to shore but others were collected by boat 50–100 m offshore, as were algae. Fish tend to feed on the east side of the lake and were caught in two extended areas on either side of the outlet, whereas clams were harvested between Inlet 3 and the outlet. Most samples were collected three times during the summer and fall of 2003 (May 29–30, July 28–29 and October 1–2). Additional measurements of water concentrations were made in early November. Air concentrations were measured only in August and October as monthly averages and algae and clams were not available in October. Replicate samples were taken in some cases. All samples were analyzed for their HTO content, and OBT concentrations were determined for the sediments, plants and animals.

Given the measured HTO concentrations in water, sediments and air, participants in the scenario were asked to calculate:

(1) HTO and non-exchangeable OBT concentrations in cattails and worts for the May sampling period for the near-shore portions of sites S1, S2 and S3. For cattails, concentrations were requested for both the above water and below water parts of the plant.
(2) HTO and non-exchangeable OBT concentrations in algae for the May sampling period for the offshore portions of sites S1, S2 and S3.
(3) HTO and non-exchangeable OBT concentrations in clams, bullheads and pike for each of the three sampling periods. For bullheads and pike, concentrations were requested in head, flesh and internal organs (liver, gonads, stomach and intestines).

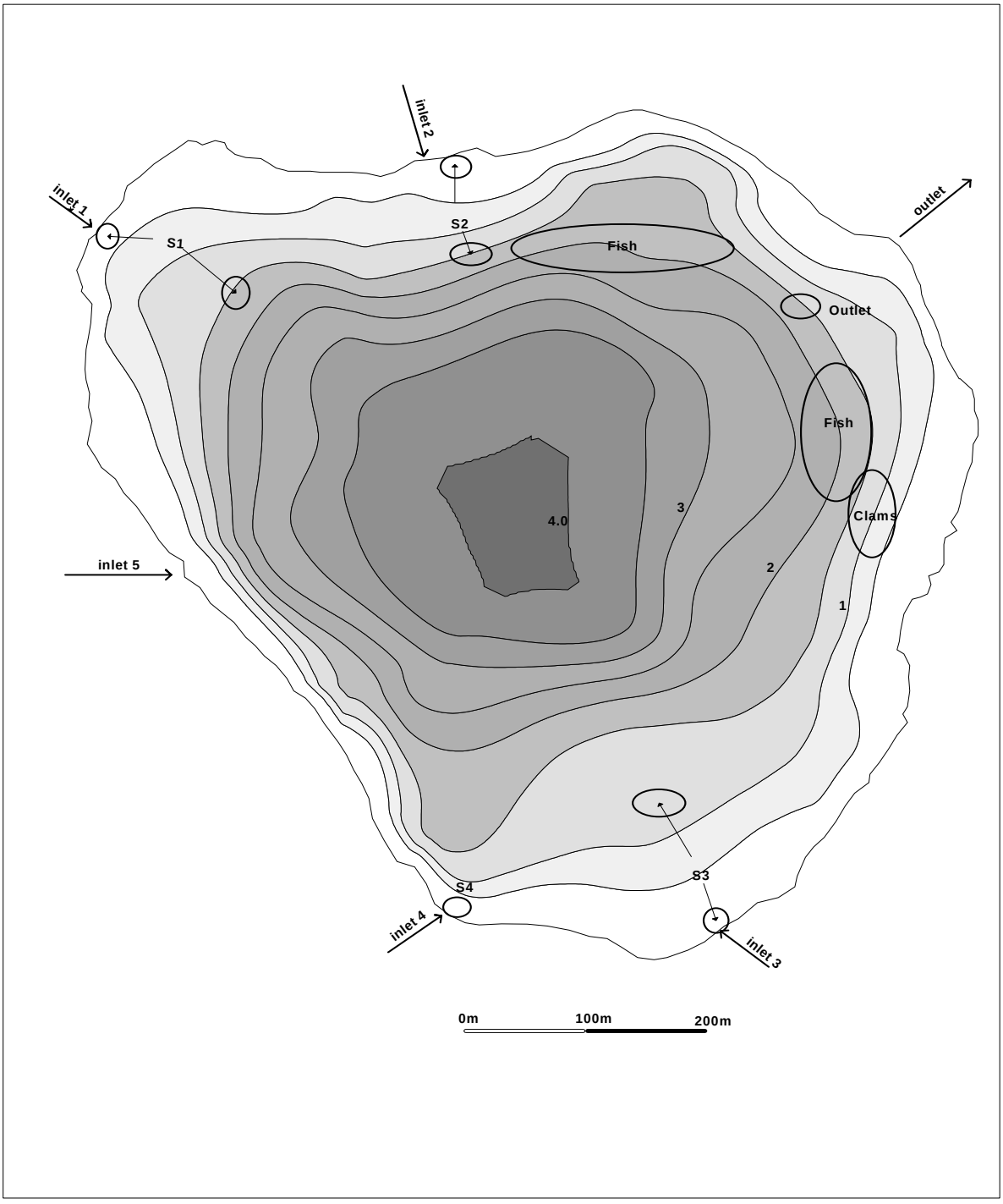

Fig. 2.1. Map of Perch Lake showing inlets, the outlet, depth contours in m and the sampling locations.

(4) non-exchangeable OBT concentrations in sediments for the May sampling time for the near-shore portions of sites S1, S2 and S3.
(5) 95% confidence intervals on all predictions in (1)–(4).

The data included in the scenario represented a relatively small subset of all the data collected in the experimental programme. The full data set has been presented and analyzed by Kim et al. [8]. The full scenario description is given in Appendix I.1.

2.2. Observations

2.2.1. Measured concentrations

Measured HTO concentrations in air moisture, lake water and sediment water are shown in Table 2.1. These are the concentrations that were supplied to the participants to drive their models. Observed HTO and OBT concentrations in plants, animals and sediments, which were the endpoints of the scenario, are given in Tables 2.2 and 2.3. The OBT concentrations are given in units of Bq L^{-1} of combustion water.

Counting errors in the HTO concentrations for lake water, plants and aquatic animals were generally less than 2%, but reached about 10% in some cases. These errors likely represent the full uncertainty for the lake water samples, which are easy to collect and analyse. Additional differences of perhaps 30% would be expected from sample to sample in plants and animals due to natural variability. Counting errors in the sediment concentrations were larger, reaching up to 25% in some cases, and the total uncertainty may be somewhat greater because of difficulties in keeping the sediment pore water distinct from the lake water. Uncertainties in air concentrations arose due to counting errors and the performance of the samplers, and are estimated to be about 30%. Counting errors for OBT concentrations were usually less than 5% but additional uncertainty arose due to difficulties in removing exchangeable OBT from the samples and in the combustion process. The total uncertainty in the OBT measurements is estimated to be about 20%, although greater variation must be expected among individual plants and animals.

Table 2.1. Measured HTO concentrations in water, sediment water and air moisture.

Month	Compartment		HTO Concentrations (Bq L^{-1})				
			S1	S2	S3	S4	Outlet
May	Surface water	– offshore	4350	5450	4730		
	Sediment water	– offshore	4730	10890	1320		
			3330	13570			
			3830	13210			
July	Surface water	– offshore	4640	4590	4620		4660
		– from shore near inlet	4150	3330	3800	91	
	Bottom water	– offshore*	4480	4460	4420		4620
		– from shore near inlet‡	3900	2570	3580		
	Sediment water	– from shore near inlet	2300	7120	70		
Oct	Surface water	– from shore near inlet	2030	9290	139		
	Bottom water	– from shore near inlet‡	2080	9190	113		
	Sediment water	– from shore near inlet	1500	7420	84		
			1650	4550			
	Air	– August	740	1970	510		
		– October	660	1770	260		
Nov	Surface water	– offshore	3840	5270	3770		
	Bottom water	– offshore*	3480	9350	3770		

* Collected at a depth of about 1.5 m.
‡ Collected at a depth of about 0.4 m.

Table 2.2. Observed HTO and OBT concentrations in plants and sediments in May.

Compartment		HTO (Bq/L)			OBT (Bq/L combustion water)		
		S1	S2	S3	S1	S2	S3
Cattails	– emergent	1970	8080	1180	1500	4100	971
	– submerged	3390	9760	1360	2120	3760	655
Worts		4680	6020	4520	2500	3230	1580
Algae		6630	5490	4990	2610	3200	2410
Sediments		See Table 2.1			1960	2970	488

Table 2.3. Observed HTO and OBT concentrations in clams and fish.

Fish Type		HTO (Bq/L)			OBT (Bq/L combustion water)		
		May	July	October	May	July	October
Clams		5750	4100	–	3270	3810	–
Bullheads	– head	5270	4070	3230	3820	3160	4110
	– flesh	5310	4050	3230	3970	3480	3820
	– internal organs	5240	4040	3620	3610	3340	3520
Pike	– head	5120	4100	3470	3630	4050	4480
	– flesh	5020	4130	3460	3950	3710	4500
	– internal organs	5170	4100	3510	3780	3460	4610

2.2.2. Analysis of observations

The following conclusions can be drawn from an analysis of the full Perch Lake data set [8]:

2.2.2.1. HTO Concentrations

— Within experimental uncertainty, the HTO concentrations in the aqueous parts of algae and worts are indistinguishable from the HTO concentrations in the water surrounding them (plant/water = 0.94 ± 0.27; n = 12; 1 outlier ignored).

— HTO concentrations in the submerged parts of cattails are the same as HTO concentrations in sediment pore water (plant/sediment = 1.06 ± 0.29; n = 9).

— HTO concentrations in the emergent parts of cattails (C_{ec}) are well predicted by the equation $C_{ec} = 1.1\ (C_{am} + C_{sed})/2$, where C_{am} and C_{sed} are the HTO concentrations in air moisture and sediment water (predicted/observed = 1.03 ± 0.21; n = 9). The factor 1.1 is the ratio of vapour pressures between water and HTO, and is introduced by analogy with the model for terrestrial plants [7].

— HTO concentrations in clams are the same as HTO concentrations in bottom waters averaged over all offshore locations (clam/water = 1.05 ± 0.14; n = 2).

— HTO concentrations in bullheads are indistinguishable from the HTO concentrations in bottom waters averaged over inshore and offshore locations (fish/water = 0.96 ± 0.06; n = 3).

— HTO concentrations in pike are the same as HTO concentrations in water averaged over the entire lake, including surface and bottom water and onshore and offshore water (fish/water = 0.96 ± 0.04; n = 3).

— HTO concentrations in the flesh, head and internal organs of the fish show no significant differences.

2.2.2.2. OBT Concentrations

- OBT concentrations in the combustion water of algae and worts are proportional to the HTO concentrations in the aqueous part of the respective plants, averaged up to the time of sampling. The mean observed OBT/HTO ratio is 0.48, with a standard deviation ± 0.08 (n = 13).
- OBT concentrations in all parts of cattails are proportional to the HTO concentrations in the emergent part of the plant, averaged up to the time of sampling. The mean observed OBT/HTO ratio is 0.70, with a standard deviation ± 0.19 (n = 18).
- OBT concentrations in clams, bullheads and pike are proportional to the HTO concentrations in water, averaged spatially over the locations accessed by the species in question and temporally up to the time of sampling. The mean observed OBT/HTO ratio is 0.79, with a standard deviation ± 0.09 (n = 8).
- OBT concentrations in the flesh, head and internal organs of the fish show no significant differences.
- OBT concentrations in sediments are about 60% of the OBT concentration in plants (n = 9).

The OBT concentrations in all plants are less than the corresponding HTO concentrations primarily because of isotopic discrimination in the formation of OBT. Similarly, animal OBT concentrations are less than HTO concentrations because of metabolic processes that tend to convert OBT to HTO.

2.3. Model descriptions

Eight participants submitted results for this scenario (Table 2.4). All participants treated the scenario as a blind test of their models and submitted results before the observed concentrations were made known to them.

The Perch Lake scenario tested models that predict tritium concentrations in an aquatic ecosystem subject to a continuous release of HTO. It was a fairly simple scenario in the sense that releases to the lake have been going on for many years at roughly the same rate, and tritium concentrations in various parts of the ecosystem are likely to be in equilibrium. However, the scenario showed a number of complicating factors. Since tritium enters the lake through the sediments, concentrations in sediment pore water are generally higher than those in lake water, which in turn are higher than those in air. The sediments themselves show a spatial gradient in concentration, with larger values in the parts of the lake closest to the subsurface tritium plume.

Table 2.4. Participants in the Perch Lake Scenario.

Participant	Affiliation	Designation in text
A. Golubev	VNIIEF, Russia	VNIIEF
F. Siclet	EDF, France	EDF
M. Saito	Safety Reassurance Academy, Japan	SRA
F. Baumgärtner	Technische Universität München, Germany	BioM
D. Galeriu	IFIN-HH, Romania	IFIN
Japanet*	Japan	J
P. Marks	GE Healthcare, U.K.	GE
T. Nedveckaite	Institute of Physics, Lithuania (LIETDOS_W model)	L

* Participants from NIRS, Ibaraki University, Kumamoto University, Toyama University and Kyoto University, led by K. Miyamoto and Y. Inoue from NIRS.

Water concentrations in a narrow zone close to shore may be higher or lower than those in the main body of the lake, depending on the tritium concentration in the water in the streams flowing into the lake. Concentrations in sediments, lake water and air all varied gradually with time during the study period. Finally, the sediments were composed of a mixture of sand and gyttja (decomposing organic matter), with proportions varying through the lake. In the face of this variability, the modelers had to make a number of decisions: which source compartments (sediments, water or air) contributed tritium to the plants and animals for which predictions were requested; how to average over space to reflect the concentrations seen by the fish, which move freely throughout the lake; how to average over time when calculating concentrations of OBT, which has a long biological half life in all organisms; and how to estimate the required water concentrations when the relevant data was missing or incomplete in the scenario description.

Once these decisions were made, most modelers assumed the HTO concentration in a given endpoint was equal to the average water concentration in the source compartment(s). The exception was L, which assumed that HTO concentrations in plants and animals were slightly lower than in water. The OBT concentration in a given endpoint was generally based on the corresponding HTO concentration, with some allowance made for isotopic discrimination in the case of plants and metabolic processes in the case of animals. The IFIN model generated predictions for each plant type that were representative of a whole lake average, using data from Cornett et al. [9] to augment the information in the scenario description on bottom water concentrations. Two participants (IFIN and GE) used dynamic models to estimate OBT concentrations in algae and all animals, and a third model (EDF) took a similar approach for fish. In each case, these models took account of the growth rate of the animal, ingestion and excretion rates and internal metabolic/catabolic processes to describe the incorporation of OBT in the animal and the conversion between OBT and HTO. The participants showed considerable variability in their approach to modeling sediments.

The BioM model gives different OBT endpoints than those of the other models, predicting the concentration of buried tritium rather than the tritium traditionally considered to be organically (or carbon) bound. Buried tritium is tritium in exchangeable positions that is not removed by the conventional rinsing process. It consists primarily of tritium in large molecules that becomes hidden from the effects of washing when the free water in the sample is extracted by freeze drying or azeotropic distillation. A smaller part consists of tritium in hydrate bonds that is similarly not removed by washing, but this is not accounted for in the model. Buried tritium appears as part of the experimental yield when the sample undergoes traditional analysis for OBT, but is converted to HTO as soon as it is ingested. BioM

calculates the concentration of buried tritium from the HTO concentration in the sample assuming a two-step exchange process and taking into account the proportion of carbohydrates, proteins and DNA in the tissues. The difference between the observed OBT concentration and the predicted buried tritium concentration gives the organically bound (or carbon bound) tritium concentration for the BioM model, if the tritium in the hydration shells is neglected.

The participants estimated the uncertainties in their predictions using very different methods. One modeler (L) carried out a rigorous Monte Carlo uncertainty analysis using lognormal distributions for the HTO concentrations in water and the bioaccumulation factors. At the opposite end of the spectrum, IFIN used expert judgment, arguing that the main source of uncertainty was the lack of detailed information on HTO concentrations in water as a function of time and space in the lake. J also used expert judgment, setting the uncertainty in a given endpoint at ±20% of the water concentration used to predict that endpoint. Between these extremes, EDF, SRA and BioM used the variability in the observed water concentrations as the basis for their uncertainty estimates but even here the individual approaches were quite different. EDF carried out a perturbation analysis to estimate uncertainties in most OBT concentrations and used the range of predictions from different conceptual models to arrive at the uncertainty in sediment OBT concentrations.

Details of the models are introduced in the following sections as they are needed to explain the results. Full model descriptions are given in Appendix II.1.

2.4. Comparison of predictions and observations

2.4.1. Overall results

When the predictions of all the models were averaged for a given endpoint, the results agreed well with the corresponding observation (Table 2.5). The mean predictions lay within 30% of the observations for all HTO concentrations. Similar agreement was found for the OBT concentrations, except in the case of sediments and the underwater parts of cattails, where concentrations were overestimated by factors of 2.3 and 1.7, respectively. Most participants derived the OBT concentrations in submerged cattails from the HTO concentration in the same part of the plant. This leads to overestimates since the data suggest that OBT is formed in the emergent parts and translocated to the submerged parts. HTO concentrations in the emergent parts are low because of losses to the relatively uncontaminated air, and the OBT produced will be correspondingly low.

OBT in sediments is expected to arise from decaying plant and animal material deposited on the lake bottom, with the greatest contribution coming from plants. The sediment concentration was observed to be lower than the concentration in plants by about a factor of 2. This could be due to the increasing age of the organic material in deeper parts of the sediments, which could result in decreasing activity due to decay or breakdown of OBT as the organic matter decomposes. Most participants assumed concentrations were equal in plants and sediments and overestimated the sediment concentrations.

Table 2.5. Comparison of predictions averaged over all models to the observations for each endpoint.

Endpoint	Ratio of mean prediction to observation	
	HTO	OBT
Algae	0.92	1.2
Worts	0.83	1.3
Submerged cattails	1.2	1.7
Emergent cattails	1.3	1.4
Bullhead flesh	1.1	0.87
Pike flesh	1.0	0.71
Clams	0.95	0.91
Sediments	*	2.3

* HTO concentrations in sediments were given as part of the scenario description.

Table 2.6. Range of model predictions for each endpoint.

Endpoint	Ratio of highest to lowest prediction	
	HTO	OBT
Algae	1.8	2.6
Worts	1.7	4.1
Submerged cattails	93	103
Emergent cattails	6.5	103
Bullhead flesh	3.3	6.1
Pike flesh	2.6	7.8
Clams	2.8	5.2
Sediments	*	97

* HTO concentrations in sediments were given as part of the scenario description.

The results shown in Table 2.5 indicate that, with the exception of OBT in sediments and the underwater parts of cattails, the modelers as a group have a good conceptual understanding of the behaviour of tritium in the Perch Lake ecosystem and can predict HTO and OBT concentrations that, in an average sense, agree well with the observations. However, the scatter in the predictions of individual models was substantial. Table 2.6 shows the ratio of the largest prediction to the smallest for each endpoint in the scenario. The ratios range from 1.7 to more than 100 and are larger for OBT than for HTO. The largest values occur for sediments and the emergent parts of cattails, where the modelers showed the greatest divergence in their conceptual approaches.

Results for each scenario endpoint are discussed in turn below. For the plant and sediment endpoints, emphasis will be given to sampling site S3, where spatial gradients are expected to be smallest. For the animal endpoints, the discussion will focus on the results for July, for which there is the largest amount of information on HTO concentrations in water and sediments.

2.4.2. Algae

Predictions for the HTO concentration in algae at sampling site S3 in May are compared with the observation in Figure 2.2. Because algae is completely submerged in water, and because tritium in so mobile in the aqueous phase, the HTO concentration in algae collected at a given time and place is expected to equal the local water concentration. This expectation was borne out in the analysis of the full Perch Lake dataset [8] and is evident at site S3 in May, where the HTO concentration in algae (4990 Bq/L) was within 5% of the water concentration (4730 Bq/L). Five of the participants (EDF, SRA, BioM, IFIN and J) assumed the HTO concentration in algae was equal to the local water concentration and so achieved a good result (Figure 2.2). GE is a dynamic model and overestimated the observation slightly, but even here the prediction lay within the uncertainty bounds of the data. VNIIEF assumed that the algae were in equilibrium with water concentrations averaged over surface and bottom layers and underestimated the observation. It is not clear if this underprediction is significant because the modeler did not estimate the uncertainties in his concentrations. Participant L did not submit predictions for algae.

The results for Site S2 followed the same pattern as for S3, with all models but VNIIEF producing results in good agreement with the observation. At S1, all of the models predicted a concentration in algae close to the water concentration (4350 Bq/L) but for some reason the observed concentration in algae at this site was substantially higher at 6630 Bq/L.

Because of the slow turnover rate of OBT in algae and other plants, OBT concentrations are expected to depend on the plant HTO concentration averaged over the few weeks prior to the sampling time. It was not possible to test such a dependence using the Perch Lake data since no water measurements were made prior to the May sampling period. Instead, most modelers based their OBT prediction on the predicted HTO concentration in the algae. These predictions showed greater scatter than those for HTO (Figure 2.3). Two modelers (IFIN and GE) attempted to simulate the formation of OBT using dynamic models that took into account the growth rate and dry fraction of the algae and the time-dependent water concentration, and both were relatively successful. The other participants assumed the OBT concentration was proportional to the HTO concentration, with the proportionality constant F_D allowing for processes such as isotopic discrimination. Most modelers took a value of F_D from the literature, with the chosen values ranging from 0.5 to 0.8 (Table 2.7). The BioM model calculated a somewhat lower value of 0.41 but this and the model prediction itself applies to buried tritium rather than OBT. The variation in F_D, coupled with the variation in the predicted HTO concentration in the plants, resulted in OBT predictions that varied by more than a factor of 2. Each individual prediction was within a factor of 1.7 of the observation, although in one case (J) the difference between prediction and observation was significant even when uncertainties were taken into account. Very similar results were obtained for sites S1 and S2. The full Perch Lake data set implies that $F_D = 0.46 \pm 0.08$ for algae, in agreement with the results of Blaylock et al. [10].

The 95% confidence intervals shown in Figures 2.2 and 2.3 vary greatly from model to model, reflecting the different approaches taken by the participants in estimating their uncertainties. The confidence interval on the OBT concentration for model J is clearly an underestimate since the prediction does not agree with the observation even when uncertainties are taken into account. On the other hand, the confidence interval estimated by EDF (which reflects the variability in the observed water concentrations over all time and space) is so large that the prediction loses a lot of its usefulness. Similar variability arose for the other endpoints and will be discussed further in Section 2.5.

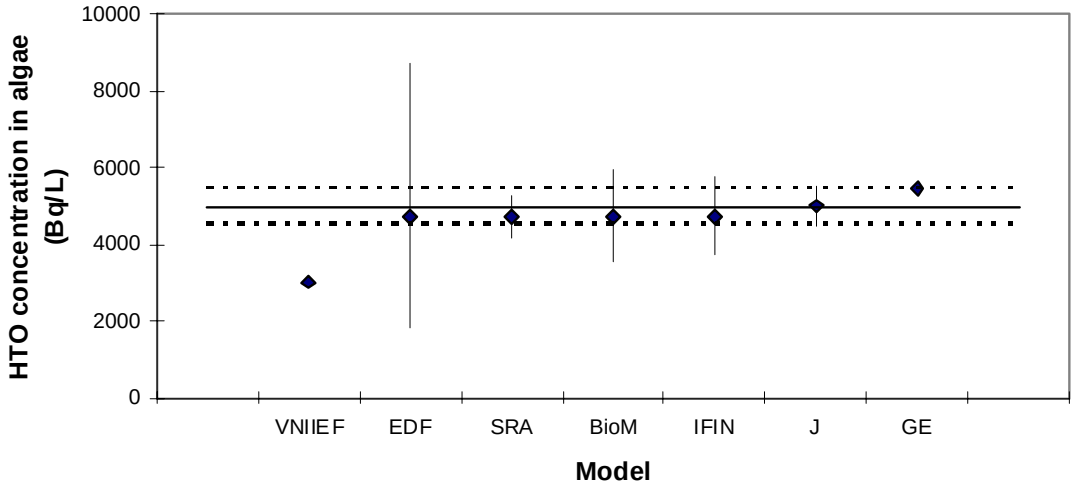

Fig. 2.2. HTO concentrations in algae at site S3 in May. The model predictions are shown as solid diamonds with the vertical lines representing 95% confidence intervals as estimated by the modelers. The solid horizontal line is the observation with the 95% confidence interval indicated by the dashed lines. VNIIEF and GE did not provide uncertainty estimates and L did not submit results for this endpoint. The offshore water concentration at S3 in May was 4730 Bq/L.

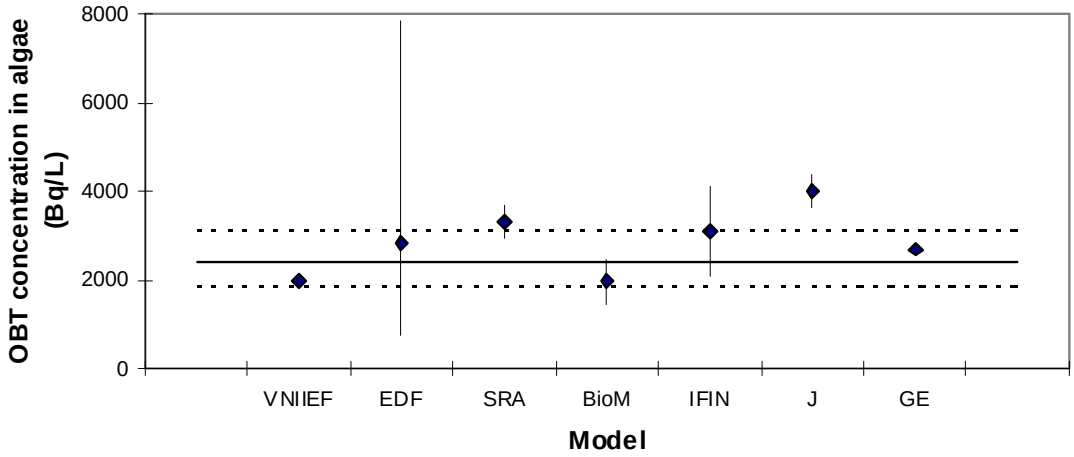

Fig. 2.3. OBT concentrations in algae at site S3 in May. The model predictions are shown as solid diamonds with the vertical lines representing 95% confidence intervals. The solid horizontal line is the observation with the 95% confidence interval indicated by the dashed lines. VNIIEF and GE did not provide uncertainty estimates and L did not submit results for this endpoint. The observed HTO concentration in algae at S3 in May was 4990 Bq/L.

Table 2.7. OBT/HTO ratios for plants.

Participant	F_D = OBT/HTO			
	Algae	Worts	Cattails	
			Submerged	Emergent
VNIIEF	0.65	0.8	0.8	0.8
EDF	0.6	0.6	1.0	1.0
SRA	0.7	0.7	‡	0.7
BioM*	0.41	0.33	‡	0.33
IFIN	0.66¶	0.8	0.8	0.8
J	0.8	0.8	‡	0.8
GE	0.5#	–	–	–
L	–	0.75	0.82	0.66
Observed	0.46	0.48	0.70†	0.70

* Calculated for buried tritium from a two-step exchange process, taking into account the proportion of carbohydrates, proteins and DNA in the tissues.
¶ Calculated from a time-dependent model that depends on the algal growth rate and the HTO concentration in water.
# Calculated from a time-dependent model that depends on the rates of algal metabolism and catabolism.
‡ OBT concentration in submerged cattails assumed equal to concentration in emergent parts.
† Ratio of OBT concentration in submerged cattails to HTO concentration in emergent parts.

2.4.3. Worts

Predictions for the HTO concentration in worts at sampling site S3 in May are compared with the observation in Figure 2.4. As was the case for algae, the HTO concentration in worts collected at a given time and place is expected to equal the local water concentration, and all modelers made this assumption. Unfortunately, the worts were collected near shore in May and the water samples were taken off shore, so a local water concentration was not available. The participants approximated the missing data in various ways. SRA adopted the near shore water concentration observed in July at S3, J took the May offshore value at S3, and EDF reduced the observed offshore value at S3 in May by the ratio of near shore to offshore concentrations at S3 in July. As a result, the predictions for worts show greater scatter than for algae, but all lie within 50% of the observation and all agree with the observation when uncertainties are taken into account.

The results for S1 showed somewhat less scatter than for S3, but those for S2 showed greater scatter. At both S1 and S2, all of the predictions underestimated the observations. However, this may not be significant given the difficulty in estimating the water concentration at the location where the worts were sampled.

All modelers assumed that the OBT concentration in worts was proportional to the predicted HTO concentration. The OBT predictions showed greater scatter than those for HTO, ranging over a factor of 4 (Figure 2.5). This scatter was due to the variability in both the predicted HTO concentrations and the values chosen for the proportionality constant F_D, which ranged from 0.33 to 0.8 (Table 2.7). Only three of the results agree with the observation when uncertainties are taken into account. All but one of the predictions overestimate the observation, but this may be the fault of the observation, which appears low in relation to the measured HTO concentration in the plants. Similar results were obtained for sites S1 and S2, although here the model predictions scatter more uniformly about the observations. The full Perch Lake data set implies that $F_D = 0.48 \pm 0.19$ for worts.

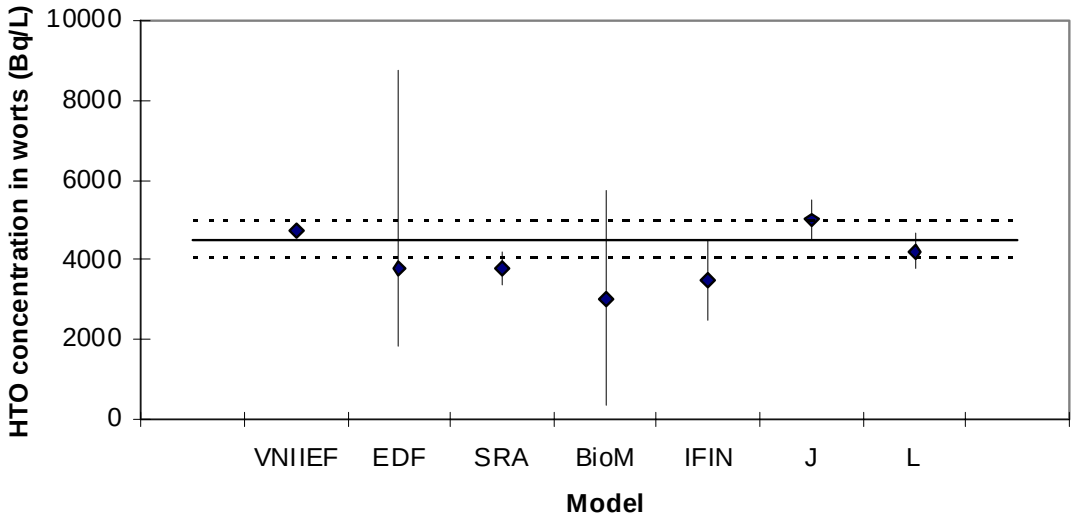

Fig. 2.4. HTO concentrations in worts at site S3 in May. The model predictions are shown as solid diamonds with the vertical lines representing 95% confidence intervals as estimated by the modelers. The solid horizontal line is the observation with the 95% confidence interval indicated by the dashed lines. VNIIEF did not provide uncertainty estimates and GE did not submit results for this endpoint. The HTO concentration in near-shore water at S3 in May was not measured.

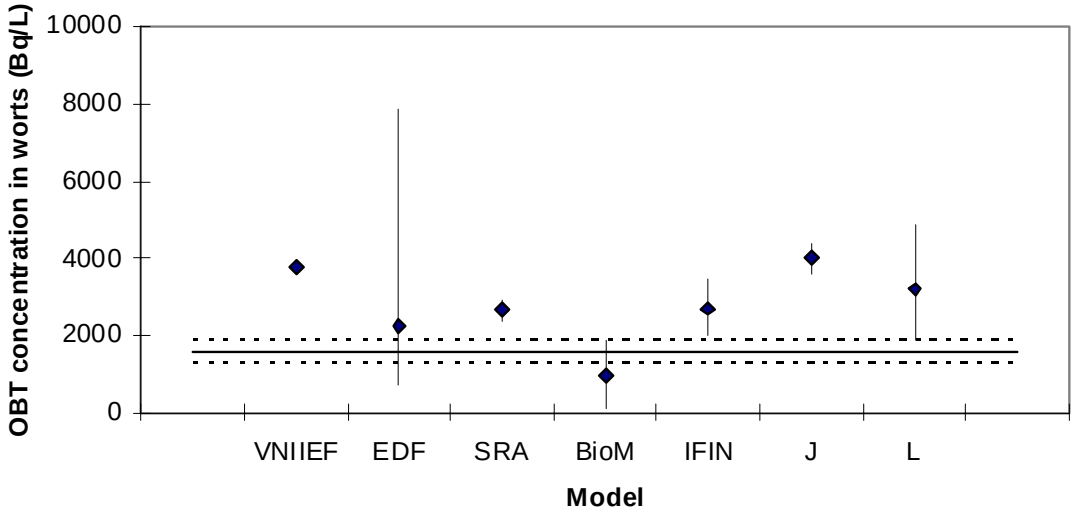

Fig. 2.5. OBT concentrations in worts at site S3 in May. The model predictions are shown as solid diamonds with the vertical lines representing 95% confidence intervals. The solid horizontal line is the observation with the 95% confidence interval indicated by the dashed lines. VNIIEF did not provide uncertainty estimates and GE did not submit results for this endpoint. The observed HTO concentration in worts at S3 in May was 4520 Bq/L.

2.4.4. Cattails

2.4.4.1. HTO Concentrations in submerged cattails

Predictions for the HTO concentration in the below-water parts of the cattails at sampling site S3 in May are compared with the observation in Figure 2.6. Because cattails are rooted in the sediments, their HTO concentrations are expected to equal the concentration in sediment water. This approach was taken by three modelers (VNIIEF, SRA and BioM). Since the near-shore sediment concentration was not measured in May, two of the modelers (VNIIEF and BioM) used the off-shore value instead and obtained a result in close agreement with the observation. The third modeler (SRA) used the near-shore value for July and underpredicted severely. Four participants (EDF, IFIN, J and L) modeled the cattails in the same way as worts, setting the HTO concentration equal to the local lake water concentration. This approach overestimated the observation in each case, with none of the predictions agreeing with the observation even when uncertainties were taken into account.

The predictions for sampling site S1 all lay in the range 2000 Bq/L to 4000 Bq/L and all agreed reasonably well with the observation (3390 Bq/L). The good performance here is due to the fact that the sediment and water concentrations were similar and roughly constant in May and July. The scatter in the predictions for site S2 was about the same as for S3, ranging over a factor of 3.5. Here the models that were based on the water concentration underpredicted the observation by a factor of about 2.5, since the water concentration was less than the sediment concentration. In contrast, the models based on sediment concentration returned predictions within 50% of the observation.

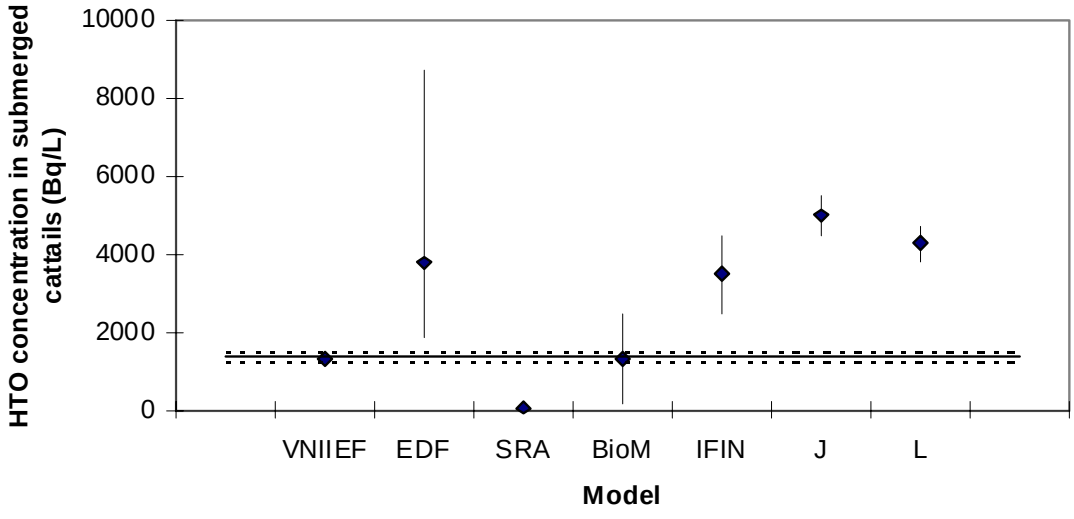

Fig. 2.6. HTO concentrations in submerged cattails at site S3 in May. The model predictions are shown as solid diamonds with the vertical lines representing 95% confidence intervals as estimated by the modelers. The solid horizontal line is the observation with the 95% confidence interval indicated by the dashed lines. VNIIEF did not provide uncertainty estimates and GE did not submit results for this endpoint.

2.4.4.2. HTO Concentrations in emergent cattails

Predictions for the HTO concentration in the emergent parts of the cattails sampled at site S3 in May are compared with the observation in Figure 2.7. As noted in Section 2.2.2, cattail concentrations are well predicted by the average of the concentrations in sediment water and air moisture. Three modelers (VNIIEF, EDF and SRA) explicitly took the contribution from air moisture into account. EDF took an average of the air and surface water concentrations, but would have done better to average air and sediment water. SRA assumed the cattail concentration was made up of 30% air and 70% sediment water (where the air concentration was set to 0) but underestimated severely because of an inappropriate choice for the sediment concentration. VNIIEF used a weighting of 75% air and 25% sediment water and produced a good result by using the offshore sediment water concentration measured at S3 in May. Participant J modeled emergent cattails in the same way as all other plants, setting the HTO concentration equal to the local water concentration, and overestimated the observation. IFIN and L lowered their predictions for cattails below those for other plants in recognition of the contribution from the air, but still overestimated the observation. The BioM result is also an overestimate since it predicts that the cattail concentration is slightly higher than the sediment concentration.

The predictions for sampling site S1 showed less scatter than those for S3 because of the similarity in the water and sediment concentrations at this site. The predictions ranged from about 1000 Bq/L to 4000 Bq/L compared to the observed value of 1970 Bq/L. The range in predictions for site S2 was larger (a factor of 7) because the sediment concentrations were more than twice the water concentrations. The models that were based on the water concentration underpredicted the observation whereas those based on sediment concentration overpredicted.

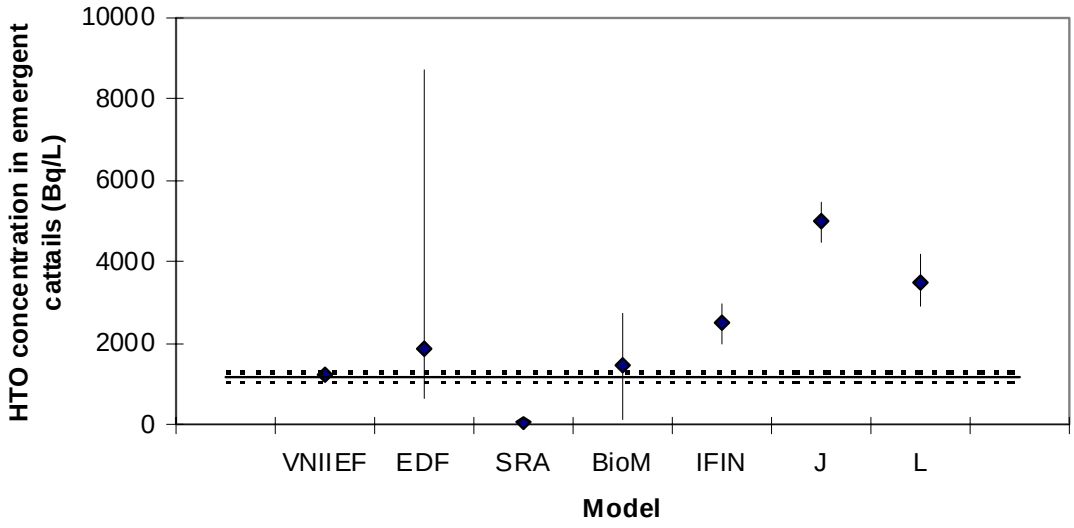

Fig. 2.7. HTO concentrations in emergent cattails at site S3 in May. The model predictions are shown as solid diamonds with the vertical lines representing 95% confidence intervals as estimated by the modelers. The solid horizontal line is the observation with the 95% confidence interval indicated by the dashed lines. VNIIEF did not provide uncertainty estimates and GE did not submit results for this endpoint.

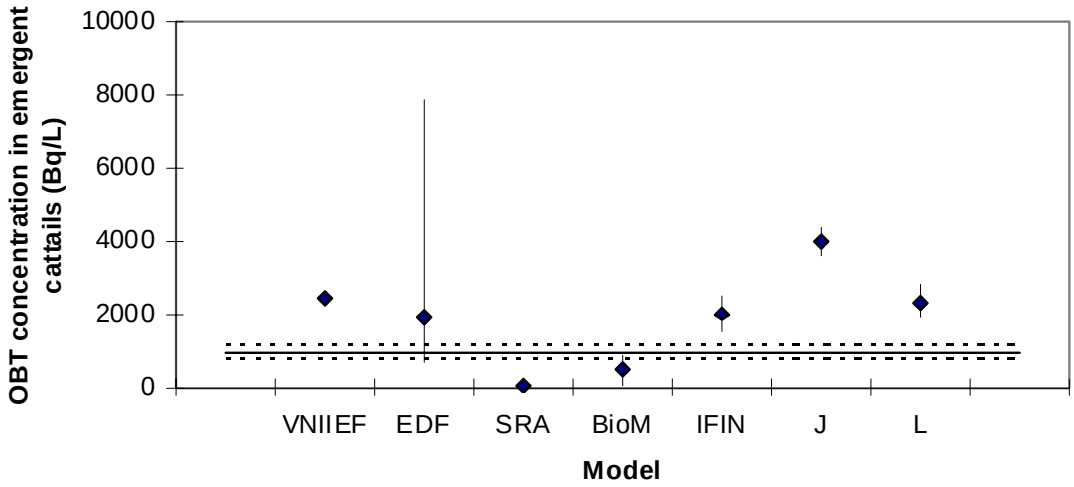

Fig. 2.8. OBT concentrations in emergent cattails at site S3 in May. The model predictions are shown as solid diamonds with the vertical lines representing 95% confidence intervals as estimated by the modelers. The solid horizontal line is the observation with the 95% confidence interval indicated by the dashed lines. VNIIEF did not provide uncertainty estimates and GE did not submit results for this endpoint.

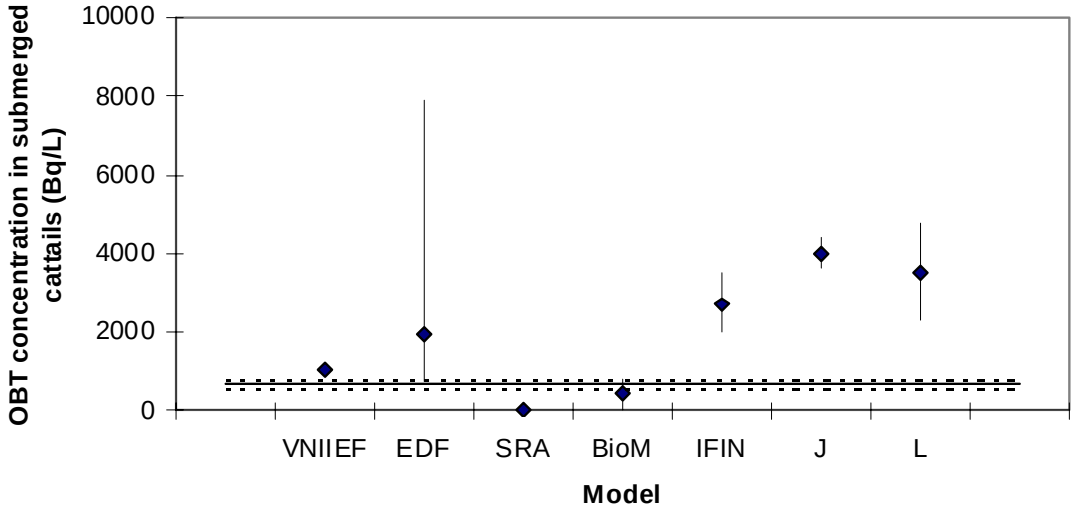

Fig. 2.9. OBT concentrations in submerged cattails at site S3 in May. The model predictions are shown as solid diamonds with the vertical lines representing 95% confidence intervals as estimated by the modelers. The solid horizontal line is the observation with the 95% confidence interval indicated by the dashed lines. VNIIEF did not provide uncertainty estimates and GE did not submit results for this endpoint.

2.4.4.3. OBT Concentrations in cattails

Analysis of the full Perch Lake data set indicates that OBT concentrations are the same in both the emergent and submerged parts of the cattails, with a magnitude equal to 0.7 times the HTO concentration in the emergent part [8]. This suggests that the OBT is formed primarily by photosynthesis in the emergent part and translocated to the submerged parts. Most modelers assumed that the OBT concentration in the emergent part was proportional to the HTO concentration in that part, with a proportionality constant F_D equal to that in the last column of Table 2.7. The results show considerable variability (Figure 2.8), due primarily to the differences among the predicted HTO concentrations, with some contribution from the values used for F_D. Only two predictions agree with the observation when uncertainties are taken into account. Three of the modelers (SRA, BioM and J) assumed that the OBT concentration in the underwater parts was the same as that in the emergent parts. Most of the other modelers calculated the OBT concentration in the submerged parts from the HTO concentration in the submerged parts, using the F_D values in the fourth column of Table 2.7. The comparison between predictions and observations for this endpoint (Figure 2.9) shows much the same pattern as for the emergent parts in Figure 2.8, with agreement in only three cases when uncertainties are taken into account. The results for sampling sites S1 and S2 are very similar to those for S3.

2.4.5. Clams

Predictions for the HTO concentration in clams in July are compared with the observation in Figure 2.10. Because clams live at the sediment/water interface, their HTO concentration is expected to equal the local bottom water concentration at the time of sampling. Most participants made this assumption but, in the absence of measured water or sediment concentrations in the area where the clams were harvested, they estimated the water concentrations in different ways. In the case of EDF, the concentrations were calculated as the average of the near shore and offshore sediment concentrations for the three sampling sites; for SRA, as the average of the deep and surface water concentrations at S1 and S3 and the sediment water concentration at S3; and for IFIN, as the average of the bottom water and sediment concentrations over time throughout the lake. Despite these different approaches, the predictions agreed with the observation for each model in which uncertainties were estimated (Figure 2.10), and five of the eight predictions lay within 12% of the observation. Similar agreement was obtained for the May sampling period. The uncertainties were large for some models, reflecting the difficulties the modelers had in estimating the water concentrations experienced by the clams. Analysis of the full Perch Lake data set [8] indicates that the clam concentration in July (4100 Bq/L) lay within 10% of the average offshore bottom water concentration (4495 Bq/L).

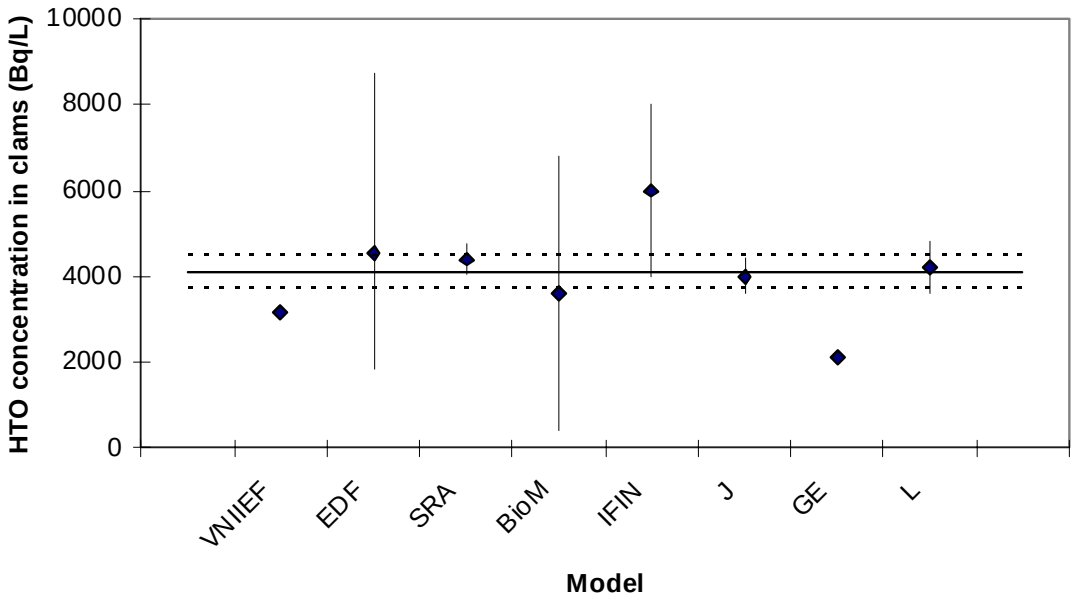

Fig. 2.10. HTO concentrations in clams in July. The model predictions are shown as solid diamonds with the vertical lines representing 95% confidence intervals as estimated by the modelers. The solid horizontal line is the observation with the 95% confidence interval indicated by the dashed lines. VNIIEF and GE did not provide uncertainty estimates for this endpoint.

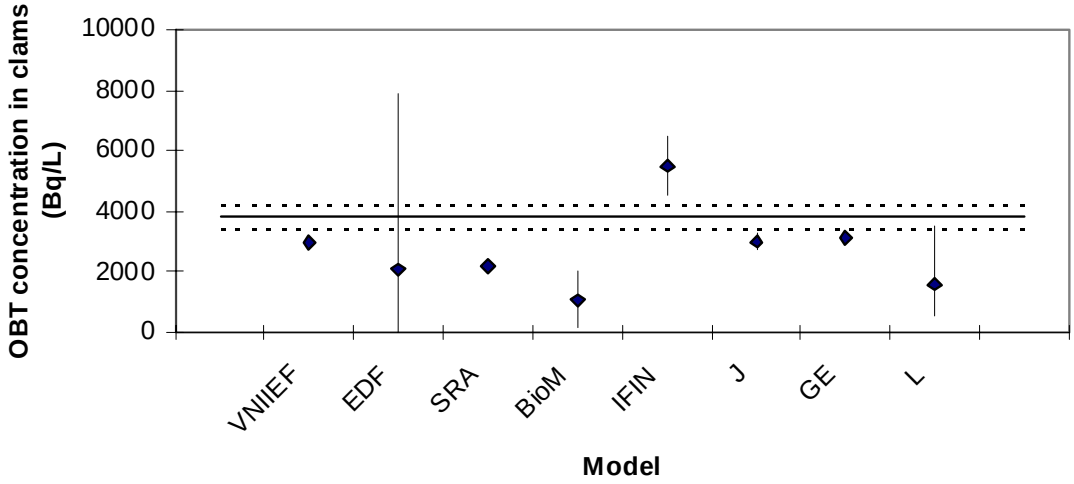

Fig. 2.11. OBT concentrations in clams in July. The model predictions are shown as solid diamonds with the vertical lines representing 95% confidence intervals as estimated by the modelers. The solid horizontal line is the observation with the 95% confidence interval indicated by the dashed lines. VNIIEF and GE did not provide uncertainty estimates for this endpoint.

Table 2.8. OBT/HTO ratios for aquatic animals.

Participant	F_M = OBT/HTO						
	Clams	Bullheads			Pike		
		Flesh	Head	Organs	Flesh	Head	Organs
VNIIEF	0.75–0.95	0.4	0.3	0.5	0.27	0.3	0.2
EDF[§]	0.45	0.52–0.57 depending on the month					
SRA	0.5	0.7	0.64	0.66	0.7	0.64	0.66
BioM*	0.30	0.3	0.1 for gonads		0.3	0.1 for gonads	
IFIN[†]	0.92	0.93–1.2	Higher for viscera		1.0	Higher for viscera	
J	0.8	0.8	0.8	0.8	0.8	0.8	0.8
GE[‡]	1.48	1.48–2.05 depending on the month					
L	0.38	0.38	0.38	0.38	0.38	0.38	0.38
Observed	0.75		0.77			0.84	

[§] Animal OBT/water HTO = 0.45 for clams and all parts of fish.

* Calculated from a two-step exchange process for buried tritium, taking into account the proportion of carbohydrates, proteins and DNA in the tissues.

[†] Calculated from a time-dependent model that depends on mass, metabolic rate and OBT residence time.

[‡] Calculated from a time-dependent model that depends on the rates of metabolism, catabolism, ingestion and excretion.

Clams are filter feeders, eating phytoplankton and zooplankton but also retaining detritus. Most OBT in clams and other aquatic animals is the result of direct incorporation of OBT taken in with the diet. However, only two of the participants (IFIN and GE) simulated OBT formation in this way, using dynamic models that took into account the metabolism/catabolism of the animals and the time-dependent water concentrations. IFIN overestimated the observation for clams by about 50% whereas GE underestimated by about 20% (Figure 2.11). The latter model predicted an OBT/HTO ratio of 1.5, implying bioaccumulation of tritium in the organic material of the clams. Most of the remaining participants assumed the OBT concentration was proportional to the HTO concentration in the clams, with the proportionality constant, F_M, accounting for metabolic processes. Most modelers took a value of F_M from the literature, with the chosen values ranging from 0.30 to 0.95 (Table 2.8). In most cases, the HTO concentrations used were those predicted for July, even though the slow turnover rate of OBT in animals implies that they should be based on HTO concentrations integrated over the few weeks prior to sampling. The predictions showed greater scatter than those for HTO (Figure 2.11). The variations in F_M, coupled with the variations in the predicted HTO concentration in the clams, resulted in OBT predictions that varied by more than a factor of 5. Seven of the eight models underpredict and only two of the predictions agree with the observation even when uncertainties are taken into account. Despite the added complexity in predicting OBT, the uncertainties assigned to several of the OBT predictions were smaller than those for the corresponding HTO concentrations.

The results for May showed more scatter but less bias than those for July, with half of the models overestimating the observation and half underestimating. Based on an analysis of the full data set, Kim et al. [8] found good agreement between predictions and observations when the OBT concentrations in clams were calculated by multiplying the HTO concentration in bottom water (averaged over the entire lake and over time up to the time of sampling) by a metabolic factor $F_M = 0.75$.

2.4.6. Bullheads

Bullheads are benthic fish that move freely throughout the lake near the sediment/water interface. They are omnivorous, eating a variety of molluscs, insects, leeches, worms, algae, plant material and small fish. Because of the rapid rate of equilibrium between HTO in lake water and fish, the HTO concentration in bullheads is expected to equal the average concentration in the water encountered by the fish in the hour or two prior to sampling. The analysis of the full Perch Lake dataset showed that the observed HTO concentrations in bullheads were essentially equal to the concentration in bottom waters averaged over the entire lake at the time the fish were sampled. EDF, BioM, IFIN and L all based their predictions on the average HTO concentration in offshore waters only and slightly overestimated the observation (Figure 2.12), since offshore waters had a higher concentration than near-shore waters. The high result of SRA is due to the fact that, in this model, half of the tritium in the fish was assumed to come from sediment waters, which had high concentrations at some times and locations in the lake. The other participants adopted a water concentration lower than the average observed concentration for bottom waters and underestimated the observation. The predictions of SRA and J do not agree with the observations even when uncertainties are taken into account. The predictions for May and October show more scatter than for July, likely because the HTO concentrations in the environment were less well characterized and it was more difficult to define a representative water concentration for the bullheads.

All models but one predicted equal HTO concentrations in all parts of the fish, in agreement with the observations. The exception was VNIIEF, where the concentrations in internal organs were sometimes higher and sometimes lower than in the flesh and head. In this model, HTO in the head is assumed to come from the water column and HTO in the organs from the diet of the fish; HTO in the flesh comes partly from the water and partly from the diet.

Predicted and observed OBT concentrations in bullhead flesh in July are shown in Figure 2.13. Two of the process-oriented models (IFIN and GE) substantially overestimated the observation and both predicted OBT/HTO ratios in the fish greater than one. The other dynamic model (EDF) slightly underestimated the observation. As was the case for clams, most of the remaining participants assumed the OBT concentration was proportional to the HTO concentration, with the proportionality constant F_M shown in Table 2.8. Kim et al. [8] found good agreement between predictions and observations when the OBT concentrations in bullheads were calculated from the HTO concentration in bottom water averaged over the entire lake and over time up to the time of sampling, with $F_M = 0.77$. Most modelers used a lower value, which explains in part why most predictions underestimate the OBT concentration in bullheads. The differences in model formulation and parameter values adopted by the various participants resulted in OBT predictions that ranged over more than a factor of 6. Individual predictions differed from the observation by up to a factor of 4, and in only three cases did the prediction and observation agree when uncertainties were taken into account. Very similar results were obtained for the May and October sampling periods.

Half of the models (VNIIEF, SRA, BioM and IFIN) showed different OBT concentrations in the different parts of the fish, reflecting the different proportions of proteins, carbohydrates and fat in the flesh, head and internal organs. The differences were small for SRA (10%) and IFIN but more substantial for VNIIEF (67%) and BioM (a factor of 3 between flesh and gonads, but this result applies to buried tritium rather than OBT). In contrast, the data show that OBT concentrations in the flesh, head and internal organs of the bullheads are not significantly different, an assumption made by models EDF, J, GE and L.

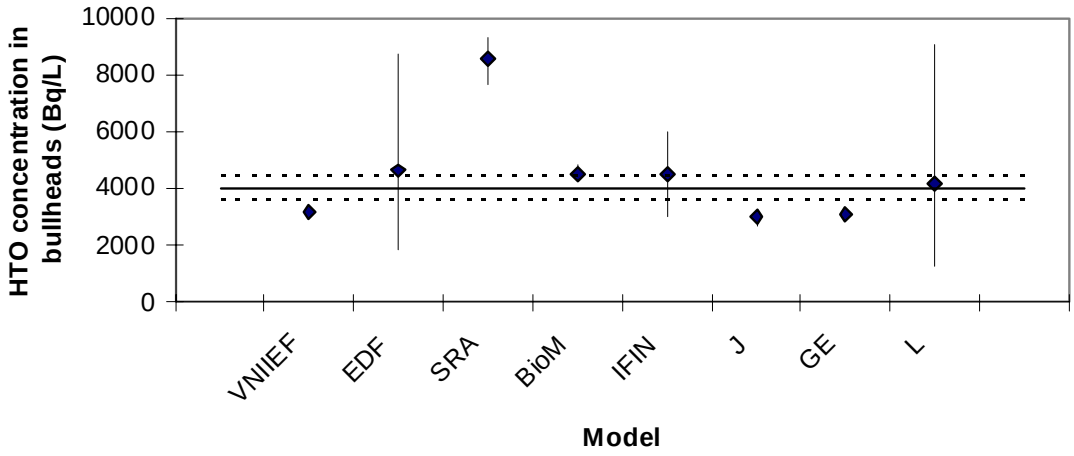

Fig. 2.12. HTO concentrations in bullheads in July. The model predictions are shown as solid diamonds with the vertical lines representing 95% confidence intervals. The solid horizontal line is the observation with the 95% confidence interval indicated by the dashed lines. VNIIEF and GE did not provide uncertainty estimates for this endpoint. The observed HTO concentration in bottom waters averaged over the entire lake for July was 4000 Bq/L.

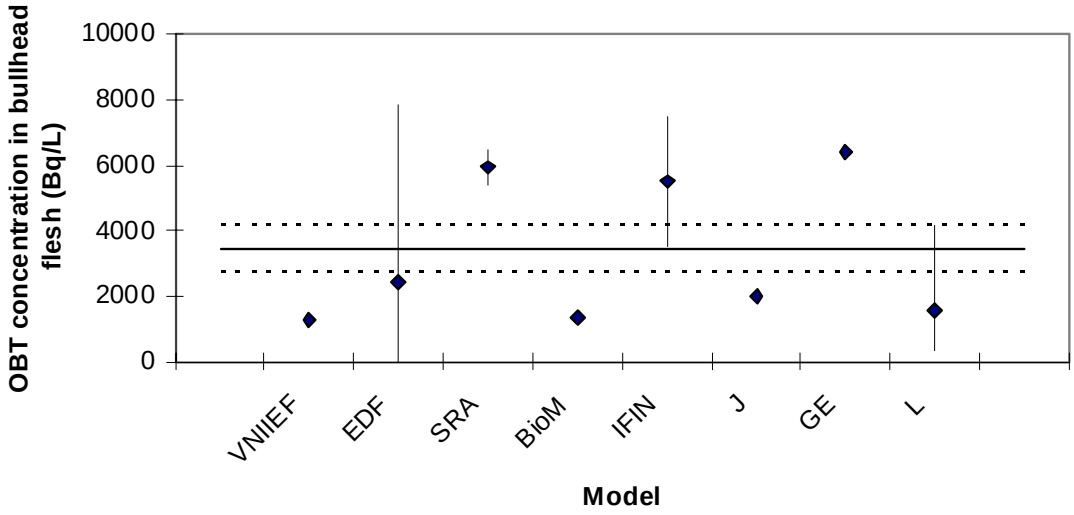

Fig. 2.13. OBT concentrations in bullhead flesh in July. The model predictions are shown as solid diamonds with the vertical lines representing 95% confidence intervals. The solid horizontal line is the observation with the 95% confidence interval indicated by the dashed lines. VNIIEF and GE did not submit uncertainty estimates for this endpoint. The observed HTO concentration in bottom waters averaged over the entire lake over the May and July sampling periods was 4655 Bq/L.

2.4.7. Pike

Five participants (EDF, BioM, J, GE and L) modeled pike in the same way as bullheads and predicted the same tritium concentrations for both types of fish. These modelers felt either that the foraging habits of bullheads and pike were sufficiently similar that they could be modeled in the same way, that there was too little information to attempt to model them differently, or that any differences in habits would not translate into significant differences in concentration in a well-mixed system such as Perch Lake. For the IFIN model, results for pike and bullheads differed by less than 10%, whereas the results for VNIIEF were within 45%. SRA predicted concentrations in pike that were a factor of 2 lower than those in bullheads on the assumption that sediment water plays less of a role in determining tritium levels in pike than in bullheads. In fact, the experimental data indicate that concentrations in the two types of fish are identical within measurement error. As piscivores that move freely throughout the lake, pike differ from bullheads in the parts of the lake they access and the type of food they eat. However these differences in behaviour do not result in significant differences in concentrations in Perch Lake.

The observed and predicted HTO concentrations in pike in July are shown in Figure 2.14. The overall results are good and only two predictions (those for J and GE) do not agree with the observation when uncertainties are taken into account. The predictions for VNIIEF and SRA are much better for pike than they were for bullheads. In contrast, most of the models underestimate the observed OBT concentration in pike flesh for July (Figure 2.15) because they underestimate the metabolic factor F_M. Similar results were obtained for the May and October sampling periods.

As was the case for bullheads, the observed tritium concentrations were the same to within measurement error in all parts of the pike. Of all the predictions, only those of VNIIEF and BioM are inconsistent with this finding.

2.4.8. Sediments

There is no evidence that OBT discharges directly to the lake with groundwater. If this is the case, sediment OBT must arise from decaying plant and animal material deposited on the lake bottom, with the vast majority expected to come from plants. The experimental data suggest that the mean sediment/plant ratio is 0.61 ± 0.20. Since most sediments were collected from shore, only those plants found close to shore (worts and cattails) were considered in this calculation. Also, the plant concentrations were averaged over time up to the time of sampling, to account in a small way for the fact that the sediments, which were collected to a depth of 15 cm, are averages of the material deposited over a considerable length of time. The sediment concentrations are believed to be lower than those in plants due to radioactive decay and/or the breakdown over time of OBT in the decomposing plant material.

Predicted and observed sediment OBT concentrations at sampling site S3 in May are shown in Figure 2.16. The predictions range over a factor of 100 and only two of the six predictions agree with the observation when uncertainties are taken into account. The variation is due to the very different assumptions made by each modeler in calculating the sediment concentrations:

— VNIIEF: the sediment OBT concentration was assumed equal to the HTO concentration in detritus formed in surface waters in May.

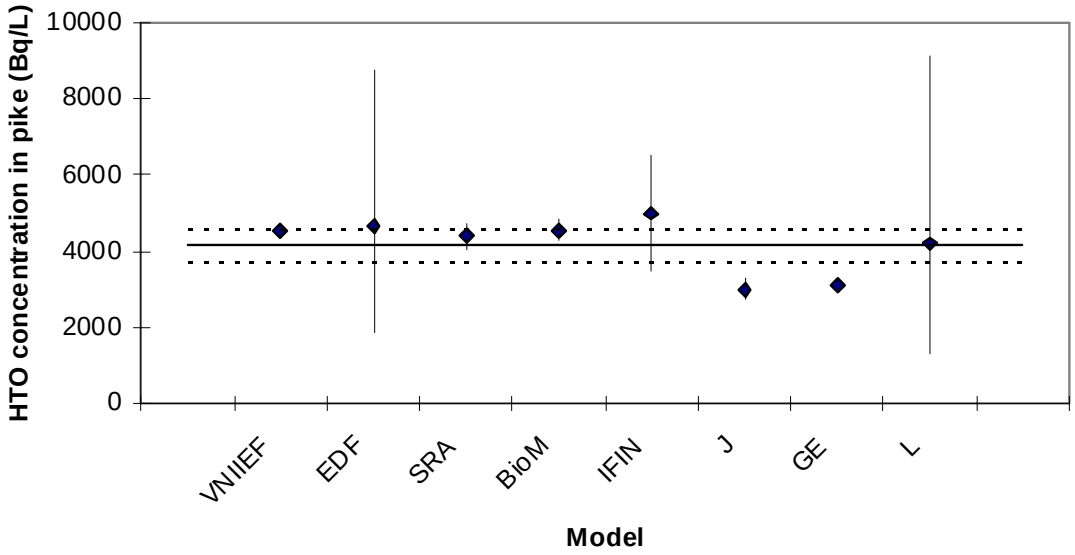

Fig. 2.14. HTO concentrations in pike in July. The model predictions are shown as solid diamonds with the vertical lines representing 95% confidence intervals. The solid horizontal line is the observation with the 95% confidence interval indicated by the dashed lines. VNIIEF and GE did not provide uncertainty estimates for this endpoint. The observed HTO concentration averaged over the entire lake for July was 4130 Bq/L.

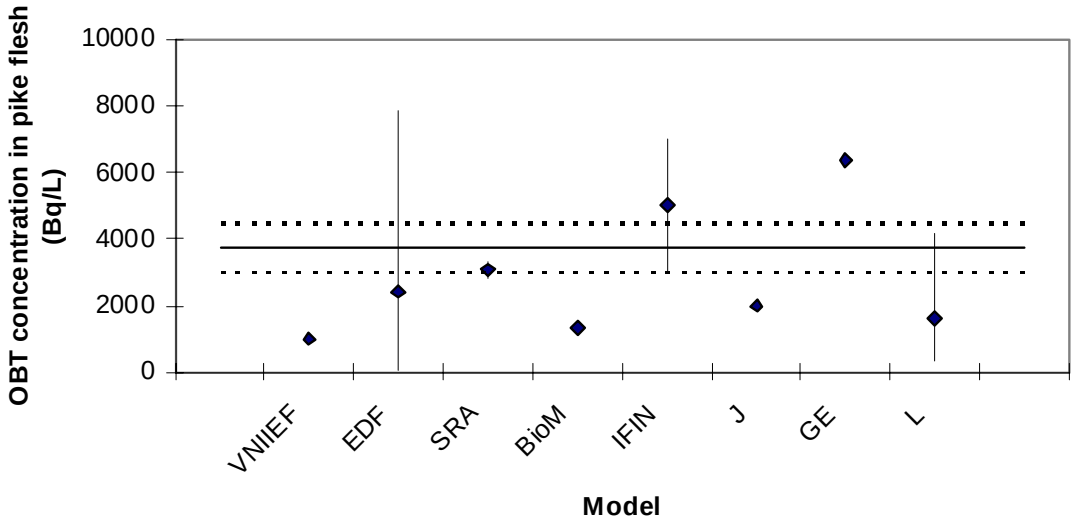

Fig. 2.15. OBT concentrations in pike flesh in July. The model predictions are shown as solid diamonds with the vertical lines representing 95% confidence intervals. The solid horizontal line is the observation with the 95% confidence interval indicated by the dashed lines. VNIIEF and GE did not provide uncertainty estimates for this endpoint. The observed HTO concentration averaged over the entire lake over the May and July sampling periods was 4720 Bq/L.

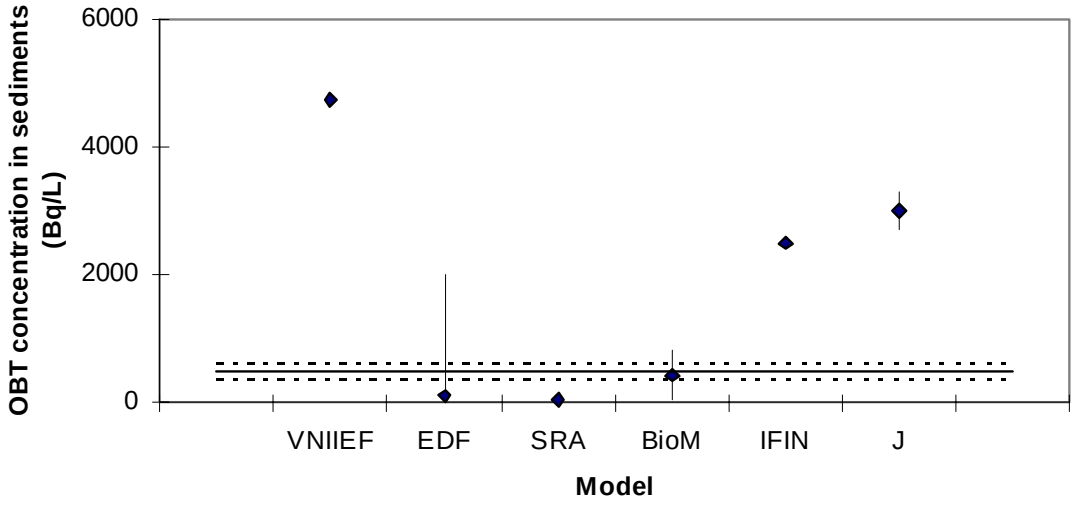

Fig. 2.16. OBT concentrations in sediments at site S3 in May. The model predictions are shown as solid diamonds with the vertical lines representing 95% confidence intervals. The solid horizontal line is the observation with the 95% confidence interval indicated by the dashed lines. GE and L did not submit predictions for this endpoint. The observed OBT concentration in worts and cattails at S3 in May was 1070 Bq/L.

- EDF: the sediment OBT concentration at S3 was assumed to be in equilibrium with the OBT concentration in the organic matter of decomposing terrestrial vegetation, which was assumed to equal 60% of the air HTO concentration.
- SRA: the sediment OBT concentration was assumed equal to 0.63 times the HTO concentration in the near-shore sediment water.
- BioM: the concentration of buried tritium in sediment was assumed to equal the predicted concentration of buried tritium in the submerged part of cattails.
- IFIN: the sediment OBT concentration was estimated from the predicted OBT concentration in macrophytes and benthic algae, which in turn depend on the HTO concentration in bottom waters.
- J: the sediment OBT concentration was set equal to the mean of the predicted plant and animal OBT concentrations.

Most of these assumptions were reasonable, but only BioM produced a result in good agreement with the observation. This must be considered fortuitous since BioM predicts the concentration of buried tritium whereas the observation is of organically bound tritium. The other models did not do as well because they all overestimated the concentrations in the plants that were assumed to make up the sediments.

The results for sites S1 and S2 showed somewhat less scatter than for S3, although the predictions still ranged over a factor of 3 or 4, and most of the models continued to overestimate the sediment concentrations.

2.5. Discussion and conclusions

The Perch Lake scenario provided a good test of models that predict tritium concentrations in the various compartments of a freshwater ecosystem at steady state. Apart from a narrow zone close to shore near the inlets, the lake is well mixed with respect to HTO concentrations in the water, and concentrations change only slowly over time. Therefore the water concentrations to which the fish are exposed, and the concentrations in the plants and animals that make up their diets, can be estimated with some confidence. Moreover, the concentrations in sediments are substantially different from those in the lake water itself, which makes it possible to say whether the tritium in plants and fish came from the water or the sediments. On the other hand, the scenario was not ideal since some relevant information was missing or incomplete, and this contributed to the differences between predictions and observations. But many real assessments must be carried out with even less information, and discrepancies of a similar magnitude must be expected in practice.

A number of conclusions regarding the relationship between tritium concentrations in the various parts of the Perch Lake ecosystem can be drawn from an analysis of the full data set [8] and the results discussed here:

- The HTO concentration in a given plant or animal is equal to the concentration in water, sediments or air to which the organism was exposed in the hour or two prior to sampling. For algae and worts, this is the local concentration in water. For submerged cattails it is the sediment water concentration and for emergent cattails, an average of air and sediment concentrations. Concentrations in clams and bullheads are the same as the concentrations in local bottom waters, and bottom waters averaged over the entire lake, respectively. HTO concentrations in pike reflect an average of both bottom and surface waters over the entire lake.
- The OBT concentration in algae and worts is about half the HTO concentration in the plant. The OBT concentration in the emergent parts of cattails is about 70% of the HTO concentration. The OBT concentration in the submerged parts of cattails is the same as in the upper part, indicating that the OBT forms in the emergent parts and is translocated to the parts below water.
- The OBT concentration in clams, bullheads and pike is about 80% of the HTO concentration in the water to which the animal is exposed.
- The OBT concentration in sediments is about 60% of the OBT concentration in the aquatic plants that make up most of the organic fraction of the sediments. The sediment concentrations are believed to be lower than those in plants because of radioactive decay and/or the breakdown over time of OBT in the decaying plant material.
- The OBT concentration in each compartment should be calculated from the HTO concentration averaged over the few weeks prior to sampling.
- Within measurement error, there is no significant difference between the HTO or OBT concentrations in different parts of the fish.

When the predictions of all the models were averaged for a given endpoint, the mean lay within 30% of the observation in each case except for OBT concentrations in sediments and the underwater parts of cattails. With these exceptions, the modelers as a group have a good conceptual understanding of the behaviour of tritium in the Perch Lake ecosystem and can predict HTO and OBT concentrations that, in an average sense, agree well with the observations. However, the difference between prediction and observation for an individual model could be as large as a factor of 25. More typically, the predictions of a given model for

HTO concentrations in plants and animals lay within 30% of the corresponding observation, and the predictions of OBT concentrations within a factor of about 2. These differences for OBT are significant even when uncertainties are taken into account. The models were equally as likely to overpredict as to underpredict the HTO concentrations in plants. They tended to be conservative for HTO concentrations in animals and OBT concentrations in plants but to underestimate OBT concentrations in animals.

There were several reasons for the mispredictions:

- An inappropriate choice for the source compartment from which the plant or animal draws its tritium. In particular, the submerged parts of cattails are in equilibrium with sediment water rather than lake water; clams and bullheads are in equilibrium with bottom water rather than sediment water; and OBT in submerged cattails is translocated from the emergent parts of the plant rather than being formed in place.
- An inappropriate choice of surrogate values when HTO concentrations in the source compartment were not available. The modelers had particular difficulty in defining the source terms for worts and cattails, since near-shore water and sediment concentrations were not measured in May. Similarly, no sediment or water concentrations were measured in the area where the clams were harvested.
- An inappropriate choice for the discrimination and metabolic factors, F_D and F_M, used to calculate OBT concentrations from the HTO concentrations.
- Inappropriate spatial averaging, particularly for fish. The best prediction of HTO concentration in bullheads was obtained by averaging the bottom waters over the entire lake, including near-shore and offshore zones. Similarly, the best prediction of HTO concentration in pike occurs by averaging over the water column as well as over the entire lake.
- Lack of time-averaging when calculating OBT concentrations. Apart from the dynamic results for algae, clams and fish generated by IFIN and GE, none of the models considered any sort of time-averaging in calculating OBT concentrations in plants or animals. In contrast, the observed OBT concentrations correlate better with the time-averaged HTO concentrations than with point concentrations.

No one model stood out as generating predictions superior to the others. The level of agreement between predictions and observations was about the same for the dynamic models as for the steady-state models, although the dynamic models tended to have the highest predictions for OBT concentrations in clams, bullheads and pike. None of the models were satisfactory for sediments.

The results of the BioM model, which calculates the concentration of buried tritium rather than the tritium traditionally considered to be organically bound, were generally lower than those of the other models for the OBT endpoints. However, the BioM predictions made up a substantial proportion (between 25% and 90% depending on the endpoint) of the measured OBT concentrations. If the results of this model are correct, this implies that the fraction of carbon bound tritium in the OBT yielded by conventional analytical techniques is much lower than normally believed. This could have consequences for dose estimation, although such consequences may be small since the dose conversion factors for OBT are based on OBT concentrations measured in the traditional way. The results of the BioM model indicate that the formation of buried tritium is better modeled as a two-step exchange process rather than as a one-step process.

Table 2.9. 95% confidence intervals based on the differences between predictions and observations.

Endpoint	95% confidence interval
HTO in algae, worts and all animals	BE* ± 30%
HTO in cattails	BE/2 to 2 BE
OBT in algae, worts	BE/2 to 2 BE
OBT in cattails	BE/3 to 3 BE
OBT in animals	BE/2.5 to 2.5 BE
OBT in sediments	BE/10 to 10 BE

* Best estimate.

Despite that fact that two models predicted OBT/HTO ratios greater than one for some endpoints, there is no evidence in the Perch Lake data of tritium bioaccumulation in OBT formation. Ratios greater than one are confined to non-equilibrium situations such as those that exist in Cardiff Bay, where tritiated organic material is released directly to the water body [11, 12].

Given the large variation in the confidence intervals estimated by the various participants, no definitive conclusions can be drawn regarding the uncertainties in the model predictions. Ideally, the confidence intervals would take into account the uncertainties in the HTO concentrations in water, sediments and air used to drive the models; in the conceptual models themselves to cover uncertainties in the appropriate source compartments and spatial and temporal averaging; in estimating values to replace missing data; and (for OBT concentrations only) in the parameters F_D and F_M. The dynamic models used by some participants would have additional sources of uncertainty associated with the extra parameters that are needed to describe the growth of the organisms and the metabolic processes that occur in them. The uncertainties are limited to some extent by specific activity concepts, since concentrations in a given compartment cannot be higher than concentrations in a donor compartment. Table 2.9 lists approximate 95% confidence intervals for the various endpoints based on an overall assessment of the differences between the observations and the predictions submitted by the participants. Hopefully the lessons learned in this scenario will help to reduce the uncertainties in future studies that require the estimation of steady-state tritium concentrations in freshwater ecosystems.

CHAPTER 3. THE PICKERING SCENARIO

3.1. Scenario description

This scenario is based on data collected in the vicinity of Pickering Nuclear Generating Station (PNGS), a collection of eight CANDU reactors on the north shore of Lake Ontario. The surrounding environment contains slightly elevated levels of tritium due to continuous, routine discharge from the reactors. The releases have been going on for many years and concentrations in various parts of the local environment are likely to be in equilibrium. A large number of environmental and biological samples were collected in 2002 from four sites in the vicinity of the station. HTO concentrations were measured in air, precipitation, soil, drinking water, plants (including the crops that make up the diet of the local farm animals) and products derived from the animals themselves; OBT concentrations were measured in the plant and animal samples. These data were used as a test of models that predict the long-term average tritium concentrations in terrestrial systems due to chronic releases.

The samples were taken at two dairy farms (DF8 and DF11), a hobby farm (F27) and a small garden plot (P2) (Figure 3.1). All of the sampling sites were located to the northeast of PNGS; the two dairy farms lay about 10 km from the station, the hobby farm about 7 km and the garden plot about 1 km. The two dairy farms yielded much the same sort of samples, including pasture grasses, a variety of grains, milk and meat. In contrast, F27 produced mainly fruit, garden vegetables, chickens and eggs. A limited number of plants are grown at P2 for research purposes and raspberry leaves and grass were sampled.

The cows at DF8 and DF11 were fed total mixed ration (TMR), a blend of various feeds harvested in the previous year. Most components of the mixture were obtained locally. Estimates of the total food intake by the cows were available from the owners. The chickens raised at F27 were essentially free-range and their food intake was not regulated or monitored. As a result, the make-up of their diet and their intakes could only be estimated. The amount of drinking water ingested by the cows and chickens was not monitored.

Tritium concentrations in air and precipitation were available from a monitoring programme carried out by the utility. Air concentrations at P2 were measured monthly using an active air sampler, and were considered reliable. However, at DF8, DF11 and F27, air concentrations were available only as annual averages from passive diffusion samplers. For a number of reasons, these data were considered untrustworthy and were replaced with the predictions of a sector-averaged atmospheric dispersion model that produced concentrations in good agreement with the observations at P2, DF8 and DF11.

All of the other samples were collected in two field campaigns conducted in 2002, the first from July 8–10 and the second from September 16–18. All of the samples collected in July were dried before the HTO could be extracted and so were suitable for OBT analysis only. The September samples were frozen in their fresh state and were analysed for both HTO and OBT. At the dairy farms, samples were collected of each of the plants that made up the animal diets, as well as separate samples of TMR. At F27, additional measurements were made of garden vegetables, root crops and fruit. The meat samples from DF8 and DF11 came from calves that were either stillborn or died from complications at birth. The mothers were three years old or younger and were raised exclusively on these farms. Additionally, composite milk samples consisting of a mixture of milk from all cows in the herd were collected in July at both farms. The only animal products sampled at F27 in the July campaign were eggs. In September, in addition to eggs, blood and flesh were also analysed from a single chicken.

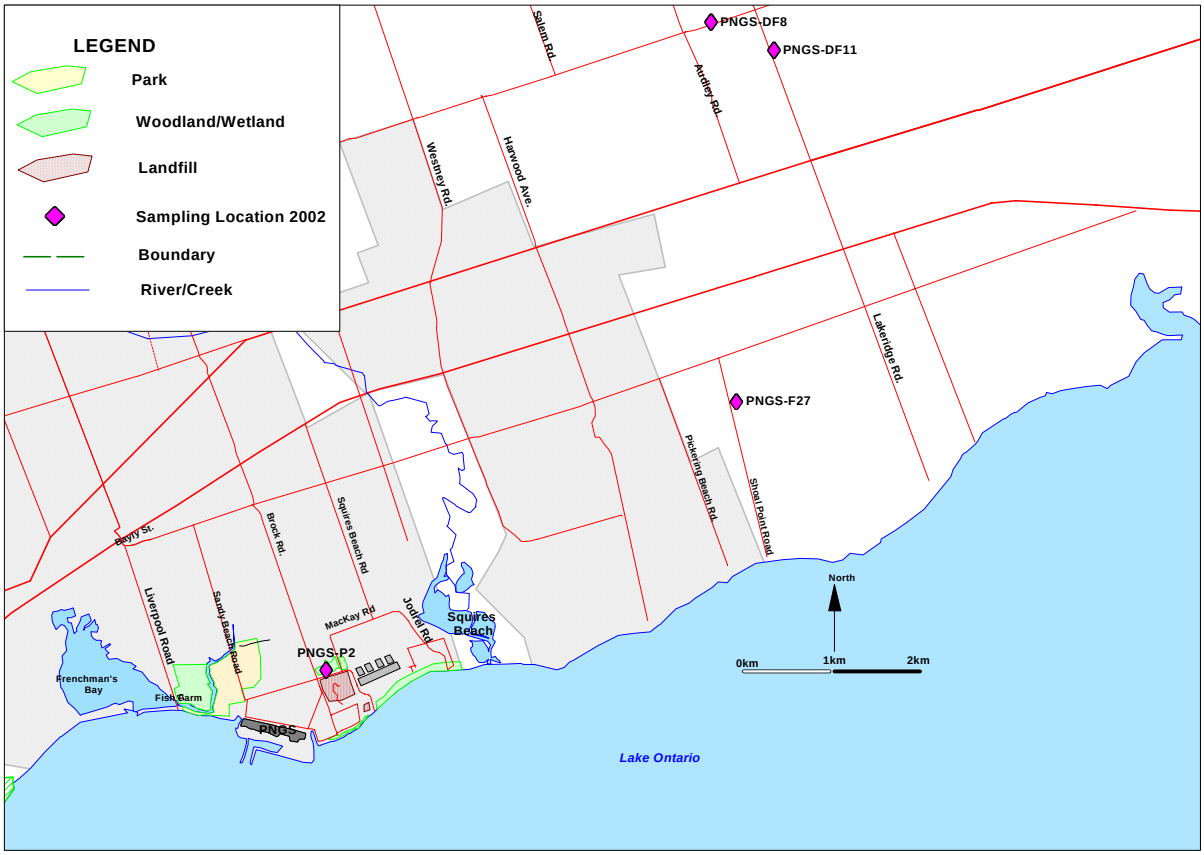

Fig. 3.1. Map of the study area showing PNGS and the sampling sites.

Samples of water were taken from the deep wells that supply drinking water for the cows at farms DF8 and DF11 in the September sampling period. The concentration in drinking water at F27, which comes from a shallow well, was available as a six month average from the routine monitoring programme carried out by the utility. Soil cores were collected at a single location at each site from undisturbed grassed areas or where the soil had lain fallow for some time.

Given the measured HTO concentrations in air, precipitation and drinking water, participants in the scenario were asked to calculate:

(1) HTO and non-exchangeable OBT concentrations in the sampled plants and animal products for each site and each sampling period.
(2) HTO concentrations in the top 5 cm soil layer for each site and each sampling period.
(3) 95% confidence intervals on all predictions.

The full scenario description is given in Appendix I.2.

3.2. Observations

3.2.1. Measured concentrations

Estimates of HTO concentrations in air and drinking water are shown in Table 3.1; HTO concentrations in monthly precipitation are given in Table 3.2. These are the concentrations that were supplied to the participants to drive their models. Observed concentrations in soil, plants and animal products, which were the endpoints of the scenario, are given in Tables 3.3, 3.4 and 3.5, respectively. The OBT concentrations are given in units of Bq L^{-1} of combustion water.

The observed concentrations in all environmental compartments were relatively low, although they were at least a factor 4–5 above background. Counting errors for both HTO and OBT samples were less than 10% in most cases. An additional uncertainty of about 30% must be added to the plant and animal concentrations to account for natural variability. A further error of perhaps 50% must also be added to the air concentrations at DF8, DF11 and F27, which were estimated using an atmospheric dispersion model.

Table 3.1. Measured HTO concentrations in air and drinking water. The air concentrations include a background contribution of 0.19 Bq m^{-3}.

Compartment	DF8	DF11	F27	P2
Air concentration (Bq m^{-3})				
2002 May	1.01	1.01	1.56	24
June	1.39	1.39	2.14	33
July	0.93	0.93	1.43	22
August	0.88	0.88	1.36	21
September	0.67	0.67	1.04	16
Air concentration (Bq m^{-3})				
2001 May	0.49	0.49	0.77	12
June	2.83	2.83	4.40	69
July	0.86	0.86	1.34	21
August	1.23	1.23	1.92	30
September	0.66	0.66	1.02	16
Drinking water concentration (Bq L^{-1}) 2002 September	18.6	21.1	24.3*	Not relevant

* Average value for June–December 2002.

Table 3.2. Measured monthly HTO concentration in precipitation in 2002.

Month	HTO Concentration in Precipitation (Bq L^{-1})		
	DF8	F27	P2
January	not available	not available	3670
February	not available	18	1350
March	not available	24	347
April	24	29	474
May	69	14	525
June	85	61	579
July	9	14	205
August	49	19	442
September	13	22	452

Table 3.3. Measured HTO concentration in soil water for the September sampling period.

Site	Soil water concentration ($Bq\ L^{-1}$)
DF8	22.5
DF11	18.7
F27	32.9
P2	552

Table 3.4. Measured HTO and OBT concentrations for the sampled crops.

Crop type	Site	Month	Plant type	Concentration ($Bq\ L^{-1}$)	
				HTO	OBT
Forage	DF8	July	Hay¤	–	79.4
			Haylage¤	–	82.0
		September	Alfalfa	21.4	25.7
			Baled hay¤	46.5	17.2
			Haylage	86.7	23.5
			Corn silage	31.0	25.0
	DF11	July	Alfalfa	–	43.9
			Baled hay	–	20.2
			Haylage	–	46.5
		September	Alfalfa	22.2	31.0
			Baled hay	27.8	22.2
			Haylage	10.6	31.3
			Corn silage	20.5	31.9
	F27	July	Grass	–	31.0
		September	Grass	30.2	20.3
	P2	September	Grass	2253	730
			Raspberry leaves	1564	677
Grain	DF8	July	Barley	–	50.8
		September	Feed Corn	76.0	28.5
			Barley	72.1	40.1
	DF11	July	Feed corn	–	27.9
		September	Feed corn	163.8	20.8
	F27	July	Spring wheat	–	27.4
		September	Feed corn	34.8	15.6
			Spring wheat	38.9	26.9
Total Mixed Ration	DF8	July	TMR*	–	42.5
		September	TMR	38.7	26.1
	DF11	July	TMR*	–	38.4
		September	TMR*	38.2	22.5
Root crops	F27	July	Mixed vegetables‡	–	42.0
	F27	September	Carrots and potatoes	38.5	40.6
			Beet	30.7	17.2
			Garlic	–	40.9
Fruit and fruit vegetables	F27	September	Tomato	35.5	27.0
			Cucumber	–	54.0
			Soya meal	61.5	20.3
			Apple	38.7	30.9
			Pear	–	38.6
			Raspberry	–	24.5

¤ Hay refers to fresh cut pasture; baled hay is dried pasture; haylage is hay that has been stored in a silo.
* Produced in 2001.
‡ Beet, cabbage, hot pepper, onion, dill, potato, spinach.

Table 3.5. Measured HTO and OBT concentrations in the sampled animal products.

Site	Month	Animal product	Concentration (Bq L^{-1})	
			HTO	OBT
DF8	July	Milk	–	33.9
	September	Calf flesh	27.5	31.3
		Calf heart	26.9	26.9
DF11	July	Milk	–	21.3
	September	Calf flesh	29.4	32.8
		Calf heart	33.2	20.0
F27	July	Egg	–	44.0
		Composite egg	–	23.1
		Immature egg	–	19.1
	September	Egg	33.7	26.2
		Chicken blood	33.5	21.8
		Chicken flesh	–	20.3

Table 3.6. Average OBT concentrations (Bq L^{-1} combustion water) in the grouped samples.

Sample Type	DF8 and DF11 combined		F27		P2
	July	September	July	September	September
Soil		20.6±1.9 (2)		32.9	552
Plants					
Forage	54.4±23.4 (5)	26.0±4.8 (8)	31.0	20.3	704±27 (2)
Grain	39.4±11.5 (2)	29.8±7.9 (3)	27.4	21.3±5.7 (2)	
Root crops			42.0	32.9±11.1 (3)	
Fruit and fruit vegetables				32.6±11.1 (6)	
Animal Products					
Milk – DF8	33.9				
– DF11	21.3				
Calf flesh/heart – DF8		29.1±2.2 (2)			
– DF11		26.4±6.4 (2)			
Eggs			28.7±10.9 (3)	26.2	
Chicken flesh/blood				21.1±0.8 (2)	

Note: Where more than one sample of a given type was collected, the average and standard deviation of the measurements are listed. The numbers in brackets beside the concentrations are the number of samples in the average.

3.2.2. Discussion of observations

For the plant samples, a quantitative comparison between predictions and observations will be made for the OBT concentrations only. The HTO concentrations in plants reflect conditions in the few hours before sampling. In contrast, the air concentrations that control tritium levels in plants are available in the scenario only as averages over a month at least. This means that the predicted HTO concentrations in plants must also be averages over the growing season. This mismatch in averaging times implies that no meaningful conclusions can be drawn from a comparison of predicted and observed HTO concentrations in plants. Rather, the predictions will be used to help explain differences among model results for OBT concentrations. On the other hand, the residence time for HTO in soil and animal products is a few days and for OBT in plants and animals a few weeks, sufficiently long that concentrations in these compartments better reflect average air concentrations and provide more reliable endpoints for discussion.

To keep the number of results to a manageable level, the various plant samples were grouped into five broad categories: forage (hay, baled hay, haylage, corn silage, alfalfa, grass and raspberry leaves), grain (corn, barley and spring wheat), TMR, fruit and fruit vegetables (apples, pears, raspberries, tomatoes, cucumber and soya meal) and root crops (mixed vegetables, potatoes, carrots, beets and garlic). Similarly, the animal products were grouped into four categories: milk, eggs, calf flesh (including calf heart) and chicken flesh (including chicken blood). Moreover, the plant and soil samples from DF8 and DF11 were combined in the analysis since the farms were so close together and the crops grown were similar. In contrast, the animal and TMR data were analysed separately because the cows had different diets. A separate analysis was also carried out for each sampling period. The average observed OBT concentrations for each of these categories are shown in Table 3.6.

Concentrations in all compartments were lower than those in air moisture, as required by specific activity concepts. The plant concentrations were higher in July than in September at all locations but the animal concentrations were the same at both sampling times, perhaps because the concentration in drinking water, which contributes significantly to the total tritium intake, varied little over time. At F27, the concentrations in vegetables and fruit were higher than in forage or grain. The standard deviations of the measured values were relatively low (< 30%) for all categories except forage at the dairy farms in July, vegetables, fruit and root crops at F27 in September and eggs at F27 in July.

Some of the variability evident in Table 3.6 can be reduced by normalizing the observations by the HTO concentration in air moisture, which controls concentrations in the other compartments and which varied over time and space during the study. The air moisture concentrations (in Bq L^{-1}) were derived from the air concentrations in Table 3.1 (in Bq m^{-3}) by dividing by 0.012 kg m^{-3}, the average absolute humidity over the growing season. The normalized results are shown in Table 3.7. The ratios for a given sample type incorporate data from all sampling locations and times. For rain, the ratios are based on monthly concentrations in rain and air moisture. For the other HTO endpoints, the observations are scaled by the air concentration in the month prior to sampling, the shortest interval available. For the OBT endpoints, the observations are scaled by the air concentrations averaged over the two months before sampling, to reflect the longer residence time of OBT in plants and animals.

The rain/air ratios show considerable variability, ranging from 0.11 to 0.82. Concentrations in rain depend strongly on the frequency with which rain falls when the plume is present and are unlikely to show stable values over averaging time as short as a month. The overall mean ratio of 0.32 falls within the range of values (0.041 – 0.44) found in other studies [3, 13]. The four measured soil/air ratios were all very similar at about 0.33 and also agree with the data of Davis et al. [13] and BIOMASS [3]. The normalized drinking water concentrations show little variability, with a mean value of 0.29, but the significance of this is not clear. The drinking water samples were taken from wells and the concentrations are likely to be driven more by local hydrology than air concentrations. The normalized plant OBT concentrations varied between 0.14 and 0.83. The values for forage, grain and TMR are consistent with a plant HTO/air moisture ratio of 0.6–0.7, together with an isotopic discrimination factor of 0.7 in the formation of OBT. The normalized OBT concentrations for root crops, fruit and fruit vegetables, which take a lot of their tritium from the soil, tend to be lower than those for the other types of plants, which are influenced more by concentrations in air moisture. Animal OBT/air ratios ranged from 0.13 to 0.46. On average, the OBT concentrations in animal products were lower than the HTO concentrations, and lower than the OBT concentrations in the feed.

Table 3.7. Observations normalized by HTO concentrations in air moisture.

Sample Type	Mean	Standard Deviation	Minimum	Maximum	Number of Samples
Monthly rain (HTO)	0.32	0.23	0.11	0.82	15
Soil (HTO)	0.33	0.03	0.29	0.36	4
Drinking water (HTO)	0.29	0.03	0.24	0.33	3
Plants (OBT)					
Forage	0.41	0.18	0.19	0.83	17
Grain	0.33	0.15	0.14	0.57	8
TMR	0.38	0.04	0.32	0.43	4
Fruit and fruit vegetables	0.30	0.10	0.19	0.50	6
Root crops	0.30	0.09	0.16	0.38	4
Animal products (HTO)					
Milk	–	–	–	–	0
Calf flesh/heart	0.45	0.04	0.41	0.51	4
Eggs	0.34				1
Chicken flesh/blood	0.34				1
Animal Products (OBT)					
Milk	0.28	0.06	0.22	0.35	2
Calf flesh/heart	0.39	0.07	0.28	0.46	4
Eggs	0.20	0.07	0.13	0.29	4
Chicken flesh/blood	0.19	0.01	0.19	0.20	2

Note: Results for a given sample type incorporate data from all sampling locations and times.

3.3. Modelling approaches

Eight participants submitted results for this scenario (Table 3.8). All participants treated the scenario as a blind test of their models and submitted results before the observed concentrations were made known to them.

The Pickering scenario tested models that predict tritium concentrations in a terrestrial ecosystem subject to a continuous release of HTO. It was a fairly simple scenario in the sense that releases have been going on for many years at roughly the same rate, and tritium concentrations in various parts of the ecosystem are likely to be in equilibrium. The approaches taken by the various participants to model this scenario varied widely. FSA used the STAR H-3 model, a dynamic compartment model that is formulated in terms of a series of coupled first-order differential equations. Rate constants for the transfers between compartments were derived from consideration of the hydrogen inventories of the compartments and the hydrogen fluxes between them. Predictions for the Pickering scenario, which is an equilibrium situation, were obtained from the steady-state solution to the equations. IRSN, GE, LIET and LLNL used in-house models that are well established in their respective institutions. The IRSN and GE models are similar in structure to STAR H-3, whereas LIET and LLNL are based for the most part on simple analytical equations that describe transfers between most compartments using empirically-based bulk parameters.

TUM, IFIN and SRA used less formal approaches, developing the computational tools needed to make their predictions in an *ad hoc* fashion. For the most part, these models were also analytical in structure and employed well known empirical relationships between concentrations in the various environmental compartments. All of the modellers grouped the plants and animals into a small number of categories to facilitate their calculations.

Table 3.8. Participants in the Pickering Scenario.

Participant	Affiliation	Model	Designation in text
F. Baumgärtner	Technische Universität München, Germany	BioM	TUM
R. Peterson	Lawrence Livermore National Laboratory, USA	DCART	LLNL
T. Nedveckaite	Institute of Physics, Lithuania	LIETDOS	LIET
P. Marks	GE Healthcare, U.K.	–	GE
D. Galeriu	National Institute of Physics and Nuclear Engineering – Horia Hulubei, Romania	–	IFIN
M. Saito	Safety Reassurance Academy, Japan	–	SRA
S. le Dizès-Maurel	Institut de Radioprotection et de Sûreté Nucléaire, France	TOCATTA	IRSN
D. Cutts	Food Standards Agency, UK	STAR H-3	FSA

The TUM model gives different OBT endpoints than those of the other models, predicting the concentration of buried tritium rather than the tritium traditionally considered to be organically (or carbon) bound. Buried tritium is tritium in exchangeable positions that is not removed by the conventional rinsing process. It consists primarily of tritium in large molecules that becomes hidden from the effects of washing when the free water in the sample is extracted by freeze drying or azeotropic distillation. A smaller part consists of tritium in hydrate bonds that is similarly not removed by washing, but this is not accounted for in the model. Buried tritium appears as part of the experimental yield when the sample undergoes traditional analysis for OBT, but is converted to HTO as soon as it is ingested. TUM calculates the concentration of buried tritium from the HTO concentration in the sample assuming a two-step exchange process and taking into account the proportion of carbohydrates, proteins and DNA in the tissues. The difference between the observed OBT concentration and the predicted buried tritium concentration gives the organically bound (or carbon bound) tritium concentration for the TUM model, if the tritium in the hydration shells is neglected.

Although the models used by the various participants were very different in formulation, they were all based on the same pool of environmental tritium data. The rate constants used by the compartment models were derived from the same data that provided the bulk parameters used by the analytical models. Thus the differences in model structure do not necessarily imply similar differences in predictions.

The modellers used air concentrations averaged over different time intervals to drive their models. In the LLNL model, the mean air concentration from May to July was used to calculate concentrations in the samples collected in July, and the mean air concentration from May to September to calculate concentrations in the September samples. The IFIN approach was to base HTO concentrations on the air concentration in the month prior to sampling and the OBT results on the air concentration averaged over the two months before sampling. In the IRSN model, the July and September air concentrations were used to drive the predictions for the two sampling periods. The other models adopted variations on these approaches.

The FSA results are based on an absolute humidity value appropriate to UK conditions instead of the value specified in the scenario. Use of the scenario specific value for this parameter would have decreased the FSA predicted concentrations in all endpoints by approximately 1/3.

The participants also estimated the uncertainties in their predictions using very different methods. Three modellers (IRSN, LIET and LLNL) carried out a rigorous Monte Carlo uncertainty analysis using Latin Hypercube techniques to sample distributed parameters. At the opposite end of the spectrum, IFIN used expert judgment to estimate his uncertainties. Between these extremes, SRA carried out an analytical analysis, on the assumption that the uncertainty in each input parameter was ±20%. TUM, GE and FSA did not submit uncertainty estimates.

Details of the models are introduced in the following sections as they are needed to explain the results. Full model descriptions are given in Appendix II.2.

3.4. Comparison of predictions and observations

3.4.1. Soil water

Predictions for the HTO concentration in soil water at DF8 and DF11 combined are compared with the observation in Figure 3.2. Five of the six models that submitted predictions for this endpoint produced results in good agreement with the observation even though they were all very different in structure. LLNL assumed the soil water concentration equalled 30% of the air moisture concentration, following the recommendation of BIOMASS [3]. IFIN assumed that the tritium in soil arose primarily from washout and set the soil water concentration equal to the sum of the concentration in rain plus 10% of the concentration in air moisture. SRA used a more complex analytical equation that described the balance between average tritium sources (wet and dry deposition) and sinks (infiltration, plant uptake and re-emission) in the root zone. The FSA and IRSN models are similar to this since, at steady state, the coupled differential equations on which they are based lead to solutions that are essentially a balance between sources and sinks.

The predictions of these five models for soil water concentrations were as good or better at F27 and P2 as they were at the dairy farms. Thus, good model performance for this data set can be achieved with models of very different complexity. In contrast, the predictions of the LIET model overestimated the observed soil water concentrations by about a factor of two at all sites. This model obtained the soil concentrations by balancing gains and losses in a two-compartment model of air and soil. The soil concentration was expressed in terms of the concentration in rain, the soil water content, the average rainfall rate, the depth of the root zone and the rate constant for losses from soil due to evapotranspiration, infiltration and runoff. The overprediction may have been due to an inappropriate choice of values for those parameters that were not defined in the scenario description.

The 95% confidence intervals shown in Figure 3.2 are fairly consistent from model to model, despite the different approaches taken by the participants in estimating their uncertainties. The confidence interval for LIET is clearly an underestimate since the prediction does not agree with the observation even when uncertainties are taken into account. The confidence intervals for the other endpoints were similar and will be discussed further in Section 3.5.

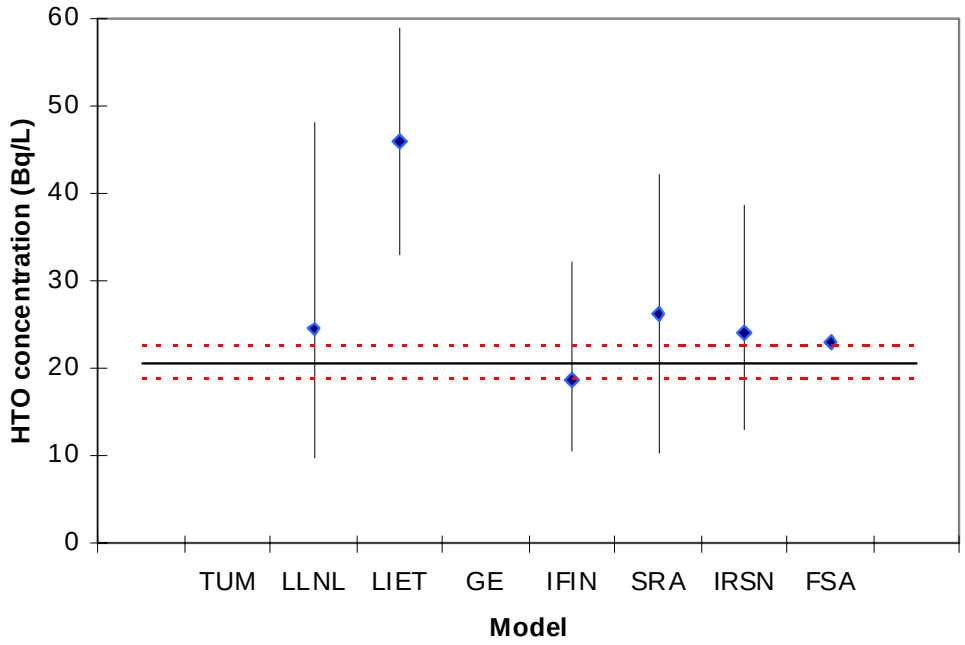

Fig. 3.2. HTO concentration in soil water for the September sampling period at DF8 and DF11 combined. The model predictions are shown as solid diamonds with the vertical lines representing 95% confidence intervals as estimated by the modelers. The solid horizontal line is the observation with the 95% confidence interval indicated by the dashed lines. FSA did not estimate uncertainties and TUM and GE did not submit results for this endpoint.

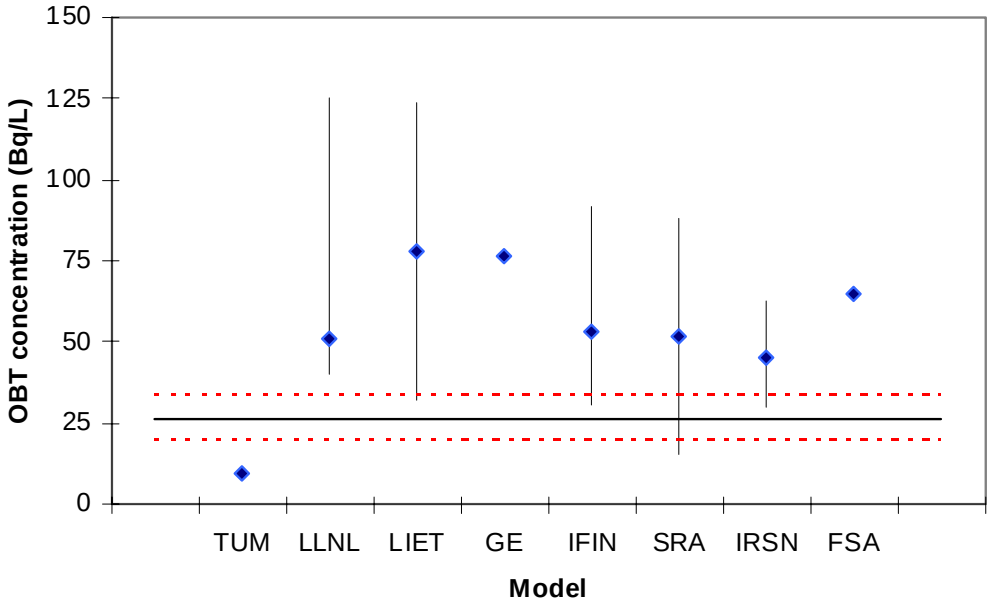

Fig. 3.3. OBT concentration in forage crops for the September sampling period at DF8 and DF11 combined. TUM, GE and FSA did not estimate uncertainties for this endpoint.

3.4.2. Forage

Predictions of the OBT concentration in forage crops at DF8 and DF11 combined for the September sampling period are compared with the observation in Figure 3.3. The GE result, which was reported in Bq kg^{-1} fresh weight, was converted to Bq L^{-1} water equivalent assuming a water fraction of 0.75 for fresh forage and a water equivalent factor of 0.59. With the exception of TUM, the scatter in the predictions was relatively small. However, all models overestimated the observed concentration, by up to a factor of 3 in the case of LIET and GE, and by a factor of 2.3 on average. The results of four models (LIET, IFIN, SRA and IRSN) marginally agreed with the data when uncertainties were taken into account. The TUM model underestimated the observation, but this was expected since this model predicts the concentration of buried tritium rather than fixed OBT. Similar results were obtained for DF8 and DF11 in July, although the degree of overprediction was not as large, and the results of all five models that estimated uncertainties agreed with the observation when the uncertainties were taken into account. However, the better agreement in July could be primarily a result of anomalously large measured concentrations in hay and haylage at DF8 rather than improved model performance. All of the models overestimated the OBT concentrations in grass at F27 by a factor of at least 3, and in grass and raspberry leaves at P2 by a factor of 2 on average.

OBT concentrations depend on the HTO concentration in the plant leaves and the rate at which that HTO is converted to OBT. The reasons for the misprediction of OBT concentrations evident in Figure 3.3 must be sought in these processes and they way they were modelled. The various participants determined the HTO concentration in plants in very different ways. Six models (FSA, IRSN, SRA, GE, LIET and LLNL) explicitly took into account the transfers of tritium to the plant from air and soil. FSA, GE and IRSN did this by specifying appropriate rate constants for use in their numerical models and calculating plant HTO concentrations at steady state. SRA used an analytical equation that balanced uptake and loss, with the roles of rainfall and air-plant transfer expressed explicitly:

$$C_{pw} = \alpha \left[\frac{C_a + I_w C_{sw} r}{\rho_s + \alpha\ I_w r} \right], \tag{3.1}$$

where:

C_{pw} is the HTO concentration in plant water;
$\alpha = 1.1$ is the ratio of the vapour pressure for water vapour to that of HTO;
C_a is the HTO concentration in air;
I_w is the average rainfall intensity;
C_{sw} is the HTO concentration in soil water;
ρ_s is the saturated vapour density of the air; and
r (= 67 s m^{-1}) is the exchange resistance for HTO and water between the plant leaf and the atmosphere.

LLNL and IFIN calculated the plant HTO concentration using Murphy's [7] analytical model, which distinguishes the contributions of air moisture and soil water to the HTO concentration in the plants:

$$C_{pw} = \alpha\ [RH\ C_{am} + (1\text{-}RH)\ C_{sw}], \tag{3.2}$$

where:

RH is the relative humidity; and
C_{am} is the HTO concentration in air moisture.

LIET used an equation similar to Equation (3.2) but with a slightly larger contribution from the soil. The remaining model (TUM) took a more empirical approach, assuming that C_{pw} was equal to the mean of the HTO concentration in drinking water and in rainfall (averaged over the 2–3 months prior to sampling); where the drinking water concentration was not available in July, C_{pw} was set equal to the average concentration in rain.

The predictions of the eight models for the HTO concentration in plant water for forage crops at the dairy farms are shown in Table 3.9. The results vary over a factor of more than 2 for July and more than 3 for September. The scatter is about a factor of two even for the six models that are theoretically based. Also shown in Table 3.9 are the plant concentrations normalized by the average air moisture concentrations in the month prior to sampling (103 and 64.6 Bq L^{-1} for the July and September sampling periods respectively). Some of the predictions show a plant/air ratio greater than 1, and most have a ratio greater than 0.65, the long-term average value observed in forage crops [14], but this could easily be due to the mismatch in averaging times for air and plant. The HTO predictions show a pattern similar to that evident in Figure 3.3 and explain most of the variability in the OBT results. The high plant/air ratios are likely responsible for some of the overprediction. Unfortunately, long-term average HTO measurements in plant water are not available to help identify the best predictions.

The other processes controlling OBT concentration are the rates of OBT formation and loss in the plant. The numerical models (FSA, IRSN and GE) accounted for these processes directly. In the analytical and empirical models, the OBT concentration was calculated as a fixed fraction of the HTO concentration. The TUM model calculated the concentration of buried tritium rather than OBT itself using a two-step exchange process that accounted for the number of exchangeable hydrogen positions in the carbohydrates and proteins of the plant in question.

The OBT/HTO ratios for each model are shown in Table 3.10. All but one of the ratios are high compared to observed ratios in the field [14], which tend to scatter about 0.7. Three of the models, including two of the numerical models, predict OBT concentrations larger than the corresponding HTO concentrations. The value used by IFIN was chosen to be deliberately conservative. These large values explain part of the general overprediction of OBT concentrations in the forage crops.

No data are given in Table 3.10 for the TUM model, which calculates the concentration of buried tritium rather than fixed OBT. The predictions for buried tritium lay between one third and one half of the observed OBT concentrations. If these predictions are correct, buried tritium makes up a significant proportion of what is traditionally called OBT.

Table 3.9. Predicted HTO concentrations in plant water for forage crops at the dairy farms.

Model	HTO Concentration			
	July		September	
	Plant (Bq L^{-1})	Plant/Air	Plant (Bq L^{-1})	Plant/Air
TUM	47	0.46	24.8	0.38
LLNL	85.5	0.83	72.9	1.13
LIET	97	0.94	97	1.50
GE	100	0.97	71	1.10
IFIN	74	0.72	53	0.82
SRA	54.9	0.53	44.9	0.70
IRSN	–	–	50.2	0.78
FSA	78	0.76	56.0	0.87

Table 3.10. OBT/HTO ratios in forage crops at DF8 and DF11.

Model	OBT/HTO ratio
LLNL	0.7
LIET	0.8
GE	1.1
IFIN	1.0
SRA	1.1
IRSN	0.9
FSA	1.2

Table 3.11. Average factor by which the predictions overestimated the observations for OBT in plants.

Crop type	Site	Month	Mean P/O ratio
Forage	DF8 and DF11	July	1.4
		September	2.3
	F27	July	3.4
		September	4.5
	P2	September	1.9
Grain	DF8 and DF11	July	1.8
		September	1.9
	F27	July	3.3
		September	4.0
Root crops	F27	September	2.6
Fruit and fruit vegetables		September	2.6

Table 3.12. Values adopted by the various modelers for food and drinking water ingestion rates.

Model	Ingestion rate of cows at DF11 (kg dry d^{-1})	Ingestion rate of chickens at F27 (kg dry d^{-1})	Drinking water ingestion rates (L d^{-1})	
			Cows	Chickens
LLNL	16.4	0.139	80	0.29
LIET	14	0.1	35	0.2
IFIN	19	0.2	70	0.3
SRA	10	0.1	90	0.2
IRSN	10	0.2	75	0.3
FSA	115 (fresh wt)	0.5 (fresh wt)	60	0.2

3.4.3. Grain, fruit vegetables, fruit and root crops

Two modellers (IRSN and FSA) assumed that the HTO concentration was the same in the edible portions of grain, fruit vegetables, root crops and fruit as it was in forage. The other modellers reduced the HTO concentrations in these plants to account for the fact that they draw more of their tritium from soil water than the forage crops do. However, all of the modellers assumed that HTO was taken up by the leaves of all plant types in the same way, that OBT was formed in the leaves by photosynthesis, and that the OBT was translocated to the edible portion of the plant without change in concentration. Thus, each participant predicted the same OBT concentration in all crops sampled at the same time and place. Leaving the TUM results aside for the moment, all of the models overestimated the OBT concentrations in all crop types at all sampling sites and times. The degree of overprediction for the various crops is shown in Table 3.11 in terms of the mean ratio of predictions to observations (the mean P/O ratio). The TUM and GE results were not included in these factors, since TUM did not calculate traditional fixed OBT *per se* and the very high GE predictions suggest a mistake may have been made. There is a tendency for the ratios to be higher at F27 than elsewhere. This conclusion cannot be stated definitively for forage and grain since the results are based on one or two samples only and the measured concentrations may be unreliable. But the overprediction for fruit, fruit vegetables and root crops must be accepted as real and suggests that the models are not performing as well for these crops as for forage and grain. The results for fruit and fruit vegetables measured at F27 in September are shown in Figure 3.4, where the mean overprediction was 2.6.

3.4.4. Total Mixed Ration (TMR)

The calculation of TMR concentrations required special consideration for two reasons:

(1) not all of the components of TMR were contaminated; and
(2) most of the TMR fed to the cows in 2002 was grown in 2001.

The LLNL, IFIN and SRA models took both of these factors into account, calculating concentrations in the various components of the 2001 TMR using the air concentrations measured in 2001, and forming the TMR concentration itself from an average of the component concentrations weighted by their fractional contribution to the total make-up of the TMR (with the uncontaminated components assumed to have background tritium levels). IRSN accounted for the higher air concentrations in 2001 but not the uncontaminated portion of the TMR; LIET accounted for the uncontaminated portion but not the higher air concentrations. GE took neither of these factors into account but instead set the TMR concentration equal to the concentration of the forage crops (on a fresh weight basis). FSA did not submit predictions for TMR.

Predictions for the OBT concentration in the TMR sample collected at DF11 in July (which was composed of crops harvested in 2001) are shown in Figure 3.5. Similar results were obtained for DF8 and the September sampling period. All of the models overestimate the observed concentration, although not as severely as some of the other endpoints. Predictions of five of the six models agree with the observation when uncertainties are taken into account.

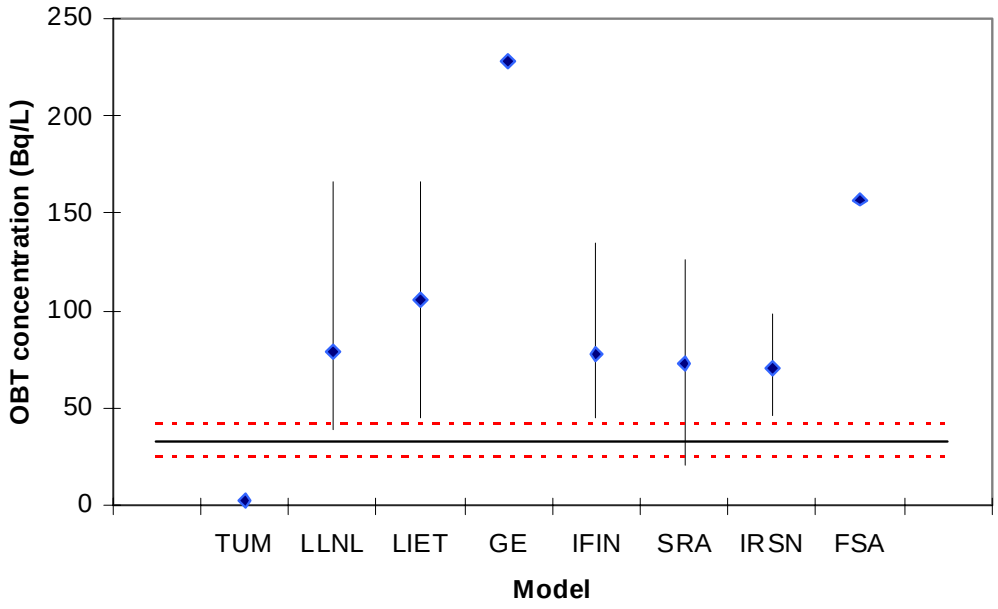

Fig. 3.4. OBT concentration in fruit and fruit vegetables for the September sampling period at F27. TUM, GE and FSA did not estimate uncertainties for this endpoint.

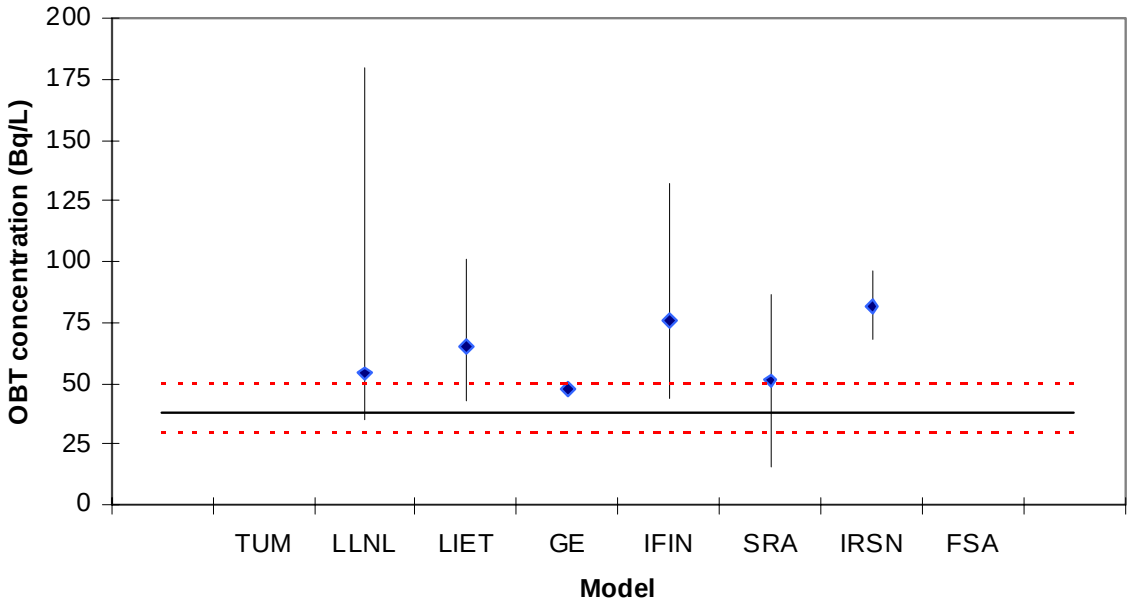

Fig. 3.5. OBT concentration in the TMR sample collected in July at DF11. TUM and FSA did not submit predictions for this endpoint.

3.4.5. Milk and beef

3.4.5.1. HTO concentrations

Predictions of the average HTO concentration in calf flesh and heart for the samples taken at DF8 in September are compared with the observation in Figure 3.6. With the exception of FSA, the predictions ranged over less than a factor of two and all agreed with the observed value when uncertainties were taken into account. Similarly good agreement was obtained for the HTO concentrations in calf flesh and heart at DF11 in September, even though the diet of the cows was not well known at that site. The assumptions made by the various modellers regarding the ingestion rate of the cows at DF11 are shown in Table 3.12 The differences in the assumed value would have contributed to the variability in the predicted concentrations.

Unfortunately, HTO concentrations were not measured in the milk samples so the predictions could not be compared with observations. But the predictions of most of the models show the same relatively small scatter evident in Figure 3.6 at both DF8 and DF11. When FSA, which appears to be an outlier, was left out of the calculations, the mean predicted HTO concentration in milk was about 30 Bq L^{-1} at both sites, with a standard deviation of less than 30%.

The agreement in the predicted HTO concentrations was achieved despite the fact that the models used by the various participants were quite different. In their numerical models, FSA and IRSN specified rate constants that described the uptake of tritium by the animal through inhalation and ingestion, and losses due to elimination, and solved for the concentrations at steady state. LLNL assumed that the animal HTO concentration was equal to the average concentration of the water pools accessed by the animal (plant water, plant organic matter, drinking water and inhalation/skin absorption), weighted by the fraction that each pool contributed to the total water intake. IFIN used a model based on the metabolism of hydrogen and carbon in the body to derive transfer parameters specific to the animal in question and its diet. SRA used the experimental data of Kirchmann et al. [15, 16] to derive the tritium specific activity in animal products given the specific activity in the diet and the drinking water. LIET expressed the animal concentrations in terms of the fraction of daily tritium intake that appears in the animal product, with separate values for transfer from HTO in food to HTO in animal product, from OBT in food to HTO in animal product, from HTO in food to OBT in animal product and from OBT in food to OBT in animal product. TUM assumed that the animal concentration was equal to the mean of the HTO concentration in drinking water and in rainfall averaged over the 2–3 months prior to sampling. GE did not calculate animal concentrations.

The similarity in predictions despite the divergence in model structure can be attributed in part to the fact that drinking water is a major contributor to tritium body burden and that drinking water concentrations were provided with the scenario. The ingestion rates assumed by the modelers (Table 3.12) imply that drinking water contributed between 50 and 80% to the total tritium body burden of the cows. Thus, knowing the tritium concentration in drinking water helped to damp the effect of the overprediction of food concentrations.

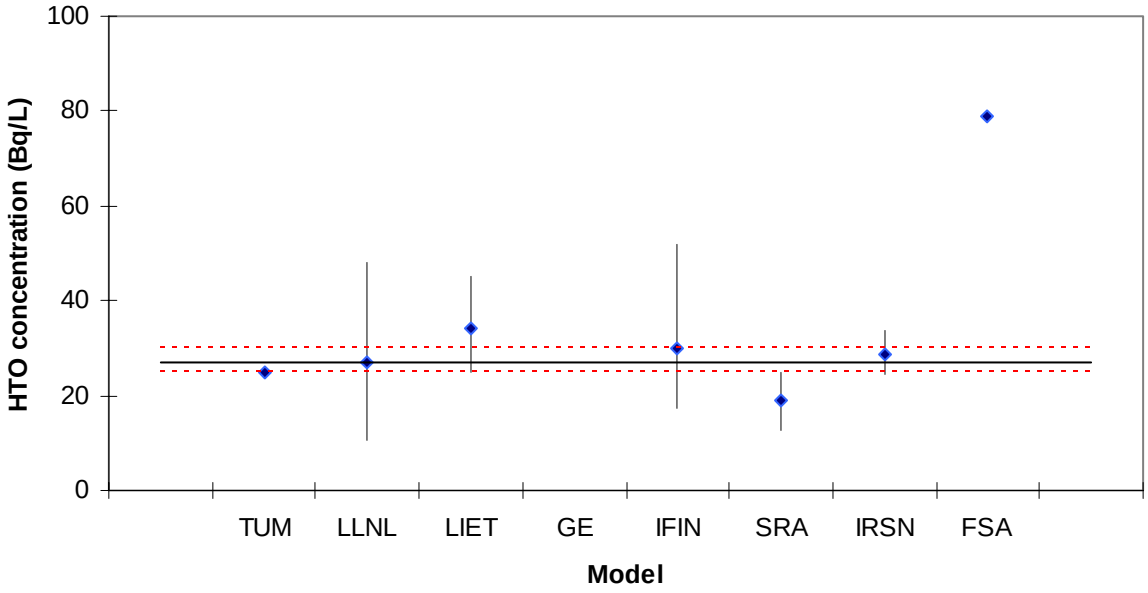

Fig. 3.6. Average HTO concentration in calf flesh and heart at DF8 in September. GE did not submit a prediction for this endpoint and TUM and FSA did not estimate uncertainties.

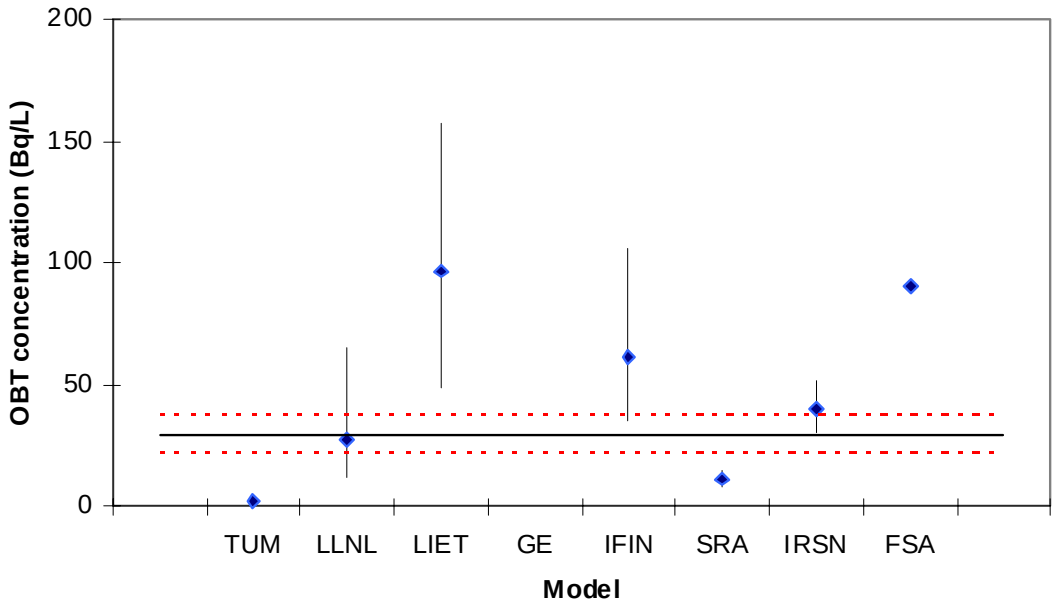

Fig. 3.7. Average OBT concentration in calf flesh and heart at DF8 in September. GE did not submit a prediction for this endpoint and TUM and FSA did not estimate uncertainties.

3.4.5.2. OBT concentrations

Predictions of the average OBT concentration in calf flesh and heart for the samples taken at DF8 in September are compared with the observation in Figure 3.7. The agreement between predictions and observations is worse than it was for HTO. The predictions show greater scatter, ranging over a factor of 10, and only three agree with the observed value when uncertainties are taken into account. Most of the models overpredict the observation, with a mean P/O ratio of 1.6. Similar results were obtained for the OBT concentrations in calf flesh and heart at DF11, where the mean P/O ratio increased to 2. Results for milk were also similar, with considerable scatter in predictions at both sites and mean P/O ratios of 1.2 and 2.3 at DF8 and DF11, respectively.

Four participants considered HTO and OBT to be coupled within the cow and solved for the concentrations of the two species simultaneously using the same model. Thus the numerical models of FSA and IRSN, the metabolic model used by IFIN and the transfer parameter model of LIET returned OBT concentrations as well as HTO. SRA used the empirical data of Kirchman et al. [15, 16] for both HTO and OBT. LLNL set the OBT concentration equal to the HTO concentration and TUM assumed an exchange process model to calculate the concentration of buried tritium. The differences in these models and their parameter values resulted in the scatter evident in Figure 3.7. Differences in assumptions for the food ingestion rate at DF11 and in the water ingestion rates at both sites (Table 3.12) would also have contributed to the variability in the predicted concentrations.

The models differed in their predictions of the ratio of OBT to HTO concentrations in milk and calf flesh. One model (RSA) produced an OBT/HTO ratio of about 0.6. Two other models (LLNL and FSA) predicted a ratio close to 1. In the remaining models (LIET, IFIN and IRSN), the OBT concentrations exceeded the HTO concentrations, by a factor of 2 on average. In fact, the data show that the HTO and OBT concentrations in calf flesh are about the same. This observation may be specific to the conditions of this scenario and not generally applicable. The primary source of HTO for the cows was drinking water whereas the main source of OBT was TMR, and concentrations in these two sources were essentially independent.

The data show that the OBT concentration in milk or flesh in July was about 30% lower than the concentration of OBT in TMR grown in 2001. In September, the situation was reversed, with the OBT concentration in milk or flesh about 20% greater than that in TMR. The latter finding is surprising since much of the OBT ingested by the cow is expected to be converted to HTO during digestion, and little of the HTO ingested is converted to OBT. Most modelers predicted animal concentrations lower than TMR concentrations, by factors that ranged from 0.25 for SRA to 0.8 for IFIN and IRSN. In contrast, the results for LIET and FSA showed animal concentrations as much as 50% greater than those in TMR.

With two exceptions, the models predicted that the OBT concentrations in flesh and milk were about the same. The exceptions were LIET and FSA, which predicted flesh concentrations greater or less than those in milk depending on the site and the time of sampling. Observations are not available to test these predictions since milk and flesh were never sampled at the same time.

3.4.6. Chicken and eggs

3.4.6.1. HTO Concentrations

Predictions of the HTO concentration in eggs for the sample taken at F27 in September are compared with the observation in Figure 3.8. The performance of the models is not as good for eggs as it was for milk or calf flesh. The predictions show considerable scatter, with only three agreeing with the observation when uncertainties are taken into account. Three of the results overestimated the observation by factors ranging from 2 to 4. Similar results were obtained for the HTO concentrations in chicken blood in September. The scatter was much the same for the predicted concentrations in eggs in July, although in this case no observation was available for comparison. The participants used the same models for chickens and eggs as they did for milk and calf flesh, so the poorer performance here must be due to the parameter values used in the models. In particular, the feed and water ingestion rates for the chickens were not known and the modellers made very different assumptions about their values (Table 3.12), which would have contributed to the variability in the predicted concentrations. Also, the models assume all drinking water was contaminated, when in reality the chickens may have drawn their water from uncontaminated sources.

3.4.6.2. OBT concentrations

Predictions of the OBT concentration in eggs for the sample taken at F27 in September are compared with the observation in Figure 3.9. The scatter among the models was less than it was for HTO, but the level of agreement between predictions and observations was worse, with all of the models apart from TUM overpredicting the measured value, by a factor of 3.2 on average. Only the LLNL model agreed with the observation when uncertainties were taken into account. Similar results were obtained for the OBT concentration in eggs in July. Results were worse for chicken blood and flesh in September, where the mean P/O ratio increased to 4.5.

With one exception, the models consistently predicted higher OBT than HTO concentrations in eggs and blood, with the OBT/HTO ratio varying from 1.2 to 2.5. The exception was LIET, which predicted an OBT/HTO ratio of 0.47 for eggs in July, 0.78 for eggs in September and 1.04 for blood in September. In fact, the data show that the OBT concentration was less than the HTO concentrations, with an OBT/HTO ratio of 0.78 for eggs and 0.63 for blood. As was the case for cows, this observation may not be generally applicable outside of this scenario.

The data show that the OBT concentration in eggs and chicken flesh in September was about the same as the average OBT concentration in the feed eaten by the chickens. Most of the modelers (LIET, SRA, IRSN and FSA) reproduced this observation. In contrast, LLNL predicted an animal/feed ratio of 0.57 and IFIN a ratio of 1.4 for eggs and 1.8 for flesh.

For all models, the predicted HTO concentrations in eggs were essentially identical to the HTO concentrations in chicken flesh and blood, in agreement with the observation. With two exceptions, the models also predicted that the OBT concentrations in flesh and eggs were about the same, a conclusion again supported by the observations. The exceptions were LIET and IFIN, which both predicted flesh concentrations about 30% greater than those in eggs.

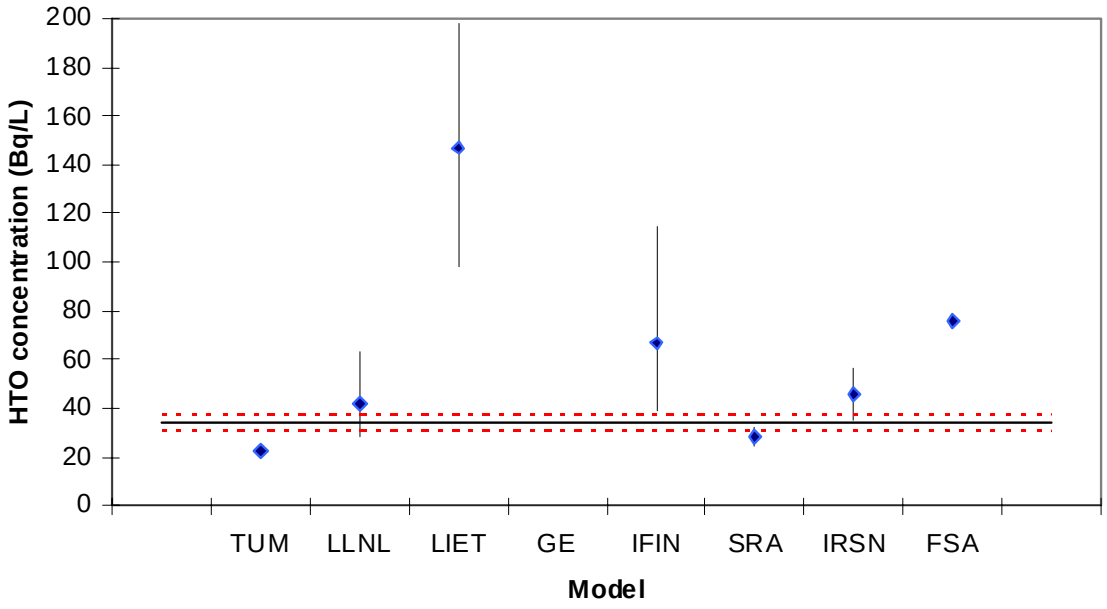

Fig. 3.8. HTO concentration in eggs at F27 in September. GE did not submit a prediction for this endpoint and TUM and FSA did not estimate uncertainties.

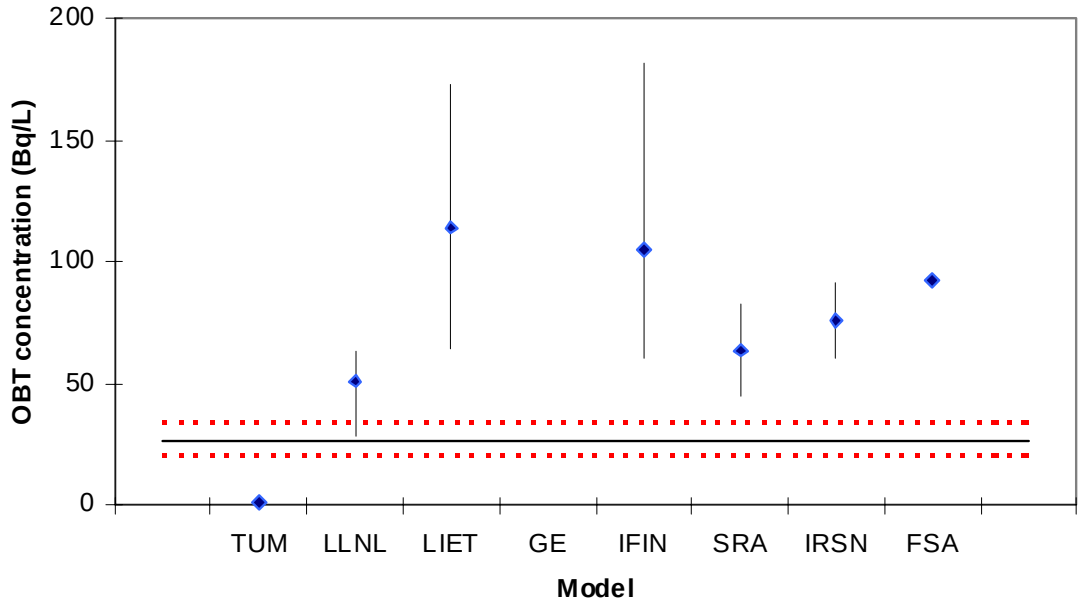

Fig. 3.9. OBT concentration in eggs at F27 in September. GE did not submit a prediction for this endpoint and TUM and FSA did not estimate uncertainties.

3.5. Discussion and conclusions

The Pickering scenario provided a good test of models that predict tritium concentrations in the various compartments of an agricultural ecosystem at steady state. Reliable estimates of HTO concentrations were available in air moisture, precipitation and drinking water as input to the models. Most of the information required to evaluate the animal pathways was available without the need for the assumptions that usually have to be made about diet or the fraction of feed that is contaminated. On the other hand, the scenario was not ideal since some information on ingestion rates was incomplete or missing, and this contributed to the differences between predictions and observations. But many real assessments must be carried out with even less information and difficulties of this sort must be expected in practice.

The models used by the participants in their calculations varied from numerical dynamic compartment models (solved for steady-state conditions) to simple analytical models based on empirical data. Similarly, different parameters appeared in the different models, although all were based on the same pool of environmental tritium data. For these reasons, it was often difficult to explain why one model produced a different result than another, or why a specific model result differed from the corresponding observation.

Despite their differences, all models but one performed well for HTO in soil, predicting concentrations that agreed with each other and with the observations when uncertainties were taken into account. In contrast, all of the models significantly overestimated the OBT concentrations in plants, by an average factor of 1.9 at the dairy farms and 3.4 at F27. This appears to be due in part to overprediction of the concentration of HTO in the plant leaves, where OBT is formed by photosynthesis. For most models, the ratio of predicted HTO concentration in plant leaves to observed HTO concentration in air moisture was substantially larger than the value of 0.65 that has been observed in other studies. Additionally, the models appear to underestimate the effect of isotopic discrimination in OBT formation. Most of the predicted OBT/HTO ratios for the plant leaves were larger than the value of 0.7 observed elsewhere.

These two factors alone could explain overestimates of as much as a factor of two in the predicted OBT concentrations for several of the models, and resolve the differences between predictions and observations for forage and grain at the dairy farms. Additional reasons must be found to explain the more severe overpredictions at F27. One possibility may lie in the fact that most of the samples taken at this site were root crops, fruit and fruit vegetables. OBT that appears in the edible parts of these plants must be translocated from the leaves where it is formed, and a reduction in concentration may occur during the translocation process. This cannot explain the large overestimates for forage crops at F27 but the observed values for these plants may not be reliable since they were based on one or two samples only.

A second explanation may lie with the air concentrations provided as part of the scenario description. The measured concentrations at F27 were lower than those observed at the dairy farms. This was thought unlikely since the wind blows with equal frequency toward F27 and the dairy farms, and F27 is closer to the reactors. Moreover, the measurements were made with passive samplers, for which the uncertainty is large. It was therefore assumed that the measurements were in error, and, as noted in Section 3.1, they were replaced with predictions from a sector-averaged Gaussian plume model, which produced results in good agreement with the observed air concentrations at P2 and the dairy farms. If the measured concentrations were indeed correct and had been used in the models, the predicted plant concentrations would have been lower by a factor of 2, removing a lot of the discrepancy between

predictions and observations at F27. A quantitative assessment of the air concentrations used to drive the models is given in Appendix III, based on data that became available only after work on the scenario had been finalized.

No conclusions could be drawn about the ability of the models to predict HTO concentrations in plants. HTO is very mobile in plants and the observed concentrations reflect the air concentrations in the hour or two before sampling. It is unlikely that this will match the long-term average air concentration used to drive the models, with the result that predicted and observed values cannot necessarily be expected to agree.

Most of the models predicted HTO concentrations in milk and calf flesh that were in good agreement with the observations. This may be due in large part to the importance of drinking water concentrations, which were provided in the scenario description, to the body burden of the animal. Model performance was not as good for OBT, which was overestimated in most cases. The models did not do as well for eggs and chickens as for milk and calf flesh, partly because the concentrations in chicken feed were overestimated to a greater extent than in cow feed and partly because the ingestion rates of feed and drinking water were not known for the chickens. Most of the models did not correctly reproduce the observed OBT/HTO ratio in the animals, and some predicted higher OBT concentrations in animals than in their feed, which seems unlikely in reality. Most models predicted that concentrations in milk were similar to concentrations in calf flesh, and that concentrations in eggs were similar to concentrations in chicken flesh, in agreement with the observations.

No one model stood out as generating predictions superior to the others for HTO concentrations in soil water or OBT concentrations in plants. Generally speaking, the level of agreement between predictions and observations was about the same for the numerical models as for the analytical models, although the numerical models tended to be responsible for all of the very high predictions. All of the models were satisfactory for HTO concentration in milk and calf flesh. However, the LLNL model stood out as the only model that reproduced the observed concentrations in all of the animal endpoints within the estimated uncertainties. The IRSN also did well in this regard. Despite the fact that some models predicted OBT/HTO ratios greater than one for some plants, and OBT concentrations in animals that exceeded the OBT concentration in their feed, there is no evidence in the Pickering data of tritium bioaccumulation in the terrestrial pathways.

The results of the TUM model, which calculates the concentration of buried tritium rather than the tritium traditionally considered to be organically bound, were lower than those of the other models for the OBT endpoints. The TUM predictions made up a significant proportion (40%) of the measured OBT concentrations only for forage; for fruit, fruit vegetables, calf flesh, calf heart and eggs, buried tritium made up less than 5% of the measured concentration. The results of the TUM model indicate that the formation of buried tritium is better modeled as a two-step exchange process rather than as a one-step process.

The uncertainties estimated by the various participants differed somewhat from model to model and endpoint to endpoint, but were roughly consistent with a confidence interval (97.5^{th} percentile divided by the 2.5^{th} percentile) of a factor 3. In general, the modellers estimated higher uncertainties for OBT concentrations than for HTO, which is reasonable given that the uncertainties in OBT include those for HTO plus additional ones specific to OBT itself. The uncertainty estimates for the animal endpoints were generally lower than those for plants, which is justified based on model performance for HTO in milk and calf flesh but not for HTO in eggs and chicken flesh or OBT in any animal product.

CHAPTER 4. THE PINE TREE SCENARIO

4.1. Background and objectives

4.1.1. Introduction

In the Tritium Working Group (TWG) of the IAEA BIOMASS Programme from 1996 to 2000, two atmospheric source scenarios for model-data comparison exercises were proposed by Canada and France. Both were concerned with the transport of tritium in the vicinity of long-term or chronic atmospheric sources of tritiated water vapour (HTO). The sites were located in inland areas subject to temperate climates. Modelers were requested to predict tritium concentrations in sample species such as air, rain, soil water and plant water, with special focus on organically bound tritium (OBT) in plants and on the relationships between air HTO, plant tissue free water tritium (TFWT) and plant OBT concentrations. Compared with these two scenarios, the EMRAS pine tree scenario has unique features in the following aspects. First, it deals with a sub-tropical climate, which may affect the tritium behavior in the environment differently from a temperate climate. Secondly, the tritium sources are located along the Pacific coast, which may have a specific influence on atmospheric dispersion. Thirdly, it is the first model-data intercomparison exercise that treats sub-surface infiltration (groundwater) pathways following long-term atmospheric releases. Finally, it involves monthly variations of plant OBT concentrations over a few years, which may help to understand the seasonal variations of OBT in an evergreen pine tree. If we take into account the long residence time and translocation of OBT in plants, it is useful to compare OBT concentrations in four seasons in consecutive years. The Canadian BIOMASS scenario requested OBT concentrations in grass only at three times in a 2 month period in the summer, and the French scenario requested annual average OBT concentrations in a deciduous birch tree. Thus neither scenario addressed the long-term behavior of plant OBT, including winter seasons, a deficiency that is rectified in the EMRAS Pine Tree scenario.

4.1.2. Need for the present study

We learned from the BIOMASS scenarios that the uncertainty associated with the prediction of OBT concentrations in plants depends largely on the uncertainty in the tritium concentration in air moisture. The plant OBT concentration is calculated by multiplying the plant TFWT concentration by a discrimination factor, while the TFWT concentration is usually expressed as a function of the HTO concentrations in air and soil. These relationships have been validated in temperate climates and inland areas such as Europe and North America, where rainfall, air temperature and air humidity are all relatively low. For tritium discharge sources located along the sea coast, alternating wind directions between day and night time are common and may affect the atmospheric dispersion of the airborne plume. Especially during the day, onshore winds sometimes result in trapping conditions that have never been considered in past modeling scenarios. The Pine Tree scenario provides the opportunity to test models that predict tritium concentrations in various sample species (endpoints) due to multiple tritium sources located along the Pacific coast in Tokaimura, Japan.

In the French scenario of BIOMASS, the OBT concentrations measured in the leaves of one plant type were a factor of two different from the concentrations in the annual rings of a second plant type. There is a need to confirm this difference for different components of the same plant species, and to provide possible explanations for the difference. Since humans and animals eat different components of plants (leaves, stems, fruits and roots), it is important to

take into account differences of OBT concentration between the various plant parts for reliable tritium dose assessments.

In BIOMASS, two exercises on sub-surface pathways were conducted as model inter-comparison exercises without observational data. Suitable test data, which are essential for validating soil and hydrological models, were not found despite a concerted search at the time. The EMRAS Pine Tree scenario includes a dataset of monthly HTO concentrations in groundwater for a few years and meets the need not realized in the BIOMASS programme.

4.1.3. Specific objectives

The Pine Tree scenario was provided to evaluate the suitability of current modeling approaches for predicting monthly and yearly mean tritium concentrations in sample species (air moisture, rain, pine needle TFWT and OBT, pine annual ring OBT, and groundwater) in the vicinity of multiple tritium sources, taking into account such features and conditions as: (i) a short-term incidental release from one of the tritium sources; (ii) a sea coast location for all sources, which were subject to diurnal wind direction changes; (iii) a sub-tropical climate characterized by high humidity and rainfall intensity; (iv) OBT production and translocation related to pine tree physiology; and (v) groundwater and tritium movement through a shallow sandy gravel layer.

4.2. Scenario description

The Pine Tree scenario involved the continuous release of tritium from four sources near Tokaimura, Ibaraki Prefecture, Japan, and requested the calculation of tritium concentrations in air moisture, rain, pine trees and groundwater in the vicinity of the sources. As shown in Figure 4.1, two heavy water moderated research reactors (JRR2 and JRR3) and a waste treatment facility (WTF) are located at the JAERI[1] site and the Tokai Reprocessing Plant (called the Nuclear Fuel Reprocessing Plant, NFRP in this report) is situated at the JNC* site in Tokaimura. These facilities have released HTO vapor into the atmosphere continuously for many years. The most frequent wind direction at the site is north-east to south-west, as shown in Figures I.3.9 and I.3.10 in the Scenario Description (Appendix I.3). Since 1981, the National Institute of Radiological Sciences (NIRS) has conducted a monthly monitoring programme, including measurements of tritium concentrations in rain, groundwater and pine trees in the vicinity of JAERI and JNC. Among many sampling points, data from P3, MS2 and G4 were selected for the scenario because of their distinct source-distance relationships.

Since 1984, JAERI has conducted a monthly monitoring programme including measurements of HTO concentrations in air, rain and pine needles at MP7, and HTO concentrations in rain at MS2.

[1] The Japan Atomic Energy Research Institute (JAERI) and the Japan Nuclear Cycle Development Institute (JNC) were unified into the Japan Atomic Energy Agency (JAEA) on 2005 October 1. The old names of JAERI and JNC are used in this report to maintain consistency with the organization names used in published papers related to this report.

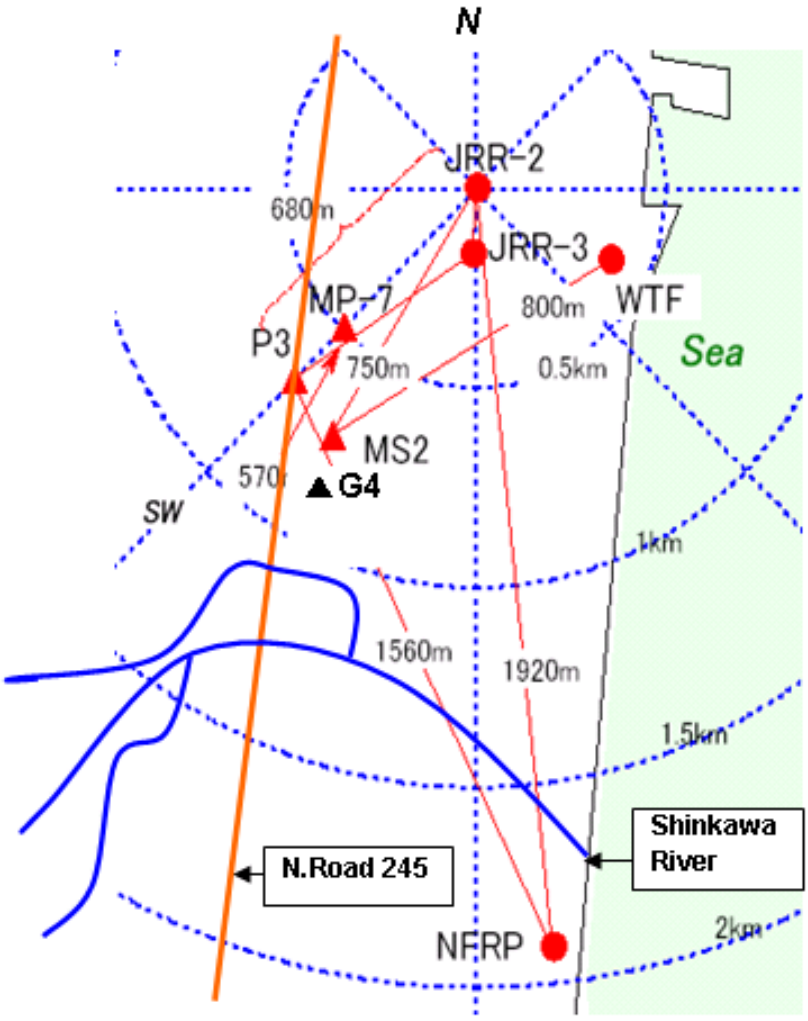

Fig. 4.1. Map of the four tritium sources JRR2, JRR3, WTF of JAERI, and NFRP of JNC (closed circles) and the four tritium sampling points MP7 of JAERI and P3, MS2 and G4 of NIRS (triangles) in Tokaimura, Japan.

All the main tritium sources as well as the sampling points P3, MS2 and G4 in the scenario were located within a rectangle measuring 1.0 km east-west and 2.0 km north-south (Figure 4.1). The area is covered with sand dunes, the height of which increases away from the coastline to about 24 m above the sea level. A detailed description of the area, including the direction and distance of the sampling points from the sources, soil characteristics, geological structure (including parameter values for groundwater flow calculation), meteorological data and atmospheric tritium discharge rates from the four sources were provided in the scenario description.

Modelers were requested to calculate the following endpoints:

(1) Monthly-average HTO concentrations in air moisture and precipitation, and TFWT and non-exchangeable OBT (nOBT) in pine needles from 1982 to 1986 at sampling point P3;

(2) Annual-average HTO concentrations in air moisture and precipitation, OBT in pine tree rings, and TFWT and OBT in needles of pine trees separately collected from the tree at the sampling point MS2. All predictions were to be for the period 1984 to 1987 at MS2;
(3) Monthly-average tritium concentrations in groundwater at the well G4 from 1984 to 1987; and
(4) 95% confidence intervals on each prediction.

The full scenario description is provided in Appendix I.3.

4.3. Observations

4.3.1. Sampling

From 1981, NIRS collected monthly rain water using a funnel attached to a long pipe. No effort was made to avoid tritium exchange between air moisture and the rain water accumulated in the pipe. Groundwater samples were collected from the taps of residents. New pine needle samples were collected from new growth branches at heights of 1.0 to 1.5 m above the ground; these samples were stored in double-sealed plastic bags until they could be analyzed. The red pine trees in the Tokaimura area are up to 10 m high. For the annual-ring OBT analysis, a pine tree trunk sample was collected in December 1987 close to MS2.

4.3.2. Background samples

The contribution of tritium discharged from the tritium sources to the environmental concentrations was calculated from the observations by subtracting the background tritium levels. The background concentrations in rain, groundwater and annual-ring samples were determined by NIRS at locations far from nuclear facilities. Background concentrations in air moisture, pine needle TFWT and pine needle OBT in Japan were taken from published papers. These background data are shown in Table 4.1.

4.3.3. Experimental procedures

Rain samples were purified by distillation and counted by low background liquid scintillation counting (LSC) techniques. Groundwater samples were normally electrolytically enriched before LSC. Needle TFWT was extracted on a cold finger as ice by vacuum distillation, purified by distillation by adding a small amount of $KMnO_4$, and counted by LSC. OBT concentrations in pine needles were obtained from the combustion water of the dry samples using an oxygen plasma asher (oxidizer) and purified by distillation. Detailed techniques of analysis are published elsewhere [17–21].

Table 4.1. Background tritium concentrations in Japan from 1982 to 1987.

Quantity	Air moisture	Rain	Pine needle TFWT	Pine needle OBT	Groundwater
	1984–1988	**1982–1987**	**1983**	**1983**	**1980–1988**
Mean (Bq/L)	1.9	1.1	1.7	2.4	2.2
2SD*	0.2	0.4	1.1	1.3	0.6
Location	Fukuoka	Chiba	Whole of Japan	Whole of Japan	Ibaraki

*SD: standard deviation of the mean.

4.3.4. Uncertainties in counting

The lower detection limit was estimated to be 1.2Bq/L, a value 3 standard deviations (SD) below the net counting rate when 8 ml of water was directly counted. The OBT concentrations in all samples exceeded this limit except for the concentrations in the tree rings collected in Chiba city in the late 1980s. The precision (reproducibility) was estimated to be 11–20% (2SD of the mean) by analyzing identical samples of two different tree rings two to three times. Uncertainties as 2 SD of the mean ranged from 11% to 31% for the OBT concentration in tree rings at MS2 from 1984 to 1987 [21].

4.3.5. Air moisture estimates at P3 and MS2

NIRS did not carry out air moisture sampling at P3 or MS2. JAERI collected air moisture continuously using molecular sieve columns at MP7, but not at MS2. JAERI also collected monthly rain at MP7 and MS2 [22]. The air HTO concentration in Bq/m^3 reported by JAERI was converted to Bq/L water using the absolute humidity of each month averaged over the six years from 1982 to 1987. This conversion may have introduced an error of about 10% into the observed air moisture concentration in Bq/L water at MP7.

Ratios of annual mean tritium concentration in rain at P3 and MP7 and at MS2 and MP7 from 1984 to 1987, which were calculated from NIRS data for P3 and MS2 and JAERI data for MP7, are shown in Figure 4.2. The rain concentrations are similar at the three sites, suggesting that the concentrations in air moisture are also similar. Thus it is reasonable to assume that JAERI's air moisture data at MP7 apply also at P3 and MS2 as reference values, with uncertainties of about 30% for P3 and 80% for MS2.

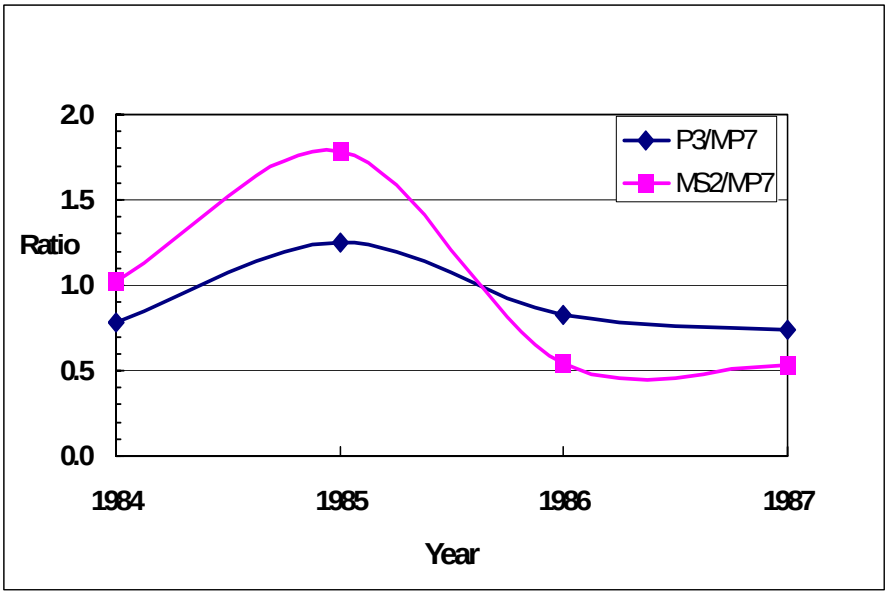

Fig. 4.2. Ratios of yearly tritium concentration in rain at P3 and MP7, and at MS2 and MP7 from 1984 to 1987.

Table 4.2. Participants and the models in the Pine Tree scenario.

Participating Group	Affiliation	Model name	Designation used in text
K. Miyamoto K. Yamamoto	NIRS, Japan Y First, Japan	Tritium-EESAD ERMA	NIRS
M. Saito	Safety Reassurance Academy, Japan	TriSat	SRA
S.R. Peterson	Lawrence Livermore National Lab, USA	DCART	LLNL
D. Galeriu A. Melintescu	Institute of Atomic Physics and Nuclear Engineering, "Horia Hulubei", Romania	DISPT	IFIN
F. Siclet E. Gilbert T. Kestens	Electricité de France, France	ADMS3, ARGUS	EDF

Table 4.3. Participants and their calculated endpoints.

Participant	Number of calculations until final results	Air	Rain	Needle TFWT	Needle nOBT	Ring nOBT	Ground-water
NIRS	2	○	○	○	○	○	○
SRA	3	○	○	○	○	○	○
LLNL	1	○	○	○	○	○	–
IFIN	1	○	○	○	○	○	○
EDF	1	○	○	–	–	–	○

4.4. Participants and their models

4.4.1. Participants and model names

The five modeling groups that submitted results for the Pine Tree scenario are shown in Table 4.2, together with affiliations, model names and designations used in text. The endpoints calculated by each group are shown in Table 4.3. Observed values were revealed after the submission of the second set of results.

4.4.2. Modeling approaches

The detailed approaches used in each model are described in Appendix II.3. The models and calculation conditions assumed for pathways from air to pine tree are summarized in Table 4.4 and those from air to groundwater in Table 4.5.

4.4.2.1. Modeling approaches for atmospheric dispersion

Most modelers used a Gaussian plume model to calculate atmospheric dispersion. The exception was NIRS, which applied a random walk model that has been proven to generate results essentially identical to those of the Gaussian model for steady-state conditions. Within this overall similarity in approach, there were some differences in the way individual dispersion processes were treated. All modelers except NIRS considered all four HTO sources separately. In contrast, NIRS ignored the NFRP at JNC on the assumption that it makes a minor contribution at the sampling (target) sites due to its large effective release height, its location in a sector into which the wind blows infrequently and its large distance from the target sites.

Table 4.4. Models and calculation conditions for pathways from air to pine tree*.

Model characteristic		NIRS	SRA	IFIN	LLNL	EDF
Type of dispersion model		Random walk	Sector-averaged Gaussian plume	Sector-averaged Gaussian plume	Sector-averaged Gaussian plume	Advanced Gaussian plume
Code name		Tritium-EESAD	TriSat	DISPT	CAP88-PC, DCART	ADMS3
Number of sources		3 (NFRP ignored)	4	4	4	4
Receptor size		100 m × 100 m	Sector-averaged	Sector-averaged	Sector- averaged	100 m × 100 m
Roughness length, m		–	–	–	0.01	0.5
Wind data used to estimate wind speed at stack height		JAERI:40m	JAERI:40m, JNC:70m	JAERI:40m, JNC:70m	JAERI:10m, JNC:10m	JNC 10m
Plume rise		Not calculated	Not calculated	Equation in the scenario	Equation in the scenario	ADMS3 equations
Dispersion parameter, σ_z		Pasquill-Gifford	Briggs	$ax^{0.711}$	Briggs	Based on Monin-Obukhov theory
Dry deposition velocity, m s^{-1}		0.005	0.003	Soil concentration includes $0.1C_{air}$	Dry deposition not calculated	Dry deposition not calculated
Washout coefficient, s^{-1} (J= rain intensity, mm h^{-1})		5.0E-5$J^{0.8}$	7.3E-5	1E-4 $J^{0.8}$	Variable from 7E-6 to 1.3E-4	7.3E-5
Re-emission		Considered	Considered	Considered	Not calculated	Not calculated
Soil concentration		$0.3C_{air}$	Equal to rain concentration	0.9 × rain concentration + 0.1 × air concentration	Equal to rain concentration	Not calculated
Needle TFWT concentration		$0.57C_{air}+0.43C_{soil}$	1.1 [RH × C_{air} + (1-RH) × C_{soil}]	1.1 [RH × C_{air} + (1-RH) × C_{soil}]	1.1 [RH × C_{air} + (1-RH) × C_{soil}]	Not calculated
Needle OBT	Equation	0.8 × C_{TFWT}	0.73 × C_{TFWT}	0.5 oldOBT+ 0.5 newOBT (newOBT = 0.6 × C_{TFWT})	0.7 × C_{TFWT}	Not calculated
	Photosynthesis period	Entire year	April–August	April–October	The entire year	–
	Retention period	6 months	2 years	Equilibrium	Equilibrium	–
Ring OBT		0.5 × needle OBT	1.0 × needle OBT	1.0 × needle OBT	0.57 × needle OBT	Not calculated

*Some expressions or units in this table differ from those in the model descriptions to aid in the comparison.

Table 4.5. Models and parameters for the groundwater (GW) pathway.

Model characteristic	**NIRS**	**SRA**	**IFIN**	**EDF**
Modeler Code name	K. Miyamoto ERMA	M. Saito TriSat	D. Galeriu	T. Kestens ARGUS
Input data or wet deposition area	Rain concentration at MS2	Rain concentration at MS2	From 2 km north of JRR2 to 800 m south (G4) of JRR2	Area 200 m wide by 500 m long, 300–800 m south of JRR2-3
Unsaturated soil layer Total porosity of surface soil	–	–	–	0.53
Water content, %	–	–	–	28.4
Thickness of unsaturated layer, m	15	15	–	15
Vertical water velocity, m a^{-1}	5.5	5	–	5.5
Vertical dispersivity, m	–	–	–	1
Travel time of HTO from soil surface to GW table, a	2.7	3	1	2.7
Saturated layer Thickness of water table, m	–	–	1m at 2 km N of JRR2 to 10 m at Shinkawa river	5
Number of dimensions	–	–	2 (x, z)	2 (x, y)
Hydraulic conductivity, m s^{-1}	–	–	–	6 × E-4
Longitudinal pore water velocity	–	–	30 m $month^{-1}$	0.2 m day^{-1}
Vertical pore water velocity, m $month^{-1}$	–	–	0.3	–
Longitudinal dispersivity, m	–	–	–	10
Transverse dispersivity, m	–	–	–	1
Turnover rate of aquifer, a^{-1}	0.17	–	–	–
Dilution factor	–	0.3	–	–

SRA, IFIN and LLNL used the sector-averaged form of the Gaussian plume model and calculated air concentrations averaged over the sector. On the other hand, NIRS and EDF used an averaging area of 100 m × 100 m, which was smaller than that of the Gaussian model at the downwind distances of the target sites.

NIRS and SRA did not take plume rise into account while other modelers estimated plume rise by different methods. LLNL used the momentum driven plume rise model in the dispersion code CAP88-PC, where plume rise = 1.5VD/U, where V is the stack gas exit velocity (m/s), D is the inside stack diameter (m) and U is the wind speed (m/s). The wind speed used in the models should ideally be the speed at the effective release height (physical stack height + plume rise) of the plume. Since they did not calculate plume rise, NIRS and SRA used the wind speed at the physical stack height. Using the ADMS3 code, EDF recalculated the wind speed at the emission height of each stack based on meteorological data observed 10 m above ground on the JNC meteorological tower.

The vertical dispersion parameter, σ_z, is important in predicting tritium concentrations in air at the target points. The modelers used a number of different approaches to calculating σ_z, as presented in Table 4.4.

Washout of HTO from the air to the ground by rain is an important process for determining tritium concentrations in rain, soil and groundwater. Most modelers calculated wet deposition and rain concentrations using a washout coefficient, although the value of the coefficient differed from modeler to modeler, as shown in Table 4.4. Consideration of dry deposition and re-emission of HTO from the ground surface depended on each model.

4.4.2.2. Modeling approaches for pine trees

All modelers estimated the concentration of TFWT in pine needles using an equation of the form:

$$C_{TFWT} = \gamma \{RH*C_a+(1-RH)*C_s\}, \quad (4.1)$$

where:

γ (=1.1) is an isotopic discrimination factor;
RH is the relative humidity;
C_a is the HTO concentration in air moisture; and
C_s is HTO concentration in soil moisture.

NIRS adopted a mean equivalent value for RH based on reference searches as presented in Table 4.4. Modelers calculated C_{OBT} in pine needles by multiplying C_{TFWT} by a proportionality constant of 0.6 to 0.8, which is considered an isotopic discrimination factor in the photosynthesis process. The modelers made different assumptions about the period of OBT photosynthesis, ranging from five months (from April to August) by SRA to the full year by NIRS and LLNL. NIRS assumed that the pine needle OBT concentration equaled the average value over the six months before sampling. Although new-growth needles were always collected from new-growth branches, IFIN assumed that half the needle OBT concentration was made up of old OBT produced in the previous year and translocated to the new growth.

The OBT concentrations in the annual rings of the pine tree were calculated by multiplying the needle OBT concentrations by values ranging from 1.0 (no isotopic discrimination) to about 0.5. LLNL and NIRS applied values of 0.57 and 0.50, respectively, which are assumed

to be isotopic discrimination factors in a metabolic translocation process of OBT from pine needles to the woody parts of the annual rings [23].

4.4.2.3. Modeling approaches for groundwater

Four models participated in the prediction of HTO concentration in groundwater. The models and parameter values for the pathway from soil surface to groundwater are presented in Table 4.5. The models fall into two categories. The first is a compartment model, where wet deposited HTO infiltrates the unsaturated soil layer and, after a certain travel time, reaches the saturated layer of the groundwater aquifer where instant mixing is assumed. NIRS and SRA adopted this simple approach, which requires few parameters. They assumed that the tritium concentration in groundwater at G4 equaled the monthly-average concentration in rain deposited on the soil surface at MS2, with a travel time of about 2.7–3 years to reach the water table after wet deposition. Another parameter required by NIRS is the turnover rate ($0.17\ a^{-1}$) of water in the groundwater aquifer. SRA used a factor of 0.3 as a dilution factor for tritium in the pathway from soil surface to groundwater.

The second category of groundwater model, as adopted by IFIN and EDF, was relatively more complex and required many parameters to run. EDF fully utilized the information given in the scenario description regarding the geological formation and the groundwater flow, with the assumption that the model area was limited to a region 500 m long by 200 m wide starting 300 m southwest of JRR2 and JRR3. Only tritium deposited in this limited area by precipitation affected the tritium concentration in the groundwater at G4. EDF needed many parameter values to solve their dispersion model as listed in Table 4.5. On the other hand, IFIN assumed a different groundwater scenario in which the aquifer started 2 km north of JRR2 and flowed south through G4. In this case, wet-deposited tritium from a wide area affected the tritium concentration in groundwater at G4.

4.5. Comparison of predictions with observations

Before model performance was evaluated, the internal consistency of predictions and observations was examined and discussed.

4.5.1. Internal consistency between predictions of each model

The means of predicted to predicted (P_x/P_{air}) ratios of the yearly mean tritium concentration (P_x) for each endpoint (x) to that for air moisture were compared between models. The endpoints considered were rain, pine needle TFWT, pine needle OBT and ring OBT.

When the air concentration varies with time, the predicted concentration in each endpoint is expected to vary with time in a similar fashion, but the pattern and concentration levels may differ from those of air depending on factors in the tritium transport process such as isotopic dilution, the rate at which equilibrium is achieved, isotopic discrimination and time delays between adjacent compartments. The P_x/P_{air} ratio and the factors that influence it for each endpoint are listed in Table 4.6.

Even if elevated OBT concentrations are produced after an incidental release of tritium, the effect of isotopic discrimination and isotopic dilution by less contaminated OBT produced thereafter means that the P_{OBT}/P_{air} ratio rarely exceeds unity. Similarly, the large isotopic dilution that occurs as the HTO plume moves into the groundwater (GW) aquifer suggests that the P_{GW}/P_{air} ratio rarely exceeds unity even if the concentrations in rain are elevated. In all cases where the P_x/P_{air} ratio is above unity, the mechanisms should be clarified.

Table 4.6. Expected predicted to predicted (P_x/P_{air}) ratio of tritium concentrations in the scenario endpoints (x) and the concentration in air moisture in dynamic conditions.

Endpoint (x)	Influence factors* for P_x/P_{air} ratio	Expected P_x/P_{air} ratio
Rain	Isotopic exchange rate with air HTO in the plume	< 1 (≥ 1)**
Plant TFWT	Rapid isotopic equilibrium with air HTO; contribution of soil HTO	< 1
Plant OBT	Isotopic discrimination, translocation of OBT, different photosynthesis rates between day and night	< 1, (≥ 1)**
Groundwater	Time delay from air HTO	< 1, (≥ 1)**

* Large isotopic dilution by less contaminated water pools always occurs.
** The ratio may be above unity for short times under dynamic conditions.

Table 4.7. The means of predicted to predicted (P_x/P_{air}) ratios of yearly mean tritium concentration in each endpoint (x) to that in air at P3 averaged over 1982–1986.

Modeller	Rain to air		Needle TFWT to air		Needle OBT to air	
	Mean ratio*	SD	Mean ratio*	SD	Mean ratio*	SD
NIRS	0.27‡	0.06	0.76	0.08	0.77	0.17
SRA	1.22	0.22	1.00	0.04	1.14	0.69
LLNL	0.60	0.14	0.97	0.01	0.73	0.01
IFIN	0.55	0.14	0.97	0.03	0.50	0.04
EDF	5.62	3.66	np**	np**	np**	np**

* The mean P_x/P_{air} ratios and the standard deviations for 1982–1986 were calculated from the mean ratios for each year.
‡ Annual means calculated from monthly data.
** Not predicted.

Table 4.8. The means of predicted to predicted (P_x/P_{air}) ratios of yearly mean tritium concentration in each endpoint (x) to that in air at MS2 averaged over 1984–1987.

Modeller	Rain to air		Needle TFWT to air		Needle OBT to air		Ring OBT to air	
	Mean ratio*	SD	Mean ratio*	SD	Mean ratio*	SD	Mean ratio*	SD
NIRS	0.22	0.03	0.70	0.04	0.58	0.05	0.37	0.03
SRA	1.63	0.58	1.22	0.12	0.76	0.24	0.66	0.18
LLNL	0.69	0.27	0.98	0.02	0.73	0.02	0.42	0.01
IFIN	0.50	0.05	0.98	0.03	0.50	0.07	0.51	0.10
EDF	3.83	0.94	np**	np**	np**	np**	np**	np**

* The mean P_x/P_{air} ratio and the standard deviations for 1984–1987 were calculated from the mean ratios for each year.
** Not predicted.

Table 4.9. Observed to observed ratios (O_x/O_{air}) of tritium concentration in each endpoint (x) at P3 to that of air at MP7.

Endpoint	Ratio, 1984	Ratio, 1985	Ratio, 1986	Mean ratio	SD*
Rain	0.36	0.38	0.27	0.34	0.06
TFWT	1.88	4.20	0.71	2.26	1.78
Needle OBT	1.09	1.35	nd**	1.22	0.18

* Standard deviation of the mean from 1984 to 1986.
** No data.

Table 4.10. Observed to observed ratios (O_x/O_{air}) of tritium concentration in each endpoint (x) at MS2 to that of air at MP7.

Endpoint	Ratio, 1984	Ratio, 1985	Ratio, 1986	Ratio, 1987	Mean ratio	SD*
Rain	0.43	0.43	0.13	0.18	0.29	0.16
TFWT	1.62	4.00	0.63	1.03	1.82	1.51
Needle OBT	0.68	1.05	0.38	1.08	0.80	0.33
Ring OBT	0.43	0.37	0.13	0.17	0.28	0.15

* Standard deviation of the mean from 1984 to 1987.

Table 4.11. The means of observed to observed (O_{OBT}/O_{TFWT}) ratios of needle OBT to needle TFWT concentrations at P3 and MS2.

Averaging time and location	OBT/TFWT Ratio	SD
Mean ratio for 1984 and 1985 at P3	0.54	0.43
Mean ratio for 1984 and 1987 at MS2	0.44	0.41

Table 4.12. Means of predicted to observed (P_x/O_x) ratios of tritium concentration for each endpoint (x) at P3 for 1982 to 1986.

Modeller	Air, 1984–1986		Rain, 1982–1986		TFWT, 1982–1986		Needle OBT, 1982–1986	
	Ratio	SD	Ratio	SD	Ratio	SD	Ratio	SD
NIRS	0.92	0.21	0.86	0.27	0.92	0.73	0.74	0.36
SRA	0.46	0.13	2.00	0.76	0.63	0.55	0.52	0.14
LLNL	0.32	0.14	0.58	0.15	0.35	0.24	0.21	0.07
IFIN	0.42	0.13	0.82	0.43	0.53	0.41	0.21	0.08
EDF	0.21	0.07	3.71	1.21	np*	np*	np*	np*

* Not predicted.

Table 4.13. Means of predicted to observed (P_x/O_x) ratios of tritium concentration for each endpoint (x) at MS2 for 1984–1987.

Modeller	Air		Rain		TFWT		Needle OBT		Ring OBT	
	Ratio	SD	Ratio	SD	Ratio	SD	Ratio	SD	Ratio	SD
NIRS	0.74	0.18	0.66	0.30	0.39	0.19	0.61	0.23	1.15	0.46
SRA	0.38	0.17	2.31	1.07	0.34	0.19	0.35	0.06	1.08	0.67
LLNL	0.23	0.08	0.60	0.26	0.18	0.10	0.24	0.09	0.44	0.21
IFIN	0.37	0.13	0.76	0.39	0.27	0.14	0.24	0.06	0.86	0.51
EDF	0.18	0.06	2.72	1.40	np*	np*	np*	np*	np*	np*

* Not predicted.

The mean P_x/P_{air} ratios for each endpoint for each model are presented in Tables 4.7 and 4.8 for sampling sites P3 and MS2, respectively. Also shown are the standard deviations (SD) in the ratios, which indicate the variation in the mean ratio from year to year. The SDs were used here to judge if the mean P_x/P_{air} ratio is less than or greater than unity when uncertainties are taken into account. The ratios for each endpoint at P3 and MS2 showed similar values or tendencies among the models. When the SDs are taken into account, the P_{rain}/P_{air} and P_{TFWT}/P_{air} ratios predicted by NIRS, LLNL and IFIN are below unity and are considered to be reasonable. On the other hand, some of the ratios predicted by SRA and EDF are above unity when the SDs are taken into account. These are considered to be questionable and may need clarification.

4.5.2. Internal consistency between observations

The observed to observed (O_x/O_{air}) ratios of tritium concentration for each endpoint (rain, pine needle TFWT, pine needle OBT and ring OBT) to the concentration in air moisture are presented in Tables 4.9 and 4.10 for sampling sites P3 and MS2, respectively. The O_x/O_{air} ratios can be greater than unity in dynamic conditions but such values should be confirmed and the responsible mechanism clarified.

When discussing the O_x/O_{air} ratios, we must take into account the timing of the exposure of the samples to the air and the different OBT photosynthesis rates between daytime and night time. Since the air moisture was continuously collected for whole days, including daytime and night time, and the rain was accumulated monthly, the timing of the exposure is not an issue for the O_{rain}/O_{air} ratio. The mean O_{rain}/O_{air} ratios presented in Tables 4.9 and 4.10 are around 0.3, which is consistent with other measured values.

There are a number of reasons for O_{TFWT}/O_{air} and O_{OBT}/O_{air} ratios above unity. Firstly, O_{TFWT} reflects the daytime air concentration while O_{air} reflects the 24 hour air concentration. The pine needles were always collected around noontime and thus their TFWT and OBT concentrations were directly influenced by the daytime air and not the 24 hour air. Analyses of wind direction frequency data at JAERI for daytime (6hr–18hr) and nighttime (18–6hr) for four seasons from 1981 to 1987 showed that i) during both the day and night, winds from the NE were dominant in spring and summer, and winds from the NW were dominant in autumn and winter, and ii) the frequency of occurrence of winds from the NE and adjacent directions (onshore windw) increased a little during the day even in autumn and winter, and the frequency of winds from the NW and adjacent directions (offshore winds) increased a little at night even in spring and summer. Thus the probability that the pine needles were exposed to onshore winds (which brings contaminated air from the three tritium sources at JAERI over sampling points P3, MS2 and MP7) is higher during the day than at night throughout the year. Consequently, the daytime air concentration tends to be higher than that of the 24 hour air and the O_{TFWT}/O_{air} and O_{OBT}/O_{air} ratios tend to be higher than unity (called the “downwind effect” hereafter).

Secondly, the air over the sea is stable during the day due to cooling by sea water. When this air blows onshore, it becomes unstable due to warming by the land surface. The thickness of the unstable layer, which is called the internal boundary layer, increases with distance from the coast. When tritium is released into this internal boundary layer, upward dispersion is limited because the stable sea air caps any further vertical transport. The tritium is constrained to disperse within the internal boundary layer, which causes an elevation of the surface air concentration (called the “trapping effect” hereafter). As a result, the daytime O_{TFWT} value often tends to be higher than the nighttime value, in which case the observed O_{TFWT}/O_{air} ratio

can be above unity (a maximum value of 4.2 was observed at P3 in 1985), as shown in Tables 4.9 and 4.10. The trapping effect is not an issue for the NFRP in JNC because of its large effective stack height.

Thirdly, during the day, the pine needles are biologically active and produce a large amount of OBT, whose concentration tends to be high due to exposure to the elevated air concentrations in effect during the day. However, at night, the pine needles are biologically less active and produce lesser amounts of OBT, whose concentration tends to be low due to exposure to air that blows mostly offshore and is essentially uncontaminated. As a result, the observed OBT concentration (O_{OBT}) at daytime tends to be higher than that of the 24 hour air concentration, and thus the O_{OBT}/O_{air} ratios tend to be higher than the P_{OBT}/P_{air} ratios, which are calculated for the whole day (called the photosynthesis rate effect hereafter). Thus the O_{OBT}/O_{air} ratios that sometimes lie above unity (a maximum of 1.35 was observed at P3 in 1985; Tables 4.9 and 4.10) are considered reasonable.

The means of observed to observed ratios of needle OBT to needle TFWT concentrations at P3 and MS2 (O_{OBT}/O_{TFWT}) have almost the same values (0.54 and 0.44, respectively; Table 4.11). The isotopic discrimination factor D_p in the formation of OBT from TFWT in controlled conditions ranges from 0.54 for barley to 0.83 for maize, with a mean of 0.70 ±0.12 [24]. This suggests that the value of 0.5 for the O_{OBT}/O_{TFWT} ratio in pine needles (which was obtained in dynamic conditions in the field) can be attributed primarily to isotopic discrimination. Given these interpretations, all the observations are believed to be internally consistent for dynamic conditions, and can be used with confidence for the discussion of the P/O ratios in the following sections.

4.5.3. Predictions and observations of tritium concentrations in air moisture

Predicted monthly variations of tritium concentrations in air moisture at P3 are shown in Figure 4.3, together with the observed concentrations at MP7. All the predictions vary almost coincidently with each other and with the observations over the entire study period, but the predictions for P3 generally underestimate the observations at MP7 from 1984 to 1986. Predicted yearly variations of tritium concentrations in air moisture at MS2 are compared with each other and with the observations at MP7 in Figure.4.4. They also vary in parallel with each other and the predictions underestimate the observations.

The means of predicted to observed ratios (P_x/O_x) for each endpoint (x) were calculated from the yearly values for each year of the study, and are presented in Tables 4.12 and 4.13 for sampling sites P3 and MS2, respectively. The means of P_{air}/O_{air} at P3 from 1984 to 1986 ranged from 0.92±0.21 for NIRS to 0.21±0.07 for EDF. The means of P_{air}/O_{air} at MS2 for 1984–1987 ranged from 0.74±0.18 for NIRS to 0.18±0.06 for EDF. The order of mean P_{air}/O_{air} ratios was NIRS > SRA> IFIN> LLNL> EDF for P3 and MS2. The concentrations predicted for MS2 were about 80% of the values predicted for P3.

Taking account of the standard deviation of the mean of the P_{air}/O_{air} ratios, and an estimated error of 30% to 80% when the observed air concentration at MP7 is assumed to apply at P3 and MS2, the NIRS model performed very well at both sampling sites. This agreement may be fortuitous and due in part to compensatory errors, since the NIRS model ignores plume rise (which could result in an overestimate of the concentrations) and trapping (which could result in an underestimate).

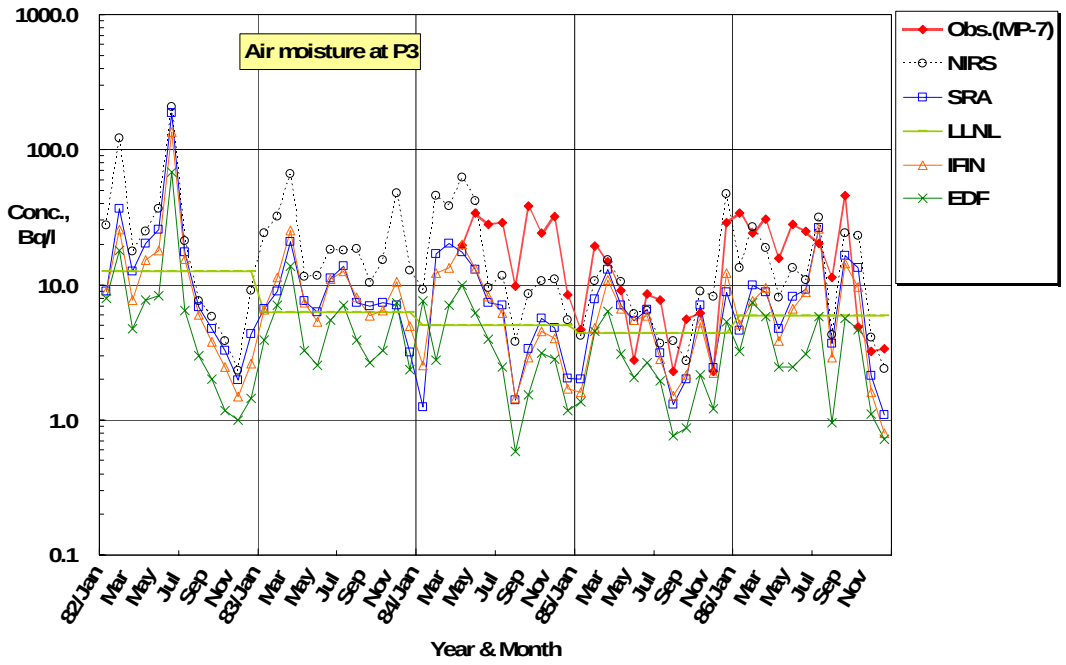

Fig. 4.3. Predicted and observed monthly variations of tritium concentration in air moisture at P3 from 1982 to 1986.

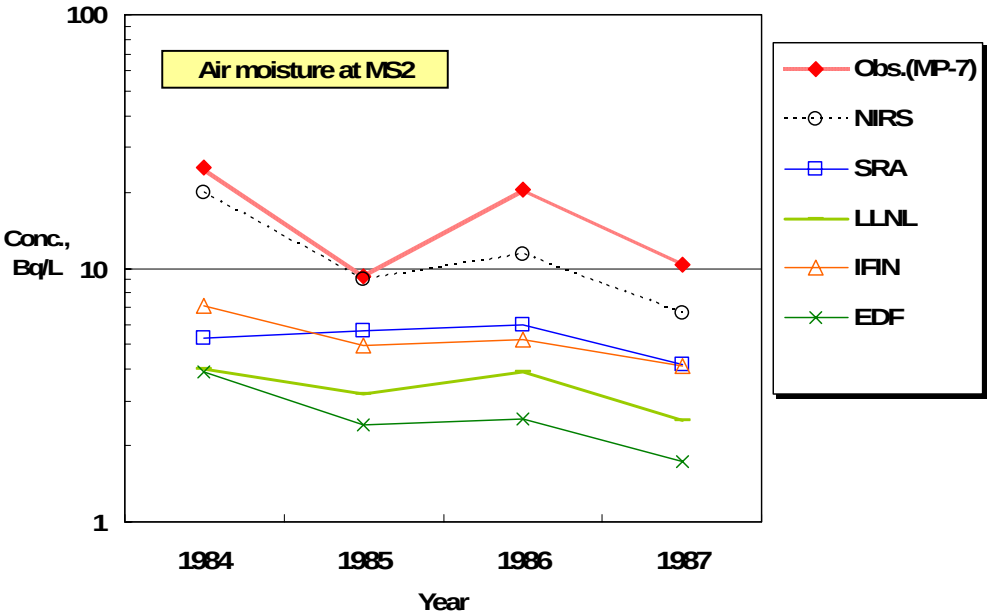

Fig. 4.4. Predicted and observed yearly variations of tritium concentration in air moisture at MS2 from 1984 to 1987.

The other models underestimated the air moisture concentrations at P3 and MS2 by factors of 2 to 5, as shown in Tables 4.12 and 4.13. The reasons for this can be attributed to the parameter values in the atmospheric dispersion equations, as listed in Table 4.4. The relevant parameters are the wind speed at the effective stack height and the vertical dispersion parameter σ_z. The wind speed is normally estimated by extrapolating the wind data observed at different heights to the effective stack height using a power law function. However, data from the 10 m, 20 m and 40 m levels on the JAERI meteorological tower indicate a linear relationship between wind speed and height. Thus models with a power law function will estimate wind speeds that are too high and air HTO concentrations that are too low. In the EDF model, the wind speed at the effective stack height was estimated by extrapolating the speed observed 10 m above ground at JNC, rather than the speed at the greatest measurement height, viz. 40 m on the JAERI meteorological tower. This will probably amplify the errors in the power function extrapolation and may help to explain the low predictions of the EDF model.

The various modelers calculated the vertical dispersion parameter σ_z in different ways and obtained very different results in some cases. For example, the SRA and NIRS models gave smaller σ_z values than IFIN by a factor of 2–5, depending on the stability class and the distance from source to receptor. The prediction of higher air HTO concentrations by NIRS compared to IFIN may be attributed partly to the use of lower σ_z values.

Other causes for the underestimation may be the following:

— Ignoring differences in elevation between the base of the stacks and the target points. P3 and MS2 are located about 20 m and 35 m above sea level, respectively, whereas the three tritium sources at JAERI are located between about 10 m and 15 m above sea level. In ignoring these differences, the models will under-predict the air HTO concentrations because they overestimate the height of the plume as it passes over the target points.

— Ignoring trapping in coastal areas. A simulation of pollutant dispersal under typical conditions in coastal Japan has shown that when a continuous source with an effective stack height of 52.5 m is located at the coastline, the air concentration is largest 700–800 m from the source [25]. Similar conditions may have sometimes happened at Tokaimura, leading to large concentrations at the target points P3 and MS2, but were not simulated by the models.

4.5.4. Predictions and observations of tritium concentrations in rain

Predicted and observed monthly tritium concentrations in rain from 1982 to 1986 at P3 and yearly concentrations at MS2 from 1984 to 1987 are shown in Figures 4.5 and 4.6, respectively. At both sites, the predictions scatter around the observations. The predictions of most models for P3 track each other well, including the sharp peak in June 1982 when an incidental HTO release occurred from JRR3. The EDF predictions stand apart due to their higher level and some sharp peaks in the middle of 1984.

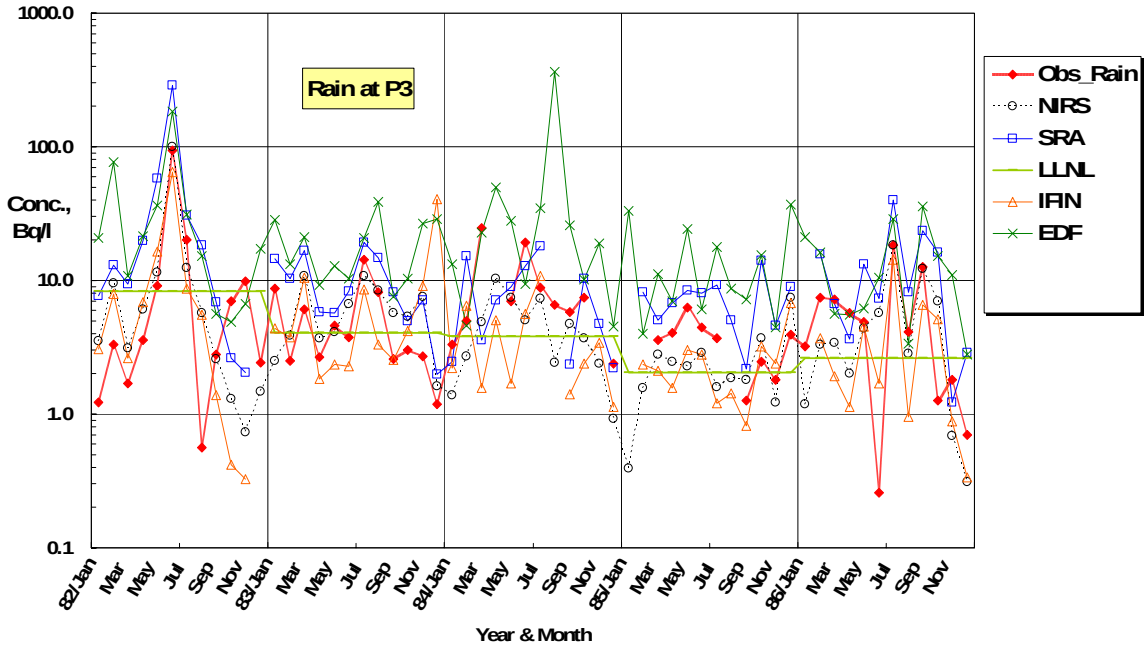

Fig. 4.5. Predicted and observed monthly tritium concentrations in rain at P3 from 1982 to 1986.

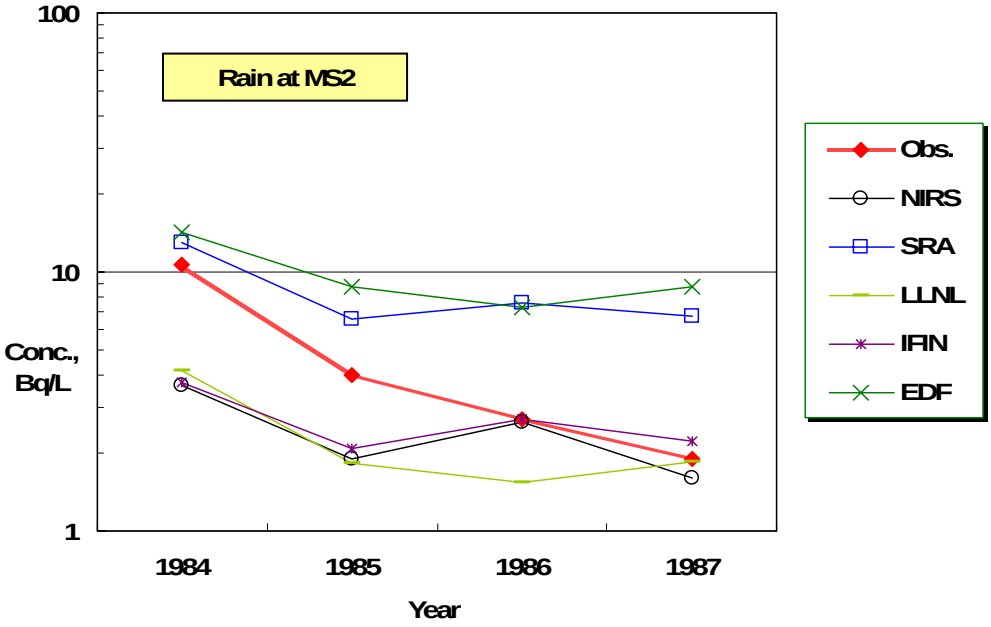

Fig. 4.6. Predicted and observed yearly tritium concentrations in rain at MS2 from 1984 to 1987.

The means of yearly P_{rain}/O_{rain} ratios at P3 from 1982 to 1986 and those at MS2 from 1984 to 1987 are shown in Tables 4.12 and 4.13, respectively. The models divide into two groups depending on whether the ratio is above or below unity. P_{rain}/O_{rain} ratios above unity are predicted by EDF and SRA, the models for which the P_{rain}/P_{air} ratios are also above unity. P_{rain}/O_{rain} ratios below unity are predicted by IFIN, NIRS and LLNL, the models that also predict P_{rain}/P_{air} ratios below unity. This systematic difference may be caused by the models and washout coefficients used to calculate concentrations in rain. The P_{rain}/O_{rain} ratios of 3.71 and 2.72 predicted by EDF are difficult to accept given that the P_{rain}/P_{air} ratios for this model are 5.62 and 3.83, more than 10 times higher than the mean O_{rain}/O_{air} ratios of 0.34 and 0.29. The P_{rain}/O_{rain} ratios of NIRS, IFIN and LLNL lie in the range 0.58 to 0.86, which agrees with the O_{rain}/O_{air} ratios within a factor of two to three and thus are more acceptable.

4.5.5. Predictions and observations of TFWT concentrations in pine needles

The predicted and observed monthly and yearly TFWT concentrations in pine needles at P3 and MS2 are shown in Figures 4.7 and 4.8, respectively. The means of predicted to observed ratios (P_{TFWT}/O_{TFWT}) are listed in Tables 4.12 and 4.13. Since all models calculated the TFWT concentration using an equation similar to Equation (4.1), the predicted monthly patterns of TFWT concentrations at P3 and MS2 are similar to those of the air HTO concentrations (Figures 4.3 and 4.4).

The mean observed TFWT concentrations were higher than the predictions both at P3 and MS2. Individual models underestimated the observations at P3 by up to a factor of 3 and at MS2 by up to a factor of 5. Since these factors are almost the same as the P/O ratios for air, the underestimate of the TFWT concentrations appears to be due primarily to the underprediction of the air concentrations.

The observed TFWT concentrations were higher than the predictions at both P3 (Figure 4.7) and MS2 (Figure 4.8) in 1984 and 1985, the years in which the observed mean O_{TFWT}/O_{air} ratios were much greater than 1 (Tables 4.9 and 4.10). Due to a combination of the downwind effect and the trapping effect associated with onshore winds during the day, which lead to high O_{TFWT}/O_{air} ratios (Section 4.5.2), the observed TFWT concentrations in pine needles collected near noontime tend to be higher than the predicted concentrations, which were calculated on a 24 hour basis.

4.5.6. Predictions and observations of OBT concentrations in pine needles

Predicted and observed monthly OBT concentrations at P3 from 1982 to 1986 and yearly concentrations at MS2 from 1984 to 1987 are shown in Figures 4.9 and 4.10, respectively. The mean predicted to observed (P_{OBT}/O_{OBT}) ratios of yearly average OBT concentration at P3 and MS2 are presented in Tables 4.12 and 4.13, respectively. All of the models underpredicted the observed OBT concentrations by up to a factor of 5; the magnitude of the underprediction was similar at P3 and MS2. All models calculated the OBT concentration at a given time by multiplying the TFWT concentration by an isotopic discrimination factor between 0.6 and 0.8 (Table 4.4). One model assumed that the concentration in the new growth was made up partly of OBT produced in the current year and partly of OBT formed in the previous year and translocated to the new growth.

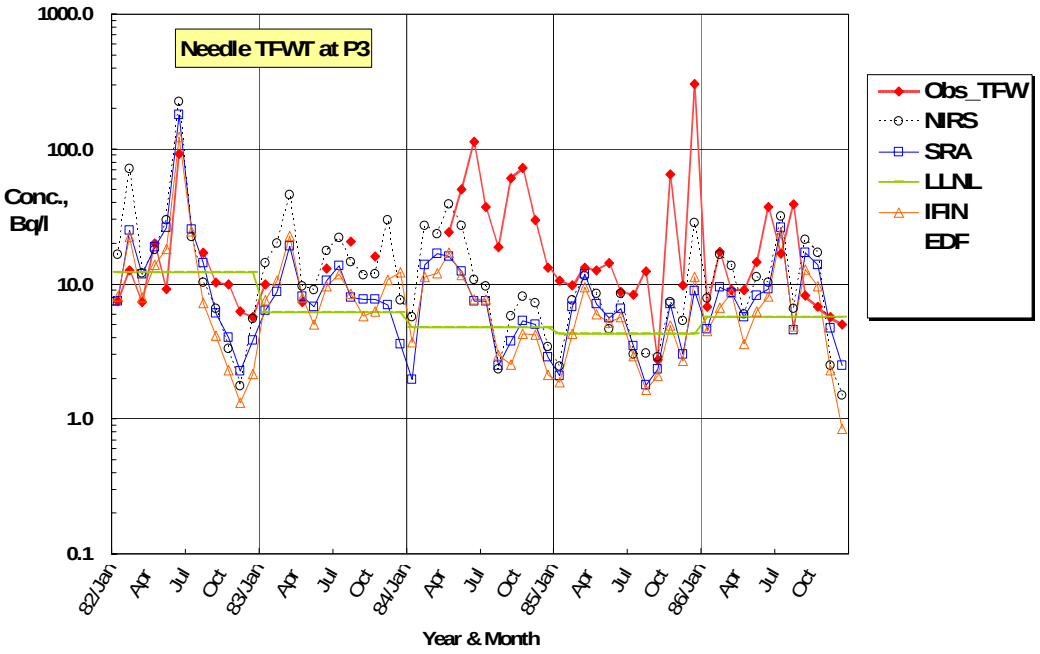

Fig. 4.7. Predicted and observed monthly tritium concentrations (Bq/l) in pine needle at sampling point P3 from 1982 to 1986.

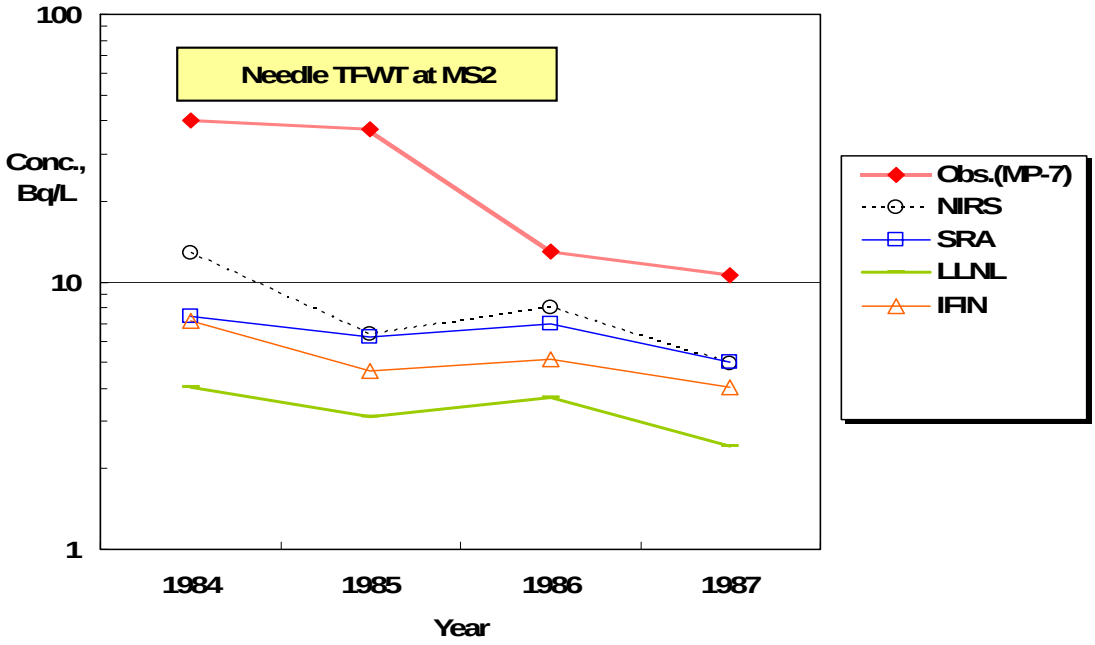

Fig. 4.8. Predicted and observed yearly tritium concentrations in pine needles at sampling point MS2 from 1984 to 1987.

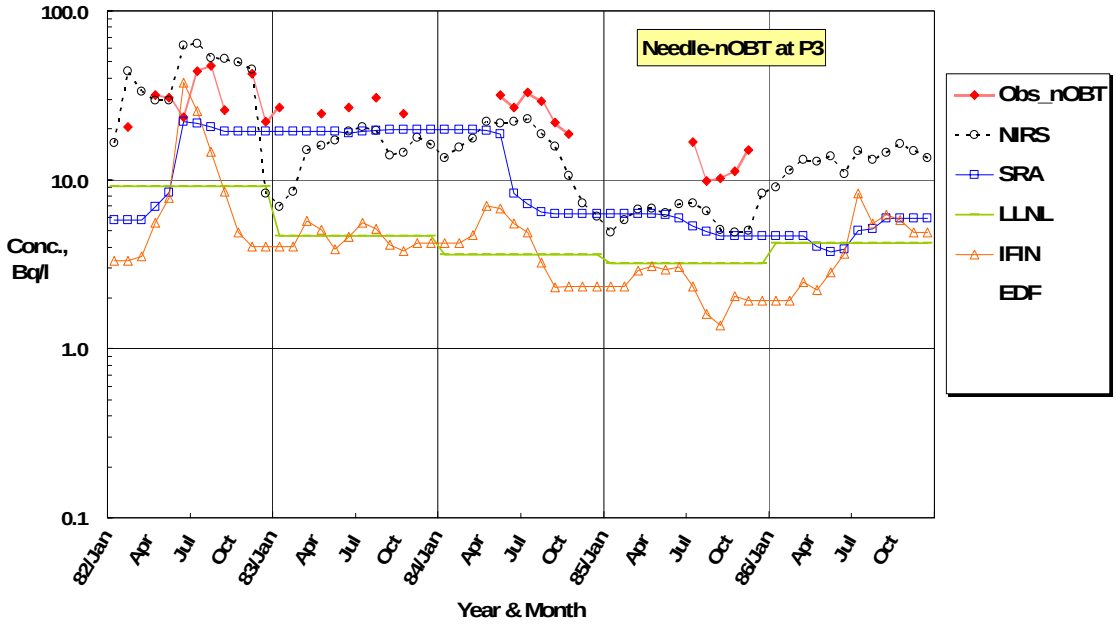

Fig. 4.9. Predicted and observed monthly OBT concentrations (Bq/l) in pine needles at P3 from 1982 to 1986.

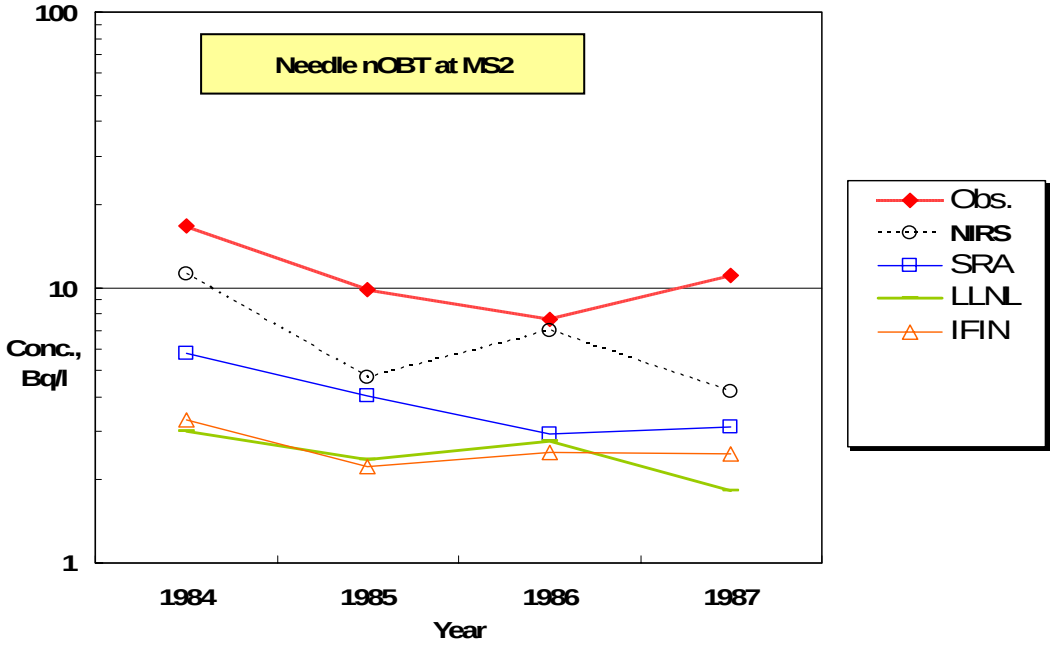

Fig. 4.10. Predicted and observed yearly OBT concentrations (Bq/l) in pine needles at MS2 from 1984 to 1987.

The NIRS and SRA predictions of OBT were almost always several times higher than those of IFIN and LLNL (Figure 4.9) whereas all predictions of TFWT concentrations were about the same (Figure 4.7). This result may have derived from the different assumptions made in the models regarding the photosynthesis period for OBT production, and the retention and translocation in pine trees, particularly as these relate to the high tritium concentration in air in June 1982. NIRS made the conservative assumptions that OBT is photosynthesized at the same rate throughout the year and that the OBT concentration at the time of sampling is an average over the 6 months before sampling. This resulted in predicted OBT concentrations of up to several tens of Bq/L in the second half of 1982, due to predicted TFWT concentrations that reached as high as about 200 Bq/L in June 1982.

The IFIN model was the only model that took account of the specific plant physiology of an evergreen conifer. The model estimated the average net photosynthetic rate from temperature and solar radiation intensity, which resulted in an OBT production period from April to October. In addition, the model assumed a low retention rate of newly photosynthesized OBT in leaves and a large translocation rate to roots and trunk. As a consequence, it assumed that the monthly average OBT concentration in needles during the summer consisted of equal parts old and new OBT, where the new OBT depended on the TFWT concentration. For example, the OBT concentration in needles in August was calculated as $OBT_{Aug} = 0.5 \times OBT_{py} + 0.5 \times 0.6 \times TFWT_{cy.}$, where OBT_{py} is the OBT concentration in the previous year, $TFWT_{cy}$ is the HTO concentration in needles in the current year (averaged over the previous few months), and 0.6 is the isotopic discrimination factor. The assumptions of a low contribution of new OBT and a rapid turnover of old OBT, together with predictions of low TFWT concentrations, may have resulted in OBT predictions by IFIN that were lower and changed more rapidly than those of NIRS or SRA.

The SRA model assumed that OBT was produced over the period from April to August and retained for two years. Although SRA and IFIN predicted similar time variations of TFWT concentrations, the long retention time adopted by SRA resulted in high OBT concentrations from June 1982 through May 1984, due to the influence of high air and TFWT concentrations in June 1982.

The LLNL model assumed that the OBT concentration was the TFWT concentration multiplied by an isotope discrimination factor of 0.7, without any assumptions concerning photosynthesis periods, retention or translocation of OBT. Thus its predicted yearly average OBT concentrations were simply 0.7 times the TFWT concentrations.

4.5.7. Predictions and observations of OBT concentrations in tree rings

Predicted and observed OBT concentrations in the annual rings of the pine tree collected at MS2 are shown in Figure 4.11, together with the observed needle OBT concentration at MS2 for comparison. Since SRA and IFIN assumed no isotopic discrimination between needles and rings, the ring OBT concentrations predicted by these models were almost the same as the needle concentrations. Since NIRS and LLNL assumed an isotopic discrimination factor of 0.5 and 0.57 respectively, the OBT concentrations in rings predicted by NIRS and LLNL were about half the OBT concentrations in the needles.

As seen in Figure 4.11, the ring OBT concentrations of each model agree fairly well with each other except for 1984, when the observed TFWT concentration was irregularly high. The predicted to observed ($P_{ringOBT}/O_{ringOBT}$) ratios for ring OBT concentrations averaged over the period 1984–1987 were 1.15 for NIRS, 1.08 for SRA, 0.44 for LLNL and 0.86 for IFIN. All of the models predicted the observed ring OBT concentration to within a factor of about 2.

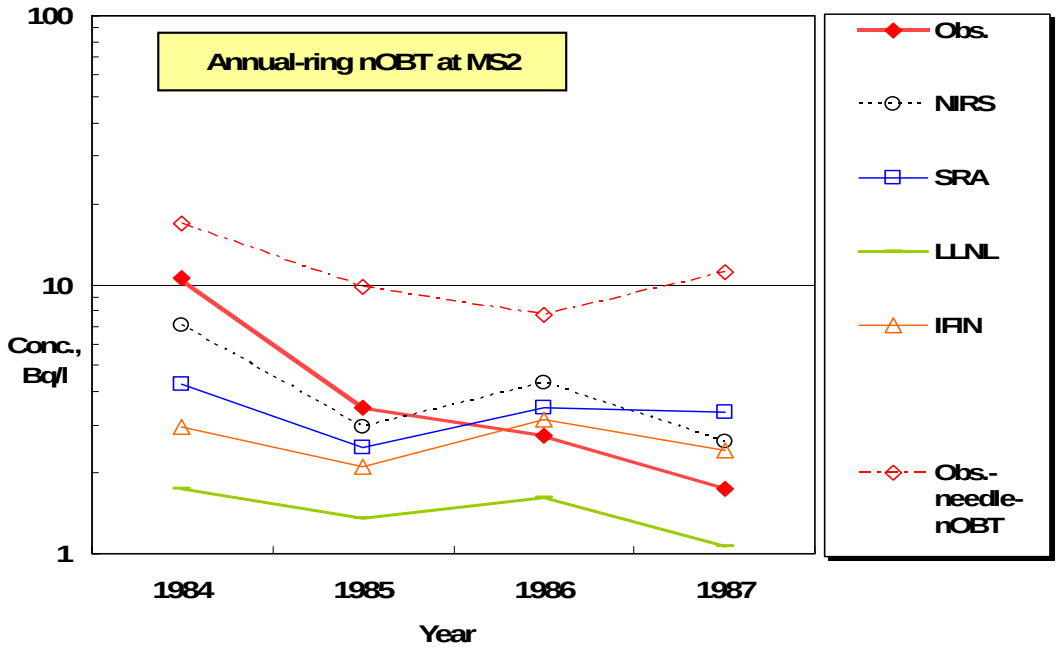

Fig. 4.11. Observed and predicted yearly OBT concentrations in tree rings at MS2 from 1984 to 1987. Needle OBT concentrations observed at MS2 are also plotted for comparison.

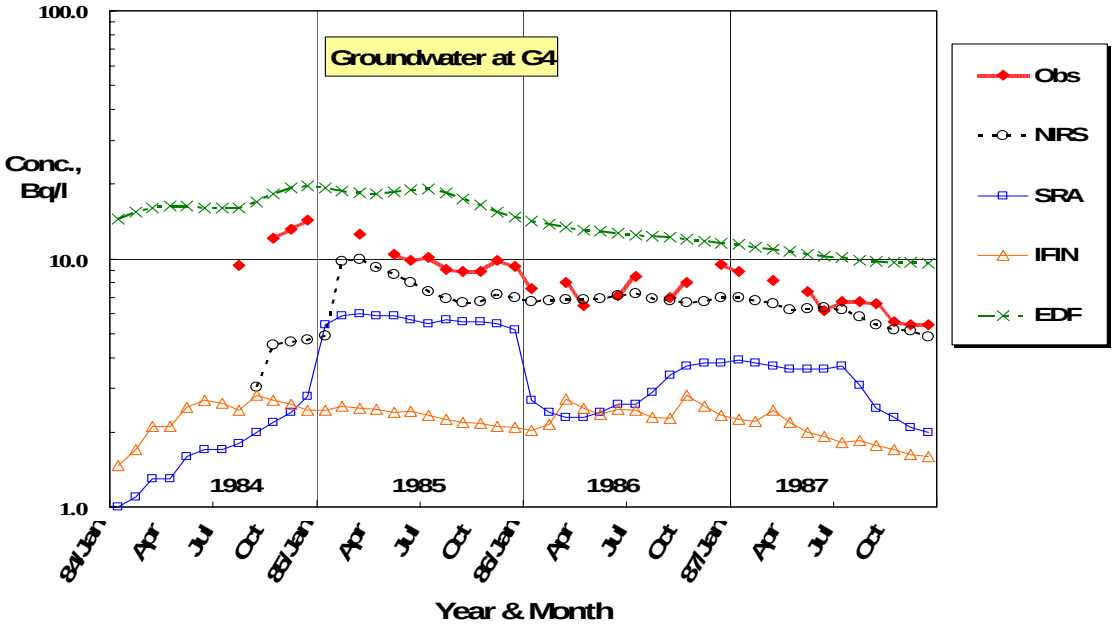

Fig. 4.12. Predicted and observed monthly tritium concentrations in groundwater at G4.

Table 4.14. Predicted to observed (P_{GW}/O_{GW}) ratios of yearly mean tritium concentration in groundwater at G4 from 1984 to 1987 and the means of 1985 to 1987.

Modeller	1984		1985		1986		1987		1985–1987	
	Ratio	SD	Ratio	SD	Ratio	SD	Ratio	SD	Mean	SD
NIRS	0.34	0.09	0.78	0.17	0.89	0.11	0.89	0.19	0.85	0.06
SRA	0.14	0.05	0.57	0.07	0.37	0.09	0.47	0.14	0.47	0.10
IFIN	0.19	0.05	0.24	0.03	0.31	0.05	0.29	0.07	0.28	0.04
EDF	1.37	0.27	1.80	0.26	1.63	0.22	1.53	0.28	1.65	0.14

It is worth noting that the data for 1984, 1985 and 1986 (but not 1987) show a yearly mean concentration ratio of ring OBT to needle OBT of about 0.5. This value is interpreted as an isotopic discrimination factor arising during translocation of needle OBT to ring OBT.

4.5.8. Predictions and observations of tritium concentrations in groundwater

The predicted and observed monthly tritium concentrations in groundwater at G4 from 1984 to 1987 are shown in Figure 4.12. The yearly means of predicted to observed ratios of the groundwater concentrations are presented in Table 4.14.

The means of the P_{GW}/O_{GW} ratios for each model (the last two columns of Table 4.14) were based on the three years of data from 1985 to 1987, excluding the 1984 data, when most of the predicted concentrations were changing rapidly. Given that the tritium discharge rates and meteorological data were specified starting only in 1981, and that a delay time of about 3 years was assumed for wet-deposited tritium to reach the groundwater aquifer, the predicted time variation in 1984 varied strongly depending on the initial 1981 conditions assumed by the modelers. The peak concentration predicted by all models except that of IFIN occurred at the beginning or middle of 1985 as shown in Figure 4.12, which corresponds most probably to the high release from JRR3 in June 1982.

The mean P_{GW}/O_{GW} ratios for 1985−1987 indicate that EDF overestimated the observed concentration by a factor of 1.65, and NIRS, SRA and IFIN underestimated by factors of 0.85, 0.47 and 0.28, respectively. In other words, all models predicted the observed groundwater concentration within a factor of about 3 except for 1984.

The EDF results, which were obtained with the groundwater dispersion model ARGUS, overestimated the observations by an average of 65%. EDF demonstrated through additional calculations that this overestimate could be reduced by 30% by assuming an aquifer thickness of 7 m rather than 5 m. Part of the overprediction was also ascribed to the fact that EDF overestimated the observed rain concentration by a factor of 2.7 at MS2 (Table 4.13). As a conclusion, the sophisticated ARGUS model proved to be precise enough to predict the time variation of groundwater concentration as long as the input rain concentrations were predicted correctly. The good performance of the model was judged to be due to an appropriate assumption of a limited area of wet deposition and a suitable selection of parameter values based on the relatively detailed information on geological structure, infiltration rate, soil layer depth and groundwater flow rate given in the scenario description.

IFIN also applied a dispersion model to the groundwater calculations, but predicted concentrations that were consistently lower than those of any other model, as shown in Figure 4.12. This was due in part to an underestimate of the rain concentration at MS2, and in part to the assumption of a wide wet deposition area starting 2 km north of JRR2 to the Shinkawa river through G4, which resulted in excessive dilution of tritium by the southward movement of less contaminated groundwater.

NIRS and SRA used so-called piston models in their calculations. Wet-deposited tritium at MS2 was assumed to infiltrate the soil compartment, enter the groundwater aquifer and run off to the Shinkawa river with instant mixing and no dispersion in any compartment. Only a few parameters were required for their calculations, as listed in Table 4.5. The mean monthly groundwater concentrations predicted by NIRS were only 15% lower than the observations (Table 4.14). The success of this simple model may be due to the small, shallow nature of the groundwater system, with rapid mixing in an aquifer of limited area, in addition to the use of appropriate parameter values based on expertise accumulated by NIRS staff in the area concerned.

The mean monthly groundwater concentration predicted by SRA was about a factor of two lower than the observations in spite of the fact that the rain concentrations were overestimated by more than a factor of 2. If the dilution factor used in the model were increased from 0.3 to 0.6 (Table 4.5), the predicted groundwater concentrations would become closer to the observations, although the basis for selecting the value of the dilution factor is not clear.

4.5.9. 95% confidence intervals

Only LLNL carried out a rigorous uncertainty analysis and reported 95% confidence intervals for all scenario endpoints. IFIN reported 95% confidence intervals based on expert judgment without statistical analysis: a factor 3 for air moisture and a factor 5 for needle OBT and ring OBT. No factors were given for needle TFWT predictions, for which the uncertainty was expected to be large due to the fact that the measured value came from a single batch sample in a month. Other modelers did not report any uncertainties. In this situation, no conclusions can be drawn regarding the overall uncertainties for any of the endpoints in the scenario.

4.6. Summary and conclusions

The Pine Tree scenario requested modelers to predict time-dependent monthly or yearly tritium concentrations in a variety of endpoints including air moisture, rain, TFWT and OBT in pine needles, OBT in annual tree rings and HTO in groundwater in the vicinity of multiple tritium sources located along the Pacific coast in Tokaimura, Japan. Monthly tritium release rates from three sources, yearly release rates from a fourth source, and hourly meteorological data were provided on a CD separately from the scenario description. Five models participated in the exercise. One model did not submit groundwater concentrations and predicted only mean yearly concentrations for the rest of the endpoints. Another model predicted concentrations in air moisture, rain and groundwater, but not in the pine tree.

All models were based on similar concepts but the equations and parameters used for tritium transfer in each process differed among models. Most modelers used a Gaussian plume model to calculate air concentrations but one participant used a random walk model. Similarly, simple piston compartment models and sophisticated dispersion compartment models were used for groundwater movement. The differences between predictions and observations proved to depend less on the differences in the models themselves and more on the choice of parameter values and the ways in which local conditions were taken into account, particularly the meteorological characteristics specific to the Pacific coast in Japan and the relationship between the sampling method used (continuous or batch) and the exposure timing (24 hours or daytime only) of each sample type. Some aspects of plant physiology, such as the difference in photosynthesis rate between day and night and between seasons, and the translocation of OBT, proved to be quite important in predicting the OBT concentration in plants.

For a given model, the accuracy of the predicted tritium concentrations in rain, needles, rings or groundwater depended on the ability of the model to predict the air concentrations accurately. Good agreement between predictions and observations for rain, needles, rings or groundwater was likely the result of compensatory errors if the model performed poorly with respect to the concentration in air.

The internal consistency of the predictions (P) of each model was examined based on the mean P_x/P_{air} ratios of yearly mean tritium concentration in a given endpoint (x) to the concentration in air. Most of the five models showed mean P_x/P_{air} ratios close to or below unity when the variance in the ratios was taken into account, indicating that most predictions were internally consistent. However, one model showed an unacceptably high P_{rain}/P_{air} ratio, suggesting that it may have a problem in modeling wet deposition.

The internal consistency of the observations (O) was also examined in terms of the O_x/O_{air} ratios of tritium concentrations in the various endpoints (x) to the concentration in air. The yearly mean O_{TFWT}/O_{air} ratios showed values much greater than unity at two target points in two years of the study. These high ratios likely arose from the fact that the pine needles were always sampled during the day. The air concentration during the day (and thus the observed TFWT concentration) tends to be high due to the frequent onshore winds that carry contaminated air to the target points and sometimes cause the trapping effect. In contrast, the 24 hour air concentration from which the TFWT concentrations were predicted tends to be lower because the frequency of offshore winds, which are associated with lower concentrations, increases at night.

The air moisture concentrations predicted by three of the five participating models lay within 40% to 80% of the observed concentrations, which is considered good modeling performance. The remaining two models underestimated the observed concentrations by a factor of 3 to 5, which suggests relatively poor performance, perhaps because the wind speeds or dispersion parameters used to calculate the air concentrations were overestimated. Ignoring the probable trapping effect is probably a common cause for all models to underestimate the air moisture concentration.

Since the scenario involved a simple groundwater system with relatively detailed information on the geological structure and water movement in the unsaturated and saturated soil layers, the complex dispersion compartment models were able to predict the time evolution of tritium concentrations in the groundwater to within a factor of 2 if appropriate assumptions and parameter values were applied. Even the simple piston compartment models that assumed instant mixing of input tritium performed well as long as key parameter values such as the turnover rate or dilution factor in the aquifer were known beforehand from other sources.

The key conclusions to come out of the Pine Tree scenario are:

(1) the air concentration, which drives concentrations of the other environmental compartments, is affected by local meteorology such as the trapping effect when the sources are located along the sea coast;
(2) the measured TFWT and OBT concentrations, which were obtained from samples collected during the day, reflect daytime meteorological conditions; and
(3) the plant OBT concentration is affected by the physiology of OBT production, OBT translocation and associated hydrogen isotope effects. All of these aspects are worthy of further study.

CHAPTER 5. THE SOYBEAN SCENARIO

5.1. Scenario description

The soybean scenario addresses tritium absorption by soybean foliage and subsequent tritium behaviour in the plant. To provide data for model testing, soybean plants were exposed to elevated levels of airborne tritium in a glove box. The exposure was carried out acutely for one hour at various stages in the growth of the soybeans. The tritium behaviour in the plant body and pods was observed by sampling the various plant parts and determining the concentrations in them.

The full scenario description is given in Appendix I.4. Briefly, a total of six pots (SB1 to SB6) were tested, with the exposures occurring at different stages of growth. The sowing was made on May 22, flowering was observed on July 7, and harvest was done on October 5. The exposures were made on July 2, July 13, July 30, August 9, August 24 and September 17 for SB1 to SB6, respectively. SB1 and SB4 were sampled several times between exposure and harvest to measure the tritium concentrations of each plant part as a function of time. The other plants were sampled and analyzed twice, at the end of the exposure and at harvest. The surface soil of the pots was covered by vinyl paper during the exposure in order to prevent tritium from depositing to the soil. Following exposure, the plants were removed from the glove box and cultivated as usual outdoors.

Information on biomass growth rates, tritium concentrations in air in the glove box during the exposure, background tritium concentrations and meteorological conditions were given as part of the scenario. Modellers were asked to predict the following:

(1) HTO concentrations in the free water of the plant body and pods (tissue free water tritium –TFWT) in the SB1 and SB4 experiments at the times the plants were sampled;
(2) the non-exchangeable OBT concentrations in the plant body and pods at harvest for each of the six experiments (SB1 to SB6); and,
(3) the 95% confidence intervals on all predictions.

5.2. Observations

The observed concentrations corresponding to the requested predictions are shown in Tables 5.1–5.3. The free water tritium and organically bound tritium concentrations were normalized by the mean activity of the air moisture in the glove box during the exposure. The normalized quantities make it easier to compare the trend of the calculations and observations across experiments, particularly for OBT, since the mean activities in air moisture in the glove box differed from experiment to experiment.

The observations have associated uncertainties that arose from sampling and counting; the supporting data (e.g. meteorological data and light intensity) also have related uncertainties. A Quantulus 1220 liquid scintillation counter (Wallac) was used to measure the tritium concentrations in the plant samples, with a counting error of about 10%. It is difficult to assign quantitative values to the other sources of uncertainty. The errors in the OBT measurements would be higher than in the HTO concentrations because of difficulties in removing exchangeable OBT and combusting the dry matter. Some variability must be expected between plants, although this was kept to a minimum in the experiments by analyzing composite samples taken from a number of plants.

Table 5.1. Observed and normalized TFWT for SB1 experiment.

Time and date	Time after exposure (hr)	TFWT (Bq/mL)	Normalized TFWT*
In the plant body (stem and leaves)			
10:40 July 2	0.2	9580	1.23E-01
11:30 July 2	1	1050	1.35E-02
July 3	24	3.92	5.05E-05
July 7	120	1.32	1.70E-05
July 16	336	0.33	4.25E-06
August 10	936	0.11	1.42E-06
September 7	1608	0.06	7.73E-07
October 5	2280	0.06	7.73E-07
In the pods (shell and seeds)			
August 10	936	0.21	2.70E-06
September 7	1608	0.06	7.73E-07
October 5	2280	0.06	7.73E-07

* Tissue free water tritium concentration in the plant divided by the average tritium concentration in air moisture during the exposure (7.77 E+04 Bq/mL for SB1)

Table 5.2. Observed and normalized TFWT concentrations for SB4 experiment.

Time and date	Time after exposure (hr)	TFWT (Bq/mL)	Normalized TFWT*
In the plant body (stem and leaves)			
10:40 August 9	0.2	7000	1.33E-01
11:30 August 9	1	3200	6.08E-02
August 10	24	25.9	4.92E-04
August 14	120	2.1	3.99E-05
August 23	336	0.8	1.52E-05
September 10	768	0.27	5.13E-06
October 5	1368	0.14	2.66E-06
In the pods (shell and seeds)			
10:40 August 9	0.2	10500	1.99E-01
11:30 August 9	1	8000	1.52E-01
August 10	24	2700	5.13E-02
August 14	120	63.5	1.21E-03
August 23	336	1.49	2.83E-05
September 10	768	0.84	1.59E-05
October 5	1368	0.26	4.94E-06

* Tissue free water tritium concentration in the plant divided by the average tritium concentration in air moisture during the exposure (5.27×10^4 Bq/mL for SB4).

Table 5.3. Observed non-exchangeable organically bound tritium (OBT) concentration in plant parts at harvest for experiments SB1 to SB6.

Case	Mean activity of air moisture during exposure (Bq/mL)	OBT concentration at harvest (Bq/mL)[1]							
		Body				Pods			
		Stem	Leaves	Avg.	Nor.avg.[2]	Shell	Seeds	Avg.	Nor.avg.[2]
SB1	7.77×10^4	18.0	14.0	16.0	2.06E-04	0.83	0.5	0.67	8.63E-06
SB2	1.47×10^5	59.8	50.8	55.3	3.75E-04	3.5	3.7	3.6	2.44E-05
SB3	1.14×10^5	37.8	17.7	27.8	2.44E-04	101.3	19.3	60.3	5.28E-04
SB4	5.27×10^4	19.8	8.8	14.3	2.71E-04	74.7	200.0	137.4	2.61E-03
SB5	9.19×10^4	44.3	13.5	28.9	3.14E-04	73.3	214.2	143.8	1.56E-03
SB6	1.37×10^5	180	19.5	99.8	7.28E-04	33.5	77.0	55.2	4.03E-04

[1] One gram of dry matter yields about 0.6 mL of combustion water.
[2] Normalized OBT: average OBT concentration divided by the mean activity of air moisture.

Table 5.4. Participants in the Soybean Scenario.

Participant	Affiliation	Designation used in the text
Phil Davis	AECL, Canada	AECL
Yves Belot	Consultant, France	Belot
Françoise Siclet	EDF, France	EDF
Wolfgang Raskob	FzK, Germany	FzK
Masahiro Saito	SRA, Japan	SRA
Kiriko Miyamoto	Japanet, Japan	Japanet
Hansoo Lee	KAERI, Korea	KAERI
Dan Galeriu	IFIN, Romania	IFIN
Alexei Golubev	VNIIEF, Russia	VNIIEF
Darren Cutts	FSA, United Kingdom	FSA
Paul Marks	GE HealthCare, United Kingdom	GE
Ring Peterson	LLNL, United States	LLNL

The TFWT concentrations in the plant body drop off much more quickly in experiment SB1 than in SB4, with values an order of magnitude or more lower between 24 and 120 hours post-exposure. This suggests that the tritium dynamics in the plants depend on the timing of the exposure relative to the growth stage of the plant. The difference in results may also be caused by differences in the growth rates of the plants and differences in the meteorological conditions that they experienced after the exposure.

The normalized TFWT concentration in the pods is higher than in the plant body for SB4, in particular from the time just after exposure to 120 hours elapsed. The TFWT in the plants decreased more rapidly than in the pods. This implies that the exchange rate of TFWT from the plant body to the air is higher than from the pods since most plant-to-air transfer occurs through the leaves. It also suggests that the transfer rate between the pods and the body is not high enough to preserve the equilibrium between the two parts of the plant. The TFWT concentration in the pods eventually dropped down to approximately the same level as that in the plant body, indicating that the TFWT comes into equilibrium throughout the plant after a sufficiently long time.

Table 5.3 shows the OBT concentrations at harvest for each experiment. For the plant body, separate concentrations are given for stems and leaves, as well as an average over the two compartments. For experiments SB3 through SB6, the concentrations in stems are quite different than in leaves, so the average must be treated with caution. A similar comment applies to shells and seeds and the average over the two compartments. However, the endpoint for the calculations was the plant body (stem + leaves) and the results submitted by most participants did not distinguish between shell and seeds. Thus, for simplicity, only two endpoints (plant body and pods) are considered here.

5.3. Comparison of predictions and observations

Twelve participants submitted predictions for the soybean scenario (Table 5.4), including KAERI. The scenario was not a blind test for KAERI, which provided the test data, but the KAERI model and predictions are included in the report since they provide insight into the results. Full descriptions of the models used to carry out the calculations are given in Appendix II.4.

A generalized equation for the build-up of HTO concentration in the plant body during exposure can be expressed as an activity balance that includes tritium absorption for input and transpiration for output:

$$A\frac{dC_{pb}}{dt} = C_a - BC_{pb}, \qquad (5.1)$$

where:

C_{pb} and C_a are the HTO concentrations in the plant body and in air, respectively; and
A and B are the parameters required to sustain the proper activity balance between air and plant body.

If the tritium concentration in air is constant, then the solution of Equation (5.1) gives Belot's equation [26]. Once the exposure is terminated and the chamber is opened, the air concentration to which the plants are exposed drops to natural background levels. Equation (5.1) is then employed again with the air concentration set to zero in order to predict the loss of tritium from the plant.

Most models take into account plant growth in calculating the HTO concentrations. Although plant growth rate data were given as part of the scenario, some modelers (AECL, FzK, IFIN) calculated it based on CO_2 assimilation or other approaches (VNIIEF) since there was considerable variability in the given data.

The transfer of HTO from the plant body to other organs was modeled as an instantaneous equilibrium with different partitioning factors for shells and seeds (AECL, SRA, FSA, GE, KAERI, LLNL) or with a single factor for the pods as a whole (Belot, FzK).

In some models, OBT formation was treated as an equilibrium, with appropriate parameters relating the OBT and HTO concentrations in each organ (Belot, Japanet). Some codes allowed the OBT concentration to be diluted by new, uncontaminated growth (AECL, IFIN, LLNL, VNIIEF). Other models related OBT formation to HTO concentrations using forward and backward transfer rates for the plant body and forward transfer rates only for the pods (FSA, FzK, KAERI, SRA). In these cases, plant growth was incorporated into the calculations by adding the plant growth balance equation. Most models also account for the reverse transfer from OBT to HTO by introducing rate constants for the plant body and the pods (SRA, FSA, GE, KAERI, LLNL). In this way the models describe the different rates of decrease of tritium in the plant body and the pods.

One of the participants in the Working Group, Franz Baumgartner of the Technical University of Munich, contributed a paper discussing a conceptual model that describes tritium transfer from water to biomolecules by energy balance between hydrogen isotopes, i.e. by minimizing the free energy of the isotopes. Although no results were submitted for this model, it is described in Appendix II.4 as well.

Four participants (LLNL, Japanet, AECL and IFIN) submitted estimates of the 95% confidence intervals on the predicted concentrations. LLNL carried out a numerical Monte Carlo uncertainty analysis using input parameters with normal, triangular or uniform distributions. The uncertainties estimated by Japanet for the TFWT concentrations were based on a 10% variation in the rate constant of HTO loss from the plant; for OBT, the uncertainties were based on the standard deviations of the mean HTO concentration in air moisture during the exposure. The AECL estimates were based on an uncertainty analysis of UFOTRI, a code similar to ETMOD, for a scenario from BIOMOVS II that was similar to the soybean scenario [1]. The uncertainties are not shown in the figures to prevent them from becoming too busy, but are discussed in Section 5.3.4.

5.3.1. HTO concentrations for SB1

Normalized HTO concentrations in the plant body and in the pods for experiment SB1 are shown as a function of time in Figures 5.1 and 5.2, respectively. The predictions of most participants for the plant body lay close together in the early part of the experiment (up to 1 hr after the exposure). All predictions lay above the observed data but by less than an order of magnitude in most cases. The reason for this is not clear. When the exposure was finished, a fan was used to remove the tritium from the glove box. This may have caused extreme mixing that facilitated the removal of tritium from the plant body. Another reason for low uptake by the plants may have been the high temperatures in the chamber, which may have affected the behavior of the stomata. Alternatively, the models themselves may have been in error, with uptake rates that were too high or initial loss rates that were too low.

The predictions of the various models diverged significantly after 1 hour. EDF, FzK and IFIN predicted the observations closely in the beginning, but the calculations showed a sudden change after 1 hr, resulting in predictions that were lower than the observations at later times. GE, KAERI and SRA predictions were higher than the measurements through the entire observation time. The predictions as a whole show no obvious bias but the results of individual models are more than three orders of magnitude different from the observations in some cases.

The predictions of normalized HTO concentration in the pods in SB1 (Figure 5.2) varied from 10^{-4} to 10^{-9}, whereas the observations lay in the range of 10^{-6}. According to the observations, the HTO concentrations were roughly the same in all parts of the plant at these times. Most of the models reproduced this observation and thus over- or underestimated the concentration in the pods to the same extent that they over- or underestimated the concentrations in the plant body. LLNL assumed that the pods were not growing at the time of exposure for SB1 and that HTO in the pods when they started to grow equaled the HTO in the leaves. This assumption accounted for the low predictions of LLNL in Figure 5.2.

5.3.2. HTO concentrations for SB4

The predicted HTO concentrations in the plant body for experiment SB4 (Figure 5.3) show the same patterns as the predictions for SB1. The results of all participants are fairly closely grouped and higher than the observations at the beginning of the experiment, but after 24 hours they become distributed over a range of 10^5, with some overestimates and some underestimates. As was the case for SB1, the discrepancy could be explained by the use of uptake rates that were too high or initial loss rates that were too low.

The predictions and observations of normalized HTO concentration in the pods for SB4 are shown in Figure 5.4. At the beginning of the experiment, the predictions range over a factor of 100 and bracket the observations. At later times, the predictions range over five orders of magnitude and tend to underestimate the observations. Most of the models are unable to account for the relatively long residence time of HTO in the pods.

The HTO concentrations in all parts of the plants at harvest were about 2 orders of magnitude higher than the levels expected of plants growing in an environment with an average air concentration of 0.04 Bq m^{-3}. There are two possible explanations for this:

(1) The HTO concentrations are maintained at a relatively high level by the slow breakdown of OBT in the plant.

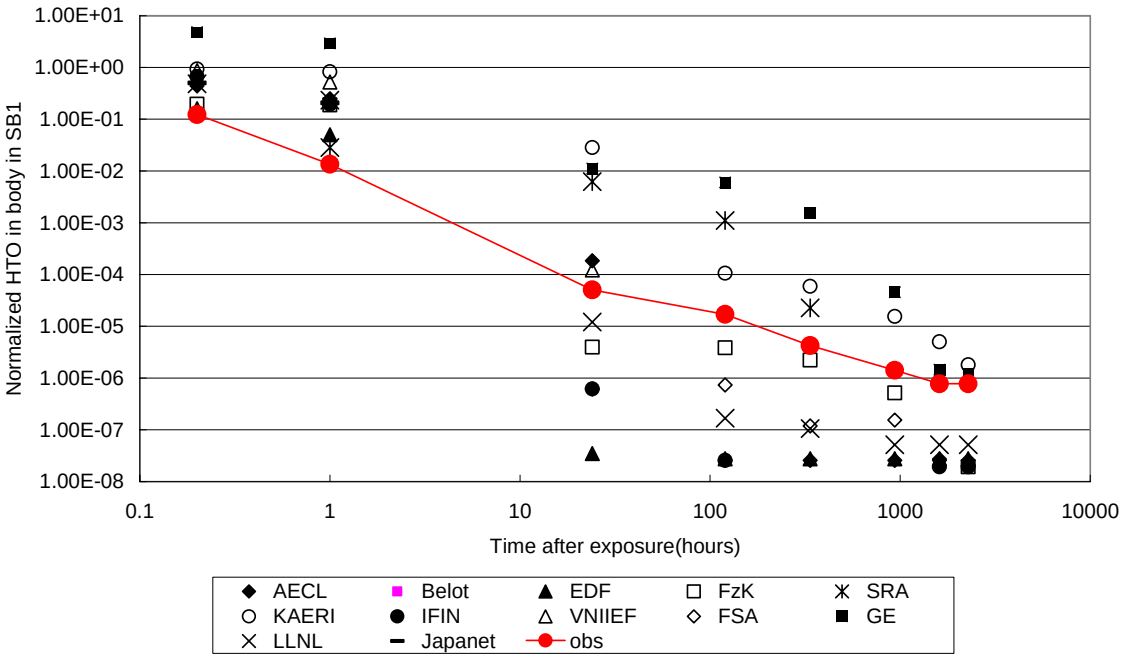

Fig. 5.1. Predicted and observed normalized HTO concentration in plant body in SB1

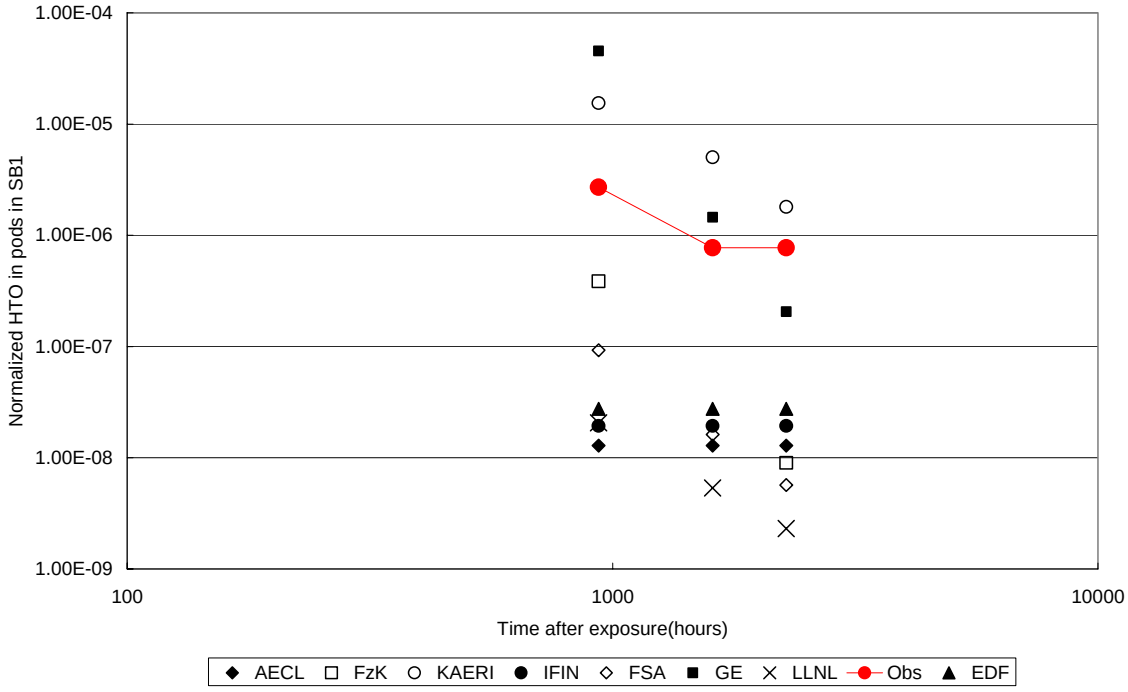

Fig. 5.2. Predicted and observed normalized HTO concentration in pods in SB1.

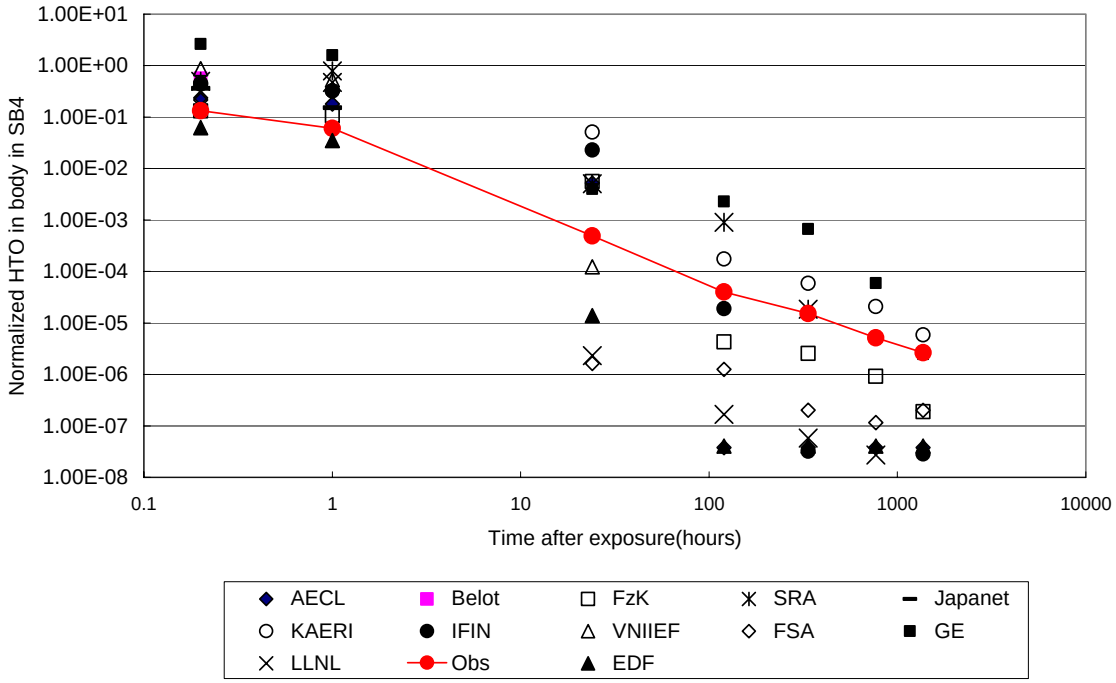

Fig. 5.3. Predicted and observed normalized HTO concentration in plant body in SB4.

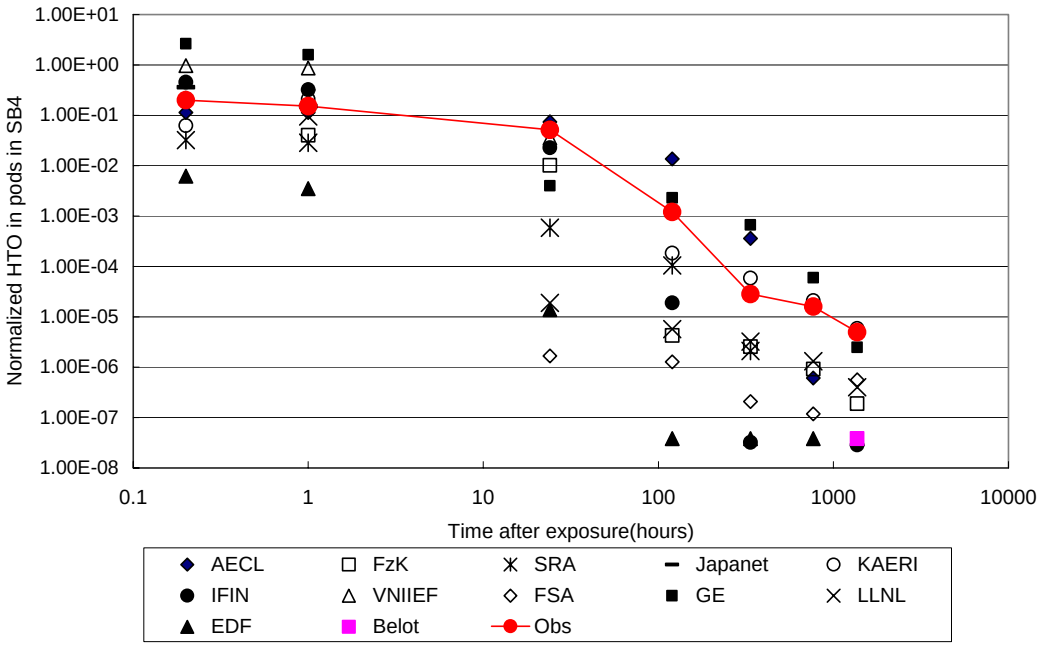

Fig. 5.4. Predicted and observed normalized HTO concentration in pods in SB4.

(2) The high concentrations may occur as the result of a reverse transfer of HTO from stem or roots to leaves and pods. In the pre-fruiting period, part of the HTO is transferred to stem and roots. At the fruiting period, when the HTO in the leaves and pods is almost exhausted by translocation or transpiration, the HTO in the stem or roots is recycled to the leaves and pods, maintaining the concentration at the residual level.

In theory, elevated concentrations could also be maintained by root uptake if the soil was contaminated during exposure. However, this is believed to be unlikely because of the care taken in applying the vinyl covering to the soil and the post-exposure dilution of soil water concentrations with clean irrigation water.

5.3.3. OBT concentrations for SB1 to SB6

The predictions and observations for OBT concentrations for experiments SB1 to SB6 are plotted in Figures 5.5 and 5.6 for the plant body and the pods, respectively. The observed concentrations in the plant body increased slightly as the time between exposure and harvest decreased. This likely reflects the fact that the OBT in plants exposed at later times had less time to breakdown and was less subject to dilution with new, uncontaminated dry matter production. The predictions of most models were fairly constant with time and followed the observed tendency well, even though the absolute values were dispersed over two orders of magnitude. The predictions tended to underestimate the observations, more so for the first three experiments than for the last three. The AECL model under-predicted severely for SB3–SB6. This model assumed that all OBT formed in the leaves after flowering was translocated to the pods and set the leaf concentration to background levels. This assumption is not supported by the observations.

The OBT concentration in the pods is crucial for estimating the effects of contaminated foodstuffs in the diet. This concentration initially increased as the time between exposure and harvest decreased, reaching a maximum for SB4 when the plants were growing very actively (Figure 5.6). Concentrations dropped off as the exposure took place closer to harvest, perhaps because the translocation rate to the grain decreased as the grain became riper. Moreover, the leaves started to fall in the later experiments, reducing the amount of tritium absorption through the leaves and making less tritium available for OBT formation. The predictions of some models captured this variation well while others remained almost constant or increased only slightly with exposure time. The very low predictions by the AECL, LLNL, EDF and IFIN models for SB1, in which the pods had not yet started to form at the time of exposure, occurred because the HTO concentrations in these models drop off very quickly with time and were essentially negligible when the pods began to form. The low concentration predicted by AECL for SB2 has a similar explanation.

The amount of OBT formed in a plant depends on the time-integrated HTO concentration in its leaves rather than on the instantaneous HTO concentration at any given time. Accordingly, ratios of OBT at harvest to the HTO concentration in the plant body integrated over the first 24 hours following exposure were calculated for each model and compared with the observations in Figure 5.7 to provide insight into the behaviour of the models. The calculated ratios were lower than the observed ratios for both SB1 and SB4, whether the ratio was based on the OBT in the plant body or in the pods. The models generate a significantly smaller amount of OBT per unit time-integrated HTO concentration than the plants produce in reality. The models that overpredict the OBT concentration in the plants do so only because they overpredict the initial time-integrated HTO concentration. This is of concern since it is the OBT concentration that is important in determining dose.

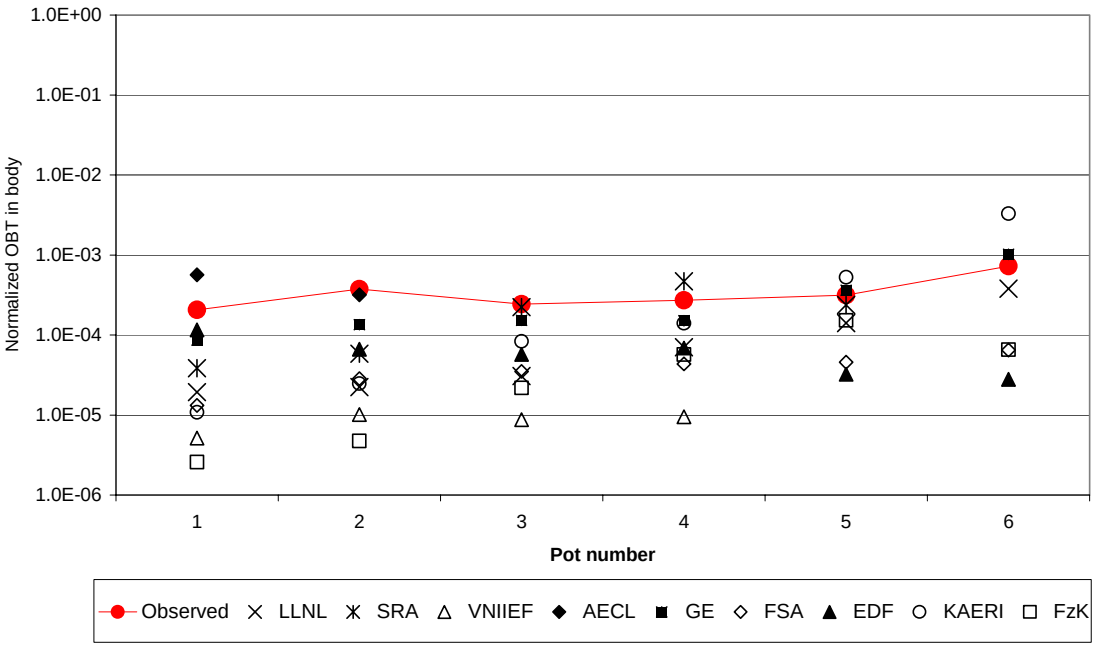

Fig. 5.5. Predicted and observed OBT concentrations in the plant body at harvest (average of stem and leaves). AECL predictions for SB3 to SB6 were ~ 10^{-8} and are not plotted.

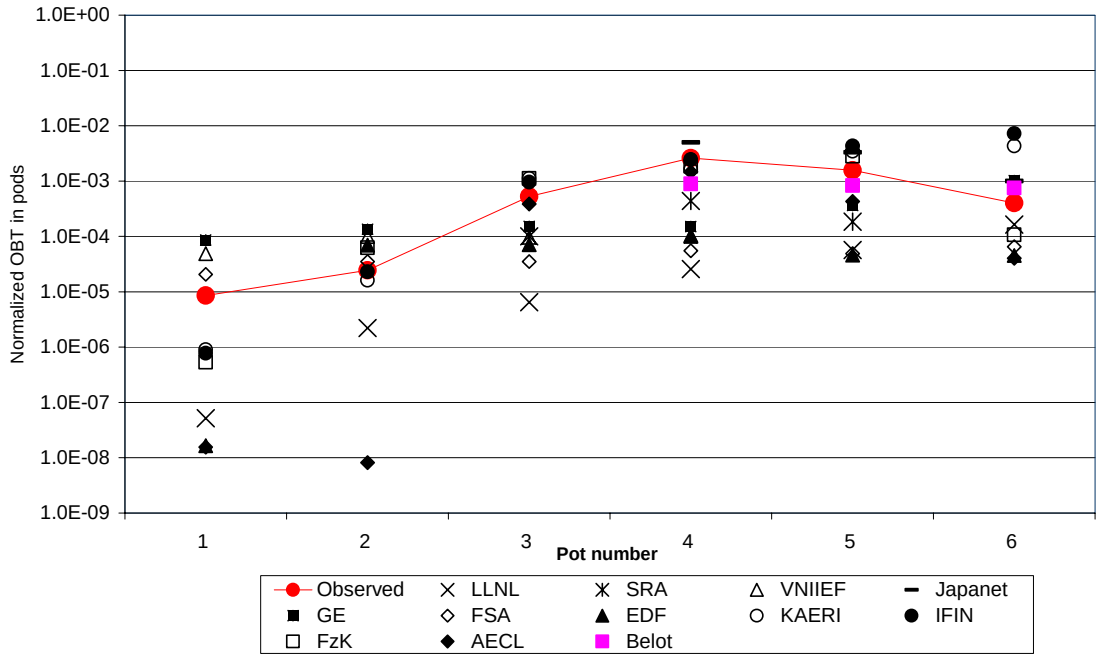

Fig. 5.6. Predicted and observed OBT concentrations in the pods at harvest (average of shell and seeds)

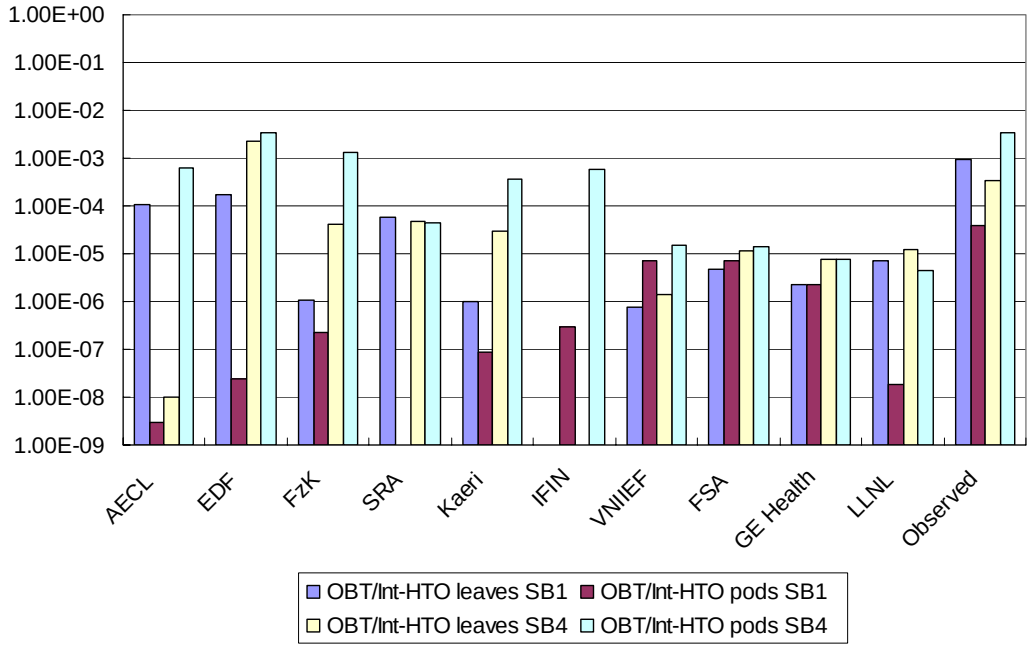

Fig. 5.7. The ratio of OBT in plant parts to the HTO concentration integrated for 24 hrs.

In the SB1 experiment, the observed OBT/time-integrated HTO ratio was higher in the leaves than in the pods. Most of the OBT remained in the plant body since the exposure was carried out before flowering. All models except VNIIEF and FSA reproduced this behaviour. In contrast, for SB4, the ratio was higher in the pods than in the leaves since most of the OBT was translocated to the pods as this exposure was conducted during the active fruiting period. Again, all of the models with the exception of SRA and LLNL were able to simulate this result.

5.3.4. Uncertainty analysis

Four participants (LLNL, Japanet, AECL and IFIN) calculated the uncertainties on their predictions and arrived at very different conclusions. The Japanet estimates were very low, with the upper and lower confidence limits lying just 5% from the best estimate. In the case of AECL, the 95% confidence interval (the 97.5th percentile divided by the 2.5th percentile) was estimated to cover a factor of 10 for TFWT concentrations in the plant body and a factor of 4 for OBT concentrations in pods at harvest. The uncertainties were largest for concentrations predicted immediately after exposure and decreased slightly thereafter. The confidence intervals on TFWT estimated by both LLNL and IFIN depended strongly on the time after exposure. The intervals were relatively low (~ a factor of 2–5) immediately after exposure and again at very long times. At intermediate times, the confidence intervals were larger, with values as high as a factor of 100 at t = 24 hours for SB1. For OBT concentrations in the pods, the LLNL and IFIN uncertainties depended on the growth stage of the plant at the time of exposure but the confidence intervals generally lay between factors of 10 and 30.

Given the large variation in the confidence intervals estimated by the various participants, no definitive conclusions can be drawn regarding the uncertainties in the model predictions. Ideally, the confidence intervals would take into account the uncertainties in the HTO concentrations in air moisture used to drive the models; in the various transfer parameters required by the models; in specifying the growth rates of the plants; and in the structure of the models themselves. The best estimate of uncertainty can perhaps be obtained from an overall assessment of the scatter in the predictions submitted by the participants. These suggest that the confidence intervals on TFWT concentrations are about a factor of 10 shortly after exposure, increasing to a factor of 1000 or more at later times. The greater uncertainty at longer times is probably due to differences in how the models treat residual HTO due to sequestration or the breakdown of OBT. The confidence intervals on the OBT concentrations in the pods at harvest are about a factor of 100 or less, with the experiments at later stages of plant growth having the lower uncertainties. The confidence intervals are generally smaller for OBT than for TFWT, reflecting the fact that HTO varies rapidly over time whereas OBT integrates.

5.4. Summary and conclusions

The soybean scenario tested the rate of tritium transfer between air and plant and the rate of OBT formation. Six experiments were carried out using a glove box to expose plants at different stages of growth. Two of the experiments were designed to study the time-dependent HTO concentration in various parts of the soybeans. After the exposure, the soybean parts were sampled with time to quantify the rate of transfer from leaves to other plant parts or to the air as time elapsed. In all experiments, the OBT concentrations were measured in the plants parts at harvest.

The observations were normalized to the air moisture concentrations in the exposure chamber so that a more meaningful comparison of the results could be made across experiments. The HTO concentrations in the pods were higher than in the plant body in the early period after the exposure, since the transpiration to air from the pods was lower than from the plant body. The OBT concentration in the pods at harvest initially increased as the time between exposure and harvest decreased, with the highest concentration occurring for the exposure time closest to the active fruiting period. For exposure at later growth stages, the OBT concentration decreased slightly due to low translocation rates or lesser numbers of leaves supplying tritium from the air.

Twelve participants submitted predictions and one submitted a theoretical paper concerning tritium transfer from water to biota. The models for tritium transfer from air to leaves were generally based on an activity balance, yielding the HTO concentrations in the plant body or pods. Some participants used equilibrium assumptions to calculate OBT concentrations based on the HTO levels whereas others used compartment models to simulate HTO and OBT concentrations simultaneously and time-dependently.

The predictions of HTO concentrations in the plant body for SB1 were higher than the observations in the first hour after exposure. This might be due to the vigorous mixing used to remove the tritium from the glove box after the experiment, which may have accelerated the transfer of tritium from the leaves to the air. Alternatively, the discrepancy may be explained by the use of incorrect values for the transfer parameters in the models. After an hour, the predictions dispersed widely but followed the observed trend to decreasing HTO concentrations with time. Predictions for the normalized HTO concentration in the pods in SB1 ranged widely again but scattered around the observations.

The results for the HTO concentration in the plant body for SB4 were similar to those for SB1. For both experiments, the concentrations at harvest were well above background levels. There are a number of possible explanations for this observation, but a definitive conclusion must await additional experimental evidence. The generally poor predictions at longer times are of no practical significance because the concentrations are extremely low at this point. The models are all conservative for the first few hours, the period that is important for the production of OBT.

OBT concentration is the essential information necessary for assessing ingestion doses. Most participants were able to reproduce the slight increase in the normalized OBT concentrations that was observed in the plant body at harvest as the time between exposure and harvest decreased. Similarly, most participants were able to simulate the variation in the normalized OBT concentration in the pods with exposure time by considering the plant growth rate in their models. However, most of the models underestimated the observed OBT concentrations, and the scatter in the predictions, while less than that for HTO, remained substantial. The models do not produce as much OBT per unit time-integrated HTO concentration as the plants were observed to produce. The models would have underestimated the OBT concentration by more than they did if they had not overpredicted the initial time-integrated HTO concentration.

Four participants carried out uncertainty analyses and reported the 95% confidence interval on their predictions. These differed substantially and no definitive conclusions can be drawn regarding the uncertainties of the models. An overall assessment of the scatter in the predictions suggests that the confidence intervals on TFWT concentrations are about a factor of 10 shortly after exposure, increasing to a factor of 1000 or more at later times. These large uncertainties are of little significance because the concentrations themselves are very low at these times. The confidence intervals on the OBT concentrations in the pods at harvest are about a factor of 100 or less, with the experiments at later stages of plant growth having the lower uncertainties.

CHAPTER 6. THE PIG SCENARIO

6.1. Introduction

At the 2005 EMRAS Plenary Meeting in Vienna, the Tritium/C14 Working Group decided to adopt a scenario to test models that describe the transfer of tritium in large farm animals. As a world average, meat, milk, eggs and fish supply 16% of human food energy and 36% of protein. Pig meat consumption ranks first among various meats and is predicted to increase. Pigs are not very economic in terms of land requirements but they are efficient in terms of water consumption per unit energy or protein produced. As a consequence, we chose to base the animal scenario on pigs.

6.2. Scenario description

The scenario was split into two parts. The first part was based on unpublished observational data and provided a blind test of the models. Participants were asked to predict the dynamics of total tritium in urine and faeces and the concentrations of tritiated water (HTO) and organically bound tritium (OBT) in organs for a pregnant sow fed an OBT diet for 84 days before delivery. The genotype and initial mass of the sow were given, as well as the composition, OBT concentration and intake dynamics of the diet.

The second part of the scenario was a model intercomparison exercise based on hypothetical data. This exercise was necessary because the sow considered in the blind test was about 200 kg in weight, much heavier than animals used for human consumption, which are normally sacrificed near 110 kg. In the absence of relevant experimental observations, two exercises were proposed. In the first, the pig was fed a diet contaminated with HTO for 50 days between 55 and 105 days of age, the mid period between weaning and sacrifice. The diet at early and later times was uncontaminated. Modellers were asked to predict the total tritium in urine, HTO and OBT concentrations in faeces, and the OBT concentration in muscle from the time the pig was 55 to 155 days old. The second exercise considered a short-term OBT intake at various ages of the pig. Modellers were asked to predict the meat and liver OBT concentrations at sacrifice for different pig genotypes.

The scenario descriptions are discussed briefly below and are given in full in Appendix I.5.

6.2.1. Blind test

Data for the blind test were obtained from experiments carried out by M. van Hess and colleagues at SCK-CEN, Belgium. Results from one of these experiments, in which a pregnant sow was fed OBT during gestation, delivery and lactation, were published [27]. However, data from a prior experiment involving a sow that was slaughtered just before delivery were not published. These data were provided by van Hess in the form of a personal communication to N. Beresford (CEH, UK) as the basis for the scenario. Concentrations of total tritium in urine and OBT in fecal dry matter are given as a function of time in Table 6.1. HTO and OBT concentrations in various organs of the sow at slaughter are given in Table 6.2. This study pre-dated the publication on the sow that was allowed to live through delivery [27] and records on the experimental protocol were only partially recovered.

We observe from Table 6.2 that the organs differ in OBT concentration by a factor 3, with the lowest value in muscle and the highest in liver, and an average value that is close to the OBT concentration in blood.

Table 6.1. Concentrations of total tritium in urine and OBT in faeces for a pregnant sow.

Days after start of contamination	Total tritium in urine		OBT in faeces	
	(nCi/ml)	(Bq/ml)	(nCi/g dry wt)	(Bq/g dry wt)
7	1.53	56.6	43.91	1624.7
14	2.09	77.3	54.08	2001.0
21	1.88	69.6	57.44	2125.3
28	2.41	89.2	57.26	2118.6
36	2.73	101.0	58.44	2162.3
42	2.79	103.2	61.71	2283.3
49	2.55	94.4	53.95	1996.2
56	2.83	104.7	55.83	2065.7
63	2.91	107.7	51.70	1912.9
70	3.08	114.0	50.43	1865.9

Table 6.2. HTO and OBT concentrations in sow organs at delivery.

Organ	Dry weight (% fresh wt)	HTO concentration		OBT concentration	
		(nCi/ml)	(Bq/ml)	(nCi/g dry wt)	(Bq/g dry wt)
Heart	21.70	1.31	48.5	6.52	241.2
Lungs	23.45	1.26	46.6	4.79	177.2
Liver	26.09	1.37	50.7	8.22	304.1
Jejunum	22.40	1.31	48.5	5.26	194.6
Ileum	20.16	1.25	46.3	5.97	220.9
Colon	24.26	1.21	44.8	4.07	150.6
Kidney	23.68	1.36	50.3	6.17	228.3
Muscle	26.98	1.33	49.2	2.70	99.9
Brain	22.16	1.32	48.8	3.10	114.7
Little brain	26.23	–	–	5.67	209.8
Blood	–	1.13	41.8	5.14	190.2

The modellers were given the composition and total amount of the diet, but no information on water intake, urine production or the number of piglets in the litter. From the published paper [27], we deduce a piglet number of 8–9, which was normal for livestock practices of the early 1980s. Literature values for sow water intake start from a low of 6–8 L/d (perhaps at the start of gestation) to 20 L/d (at delivery and lactation); water intake also increases with feed intake [28]. The water intake range suggested in the scenario might be an underestimate and this might influence model results.

Pregnant sows increase food intake for purposes of maintenance, activity, pregnancy (gestation and development of mammary glands) and maternal growth (body reserves to be used later in lactation). This information was not known and had to be assessed by the modellers, or at least considered in estimating the uncertainties in their predictions. Intake and partition is most conveniently addressed in terms of metabolisable energy (ME). The ME intake can be estimated from the diet composition and amount. Values for dry potato and dry milk are included in many nutritional tables, and values for algae can be obtained by assuming similarity to grass or alfalfa. Considering the nutritional tables from Romania [29], the UK [30], the USA [28] and France [31], we obtain an average value of 16.5 MJ/kg dry mass, with about 5% variability. Uterine energy deposition (ME_{preg}) can be assessed using the literature [32] and is given in Figure 6.1. The maintenance energy of the sow depends on body weight and an agreed value is $ME_{main} = 0.43 \cdot BW^{0.75}$. Here we can ignore any thermal stress, as we are discussing a controlled experiment. An approximate value for the activity energy need of the sow (ME_{act}) is available in Noblet et al. [32]. The potential maternal growth of the sow (ME_{growth}) can be estimated as the balance between ME intake and the sum of ME_{main},

ME_{act} and ME_{preg}. The intake and partition of metabolisable energy for this scenario, as well as the mass gain of the sow, is summarized in Table 6.3.

A gain in mass immediately before delivery is not realistic, as at this moment feed intake is increased to allow for milk production. The values in Table 6.3 imply that the sow will have a maternal weight gain close to 20 kg, in agreement with the range of 20–30 kg found in the literature. Most of the mass gain will be in adipose tissue, but the weight of the visceral organs will also increase to reflect the increased intake [32].

As a conclusion of this short analysis of processes in the gestation period, we expect that muscle mass will not change significantly, but some weight gain will occur in the viscera, which should be taken into account in the models. The uncertainty in the sow water intake will influence model results for total tritium concentration in urine. Similarly, the modelers were required to estimate the digestible fraction of the diet in order to predict the OBT concentration in faeces. According to recent French work [31], this fraction has a value of about 0.85.

The prediction of tritium concentrations in urine and faeces requires knowledge of pig waste. Some relevant information is available from the FAO [33]:

> *"The production of solid pig waste ranges from 0.6 to 1.0% of dry matter per day calculated on body weight. Low-digestibility rations yield relatively more manure. With an increase of body weight, the quantity of pig waste decreases significantly. Faeces represent about 46% and urine 54% of wastes on a fresh weight basis, but on a dry basis faeces represent 77% and urine 23%. The pH of pig manure is in the range 7.2–8.3."*

This reference indicates that waste fresh mass is given by $1.4 \cdot BW^{0.25}$ and provides an idea of the mass and composition of urine and faeces.

6.2.2. Model intercomparisons

The blind test was not particularly applicable for normal radiological assessments of tritium transfer through the food chain because the sow was much heavier than is usual for pigs at slaughter. Intercomparison exercises involving smaller animals were added to make the scenario more useful. The first exercise, which involved HTO intake over a period of 50 days, was promoted as an example of a waste management scenario in which the contamination arises from drinking water from a well. The second exercise had two goals: to consider tritium dynamics following a short-term intake of OBT; and to consider the influence of pig genotype on the tritium concentrations in meat and liver. The exercises were built without experimental data but both incorporated hypothetical data on pig growth following the modeling results of van Milgen and Noblet [34] and Noblet et al. [32].

Table 6.3. Metabolisable energy (ME) intake and partition to maintenance, activity, pregnancy and growth.

Day of gestation	Days after start of contamination	ME intake (MJ/d)	ME_{main} (MJ/d)	ME_{act} (MJ/d)	ME_{preg} (MJ/d)	ME_{growth} (MJ/d)	Mass gain (kg/d)
30–51	0–21	30.7	21.1	1.33	1.4	6.84	0.18
52–76	22–46	34.0	21.6	1.35	2.2	8.88	0.23
77–109	47–79	38.1	22.3	1.40	3.2	11.2	0.29
110–114	80–84	49.6	23.1	1.45	4.4	20.6	0.57

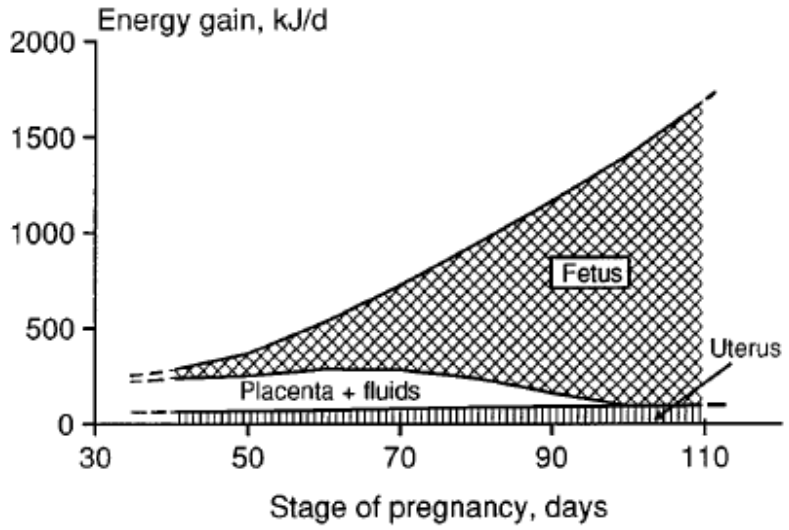

Fig. 6.1. Uterine energy deposition in a sow bearing 12 piglets

6.3. Model descriptions

The models used to calculate results for the Pig Scenario varied in complexity. The simplest model (STAR-H3) was one of the oldest, being formulated in 1995–1998. STAR-H3 has a single organic compartment representing the slow turnover of OBT, with a turnover rate for all animals of 0.03 d^{-1} (half-time of 23 d). In STAR-H3, the animals are assumed not to grow over time. The model is implemented on a software platform (AMBER) that allows only pasture as intake. STAR-H3 was not applied in this scenario by the model developers but by a combination of participants from the National Institute of Physics and Nuclear Engineering – Horia Hulubei (IFIN-HH) and Lawrence Livermore National Laboratory (LLNL). At LLNL, STAR-H3 was applied as prescribed, with the given pig diet replaced by pasture. AT IFIN, the model was reconstructed from references and judgement to allow more realistic inputs. The modified model, termed STAR-H3(DG), was used to execute the LNLL examples with the same pasture intakes to ensure the accuracy of the reconstruction. The model was then run with the diet as given in the scenario description for the blind test. STAR-H3(DG) does not allow for pig growth and was not used in the model intercomparison exercises.

Electricité de France (EDF) also used a simple model (OURSON) with a single organic compartment. OURSON assumes that all OBT in the diet enters the organic compartment. A dynamic equation is derived for the specific activity (SA) in the compartment, taking into account growth dilution and the difference in feed and compartment concentrations. The rate of transfer to HTO in the body is given by the digestible intake per unit body dry weight. There is no transfer from body HTO to body OBT. The HTO concentration in urine is assumed to be the same as that in the body; similarly, the OBT concentration in urine urea is taken to equal that in the body. Faeces OBT corresponds to the OBT in the non-digestible fraction of food, where it is assumed that the OBT SA is identical in the digestible and non-digestible fractions. The whole body OBT is considered to be representative of the muscle compartment. Concentrations in other organs are derived from the concentration in muscle using correction factors based on the fat and protein contents of each organ, the fat and protein turnover rates, and the hydrogen contents of fats, proteins and carbohydrates.

Atomic Energy of Canada Limited (AECL) carried out the calculations using the animal model from the ETMOD code, a process-oriented code that considers the detailed dynamics of HTO. ETMOD does not have an animal organic compartment, assuming that all tritium in the animal is in the form of HTO. Accordingly, AECL submitted results for the total tritium concentration in urine only.

Two of the models participating in the Pig Scenario, MCT and PRISM, were of moderate complexity. MCT is a model with two organic compartments, one with a fast turnover rate (half-life 30 days) and one with a slow turnover (half-life 450 days). The model also includes an inorganic compartment representing body water. MCT was developed initially for humans but was modified for these calculations to reflect the mass of the sow. In the pig version, organically bound hydrogen is split equally between the two organic compartments. About 70% of OBT intake enters the fast OBT compartment and the rest is converted immediately to HTO and enters the body water compartment. There is no transfer from the fast to the slow OBT compartment.

The PRISM software is a modeling platform for probabilistic applications in which specific models for tritium and C-14 have been implemented. The current standard version is PRISM HC [35]. This version was extended for the Pig Scenario to treat the urine and faeces endpoints [36]. PRISM HC uses a simplified model of the gastrointestinal tract. OBT intake is partitioned between body water and two organic compartments, one of which is labile (fast turnover) and the other non-labile (slow turnover). A fraction 0.79 (range 0.61–0.94) of the OBT is immediately converted to HTO and distributed to body water. The rest enters the organic compartments, with twice as much going to the labile compartment as to the non-labile compartment. Similarly, the hydrogen content of the labile compartment is twice that of the non-labile compartment on average, but the range is very large (from 1/9 to 9). The loss rate from body water is 0.13 d^{-1} (0.06–0.19 d^{-1}), higher than in MCT (0.077 d^{-1}), but the range includes the MCT value. The loss rate from the labile organic compartment is 1.1×10^{-3} d^{-1} (5.5×10^{-4} – 2.2×10^{-3} d^{-1}) whereas from the non-labile compartment it is 7.32×10^{-5} d^{-1} (3.66×10^{-5} – 1.46×10^{-4} d^{-1}). Note that these rates are much lower than in MCT and the transfers are directly to faeces and urine and not through body water as an intermediate pathway.

It was observed that the PRISM results submitted by the Food Standards Agency (FSA) differed substantially from the experimental observations and from the predictions of the other models. To clarify this, IFIN used available documentation (supplied by the model developers and FSA) to independently reconstruct the model under the ModelMaker platform. The reconstructed model was run with average values of the PRISM HC transfer parameters, and results are reported as PRISMDG.

The MAGENTC model (Mammal GENeric model for Tritium and Carbon transfer) was developed by IFIN over the last three years with inputs from Japan (H. Takeda, NIRS) and the UK (N. Beresford, CEH; N. Crout, Nottingham University). The model starts with the basic assumption that the turnover rates of organically bound tritium and carbon in organs can be assessed using net maintenance energy turnover rates. The model has six organic compartments and distinguishes between organs with high transfer and metabolic rates (viscera), storage organs with very low metabolic rates (adipose tissue), and ‘muscle’ with intermediate metabolic and transfer rates. Dry matter intake is partitioned to metabolisable and excreted fractions. The former, in the case of tritium, distinguishes exchangeable and non-exchangeable fractions. The exchangeable fraction is converted to HTO and transfers directly to body water compartments, whereas the non-exchangeable fraction is absorbed in

the systemic circuit (blood plasma) after digestion. While MAGENTC is a research grade model, two major simplifications are included: a single respiration rate and a single metabolic rate for all organs. Model parameter values were established independently of any tritium or C-14 experimental data. Generic values were used in the blind scenario, but more refined values for pig nutrition, growth, metabolism and physiology were used in more recent applications. The biokinetic rates for muscle and viscera used in the Pig Scenario are shorter than those for the labile and non-labile compartments in PRISM HC.

A summary of the participating models and users is shown in Table 6.4. Full descriptions of all the models are presented in Appendix II.5.

6.4. Results of the blind test

Predicted and observed concentrations of total tritium in urine for the blind test are shown in Figure 6.2, and predicted-to-observed (P/O) ratios are given in Table 6.5. FSA overestimates by many orders of magnitude whereas most other predictions lie within a factor 10 of the observations. Because the reconstructed version of PRISM (PRISMDG) gives good results, the FSA overestimate may be due to inappropriate use of the model by the user, most likely in matching the model output to the scenario requirements. The overestimate of a factor 4–6 by STAR-H3 is explained by the fact that, in this model, all OBT intake is distributed to body water and the excretion rate assumed is too high for a pig. The underestimate in MCT is due to the low excretion rate and the partition of intake OBT to the body water compartment. The underestimate of a factor 3–10 in the EDF results is due to the model assumption that all OBT input appears in the body organic compartment. The IFIN and AECL predictions agree well (within 20% at most times) with the experimental data.

The concentration of OBT in faeces was predicted only by MCT, FSA, EDF and IFIN; the P/O ratios for this endpoint are given in Table 6.6. Faeces contamination is expected to be similar to the contamination of undigested feed, but in fact it is four times higher than the average concentration in the diet (Table 6.1). This explains the underprediction by MCT, EDF and IFIN. The overprediction by FSA remains to be explained.

The sow was fed a mixture of dry potato, dry cow milk and dry algae. It is known that the composition of faeces differs from that for feed, as shown in Table 6.7. It is possible that the inhomogeneity of feed compound activity and fibre enhancement in pig faeces explains the enhanced activity in the faeces.

Predictions of organ HTO and OBT concentrations were supplied by FSA, MCT, EDF and IFIN (using STAR and PRISM as well as MAGENTC). The P/O ratios for HTO are given in Table 6.8. With the exception of FSA, all models give good predictions, although EDF underestimates by a factor 5. Table 6.9 gives the P/O ratios for OBT in organs. STAR-H3(DG), as expected, underestimates by a factor 10 due to the model assumption that OBT intakes enter the high turnover compartment (body water). The EDF predictions, which were obtained on the assumption that all OBT in the diet enters the organic compartment, are close to the observations, although the concentration in muscle is overestimated by a factor of 3. The reasons for this are not clear and should be investigated further. MCT overestimates by a factor between 2 and 4, and IFIN (using generic parameter values) by a factor 2. We note the large range of overestimation in the FSA results, which are unexplained. The reconstructed version of PRISM overestimates by only 50%.

Table 6.4. Participating models and users.

Model	User	Affiliation	Designation
MCT	M Saito	Kyoto, Japan	MCT
STAR-H3	D Galeriu, R Peterson	National Institute of Physics and Nuclear Engineering – Horia Hulubei (IFIN-HH), Romania Lawrence Livermore National Laboratory (LLNL), U.S.A.	STAR-H3(DG)
MAGENTC	D Galeriu, A Melintescu	IFIN, Romania	IFIN
PRISM HC	P Kennedy	Food Standards Agency (FSA), U.K.	FSA
PRISM HC reconstructed	D Galeriu, A Melintescu	IFIN, Romania	PRISMDG
OURSON	F Siclet	Electricité de France (EDF), France	EDF
ETMOD	V Korolevych	Atomic Energy of Canada Limited (AECL), Canada	AECL

Table 6.5. Predicted-to-observed ratios for total tritium in urine.

Days after start of contamination	MCT	IFIN	STAR-H3(DG)	FSA	PRISMDG	EDF	AECL
7	0.02	0.64	6.26	17675	1.34	0.09	0.81
14	0.11	0.85	4.88	34495	1.39	0.14	0.92
21	0.24	1.20	5.46	82942	1.73	0.23	1.21
28	0.28	1.06	4.27	98812	1.41	0.24	1.07
36	0.30	1.02	3.77	123077	1.26	0.27	1.01
42	0.36	1.04	3.70	146154	1.24	0.30	1.01
49	0.46	1.18	4.05	199568	1.37	0.37	1.16
56	0.43	1.09	3.66	212098	1.23	0.37	1.09
63	0.47	1.08	3.56		1.20		
70	0.56	1.03			1.14		

Table 6.6. Predicted-to-observed ratios for OBT in faeces.

Days after start of contamination	MCT	FSA	IFIN	EDF
7	0.69	2.46	2.20	3.60
14	0.42	3.93	1.10	1.80
21	0.33	4.86	0.73	1.20
28	0.28	5.64	0.55	0.90
36	0.23	6.31	0.43	0.70
42	0.21	6.62	0.37	0.60
49	0.19	7.14	0.31	0.51
56	0.17	7.51	0.28	0.45
63	0.16		0.24	
70	0.17		0.22	

Table 6.7. Composition of pig feed and faeces [33].

Constituent	Unit	Feed	Faeces	Faeces/feed ratio
Gross energy	MJ/kg	18.0	17.9	–
Ether extract (crude fat)	%	5.27	4.72	0.90
Ash	%	6.7	17.4	2.59
Crude fibre	%	5.7	18.2	3.19
Acid detergent fibre	%	6.8	24.3	3.57
Neutral detergent fibre	%	20.6	44.6	2.17
Lignin	%	1.1	4.9	4.45
Cellulose	%	5.2	16.9	3.25
Hemicellulose	%	13.8	20.3	1.47

Table 6.8. Predicted-to-observed ratios for HTO in organs (84 days after start of contamination).

Organ	MCT	FSA	IFIN	PRISMDG	STAR-H3(DG)	EDF
Heart	0.54	33.4	2.17	1.31	0.81	0.19
Lungs	0.56	11.7	2.25	1.36	0.84	0.20
Liver	0.51	5.39	2.07	1.25	0.77	0.18
Jejunum	0.54	11.2	2.17	1.31	0.81	0.19
Ileum	0.56	38.4	2.27	1.37	0.85	0.20
Colon	0.58	5.89	2.35	1.42	0.88	0.21
Kidney	0.52	29.2	2.09	1.26	0.78	0.18
Muscle	0.53	0.42	2.13	1.29	0.80	0.19
Brain	0.53	7.70	2.15	1.30	0.80	0.19
Blood	0.62	2456	2.51	1.52	0.94	0.22

Table 6.9. Predicted-to-observed ratios for OBT in organs (84 days after start of contamination).

Organ	MCT	FSA	IFIN	PRISMDG	STAR-H3(DG)	EDF
Heart	2.05	9.89	1.40	1.51	1.29	1.29
Lungs	2.79	4.11	1.90	2.06	0.13	1.30
Liver	1.92	1.04	1.11	1.20	0.08	0.84
Jejunum	3.00	3.23	1.73	1.88	0.12	1.09
Ileum	2.24	13.0	1.53	1.65	0.10	0.96
Colon	3.28	2.23	2.24	2.42	0.15	1.40
Kidney	2.17	8.46	1.48	1.60	0.10	1.17
Muscle	4.44	0.23	1.90	3.65	0.23	3.11
Brain	3.91	4.69	–	3.17	0.20	1.65
Blood	3.04	970	1.27	1.92	0.12	1.22

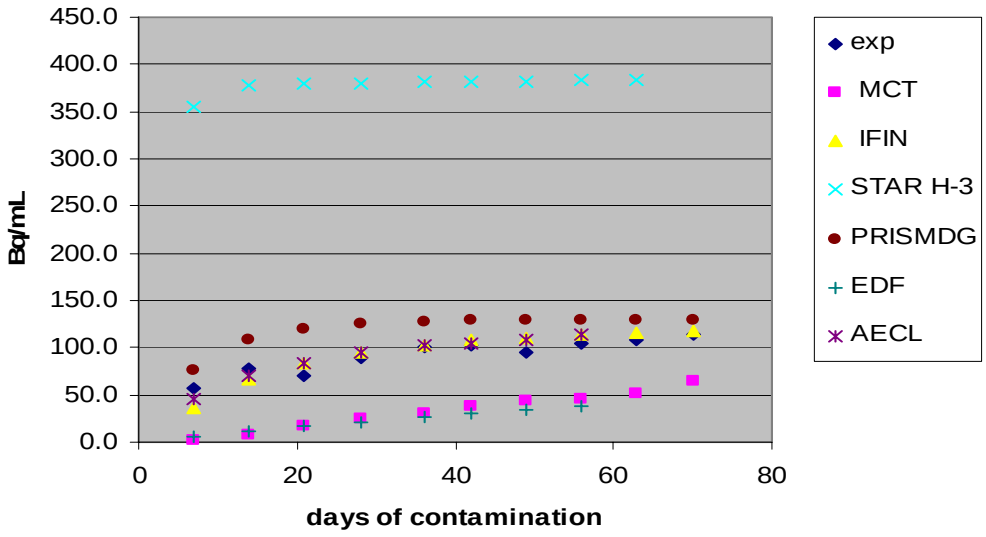

Fig. 6.2. Predictions and observations of total tritium concentrations in urine. Results for FSA are very high and are not shown.

With the exception of FSA and STAR, all models give reliable predictions of HTO and OBT concentrations in organs. STAR was developed assuming pasture intake and the model structure must be changed if performance is to improve. The poor FSA results are likely due to user error and not to any deficiency in the model. The results of the blind test give confidence that both simple and complex models can be used to predict tritium concentrations in pig meat if only OBT intake is considered.

6.5. Results of the intercomparison exercises

Only four models (IFIN, MCT, FSA and AECL) participated in the intercomparison exercises. Moreover, AECL submitted results for the urine concentrations only, and the FSA results are suspect given the poor performance of this model in the blind test. The conclusions that can be drawn from such little information are limited. Predictions for the first exercise, in which the diet of a growing pig was contaminated with HTO for 50 days starting when the pig weighed 20 kg, are given in Table 6.10. Concentrations in urine are expected to be slightly less than those in drinking water (10 Bq/ml) because of dilution with metabolic water. This is the case for IFIN, MCT and AECL but the FSA results are much higher. Once the contamination stops at day 50, the urine concentrations should decay. This was again the case for IFIN, MCT and AECL, but not for FSA. Similar results were obtained for HTO in faeces.

Table 6.11 shows the model predictions for OBT concentrations in meat for the first intercomparison exercise. There are orders of magnitude difference between models, with FSA showing the highest results. The decay in meat, after the contamination stops at day 50, is slower in FSA than in IFIN or MCT. Kirchmann et al. [15] indicates a half-time in urine near 4 days, based on an experiment in which pigs were offered tritiated water for 28 days starting from the age of 8 weeks; in contrast, van Hess et al. [27] observed a half-time of about 100 days for muscle after OBT intake. At the end of Kirchmann's experiment, muscle OBT made up 0.6% of the total activity intake. The IFIN prediction at the end of HTO intake (0.49 %) is closest to this value (Table 6.11). The FSA result is higher by a factor 10, whereas that for MCT is lower by a factor 5.

HTO concentrations in faeces were predicted by FSA, MCT and IFIN (Table 6.12). The FSA results are again unexpected high. At the end of the contamination period, the MCT predictions for HTO in urine and feces indicate a half-time of 8 days, double the experimental result for a similar pig [15]. Here and elsewhere in the first intercomparison exercise, there is a need to clarify the FSA results. Also, more model predictions are needed before useful conclusions can be drawn.

For the second intercomparison exercise, in which pigs of different genotypes were fed OBT for one day at different stages of their growth, only IFIN and FSA supplied predictions (Table 6.13). Two contrasting genotypes were considered but FSA preserved the same organ partitioning for both types, whereas IFIN used a conventional and obese one. Both models showed that the genotype has little effect on OBT concentrations in meat, but the IFIN results suggest that genotype is more important for concentrations in liver. There are significant differences between the model predictions that remain to be explained.

Table 6.10. Total tritium concentration in urine for the intercomparison exercise involving 50 days of HTO intake.

Days after start of contamination	Total tritium concentration in urine (Bq/ml)			
	FSA	IFIN	MCT	AECL
7	9.55E+04	8.20	3.45	8.15
14	2.48E+05	8.90	5.23	9.077
21	4.76E+05	8.90	6.27	9.204
42	1.13E+06	8.80	7.72	9.254
50	1.33E+06	8.70	8.00	9.261
60	1.48E+06	1.00	3.50	1.302
70	1.53E+06	0.20	1.55	0.17
100	1.56E+06	0.01	0.15	0.0005

Table 6.11. OBT concentration in meat for the intercomparison exercise involving 50 days of HTO intake.

Days after start of contamination	OBT concentration in meat (Bq/kg fresh weight)		
	FSA	IFIN	MCT
7	9.21E+03	7.50E+01	3.9E+00
14	1.58E+04	1.65E+02	1.2E+01
21	2.33E+04	2.27E+02	2.1E+01
42	3.90E+04	3.19E+02	4.8E+01
50	4.16E+04	3.35E+02	5.8E+01
60	3.91E+04	2.85E+02	6.2E+01
70	3.69E+04	2.23E+02	5.8E+01
100	3.19E+04	1.22E+02	4.0E+01

Table 6.12. HTO concentration in faeces for the intercomparison exercise involving 50 days of HTO intake.

Days after start of contamination	HTO concentration in faeces (Bq/ml)		
	FSA	IFIN	MCT
7	354	10.0	5.41
14	929	10.0	6.66
21	1810	10.0	7.39
42	4480	10.0	8.40
50	5350	10.0	8.60
60	6130	1.20	5.45
70	6560	0.20	4.09
100	7390	0.01	3.11

Table 6.13. OBT concentrations in meat and liver after short-term OBT intake at various stages of growth.

Mass at intake (kg)	OBT concentration in meat at sacrifice (Bq/kg fresh weight)				OBT concentration in liver at sacrifice (Bq/kg fresh weight)			
	Genotype 1		Genotype 2		Genotype 1		Genotype 2	
	IFIN	FSA	IFIN	FSA	IFIN	FSA	IFIN	FSA
20	575	263	617	269	62	3621	48	3708
40	1775	408	1380	381	170	5521	93	5226
60	2851	529	2078	452	350	7291	126	6221
80	3982	647	2800	517	1192	8925	168	7128
100	5001	739	3900	581	6000	10187	1330	7751

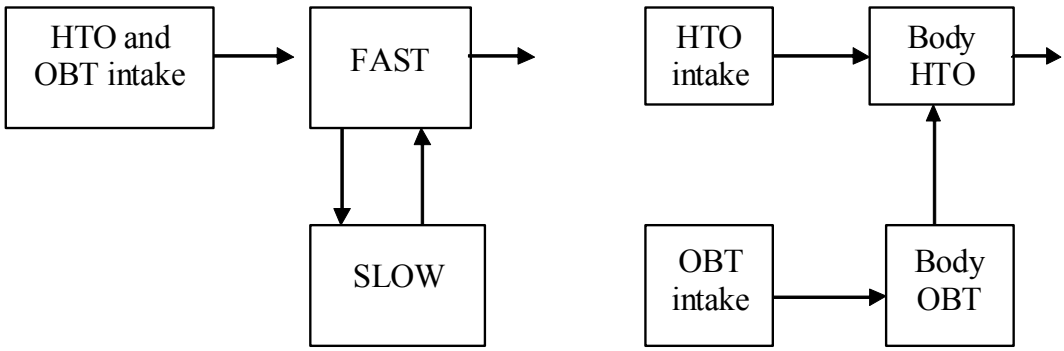

Fig. 6.3. Flowchart of the simple models STAR (on the left) and OURSON (on the right).

6.6. Conclusions and recommendations

The two simple models, STAR-H3 and OURSON, differ in terms of their partitioning of tritium following intake and their transfers from HTO to OBT and OBT to HTO (Figure 6.3). In STAR, OBT taken in with feed enters only the fast (body water) compartment, while in OURSON it enters only the slow (body OBT) compartment. The metabolisation of OBT from body HTO is modeled in STAR but is ignored in OURSON.

The scenario gives the intake of tritium as OBT, a fraction of which will be in exchangeable form. There are processes in animal digestion that increase the fraction of exchangeable OBT (mostly from carbohydrates), and the stomach and intestines will contain not only non-exchangeable OBT but also tritiated water, which is absorbed and distributed to body water. Thus, in reality, organic tritium taken in with feed is distributed between body OBT and body HTO, and not entirely to one or the other, as in STAR and OURSON. Because STAR sends all organic intake to body water, it overpredicts total tritium concentrations in urine and underpredicts OBT concentrations in pig organs. In contrast, because OURSON sends all organic intake to the body OBT compartment, it underestimates total tritium concentrations in urine and HTO concentrations in meat, and overestimates OBT concentrations in organs.

The biological half-life of OBT is comparable in both models. There are experimental data showing the existence of OBT in organs after an HTO intake, a transfer pathway that is not considered in OURSON, or in the AECL model. The above analysis suggests changes that could lead in the future to an improved simple model for tritium transfer in large animals.

Two of the participating models, MCT and PRISM, consider two organic compartments (Figure 6.4). The transfer pathways and many transfer rates differ between the models but both give predictions that are relatively close to the observations. (This statement is based on the results obtained with the reconstructed version of PRISM and not on those obtained by FSA, which appear to be incorrect.) MCT does not consider the fraction of input organic tritium that is directly absorbed in the body OBT, which explains the underprediction in urine. Both models have fast and slow OBT compartments but MCT transfers catabolic OBT to body water, whereas PRISM transfers it out of the body, which is perhaps an oversimplification. The parameter values used in MCT reflect human properties and should be adapted more to pig metabolism. However, it is premature to designate either MCT or PRISM as the better model, as the blind test covered a single situation only.

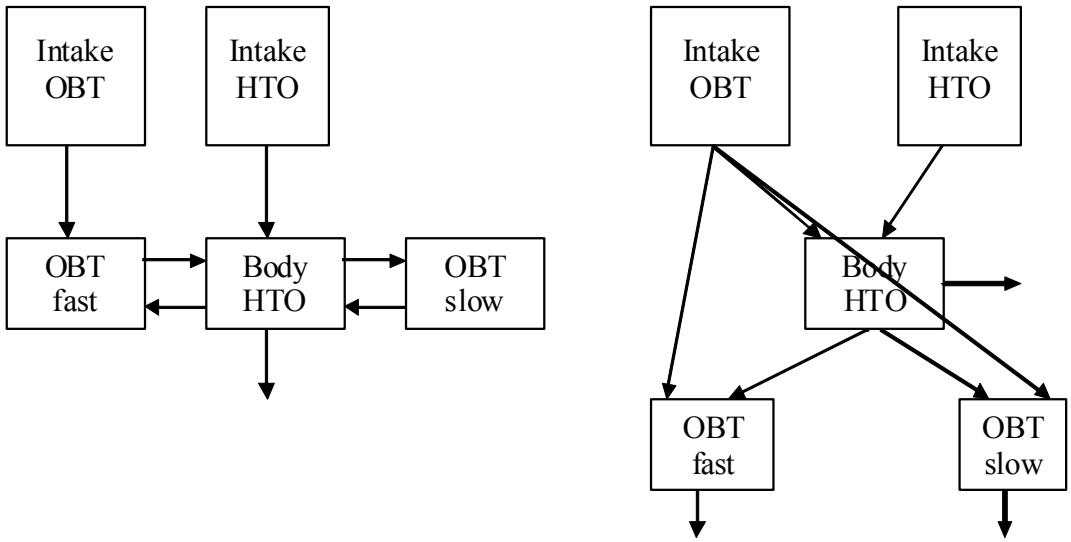

Fig. 6.4. Flowchart of the models MCT (on the left) and PRISM (on the right).

MAGENTC was developed as a research model and is more complex than the other models in the scenario. Its performance is marginally better than that of MCT and PRISM for the blind test, and gives results that are closer to observations in similar experiments involving HTO intake in pigs.

Few models participated in the intercomparison exercises and, because the FSA results are likely incorrect, no firm conclusions can be drawn. For the case of prolonged HTO intake, the IFIN model seems to give reliable predictions based on the available experimental data for pigs. In the second intercomparison, only FSA and IFIN participated. The results of MAGENTC compare favourably with data from many other experiments, so we conclude that genotype is not important for the radiological assessment of tritium in meat (although it may be in liver).

To the best of our knowledge, this scenario was the first to attempt a limited blind test and model intercomparison for tritium transfer in large farm animals. More tests and intercomparisons are needed in order to define the best operational model. Also, in practice, we must be aware of the influence that the user has on model performance. The results presented here give hope that a simple operational model can soon be developed that is based on parameter values reflecting pig metabolism and that satisfies the requirements of robustness needed today in radiological assessments.

CHAPTER 7. THE MUSSEL UPTAKE SCENARIO

7.1. Background and objectives

Although steady-state models often provide practical tools to estimate free-water tritium (HTO) concentrations (and to a lesser extent, organically bound tritium (OBT) concentrations) [8, 37–40], aquatic organisms are occasionally exposed to short-term, elevated tritium concentrations in watersheds that have fluctuating tritium levels. Depending upon the nature and the duration of such events, in some cases, steady-state models may or may not be predictive of actual organism tritium concentrations [37]. Therefore, it is important to calibrate organisms that might serve as tritium biomonitors, in order to interpret organism responses to such fluctuations in terms of their exposure levels to tritium, as well as their biological responses [41–44].

In general, the rates of HTO uptake and OBT formation are not well known under dynamic exposure conditions, but can be studied by transplanting biomonitoring species, such as freshwater mussels, from areas with low tritium concentrations to areas with elevated tritium levels [42, 45–63]. In this way, changes in HTO and OBT concentrations can be monitored to quantify responses to dynamic exposure conditions.

This was accomplished in the present study through an experiment involving the transplantation of mussels in cages from areas with low tritium concentrations to Perch Lake, a small Canadian Shield lake located on AECL's Chalk River Laboratories site with an aquatic tritium concentration of approximately 4500 Bq/L [8, 64, 65]. The results of this study provided the observations for a model validation scenario for the EMRAS Tritium/C14 Working Group.

7.1.1. Scenario objective

The objective of this scenario was to conduct a model validation exercise to compare observed temporal changes in HTO and OBT concentrations in freshwater Barnes mussel (*Elliptio complanata*) tissues to predicted concentrations in response to abrupt increases in tritium exposure levels. Modelled values were calculated for scenarios in which mussels were exposed to tritium through the water pathway alone, or through both water and sediments.

7.2. Scenario description

A detailed scenario description, which was developed and provided to the EMRAS Tritium/C14 Working Group [64], can be found in Appendix I.6. The scenario focused on the prediction of dynamic tritium data that were measured in freshwater Barnes mussel (*Elliptio complanata*) tissues at discrete time points following transplantation from a site with background tritium concentrations to Perch Lake.

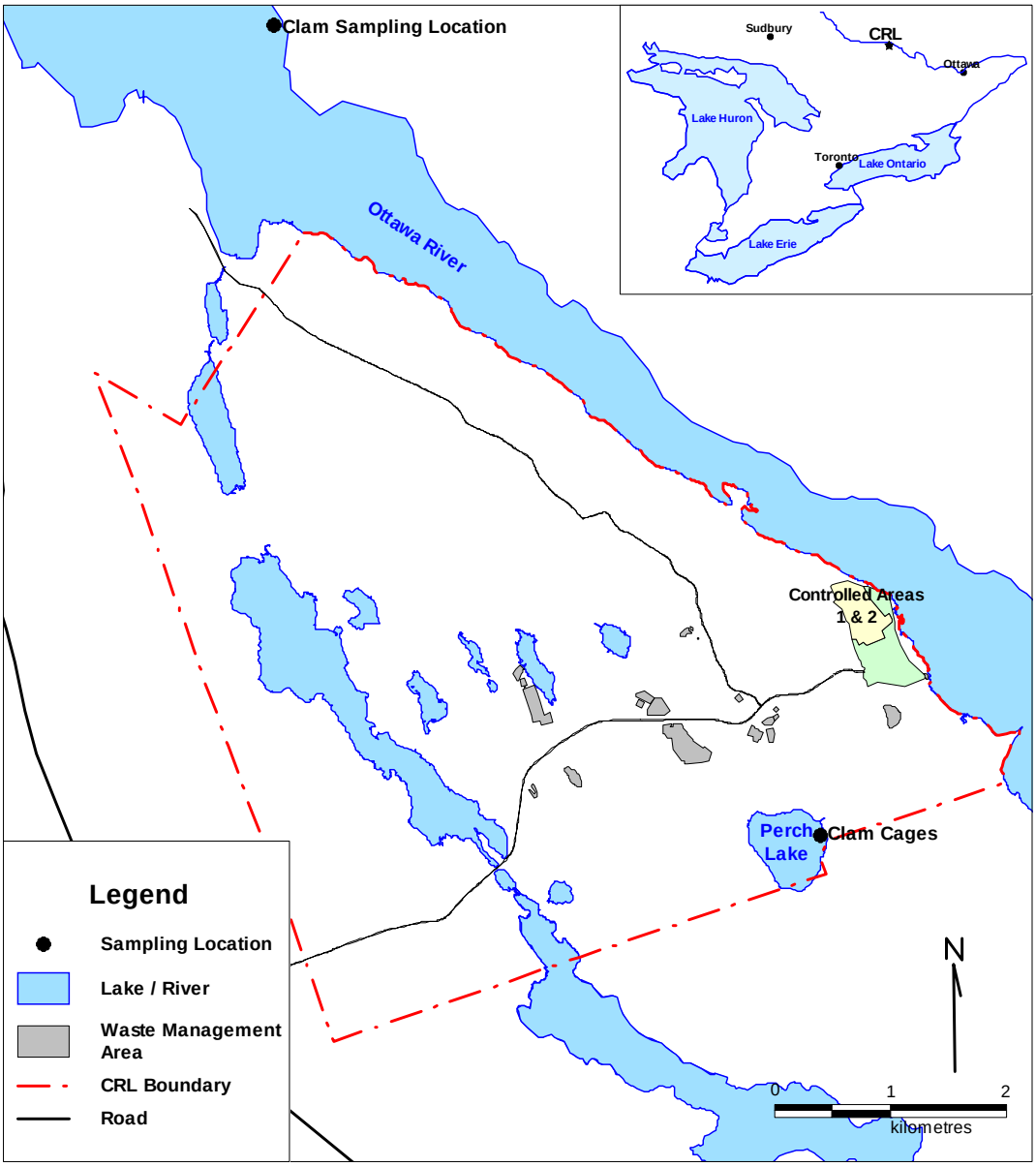

*Fig. 7.1. Map depicting the location of the reference site in the Ottawa River where freshwater mussels (*Elliptio complanata*) were collected, relative to the site of mussel transplantation in Perch Lake on AECL's Chalk River Laboratories site.*

7.2.1. Site description

Perch Lake (Figure 7.1) is situated downstream of two historic CRL Waste Management Areas (WMAs) on Atomic Energy of Canada Limited (AECL)'s Chalk River Laboratories (CRL) site. The lake receives inputs of tritium via groundwater that migrates to surface streams and the lake from these WMAs. Surface water enters Perch Lake via five small inflowing streams through gauged weirs at Inlets 1, 2, 3, 4 and 5. Surface water leaves the lake through one outflowing stream (Perch Creek) at Perch Lake Outlet [66, 67].

Tritium, in the form of HTO, enters the lake primarily via groundwater discharge through the underlying lake sediments and through surface water at the Inlet 2 inflowing stream. The stream at Inlet 1 also has slightly elevated levels of tritium, whereas inflowing streams at Inlets 3, 4 and 5 have relatively low levels of tritium [68]. The spatial distribution of HTO in the lake is not known quantitatively, although it is believed that the lake is well-mixed, with a mean tritium concentration of approximately 4500 Bq/L in the vicinity of the mussel transplantation cages. The cages were deployed in a shallow, sandy substrate where many mussels can be found naturally.

7.2.2. Model input data

Input data summarizing initial tritium concentrations in mussel tissues and environmental media, temporal changes in Perch Lake water temperatures, and mussel sizes both at the time of transplantation and at the time of harvest were provided to modellers participating in the scenario. These input data have been compiled in Tables 7.1–7.5.

A summary of the experimental methodologies that were applied to generate the measured values, and the uncertainty surrounding them, is provided in Section 7.3 below.

7.3. Observations

7.3.1. Study design

Two pairs of mussel transplantation cages were built and deployed in Perch Lake in early July 2004. The transplantation cages had dimensions of 96 cm (length) × 96 cm (width) × 12 cm (height) and were constructed using 2" × 2" cedar boards and chicken wire. Each cage was built with an 8 × 8 design, resulting in a total of 64 compartments per cage [64]. Individual cage compartments had surface area dimensions of 12 cm × 12 cm with one animal per compartment to provide the mussels with adequate space without overcrowding.

Test mussels were collected on 5–7 July 2004 from a nearby reference site in the Ottawa River (Figure 7.1) where tritium concentrations were less than 10 Bq/L HTO in water. During collection, each mussel was carefully examined to assess its suitability for the study. Mussels with total shell lengths of 90 to 111 mm were selected to standardize size and filtration rates, to ensure adequate tissue biomass for tritium analysis and to take account of the dominant mussel size distribution that was present at the background site to reduce the sampling time required. Damaged or unhealthy mussels (e.g. those incapable of closing their shells) were not selected. HTO concentrations in the soft tissues of the reference mussels were less than 10 Bq/L. OBT levels were less than 15 Bq/L for mussels that were frozen immediately after collection, and 45 Bq/L for mussels that were stored in lidded buckets at the CRL site over a period of three days.

Upon collection, mussels were placed into lidded, plastic buckets containing water from the reference site to prevent uptake of tritium prior to initiation of the study. The mussels were then transported to the CRL site and individuals were quickly measured, weighed and alpha-numerically numbered with a cage number and cage compartment number using a Dremel™ engraver for tracking purposes. Labelled clams were separated by placing them into labelled nylon bags and replaced into the lidded buckets of water from the reference site until initiation of the transplantation into Perch Lake, which was carried out on the same day as mussel collection.

Table 7.1. Summary of mean monthly Perch Lake surface water and local air temperatures collected over the course of the Perch Lake mussel transplantation study between July and early October 2004.

Month	Mean ± Standard Error [n] (Minimum to Maximum)		Mean Surface Water-to-Air Ratio	Comments
	Perch Lake Surface Water Temperature (^{o}C)	Local Air Temperature (^{o}C)		
July	22.3 ± 0.25 [25] (19.0 to 25.9)	20.1 ± 0.27 [25] (15.3 to 25.5)	1.11	Represents sampling conducted over the period between July 7th and 31st.
August	16.7 ± 0.16 [31] (15.2 to 20.5)	17.8 ± 0.33 [31] (12.0 to 24.3)	0.94	Represents sampling conducted over the course of the entire month.
September	14.9 ± 0.10 [23] (13.9 to 16.4)	16.1 ± 0.40 [23] (9.5 to 21.3)	0.93	Represents sampling conducted over the month, with the exception of September 11th to 17th during which the data were lost.
October	13.8 ± 0.03 [6] (13.4 to 14.2)	10.0 ± 0.38 [6] (5.0 to 14.8)	1.38	Represents sampling conducted over the period between October 1st and 6th.

Table 7.2. Summary of weight and length measurements of freshwater mussel specimens at the start of the transplantation study relative to the weight and length at the time of mussel harvest.

Cell No.	Cage No.	Mussel Measurements (Time 0)				Fresh Weight at Harvest Time (g)	Fresh Weight at Harvest-to-Initial Fresh Weight Ratio
		Fresh Weight (g)	Shell Length (mm)	Shell Width (mm)	Shell Height (mm)		
A1	Cage No. 1	64.40	96	46	24	59.49	0.92
	Cage No. 2	60.03	92	49	23	59.46	0.99
	Cage No. 3	100.77	111	58	28	99.50	0.99
	Cage No. 4	78.33	98	49	24	78.89	1.01
A2	Cage No. 1	95.19	98	54	28	91.48	0.96
	Cage No. 2	57.35	92	45	21	65.10	1.14
	Cage No. 3	74.09	96	51	27	71.71	0.97
	Cage No. 4	64.90	95	49	25	64.36	0.99
A3	Cage No. 1	62.94	90	48	25	58.50	0.93
	Cage No. 2	68.62	93	46	26	65.10	0.95
	Cage No. 3	122.57	109	57	33	120.52	0.98
	Cage No. 4	97.13	103	53	27	95.99	0.99
A4	Cage No. 1	83.50	103	49	27	81.06	0.97
	Cage No. 2	61.38	90	45	24	61.58	1.00
	Cage No. 3	62.44	94	46	26	59.449	0.95
	Cage No. 4	60.93	94	45	24	61.23	1.00
A5	Cage No. 1	79.23	99	50	26	76.46	0.97
	Cage No. 2	91.42	105	51	30	90.00	0.98
	Cage No. 3	85.65	103	50	28	85.2	0.99
	Cage No. 4	90.77	105	53	28	90.05	0.99

Table 7.2. (Continued)

Cell No.	Cage No.	Mussel Measurements (Time 0)				Fresh Weight at Harvest Time (g)	Fresh Weight at Harvest-to-Initial Fresh Weight Ratio
		Fresh Weight (g)	Shell Length (mm)	Shell Width (mm)	Shell Height (mm)		
A6	Cage No. 1	102.05	102	56	27	94.02	0.92
	Cage No. 2	58.94	93	47	23	59.07	1.00
	Cage No. 3	87.57	104	56	28	86.55	0.99
	Cage No. 4	77.47	103	51	25	74.06	0.96
A7	Cage No. 1	69.89	95	49	24	68.55	0.98
	Cage No. 2	74.51	96	52	26	71.98	0.97
	Cage No. 3	56.50	92	52	20	56.006	0.99
	Cage No. 4	100.44	109	57	29	100.61	1.00
A8	Cage No. 1	83.58	96	51	27	82.54	0.99
	Cage No. 2	72.89	94	50	26	72.13	0.99
	Cage No. 3	61.72	92	46	25	60.38	0.98
	Cage No. 4	70.48	90	51	25	69.21	0.98
B1	Cage No. 1	73.07	96	46	27	71.30	0.98
	Cage No. 2	90.96	100	54	30	89.41	0.98
	Cage No. 3	82.79	101	53	26	82.79	1.00
	Cage No. 4	69.16	90	49	25	69.7	1.01
B2	Cage No. 1	75.31	95	48	26	73.67	0.98
	Cage No. 2	98.10	105	54	32	97.78	1.00
	Cage No. 3	86.19	107	55	25	84.85	0.98
	Cage No. 4	117.87	109	59	31	116.1	0.98
B3	Cage No. 1	77.75	95	51	27	76.64	0.99
	Cage No. 2	79.26	95	52	29	78.41	0.99
	Cage No. 3	75.66	99	53	27	75.86	1.00
	Cage No. 4	73.90	100	51	26	72.96	0.99
B4	Cage No. 1	94.55	104	54	28	92.13	0.97
	Cage No. 2	73.14	94	51	27	71.56	0.98
	Cage No. 3	72.95	98	51	26	72.2	0.99
	Cage No. 4	85.76	102	52	26	84.92	0.99
B5	Cage No. 1	66.31	94	49	26	65.89	0.99
	Cage No. 2	70.63	94	53	27	68.25	0.97
	Cage No. 3	74.28	103	51	27	72.62	0.98
	Cage No. 4	73.64	100	49	24	75.6	1.03
B6	Cage No. 1	98.34	106	56	27	96.76	0.98
	Cage No. 2	62.84	90	51	35	61.23	0.97
	Cage No. 3	101.33	110	54	30	100.94	1.00
	Cage No. 4	83.43	104	52	25	82.43	0.99
B7	Cage No. 1	70.41	95	49	26	67.7	0.96
	Cage No. 2	65.22	96	47	27	64.2	0.98
	Cage No. 3	91.92	100	54	28	91.7	1.00
	Cage No. 4	77.91	93	50	26	78.04	1.00
B8	Cage No. 1	70.29	103	47	22	69.64	0.99
	Cage No. 2	70.75	90	51	29	70.73	1.00
	Cage No. 3	74.20	99	50	28	74.34	1.00
	Cage No. 4	78.51	98	49	26	77.8	0.99
C1	Cage No. 1	67.95	97	47	25	67.76	1.00
	Cage No. 2	73.15	100	46	26	72.02	0.98
	Cage No. 3	102.75	108	53	31	98.87	0.96
	Cage No. 4	69.39	95	47	27	67.49	0.97

Table 7.2. (Continued)

Cell No.	Cage No.	Mussel Measurements (Time 0)				Fresh Weight at Harvest Time (g)	Fresh Weight at Harvest-to-Initial Fresh Weight Ratio
		Fresh Weight (g)	Shell Length (mm)	Shell Width (mm)	Shell Height (mm)		
C2	Cage No. 1	80.67	104	54	25	80.97	1.00
	Cage No. 2	62.98	94	58	26	61.20	0.97
	Cage No. 3	68.65	97	47	24	68.64	1.00
	Cage No. 4	84.76	100	50	27	84.32	0.99
C3	Cage No. 1	57.44	93	45	23	57.177	1.00
	Cage No. 2	77.36	100	55	26	74.69	0.97
	Cage No. 3	71.25	99	48	27	69.43	0.97
	Cage No. 4	57.55	95	47	21	57.505	1.00
C4	Cage No. 1	79.36	104	52	25	77.4	0.98
	Cage No. 2	79.90	98	48	28	80.56	1.01
	Cage No. 3	83.91	105	53	29	83.87	1.00
	Cage No. 4	94.57	105	55	26	94.43	1.00
C5	Cage No. 1	73.39	96	50	25	70.86	0.97
	Cage No. 2	63.48	95	52	23	62.24	0.98
	Cage No. 3	84.51	103	51	29	84.16	1.00
	Cage No. 4	67.19	102	50	22	65.26	0.97
C6	Cage No. 1	86.02	99	49	30	85.12	0.99
	Cage No. 2	81.52	100	52	26	80.2	0.98
	Cage No. 3	78.38	104	51	26	76.1	0.97
	Cage No. 4	94.18	105	50	29	93.12	0.99
C7	Cage No. 1	83.06	101	52	26	82.55	0.99
	Cage No. 2	82.38	102	59	30	81.61	0.99
	Cage No. 3	70.38	98	47	27	67.64	0.96
	Cage No. 4	78.38	100	51	27	76.63	0.98
C8	Cage No. 1	74.35	101	46	26	73.06	0.98
	Cage No. 2	119.84	109	57	33	115.86	0.97
	Cage No. 3	81.21	104	54	27	81.16	1.00
	Cage No. 4	80.26	98	50	27	81.31	1.01
D1	Cage No. 1	101.37	103	58	27	97.39	0.96
	Cage No. 2	113.44	110	56	30	112.9	1.00
	Cage No. 3	117.32	106	60	30	116.93	1.00
	Cage No. 4	70.64	95	50	24	69.49	0.98
D2	Cage No. 1	101.61	101	55	29	99.5	0.98
	Cage No. 2	96.75	104	56	30	94.91	0.98
	Cage No. 3	78.61	102	55	28	78.68	1.00
	Cage No. 4	80.66	99	52	26	81.01	1.00
D3	Cage No. 1	83.65	102	50	25	82.31	0.98
	Cage No. 2	97.71	101	59	30	95.74	0.98
	Cage No. 3	77.04	100	50	26	77.41	1.00
	Cage No. 4	81.01	101	51	25	81.39	1.00
D4	Cage No. 1	68.54	96	49	29	66.12	0.96
	Cage No. 2	116.83	110	51	33	113.79	0.97
	Cage No. 3	71.61	94	50	26	70.53	0.98
	Cage No. 4	82.94	104	51	26	80.45	0.97
D5	Cage No. 1	69.29	95	49	26	69.18	1.00
	Cage No. 2	68.78	93	53	25	67.99	0.99
	Cage No. 3	103.58	109	55	30	100.6	0.97
	Cage No. 4	78.11	99	51	25	77.81	1.00

Table 7.2. (Continued)

Cell No.	Cage No.	Mussel Measurements (Time 0)				Fresh Weight at Harvest Time (g)	Fresh Weight at Harvest-to-Initial Fresh Weight Ratio
		Fresh Weight (g)	Shell Length (mm)	Shell Width (mm)	Shell Height (mm)		
D6	Cage No. 1	78.06	99	49	27	76.21	0.98
	Cage No. 2	98.91	104	50	30	97.65	0.99
	Cage No. 3	74.73	93	53	24	75.21	1.01
	Cage No. 4	86.86	105	51	26	84.54	0.97
D7	Cage No. 1	74.73	99	50	25	72.37	0.97
	Cage No. 2	56.23	94	50	24	55.53	0.99
	Cage No. 3	91.28	99	54	29	90.39	0.99
	Cage No. 4	74.43	100	51	26	74.86	1.01
D8	Cage No. 1	68.01	95	45	25	67.69	1.00
	Cage No. 2	78.77	94	52	28	76.85	0.98
	Cage No. 3	76.94	96	51	24	77.54	1.01
	Cage No. 4	67.74	91	45	26	65.99	0.97
E1	Cage No. 1	70.48	101	50	23	70.61	1.00
	Cage No. 2	94.40	100	58	30	93.63	0.99
	Cage No. 3	75.84	100	51	27	74.22	0.98
	Cage No. 4	56.26	93	46	24	56.267	1.00
E2	Cage No. 1	83.36	104	53	26	80.08	0.96
	Cage No. 2	93.48	100	52	30	89.86	0.96
	Cage No. 3	85.21	96	51	29	83.04	0.97
	Cage No. 4	74.88	94	52	25	74.19	0.99
E3	Cage No. 1	75.97	96	50	27	75	0.99
	Cage No. 2	87.74	104	53	29	85.62	0.98
	Cage No. 3	108.61	101	54	34	105.06	0.97
	Cage No. 4	67.46	100	50	21	67.53	1.00
E4	Cage No. 1	94.02	106	55	32	91.5	0.97
	Cage No. 2	84.80	101	54	29	83.68	0.99
	Cage No. 3	121.49	106	58	32	120.72	0.99
	Cage No. 4	82.10	91	50	28	82.6	1.01
E5	Cage No. 1	68.08	97	48	25	66.73	0.98
	Cage No. 2	78.27	98	50	29	75.46	0.96
	Cage No. 3	71.57	98	50	25	70.37	0.98
	Cage No. 4	93.52	106	54	26	94.4	1.01
E6	Cage No. 1	94.80	99	50	29	88.33	0.93
	Cage No. 2	59.17	90	48	24	58.416	0.99
	Cage No. 3	67.72	94	49	26	66.59	0.98
	Cage No. 4	79.62	100	54	24	77.65	0.98
E7	Cage No. 1	76.23	96	54	25	73.29	0.96
	Cage No. 2	90.52	102	57	29	88	0.97
	Cage No. 3	67.71	98	46	25	68.7	1.01
	Cage No. 4	68.97	94	47	26	67.4	0.98
E8	Cage No. 1	72.53	96	48	26	71.23	0.98
	Cage No. 2	84.61	102	53	28	81.36	0.96
	Cage No. 3	91.71	100	54	28	89.95	0.98
	Cage No. 4	64.47	94	48	25	63.28	0.98
F1	Cage No. 1	82.47	100	56	25	78.14	0.95
	Cage No. 2	106.65	108	55	31	105.95	0.99
	Cage No. 3	118.56	106	56	35	115.79	0.98
	Cage No. 4	72.55	102	50	23	70.81	0.98

Table 7.2. (Continued)

Cell No.	Cage No.	Mussel Measurements (Time 0)				Fresh Weight at Harvest Time (g)	Fresh Weight at Harvest-to-Initial Fresh Weight Ratio
		Fresh Weight (g)	Shell Length (mm)	Shell Width (mm)	Shell Height (mm)		
F2	Cage No. 1	71.93	92	45	26	69.54	0.97
	Cage No. 2	83.38	100	53	30	81.72	0.98
	Cage No. 3	93.37	108	55	27	87.03	0.93
	Cage No. 4	75.37	97	51	24	74.34	0.99
F3	Cage No. 1	64.14	95	46	25	61.8	0.96
	Cage No. 2	70.93	99	49	26	70.59	1.00
	Cage No. 3	84.16	98	54	28	82.23	0.98
	Cage No. 4	77.31	100	50	27	76.95	1.00
F4	Cage No. 1	64.66	90	43	27	63.85	0.99
	Cage No. 2	62.23	94	52	25	60.1	0.97
	Cage No. 3	52.74	95	44	22	51.241	0.97
	Cage No. 4	56.74	92	46	24	56.236	0.99
F5	Cage No. 1	57.42	96	46	20	56.668	0.99
	Cage No. 2	66.86	94	52	27	66.36	0.99
	Cage No. 3	86.67	96	56	27	86.99	1.00
	Cage No. 4	61.29	93	48	23	61.02	1.00
F6	Cage No. 1	62.56	91	45	24	61.05	0.98
	Cage No. 2	81.23	96	55	28	81.23	1.00
	Cage No. 3	87.95	99	51	27	85.63	0.97
	Cage No. 4	85.34	101	50	26	85.03	1.00
F7	Cage No. 1	77.95	96	50	25	75.62	0.97
	Cage No. 2	86.17	100	50	30	83.18	0.97
	Cage No. 3	78.95	101	50	25	75.58	0.96
	Cage No. 4	88.66	105	51	25	86.43	0.97
F8	Cage No. 1	103.22	102	52	32	100.25	0.97
	Cage No. 2	80.08	98	50	27	78.4	0.98
	Cage No. 3	78.25	96	56	27	76.98	0.98
	Cage No. 4	79.17	96	50	26	78.81	1.00
G1	Cage No. 1	93.02	100	50	29	90.27	0.97
	Cage No. 2	84.70	102	56	28	82.26	0.97
	Cage No. 3	75.21	92	49	29	74.76	0.99
	Cage No. 4	97.28	101	53	28	96.13	0.99
G2	Cage No. 1	87.85	100	51	27	85.82	0.98
	Cage No. 2	81.72	96	52	29	80.41	0.98
	Cage No. 3	88.85	100	50	29	84.76	0.95
	Cage No. 4	68.91	100	49	24	68.65	1.00
G3	Cage No. 1	81.58	98	52	27	79.63	0.98
	Cage No. 2	92.11	101	59	28	92.06	1.00
	Cage No. 3	73.52	95	48	27	71.62	0.97
	Cage No. 4	57.64	95	43	25	57.56	1.00
G4	Cage No. 1	78.90	103	49	25	75.92	0.96
	Cage No. 2	76.98	101	49	28	75.28	0.98
	Cage No. 3	96.64	104	51	30	92.47	0.96
	Cage No. 4	65.54	95	49	25	65.23	1.00
G5	Cage No. 1	81.23	98	50	26	78.49	0.97
	Cage No. 2	85.68	103	54	27	85.27	1.00
	Cage No. 3	87.76	99	52	26	87.03	0.99
	Cage No. 4	59.86	93	46	24	59.814	1.00

Table 7.2. (Continued)

Cell No.	Cage No.	Mussel Measurements (Time 0)				Fresh Weight at Harvest Time (g)	Fresh Weight at Harvest-to-Initial Fresh Weight Ratio
		Fresh Weight (g)	Shell Length (mm)	Shell Width (mm)	Shell Height (mm)		
G6	Cage No. 1	75.92	104	50	26	72.72	0.96
	Cage No. 2	69.04	93	49	24	67.95	0.98
	Cage No. 3	87.04	94	51	26	85.87	0.99
	Cage No. 4	78.69	101	48	26	78.23	0.99
G7	Cage No. 1	82.61	99	51	26	78.7	0.95
	Cage No. 2	102.42	109	58	28	94.75	0.93
	Cage No. 3	90.70	105	52	29	87.91	0.97
	Cage No. 4	77.30	95	50	28	77.06	1.00
G8	Cage No. 1	101.38	101	55	30	95.56	0.94
	Cage No. 2	111.92	105	54	32	108.58	0.97
	Cage No. 3	77.33	93	51	27	75.57	0.98
	Cage No. 4	71.08	95	49	26	71.36	1.00
H1	Cage No. 1	99.11	99	51	29	97.53	0.98
	Cage No. 2	58.79	95	49	23	56.92	0.97
	Cage No. 3	78.30	96	50	27	75.04	0.96
	Cage No. 4	88.84	99	52	28	89.2	1.00
H2	Cage No. 1	102.84	106	58	29	99.02	0.96
	Cage No. 2	76.84	100	52	27	73.43	0.96
	Cage No. 3	73.16	101	51	22	70.6	0.97
	Cage No. 4	70.65	97	48	25	68.19	0.97
H3	Cage No. 1	89.06	105	54	27	84.9	0.95
	Cage No. 2	91.36	105	57	27	89.78	0.98
	Cage No. 3	76.54	97	50	27	74.96	0.98
	Cage No. 4	62.94	91	48	25	60.85	0.97
H4	Cage No. 1	71.87	92	48	24	71.17	0.99
	Cage No. 2	97.37	104	60	30	91.01	0.93
	Cage No. 3	78.72	94	49	27	77	0.98
	Cage No. 4	78.80	100	50	26	77.18	0.98
H5	Cage No. 1	99.63	107	59	29	98	0.98
	Cage No. 2	82.38	102	54	29	79.17	0.96
	Cage No. 3	93.95	105	54	28	92.17	0.98
	Cage No. 4	59.08	91	46	23	58.193	0.98
H6	Cage No. 1	86.78	101	50	27	81.68	0.94
	Cage No. 2	79.57	96	51	30	75.8	0.95
	Cage No. 3	79.56	101	51	25	77.41	0.97
	Cage No. 4	75.75	98	51	25	74.1	0.98
H7	Cage No. 1	87.75	100	51	28	85.58	0.98
	Cage No. 2	92.28	99	55	30	89.54	0.97
	Cage No. 3	87.52	102	51	26	85.56	0.98
	Cage No. 4	76.51	94	50	25	74.86	0.98
H8	Cage No. 1	99.67	107	56	27	96.14	0.96
	Cage No. 2	67.62	96	49	26	66.23	0.98
	Cage No. 3	73.50	101	48	25	71.24	0.97
	Cage No. 4	65.86	93	49	25	64.06	0.97

Table 7.3. Summary of tritium concentrations in Perch Lake surface waters (provided as model input data) [64].

Time After Mussel Transplantation	Cage Numbers	Arithmetic Mean HTO in Water (Bq/L)	Standard Error	n	Minimum	Maximum
0 hours (all cages)	Cages 1 and 2	4796	26.9	6	4689	4880
	Cages 3 and 4	4698	27.7	6	4636	4799
1 hour (all cages)	Cages 1 and 2	4766	23.8	6	4685	4830
	Cages 3 and 4	4749	30.3	6	4646	4844
2 hours (all cages)	Cages 1 and 2	4664	31.7	6	4575	4795
	Cages 3 and 4	4713	19.7	6	4638	4766
4 hours (all cages)	Cages 1 and 2	4681	22.5	6	4598	4747
	Cages 3 and 4	4724	26.9	6	4660	4835
7 hours (all cages)	Cages 1 and 2	4712	29.9	6	4611	4804
	Cages 3 and 4	4686	29.9	6	4566	4769
19 hours (all cages)	Cages 1 and 2	4783	19.1	6	4716	4840
	Cages 3 and 4	4368	18.9	6	4329	4456
24 hours (all cages)	Cages 1 and 2	4731	25.5	6	4677	4832
	Cages 3 and 4	4441	23.5	6	4371	4522
48 hours (all cages)	Cages 1 and 2	4698	27.7	6	4636	4799
	Cages 3 and 4	4476	49.9	6	4329	4648
96 hours (all cages)	Cages 1 and 2	4629	15.9	6	4597	4699
	Cages 3 and 4	4583	30.9	6	4526	4722
8 days (all cages)	Cages 1 and 2	4690	15.2	6	4634	4749
	Cages 3 and 4	4323	33.2	6	4200	4431
14 days (all cages)	Cages 1 and 2	4416	33.4	6	4298	4533
	Cages 3 and 4	4163	12.8	6	4128	4212
18 days (Cages 1 and 2)	Cages 1 and 2	4352	21.3	6	4276	4438
19 days (Cages 3 and 4)	Cages 3 and 4	4417	14.6	6	4374	4470
25 days (Cages 1 and 2)	Cages 1 and 2	4367	19.3	6	4299	4420
27 days (Cages 3 and 4)	Cages 3 and 4	4093	24.5	6	3985	4143
36 days (Cages 1 and 2)	Cages 1 and 2	4298	33.2	6	4191	4393
35 days (Cages 3 and 4)	Cages 3 and 4	4231	29.3	6	4150	4328
42 days (Cages 1 and 2)	Cages 1 and 2	4130	16.8	6	4079	4182
41 days (Cages 3 and 4)	Cages 3 and 4	4048	20.6	6	3977	4094
[a] 77 days	Perch Lake	4065	15.3	3	4038	4091
86 days (Cages 1 and 2)	Cages 1 and 2	3985	35.4	4	3930	4088
84 days (Cages 3 and 4)	Cages 3 and 4	4025	23.9	4	3955	4062

Measurement error for HTO was <1%.

[a] Triplicate water samples were collected in the area where the plankton samples were taken. Water data are likely representative of a well-mixed condition in the lake.

Table 7.4. Summary of tritium concentrations in Perch Lake sediments (provided as model input data) [64].

Time After Mussel Transplantation	Cage Numbers	Arithmetic Mean HTO in Sediments (Bq/L) ± Standard Error [n]	OBT ± Counting Error
0 hours (all cages)	Cages 1 and 2	n.a.	n.a.
	Cages 3 and 4	4303 ± 7.0 [2]	1020 ± 26
1 hour (all cages)	Cages 1 and 2	3944 ± 17.5 [2]	994 ± 23
	Cages 3 and 4	n.a.	n.a.
2 hours (all cages)	Cages 1 and 2	n.a.	n.a.
	Cages 3 and 4	n.a.	n.a.
4 hours (all cages)	Cages 1 and 2	n.a.	n.a.
	Cages 3 and 4	n.a.	n.a.
7 hours (all cages)	Cages 1 and 2	n.a.	n.a.
	Cages 3 and 4	n.a.	n.a.
19 hours (all cages)	Cages 1 and 2	4020 ± 5.0 [2]	700 ± 7
	Cages 3 and 4	3828 ± 26.0 [2]	1248 ± 50
24 hours (all cages)	Cages 1 and 2	n.a.	n.a.
	Cages 3 and 4	n.a.	n.a.
48 hours (all cages)	Cages 1 and 2	n.a.	n.a.
	Cages 3 and 4	n.a.	n.a.
96 hours (all cages)	Cages 1 and 2	n.a.	n.a.
	Cages 3 and 4	n.a.	n.a.
8 days (all cages)	Cages 1 and 2	3956 ± 37.0 [2]	571 ± 9
	Cages 3 and 4	3820 ± 25.0 [2]	1403 ± 66
14 days (all cages)	Cages 1 and 2	n.a.	n.a.
	Cages 3 and 4	n.a.	n.a.
18 days (Cages 1 and 2)	Cages 1 and 2	n.a.	n.a.
19 days (Cages 3 and 4)	Cages 3 and 4	n.a.	n.a.
25 days (Cages 1 and 2)	Cages 1 and 2	n.a.	n.a.
27 days (Cages 3 and 4)	Cages 3 and 4	3885 ± 9.0 [2]	1159 ± 33
36 days (Cages 1 and 2)	Cages 1 and 2	3830 ± 27.5 [2]	704 ± 17
35 days (Cages 3 and 4)	Cages 3 and 4	n.a.	n.a.
42 days (Cages 1 and 2)	Cages 1 and 2	n.a.	n.a.
41 days (Cages 3 and 4)	Cages 3 and 4	n.a.	n.a.
86 days (Cages 1 and 2)	Cages 1 and 2	n.a.	n.a.
84 days (Cages 3 and 4)	Cages 3 and 4	3557 ± 28.3 [2]	1829 ± 28 (Cage 3) 1981 ± 57 (Cage 4)
All Data	**Cages 1 and 2**	**3937 ± 28 [8]**	**742 ± 89 [4]**
	Cages 3 and 4	**3879 ± 91 [10]**	**1440 ± 157 [6]**

n.a. – data not available, since only a subset of sediment samples were analyzed.

Table 7.5. Summary of HTO and OBT concentrations measured in mussel soft tissues following transplantation from a background location on the Ottawa River to Perch Lake.

Time After Mussel Transplantation	Time (days)	Cage Numbers	Measured HTO (Bq/L) ± Standard Error	Measured OBT (Bq/L) ± Counting Error
0 hours	0	not applicable	< 10	45
1 hour	0.04	Cages 1 and 2	4425 ± 5.8	168 ± 1
		Cages 3 and 4	3042 ± 22	134 ± 7.5
2 hours	0.08	Cages 1 and 2	4599 ± 23	150 ± 7
		Cages 3 and 4	4382 ± 13	244 ± 11.5
4 hours	0.17	Cages 1 and 2	4501 ± 27	176 ± 19
		Cages 3 and 4	4472 ± 25	231 ± 30
7 hours	0.29	Cages 1 and 2	4594 ± 22	159 ± 1
		Cages 3 and 4	4422 ± 14	233 ± 14
19 hours	0.79	Cages 1 and 2	4515 ± 9.8	208 ± 16
		Cages 3 and 4	4231 ± 9.2	217 ± 10.5
24 hours	1	Cages 1 and 2	4131 ± 44	227 ± 7
		Cages 3 and 4	4205 ± 27	201 ± 9.5
48 hours	2	Cages 1 and 2	4481 ± 15	879 ± 29
		Cages 3 and 4	4151 ± 9.8	934 ± 138
96 hours	4	Cages 1 and 2	4126 ± 19	802 ± 89
		Cages 3 and 4	4379 ± 17	1090 ± 36.5
8 days	8	Cages 1 and 2	4147 ± 8.1	1013 ± 55
		Cages 3 and 4	3796 ± 12	1236 ± 268.5
14 days	14	Cages 1 and 2	4050 ± 11	1147 ± 42
		Cages 3 and 4	3951 ± 17	999 ± 114
18 days	18	Cages 1 and 2	4078 ± 20	1198 ± 230
19 days	19	Cages 3 and 4	4209 ± 26	1330 ± 11.5
25 days	25	Cages 1 and 2	4234 ± 31	1179 ± 102
27 days	27	Cages 3 and 4	3904 ± 18	1498 ± 80
36 days	36	Cages 1 and 2	4185 ± 13	1657 ± 186
35 days	35	Cages 3 and 4	4008 ± 13	1809 ± 54
42 days	42	Cages 1 and 2	3936 ± 19	1844 ± 132
41 days	41	Cages 3 and 4	3880 ± 13	1900 ± 90.5
86 days	86	Cages 1 and 2	3791 ± 21	1206 ± 125
84 days	84	Cages 3 and 4	3745 ± 16	1016 ± 68.5

Two sets of exposure conditions were established in Perch Lake. These included exposure to tritium via the surface water pathway only (Cages 1 and 2), and exposure via both sediments and surface water (Cages 3 and 4). Cages 1 and 2 were positioned on cement blocks at a depth of approximately 0.75 m, whereas Cages 3 and 4 were placed at the sediment-to-water interface at a depth of approximately 0.4 m. Each compartment in Cages 3 and 4 was filled with 5 to 10 cm of sandy surface sediments originating from the area surrounding the cages, a depth that enabled mussels to position themselves in an upright position with their siphons pointed upwards, as they do in natural systems. The sediments were added to the cages several hours prior to transplantation of the mussels to allow settling of any suspended particulates.

Mussel Cages 1 and 2 were deployed in Perch Lake on 5 July 2004 at 14:00 hours, whereas Cages 3 and 4 were deployed on 7 July 2004 at 14:00 hours. Upon initiation of mussel transplantation (at time 0), individuals were first transferred from the buckets containing water from the reference site to buckets containing water from Perch Lake, such that all mussels received initial tritium exposure at approximately the same time, despite the 10 to

15 minute time period required to transfer all the mussels from buckets to the numbered cage compartments.

Following transplantation into the cage compartments, mussels were visually monitored. In general, in Cages 3 and 4 (which contained sediments), mussels began positioning themselves in an upright position within five minutes of transplantation. In addition, after being placed into the cage compartments, the mussels in Cages 1 and 2 (without sediments) began filtering within less than five minutes. No mussel mortality occurred in any of the four cages over the course of the 86 to 88 day study.

Whole-mussel fresh weights were measured just prior to transplantation, as well as following mussel harvest (Table 7.2 and [64]). In general, mussels did not show increased weight gain over the course of the study, as indicated by an arithmetic mean post-harvest-to-initial mussel fresh weight ratio of 0.981. This lack of mussel growth was not surprising, since the mussels used in this study were likely 14 to 15 years old [69]. The small weight losses that were noted for some individual mussels may have been due to the fact that the mussels were processed while they were still frozen (to prevent exchange of mussel free-water tritium with the atmosphere) and some water loss may have occurred as ice was lost from mussel tissues. In addition, it is possible that some weight loss occurred as female mussels released their eggs during reproduction.

7.3.2. Generation of model input data – experimental methodologies and observations

7.3.2.1. Monitoring of water temperatures in Perch Lake

Perch Lake surface water temperatures were recorded continuously during July–October 2004 using a Model 107b Campbell Scientific Inc. Temperature Probe and data logger set to integrate values over 5 minute time intervals (Figure 7.2 and [64]). The probe was positioned in the vicinity of the mussel cages, a few centimetres above the sediment-water interface.

Surface water temperatures were provided to modellers as input to their models [64]. In general, mean monthly surface water temperatures (± standard error) of 22.3 ± 0.25 ^{o}C, 16.7 ± 0.16 ^{o}C, 14.9 ± 0.10 ^{o}C and 13.8 ± 0.03 ^{o}C were measured in Perch Lake in July, August, September and October 2004, respectively. Corresponding air temperatures measured at the ground surface showed a fairly similar trend, with mean monthly values (± standard error) of 20.1 ± 0.27 ^{o}C, 17.8 ± 0.33 ^{o}C, 16.1 ± 0.40 ^{o}C and 10.0 ± 0.38 ^{o}C, representing water-to-air temperature ratios of 1.11, 0.94, 0.93 and 1.38 for July, August, September and October, respectively (Table 7.1). Water temperature measurements were not available over the period from 11–17 September 2004, although in general, water temperature corresponded well with air temperatures (Figure 7.2), which were available when data gaps occurred for the water.

7.3.2.2. Sample collection and processing

Surface water, sediment and mussel samples were collected on an expanding time-step over the course of the study period (Tables7.3–7.5). Upon collection, mussels were immediately placed into air-tight mason jars to avoid tritium exchange with the atmosphere, and the jars containing the mussels were frozen until processing for tritium analysis could be carried out. In general, it was necessary to composite soft tissues from 3 to 4 individual mussels to reach the biomass required for HTO and OBT analysis. The mean water content of mussel tissue was 89% (by weight), with little variability among individual animals.

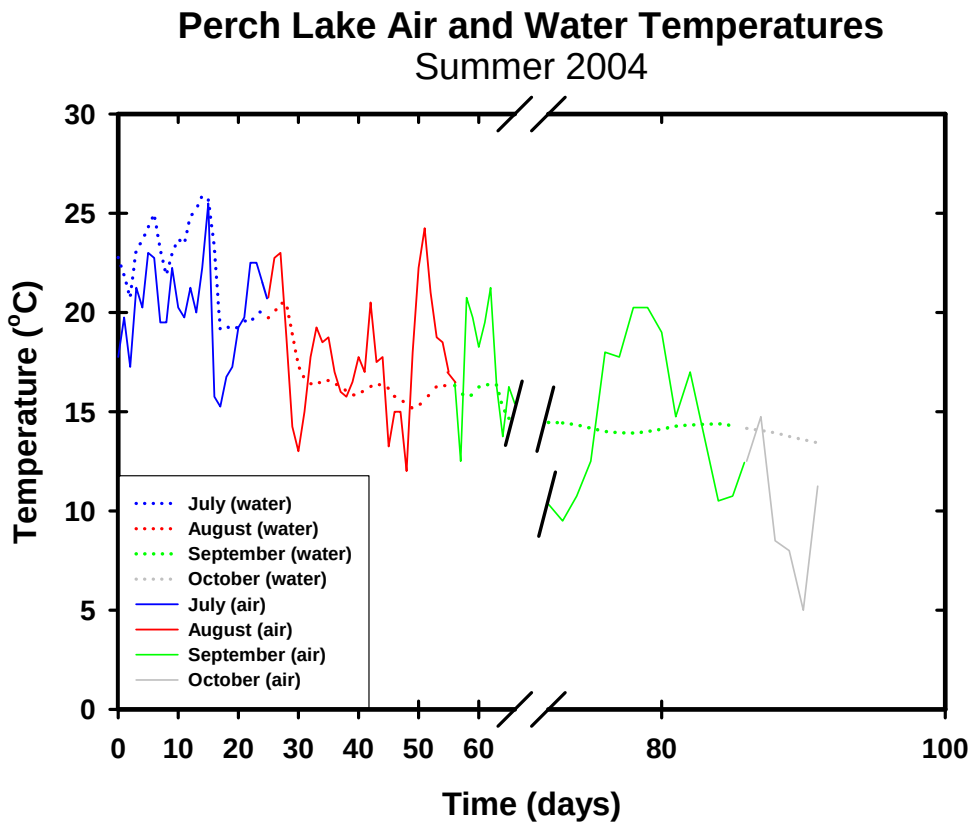

Fig. 7.2. Perch Lake surface water temperatures relative to air temperatures. Temperature measurements were not available over the period between 11 and 17 September 2004.

Both water and sediment samples were collected in triplicate at each sampling time in the vicinity of each of the mussel cages. In doing so, water sample bottles were opened at the depth where the mussels were filtering and the samples were subsequently left standing for at least 4 hours to allow suspended sediments to settle.

Sediment samples were collected by hand at a depth of 5 to 10 cm and were placed in Ziplock™ bags that were sealed at depth. Sediment porewater was extracted from a subset of these samples by freeze-drying at a pressure between 10^{-4} and 10^{-5} Torr and a temperature of 0 to -4° C, and the porewater was analyzed for HTO concentration by liquid scintillation counting (LSC). The remaining solid sediment material was washed with tritium-free water to remove the exchangeable OBT. Sediments were oven-dried until no change in mass occurred and dried sediments were combusted in a combustion tube with oxygen flow. The combustion water was analyzed by LSC to determine OBT concentrations, which served as input data for the scenario.

Plankton samples were collected in the Perch Lake water column on 20 September 2004 just offshore of the mussel cages to quantify tritium levels in mussel dietary items (as an input parameter for modeling purposes). HTO levels of 4153, 4101 and 4068 Bq/L were measured in the plankton samples. Corresponding HTO concentrations in Perch Lake surface waters at the time of plankton sampling were 4091, 4066 and 4038 Bq/L, respectively.

It was not possible to measure OBT in individual plankton samples due to the relatively large biomass required for OBT analysis and the relatively large water content present in plankton samples. As a result, OBT levels were measured in a single composite plankton sample, which had a value of 2914 ± 42 Bq/L.

7.3.2.3. Sample tritium analyses

HTO analysis

HTO concentrations were analyzed in water, sediment, mussel and plankton samples collected in 2004 (Tables7.3–7.5).

Surface water samples were analyzed for tritium in accordance with a standard procedure that has been developed by AECL (ETB-ERM-602 Rev 2.2, 1999). Briefly, 2 mL of water sample were mixed with 10 mL of Ultima Gold scintillation cocktail and placed in a 20 mL polyethylene Packard™ scintillation vial [70–72]. The samples were then counted for 30 minutes using a Beckman 6500 LSC in AECL's environmental laboratories in Building 513 (B513) at CRL. Tritium analysis of a few background samples was performed at AECL's Low Background Environmental Laboratory (Building 560, (B560)) using a Quantulus 1220 LSC (Wallac, Finland). The lower limits of detection (LLD) for the HTO measurements were approximately 1.0 Bq/L for the Quantulus and 60 Bq/L for the Beckman LSC.

The free-water (HTO) of the mussels, plankton and sediment samples was extracted using a freeze-drying system in AECL's environmental labs in B513 at CRL or in B560, depending upon the expected HTO level in a given sample. For example, mussels collected within 24 hours of transplantation were analyzed in B560, whereas other samples, including Perch Lake sediments, were analyzed in B513. The samples were loaded into vacuum flasks and exposed to dry ice traps at vacuum pressure for 24 hours. Incompletely dried samples were placed in a drying oven at 60°C for 24 hours. Tritium concentrations in the free-water were determined using the Quantulus 1220 LSC in B560 or the Beckman 6500 in B513. For the Quantulus LSC, 10 mL of water were mixed with 10 mL of Ultima Gold cocktail.

OBT analysis

Mussel and sediment dry matter remaining after the HTO analysis was chopped and homogenized using scissors and mixed with 30 to 50 mL of tritium-free-water to remove the exchangeable OBT. The samples were then refrozen and subjected to a second round of cryogenic distillation under vacuum. This process was repeated at least twice, until the tritium concentration of the rinse-water was less than 4.0 Bq/L. Most samples reached this value following the second rinse. The completely rinsed mussel samples were then combusted using a Parr bomb with pressurized oxygen. The sediment samples were combusted using a furnace type combustion tube with oxygen flow. Samples collected within 24 hours of transplantation were measured for OBT at B560. The combusted water from these samples was made up to 10 mL with tritium-depleted water and combined with 10 mL of Ultima Gold XR to measure the OBT concentrations. OBT in the remaining samples (that had been collected more than 24 hours after transplantation) were measured in B513. In such cases, 2 mL of the combustion water were mixed with 10 mL of Ultima Gold AB (Perkin-Elmer).

Counting errors for OBT concentrations were generally less than 5%, but additional uncertainty arose due to difficulties in removing exchangeable OBT from the samples and in the combustion process. The total uncertainty in the OBT measurements is estimated to be approximately 25%.

Table 7.6. Models and modellers participating in the Perch Lake uptake scenario.

Model Name	Lead Modeller	Affiliation	Country
NIRS	Kiriko Miyamoto	National Institute of Radiological Sciences (NIRS)	Japan
SRA	Masahiro Saito	Kyoto University Safety Reassurance Academy (SRA)	Japan
AQUATRIT	Dan Galeriu and Anca Melintescu	Institute of Atomic Physics and Nuclear Engineering, Horia Hulubei (IFIN-HH)	Romania
EDF	Francoise Siclet	Electricité de France (EDF)	France
BIOCHEM	Franz Baumgärtner	Technical University Munich, Institute of Radiochemistry	Germany

Table 7.7. Summary of key model assumptions.

Model Name	Country	Type of Model	No. of Compartments	Model Compartments*	Does Model Account for Water Temperature?	Does Model Assume Dietary Assimilation to Dilute OBT?
NIRS	Japan	Dynamic	3	HTO, OBT-1, OBT-2	No	No
SRA	Japan	Dynamic	3	HTO, OBT-1, OBT-2	No	Yes
AQUATRIT	Romania	Dynamic	2	HTO, OBT	No	Yes
EDF	France	Dynamic	2	HTO, OBT	No	Yes
BIOCHEM	Germany	Steady state	4	HTO, CBT, YBT, XBT	Yes	No

* HTO: free-water tritium; OBT: organically-bound tritium; CBT: carbon-bound tritium; YBT: h**y**drate-**b**ound **t**ritium; XBT: tritium that is bound to oxygen, nitrogen or sulphur atoms (representing a form of exchangeable OBT).

7.4. Model descriptions

A total of five models from Japan, Romania [73], France and Germany [4, 5, 74, 75] participated in the mussel uptake scenario (Table 7.6). The modelling teams were asked to predict temporal changes in mussel HTO and OBT concentrations, along with the 95% confidence intervals on each model prediction, using the model input data that were provided.

A summary of the key assumptions of each modelling approach is provided in Table 7.7; detailed descriptions of each model can be found in Appendix II.6.

7.5. Results and discussion

7.5.1. Modelled-to-measured comparisons

7.5.1.1. Prediction of mussel HTO

Both the NIRS and SRA models under-predicted HTO uptake rates over the initial 8 days of the study period, after which the values predicted by NIRS fell within 1.04 to 1.23 fold of the measured values and the values predicted by SRA fell within 1.01 to 1.08 fold of the observations for all mussel cages (Figure 7.3).

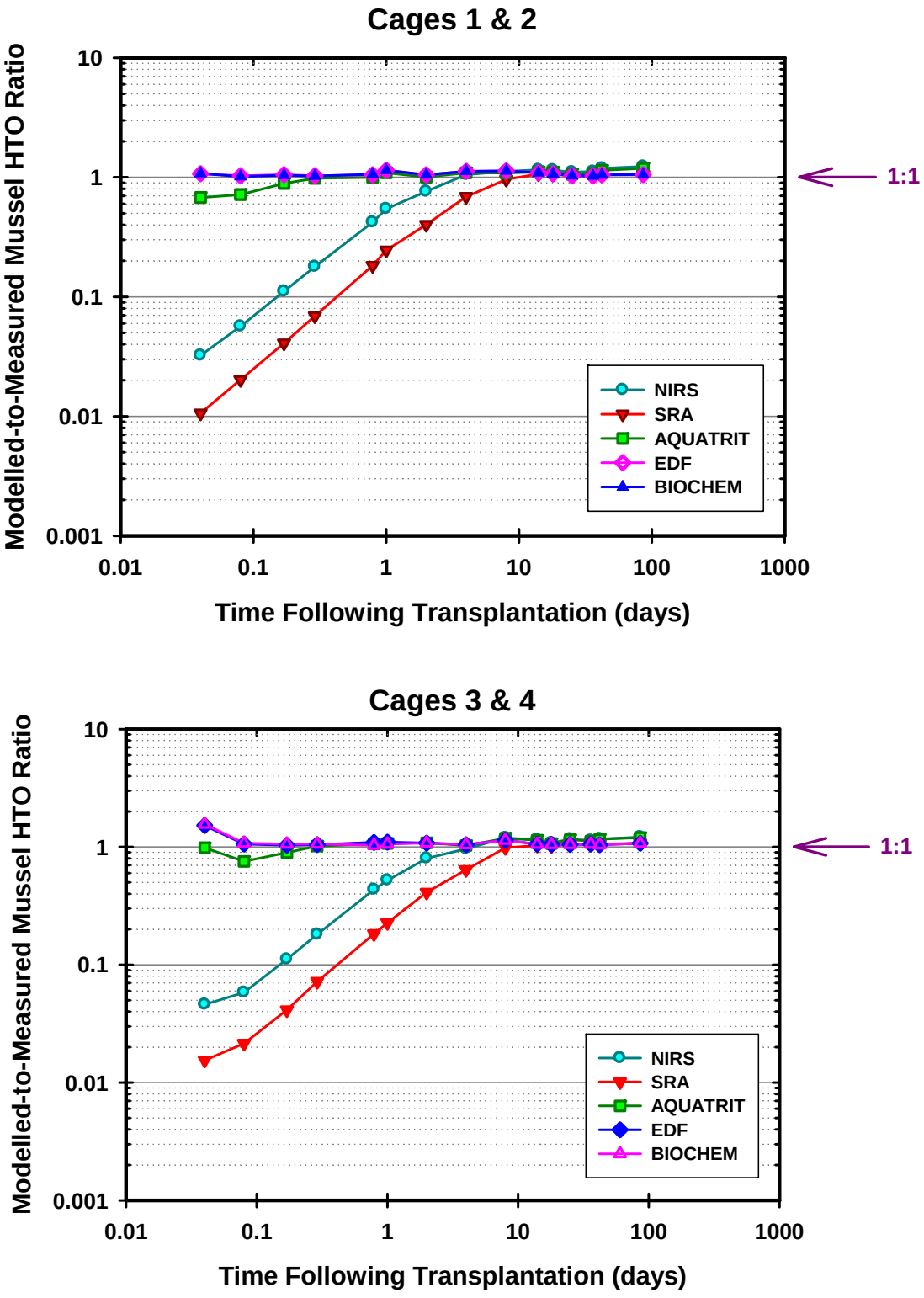

Fig. 7.3. Inter-model comparison of modelled-to-measured HTO concentration in soft tissues of transplanted mussels.

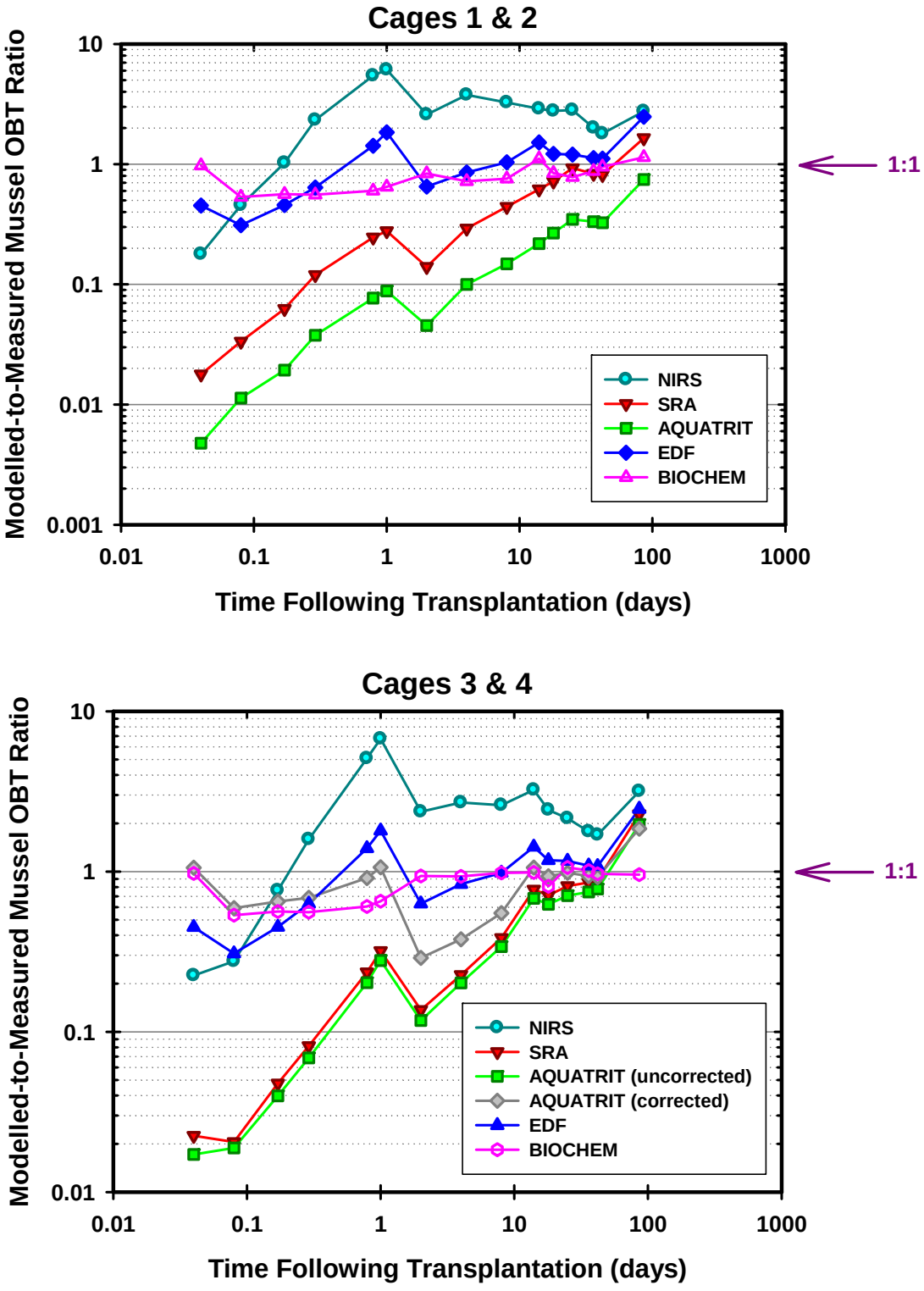

Fig. 7.4. Inter-model comparison of modelled-to-measured OBT concentration in soft tissues of transplanted mussels. Uncorrected values predicted by the AQUATRIT model do not account for elevated tritium concentrations in mussel dietary items in Perch Lake, whereas corrected values assume that mussels are feeding on food with tritium levels that are at steady state with Perch Lake HTO levels.

By comparison, mussel HTO concentrations that were predicted using AQUATRIT were very close to measured values at all sampling time points, with modelled-to-measured ratios that ranged from 0.7 to 1.2 (for Cages 1 and 2) and from 0.8 to 1.2 (for Cages 3 and 4) (Figure 7.3).

With the exception of the one hour time point for Cages 3 and 4 (for which predicted values were approximately 1.5 fold higher than measured values), the EDF model showed good predictive power throughout the study, with modelled-to-measured ratios that ranged from 1.03 to 1.15. Similarly, with the exception of the Cage 3 and 4 one hour time point (which showed a modelled-to-measured ratio of 1.6), the BIOCHEM model predictions fell within 1.01 to 1.15 fold of the measured values.

7.5.1.2. Prediction of mussel OBT

The NIRS model initially under-estimated mussel OBT concentrations by 2 to 6 fold, then over-estimated the measured values by 2 to 7 fold, and finally began to approach the measured values 36 after transplantation (Figure 7.4).

The SRA model also initially under-estimated OBT until approximately 14 days (for Cages 3 and 4) to 18 days (for Cages 1 and 2) had passed, after which predicted values fell close to measured values. Between 18 and 42 days, modelled-to-measured OBT ratios lay between 0.7 and 0.9 for all mussel cages, although SRA slightly over-estimated mussel OBT concentrations on Day 86, showing modelled-to-measured ratios of approximately 1.7 (for Cages 1 and 2) and 2.3 (for Cages 3 and 4), respectively (Figure 7.4).

OBT concentrations in mussels receiving tritium exposure via water only (i.e., Cages 1 and 2) were under-estimated by the AQUATRIT model until almost the end of the study period by factors of 210 after 1 hour to 1.3 after 86 days (Figure 7.4). By comparison, in general, AQUATRIT OBT predictions for mussels exposed to tritium via both water and sediments (Cages 3 and 4) were closer to measured values, particularly when it was assumed that mussels were feeding on food (e.g., plankton) that was at steady state with respect to HTO levels in Perch Lake. Predictions based on this assumption are reflected by the 'corrected' OBT predictions for the AQUATRIT model, whereas 'uncorrected' OBT predictions do not account for the presence of tritium in the mussel food source (Figures 7.4 and 7.5). In general, uncorrected OBT predictions for mussels receiving tritium exposure via water plus sediments had modelled-to-measured OBT concentrations that fell between 0.02 and 0.8 (excluding the 86 day time point, which was over-estimated by most models), whereas those that had been corrected for food based on Perch Lake HTO concentrations ranged from 0.3 to 1.06 (Figure 7.4).

OBT concentrations were under-estimated by the EDF model by approximately 2 to 3 fold during the first four hours following transplantation. Thereafter, EDF model predictions were very close to measured values and remained so until the last data point, which was over-estimated by most models.

Over the first day, the BIOCHEM model initially slightly under-estimated mussel OBT concentrations by factors of approximately 1.5 to 2 fold (Figure 7.4). After the first day, modelled-to-measured OBT ratios of 0.7 to 1.1 were predicted by BIOCHEM.

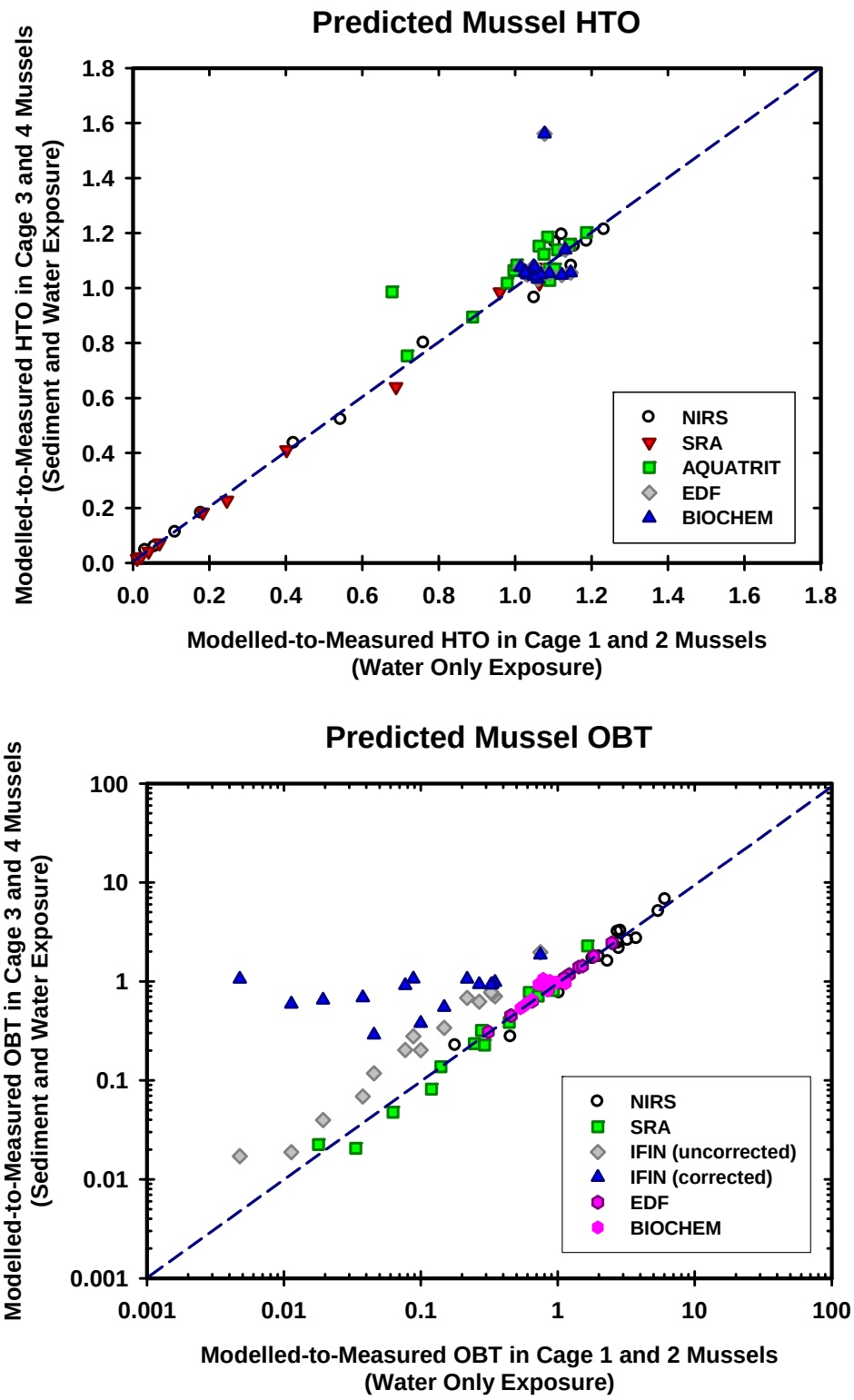

Fig. 7.5. Inter-model comparison of modelled-to-measured HTO and OBT concentrations for mussels in Cages 1 and 2 relative to those for mussels in Cages 3 and 4. Cage 1 and 2 mussels received tritium exposure from the water pathway only. Cage 3 and 4 mussels received tritium exposure from both the sediment and water pathways.

7.5.1.3. Inter-model comparisons

It is not only important to appraise the similarities and differences in predicted HTO and OBT concentrations at a given time point, but also the rate of increase of these concentrations over time. This was done through linear regression analysis (Tables 7.8 and 7.9). In addition, analysis of covariance (ANCOVA) was conducted to test whether or not there were significant differences in slope (which reflects the rate of change of modelled-to-measured HTO or OBT concentration in mussel tissues with time after transplantation).

7.5.2. Tritium dynamics

7.5.2.1. Mussel HTO dynamics

With the exception of the BIOCHEM model predictions, no statistically significant difference in mussel HTO concentration was predicted between mussels receiving tritium exposure from water only (in Cages 1 and 2) or from water plus sediments (in Cages 3 and 4) (Table 7.8).

For the initial time period when the observed rate of change of HTO concentration was relatively constant, EDF and BIOCHEM model results did not differ statistically in their predicted rates of HTO increase for mussels receiving exposure via water only (ANCOVA, $p = 0.742$; Table 7.8; Figure 7.3). Rates of HTO increase in Cage 1 and 2 mussels were significantly different for all other models, with slopes of 0.97, 0.88, 0.15, 0.037 and 0.029 for the SRA, NIRS, AQUATRIT, BIOCHEM and EDF models, respectively (Table 7.8).

Similarly, for mussels that had been exposed to tritium via both water and sediments (in Cages 3 and 4), the initial rates of HTO increase in mussel soft tissues differed significantly between all models (ANCOVA, $p \leq 0.0224$), with slopes of 0.94, 0.87, 0.13, 0.037 and –0.010 for the SRA, NIRS, AQUATRIT, EDF and BIOCHEM models, respectively (Table 7.8).

In addition, it is interesting to note that for all models, the rate of HTO increase between the 1 hour and 2 hour time points was predicted to occur relatively more slowly in mussels that received tritium exposure via both water and sediments than for mussels that were exposed to tritium via water only (Figure 7.3).

7.5.2.2. Mussel OBT dynamics

Although all models tended to predict similar final mussel HTO concentrations regardless of whether mussels received tritium exposure from water only or from water and sediments, the same was not necessarily true for all models with respect to the prediction of mussel OBT (Figure 7.4).

Water-only pathway

In most cases, the predicted patterns of mussel OBT formation for exposure to water only (Cages 1 and 2) were similar among all models (Figure 7.4). Despite this similarity, however, the initial rates of OBT formation and the initial OBT concentrations in mussel tissues often greatly differed among the models, as reflected by relatively large differences in the y-intercepts on plots of OBT concentration versus time (Table 7.9). For example, although the initial rates of OBT increase did not significantly differ for the AQUATRIT and BIOCHEM models, BIOCHEM estimated an initial mussel OBT concentration of 0.63 one hour after transplantation, compared to a y-intercept value of 0.08 for AQUATRIT. This represents an 8 fold difference between the initial OBT predictions of the two models. This suggests that the initial conditions assumed by a particular model can play a significant role in determining the initial concentration and possibly the predicted rate of increase in the concentration.

Table 7.8. Summary of outcomes of linear regression and Analysis of Covariance (ANCOVA) analyses for modelled-to-measured initial rate of HTO uptake by mussels following transplantation into Perch Lake.

Model	CageNos.	Linear Regression Analysis: Range Considered in Linear Regression		$LOG\left(\frac{Predicted\,[HTO]_{mussel}}{Measured\,[HTO]_{mussel}}\right) = m \cdot LOG(time) + b$			Analysis of Covariance (ANCOVA)	
		Start Time (days)	End Time (days)	Slope, m	y-intercept, b	r^2 -value	p-value	Interpretation
NIRS	1 and 2	0.04	1	0.876	-0.277	99.96%	0.8322	[a] Equal slopes
	3 and 4	0.08	1	0.873	-0.278	99.98%		
SRA	1 and 2	0.04	1	0.969	-0.630	99.94%	0.1704	[a] Equal slopes
	3 and 4	0.08	1	0.942	-0.643	99.95%		
AQUATRIT	1 and 2	0.04	1	0.145	0.0382	92.4%	0.7388	[a] Equal slopes
	3 and 4	0.08	1	0.133	0.0451	88.1%		
EDF	1 and 2	0.08	1	0.0287	0.0398	46.1%	0.7116	[a] Equal slopes
	3 and 4	0.08	1	0.0209	0.038	65.4%		
BIOCHEM	1 and 2	0.08	1	0.0369	0.0421	64.9%	0.0288	[b] Unequal slopes
	3 and 4	0.08	1	-0.0104	0.0184	56.3%		

[a] Equal rates of HTO increase for mussels receiving exposure from sediments and water compared to mussels exposed to water only.
[b] HTO uptake rates are predicted to be marginally significantly faster for mussels exposed to HTO via water only compared to those exposed via both water and sediments.

Table 7.9. Summary of outcomes of linear regression and Analysis of Covariance (ANCOVA) analyses for modelled-to-measured initial rate of OBT formation uptake by mussels following transplantation into Perch Lake.

Model	Cage Nos.	Linear Regression Analysis: Range Considered in Linear Regression		$\text{LOG}\left(\frac{Predicted\ [OBT]_{mussel}}{Measured\ [OBT]_{mussel}}\right) = m \cdot \text{LOG}(time) + b$			Analysis of Covariance (ANCOVA)	
		Start Time (days)	End Time (days)	Slope, m	y-intercept, b	r^2 -value	p-value	Interpretation
NIRS	1 and 2	0.04	1	4.48	5.51	90.8%	0.294	[a] Equal slopes
	3 and 4	0.08	1	5.94	5.87	90.5%		
SRA	1 and 2	0.04	1	0.194	0.253	92.5%	0.210	[a] Equal slopes
	3 and 4	0.08	1	0.270	0.276	90.3%		
[c] AQUATRIT	1 and 2	0.04	1	0.062	0.080	92.6%	0.0033 (uncorr.)	[b] Unequal slopes
	3 and 4 (uncorrected)	0.08	1	0.234	0.239	89.5%	0.0013 (corr.)	[b] Unequal slopes
	3 and 4 (corrected)	0.08	1	0.411	0.987	89.3%		
EDF	1 and 2	0.08	1	1.38	1.63	91.0%	0.932	[a] Equal slopes
	3 and 4	0.08	1	1.35	1.59	91.0%		
BIOCHEM	1 and 2	0.08	1	0.090	0.626	84.6%	0.876	[a] Equal slopes
	3 and 4	0.08	1	0.095	0.630	85.2%		

[a] Equal rates of OBT increase for mussels receiving exposure from sediments and water compared to mussels exposed to water only.
[b] OBT uptake rates are predicted to be marginally significantly faster for mussels exposed to OBT via water only compared to those exposed via both water and sediments.
[c] Uncorrected values predicted by the AQUATRIT model do not account for elevated tritium concentrations in mussel dietary items in Perch Lake, whereas corrected values assume that mussels are feeding on food with tritium levels that are at steady state with Perch Lake HTO levels.

Sediment plus water pathways

Similar trends and relative OBT formation rates were found between Cages 1 and 2 (water only) and Cages 3 and 4 (water plus sediments) for most models. This suggests that the models did not predict significant differences in OBT formation, regardless of exposure pathway (Table 7.9). The exception was the two AQUATRIT runs that predicted OBT in mussels consuming uncontaminated food and food with tritium levels that reflected Perch Lake tritium concentrations.

As for HTO, for all models, the rate of OBT formation between the 1 hour and 2 hour time points was predicted to occur relatively more slowly in mussels that received tritium exposure via both water and sediments than via water only (Figure 7.4). Similar trends were also predicted by the EDF and BIOCHEM models for mussels receiving tritium exposure via water only, as indicated by the relatively less steep slope between the 1 hour and 2 hour time points compared to later times (Figure 7.4).

Evaluation of the rate of change of OBT concentration over time indicated that no significant differences in the initial rates of OBT formation occurred between the SRA and AQUATRIT models, although significant differences existed in the predictions of all other models.

In addition to the rate of change of OBT formation, it is also important to compare the initial starting conditions (or the y-intercepts) that are predicted by each model in the linear range when plotting changes in modelled-to-measured OBT concentrations in mussels over time. In general, although the rate (or slope) of OBT formation did not differ between the SRA and AQUATRIT models, the assumed starting conditions did (assuming that mussels were consuming contaminated food items), with y-intercepts of 0.276 and 0.987, respectively (Table 7.9). This suggests that, although mussel starting conditions were not assumed to be the same, the factors leading to OBT formation may have been similar. A range of y-intercepts were predicted for Cage 3 and 4 mussels by the NIRS, EDF and AQUATRIT models, with values of 5.87, 1.59 and 0.630, respectively. By comparison, similar y-intercepts were predicted by the SRA model and the AQUATRIT model run that assumed mussels were consuming uncontaminated food (Table 7.9).

7.5.3. Pathways analysis for tritium uptake by mussels

In general, with the exception of individual predictions that were made using the AQUATRIT, EDF and BIOCHEM models, mussel HTO uptake was predicted to be similar for mussels exposed to HTO via water only (in Cages 1 and 2) and those exposed via both water and sediments (in Cages 3 and 4) (Figure 7.5). In the exceptional cases, which tended to occur within the first hour of transplantation, a relatively higher HTO uptake was predicted for mussels that had been added to the cages where they had access to both sediments and water. It is possible that these mussels (which were exposed to higher suspended matter content) were initially filtering more slowly as they took time to optimally position themselves in the sediments and made use of available suspended matter, whereas mussels expose to water only began to filter more quickly upon transplantation. This may have resulted in the slight over-estimation of mussel HTO levels at the first time point predicted by the AQUATRIT, EDF and BIOCHEM models for animals exposed to water plus sediments relative to those exposed to water only.

With the exception of the two AQUATRIT model runs, predicted OBT uptake was similar when mussels were exposed to tritium via water alone compared to when they were exposed

via both water and sediments (Table 7.9; Figure 7.5). However, it is interesting to note that for all models, when mussels received tritium exposure via both water and sediment, the rate of uptake was initially predicted to be slower than when they were exposed via water only (Figures 7.3 and 7.4).

In the case of the AQUATRIT model (for both the scenario that assumed uncontaminated food and the scenario in which tritium concentrations in mussel dietary items were assumed to be at steady state with those in Perch Lake), it appears that some OBT contribution from the sediments was assumed. This suggests that predicted OBT concentrations for mussels receiving tritium exposure via both water and sediments were higher than those predicted for mussels receiving tritium exposure from water only (Figure 7.5). This concurs with the similarity in assumed initial starting conditions for tritium concentration among the models (with the exception of AQUATRIT) for Cages 1 and 2 and for Cages 3 and 4, as indicated by the similarities in the y-intercepts between the different cage conditions (Table 7.9). However, for AQUATRIT, when it was assumed that mussels consumed uncontaminated food, OBT levels in mussels that received tritium exposure via water only were proportional to those in mussels that receive exposure via both water and sediments (Figure 7.5). In comparison, such a relationship did not exist when mussels were assumed to assimilate dietary items that contained tritium at Perch Lake levels. Instead, in the latter case, it seemed that mussel OBT levels were being driven by the concentration in the sediments, and remained relatively constant with respect to changes in OBT concentrations in mussels that received exposure via water only.

7.6. Summary and conclusions

In general, a number of consistencies in model predictions, in terms of either the under-estimation or the over-estimation of measured HTO and/or OBT concentrations, were identified, as discussed in the sections that follow. Such under- and over-predictions were evaluated, to the extent possible, to determine whether they could be attributed to similarities in tritium transfer or formation coefficients leading to differences between modelled and measured values, or whether they were due to unexpected fluctuations in measured data as influenced by analytical or biological factors.

7.6.1. Under-estimates of initial tritium accumulation rates

In all cases where mussels received tritium exposure via both sediments and water and in a number of cases where exposure occurred via water only, the rate of HTO and OBT accumulation by mussels was relatively slow between the 1 hour and 2 hour sampling time points (Figures 7.3 and 7.4).

7.6.2. Over-estimates of OBT concentrations in mussels at the final time point

With the exception of the BIOCHEM model (with assumed OBT loss during reproduction) and Cage 1 and 2 mussels for AQUATRIT (which under-estimated OBT at all time points), all models over-estimated mussel OBT concentrations at the final experimental time point (Figure 7.4). Evaluation of measured data indicates that these over-estimations were likely related to unexpectedly low measured OBT levels in harvested mussels at the last sampling point [65].

These lower-than-expected OBT concentrations may be attributed to a number of factors possibly related to mussel biology. As discussed in Section 7.3.1 above, mussels selected for use in the transplantation study ranged from approximately 90 to 111 mm total shell length.

Based on available literature data on mussel length-to-age relationships [69], it is likely that the mussels collected for this study were more than 14 years old. Mussel growth typically occurs between April and September and depends upon water temperature, food availability, water currents and water chemistry. Since unionid mussels (Family Unionidae) such as *Elliptio complanata* typically reach sexual maturity between 6 and 12 years of age, it is likely that the transplanted mussels were sexually mature and, due to their relatively large size, it would be expected that the test animals were likely expending a relatively large proportion of their energy towards reproduction, as opposed to growth of somatic tissues. This could be indirectly confirmed through consideration of the mussel reproductive cycle and the mussel growth data collected over the course of the study, as well as the timing of mussel sampling with respect to the relatively sudden decline in mussel OBT at the last data point.

In terms of reproduction, unionid mussels have separate sexes. During reproduction, the unfertilized eggs are deposited into the water tubes of the gills of the females and the males release their sperm into the water column. The sperm is then drawn in by the females, allowing the eggs to become fertilized. The embryos are retained inside the females for a short period during their early stages of development, representing a period of rapid growth. Therefore, it is possible that following transplantation into Perch Lake, growing tissues, such as those of gonad tissues and mussel embryos, would incorporate tritium at a faster rate than other tissues.

Unlike other families of freshwater mussels, Unionidae are considered short-term breeders and are gravid between April and August (as opposed to long-term breeders, which fertilize their eggs in mid-summer and carry them until the following spring or summer). Mussel larvae, or glochidia, are released by females into the water column and later become a temporary, but obligatory, parasite on fish. They then leave the host fish and deposit in the lake sediments as juvenile mussels. Therefore, it is possible that OBT was formed in reproductive tissue following mussel transplantation into Perch Lake; however, with release of glochidia into the water column between mid-August (when the second last mussel sample was taken) and early October (which represented the final sampling point), mean OBT levels in the mussels declined. In addition, the fresh weights of individual mussels just prior to transplantation relative to those at time of harvest indicate a lack of growth, and in some cases, slight declines in mussel fresh weights over the course of the study, suggesting that the female mussels lost weight with the release of larvae into the water column.

7.6.3. Variability in model predictions and future work

A number of factors could potentially account for the observed differences between modelled and measured HTO and OBT concentrations in the mussels. These include differences in the assumed initial starting conditions to which the transplanted mussels were exposed; the assumed HTO transfer rate into mussel tissue (which could, in turn, be influenced by physical factors such as diffusion rates and/or concentration gradients, as well as biological properties such as mussel filtration rates); assumed OBT formation rates; the expected importance of various tritium exposure pathways in terms of the HTO and OBT inventories in mussel tissues; and/or assumptions with respect to tritium speciation in the body in key biological compartments and the relative importance of these tritium species and compartments. Such factors may or may not be captured by all models, and in cases where similar processes are assumed to occur, numerical values of relevant transfer parameters may or may not be the same between models.

Accumulation processes for OBT are complex relative to those for HTO, and can be influenced by exposure pathway (which may include OBT formation following uptake of HTO and/or direct dietary uptake), as well as physiological metabolism, whereby HTO diffuses into cells and is subsequently converted to OBT. Such OBT formation mechanisms likely depend more upon initial exposure conditions than on those that obtain later on.

Furthermore, the tritium community is becoming aware of several new issues based on the findings of HTO exposure experiments in plants. Recently, new OBT species (buried tritium and hydrate-bound tritium), as well as the distinction between different OBT formation rates (i.e., fast versus slow) have been suggested as factors that should be considered in predicting tritium doses to humans and biota [4, 5, 74, 75]. For example, the BIOCHEM model is focussed on the estimation of buried tritium, as well as physical diffusion processes that can influence OBT levels in mussel tissues. In doing so, the model assumes that contributions of carbohydrate (and carbon-bound tritium) to the total OBT inventory in mussel tissues are negligible, and that OBT uptake through dietary pathways (such as ingestion of plankton) is insignificant due to the lack of mussel growth. Although only buried tritium is considered in the BIOCHEM model, the model still over-estimates total mussel OBT concentrations. This implies that buried tritium represents the dominant form of OBT in mussels. Further experimental work is clearly required to confirm these assumptions. In addition, the uncertainty in OBT analysis is estimated to be larger than expected previously.

Such factors, as well as the way in which each model accounts for each factor, may explain the variability among model predictions, particularly for OBT. To date, only a few experiments have been designed to validate the various models and, in order to improve the understanding of tritium, and especially OBT, behaviour in abiotic and biotic environments, more scenarios and accurate datasets are required.

Future work could focus on characterization of key parameter values, such as the biological half-life of OBT, OBT formation rates over various time scales and the influence of exposure pathway on OBT accumulation, which may influence OBT concentrations in freshwater biota. Furthermore, uncertainty and sensitivity analysis, particularly for the long-term context, are required to gain additional insights into the key parameters that should be included in OBT models. However, as a necessary first step, further work is underway to gain understanding of the similarities and differences in the parameter values and the assumptions that have been applied in running the models that participated in this scenario.

CHAPTER 8. THE MUSSEL DEPURATION SCENARIO

8.1. Background and objectives

Hydrogen is ubiquitously distributed throughout the biosphere, primarily as part of water molecules. As tritium enters the environment, it exchanges with these molecules, forming tritiated water (HTO) [76–78]. In this form it is extremely mobile and able to quickly transfer between environmental compartments as part of the hydrologic cycle [79]. Due to this mobility, tritium can represent a key radionuclide in the aquatic environment, potentially contributing significantly to the doses received by aquatic biota in surface waters receiving radionuclide inputs, particularly under accidental release conditions. Following tritium uptake, aquatic biota convert HTO into organically-bound tritium (OBT), a form with a relatively slow turnover rate compared to aqueous forms. Therefore, depending on the form in which tritium is found in the body, reductions in environmental tritium concentrations may or may not lead to rapid declines in doses to aquatic organisms.

In many cases, steady-state models provide practical tools to estimate free-water tritium concentrations (and, to a lesser extent, OBT concentrations) following exposure. However, aquatic organisms are occasionally exposed to short-term, elevated tritium levels in water when tritium is released accidentally to aquatic systems. Tritium can later be eliminated by an organism once tritium concentrations have declined in the water. Depending upon the nature and the duration of such events, steady-state models may or may not be predictive of true organism concentrations. Dynamic models may be required to simulate the rates at which HTO and OBT concentrations change in an organism as conditions change and as the organism responds to those changes.

In general, the rates of HTO and OBT depuration are not well known under dynamic exposure conditions, but can be studied by transplanting biomonitoring species, such as freshwater mussels, from areas with elevated tritium concentrations to areas with relatively low tritium levels [42–44, 58]. In this way, changes in HTO and OBT concentrations can be monitored to quantify organism responses to dynamic exposure conditions. Such data can then be used to improve capabilities to predict tritium dynamics in aquatic organisms through model validation exercises.

8.1.1. Scenario objective

The objective of this scenario was to conduct a model validation exercise to compare observations and predictions of time-dependent tritium concentrations in freshwater mussels subject to an abrupt decline in ambient tritium levels. The study was designed to complement the dynamic mussel uptake scenario that was carried out by the EMRAS Tritium/C14 Working Group in 2004/2005.

8.2. Scenario description

The detailed dynamic Perch Lake mussel depuration scenario [80] can be found in Appendix I.7. The scenario focused on the prediction of dynamic tritium concentrations that were measured in freshwater Barnes mussels (*Elliptio complanata*) at discrete times following transplantation of the mussels from a site with measurable tritium levels to a site with significantly lower tritium concentrations.

8.2.1. Site descriptions

8.2.1.1. Mussel source water body (Perch Lake)

At the start of the study, Barnes mussels (*Elliptio complanata*) with total shell lengths ranging from 71 to 105 mm (geometric mean = 82.6 mm) were collected from Perch Lake, a small Canadian Shield lake that has received chronic, low-level tritium inputs over several decades from two historic upgradient Waste Management Areas (WMAs). Located on the site of Chalk River Laboratories (CRL), Perch Lake contains measurable amounts of tritium, which enters in the form of HTO via discharges through the sediments from below, as well as via two inflowing streams [66, 67].

Mussels for transplantation were collected in an area of the lake that is well-mixed, with relatively uniform tritium exposure concentrations at a given time. The mean tritium water concentration was 3539 ± 73 Bq/L at the time of mussel collection (Table 8.1;Figure 8.1).

The sediments in the vicinity of the mussel collection site are primarily sandy in nature, with some accumulation of decomposing organic matter (or gyttja). The sediments are approximately 50% water by weight.

8.2.1.2. Mussel receiving water body (Upper Bass Lake)

Upper Bass Lake, the site of the mussel transplantation, has significantly lower tritium concentrations than Perch Lake, with a mean concentration of 61.3 ± 2.8 Bq/L (Table 8.1; Figures 8.1 and 8.2). The lake (Figure 8.3) is relatively small in comparison to Perch Lake, with a surface area of approximately 55 450 m^2, or 12% of the Perch Lake area. However, Upper Bass Lake is approximately 2 fold deeper than Perch Lake, with a mean depth of 4 metres and a maximum depth exceeding 8 metres. Upper Bass Lake has a substantially smaller volume (266 405 m^3) compared to the 910 000 m^3 volume of Perch Lake.

The sediments in Upper Bass Lake are similar to those in Perch Lake, consisting of sand and gyttja, with primarily sandy sediments mixed with some organic matter in the vicinity of the mussel cages.

8.2.2. Model input data

Model input data, including initial tritium concentrations in mussel tissues and environmental media from Perch Lake (the source water body for the mussels), temporal changes in water temperatures and tritium levels in Upper Bass Lake (the mussel receiving water body), and mussel sizes both at the time of transplantation and at the time of harvest, were provided to modellers participating in the scenario, as described in the sections that follow.

Table 8.1. Free-water tritium (HTO) and/or organically-bound tritium (OBT) concentrations in surface water and Barnes mussels collected at the mussel source location in Perch Lake, as well as in resident fish inhabiting Upper Bass Lake. Values measured for freshwater Barnes mussels *(Elliptio complanata)* represent the initial tritium levels at Time 0 of the study, whereas values for largemouth bass represent the typical concentrations present in Upper Bass Lake.

Sample Type	Source	HTO (Bq/L)	OBT (Bq/L)
Surface Water	Perch Lake	3568 3644 3325 3617	n.a.
	Mean ± SE :	3539 ± 72.9	n.a.
	Mussel Transfer Buckets (originally from Perch Lake)	3581 3534 3617	n.a.
	Mean ± SE :	3577 ± 24.0	n.a.
	[a] Upper Bass Lake	61.3 ± 2.83 [59] (12 to 115)	n.a.
Sediments	Perch Lake	3000	700
	[a] Upper Bass Lake	66.0 ± 5.34 [4] (60 to 82)	26.8 ± 5.74 [4] (15 to 42)
Barnes Mussels	Perch Lake	2946 ± 8	2287 ± 25
Largemouth Bass	Upper Bass Lake	70 ± 1	122 ± 3
Perch Lake Mussel-to-Upper Bass Lake Bass Tritium Concentration Ratio:		**42**	**19**

n.a. – Not applicable.
SE – Standard Error.
[a] Arithmetic Mean ± Standard Error [n].
(Minimum to Maximum).

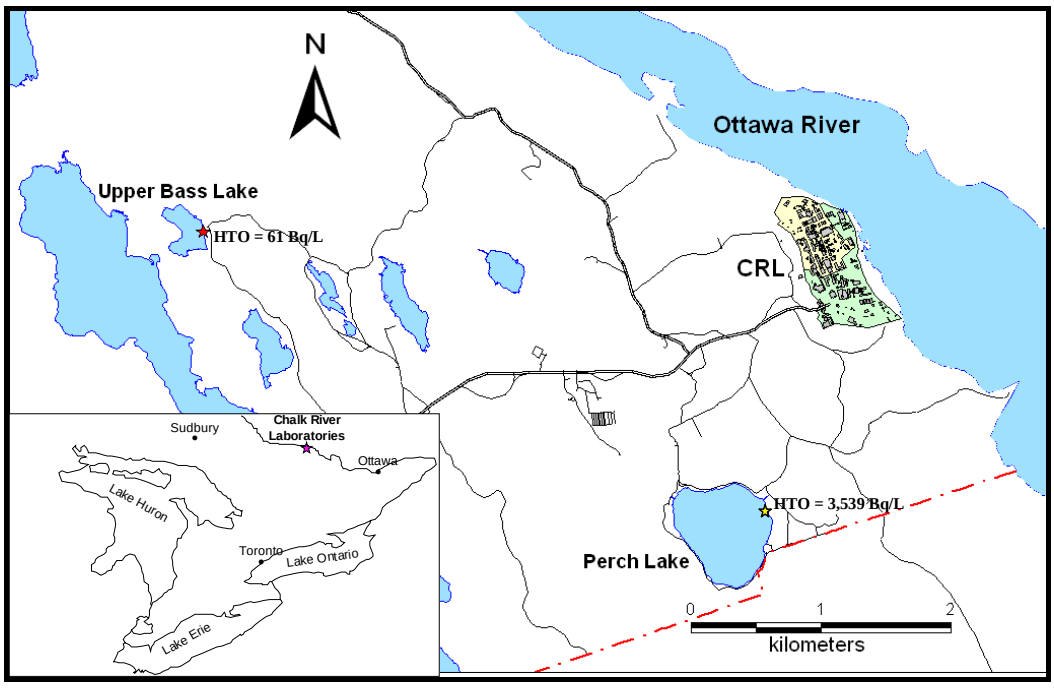

Fig. 8.1. Map depicting the source location in Perch Lake where freshwater Barnes mussels (Elliptio complanata) were collected, relative to the site of mussel transplantation in Upper Bass Lake on AECL's Chalk River Laboratories site.

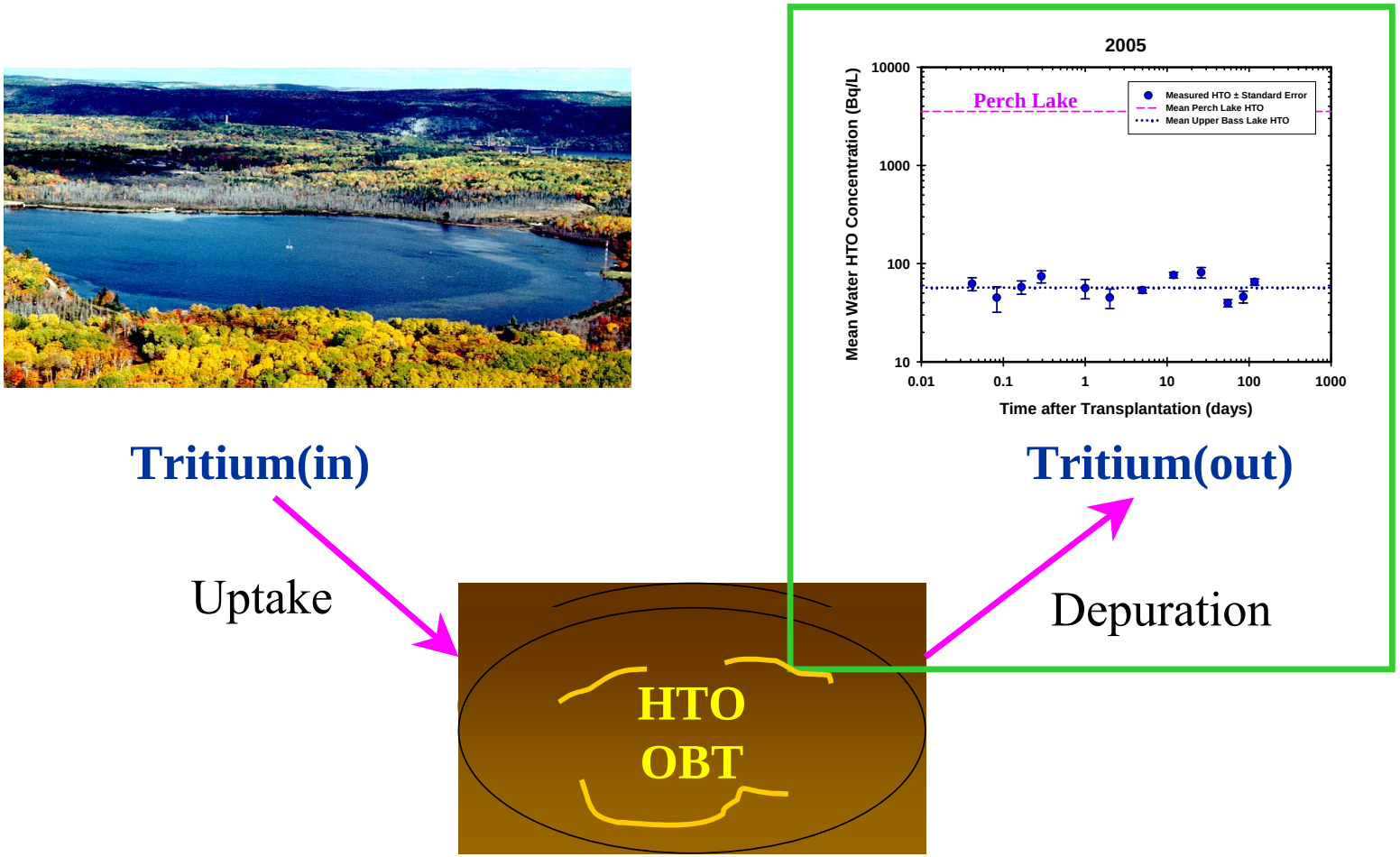

Fig. 8.2. Temporal trends in Upper Bass Lake tritium concentrations over the course of the mussel depuration study.

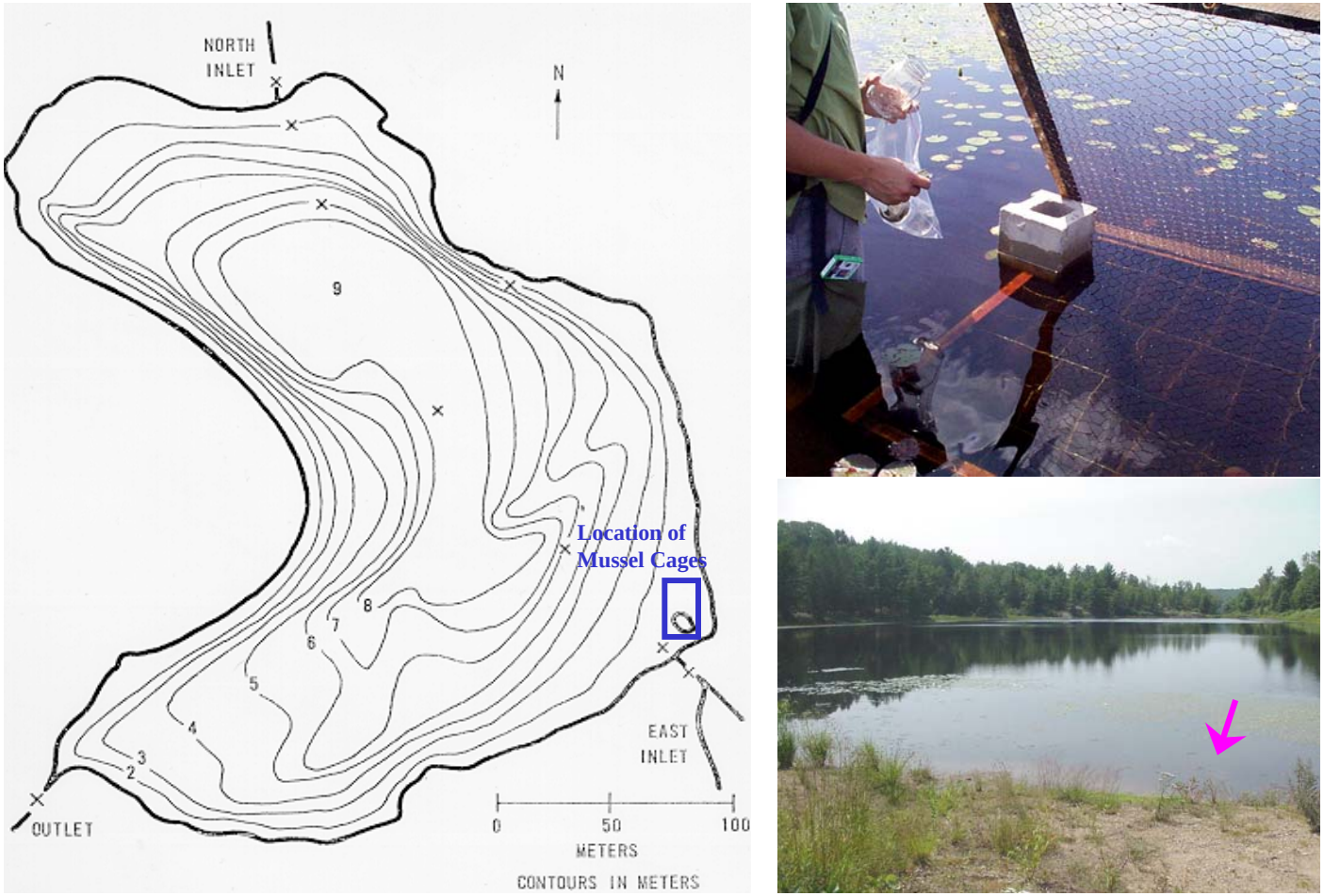

Fig. 8.3. Map of Upper Bass Lake depicting the location of inflowing and outflowing streams, depth contours (in metres) and the location of the mussel transplantation cages. The pink arrow in the bottom right panel indicates the location of the mussel transplantation cages, which are shown in detail in the upper right panel.

8.2.2.1. Perch Lake tritium levels: the initial condition

At the time of mussel collection from Perch Lake, mean HTO concentrations (± standard deviation) of 3539 ± 146 Bq/L were measured in Perch Lake surface water, with values of 3000 ± 13 and 2946 ± 8 Bq/L in sediments and mussel soft tissues, respectively (Table 8.1). Perch Lake sediments and mussels showed OBT concentrations of 700 ± 11 and 2287 ± 25 Bq/L, respectively (based on single, composite samples).

8.2.2.2. Upper Bass Lake parameter values

Steady state tritium levels in the Upper Bass Lake receiving water body

Temporal changes in tritium concentrations in Upper Bass Lake environmental media, including sediments and surface waters, were quantified over the course of the study. HTO concentrations in surface water and sediment porewater, OBT in sediment particulates, and both HTO and OBT in resident largemouth bass collected in Upper Bass Lake, are provided in Tables 8.1 and 8.2, as discussed in the sections that follow.

Surface Water: In general, HTO concentrations in the vicinity of the mussel cages did not show pronounced seasonal changes over the course of the study (Figure 8.4). With few exceptions, no significant differences in concentrations occurred between experimental time points (Table 8.2). For example, using a one-way ANOVA, no significant differences in Upper Bass Lake surface water HTO concentrations existed between measurements taken 2 hours after transplantation (45 ± 13 Bq/L), 48 hours (45 ± 10 Bq/L), 120 hours (54 ± 3.8 Bq/L), 55 days (40 ± 3.4 Bq/L) and 85 days (46 ± 6.4 Bq/L); however, notable exceptions did occur on Day 40 (95 ± 6.5 Bq/L), which showed significantly higher HTO levels than for the time points listed above, as well as on Day 12 (77 ± 5.2 Bq/L) compared to Day 55 (40 ± 3.4 Bq/L) ($p \leq 0.001$, one-way ANOVA, Holm-Sidak Multiple Pairwise Comparisons).

Sediments: Although sediments were collected in Upper Bass Lake at each sampling time, tritium concentrations were measured for only a subset of the data, including the 2 hour, 12 day, 55 day and 117 day time points (Table 8.2). HTO levels in Upper Bass Lake sediment porewaters were fairly similar at the time points when measurements were taken, showing values that varied by at most 1.4 fold between sampling times (Table 8.2 and Figure 8.4). Sediment OBT concentrations were slightly more variable, differing by a factor of approximately 1.3 to 2.8 (Figure 8.5).

Tritium in Resident Largemouth Bass: A composite sample of resident largemouth bass (a common fish species in Upper Bass Lake) collected during July 2005 showed an HTO concentration (± 1 sigma counting error) of 70 ± 1 Bq/L and an OBT concentration of 122 ± 3 Bq/L (Table 8.1). It is interesting to note that the OBT levels were approximately 1.7 times higher than the HTO concentrations. This may have been due to short time-scale fluctuations in surface water HTO concentrations, which would have been reflected almost immediately in mussel HTO levels but not in OBT concentrations. HTO levels tend to be more transient, representing a snapshot of the ambient HTO concentrations at the time when sampling was conducted [37, 38]. The larger OBT concentrations may also reflect decreased analytical sensitivity and larger uncertainties in OBT concentrations for small combustion volumes.

Table 8.2. Tritium concentrations in water, sediments and mussel tissues of Upper Bass Lake over the course of the depuration study.

Date of Mussel Sampling	Time after Mussel Transplantation	Water HTO Concentration (Bq/L)	Sediment Tritium Concentration		Mussel Tritium Concentration	
			Porewater HTO ± 1 Sigma (Bq/L)	OBT ± 1 Sigma (Bq/L)	HTO ± 1 Sigma (Bq/L)	OBT ± 1 Sigma (Bq/L)
30 June 2005 (11:00 am)	0 hour	68 59 92	n.a.	n.a.	2946 ± 8	2287 ± 25 (from Perch Lake)
30 June 2005	1 hour	48 59 80	n.a.	n.a.	817 ± 10	2847 ± 18
30 June 2005	2 hours	70 26 39	82 ± 1	42 ± 5	68 ± 2	2625 ± 42
30 June 2005	4 hours	73 58 42	n.a.	n.a.	64 ± 2	2684 ± 6 2645 ± 40
30 June 2005	7 hours	79 89 54	n.a.	n.a.	64 ± 1	2815 ± 22
1 July 2005	24 hours	33 76 60	n.a.	n.a.	65 ± 3	2605 ± 24 2593 ± 31
2 July 2005	48 hours	38 32 65	n.a.	n.a.	61 ± 1	2627 ± 15
5 July 2005	120 hours (5 days)	58 62 49 38 62 53	n.a.	n.a.	60 ± 2	2616 ± 10
12 July 2005	288 hours (12 days)	84 72 69 96 59 79	61 ± 1	15 ± 8	72 ± 4	2419 ± 9 2371 ± 29
26 July 2005	624 hours (26 days)	12 70 81	n.a.	n.a.	66 ± 1	2254 ± 9
9 August 2005	960 hours (40 days)	74 115 100 77 101 102	n.a.	n.a.	80 ± 2	1826 ± 15
24 August 2005	1320 hours (55 days)	45 49 33 31 40	60 ± 1	22 ± 7	72 ± 4	1897 ± 11 1728 ± 33
23 September 2006	2040 hours (85 days)	36 47 69 40 26 58	n.a.	n.a.	66 ± 1	1845 ± 8
25 October 2005	2808 hours (117 days)	76 61 55 51 67 81	missing	28 ± 6	59 ± 3	1621 ± 11 1530 ± 17

n.a. – measurement not available.
Measurement error of HTO was <5%.

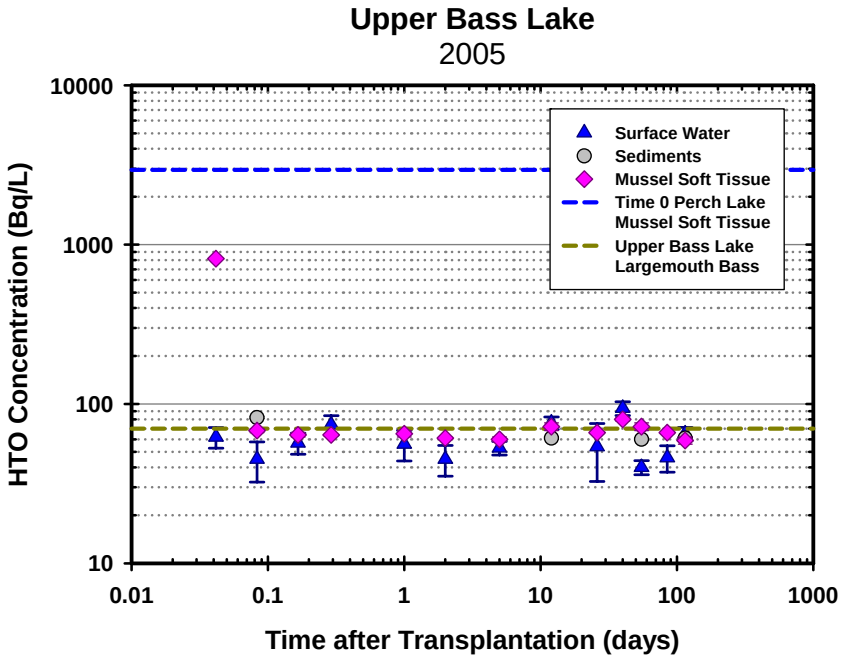

Fig. 8.4. Temporal trends in HTO concentrations in Upper Bass Lake surface waters and sediments collected in the vicinity of the mussel transplantation cages over the course of the experiment. Also shown are HTO levels in mussel soft tissues, in Perch Lake mussels just prior to transplantation (Time 0) and in Upper Bass Lake largemouth bass hypaxial muscle tissue.

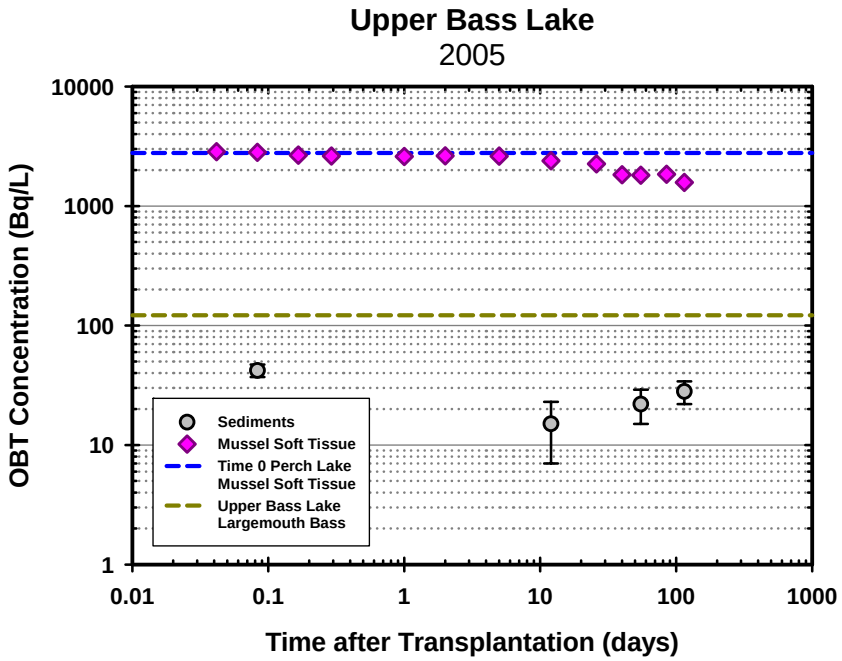

Fig. 8.5. Temporal trends in OBT concentrations in Upper Bass Lake sediments collected in the vicinity of the mussel transplantation cages over the course of the experiment. Also shown are the OBT levels in mussel soft tissues, in Perch Lake mussels just prior to transplantation (Time 0) and Upper Bass Lake largemouth bass hypaxial muscle tissue.

It was not possible to compare tritium concentrations in Upper Bass Lake Barnes mussels or other large-bodied mussel species to those collected from Perch Lake, since no large-bodied mussels have been found in Upper Bass Lake. Instead, tritium levels in largemouth bass were compared to those in Perch Lake mussels (Table 8.1). The measured HTO levels in the mussels (2946 Bq/L) were larger than those in the bass (70 ± 1 Bq/L) by a factor of 42. OBT concentrations in Perch Lake mussels (2287 Bq/L) were also higher, exceeding those measured in Upper Bass Lake largemouth bass (122 ± 3 Bq/L) by a factor of approximately 19 (Table 8.1).

Based on tritium measurements taken for resident Perch Lake biota in 2004 under steady state conditions, it is expected that tritium levels in Upper Bass Lake bass would be representative of those measured in resident mussels, if present. For example, mean HTO concentrations (± standard error) in Perch Lake mussels (4925 ± 825 Bq/L) did not significantly differ from those measured in either brown bullhead, a benthivorous fish (4663 ± 610 Bq/L) or northern pike, a piscivorous fish (4607 ± 497 Bq/L) (Table 8.3; one-way ANOVA, $p = 0.933$). Similarly, no significant differences occurred between mean OBT concentrations in Perch Lake mussels (3540 ± 270 Bq/L), bullheads (3563 ± 237 Bq/L) and pike (3763 ± 23.3 Bq/L) (Table 8.3; one-way ANOVA, $p = 1.000$). Based on this similarity in the tritium concentrations between Perch Lake fishes and mussels, it is assumed that if mussels were present in Upper Bass Lake, they would likely be comparable to largemouth bass in terms of their tritium levels.

Mussel mortality and growth

Whole-mussel fresh weights were measured just prior to mussel transplantation into Upper Bass Lake, as well as following mussel harvest [80]. In general, mussels did not show increased weight gain over the course of the 117 day tritium elimination study, as indicated by the geometric mean post-harvest-to-initial mussel fresh weight ratio of 0.98 (Table 8.4). This is not surprising since the mussels transplanted as part of this study were likely greater than 14 years old [69]. In addition, no mussel mortality occurred over the course of the transplantation experiment.

The small weight losses that were noted for some individual mussels may have been due to the fact that the mussels had been processed while they were still frozen (to prevent exchange of mussel free-water tritium with the atmosphere) and some water loss may have occurred as ice was lost from mussel tissues. In addition, it is possible that some weight loss occurred as female mussels released their eggs during reproduction.

Temporal trends in Upper Bass Lake water temperatures

Modellers were provided with Upper Bass Lake water temperatures for the period of the mussel depuration experiment, since temperature influences biological parameter values such as mussel filtration rates, growth and metabolism that could influence rates of HTO uptake and OBT formation [57, 81, 82]. Mean monthly surface water temperatures (± standard error) of 24.2 ± 0.07 ^{o}C, 25.3 ± 0.38 ^{o}C, 23.3 ± 0.31 ^{o}C, 19.8 ± 0.36 and 13.2 ± 0.55 ^{o}C were measured in Upper Bass Lake in June, July, August, September and October 2005, respectively (Table 8.5 and Figure 8.6;[80].

Table 8.3. Comparison of mussel HTO and OBT concentrations relative to those measured in benthic fish (brown bullheads) and piscivorous fish (northern pike) under steady state conditions. Animals were collected in Perch Lake in 2004.

Species	Tissue	Month	Mean HTO (Bq/L)	Mean OBT (Bq/L)
Barnes Mussel	soft tissue	May	5750	3270
(*Elliptio complanata)*	soft tissue	July	4100	3810
		Mean:	**4925**	**3540**
		Standard Error:	**825**	**270**
Brown Bullhead	head, muscle and	May	5273	3800
(*Ameirus nebulosus*)	internal organs	July	4053	3327
		Mean:	**4663**	**3563**
		Standard Error:	**610**	**237**
Northern Pike	head, muscle and	May	5103	3787
(*Esox lucius*)	internal organs	July	4110	3740
		Mean:	**4607**	**3763**
		Standard Error:	**497**	**23.3**
		Mean Mussel-to-Mean Bullhead:	**1.06**	**0.993**
		Mean Mussel-to-Mean Pike:	**1.07**	**0.941**

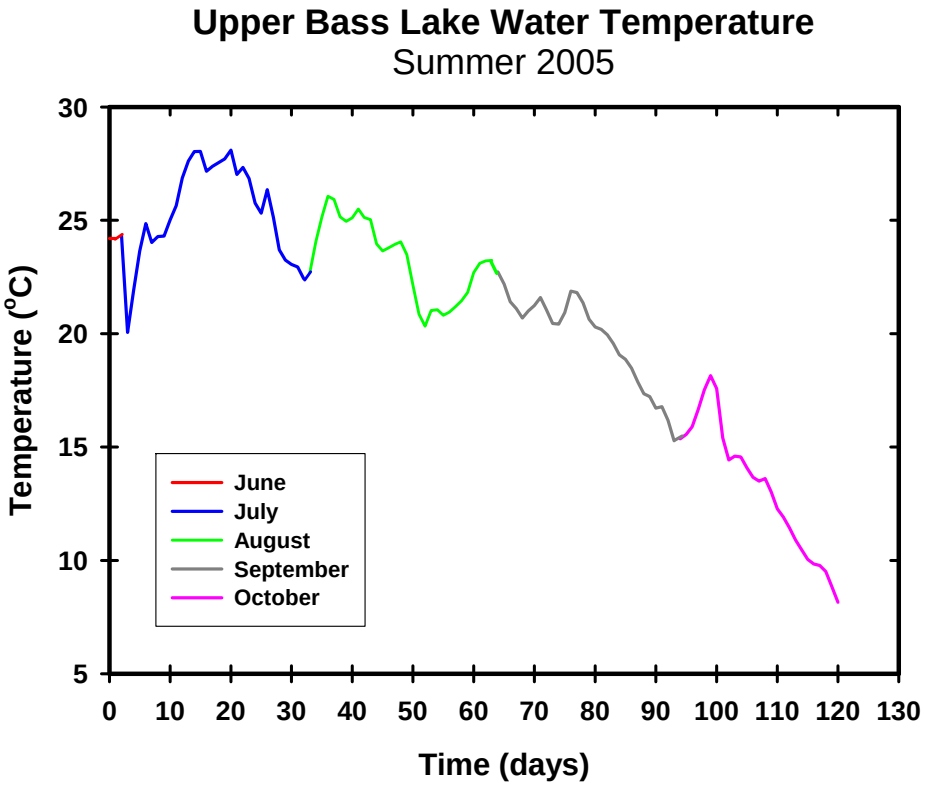

Fig. 8.6. Upper Bass Lake surface water temperatures taken between 30 June and 27 October 2005. Individual data points represent temperature values that have been integrated over 5 minute time intervals, following continuous measurement.

Table 8.4. Weight and length measurements of freshwater mussels *(Elliptio complanata)* transplanted from Perch Lake to Upper Bass Lake.

Time After Mussel Transplantation	Cage No.	Mussel No.	Initial Mussel Measurements (at Time 0)				Mussel Measurements at Harvest Time		Final-to-Initial Measurement Ratio	
			Initial Fresh Weight (g)	Initial Shell Length (mm)	Initial Shell Width (mm)	Initial Shell Height (mm)	Final Fresh Weight (g)	Final Shell Length (mm)	Fresh Weight at Harvest-to-Initial Fresh Weight Ratio	Shell Length at Harvest-to-Initial Shell Length Ratio
0 hours (from Perch Lake) 30 June 2005 11:00 am	[a] n.a.	6	n.a.	n.a.	n.a.	n.a.	39.86	78	n.a.	n.a.
	[a] n.a.	7	n.a.	n.a.	n.a.	n.a.	59.40	84	n.a.	n.a.
	[a] n.a.	8	n.a.	n.a.	n.a.	n.a.	39.74	74	n.a.	n.a.
	[a] n.a.	9	n.a.	n.a.	n.a.	n.a.	40.55	78	n.a.	n.a.
	[a] n.a.	10	n.a.	n.a.	n.a.	n.a.	33.91	71	n.a.	n.a.
1 hour (0.04 days)	2	C5	43.50	82	42	22	42.755	82	0.98	1.00
	2	D2	48.49	80	42	23	48.721	82	1.00	1.03
	3	B3	74.91	90	45	30	72.36	90	0.97	1.00
	3	D3	52.32	78	42	27	51.267	78	0.98	1.00
	4	D5	67.46	87	49	26	66.37	87	0.98	1.00
[b] 2 hours (0.08 days)	4	[c] B3	67.39	91	49	25	67.12	92	1.00	1.01
	4	[c] H5	118.34	103	51	33	117.06	103	0.99	1.00
	4	[c] B7	65.66	91	44	27	65.03	92	0.99	1.01
	2	[c] A2	78.23	92	48	28	80.53	92	1.03	1.00
	2	[c] C8	68.75	84	45	28	67.5	89	0.98	1.06
	4	[d] C2	55.06	88	46	22	54.48	87	0.99	0.88
	4	[d] E3	53.07	82	40	26	52.21	83	0.98	1.01
	4	[d] F4	38.07	72	39	21	37.123	73	0.98	1.01
	2	[d] F5	44.52	78	42	22	47.271	83	1.06	1.06
	2	[d] C8	68.75	84	45	28	67.125	78	0.98	0.93
[b] 4 hours (0.17 days)	2	[c] D5	62.76	90	46	26	61.85	91	0.99	1.01
	2	[c] A3	40.39	78	40	21	36.838	79	0.91	1.01
	2	[c] D7	49.74	83	44	25	51.443	79	1.03	0.95
	2	[c] F8	33.89	71	38	20	33.22	72	0.98	1.01
	4	[c] D4	77.75	88	45	30	75.88	89	0.98	1.01
	4	[d] A5	80.66	88	45	33	79.270	90	0.98	1.02
	3	[d] H4	54.08	79	41	22	53.590	80	0.99	1.01
	3	[d] E1	46.30	78	37	26	46.312	77	1.00	0.99
	4	[d] F8	43.14	75	40	23	40.804	76	0.95	1.01
	4	[d] E7	41.16	77	041	21	40.989	78	1.00	1.01

Table. 8.4. (Conitnued)

Time After Mussel Transplantation	Cage No.	Mussel No.	Initial Mussel Measurements (at Time 0)				Mussel Measurements at Harvest Time		Final-to-Initial Measurement Ratio	
			Initial Fresh Weight (g)	Initial Shell Length (mm)	Initial Shell Width (mm)	Initial Shell Height (mm)	Final Fresh Weight (g)	Final Shell Length (mm)	Fresh Weight at Harvest-to-Initial Fresh Weight Ratio	Shell Length at Harvest-to-Initial Shell Length Ratio
7 hours (0.29 days)	2	A6	52.38	80	41	26	52.492	80	1.00	1.00
	2	G7	41.32	71	38	23	40.834	71	0.99	1.00
	4	A2	62.21	91	46	25	61.250	91	0.98	1.00
	4	E5	82.67	98	50	27	84.36	98	1.02	1.00
	4	H8	68.86	94	46	24	68.67	96	1.00	1.02
[b] 24 hours (1 day)	3	[c] A6	63.11	89	46	26	61.870	89	0.98	1.00
	3	[c] C1	46.56	81	42	22	46.307	81	0.99	1.00
	4	[c] D8	42.00	82	40	20	40.814	82	0.97	1.00
	2	[c] E6	45.17	78	42	25	45.579	78	1.01	1.00
	2	[c] F1	47.75	80	43	24	47.291	80	0.99	1.00
	3	[d] D6	63.63	81	45	26	64.92	82	1.02	1.01
	2	[d] H2	47.79	81	43	25	46.447	82	0.97	1.01
	3	[d] G2	41.30	76	39	21	41.329	76	1.00	1.00
	4	[d] E6	73.63	91	47	28	70.37	91	0.96	1.00
	4	[d] A6	49.12	80	43	22	47.743	81	0.97	1.01
48 hours (2 days)	2	B7	56.89	81	41	25	55.164	82	0.97	1.01
	2	E1	48.14	77	38	26	47.475	76	0.99	0.99
	4	B8	43.87	79	41	22	43.936	80	1.00	1.01
	4	D7	45.46	79	42	21	45.397	79	1.00	1.00
	4	E1	60.63	87	47	26	58.488	88	0.96	1.01
120 hours (5 days)	3	C3	59.36	82	44	26	58.004	81	0.98	0.99
	3	D5	44.41	80	42	22	44.500	81	1.00	1.01
	4	B6	51.18	83	44	22	50.525	84	0.99	1.01
	4	C2	55.06	88	46	22	53.96	88	0.98	1.00
	4	E3	53.07	82	40	26	50.521	84	0.95	1.02
	4	C3	62.90	86	46	28	63.27	87	1.01	1.01

Table 8.4. (Continued)

Time After Mussel Transplantation	Cage No.	Mussel No.	Initial Mussel Measurements (at Time 0)				Mussel Measurements at Harvest Time		Final-to-Initial Measurement Ratio	
			Initial Fresh Weight (g)	Initial Shell Length (mm)	Initial Shell Width (mm)	Initial Shell Height (mm)	Final Fresh Weight (g)	Final Shell Length (mm)	Fresh Weight at Harvest-to-Initial Fresh Weight Ratio	Shell Length at Harvest-to-Initial Shell Length Ratio
[b] 288 hours (12 days)	2	[c] F3	44.15	80	40	23	43.579	80	0.99	1.00
	2	[c] C1	51.02	83	42	22	49.694	84	0.97	1.01
	2	[c] E8	64.07	87	46	26	63.86	87	1.00	1.00
	2	[c] B4	48.91	82	43	23	48.077	82	0.98	1.00
	2	[c] D4	37.26	75	38	22	36.099	76	0.97	1.01
	4	[d] G8	44.66	84	44	21	43.508	84	0.97	1.00
	3	[d] E3	58.97	86	43	27	59.349	86	1.01	1.00
	3	[d] H2	49.55	84	42	24	47.135	85	0.95	1.01
	3	[d] G5	65.34	85	48	25	65.100	87	1.00	1.02
	3	[d] H3	40.68	79	41	21	41.081	79	1.01	1.00
624 hours (26 days)	3	F3	48.89	83	43	23	47.485	83	0.97	1.00
	4	D2	42.55	80	40	21	42.583	81	1.00	1.01
	4	F7	47.69	77	40	25	46.079	78	0.97	1.01
	4	G6	100.11	105	53	30	97.420	87	0.97	0.83
	4	H3	34.99	78	39	18	35.609	78	1.02	1.00
960 hours (40 days)	2	C2	55.53	76	43	25	55.639	78	1.00	1.03
	2	D1	39.40	74	38	21	39.784	75	1.01	1.01
	2	G5	35.06	73	38	22	35.543	73	1.01	1.00
	2	H8	43.60	83	42	21	45.409	84	1.04	1.01
	3	E7	68.67	85	46	28	66.830	87	0.97	1.02
1320 hours (55 days)	2	C6	61.27	85	44	26	60.210	85	0.98	1.00
	2	E4	46.79	77	40	24	46.431	79	0.99	1.03
	3	D8	64.23	85	44	28	65.470	85	1.02	1.00
	2	A5	54.61	80	43	27	55.273	80	1.01	1.00
	3	C8	38.04	78	39	21	36.693	76	0.96	0.97
	4	B2	67.45	89	46	26	66.680	89	0.99	1.00
	3	E6	42.29	77	40	24	42.063	76	0.99	0.99
	2	A8	74.02	89	48	27	75.930	88.5	1.03	0.99

Table 8.4. (Continued)

Time After Mussel Transplantation	Cage No.	Mussel No.	Initial Mussel Measurements (at Time 0)				Mussel Measurements at Harvest Time		Final-to-Initial Measurement Ratio	
			Initial Fresh Weight (g)	Initial Shell Length (mm)	Initial Shell Width (mm)	Initial Shell Height (mm)	Final Fresh Weight (g)	Final Shell Length (mm)	Fresh Weight at Harvest-to-Initial Fresh Weight Ratio	Shell Length at Harvest-to-Initial Shell Length Ratio
2040 hours (85 days)	2	A4	60.35	83	43	25	59.30	84	0.98	1.01
	2	G8	42.05	81	41	22	39.60	82	0.94	1.01
	3	E2	55.12	83	40	27	55.99	84	1.02	1.01
	3	F4	59.15	83	46	25	59.2	84	1.00	1.01
	4	D3	62.56	85	45	28	57.4	87	0.92	1.02
[b] 2808 hours (117 days)	2	[c] E3	45.40	82	42	23	44.4	85	0.98	1.04
	2	[c] E7	45.35	77	40	24	39.4	77	0.87	1.00
	2	[c] G1	43.43	80	41	23	45.3	80	1.04	1.00
	2	[c] H3	50.60	79	42	26	46.2	79	0.91	1.00
[b] 2808 hours (117 days)	3	[c] B2	73.99	91	48	28	71.9	92	0.97	1.01
	3	[d] C6	54.23	82	41	24	56.2	83	1.04	1.01
	3	[d] G6	53.29	82	40	25	53.80	84	1.01	1.02
	4	[d] A3	47.83	79	41	22	46.3	79	0.97	1.00
	4	[d] A8	75.18	91	47	28	74.4	93	0.99	1.02

[a] n.a. – not available.
[b] Duplicate composite mussel samples taken and measured for QA purposes.
[c] Represent mussels that were included in Composite 1.
[d] Represent mussels that were included in Composite 2.

Table 8.5. Mean monthly Upper Bass Lake surface water temperatures collected over the course of the depuration study between late June and October 2005.

Month	No. of Daily Water Temperature Measurements	Mean Daily Upper Bass Lake Surface Water Temperature (^{o}C) ± Standard Error	Minimum to Maximum	Comments
June	2	24.2 ± 0.0	n.a.	Represents sampling conducted over the period between 29th and 30th June 2005.
July	31	25.3 ± 0.38	20.1 to 28.1	Represents sampling conducted over the month of July 2005.
August	31	23.3 ± 0.31	20.3 to 26.1	Represents sampling conducted over the month of August 2005.
September	30	19.8 ± 0.36	15.3 to 22.7	Represents sampling conducted over the month of September 2005.
October	24	13.2 ± 0.55	8.2 to 18.2	Represents sampling conducted over the period between October 1st and 24th, 2005.

8.2.2.3. Analysis of measured mussel cxoncentrations

Tritium depuration by transplanted mussels

As expected, HTO concentrations in mussel soft tissues rapidly decreased upon mussel transplantation into Upper Bass Lake, reaching steady state with the lake water within approximately 2 hours (or 0.08 days) (Figure 8.4 and Table 8.2). In contrast, mussel OBT loss (Figures 8.5 and 8.7) following transplantation occurred much more slowly (Figure 8.4). OBT depuration rates were initially high and then decreased, eventually levelling off 40 days after transplantation (Figure 8.7). The time-dependent mussel OBT concentration can be represented by an exponential function (Figure 8.7):

$$OBT_{mussel} = 2627 \cdot e^{-0.005 \cdot t} \ (r^2 = 87.7\%) \quad (8.1)$$

where t is time in days after transplantation.

Despite the predictable trends in both short-term and long-term HTO and OBT depuration, comparison of mussel OBT concentrations relative to mussel HTO levels did not produce any clear trends (Figure 8.8). This was not surprising due to the expected differences in the rates of HTO relative to OBT depuration by mussels.

Estimation of time to mussel equilibration

Although Barnes mussels reached steady state within approximately 2 hours with respect to HTO concentrations in Upper Bass Lake surface waters, OBT equilibration occurred over a much longer time-frame. As a result, under conditions where HTO levels have declined significantly in a freshwater ecosystem due to mitigation, remediation and/or reduced emissions, a key question arises with respect to the capacity of mussels to eliminate OBT from their tissues. In other words, how long does it take for improved environmental quality to be reflected in OBT concentrations in aquatic biota in natural ecosystems?

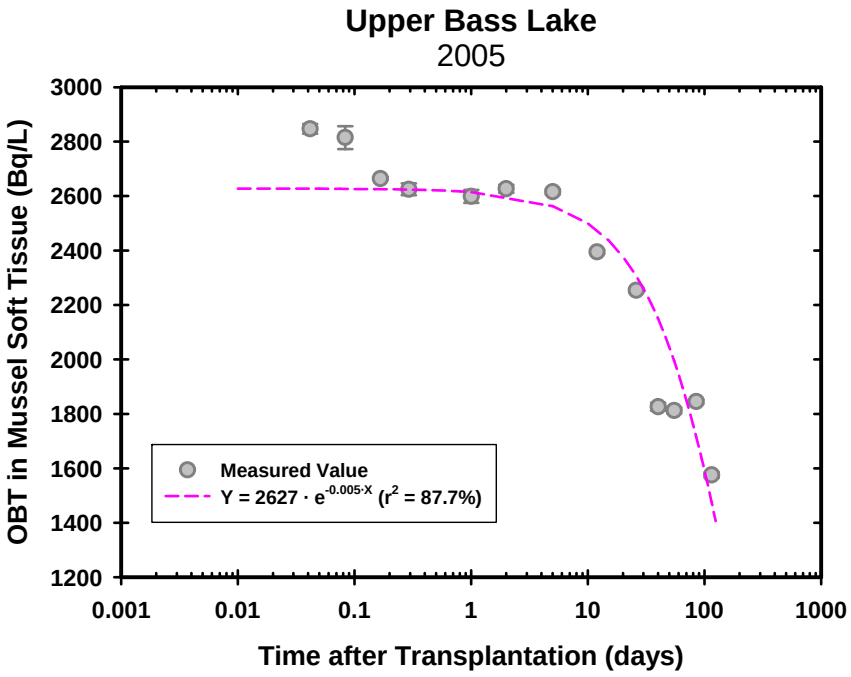

Fig. 8.7. Temporal changes in OBT concentrations in Upper Bass Lake mussels following transplantation from Perch Lake. The estimated long-term temporal decline in OBT concentrations is represented by the dashed pink line.

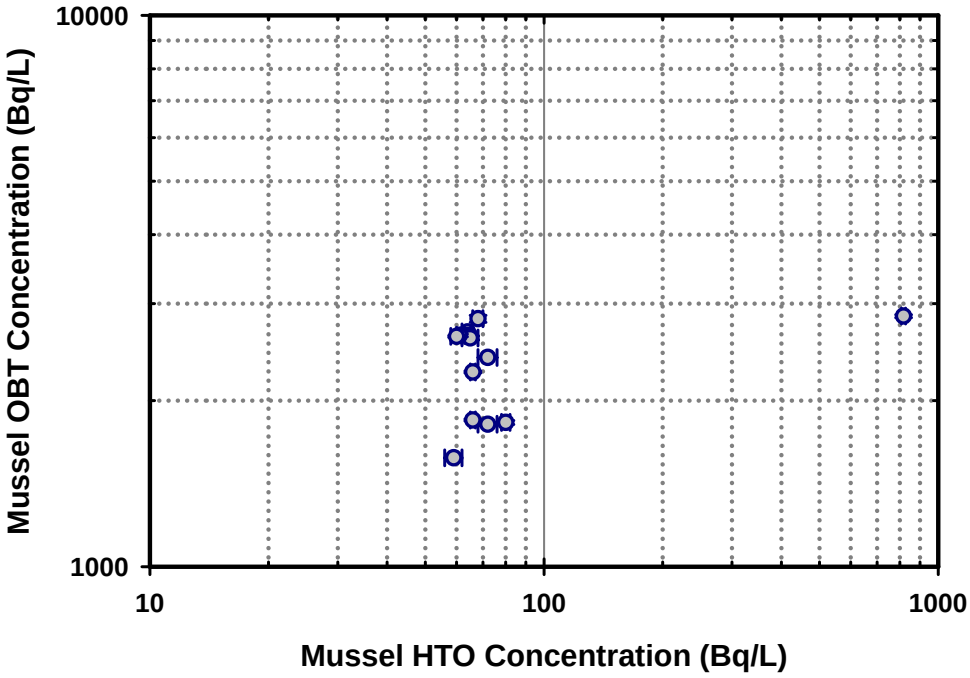

Fig. 8.8. Relationship between mussel OBT concentrations and mussel HTO concentrations measured in soft tissues over the course of the mussel depuration experiment.

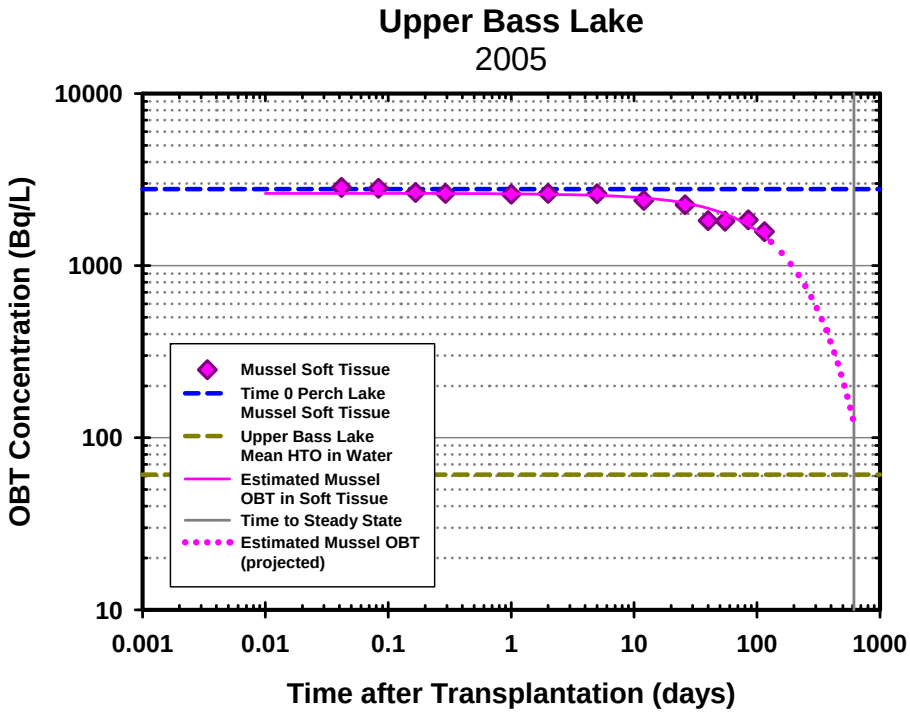

Fig. 8.9. Time required for OBT in mussels to reach equilibrium with HTO in Upper Bass Lake following transplantation from Perch Lake, as estimated using Equation (8.1). The estimated equilibration time is approximately 2 years.

OBT data collected over the course of this study show that steady state was not reached by Barnes mussels over the 117 day period following mussel transplantation (Figure 8.5). In fact, assuming that Equation (8.1) is representative of longer-term trends in OBT depuration in mussel tissues and that no significant changes in OBT levels in resident Upper Bass Lake biota occur, a period of approximately 2 years would be required for mussel OBT to reach steady state, with a 46 fold decrease in mussel OBT levels over that time (Figure 8.9 and Table 8.8). This is equivalent to a biological half-life of approximately 0.34 years (123 days).

8.3. Observations: methodologies and generation of model input data

8.3.1. Mussel transplantation

Three mussel transplantation cages were built and deployed in Upper Bass Lake in late June 2005 to quantify rates of temporal changes in HTO concentration and OBT formation in mussel soft tissues following an abrupt decrease in ambient tritium levels. The transplantation cages had dimensions of 96 cm (length) × 96 cm (width) × 12 cm (height) and were constructed using 5.08 cm × 5.08 cm cedar boards and chicken wire. Each cage was built with an 8 × 8 design, resulting in a total of 64 compartments per cage [80]. Individual cage compartments had surface areas of 12 cm × 12 cm with one animal per compartment to provide mussels with adequate space without overcrowding. Cages were placed at the sediment-to-water interface at a water depth of 0.5 to 1 metre on 29 June 2005, one day prior to mussel transplantation, to allow conditions to reach equilibrium (Figure 8.3). No sediments were added to the compartments.

Mussels were collected from Perch Lake on 30 June 2005 and placed into lidded, plastic buckets containing water from the mussel collection site to prevent tritium elimination by mussels prior to initiation of the study. Damaged or unhealthy mussels (e.g. those incapable of closing their shells) were not selected. Mussels were then transported to the laboratory on the Chalk River site. Individuals were quickly weighed and measured to quantify whole animal fresh weights and total shell lengths, widths and heights. The shell of each mussel was etched using a Dremmel™ etching tool with a unique alphanumeric code representing the cage number and compartment for tracking purposes [80]. Individual mussels were separated by placing them into labelled nylon bags. The animals were then replaced into the lidded buckets of Perch Lake water until initiation of the transplantation, which was carried out on the same day as mussel collection. Only one mussel was removed from a bucket of Perch Lake water at a time during measuring to minimize HTO exchange prior to study initiation. Concentrations of HTO and OBT in Perch Lake surface waters, in the buckets of Perch Lake water in which mussels were held during transport and measuring, and in mussels collected from the Perch Lake mussel source are provided in Table 8.1. HTO concentrations in soft tissues of the collected mussels were 2946 ± 8 Bq/L, with OBT levels of 2287 ± 25 Bq/L.

Mussel transplantation took place on 30 June 2005 at 11:00 hours. The mussels were transferred from the lidded buckets containing water from the Perch Lake source to buckets containing water from Upper Bass Lake. In this way, all mussels were introduced to the exposure conditions in Upper Bass Lake at approximately the same time, despite the 10 to 15 minute period required for mussel transfer from buckets to the numbered cage compartments.

Upon placement in the cages, the mussels began filtering within less than five minutes. No mussel mortality occurred in any of the cages over the course of the 117 day study. Algal growth, which accumulated on the cages over the course of the study, was not removed, as it did not appear to obstruct water flow within the cages.

During mussel transfer, care was taken to ensure that no Perch Lake water was spilled in the vicinity of Upper Bass Lake. Once mussels were transferred to the buckets containing Upper Bass Lake water, the lids on the Perch Lake water buckets were securely replaced and the water was later returned to Perch Lake.

8.3.2. Sample collection

Mussels were collected at each of 14 sampling times on an exponential time-step over a 117 day period (Table 8.2). Upon harvest, whole-mussel fresh weights, and shell lengths, widths and heights were measured. Mussels were then immediately placed into air-tight Mason™ jars to avoid tritium exchange with the atmosphere. The jars were then frozen until tritium analysis could be carried out. In general, it was necessary to composite soft tissues from 3 to 4 individuals to gain the biomass required for each HTO and OBT analysis. The water content of mussel tissue was approximately 89% (by weight), with little variability among individual animals.

Complementary water samples were collected in triplicate at each sampling time in the vicinity of the mussel cages at the depth where the mussels were filtering. The samples were then left standing to allow any suspended sediments to settle out prior to analysis. In addition, sediment samples were collected by hand at a depth of 5 to 10 cm from the sediment surface in the vicinity of the mussel cages at each sampling time. These were placed into Ziplock™ bags that were sealed at depth, and later transferred to air-tight Mason™ jars to prevent tritium exchange.

Four resident largemouth bass (*Micropterus salmoides*) were collected on 20 July 2005 from Upper Bass Lake by rod and reel. The bass were euthanized and dissected to sample hypaxial muscle for tritium analysis and to quantify typical HTO and OBT concentrations in Upper Bass Lake aquatic animals. Upon dissection, a composite of the muscle samples taken from the four specimens were immediately placed into an air-tight Mason™ jar and frozen until HTO and OBT analysis could be carried out.

8.3.3. Sample tritium analyses

8.3.3.1. HTO analysis

HTO concentrations were analyzed in water, sediment, mussel and largemouth bass samples collected in 2005.

Surface water samples were analyzed for tritium in accordance with a standard procedure developed by AECL. Briefly, 2 mL of water sample were mixed with 10 mL of Ultima Gold scintillation cocktail and placed in a 20 mL polyethylene Packard™ scintillation vial. The samples were then counted for 30 minutes using a Beckman 6500 Liquid Scintillation Counter (LSC) in Building 513 (B513) at CRL. Tritium analysis of the background samples was performed at the Low Background Environmental Laboratory at CRL (Building 560 (B560)) using a Quantulus 1220 LSC (Wallac, Finland). The lower limits of detection (LLD) for the HTO were approximately 1.0 Bq/L for the Quantulus and 55 Bq/L for the Beckman LSC.

The free-water of the mussel soft tissue, fish hypaxial muscle and a subset of sediment samples was extracted using a freeze-drying system in B560. The pressure during freeze-drying fell between 10^{-4} and 10^{-5} Torr and the temperature was in the range of 0 to -4^{o} C. Tritium concentrations in the free-water were determined using the Quantulus 1220 LSC in B560, where each 10-mL water sample was mixed with 10 mL of Ultima Gold LLT™ cocktail.

8.3.3.2. OBT analysis

The mussel and sediment dry matter remaining after HTO extraction was chopped using scissors and mixed with 30 to 50 mL of tritium-free water to remove the exchangeable OBT. The samples were then refrozen and subjected to a second round of cryogenic distillation under vacuum. This process was repeated at least twice, until the tritium concentration of the rinse-water was less than 4.0 Bq/L. Most samples reached this level following the second rinse. The rinsed mussel samples were then combusted using a Parr bomb with pressurized oxygen. The sediment samples were combusted using a furnace type combustion tube with oxygen flow. As for HTO analysis (Section 8.3.3.1), the combustion water from these samples was made up to 10 mL with tritium-depleted water and combined with 10 mL of Ultima Gold XR to measure the OBT concentrations. All OBT measurements were carried out at B560.

Counting errors for OBT concentrations were generally less than 10%, but additional uncertainty arose due to difficulties in removing exchangeable OBT from the samples and in the combustion process. The total uncertainty in the OBT measurements is estimated to be approximately 25%.

8.3.4. Monitoring water temperature

Surface water temperatures were provided to modellers as input to their models. Upper Bass Lake surface water temperatures were measured continuously between 29 June and 24 October 2005 using two Model 107b Campbell Scientific Inc. temperature probes. The data loggers were set to integrate values over 5 minute time intervals (Appendix I.7, Table I.7.5). The probes were positioned in the littoral zone of the lake at the sediment-water interface at a water depth of approximately 0.5 metres adjacent to the mussel cages.

8.4. Model descriptions

Four models, including NIRS from Japan, AQUATRIT from Romania [73], EDF from France and BIOCHEM from Germany [4, 5, 74, 75], participated in the scenario (Table 8.6). The modellers were asked to predict temporal changes in mussel HTO and OBT concentrations, along with the 95% confidence intervals on the predictions, using the model input data that were provided in the scenario description [80].

The assumptions for each model are listed in Table 8.7. In each case, the models were identical to those used in the mussel uptake scenario, and detailed descriptions can be found in Appendix II.6 of the final report for that scenario. Additional information on the application of the BIOCHEM model to the depuration scenario is given in Appendix II.7. Two runs of the AQUATRIT model were carried out. Mussel dietary items were assumed to be uncontaminated in Run 1, and contaminated to the same level as the Upper Bass Lake environment in Run 2.

8.5. Results and discussion

8.5.1. Modelled-to-measured comparisons

8.5.1.1. Prediction of mussel HTO

Modellers were asked to estimate tritium concentrations in mussel soft tissues at each sampling point to follow the loss of tritium over time after transplantation. As expected [39, 40], the experimental data showed that the HTO concentration in the mussels quickly reached the concentration in lake water, achieving steady state within 2 hours (e.g., Figure 8.4; Table 8.2). However, of the three models that provided estimates of mussel HTO concentrations (AQUATRIT did not submit results for this endpoint), two (NIRS and BIOCHEM) over-estimated the observations in the first few hours after transplantation and the other (EDF) under-estimated. NIRS over-estimated the time required to achieve equilibrium by about one day and BIOCHEM by about two days (Figure 8.10; Table 8.9). These deficiencies can be simply corrected by increasing the rate at which HTO is transferred from the mussel soft tissues to the water. The EDF model under-predicted the mussel HTO concentration one hour after transplantation, suggesting that the model over-estimated the rate of tritium loss by mussels by more than an order of magnitude (Figure 8.10; Table 8.9). This can be corrected by modifying model parameters such that a slower rate of HTO depuration is obtained. Once steady state was reached in mussel HTO, all models produced excellent predictions within a factor of 2 of the measured values.

Table 8.6. Models and modellers participating in the mussel depuration scenario [80].

Country	Model Name	Lead Modeller(s)	Affiliation	Predictions Made
Germany	BIOCHEM	Franz Baumgärtner	Technical University Munich, Institute of Radiochemistry	HTO and OBT
France	EDF	Francoise Siclet	Electricité de France (EDF)	HTO and OBT
Japan	NIRS	Kiriko Miyamoto	National Institute of Radiological Sciences (NIRS)	HTO and OBT
Romania	AQUATRIT	Dan Galeriu and Anca Melintescu	Institute of Atomic Physics and Nuclear Engineering, Horia Hulubei (IFIN-HH)	OBT

Table 8.7. Summary of key model assumptions.

Model Name	Country	Type of Model	No. of Compartments	Model Compartments[a]	Does Model Account for Water Temperature?	Does Model Assume Dietary Assimilation to Dilute OBT?
BIOCHEM	Germany	Steady state	4	HTO, CBT, YBT, XBY	Yes	No
EDF	France	Dynamic	2	HTO, OBT	No	Yes
NIRS	Japan	Dynamic	3	HTO, OBT-1, OBT-2	No	No
AQUATRIT	Romania	Dynamic	2	HTO, OBT	No	Yes

[a] HTO: free-water tritium; OBT: organically-bound tritium; CBT: carbon-bound tritium; YBT: hydrate-bound tritium; XBT: tritium that is bound to oxygen, nitrogen or sulphur atoms, as designated by an 'X' (which represents a form of exchangeable OBT)

Table 8.8. Estimated time required for HTO and OBT concentrations in Barnes mussels to reach equilibrium with water HTO concentrations, based on tritium bioelimination rates measured for animals transplanted from Perch Lake into Upper Bass Lake.

Parameter	[a] Steady State Mussel Tritium Concentration ± 1 Sigma Counting Error (Bq/L)	[b] Time Required to Reach Tritium Steady State	Relevant Figure(s)
HTO Concentration	70 ± 1 (bass) 61 ± 2.8 (water)	2 hours	Figure 8.4
[b] OBT Concentration	61 ± 2.8 (water)	2.1 years	Figures 8.5 and 8.9

[a] Assuming that steady-state tritium concentrations in resident largemouth bass in Upper Bass Lake are comparable to steady-state mussel tritium concentrations.

[b] Assuming that the trends depicted in Figure 8.7 are representative of trends over longer time periods. Note that Upper Bass Lake largemouth bass showed OBT levels of 122 Bq/L and were not believed to be at steady state with the lake; therefore, surface water HTO levels were used as the steady-state baseline.

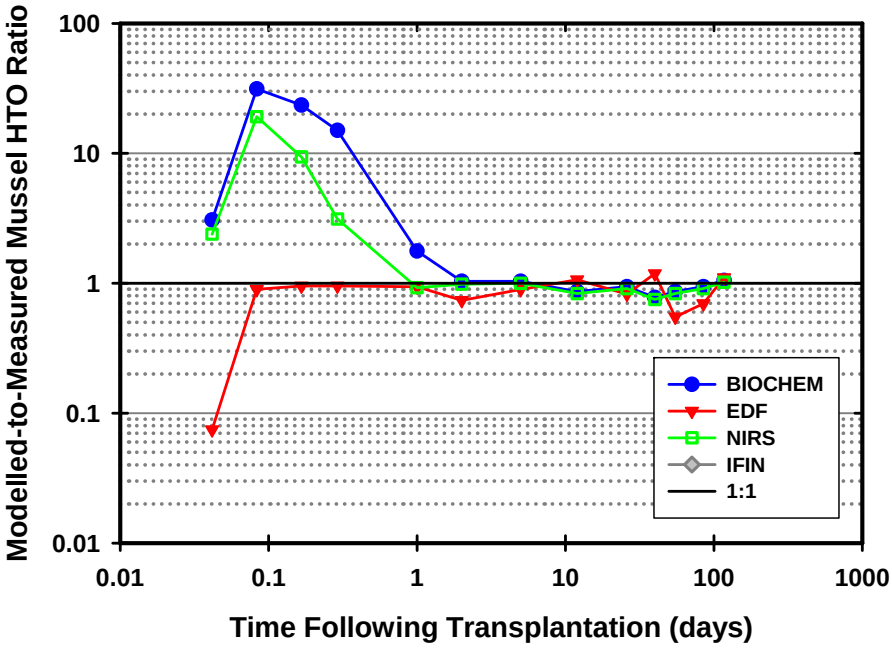

Fig. 8.10. Inter-model comparison of modelled-to-measured HTO concentration in soft tissues of transplanted mussels. IFIN did not submit results for this endpoint.

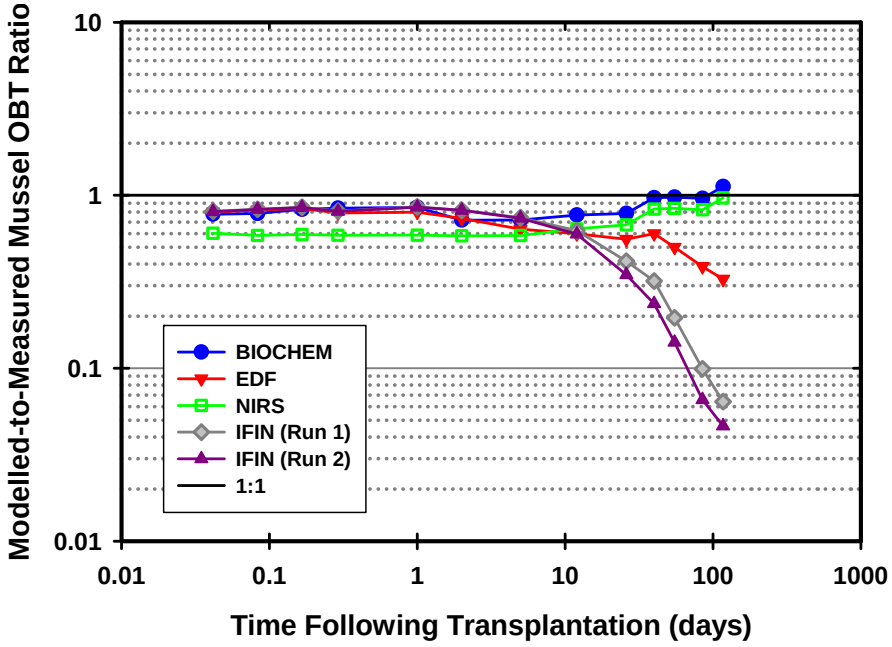

Fig. 8.11. Inter-model comparison of modelled-to-measured OBT concentrations in soft tissues of transplanted mussels. The IFIN results designated "Run 1" were obtained by assuming that mussel dietary items were uncontaminated. The results designated "Run 2" were obtained under the assumption that mussels feed on food with tritium levels at steady state with Upper Bass Lake HTO levels.

Table 8.9. Modelled-to-measured tritiated water (HTO) concentrations in mussel soft tissues at each time point over the course of the mussel depuration study.

Sampling Time (days)	Modelled-to-Measured HTO in Mussel Soft Tissue			
	BIOCHEM	EDF	NIRS	AQUATRIT
0.042	3.1	0.075	2.4	n.a.
0.083	31	0.90	19	n.a.
0.17	23	0.95	9.4	n.a.
0.29	15	0.95	3.1	n.a.
1	1.8	0.94	0.92	n.a.
2	1.0	0.74	0.98	n.a.
5	1.0	0.89	1.0	n.a.
12	0.86	1.1	0.83	n.a.
26	0.94	0.82	0.91	n.a.
40	0.78	1.2	0.75	n.a.
55	0.86	0.55	0.83	n.a.
85	0.94	0.70	0.91	n.a.
117	1.1	1.1	1.0	n.a.

n.a. – not available.

Table 8.10. Modelled-to-measured organically-bound tritium (OBT) concentrations in mussel soft tissues at each time point over the course of the mussel depuration study.

Sampling Time (days)	Modelled-to-Measured OBT in Mussel Soft Tissue				
	BIOCHEM	EDF	NIRS	AQUATRIT (Run 1)	AQUATRIT (Run 2)
0.042	0.78	0.80	0.60	0.81	0.80
0.083	0.79	0.82	0.59	0.83	0.83
0.17	0.83	0.84	0.59	0.85	0.85
0.29	0.84	0.79	0.59	0.81	0.81
1	0.85	0.80	0.59	0.86	0.85
2	0.72	0.73	0.58	0.82	0.82
5	0.72	0.64	0.58	0.74	0.74
12	0.77	0.60	0.64	0.62	0.60
26	0.78	0.56	0.67	0.42	0.35
40	0.97	0.60	0.83	0.32	0.24
55	0.97	0.50	0.84	0.20	0.14
85	0.96	0.39	0.82	0.099	0.066
117	1.1	0.33	0.96	0.064	0.046

8.5.1.2. Prediction of mussel OBT

All models predicted OBT concentrations in mussel soft tissues over the first 12 days following transplantation quite well, producing results that lay within a factor of 2 of the measured values and showing no clear temporal trend about a modelled-to-measured ratio of unity (Figure 8.11; Table 8.10). However, after 12 days, two models (AQUATRIT and, to a lesser extent, EDF) began to over-predict the rate of OBT depuration, resulting to under-estimates of mussel OBT levels of 16 fold, 22 fold and 3 fold for AQUATRIT Run 1 (which assumed mussel dietary items were uncontaminated), AQUATRIT Run 2 (which assumed mussel dietary items reflected ambient tritium concentrations in Upper Bass Lake) and EDF,

respectively. By comparison, the BIOCHEM and NIRS model predictions showed good agreement in mussel OBT concentrations throughout the 117 day study, likely because these models account for both fast and slow OBT compartments.

8.6. Summary and conclusions

8.6.1. Experimental observations

Under conditions where HTO concentrations decrease in a freshwater system, the rate at which mussels eliminate OBT from their tissues is of interest, particularly in cases where tritium doses represent a significant proportion of the total dose. Specifically, such relationships can provide insight into estimating potential changes in HTO and OBT exposure and dose rates to aquatic biota following mitigation, remediation and/or improvements in processes that lead to reduced emissions.

The 2005 Upper Bass Lake mussel transplantation study focused on quantifying rates of HTO and OBT depuration by mussels exposed to a sudden and significant decrease in ambient tritium concentrations. A predictive relationship (Equation 8.1) was developed to estimate the time rate of change of OBT concentrations in mussels that had been transplanted from a lake with relatively elevated tritium levels to a lake with significantly lower levels. Following transplantation, the mussels reached steady state within approximately 2 hours with respect to HTO concentrations in surface waters. Once equilibrium had been reached, mussel HTO concentrations tracked those in surface waters fairly well, falling within a factor of 1.06 to 1.8 (Figure 8.4). These results support those from a complementary study involving temporal changes in mussel HTO uptake and OBT formation following an abrupt increase in ambient tritium concentrations [83]. In the latter study, it also took approximately 2 hours for transplanted mussel HTO concentrations to reach steady state with the new HTO conditions.

In contrast, mussel OBT concentrations did not reach steady state over the 117 day period of the 2005 depuration study. Assuming that no significant changes in Upper Bass Lake tritium dynamics occur, that predictive relationships describing OBT formation rates by mussels following transplantation are representative of longer time-periods and that seasonal changes in Upper Bass Lake water temperatures do not result in slower OBT loss rates by mussels, it is expected that approximately two years would be required for mussel OBT concentrations to reach steady state. That said, it is likely that OBT formation rates by mussels may be slower at colder water temperatures, such as those that occur during the winter. Because this study was carried out over the summer months, it may in fact over-estimate annual OBT depuration rates. Additional work is required to measure/validate rates of tritium depuration by transplanted mussels over a full year period. In addition, younger mussels, which are actively growing, would likely equilibrate more rapidly than the older mussels that were considered in this study.

In contrast to these results, OBT in mussel soft tissues following an abrupt increase in ambient tritium levels, as discussed in the mussel uptake scenario, was estimated to take much longer than 2 years to reach steady state. In fact, taking account of the spring and summertime variability in tritium uptake and concentrations in the lake, it was estimated that adult mussels would take 7 to 15 years to reach steady state under conditions where there is a significant increase in ambient tritium concentrations.

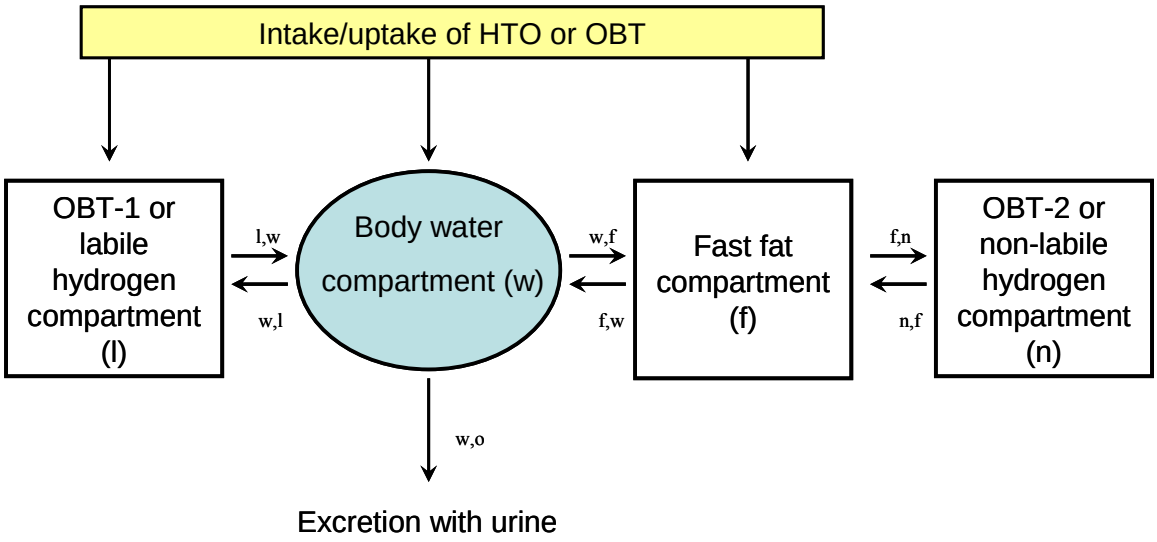

Fig. 8.12. Four-compartment model for tritium metabolism, applied for uptake of HTO and OBT by humans. The four compartments are body water (w); labile OBT with a high turnover rate (l); a fat compartment with a fast turnover of non-labile OBT (f); and non-labile OBT with a slow turnover rate (n). The λ parameters represent rate constants for tritium transfer among compartments and relate to the half-lives in these compartments [84, 85].

The findings of the depuration study described here and of the complementary uptake study [64, 83] suggest that, although mussel HTO levels can quickly increase following an increase in ambient tritium levels, they will quickly decrease again once the tritium source is removed. By comparison, the rate of OBT increase in mussel tissues occurs much more slowly than for HTO, allowing time to rectify the situation before tritium can accumulate in the slower OBT compartments in the body. In addition, it is important to note that in cases where OBT has formed in tissues, once the tritium source is removed, the rate of loss from the body is expected to occur over a much shorter time-frame than it took for the OBT to form.

8.6.2. Modelled-to-measured comparisons

The model testing exercise carried out here suggests that, although it is often possible to reach agreement between predicted and measured data for HTO over the course of the study, the same is not necessarily true when predicting OBT dynamics. OBT formation processes in the body are relatively complex and can be influenced by, among other things, 'dilution' with new organic material incorporated during feeding. For example, models such as EDF and AQUATRIT assume that newly-formed organic matter has the same OBT concentration as the dietary items being consumed by the mussels. These models began to under-predict the dynamics of OBT loss in mussel soft tissues after approximately 12 days. By comparison, models such as BIOCHEM and NIRS, both of which distinguish compartments with slow and fast OBT turnover, generated predictions in good agreement with the measured values over the entire 117 days of the study.

It is interesting to note that the most recent human dosimetry models for OBT [84–86] also include fast and slow OBT compartments. For example, Etnier et al. [85] proposed a four-compartment tritium model, consisting of tritium in body water as well as three additional

compartments that represent tritium retention in various types of organic molecules (as depicted in Figure 8.12). These include a rapid turnover compartment of labile OBT, a fat compartment with rapid turnover of non-labile OBT, and a slow turnover compartment of non-labile OBT. Similarly, the results of the mussel depuration study suggest that OBT compartments with varying biological half-lives also occur in freshwater mussels.

Two OBT pools corresponding to mussel somatic tissue and mussel reproductive tissue could also be discerned in the results of the tritium uptake study [83]. The modelled-to-measured values for OBT formation indicated that models that took account of biological processes, such as tritium loss with egg production and release, tended to better predict OBT concentrations in mussel soft tissues over time than models that did not include these process. This suggests that the reproductive tissue (or egg) compartment in mussels could be comparable to the fat compartment with rapid turnover that has been included in human dosimetry models for tritium. Such information may be useful in the development of biokinetic dose models for tritium in freshwater mussels and can also be used to establish the relative contributions of HTO versus OBT to biota dose.

More experimental work is clearly needed to gain fundamental understanding of the physical and biological factors that can influence OBT dynamics and the role they play in contributing to the doses received by aquatic biota in water bodies receiving tritium inputs. The results of such studies can then be made available to model validation programs to help establish the confidence that can be placed in the predictions of environmental tritium models. Sensitivity analysis of the models will isolate the variables that play a key role in driving radionuclide transport in natural systems. The results of such studies will ultimately lead to improved international modelling capabilities for key drivers of radiological dose.

CHAPTER 9. SCENARIOS BASED ON HYPOTHETICAL DATA

9.1. Introduction

Nuclear plants, whether civilian or military, may accidentally release tritium to the environment. Hydrogen, as a major biological element, has a relatively complicated environmental behavior depending on its initial chemical form, its transformation from one form to another, and on the climatic and soil conditions at the time of release [87]. A lot of experimental work has been performed to improve environmental tritium models and many international programmes [1–3] have included inter-comparison exercises based on activities in various environmental compartments. Tritium impact has been particularly studied to evaluate the safety of fusion reactors. It seems presently interesting to go a step further and use model intercomparison exercises to provide guidance in managing an emergency situation.

The objective of this study is to analyse the consequences of an acute atmospheric release of tritium, by considering various pathways in terms of activity in biosphere compartments and products, as well as the contribution of the various forms of tritium (HT, HTO and OBT) to total dose. The study aims to give practical guidance to decision-makers in the case of a severe release, taking account of the prevailing conditions during the release. The study has produced a set of results/guidelines that could be used by authorities to reduce the consequences of the release, if needed. This may require a harmonisation of crisis management on a technical/scientific basis within an international framework.

An integrated approach will be followed, in that the study will encompass immediate atmospheric impacts, further impacts on the food chain and ultimately dose to humans. The intent is to:

- establish a classification of different pathways;
- define the importance of different parameters to total dose; and
- assist in the definition of derived intervention levels.

9.2. Scenarios

Three scenarios are defined based on the three meteorological cases shown in Table 9.1. In each case, the following conditions apply (Table 9.2):

- the source term is 10 g of tritium in HTO or HT form;
- consequences are calculated at downwind distances of 1 km, 3 km, 10 km and 30 km;
- the site is at 45° latitude with a temperate climate; and
- the accident occurs at the end of June.

The food consumption rates assumed in the study come from the international BIOMASS exercise as shown in Table 9.3. The crop yield, percentage of dry matter, and time between accident and harvest for crops directly contaminated by deposition from the air are shown in Table 9.4 for each crop type considered.

A full description of the scenarios is given in Appendix I.8.

Table 9.1. Meteorological characteristics of the scenarios.

Parameter	Case 1	Case 2	Case 3
Time of day of release	midday	midday	midnight
Wind speed (m s^{-1})	2	5	2
Direction (mean ± standard deviation) (true)	45 ± 15	45 ± 5	45 ± 3
Diffusion conditions	unstable	neutral	stable
Weather	fine	cloudy	clear
Pasquill stability class	A	D	F
Solar radiation (W/m²)	700	300	0
Temperature (°C)	20	20	10
Rain	none	15 mm before the end of release	none
Relative humidity (%)	70	70	95

Table 9.2. General characteristics of the scenarios.

Parameter	Value
Release amount (HTO or HT)	10 g (3.7 E15 Bq) at a constant rate
Release duration	1 hour
Effective release height	20 m point source (no plume rise or building wake effects)
Latitude	45° N
Date	End of June
Day length, from sunrise to sunset	19.5 hours
Potential evapotranspiration	3.2 mm/day
Soil water content	30% by volume
Soil density	1.2 kg/L
Soil depth: garden vegetables/wheat	20 cm / 40 cm
Average rainfall during summer	60 mm/month
Irrigation of garden vegetables	Yes
Irrigation of wheat	No

Table 9.3. Human food consumption rates and vegetable characteristics.

Food category	Food product	Adult	Infant (1–2 yr)	Harvest and time of consumption
		g/day		
Salad vegetables	Green, leafy vegetables	130	80	In harvest period
Root vegetables	Radish, turnip	30	15	In harvest period
	Potatoes	200	100	Harvest in August, 8 months
	Carrots	50	25	In harvest period
	Total	**280**	**140**	
Fruit vegetables	String beans	50	25	In harvest period
	Peas	50	25	In harvest period
	Tomatoes	100	50	Harvest starts mid-July
	Total	**200**	**100**	
Cereals	Wheat	430	40	Harvest starts in August, 1 year
Milk	Milk*	500	440	
Meat	Beef	140	60	
	Chicken and eggs	100	50	
	Total	**240**	**110**	

* Including butter and cheese.

Table 9.4. Crop yield and time between accident and harvest for directly contaminated crops.

Product	Yield per crop (kg fw/m^2)	% Dry matter	Minimum time between accident and beginning of harvest	Maximum time between accident and end of harvest	Number of crops/year after accident
Salad vegetables	3	8	0*	1 month	4
Radish and turnip	1	20	0*	3 weeks	3
Potatoes	3	21	2 months	3 months	1
Carrots	2.5	16	2 weeks	2 months	2
Peas	1	25	0*	1 month	2
Beans	0.4	25	0*	1 month	3
Tomatoes	3	6	4 weeks	3 months	1
Cereals	0.8	86	4 weeks	7 weeks	1
Grass	0.7	15	0*	2 months	4

* It is assumed that these crops are ready for harvest when the release occurs, i.e. leaves from these crops would have been exposed to atmospheric tritium. Taking salad vegetables as an example, the crop lasts for one month, at which time a new crop is planted, for which only soil contamination/root uptake has to be considered. New garden crops are sown after each harvest. It is assumed that contamination of the surface environment ends in November, when all crops have been harvested and the tritium has migrated down to the water table. Cows are assumed to eat hay harvested before the accident during the winter. But they also may eat contaminated maize (whole plant) from November to March (35 kg/day, 35% dry matter). Tests of the sensitivity of the model predictions to this particular point may be done if judged necessary.

Table 9.5. Participants in the hypothetical scenarios.

Participant	Affiliation	Designation in text
P. Davis	Atomic Energy of Canada Limited (AECL), Canada	Canada
D. Galeriu A. Melintescu	Institute of Atomic Physics and Nuclear Engineering (IFIN-HH), Romania	Romania
H. Lee	Korea Atomic Energy Research Institute (KAERI), Korea	Korea
K. Miyamoto	National Institute of Radiological Sciences (NIRS), Japan	Japanet
L. Patryl P. Guétat	CEA, DAM, DIF, F91297 Arpajon, Cedex, France	France
W. Raskob	Institut fur Kern und Energietechnik (IKET), Germany	Germany
P.M. Ravi	Bhabha Atomic Research Centre (BARC), India	India
M. Saito	Safety Reassurance Academy, Kyoto University, Japan	Japan K

9.3. Participating models

Eight participants submitted results for the three scenarios (Table 9.5). Tables 9.6–9.8 compare different aspects of the models. Full model descriptions are presented in Appendix II.8.

9.3.1. Atmospheric dispersion

Most participants calculated air concentrations using a Gaussian plume model with constant wind direction during the release. The exception was Japanet, which used a random walk model. For complex models such as UFOTRI, the weather was constant only for the first hours. Thereafter, it changed according to a typical weather sequence which was not specified. Mixing heights were different between models. Lateral and vertical dispersion parameters were generally calculated using Briggs equations and Pasquill stability classes, although France used Doury's model and Romania used the Mol parameters.

Table 9.6. Model descriptions – Atmospheric dispersion.

Model name	Type of model	Lateral dispersion	Vertical dispersion	Deposition
ETMOD (Canada)	Gaussian plume model. Wind direction remains constant	Briggs dispersion parameters [88]	Smith-Hosker approach [89]	Deposition velocity determined by the multiple resistance approach.
RODOS (Romania)	Gaussian plume model	SCK Mol dispersion parameters	SCK Mol dispersion parameters	Dry deposition velocity determined by the multiple resistance approach.
KAERI model (Korea)	Gaussian plume model	Briggs rural dispersion parameters [90]		Tritium in air moisture is assumed to be in equilibrium with plant water, with a plant/air ratio of 0.5.
Japanet model (Japan)	EESAD Code (Random walk model): Movement of Lagrangian particles is determined by the mean three-dimensional wind speed and diffusion due to air turbulence. Mixing height is set to 800 m.	Dispersion parameters are calculated by the Pasquill-Meade equation	Dispersion parameters are calculated by the Pasquill-Meade equation	Wet deposition is calculated using a washout coefficient = 5.0×10^{-5} $J^{0.8}$ s^{-1} , where J is rain intensity in $mm.h^{-1}$. Dry deposition is calculated using a deposition velocity of 0.005 $m.s^{-1}$ .Tritium deposited on surface soil infiltrates to lower depths at a rate determined by the rate constant k_{perm}.
Gazaxi (France)	Gaussian plume model with correction for deposition/depletion due to rain	Doury lateral and vertical dispersion parameters [91]		Wet deposition velocity calculated using Chamberlain's equations [92]. Dry deposition velocity = 3.10^{-3} $m.s^{-1}$ [87].
UFOTRI (Germany)	Gaussian trajectory model	Briggs dispersion parameters	Briggs dispersion parameters	Time-dependent deposition velocity determined by the multiple resistance approach
Indian model (India)	Double gaussian equation with correction for deposition/depletion due to rain. Concentration in air moisture is calculated from air moisture data.	Pasquill-Gifford dispersion parameters [93]		Wet deposition calculated using a wet deposition velocity [94]. Dry deposition calculated using a dry deposition velocity.
Japan K model (Japan)	Gaussian dispersion model			Washout coefficient = $4.6.10^{-4}$ s^{-1}. Tritium exchange between air and soil assumed to occur quickly and to result in concentrations that were in equilibrium throughout the tritium release. Depletion and reemission assumed to compensate each other; thus no secondary plume was considered.

Table 9.7. Model descriptions – Behaviour in the biosphere (Part 1).

Model name	Air-plant transfer	Air-soil transfer	Tritium re-emission	Soil-plant transfer
ETMOD (Canada)	Air to plant transfer is a diffusion process that depends on the exchange velocity and the concentration gradient between air and leaf. Exchange velocity = 0 when stomata are closed (night). Root crops take up tritium only from soil water with the transpiration stream.	Dry deposition to soil is modelled using a deposition velocity, values of which are determined by the multiple resistance approach. Wet deposition is also modelled using an effective deposition velocity, which is calculated as the product of a washout ratio and the rainfall rate. The time-dependent HTO profile in soil is determined by an advection-diffusion equation that considers diffusion, advection by infiltration, loss due to plant uptake and re-emission.	Air concentrations from re-emission are calculated by multiplying the plant-to-air emission rate by a dispersion factor. The area over which the plume is likely to travel is discretized into terrain elements, each of which is treated as a Gaussian point source with an initial lateral dispersion parameter that reflects the crosswind width of the element.	Tritium is taken up from soil via the transpiration stream, which has a concentration equal to the concentration in soil water.
RODOS (Romania)	The exchange velocity depends on atmospheric, boundary layer, and canopy resistances. The transfer rate depends on the concentration gradient and exchange velocity.	The exchange velocity depends on atmospheric and soil resistances.	The same approach as in air-plant transfer is used, but the gradient between air and plant concentrations is reversed.	This transfer depends on the transpiration flux and the HTO concentration in the root zone.
KAERI model (Korea)	The tritium loss rate from plant water to the atmosphere compartment was determined on the assumption that the half-time of the loss was proportional to the water content of the plant. Its reference value (0.347 h^{-1}) was obtained on the assumption that the half-time was one hour during the daytime when the water content was 0.4 $kg.m^{-2}$. The water content of the plant was calculated by multiplying the water fraction by the yield of the wet crop. The tritium transfer rate from air to plant was determined on the assumption that the equilibrium ratio of tritium concentrations in air and plant compartments was 0.5. For releases occurring at night (Case 3), the rate constants of tritium transfer between air and plant were assumed to be 10% of the values for daytime conditions. The transfer rate of tritium from HTO to OBT compartments was assumed to decrease exponentially with the half-time of the growth period of the plant.	Soil deposition was determined by both dry deposition and rainfall. For Case 2, it was assumed that rain started 15 minutes before the end of the tritium release, and that there was no water emission from surface soil to the atmosphere during the rainfall.	The transfer rate of tritium from the soil surface to the atmosphere was determined from the balance of the tritium fluxes among the plant, soil and atmosphere compartments.	Plant absorption of water from the surface soil, soil layer 2, and soil layer 3 was assumed to be 0.2, 0.4, and 0.4 of the total plant absorption, respectively. Total plant absorption was determined from the balance of tritium fluxes among the plant, soil and atmosphere compartments. Similarly, transfer rates between the soil compartments were determined from the balance of tritium fluxes among the compartments. The rate of loss of water from soil layer 3 to deeper soil was assumed to occur at a constant rate of 3.42×10^{-4} h^{-1} [95].

Table. 9.7. (Continued).

Model name	Air-plant transfer	Air-soil transfer	Tritium re-emission	Soil-plant transfer
Japanet model (Japan)	The HTO concentration used to calculate the OBT concentration in crops was set to the environmental concentration (air and surface soil) immediately after plume passage. A representative HTO concentration in the plant was defined as the geometric average concentration between the time of release and the time harvest began. The specific activity ratio (SAR) method was used in the calculation of HTO or OBT concentrations in the plant.	The HTO concentration on the surface soil after deposition decreased by infiltration to greater depths.	The re-emission rate from surface soil to air was experimentally derived from the difference between the HTO concentration on the surface soil and in the air above the soil. The re-emitted tritium activity was added to the air concentration in the current time step and then eliminated in the next time step.	HTO and OBT concentrations in plants were separately calculated from literature values of the plant/soil and plant/air specific activity ratios for HTO or OBT.
Gazaxi (France)	The diffusion process depends on the exchange velocity, which is proportional to the foliar index and inversely proportional to the foliar resistance (300 $s.m^{-3}$ for daytime conditions and 3000 $s.m^{-3}$ at night). The HTO concentration in plant water is evaluated for 2 phases (incorporation during the release and depletion after the accident up to harvest). An average concentration is used for crops in continuous production (i.e., lettuce, tomatoes and so on). HTO transfer from the air pathway is neglected at harvest for annual crops (root crops, cereals, etc.).	The soil pathway is modelled as a diffusion process involving dry and wet deposition on the soil: Dry deposition: Independently from air-plant transfer, a direct air-soil transfer is assumed to occur with a deposition velocity of 3 10^{-3} $m.s^{-1}$ (range $10^{-3} - 10^{-2}$). Wet deposition: Based on the model of Chamberlain and Eggleton, which depends on the characteristics of rain drops through and below the plume.	No deposition/re-emission is considered in calculating the HTO air concentration. Soil water activity is calculated using a decay constant defined as the ratio of the daily evapotranspiration rate divided by the soil water content of the root zone.	Calculation of crop concentrations due to root uptake is performed for one crop cycle assuming full equilibrium between plant and soil water and an exponential decrease due to evapotranspiration.

Table. 9.7. (Continued).

Model name	Air-plant transfer	Air-soil transfer	Tritium re-emission	Soil-plant transfer
UFOTRI (Germany)	The exchange reaction of the plant with atmospheric tritium takes place via the water circulation in the leaves and is recalculated every hour. The mechanisms of the plant/atmosphere exchange are described according to the 'big leaf' approach. There the aerodynamic, boundary layer and stomatal resistances determine the sensible and latent heat fluxes at the earth's surface. At night, when the stomata are closed, the stomatal resistance is replaced by the epidermal resistance, which is a factor of 15 higher than the minimum stomatal resistance. To determine the HTO exchange between the atmosphere and the vegetation, the model of Belot has been used.	Dry deposition: depends on atmospheric stability and properties of the soil. Is recalculated every hour. Wet deposition: washout from the whole plume. The washout coefficient depends on the rain intensity.	For plants, re-emission is based on the transpiration of water from the crop, which is modelled according to Monteith's approach. For soil, the re-emission processes are modelled by coupling the re-emission of HTO to the evaporation of water from the soil.	The amount of water taken up by the plant is assumed to equal the amount of water lost to the atmosphere by transpiration. The HTO content in the water is modelled taking into account the matrix forces in three layers (0–5, 5–15 and 15–30 cm).
Indian Model (India)	A transpiration model is used. After release, plant water is lost by transpiration at a rate of $0.1\ h^{-1}$.	Dry and wet deposition used.	Re-emission is not considered.	A transpiration model is used.
Japan K model (Japan)	Free water tritium in the plant reaches equilibrium with air moisture by the end of the exposure period. Leafy vegetables take up tritium through both the air pathway and the soil pathway. Root vegetables take up tritium only from the soil pathway.		Re-emission is not modeled explicitly since depletion is assumed to balance re-emission .	

Table 9.8. Model descriptions - Behaviour in the biosphere (Part 2).

Model name	Dry matter production in the plant	OBT production	Concentration in animals	Doses
ETMOD (Canada)	CO_2 consumption model [96] depending on: Air temperature, resistance to CO_2 uptake by the plant, and photosynthetically active radiation. A production rate based on net photosynthesis.	The T/H ratio in OBT is assumed to be 60% of the T/H ratio in plant water. OBT formation does not occur at night. OBT concentrations decrease with dilution by new uncontaminated dry matter. The model does not account for the conversion of OBT to HTO.	Dynamic model using simple mass balance equation. OBT ingested by animals is converted to HTO. OBT concentrations are not estimated	The dose from skin absorption is assumed to equal the dose from inhalation.
RODOS (Romania)	Dry matter production is given by gross photosynthesis minus growth and maintenance respiration. Gross photosynthesis is modelled using WOFOST (a crop growth model developed by the Wageningen School, Holland).	OBT formation depends on the net photosynthesis rate and the HTO concentration in leaf water.	Concentrations in animals were calculated from integral convolutions involving intakes, transfer factors, and biological loss rates.	The dose from skin absorbtion is assumed to equal half the dose from inhalation.
KAERI model (Korea)	No time-dependent equation for plant growth was considered. The dry weight of each plant was calculated from the yield of the wet crop and the percent dry matter given in the scenario description.	OBT production was determined by multiplying the fraction of hydrogen in the organic part of the plant (0.08 for all plants) by the dry weight of the plant.	Grass concentrations were assumed to be constant at the value in effect 30 days after the release Chickens eat uncontaminated grain harvested in the previous year, implying that doses from chicken are negligible	Plants are harvested several times until the end of November following the harvest schedules given in the scenario description. Ingestion doses are calculated for each harvest time and summed.
Japanet model (Japan)	The dry matter fraction of each plant was assumed to be constant from exposure to harvest.	The OBT concentration was separately calculated from literature values of the plant/soil and plant/air specific activity ratios for OBT.		Doses from the food pathways (via crops or animal products) are calculated for the first harvest only. Ingestion doses from crops after the second harvest are negligible. Doses from inhalation and skin absorption are caused by HTO (vapour) only.

Table 9.8. (Conitnued).

Model name	Dry matter production in the plant	OBT production	Concentration in animals	Doses
Gazaxi (France)	An average dry matter production rate is calculated by using the yield at maturity and the duration of linear growth.	All organic tritium is assumed to be organically bound tritium. The OBT concentration is deduced from the time-integrated HTO concentration divided by the appropriate time of integration (growth or harvest), with an isotopic discrimination factor of 0.53.	Animal integrated activity is modelled using the integrated activity in feed and a transfer coefficient. Animals are assumed to stay outside during the accident and to graze all the time. All dry matter of milk and meat is assumed to be OBT. No account is taken of animal inhalation.	All plant and animal products consumed by humans are assumed to be harvested at the same location. This is also true for animal consumption. Integration is done for the time up to harvest for the different crops present at the time of the accident. No decrease in concentration is assumed to occur after harvest. Consumption of harvested products may last for 1 year in the case of wheat. The dose from skin absorption is assumed to equal 40% of the inhalation dose.
UFOTRI (Germany)	A photosynthesis submodel calculates the build-up of organic matter. The model distinguishes between the linear growth phase and other phases.	A photosynthesis submodel calculates the build-up of organic matter and this is linked with the build-up of OBT.	A compartment model is used for the transfer of activity to animals, taking into account the exchange processes cow/atmosphere, cow/plant and cow/soil; There is a direct transfer from milk HTO to milk OBT; Animals are assumed to stay outside during the accident and to graze all the time; Animal inhalation is considered.	All plant and animal products consumed by humans are assumed to be harvested at the same location. This is also true for animal consumption; Integration is done for the time up to harvest for the different crops present at the time of the accident. Consumption of harvested products lasts for 1 year in the case of wheat and potatoes; The skin absorption dose is modelled separately and makes up 50% of the direct inhalation dose via the lung.

Table 9.8. (Conitnued).

Model name	Dry matter production in the plant	OBT production	Concentration in animals	Doses
Indian Model (India)	The dry matter content of the plants was taken from the scenario description.	A fixed rate is used for HTO to OBT conversion: OBT = 0.06% HTO in the plant at the end of the release. This value is constant throughout the consumption period; OBT=0.7% HTO in milk.	The source of HTO and OBT in animals is due to inhalation of contaminated air and ingestion of contaminated feed. A fraction 0.0158 of the daily activity intake (Bq/d) is transferred to each liter of milk. The biological half life of HTO in cows is 3.1 days.	The skin absorption dose is equivalent to the inhalation dose. Ingestion doses are based on integrated intakes throughout the harvesting period.
Japan K Model (Japan)				Consumption of contaminated foods continues until the end of November. Dose coefficients come from ICRP Publication 56.

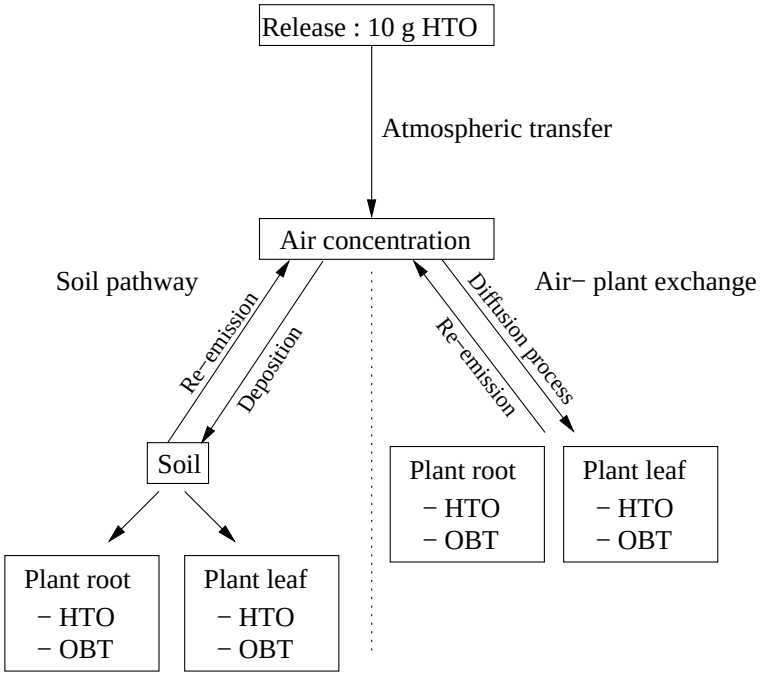

Fig. 9.1. HTO exchange between air, plants and soil.

9.3.2. Depletion, deposition and re-emission

The participants modelled dry and wet deposition using a deposition velocity which was either calculated or defined. Plume depletion due to deposition of airborne material to the underlying surface was also modeled by some participants.

Air concentrations from re-emission by plants (Figure 9.1) were calculated by Canada, Germany and Romania. Other participants assumed either that re-emission compensated for depletion, or that there was no re-emission at all, and did not calculate air concentrations from re-emission. Regardless of the way the models treated re-emission, all allowed plant concentrations to decrease through loss of tritiated water to the air.

Air concentrations from re-emission by soil (Figure 9.1) were modelled by Germany, Japanet and Korea. This process was not modelled by the other participants but some, such as France, calculated soil depletion due to water transpiration in plants.

9.3.3. Air – plant transfer

Two air-plant pathways were modelled:

- directly via air, representing the exchange of tritium from air to plant leaves by simple diffusion. Most participants calculated the plant activity using a diffusion equation depending on an exchange velocity and driven by the gradient between the tritium concentration in air moisture and in plant water. The exchange from air to plants is reversible, and the plants lose tritium to the air when the plume has passed;
- indirectly via soil, representing the exchange of tritium from air to soil and then from soil to plants by root uptake.

The exchange velocity depends on parameters which can have very different values between models. For example, Canada set the exchange velocity to zero at night because they assumed the stomata are closed and no exchange takes place at night.

9.3.4. OBT

A conversion coefficient is used in the models to convert HTO to OBT which can be defined (Japan K, Japanet and India) or calculated from dry matter production (Canada, France, Germany). No models account for OBT to HTO conversion.

9.3.5. Concentrations in animals

All participants considered the ingestion of contaminated food when calculating the tritium activity in animals. Only the Indian and German models considered animal activity from inhalation. In the first step, the participants calculated HTO and OBT concentrations in animal feed. Animal OBT and HTO activities were then calculated using either integrated concentrations (analytical approach) or fully dynamic models.

9.3.6. Dose

Participants calculated the committed effective dose for adults from inhalation, skin absorption and ingestion. In the Canadian model, the dose from skin absorption was conservatively assumed to equal the inhalation dose whereas other models used an inhalation ratio or did not account for skin absorption.

9.4. Atmospheric dispersion results

This section compares the atmopheric dispersion predictions of the various models. All participants submitted integrated air concentrations (Bq.s.m^{-3}) and lateral and vertical dispersion parameters (m), which were calculated using the models defined in Section 9.3.

9.4.1. Integrated air concentrations

9.4.1.1. Case 1: Daytime conditions, fine weather, unstable, wind speed 2 m s^{-1}

Integrated air concentrations calculated by the participants are shown as a function of distance in Figure 9.2. The results vary substantially. Whatever the distance, there is more than a factor 10 difference among the predictions (e.g., 2.10^9 to 7.10^{10} at 500 m). The French results are the highest at 7.10^{10} Bq.s.m^{-3}.

9.4.1.2. Case 2: Daytime conditions, rain, neutral stability, wind speed 5 m s^{-1}

Integrated air concentrations calculated by the participants are shown as a function of distance in Figure 9.3. At short distances, there is about a factor 10 difference among the predictions. This increases to a factor of 100 at 10 km and more than a factor of 1000 at 30 km. These differences are probably due to the differences in the way the models address plume depletion by wet deposition.

9.4.1.3. Case 3: Night-time conditions, fine weather, stable, wind speed 2 m s^{-1}

Integrated air concentrations calculated by the participants are shown as a function of distance in Figure 9.4. At short distances, the predictions of all the participants are fairly close, less than a factor 10. The differences increase with distance but remain less than a factor 100 at 30 km.

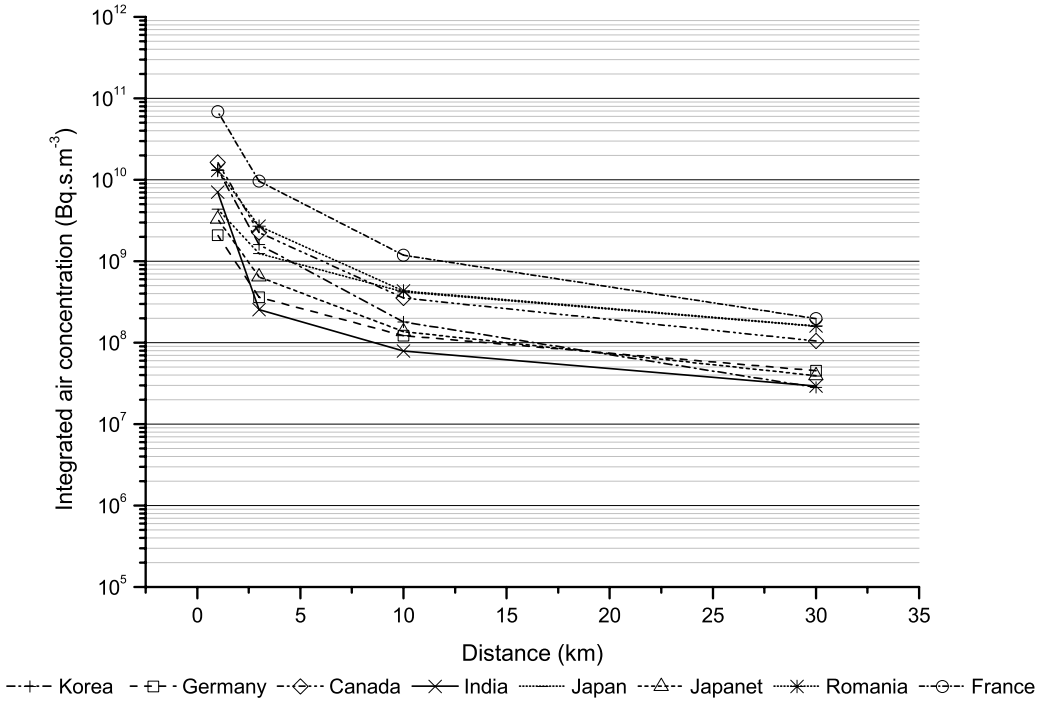

Fig. 9.2. Integrated air concentrations – Case 1.

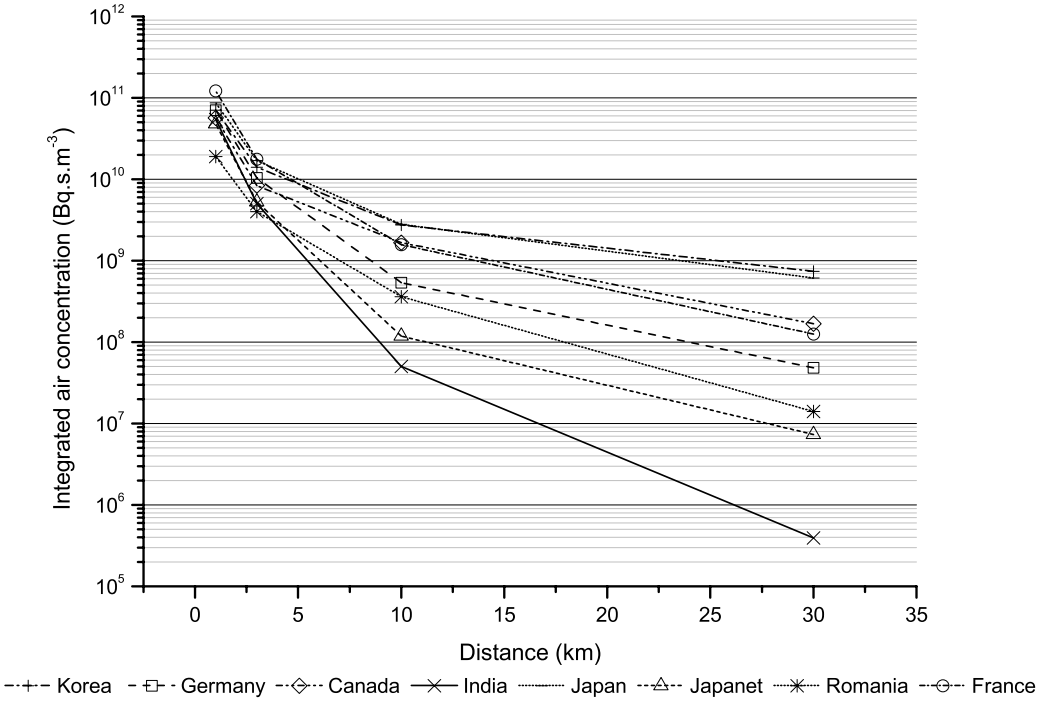

Fig. 9.3. Integrated air concentrations – Case 2.

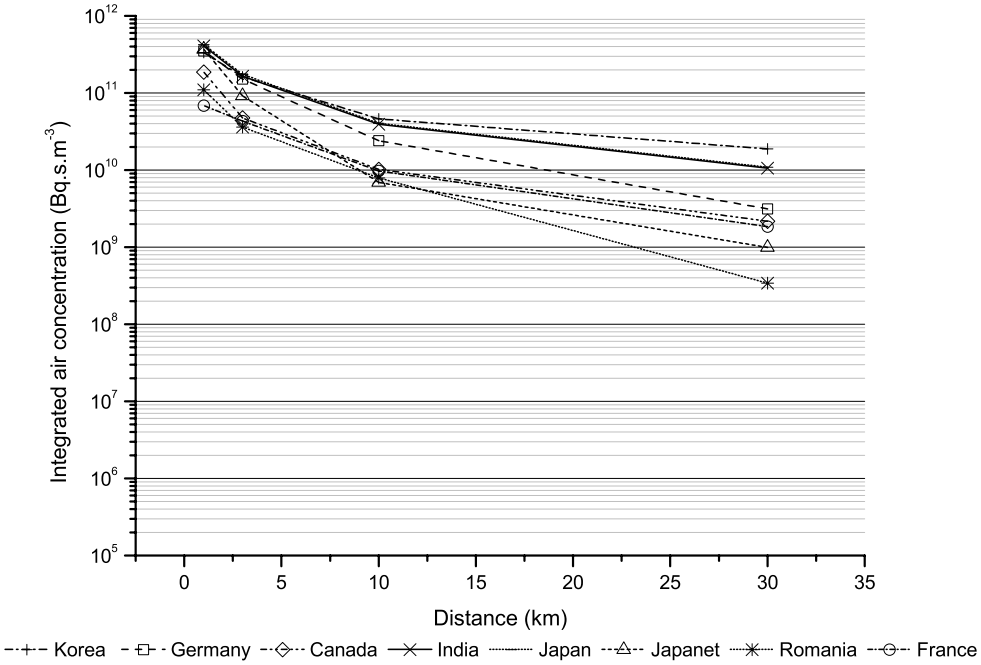

Fig. 9.4. Integrated air concentrations – Case 3.

9.4.2. Lateral (σ_y) and vertical (σ_z) dispersion parameters

Except for Japanet, all participants used the Gaussian plume model to calculate the concentration of tritium in air. To try to explain the differences in the results, each participant submitted their estimates of the vertical and lateral dipersion parameters. Figure 9.5 shows these parameters for each participant and for several sigma schemes found in the literature (Briggs rural [97], Briggs urban [97], Pasquill-Gifford [97], Doury [91] and Karlsruhe-Jülich).

The lateral dipersion parameters calculated by the participants are fairly closely grouped in Cases 1 and 2, with agreement within a factor of 2 on average regardless of the downwind distance. Deviations are noticeably higher (by about a factor of 7) for Case 3.

With the exception of France and Romania, all participants calculated lateral dispersion using either the Pasquill-Gifford or Briggs rural models, which yield similar results. France, using the Doury model, also obtained results close to those of the other participants with the exception of Case 3. Only in the Doury model is lateral dispersion unaffected by atmospheric stability. The SCK-Mol parameters used by Romania tend to be slightly higher than those of the other participants at short distances, but converge further downwind.

The vertical dispersion parameters predicted by the various models were very different for Case 1, ranging from 150 m to 5000 m at 3 km. The Doury model used by the French gave the lowest σ_z value and the Pasquill-Guifford model used by Japanet yielded the highest. In Case 2, the vertical dispersion parameters were fairly closly grouped regardless of the distance. The range was about 30–90 m and 110–380 m at distances of 1 km and 10 km, respectively. In Case 3, the Doury model yielded the lowest values and the Romanian model the highest. For a 30 minute release, it is well known that Doury's model underestimates the vertical dispersion parameters and overestimates air concentrations by a factor of about 5 compared to experimental data and Pasquill's parameters.

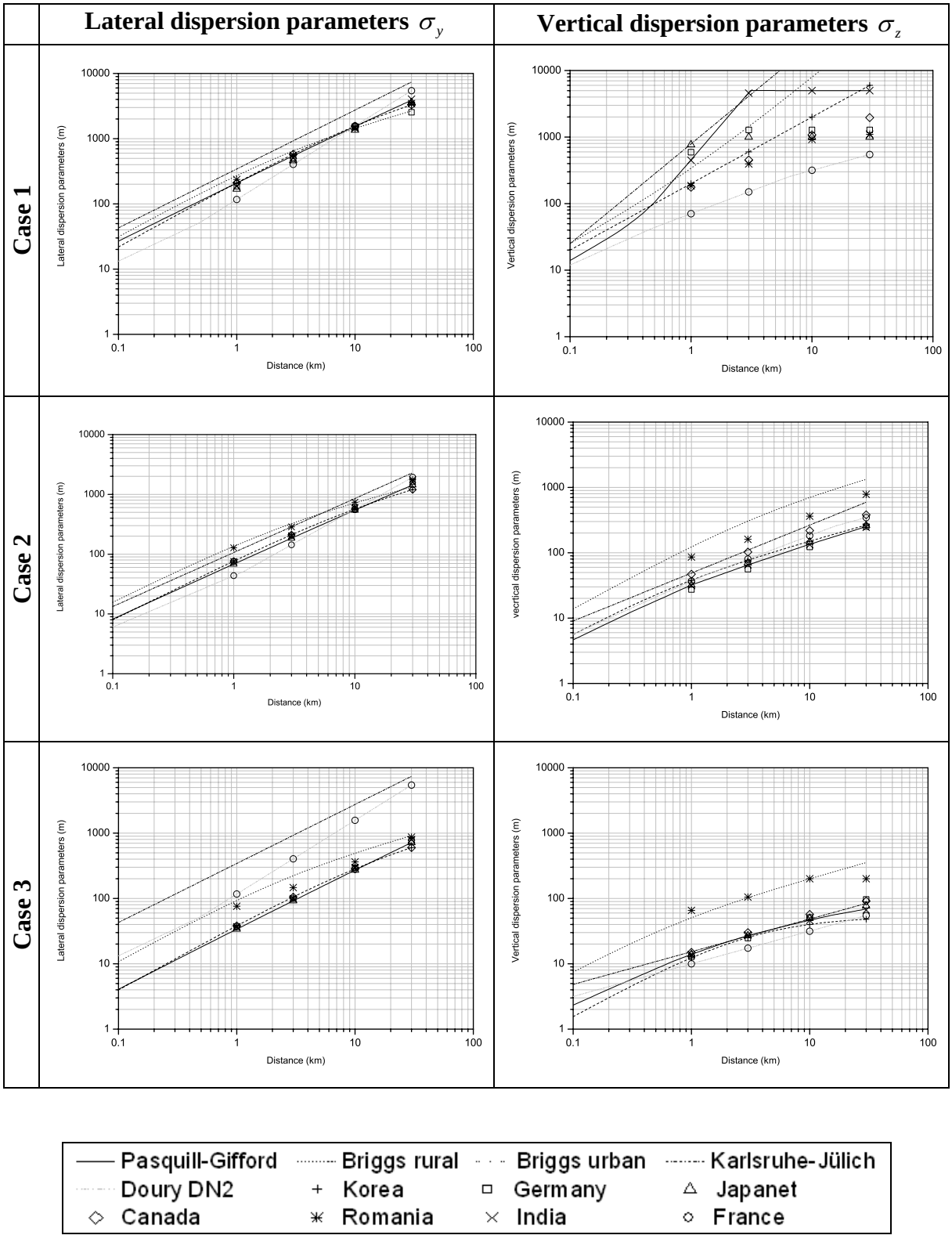

Fig. 9.5. Lateral (σ_y) and vertical (σ_z) dispersion parameters.

9.4.3. Discussion

Case 1: At short downwind distances, σ_z seems to be the main parameter influencing air concentration. The French results prove this rule, particulary for Case 1.

Plume levels reached mixing heights of 1000 m, 1280 m and 3000 m for the Japanet, German and Indian models, respectively. In the rest of the models, mixing heights either were not set or were not reached by the calculated plumes.

Case 2: Whatever the downwind distance, the lateral and vertical dispersion parameters were similar among participants. In contrast, there is a clearly visible discrepancy in integrated air concentrations. One possible explanation may be the different approaches to modeling rain and its effect on plume depletion.

Case 3: The lateral and vertical dispersion parameters were fairly closely grouped for those participants using the Pasquill or Briggs models. At shorter distances, the integrated air concentrations were also grouped, varying by less than a factor of 10. The range increased with distance, which may be explained by the ways in which the various participants modeled (or ignored) plume depletion or re-emission.

France is set apart from the other participants by its higher σ_y values and lower σ_z values. These two parameters appear to have balanced each other out, resulting in integrated air concentration that lay within the range of those predicted by the other participants.

9.5. Dose results for an HTO release

9.5.1. Total doses

The total doses predicted by each participant at each downwind distance are shown in Appendix IV and plotted in Figure 9.6.

Case 1: At 1 km, the mean total dose averaged over all models was approximately 2 mSv. The largest dose was calculated by France: 9.7 mSv. All other predictions were less than 0.9 mSv. Whatever the distance, there was more than a factor 15 difference among the predictions of the various models. This discrepancy can be explained in large part by the variability in the atmospheric dispersion results.

Case 2: At 1 km, the mean total dose was approximately 17 mSv, ranging from a low of 2 for Canada to a high of 39 for France and Japanet. At longer distances, the discrepancy increased considerably, reaching 10^4 at 30 km. This can be explained by the differences in the way the various participants modeled rain, wet deposition and tritium transfer through the biosphere, and by the values they used for the washout coefficient. Most probably, at long distances, the models which give the highest doses do not take into account plume depletion by deposition.

Case 3: At 1 km, the mean total dose calculated by the participants was approximately 26 mSv. The discrepancy among the results increased with distance, from a factor 30 at 1 km to a factor 95 at 30 km. This variability can be explained on the one hand by the variability in the atmospheric dispersion results and on the other by the photosynthesis models used by the various participants, which used incorporation rates that ranged from 0 to a value equivalent to a sunlight situation.

Case 1

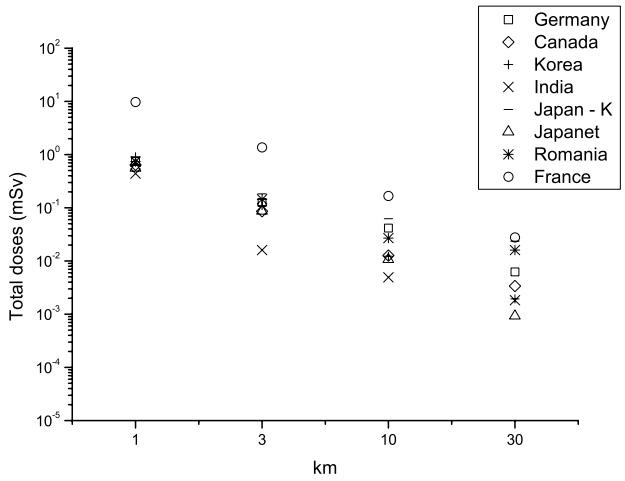

Case 2

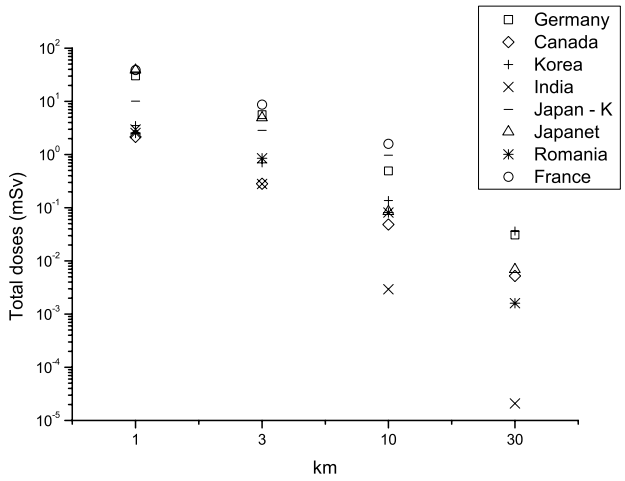

Case 3

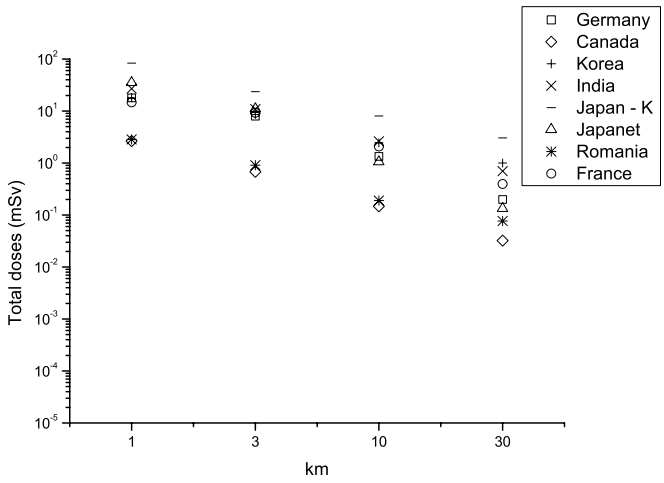

Fig. 9.6. Total doses following an HTO release.

9.5.2. Breakdown of normalized total dose by exposure pathway

Figure 9.7 shows a breakdown of the total doses by exposure pathway at 1 km. In constructing this figure, the doses were normalized by the average predicted integrated air concentration for each case:

- Case 1: 6.10^{9} Bq.s.m^{-3};
- Case 2: 3.10^{10} Bq.s.m^{-3};
- Case 3: 3.10^{11} Bq.s.m^{-3}.

In this way, results can be compared across cases. Figure 9.8 shows the relative contributions of the different pathways to the total dose. The detailed dose predictions of each model for the three meteorological cases at a downwind distance of 1 km are listed in Appendix V.

Case 1: All normalized total doses are below 2.1 mSv, and below 0.75 mSv without the cereal pathway. Inhalation doses are practically identical for all participants and represent a minor part of the total dose. Transcutaneous exposure (skin absorption) represents a few tens of percent of the inhalation dose, and is given for completeness. Garden vegetables represent a significant part of the total dose (from 10% to 60%). Animal products represent generally 30% or less. The cereal pathway is the most variable, contributing between 20% and 80% depending on the model.

Case 2: The normalizing air concentration is a factor 5 higher for Case 2 than for Case 1. For each participant, the contribution of the different pathways is practically the same as in Case 1.

For these two "daylight" situations (Cases 1 and 2), 3 groups of models can be distinguished:

- Korea – Japan K – Romania – India: the dose from green vegetables is greater than or equivalent to the dose from cereals;
- Germany – Japanet – France: the dose from cereals largely dominates the total dose;
- Canada: all pathways contribute a similar amount to the total dose.

At the same level of integrated air concentration, rain increases the total dose by a factor of 1.35 to 2 for Germany, Romania and France. This effect does not appear in the results for Korea, Japan K, Canada or India.

Case 3: The normalizing air concentration is a factor 50 higher for Case 3 than for Case 1. The relative importance of the different pathways is about the same as for Case 1, except for Canada. There is no OBT formation at night in the Canadian model, so that the contribution from the ingestion pathways is very small. The variability in the rate of tritium incorporation into organic compounds plays a major role in determining the relative importance of the different pathways.

Case 1 – Normalized by 6.10^{9} Bq.s.m^{-3}

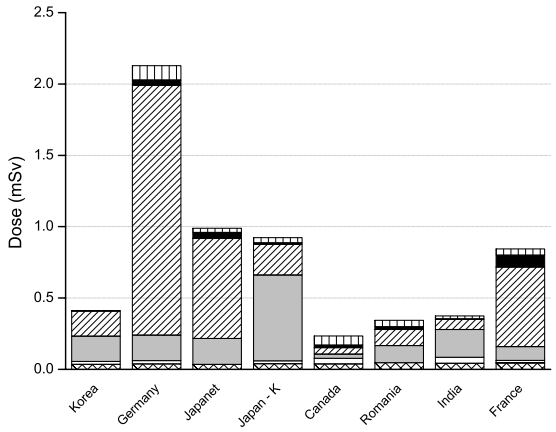

Case 2 – Normalized by 3.10^{10} Bq.s.m^{-3}

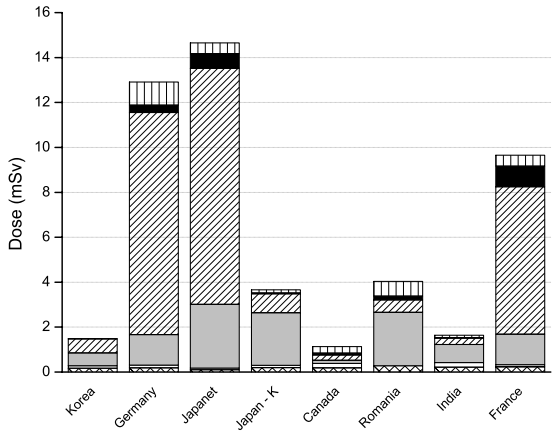

Case 3 – Normalized by 3.10^{11} Bq.s.m^{-3}

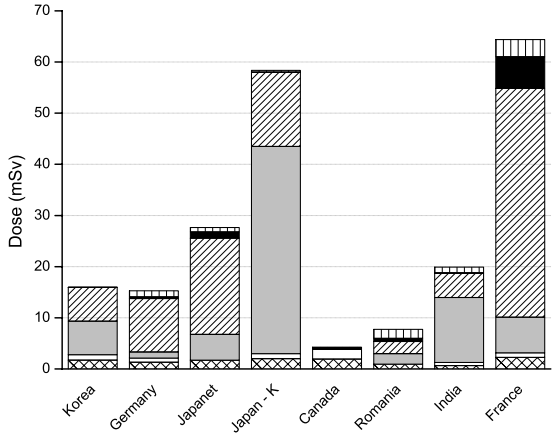

Fig. 9.7. Breakdown of normalized total dose by exposure pathway at 1 km.

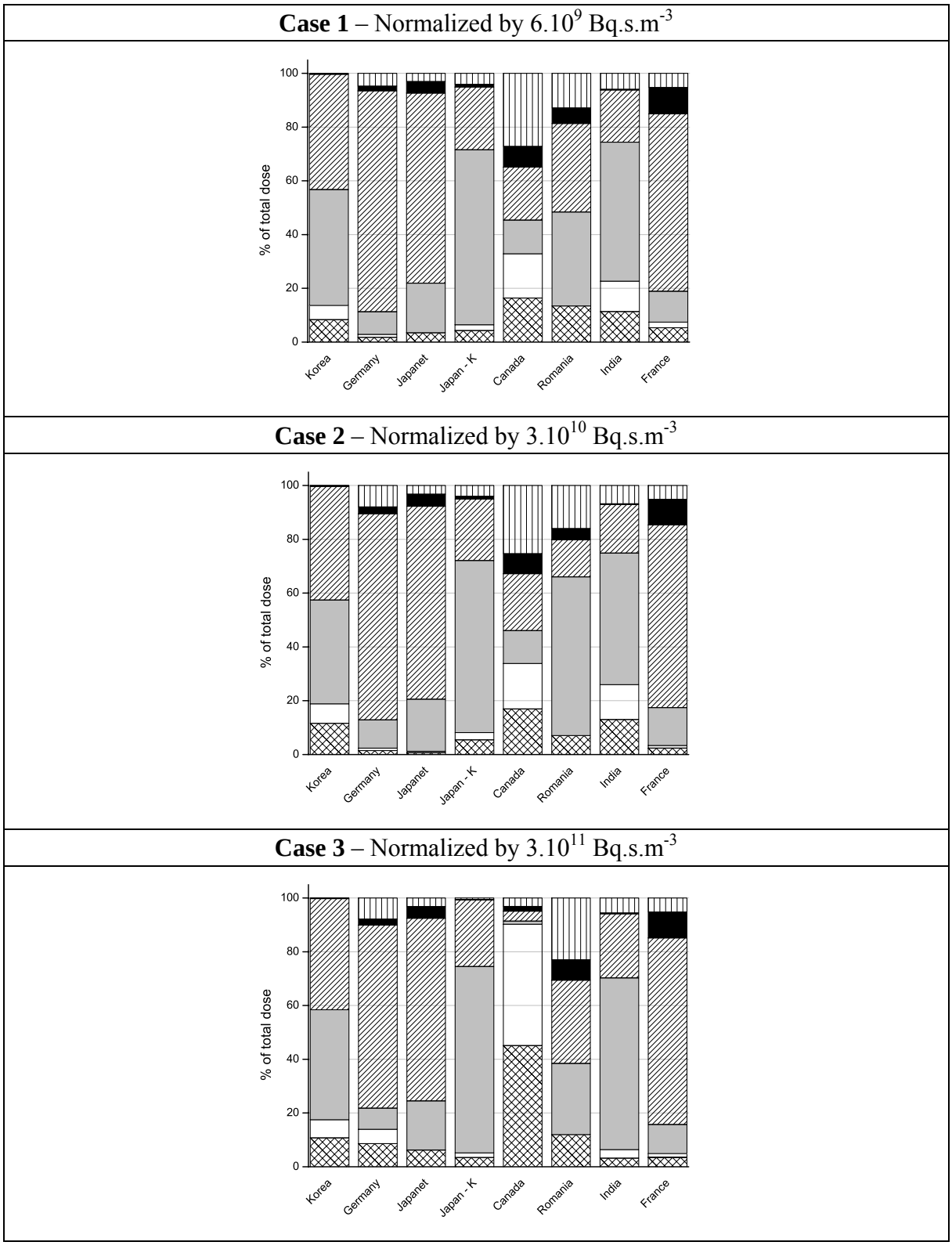

Fig. 9.8. Contribution of the exposure pathways to the total dose at 1 km.

9.5.3. Breakdown of ingestion dose by chemical nature and exposure pathway (air or soil)

Figure 9.9 shows the origin of the ingestion doses considering on the one hand the air pathways (air–vegetable and air–grass–animal) and on the other hand the soil pathways (air–soil, soil–vegetable and soil–grass–animal). The air and soil pathways are also broken down by the two chemical forms of tritium, HTO and OBT. Two participants (Korea and Romania) did not distinguish between air and soil pathways.

Case 1: The OBT dose is predicted to be greater than the HTO dose by most participants except Canada (where the two doses are similar) and Japan K (where the HTO dose dominates). The air pathway is generally dominant, with the contribution of the soil pathway varying from negligible to an amount equivalent to the air pathway. This means that the main part of the dose comes from OBT formed in plants growing during the relase and exposed to the airborne plume. There is no need for intervention in this case because the doses are much less than 5 mSv, the lowest level at which intervention is desirable.

Case 2: There is no significant change in the relative importance of the pathways compared to Case 1 and the same conclusions can be drawn. The soil contribution increases slightly but remains less than the air pathways. For all participants, the exposure remains below 5 mSv during the first weeks but increases significantly in the following months with the consumption of cereals and, to a lesser extent, potatoes. Half of the participants find total doses over 5 mSv without intervention.

Case 3: There is again no significant change in the relative importance of the pathways except for Canada, where OBT formation is assumed not to occur at night and the air pathway for HTO decreases in importance. For Germany and Romania, the OBT contribution by the air pathway is reduced but remains dominant. The results for the other participants show no differences between night-time and daytime releases. The French model does not reduce the OBT formation rate at night relative to the daytime rate.

In all cases, the variability in the results reaches one order of magnitude for the normalized doses. Two extreme situations have been assessed, one with no OBT production by the air pathway at night (Canada) and the other with night-time production equal to daytime production (France). Germany and Romania use elaborate models that show that OBT production via the air pathway during the night is reduced but remains important (compare Cases 1 and 3 in Figure 9.9). Relative to these results, the French approach overestimates the ingestion dose by a factor of 3 and the Canadian approach underestimates by a factor of 2. The relatively small underestimate by Canada appears to be the result of compensatory errors in the processes contributing to the ingestion dose, since this model underestimates deposition on soil by a factor of 10, underestimates the rate of HTO incorporation in plants by a factor of 5 (Cases 1 and 3) and underestimates the OBT prodution rate by a factor of 2.

9.5.4. Intervention levels

In the event of an accident, it is valuable to be able to use environmental measurements to determine quickly the real impact of the release. In this regard, it is useful to establish the relation between the instantaneous activity in plants and the total dose to people if no countermeasures are adopted. Intervention levels are derived here based on a committed effective dose of 5 mSv, which includes all exposure pathways (inhalation, skin absorption and ingestion).

Case 1

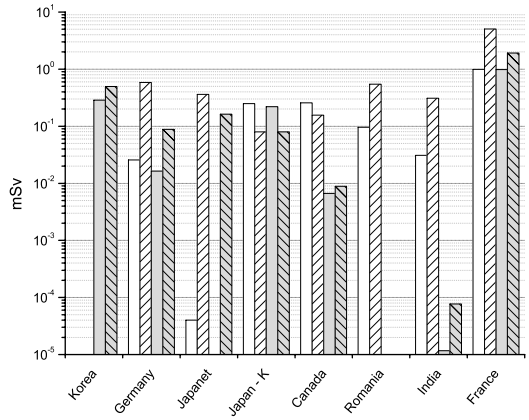

Case 2

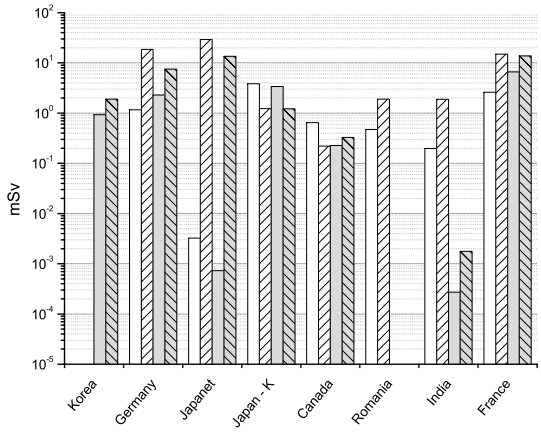

Case 3

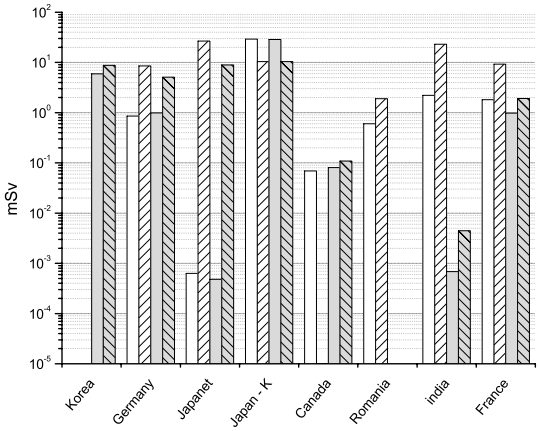

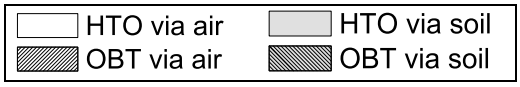

Korea and Romania did not break their results down by air and soil pathways

Fig. 9.9. Ingestion dose versus chemical nature and exposure pathway (air or soil) (not normalized).

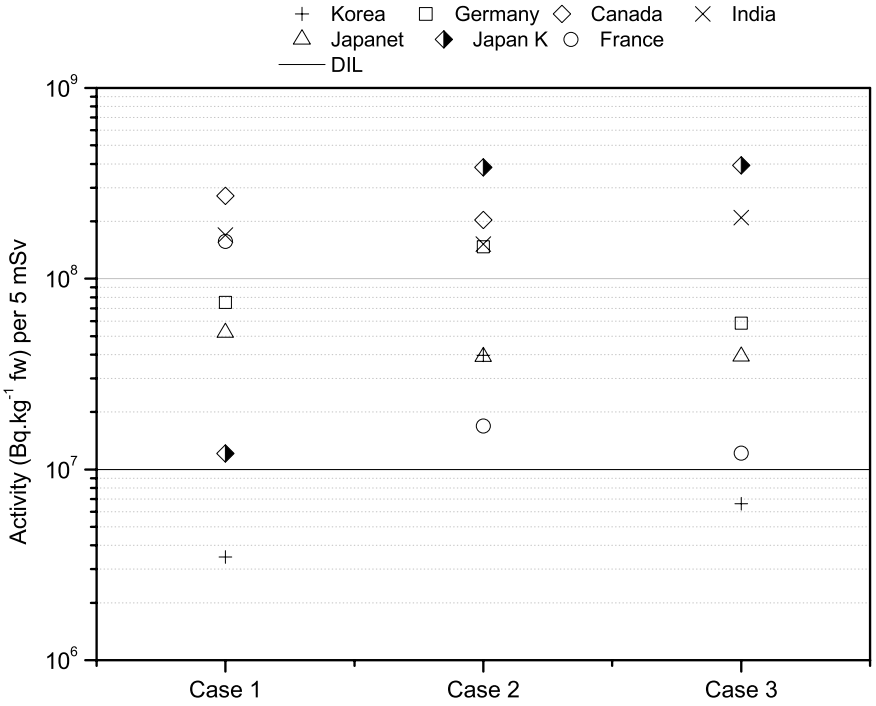

Fig. 9.10. HTO activity in salad vegetables 1 h after the release corresponding to a 5 mSv committed effective dose at 1 km.

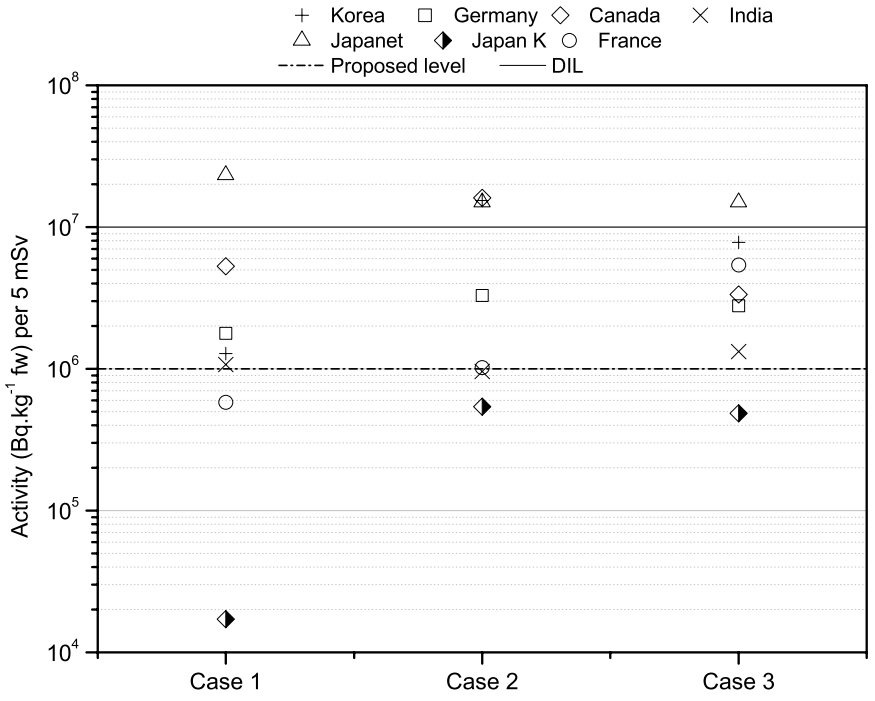

Fig. 9.11. HTO activity in salad vegetables 48 h after the release corresponding to a 5 mSv committed effective dose at 1 km.

Figure 9.10 shows the HTO activities in salad vegetables 1 hour after the release that correspond to a 5 mSv committed effective dose from all pathways. Figure 9.11 shows the corresponding activities 48 hours after the release. It is important to note that the decrease in environmental tritium levels with time leads to different activities, which is generally not taken into account in the definition of food intervention levels for other radionuclides. Between 1 h and 48 h, vegetable activity decreases because of the release of tritium to air by transpiration, although this decrease is limited by the incorporation of tritium into organic matter and by plant uptake of some tritiated water deposited on the soil.

According to the US DOE [98], the Derived Intervention Level (DIL) for tritium-contaminated crops and animal feed is 1.10^7 Bq.kg^{-1}. It must be noted that in this publication, the duration of ingestion is 8 days and the quantity of food consumed is not stated. Better practice is to base the DIL on the results of models that integrate the dose over 1 year, as considered in this exercise. Figures 9.10 and 9.11 show that:

— there is no effect of meteorological conditions on the results in the cases studied;
— between 1 h and 48 h, most models predict that the total tritium activity decreases by about a factor of 10;
— 10^7 Bq.kg^{-1} appears to be the minimum value on which to base the DIL at one hour (Figure 9.10), but seems to be high at 2 days as the concentration has dropped by at least a factor of 10 (Figure 9.11).

Given the daily food consumption rates in this exercise, a single reference value of 10^7 Bq.kg^{-1} fresh weight in salad vegetables should be used to determine countermeasures during the first day after the release. It would be better to take into account the decrease of activity with time and use a reference value of 10^6 Bq.kg^{-1} after two days.

9.6. Dose results for an HT release

Four countries submitted results for an HT release under the conditions of Case 1, and three countries submitted results for Cases 2 and 3. Detailed predictions of each model are shown in Appendix VI. Figure 9.12 shows the breakdown of the total dose by exposure pathway at 1 km and Figure 9.13 shows the relative contributions of the different pathways to the total dose. The doses have been normalized by the average predicted integrated air concentration in each case:

— Case 1: 6.10^9 Bq.s.m^{-3};
— Case 2: 3.10^{10} Bq.s.m^{-3};
— Case 3: 3.10^{11} Bq.s.m^{-3}.

Case 1: At 1 km, the maximum dose was calculated by France: 0.3 mSv. When normalized by the air concentration, doses were between 0.003 and 0.025 mSv. As was the case for the HTO results, the differences in the predicted doses can be explained mainly by the variability in the atmospheric dispersion models. For releases of half an hour, it is well known that Doury's model overestimates air concentrations and therefore doses.

For Canada, France and Germany, the main exposure pathway is cereal ingestion. For Japan K, the garden vegetable pathway is more important than cereal ingestion. The contribution of the inhalation pathway to total dose was calculated to be negligible.

Case 1 – Normalized at $6.10^{9}\ Bq.s.m^{-3}$

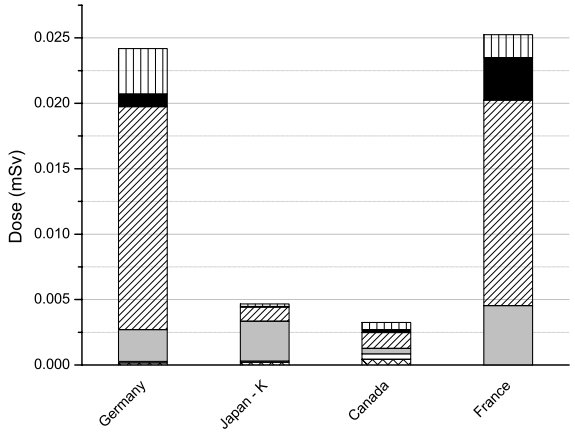

Case 2 – Normalized at $3.10^{10}\ Bq.s.m^{-3}$

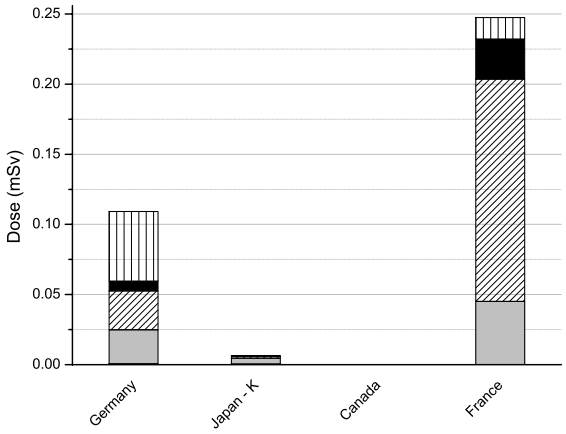

Case 3 – Normalized at $3.10^{11}\ Bq.s.m^{-3}$

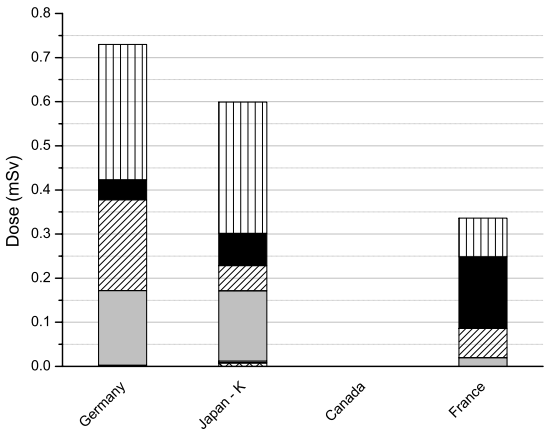

Fig. 9.12. Breakdown of normalized total dose by exposure pathway at 1 km for an HT release.

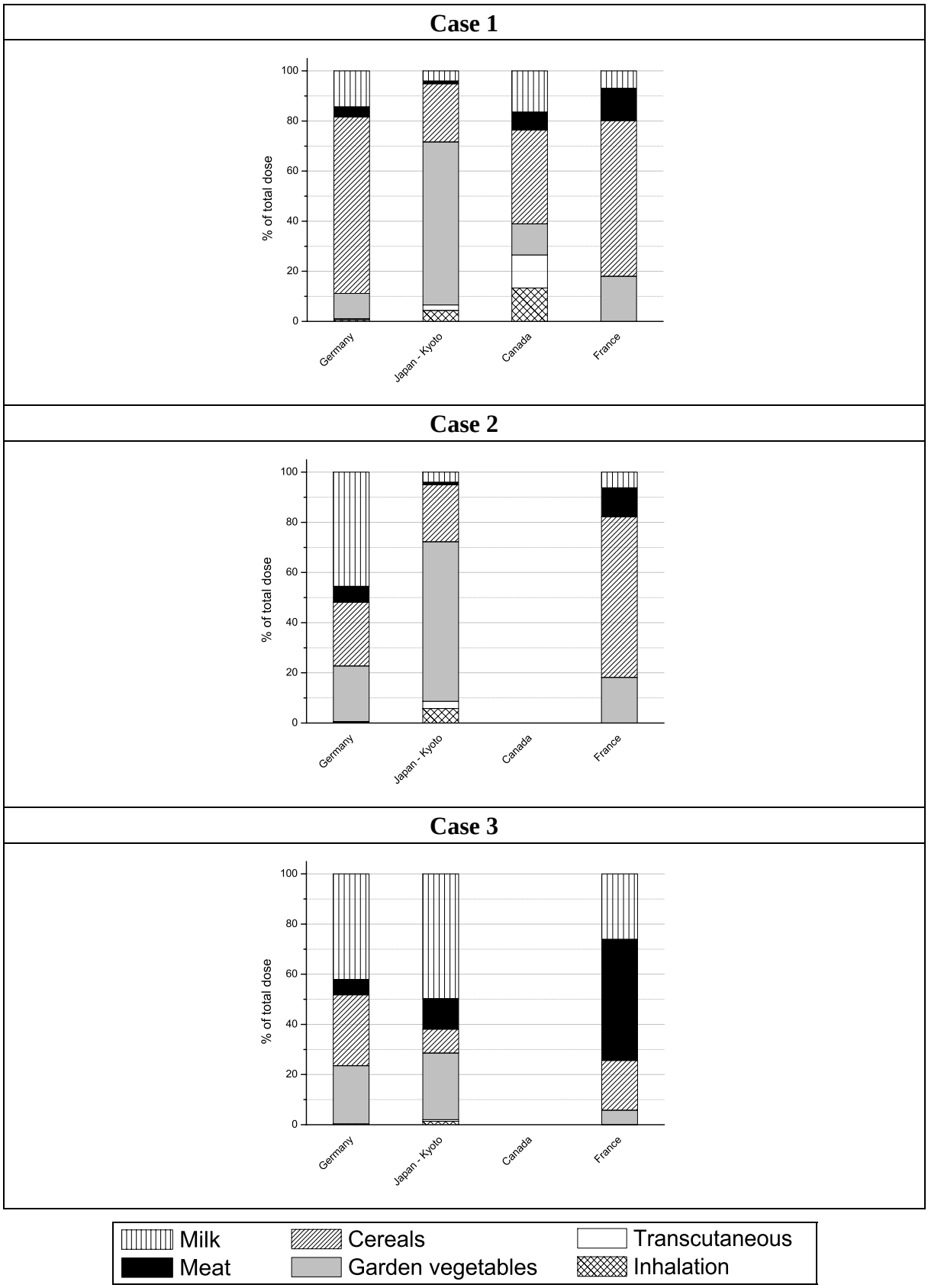

Fig. 9.13. Contribution of the exposure pathways to total dose at 1 km for an HT release.

Case 2: At 1 km, the total doses predicted by the various models lay between 0.02 mSv and 1 mSv. When normalized by the air concentration, the doses ranged between 0.007 and 0.25 mSv. The difference between the German and French results is small (about a factor 2). The total dose for Japan K is much lower; this is most probably due to permanent leaching of the soil in the Japanese model.

For France and Japan K, the relative importance of the different pathways was more or less the same for Cases 1 and 2. For Germany, the relative importance of milk increased significantly from Case 1 to Case 2. Nevertheless, ingestion remained the main pathway of exposure in Case 2, as it was in Case 1.

Case 3: At 1 km, the total doses predicted by the various models ranged between 0.07 mSv and 1 mSv. When normalized by the air concentration, the doses lay between 0.34 and 0.73 mSv. This shows that atmospheric dispersion explains most of the varibility in the results. The contribution of animal products (milk and meat) to the total dose is greater in Case 3 for all participants than in Case 1 or 2. Ingestion of vegetable products (cereals and garden vegetables) is the second most important pathway.

Whatever the meteorological conditions or downwind distance, the release of 10 g of HT leads to exposures below 1 mSv. Doses following an HT release are significantly lower than those for an HTO release. For Cases 1, 2 and 3, respectively, the total dose from the HT release represents 1.5% (0.5–3%), 1.2% (0.9–2.5%) and 2.1% (0.5–4.8%) of the total dose from the HTO release.

9.7. Conclusions

The objective of this study was to analyse the consequences of 10 g of tritium released to the atmosphere as either HTO or HT for three meteorological scenarios. The following exposure pathways were considered: inhalation, skin absorption and ingestion of animal and vegetable products. In the environment, the transformation from HTO to OBT, and from HT to HTO and then to OBT, was taken into account. The study has led to proposed guidelines that could be used by authorities to manage a crisis involving a tritium release.

Eight participants submitted results for the three scenarios: Canada, France, Germany, India, Japan (Kyoto), Japan (Japanet), Korea and Romania. The participants used models ranging from simple to complex.

Atmospheric dispersion modelling, which was the first step in the assessment, was the main source of variability in the predicted doses. Even though the stability of the atmosphere was given in the scenario description, the predicted air concentrations showed significant differences because the participants did not use the same methods for calculating the lateral and vertical dispersion parameters. Also, the participants used different approaches to modelling plume depletion by rain, which increased the variability in the predictions at the longest downwind distances for Case 2.

Predicted concentrations in the various biosphere compartments and food products also varied by an order of magnitude depending on the models used, especially for Case 3 (night release). Nevertheless, all participants found that food ingestion, mainly from plant products, was the dominant exposure pathway. At short distances, the presence or absence of rain did not change the overall results very much.

For the night release, the models varied between two extreme situations: no OBT production following HTO uptake from the air, and OBT production at the daytime rate. More work is required to reach consensus on this point.

Doses for the HT release represent about 1% (range 0.5 to 5%) of the doses for the HTO release according to the models and meteorological conditions considered in this study.

From the results of this intercomparison, a Derived Intervention Level (DIL) has been established based on the activity in salad vegetables that corresponds to a total dose over all exposure pathways of 5 mSv. We propose a DIL of 10^7 $Bq.kg^{-1}$ fresh weight for the activity in salad vegetables measured during the first day after the release, and a value of 10^6 $Bq.kg^{-1}$ on the following day; both of these values are independent of the weather conditions in effect during the release.

CHAPTER 10. THE RICE SCENARIO

10.1. Scenario description

This scenario is based on 10 years of monitoring data collected between 1991 and 2001 by the Japan Atomic Energy Agency (JAEA) around the Tokai reprocessing plant (TRP) in the east end of Tokai-mura, Japan. The monitoring data include airborne ^{14}C release rates, and ^{14}C concentrations in atmospheric CO_2 and rice grain. These data were used as a test of models that predict steady-state ^{14}C concentrations in rice plants growing near a continuous atmospheric source of ^{14}C.

Figure 10.1 shows a map of the study area including the TRP and the environmental monitoring sites. Carbon-14 has been released as $^{14}CO_2$ from three stacks of the TRP (the "main stack", the "sub-1 stack" and the "sub-2 stack") with careful weekly monitoring. The atmospheric $^{14}CO_2$ samples were collected at five monitoring stations (ST-1 to ST-4 and ST-N) on a monthly basis. Two of these stations, ST-3 and ST-4, were located to the southwest of the TRP, which is the most frequent wind direction in this area. ST-2 and ST-N were control sites, situated 4.2 km to the northwest and 14.6 km to the west-northwest of the TRP, respectively. ST-1 was the nearest station to the TRP. Rice grain samples were collected every year at three sites (R-1 to R-3) normally in late September, the harvest season of rice. The R-1 and R-2 sites were located 1.9 km west-southwest and 1.0 km west of the TRP, respectively, whereas R-3 was about 12 km to the west. The distance and direction of all the monitoring stations from the main stack are summarized in Table 10.1.

The scenario provided data on weekly ^{14}C release rates, stack height, inner stack diameter, and the exhaust velocity and temperature of the stack gases. Also available were hourly meteorological data observed at the stack height, the annual average background level of ^{14}C in Japan, and information on the management schedule of a paddy field in Tokai-mura and the growth of rice plants. Participants in the scenario were asked to calculate:

(1) Monthly mean ^{14}C concentrations in air at four monitoring stations (ST-1 to ST-3 and ST-N) from May to October (i.e. the rice growing season) for 1992 to 1997;
(2) Carbon-14 concentrations in rice grain collected at all monitoring sites (R-1 to R-3) for 1992 to 2001; and
(3) 95% confidence intervals on all predictions.

The full scenario description is given in Appendix I.9.

Table 10.1. Distance and direction of the sampling sites from the main stack.

Sampled quantity	Site	Distance and direction from main stack	Notes
$^{14}CO_2$ in air	ST-1	0.5 km northwest	
	ST-2	4.2 km northwest	
	ST-3	2.8 km southwest	
	ST-4	5.2 km west-southwest	Control
	ST-N	14.6 km west-northwest	Control
Rice grain	R-1	1.9 km west-southwest	
	R-2	1.0 km west	
	R-3	11.8 km west	Control

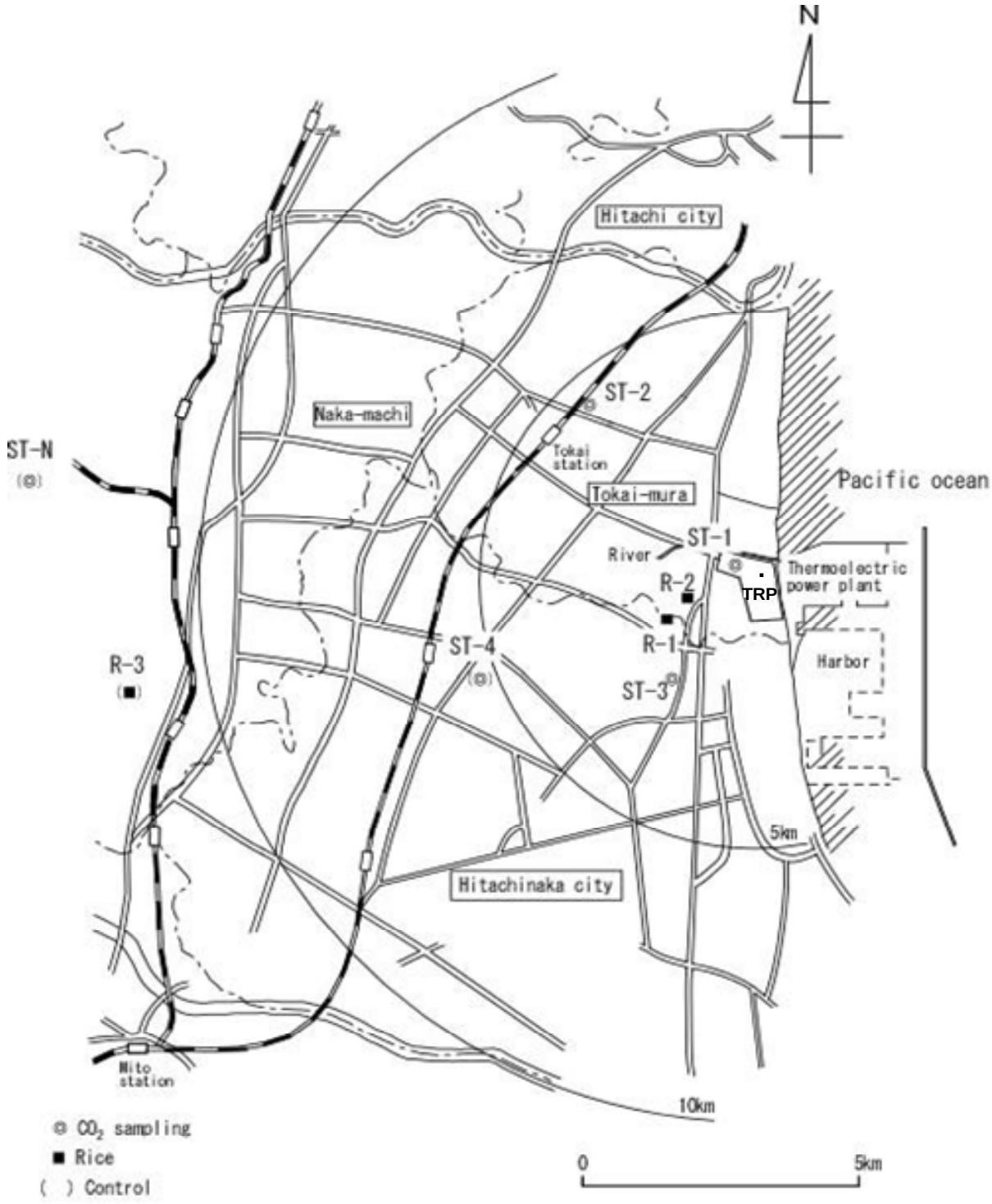

Fig. 10.1. Map of the study area including the TRP and the environmental monitoring sites.

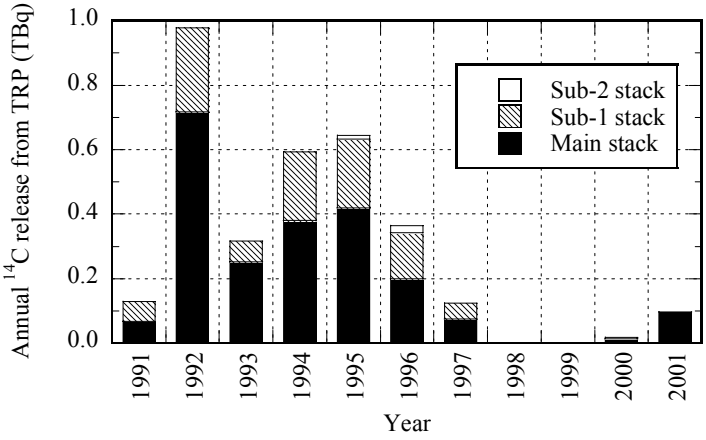

Fig. 10.2. Annual ^{14}C release from the three TRP stacks.

10.2. Observations

10.2.1. Carbon-14 release rates

The annual ^{14}C releases from the three stacks of the TRP are shown in Figure 10.2. Reporting of these data officially started in October 1991 for the main and sub-1 stacks. As for the sub-2 stack, airborne release data have been reported since September 1994, when discharges began. Therefore, the ^{14}C releases shown in Figure 10.2 for the main and sub-1 stacks in 1991 correspond to the 3 month period October to December, and the data for the sub-2 stack in 1994 to the four month period from September to December. Through 10 years of TRP operation, the maximum annual ^{14}C release was 0.98 TBq in 1992. A fire and explosion accident at a bituminization demonstration facility in March 1997 stopped TRP operations until July 2000. During this period, the ^{14}C concentrations in the stack gases were always less than an authorized detection limit of 40 Bq cm^{-3}. The primary source of airborne ^{14}C release from the TRP in all years has been the main stack. Almost all of the ^{14}C release was apportioned to the chemical form $^{14}CO_2$ [99]. Prior to the accident, ^{14}C releases from the sub-1 stack accounted for 21–48% of the total airborne release, but no releases have occurred from this stack since then. The ^{14}C releases from the sub-2 stack made only a small contribution to the total release in all years [100].

10.2.2. Carbon-14 in atmospheric CO_2

The ^{14}C concentrations in atmospheric CO_2 at the five monitoring stations are presented in Figure 10.3, together with the background level of ^{14}C in Japan [101]. The figure demonstrates that the $^{14}CO_2$ concentrations at ST-N as a control site, 14.6 km west-northwest of the main source, were the same as background concentrations. In contrast, the ^{14}C concentrations obtained at the other monitoring stations were slightly elevated, especially at ST-3, which is located southwest of the TRP. Our data on wind direction, observed at the height of ^{14}C discharge, show that winds blow most frequently from the northeast, with a frequency of 20.2% in the 2001 fiscal year [102]. Figure 10.4 shows, as an example, the monthly $^{14}CO_2$ monitoring data at three stations (ST-3, ST-4 and ST-N) in fiscal 1992 and the corresponding monthly ^{14}C release from the TRP. There is a weak, though positive, correlation between the $^{14}CO_2$ concentration at ST-3 and the release rates, suggesting a contribution of TRP-derived ^{14}C to the $^{14}CO_2$ concentration at ST-3. The data also indicate that, outside the periods of ^{14}C release, the $^{14}CO_2$ concentrations are around background, even at the ST-3 site.

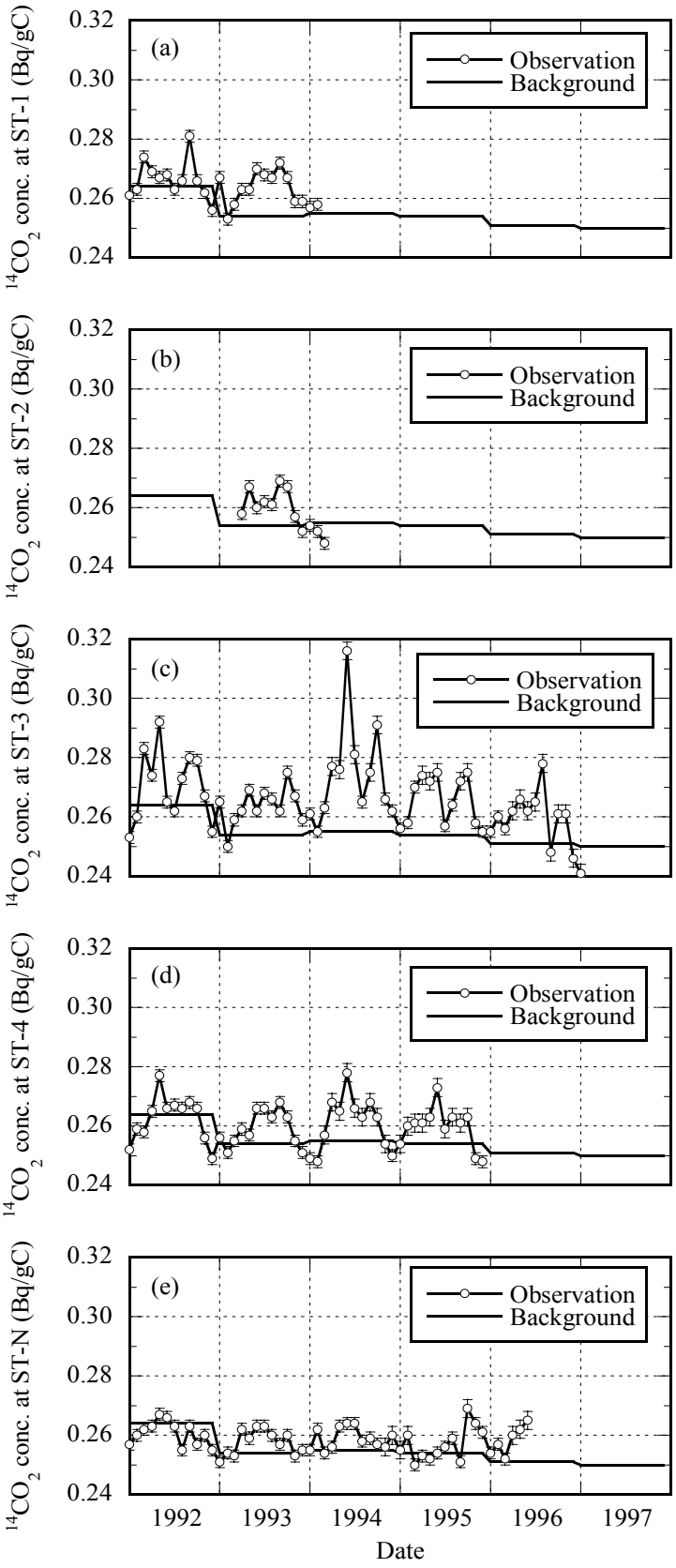

Fig. 10.3. Concentrations of $^{14}CO_2$ in air at (a) ST-1; (b) ST-2; (c) ST-3; (d) ST-4; and (e) ST-N. The error bars indicate the counting error (1σ) of the activity measurements.

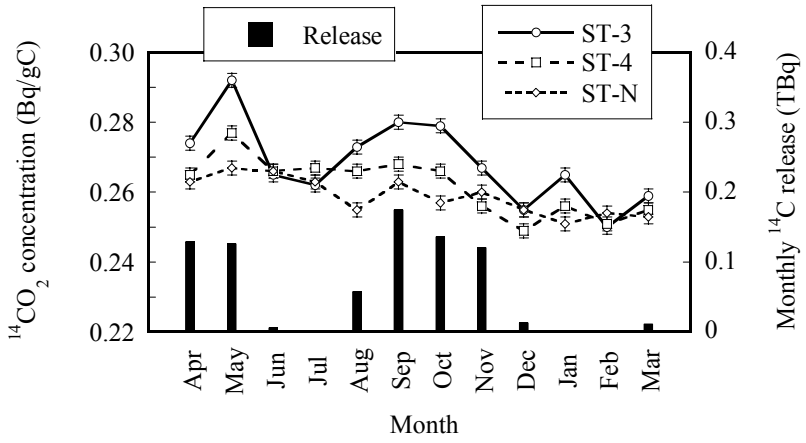

Fig. 10.4. Monthly $^{14}CO_2$ concentrations at three monitoring stations in fiscal 1992 and the corresponding monthly ^{14}C release from the TRP. The error bars indicate the counting error (1σ) of the activity measurements.

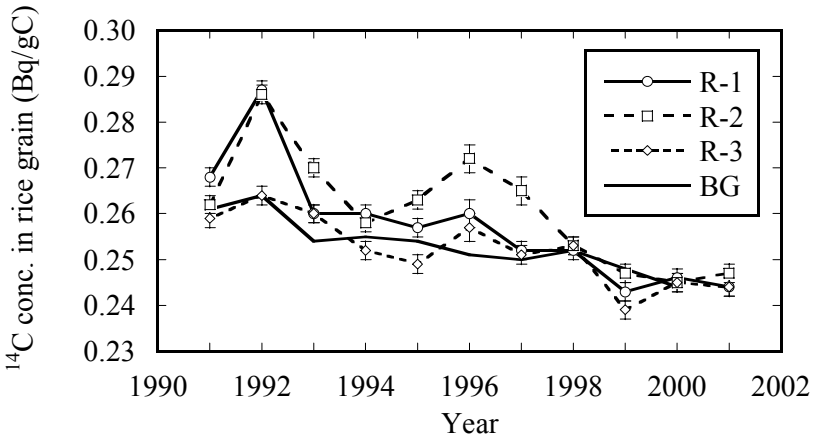

Fig. 10.5. Concentrations of ^{14}C in rice grain samples. The error bars indicate the counting error (1σ) of the activity measurements.

Table 10.2. Participants in the ^{14}C rice scenario.

Participant	Affiliation	Designation in text
P. Davis	Atomic Energy of Canada Limited, Canada	AECL
F. Siclet	Electricité de France, France	EDF
D. Galeriu and A. Melintescu	National Institute of Physics and Nuclear Engineering, Horia Hulubei, Romania	IFIN
M. Saito	Safety Reassurance Academy, Japan	SRA
S. Uchida et al.[a]	National Institute of Radiological Sciences, Japan	UTTY

[a] S. Uchida, H. Takeda, K. Tagami, T. Takahashi and K. Yamamoto.

10.2.3. Carbon-14 in rice grain

Concentrations of ^{14}C in rice grain samples collected between 1991 and 2001 are plotted in Figure 10.5, together with the background level of ^{14}C in Japan [101]. In the 1991 samples, there was no obvious ^{14}C enhancement above background, although the TRP presumably had released some amount of ^{14}C into the atmosphere since the commencement of operations in 1977. This implies that accumulation of TRP-derived ^{14}C on the paddy fields is apparently negligible, at least as of 1991.

The ^{14}C concentrations in the rice grain sampled at R-3, about 12 km west of the main stack, gradually decreased from 0.259 Bq/gC in 1991 to 0.244 Bq/gC in 2001. This decreasing trend was the same as that of the background ^{14}C concentration. In contrast, ^{14}C concentrations slightly higher than background were detected in the samples from the R-1 and R-2 sites. The 1992 samples had the highest ^{14}C concentrations, probably reflecting the largest annual ^{14}C release (0.98 TBq). In contrast, the increases in ^{14}C concentrations seemed to be insignificant in the 1994 and 1995 samples, despite the relatively large annual ^{14}C releases in these years (Figure 10.2). This may be related to the difference in the monthly ^{14}C release patterns in different years [100]. The TRP normally had two reprocessing campaigns a year, the first typically covering the last ten days of September or later to December, and the second from January–March to the last ten days of June. In other words, the monthly ^{14}C releases were normally small during July to September. However, in 1992, the TRP exceptionally began the first campaign during the last ten days of August, with a maximum monthly release of 0.18 TBq in September. On the other hand, in 1994, the maximum monthly release was 0.13 TBq in June, with the release of only 0.02 TBq in September. The monitoring data at ST-3 (Figure 10.3) show a peak in the $^{14}CO_2$ concentration (0.316 Bq/gC) in June. It has been reported that the assimilated-carbon retention percentages in ears at the harvest stage of rice are approximately 7%, 28% and 82% of the total, respectively, when carbon atoms were assimilated in the rice plant at three different growth stages, i.e. vegetative, flowering and milky [103]. This indicates that, in the late ripening period, photosynthates are efficiently translocated to the harvest organs. According to the management schedule of paddy fields, the late ripening period of rice plants in the Tokai-mura area coincides with the period from late August to late September. The monitoring data thus suggest that the timing of ^{14}C releases, as well as the quantity, is an important factor affecting the ^{14}C concentration in rice grain.

In 1996 and 1997, higher ^{14}C concentrations were observed for the rice grain samples at R-2 compared to those at R-3. However, there were no noticeable ^{14}C releases from the TRP from June to the end of September in either of these years. The reason for the higher ^{14}C concentrations at R-2 remains unclear, although it is possible that they are caused by ^{14}C releases from a boiling water reactor and a gas cooled reactor in Tokai-mura. These reactors are located in about 3–4 km north-northeast of the TRP.

10.3. Modeling approaches

Five participants submitted results for this scenario (Table 10.2). All participants treated the scenario as a blind test of their models and submitted results before the observed concentrations were made known to them.

The rice scenario tested models that predict ^{14}C concentrations in rice grown in the vicinity of continuous atmospheric ^{14}C sources. Predictions of the rice concentrations were made by first estimating the $^{14}CO_2$ concentrations in the atmosphere and then modeling the transfer from air to the rice plant. Tables 10.3 and 10.4 summarize the different modeling parameters and assumptions among the models.

Table 10.3. Models, assumptions and parameter values for calculating ^{14}C concentration in air.

Model characteristic	AECL	EDF	IFINa	IFINb	SRA	UTTY
Type of model	Sector-averaged Gaussian plume model	Gridded Gaussian plume model (ADMS3)	Sector-averaged Gaussian plume model	Sector-averaged Gaussian plume model	Sector-averaged Gaussian plume model	Sector-averaged Gaussian plume model
Receptor size	Sector (16×22.5^o)	100×100 m grid	Sector (32×11.3^o)	Sector (32×11.3^o)	Sector (16×22.5^o)	Sector (16×22.5^o)
Number of sources	3 for ST-1; single for other receptors	3	3	3	3	Single
Plume rise estimation	Briggs' equations	Jet equation in the ADMS3 tool	Equation in the scenario	Equation in the scenario	Equation in the scenario	Equation in the scenario
Wind data used for calculation	100 m above sea level	10 m above sea level[a]	100 m above sea level	100 m above sea level	100 m above sea level	100 m abovee sea level
Wind velocity adjustment	Reduction by a factor 0.75–0.9	Automatic treatment by ADMS3	None	None	None	None
Roughness length	0.4 m	0.5 m			Not required	Not required
Equation for vertical dispersion parameter	Smith-Hosker approach	Based on Monin-Obhukov similarity theory	$\sigma_z = a \cdot x^{0.711}$, a depends on stability class	$\sigma_z = a \cdot x^{b}$, a and b depend on stability class	Equations in Japanese Meteorological Guideline[b]	Equations in Japanese Meteorological Guideline[b]
Dry deposition	0.003 m s^{-1}	Not considered	Not considered	Not considered	Not considered	Not considered
Wet deposition	Not considered	Not considered	Not considered	Not considered	Not considered	Not considered
Other considerations and remarks	The sectors in the dispersion model were centered on the receptor of interest.					

[a] Data at 10 m above sea level was entered into the model, which calculated wind speed and direction at emission height.
[b] Meteorological Guideline for the Safety Analysis of Nuclear Power Plants" by the Nuclear Safety Commission of Japan

$\sigma_z = \sigma_0 \cdot x^{a_1+a_2\cdot\log x+a_3\cdot(\log x)^2}$, σ_0, a_1, a_2 and a_3 are constants each depending on the stability class.

Table 10.4. Models and assumptions for calculating ^{14}C uptake in rice.

Model characteristic	AECL	EDF	IFINa	IFINb	SRA	UTTY
Type of model	Specific activity equilibrium model	Dynamic compartment model	Rice growth and ^{14}C transfer to grain	Rice growth and ^{14}C transfer to grain	Specific activity equilibrium model	Dynamic compartment model
Period considered for rice ^{14}C calculations	May to October	May to September	Dependent on temperature	Dependemt on temperature	August and September	May to September
Compartment composition	–	One vegetative and one for ear	–	–	–	Two for organic, one for inorganic and two for environment[b]
Growth curves	–	Logistic curve (fitted to the scenario data)	Logistic curve	Logistic curve	–	Sigmoidal curve
Dark respiration	–	Not considered	Not considered	Not considered	–	Modeled
Other considerations and remarks		Considers remobilization of plant ^{14}C through respiration[a]				Considers two pathways of carbon transfer to ear[c]

[a] The remobilization rate was determined to be 0.01 day^{-1} from the data given in the scenario.
[b] The two organic compartments comprise the stem-leaf-root and ear. The two environmental compartments are air and soil.
[c] Translocation of photosynthates from stems, leaves and roots and direct transfer of carbon from the inorganic pool.

10.3.1. Modelling approaches for atmospheric ^{14}C dispersion

In the case of continuous releases, the diffusion of the contaminant (^{14}C in this scenario) in the direction of the wind is relatively small compared to advective transport by the wind itself. The models adopted to predict transfer under these conditions are termed plume models, of which the best known is the sector-averaged Gaussian plume model:

$$C(x, \theta_i, z) = \frac{1}{\sqrt{2\pi}} \cdot \frac{f_i \cdot Q}{x \cdot \Delta\theta} \cdot \sum_{s=A}^{F} \frac{f_s}{u_s \cdot \sigma_{z,s}} \cdot \left[\exp\left(-\frac{(z-h_e)^2}{2\sigma_{z,s}^{\ 2}} \right) + \exp\left(-\frac{(z+h_e)^2}{2\sigma_{z,s}^{\ 2}} \right) \right] \quad (10.1)$$

where:

$C(x, \theta_i, z)$ is the activity concentration in air (Bq m^{-3}) at downwind distance x (m) and height z (m) in sector θ_i;
f_i is the frequency with which the wind blows into sector θ_i;
Q is the release rate (Bq s^{-1});
$\Delta\theta$ is the sector width (radians);
f_s is the frequency of occurrence of stability class s;
u_s is the average wind speed for stability class s (m s^{-1});
$\sigma_{z,s}$ is the vertical dispersion parameter for stability class s (m); and
h_e is the effective release height (m).

The model assumes an ideal steady-state of constant meteorological conditions over long distances, idealized plume geometry, uniform flat terrain, complete conservation of mass and an exact Gaussian distribution. Gaussian plume models require the categorization of the meteorological conditions into six Pasquill-Gifford stability categories (classes A to F) in which A represents the most unstable conditions, D is neutral and F is most stable. The stability category determines the vertical dispersion parameter (the standard deviation of the distribution of air concentration about the axis of the plume). All participants except for EDF employed a sector-averaged Gaussian plume model for calculating air $^{14}CO_2$ concentrations in the scenario, although there were some differences among the models, mainly in the parameterization of the vertical dispersion parameter and the treatment of plume rise. EDF employed a gridded Gaussian plume model as described below.

The AECL model used the Smith-Hosker approach for obtaining the vertical dispersion parameter, with a surface roughness length of 0.4 m. IFIN tested two models (hereafter referred to as IFINa and IFINb), both of which used a power function with two constants to express $\sigma_{z,s}$. In IFINa, only one constant depended on stability class, whereas both of the constants depended on stability class in IFINb. SRA and UTTY calculated $\sigma_{z,s}$ using the formula given in "Meteorological Guideline for the Safety Analysis of Nuclear Power Plants" by the Nuclear Safety Commission of Japan [104]. EDF used a personal-computer-based atmospheric dispersion modeling system, ADMS3, developed by Cambridge Environmental Research Consultants. This model is also based on Gaussian plume concepts, but the dispersion parameters are derived from surface similarity theory through the Monin-Obukhov length. The model was run at hourly time steps and the hourly predictions were averaged to obtain monthly mean results. The output grid resolution chosen by the modeler was 100×100 m.

All participants except EDF based their calculations on meteorological data obtained at a height of 100 m, the height of the ^{14}C release points at the TRP. EDF used the data obtained

10 m above the ground near the ST-1 sampling site. The ADMS code internally calculates the wind speed and direction at the emission height, taking into account similarity theory and the Eckman spiral. In the AECL model, the 100 m wind speeds were reduced by a factor between 0.75 for near-field receptors and 0.9 for far-field receptors, to account for the fact that the plume encounters lower wind speeds as it diffuses down to the ground. Of the five models, only the AECL model considered plume depletion due to dry deposition, with a deposition velocity of 0.003 m s^{-1}. No wet deposition or re-emission of ^{14}C was taken into account in any of the models.

The modeling of the discharge source is an important factor in any prediction of atmospheric dispersion. TRP has three 90 m stacks and their release points are situated 96 m above sea level. The scenario presented a set of source data that included the ^{14}C release rate and the temperature and exit velocity of the effluent for each stack. The AECL model considered each of the three sources separately in calculating air concentrations at the nearest receptor ST-1, which was within 500 m of the stacks, but a single generic source for the other receptors, which were further downwind. In other words, for all receptors except ST-1, AECL assumed that the entire release from the main, sub-1 and sub-2 stacks was discharged from a virtual stack with average values for the exit velocity, stack gas temperature and stack diameter, and located at the position of the main stack. EDF, IFIN and SRA took explicit account of the three emission sources for all the receptors. UTTY assumed that all discharged ^{14}C was from the main stack, and used the parameters for the main stack in the calculations.

Carbon-14 released from the stacks undergoes plume rise, ascending above the original release height because of the vertical momentum and buoyancy of the stack gases. The effective release height, h_e, in the Gaussian dispersion model (Equation 10.1) is evaluated by adding plume rise to the physical height of the release. The AECL model calculated plume rise using Briggs' equations, which take into account both momentum and buoyancy. SRA and UTTY, and the two IFIN models, used the equation given in the scenario in evaluating plume rise, considering the momentum flux only. For EDF, the model in ADMS3 calculated the plume rise internally, using stack height, diameter, exit velocity and the ^{14}C emission rate.

10.3.2. Modelling approaches for ^{14}C concentrations in rice

The approaches taken by the various participants to model the uptake of ^{14}C by rice varied widely. In the AECL model, the concentrations in rice were simply set equal to the local air concentration (on a Bq/gC basis) averaged over the rice growing period (May to October), on the assumption of specific activity equilibrium between rice plant and air. The SRA model also assumed specific activity equilibrium, but the rice concentrations were determined as the air concentration averaged over the flowering-harvest stage of the rice plant (August and September), assuming that ^{14}C taken into the plant body appears in the rice grain only during this stage.

IFIN used a model describing the incorporation of ^{14}C in rice grain. The model was linked to the growth of dry matter in the plant, which was given by a logistic function. The model considered the incorporation of airborne ^{14}C during three development stages of the plant. The advance in development stage was dependent on the air temperature exceeding a specific temperature, thus making it possible to take into account the effects of year-to-year temperature variability on rice growth. EDF and UTTY employed dynamic multi-compartment models, simulating the incorporation of ^{14}C into new dry matter during plant growth, and the translocation of the photosynthetic assimilate from the vegetative parts of the plant to the grain. In the EDF model, the rice plant was represented by two compartments (the

vegetative part and the ear) with their own growth rates. The model considered two origins of ^{14}C contamination of the ear: ^{14}C from the air at the time of grain growth, and ^{14}C fixed in the vegetative part and remobilized to the grain by respiration.

The UTTY model consisted of two organic compartments (stem-leaf-root and ear), one inorganic compartment (the whole plant) and two environmental compartments (air and soil). The model considered carbon uptake to the inorganic compartment from the environmental compartments, and two pathways from the inorganic compartment to the ear: (1) uptake and temporary storage in the stems, leaves and roots, followed by translocation of photosynthates to the ear; and (2) direct transfer of photosynthates to the ear with no storage in the stems, leaves or roots.This model hence assumes that carbon is readily exchangeable between the environmental compartments and the plant inorganic compartment due to light respiration, and that inorganic carbon is rapidly converted into the organic form during compartment-to-compartment transfers. The growth curves were given as logistic functions in the EDF model and sigmoidal functions in UTTY. The UTTY model considered dark respiration in the nighttime.

Full model descriptions are given in Appendix II.9.

10.4. Comparison of predictions and observations

10.4.1. Atmospheric $^{14}CO_2$ concentrations

Predictions of the $^{14}CO_2$ concentrations in air at ST-1 are compared with the observations in Figure 10.6. "Excess $^{14}CO_2$ concentration" in the figure is defined as the difference between measured and background concentrations for observations, and as the incremental contribution due to TRP-derived ^{14}C for predictions.

All the predictions, except the UTTY result for May, underestimated the observed air concentrations in the period May to August 1993, during which there was only a small quantity of ^{14}C discharged from the TRP. The difference between predictions and observations may be attributed mainly to an error in estimating the observed excess $^{14}CO_2$ concentrations. The annual average background concentration of ^{14}C given in the scenario description, which was determined from the ^{14}C activity in ethanol extracted from wine made in several prefectures in Japan, decreased from 0.264 Bq/gC in 1992 to 0.244 Bq/gC in 2000 [101]. However, the decrease was non-linear, and the concentration in 1993 was low compared to the concentrations in 1992 and 1994. This appears to have led to a high excess $^{14}CO_2$ concentration in 1993 for the observation, which resulted in an apparent under-prediction by the models.

Figure 10.7 shows the comparison between the model predictions of monthly air $^{14}CO_2$ concentrations and the observations at sampling point ST-N, a control site about 14.6 km west-northwest of the discharge sources. As at ST-1, the observed excess $^{14}CO_2$ concentrations at ST-N in 1993 always exceeded those predicted by the models. Additionally, the $^{14}CO_2$ concentrations observed at ST-N in 1993 seem to be high compared to the annual background level, as shown in Figure 10.3(e), suggesting that in 1993 the background ^{14}C concentrations in this area were actually higher than those estimated from the wine samples. We therefore decided to use the observations at ST-N as the background concentrations in this area, and re-defined the excess $^{14}CO_2$ concentration for observations as the difference between the concentrations measured at the sampling point of interest and at ST-N.

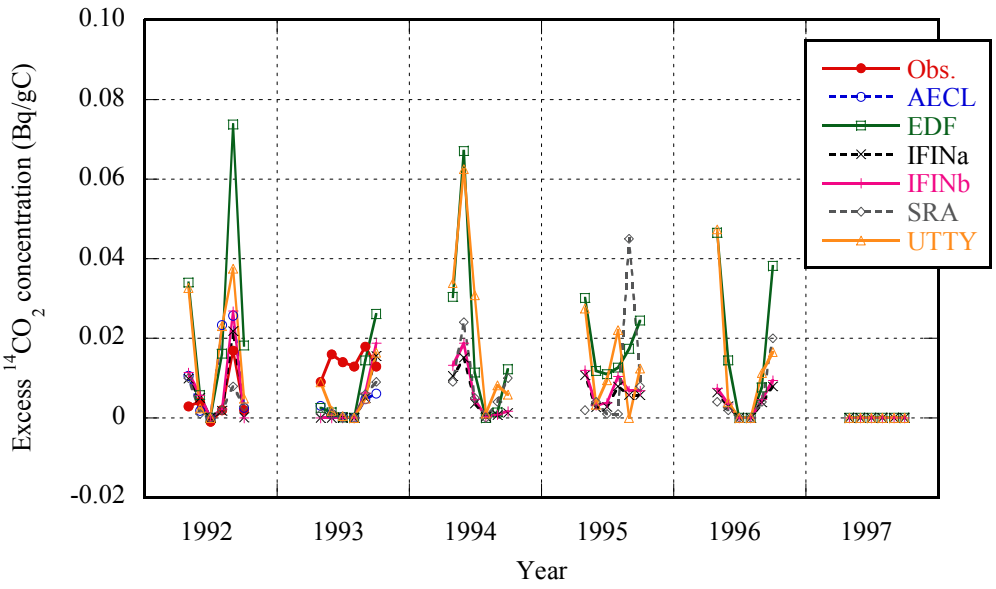

Fig. 10.6. Monthly variation of predicted and observed $^{14}CO_2$ concentrations in air at sampling point ST-1 from May to October for 1992 to 1997. "Excess $^{14}CO_2$ concentration" on the y-axis means the ^{14}C concentration due to releases from the TRP. The observed excess $^{14}CO_2$ concentrations were determined by subtracting the annual average background levels given in the scenario description from the measured concentrations.

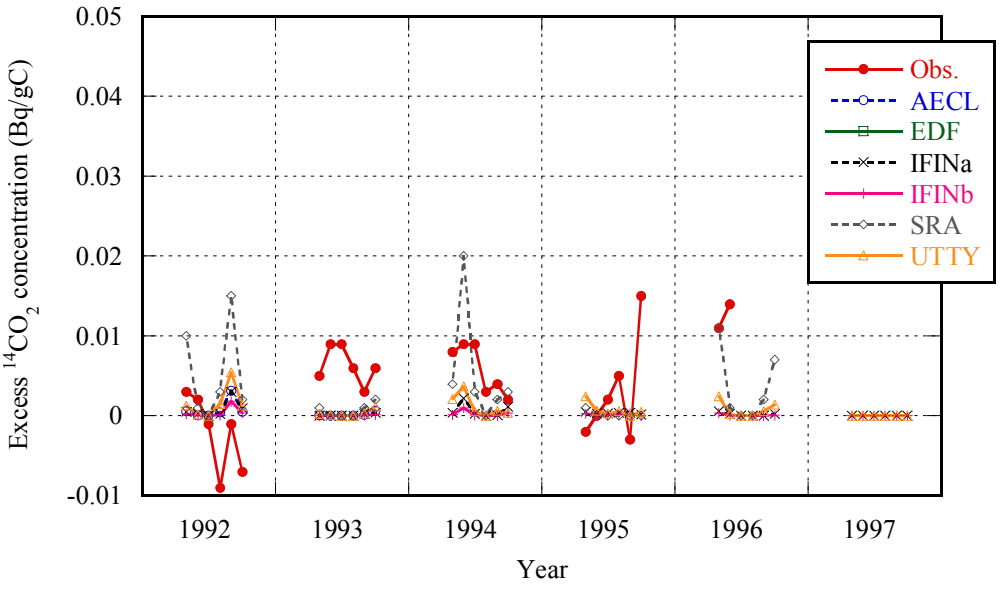

Fig. 10.7. Monthly variations of predicted and observed $^{14}CO_2$ concentrations in air at ST-N from May to October for 1992 to 1997. "Excess $^{14}CO_2$ concentration" on the y-axis means the ^{14}C concentration due to releases from the TRP. The observed excess $^{14}CO_2$ concentrations were determined by subtracting the annual average background levels given in the scenario description from the measured concentrations.

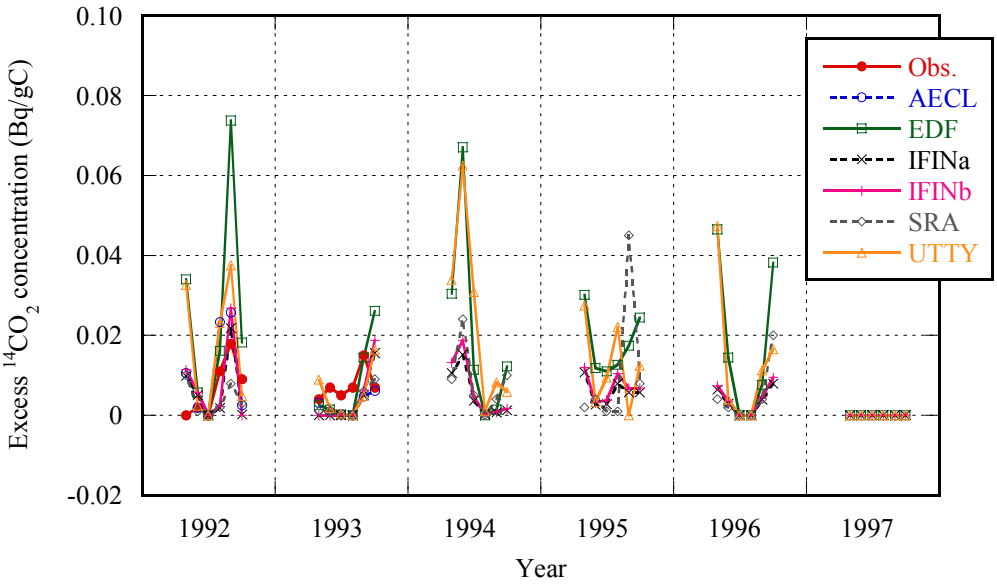

Fig. 10.8. Monthly variations in predicted and observed $^{14}CO_2$ concentrations in air at ST-1 from May to October for 1992 to 1997. "Excess $^{14}CO_2$ concentration" on the y-axis means the ^{14}C concentration due to releases from the TRP. The observed excess $^{14}CO_2$ concentrations were determined by subtracting the concentrations measured at ST-N from those at ST-1.

Figure 10.8 compares the predictions of the excess $^{14}CO_2$ concentrations in air at ST-1 with the observations estimated using this modified approach. The AECL and IFIN predictions agreed in both magnitude and trend with the observed concentrations in 1992, when the TRP recorded the largest annual ^{14}C discharge during the period of interest in this scenario. The remaining three models also predicted well the spike of ^{14}C concentration in September 1992, although the SRA model underestimated this result. The EDF and UTTY models almost always produced higher concentrations at ST-1 than the other models through the entire period. The various predictions, however, agreed with each other and with the observations to within a factor of 3, even for the sampling site very close to the discharge sources. The concentration observed in May 1992 was quite low, although the amount of ^{14}C discharged was comparable to that in October 1992 (see Figure I.9.6 in Appendix I.9).

Plume rise is potentially an important factors explaining the differences in predictions, particularly for sampling site ST-1, which was located very close to the stacks (within about 500 m), and the effective release height (stack height + plume rise) was relatively high. In the case of the equation given in the scenario description, plume rise was estimated from the exit velocity of the stack gases, the stack diameter, and the wind speed at the top of the stack; additional variables (stability class, difference in temperature between stack gases and ambient air, and vertical air temperature gradient) are required for Briggs' plume rise equations, which were used in the AECL model. Table 10.5 compares the values of plume rise derived from these two approaches for the stack and the meteorological conditions of this scenario. The predictions from Briggs' equations lead to larger plume rise than those from the scenario equation for atmospheric stability classes D, E and F, while on average they give lower values for the unstable classes (A, B and C). This suggests the possibility that the air

concentrations predicted by AECL could be lower than the others, considering that stability classes D and F appeared frequently in the meteorological file (for example, in 1992 the frequencies of classes A through F were 0.8%, 15.7%, 8.6%, 41.2%, 4.3% and 29.4%, respectively).

On the other hand, the AECL model reduced the 100 m wind speeds by a factor between 0.75 and 0.9 in the dispersion calculations, in order to account for the fact that the plume encounters lower wind speeds as it diffuses down to the ground. In this regard, the AECL predictions will be higher than those of the other models since air concentrations are inversely proportional to wind speed in the Gaussian plume equation (Equation 10.1). These opposite effects in the AECL model may result in predictions that are similar to those of the other models, not only for September 1992 at ST-1 but also for the entire period at all sampling stations (see Figures 10.7–10.9 and 10.12). Thus, it was not easy to identify plume rise as a key factor for explaining the differences in the predicted air concentrations in this scenario. The models also adopted different approaches with respect to other processes, including vertical dispersion and plume depletion. However, the UTTY model with no plume rise produced a significant overprediction of air concentrations in the first round of calculations, suggesting the importance of plume rise in modeling atmospheric dispersion.

Predictions and observations for $^{14}CO_2$ concentrations in air at ST-2 are plotted in Figure 10.9. Observations were available only for 1993 at ST-2. All models showed similar monthly trends, but UTTY produced significantly larger predictions than the other models.

IFIN, SRA and UTTY assumed basically similar dispersion processes in their models, but showed some differences in the vertical dispersion parameter and the number of sectors, as summarized in Table 10.3. Figure 10.10 compares the vertical dispersion parameters used in these models, and Table 10.6 lists the parameter values for the ST-1, ST-2 and ST-N sites. For stability classes C to F, the SRA and UTTY models gave smaller dispersion parameters than the IFINa model by a factor of 2–5, depending on stability class and distance from source to receptor. The dispersion parameters of the IFINb model were higher than those of IFINa by a factor of about 2 or less for stability classes A to D, whereas they were lower by a factor of about 2 or less in most cases for classes E and F. The only difference between the two IFIN models was the way in which the vertical dispersion parameter was calculated. The excess $^{14}CO_2$ concentrations predicted by the two IFIN models are compared in Figure 10.11. The IFINb predictions were, in general, 20% higher than the IFINa results for ST-1, the nearest sampling site from the source (0.5 km), and were almost half the IFINa results for ST-2 (4.2 km) and ST-N (14.6 km). These results directly reflect the difference in the vertical dispersion parameters.

Table 10.5. Plume rise estimated by different equations.

Stability class	Plume rise (m)	
	Scenario equation [a]	Briggs' equations [b]
A	58	7–48
B	32	6–31
C	21	6–26
D	29	8–75
E	23	9–77
F	36	26–59

[a] Determined only for the main stack from the stability-class-averaged wind speeds.
[b] The range was determined for all stacks for each stability class from the monthly-averaged meteorological data. The lowest plume rise always occurred for the sub-1 stack and the highest for the main stack.

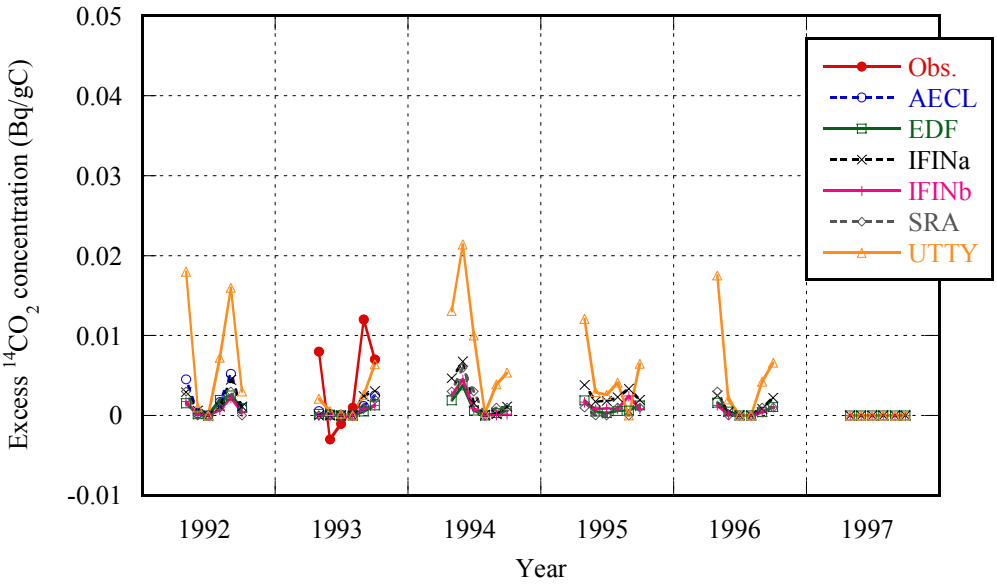

Fig. 10.9. Monthly variations in predicted and observed $^{14}CO_2$ concentrations in air at ST-2 from May to October for 1992 to 1997. "Excess $^{14}CO_2$ concentration" on the y-axis means the ^{14}C concentration due to releases from the TRP. The observed excess $^{14}CO_2$ concentrations were determined by subtracting the concentration measured at ST-N from that at ST-2.

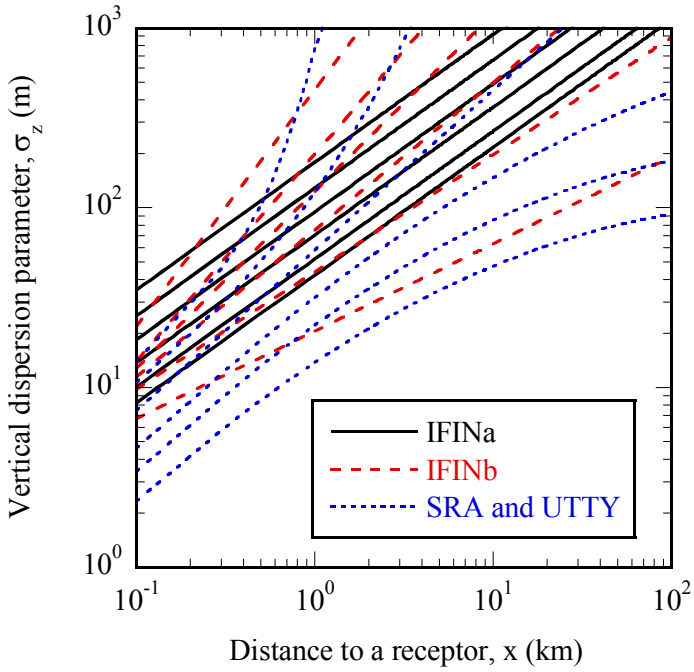

Fig. 10.10. Comparison of vertical dispersion parameters among the IFIN, SRA and UTTY models. The uppermost line for each model corresponds to stability class A and the lowermost line to class F.

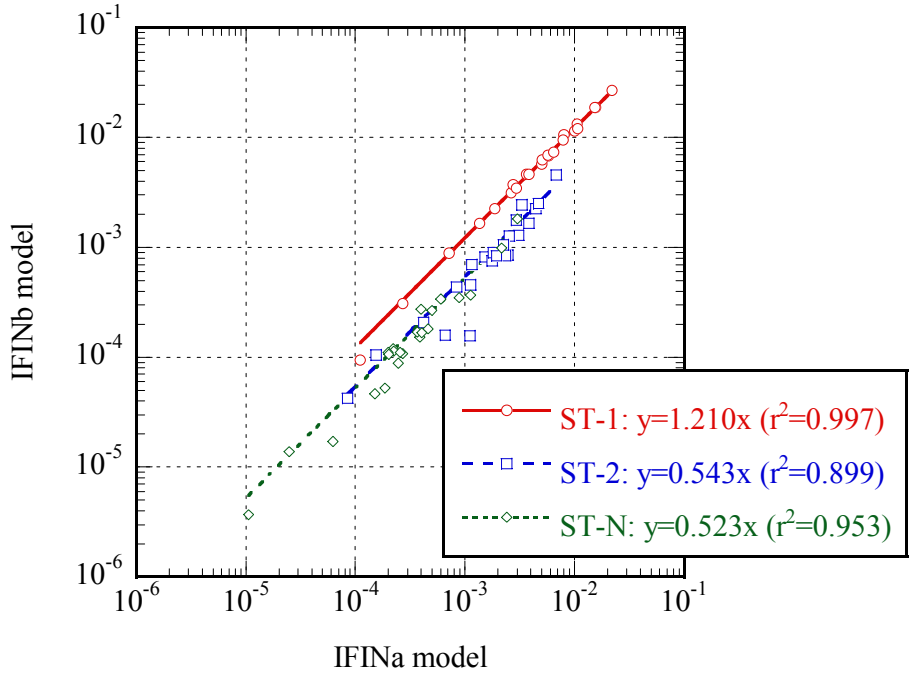

Fig. 10.11. Excess $^{14}CO_2$ concentrations predicted by the IFINa and IFINb models.

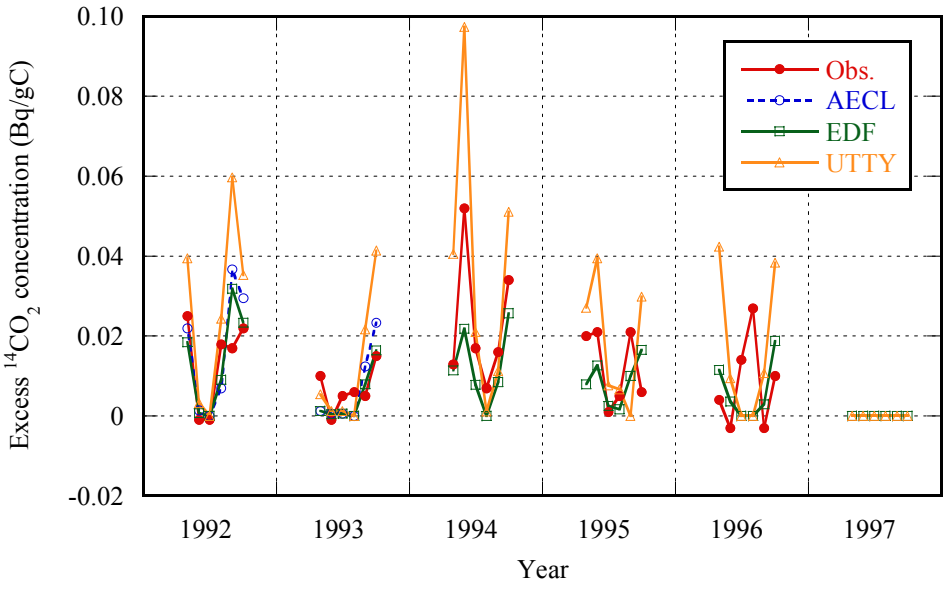

Fig. 10.12. Monthly variations in predicted and observed $^{14}CO_2$ concentrations in air at ST-3 from May to October for 1992 to 1997. "Excess $^{14}CO_2$ concentration" on the y-axis means the ^{14}C concentration due to releases from the TRP. The observed excess $^{14}CO_2$ concentrations were determined by subtracting the concentration measured at ST-N from that at ST-3. IFIN and SRA did not submit results for this endpoint.

Table 10.6. Values of the vertical dispersion parameter (in m) in the IFIN, SRA and UTTY models for three sampling sites.

SC[a]	ST-1[b]			ST-2[b]			ST-N[b]		
	IFa[c]	IFb[c]	S&U[c]	IFa	IFb	S&U	IFa	IFb	S&U
A	109.5	182.9	103.5	497.4	1000[d]	1000[d]	1000[d]	1000[d]	1000[d]
B	78.8	89.5	50.4	358.0	1000[d]	1000[d]	868.1	1000[d]	1000[d]
C	58.1	62.4	31.3	263.8	507.7	208.6	639.7	1000[d]	631.1
D	43.1	42.8	18.3	195.9	243.8	87.0	475.2	675.6	182.0
E	31.7	28.0	13.2	143.9	112.2	55.0	349.1	252.7	100.7
F	25.8	14.7	8.5	117.2	41.3	31.8	284.2	75.8	54.9

[a] SC: Atmospheric stability class.
[b] The sampling sites ST-1, ST-2 and ST-N were located 0.5 km, 4.2 km and 14.6 km distant from the main stack, respectively.
[c] "IFa", "IFb" and "S&U" represent "IFINa", "IFINb" and "SRA and UTTY", respectively.
[d] The models have a cut-off of 1000 m for the vertical dispersion parameter.

Although the SRA and UTTY models used a similar approach to modeling most atmospheric dispersion processes, the two models predicted quite different air concentrations for each sampling site: UTTY predicted higher concentrations than SRA at ST-1 and ST-2 (Figures 10.8 and 10.9), and SRA predicted higher concentrations at ST-N (Figure 10.7). The only difference between the two models was the number of emission sources considered (Table 10.3). This is unlikely to explain the inconsistent results, since the assumption of the UTTY model that all the discharge occurred through the main stack is quite reasonable, because the main stack had three to four times higher release rates than the other two stacks (see Table I.9.1 in Appendix I). Another possible cause for the different predictions of the UTTY and SRA models may have been the pre-processing of the raw meteorological data into the input format required for model calculations.

Figure 10.12 compares the predictions of monthly $^{14}CO_2$ concentrations in air with the observations at sampling point ST-3, where concentrations were most elevated by TRP-derived ^{14}C. Three of the five participants submitted predictions for this endpoint. With the exception of 1996, when high concentrations were unexpectedly observed as mentioned above, all models performed well in reproducing the observations.

The UTTY predictions showed the highest concentrations for all sites. EDF also predicted high concentrations for ST-1, the nearest receptor, but did not do so for ST-2 or ST-3. It is difficult to find specific explanations for these trends because of the many different parameter values and assumptions used in the models, as shown in Table 10.3.

Figure 10.13 shows the predicted to observed (P/O) ratios of excess $^{14}CO_2$ concentration for all models for sampling sites ST-1, ST-2 and ST-3. The figure demonstrates that the P/O ratio is often much less than a factor of 3, although sometimes it is more, especially at ST-1 and ST-2. Three participants (AECL, EDF and IFIN) reported the uncertainties on their predictions. AECL did not carry out an uncertainty analysis for this scenario but made uncertainty estimates based on results of previous analyses of similar situations. Their 2.5% and 97.5% confidence limits on the predicted seasonal air concentrations (excess $^{14}CO_2$ concentrations) ranged from BE/7 to BE/2, and from 2·BE to 7·BE, respectively, in terms of the best estimate (BE) predictions. The uncertainties were high (BE/7 and 7·BE) close to the source where the predictions were very sensitive to the effective release height and the vertical dispersion parameter. The uncertainties decreased further downwind.

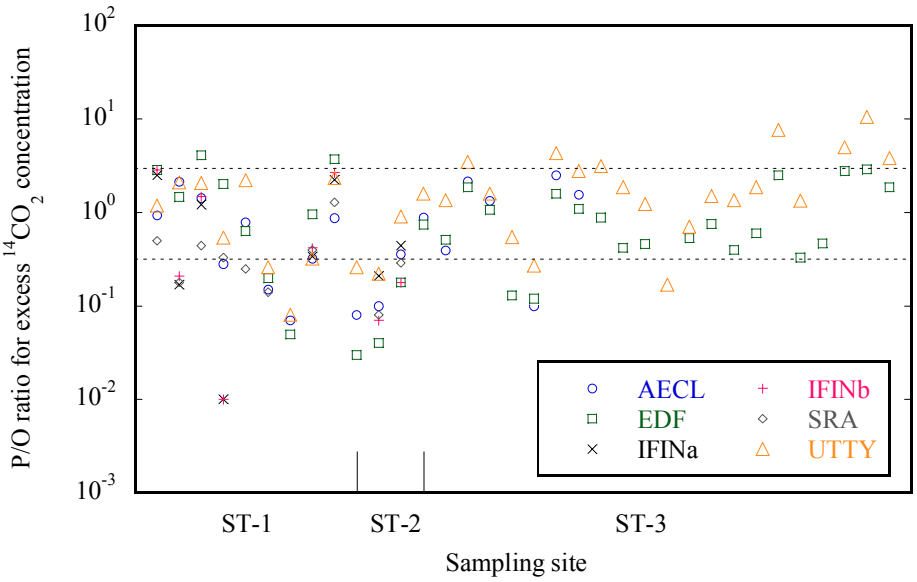

Fig. 10.13. Predicted to observed (P/O) ratios of monthly excess $^{14}CO_2$ concentrations in air for three sampling sites. Dashed lines in the figure indicate a factor of 3 difference between predictions and observations. No data were plotted in the case that the predicted value equaled zero, or that the observed excess $^{14}CO_2$ concentration had a negative value.

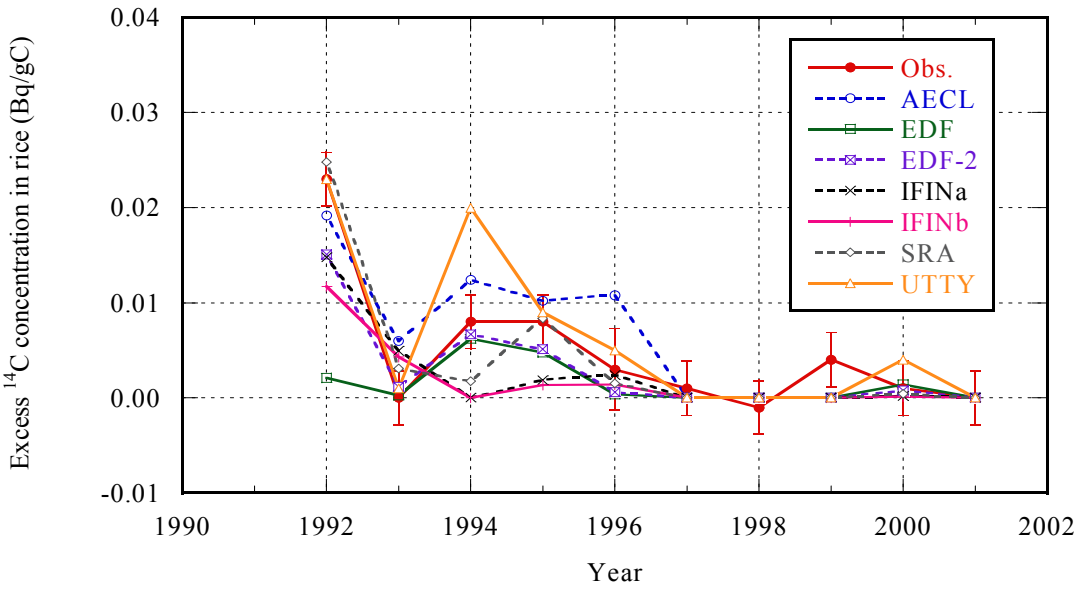

Fig. 10.14. ^{14}C concentrations in rice at R-1 from 1992 to 2001. "Excess ^{14}C concentration" on the y-axis means the ^{14}C concentration due to releases from the TRP. The observed excess ^{14}C concentrations were determined by subtracting the concentration measured at R-3 from that at R-1. The error bars on the observations were derived from the counting errors (1σ) of the activity measurements. The results marked EDF-2 were obtained with a linear rice growth model (as opposed to a logistic curve) in the EDF model.

IFIN also did not carry out a full uncertainty analysis for this scenario. Based on their previous experience, they tentatively assessed 95% confidence intervals similar to those of AECL, with lower and upper limits of BE/3 and 4·BE, respectively for the excess air concentrations. The EDF predictions had about BE/10 and 10·BE for the 2.5% and 97.5% confidence limits, respectively.

The uncertainties in the observed excess $^{14}CO_2$ concentrations are also quite high because the measured values are only slightly above background. Given the magnitude of the uncertainties, it is clear that the predictions and observations agree when the uncertainties are taken into account. Thus, good model performance for the predicted air concentrations in this scenario can be achieved even with a simple Gaussian plume model with very different parameters and assumptions. It should be again noted that the Gaussian plume model assumes constant airflow and turbulence characteristics over the plume travel distance, implying that the wind speed and direction are uniform from source to receptor, that the surface roughness remains constant with downwind distance, and that the terrain over which the plume travels remains flat.

10.4.2. Carbon-14 concentrations in rice

Predictions of the ^{14}C concentrations in rice at R-1, R-2 and R-3 are compared with the observations in Figures 10.14–10.16, respectively. As in the case of air concentrations, we assumed the concentrations at control point R-3 (about 11.8 km from the sources) were equal to background levels, and defined the excess ^{14}C concentrations in rice as the difference between the concentrations measured at the sampling point of interest and at R-3. Most models predicted no or little incremental contribution of TRP-derived ^{14}C at the control site R-3 (Figure 10.16). In general, the predictions for R-1 were in better agreement with the observations than those for R-2. The main reason for this is related to the potential anomaly, mentioned above, in the observed data at R-2 for 1996 and 1997, where the ^{14}C discharges from the stacks were lower than for other years, but the observed concentrations in rice were higher. Overall, the rice concentrations predicted by EDF and IFIN were lower than the observations.

All the models except for EDF predicted the excess ^{14}C concentrations in rice in 1992 at R-1 and R-2 within a factor of 2. The EDF predictions were one order of magnitude lower than the other predictions and the observations in 1992. However, the air concentrations predicted by EDF were comparable to those of the other participants at ST-3, the nearest air sampling point to R-1, and were considerably higher at ST-1, the nearest to R-2, implying that the under-predictions in rice concentrations by EDF resulted from the rice model itself, and particularly the type of growth model. EDF used a logistic function to describe rice grain growth. To check the influence of the growth function on the ^{14}C concentration at harvest, the logistic function was replaced by a linear function (Figure 10.17), which increased the predicted concentrations by a factor of 7. This is due to the absence of discharge in August at a time when the logistic growth rate is highest. In the following years, the differences between the two growth functions were much smaller (Figures 10.14 and 10.15). These results indicate that the rice growth function is one of the key assumptions affecting the predictions of dynamic rice models. In Figure 10.18, the results of the EDF models are compared to the predictions of a simple steady-state model based on the specific activity in air averaged over the period May to September.

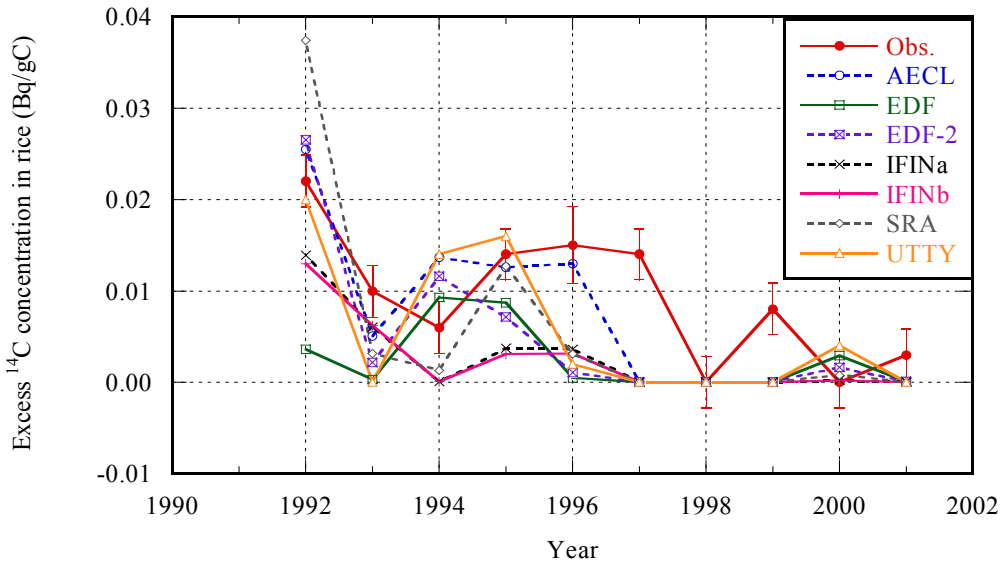

Fig. 10.15. ^{14}C concentrations in rice at R-2 from 1992 to 2001. "Excess ^{14}C concentration" on the y-axis means the ^{14}C concentration due to releases from the TRP. The observed excess ^{14}C concentrations were determined by subtracting the concentration measured at R-3 from that at R-2. The error bars on the observations were derived from the counting errors (1σ) of the activity measurements. The results marked EDF-2 were obtained with a linear rice growth model (as opposed to a logistic curve) in the EDF model.

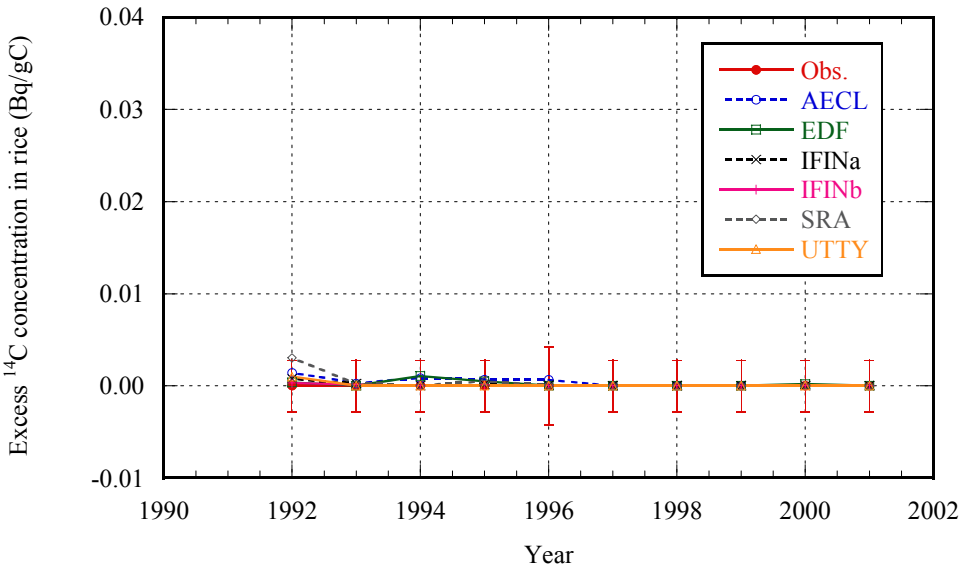

Fig. 10.16. ^{14}C concentrations in rice at R-3 from 1992 to 2001. "Excess ^{14}C concentration" on the y-axis means the ^{14}C concentration due to releases from the TRP. The observed excess ^{14}C concentration was assumed to be zero, i.e., it was assumed there was no incremental contribution of TRP-derived ^{14}C to the concentration at R-3. The error bars on the observations were derived from the counting errors (1σ) of the activity measurements.

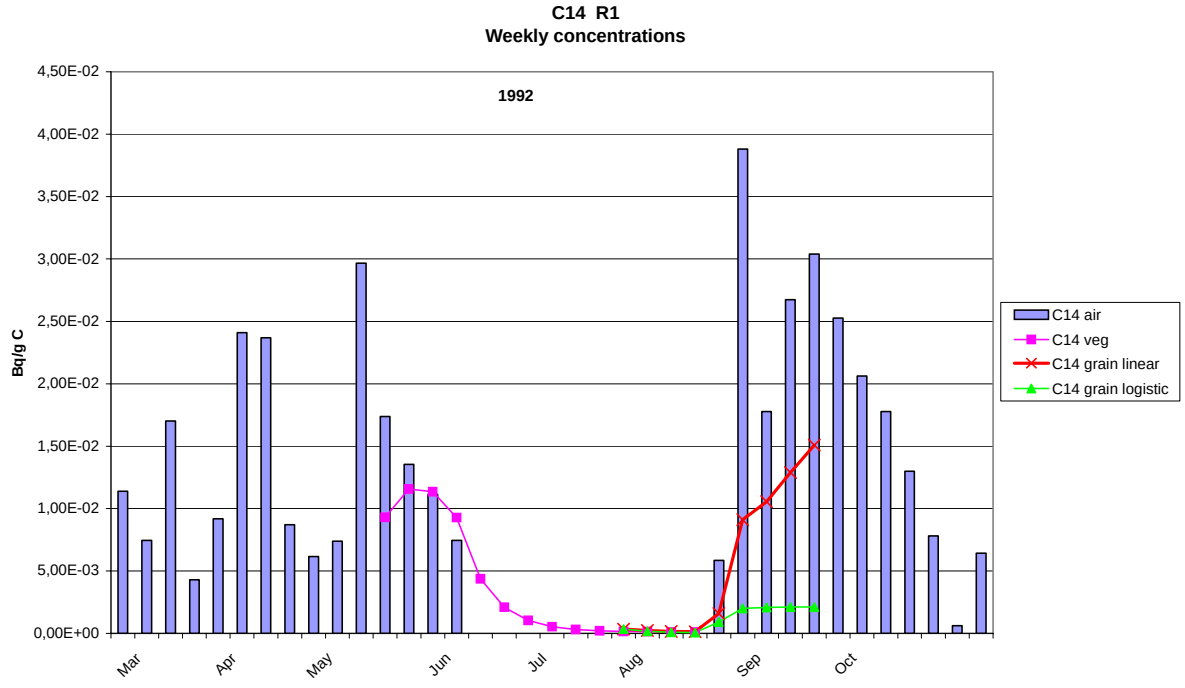

Fig. 10.17. Relation between rice growth curve and predicted ^{14}C concentrations in rice grain in 1992 in the EDF model.

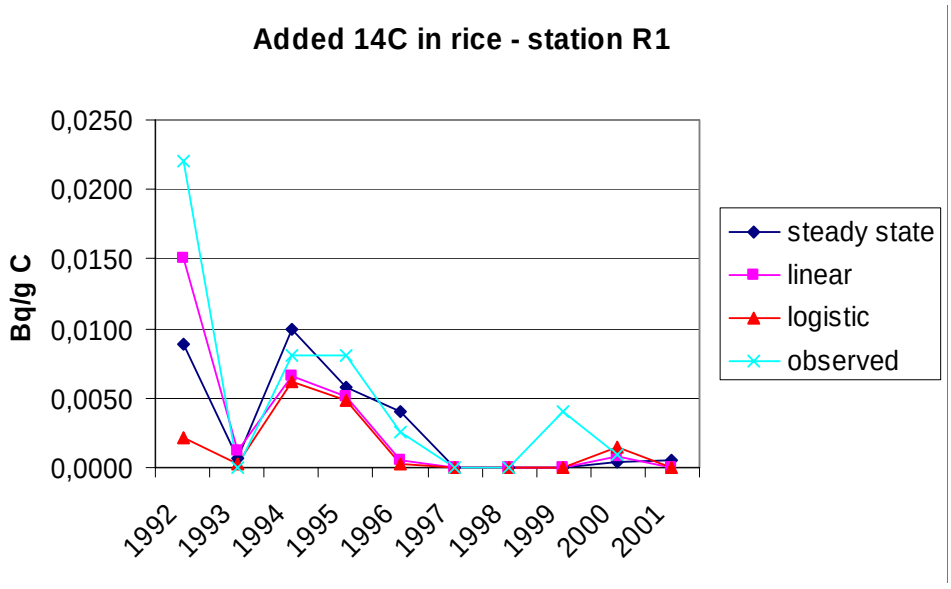

Fig. 10.18. Comparison of the ^{14}C concentration in rice predicted by the dynamic EDF models and a steady-state model based on specific activity concepts.

Table 10.7. Excess $^{14}CO_2$ concentrations in rice (in Bq/gC) predicted by the SRA model for 3 averaging periods at R-1 and R-2.

Site	R-1			R-2		
Year \ Period[a]	M–O	A–S	M–S	M–O	A–S	M–S
1992	0.018	0.025	0.017	0.018	0.037	0.019
1993	0.004	0.003	0.002	0.003	0.003	0.002
1994	0.016	0.002	0.017	0.017	0.001	0.017
1995	0.012	0.008	0.010	0.013	0.013	0.010
1996	0.007	0.001	0.006	0.011	0.003	0.009

[a] "M–O", "A–S" and "M–S" mean "May to October", "August to September" and "May to September", respectively.

AECL and UTTY over-predicted the ^{14}C concentrations in rice in 1994 for both the R-1 and R-2 sites, whereas IFIN and SRA under-predicted. In 1994, the TRP released a large quantity of ^{14}C in June and minor quantities in September, as mentioned previously. AECL and SRA both employed specific activity models that assumed the concentrations in rice equal to the concentrations in local air, but with different averaging times: May to October for AECL and August to September for SRA. The UTTY model took into account the translocation of photosynthates formed in the plant body before flowering to the ears, as well as the direct transfer of photosynthates formed during ripening to the ears. Thus the over-predictions in the AECL and UTTY models may be due to an inappropriately large assimilation of ^{14}C in June to the concentration in the ears at harvest.

IFIN defined a parameter DVS to indicate the development stage of the plant in their rice model. DVS had a value of 0 at emergence, 1 at flowering and 2 at harvest, and was a function of air temperature accumulated from the time of emergence. The DVS value controlled the relative contribution of two grain formation processes: (1) the daily new dry matter produced in the plant and translocated to the grain; and (2) the translocation of dry matter produced previously to the grain. No grain formation occurred for DVS<0.8 (i.e. before flowering); a linear relationship held for 0.8 < DVS < 1.2; and all new dry matter appeared in the grain for DVS >1.2. Therefore, the local ^{14}C concentration in air before flowering (strictly, before the stage corresponding to DVS = 0.8) never directly affected the ^{14}C concentration in rice at harvest, which may explain the lower predicted rice concentrations for 1994.

Specific reasons for the differences in the predicted concentrations in rice were difficult to identify because the models differed with respect to atmospheric dispersion. We therefore made a comparison of rice concentrations normalized against air concentrations to enable a thorough comparison of the different rice models. The comparison was based on limited predictions by IFINa, SRA and UTTY of monthly air concentrations from May to October at R-1 and R-2.

Table 10.7 presents excess $^{14}CO_2$ concentrations calculated with the SRA specific activity model averaged over the three different periods: May to September (corresponding to the period for calculating rice concentrations in the AECL model), August to September (in the SRA model), and May to September (in the UTTY model), at R1 and R2 for 1992–1996. The table indicates that SRA predicts significantly lower excess rice concentrations in 1992 and higher concentrations in 1994 when adopting the longer averaging period. This result explains

the discrepancy between the SRA and AECL predictions (Figures 10.14 and 10.15), considering that even the highest rice concentration was only about 10% above background. It is therefore concluded that the rice concentrations predicted using the specific activity model depend strongly on the averaging period used.

For two of the dynamic models (IFINa and UTTY), Table 10.8 shows the gross rice ^{14}C concentrations normalized against the gross local air concentrations (May to September averaging period only; hereafter referred to as "R/A_{M-S}") at both R-1 and R-2. The UTTY values were all less than or equal to unity. For 1992 and 1994, they ranged from 0.90 to 0.92, indicating that the gross rice concentrations were always about 10% lower than the gross local air concentrations averaged over the rice growing period considered in the UTTY model. The IFIN values of R/A_{M-S} were close to unity for 1992 and 1993, but gave a slightly lower value of 0.96 in 1994. The values greater than unity probably arose because the period when the air concentration affects the rice concentration depends on air temperature in the IFIN rice model. The ^{14}C discharges from the TRP showed a contrasting pattern between 1992 and 1994: large discharges in September (milky stage) in 1992 and in June (vegetative stage) in 1994. The IFINa model produced relatively high air concentrations (0.290–0.296 Bq/gC including background) for these months at both sites, whereas the corresponding air concentrations averaged over May to September were estimated to be about 0.278 and 0.267 Bq/gC (corresponding to excess rice concentrations of 0.014 and 0.012 Bq/gC). Thus, the negligible contribution of TRP-derived ^{14}C (0.255 Bq/gC including background) predicted for 1994 by the IFINa model may be attributed mainly to an under-prediction by the rice model.

The considerably lower R/A_{M-S} values of 0.59–0.81 obtained for 1995 and 1996 mean that IFIN's rice model estimates the rice concentrations to be about 20–40% lower than the local air concentrations averaged over May to September. In 1995 and 1996, the IFINa model predicted high air concentrations (0.399–0.526 Bq/gC including background) in September at both sites. This suggests that the September air concentration does not always contribute predominantly to the rice concentration at harvest in IFIN's model.

Figure 10.19 presents P/O ratios of excess ^{14}C concentrations in rice for all models and years for sites R-1 and R-2. The figure shows that most P/O ratios for AECL, EDF-2, SRA and UTTY fall within a factor of 3. The IFIN models give significantly low P/O values in 1994, due probably to the reasons mentioned previously. EDF sometimes gives low P/O ratios. AECL reported that the uncertainties in the predicted rice concentrations were the same as those in the predicted air concentrations because the uncertainty in ^{14}C transfer was likely to be much less than the uncertainty in atmospheric dispersion for specific activity models. IFIN tentatively assessed 95% confidence intervals with a lower limit of BE/3 and an upper limit of $5 \cdot BE$ for the rice concentration predictions. The EDF uncertainties were no higher than those of AECL or IFIN. Taking the uncertainties into account, most model predictions of the excess ^{14}C concentrations in rice grain agreed with the observations. The specific activity and dynamic models performed equally well for the conditions of this scenario, i.e. the prediction of steady-state ^{14}C concentrations in rice growing near a continuous atmospheric source of ^{14}C. Good performance in predicting ^{14}C concentration in rice grain thus can be achieved by models with very different structures and assumptions.

Table 10.8. R/A_{M-S} values for the IFINa and UTTY predictions.

Site	R-1		R-2	
Year \ Period	IFINa	UTTY	IFINa	UTTY
1992	1.01	0.91	1.00	0.90
1993	1.01	0.98	1.02	0.99
1994	0.96	0.92	0.96	0.92
1995	0.80	0.95	0.81	1.00
1996	0.59	0.90	0.61	0.92

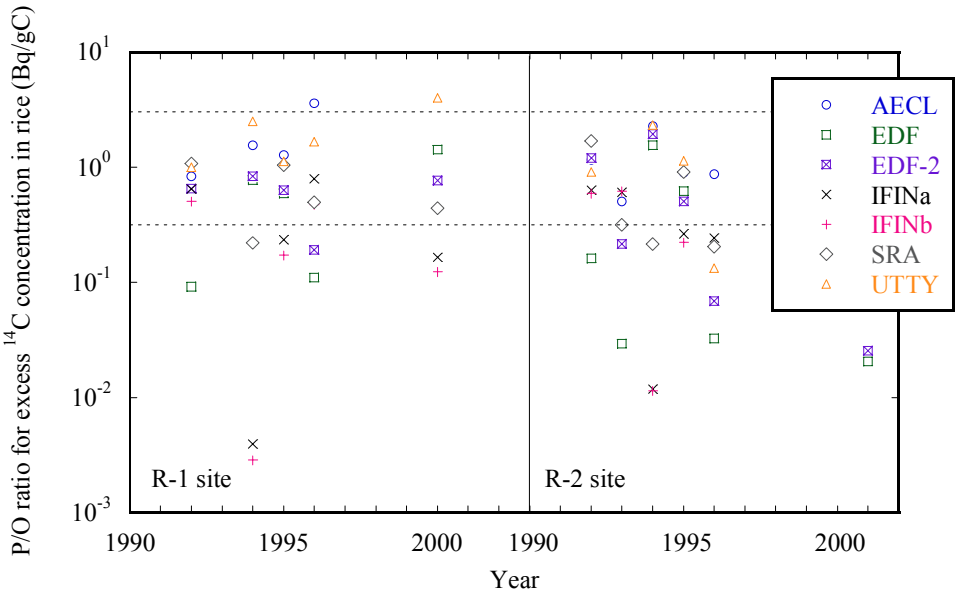

Fig. 10.19. Predicted to observed (P/O) ratios of excess ^{14}C concentrations in rice for two sampling sites. Dashed lines in the figure indicate a factor of 3 difference between predictions and observations. No data were plotted in the case that the predicted value equaled zero, or that the observed excess ^{14}C concentration had a negative value.

10.5. Conclusions

The rice scenario was based on long-term monitoring data collected by JAEA around the Tokai reprocessing plant (TRP) in eastern Japan. The scenario provided a good test of models that predict steady-state ^{14}C concentrations in air and rice plants growing close to a continuous atmospheric source of ^{14}C. Participants in the scenario were provided with information on the exhaust stacks, weekly discharge rates, hourly meteorological data, background ^{14}C levels in Japan and the growth of rice plants. From these data, the participants were asked to calculate monthly average ^{14}C concentrations in air at four sites over a 6 year period, and ^{14}C concentrations in rice grain at harvest at three different sites for each year from 1992 to 2001.

Five participants submitted predictions for this scenario. Each used a Gaussian plume model to predict air concentrations, but adopted different approaches to calculating plume rise, vertical dispersion and plume depletion during its journey from source to receptor. Despite

these differences in approach, the various predictions agreed well with each other and with the observations when background ^{14}C levels were subtracted and uncertainties were taken into account. Thus, the main conclusion of this study was that simple Gaussian plume models with different parameters and assumptions can provide reasonably accurate predictions of average air concentrations, even close (within 500 m) to tall stacks. No one model produced consistently superior predictions over all sites and times.

Two participants (AECL and SRA) set the ^{14}C concentrations in rice grain equal to the concentrations in air (on a Bq/gC basis), on the assumption of specific activity equilibrium between plant and air. The averaging time of the air concentrations is a key factor in specific activity models, particularly in the case of dynamic changes in local air concentrations during plant growth. The AECL and SRA models performed equally well although they used quite different averaging times (May to October in the case of AECL, and August to September in the case of SRA). Carbon-14 appears in the grain via direct incorporation during growth but also via translocation from the vegetative parts of the plant. Thus, although the rice grains begin to form only in August, the longer averaging period may be more appropriate if translocation makes a significant contribution to the total ^{14}C content of the grain.

The other participants employed dynamic multi-compartment models to calculate concentrations in rice, simulating the incorporation of ^{14}C into new dry matter during plant growth and the translocation of the photosynthetic assimilate from the vegetative parts of plant to the grain. The use of different rice growth curves in these models gave very different predictions for the concentrations at harvest when the ^{14}C discharge rates varied in time. Growth curves that predicted the largest growth rates when the discharge rates were greatest gave higher concentrations than curves for which the maximum growth and discharge rates occurred at different times.

Most models, including both the specific activity and dynamic models, predicted the rice concentrations within a factor of 3 of the observed data, although the highest observed concentrations were only about 10% above background. In other words, for the scenario presented here, the specific activity models (which are relatively simple) produced predictions that were similar to those of the dynamic models (which are relatively more complex). However, this scenario applies to steady-state conditions for which the differences in predictions among models of different complexity is expected to be small. It is therefore concluded that the rice models tested are all adequate for steady-state conditions (chronic releases). However, the adequacy of the models, and of specific activity models especially, is less clear in the case of dynamic releases (e.g. accidental releases). Therefore, different models with different levels of complexity may be required to address the diversity of applications for which environmental ^{14}C models are needed.

CHAPTER 11. THE POTATO SCENARIO

11.1. Scenario description

The scenario for ^{14}C transfer in crops is based on unpublished data contained in a PhD thesis from Imperial College, UK [105]. The crops investigated were cabbage, beans and potatoes. We decided to base the scenario on potatoes because they are widely used.

Approximately two hundred potato tubers (*Solanum tuberosum* cv. Romano) were placed in dark storage on July 5, 1995 and left to chit (sprout). Some tubers were split to produce sufficient plants to transfer three to each of one hundred pots on August 4, 1995. Some of the plants were later thinned to two per pot. The pots had dimensions 40×40×40 cm and each was filled with Fison's Levington multi-purpose peat-based compost.

The crops were exposed to $^{14}CO_2$ in the MAFF/CARE wind tunnel. This allowed the exposure to take place under realistic atmospheric boundary layer conditions, while providing adequate containment for the $^{14}CO_2$. The experimental layout given in the scenario description shows four plants in each pot. This was the case for cabbage and beans, but only 2–3 plants per pot were used in the potato experiments. The wind tunnel has the capacity to accommodate thirty pots. Twenty of these constituted the 'fetch' of the canopy and facilitated the build up of a turbulent boundary layer. The remaining ten pots provided the plant material to be sampled as part of the experiment, enabling a maximum of thirty potato plants to be sampled for each exposure (but generally 20 plants in the later development stage).

The potato plants were fumigated with $^{14}CO_2$ for approximately 10 hours within the wind tunnel at six stages of the crop's growth cycle. The schedule of fumigations is given in Table 11.1, which shows the number of days after sowing at which fumigation occurred (the stage of development) and the fumigation date. Following exposure, one-sixth of the plants in the experimental section were selected at random and sampled immediately to measure the activity concentration of ^{14}C fixed by the crop (harvest H1). The remainder of the crop was transported to a walled garden at Imperial College and sampled a further five times until maturity (harvests H2 to H6) at intervals that varied in frequency according to the age of the crop at fumigation, as given in Table 11.2.

Information on the ^{14}C air activity concentration as a function of time during each fumigation, the time-integrated ^{14}C air concentrations, and the ranges of temperature and photosynthetically active radiation (PAR) in the tunnel during each experiment are given in Tables 11.3–11.5, respectively. The average dry weight of the roots, leaves, stems and tubers in all experiments for every harvest time, and the dry weight fractions for each harvest, are given in the scenario description.

It should be noted that normal development for potatoes requires about 140 days to maturity, which was not available for these experiments. The late chitting and sowing dates meant that the plants were growing later in the season than normal, and were exposed to fall rather than summer weather. It is possible that the tubers were not fully mature at final harvest.

Modelers were asked to calculate the following:

(1) the ^{14}C concentration in the leaves at each sampling time (H1 to H6) for each experiment [Bq/g dry matter (dm)];
(2) the carbon concentration in the tubers at final harvest (H6) for each experiment [Bq/g dm]; and
(3) the 95% confidence intervals on all predictions.

The full scenario description is given in Appendix I.10.

Table 11.1. Fumigation schedule for experiments in which potato plants were exposed to $^{14}CO_2$.

Designation of Experiment	Time of Fumigation (Days after sowing)	Fumigation date
P1	21	August25, 1995
P2	33	September 7, 1995
P3	47	September 21, 1995
P4	61	October 5, 1995
P5	74	October 18, 1995
P6	89	November 2, 1995

Table 11.2. Potato sampling schedule.

Harvest	P1		P2		P3		P4		P5		P6	
	Age*	T**	Age	T	Age	T	Age	T	Age	T	Age	T
H1	21	0	33	0	47	0	61	0	74	0	89	0
H2	31	10	38	5	53	6	65	4	79	5	90	1
H3	38	17	44	11	58	11	72	11	83	9	93	4
H4	48	27	58	25	68	21	83	22	87	13	95	6
H5	72	51	79	46	83	36	90	29	93	19	97	8
H6	97	76	97	64	97	50	97	36	100	26	100	11

* Days after sowing.
** Days after exposure.

Table 11.3. C-14 air concentration above the potatoes.

P1		P2		P3		P4		P5		P6	
Time (min)	Air conc (Bq/m3)	Time (min)	Air conc (Bq/m3)	Time (min)	Air conc (Bq/m3)	Time (min)	Air conc (Bq/m3)	Time (min)	Air conc (Bq/m3)	Time (min)	Air conc (Bq/m3)
32	65121	32	47090	31	68339	31	55009	30	57453	30	30450
99	43715	99	29804	100	42376	98	34387	97	36612	96	21067
166	21521	166	16279	167	24373	165	18999	163	19576	162	12966
233	12095	233	8297	236	11749	230	10269	236	9906	228	7152
300	6577	301	4405	303	6361	294	5774	304	5028	295	4086
368	3667	369	2490	371	2983	360.5	3359	370	2858	361	2461
435	2325	438	1393	438	1827	430.5	1686	436	1646	426	1452
501	1460	505	801	504	839	496.5	985	501	954	492	900
569	701	570	565	570	694	567	651	568.5	607	566	507

Table 11.4. C-14 integrated air concentrations.

Experiment	Time-integrated air concentration (MBq m^{-3} min)
P1	9.764
P2	6.983
P3	9.647
P4	8.089
P5	8.307
P6	4.774

Table 11.5. Temperature and PAR ranges during fumigation.

Experiment	Range in Temperature (^oC)	Range in PAR (W/m^2)
P1	23–27	70–150
P2	21–26	50–160
P3	20–23	40–160
P4	19–24	30–130
P5	19–13	30–130
P6	17–20	30–130

11.2. Observations

11.2.1. Experimental data

Average values and standard deviations of the following parameters were collected at each harvest following each fumigation:

- fresh and dry weights of each plant component and of the total plant,
- ^{14}C concentrations on dry and wet weight bases for each plant component and for the total plant, and
- ^{14}C inventories for each component and for the total plant (absolute and as a fraction of plant inventory)

The measured ^{14}C concentrations in the plant leaves at each harvest time for each exposure are given in Table 11.6. The ^{14}C concentrations in the tubers at final harvest are shown in Table 11.7.

The standard deviations of the measured ^{14}C activities are quite large, reflecting field variability of leaf properties and illumination, as well as variability in tuber growth rates.

11.2.2. Carbon-14 concentrations in potato plants

The ^{14}C activity concentrations in potato tissues generally fell after exposure in experiments P1 and P2, but the decrease was not very pronounced. The concentrations in experiments P3 to P6 showed very little reduction with time following exposure. In experiments P3 to P5, the edible tubers possessed the highest concentrations among all the plant tissues, either throughout the time course in the case of P3 and P4, or at final harvest in the case of P5. Table 11.8 indicates that, for all experiments, the ^{14}C inventory in all plants was conserved up to the final harvest, indicating that any respiratory losses after exposure were negligible. It can therefore be concluded that the reductions in ^{14}C concentrations in plant tissues in the first two to three cohorts of the experiment were solely due to translocation to newly-developing tissues, notably edible tuber tissues, which commenced growth 40 days after sowing, i.e. between exposures P2 and P3. From exposure P3 onwards, the tubers always accounted for the greater part of the total plant ^{14}C inventory and, with tuber biomass exceeding all other tissue biomass by several fold, it is clear that once tuber initiation has begun these edible tissues represent the most important sink for any ^{14}C fixed during a contamination event.

There was no significant decrease in the rate of photosynthesis between experiments P1 to P6. The leaf concentrations were higher in P1 than P6 due to the much greater export of ^{14}C from the leaves during P6. By P6 H2 (1 day after exposure) 68% of plant ^{14}C had been transported to the tubers. The proportion of the total transfer constituted by transfer to the tubers increased with plant age from 27% at P1 to approximately 95% at P6.

The within-harvest covariance on the fixation rate for the 6 potato experiments was relatively constant at approximately 50%. This may be due to the reduction in the number of plants used in the wind tunnel in the later exposures and the different growth profiles of the potato foliage.

Table 11.6. C-14 concentrations in leaves.

Experiment	Age (days)	^{14}C concentration in leaves (Bq/g dm)	Standard deviation in concentration
P1	21	1126.28	373.88
	31	312.68	115.74
	38	215.48	55.42
	48	224.70	148.77
	72	106.04	50.65
	97	101.38	38.49
P2	33	482.90	218.91
	38	393.72	187.15
	44	482.36	138.56
	58	279.77	240.01
	79	187.17	119.13
	97	47.13	27.44
P3	47	291.42	213.58
	53	307.33	147.54
	58	196.77	115.31
	68	322.20	88.31
	83	176.95	157.47
	97	107.55	121.41
P4	61	361.98	207.07
	65	42.58	13.75
	72	95.43	78.95
	83	191.30	26.68
	90	132.30	43.83
	97	28.60	Not available
P5	74	456.58	296.46
	79	119.27	87.12
	83	89.73	118.62
	87	79.33	33.46
	93	46.87	29.90
	100	55.27	16.97
P6	89	68.86	37.59
	90	65.68	22.31
	93	27.40	9.70
	95	77.67	51.23
	97	26.43	28.48
	100	76.10	59.68

Table 11.7. C-14 concentration in tubers at final harvest.

Experiment	Age at fumigation (days)	^{14}C concentration in tubers (Bq/g dm)	Standard deviation in concentration
P1	21	15.20	6.48
P2	33	12.98	9.14
P3	47	224.60	141.28
P4	61	181.45	124.52
P5	74	158.70	56.92
P6	89	43.00	41.15

Table 11.8. Results of single factor ANOVA to determine the significance of the change of total ^{14}C inventory in the total plant from harvest to harvest within each exposure experiment.

Experiment	F value	F critical	P value	Significant Loss?
P1	0.59	2.62	0.71	No
P2	1.7	2.74	0.18	No
P3	0.43	3.03	0.82	No
P4	1.09	2.96	0.41	No
P5	2.52	2.9	0.08	No
P6	0.73	2.96	0.61	No

11.2.3. Relationship between tuber size and ^{14}C content

As potato tubers are composed mostly of imported carbon, it is reasonable to expect that large tubers import more ^{14}C than small ones in contaminated plants. Oparka [106] described a linear relationship between tuber size and ^{14}C inventory. This may have some importance for radiological dose assessment because potatoes may be graded by tuber size before consumption e.g. large tubers are used for baking potatoes.

All tubers were weighed and analyzed individually from selected plants. Up to thirty tubers were found on some plants, although only a few of them developed to edible size. In order to reduce the amount of analysis necessary, all tubers which remained undeveloped were homogenized and analyzed as a single sample, which provided an average concentration. The remaining tubers were weighed and analyzed for ^{14}C content individually. Time constraints allowed the tubers from only 26 individual plants to be analyzed in this way. The plants were chosen to give a cross section of exposure timings and plant ages. The number of measured tubers on a plant ranged from 3 to 9 and from 0.02 to 30 g dm.

Only one individual plant from Experiment P1 was investigated in this way. This individual was exposed 21 days after sowing and harvested 79 days later. Tuber initiation took place approximately 11 days after the exposure. At this stage, there was no correlation between tuber size and ^{14}C inventory, which was approximately equal for all tubers. The smallest tuber consequently had the highest concentration (426 Bq g^{-1}). This was 14 times higher than the average tuber concentration of the whole individual. This tuber was only 0.07 g dm (0.44 g fresh weight (fw)) so it would not be eaten.

The plants in experiment P2 were exposed 33 days after planting, at a time when the tubers were starting to develop. Four individuals were analyzed from experiment P2, one from each of the harvests at 11, 25, 46 and 64 days post-exposure. The tubers from the individuals harvested 25 and 64 days after exposure displayed significant ($p< 0.05$) linear correlations between tuber size and ^{14}C inventory. However, the individuals sampled at 11 and 46 days post-exposure did not exhibit such a relationship.

In the individual plant harvested 64 days following exposure, the second largest tuber imported 82 times more ^{14}C than the smallest tuber. The ^{14}C activity concentrations in the larger tubers from this plant did not reflect this difference in ^{14}C content due to dilution with stable carbon. These results are equivocal in that two individuals suggest a linear relationship while two others do not.

11.2.3.1. Potatoes exposed after tuber initiation

Five individuals were sampled from experiment P3, one from each harvest except H3. Six individuals were sampled from Experiment P4. The significance of the correlation coefficient of a linear fit of tuber size and ^{14}C inventory is shown for each sample in Table 11.9. With the exception of one individual, the correlation was significant in all cases. The non-significant result may possibly be caused by the proximity of the sampling time to the exposure. The results from these two exposures support Oparka's [106] observations more strongly than those from Experiments P1 and P2. It is possible that the stronger linear relationships are due to the exposure timing in these experiments. In P1 and P2, the exposures took place before tuber initiation.

The differences in the maximum and minimum tuber ^{14}C contents, divided by the minimum contents, are displayed in the third column of Table 11.9. The fourth column shows the corresponding concentration factors.

Table 11.9. Significance of linear fits to ^{14}C inventory against tuber size.

Individual taken from	Significance of R value	Maximum Inventory factor	Maximum concentration factor
P3 H1	5%	1884	54
P3 H2	0.1%	65	3
P3 H4	1%	21	3
P3 H5	5%	1643	27
P3 H6	5%	33804	124
P4 H1	Not significant	959	511
P4 H2	1%	178	9.1
P4 H3	1%	40	3
P4 H4	1%	4494	113
P4 H5	0.1%	1544	47
P4 H6	5%	1472	472

The difference in ^{14}C content between tubers on an individual plant varied by a factor of up to 33804. The corresponding concentration factor for this plant was 124. The import of ^{14}C is accompanied by the import of stable carbon, which leads to a reduction in ^{14}C concentration. However, the level of dilution was not sufficient to make the concentrations equal in tubers of all sizes.

With the exception of the sample from P4 H1, the largest differences in ^{14}C concentration occurred at final harvest for Experiments P3 and P4. The concentrations ranged from 2.1 to 256 Bq g^{-1} for the individual sampled from P3 H6 and from 1.24 to 585 Bq g^{-1} for the plant from P4 H6. The average 'pooled' tuber ^{14}C concentrations were 124.7 Bq g^{-1} and 269 Bq g^{-1} for these samples. This indicates that the tuber ^{14}C concentrations in the largest tubers can be approximately double the average measured values.

11.2.3.2. Potatoes exposed close to senescence

Ten potato plants from experiments P5 and P6 were also analyzed for the ^{14}C content of individual tubers. Only one of the ten plants exhibited a significant relationship between tuber weight and ^{14}C inventory. There were, however, large differences between the amounts of ^{14}C imported into individual tubers. The maximum range of concentrations was from 0.69 Bq g^{-1} to 154 Bq g^{-1} at P5 H5. The 'pooled' average activity concentration for tubers on this plant was 55.7 Bq g^{-1}. Therefore the maximum activity concentration was approximately 3 times greater than the average.

In plants from experiments P5 and P6, one or two tubers constituted large sinks for ^{14}C with very little imported into the other tubers. These tubers were usually (but not exclusively) the largest tubers. This dominance of one or two tubers may have been due to ontogenic effects at this stage of plant development. Additionally, the collapse of the haulm during these two experiments may have favored carbohydrate supply to one or two tubers over the others.

11.2.3.3. Summary

The relationship between tuber size and ^{14}C content appears to be dependent on the timing of the exposure. The results from exposures carried out before tuber initiation are inconclusive with respect to the assumption of a linear dependence between size and tuber ^{14}C content. They do, however, illustrate that there may be differences between individual tuber ^{14}C contents and concentrations.

Plants exposed during tuber bulking (i.e., the period of time during which tubers experience rapid growth) did show a linear relationship. There were very large differences in ^{14}C content and concentration between individual tubers. Large tubers could contain approximately twice the average concentration. The increased import of ^{14}C was not entirely matched by an increase in stable carbon. This could be due to the changing ratio of ^{14}C in the translocated carbon with time.

Plants exposed after the collapse of the haulm exported ^{14}C to one or two dominant tubers. Such tubers could contain up to three times the average concentration of ^{14}C. The implications of these observations are that a critical group may increase its dose from the ingestion of potatoes by eating larger tubers.

11.2.4. Partition fractions

The rate of transfer of ^{14}C between plant compartments was not solely dependent on the 'sink demand' but also on the chemical partitioning of the ^{14}C. The initial ^{14}C incorporation in the plants was low for experiments P1 and P6 and higher for P2–P5 (Figure 11.1). This cannot be explained by the illumination levels or air temperatures in the wind tunnel, which were roughly constant for the first three fumigations and somewhat lower for the last three (Table 11.5). For P1, the low incorporation is explained by the low leaf area index at this development stage; for P6, both plant senescence and low leaf area index contributed to the low incorporation.

Time-dependent partition fractions for each plant part were calculated from the ^{14}C inventories in leaves, stems, roots and tubers for each fumigation and sampling time. We give an example for leaves in Figure 11.2. Due to the late seeding, the plants were unable to complete their normal development by the end of the study, which may explain the high partition fractions for the last fumigation (P6). The initial partition fractions in leaves can also vary substantially depending on genotype and the amount of fertilization [107].

There was a significant drop in the partition fractions for leaves and stems combined just before final harvest in all fumigations (Figure 11.3). This reflects a translocation of labile photosynthates to tubers at senescence. This is a physiological process well established in many perennial plants, including potatoes. However, it is included only in very advanced growth models, and not usually in those applied to radiological contamination. Significant translocation also occurs from stems to storage organs at the start of tuber formation. About 20–40% of the dry matter in the stems is translocated to the tubers at this time.

11.3. Modeling approaches

Four participants submitted results for this scenario (Table 11.10). The participants from Romania carried out calculations with two models, one simple (Scottish) and the other more complex (WOFOST). All participants treated the scenario as a blind test of their models and submitted results before the observed concentrations were made known to them. However, the participants from Japan submitted revised predictions after the data had been disclosed.

The OURSON model is a dynamic model primarily developed to evaluate radionuclide concentrations in the aquatic and terrestrial environments following liquid discharges. It assumes that the incorporation of ^{14}C in the plant results from photosynthetic carbon assimilation and that translocation occurs between the leaves, where photosynthesis takes place, and the storage organs. The net photosynthetic carbon assimilation rate, which is a function of leaf biomass, corresponds to the total growth rate of the plant. The allocation of photosynthates to different parts of the plant depends on the growth stage.

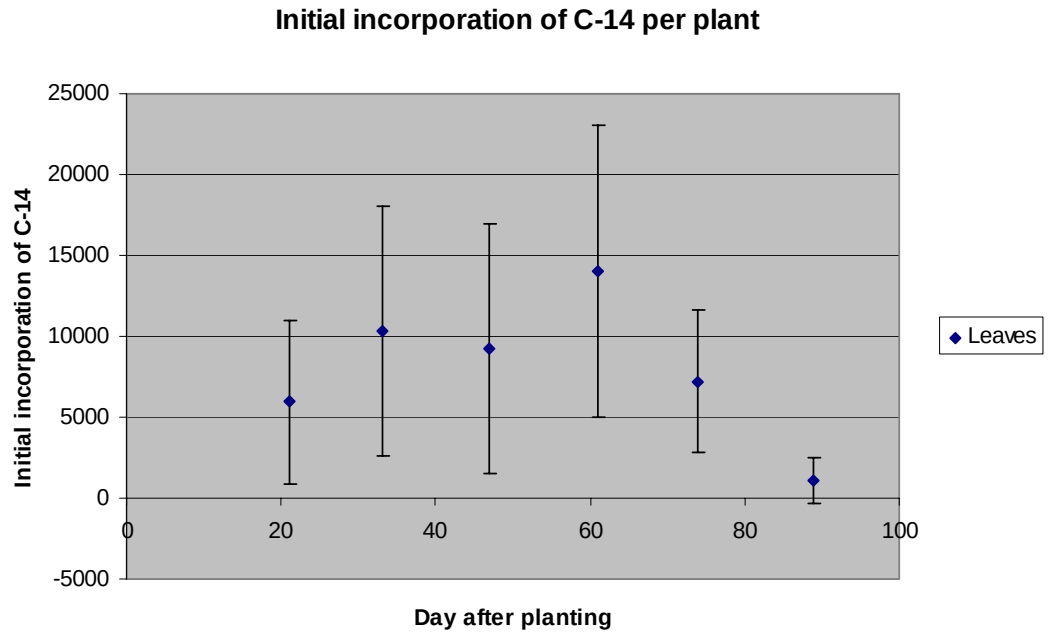

Fig. 11.1. The initial incorporation of ^{14}C per plant.

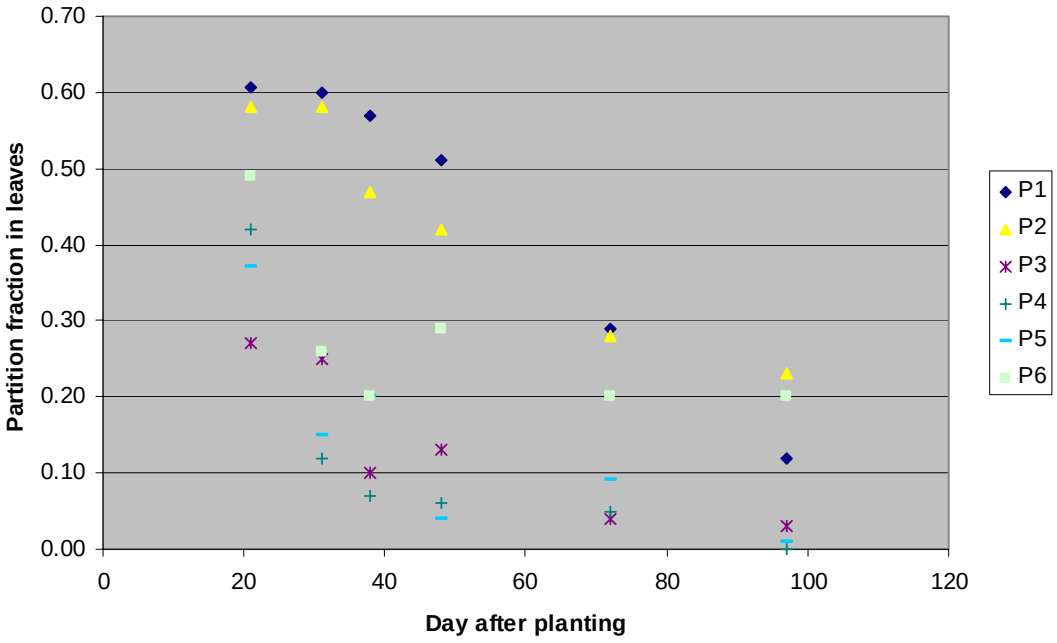

Fig. 11.2. Time evolution of partition fraction in leaves for each fumigation.

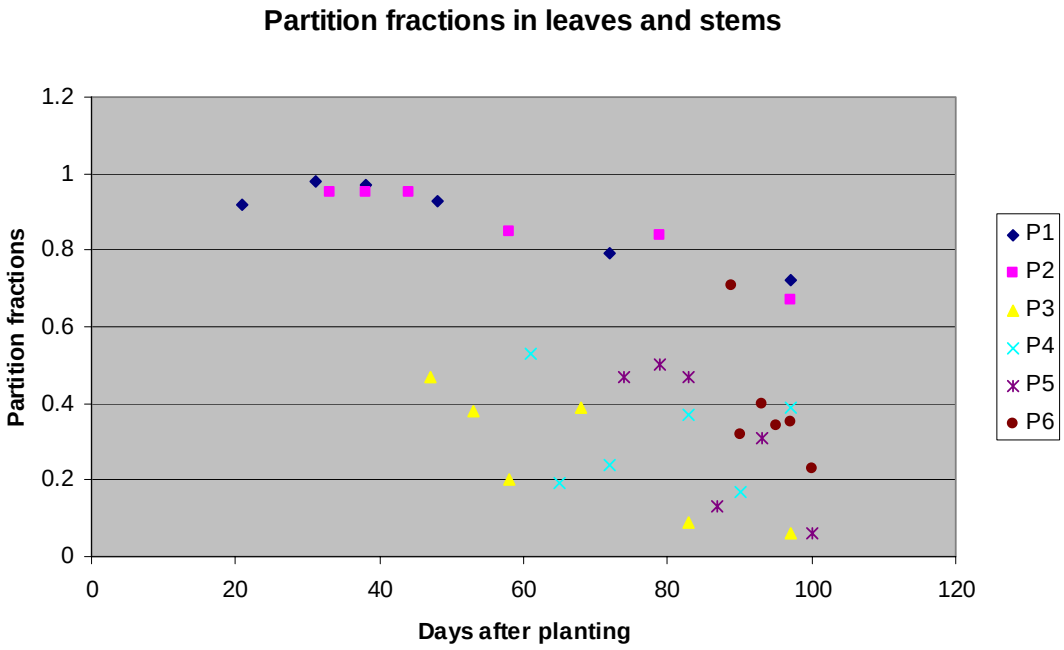

Fig. 11.3. Time evolution of partition fraction in leaves and stems combined for each fumigation.

Table 11.10. Participants in the Potato Scenario.

Participant	Affiliation	Model	Designation in the text
F. Siclet	Electricite de France, France	OURSON	EDF
P. Kennedy	Food Standards Agency, UK	PRISM3	FSA
A. Melintescu and D. Galeriu	National Institute for Physics and Nuclear Engineering, Romania	WOFOST Scottish	WOFOST Scottish
S. Uchida et al. [a]	National Institute of Radiological Sciences, University of Kyoto, and Yfirst Inc., Japan	MOGRA	UTTY UTTY revised

[a] S. Uchida, H. Takeda and K. Tagami (NIRS); T. Takahashi (Kyoto Univ.); and K. Yamamoto (Yfirst Inc.)

PRISM3 is a dynamic compartment model that considers biological and environmental compartments, including separate compartments for soil water and soil organic matter. It is designed to be conservative for use in regulatory assessments. The external parts of the plant are not explicitly represented, as all sources are considered to be gaseous. Root storage is not considered due to rapid redistribution of ^{14}C.

WOFOST is a model developed by the Wageningen School in The Netherlands for plant growth. The photosynthesis sub-model in WOFOST, with default parameter values for potatoes, was used to predict time-dependent photosynthetically active radiation (PAR), leaf area index (LAI), and maximum leaf photosynthesis rate.

The Scottish model [108] considers dry matter production only, according to the following equation:

$$\Delta W = L_e \, PAR \, L_i \qquad (11.1)$$

where:

ΔW is the dry mass increment (g m^{-2} d^{-1});
L_e is the light use efficiency (g/MJ);
PAR is the incoming photosynthetically active radiation (MJ m^{-2} d^{-1}); and
L_i is the light interception, which depends on the leaf area index (LAI) and the extinction coefficient for PAR

The initial partition for leaves differs by a factor 2 for the two genotypes considered by the WOFOST and Scottish models.

The UTTY model is a dynamic compartment model that was developed using the MOGRA tool (Migration Of GRound Additions). It considers two organic compartments (stem-leaf-root and tuber), one inorganic compartment (the whole plant) and two environmental compartments (air and soil). This model is essentially the same as the UTTY model used in the EMRAS rice scenario, with the tuber compartment replacing the rice grain compartment and the plant growth model modified to reflect potatoes.

Full descriptions of all the models are given in Appendix II.10.

11.4. Results

11.4.1. Carbon-14 concentrations in leaves

The predictions of ^{14}C concentrations in leaves following the P1 fumigation are shown in Figure 11.4. Generally, the WOFOST and Scottish models underestimate the data, although by less than a factor of 5. The remaining models all overestimate the observations, by up to a factor of 5 for FSA, a factor between 3 and 6 for EDF, and up to a factor of 20 for UTTY. The predictions of UTTY revised are better, overestimating the observations by less than a factor of 4.

The results for experiment P2 are shown in Figure 11.5. The WOFOST and Scottish models underestimate the data for the first five samplings by up to a factor of 5, but overestimate H6 by a similar margin. FSA overestimates at all sampling times but by a significant amount (a factor of 25) only for H6. EDF overestimates by a factor of 11 at H1, by a factor of 6 at H6, and by a factor close to 1 at other sampling times. UTTY overestimates at H1 by a factor of 17, at intermediate times by a factor of about 7, and at H6 by a factor of 20. The predictions of UTTY revised are better, overestimating by a factor between 1 and 3.

For the P3 fumigation, the WOFOST and Scottish models overestimate the observations by a factor less than 6, except for the last sampling where the overestimate increases to a factor greater than 10 (Figure 11.6). The large overestimation for H6 is believed to be due to the use of the green leaf mass reported in the scenario description and the neglect of the contaminated dead leaves. The results for FSA are similar to those of WOFOST and Scottish. EDF overestimates by as much as a factor of 3, UTTY by a factor between 10 and 24, and UTTY revised by a factor less than 2.

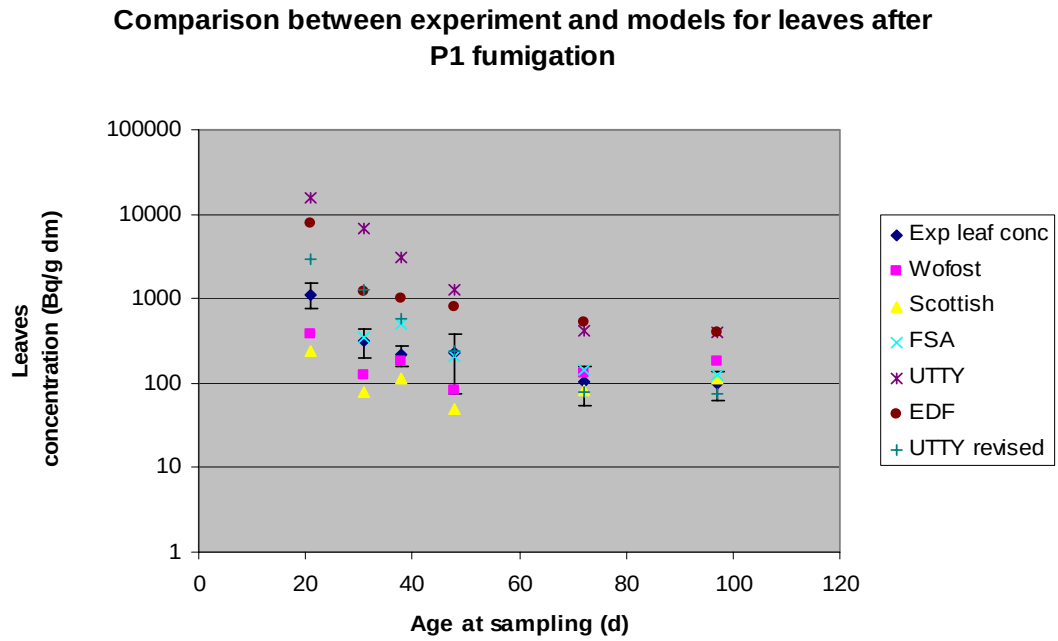

Fig. 11.4. Comparison between predictions and observations for the ^{14}C concentration in leaves following the P1 fumigation

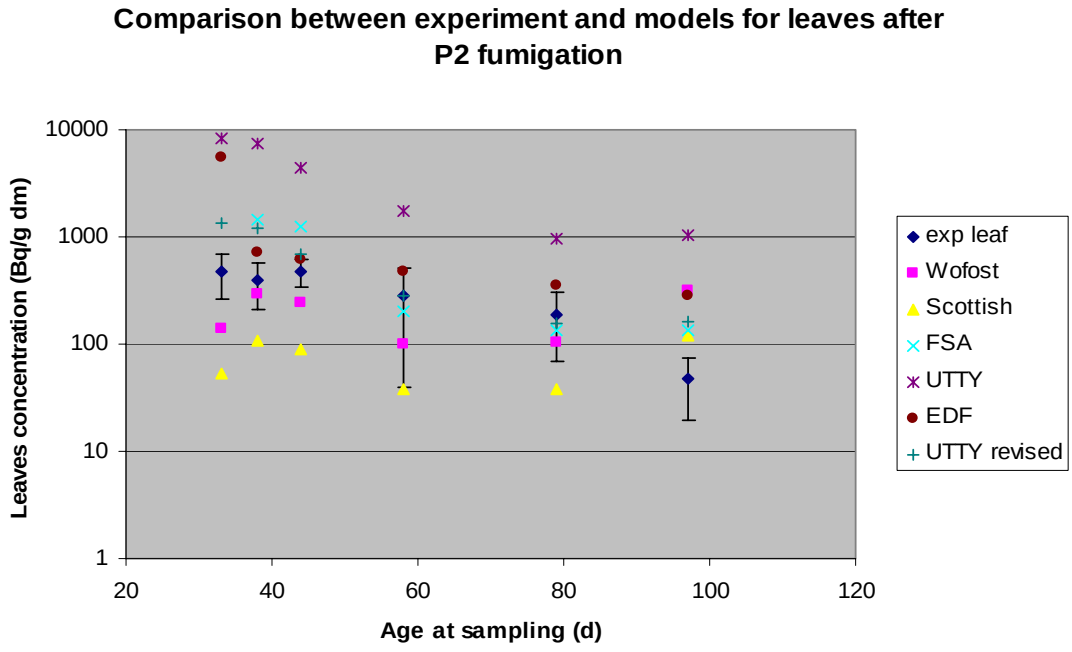

Fig. 11.5. Comparison between predictions and observations for the ^{14}C concentration in leaves following the P2 fumigation.

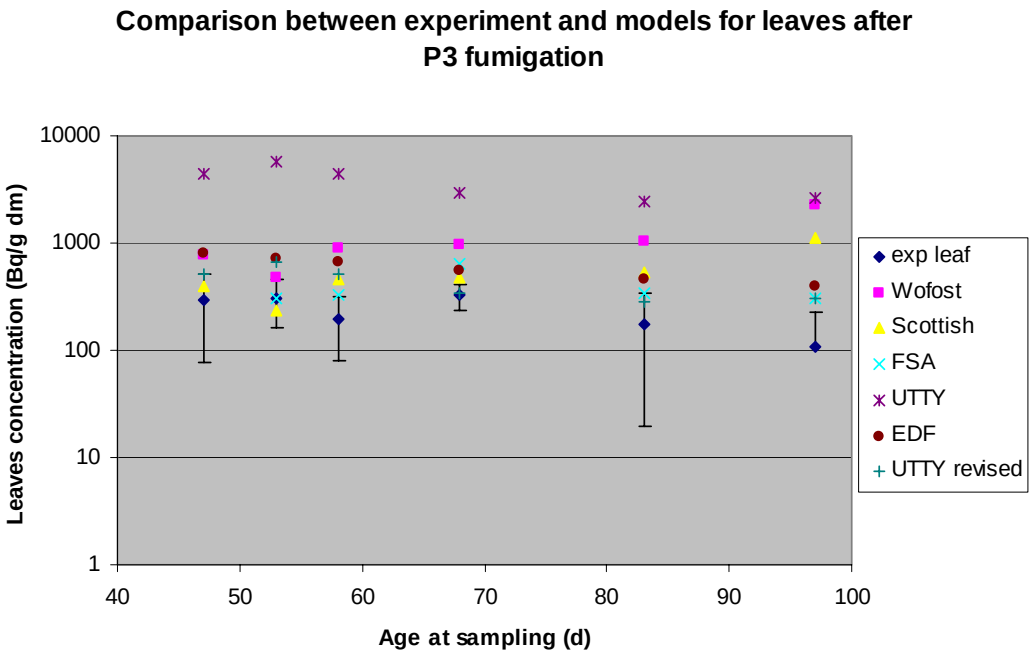

Fig. 11.6. Comparison between predictions and observations for the ^{14}C concentration in leaves following the P3 fumigation

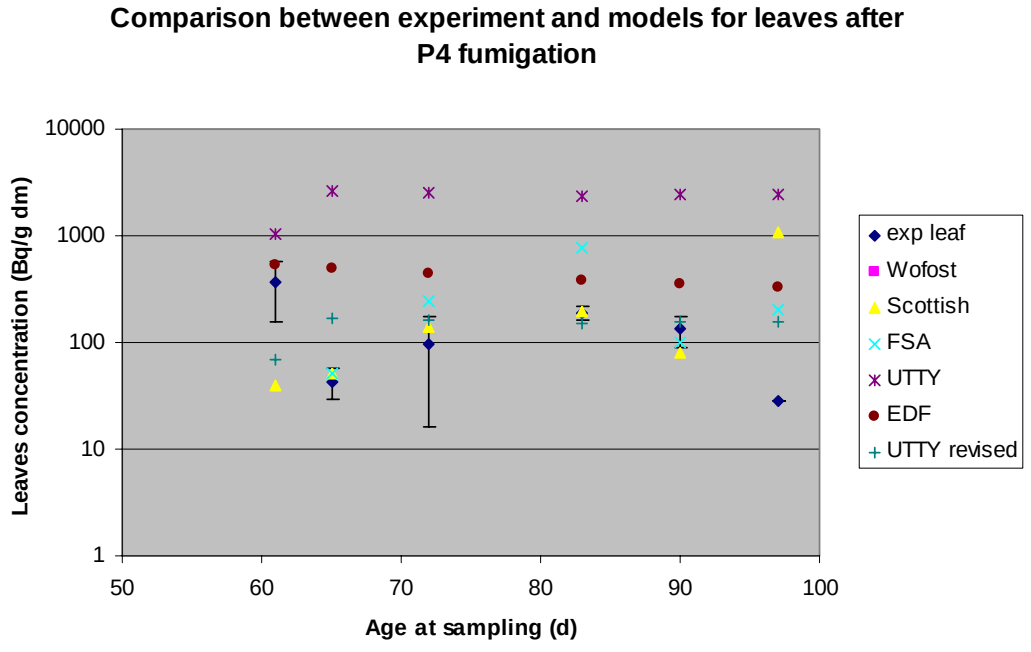

Fig. 11.7. Comparison between predictions and observations for the ^{14}C concentration in leaves following the P4 fumigation.

For the P4 fumigation (Figure 11.7), WOFOST with its default parameter values does not predict any ^{14}C in the leaves. The Scottish model underestimates at H1 by a factor of 10, and at H6 by a factor 40, but the predictions at intermediate times are quite good. The FSA predictions agree with the observations when uncertainties are taken into account with the exception of the last sampling, when it overestimates by a factor near 30. EDF overestimates by a factor between 1 and 11, UTTY by a factor between 10 and 80, and UTTY revised by a factor between 1 and 5. All models significantly overestimate the observed concentration at H6.

For the P5 fumigation (Figure 11.8), WOFOST predicts that the ^{14}C concentration in the leaves is zero. The Scottish model underestimates the observations, by a factor of 5 at the beginning of the experiment and by smaller factors at later times. FSA also overpredicts, by a factor of 10 at H1 and a factor of 50 at H6. EDF reproduces the observed concentration well at H1 but overestimates by a factor of 7 at the other sampling times. UTTY and UTTY revised both underestimate by a factor 10 at H1 and then predict no ^{14}C in the leaves.

For the P6 fumigation (Figure 11.9), WOFOST, UTTY and UTTY revised do not predict any ^{14}C in the leaves. The Scottish model underestimates the data by a factor less than 2. The FSA model also underestimates by up to a factor of 6. The EDF model overestimates the ^{14}C concentrations by a factor between 2 and 7.

11.4.2. Discussion of predicted leaf concentrations

Considering the uncertainty in the experimental data (Tables 11.6 and 11.7) and the complex processes of partition and translocation involved in this scenario, the predictions cannot be expected to agree with the observations to better than a factor 5. All the models tend to substantially overestimate the leaf concentration at the last sampling point, close to senescence, when translocation from leaves to tubers is ignored by the models.

Generally, UTTY significantly overestimated the ^{14}C concentration in leaves. They hypothesize that, in their model, the ^{14}C in the plant inorganic compartment included some residual ^{14}C picked up after the 10 hour exposure itself, implying that each part of the potato plant (stem, leaf and tubers) was effectively exposed for more than 10 hours. C-14 transfer to the inorganic compartment should become zero immediately after the exposure, when the ^{14}C concentration in air drops to zero. The model will be improved in this regard in the future but, to correct the problem for this scenario, additional calculations were carried out with a reduced air concentration, chosen so that the time-integrated ^{14}C amount in the organic compartment reflected the 10 hour exposure time. These calculations were submitted as the UTTY revised model, which showed much better performance than the original model. The ratio of the ^{14}C concentration in air during the 10 hour exposure to the time-integrated ^{14}C content in the inorganic compartment was different in each experiment because the plant growth rate was different. The improved performance of the UTTY revised model was due to an imposed decrease in the ^{14}C air concentration to which the potatoes were exposed, and not to any change in the conceptual model.

The EDF model overestimated most of the experimental data, by a factor of about 5 on average, perhaps because it does not consider light and temperature effects on the photosynthetic rate, which is set to a maximum value.

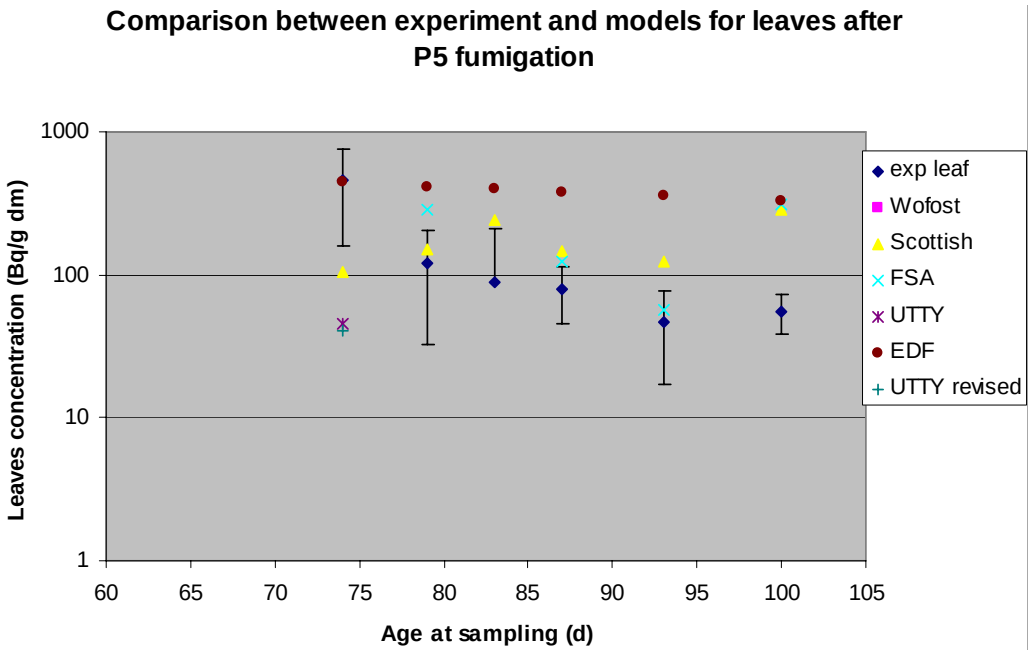

Fig. 11.8. Comparison between predictions and observations for the ^{14}C concentration in leaves following the P5 fumigation

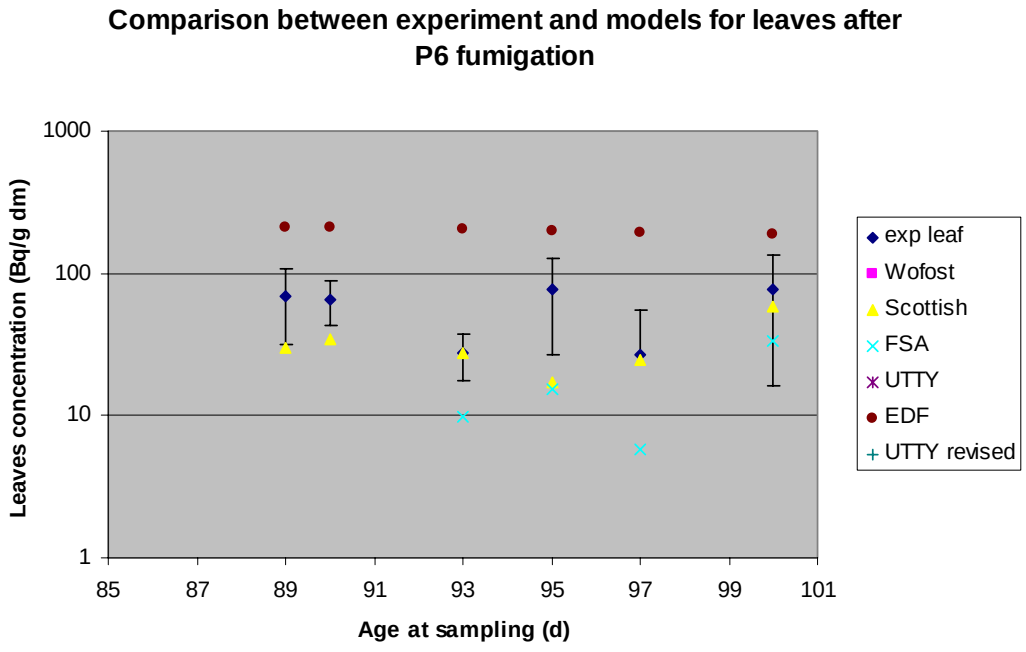

Fig. 11.9. Comparison between predictions and observations for the ^{14}C concentration in leaves following the P6 fumigation.

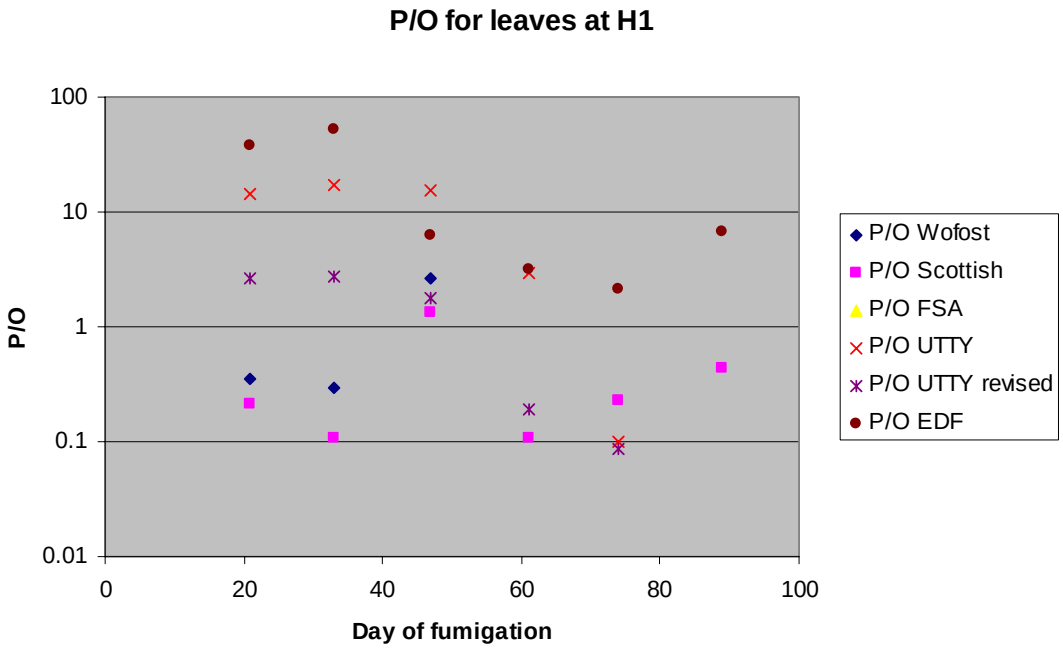

Fig. 11.10. Predicted to observed ratio for C-14 concentration in leaves at the H1 sampling.

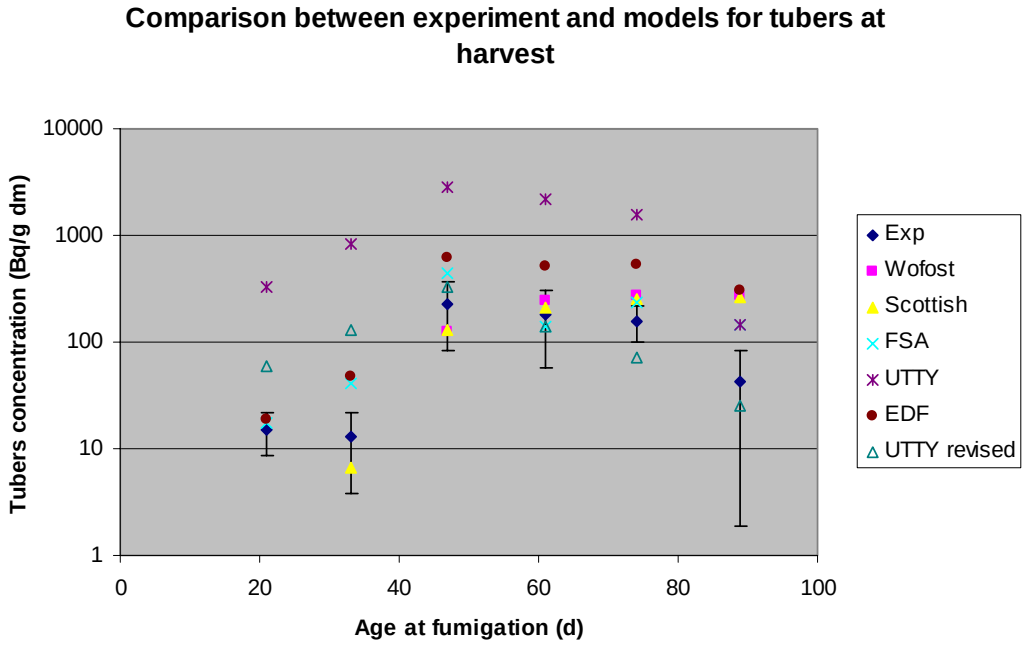

Fig. 11.11. Comparison between predictions and observations of ^{14}C concentrations in tubers at final harvest.

In all cases, the FSA model predicted zero concentration in the leaves at the first sampling time, which is not reasonable. FSA has indicated that finite concentrations can be obtained by changing the time of H1 to one day after the start of the exposure. The inference is that the H1 time point was interpreted to be either before or during fumigation in the model runs, suggesting that this is likely a problem of the user interface.

The analysis of ^{14}C dynamics in leaves must start with the initial contamination immediately after fumigation (sampling time H1). Figure 11.10 shows the predicted to observed ratios for ^{14}C concentration in leaves at this time. The EDF and UTTY models overestimated by a factor of 10 or more, UTTY revised overestimated by a factor of about 2, and WOFOST and the Scottish models underestimated by a factor of about 5. As noted above, FSA predicted zero concentration in leaves at H1, which was not in agreement with observation. The WOFOST model did not predict any ^{14}C concentration in leaves at H1 for the last three experiments. This is explained by an improper choice for the partition fractions that describe the translocation of new photosynthates to the various plant parts for the cultivar assumed in this scenario, as discussed in the full model description (Appendix II.10).

After the initial day of contamination, the dynamics in leaves depends strongly on translocation (reallocation) of photosynthates to other plant parts – stems, new leaves, roots and tubers. Differences among model predictions can be explained by the different assumptions made with regard to the partition fractions, which depend on the development stage of the plant and the specific genotype.

11.4.3. Carbon-14 concentrations in tubers

The concentrations in the tubers are of greater radiological significance than those in the leaves, since the tubers comprise the edible part of the plant. The best results were given by FSA, where the predictions agreed with the observations to within a factor of 3 for all fumigations (Figure 11.11). EDF overestimated by up to a factor of 6. UTTY overestimated substantially by a factor between 3 and 68. UTTY revised performed better, but still overestimated by a factor between 1 and 10. The WOFOST and Scottish models did not predict any contamination in tubers for the first fumigation, underestimated for the second fumigation, and overpredicted by a factor of 6 for the last fumigation. For intermediate experiments, the predictions lay within a factor of 2 of the observations.

For all models, the predicted ^{14}C concentrations in the tubers were better than those in the leaves. This may be partially the result of compensatory errors, at least for those models that greatly overpredicted the initial contamination of the potato plant.

11.5. Discussion and conclusions

The Potato Scenario provided a good test of models that predict ^{14}C concentrations in plants following an acute exposure to ^{14}C in air. The uncertainty in the experimental data was quite large, but this reflects natural conditions because the variability in ^{14}C concentrations in field plants is also large. The main limitations in the data arose from the late seeding (August 4) and the abrupt and early senescence of the plants, which was caused by the onset of autumn weather conditions shortly after exposure. Most models assumed the plants developed normally, which was not the case in the scenario.

The following conclusions can be drawn from the results of this scenario:

- The plant genotype is important in determining ^{14}C concentrations, because the partitioning of new photosynthate to leaves, stems and tubers depends on the cultivar.
- Respiration dynamics is important shortly after fumigation, because the slow respiration rate has a half time of about 2 days.
- Translocation from stems to tubers is also important when the fumigation occurs at the start of tuber formation. There are indications in the data that, at plant senescence, carbon is translocated from leaves and stems to tubers.
- A simple model can be used for the initial incorporation of ^{14}C into the plant, but a process-level model is required to assess partitioning if uncertainties are to be kept relatively low.
- The low rate of ^{14}C incorporation in the plant during the last exposure may have been due to the weather conditions at the time, which were not known for inclusion in the scenario description.
- The relatively good predictions of ^{14}C concentrations in tubers should be analysed to see if they are the result of compensatory errors.
- The large uncertainties in the experimental data make it difficult to draw firm conclusions regarding model performance.

Even though the experimental data on ^{14}C dynamics in leaves are poorly reproduced by most of the models, the predicted concentrations in tubers almost always agree with the observations to better than a factor of 10.

REFERENCES

[1] SWEDISH RADIATION PROTECTION INSTITUTE, BIOMOVS II, Tritium in the Food Chain: Intercomparison of model predictions of contamination in soil, crops, milk and beef after a short exposure to tritiated water vapour in air, Published on behalf of the BIOMOVS II Steering Committee by SSI, Sweden, ISBN 91-972134-7-0 (1996).

[2] SWEDISH RADIATION PROTECTION INSTITUTE, BIOMOVS II, Tritium in the Food Chain: Comparison of predicted and observed behaviour; A: Re-emission from soil and vegetation, B: Formation of organically bound tritium in grain of spring wheat, Published on behalf of the BIOMOVS II Steering Committee by SSI, Sweden, ISBN 91-972958-2-5 (1996).

[3] INTERNATIONAL ATOMIC ENERGY AGENCY, Modelling the environmental transport of tritium in the vicinity of long-term atmospheric and subsurface sources, IAEA-BIOMASS-3, IAEA, Vienna (2003).

[4] BAUMGÄRTNER, F., DONHÄRL, W., Non-exchangeable organically bound tritium (OBT): its real nature, Anal. Bioanal. Chem., 379, 204–209 (2004).

[5] BAUMGÄRTNER, F., Accumulative tritium transfer from water into biosystems, Fusion Science and Technology, 48, 787–790 (2005).

[6] KIM, S-B., DAVIS, P.A., Experimental investigation of buried tritium, AECL Report 153-121210-440-004 (2006).

[7] MURPHY, C.E., Jr., The relationship between tritiated water activities in air, vegetation and soil under steady-state conditions, Health Physics, 47, 635–639 (1984).

[8] KIM, S-B., WORKMAN, W.J.G., DAVIS, P.A., YANKOVICH, T., Tritium concentrations in the Perch Lake ecosystem, AECL document CTD-03700-ENA-003, Chalk River Laboratories, Chalk River, Ontario (2004).

[9] CORNETT, R.J., RISTO, B.A., LEE, D.R., Measuring groundwater transport through lake sediments by advection and diffusion, Water Resources Research, 25, 1815–1823 (1989).

[10] BLAYLOCK, B.G., HOFFMAN, F.O., FRANK, M.L., Tritium in the aquatic environment, CONF-860214-2, Oak Ridge National Laboratory, Oak Ridge, Tennessee (1986).

[11] WILLIAMS, J.L., RUSS, R.M., MCCUBBIN, D., KNOWLES, J.F., An overview of tritium behaviour in the Severn Estuary, J. Radiological Protection, 21, 337–344 (2001).

[12] LAMBERT, B., Welsh tritium, J. Radiological Protection, 21, 333–335 (2001).

[13] DAVIS, P.A., KOTZER, T.G., WORKMAN, W.J.G., Environmental tritium concentrations due to continuous atmospheric sources, Fusion Science and Technology, 41, 453–457 (2002).

[14] PETERSON, S-R., DAVIS, P.A., Tritium doses from chronic atmospheric releases: a new approach proposed for regulatory compliance, Health Physics, 82, 213–225 (2002).

[15] KIRCHMANN, R., CHARLES, P., VAN BRUWAENE, R., REMY, J., Distribution of tritium in the different organs of calves and pigs after ingestion of various tritiated feeds, Current Topics in Radiation Research, Q 12, 291 (1977).

[16] KIRCHMANN, R., REMY, J., CHARLES, P., KOCH, G., Distribution and incorporation of tritium in different organs of ruminants, IAEA-SM-172/81, IAEA, Vienna (1985).

[17] IWAKURA, T., KASIDA, S., INOUE, Y., A low-background scintillation counter for measuring low-level tritium, In: Behaviour of Tritium in the Environment, IAEA-SM-232/32, 163–171 (1979).
[18] TANAKA-MIYOMOTO, K., INOUE, Y., IWAKURA, T., Tritium concentrations of groundwater in Naka Terrace, Ibaraki Prefecture, Japan, Journal of Environmental Radioactivity, 5, 219–227 (1987).
[19] INOUE, Y., IWAKURA, T., Tritium concentration in Japanese rice, Journal of Radiation Research, 31, 311–323 (1990).
[20] HISAMTSU, S., KATSUMATA, T., TAKIZAWA, Y., INOUE, Y., ISOGAI, K., Interlaboratory comparison of low-level organic tritium measurement in environmental samples, Radioisotopes, 39, 457–463 (1990).
[21] FUMA, S., INOUE, Y., Simplified and sensitive analysis of organically bound tritium in tree rings to retrospect environmental tritium levels, Appli. Radiat. Isot., 46, 991–997 (1995).
[22] MATSUURA, K., SASA, Y., NAKAMURA, C., KATAGIRI, H., Levels of tritium concentration in the environmental samples around JAERI Tokai, J. Radioanaly. and Nucl. Chem. Articles, 197, 295–307 (1995).
[23] INOUE, Y., MIYAMOTO, K., FUMA, S., TAKEDA, H., Unique features of a pine tree for monitoring and modeling of environmental tritium, Fusion Science and Technology, 48, 508–511 (2005).
[24] INTERNATIONAL ATOMIC ENERGY AGENCY, Handbook of Parameter Values for the Prediction of Radionuclide Transfer in Temperate Environments, Technical Reports Series 364, IAEA, Vienna (in press).
[25] KIMURA, F., TAKEUCHI, K., A numerical experiment on fumigation by sea breeze, Meteorology and Geophysics, 29, 17–28 (1978).
[26] BELOT , Y., GAUTHIER, D., CAMUS, H., CAPUT, C., Prediction of the flux of tritiated water from air to plant leaves, Health Physics, 37, 575 (1979).
[27] VAN HESS, M., ET AL., Retention in young pigs of organically bound tritium given during pregnancy and lactation, Radiation Protection Dosimetry, 16, 123 (1986).
[28] NATIONAL ACADEMY PRESS, National Academy of Sciences. Nutrient Requirements of Swine, Tenth Revised Edition, NAC, Washington D.C. (1998).
[29] STOICA, I., Animal Nutrition and Feeding, Ed Coral-Sanivet, Bucharest (in Romanian) (1997).
[30] MCDONALD, P., EDWARDS, R.A., GREENHALGH, J.F.D., MORGAN, C.A., Animal Nutrition, Fifth Edition, Longman Scientific and Technical Publishers, Harlow (1995).
[31] Institut National de Recherche Agronomique, INRA (2008). http://www.inapg.fr/dsa/adz/tables/; http://www.inapg.fr/dsa/afz/tables/fichiers/FeedMix2004.pdf; http://www.inapg.fr/dsa/afz/tables/fichiers/jn233.pdf.
[32] NOBLET, J., DOURMAD, J.Y., ETIENNE, M., LE DIVIDICH, J., Energy metabolism in pregnant sows and newborn pigs, J. Anim. Sci., 75, 2708–2714 (1997).
[33] FOOD AND AGRICULTURE ORGANIZATION, Feed from animal wastes: state of knowledge, FAO Animal Production and Health Paper 18, (1980). http://www.fao.org/DOCREP/004/X6518E/X6518E00.HTM
[34] VAN MILGEN, J., NOBLET, J., Partitioning of energy intake to heat, protein and fat in growing pigs, J. Anim. Sci., 81(E. Suppl. 2), E86–E93 (2003).

[35] MAUL, P.R., WATSON, C.E., THORNE, M.C., Probabilistic modelling of C-14 and H-3 uptake by crops and animals, Qunitessa Report QRS-1264A-1, Version 3.0 (2005).
[36] WALKE, R., THORNE, M., EMRAS model comparisons Adaptation of PRISM H-3 Model to Partition Excretion, Quintessa Report QRS-3004B-TN1, Version 1.0 (2007).
[37] KOTZER, T., YANKOVICH, T.L., WORKMAN, W., Natural concentrations of tritium (OBT, FWT) in fish and associated media, COG report (2001).
[38] KOTZER, T., YANKOVICH, T.L., Concentrations of tritium (OBT, FWT) in fish and associated media, TK-01-01 (2001).
[39] ADAMS, L.W., PETERLE, T.J., WHITE, G.C., Tritium behaviour in aquatic plants and animals in a freshwater marsh ecosystem, In: Behaviour of Tritium in the Environment, IAEA-SM-232/50, pp. 231–245 (1979).
[40] BLAYLOCK, B.G., FRANK, M.L., Distribution of tritium in a chronically contaminated lake, In: Behaviour of Tritium in the Environment, IAEA-SM-232/74, pp. 247–256 (1979).
[41] CAMPBELL, P.G.C., LEWIS, A.G., CHAPMAN, P.M., CROWDER, A.A., FLETCHER, W.K., IMBER, B., LUOMA, S.N., STOKES, P.M., WINFREY, M., Biologically Available Metals in Sediments, NRCC No. 27694, pp. 298 (1988).
[42] ELDER, J.F., COLLINS, J.J., Freshwater molluscs as indicators of bioavailability and toxicity of metals in surface-water systems, Rev. of Environ. Contam. and Toxicol., 122, 37–79 (1991).
[43] PHILLIPS, D.J., The use of biological indicator organisms to monitor trace metal pollution in marine and estuarine environments – a review, Environ. Pollut., 13, 281–317 (1977).
[44] PHILLIPS, D.J.H., Quantitative aquatic biological indicators, Elsevier, London, pp. 460 (1980).
[45] BAYNE, B.L., BROWN, D.A., BURNS, K., DIXON, D.R., IVANOVICI, A., LIVINGSTONE, D.R., LOWE, D.M., MOORE, M.N., STEBBING, A.R., WIDDOWS, J., The Effects of Stress and Pollution on Marine Animals, Praeger: New York, pp. 381 (1985).
[46] CLARKE, A.H., *Elliptio complanata* (Lightfoot, 1786) Eastern Elliptio, In: The Freshwater Molluscs of Canada. National Museum of Natural Sciences, Ottawa. pp. 266–269 (1981).
[47] CURRY, C.A., The freshwater clam (*Elliptio complanata*), A practical tool for monitoring water quality, Water Poll. Res. Canada, 13, 45–52 (1977/78).
[48] DECHNO, A.W., LUOMA, S.N., Geopolymers (humic and fulvic acids): Sink or trophic transfer-vehicle for metals to bivalves, Proc. of the 13th Annual Meeting of the Society of Environmental Toxicology and Chemistry, Cincinnati, Ohio (1992).
[49] JACKIM, E., MORRISON, G., STEELE, R., Effects of environmental factors on radiocadmium uptake by four species of marine bivalves, Mar. Biol., 40, 303–308 (1977).
[50] GREIG, R.A., NELSON, B.A., NELSON, D.A., Trace metal content in the American oyster, Mar. Pollut. Bull., 6(5), 72–73 (1975).
[51] HINCH, S.G., STEPHENSON, L.A., Size- and age-specific patterns of trace metal concentrations in freshwater clams from an acid-sensitive and a circumneutral lake, Can. J. Zool., 65, 2436–2442 (1987).
[52] KAUSS, P.B., GRIFFITHS, M., MELKIC, A., Use of freshwater clams in monitoring trace contaminant source areas, In: Proc. of the 2nd O.M.O.E. Technol. Transfer Conf. Toronto, Ontario, December 1981, pp. 371–388 (1981).

[53] KAUSS, P.B., HAMDY, Y.S., Biological monitoring of organochlorine contaminants in the St. Clair and Detroit Rivers using introduced clams, *Elliptio complanata*, J.G.L.R., 11(3), 247–263 (1985).
[54] LOBEL, P.B., MOGIE, P., WRIGHT, D.A., WU, B.L., Metal accumulation in four molluscs, Marine Pollution Bulletin, 13(5), 170–174 (1982).
[55] Lobel, P.B., Wright, D.A., Total body zinc concentration and allometric growth ratios in *Mytilus edulis* collected from different shore levels, Mar. Biol., 66, 231–236 (1982).
[56] LUTEN, J., BOUQUET, W., BURGGRAAF, M., RUS, J., Accumulation, elimination and speciation of Cd and Zn in mussels: *Mytilus edulis* in the natural environment, Bull. Environ. Contam. Toxicol., 37, 579–586 (1986).
[57] MATTESON, M.R., Life history of *Elliptio complanatus* (Dillwyn, 1817), Amer. Midl. Nat., 40(3), 690–723 (1948).
[58] PHILLIPS, D.J.H., Trace metals in the common mussel *Mytilus edulis* and in the alga *Fucus vesiculosus* from the region of the sound (Oresund), Environ. Pollut. (Ser. A), 18, 31–43 (1979).
[59] RUBENSTEIN, N.I., LORES, E., GREGORY, N.R., Accumulation of PCBs, mercury and cadmium by *Nereis virens, Mercenaria mercenaria* and *Palaemonetes pugio* from contaminated harbor sediments, Aquat. Toxicol., 3(3), 249–260 (1983).
[60] SERVOS, M.R., MALLEY, D.F., MACKIE, G.L. LAZERTE, B.D., Lack of bioaccumulation of metals by *Elliptio complanata* (Bivalvia) during snowmelt in three South-Central Ontario streams, Bull. Environ. Contam. Toxicol., 38, 762–768 (1987).
[61] TATUM, H.E., Bioaccumulation of polychlorinated biphenyls and metals from contaminated sediment by freshwater prawns, *Macrobrachium rosenbergii* and clams, *Corbicula fluminea*, Arch. Environ. Contam. Toxicol., 15(2), 171–183 (1986).
[62] TESSIER, A., CAMPBELL, P.G.C., AUCLAIR, J.C., BISSON, M., Relationships between the partitioning of trace metals in sediments and their accumulation in the tissues of the freshwater mollusc *Elliptio complanata* in a mining area, C.J.F.A.S., 41, 1463–1472 (1984).
[63] TESSIER, A., COUILLARD, Y., CAMPBELL, P.G.C., AUCLAIR, J.C., Modeling Cd partitioning in oxic lake sediments and Cd concentrations in the freshwater bivalve *Anodonta grandis*, Limnol. Oceanogr., 38(1), 1–17 (1993).
[64] YANKOVICH, T.L., KIM, S.B., EMRAS Tritium/C14 Working Group: The Dynamic Perch Lake Mussel Transplantation Scenario Description (Revision 1), AECL Environmental Technologies Branch Memorandum No. ETB-05-99 (Revision 1), 27 July 2005 (2005).
[65] YANKOVICH, T.L., KIM, S.B., BAUMGÄRTNER, F., GALERIU, D., MIYAMOTO, K., SAITO, M., SICLET, F., EMRAS Tritium/C14 Working Group: The dynamic Perch Lake mussel transplantation scenario – Modelled-to-measured comparison, AECL ETB Technical Memorandum No. ETB-06-270 (Rev. 0). 1 November 2006 (2006).
[66] MERRITT, W.F., RISTO, B.A., Calibration and history of the Perch Lake weirs, In: Hydrological Studies on a Small Basin on the Canadian Shield (P.J. Barry, editor), Atomic Energy of Canada Limited Report, AECL-5041/1, 299–310 (1975).
[67] SLATER, J.E., Water survey of Canada hydrometric program at Perch Lake, In: Hydrological Studies on a Small Basin on the Canadian Shield: A Final Summary of the Perch Lake Evaporation Study 1965–1974, Atomic Energy of Canada Limited, AECL–5041/I, pp. 238–297 (1975).

[68] NIEMI, T., Annual Program Report: 2004 Annual report of radiological monitoring results for Chalk River and Whiteshell Laboratories sites, Volume 3: Environmental Monitoring – Chalk River, AECL-MISC-362-04-CRL, April 2005, Vol. 3 (Rev. 0) (2005).
[69] NEGUS, C., A quantitative study of growth and production of unionid mussels in the River Thames at Reading, J. Anim. Sci., 35, 513–532 (1966).
[70] WORKMAN, W.J.G., BROWN, R.M., Methods for the measurement of tritium in environmental materials, May 1992 (1992).
[71] WORKMAN, W.J.G., Procedure for the analysis of tritium on the Quantulus Liquid Scintillation Counter, ETB-ERM-601 Rev 1.0 (1999).
[72] WORKMAN, W.G.J., Procedure for the analysis of tritium on the Quantulus Liquid Scintillation Counter, ETB-ERM-601, Rev. 1.0 (2000).
[73] GALERIU, D., HELING, R., MELINTESCU, A., The dynamics of tritium-including OBT- in the aquatic food chain, Fusion Science and Technology, 48(1), 779–782 (2005).
[74] BAUMGÄRTNER, F., Theoretical foundation and experimental proof of the accumulating transfer of tritium from water into DNA and other biomolecules in vitro and in vivo, Radiation Biology and Radioecology, 40(5), 495–499 (2000).
[75] BAUMGÄRTNER, F., KIM, M.-A., Tritium/protium fractionation near and inside DNA, J. Radioanal. & Nuclear Chem., 243, 95–98 (2000).
[76] DAVIS, P.A., ZACH, R., STEPHENS, M.E., AMIRO, B.D., BIRD, G.A., REID, J.A.K., SHEPPARD, M.I., SHEPPARD, S.C., STEPHENSON, M., The disposal of Canada's fuel waste: The biosphere model, BIOTRAC, for postclosure assessment, AECL-10720, COG-93-10, pp. 531 (1993).
[77] WEISS, W., BULLACHER, J., ROETHER, W., Evidence of pulsed discharges of tritium from nuclear energy installations in Central Europe precipitation, In: Behaviour of Tritium in the Environment, IAEA-SM-232/18, pp. 17–30 (1979a).
[78] WEISS, W., ROETHER, W., DREISIGACKER, E., Tritium in the North Atlantic Ocean: Inventory, input and transfer into the deep water, In: Behaviour of Tritium in the Environment, IAEA-SM-232/98, pp. 315–336 (1979b).
[79] NATIONAL COUNCIL ON RADIATION PROTECTION, Tritium in the environment, National Council on Radiation Protection and Measurements, NCRP, Washington, DC. NCRP Report No. 62 (1979).
[80] YANKOVICH, T.L., KIM, S.B., The dynamic Perch Lake mussel transplantation scenario for tritium depuration: Input into the EMRAS Tritium/C14 Working Group, COG Technical Note, TN-06-3022 (2006).
[81] JORGENSEN, C.B., LARSEN, P.S., RIISGARD, H.U., Effects of temperature on the mussel pump, Marine Ecology Progress Series, 64, 89–97 (1990).
[82] AMYOT, J.-P., DOWNING, J.A., Locomotion in Elliptio complanata *(Mollusca: Unionidae)*, A reproductive function? Freshwater Biology, 39, 351–358 (1998).
[83] YANKOVICH, T.L., KOARASHI, J., KIM, S.B., DAVIS, P.A., International study on the validation of models for the environmental transfer of tritium and carbon-14, Proceedings of the International Conference on Environmental Radioactivity: From Measurements and Assessments to Regulation, 23–27 April 2007, Vienna (2007).
[84] MCKONE, T.E., BRAND, K.P., SHAN, C., Environmental health-risk assessment for tritium releases at the National Tritium Labeling Facility at Lawrence Berkeley National Laboratory, April 1997, LBL-37760/UC-2000 (1997).
[85] ETNIER, E.L., TRAVIS, C.C., HETRICK, D.M., Metabolism of Organically Bound Tritium in Man, Radiat. Res., 100, 487–502 (1984).

[86] HILL, R.L., JOHNSON, J.R., Metabolism and Dosimetry of Tritium. Health Phys., 65, 628–647 (1993).
[87] BELOT, Y., ROY, M., METIVIER, H., Le tritium dans l'environnement, Technical Report, IPSN (1996).
[88] BRIGGS, G.A., Diffusion estimation for small emissions, 1973 Annual Report, Environmental Research Laboratories, Air Resources Atmospheric Turbulence and Diffusion Laboratory, National Oceanic and Atmospheric Administration (1973).
[89] SMITH, F.B., A scheme for estimating the vertical dispersion of a plume from a source near ground level, In: Proceedings of the third meeting of the Expert Panel on Air Pollution Modelling, Volume 14, NATO Committee on the Challenges of Modern Society (1972).
[90] TILL, J.E., MEYER, H.R., Radiological Assessment: A Textbook on Environmental Dose Analysis, GPO Sales Program, US Nuclear Regulatory Commission, Washington, DC (1983).
[91] DOURY, A., Vademecum des transfert atmospheriques, Techncial Report 440, CEA Centre d'Etudes Nuclaires, Department de la Suret Nuclaire (1981).
[92] CHAMBERLAIN, A.C., EGGLETON, E.J., Washout of tritiated water vapour by rain, Air Water Pollution, 8, 135–149 (1964).
[93] HUKKOO, R.K., BAPAT, V.N., SHIRVAIKAR, V.V., Manual of dose evaluation from atmospheric releases, Bhabha Atomic Research Centre Report, BARC-1412 (1988).
[94] DUBE, B., SAXENA, V., TIWARI, S.N., KUMAR, A., VARAKHEDKAR, V.K., KUMAR, M., SUNDARARAJAN, P., GAUTAM, Y.P., SHARMA, L.N., Environmental radiological monitoring around Narora Atomic Power Station (1990–1999), Radiation Protection and Environment, 1–19, 15–20 (2000).
[95] RASKOB, W., UFOTRI: Description of the new version of the tritium model UFOTRI, including user guide, KfK-Report 5194, Kernforschungszentrum Karlsruhe (1994).
[96] WEIR, A.H., BRAGG, P.L., PORTER, J.R., RAYNER, J.H., A winter wheat crop simulation model without water or nutrient limitation, Journal of Agricultural Science 102 (1984).
[97] BOUDEL, R.W., FOX, L.D., TURNER, B., STERN, A.C., Fundamentals of Air Pollution – Third Edition, ISBN-0-12-118930-9 (1994).
[98] UNITED STATES DEPARTMENT OF ENERGY, Guidance on deriving intervention levels for tritium-contaminated crops and animal feed for DOE emergency planning and response activities, UD DOE (2006).
[99] KOARASHI, J., AKIYAMA, K., ASANO, T., KOBAYASHI, H., Chemical composition of ^{14}C in airborne release from the Tokai reprocessing plant, Japan, Radiation Protection Dosimetry, 114, 551–555 (2005).
[100] KOARASHI, J., TAKEISHI, M., KOBAYASHI, H., Carbon-14 source, distribution and behavior around Tokai reprocessing plant, Proceedings of International Symposium on Environmental Modeling and Radioecology, 18-20 October, Rokkasho, Aomori, Japan, pp. 223–230 (2006).
[101] FUMA, S., INOUE, Y., MIYAMOTO, K., TAKEDA, H., IWAKURA, T., ARAI, K., KASHIDA, Y., ICHIMASA, Y., Environmental background ^{14}C level in Japan in 1990s, Radioisotopes, 51, 381–391 (in Japanese with English abstract) (2002).
[102] NAKANO, M., ONUMA, T., TAKEYASU, M., TAKEISHI, M., Analysis of meteorological data for the atmospheric diffusion calculation (FY1995-2004), JAEA-Technology 2006–008 (in Japanese with English abstract) (2006).

[103] OSAKI, M., TANAKA, A., Current photosynthates and storage substances as the respiratory substrates in the rice plant, Japanese Journal of Soil Science and Plant Nutrition, 50, 540–546 (in Japanese with English abstract) (1979).
[104] NUCLEAR SAFETY COMMISSION OF JAPAN, Meteorological Guideline for the Safety Analysis of Nuclear Power Plants, NSCJ, Taiseishuppanshya, Tokyo (in Japanese) (2000).
[105] TUCKER, S.M., ^{14}C dynamics in crops following short-term exposure to atmospheric $^{14}CO_2$, PhD Thesis, Imperial College, UK (1998).
[106] OPARKA, K.J., Changes in partitioning of current assimilate during tuber bulking in potato (*Solanum tuberosum* L.), cv Maris Piper. Ann. Bot., 55, 705–713 (1985).
[107] KARVONEN, T., KLEEMOLA, J., CROPWATN: prediction of water and nitrogen limited potato production, In: Modelling and parameterization of the soil-plant-atmosphere system, A comparison of potato growth models, P. Kabat, et al., (Eds.), Wageningen Press, 335–369 (1995).
[108] KOOMAN, P.L., SPITTERS, C.J.T., Coherent set of models to simulate potato growth, In: Modelling and parameterization of the soil-plant-atmosphere system, A comparison of potato growth models, P. Kabat, et al., (Eds.), Wageningen Press 253–274 (1995).

APPENDIX I. SCENARIO DESCRIPTIONS

I.1. Perch Lake Scenario Description

I.1.1. Background

Located on the site of Chalk River Laboratories (CRL), Perch Lake contains trace amounts of tritium due to leakage from a nearby waste management area. The releases have been going on for many years and concentrations in various parts of the lake ecosystem are likely to be in equilibrium. Tritium concentrations in lake water, sediments, aquatic plants, fish, clams and air were collected three times during the summer and fall of 2003 at three locations in the lake. These data are offered here as a test of models that predict the long-term average tritium concentrations in aquatic systems due to chronic releases.

I.1.2. Site description

Perch Lake (Figure I.1.1) is a small, shallow freshwater Canadian Shield lake. Its largest fetch is about 800 m and it has a surface area of 4.5×10^5 m^2. It has a mean depth of 2.0 m, a maximum depth of 4.1 m and a total volume of 9.1×10^5 m^3. It drains a watershed of area 5.65×10^6 m^2. The lake can be considered unstratified, although there is weak stratification in deeper areas in the summer, when surface waters are approximately 5^oC higher than those at lake bottom. The lake is usually ice covered from early December to mid April. Mean monthly water temperatures are 13, 19, 24, 23, 19 and 11^o C for the months of May through October. The turnover time of lake waters is about two years.

Sediments in the lake are composed of sand and gyttja (decomposing organic material). The average dry bulk density is 185 kg m^{-3} but this varies substantially across the lake depending on the local composition of the sediments. The sediments near Inlet 1 are largely organic in composition, those near Inlets 2 and 3 contain more sand and those near Inlet 4 and the outlet are primarily sand. The sediments are 89% water by weight and the sedimentation rate is 0.16 kg m^{-2} a^{-1}, or 0.06 cm a^{-1}.

Perch Lake is contaminated by tritium migrating through an extensive sand aquifer from a waste management area (WMA) located about 750 m to the north. The WMA was in operation for about 40 years until it was shut down in 1999. The tritium forms a well-defined underground plume that is narrow near the source but broadens to a width of about 1000 m by the time it reaches the lake. Tritium in the form of HTO discharges into the lake through the sediments from below and also through a stream (Inlet 2 in Figure I.1.1) that flows above the underground plume. Inlet 1 shows slightly elevated levels of tritium but Inlets 3, 4 and 5 are all uncontaminated. The rate and distribution of HTO releases to the lake are not known quantitatively.

I.1.3. Tritium measurements

Water, sediment, plant and air samples were collected primarily from three locations in Perch Lake: at S1, located near Inlet 1; at S2 near Inlet 2; and at S3 near Inlet 3 (Figure I.1.1). A few samples were also taken at S4 near Inlet 4 and near the outlet of the lake. Most of the plant and sediment samples were collected from shore at the edge of the lake. Some of the water samples were also taken close to shore but others were collected by boat 50-100 m offshore, as were algae. Fish tend to feed on the east side of the lake and were caught in two extended areas on either side of the outlet, whereas clams were harvested between Inlet 3 and the outlet. Most samples were collected three times during the summer and fall of 2003 (May 27-28, July 28-29 and September 28-October 1). Additional measurements of water concentrations were made in early November. Air concentrations were measured only in August and September as monthly averages and algae were not available in September, as they had all died off. Replicate samples were taken in some cases.

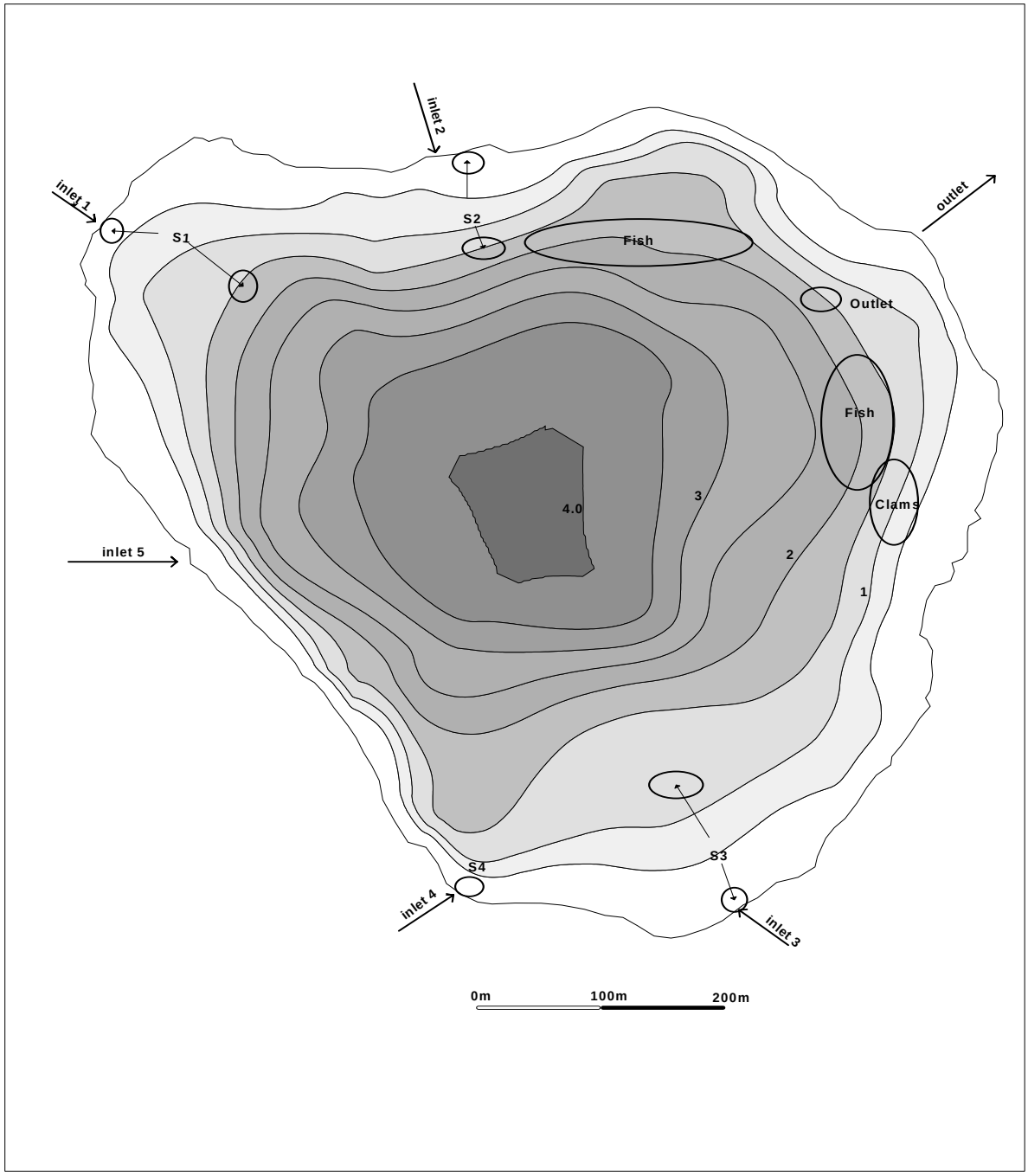

Fig. I.1.1. Map of Perch Lake showing inlets, the outlet, depth contours in m and the sampling locations.

I.1.3.1. Water

Water samples were collected near the surface of the lake and at deeper levels by opening sampling bottles at the desired depth. The samples were left standing to allow suspended sediments to settle out and then 10 ml of water was transferred to scintillation vials. HTO concentrations were determined by liquid scintillation counting (LSC).

I.1.3.2. Sediments

Sediment samples were scooped up by hand and placed in vinyl bags that were sealed at depth. This provided samples averaged over the top 15 cm or so of sediments. Water was extracted from the sediments by freeze-drying and analyzed for HTO concentration by LSC. The pressure during freeze-drying was between 10^{-4} and 10^{-5} Torr and the temperature was between 0 and -4^{o} C. The remaining solid material was washed with tritium-free water to remove the exchangeable OBT and was then completely dried in an oven, followed by combustion in a combustion tube. The combustion water was analyzed by LSC to give OBT concentrations.

I.1.3.3. Plants

Samples were taken of bladderwort *(Utricularia spp.)*, hornwort *(Ceratophylum demersum)* and cattails *(Typha latifolia)*, and of algae belonging to the phylum Chlorophyta. Bladderwort and hornwort are both unrooted plants that are completely submerged and obtain their nutrients from the water. They consist of a long thin stem that supports masses of delicate, needle-shaped, whirled leaves. These two species were composited for analysis. The cattails are rooted in the top 5-10 cm of the sediments, from which they draw their nutrients. They extend above the water into the air, and the submerged and emergent parts were analysed separately. Algae were scooped out of the water by hand and placed in a sampling jar after allowing the water to drain away. The bladderwort, hornwort and cattails were sampled from shore at the edge of the lake whereas the algae were collected further offshore. The water in all plant samples was extracted by freeze-drying and HTO concentrations were determined by LSC. The solid matter was washed with tritium-free water and was then oven-dried and combusted in a combustion bomb. LSC of the combustion water yielded non-exchangeable OBT concentrations.

Table I.1.1 shows measured water contents of the aquatic plants. No data could be found on the nutrient composition (protein, fat and carbohydrate) of these plants.

I.1.3.4. Aquatic animals

The aquatic animals collected included clams *(Elliptio complanata)*, bullheads *(Ameiurus nebulosus)* and pike *(Esox lucius)*. Bullheads are small benthic fish and pike are larger piscivores. Both types of fish likely move throughout the lake, eating other fish and invertebrates. The fish were caught in nets and the clams were pulled individually from the sediments by hand. The fish samples were divided into three parts (flesh, head and internal organs), each of which was analyzed separately. About five pike, 20 bullheads and 12 clams were combined to provide enough mass for each analysis. The fish caught in May were significantly smaller (mean weight 40 g for the bullheads and 200 g for the pike) than those caught in September (70 g for the bullheads and 400 g for the pike), although there was a large variation in size at all sampling times. Water was extracted from the samples by freeze-drying and analyzed by LSC. The solid matter was washed with tritium-free water, oven-dried and combusted in a combustion bomb for subsequent OBT analysis by LSC.

Table I.1.1. Plant water contents.

Plant type	Water Content (% by weight)
Algae	88.0
Bladderwort, hornwort	95.0
Cattail – below water	93.5
Cattail – above water	85.1

Table I.1.2. Number of grams of nutrient in 100 g of edible portion of pike, carp (a surrogate for bullheads) and clams.

Nutrient	Pike	Carp (Bullhead)	Clam
Protein	18.2	18.9	10.5
Fat	1.2	7.1	1.3
Carbohydrate	0	0	3.1
Water equivalent factor	0.645	0.709	0.577

Table I.1.3. Water contents of fish and clams.

Organism	Water content (% by weight)
Clam	89.0
Bullhead – flesh	82.3
Bullhead – head	76.8
Bullhead – internal organs	82.3
Pike – flesh	77.7
Pike – head	73.9
Pike – internal organs	81.0

Table I.1.4. Total weight and organ weights (g) of fish caught September 28 – October 1.

Fish	Total weight	Organ				Total organ	Comments
		Liver	Gonads	Stomach	Intestines		
Pike	258	2.08	2.43	4.32	4.02	12.85	Male, stomach empty
Pike	453	4.81	5.09	6.23	7.90	24.03	Male
Pike	178	1.84	0.81	3.70	4.10	10.45	Tail damage
Pike	558	5.54	10.65	10.19	7.61	33.99	Female
Bullhead	69.1	0.50	0.22	0.66	1.02	2.400	Female
Bullhead	120	3.76	0.39	11.21	7.39	22.75	Exceptionally large male; stomach contained a sunfish

Table I.1.2 gives some information, taken from the literature, on nutrient composition and water equivalent factors for the fish and clams. Nutrient data could not be found for bullheads so values are given for carp, which are believed to be a reasonable surrogate. The data are for the edible portion of the organisms and may not reflect the composition of the internal organs. Table I.1.3 shows measured water contents of the fish and clams. The total weight and organ weights of some of the fish caught in the sampling campaign of September 28 - October 1 are given in Table I.1.4.

I.1.3.5. Air

The tritium in the air above Perch Lake comes primarily from evapotranspiration from the lake and the adjacent wetland. Fluxes from the wetland to the air during daytime in the summer are about 1-3 Bq m^{-2} s^{-1}. Monthly-averaged air samples were collected with passive diffusion samplers in the months of August and September at sites S1, S2 and S3. The samplers were located 1-2 m from the shoreline at a height of 1 m. Analysis by LSC provided concentrations in Bq m^{-3} air, which were converted to Bq L^{-1} air moisture using the measured average monthly temperature and an estimated relative humidity of 75%.

I.1.3.6. Uncertainties

Counting errors in the HTO concentrations in lake water, plants and aquatic animals were generally less than 2% but reached 10% in some cases of low concentrations. Total uncertainties in the HTO concentrations in sediment water were somewhat larger because of the difficulties in keeping lake water out of the sample. Replicate sediment samples from the same location showed differences of about 30%. A similar variation among individual plant and animal samples would be expected because of natural variability but may not be evident in the composite samples that were analysed. Uncertainties in air concentrations arose due to counting errors, and to uncertainties in the performance of the passive samplers and in determining the volume of air sampled. The total uncertainties in the air concentrations are estimated to be less than about 30%.

Counting errors for OBT concentrations were usually less than 5% but additional uncertainty arose due to difficulties in removing exchangeable OBT from the samples and in the combustion process. The total uncertainty in the OBT measurements is estimated to be about 20%. Differences among replicate samples from the same location may be larger because of natural variability.

I.1.4. Input data

Measured HTO concentrations in water, sediment water and air moisture are shown in Table I.1.5. Where more than one value is listed for a given parameter, separate samples were taken close to the same location. Concentrations of the water and sediment samples collected from shore may not reflect concentrations in the main body of the lake. At sampling sites S1, S3 and S4, the near-shore samples were taken close to the inlets of the associated streams and concentrations may have been diluted by the relatively clean inflow. In contrast, the near-shore samples taken at S2 may be higher than those further out in the lake since concentrations in Inlet 2 are relatively high. Air concentrations were highest near S2, which is directly over the underground plume, and decreased from August to September.

Table I.1.5. Measured HTO concentrations in water, sediment water and air moisture.

Month	Compartment	HTO Concentrations (Bq L^{-1})				
		S1	S2	S3	S4	Outlet
May	Surface water – offshore	4350	5450	4730		
	Sediment water – offshore	4730	10890	1320		
		3330	13570			
		3830	13210			
July	Surface water – offshore	4640	4590	4620		4660
	Surface water – from shore near inlet	4150	3330	3800	91	
	Deep water – offshore*	4480	4460	4420		4620
	Deep water – from shore near inlet‡	3900	2570	3580		
	Sediment water – from shore near inlet	2300	7120	70		
Sept	Surface water – from shore near inlet	2030	9290	139		
	Deep water – from shore near inlet‡	2080	9190	113		
	Sediment water – from shore near inlet	1500	7420	84		
		1650	4550			
	Air – August	740	1970	510		
	Air – September	660	1770	260		
Nov	Surface water – offshore	3840	5270	3770		
	Deep water – offshore*	3480	9350	3770		

* Collected at a depth of about 1.5 m.
‡ Collected at a depth of about 0.4 m.

Based on single measurements made from shore at the outlet of the lake in 2001, HTO concentrations in surface water were 6330 Bq L^{-1} in June and 6660 Bq L^{-1} in December.

The rate and distribution of HTO releases to the lake are too poorly known to allow concentrations in lake water to be predicted using a model. The concentrations needed for the scenario calculations must therefore be estimated from the data in Table I.1.5. Similarly, no information is available on rates of eutrophication, biomass production or decay in the lake, or on OBT concentrations in soils of the watershed, to help in estimating OBT concentrations in sediments.

I.1.5. Scenario calculations

Using the information provided above, calculate:

(1) HTO and non-exchangeable OBT concentrations in cattails, and in bladderwort and hornwort combined, for the May sampling period for the near-shore portions of sites S1, S2 and S3. For cattails, give concentrations for both the above water and below water parts of the plant. Also, calculate HTO and non-exchangeable OBT concentrations in algae for the May sampling period for the offshore portions of sites S1, S2 and S3. For HTO, give the results in Bq L^{-1}; for OBT, give the concentration in the combustion water (i.e., Bq L^{-1} water equivalent).

(2) HTO and non-exchangeable OBT concentrations in clams, bullheads and pike for each of the three sampling periods. For bullheads and pike, give concentrations in head, flesh and internal organs (liver, gonads, stomach and intestines). Give the results in Bq L^{-1} for HTO and Bq L^{-1} water equivalent for OBT.

(3) non-exchangeable OBT concentrations in sediments for the May sampling time for the near-shore portions of sites S1, S2 and S3, in units of Bq L^{-1} water equivalent.

(4) 95% confidence intervals on all predictions in (1)–(3).

I.2. Pickering Scenario Description

I.2.1. Background

Small amounts of tritium are released continuously from the CANDU reactors that make up Pickering Nuclear Generating Station (PNGS) on the north shore of Lake Ontario. The releases have been going on for many years and concentrations in various parts of the environment are likely to be in equilibrium. A large number of environmental and biological samples were collected in 2002 from four sites in the vicinity of the station. HTO concentrations were measured in air, precipitation, soil, drinking water, plants (including the crops that make up the diet of the local farm animals) and products derived from the animals themselves; OBT concentrations were measured in the plant and animal samples. These data are offered here as a test of models that predict the long-term average tritium concentrations in terrestrial systems due to chronic releases.

I.2.2. Site description

PNGS is made up of two units, each consisting of four reactors. Unit A has been shut down for several years but still releases significant amounts of tritium. Unit B was running at full power during the study period. The land surrounding the station is gently rolling and supports a mixture of uses, including industrial, recreational, agricultural and residential.

The samples were taken at two dairy farms (DF8 and DF11), a hobby farm (F27) and a small garden plot (P2) (Figure I.2.1 and Table I.2.1). All of the sampling sites were located to the northeast of PNGS; the two dairy farms lay about 10 km from the station, the hobby farm about 7 km and the garden plot about 1 km. As dairy farms, DF8 and DF11 yielded much the same sort of samples, including corn, pasture grasses, a variety of grains, milk and meat. In contrast, F27 produced mainly fruit, garden vegetables, chickens and eggs. A limited number of plants are grown at P2 for research purposes and raspberry leaves and grass were sampled.

Meteorological data for the Pickering area are given in Table I.2.2. The air temperatures were measured locally in 2002. The solar radiation data represent long-term average conditions at Toronto, about 25 km west of Pickering. The precipitation data are long-term averages for the Pickering area. The fraction of time that rain falls when the wind blows toward F27 is 0.125; the analogous number for DF8, DF11 and P2 is 0.115. These frequencies are based on long-term average data for Toronto and are believed to be overestimates. The average absolute humidity for the 2002 growing season for the area was 0.012 kg m^{-3}.

I.2.3. Farm practices

The cows at DF8 and DF11 are fed total mixed ration (TMR), a blend of various feeds harvested in the previous year. The make-up of the TMR at the two farms is shown in Table I.2.3. The corn silage, feed corn, baled hay, haylage and barley are all obtained locally. The silos containing corn silage are filled annually in September. The haylage silos are filled two to three times per year, depending on the growing season. All of the other feed components (brewer's grain, dairy supplement, limestone) are purchased from remote locations and are assumed to contain only background levels of tritium. The total food intake by the cows was estimated by the owners to be 19.0 and 8.8 kg dry weight per day for farms DF8 and DF11, respectively. The latter value is believed to underestimate the true intake.

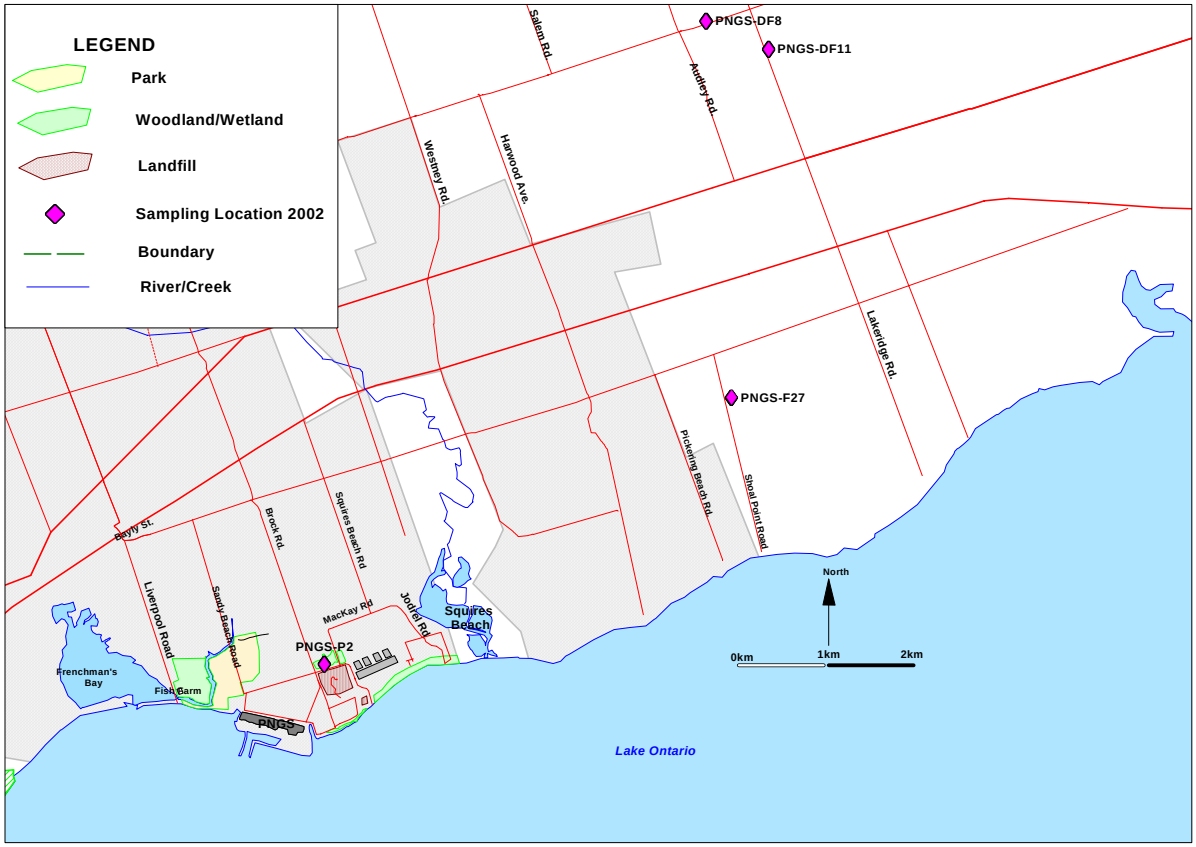

Fig. I.2.1. Map of the study area showing the tritium release points (PNGS) and sampling sites (red polygons).

Table I.2.1. Location and description of the sampling sites.

Site	Distance from Unit A (m)	Description
DF8	10 520	Dairy farm, growing pasture grasses, corn and a variety of grains, and raising dairy cows
DF11	10 405	Dairy farm, growing pasture grasses, corn and a variety of grains, and raising dairy cows
F27	7125	Hobby farm, growing fruit, pasture grasses and garden vegetables, and raising chickens
P2	1150	Research garden plot growing berries and surrounded by grass

Table I.2.2. Meteorological data for the Pickering area.

Month	Air Temperature (C)		Solar Radiation (W m^{-2})		Rainfall (mm)
	Daily mean	Mean daily max	Daily mean	Mean daily max	
May	9.2	14.5	230	658	72.5
June	16.3	21.9	254	708	64.5
July	20.9	27.6	254	717	68.4
August	20.5	27.3	216	642	77.6
Sept	18.6	25.2	163	528	66.9

Table I.2.3. Ratios of feed components in TMR.

Type of feed	DF8 (%)	DF11 (%)
Corn silage	45.5	41.9
Feed corn	13.9	22.9
Haylage	12.7	19.6
Brewer's grain	12.7	0
Dairy supplement	7.4	13.8
Baled (dried) hay	4.6	1.9
Barley	3.0	0
Limestone	0.1	0

Table I.2.4. Estimated composition of the chicken diet at F27.

Type of Feed	% of Diet
Grass	10
Chicken greens (leafy material such as lettuce, beet tops, etc.)	10
Feed corn	30
Oyster shells	3
Apples	5
Carrots	5
Potatoes	5
Green beans	7
Other sources	25

The chickens raised at F27 were essentially free-range and their food intake was not regulated or monitored. As a result, the make-up of their diet and their intakes could only be estimated (Table I.2.4). The feed corn in their diet was purchased from DF11, and the "other sources" consisted largely of table scraps.

The amount of drinking water ingested by the cows and chickens was not monitored. Irrigation was not carried out to any significant extent at any of the farms during the study period.

I.2.4. Tritium measurements

All of the samples were collected in two field campaigns carried out in 2002, the first from July 8 to 10 and the second from September 16 to 18. All of the samples collected in July were oven-dried before the HTO could be extracted and so were suitable for OBT analysis only. The September samples were frozen in their fresh state and were analysed for both HTO and OBT.

I.2.4.1. Air

Air concentrations at the sites are measured routinely as part of a monitoring program carried out by the utility. Active molecular sieve samplers provided monthly-average concentrations at P2 and annual average concentrations were available from passive diffusion samplers at the other sites. The background air concentration due to tritium sources other than PNGS is 0.19 Bq m^{-3}. Tritium concentrations in the samples were determined using liquid scintillation counting (LSC) techniques.

I.2.4.2. Precipitation

Precipitation is collected monthly by the utility at DF8, F27 and P2 using gauges with an oil layer to prevent the transfer of tritium between air and water. The water collected was analysed for its tritium content using LSC.

I.2.4.3. Plants

At the farm sites, samples were collected of each of the plants that made up the animal diets, as well as separate samples of TMR. At F27, additional measurements were made of garden vegetables, root crops and fruit. Table I.2.5 lists the samples collected and their measured water contents. Water equivalent factors (the fraction by weight of water produced when a dry sample is combusted) are also listed. However, these are literature values since the measured values seem low, likely because of the difficulty in collecting all of the water following combustion. Published values of plant yields are also shown in Table I.2.5 for those crops for which data are available. The water in the September samples was extracted by freeze-drying, and HTO concentrations were determined by LSC. The dry matter in the July and September samples was washed with tritium-free water and then oven-dried and combusted in a combustion bomb. LSC of the combustion water yielded non-exchangeable OBT concentrations.

I.2.4.4. Animal Products

The meat samples from DF8 and DF11 came from calves that were either stillborn or died from complications at birth. The mothers were three years old or younger and were raised exclusively on these farms. A local veterinarian dissected the calves and provided samples of flesh and heart. Additionally, composite milk samples consisting of a mixture of milk from all cows in the herd were collected in July at both farms.

The only animal products sampled at F27 in the July campaign were eggs. Two eggs from mature layers (24-65 weeks old) were combined and a further measurement was made of a composite sample of about 12 eggs. In addition, an immature egg taken from the body cavity of a slaughtered chicken was analysed. In September, in addition to eggs, blood and flesh were also analysed from a single chicken that was probably less than 24 weeks old, as there were no mature yolks in its body cavity. HTO and OBT concentrations in all animal products were determined using the same procedures as for plants.

The animal products sampled during the study are listed in Table I.2.6, together with measured water contents and literature values of the water equivalent factors.

I.2.4.5. Drinking Water

Samples of water were taken from the deep wells that supply drinking water for the cows at farms DF8 and DF11 in the September sampling period. Concentrations in drinking water at F27, which comes from a shallow well, are available from routine monitoring by the utility, but not for each month. The value given below in Table I.2.8 is the average for June to December.

Table I.2.5. Measured water contents and published yields and water equivalent factors for the sampled crops.

Crop type	Site	Month	Plant type	Water content (%)	Water equivalent factor	Yield (kg fw m^{-2})
Forage	DF8	July	Hay¤	78.4	0.587	0.47
			Haylage¤	70.5	0.594	0.47§
			Barley	10.5	0.567	0.28
			TMR*	51.9	0.582	
		September	Alfalfa	76.4	0.592	0.40
			Baled hay¤	13.8	0.584	0.47§
			Corn silage	61.5	0.579	2.7§
			Haylage	63.7	0.594	0.47§
			Feed corn	25.2	0.572	2.7
			Barley	12.6	0.567	0.28
			Soya meal	11.6	0.600	0.24§
			TMR	54.9	0.582	
	DF11	July	Alfalfa	78.0	0.592	0.40
			Baled hay	15.9	0.584	0.47§
			Haylage	34.5	0.594	0.47§
			Feed corn	20.1	0.572	2.7
			TMR*	41.7	0.578	
		September	Alfalfa	73.0	0.592	0.40
			Baled hay	11.5	0.584	0.47§
			Corn silage	60.2	0.579	2.7§
			Haylage	36.9	0.594	0.47§
			Feed corn	22.4	0.572	2.7
			TMR*	39.2	0.578	
	F27	July	Grass	56.1	0.587	
			Spring wheat	13.3	0.617	0.33
			Soya meal	10.8	0.600	0.24§
		September	Grass	76.1	0.587	
			Feed corn	5.0	0.572	2.7
			Spring wheat	10.0	0.617	0.33
			Soya meal	6.0	0.600	0.24§
	P2	September	Raspberry leaves	54.8	0.470	
			Grass	75.9	0.587	
Garden vegetables	F27	July	Mixed vegetables‡	87.4	0.537	
		September	Tomato	81.0	0.543	2.0
			Cucumber	94.0	0.520	1.7
Fruit	F27	September	Apple	80.0	0.575	1.9
			Pear	83.2	0.560	0.68
			Raspberry	85.1	0.562	0.16
Root crops	F27	September	Carrots and potatoes	81.1	0.543	3.0
			Beet	87.4	0.523	2.3
			Garlic	55.3	0.549	1.7

¤ Hay refers to fresh cut pasture; baled hay is dried pasture; haylage is hay that has been stored in a silo.
* Produced in 2001.
‡ Beet, cabbage, hot pepper, onion, dill, potato, spinach.
§ Yield of parent plant in the field.

Table I.2.6. Measured water contents and published water equivalent factors for the sampled animal products.

Site	Month	Animal product	Water content (%)	Water equivalent factor
DF8	July	Milk	85.9	0.746
	September	Calf flesh	75.7	0.646
		Calf heart	76.6	0.753
DF11	July	Milk	87.5	0.746
	September	Calf flesh	75.5	0.646
		Calf heart	76.3	0.753
F27	July	Egg	74.8	0.803
		Composite egg	71.5	0.803
		Immature egg	47.2	0.803
	September	Egg	76.0	0.803
		Chicken blood	80.0	Unknown
		Chicken flesh	74.4	0.697

Table I.2.7. Water content of the sampled soils (% wet weight).

Month	DF8	DF11	F27	P2
July	–	12.9	25.9	–
September	19.4	14.0	15.0	26.1

Table I.2.8. Measured HTO concentrations in air and drinking water. The air concentrations include a background contribution of 0.19 Bq m^{-3}.

Compartment	DF8	DF11	F27	P2
Air concentration (Bq m^{-3})				
2002 May	1.01	1.01	1.56	24
June	1.39	1.39	2.14	33
July	0.93	0.93	1.43	22
August	0.88	0.88	1.36	21
September	0.67	0.67	1.04	16
Air concentration (Bq m^{-3})				
2001 May	0.49	0.49	0.77	12
June	2.83	2.83	4.40	69
July	0.86	0.86	1.34	21
August	1.23	1.23	1.92	30
September	0.66	0.66	1.02	16
Drinking water concentration (Bq L^{-1}) 2002 September	18.6	21.1	24.3*	Not relevant

* Average value for June-December 2002.

Table I.2.9. Measured monthly HTO concentrations in precipitation.

Month	HTO Concentration in Precipitation (Bq L^{-1})		
	DF8	F27	P2
January	not available	not available	3670
February	not available	18	1350
March	not available	24	347
April	24	29	474
May	69	14	525
June	85	61	579
July	9	14	205
August	49	19	442
September	13	22	452

I.2.4.6. Soil

Soil cores were collected at a single location at each site. Three cores 15 cm in diameter and 5 cm deep were taken at each location and composited for analysis. The cores were collected from undisturbed locations in grassed areas or where the soil had lain fallow for some time. No detailed analysis of physical properties was done but the soils at DF8, DF11 and P2 are believed to be loams or clay loams with bulk density, pH and organic content around 1.08 g cm^{-3}, 7.3 and 5.2% dry weight, respectively. At F27, where the cores were taken beside a road, the soil contained more sand. The samples were analysed for their HTO and OBT concentrations using the procedures discussed above for plant and animal samples. Water contents are listed in Table I.2.7.

I.2.4.7. Uncertainties

The observed concentrations in all environmental compartments were relatively low, although they were at least a factor 4-5 above background. Counting errors for both HTO and OBT samples were less than 10% in most cases. A further error of perhaps 30% must be added to the air concentrations to account for the uncertainty in the passive diffusion sampler data at DF8, DF11 and F27. An additional uncertainty of about 30% must also be added to the plant and animal concentrations to account for natural variability.

I.2.5. Input data

Best estimates of the HTO concentrations in air and drinking water at the study sites are shown in Table I.2.8. HTO concentrations in monthly precipitation are given in Table I.2.9.

I.2.6. Scenario calculations

From the information provided above, calculate:

(1) HTO and non-exchangeable OBT concentrations in the plants and animal products listed in Tables I.2.5 and I.2.6. For HTO give the results in Bq L^{-1}; for OBT give the concentration in the combustion water (i.e., Bq L^{-1} water equivalent).
(2) HTO (Bq L^{-1}) concentrations in the top 5-cm soil layer for each site for each sampling period.
(3) 95% confidence intervals on all predictions.

The predicted HTO concentrations in plants should reflect average conditions over the growing season and not the measured concentrations at the sampling times. HTO is very mobile in plants and concentrations are strongly dependent on the air concentration in effect in the few hours before sampling. Since these concentrations (or the meteorological and source term data required to calculate them) are not available, no attempt will be made to compare predicted and observed HTO concentrations in plants. Rather, the predictions will be used to help explain differences among model results for OBT concentrations.

I.3. Pine Tree Scenario Description

I.3.1. Background

The main purpose of the pine tree scenario is to test models by comparing their prediction with observations of TFWT and OBT concentrations in pine trees, and HTO concentrations in groundwater. The major observed data were results of the NIRS monitoring program conducted monthly in the vicinity of nuclear sites in Tokaimura, Japan, where a few sources have released HTO vapor into the atmosphere continuously for many years. The scenario is characterized by such features as a subtropical environment, relatively simple wind direction frequencies (especially when it rains), reliable discharge rate data, and additional supportive measurements of tritium in air vapor and precipitation.

I.3.2. Site description and measurements

I.3.2.1. Location of nuclear facilities

The Tokiamura village is basically a flat land of agriculture such as rice plant, vegetable and fruit plants. An overview of the Tokaimura village is shown in Figure I.3.1. The population of Tokaimura is about 35,400. The Japan Atomic Energy Research Institute (JAERI), the Japan Nuclear Cycle Development Institute (JNC) (previously the Power Reactor and Nuclear Fuel Development Corporation (PNC)), and other nuclear facilities are located in the east end of Tokaimura village (longitude 140.6E, latitude 36.5N), Ibaraki Prefecture Japan, facing the Pacific ocean. The locations of the main nuclear facilities and sampling sites are shown in Figure I.3.2.

As can be seen in Figures I.3.1 and I.3.2, the major nuclear facilities in Tokaimura are situated in a 1000-m wide zone between the east coast facing the Pacific Ocean and National Road No. 245, which runs north-south along the west boundaries of the JAERI and JNC sites. All the major tritium discharge sources, as well as the NIRS tritium sampling points in the scenario, are located within a rectangle 1 km east-west by 2 km north-south. The elevation of the sand dune terrain increases from sea level at the coast line to about 24 m above sea level at road 245. Most of the facility buildings at JAERI and JNC are located about 10-20 m above sea level. The highest hill top of the sand dunes is 35.7 m above sea level and located near the site boundary of JAERI in the SSW direction from the two heavy-water moderated research reactors JRR-2 and JRR-3. JAERI Monitoring Station 2 (MS-2) is located near the top of this hill.

I.3.2.2. Geological formation and a supposed groundwater aquifer in Shinkawa River Basin in Shuku district

The Tokaimura village is situated on part of the diluvial Naka Terrace. Three small streams are combined into the main Shinkawa River in the Shuku district, which flows along the north boundary of JNC (PNC) into the Pacific Ocean, as shown in Figure I.3.2. The Quaternary formation of Naka Terrace, consisting of silt or sandy gravel layers, overlies a hardened pelite layer (Miocene-Pliocene). The Pleistocene deposits of Naka terrace formed the broad wave-cut platform and the buried river channels of ancient rivers. Both the JAERI and JNC sites are situated on a shallow buried river channel that was cut by the ancient Shinkawa River. Later this was covered with quaternary formations when the area lay below sea level. Although groundwater is not so plentiful because of the thinness of soil deposits over the hardened pelite base rock, this groundwater, as well as water from the Kuji River (see Figure I.3.1) supplied to the inhabitants in a local public water supply, is used for drinking or irrigation of fruit trees or upland rice fields.

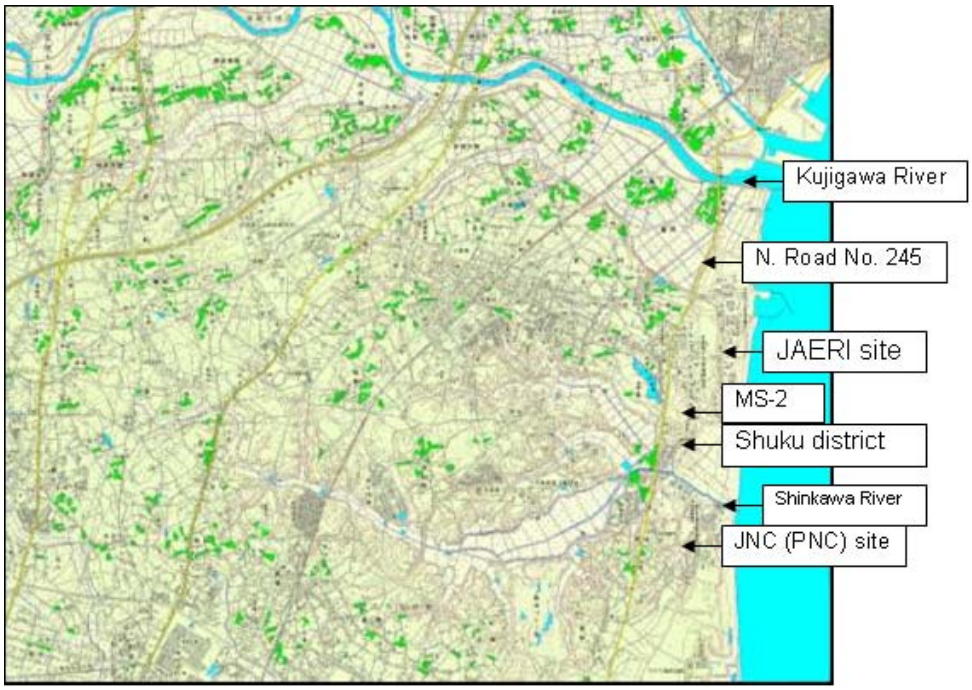

Fig. I.3.1. Map of Tokaimura village with key nuclear facilities and landmarks.

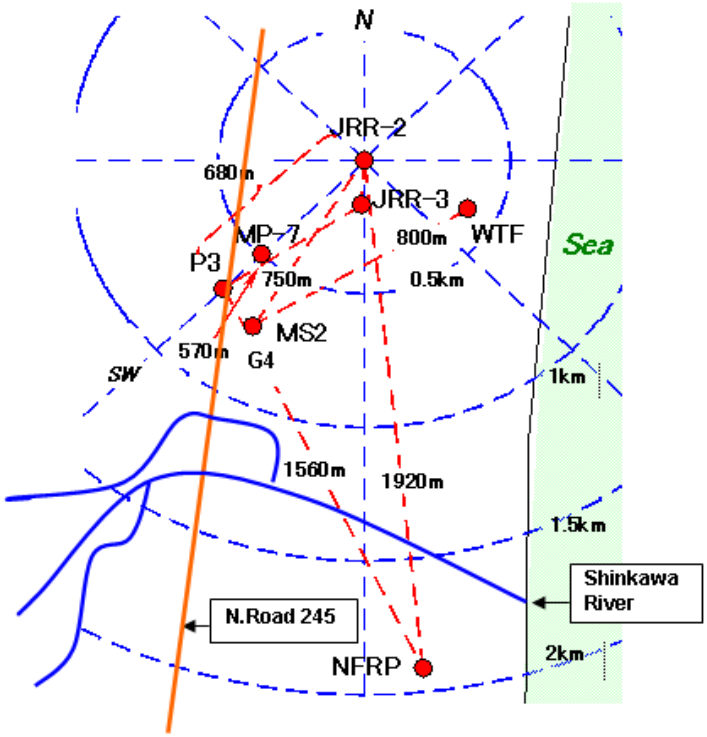

Fig. I.3.2. Directions and distances of sampling points MP-7, P3, MS2 and G4 from the tritium discharge sources JRR-2, JRR-3, WTF and NFRP in Tokaimura, Ibaraki Prefecture. The distance between stacks of JRR-2 and JRR-3 is approximately 170m.

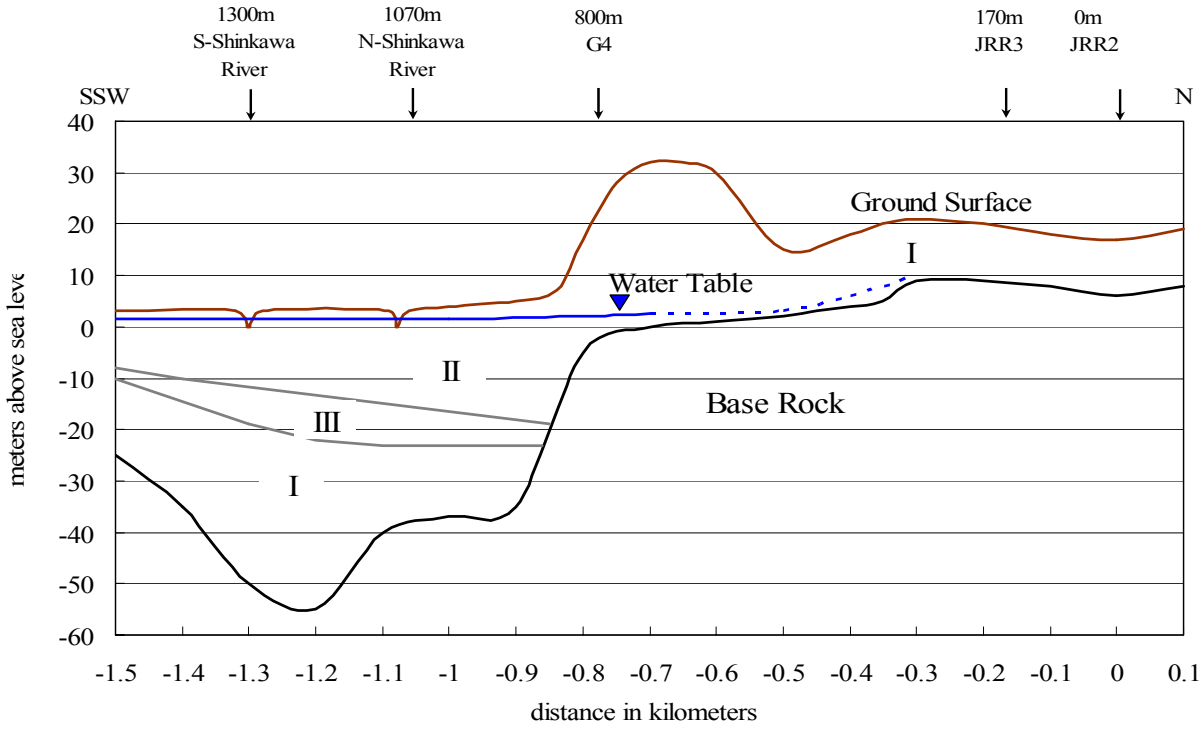

Fig. I.3.3. Supposed and simplified geological model along a line connecting the points of northern JRR2, south south-west G4, and Shinkawa River. I: Sand/Silt, II: Gravel/Sand, III: Silt/Clay

Figure I.3.3 shows a supposed simplified geological cross-section and a groundwater aquifer along a line (the inner land line) connecting the points JRR2 at the north, G4 at the south-southwest and the Shinkawa river. Figure I.3.3 was drawn based on information from a limited number of soil cores in the area, taking into account a published, detailed geological section along a line (the seaside line) which runs about 500m east and almost parallel to the inner land line described above. Since the levels of both ground surface and base rock in the area surrounding JRR2 and JRR3 along the inner land line seem about 10 m higher than those along the seaside line, the groundwater may mainly flow eastward in the direction of the sea. Even if the groundwater flows southward from the JRR2 and JRR3 area, it might be blocked by ascending ground surface and base rock about 300 m south of JRR2, provided that the amount of groundwater is not so plentiful and the mean residence time of groundwater is relatively short, e.g. about half a year.

The infiltration rate of water into the unsaturated soil layer was estimated to be about half the annual precipitation of 500 – 700 mm (0.5 - 0.7 m). The vertical pore water velocity in the unsaturated soil layer was estimated to be about 5.5 m/y based on experimental data obtained by tracing HDO depth profiles for several months after mixing D_2O with surface soil in a field in the northern part of the JAERI site. The mean horizontal flow rate was estimated to be about 0.2 m/day based on Darcy's law applied to the area between a well close to G4 and a well close to the Shinkawa river, where groundwater flows southward into the Shinkawa River. Most of the well water in the Shuku district was probably taken from subsurface groundwater at a depth from several meters to 20 m. More than 10 monthly groundwater

samples were taken from the resident wells in the area outside the south boundary of the JAERI for tritium analyses. The distribution or contour lines of tritium concentration in subsurface groundwater in the area showed an evident relationship between the excess tritium concentration and the distance in a southwest direction from JAERI. A horizontal gradient in the tritium concentration suggested that tritium reaching the groundwater layer gradually drains into the ocean through the Shinkawa basin due to an inflow of groundwater from the upper inland basin. The groundwater sampling well at G4 in Figure I.3.3, where groundwater tritium concentration is requested for prediction in this scenario, was bored in the early 1980s at a point halfway down the southern slope of the 35.7-m sand dune hill, about 800 m SSW of JRR-2, as indicated in Figure I.3.3. At G4, the depth from the soil surface to the top of the groundwater aquifer is estimated to be 15 – 20 m.

I.3.2.3. Surface soil characteristics

Both the JAERI and JNC (PNC) sites are located in an area covered with sand dunes along the coast. The environment surrounding both sites is a grove mainly of pine trees on sandy soil with a total porosity of 0.53 (the volume ratio of the air-filled and liquid-filled pore space to the total, which includes the solid phase space). The soil characteristics from the surface to 20 cm depth are shown in Table I.3.1, and the water content of the surface soil from 0-60 cm, as observed at MS2 in 1986, is shown in Table I.3.2. The profiles of soil water content from 5 cm to 100 cm depth were almost constant at each sampling.

I.3.2.4. Parameter values related to groundwater flows

Parameter values which may be applicable to groundwater flows in the area are listed in Table I.3.3. The locations where the parameter values were obtained or estimated are also indicated.

I.3.2.5. Vegetation

There are various species of vegetation in the area, but Japanese red and black pine trees about 10-m high are the dominant species. The depth of pine tree roots is observed to be mostly within about 1m of the soil surface. Pine tree needle samples were taken monthly about 1.0-1.5 m above the ground at several points around the JAERI site from 1982. As the pine tree branch and needles grow actively from spring to summer and stay for a few years, pine needles grown in individual years are easily identified and were separately collected at sampling. A pine tree trunk sample was taken near MS-2 near the top of the 35.7-m sand dune. A view of a typical pine tree grove is shown in Figure I.3.4. It is likely that tritium reaches the trees from both air and root pathways.

I.3.2.6. Detection limit, precision and uncertainty of tritium measurement

The lower detection limit is evaluated to be 1.2 Bq/L based on 3 standard deviations (SD) of the net counting rate when 8 ml of combustion water are counted. All the OBT concentration data exceeded the lower detection limit except for the tree rings in Chiba city in the late 1980s (a natural or background level sample). The precision (reproducibility) was evaluated to be 11-20% (2 SDs of the mean) on the basis of 2 or 3 replicate analyses of identical tree ring samples obtained in different years. Uncertainties (as 2 SDs of OBT concentrations in tree rings at MS2 from 1984 to 1987) ranged from 11% to 31%.

Table I.3.1. Typical soil characteristics of the surface soil layer around JAERI.

Depth (cm)	Texture (%)				Soil pH		Organic matter (%)
	Silt	Sand		Gravel	KC1	H_2O	
		Fine	Coarse				
	(<0.075)	(0.075–0.25)	(0.25–2.0)	(>2 mm)			
0–5	2.8	17.1	79.9	0.2	5.1	5.7	2.5
5–10	1.9	16.2	81.7	0.2	–	–	–
10–15	1.6	16.4	81.9	0.1	–	–	–
15–20	1.5	16.6	81.8	0.1	6.3	7.1	1.0

Table I.3.2. Soil water content (% by weight) in surface soil from 0–60 cm depth at MS2 in 1986.

Date (1986)	20-Jan	23-Jun*	8-Jul	16-Jul	18-Sep	2-Oct	21-Oct	13-Nov	2-Dec	Mean
Water content (%)	2.20	1.90	2.93	2.70	4.46	3.23	2.46	3.59	2.05	2.84

* Soil depth 0–40 cm.

Table I.3.3. Parameter values suggested for predicting groundwater flows.

Parameter	Value	Remarks
Porosity for coastal soil Total porosity of surface soil	0.4 0.53	Tokaimura coast
Evaporation/Evapotranspiration rate	~ 62% of annual precipitation	Ibaraki Prefecture
Potential recharge	~ 0.7 m/y	Ibaraki Prefecture
Vertical pore water velocity in unsaturated soil layer	~ 5.5 m/y	JAERI site
Estimated depth from soil surface to the top of groundwater aquifer at G4	~ 15 to 20 m	Rough estimate for the point G4
Hydraulic conductivity, K	~ 6 x 10^{-4} m/s	Between G4 and Shinkawa River
Longitudinal pore water velocity, U_x	~ 0.2 m/d	Between G4 and Shinkawa River
Empirical longitudinal dispersivity on a field scale of 1km	~ 10 m	General text book value

Fig. I.3.4. A view of a pine tree grove on the sand dunes looking toward the Pacific Ocean from the east boundary of the JAERI site.

Table I.3.4. The discharge sources and their discharge parameters.

Parameter	Discharge sources			
	JRR-2	JRR-3	WTF	NFRP
Stack height, m	40	40	30	90
3WD, m	28.5	31.5	26.5	139.2

Table I.3.5. Tritium samples and their sampling locations.

Sampling points (Figure I.3.2)	Samples	Tritium forms measured	Responsible organization	Direction and distance (m) from the tritium discharge sources			
				JRR-2	JRR-3	WTF	NFRP
MP-7	air vapor	HTO	JAERI				
	rain	HTO	JAERI	SSW	SW	WSW	NNW
	pine needles	TFWT	JAERI	510	400	720	1610
P3	rain	HTO	NIRS	SW	SW	WSW	NNW
	pine needles	TFWT & OBT	NIRS	680	570	820	1560
MS2	rain	HTO	NIRS	SSW	SSW	SW	NNW
	pine needles	TFWT & OBT	NIRS	750	580	800	1300
	tree-rings	OBT	NIRS				
G4	groundwater	HTO	NIRS	SSW 800	SSW 630	SW 850	NWN 1260

I.3.3. Tritium discharge sources and sampling points

The major tritium sources that affected tritium levels in the Shuku district near MS-2 were the two heavy-water moderated research reactors JRR-2 and JRR-3 and a waste treatment facility (WTF) on the JAERI site in the north-east, and a small-scale nuclear fuel reprocessing plant (NFRP) at JNC (PNC) in the south. The JRR-2, JRR-3 and WTF discharged HTO continuously into the atmosphere whereas the NFRP discharged HT as well as HTO. The average discharge rate of HT was recently studied and proved to be in the range of 20-30% of the total tritium when spent nuclear fuels were being reprocessed and almost 0% when reprocessing was not occurring. Thus the conversion to HTO resulting from the oxidation of HT by the surface soil could be ignored.

The stack height and discharge parameter 3WD of each HTO discharge source are indicated in Table I.3.4. Plume rise should be calculated by applying the monthly mean wind speed to the equation $\Delta H = 3WD/U$, where ΔH is plume rise (m); W is the exit velocity of the stack gases (m/s); D is the inside diameter of the stack (m); and U is the monthly mean wind speed (m/s). Then the effective stack height can be derived by adding ΔH to the physical height of the stack.

From the end of 1981, NIRS started a tritium monitoring program in the general Tokaimura area, with intensive measurements near the nuclear site boundaries, including the Shuku district. Samples of precipitation, river water, seawater, groundwater and plants such as pine needles and moss were collected on a monthly basis. NIRS often found a relatively good relationship between elevated tritium concentrations in the Shuku district and the distance of the sampling locations from the tritium discharge sources at JAERI. The monthly TFWT and OBT concentrations in pine needles, monthly precipitation and groundwater were determined in the Shuku district intensively for the period 1982 to 1986. Additionally, a pine tree trunk was sampled near MS-2 near the top of the sand dune in December 1987. OBT concentrations in this sample made it possible to determine the past environmental tritium levels retrospectively to 1961. These data are offered for testing models that predict the long-term

average tritium concentrations in the environment due to chronic atmospheric releases. Near some of NIRS sampling points, JAERI also measured monthly tritium concentrations in air vapor and precipitation, and tissue free water in pine needles. Tritium samples and their sampling locations are summarized in Table I.3.5 in relation to the four tritium sources.

I.3.4. Tritium discharge rates

JNC provided monthly HTO discharge rates from NFRP from January to December each year. JAERI provided similar data for JRR-2 and JRR-3, but for the Waste Treatment Facility (WTF) only yearly data were provided starting in April and ending in March of the following year. The monthly discharge rates from 1981 to 1987 are plotted in Figures I.3.5 (JRR-2), I.3.6 (JRR-3) and I.3.7 (NFRP). The annual discharge rates of the four tritium sources are shown in Figure I.3.8. The numerical values are summarized in Tables I-1.1 and I-1.2 in Annex I-1. The WTF discharge rates will cause an error in model predictions to a certain extent when the annual rates are divided into monthly rates and assigned to individual months.

Note that an incidental release of HTO with a small leakage of D_2O from a pipe occurred in JRR-3 during a week in June in 1982. This led to a monthly discharge rate of 1.6×10^{12} Bq, which was one order of magnitude higher than the usual monthly discharge rate (Figure I.3.6). This incident may have affected the tritium concentration in precipitation, groundwater and pine needles in the months immediately following.

I.3.5. Meterological data

Both monthly and annual average meteorological data from 1981 to 1987 for JAERI (File name: JAERI_met_aver3.xls) and JNC (JNC_met_aver7.xls) were tabulated by averaging the original hourly data from JAERI and the 10-minute data from JNC observed at different heights on their respective meteorological towers. The JNC data are provided with the scenario text in electronic form. The JAERI data will be provided on request for each modeler who carries out calculations. The datasets contain wind roses (16 directions) and wind speeds measured at different heights, stability classes (A to G), precipitation intensities, precipitation frequencies, air temperatures, relative humidities (JNC) or dew point temperatures (JAERI), net radiation (JNC) or solar radiation and radiation balance (JAERI), and so on. The method used to classify atmospheric stability is shown in Table I.3.6. The JAERI measurements of atmospheric stability class are indicated using numbers from 1 to 10, which correspond to stability classes A to G as shown in a separate file (JAERI_met_cmnt.txt).

The wind roses observed at JAERI and JNC were quite similar to each other, and the roses observed at 70m at JNC (PNC) during fine and rainy weather are shown as examples in Figures I.3.9 and I.3.10, respectively. The annual mean wind rose fluctuated less from year to year during fine weather than during rainy weather. The NE sector (wind blowing from northeast to southwest) was by far the dominant wind direction (20 to 38%) during rain and this is a special feature of weather in the area. Stability classes D and G were dominant at the JAERI site but D was overwhelming frequent at JNC (PNC) from 1981-1987. Washout may play a key role in the prediction of tritium concentration in precipitation, groundwater, and so on. Two washout factors Λ were reported by separate research groups in field studies around the nuclear facilities, one on the Japan coast and the other on the Pacific side of Tokaimura. The reported values were 7.3×10^{-5} s^{-1} and 4.6×10^{-4} s^{-1} respectively, both at precipitation intensities of 2 mm/h.

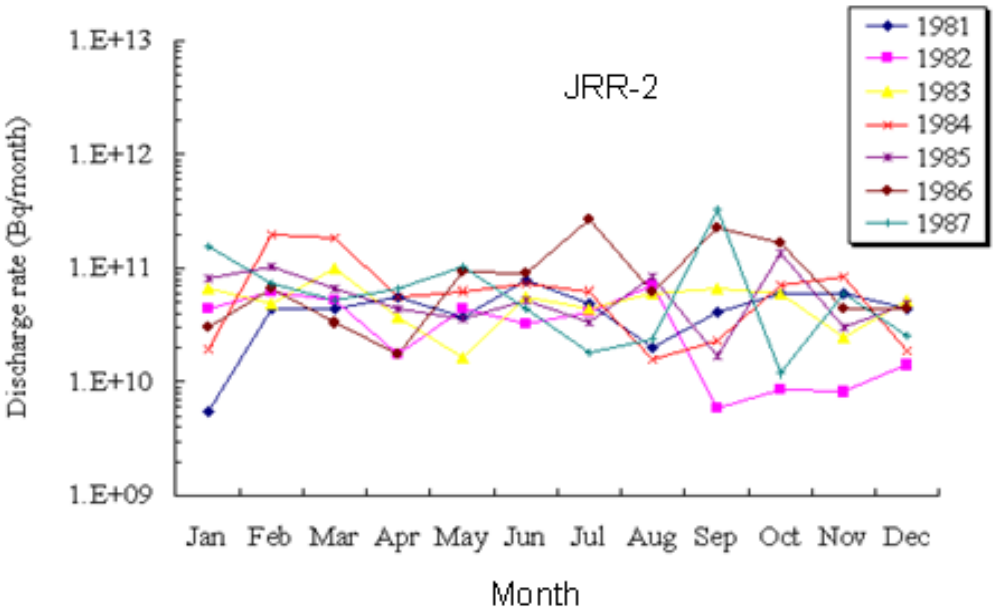

Fig. I.3.5. Monthly atmospheric discharge rates of HTO from JRR-2.

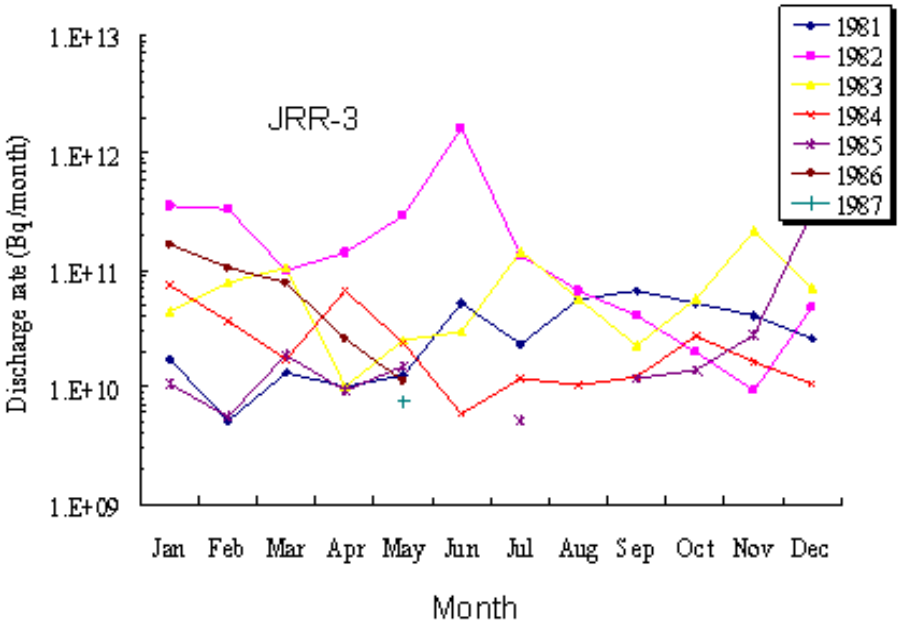

Fig. I.3.6. Monthly atmospheric discharge rates of HTO from JRR-3.

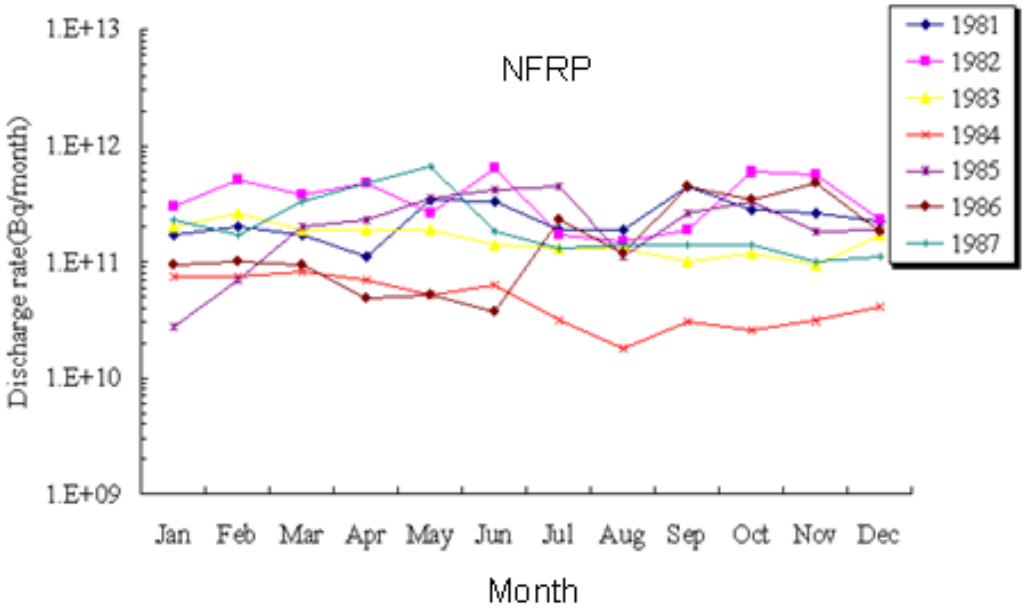

Fig. I.3.7. Monthly atmospheric discharge rates of HTO from NFRP.

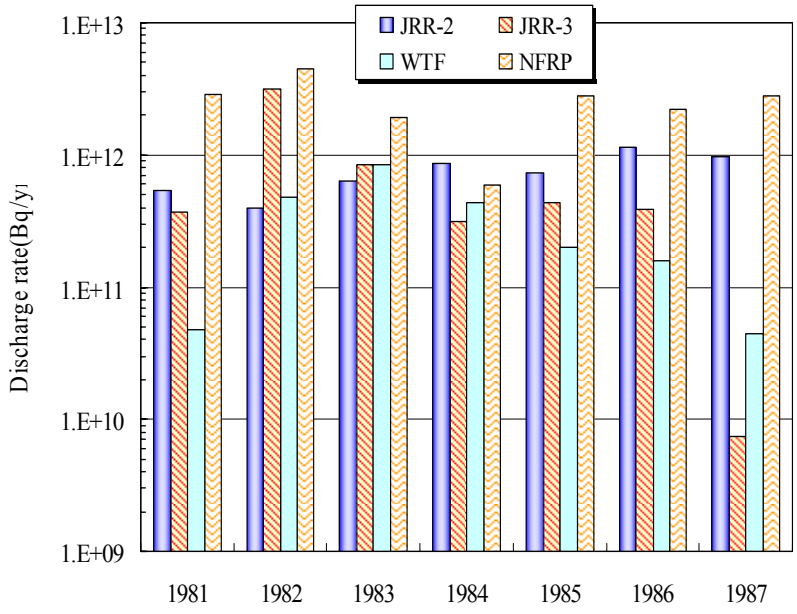

Fig. I.3.8. Annual discharge rates of the four tritium sources. The WTF data were obtained for annual periods starting in April and ending in March of the following year.

Table I.3.6. Classification of atmospheric stability for safety assessment of nuclear power plants in Japan.

Wind speed* (U) m/s	Solar radiation** (T) kW/m^2				Radiation balance** (Q) kW/m^2		
	T≥0.60	0.60>T≥ 0.30	0.30>T≥ 0.15	0.15>T	Q≥-0.020	-0.020> Q ≥ -0.040	-0.040>Q
U<2	A	A–B	B	D	D	G	G
2≤U<3	A–B	B	C	D	D	E	F
3≤U<4	B	B–C	C	D	D	D	E
4≤U<6	C	C–D	D	D	D	D	D
6≤U	C	D	D	D	D	D	D

* Measured at the ground surface.
** Solar radiation used during the day and radiation balance at night.

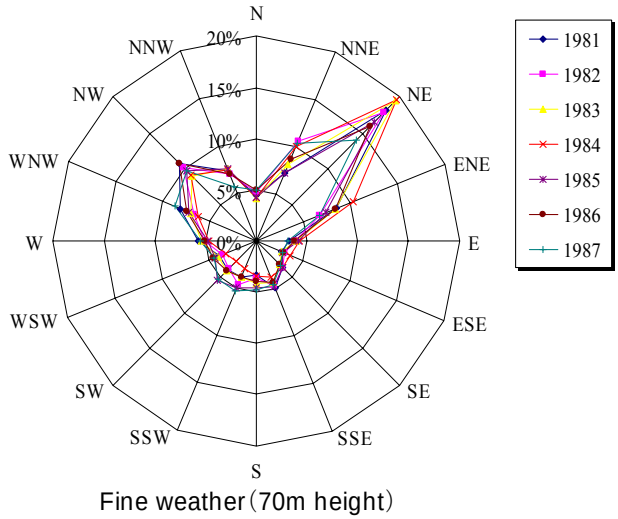

Fig. I.3.9. Annual average wind rose at 70 m at the JNC (PNC) Tokai site from 1981–1987 during fine weather.

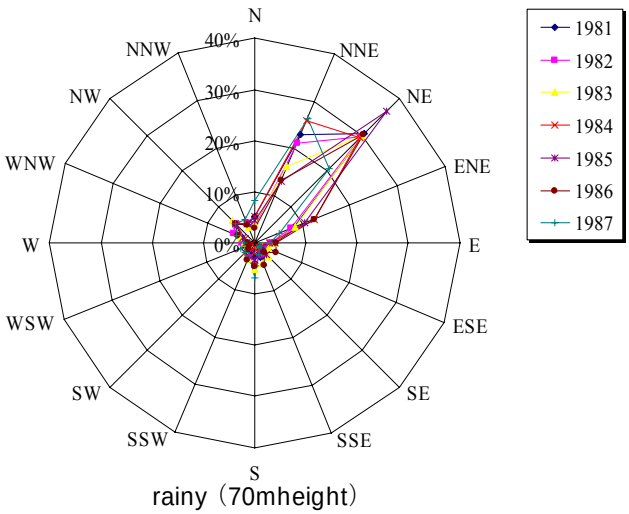

Fig. I.3.10. Annual average wind rose at 70 m at the JNC (PNC) Tokai site from 1981–1987 during rainy weather.

I.3.6. Calculation end points

Using the HTO discharge rates for the four tritium sources, and the meteorological data given with the scenario text, modelers are requested to calculate the following end points:

(1) Monthly tritium concentrations in air moisture, precipitation, tissue free water (TFWT) and non-exchangeable OBT (nOBT) in pine tree needles from 1982 to 1986 at P3;
(2) Yearly tritium concentrations in air moisture, precipitation and nOBT in pine tree trunk year-rings, and TFWT and nOBT in needles of pine trees collected separately from the trunk at MS2. All predictions are to be for the period from 1984 to 1987 at MS-2.
(3) Monthly tritium concentrations in groundwater at the well G4 from 1984 to 1987;
(4) 95% confidence intervals on each prediction.

All results should be reported for the excess tritium concentration caused by the atmospheric HTO discharges from the four sources, not including the contribution from natural and fallout tritium. These will be compared with observations from which background levels have been subtracted. The predictions should be presented in Bq/L water or water equivalent, taking into account the fact that the OBT samples were washed with tritium free water and dried before combustion. Please contact Yoshikazu Inoue (y_inoue@nirs.go.jp) or Kiriko Miyamoto (kiriko@nirs.go.jp) if you have any questions.

Acknowledgement

The author is grateful to the Japan Atomic Energy Research Institute (JAERI) and the Japan Nuclear Cycle Development Institute (JNC) (which were unified into the Japan Atomic Energy Agency (JAEA) as of 1st October 2005) for their cooperation in providing their source data in electronic form.

ANNEX I-1. NUMERICAL VALUES FOR TRITIUM DISCHARGE RATES

Table I-1.1. Monthly discharge rates of HTO from JRR-2 and JRR-3, and the annual discharge rate of HTO from WTF at JAERI.

Year	Facilities	Jan	Feb	Mar	Apr	May	Jun	Jul	Aug	Sep	Oct	Nov	Dec	Annual
		Bq/month												Bq/year
1981	JRR-2	5.6E+09	4.4E+10	4.4E+10	5.6E+10	3.7E+10	7.8E+10	4.8E+10	2.0E+10	4.1E+10	5.9E+10	5.9E+10	4.4E+10	5.4E+11
	JRR-3	1.7E+10	5.2E+09	1.3E+10	1.0E+10	1.3E+10	5.2E+10	2.3E+10	5.6E+10	6.7E+10	5.2E+10	4.1E+10	2.6E+10	3.7E+11
	WTF													4.8E+10
1982	JRR-2	4.4E+10	6.3E+10	5.2E+10	1.7E+10	4.4E+10	3.2E+10	4.1E+10	7.0E+10	5.9E+09	8.5E+09	8.1E+09	1.4E+10	4.0E+11
	JRR-3	3.4E+11	3.3E+11	1.0E+11	1.4E+11	2.9E+11	1.6E+12	1.3E+11	6.7E+10	4.1E+10	2.0E+10	9.3E+09	4.8E+10	3.2E+12
	WTF													4.8E+11
1983	JRR-2	6.7E+10	4.8E+10	1.0E+11	3.7E+10	1.7E+10	5.6E+10	4.4E+10	5.9E+10	6.7E+10	5.9E+10	2.5E+10	5.2E+10	6.3E+11
	JRR-3	4.4E+10	7.8E+10	1.0E+11	1.0E+10	2.5E+10	2.9E+10	1.4E+11	5.6E+10	2.3E+10	5.6E+10	2.1E+11	7.0E+10	8.5E+11
	WTF													8.5E+11
1984	JRR-2	2.0E+10	2.0E+11	1.8E+11	5.6E+10	6.3E+10	7.4E+10	6.3E+10	1.6E+10	2.3E+10	7.0E+10	8.5E+10	1.9E+10	8.7E+11
	JRR-3	7.4E+10	3.7E+10	1.7E+10	6.7E+10	2.4E+10	5.9E+09	1.2E+10	1.0E+10	1.2E+10	2.7E+10	1.6E+10	1.1E+10	3.1E+11
	WTF													4.4E+11
1985	JRR-2	8.1E+10	1.0E+11	6.7E+10	4.4E+10	3.6E+10	5.2E+10	3.3E+10	8.5E+10	1.7E+10	1.4E+11	3.0E+10	4.8E+10	7.3E+11
	JRR-3	1.1E+10	5.6E+09	1.9E+10	9.3E+09	1.5E+10	0.0E+00	5.2E+09	0.0E+00	1.2E+10	1.4E+10	2.8E+10	3.1E+11	4.3E+11
	WTF													2E+11
1986	JRR-2	3.1E+10	6.7E+10	3.3E+10	1.8E+10	9.3E+10	8.9E+10	2.7E+11	6.3E+10	2.3E+11	1.7E+11	4.4E+10	4.4E+10	1.1E+12
	JRR-3	1.7E+11	1.0E+11	7.8E+10	2.6E+10	1.1E+10	0	0	0	0	0	0	0	3.8E+11
	WTF													1.6E+11
1987	JRR-2	1.6E+11	7.4E+10	5.2E+10	6.7E+10	1.0E+11	4.4E+10	1.8E+10	2.4E+10	3.3E+11	1.2E+10	5.9E+10	2.5E+10	9.6E+11
	JRR-3	0	0	0	0	7.4E+09	0	0	0	0	0	0	0	7.4E+09
	WTF													4.4E+10

Note 1: No tritium releases occurred after June 1986 because of JRR-3 reconstruction.
Note 2: Monthly discharge rate data for the WTF are not available, and the annual data for WTF are for the period April to March.

Table I-1.2. Monthly atmospheric discharge rates of HTO from NFRP at JNC (PNC).

Year	Jan	Feb	Mar	Apr	May	Jun	Jul	Aug	Sep	Oct	Nov	Dec	Annual
1981	1.7E+11	2.0E+11	1.7E+11	1.1E+11	3.4E+11	3.3E+11	1.9E+11	1.9E+11	4.4E+11	2.8E+11	2.6E+11	2.2E+11	2.9E+12
1982	3.0E+11	5.1E+11	3.8E+11	4.7E+11	2.6E+11	6.5E+11	1.7E+11	1.5E+11	1.9E+11	5.9E+11	5.6E+11	2.3E+11	4.5E+12
1983	2.0E+11	2.6E+11	1.9E+11	1.9E+11	1.9E+11	1.4E+11	1.3E+11	1.3E+11	1.0E+11	1.2E+11	9.3E+10	1.7E+11	1.9E+12
1984	7.4E+10	7.4E+10	8.1E+10	7.0E+10	5.2E+10	6.3E+10	3.2E+10	1.8E+10	3.0E+10	2.6E+10	3.1E+10	4.1E+10	5.9E+11
1985	2.8E+10	7.0E+10	2.0E+11	2.3E+11	3.5E+11	4.1E+11	4.4E+11	1.1E+11	2.6E+11	3.3E+11	1.8E+11	1.9E+11	2.8E+12
1986	9.3E+10	1.0E+11	9.3E+10	4.8E+10	5.2E+10	3.7E+10	2.3E+11	1.2E+11	4.4E+11	3.4E+11	4.8E+11	1.8E+11	2.2E+12
1987	2.3E+11	1.7E+11	3.3E+11	4.8E+11	6.7E+11	1.8E+11	1.3E+11	1.4E+11	1.4E+11	1.4E+11	1.0E+11	1.1E+11	2.8E+12

I.4. Soybean Scenario Description

I.4.1. Background

The soybean is one of many staple plants growing outdoors in northeast Asian countries. It is generally sown in May and harvested in October. The products are leaf, stem, shell, and seed. The seeds are used for human diet, and the remainder is sometimes used for animal feed.

The purpose of the experiments was to simulate tritium exposure of soybean plants during growth. Tritium concentrations were measured in the seed, as well as in other plant parts, for a better understanding of the tritium distribution from leaves to seeds.

I.4.2. Experiments

I.4.2.1. Sowing and growth

Commercially available soybeans were sown on May 22, 2001 in plastic pots 41 cm wide, 33 cm long and 23 cm high. A total of six pots (SB1 to SB6) were arranged outdoors. For SB1 and SB4, there were 12 plants per pot to ensure sufficient biomass to sample repeatedly during plant growth, with one or two plants taken at each sampling time. Four plants were grown in each pot for the rest of the experiments. In these cases, two plants were sampled immediately after exposure and at harvest.

The soil in the pots needed to be wet enough for the plants to grow, so there was supplemental watering two or three times a week. There were drain holes at the bottom of the pots to allow drainage of the water that infiltrated the soil. All plants seemed to grow uniformly.

The moisture content of the soil depended on the season. It was 18-19% (wet base) on July 13, 8-14% on October 5, and 8-9% on October 19. The properties of the soils in the pots are shown in Table I.4.1.

Sowing took place on May 22, and the plants began to flower on July 7. The pods seemed to grow from July 10 or later. The plants were harvested on Oct. 5. Tables I.4.2 and I.4.3 show the fresh and dry plant biomass, respectively, at the time of exposure. Tables I.4.4 and I.4.5 show the fresh and dry biomass at harvest (October 5).

The leaf area index (LAI) was not measured during the experiments; however we found a simple description for the LAI in a publication [I.1]. In general, for the soybean, LAI increases linearly from about May 25 to Aug. 10, at which point it reaches 6 or 7. It remains constant at this value until about Aug. 30, at which point it begins to decrease, dropping to 2 or 4 by about Oct.5.

I.4.2.2. Tritium exposure

The soybean pots were introduced into a glove box 95cm long, 95cm wide and 130cm high for the tritium exposure. The glove box was made of acryl and the experiments were conducted under natural solar conditions. Tritiated water (HTO) in a small vial was evaporated by a heating coil and circulated evenly throughout the box by a fan. The exposures were conducted between about 9:00 am and 10:00 am for an hour at six different stages of plant growth: July 2, July 13, July 30, August 9, August 24, and September 17 for experiments SB1 through SB6, respectively.

Table I.4.1. Physical and chemical properties of the soil.

pH		5.1
Organic matter (%)		1.56
Total nitrogen (ppm)		904.7
Cation exchange capacity (me/100g)		
Exchangeable cation (me/100g)	Ca	1.38
	Mg	0.36
	K	0.67
Sand (%)		73
Silt (%)		23
Clay (%)		4
Soil type		Sandy loam

Table I.4.2. Fresh biomass of soybean plants at time of exposure.

Exp.	Date of exposure	Biomass (g fresh weight m^{-2})				
		Stem	Leaves	Shell	Seed	Total
SB1	7/2	323.7	637.7			961.4
SB2	7/13	416.6	803.0			1219.5
SB3	7/30	789.4	1557.1	379.7		2726.2
SB4	8/9	545.8	914.6	392.8	162.6	2015.7
SB5	8/24	918.7	1555.9	939.5	754.2	4168.4
SB6	9/17	759.2	1354.0	836.8	635.9	3586.0

Table I.4.3. Dry biomass of soybean plants at time of exposure.

Exp.	Date of exposure	Biomass (g dry weight m^{-2})				
		Stem	Leaves	Shell	Seed	Total
SB1	7/2	57.6	115.6			173.2
SB2	7/13	86.5	172.8			259.3
SB3	7/30	222.5	424.7	70.5		717.7
SB4	8/9	174.3	303.5	109.5	44.5	631.8
SB5	8/24	324.0	503.3	267.4	225.1	1319.9
SB6	9/17	281.2	471.1	224.4	189.1	1165.7

Table I.4.4. Fresh biomass of soybean plants at harvest.

Exp.	Biomass (g fresh weight m^{-2})				
	Stem	Leaves	Shell	Seed	Total
SB1	1259.6	1503.0	920.0	703.0	4385.7
SB2	1529.5	2211.1	1388.2	1191.4	6320.2
SB3	1530.2	2201.0	1141.9	609.5	5482.6
SB4	1194.5	1687.1	876.0	193.9	3951.5
SB5	1356.1	1985.5	1075.2	513.8	4930.7
SB6	1205.5	2079.2	669.8	579.9	4534.4

Table I.4.5. Dry biomass of soybean plants at harvest.

Exp.	Biomass (g dry weight m^{-2})				
	Stem	Leaves	Shell	Seed	Total
SB1	370.0	552.4	448.5	358.0	1728.9
SB2	503.5	1278.6	747.5	695.3	3225.0
SB3	453.7	846.1	357.0	220.8	1877.6
SB4	329.2	617.1	261.2	79.4	1286.9
SB5	398.2	745.6	335.6	188.9	1668.3
SB6	535.3	1068.3	319.3	318.6	2241.4

The surface of the soil was covered with vinyl paper to prevent direct contact of the tritium with the soil, implying that the soybeans absorbed tritium only through their foliage. As the tritiated water evaporated in the glove box, water condensed on the inside walls. The surface of the soybean leaves might also have been covered with a condensed water film. This would reflect the situation in which tritium exposure happened in the morning.

About 1.5 L of contaminated air was drawn from the glove box every five minutes during the exposure. The air was passed through a scintillation vial that contained 20 ml of distilled water, which stripped the HTO from the air moisture.

After the exposure, an external fan was operated for about 5 minutes to remove contaminated air from the glove box. The box was then opened and the pots removed for sampling, which took about 5-7 min. The total elapsed time from the end of the fumigation to the end of sampling was 10 to 12 min, or 0.2 hr. The soybeans were then moved outdoors and the vinyl paper covering the soil surface of the pots was removed. The pots were then placed in an open field among other soybean plants.

I.4.3. Tritium measurements

I.4.3.1. Sampling and measurement

The first and fourth experiments (SB1 and SB4) were analyzed for the tritium concentration in the various parts of the soybean plants with time by sampling several times while the soybeans were growing outdoors. In the other experiments, the plants were sampled twice only, immediately after exposure and at harvest. The tissue free water tritium (TFWT) of each sample was extracted and collected by freeze drying. Residual TFWT and exchangeable organically bound tritium (OBT) in the freeze dried samples were removed by an exchange process. Then the samples were dried using P_2O_5, and combusted in an Oxidizer (Oxidizer 306, Canberra Packard). The combustion water was collected in a 20 ml scintillation vial.

The tritium concentration in each sample was measured using a liquid scintillation detector (Quantulus 1220). Measurements were made three times for 20-30 minutes each. The uncertainty of the measurements was about 10%.

I.4.3.2. Air in the glove box

The tritium concentration in the glove box during experiment SB1 is summarized in Table I.4.6. Similar data for the other experiments is available as an Excel file from the EMRAS organizers.

The HTO concentration in the glove box increased for 20-30 min during evaporation of the HTO. Once the HTO was completely evaporated, the concentration decreased gradually.

I.4.3.3. Background

Background HTO concentrations in air at the experimental site ranged as follows depending on the season:

— July 0.016–0.069 Bq/m^3;
— August 0.013–0.049 Bq/m^3;
— September 0.040–0.060 Bq/m^3.

Table I.4.6. Glove box conditions for experiment SB1 (July 2).

Time (hr:min)	Air temperature (C)	Relative humidity (%)	Solar radiation (klux)	HTO in air moisture (Bq/ml)
09:25	33.5	59.4	36.3	–
09:30 (start)	34.2	75.1	44.3	–
09:35	34.7	80.4	42.6	7.05×10^3
09:40	36.0	83.7	46.4	6.74×10^4
09:45	37.0	85.2	44.1	7.25×10^4
09:50	38.1	85.1	48.9	1.01×10^5
09:55	39.2	84.9	61.7	9.45×10^4
10:00	40.4	83.7	42.9	1.04×10^5
10:05	41.0	82.6	48.1	9.30×10^4
10:10	41.5	81.5	61.5	9.07×10^4
10:15	42.2	81.0	66.7	8.41×10^4
10:20	43.1	80.2	61.7	8.37×10^4
10:25	43.6	78.8	66.9	7.31×10^4
10:30 (end)	44.0	77.1	72.3	7.26×10^4
10:35	42.2	43.5	35.2	6.63×10^4

Table I.4.7. Instruments for measuring solar radiation.

In the glove box	Illuminance Meter (ANA-F11) Tokyo Photoelectric Company Ltd. (Japan)
On the meteorological tower	Silicon Cell Pyranometer (Model 3120) Qualimetrics, Inc. (USA)

Table I.4.8. Measurements of illuminance and radiant flux density.

Date and time		Illuminance (klux)		Radiant flux density(W/m^2)
		In the glove box	In the field, near the glove box	In the field
Dec.05	14:00	4.76	5.64	52.61
	15:30	3.41	3.69	70.02
Dec.08	11:30	43.8	51.7	426.90
	12:30	27.8	42.6	257.54
	13:30	4.8	5.0	110.78

Table I.4.9. Requested concentrations for experiment SB1.

Date	Time	Elapsed time (h)	Plant parts
July 2	10:40	0.2	Plant body*
	11:30	1	Plant body
July 3		24	Plant body
July 7		120	Plant body
July 16		336	Plant body
Aug 10		936	Plant body, pods§
Sep 7		1608	Plant body, pods
Oct 5		2280	Plan body, pods

* Stem and leaves.
§ Shell and seeds.

Table I.4.10. Requested concentrations for experiment SB4.

Date	Time	Elapsed time (h)
Aug 9	10:40	0.2
	11:30	1
Aug 10		24
Aug 14		120
Aug 23		336
Sep 10		768
Oct 5		1368

I.4.3.4. Vegetation

The leaf, stem, shell and seed of the soybean plants were sampled just after exposure and at harvest for each of the six experiments. In addition, for the first (SB1) and the fourth experiments (SB4), the various parts of the plants were sampled several times while they were growing. For SB1, the elapsed times after exposure and the sampling date were: 0.2 hr (July 2), 1 hr (July 2), 24 hrs (July 3), 120 hrs (July 7), 336 hrs (July 16), 936 hrs (August 10), 1608 hrs (Sept. 7), and 2280 hrs (Oct. 5). For SB4, they were 0.2 hr (Aug. 9), 1 hr (Aug. 9), 24 hrs (Aug. 10), 120 hrs (Aug. 14), 336 hrs (Aug. 23), 768 hrs (Sept. 10), and 1368 hrs (Oct. 5).

I.4.4. Meteorological measurements

The soybean plants were moved from the glove box after exposure and grown outdoors at a location with an elevation 20 m above sea level. Meteorological data collected on a tower near the planting area is available from the EMRAS organizers in two Excel files, one for air temperature, humidity and solar radiation and the other for wind, stability and rainfall data.

Two different types of instruments were used to measure solar radiation (Table I.4.7). Radiant flux density was measured by a pyranometer in W/m^2 on the tower whereas illuminance was measured with an illuminance meter in klux in the glove box. According to reference [I.2], the conversion factor between the two units depends on the wave length and ranges from 4.0 to 5.5 $W\ m^{-2}\ klux^{-1}$. However, the actual solar radiation in the glove box might have been less than what was observed in the free atmosphere. Local cloud conditions or the nearby forest may have affected the results, for example. The relation between the radiant flux density and the illuminance was checked and is summarized in Table I.4.8.

I.4.5. Scenario calculations

Using the information provided, please calculate:

(1) HTO concentrations in the SB1 experiment for the plant parts, dates and times shown in Table I.4.9.
(2) HTO concentrations in the plant body and the pods in the SB4 experiment for the dates and times shown in Table I.4.10.
(3) The non-exchangeable OBT concentration in the plant body (stems and leaves), the shells and the seeds at harvest for the six experiments SB1 to SB6.
(4) 95% confidence intervals for all predictions.

I.5. Pig Scenario Description

I.5.1. Model-data scenario

A pregnant sow of the Belgische Landras strain, weighing about 180 kg, was given feed contaminated with organically bound tritium (OBT) for 84 days before delivery. The food had an average concentration of 577 Bq/g dry matter (dm) and was composed of a mixture of milk powder, potato powder and dried algae, as shown in Table I.5.1.

As the pregnancy progressed, the amount of food given to the sow increased as shown in Table I.5.2. Throughout the period, water was offered *ad libitum* but intake was not monitored. Literature values for pregnant sows indicate a water consumption of 6-8 L/d. The sow was sacrificed at birth and the tritium activity in various organs was measured. In the 84-day contamination period, urine and faeces were also monitored for tritium content.

Modellers are asked to predict the following:

(1) Total tritium concentration in urine and HTO and OBT concentrations in faeces at the times shown in Table I.5.3.
(2) HTO and OBT concentrations in the organs shown in Table I.5.4 at delivery (84 days after the start of contamination).

Modellers are also asked to provide:

(1) estimates of the 95% confidence intervals on all predictions, and
(2) descriptions of the models they used following the EMRAS template.

I.5.2. Model intercomparisons

The above test is not appropriate for animals used for human consumption since pigs are sacrificed near 110 kg. In the absence of other experimental observations, two exercises based on hypothetical data are proposed:

I.5.2.1. Exercise 1: long-term HTO intake

A pig of conventional strain was given uncontaminated food and water for the first 55 days of its life, at which point it weighed 20 kg. It was then fed food and water contaminated with HTO at a level of 10,000 Bq/L for 50 days. Its feed was uncontaminated for the next 50 days, at which point it was 155 days old and weighed 110 kg, and was sacrificed. At no time was any of the feed given to the pig contaminated with OBT. Modellers are asked to predict the total tritium in urine, HTO and OBT in faeces and OBT in muscle from the time the pig was 55 to 155 days old (50 days of contaminated diet and 50 days of clean) for the times given in Table I.5.5. Estimate also the 95% confidence intervals of all predictions.

I.5.2.2. Exercise 2:Short-term OBT intake

All animals on a large pig farm are fed OBT-contaminated food for a single day at a level of 1 MBq/kg dm. Modellers are asked to predict the meat and liver OBT concentrations at sacrifice (body mass 110 kg) for the following pig mass on the day of contamination: 20, 40, 60, 80 and 100 kg.

Table I.5.1. Composition of the sow diet.

Food composition	Milk powder	Algal powder	Potato powder	Minerals
Amount (%)	41	2.3	51	5.7
Activity (%)	45.2	12.3	42.5	0
Concentration (Bq/g dm)	636.1	3085.7	480.8	0

Table I.5.2. Amount of feed given to the sow.

Time interval (days after start of contamination)	Amount of feed (kg dm/d)
0–21	1.86
22–46	2.06
47–79	2.31
80–84	3.01

Table I.5.3. Times at which predictions in urine and faeces are requested.

Day following start of contamination	Urine (Bq/ml total tritium)	Faeces	
		HTO in water fraction (Bq/ml)	OBT in dry fraction (Bq/g dm)
7			
14			
21			
28			
36			
42			
49			
56			

Table I.5.4. Organs for which predictions are requested at delivery.

Organ	Dry Matter (%)	HTO (Bq/ml)	OBT (Bq/g dm)
Heart	21.70		
Lungs	23.45		
Liver	26.09		
Jejunum	22.40		
Ileum	20.16		
Colon	24.26		
Kidney	23.68		
Muscle	26.98		
Brain	22.16		
Blood	18.54		

Table I.5.5. Times at which predictions in urine and faeces are requested.

Day following start of contamination	Urine (Bq/ml total tritium)	Faeces		Meat OBT (Bq/kg fw)
		HTO in water fraction (Bq/ml)	OBT in dry fraction (Bq/g dm)	
7				
14				
21				
42				
50				
60				
70				
100				

Table I.5.6. Generic feed intake rates.

Growth rate	Intake (kg dm/d)				
Body mass (kg)	20	35	50	80	110
Intake for slow growth	1	1.4	1.66	1.9	2
Intake for modern commercial growth	0.95	1.48	1.9	2.35	2.7

One of the aims of Exercise 2 is to determine if accurate results can be obtained by considering a single generic pig or if the specific strain and diet of the pig must be taken into account. Accordingly, the modellers are asked to assess the influence of growth rate and genotype on their results by carrying out calculations for their default pig (and default diet) and for slow-growth and fast-growth pigs, as defined below:

- A slow growth genotype needs about 165 days to grow from 20 to 110 kg. For a moderate fatness, the adipose mass is near 30% of empty body mass and the meat near 25%. (Empty body mass is the live body mass minus the content of the gastrointestinal tract.)
- Modern commercial pigs needs about 110 days to grow from 20 to 110 kg. Depending on genotype, muscle mass can be high (63%) or low (45%). Accordingly, the adipose mass fraction can vary between 15 and 28%.

Generic intakes for slow-growth and fast-growth pigs are shown in TableI.5.6. These intakes assume an *ad libitum* diet based on barley (20%), corn (60%) and soybean meal (20%) that contains 21% crude protein, 1% lysine and 14.4 MJ metabolisable energy per kg on a dry mass basis.

Total water intake is $0.3BM^{0.71}$ L/d, where BM is body mass in kg.

All assumptions regarding pig genotype, diet and intake rates should be fully documented in the model descriptions.

I.6. Mussel Uptake Scenario Description

I.6.1. Background information

Tritium can represent a key radionuclide in the aquatic environment, potentially contributing significantly to the doses received by aquatic non-human biota in surface waters receiving tritium inputs. Although in many cases, steady-state models provide practical tools for estimating free-water tritium concentrations (and to a lesser extent, OBT concentrations), aquatic organisms are occasionally exposed to short-term, elevated tritium concentrations in water when tritium is released accidentally to aquatic systems. Depending upon the nature and the duration of such events, in some cases, steady-state models may or may not reliably predict true organism concentrations.

In general, the rates of free-water tritium uptake and OBT formation are not well known under dynamic exposure conditions, but can be studied by transplanting biomonitoring species, such as freshwater mussels, from areas with background tritium concentrations to those with measurable tritium levels. In this way, changes in tissue free-water tritium (HTO) and OBT concentrations can be monitored to quantify their responses to dynamic exposure conditions.

I.6.1.1. Study objective

The objective of this study was to quantify the rates of HTO uptake and OBT formation in freshwater mussels (*Elliptio complanata*) receiving abrupt increases in their tritium exposure levels through transplantation from areas with background tritium concentrations to Perch Lake, a small, Canadian Shield lake receiving chronic, low-level tritium inputs. This information forms the basis for a model-data validation scenario for tritium uptake under dynamic exposure conditions. It complements a previous EMRAS scenario that was designed to test steady-state aquatic tritium models, also based on data from Perch Lake.

I.6.2. Site description

Located on the site of Chalk River Laboratories (CRL), Perch Lake contains trace amounts of tritium (Figure I.6.1 and I.6.2). The lake receives tritium inputs via groundwater that is migrating through an extensive sand aquifer from a waste management area (WMA) located approximately 750 m to the north of the lake. The WMA was in operation for approximately 40 years until it was shut down in 1999. The tritium forms a well-defined underground plume that is narrow near the source, but broadens to a width of approximately 1,000 m by the time it reaches the lake. Tritium, in the form of HTO, discharges into the lake through the sediments from below and also through the Inlet 2 inflowing stream (Figure I.6.2), which flows above the underground plume. Inlet 1 also shows slightly elevated levels of tritium; however, inflowing streams at Inlets 3, 4 and 5 are all uncontaminated. The rate and distribution of HTO releases to the lake are not known quantitatively, although it is believed that the lake is well-mixed in the vicinity of the mussel transplantation cages, which were deployed near the outflowing stream in the lake.

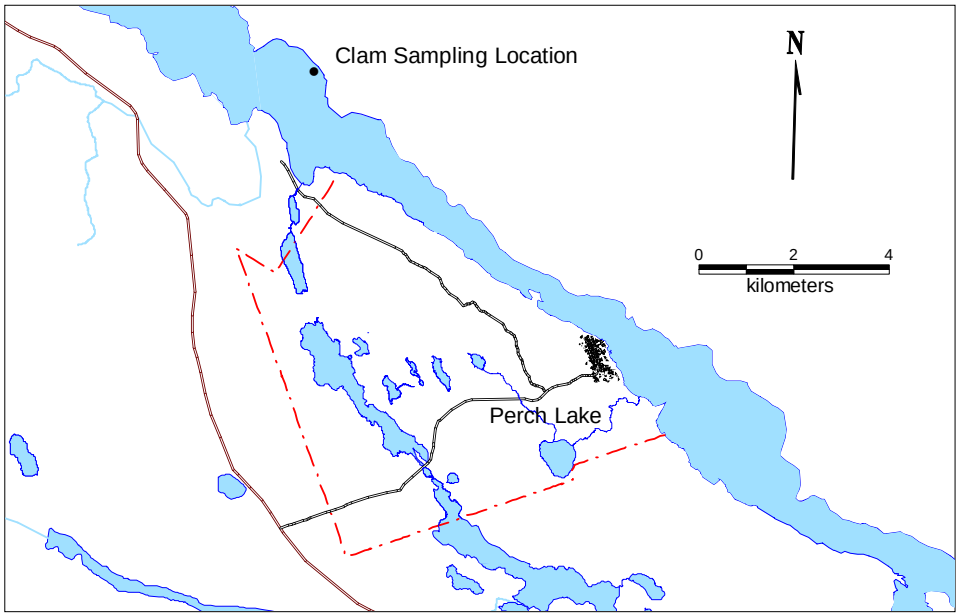

Fig. I.6.1. Map depicting the location of the reference site in the Ottawa River where freshwater mussels (Elliptio complanata) were collected, relative to the site of mussel transplantation in Perch Lake on AECL's Chalk River Laboratories site.

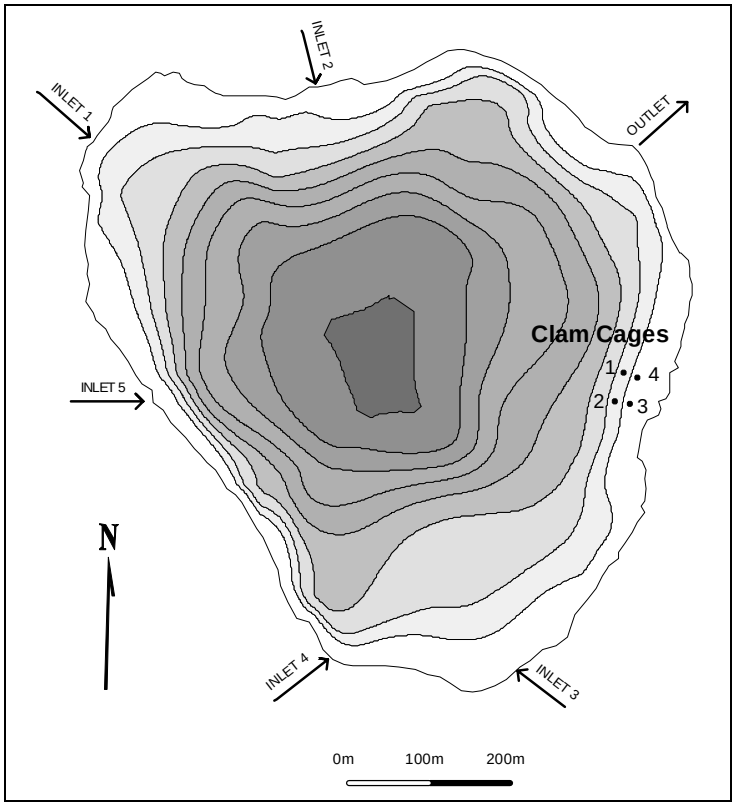

Fig. I.6.2. Map of Perch Lake depicting the location of inflowing and outflowing streams, depth contours (in metres) and locations of mussel transplantation cages.

In terms of its physical size, Perch Lake (Figure I.6.2) is a small, shallow freshwater Canadian Shield lake, with a maximum fetch of approximately 800 m, a surface area of 4.5 x 10^5 m^2 and a volume of 9.1 x 10^5 m^3. The mean depth of the lake is 2.0 m and the maximum depth is 4.1 m. The lake drains a watershed of area 5.65 x 10^6 m^2 and the residence time of water in the lake is approximately 0.5 years. Perch Lake can be considered unstratified, although there is weak stratification in deeper areas in the summer, when surface waters are approximately 5 ^oC higher than those at lake bottom. The lake is typically ice-covered from early December to mid-April. Based on historical measurements, mean monthly water temperatures are 13, 19, 24, 23, 19 and 11^o C for the months of May through October, respectively. Surface water temperatures measured in the vicinity of the mussel transplantation cages in Perch Lake over the course of this study are provided in Table I.6.1 and Figure I.6.3. These values are similar to air temperatures measured over the same time periods.

Sediments in the lake are composed of sand and gyttja (decomposing organic material). The mean dry bulk density is approximately 185 kg m^{-3} for Perch Lake sediments, but values vary substantially across the lake depending on the local composition of the sediments. The sediments in the vicinity of the mussel transplantation cages are primarily sandy in nature, with some accumulation of organic matter. These sediments consist of approximately 50% water by weight and the sedimentation rate is 0.16 kg m^{-2} a^{-1} or 0.06 cm a^{-1}.

I.6.3. Study design

Two pairs of mussel transplantation cages were built and deployed in Perch Lake in early July 2004. These cages contained freshwater mussels originating from a site with background tritium concentrations (as described in Section I.6.3.3) to quantify rates of temporal changes in HTO and OBT in mussel soft tissues. In doing so, two sets of exposure conditions were established, as summarized in Table I.6.2. These included exposure to tritium via the surface water pathway only (Cages 1 and 2), and exposure via both surface sediments and surface water (Cages 3 and 4). A more detailed description of each cage set-up is provided in Section I.6.3.3 below.

I.6.3.1. Cage design

Each mussel transplantation cage was constructed with an 8 x 8 design, resulting in a total of 64 compartments per cage (Figure I.6.4). Each compartment was assigned a unique alphanumeric code (as shown in Table I.6.3) and one animal was placed into each compartment to facilitate tracking of each animal. Cages were constructed with 2 x 2 cedar and chicken wire, with dimensions of 96 cm (length) x 96 cm (width) x 12 cm (height). Individual cage compartments had surface area dimensions of 12 cm x 12 cm.

I.6.3.2. Selection of animals

Freshwater mussels (*Elliptio complanata*) with total shell lengths in the range from 90 to 111 mm were selected for the study during sampling at the reference site. A list of whole animal fresh weights (in g), and total shell lengths, widths and heights (in mm) are provided for each animal in Table I.6.4 by cage number and compartment for tracking purposes.

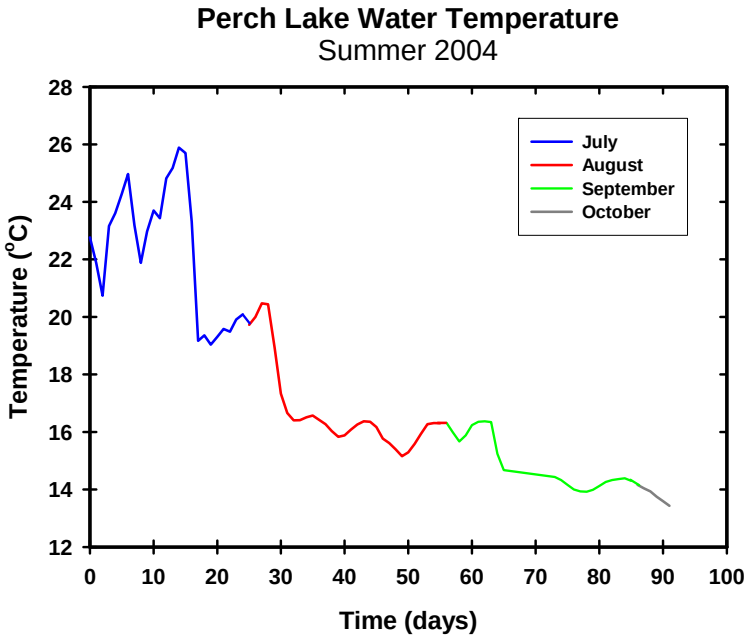

Fig. I.6.3. Depiction of changes in Perch Lake water temperatures over the course of the mussel transplantation study. Temperature measurements were integrated over 5-minute time intervals between 5 July 2004 and 6 October 2004. The experiment starting time for Cages 1 and 2 was 5 July 2004 at 14:00, whereas the starting time for Cages 3 and 4 was 7 July 2004 at 14:00. Comparable trends were observed for air temperatures.

Table I.6.1. Compilation of daily statistical Perch Lake water temperature (T) data, based on integrated measurements taken over 5-minute intervals. Temperature data were not available for the period between September 11 and 17 due to a problem with the temperature probe. Raw temperature data are available upon request.

Date	Mean Temperature T (°C)	n	Standard Error of 5-Minute Values (°C)
07-Jul-04	22.77	150	0.127
08-Jul-04	21.88	288	0.0950
09-Jul-04	20.74	288	0.0658
10-Jul-04	23.16	288	0.192
11-Jul-04	23.61	288	0.0900
12-Jul-04	24.28	288	0.102
13-Jul-04	24.97	288	0.0903
14-Jul-04	23.19	288	0.0549
15-Jul-04	21.88	288	0.0523
16-Jul-04	22.97	288	0.110
17-Jul-04	23.70	288	0.108
18-Jul-04	23.43	288	0.120
19-Jul-04	24.82	288	0.100
20-Jul-04	25.18	288	0.160
21-Jul-04	25.89	288	0.0916
22-Jul-04	25.70	288	0.0802
23-Jul-04	23.31	288	0.127
24-Jul-04	19.17	288	0.0574

Table I.6.1. (Continued).

Date	Mean Temperature T (°C)	n	Standard Error of 5-Minute Values (°C)
25-Jul-04	19.36	288	0.0088
26-Jul-04	19.04	288	0.0206
27-Jul-04	19.31	288	0.0064
28-Jul-04	19.58	288	0.0058
29-Jul-04	19.49	288	0.0088
30-Jul-04	19.91	288	0.0041
31-Jul-04	20.09	288	0.0029
01-Aug-04	19.73	288	0.0122
02-Aug-04	20.00	288	0.0056
03-Aug-04	20.47	288	0.0065
04-Aug-04	20.44	288	0.0197
05-Aug-04	18.93	288	0.0635
06-Aug-04	17.33	288	0.0172
07-Aug-04	16.66	288	0.0124
08-Aug-04	16.40	288	0.0013
09-Aug-04	16.41	288	0.0010
10-Aug-04	16.51	288	0.0028
11-Aug-04	16.57	288	0.0015
12-Aug-04	16.42	288	0.0032
13-Aug-04	16.27	288	0.0025
14-Aug-04	16.03	288	0.0072
15-Aug-04	15.83	288	0.0005
16-Aug-04	15.88	288	0.0022
17-Aug-04	16.08	288	0.0041
18-Aug-04	16.26	288	0.0029
19-Aug-04	16.37	288	0.0012
20-Aug-04	16.35	288	0.0061
21-Aug-04	16.17	288	0.0045
22-Aug-04	15.77	288	0.0129
23-Aug-04	15.61	288	0.0040
24-Aug-04	15.40	288	0.0167
25-Aug-04	15.16	288	0.0014
26-Aug-04	15.29	288	0.0047
27-Aug-04	15.59	288	0.0051
28-Aug-04	15.93	288	0.0063
29-Aug-04	16.27	288	0.0040
30-Aug-04	16.31	288	0.0003
31-Aug-04	16.30	288	0.0004
01-Sep-04	16.32	288	0.0011
02-Sep-04	15.99	288	0.0172
03-Sep-04	15.67	288	0.0010
04-Sep-04	15.88	288	0.0072
05-Sep-04	16.24	288	0.0037
06-Sep-04	16.35	288	0.0014
07-Sep-04	16.37	288	0.0017
08-Sep-04	16.34	288	0.0016
09-Sep-04	15.24	288	0.0390
10-Sep-04	14.67	177	0.0022
18-Sep-04	14.43	156	0.0007
19-Sep-04	14.33	288	0.0029
20-Sep-04	14.16	288	0.0033

Table I.6.1. (Continued).

Date	Mean Temperature T (°C)	n	Standard Error of 5-Minute Values (°C)
21-Sep-04	14.00	288	0.0023
22-Sep-04	13.93	288	0.0010
23-Sep-04	13.92	288	0.0006
24-Sep-04	13.99	288	0.0017
25-Sep-04	14.12	288	0.0023
26-Sep-04	14.26	288	0.0021
27-Sep-04	14.33	288	0.0005
28-Sep-04	14.36	288	0.0006
29-Sep-04	14.39	288	0.0004
30-Sep-04	14.30	288	0.0026
01-Oct-04	14.16	288	0.0024
02-Oct-04	14.04	288	0.0021
03-Oct-04	13.93	288	0.0023
04-Oct-04	13.75	288	0.0032
05-Oct-04	13.59	288	0.0028
06-Oct-04	13.43	171	0.0034

Table I.6.2. Transplanted freshwater mussel *(Elliptio complanata)* exposure pathways under the various test conditions.

Cage No.	Exposure Medium	
	Water	Sediments
1	X	–
2	X	–
3	X	X
4	X	X

Table I.6.3. Layout of mussel transplantation cages and mussel numbering scheme. Cages were set up as a matrix and individual mussels were numbered as alphanumerical coordinates of alphabetical ‘columns’ and numerical ‘row’ numbers to facilitate tracking of each mussel in terms of tritium uptake rates relative to mussel body size.

Row \ Column	A	B	C	D	E	F	G	H
1	A1	B1	C1	D1	E1	F1	G1	H1
2	A2	B2	C2	D2	E2	F2	G2	H2
3	A3	B3	C3	D3	E3	F3	G3	H3
4	A4	B4	C4	D4	E4	F4	G4	H4
5	A5	B5	C5	D5	E5	F5	G5	H5
6	A6	B6	C6	D6	E6	F6	G6	H6
7	A7	B7	C7	D7	E7	F7	G7	H7
8	A8	B8	C8	D8	E8	F8	G8	H8

Table I.6.4. Weight and length measurements of mussel specimens transplanted from the Ottawa River upstream of CRL to Perch Lake.

Cell No.	Cage No.	Mussel Measurements			
		Fresh Weight (g)	Shell Length (mm)	Shell Width (mm)	Shell Height (mm)
A1	Cage No. 1	64.40	96	46	24
	Cage No. 2	60.03	92	49	23
	Cage No. 3	100.77	111	58	28
	Cage No. 4	78.33	98	49	24
A2	Cage No. 1	95.19	98	54	28
	Cage No. 2	57.35	92	45	21
	Cage No. 3	74.09	96	51	27
	Cage No. 4	64.90	95	49	25
A3	Cage No. 1	62.94	90	48	25
	Cage No. 2	68.62	93	46	26
	Cage No. 3	122.57	109	57	33
	Cage No. 4	97.13	103	53	27
A4	Cage No. 1	83.50	103	49	27
	Cage No. 2	61.38	90	45	24
	Cage No. 3	62.44	94	46	26
	Cage No. 4	60.93	94	45	24
A5	Cage No. 1	79.23	99	50	26
	Cage No. 2	91.42	105	51	30
	Cage No. 3	85.65	103	50	28
	Cage No. 4	90.77	105	53	28
A6	Cage No. 1	102.05	102	56	27
	Cage No. 2	58.94	93	47	23
	Cage No. 3	87.57	104	56	28
	Cage No. 4	77.47	103	51	25
A7	Cage No. 1	69.89	95	49	24
	Cage No. 2	74.51	96	52	26
	Cage No. 3	56.50	92	52	20
	Cage No. 4	100.44	109	57	29
A8	Cage No. 1	83.58	96	51	27
	Cage No. 2	72.89	94	50	26
	Cage No. 3	61.72	92	46	25
	Cage No. 4	70.48	90	51	25
B1	Cage No. 1	73.07	96	46	27
	Cage No. 2	90.96	100	54	30
	Cage No. 3	82.79	101	53	26
	Cage No. 4	69.16	90	49	25
B2	Cage No. 1	75.31	95	48	26
	Cage No. 2	98.10	105	54	32
	Cage No. 3	86.19	107	55	25
	Cage No. 4	117.87	109	59	31
B3	Cage No. 1	77.75	95	51	27
	Cage No. 2	79.26	95	52	29
	Cage No. 3	75.66	99	53	27
	Cage No. 4	73.90	100	51	26
B4	Cage No. 1	94.55	104	54	28
	Cage No. 2	73.14	94	51	27
	Cage No. 3	72.95	98	51	26
	Cage No. 4	85.76	102	52	26

Table I.6.4. (Continued).

Cell No.	Cage No.	Mussel Measurements			
		Fresh Weight (g)	Shell Length (mm)	Shell Width (mm)	Shell Height (mm)
B5	Cage No. 1	66.31	94	49	26
	Cage No. 2	70.63	94	53	27
	Cage No. 3	74.28	103	51	27
	Cage No. 4	73.64	100	49	24
B6	Cage No. 1	98.34	106	56	27
	Cage No. 2	62.84	90	51	35
	Cage No. 3	101.33	110	54	30
	Cage No. 4	83.43	104	52	25
B7	Cage No. 1	70.41	95	49	26
	Cage No. 2	65.22	96	47	27
	Cage No. 3	91.92	100	54	28
	Cage No. 4	77.91	93	50	26
B8	Cage No. 1	70.29	103	47	22
	Cage No. 2	70.75	90	51	29
	Cage No. 3	74.20	99	50	28
	Cage No. 4	78.51	98	49	26
C1	Cage No. 1	67.95	97	47	25
	Cage No. 2	73.15	100	46	26
	Cage No. 3	102.75	108	53	31
	Cage No. 4	69.39	95	47	27
C2	Cage No. 1	80.67	104	54	25
	Cage No. 2	62.98	94	58	26
	Cage No. 3	68.65	97	47	24
	Cage No. 4	84.76	100	50	27
C3	Cage No. 1	57.44	93	45	23
	Cage No. 2	77.36	100	55	26
	Cage No. 3	71.25	99	48	27
	Cage No. 4	57.55	95	47	21
C4	Cage No. 1	79.36	104	52	25
	Cage No. 2	79.90	98	48	28
	Cage No. 3	83.91	105	53	29
	Cage No. 4	94.57	105	55	26
C5	Cage No. 1	73.39	96	50	25
	Cage No. 2	63.48	95	52	23
	Cage No. 3	84.51	103	51	29
	Cage No. 4	67.19	102	50	22
C6	Cage No. 1	86.02	99	49	30
	Cage No. 2	81.52	100	52	26
	Cage No. 3	78.38	104	51	26
	Cage No. 4	94.18	105	50	29
C7	Cage No. 1	83.06	101	52	26
	Cage No. 2	82.38	102	59	30
	Cage No. 3	70.38	98	47	27
	Cage No. 4	78.38	100	51	27
C8	Cage No. 1	74.35	101	46	26
	Cage No. 2	119.84	109	57	33
	Cage No. 3	81.21	104	54	27
	Cage No. 4	80.26	98	50	27
D1	Cage No. 1	101.37	103	58	27
	Cage No. 2	113.44	110	56	30
	Cage No. 3	117.32	106	60	30
	Cage No. 4	70.64	95	50	24

Table I.6.4. (Continued).

Cell No.	Cage No.	Mussel Measurements			
		Fresh Weight (g)	Shell Length (mm)	Shell Width (mm)	Shell Height (mm)
D2	Cage No. 1	101.61	101	55	29
	Cage No. 2	96.75	104	56	30
	Cage No. 3	78.61	102	55	28
	Cage No. 4	80.66	99	52	26
D3	Cage No. 1	83.65	102	50	25
	Cage No. 2	97.71	101	59	30
	Cage No. 3	77.04	100	50	26
	Cage No. 4	81.01	101	51	25
D4	Cage No. 1	68.54	96	49	29
	Cage No. 2	116.83	110	51	33
	Cage No. 3	71.61	94	50	26
	Cage No. 4	82.94	104	51	26
D5	Cage No. 1	69.29	95	49	26
	Cage No. 2	68.78	93	53	25
	Cage No. 3	103.58	109	55	30
	Cage No. 4	78.11	99	51	25
D6	Cage No. 1	78.06	99	49	27
	Cage No. 2	98.91	104	50	30
	Cage No. 3	74.73	93	53	24
	Cage No. 4	86.86	105	51	26
D7	Cage No. 1	74.73	99	50	25
	Cage No. 2	56.23	94	50	24
	Cage No. 3	91.28	99	54	29
	Cage No. 4	74.43	100	51	26
D8	Cage No. 1	68.01	95	45	25
	Cage No. 2	78.77	94	52	28
	Cage No. 3	76.94	96	51	24
	Cage No. 4	67.74	91	45	26
E1	Cage No. 1	70.48	101	50	23
	Cage No. 2	94.40	100	58	30
	Cage No. 3	75.84	100	51	27
	Cage No. 4	56.26	93	46	24
E2	Cage No. 1	83.36	104	53	26
	Cage No. 2	93.48	100	52	30
	Cage No. 3	85.21	96	51	29
	Cage No. 4	74.88	94	52	25
E3	Cage No. 1	75.97	96	50	27
	Cage No. 2	87.74	104	53	29
	Cage No. 3	108.61	101	54	34
	Cage No. 4	67.46	100	50	21
E4	Cage No. 1	94.02	106	55	32
	Cage No. 2	84.80	101	54	29
	Cage No. 3	121.49	106	58	32
	Cage No. 4	82.10	91	50	28
E5	Cage No. 1	68.08	97	48	25
	Cage No. 2	78.27	98	50	29
	Cage No. 3	71.57	98	50	25
	Cage No. 4	93.52	106	54	26
E6	Cage No. 1	94.80	99	50	29
	Cage No. 2	59.17	90	48	24
	Cage No. 3	67.72	94	49	26
	Cage No. 4	79.62	100	54	24

Table I.6.4. (Continued).

Cell No.	Cage No.	Mussel Measurements			
		Fresh Weight (g)	Shell Length (mm)	Shell Width (mm)	Shell Height (mm)
E7	Cage No. 1	76.23	96	54	25
	Cage No. 2	90.52	102	57	29
	Cage No. 3	67.71	98	46	25
	Cage No. 4	68.97	94	47	26
E8	Cage No. 1	72.53	96	48	26
	Cage No. 2	84.61	102	53	28
	Cage No. 3	91.71	100	54	28
	Cage No. 4	64.47	94	48	25
F1	Cage No. 1	82.47	100	56	25
	Cage No. 2	106.65	108	55	31
	Cage No. 3	118.56	106	56	35
	Cage No. 4	72.55	102	50	23
F2	Cage No. 1	71.93	92	45	26
	Cage No. 2	83.38	100	53	30
	Cage No. 3	93.37	108	55	27
	Cage No. 4	75.37	97	51	24
F3	Cage No. 1	64.14	95	46	25
	Cage No. 2	70.93	99	49	26
	Cage No. 3	84.16	98	54	28
	Cage No. 4	77.31	100	50	27
F4	Cage No. 1	64.66	90	43	27
	Cage No. 2	62.23	94	52	25
	Cage No. 3	52.74	95	44	22
	Cage No. 4	56.74	92	46	24
F5	Cage No. 1	57.42	96	46	20
	Cage No. 2	66.86	94	52	27
	Cage No. 3	86.67	96	56	27
	Cage No. 4	61.29	93	48	23
F6	Cage No. 1	62.56	91	45	24
	Cage No. 2	81.23	96	55	28
	Cage No. 3	87.95	99	51	27
	Cage No. 4	55.34	101	50	26
F7	Cage No. 1	77.95	96	50	25
	Cage No. 2	86.17	100	50	30
	Cage No. 3	78.95	101	50	25
	Cage No. 4	88.66	105	51	25
F8	Cage No. 1	103.22	102	52	32
	Cage No. 2	80.08	98	50	27
	Cage No. 3	78.25	96	56	27
	Cage No. 4	79.17	96	50	26
G1	Cage No. 1	93.02	100	50	29
	Cage No. 2	84.70	102	56	28
	Cage No. 3	75.21	92	49	29
	Cage No. 4	97.28	101	53	28
G2	Cage No. 1	87.85	100	51	27
	Cage No. 2	81.72	96	52	29
	Cage No. 3	88.85	100	50	29
	Cage No. 4	68.91	100	49	24
G3	Cage No. 1	81.58	98	52	27
	Cage No. 2	92.11	101	59	28
	Cage No. 3	73.52	95	48	27
	Cage No. 4	57.64	95	43	25

Table I.6.4. (Continued).

Cell No.	Cage No.	Mussel Measurements			
		Fresh Weight (g)	Shell Length (mm)	Shell Width (mm)	Shell Height (mm)
G4	Cage No. 1	78.90	103	49	25
	Cage No. 2	76.98	101	49	28
	Cage No. 3	96.64	104	51	30
	Cage No. 4	65.54	95	49	25
G5	Cage No. 1	81.23	98	50	26
	Cage No. 2	85.68	103	54	27
	Cage No. 3	87.76	99	52	26
	Cage No. 4	59.86	93	46	24
G6	Cage No. 1	75.92	104	50	26
	Cage No. 2	69.04	93	49	24
	Cage No. 3	87.04	94	51	26
	Cage No. 4	78.69	101	48	26
G7	Cage No. 1	82.61	99	51	26
	Cage No. 2	102.42	109	58	28
	Cage No. 3	90.70	105	52	29
	Cage No. 4	77.30	95	50	28
G8	Cage No. 1	101.38	101	55	30
	Cage No. 2	111.92	105	54	32
	Cage No. 3	77.33	93	51	27
	Cage No. 4	71.08	95	49	26
H1	Cage No. 1	99.11	99	51	29
	Cage No. 2	58.79	95	49	23
	Cage No. 3	78.30	96	50	27
	Cage No. 4	88.84	99	52	28
H2	Cage No. 1	102.84	106	58	29
	Cage No. 2	76.84	100	52	27
	Cage No. 3	73.16	101	51	22
	Cage No. 4	70.65	97	48	25
H3	Cage No. 1	89.06	105	54	27
	Cage No. 2	91.36	105	57	27
	Cage No. 3	76.54	97	50	27
	Cage No. 4	62.94	91	48	25
H4	Cage No. 1	71.87	92	48	24
	Cage No. 2	97.37	104	60	30
	Cage No. 3	78.72	94	49	27
	Cage No. 4	78.80	100	50	26
H5	Cage No. 1	99.63	107	59	29
	Cage No. 2	82.38	102	54	29
	Cage No. 3	93.95	105	54	28
	Cage No. 4	59.08	91	46	23
H6	Cage No. 1	86.78	101	50	27
	Cage No. 2	79.57	96	51	30
	Cage No. 3	79.56	101	51	25
	Cage No. 4	75.75	98	51	25
H7	Cage No. 1	87.75	100	51	28
	Cage No. 2	92.28	99	55	30
	Cage No. 3	87.52	102	51	26
	Cage No. 4	76.51	94	50	25
H8	Cage No. 1	99.67	107	56	27
	Cage No. 2	67.62	96	49	26
	Cage No. 3	73.50	101	48	25
	Cage No. 4	65.86	93	49	25

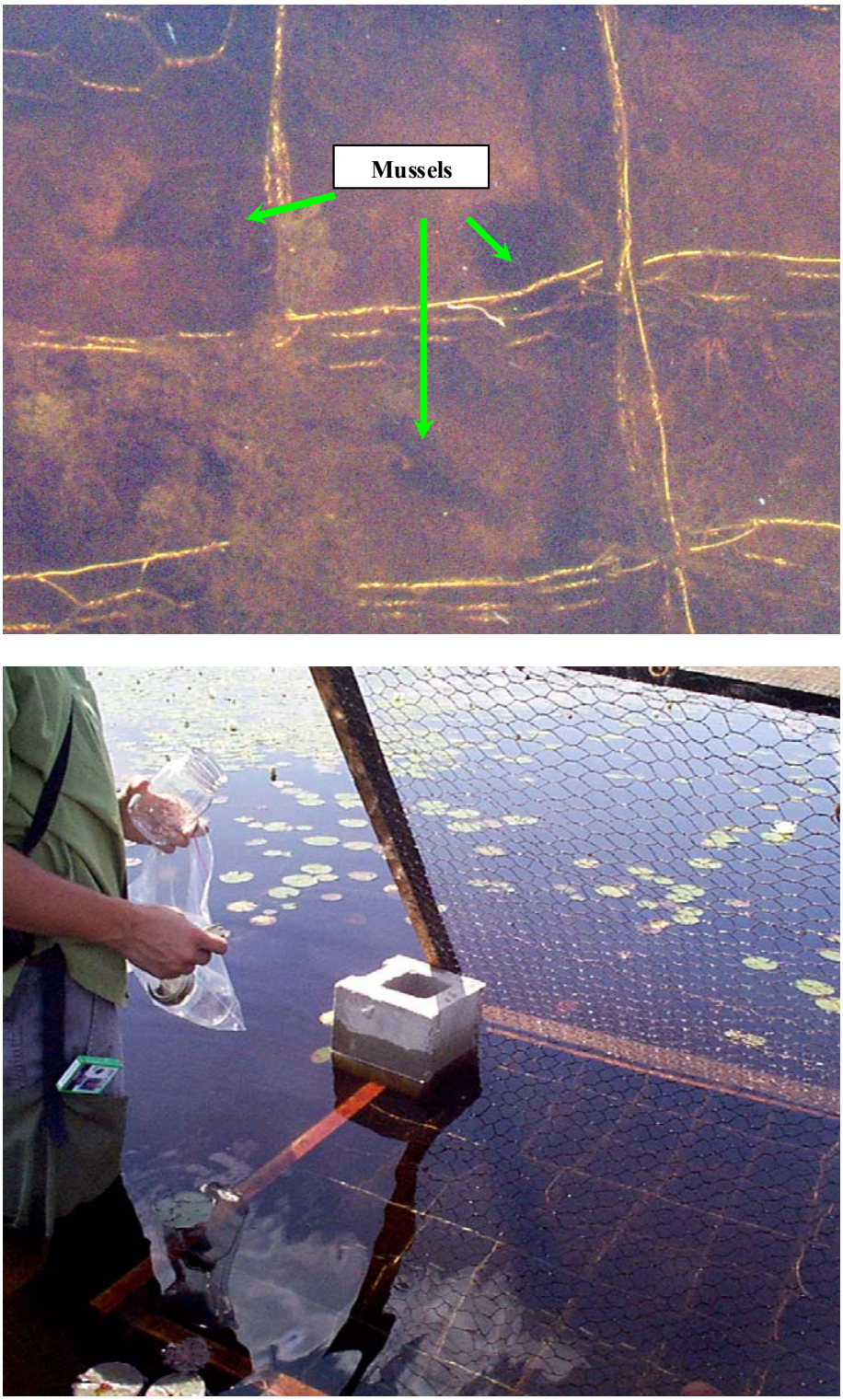

Fig. I.6.4. Photographs depicting the design of the mussel transplantation cages with sediment and water tritium exposure (top panel) and exposure from water only (bottom panel).

I.6.3.3. Mussel transplantation

Reference site

Mussels were collected from a reference area with background tritium concentrations at the mouth of the Schyan River (Quebec) in the Ottawa River, upstream of AECL's Chalk River Laboratories site (Figure I.6.1). Mussels were collected and placed into lidded, plastic buckets containing water from the reference site to prevent uptake of tritium by the mussels prior to initiation of the study. Mussels were then transported to the laboratory on the Chalk River site. Individuals were quickly measured, weighed and alpha-numerically numbered (as shown in Table I.6.4), and were separated by placing them into labeled nylon bags. Animals were then replaced into the lidded buckets of water from the reference site until initiation of the transplantation, which was carried out on the same day as mussel collection. Concentrations of HTO and OBT measured in surface waters and mussels collected from this background location are provided in Table I.6.5.

Deployment of mussel cages 1 and 2 (water exposure pathway)

Mussel Cages 1 and 2 were deployed on 5 July 2005 at 14:00 hours. Cages 1 and 2 were positioned in Perch Lake at a water depth of approximately 0.75 m. These cages were placed on cinder blocks, such that mussels only received tritium exposures through interaction with the water column. Upon initiation of the transplantation study (at time 0), mussels were transferred from the lidded buckets containing water from the reference site to buckets containing water from Perch Lake. In this way, all mussels received initial tritium exposure at approximately the same time, despite the 10 to 15 minute time period required for mussel transfer from buckets to the numbered cage compartments. Mussels began filtering less than five minutes after being placed into the cage compartments. No mussel mortality occurred in Cages 1 or 2 over the course of the 88-day transplantation study. Algal growth, which accumulated on the cages over the course of the study, was not removed, as it did not appear to alter water flow within the cages.

Deployment of mussel cages 3 and 4 (water and sediment exposure pathways)

Mussel Cages 3 and 4 were deployed on 7 July 2004 at 14:00 hours. Cages 3 and 4 were positioned in Perch Lake at the sediment-to-water interface at a water depth of approximately 0.5 m, just inshore of Cages 1 and 2 (Figure I.6.2), such that mussels received tritium exposure through the sediment and water pathways. Each cage compartment was filled with sandy surface sediments originating from the area surrounding the cages to a depth of approximately 5 to 10 cm, a depth that enabled mussels to position themselves in an upright position with their siphons pointed upwards, as they do in natural systems. The sediments were added to the cages several hours prior to transplantation of the mussels to allow settling of any suspended particulates.

As for Cages 1 and 2, upon initiation of mussel transplantation into Cages 3 and 4 (at time 0), mussels were transferred from the lidded buckets containing water from the reference site to buckets containing water from Perch Lake. Mussels were then placed into the cage compartments and were visually monitored. In general, mussels began positioning themselves in an upright position within five minutes of transplantation. Again, no mussel mortality occurred in Cages 3 or 4 over the course of the 88-day transplantation study.

I.6.4. Study measurements

I.6.4.1. Tritium monitoring

Collection of mussel samples

The composite samples taken at each time point are specified in Table I.6.6. Mussel samples were collected on an exponential time-step over the course of an 88-day period (as specified in Table I.6.7). Upon collection, mussels were immediately placed into air-tight Mason jars to avoid tritium exchange with the atmosphere. The jars and mussels were later frozen until processing for tritium analysis could be carried out. In general, it was necessary to composite soft tissues from 3 to 4 individuals to gain the biomass required for HTO and OBT analysis. The water content of mussel tissue was 89.0% (by weight), with little variability among individual animals.

Collection of surface water samples

Water samples were collected in triplicate at each sampling time in the vicinity of each of the mussel cages (Figure I.6.2). In doing so, sampling bottles were opened at the depth where the mussels were filtering. The samples were then left standing to allow suspended sediments to settle out and 10 mL of water were subsequently transferred to scintillation vials. HTO concentrations in all water samples were determined by liquid scintillation counting (LSC).

Collection of surface sediment samples

Sediment samples were collected by hand at a depth of 5 to 10 cm in the vicinity of the mussel cages at each mussel sampling time. The samples were placed in Ziplock bags that were sealed at depth. Water was extracted from a subset of sediment samples (Table I.6.7) by freeze-drying and these sediments were analyzed for HTO concentration by LSC. The pressure during freeze-drying fell between 10^{-4} and 10^{-5} Torr and the temperature ranged from 0 to -4^{o} C. The remaining solid material was washed with tritium-free water to remove the exchangeable OBT. Sediments were oven-dried until no change in mass occurred and the dried material was combusted in a combustion tube. The combustion water was analyzed by LSC to quantify OBT concentrations.

Collection of plankton

Plankton samples were collected in the Perch Lake water column on 20 September 2004 just offshore of the cages to quantify tritium levels in mussel dietary items (as an input parameter for modeling purposes). HTO levels of 4153, 4101 and 4068 Bq/L were found in the plankton samples. Corresponding HTO concentrations in Perch Lake surface waters at the time of plankton sampling were 4091, 4066 and 4038 Bq/L. In comparison, an OBT concentration of 2914 ± 42 Bq/L was measured in the composite plankton sample. Note that it was not possible to measure OBT in individual samples due to the relatively large biomass required for OBT analysis.

I.6.4.2. Monitoring of fluctuations in water temperature

Perch Lake surface water temperatures were taken continuously using a temperature probe set to integrate values over 5-minute time intervals. The probe was positioned a few centimetres above the sediment-water interface.

Table I.6.5. Free-water tritium (HTO) and organically-bound tritium (OBT) concentrations in various sample types collected at the background location in the Ottawa River, upstream of AECL's Chalk River Laboratories site. Values measured for mussels represent the initial tritium levels at the start of the study.

Sample Type	HTO (Bq/L)	OBT (Bq/L)
Surface Water	< 10	Not applicable
Freshwater Mussels	< 10	< 15

Table I.6.6. Individual mussels collected from Cages 1 to 4 in Perch Lake at each sampling time.

Time After Mussel Transplantation	Water Only Exposure		Sediment and Water Exposure		Comments
	Cage 1	Cage 2	Cage 3	Cage 4	
0 hours (all cages)	n.a.	n.a.	n.a.	n.a.	
	n.a.	n.a.	n.a.	n.a.	
	n.a.	n.a.	n.a.	n.a.	
1 hour (all cages)	A6	G5	C6	B3	
	G2	H3	E5	D8	
	H5	H7	H8	F5	
2 hours (all cages)	C4	B4	G2	A6	
	A8	E7	B5	E1	
	F3	H2	E8	E4	
4 hours (all cages)	A7	A3	A5	C3	
	B3	C6	E3	E2	
	D7	E3	G7	E6	
7 hours (all cages)	B5	B6	C5	D2	
	E6	D5	A8	E7	
	G3	E4	H3	G4	
19 hours (all cages)	B4	B3	A1	B5	Duplicate samples taken for QA purposes.
	D2	B8	C3	B6	
	H4	F1	D4	D1	
	C7	A8	E7	E5	
	E5	D1	G4	F2	
	H7	F7	G6	F8	
24 hours (all cages)	D6	F2	A3	A8	
	E3	F5	B8	C1	
	G5	D6	G5	F4	
48 hours (all cages)	C2	C4	B2	A1	
	D8	E6	E6	D5	
	F5	G3	D5	F6	
96 hours (all cages)	B2	A4	B1	A3	Duplicate samples taken for QA purposes.
	B8	A6	C4	B7	
	D5	C5	D6	D3	
	E1	E2	E2	G5	
	F4	F8	H4	C6	
	H8	G4	H7	H2	
8 days (all cages)	C8	A7	A2	A4	
	F6	C1	D7	D7	
	G4	H5	F7	F3	
14 days (all cages)	B6	B1	A4	C4	Duplicate samples taken for QA purposes.
	B7	B7	B6	B1	
	C1	D4	E1	C7	
	E7	D8	F6	F7	
	G6	G1	F8	G1	
	H6	G7	G1	H7	

Table I.6.6. (Continued).

Time After Mussel Transplantation	Water Only Exposure		Sediment and Water Exposure		Comments
	Cage 1	Cage 2	Cage 3	Cage 4	
18 days (Cages 1 & 2)	D3	D3	B7	B2	Cages 3 and 4 sampled 19 days after transplantation.
19 days (Cages 3 & 4)	F2	C7	F4	D6	
	G7	E8	H6	H8	
25 days (Cages 1 & 2)	C6	C8	A7	C5	Duplicate samples taken for QA purposes.
27 days (Cages 3 & 4)	D4	D2	C1	C8	Cages 3 and 4 sampled 27 days after transplantation.
	E4	D7	C2	F1	
	F7	E5	D8	G6	
	G1	H4	F3	H1	
	G8	F6	H5	H6	
36 days (Cages 1 & 2)	A5	A2	C8	B8	Cages 3 and 4 sampled 35 days after transplantation.
35 days (Cages 3 & 4)	D1	C3	E4	G7	
	H1	H8	H2	E3	
42 days (Cages 1 & 2)	C3	B2	A6	A2	Duplicate samples taken for QA purposes.
41 days (Cages 3 & 4)	C5	B5	B4	C2	Cages 3 and 4 sampled 41 days aftertransplantation.
	E2	E1	D1	G2	
	F1	F3	D2	G3	
	H3	G8	G3	H4	
	E8	H6	G8	H5	
86 days (Cages 1 & 2)	A1	A1	B3	A7	
84 days (Cages 3 & 4)	A2	A5	C7	B4	
	A3	C2	D3	D4	
	A4	F4	F1	E8	
	F8	G2	F2	G8	
	B1	G6	H1	H3	
	H2				

Table I.6.7. Tritium input data for use in the Perch Lake dynamic mussel transplantation scenario.

Time After Mussel Transplantation	Water HTO (Bq/L)		Surface Sediments Between Cages 1 & 2		Water HTO (Bq/L)		Surface Sediments Between Cages 3 & 4	
	Cage 1	Cage 2	HTO (Bq/L)	OBT (Bq/L)	Cage 3	Cage 4	HTO (Bq/L)	OBT (Bq/L)
0 hour (all cages)	4800	4787	–	–	4645	4799	–	–
	4847	4880	–	–	4688	4763	–	–
	4689	4775	–	–	4656	4636	–	–
1 hour (all cages)	4735	4829	–	–	4646	4729	4310	1020 ± 26
	4785	4685	–	–	4689	4792	4296	
	4830	4734	–	–	4844	4795	–	–
2 hours (all cages)	4637	4711	3926	994 ± 23	4762	4715	–	–
	4641	4625	3961	–	4685	4638	–	–
	4575	4795	–	–	4766	4709	–	–
4 hours (all cages)	4718	4636	–	–	4661	4718	–	–
	4705	4747	–	–	4711	4835	–	–
	4598	4683	–	–	4758	4660	–	–
7 hours (all cages)	4804	4611	–	–	4753	4688	–	–
	4638	4745	–	–	4653	4769	–	–
	4752	4719	–	–	4566	4685	–	–

Table I.6.7. (Continued).

Time After Mussel Transplantation	Water HTO (Bq/L)		Surface Sediments Between Cages 1 & 2		Water HTO (Bq/L)		Surface Sediments Between Cages 3 & 4	
	Cage 1	Cage 2	HTO (Bq/L)	OBT (Bq/L)	Cage 3	Cage 4	HTO (Bq/L)	OBT (Bq/L)
19 hours (all cages)	4821	4796	–	–	4456	4378	–	–
	4784	4840	–	–	4350	4356	–	–
	4743	4716	–	–	4329	4339	–	–
24 hours (all cages)	4683	4734	4015	700 ± 7	4464	4522	3802	1248 ± 50
	4832	4677	4025	–	4371	4478	3854	–
	4683	4774	–	–	4386	4427	–	–
48 hours (all cages)	4645	4799	–	–	4429	4503	–	–
	4688	4763	–	–	4371	4329	–	–
	4656	4636	–	–	4574	4648	–	–
96 hours (all cages)	4597	4615	–	–	4526	4549	–	–
	4650	4609	–	–	4547	4722	–	–
	4699	4605	–	–	4617	4534	–	–
8 days (all cages)	4678	4634	–	–	4431	4270	–	–
	4749	4697	–	–	4312	4348	–	–
	4696	4683	–	–	4200	4376	–	–
14 days (all cages)	4410	4472	3993	571 ± 9	4150	4212	3845	1403 ± 66
	4417	4533	3919	–	4128	4182	3795	–
	4298	4365	–	–	4171	4137	–	–
18 days (Cages 1 & 2)	4438	4347	–	–	4470	4415	–	–
19 days (Cages 3 & 4)	4367	4337	–	–	4385	4417	–	–
	4276	4347	–	–	4374	4443	–	–
25 days (Cages 1 & 2)	4383	4329	–	–	4136	4073	–	–
27 days (Cages 3 & 4)	4412	4420	–	–	3985	4088	–	–
	4299	4359	–	–	4132	4143	–	–
36 days (Cages 1 & 2)	4238	4393	–	–	4150	4328	3894	1159 ± 33
35 days (Cages 3 & 4)	4268	4313	–	–	4176	4272	3876	–
	4387	4191	–	–	4180	4281	–	–
42 days (Cages 1 & 2)	4102	4173	3802	704 ± 17	4069	4088	–	–
41 days (Cages 3 & 4)	4182	4137	3857	–	4094	4066	–	–
	4109	4079	–	–	3977	3991	–	–
[a] 77 days	4091	–	–	–	–	–	–	–
	4066	–	–	–	–	–	–	–
	4038	–	–	–	–	–	–	–
86 days (Cages 1 & 2)	3930	4088	–	–	4046	3955	3274	1829 ± 28 (Cage 3)
84 days (Cages 3 & 4)	3973	3949	–	–	4038	4062	3840	1981 ± 57 (Cage 4)

Measurement error for HTO was <1%.

[a] Triplicate water samples were collected in the area where plankton samples were taken. Water data are likely representative of a well-mixed condition in the lake.

Table I.6.8. Model output parameters for the dynamic Perch Lake mussel transplantation scenario (Cages 1 and 2).

Time After Mussel Transplantation	Exposure to Surface Water Only (Cages 1 and 2)			
	HTO Mussel Concentration (Bq/L)	± 95% Confidence Interval	OBT Mussel Concentration (Bq/L)	± 95% Confidence Interval
0 hour	given	given	given	given
1 hour				
2 hours				
4 hours				
7 hours				
19 hours				
24 hours				
48 hours				
96 hours				
8 days				
14 days				
18 days				
25 days				
36 days				
42 days				
77 days				
86 days				

Table I.6.9. Model output parameters for the dynamic Perch Lake mussel transplantation scenario (Cages 3 and 4).

Time After Mussel Transplantation	Exposure to both Surface Water and Sediments (Cages 3 and 4)			
	HTO Mussel Concentration (Bq/L)	± 95% Confidence Interval	OBT Mussel Concentration (Bq/L)	± 95% Confidence Interval
0 hour	given	given	given	given
1 hour				
2 hours				
4 hours				
7 hours				
19 hours				
24 hours				
48 hours				
96 hours				
8 days				
14 days				
19 days				
27 days				
35 days				
41 days				
77 days				
84 days				

I.6.5. Input data

Measured HTO concentrations in water and mussel soft tissues collected at the background location are provided in Table I.6.5. In addition, water and sediment tritium levels measured at each sampling time are summarized in Table I.6.7. Plankton HTO and OBT data are listed in Section I.6.4.1 above.

In cases where more than one value is listed for a given parameter, separate composite samples were taken close to the same location to facilitate measurement of variability.

I.6.5.1. Uncertainties

Counting errors in the HTO concentrations in Perch Lake surface waters and sediments were generally less than 2%. Counting errors for OBT concentrations are typically less than 5%, although additional uncertainty can arise due to difficulties in removing exchangeable OBT from the samples and during the combustion process. The total uncertainty in the OBT measurements is estimated to be approximately 25%. Differences among replicate samples from the same location may be larger because of natural variability.

I.6.6. Scenario calculations

Using the information provided in the sections above, participants in the scenario are asked to calculate:

(1) HTO and non-exchangeable OBT concentrations (Bq/L) in mussels exposed only via water (i.e. in Cages 1 and 2) for each measurement time-point, as specified in Table I.6.8;
(2) HTO and non-exchangeable OBT concentrations (Bq/L) in mussels exposed via both water and sediments (i.e. in Cages 3 and 4) for each measurement time-point, as specified in TableI.6.9; and
(3) 95% confidence intervals on all predictions in (1)–(2).

Results should be submitted using Tables I.6.8 and I.6.9.

I.7. Mussel Depuration Scenario Description

I.7.1. Background information

Tritium can represent a key radionuclide in the aquatic environment, potentially contributing significantly to the doses received by aquatic non-human biota in surface waters receiving tritium inputs. In many cases, steady-state models provide practical tools to estimate free-water tritium concentrations (and, to a lesser extent, OBT concentrations). However, aquatic organisms are occasionally exposed to short-term, elevated tritium levels in water when tritium is released accidentally to aquatic systems. Tritium can later be eliminated by an organism once ambient tritium concentrations have declined. Depending upon the nature and the duration of such events, steady-state models may or may not be predictive of true organism concentrations as conditions change and as the organism responds to those changes.

In general, the rates of free-water tritium and OBT elimination are not well known under dynamic exposure conditions, but can be studied by transplanting biomonitoring species, such as freshwater mussels, from areas with measurable tritium concentrations to those with significantly lower levels. In this way, changes in tissue free-water tritium (HTO) and OBT concentrations can be monitored to quantify their responses to dynamic exposure conditions.

I.7.1.1. Study objective

The objective of this study was to quantify the rates of HTO and OBT depuration from freshwater Barnes mussels (*Elliptio complanata*) that were subject to an abrupt decrease in ambient tritium levels through transplantation to a lake with low concentrations. Measurements made at the Chalk River site of AECL form the basis of a model-data validation exercise for this scenario. This study complements the mussel uptake scenario of the EMRAS Tritium/C14 Working Group, which tested models of tritium uptake by mussels following an abrupt increase in ambient tritium levels [I.3].

I.7.2. Site descriptions

I.7.2.1. Source water body for Barnes Mussels

At the start of the study, Barnes mussels (*Elliptio complanata*) were collected from Perch Lake, a small Canadian Shield lake that has received chronic, low-level tritium inputs over several decades from an upgradient Waste Management Area (WMA). Located on the site of Chalk River Laboratories (CRL), Perch Lake contains trace amounts of tritium (Figures I.7.1 and I.7.2), which discharge into the lake through the sediments from below, as well as through the Inlet 2 inflowing stream (Figure I.7.2). Inlet 1 also shows slightly elevated levels of tritium; however, inflowing streams at Inlets 3, 4 and 5 are all uncontaminated. The rate and distribution of HTO releases to the lake are not known quantitatively, although it is believed that the lake is well-mixed in the vicinity of the site where the mussels were collected for transplantation.

Sediments in the lake are composed of sand and gyttja (decomposing organic material). The mean dry bulk density is approximately 185 kg m^{-3} for Perch Lake sediments, but values vary substantially across the lake depending on the local composition of the sediments. The sediments in the vicinity of the mussel collection site are primarily sandy in nature, with some accumulation of organic matter, and are approximately 50% water by weight.

A detailed description of Perch Lake can be found in [I.3].

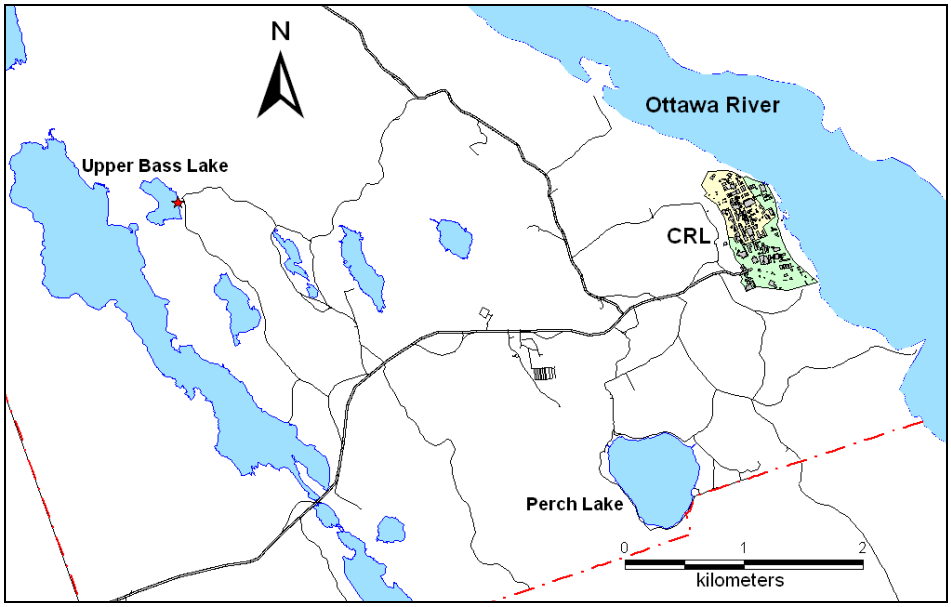

Fig.I.7.1. Map depicting the source location in Perch Lake where freshwater Barnes mussels (Elliptio complanata) were collected, relative to the site of mussel transplantation in Upper Bass Lake on AECL's Chalk River Laboratories site.

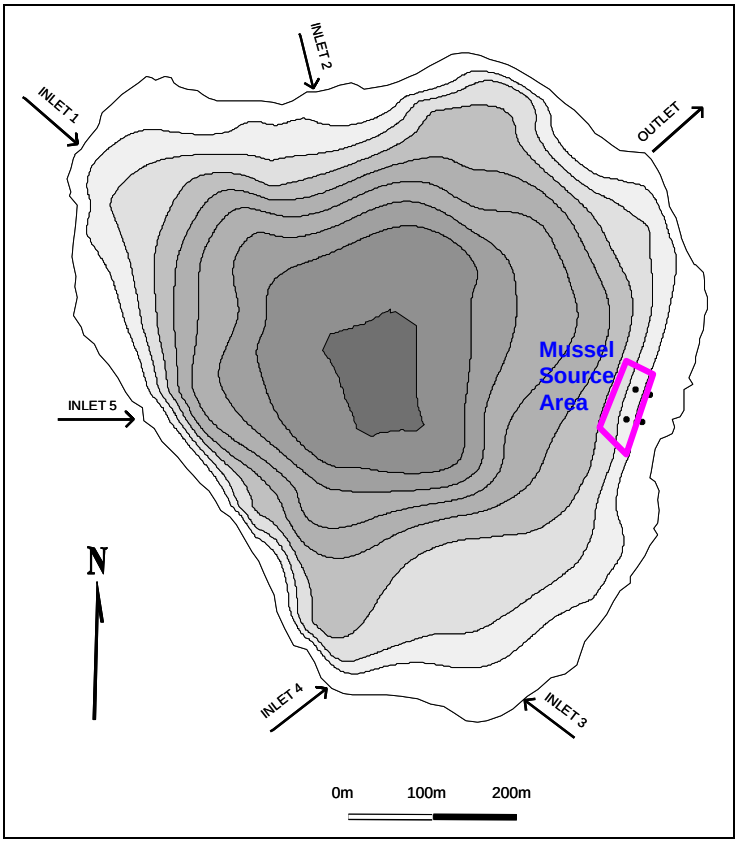

Fig. I.7.2. Map of Perch Lake depicting the location of inflowing and outflowing streams, depth contours (at 0.5 metre intervals) and the location where mussels were collected for transplantation into Upper Bass Lake.

Fig. I.7.3. Design of the mussel transplantation cages.

I.7.2.2. Receiving water body for transplantation and depuration of Barnes Mussels

Upper Bass Lake is relatively small in comparison to Perch Lake, with a surface area of approximately 55,450 m^2, representing 12% of the surface area of Perch Lake. However, Upper Bass Lake is approximately 2-fold deeper than Perch Lake, with a mean depth of 4 metres and a maximum depth exceeding 8 metres. Upper Bass Lake has a substantially smaller volume (266,405 m^3) than Perch Lake (910,000 m^3).

The sediments in Upper Bass Lake are similar to those in Perch Lake, consisting of sand and gyttja, with primarily sand mixed with some organic matter in the vicinity of the mussel cages.

I.7.3. Study design

Three mussel transplantation cages were built and deployed in Upper Bass Lake in late June 2005. In the mussel uptake experiment that was carried out in Perch Lake in 2004 [I.3], two sets of tritium exposure conditions were studied, including exposure to tritium via surface water only and exposure via both sediments and surface water. However, since the two conditions gave similar results, it was considered unnecessary to include the sediment pathway in the elimination experiment. Instead, the three transplantation cages were placed at the sediment-to-water interface and a single mussel from Perch Lake was added to each cage compartment. No sediments were added to the compartments.

Table I.7.1. Layout of mussel transplantation cages and mussel numbering scheme. Cages were set up as a matrix and individual mussels were numbered using alphabetical columns and numerical rows to facilitate tracking of each mussel.

Row \ Column	A	B	C	D	E	F	G	H
1	A1	B1	C1	D1	E1	F1	G1	H1
2	A2	B2	C2	D2	E2	F2	G2	H2
3	A3	B3	C3	D3	E3	F3	G3	H3
4	A4	B4	C4	D4	E4	F4	G4	H4
5	A5	B5	C5	D5	E5	F5	G5	H5
6	A6	B6	C6	D6	E6	F6	G6	H6
7	A7	B7	C7	D7	E7	F7	G7	H7
8	A8	B8	C8	D8	E8	F8	G8	H8

I.7.3.1. Cage design

Each mussel transplantation cage was constructed with an 8 x 8 design, resulting in a total of 64 compartments per cage (Figure I.7.3). Each compartment was assigned a unique alphanumeric code (as shown in Table I.7.1) and one animal was placed into each compartment to facilitate tracking of each animal. Cages were constructed with 2 x 2 cedar and chicken wire, with dimensions of 96 cm (length) x 96 cm (width) x 12 cm (height). Individual cage compartments had surface area dimensions of 12 cm x 12 cm.

I.7.3.2. Selection of animals

Freshwater Barnes mussels (*Elliptio complanata*) with total shell lengths ranging from 71 to 105 mm were selected for the study during sampling at Perch Lake. A list of whole animal fresh weights and total shell lengths, widths and heights are provided for each animal in Table I.7.2 by cage number and compartment.

I.7.3.3. Mussel transplantation

Reference site

As discussed in Section I.7.2.1 above, mussels were collected from an area with measurable tritium concentrations in Perch Lake on AECL's Chalk River Laboratories site (Figure I.7.1). Mussels were collected and placed into lidded, plastic buckets containing water from the collection site to prevent tritium elimination by the mussels prior to initiation of the study. The mussels were then transported to the laboratory at the CRL site.

Individuals were quickly measured, weighed and alpha-numerically numbered (as shown in Table I.7.2), and were separated by placing them into labeled nylon bags. Animals were then replaced into the lidded buckets of Perch Lake water until initiation of transplantation, which was carried out on the same day as mussel collection. Only one mussel was removed from a bucket of Perch Lake water at a time during measuring to minimize HTO exchange prior to study initiation. Concentrations of HTO measured in Perch Lake surface waters and in the buckets of Perch Lake water are provided in Table I.7.3, together with the HTO and OBT concentrations in the mussels collected from Perch Lake.

Table I.7.2. Weight and length measurements of mussels transplanted from Perch Lake to Upper Bass Lake.

Time After Mussel Transplantation	Cage No.	Mussel No.	Initial Mussel Measurements (at Time 0)				Mussel Measurements at Harvest Time		Final-to-Initial Measurement Ratio	
			Initial Fresh Weight (g)	Initial Shell Length (mm)	Initial Shell Width (mm)	Initial Shell Height (mm)	Final Fresh Weight (g)	Final Shell Length (mm)	Fresh Weight at Harvest-to-Initial Fresh Weight Ratio	Shell Length at Harvest-to-Initial Shell Length Ratio
0 hours (from Perch Lake)	[a] n.a.	6	n.a.	n.a.	n.a.	n.a.	39.86	78	n.a.	n.a.
	[a] n.a.	7	n.a.	n.a.	n.a.	n.a.	59.40	84	n.a.	n.a.
	[a] n.a.	8	n.a.	n.a.	n.a.	n.a.	39.74	74	n.a.	n.a.
	[a] n.a.	9	n.a.	n.a.	n.a.	n.a.	40.55	78	n.a.	n.a.
	[a] n.a.	10	n.a.	n.a.	n.a.	n.a.	33.91	71	n.a.	n.a.
1 hour	2	C5	43.50	82	42	22	42.755	82	0.98	1.00
	2	D2	48.49	80	42	23	48.721	82	1.00	1.03
	3	B3	74.91	90	45	30	72.36	90	0.97	1.00
	3	D3	52.32	78	42	27	51.267	78	0.98	1.00
	4	D5	67.46	87	49	26	66.37	87	0.98	1.00
[b] 2 hours	4	[c] B3	67.39	91	49	25	67.12	92	1.00	1.01
	4	[c] H5	118.34	103	51	33	117.06	103	0.99	1.00
	4	[c] B7	65.66	91	44	27	65.03	92	0.99	1.01
	2	[c] A2	78.23	92	48	28	80.53	92	1.03	1.00
	2	[c] C8	68.75	84	45	28	67.5	89	0.98	1.06
	4	[d] C2	55.06	88	46	22	42.21	77	0.77	0.88
	4	[d] E3	53.07	82	40	26	44.476	83	0.84	1.01
	4	[d] F4	38.07	72	39	21	37.123	73	0.98	1.01
	2	[d] F5	44.52	78	42	22	47.271	83	1.06	1.06
	2	[d] C8	68.75	84	45	28	37.125	78	0.54	0.93
[b] 4 hours	2	[c] D5	62.76	90	46	26	61.85	91	0.99	1.01
	2	[c] A3	40.39	78	40	21	36.838	79	0.91	1.01
	2	[c] D7	49.74	83	44	25	51.443	79	1.03	0.95
	2	[c] F8	33.89	71	38	20	33.22	72	0.98	1.01
	4	[c] D4	77.75	88	45	30	75.88	89	0.98	1.01
	4	[d] A5	80.66	88	45	33	79.270	90	0.98	1.02
	3	[d] H4	54.08	79	41	22	53.590	80	0.99	1.01
	3	[d] E1	46.30	78	37	26	46.312	77	1.00	0.99
	4	[d] F8	43.14	75	40	23	40.804	76	0.95	1.01
	4	[d] E7	41.16	77	41	21	40.989	78	1.00	1.01

Table I.7.2. (Continued).

Time After Mussel Transplantation	Cage No.	Mussel No.	Initial Mussel Measurements (at Time 0)				Mussel Measurements at Harvest Time		Final-to-Initial Measurement Ratio	
			Initial Fresh Weight (g)	Initial Shell Length (mm)	Initial Shell Width (mm)	Initial Shell Height (mm)	Final Fresh Weight (g)	Final Shell Length (mm)	Fresh Weight at Harvest-to-Initial Fresh Weight Ratio	Shell Length at Harvest-to-Initial Shell Length Ratio
7 hours	2	A6	52.38	80	41	26	52.492	80	1.00	1.00
	2	G7	41.32	71	38	23	40.834	71	0.99	1.00
	4	A2	62.21	91	46	25	61.250	91	0.98	1.00
	4	E5	82.67	98	50	27	84.36	98	1.02	1.00
	4	H8	68.86	94	46	24	68.67	96	1.00	1.02
[b] 24 hours (1 day)	3	[c] A6	63.11	89	46	26	61.870	89	0.98	1.00
	3	[c] C1	46.56	81	42	22	46.307	81	0.99	1.00
	4	[c] D8	42.00	82	40	20	40.814	82	0.97	1.00
	2	[c] E6	45.17	78	42	25	45.579	78	1.01	1.00
	2	[c] F1	47.75	80	43	24	47.291	80	0.99	1.00
	3	[d] D6	63.63	81	45	26	64.92	82	1.02	1.01
	2	[d] H2	47.79	81	43	25	46.447	82	0.97	1.01
	3	[d] G2	41.30	76	39	21	41.329	76	1.00	1.00
	4	[d] E6	73.63	91	47	28	70.37	91	0.96	1.00
	4	[d] A6	49.12	80	43	22	47.743	81	0.97	1.01
48 hours (2 days)	2	B7	56.89	81	41	25	55.164	82	0.97	1.01
	2	E1	48.14	77	38	26	47.475	76	0.99	0.99
	4	B8	43.87	79	41	22	43.936	80	1.00	1.01
	4	D7	45.46	79	42	21	45.397	79	1.00	1.00
	4	E1	60.63	87	47	26	58.488	88	0.96	1.01
120 hours (5 days)	3	C3	59.36	82	44	26	58.004	81	0.98	0.99
	3	D5	44.41	80	42	22	44.500	81	1.00	1.01
	4	B6	51.18	83	44	22	50.525	84	0.99	1.01
	4	C2	55.06	88	46	22	–	–	–	–
	4	E3	53.07	82	40	26	50.521	84	0.95	1.02
	4	C3	62.90	86	46	28	63.27	87	1.01	1.01

Table I.7.2. (Continued).

Time After Mussel Transplantation	Cage No.	Mussel No.	Initial Mussel Measurements (at Time 0)				Mussel Measurements at Harvest Time		Final-to-Initial Measurement Ratio	
			Initial Fresh Weight (g)	Initial Shell Length (mm)	Initial Shell Width (mm)	Initial Shell Height (mm)	Final Fresh Weight (g)	Final Shell Length (mm)	Fresh Weight at Harvest-to-Initial Fresh Weight Ratio	Shell Length at Harvest-to-Initial Shell Length Ratio
[b] 288 hours (12 days)	2	[c] F3	44.15	80	40	23	43.579	80	0.99	1.00
	2	[c] C1	51.02	83	42	22	49.694	84	0.97	1.01
	2	[c] E8	64.07	87	46	26	63.86	87	1.00	1.00
	2	[c] B4	48.91	82	43	23	48.077	82	0.98	1.00
	2	[c] D4	37.26	75	38	22	36.099	76	0.97	1.01
	4	[d] G8	44.66	84	44	21	43.508	84	0.97	1.00
	3	[d] E3	58.97	86	43	27	59.349	86	1.01	1.00
	3	[d] H2	49.55	84	42	24	47.135	85	0.95	1.01
	3	[d] G5	65.34	85	48	25	65.100	87	1.00	1.02
	3	[d] H3	40.68	79	41	21	41.081	79	1.01	1.00
624 hours (26 days)	3	F3	48.89	83	43	23	47.485	83	0.97	1.00
	4	D2	42.55	80	40	21	42.583	81	1.00	1.01
	4	F7	47.69	77	40	25	46.079	78	0.97	1.01
	4	G6	100.11	105	53	30	57.420	87	0.57	0.83
	4	H3	34.99	78	39	18	35.609	78	1.02	1.00
960 hours (40 days)	2	C2	55.53	76	43	25	55.639	78	1.00	1.03
	2	D1	39.40	74	38	21	39.784	75	1.01	1.01
	2	G5	35.06	73	38	22	35.543	73	1.01	1.00
	2	H8	43.60	83	42	21	45.409	84	1.04	1.01
	3	E7	68.67	85	46	28	66.830	87	0.97	1.02
1320 hours (55 days)	2	C6	61.27	85	44	26	60.210	85	0.98	1.00
	2	E4	46.79	77	40	24	46.431	79	0.99	1.03
	3	D8	64.23	85	44	28	65.470	85	1.02	1.00
	2	A5	54.61	80	43	27	55.273	80	1.01	1.00
	3	C8	38.04	78	39	21	36.693	76	0.96	0.97
	4	B2	67.45	89	46	26	66.680	89	0.99	1.00
	3	E6	42.29	77	40	24	42.063	76	0.99	0.99
	2	A8	74.02	89	48	27	75.930	88.5	1.03	0.99

Table I.7.2. (Continued).

Time After Mussel Transplantation	Cage No.	Mussel No.	Initial Mussel Measurements (at Time 0)				Mussel Measurements at Harvest Time		Final-to-Initial Measurement Ratio	
			Initial Fresh Weight (g)	Initial Shell Length (mm)	Initial Shell Width (mm)	Initial Shell Height (mm)	Final Fresh Weight (g)	Final Shell Length (mm)	Fresh Weight at Harvest-to-Initial Fresh Weight Ratio	Shell Length at Harvest-to-Initial Shell Length Ratio
2040 hours (85 days)	2	A4	60.35	83	43	25	59.30	84	0.98	1.01
	2	G8	42.05	81	41	22	39.60	82	0.94	1.01
	3	E2	55.12	83	40	27	55.99	84	1.02	1.01
	3	F4	59.15	83	46	25	59.2	84	1.00	1.01
	4	D3	62.56	85	45	28	57.4	87	0.92	1.02
[b] 2808 hours (117 days)	2	[c] E3	45.40	82	42	23	44.4	85	0.98	1.04
	2	[c] E7	45.35	77	40	24	39.4	77	0.87	1.00
	2	[c] G1	43.43	80	41	23	45.3	80	1.04	1.00
	2	[c] H3	50.60	79	42	26	46.2	79	0.91	1.00
[b] 2808 hours (117 days)	3	[c] B2	73.99	91	48	28	71.9	92	0.97	1.01
	3	[d] C6	54.23	82	41	24	56.2	83	1.04	1.01
	3	[d] G6	53.29	82	40	25	53.80	84	1.01	1.02
	4	[d] A3	47.83	79	41	22	46.3	79	0.97	1.00
	4	[d] A8	75.18	91	47	28	74.4	93	0.99	1.02

[a] n.a. – not available.
[b] Duplicate composite samples taken and measured for quality assurance purposes.
[c] Represent mussels that were included in Composite 1.
[d] Represent mussels that were included in Composite 2.

Table I.7.3. HTO and OBT concentrations in surface water and Barnes mussels collected in Perch Lake. Mussel values represent initial tritium levels at Time 0 of the study.

Sample Type	Source	HTO (Bq/L)	OBT (Bq/L)
Surface Water	Perch Lake	3,568 3,644 3,325 3,617	n.a.
	Mussel Transfer Buckets (originally from Perch Lake)	3,581 3,534 3,617	n.a.
Sediments	Perch Lake	3,000	700
Barnes Mussels	Perch Lake	2,946	2,287

n.a. – not applicable.

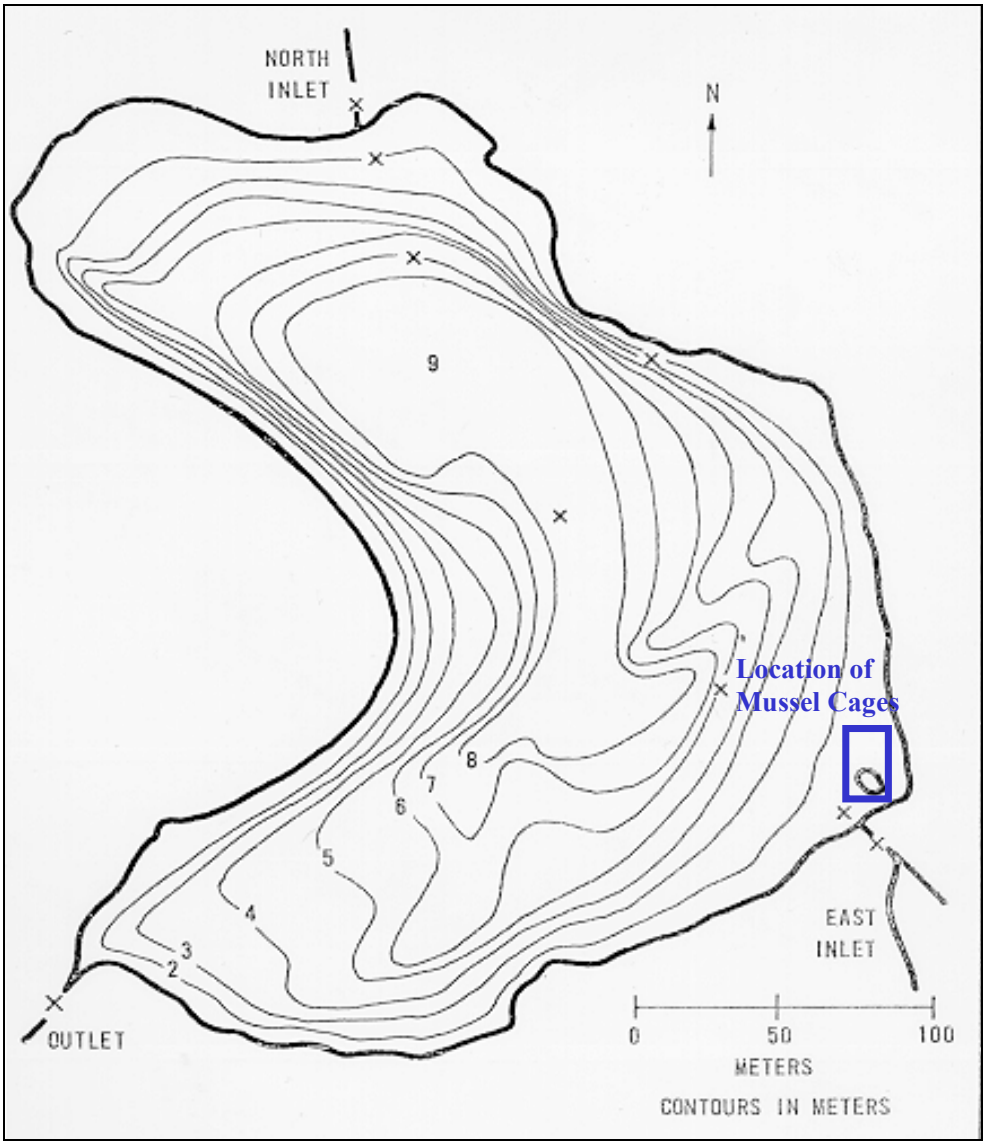

Fig. I.7.4. Map of Upper Bass Lake depicting the location of inflowing and outflowing streams, depth contours (in metres) and the location of the mussel transplantation cages.

Mussel Deployment

The three mussel cages were deployed on 29 June 2005, the day before the mussels were transplanted, to allow conditions around the cages to equilibrate before the mussels were introduced. The cages were positioned adjacent to the shoreline in Upper Bass Lake at a water depth of approximately 0.5 to 1 m (Figure I.7.4). No sediments were added to the cages.

Mussel transplantation took place on 30 June 2005 at 11:00 hours. Upon initiation of the study, mussels were transferred from the lidded buckets containing water from Perch Lake to buckets containing water from Upper Bass Lake. In this way, mussels received initial tritium exposure at approximately the same time, despite the 10 to 15 minute time period required for mussel transfer from buckets to the numbered cage compartments.

Mussels were placed into the cage compartments and began filtering within less than five minutes. No mussel mortality occurred in any of the cages over the course of the 117-day study. Algal growth, which accumulated on the cages over the course of the study, was not removed as it did not appear to alter water flow within the cages.

During mussel transfer, care was taken to ensure that no Perch Lake water was spilled in the vicinity of Upper Bass Lake. Once mussels were transferred to the buckets containing Upper Bass Lake water, the lids on the Perch Lake water buckets were securely replaced and the water was later returned to Perch Lake.

I.7.4. Study measurements

I.7.4.1. Tritium monitoring

Collection of mussel samples

Composite mussel samples were taken at each sampling time, as specified in Table I.7.2. Mussel samples were collected on an exponential time-step over the course of a 117-day period (as listed in Table I.7.2). Upon collection, mussels were immediately placed into air-tight Mason jars to avoid tritium exchange with the atmosphere, and the jars containing the mussels were frozen until processing for tritium analysis could be carried out. In general, it was necessary to composite soft tissues from 3 to 4 individuals to gain the biomass required for HTO and OBT analysis. The water content of mussel tissue is approximately 89% (by weight), with little variability among individual animals.

Collection of surface water samples

Water samples were collected in triplicate at each sampling time in the vicinity of the mussel cages (Figure I.7.4). In doing so, sampling bottles were opened at the depth where the mussels were filtering. The samples were then left standing to allow any suspended sediments to settle out and 2 mL of water were subsequently transferred to scintillation vials. HTO concentrations in all water samples were determined using a Beckman 6500 liquid scintillation counter, using a counting time of 30 minutes.

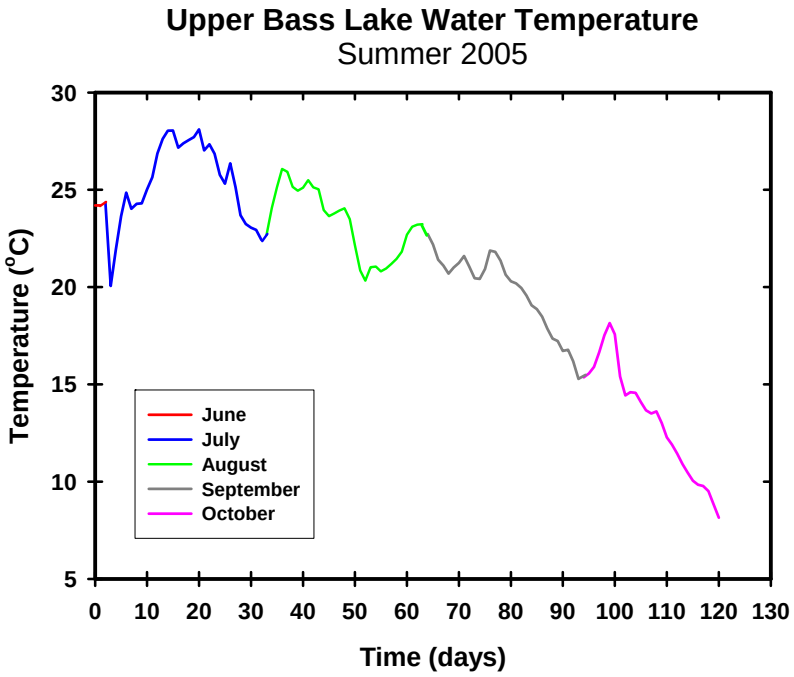

Fig. I.7.5. Upper Bass Lake water temperatures over the course of the elimination study. Temperature measurements were integrated over 5-minute time intervals between 30 June 2005 and 25 October 2005.

Collection of surface sediment samples

Sediment samples were collected by hand at a depth of 5 to 10 cm from the sediment surface in the vicinity of the mussel cages at each sampling time. The samples were placed in Ziplock bags that were sealed at depth. Sediment porewater was extracted from a subset of the samples (Table I.7.4) by freeze-drying and was analyzed for HTO concentration by LSC. The pressure during freeze-drying lay between 10^{-4} and 10^{-5} Torr and the temperature was in the range 0 to –4^{o} C. The remaining solid material was washed with tritium-free water to remove the exchangeable OBT. The samples were then oven-dried until no change in mass occurred and the dried sediments were combusted in a combustion furnace. The combustion water was then analyzed using a Quantulus 1220 liquid scintillation counter to quantify OBT concentrations in the sediments.

I.7.4.2. Monitoring water temperature

Upper Bass Lake surface water temperatures were taken continuously using a two temperature probes, each set to integrate values over 5-minute time intervals. The probes were positioned in the littoral zone of the lake at the sediment-water interface at a water depth of approximately 0.5 metres (Figure I.7.4). Mean daily water temperature data can be found in Table I.7.5 and are depicted in Figure I.7.5.

Table I.7.4. Upper Bass Lake tritium input data for use in the depuration scenario.

Date of Mussel Sampling	Time after Mussel Transplantation	[a] Water HTO Concentration (Bq/L)	Sediment Tritium Concentration	
			HTO ± 1 Sigma (Bq/L)	OBT ± 1 Sigma (Bq/L)
30 June 2005 (11:00 am)	0 hour	68 59 92	n.a.	n.a.
30 June 2005	1 hour	48 59 80	n.a.	n.a.
30 June 2005	2 hours	70 26 39	82 ± 1	42 ± 5
30 June 2005	4 hours	73 58 42	n.a.	n.a.
30 June 2005	7 hours	79 89 54	n.a.	n.a.
1 July 2005	24 hours	33 76 60	n.a.	n.a.
2 July 2005	48 hours	38 32 65	n.a.	n.a.
5 July 2005	120 hours (5 days)	58 62 49 38 62 53	n.a.	n.a.
12 July 2005	288 hours (12 days)	84 72 69 96 59 79	61 ± 1	15 ± 8
26 July 2005	624 hours (26 days)	12 70 81	n.a.	n.a.
9 August 2005	960 hours (40 days)	74 115 100 77 101 102	n.a.	n.a.
24 August 2005	1320 hours (55 days)	45 49 33 31 40	60 ± 1	22 ± 7
23 September 2006	2040 hours (85 days)	36 47 69 40 26 58	n.a.	n.a.
25 October 2005	2808 hours (117 days)	76 61 55 51 67 81	missing	28 ± 6

[a] Measurement error for HTO was <5%.
n.a. – measurement not available.

Table I.7.5. Daily Upper Bass Lake water temperatures, based on individual measurements integrated over 5-minute intervals. Temperature data were not measured for the period between July 1 and 4 due to a problem with the temperature probe; however, it was possible to estimate the missing data within a confidence of approximately 80% based on available air temperature data. Raw temperature data are available upon request.

Sampling Date	No. of Sampling Times	Mean Water Temperature (^{o}C)	Standard Error (^{o}C)
17-Jun-05	279	21.12	0.03
18-Jun-05	288	19.95	0.02
19-Jun-05	288	19.41	0.03
20-Jun-05	288	20.43	0.07
21-Jun-05	288	21.39	0.03
22-Jun-05	288	21.67	0.04
23-Jun-05	288	20.99	0.04
24-Jun-05	288	22.08	0.07
25-Jun-05	288	23.54	0.05
26-Jun-05	288	23.48	0.02
27-Jun-05	288	24.07	0.03
28-Jun-05	288	25.16	0.04
29-Jun-05	288	25.12	0.02
[a] 30-Jun-05	173	24.19	0.07
01-Jul-05	n.a.	[b] 24.33 (estimated)	n.a.
02-Jul-05	n.a.	[b] 20.05 (estimated)	n.a.
03-Jul-05	n.a.	[b] 21.92 (estimated)	n.a.
04-Jul-05	n.a.	[b] 23.65 (estimated)	n.a.
05-Jul-05	230	24.85	0.02
06-Jul-05	288	24.02	0.04
07-Jul-05	288	24.28	0.04
08-Jul-05	288	24.30	0.03
09-Jul-05	288	25.02	0.05
10-Jul-05	288	25.65	0.05
11-Jul-05	288	26.87	0.06
12-Jul-05	288	27.62	0.05
13-Jul-05	288	28.03	0.04
14-Jul-05	288	28.04	0.03
15-Jul-05	288	27.17	0.04
16-Jul-05	288	27.38	0.05
17-Jul-05	288	27.54	0.02
18-Jul-05	288	27.71	0.04
19-Jul-05	288	28.10	0.03
20-Jul-05	288	27.03	0.04
21-Jul-05	288	27.34	0.05
22-Jul-05	288	26.85	0.02
23-Jul-05	288	25.76	0.04
24-Jul-05	288	25.31	0.04
25-Jul-05	288	26.36	0.05
26-Jul-05	288	25.13	0.02
27-Jul-05	288	23.70	0.02
28-Jul-05	288	23.24	0.05
29-Jul-05	288	23.05	0.03
30-Jul-05	288	22.94	0.04
31-Jul-05	288	22.42	0.01
01-Aug-05	288	22.69	0.03
02-Aug-05	288	24.07	0.06
03-Aug-05	288	25.14	0.04
04-Aug-05	288	26.06	0.03
05-Aug-05	288	25.92	0.03

Table I.7.5. (Continued).

Sampling Date	No. of Sampling Times	Mean Water Temperature (°C)	Standard Error (°C)
06-Aug-05	288	25.15	0.04
07-Aug-05	288	24.95	0.05
08-Aug-05	288	25.11	0.05
09-Aug-05	288	25.50	0.03
10-Aug-05	288	25.12	0.02
11-Aug-05	288	25.03	0.04
12-Aug-05	288	23.96	0.02
13-Aug-05	288	23.65	0.04
14-Aug-05	288	23.79	0.04
15-Aug-05	288	23.93	0.05
16-Aug-05	288	24.05	0.04
17-Aug-05	288	23.48	0.03
18-Aug-05	288	22.14	0.02
19-Aug-05	288	20.86	0.02
20-Aug-05	288	20.33	0.02
21-Aug-05	288	21.02	0.04
22-Aug-05	288	21.06	0.03
23-Aug-05	288	20.81	0.03
24-Aug-05	288	20.95	0.04
25-Aug-05	288	21.19	0.04
26-Aug-05	288	21.45	0.04
27-Aug-05	288	21.82	0.03
28-Aug-05	288	22.69	0.04
29-Aug-05	288	23.10	0.03
30-Aug-05	288	23.21	0.03
31-Aug-05	288	23.23	0.02
01-Sep-05	288	22.72	0.03
02-Sep-05	288	22.18	0.02
03-Sep-05	288	21.41	0.02
04-Sep-05	288	21.11	0.03
05-Sep-05	288	20.69	0.03
06-Sep-05	288	21.00	0.04
07-Sep-05	288	21.24	0.03
08-Sep-05	288	21.59	0.03
09-Sep-05	288	21.04	0.03
10-Sep-05	288	20.45	0.03
11-Sep-05	288	20.42	0.03
12-Sep-05	288	20.93	0.04
13-Sep-05	288	21.88	0.04
14-Sep-05	288	21.81	0.02
15-Sep-05	288	21.36	0.03
16-Sep-05	288	20.63	0.02
17-Sep-05	288	20.29	0.03
18-Sep-05	288	20.19	0.03
19-Sep-05	288	19.95	0.02
20-Sep-05	288	19.57	0.02
21-Sep-05	288	19.06	0.03
22-Sep-05	288	18.87	0.02
23-Sep-05	288	18.48	0.02
24-Sep-05	288	17.88	0.02
25-Sep-05	288	17.35	0.01
26-Sep-05	288	17.23	0.01
27-Sep-05	288	16.72	0.02
28-Sep-05	288	16.78	0.02

Table I.7.5. (Continued).

Sampling Date	No. of Sampling Times	Mean Water Temperature (°C)	Standard Error (°C)
29-Sep-05	288	16.18	0.02
30-Sep-05	288	15.28	0.02
01-Oct-05	288	15.36	0.03
02-Oct-05	288	15.56	0.02
03-Oct-05	288	15.90	0.02
04-Oct-05	288	16.66	0.03
05-Oct-05	288	17.52	0.04
06-Oct-05	288	18.15	0.04
07-Oct-05	288	17.58	0.03
08-Oct-05	288	15.40	0.02
09-Oct-05	288	14.43	0.02
10-Oct-05	288	14.60	0.01
11-Oct-05	288	14.57	0.01
12-Oct-05	288	14.08	0.01
13-Oct-05	288	13.67	0.01
14-Oct-05	288	13.50	0.01
[c] 15-Oct-05	288	13.61	0.01
16-Oct-05	288	13.02	0.01
17-Oct-05	288	12.28	0.01
18-Oct-05	288	11.91	0.01
19-Oct-05	288	11.44	0.01
20-Oct-05	288	10.90	0.01
21-Oct-05	288	10.47	0.02
22-Oct-05	288	10.05	0.01
23-Oct-05	288	9.85	0.00
24-Oct-05	288	9.78	0.00
25-Oct-05	288	9.52	0.01
26-Oct-05	288	8.84	0.02
27-Oct-05	88	8.15	0.03

[a] Start date of the study.
[b] Data missing due to probe malfunction. Water temperatures estimated from air temperatures.
[c] End date of the study.

Table I.7.6. Model output parameters for the depuration scenario.

Time After Mussel Transplantation	Mussel Tritium Concentration (Bq/L)			
	HTO	± 95% Confidence Interval	OBT	± 95% Confidence Interval
0 hour	given		given	
1 hour				
2 hours				
4 hours				
7 hours				
24 hours				
48 hours				
120 hours				
12 days				
26 days				
40 days				
55 days				
85 days				
117 days				

I.7.4.3. Measurement of mussel body size

As discussed in Section I.7.3.3 above, whole mussel fresh weights and shell lengths were measured just prior to transplantation into Upper Bass Lake. The mussels were again measured at the final sampling time to allow quantification of any changes in fresh weight, as well as for purposes of quality assurance (with respect to shell length). These data are listed in Table I.7.2. The mussels did not show significant growth over the course of the 117-day experiment. This is not surprising since the mussels transplanted as part of this study were likely greater than 10 years old.

I.7.5. Input data

Measured HTO concentrations in surface water, sediment porewater and mussel soft tissues collected from Perch Lake (the source location of the mussels) are provided in Table I.7.3. OBT concentrations measured in Perch Lake sediments and mussel soft tissues are also listed. In addition, water and sediment tritium levels measured at each sampling time in Upper Bass Lake are presented in Table I.7.4. In cases where more than one value is listed for a given parameter, separate composite samples were taken in the vicinity of the mussel transplantation cages to facilitate measurement of variability.

I.7.5.1. Uncertainties

Counting errors in the HTO concentrations in Perch Lake surface water and sediments were generally less than 5%. Counting errors for OBT concentrations are typically less than 10%, although additional uncertainty can arise due to difficulties in removing exchangeable OBT from the samples and in the combustion process. The total uncertainty in the OBT measurements is estimated to be approximately 25%. Differences among replicate samples from the same location may be larger because of natural variability.

I.7.6. Scenario calculations

Using the information provided in the sections above, calculate:

(1) HTO and non-exchangeable OBT concentrations (Bq/L) in mussels that have been transplanted from Perch Lake to Upper Bass Lake for each measurement time, as specified in Table I.7.6;
(2) 95% confidence intervals on all predictions in (1).

Results should be submitted using Table I.7.6.

I.8. The Hypothetical Scenario Description

I.8.1. Background

The objective of the study is to analyse the consequences of an acute atmospheric release of tritium, by considering various pathways in terms of activity in biosphere compartments and products, as well as the contribution of the various forms of tritium (HT, HTO and OBT) to total exposure. This study aims to give practical guidance to decision-makers in the case of a severe release, taking account of the prevailing conditions during the release. The purpose of the study is to produce a set of results/guidelines that could be used by authorities to reduce the consequences of the release, if required. This may require a harmonisation of crisis management on a technical/scientific basis within an international framework.

An integrated approach will be followed, i.e. the study will encompass immediate atmospheric impacts and further impacts on the food chain. The intent is to:

- establish at least a classification of different pathways;
- define the importance of different parameters; and
- assist in the derivation of derived intervention levels for tritium.

The scenarios will be generic (i.e. not site specific), taking due account of previous work, and limited to the minimum number necessary for a good understanding.

The final document will distinguish between features and processes that are well established and those with uncertainties in terms of crisis management. Lack of scientific information would also be identified.

I.8.2. Scenarios

Information on parameters common to all scenarios is given in Table I.8.1. Three types of meteorological conditions are considered at the end of June and are shown in Table I.8.2 (± means 1 standard deviation). The meteorological conditions are assumed to remain constant for 6 hours. Subsequent conditions are assumed not to have a large influence on the results.

Human food consumption rates of various plant and animal products are shown in Table I.8.3. Details on crop yields and times between accident and harvest are given in Table I.8.4.

It is considered that the surface environment becomes uncontaminated in November: no further crops are grown and the tritium in the soil has migrated down to the water table. Cows are supposed to eat hay harvested before the accident during the winter, although they also may eat contaminated maize (whole plant) from November to March (35 kg/day, 35% dry matter). Tests may be done on this particular point if judged necessary (see Table I.8.5).

Human breathing rates are shown in Table I.8.6.

Table I.8.1. Parameters common to all scenarios.

Condition	Value
Release amount (HTO, HT)	10 g (3.7 E15 Bq)
Release period	1 hour (constant rate)
Effective Release height	20 m point source (no plume rise)
Latitude	45° N
Date	End of June
Day length, from sunrise to sunset	19h30
Potential evapotranspiration	3.2 mm/day
Soil water content	30% by volume
Soil density	1.2 kg/L
Soil depth : garden / wheat	20cm / 40 cm
Average rainfall during summer	60 mm/month
Irrigation of garden vegetables	Yes
Irrigation of wheat	No
Surface roughness length	0.4 m

Table I.8.2. Meteorological conditions considered.

Condition	Case 1	Case 2	Case 3
Time of day	day	day	night
Wind speed ($m.s^{-1}$)	2	5	2
Direction (°N)	45±25	45±10	45±3
Diffusion conditions	unstable	neutral	stable
Weather	fine	cloudy	clear
Pasquill stability class	A	D	F
Solar radiation (W/m^2)	700	300	0
Temperature (°C)	20	20	10
Rain	no	15mm before theend of release	no
Relative humidity (%)	70	90	95

Table I.8.3. Human food consumption rates.

Generic food type	Food product	Adult	Infant (1-2 yr)	Harvest and duration of consumption of stored products
		g/day		
Green vegetables	Salad and leafy veg.	**130**	**80**	In harvest period
Root vegetables	Radish, turnip	30	15	In harvest period
	Potatoes	200	100	Harvest in late Aug, 8 months
	Carrots	50	25	Harvest starts mid-July
	Total	**280**	**140**	
Fruit vegetables	String beans	50	25	In harvest period
	Peas	50	25	In harvest period
	Tomatoes	100	50	Harvest starts in late July
	Total	**200**	**100**	
Cereals	Wheat	**430**	**40**	Harvest starts in early Aug, 1 year
Milk	Milk (including butter and cheese)	**500**	**440**	
Meat	Beef	140	60	
	Chicken and eggs	100	50	
	Total	**240**	**110**	

Table I.8.4. Crop yield and time between accident and harvest of directly contaminated crop.

Product	Yield (kg fw/m^2 per crop)	Dry matter (%)	Minimum time between accident and beginning of harvest	Maximum time between accident and end of harvest	Number of crops per year after accident
Salads	3	8	0*	1 month	4
Radish, turnip	1	20	0	3 weeks	3
Potatoes	3	21	2 months	3 months	1
Carrots	2.5	16	2 weeks	2 months	2
Peas	1	25	0	1 month	2
Beans	0.4	25	0	1 month	3
Tomatoes[§]	3	6	4 weeks	3 months	1
Cereals	0.8	86	4 weeks	7 weeks	1
Grass	0.7	15	0	2 months	4

[§] Release occurs immediately before flowering period for tomatoes.

* It is assumed that these crops are ready for harvest when the release occurs. The crop lasts for one month, i.e. the leaves from crops consumed during this period would have been exposed to atmospheric tritium. One month after exposure, a new crop is planted, for which only soil contamination/root uptake has to be considered. In a garden, new crops are sown after each harvest.

Table I.8.5. Animal parameter values.

Animal	Fodder consumption		Breathing rate	Water intake*
	Grass	Wheat		
Cow	70 kg fw/d	2 kg fw/d	5.4 m^3/h	50 L/d
Chicken		0.1 kg fw/d	10 L/h	0.2 L/d

* Animal drinking water is assumed to be uncontaminated.

Table I.8.6. Human breathing rate (m^3/h).

Age Group	Sleeping	Awake - low activity
Adult	0.45	1.5
1 year old infant	0.15	0.35

I.8.3. Scenario endpoints

Modelers should provide the information requested in Tables I.8.7 to I.8.14.

Table I.8.7. Integrated air concentrations.

	Integrated air concentration (Bq.s.m^{-3})			
Case	1 km downwind	3 km	10 km	30 km
Case 1				
Case 2				
Case 3				

Table I.8.8. Total doses.

	Adult total dose (mSv)				Child total dose (mSv)			
Case	1 km	3 km	10 km	30 km	1 km	3 km	10 km	30 km
Case 1								
Case 2								
Case 3								

Table I.8.9. Dose by pathway – Case 1.

Pathway	Dose (mSv) - Case 1									
	Adult 1000m					Child 1000m				
	Dose via air pathway		Dose via soil pathway		Total	Dose via air pathway		Dose via soil pathway		Total
	HTO	OBT	HTO	OBT		HTO	OBT	HTO	OBT	
Inhalation										
Transcutaneous										
Leafy vegetables										
Radish, turnip										
Potatoes										
Carrots										
String beans										
Peas										
Tomatoes										
Cereals										
Beef										
Milk										
Chicken, eggs										
Total dose (mSv)										

Table I.8.10. Dose by pathway – Case 2.

Pathway	Dose (mSv) - Case 2									
	Adult 1000m					Child 1000m				
	Dose via air pathway		Dose via soil pathway		Total	Dose via air pathway		Dose via soil pathway		Total
	HTO	OBT	HTO	OBT		HTO	OBT	HTO	OBT	
Inhalation										
Transcutaneous										
Leafy vegetables										
Radish, turnip										
Potatoes										
Carrots										
String beans										
Peas										
Tomatoes										
Cereals										
Beef										
Milk										
Chicken, eggs										
Total dose (mSv)										

Table I.8.11. Dose by pathway – Case 3.

Pathway	Dose (mSv) - Case 3									
	Adult 1000m					Child 1000m				
	Dose via air pathway		Dose via soil pathway		Total	Dose via air pathway		Dose via soil pathway		Total
	HTO	OBT	HTO	OBT		HTO	OBT	HTO	OBT	
Inhalation										
Transcutaneous										
Leafy vegetables										
Radish, turnip										
Potatoes										
Carrots										
String beans										
Peas										
Tomatoes										
Cereals										
Beef										
Milk										
Chicken, eggs										
Total dose (mSv)										

Table I.8.12. Activity in food products – Case 1.

Case 1 - Activity (Bq.kg^{-1} fw) – 1000 m				
Food product	**At the end of release**	**48 hrs after end of release**	**At harvest (last salads from air pathway)**	**Next cycle of crops at harvest**
Salad and leafy veg				
Radish and turnip				
Potatoes				
Carrots				
String beans				
Peas				
Tomatoes				
Cereals				
	168 hrs after end of release		720 hrs after end of release	
Beef				
Milk				
Chicken and eggs				

Table I.8.13. Activity in food products – Case 2.

Case 2 - Activity (Bq.kg^{-1} fw) – 1000 m				
Food product	**At the end of release**	**48 hrs after end of release**	**At harvest (last salads from air pathway)**	**Next cycle of crops at harvest**
Salad and leafy veg				
Radish and turnip				
Potatoes				
Carrots				
String beans				
Peas				
Tomatoes				
Cereals				
	168 hrs after end of release		720 hrs after end of release	
Beef				
Milk				
Chicken and eggs				

Table I.8.14. Activity in food products – Case 3.

Case 3 - Activity (Bq.kg^{-1} fw) – 1000 m				
Food product	**At the end of release**	**48 hrs after end of release**	**At harvest (last salads from air pathway)**	**Next cycle of crops at harvest**
Salad and leafy veg				
Radish and turnip				
Potatoes				
Carrots				
String beans				
Peas				
Tomatoes				
Cereals				
	168 hrs after end of release		720 hrs after end of release	
Beef				
Milk				
Chicken and eggs				

The results obtained will help guide discussion on the following questions:

— What area affected by the release would require immediate action in terms of animals and crops?
— What area may come back to pre-release conditions after a few days?
— What is the need and extent for action on cereals and potatoes?
— For how long and over what area should cows be removed from pasture?
— Does a zone remain where the planting of new crops would present a problem?
— What is a reference value for tritium concentration in different foodstuffs for free trade?
— What data can be collected in support of or to confirm the assessment? Where can the most useful data be collected? When, and with what frequency? What is the time frame for data collection?
— Is any waste generated and how should it be managed?
— What is the efficiency of intervention, both in mSv and in terms of % dose saved? (For example, banning cereal consumption may save 11 mSv and 70% of the total dose.)

For this exercise, we shall consider that intervention on food products will occur for a dose level of 5 mSv per year, as there is no existing trade limit. Interventions will be considered within the optimisation principle (benefit versus cost).

Some data supplied here may not be used by all modellers, who may simplify the scenario as required. All basic assumptions should be documented.

I.9. Rice Scenario Description

I.9.1. Background

Carbon-14 (^{14}C) is one of the major radionuclides released from the nuclear fuel cycle into the environment. It has long been noted that the relatively long half-life of ^{14}C (5,730 years), together with its mobility in the environment and incorporation into man via the food-chain, leads to the long-term homogeneous irradiation of the global population. In addition, ^{14}C discharges from nuclear facilities probably result in the enhancement of local ^{14}C levels in biogenic materials and the subsequent excess exposure of the local population. The development and application of functional mathematical models for predicting short-range ^{14}C transfer in the terrestrial environment is therefore necessary to assess the local radiological impact of anthropogenic ^{14}C.

The Tokai reprocessing plant (TRP) of the Japan Atomic Energy Agency (JAEA, formerly the Japan Nuclear Cycle Development, JNC) started hot tests in September 1977. One thousand tons of spent fuel used at boiling water reactors (BWRs), pressurized water reactors (PWRs) and an advanced thermal reactor (ATR) were successfully reprocessed as of June 2002. JAEA conducted careful monitoring of ^{14}C in the airborne discharge via 90-m stacks from the TRP, and ^{14}C in atmospheric CO_2 and rice grain (which makes up a large part of the Japanese daily diet) collected around the TRP site. The monitoring data over ten years from 1991 to 2001 is useful for model-data intercomparison studies on regional ^{14}C transfer in the environment.

I.9.2. Site description

Tokai-mura is basically a flat agricultural area where crops such as rice, vegetables and fruit are grown. An overview of the Tokai-mura area is shown in Figure I.9.1. The population of Tokai-mura was about 35,400 as of 2000. The TRP of JAEA is located in the east end of Tokai-mura (longitude 140.6^{o} E, latitude 36.5^{o} N), facing the Pacific Ocean.

I.9.3. Discharge monitoring

I.9.3.1. Discharge sources

Carbon-14 has been discharged with gaseous effluent from three stacks (called the “main stack”, the “sub-1 stack” and the “sub-2 stack”) of the TRP. The dominant sources of ^{14}C discharged from the main stack are shearing and dissolution of the spent fuel and subsequent solvent extraction processes for separating uranium and plutonium from fission products. Carbon-14 released from the sub-1 and sub-2 stacks is mainly from the bituminization of low active level liquid waste and the vitrification of high active level liquid waste, respectively.

The sub-1 and sub-2 stacks were located about 210 m east-northeast and 35 m southwest of the main stack, respectively. All the stacks had physical heights of 90 m, and their release points were situated 96 m above sea level. The internal diameters of the stacks were 2.9 m for the main stack, 2.4 m for the sub-1 stack and 2.8 m for the sub-2 stack. Gaseous effluents, including ^{14}C, were continuously released from the stacks at the exhaust rates listed in Table I.9.1, but ^{14}C concentrations were less than the authorized detectable limit (40 Bq cm^{-3}) when reprocessing was not being carried out. Almost all (more than 97%) of the ^{14}C was discharged in CO_2 form during reprocessing [I.4].

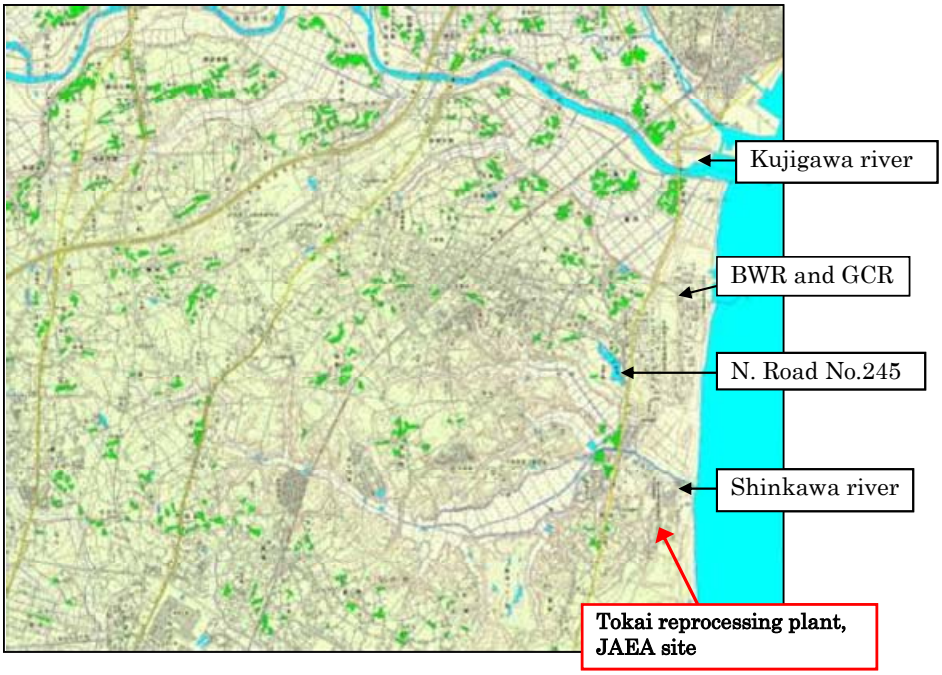

Fig.I.9.1. Overview of Tokai-mura with the Tokai reprocessing plant.

Table I.9.1. Representative discharge rates from the three TRP stacks from 1991 to 2001.

Year	Representative discharge rate ($m^3\ h^{-1}$)		
	Main stack	Sub-1 stack	Sub-2 stack
1991	4.02×10^5	1.28×10^5	–
1992	4.17×10^5	1.22×10^5	–
1993	4.17×10^5	1.22×10^5	–
1994	4.17×10^5	1.31×10^5	1.19×10^5
1995	4.17×10^5	1.28×10^5	1.13×10^5
1996	4.17×10^5	1.31×10^5	1.31×10^5
1997	4.17×10^5	8.93×10^4	1.26×10^5
1998	4.17×10^5	1.01×10^5	1.31×10^5
1999	4.17×10^5	8.93×10^4	1.26×10^5
2000	4.17×10^5	1.01×10^5	1.24×10^5
2001	4.02×10^5	8.93×10^4	1.28×10^5

The effective height of the release is not always the same as the actual physical height. The upward momentum of released effluents will tend to make the effective height greater than the actual height. Plume rise should be simply calculated by applying the mean wind speed to the following equation:

$$H = \frac{3 \cdot W \cdot D}{U} \qquad \text{(I.9.1)}$$

where:

H is plume rise (m);
W is the exit velocity of the stack gases ($m\ s^{-1}$);
D is the diameter of the stack outlet (m); and
U is the mean wind speed at the top of the stack ($m\ s^{-1}$).

The effective height of release can be derived from the physical stack height + plume rise. The temperatures of the stack discharges are provided in Tables I-2.1 to I-2.6 in Annex I-2.

I.9.3.2. Brief description of monitoring methods

Monitoring was accomplished by sampling airborne effluent from the stack before discharge. A portion of the airborne effluent was introduced into the ^{14}C sampler at a flow rate of 0.4 l min^{-1} for a week. Hydrocarbons and carbon monoxide were catalytically converted into the chemical form CO_2. All carbon was then absorbed as CO_2 in 200 ml of monoethanolamine (MEA; 2-aminoethanol) in a bubbler-type trap after the discharge stream had passed through a dehumidifier to remove water vapor in the air. Preliminary experiments demonstrated that the CO_2 absorption efficiency of the trap was almost 100%. At the end of the given sampling period, an aliquot of the MEA was mixed with liquid scintillator and methanol. The ^{14}C activity of this sample was measured using a liquid scintillation counter over 180 minutes of measurement time. The concentration of ^{14}C in the airborne effluent was evaluated using the resulting activity measurement and parameters such as the volume of MEA used for sample preparation and the total volume of air collected. The ^{14}C activity discharged in the given period was estimated by multiplying the ^{14}C concentration by the volumetric air throughput of the stack [I.5]. Weekly monitoring was accomplished typically by Wednesday-Wednesday sampling.

I.9.3.3. Data of ^{14}C discharge rates

Reporting the monitoring data of ^{14}C in airborne effluent from the TRP was officially started in October 1991 for the main and sub-1 stacks. In the case of the sub-2 stack, data on ^{14}C in airborne releases has been reported since September 1994. The numerical weekly monitoring data from October 1991 to December 2001 are provided in Tables I.2-7 to I.2-12 in Annex I-2 [I.6].

Figure I.9.2 shows the annual discharge rates of ^{14}C from the three stacks. It should be noted that a fire and explosion accident at the bituminization demonstration facility in March 1997 stopped TRP operations until July 2000. Monthly atmospheric ^{14}C discharges from the three stacks are plotted in Figures I.9.3–I.9.5. The monthly discharge from the TRP as a whole (the total from the three stacks) is shown in Figure I.9.6. The total annual ^{14}C discharge was always considerably lower than the authorized limit in the Safety Regulations for the TRP.

I.9.4. Environmental monitoring

I.9.4.1. Monitoring items and locations

Environmental monitoring of ^{14}C has been carried out mainly for two items: (1) atmospheric ^{14}C in CO_2 form; and (2) ^{14}C in polished rice grain. The atmospheric $^{14}CO_2$ has been sampled every month at five locations. Polished rice grain has been collected at three locations around the TRP in the rice harvest season. A map showing the locations of the $^{14}CO_2$ and rice grain sampling sites is presented in Figure I.9.7. Detailed information on the sampling locations and available data is summarized in Table I.9.2. Longitudinal and latitudinal data of the discharge sources and sampling locations are presented in Table I.9.3. The sampling points ST-1 and R-1 are located about 0.6 km west north-west and 2.1 km west-southwest of the sub-1 stack, respectively.

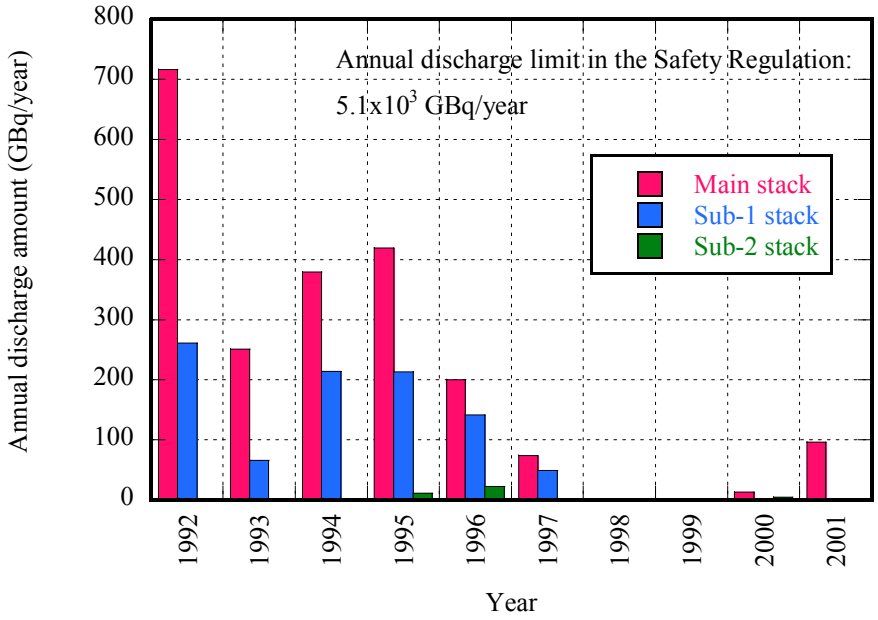

Fig. I.9.2. Annual discharge rates of ^{14}C from the three TRP stacks.

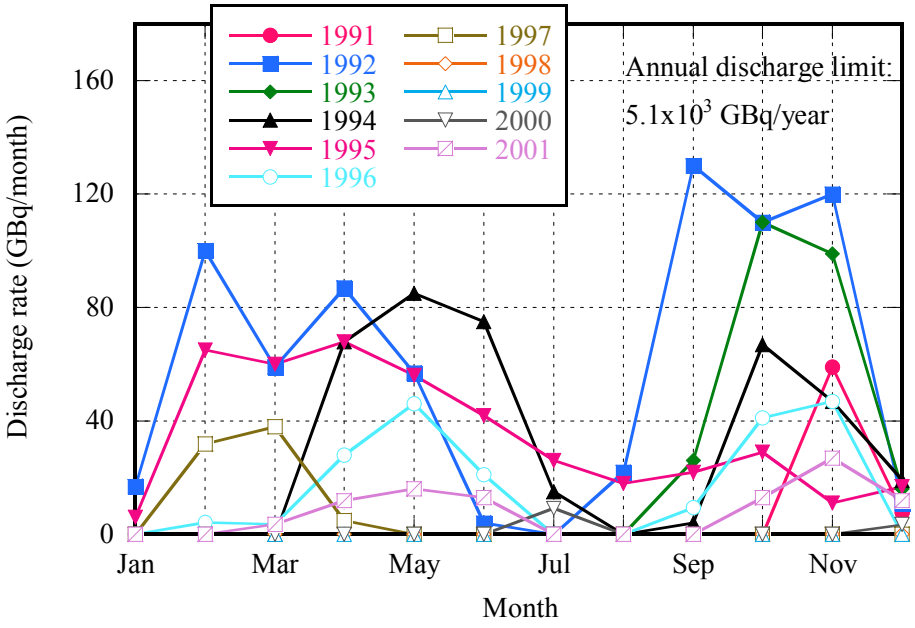

Fig. I.9.3. Monthly discharge rates of ^{14}C from the main stack.

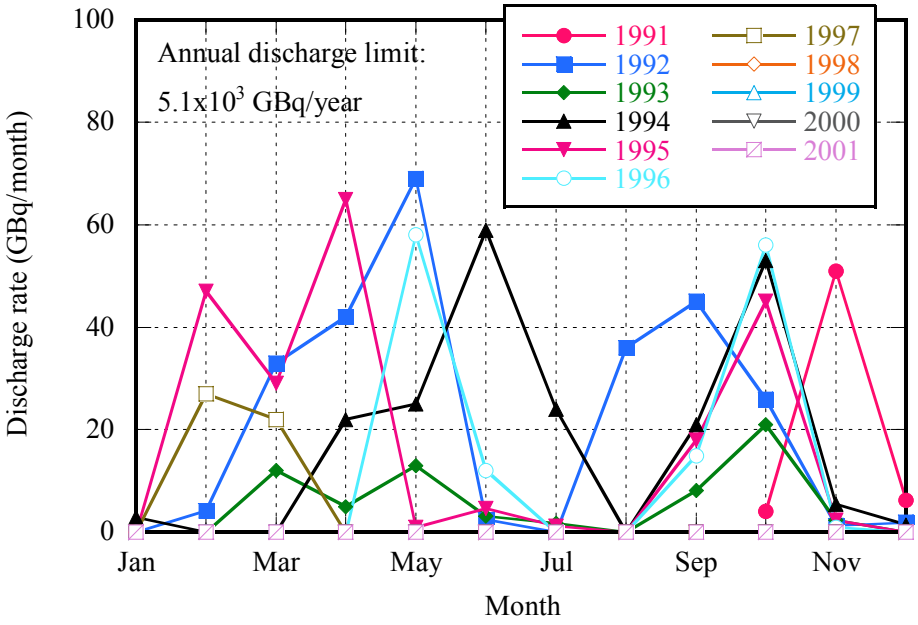

Fig. I.9.4. Monthly discharge rates of ^{14}C from the sub-1 stack.

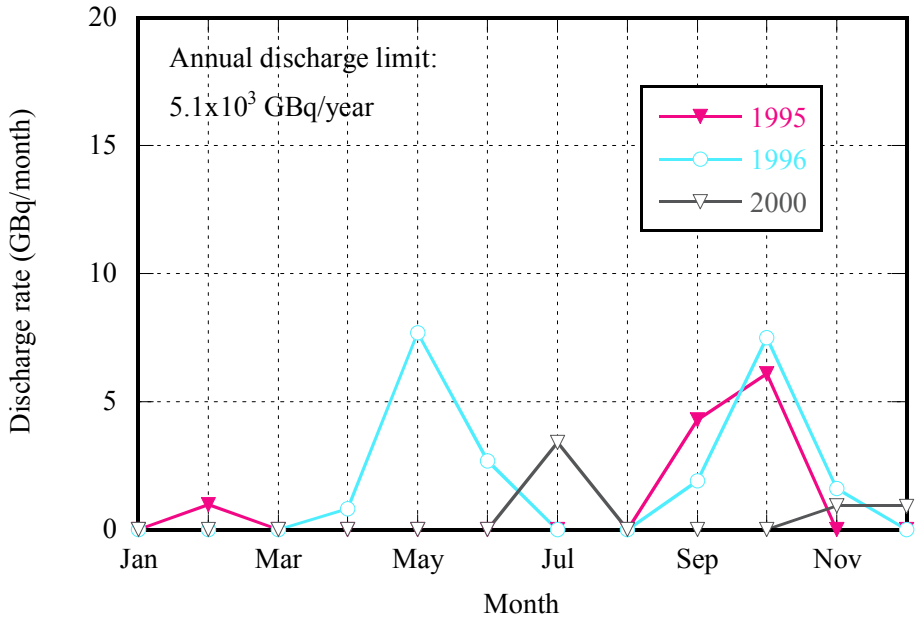

Fig.I.9.5. Monthly discharge rates of ^{14}C from the sub-2 stack.

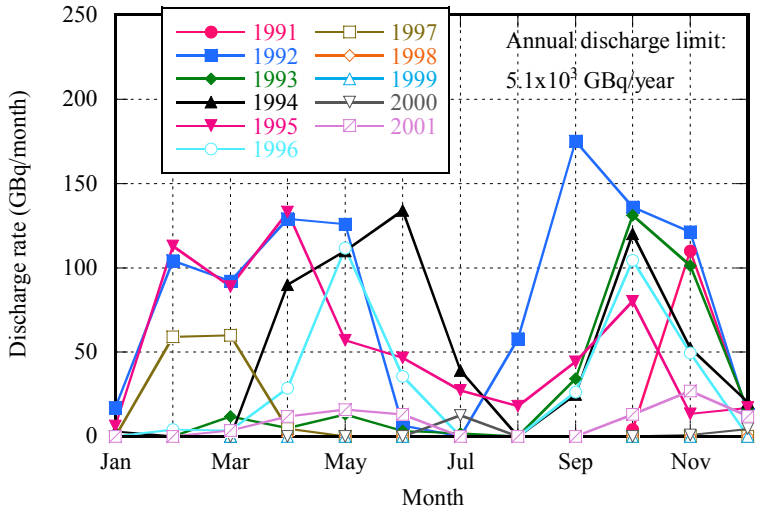

Fig. I.9.6. Monthly discharge rates of ^{14}C from the TRP as a whole.

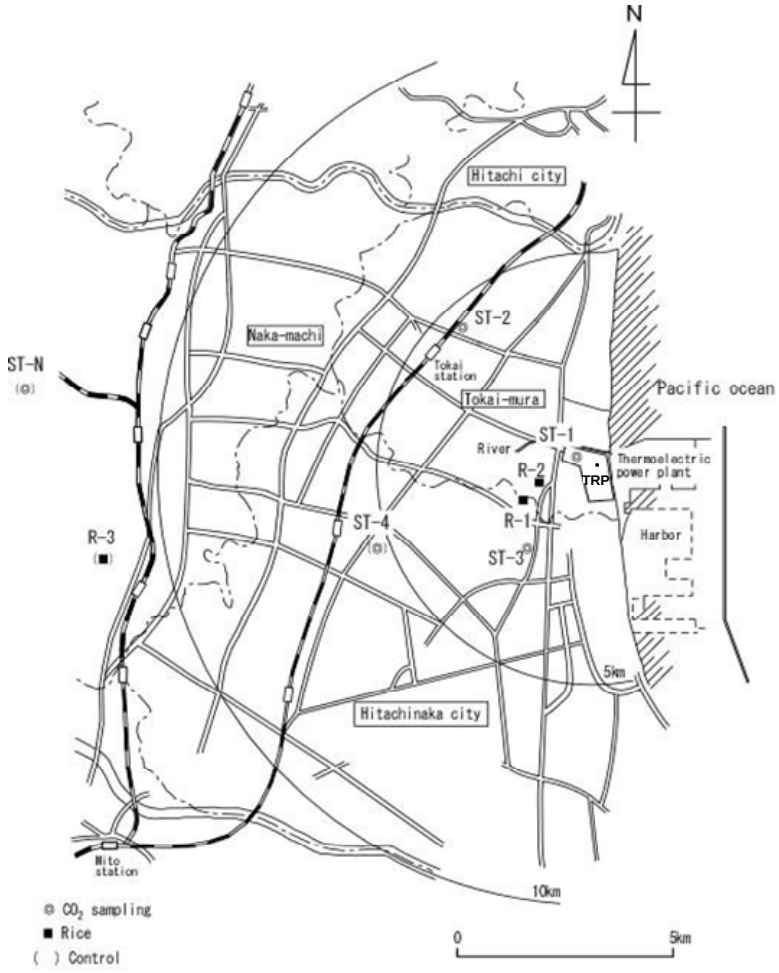

Fig. I.9.7. Map showing the sampling sites for $^{14}CO_2$ and rice grain.

Table I.9.2. Information on sampling sites and available data for 1991–2001.

Item	Location	Distance and direction from main stack	Available data	Notes
$^{14}CO_2$	ST-1	0.5 km northwest	Jan.1991–Feb.1994	
	ST-2	4.2 km northwest	Apr.1993–Mar.1994	
	ST-3	2.8 km southwest	Jan.1991–Jan.1997	
	ST-4	5.2 km west-southwest	May 1991–Dec.1995	Control
	ST-N	14.6 km west-northwest	Jan.1991–June 1996	Control
Rice grain	R-1	1.9 km west-southwest	1991–2001	
	R-2	1.0 km west	1991–2001	
	R-3	11.8 km west	1991–2001	Control

Table I.9.3. Longitude and latitude of the discharge sources and sampling sites.

Item	Location	Longitude	Latitude	Notes
Source	Main stack	36° 26’ 36.1” N	140° 36’ 19.0” E	
	Sub-1 stack	36° 26’ 38.5” N	140° 36’ 26.8” E	
	Sub-2 stack	36° 26’ 35.2” N	140° 36’ 18.1” E	
$^{14}CO_2$	ST-1	36° 26’ 46.1” N	140° 36’ 05.6” E	
	ST-2	36° 28’ 20.2” N	140° 34’ 33.7” E	
	ST-3	36° 25’ 24.0” N	140° 35’ 10.7” E	
	ST-4	36° 25’ 37.7” N	140° 32’ 55.3” E	Control
	ST-N	36° 28’ 27.2” N	140° 26’ 41.0” E	Control
Rice grain	R-1	36° 26’ 11.1” N	140° 35’ 10.3” E	
	R-2	36° 26’ 26.7” N	140° 35’ 39.9” E	
	R-3	36° 26’ 08.1” N	140° 28’ 19.5” E	Control

I.9.4.2. Brief descriptions of monitoring methods

A CO_2 sampler was used to monitor monthly $^{14}CO_2$ concentrations in the atmosphere. In the sampler, ^{14}C in CO_2 form was absorbed in an NaOH solution with stable CO_2, forming $CaCO_3$ precipitate with NH_4Cl and $CaCl_2$ after sampling. The precipitate was decomposed with H_3PO_4 to re-generate CO_2, which was converted to C_2H_2 in a reaction of metallic lithium with water, and then C_6H_6 was synthesized by polymerization of the C_2H_2. The C_6H_6 was mixed with liquid scintillator for measuring ^{14}C activity (in Bq/gC) by liquid scintillation counting. The error of the ^{14}C measurement was normally ± 0.003 Bq/gC, which represents one standard deviation associated with counting the activity.

Rice grain was completely combusted in a pressurized combustion chamber filled with oxygen. The resulting CO_2 was converted to C_6H_6 and analyzed for ^{14}C activity (Bq/gC) in the same manner as the air $^{14}CO_2$ measurement described above. The error of the ^{14}C activity was within ± 0.003 Bq/gC. The carbon-14 activity per unit weight of rice (Bq/kg-raw) also could be calculated by multiplying the concentration in Bq/gC by a factor 0.41, the carbon content (gC/g-raw) of rice.

I.9.4.3. Carbon-14 in polished rice grain in 1991

The ^{14}C activities of rice grain samples collected in 1991 showed no or little enhancement above the background level in Japan, although small amounts of ^{14}C had been discharged into the atmosphere from the TRP. This implies that the accumulation of ^{14}C discharged in the past on the paddy field was negligible as the starting point of the model calculation (1991) in this scenario.

I.9.5. Meteorological monitoring

Meteorological monitoring was made at ten minute intervals for the following variables:

(1) Wind direction and speed (m s^{-1}) 10 m above the ground;
(2) Wind direction and speed (m s^{-1}) at the top of stack, 90 m above the ground;
(3) Rainfall (mm);
(4) Atmospheric temperature (^{o}C) and relative humidity (%) 1.5 m above ground;
(5) Solar radiation (kW m^{-2}); and
(6) Atmospheric stability.

Variable (2) was monitored at the top of a meteorological observation tower built on the JAEA site. The height of the tower is about 100 m above sea level, corresponding to the physical height of the stacks. Other items were measured near the ST-1 sampling point. The meteorological data averaged over hourly periods are available as input for model calculations.

I.9.6. Other information

I.9.6.1. Background levels of ^{14}C in Japan

Fuma et al. [I.7] reported environmental background ^{14}C levels in Japan in the 1990s. They selected grapes as an indicator of ^{14}C levels in the environment, and determined the specific activities of ^{14}C in ethanol extracted from wine made from grapes cultivated in several prefectures or unknown places in Japan. The specific activities of ^{14}C gradually decreased from 0.260 Bq/gC in 1991 to 0.244 Bq/gC in 2000 (Table I.9.4).

I.9.6.2. Other nuclear facilities in Tokai-mura

It should be noted that there are other potential ^{14}C sources in Tokai-mura, such as a BWR (which began operation in November 1978) and a gas cooled reactor (GCR, which operated from July 1966 to March 1998). These reactors are located about 3-4 km north-northeast of the TRP site (Figure I.9.1).

I.9.6.3. CO_2 concentration

A thermoelectric power plant near the JAEA site (Figure I.9.7) began operation in December 2003. Therefore, CO_2 concentrations in air in the area are believed to be in the range of those in rural areas in Japan in the period 1991-2001. As an example, the CO_2 concentration 30 cm above ground in Tokai-mura was estimated to be approximately 380-390 ppmv in 2000 [I.8].

I.9.6.4. Management of a paddy field

A schedule for managing paddy fields in Tokai-mura in 1999 is presented in Table I.9.5. Panoramic photographs of paddy fields are shown in Figure I.9.8. For the period 1991 to 2001, the dates of transplanting, flowering and harvesting were 10-15 May, 15-20 August, and 18-25 September, respectively, indicating that the timing of each stage is constant within 7 days.

Table I.9.4. Environmental background ^{14}C levels in Japan in the 1990s.

Year	Specific activity of ^{14}C (Bq/gC)
1991	0.261 ± 0.002[a]
1992	0.264 ± 0.005
1993	0.254 ± 0.003
1994	0.255 ± 0.003
1995	0.254 ± 0.004
1996	0.251 ± 0.002
1997	0.250 ± 0.002
1998	0.252 ± 0.003
1999	0.248 ± 0.004
2000	0.244 ± 0.002

[a] Standard deviation (1σ) of the mean.

Table I.9.5. A schedule for managing paddy fields in 1999 in Tokai-mura.

Date	Growing stage	Days after transplanting	Depth of water (cm)	Dry/wet ratio of soil weight (%)
12 May	Transplanting	–	0–3	50.9
15 July	Midseason drainage	60	2–5	58.2
4 August	Flowering (Early ripening)	80	3–5	–
20 September	Harvest	130	0	–
28 September	After harvest	140	0	74.1

Table I.9.6. Growth of a rice plant in Hokkaido.

Days after transplanting	Growth stage	Total weight (g-dry/stock)	Weights of four components (g-dry/stock)			
			Ears	Stems, leaves and roots	Easily respired-substrate	Stored substrate
50	Vegetative	18.2	0.7	8.0	6.2	3.3
70	Flowering	54.1	6.4	23.1	14.8	9.8
100	Milky	78.5	19.2	29.3	17.0	13.0
120	Harvest	91.6	30.0	30.6	17.9	13.1

Table I.9.7. Growth of a rice plant in Ibaraki.

Days after transplanting	Total weight (g-dry/m^2)	Weight (g-dry/m^2)			
		Leaf	Stem	Ear stem	Ear
49	90	53	37	–	–
62	346	179	167	–	–
74	629	238	391	–	–
82	849	233	569	–	47
97	1152	209	520	–	423
118	1174	140	409	20	605

Fig. I.9.8. Paddy field (a) before transplanting rice plants (10 May 1999); (b) after transplanting rice plants (12 May 1999); (c) in the flowering stage (3 August 1999); and (d) in the late ripening stage (13 September 1999).

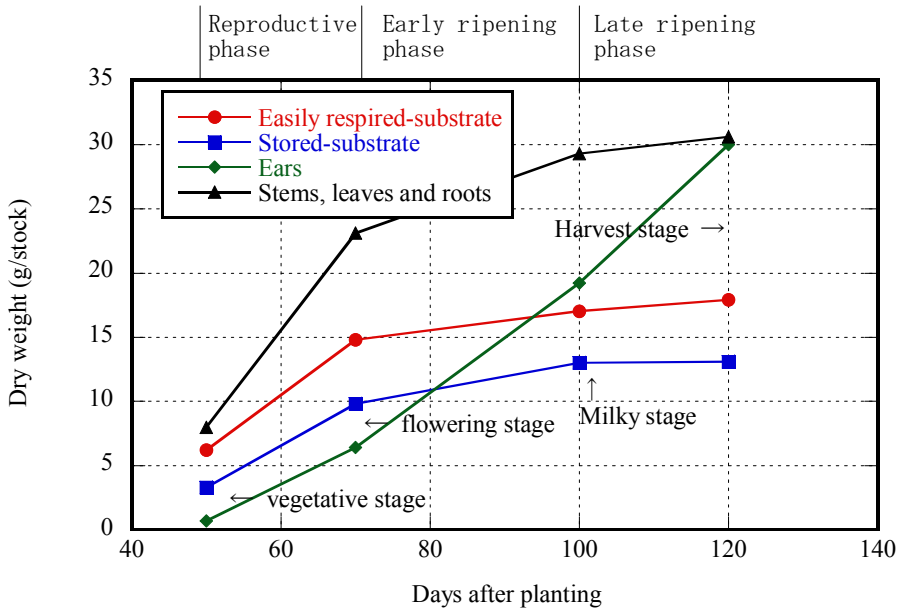

Fig. I.9.9. Growth curves of four components in rice plants.

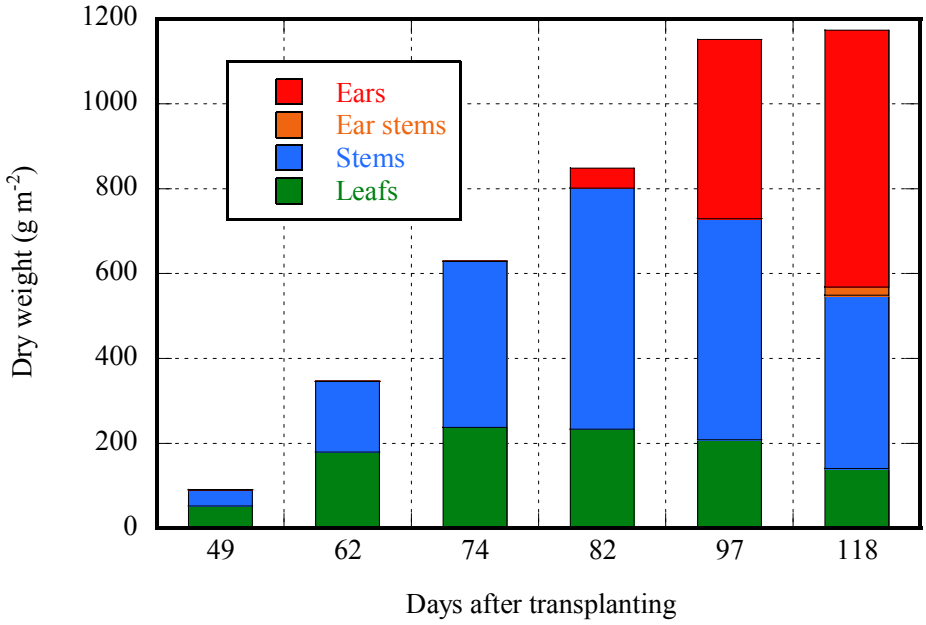

Fig. I.9.10. Growth of four components of a rice plant in Ibaraki.

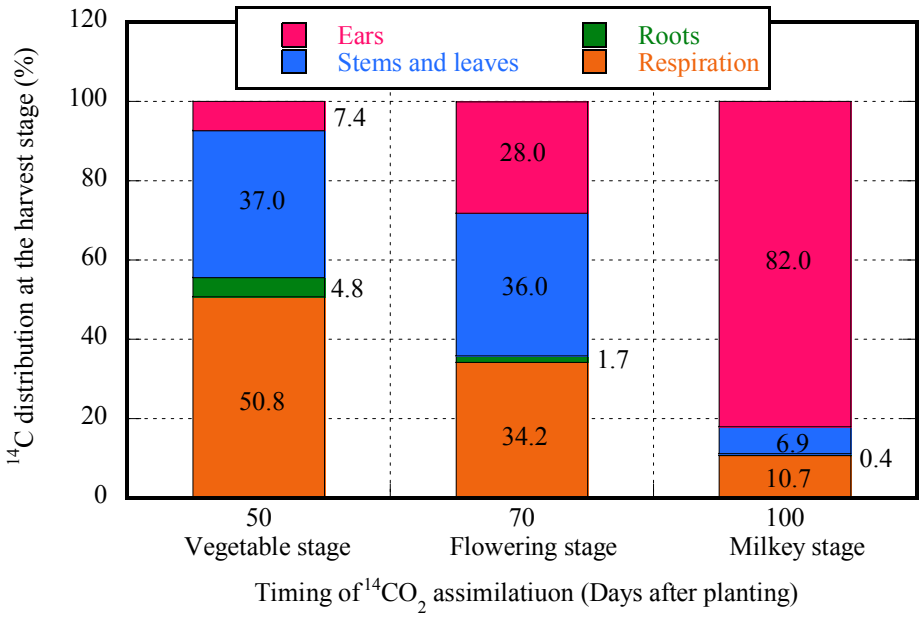

Fig. I.9.11. Distribution percentages of assimilated-^{14}C at harvest.

I.9.6.5. Growth curves of a rice plant

Osaki and Tanaka [I.9] investigated growth curves of four components of a rice plant in Hokkaido, the northernmost island of Japan. Figure I.9.9 shows growth curves determined at four stages of growth: (1) the vegetative stage; (2) the flowering stage; (3) the milky stage; and (4) the harvest stage. The easily-respired substrate and the stored substrate increased rapidly in the reproductive phase. Here, the easily-respired substrate means the photosynthesized-substrate released by respiration within a day after CO_2 assimilation. The stored substrate is temporarily stored in the plant, but is respired from the plant by harvesting. The dry weights of stems, leaves and roots had a remarkable increase until the milky stage. The dry weight of the ears showed a different growth rate, increasing sharply in the ripening phases. At the harvest stage, the dry weights of the harvest organs (the ears) and non-harvest organs (stems, leaves and roots) were almost the same (30 g dry weight per stock, where a stock is a unit bunch of pieces of rice plant). Numerical data on the growth curves is given in Table I.9.6.

Kondo [I.10] investigated the growth curves of four components (leaves, stems, ear stems and ears) of a rice plant (koshihikari) in more detail in Ibaraki in 2004. The rice plants were transplanted on 7 May. Figure I.9.10 shows growth curves determined at 6 growth stages, and numerical data are provided in Table I.9.7.

I.9.6.6. Storage and distribution of assimilated-^{14}C in rice plants

Osaki and Tanaka [I.9] also investigated storage and distribution of assimilated-^{14}C in rice plants in Hokkaido. Carbon-14 was fed to rice plants at three different growth stages (vegetative, flowering and milky), and the ^{14}C retention ratio and its distribution in three components of the plant was determined at harvest. The results are presented in Figure I.9.11. The total ^{14}C-retention percentages were approximately 50%, 65% and 90% for ^{14}C-assimilation at vegetative, flowering and milky stages, respectively. The ^{14}C-distribution percentages in ears at the harvest stage were about 7%, 28% and 82% when ^{14}C was fed at the vegetative, flowering and milky stages respectively. These data suggest that, during ripening, photosynthates are efficiently translocated to the harvest organs (ears).

I.9.7. Scenario calculations

From the information provided above, calculate:

(1) Monthly mean ^{14}C concentrations (Bq/gC) in air collected at four monitoring points (ST-1 to ST-3, and ST-N) from May to October (i.e. the rice growing season) for 1992 to 1997.
(2) Carbon-14 concentrations (Bq/gC) in rice grains collected at three monitoring points (R-1, R-2 and R-3) for 1992 to 2001.
(3) 95% confidence intervals on all predictions in (1) and (2) above.

ANNEX I-2. STACK GAS TEMPERATURES AND WEEKLY DISCHARGE RATES OF AIRBORNE ^{14}C

Table I-2.1. Temperature of stack discharges (1991–1992).

Week No.	1991				1992			
		Temperature (°C)				Temperature (°C)		
	Month	Main	Sub-1	Sub-2	Month	Main	Sub-1	Sub-2
1	Jan	24	20		Jan	25	23	
2		24	20			25	23	
3		24	21			24	23	
4		24	22			25	13	
5	Feb	24	16		Feb	25	11	
6		25	24			25	11	
7		25	26			26	21	
8		22	20			25	22	
9	Mar	25	24			25	26	
10		24	26		Mar	27	24	
11		24	24			27	27	
12		ND	ND			25	24	
13		25	24			26	26	
14	Apr	26	26		Apr	27	28	
15		26	30			26	27	
16		27	26			28	29	
17		27	27			27	29	
18	May	26	25		May	26	29	
19		29	29			24	28	
20		29	30			27	27	
21		28	29			27	27	
22	Jun	28	28			26	27	
23		30	31		Jun	28	29	
24		32	31			26	29	
25		30	30			27	27	
26		33	33			27	27	
27	Jul	33	32		Jul	29	29	
28		33	31			29	27	
29		33	30			30	27	
30		35	32			33	30	
31	Aug	33	31		Aug	34	28	
32		31	30			34	29	
33		30	29			ND	32	
34		32	31			36	32	
35		32	30			35	33	
36	Sep	32	32		Sep	31	33	
37		30	29			31	30	
38		28	28			30	29	
39		29	29			30	30	
40	Oct	28	27		Oct	29	27	
41		26	26			27	26	
42		26	27			27	26	
43		25	27			26	25	
44	Nov	24	27			24	26	
45		25	25		Nov	25	26	
46		25	27			25	24	
47		24	25			26	23	
48		26	25			26	22	
49	Dec	25	25		Dec	25	23	
50		23	23			25	23	
51		23	22			24	22	
52		22	22			23	22	
53								

ND: No data

Table I-2.2. Temperature of stack discharges (1993–1994).

Week No.	1993				1994			
		Temperature (°C)				Temperature (°C)		
	Month	Main	Sub-1	Sub-2	Month	Main	Sub-1	Sub-2
1	Jan	21	22		Jan	26	21	
2		22	13			23	19	
3		24	11			23	21	
4		26	11			24	21	
5		24	11			24	22	
6	Feb	24	13		Feb	23	22	
7		24	13			23	22	
8		25	21			25	25	
9		25	23			25	24	
10	Mar	25	24		Mar	25	24	
11		24	ND			23	23	
12		24	25			24	22	
13		25	27			24	22	
14	Apr	25	26		Apr	26	24	
15		24	26			27	25	
16		24	26			27	26	
17		24	29			28	26	
18	May	26	25		May	28	26	
19		30	27			30	27	
20		29	27			29	27	
21		30	29			28	28	
22		36	30			31	30	
23	Jun	31	29		Jun	31	29	
24		28	29			32	30	
25		30	30			32	29	
26		30	30			31	29	
27	Jul	28	28		Jul	32	30	
28		28	29			33	31	
29		28	27			35	30	
30		29	28			35	32	
31		32	29			35	30	
32	Aug	29	27		Aug	36	32	
33		31	29			37	37	
34		32	30			33	31	
35		33	29			32	30	
36	Sep	29	32		Sep	34	30	27
37		30	28			34	31	27
38		32	31			31	30	27
39		28	29			40	30	30
40	Oct	32	29		Oct	32	30	31
41		27	27			32	31	31
42		27	27			32	30	29
43		28	27			28	28	27
44		30	27			28	27	26
45	Nov	31	26		Nov	26	26	24
46		30	26			27	26	27
47		27	26			27	25	23
48		24	23			25	23	28
49	Dec	25	23		Dec	24	23	24
50		24	19			23	24	30
51		25	24			22	20	24
52		26	ND			23	19	23
53						24	19	24

ND: No data

Table I-2.3. Temperature of stack discharges (1995–1996).

Week No.	1995				1996			
		Temperature (°C)				Temperature (°C)		
	Month	Main	Sub-1	Sub-2	Month	Main	Sub-1	Sub-2
1	Jan	25	20	24	Jan	20	19	22
2		22	19	24		21	ND	22
3		22	20	23		18	16	22
4		24	29	24		19	22	22
5	Feb	26	32	23	Feb	20	18	21
6		26	32	23		30	22	23
7		26	32	23		29	22	23
8		26	33	24		30	24	23
9	Mar	26	33	24	Mar	23	24	23
10		25	31	24		25	22	22
11		26	27	23		24	22	23
12		25	26	24		23	22	22
13	Apr	25	26	23		23	24	22
14		26	28	23	Apr	25	24	22
15		28	29	23		25	23	22
16		28	28	24		25	24	22
17		28	28	25		26	26	22
18	May	27	27	24	May	27	26	24
19		28	28	25		26	26	22
20		29	29	25		27	26	23
21		30	30	26		29	24	25
22	Jun	30	28	27	Jun	29	29	27
23		29	27	26		30	28	25
24		30	28	26		30	29	24
25		30	29	25		31	30	25
26	Jul	30	29	26		30	31	25
27		31	30	25	Jul	31	30	26
28		32	31	25		32	30	25
29		32	31	25		33	31	29
30		36	33	28		34	31	27
31	Aug	35	32	25	Aug	34	30	26
32		34	32	26		34	28	28
33		35	33	26		35	31	29
34		35	33	27		33	29	25
35	Sep	33	32	26		32	28	25
36		32	31	26	Sep	31	29	26
37		29	29	26		30	29	25
38		30	30	26		31	30	26
39		32	31	26		30	32	26
40	Oct	29	31	24	Oct	30	30	26
41		28	29	25		28	28	26
42		29	29	25		27	27	24
43		27	28	25		28	28	25
44	Nov	26	27	23	Nov	28	28	25
45		24	27	22		28	27	25
46		23	25	22		28	26	22
47		22	23	21		29	26	22
48	Dec	23	19	22		27	24	21
49		24	22	22	Dec	28	25	23
50		23	21	22		26	26	24
51		22	20	21		25	21	26
52		22	19	21		22	19	26
53								

ND: No data

Table I-2.4. Temperature of stack discharges (1997–1998).

Week No.	1997				1998			
		Temperature (°C)				Temperature (°C)		
	Month	Main	Sub-1	Sub-2	Month	Main	Sub-1	Sub-2
1	Jan	21	21	25	Jan	25	15	22
2		22	17	24		26	13	22
3		22	18	25		26	13	23
4		21	17	23		26	13	21
5	Feb	24	20	23		23	13	21
6		25	20	23	Feb	24	14	21
7		27	26	20		23	14	21
8		26	25	23		23	13	21
9	Mar	26	26	23		25	14	21
10		27	26	23	Mar	23	15	20
11		25	20	24		23	20	22
12		27	20	24		24	20	21
13		26	20	25		25	20	21
14	Apr	25	20	24	Apr	25	18	21
15		26	20	24		26	21	24
16		24	20	21		27	22	28
17		24	20	24		28	24	29
18	May	27	30	25	May	27	24	29
19		27	30	26		27	25	28
20		27	30	26		28	26	28
21		25	30	25		30	27	29
22		28	30	26		29	26	28
23	Jun	28	30	25	Jun	28	25	26
24		28	30	25		29	26	26
25		30	30	25		31	26	26
26		32	30	25		32	29	25
27	Jul	34	35	26	Jul	34	32	25
28		32	35	26		33	32	26
29		32	35	25		31	29	25
30		33	35	24		32	30	25
31	Aug	35	35	25	Aug	34	32	26
32		35	35	25		33	32	26
33		33	35	25		35	33	26
34		33	35	27		34	33	26
35		34	35	27		35	33	26
36	Sep	33	35	27	Sep	33	31	26
37		32	35	26		35	31	26
38		31	35	26		34	33	25
39		29	35	26		35	30	26
40	Oct	28	23	26	Oct	32	30	26
41		28	23	26		32	29	27
42		27	24	26		31	29	27
43		27	25	25		27	25	26
44	Nov	24	22	23		28	26	26
45		25	21	21	Nov	27	24	24
46		24	21	22		25	23	23
47		24	20	22		22	20	22
48		25	21	22		24	20	22
49	Dec	25	18	21	Dec	22	19	22
50		25	18	21		24	18	22
51		25	17	22		25	18	22
52		26	15	20		24	17	23
53								

Table I-2.5. Temperature of stack discharges (1999–2000).

Week No.	1999				2000			
		Temperature (°C)				Temperature (°C)		
	Month	Main	Sub-1	Sub-2	Month	Main	Sub-1	Sub-2
1	Jan	25	16	23	Jan	25	20	26
2		22	15	22		23	21	24
3		22	15	22		24	19	23
4		25	16	23		26	17	23
5		25	16	25		25	17	22
6	Feb	24	14	23	Feb	26	22	23
7		24	15	23		26	19	24
8		24	16	22		25	16	24
9		25	17	22		26	18	24
10	Mar	25	18	22	Mar	25	19	23
11		24	17	23		26	19	25
12		26	19	25		24	20	23
13		25	20	24		24	19	24
14	Apr	25	20	24	Apr	24	22	24
15		25	22	24		24	23	23
16		28	24	25		26	24	25
17		27	27	25		25	24	24
18	May	28	25	24		25	24	25
19		29	27	24	May	27	26	25
20		29	25	27		27	26	25
21		30	26	28		26	26	25
22		31	28	28		31	28	28
23	Jun	33	29	29	Jun	29	33	28
24		32	30	29		29	27	28
25		32	27	26		30	28	28
26		32	29	26		31	30	30
27	Jul	32	30	25	Jul	34	32	33
28		32	28	25		33	31	28
29		35	32	26		35	34	28
30		38	35	27		36	35	28
31		39	36	27		35	34	28
32	Aug	37	36	28	Aug	36	36	26
33		38	34	28		35	34	26
34		37	36	27		35	33	26
35		36	34	26		35	34	25
36	Sep	36	34	27	Sep	36	34	26
37		37	34	27		34	31	26
38		35	32	27		34	34	25
39		33	30	26		32	30	26
40	Oct	33	30	26		30	28	27
41		30	27	26	Oct	29	27	28
42		29	27	26		29	28	24
43		27	23	25		27	27	23
44		29	25	28		26	24	25
45	Nov	27	23	24	Nov	25	27	25
46		27	28	24		24	25	23
47		28	24	22		24	25	22
48		28	24	22		23	23	21
49	Dec	28	20	22	Dec	23	22	23
50		27	20	22		25	23	24
51		28	18	22		26	23	24
52		26	17	23		26	22	23
53						24	17	24

Table I-2.6. Temperature of stack discharges (2001).

Week No.	2001			
		Temperature (ºC)		
	Month	Main	Sub-1	Sub-2
1	Jan	24	15	24
2		24	15	29
3		23	15	24
4		23	16	24
5	Feb	25	17	23
6		25	16	25
7		24	17	25
8		25	22	23
9	Mar	26	19	25
10		25	17	25
11		27	22	22
12		25	25	24
13		25	22	23
14	Apr	26	25	24
15		28	26	25
16		27	27	25
17		27	24	24
18	May	27	23	25
19		30	28	27
20		31	32	27
21		32	32	26
22	Jun	32	33	27
23		32	31	28
24		32	33	26
25		33	33	26
26		36	37	27
27	Jul	36	36	27
28		38	39	27
29		36	35	27
30		36	35	27
31	Aug	35	34	29
32		34	31	32
33		33	31	30
34		34	32	31
35	Sep	33	29	29
36		32	32	30
37		33	34	29
38		29	29	25
39		30	28	24
40	Oct	29	29	25
41		29	30	25
42		27	28	24
43		27	29	25
44	Nov	26	29	25
45		26	24	24
46		27	25	22
47		29	26	21
48	Dec	30	25	23
49		31	22	24
50		31	21	24
51		29	19	24
52		28	19	23
53				

Table I-2.7. Weekly release rates of airborne ^{14}C from the TRP (1991–1992).

Week No.	1991				1992			
		Stack discharge (GBq/week)				Stack discharge (GBq/week)		
	Month	Main	Sub-1	Sub-2	Month	Main	Sub-1	Sub-2
1					Jan	0.0E+00	0.0E+00	
2						0.0E+00	0.0E+00	
3						0.0E+00	0.0E+00	
4						1.7E+01	0.0E+00	
5					Feb	1.9E+01	0.0E+00	
6						2.0E+01	0.0E+00	
7						2.2E+01	0.0E+00	
8						2.3E+01	0.0E+00	
9						1.7E+01	4.2E+00	
10					Mar	1.4E+01	1.3E+01	
11						2.1E+01	1.0E+01	
12						6.5E+00	6.6E+00	
13						1.8E+01	3.3E+00	
14					Apr	2.7E+01	5.1E+00	
15						2.9E+01	1.0E+01	
16						1.5E+01	1.5E+01	
17						1.6E+01	1.2E+01	
18					May	5.9E+00	1.9E+01	
19						1.2E+01	1.9E+01	
20						1.6E+01	1.4E+01	
21						1.0E+01	1.7E+01	
22						1.3E+01	0.0E+00	
23					Jun	4.0E+00	2.5E+00	
24						0.0E+00	0.0E+00	
25						0.0E+00	0.0E+00	
26						0.0E+00	0.0E+00	
27					Jul	0.0E+00	0.0E+00	
28						0.0E+00	0.0E+00	
29						0.0E+00	0.0E+00	
30						0.0E+00	0.0E+00	
31					Aug	0.0E+00	0.0E+00	
32						0.0E+00	0.0E+00	
33						0.0E+00	0.0E+00	
34						3.8E+00	5.0E+00	
35						1.9E+01	3.1E+01	
36					Sep	3.1E+01	1.1E+01	
37						3.3E+01	1.1E+01	
38						2.8E+01	1.0E+01	
39						4.1E+01	1.3E+01	
40	Oct	0.0E+00	0.0E+00		Oct	2.3E+01	1.3E+01	
41		0.0E+00	0.0E+00			1.6E+01	9.4E+00	
42		0.0E+00	0.0E+00			1.4E+01	1.9E+00	
43		0.0E+00	4.1E+00			4.0E+01	1.2E+00	
44	Nov	0.0E+00	1.1E+00			1.6E+01	0.0E+00	
45		1.6E+01	1.7E+01		Nov	3.1E+01	0.0E+00	
46		1.6E+01	1.6E+01			3.1E+01	0.0E+00	
47		1.8E+01	6.5E+00			3.9E+01	0.0E+00	
48		9.7E+00	1.0E+01			1.5E+01	1.3E+00	
49	Dec	7.8E+00	6.3E+00		Dec	5.4E+00	2.0E+00	
50		0.0E+00	0.0E+00			5.2E+00	0.0E+00	
51		0.0E+00	0.0E+00			0.0E+00	0.0E+00	
52		0.0E+00	0.0E+00			0.0E+00	0.0E+00	
53								

"0.0E+00" indicates ^{14}C concentration of airborne effluent is below the authorized detectable limit (40 Bq cm^{-3}).

Table I-2.8. Weekly release rates of airborne ^{14}C from the TRP (1993–1994).

Week No.	1993				1994			
		Stack discharge (GBq/week)				Stack discharge (GBq/week)		
	Month	Main	Sub-1	Sub-2	Month	Main	Sub-1	Sub-2
1	Jan	0.0E+00	0.0E+00		Jan	0.0E+00	0.0E+00	
2		0.0E+00	0.0E+00			0.0E+00	0.0E+00	
3		0.0E+00	0.0E+00			0.0E+00	2.9E+00	
4		0.0E+00	0.0E+00			0.0E+00	0.0E+00	
5		0.0E+00	0.0E+00			0.0E+00	0.0E+00	
6	Feb	0.0E+00	0.0E+00		Feb	0.0E+00	0.0E+00	
7		0.0E+00	0.0E+00			0.0E+00	0.0E+00	
8		0.0E+00	0.0E+00			0.0E+00	0.0E+00	
9		0.0E+00	0.0E+00			0.0E+00	0.0E+00	
10	Mar	0.0E+00	1.0E+00		Mar	0.0E+00	0.0E+00	
11		0.0E+00	3.9E+00			0.0E+00	0.0E+00	
12		0.0E+00	4.9E+00			0.0E+00	0.0E+00	
13		0.0E+00	2.5E+00			0.0E+00	0.0E+00	
14	Apr	0.0E+00	0.0E+00		Apr	1.1E+01	6.2E+00	
15		0.0E+00	0.0E+00			1.8E+01	1.0E+01	
16		0.0E+00	1.1E+00			1.1E+01	2.9E+00	
17		0.0E+00	3.9E+00			2.7E+01	2.4E+00	
18	May	0.0E+00	4.7E+00		May	2.6E+01	0.0E+00	
19		0.0E+00	4.3E+00			1.5E+01	9.8E-01	
20		0.0E+00	2.0E+00			1.1E+01	4.0E+00	
21		0.0E+00	1.7E+00			1.4E+01	6.9E+00	
22		0.0E+00	0.0E+00			2.0E+01	1.3E+01	
23	Jun	0.0E+00	1.4E+00		Jun	2.4E+01	1.1E+01	
24		0.0E+00	8.3E-01			1.8E+01	1.3E+01	
25		0.0E+00	0.0E+00			1.6E+01	1.9E+01	
26		0.0E+00	9.1E-01			1.7E+01	1.6E+01	
27	Jul	0.0E+00	0.0E+00		Jul	4.5E+00	1.6E+01	
28		0.0E+00	1.7E+00			2.8E+00	8.1E+00	
29		0.0E+00	0.0E+00			0.0E+00	0.0E+00	
30		0.0E+00	0.0E+00			4.4E+00	0.0E+00	
31		0.0E+00	0.0E+00			3.3E+00	0.0E+00	
32	Aug	0.0E+00	0.0E+00		Aug	0.0E+00	0.0E+00	
33		0.0E+00	0.0E+00			0.0E+00	0.0E+00	
34		0.0E+00	0.0E+00			0.0E+00	0.0E+00	
35		0.0E+00	0.0E+00			0.0E+00	0.0E+00	
36	Sep	0.0E+00	0.0E+00		Sep	0.0E+00	0.0E+00	0.0E+00
37		4.3E+00	0.0E+00			0.0E+00	0.0E+00	0.0E+00
38		6.9E+00	3.2E+00			0.0E+00	1.5E+00	0.0E+00
39		1.5E+01	4.9E+00			3.9E+00	1.9E+01	0.0E+00
40	Oct	1.4E+01	5.1E+00		Oct	6.0E+00	1.6E+01	0.0E+00
41		1.8E+01	5.5E+00			6.3E+00	1.3E+01	0.0E+00
42		3.4E+01	5.2E+00			2.9E+01	1.0E+01	0.0E+00
43		3.1E+01	5.3E+00			8.8E+00	1.3E+01	0.0E+00
44		1.2E+01	0.0E+00			1.7E+01	1.6E+00	0.0E+00
45	Nov	2.3E+01	2.3E+00		Nov	2.1E+01	1.6E+00	0.0E+00
46		3.1E+01	0.0E+00			1.1E+01	1.3E+00	0.0E+00
47		1.9E+01	0.0E+00			7.6E+00	1.5E+00	0.0E+00
48		2.6E+01	0.0E+00			7.6E+00	1.3E+00	0.0E+00
49	Dec	7.2E+00	0.0E+00		Dec	1.3E+01	1.4E+00	0.0E+00
50		4.4E+00	0.0E+00			3.3E+00	0.0E+00	0.0E+00
51		4.4E+00	0.0E+00			0.0E+00	0.0E+00	0.0E+00
52		0.0E+00	0.0E+00			2.8E+00	0.0E+00	0.0E+00
53						0.0E+00	0.0E+00	0.0E+00

"0.0E+00" indicates ^{14}C concentration of airborne effluent is below the authorized detectable limit (40 Bq cm^{-3}).

Table I-2.9. Weekly release rates of airborne ^{14}C from the TRP (1995–1996).

Week No.	1995				1996			
		Stack discharge (GBq/week)				Stack discharge (GBq/week)		
	Month	Main	Sub-1	Sub-2	Month	Main	Sub-1	Sub-2
1	Jan	0.0E+00	0.0E+00	0.0E+00	Jan	0.0E+00	0.0E+00	0.0E+00
2		0.0E+00	0.0E+00	0.0E+00		0.0E+00	0.0E+00	0.0E+00
3		0.0E+00	0.0E+00	0.0E+00		0.0E+00	0.0E+00	0.0E+00
4		6.1E+00	0.0E+00	0.0E+00		0.0E+00	0.0E+00	0.0E+00
5	Feb	7.9E+00	1.5E+01	0.0E+00	Feb	4.2E+00	0.0E+00	0.0E+00
6		1.1E+01	8.4E+00	0.0E+00		0.0E+00	0.0E+00	0.0E+00
7		1.2E+01	1.2E+01	9.7E-01		0.0E+00	0.0E+00	0.0E+00
8		3.5E+01	1.2E+01	0.0E+00		0.0E+00	0.0E+00	0.0E+00
9	Mar	1.4E+01	6.4E+00	0.0E+00	Mar	0.0E+00	0.0E+00	0.0E+00
10		5.2E+00	5.9E+00	0.0E+00		0.0E+00	0.0E+00	0.0E+00
11		1.1E+01	7.8E+00	0.0E+00		0.0E+00	0.0E+00	0.0E+00
12		3.0E+01	8.9E+00	0.0E+00		0.0E+00	0.0E+00	0.0E+00
13	Apr	1.1E+01	1.1E+00	0.0E+00		3.5E+00	0.0E+00	0.0E+00
14		1.8E+01	2.4E+01	0.0E+00	Apr	1.0E+01	0.0E+00	0.0E+00
15		2.1E+01	2.5E+01	0.0E+00		3.8E+00	0.0E+00	0.0E+00
16		6.5E+00	1.5E+01	0.0E+00		9.4E+00	0.0E+00	0.0E+00
17		1.1E+01	0.0E+00	0.0E+00		5.0E+00	0.0E+00	8.0E-01
18	May	2.1E+01	0.0E+00	0.0E+00	May	2.7E+01	1.4E+00	1.9E+00
19		1.0E+01	0.0E+00	0.0E+00		7.7E+00	1.7E+01	1.9E+00
20		1.7E+01	0.0E+00	0.0E+00		7.6E+00	2.0E+01	1.9E+00
21		8.4E+00	1.0E+00	0.0E+00		4.5E+00	2.0E+01	2.1E+00
22	Jun	9.2E+00	1.4E+00	0.0E+00	Jun	1.1E+01	1.0E+01	1.8E+00
23		1.9E+01	1.3E+00	0.0E+00		2.8E+00	1.1E+00	9.3E-01
24		9.3E+00	1.1E+00	0.0E+00		3.4E+00	9.7E-01	0.0E+00
25		4.4E+00	9.5E-01	0.0E+00		4.1E+00	0.0E+00	0.0E+00
26	Jul	3.0E+00	1.2E+00	0.0E+00		0.0E+00	0.0E+00	0.0E+00
27		4.3E+00	0.0E+00	0.0E+00	Jul	0.0E+00	0.0E+00	0.0E+00
28		6.5E+00	0.0E+00	0.0E+00		0.0E+00	0.0E+00	0.0E+00
29		5.8E+00	0.0E+00	0.0E+00		0.0E+00	0.0E+00	0.0E+00
30		6.4E+00	0.0E+00	0.0E+00		0.0E+00	0.0E+00	0.0E+00
31	Aug	4.3E+00	0.0E+00	0.0E+00	Aug	0.0E+00	0.0E+00	0.0E+00
32		5.2E+00	0.0E+00	0.0E+00		0.0E+00	0.0E+00	0.0E+00
33		4.4E+00	0.0E+00	0.0E+00		0.0E+00	0.0E+00	0.0E+00
34		4.4E+00	0.0E+00	0.0E+00		0.0E+00	0.0E+00	0.0E+00
35	Sep	2.9E+00	0.0E+00	0.0E+00		0.0E+00	0.0E+00	0.0E+00
36		3.0E+00	0.0E+00	0.0E+00	Sep	0.0E+00	0.0E+00	0.0E+00
37		6.0E+00	0.0E+00	0.0E+00		0.0E+00	0.0E+00	0.0E+00
38		3.5E+00	4.5E+00	1.9E+00		4.6E+00	1.4E+00	0.0E+00
39		6.6E+00	1.4E+01	2.4E+00		4.9E+00	1.3E+01	1.9E+00
40	Oct	6.8E+00	1.2E+01	1.8E+00	Oct	1.1E+01	2.0E+01	1.8E+00
41		1.6E+01	7.7E+00	2.0E+00		7.8E+00	1.5E+01	1.7E+00
42		6.2E+00	1.7E+01	2.2E+00		1.2E+01	1.5E+01	2.0E+00
43		0.0E+00	8.9E+00	0.0E+00		1.0E+01	5.4E+00	2.0E+00
44	Nov	7.3E+00	1.2E+00	0.0E+00	Nov	1.6E+01	1.0E+00	1.6E+00
45		3.6E+00	1.1E+00	0.0E+00		1.2E+01	0.0E+00	0.0E+00
46		0.0E+00	0.0E+00	0.0E+00		4.8E+00	0.0E+00	0.0E+00
47		0.0E+00	0.0E+00	0.0E+00		6.5E+00	0.0E+00	0.0E+00
48	Dec	0.0E+00	0.0E+00	0.0E+00		7.6E+00	0.0E+00	0.0E+00
49		0.0E+00	0.0E+00	0.0E+00	Dec	0.0E+00	0.0E+00	0.0E+00
50		8.8E+00	0.0E+00	0.0E+00		0.0E+00	0.0E+00	0.0E+00
51		7.7E+00	0.0E+00	0.0E+00		0.0E+00	0.0E+00	0.0E+00
52		0.0E+00	0.0E+00	0.0E+00		0.0E+00	0.0E+00	0.0E+00
53								

"0.0E+00" indicates ^{14}C concentration of airborne effluent is below the authorized detectable limit (40 Bq cm^{-3}).

Table I-2.10. Weekly release rates of airborne ^{14}C from the TRP (1997–1998).

Week No.	1997				1998			
		Stack discharge (GBq/week)				Stack discharge (GBq/week)		
	Month	Main	Sub-1	Sub-2	Month	Main	Sub-1	Sub-2
1	Jan	0.0E+00	0.0E+00	0.0E+00	Jan	0.0E+00	0.0E+00	0.0E+00
2		0.0E+00	0.0E+00	0.0E+00		0.0E+00	0.0E+00	0.0E+00
3		0.0E+00	0.0E+00	0.0E+00		0.0E+00	0.0E+00	0.0E+00
4		0.0E+00	0.0E+00	0.0E+00		0.0E+00	0.0E+00	0.0E+00
5	Feb	8.3E+00	0.0E+00	0.0E+00		0.0E+00	0.0E+00	0.0E+00
6		6.9E+00	0.0E+00	0.0E+00	Feb	0.0E+00	0.0E+00	0.0E+00
7		7.8E+00	1.2E+01	0.0E+00		0.0E+00	0.0E+00	0.0E+00
8		8.6E+00	1.4E+01	0.0E+00		0.0E+00	0.0E+00	0.0E+00
9	Mar	9.5E+00	1.2E+01	0.0E+00		0.0E+00	0.0E+00	0.0E+00
10		7.0E+00	1.0E+01	0.0E+00	Mar	0.0E+00	0.0E+00	0.0E+00
11		0.0E+00	0.0E+00	0.0E+00		0.0E+00	0.0E+00	0.0E+00
12		1.7E+01	0.0E+00	0.0E+00		0.0E+00	0.0E+00	0.0E+00
13		4.6E+00	0.0E+00	0.0E+00		0.0E+00	0.0E+00	0.0E+00
14	Apr	4.7E+00	0.0E+00	0.0E+00	Apr	0.0E+00	0.0E+00	0.0E+00
15		0.0E+00	0.0E+00	0.0E+00		0.0E+00	0.0E+00	0.0E+00
16		0.0E+00	0.0E+00	0.0E+00		0.0E+00	0.0E+00	0.0E+00
17		0.0E+00	0.0E+00	0.0E+00		0.0E+00	0.0E+00	0.0E+00
18	May	0.0E+00	0.0E+00	0.0E+00	May	0.0E+00	0.0E+00	0.0E+00
19		0.0E+00	0.0E+00	0.0E+00		0.0E+00	0.0E+00	0.0E+00
20		0.0E+00	0.0E+00	0.0E+00		0.0E+00	0.0E+00	0.0E+00
21		0.0E+00	0.0E+00	0.0E+00		0.0E+00	0.0E+00	0.0E+00
22		0.0E+00	0.0E+00	0.0E+00		0.0E+00	0.0E+00	0.0E+00
23	Jun	0.0E+00	0.0E+00	0.0E+00	Jun	0.0E+00	0.0E+00	0.0E+00
24		0.0E+00	0.0E+00	0.0E+00		0.0E+00	0.0E+00	0.0E+00
25		0.0E+00	0.0E+00	0.0E+00		0.0E+00	0.0E+00	0.0E+00
26		0.0E+00	0.0E+00	0.0E+00		0.0E+00	0.0E+00	0.0E+00
27	Jul	0.0E+00	0.0E+00	0.0E+00	Jul	0.0E+00	0.0E+00	0.0E+00
28		0.0E+00	0.0E+00	0.0E+00		0.0E+00	0.0E+00	0.0E+00
29		0.0E+00	0.0E+00	0.0E+00		0.0E+00	0.0E+00	0.0E+00
30		0.0E+00	0.0E+00	0.0E+00		0.0E+00	0.0E+00	0.0E+00
31	Aug	0.0E+00	0.0E+00	0.0E+00	Aug	0.0E+00	0.0E+00	0.0E+00
32		0.0E+00	0.0E+00	0.0E+00		0.0E+00	0.0E+00	0.0E+00
33		0.0E+00	0.0E+00	0.0E+00		0.0E+00	0.0E+00	0.0E+00
34		0.0E+00	0.0E+00	0.0E+00		0.0E+00	0.0E+00	0.0E+00
35		0.0E+00	0.0E+00	0.0E+00		0.0E+00	0.0E+00	0.0E+00
36	Sep	0.0E+00	0.0E+00	0.0E+00	Sep	0.0E+00	0.0E+00	0.0E+00
37		0.0E+00	0.0E+00	0.0E+00		0.0E+00	0.0E+00	0.0E+00
38		0.0E+00	0.0E+00	0.0E+00		0.0E+00	0.0E+00	0.0E+00
39		0.0E+00	0.0E+00	0.0E+00		0.0E+00	0.0E+00	0.0E+00
40	Oct	0.0E+00	0.0E+00	0.0E+00	Oct	0.0E+00	0.0E+00	0.0E+00
41		0.0E+00	0.0E+00	0.0E+00		0.0E+00	0.0E+00	0.0E+00
42		0.0E+00	0.0E+00	0.0E+00		0.0E+00	0.0E+00	0.0E+00
43		0.0E+00	0.0E+00	0.0E+00		0.0E+00	0.0E+00	0.0E+00
44	Nov	0.0E+00	0.0E+00	0.0E+00		0.0E+00	0.0E+00	0.0E+00
45		0.0E+00	0.0E+00	0.0E+00	Nov	0.0E+00	0.0E+00	0.0E+00
46		0.0E+00	0.0E+00	0.0E+00		0.0E+00	0.0E+00	0.0E+00
47		0.0E+00	0.0E+00	0.0E+00		0.0E+00	0.0E+00	0.0E+00
48		0.0E+00	0.0E+00	0.0E+00		0.0E+00	0.0E+00	0.0E+00
49	Dec	0.0E+00	0.0E+00	0.0E+00	Dec	0.0E+00	0.0E+00	0.0E+00
50		0.0E+00	0.0E+00	0.0E+00		0.0E+00	0.0E+00	0.0E+00
51		0.0E+00	0.0E+00	0.0E+00		0.0E+00	0.0E+00	0.0E+00
52		0.0E+00	0.0E+00	0.0E+00		0.0E+00	0.0E+00	0.0E+00
53								

"0.0E+00" indicates ^{14}C concentration of airborne effluent is below the authorized detectable limit (40 Bq cm^{-3}).

Table I-2.11. Weekly release rates of airborne ^{14}C from the TRP (1999–2000).

Week No.	1999				2000			
		Stack discharge (GBq/week)				Stack discharge (GBq/week)		
	Month	Main	Sub-1	Sub-2	Month	Main	Sub-1	Sub-2
1	Jan	0.0E+00	0.0E+00	0.0E+00	Jan	0.0E+00	0.0E+00	0.0E+00
2		0.0E+00	0.0E+00	0.0E+00		0.0E+00	0.0E+00	0.0E+00
3		0.0E+00	0.0E+00	0.0E+00		0.0E+00	0.0E+00	0.0E+00
4		0.0E+00	0.0E+00	0.0E+00		0.0E+00	0.0E+00	0.0E+00
5		0.0E+00	0.0E+00	0.0E+00		0.0E+00	0.0E+00	0.0E+00
6	Feb	0.0E+00	0.0E+00	0.0E+00	Feb	0.0E+00	0.0E+00	0.0E+00
7		0.0E+00	0.0E+00	0.0E+00		0.0E+00	0.0E+00	0.0E+00
8		0.0E+00	0.0E+00	0.0E+00		0.0E+00	0.0E+00	0.0E+00
9		0.0E+00	0.0E+00	0.0E+00		0.0E+00	0.0E+00	0.0E+00
10	Mar	0.0E+00	0.0E+00	0.0E+00	Mar	0.0E+00	0.0E+00	0.0E+00
11		0.0E+00	0.0E+00	0.0E+00		0.0E+00	0.0E+00	0.0E+00
12		0.0E+00	0.0E+00	0.0E+00		0.0E+00	0.0E+00	0.0E+00
13		0.0E+00	0.0E+00	0.0E+00		0.0E+00	0.0E+00	0.0E+00
14	Apr	0.0E+00	0.0E+00	0.0E+00	Apr	0.0E+00	0.0E+00	0.0E+00
15		0.0E+00	0.0E+00	0.0E+00		0.0E+00	0.0E+00	0.0E+00
16		0.0E+00	0.0E+00	0.0E+00		0.0E+00	0.0E+00	0.0E+00
17		0.0E+00	0.0E+00	0.0E+00		0.0E+00	0.0E+00	0.0E+00
18	May	0.0E+00	0.0E+00	0.0E+00		0.0E+00	0.0E+00	0.0E+00
19		0.0E+00	0.0E+00	0.0E+00	May	0.0E+00	0.0E+00	0.0E+00
20		0.0E+00	0.0E+00	0.0E+00		0.0E+00	0.0E+00	0.0E+00
21		0.0E+00	0.0E+00	0.0E+00		0.0E+00	0.0E+00	0.0E+00
22		0.0E+00	0.0E+00	0.0E+00		0.0E+00	0.0E+00	0.0E+00
23	Jun	0.0E+00	0.0E+00	0.0E+00	Jun	0.0E+00	0.0E+00	0.0E+00
24		0.0E+00	0.0E+00	0.0E+00		0.0E+00	0.0E+00	0.0E+00
25		0.0E+00	0.0E+00	0.0E+00		0.0E+00	0.0E+00	0.0E+00
26		0.0E+00	0.0E+00	0.0E+00		0.0E+00	0.0E+00	0.0E+00
27	Jul	0.0E+00	0.0E+00	0.0E+00	Jul	0.0E+00	0.0E+00	9.6E-01
28		0.0E+00	0.0E+00	0.0E+00		0.0E+00	0.0E+00	1.4E+00
29		0.0E+00	0.0E+00	0.0E+00		3.4E+00	0.0E+00	1.1E+00
30		0.0E+00	0.0E+00	0.0E+00		0.0E+00	0.0E+00	0.0E+00
31		0.0E+00	0.0E+00	0.0E+00		5.8E+00	0.0E+00	0.0E+00
32	Aug	0.0E+00	0.0E+00	0.0E+00	Aug	0.0E+00	0.0E+00	0.0E+00
33		0.0E+00	0.0E+00	0.0E+00		0.0E+00	0.0E+00	0.0E+00
34		0.0E+00	0.0E+00	0.0E+00		0.0E+00	0.0E+00	0.0E+00
35		0.0E+00	0.0E+00	0.0E+00		0.0E+00	0.0E+00	0.0E+00
36	Sep	0.0E+00	0.0E+00	0.0E+00	Sep	0.0E+00	0.0E+00	0.0E+00
37		0.0E+00	0.0E+00	0.0E+00		0.0E+00	0.0E+00	0.0E+00
38		0.0E+00	0.0E+00	0.0E+00		0.0E+00	0.0E+00	0.0E+00
39		0.0E+00	0.0E+00	0.0E+00		0.0E+00	0.0E+00	0.0E+00
40	Oct	0.0E+00	0.0E+00	0.0E+00		0.0E+00	0.0E+00	0.0E+00
41		0.0E+00	0.0E+00	0.0E+00	Oct	0.0E+00	0.0E+00	0.0E+00
42		0.0E+00	0.0E+00	0.0E+00		0.0E+00	0.0E+00	0.0E+00
43		0.0E+00	0.0E+00	0.0E+00		0.0E+00	0.0E+00	0.0E+00
44		0.0E+00	0.0E+00	0.0E+00		0.0E+00	0.0E+00	0.0E+00
45	Nov	0.0E+00	0.0E+00	0.0E+00	Nov	0.0E+00	0.0E+00	0.0E+00
46		0.0E+00	0.0E+00	0.0E+00		0.0E+00	0.0E+00	0.0E+00
47		0.0E+00	0.0E+00	0.0E+00		0.0E+00	0.0E+00	0.0E+00
48		0.0E+00	0.0E+00	0.0E+00		0.0E+00	0.0E+00	9.4E-01
49	Dec	0.0E+00	0.0E+00	0.0E+00	Dec	0.0E+00	0.0E+00	0.0E+00
50		0.0E+00	0.0E+00	0.0E+00		0.0E+00	0.0E+00	9.1E-01
51		0.0E+00	0.0E+00	0.0E+00		3.7E+00	0.0E+00	0.0E+00
52		0.0E+00	0.0E+00	0.0E+00		0.0E+00	0.0E+00	0.0E+00
53						0.0E+00	0.0E+00	0.0E+00

"0.0E+00" indicates ^{14}C concentration of airborne effluent is below the authorized detectable limit (40 Bq cm^{-3}).

Table I-2.12. Weekly release rates of airborne ^{14}C from the TRP (2001).

Week No.	2001							
		Stack discharge (GBq/week)				Stack discharge (GBq/week)		
	Month	Main	Sub-1	Sub-2	Month	Main	Sub-1	Sub-2
1	Jan	0.0E+00	0.0E+00	0.0E+00				
2		0.0E+00	0.0E+00	0.0E+00				
3		0.0E+00	0.0E+00	0.0E+00				
4		0.0E+00	0.0E+00	0.0E+00				
5	Feb	0.0E+00	0.0E+00	0.0E+00				
6		0.0E+00	0.0E+00	0.0E+00				
7		0.0E+00	0.0E+00	0.0E+00				
8		0.0E+00	0.0E+00	0.0E+00				
9	Mar	0.0E+00	0.0E+00	0.0E+00				
10		0.0E+00	0.0E+00	0.0E+00				
11		0.0E+00	0.0E+00	0.0E+00				
12		0.0E+00	0.0E+00	0.0E+00				
13		3.6E+00	0.0E+00	0.0E+00				
14	Apr	0.0E+00	0.0E+00	0.0E+00				
15		3.8E+00	0.0E+00	0.0E+00				
16		4.8E+00	0.0E+00	0.0E+00				
17		3.7E+00	0.0E+00	0.0E+00				
18	May	3.1E+00	0.0E+00	0.0E+00				
19		3.8E+00	0.0E+00	0.0E+00				
20		4.7E+00	0.0E+00	0.0E+00				
21		4.6E+00	0.0E+00	0.0E+00				
22	Jun	4.9E+00	0.0E+00	0.0E+00				
23		3.3E+00	0.0E+00	0.0E+00				
24		5.1E+00	0.0E+00	0.0E+00				
25		0.0E+00	0.0E+00	0.0E+00				
26		0.0E+00	0.0E+00	0.0E+00				
27	Jul	0.0E+00	0.0E+00	0.0E+00				
28		0.0E+00	0.0E+00	0.0E+00				
29		0.0E+00	0.0E+00	0.0E+00				
30		0.0E+00	0.0E+00	0.0E+00				
31	Aug	0.0E+00	0.0E+00	0.0E+00				
32		0.0E+00	0.0E+00	0.0E+00				
33		0.0E+00	0.0E+00	0.0E+00				
34		0.0E+00	0.0E+00	0.0E+00				
35	Sep	0.0E+00	0.0E+00	0.0E+00				
36		0.0E+00	0.0E+00	0.0E+00				
37		0.0E+00	0.0E+00	0.0E+00				
38		0.0E+00	0.0E+00	0.0E+00				
39		0.0E+00	0.0E+00	0.0E+00				
40	Oct	0.0E+00	0.0E+00	0.0E+00				
41		3.3E+00	0.0E+00	0.0E+00				
42		3.5E+00	0.0E+00	0.0E+00				
43		6.0E+00	0.0E+00	0.0E+00				
44	Nov	9.7E+00	0.0E+00	0.0E+00				
45		5.9E+00	0.0E+00	0.0E+00				
46		6.1E+00	0.0E+00	0.0E+00				
47		5.4E+00	0.0E+00	0.0E+00				
48	Dec	4.0E+00	0.0E+00	0.0E+00				
49		4.3E+00	0.0E+00	0.0E+00				
50		3.8E+00	0.0E+00	0.0E+00				
51		0.0E+00	0.0E+00	0.0E+00				
52		0.0E+00	0.0E+00	0.0E+00				
53								

"0.0E+00" indicates ^{14}C concentration of airborne effluent is below the authorized detectable limit (40 Bq cm^{-3}).

I.10. Potato Scenario Description

During the Third Combined Meeting of the EMRAS Programme, held in November 2005, it was decided to initiate a scenario for C-14 transfer in crops based on unpublished data contained in a thesis from Imperial College. The crops investigated were cabbage, beans and potatoes. We decided to start the scenario with potatoes because they are widely used.

I.10.1. Experimental conditions

Approximately two hundred potato tubers (*Solanum tuberosum* cv. Romano) were placed in dark storage on July 5 1995 and left to chit (sprout). Some tubers were split to produce sufficient plants to transfer three to each of one hundred pots on August 4 1995. Some of the plants were later thinned to two per pot. The pots had dimensions 40×40×40 cm and each was filled with Fison's Levington multi-purpose peat-based compost. The plants were cultivated in a walled garden at Imperial College.

The crops were exposed to $^{14}CO_2$ in the MAFF/CARE wind tunnel. This allowed the exposure to take place under realistic atmospheric boundary layer conditions, while providing adequate containment for the $^{14}CO_2$. The experimental layout is shown in Figure I.10.1, where each pot contains four plants, as in experiments with cabbage and beans. In the potato experiment only 2-3 plants per pot were used.

The wind tunnel has the capacity to accommodate thirty pots. Twenty of these constitute the 'fetch' of the canopy and facilitate the build up of a turbulent boundary layer. The remaining ten pots provided the plant material to be sampled as part of the experiment, enabling a maximum of thirty potato plants to be sampled for each exposure (but generally 20 plants in the later development stage).

The potato plants were fumigated with $^{14}CO_2$ for approximately 10 hours within the wind tunnel at six stages (P1 – P6) of the crop's growth cycle. The schedule of fumigations is summarized in Table I.10.1, which shows the number of days after sowing at which fumigation occurred (stage of development) and the fumigation date. The date of chitting of this crop was 5th July 1995 and the planting date was 4th August 1995. Following fumigation, samples were taken immediately to measure the activity concentration of ^{14}C fixed by the crop (harvest H1) and the plants were moved outside to the garden. Subsequent samples (H2 to H6) were taken at intervals that varied in number and frequency according to the age of the crop at fumigation, as given in Table I.10.2.

The air activity concentration for each exposure period was calculated as the total activity absorbed in the trapping solution divided by the total volume of air sampled. The air profiles presented in Figure I.10.2 are plots of average air activity concentration during the sampling period plotted at the mid point of the sampling period for each of the exposure experiments. These concentrations are given numerically in Table I.10.3, and C-14 integrated air concentrations are given in Table I.10.4. The ranges of temperature and photosynthetically active radiation (PAR) in the tunnel during each experiment are given in Table I.10.5. The canopy was illuminated with a bank of six 450 W agricultural lights set to a sixteen-hour photoperiod. The temperature in the tunnel increased with time during the fumigation (Table I.10.5) and the relative humidity increased by about 10%, with an average value of 55%. The average illumination was quite constant in P2-P5, and decreased slightly with time for P1 and P6. The illumination was not uniform on all plants and the range in Table I.10.5 must be considered. The plants were under no water stress.

In experiment P1, 30 plants were used in the 10 sampling pots; 25 plants were used in P2 and 20 (2 per pot) in the rest of the fumigations.

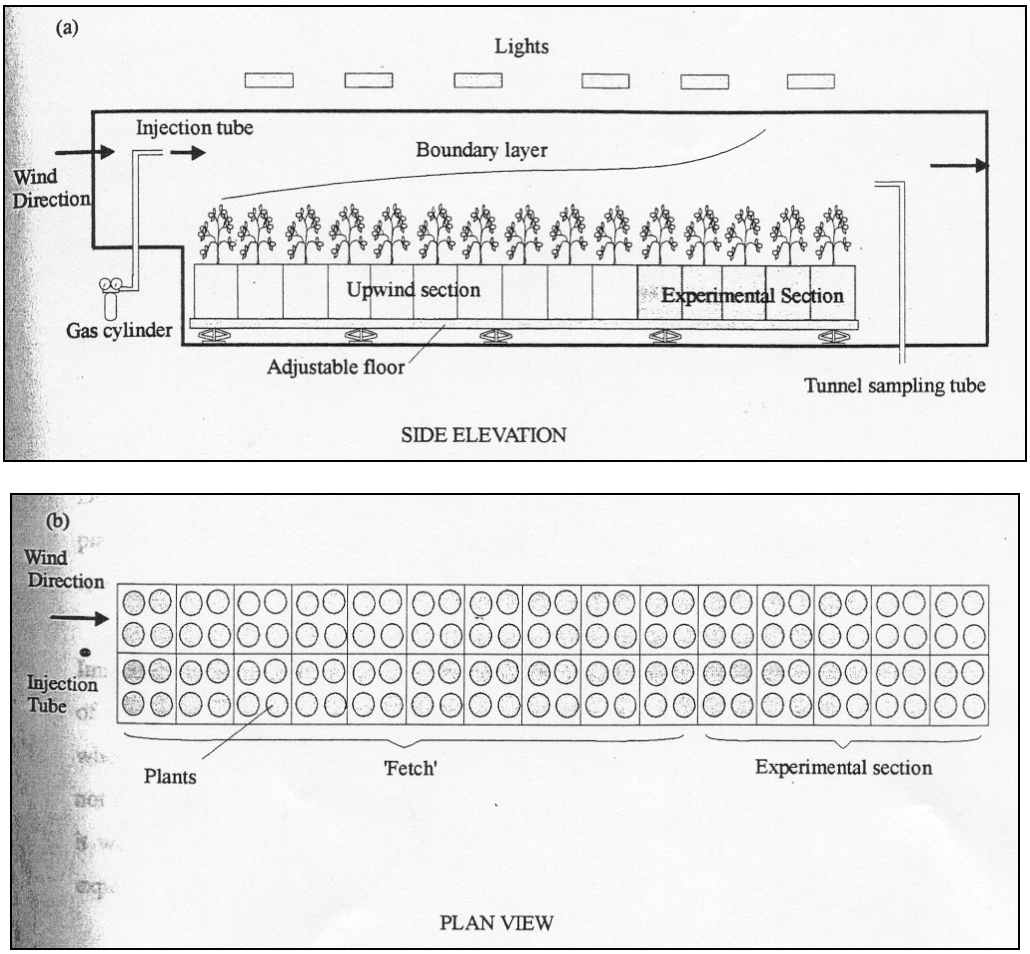

Fig. I.10.1. Experimental canopy in wind tunnel side elevation (a) and plan view (b).

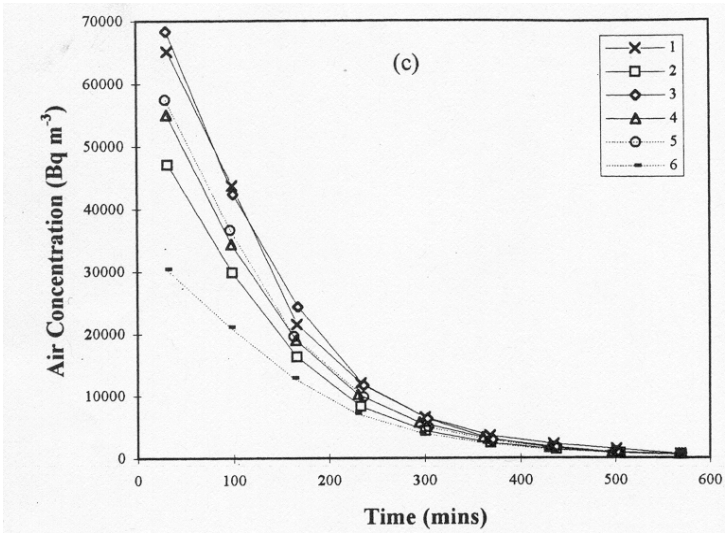

Fig. I.10.2. C-14 activity concentrations in air in the wind tunnel during exposure

Table I.10.1. Fumigation schedule for experiments in which potato plants were exposed to $^{14}CO_2$.

Code Nº of Experiment	Time of Fumigation (Days after sowing)	Fumigation date (d/m/y)
P1	21	25/8/95
P2	33	7/9/95
P3	47	21/9/95
P4	61	5/10/95
P5	74	18/10/95
P6	89	2/11/95

Table I.10.2. Potato sampling schedule.

Harvest	Experiment											
	P1		P2		P3		P4		P5		P6	
	Age*	T**	Age	T	Age	T	Age	T	Age	T	Age	T
H1	21	0	33	0	47	0	61	0	74	0	89	0
H2	31	10	38	5	53	6	65	4	79	5	90	1
H3	38	17	44	11	58	11	72	11	83	9	93	4
H4	48	27	58	25	68	21	83	22	87	13	95	6
H5	72	51	79	46	83	36	90	29	93	19	97	8
H6	97	76	97	64	97	50	97	36	100	26	100	11

* Days after sowing.
** Days after exposure.

Table I.10.3. C-14 air concentration above the potatoes.

P1		P2		P3		P4		P5		P6	
Time (min)	Air Conc (Bq/m3)	Time (min)	Air Conc (Bq/m3)	Time (min)	Air Conc (Bq/m3)	Time (min)	Air Conc (Bq/m3)	Time (min)	Air Conc (Bq/m3)	Time (min)	Air Conc (Bq/m3)
32	65121	32	47090	31	68339	31	55009	30	57453	30	30450
99	43715	99	29804	100	42376	98	34387	97	36612	96	21067
166	21521	166	16279	167	24373	165	18999	163	19576	162	12966
233	12095	233	8297	236	11749	230	10269	236	9906	228	7152
300	6577	301	4405	303	6361	294	5774	304	5028	295	4086
368	3667	369	2490	371	2983	360.5	3359	370	2858	361	2461
435	2325	438	1393	438	1827	430.5	1686	436	1646	426	1452
501	1460	505	801	504	839	496.5	985	501	954	492	900
569	701	570	565	570	694	567	651	568.5	607	566	507

Table I.10.4. C-14 integrated air concentration (IAC).

Experiment	IAC MBq m^{-3} min
P1	9.764
P2	6.983
P3	9.647
P4	8.089
P5	8.307
P6	4.774

Table I.10.5. Range of temperature (T) (ºC) and PAR (W/m^2) during fumigation.

Experiment	Tmin	Tmax	PARmin	PARmax
P1	23	27	70	150
P2	21	26	50	160
P3	20	23	40	160
P4	19	24	30	130
P5	19	23	30	130
P6	17	20	30	130

I.10.2. Biomass dynamics

The average dry weight of the roots, leaves, stems and tubers, together with standard deviations (based on 2–6 plants), in all experiments for every harvest time are given in Table I.10.6 and Figure I.10.4. The development of leaf area index (LAI) is given in Figure I.10.3. The dry weight fractions for each harvest are given in Table I.10.7.

I.10.3. Calculation endpoints

Modelers are asked to calculate the following:

(1) the carbon concentration in the leaves at each sampling time (H1 to H6) for each experiment (P1 to P6) [Bq/gdm];
(2) the carbon concentration in the tubers at final harvest (H6) for each experiment [Bq/gdm];
(3) 95% confidence intervals on all predictions.

The Modellers are also asked to supply a fully documented model description following the EMRAS template.

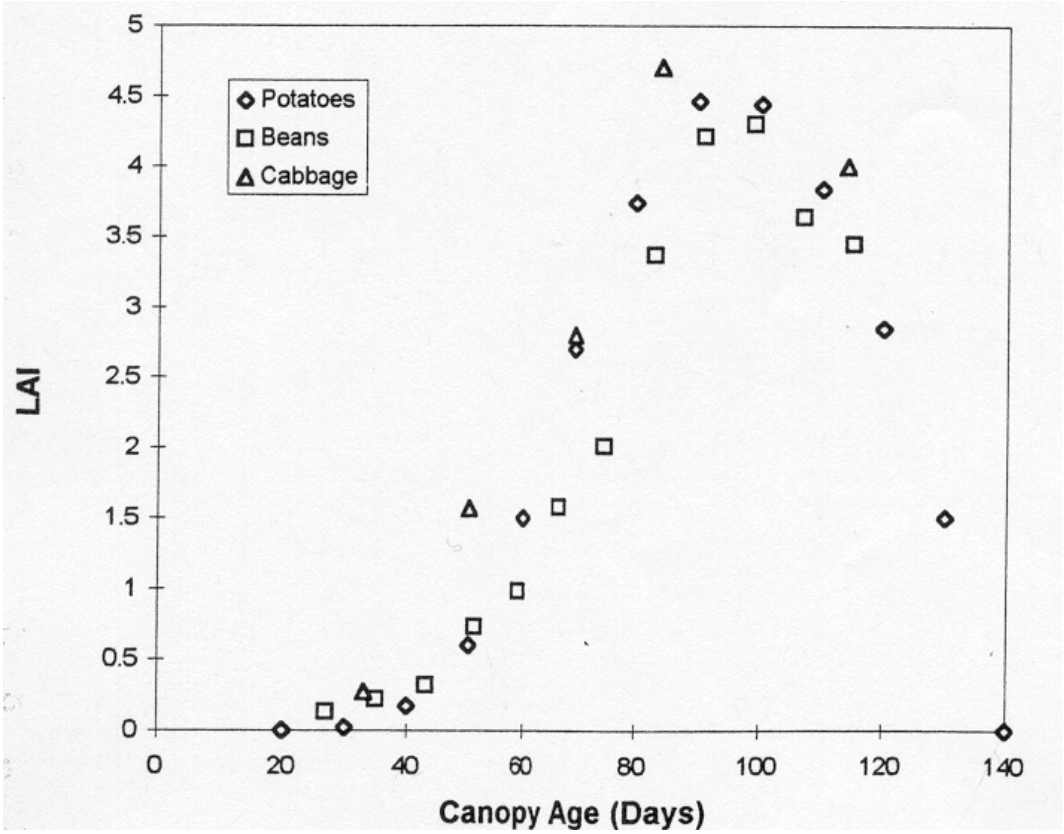

Fig. I.10.3. Leaf area index development for potatoes, beans, cabbage

Table I.10.6. Biomass dynamics for potatoes.

P1									
Harvest	**Age**	**Leaves**	**STDEV**	**Stems**	**STDEV**	**Roots**	**STDEV**	**Tubers**	**STDEV**
H1	21	*3.2*	2.3	1.7	1	7.7	4.4	–	–
H2	31	10	8.4	7.5	7.1	1.3	1.1	–	–
H3	38	7	1.2	9.6	2.2	1.8	1.3	0.3	0
H4	48	15.5	9.4	15.5	8.6	2.7	1.4	11	8.3
H5	72	9.4	8.8	11.3	6	1.4	1.4	40.7	32.6
H6	97	6.8	8.3	14.7	6.1	1.3	1	78.3	87.2
P2									
Harvest	**Age**	**Leaves**	**STDEV**	**Stems**	**STDEV**	**Roots**	**STDEV**	**Tubers**	**STDEV**
H1	33	11.2	5.1	11.9	4.7	2.9	1.5	–	–
H2	38	5.4	2.9	8	4.5	1.1	0.6	–	–
H3	44	6.5	4.6	10.9	5.6	1.9	1.1	3.8	0.7
H4	58	15.6	1.6	18.4	3	3.4	1.7	12.5	3
H5	79	15.4	15.7	14.7	8.8	1.3	1.2	45.3	47.5
H6	97	5	4.8	7.1	2.4	0.9	0.4	30.2	8.7
P3									
Harvest	**Age**	**Leaves**	**STDEV**	**Stems**	**STDEV**	**Roots**	**STDEV**	**Tubers**	**STDEV**
H1	47	7.84	2.86	12.15	5.02	3.42	1.75	9.78	7.22
H2	53	12.77	4.9	11.98	5.08	2.76	1	13.29	11.2
H3	58	6.73	5.19	9.37	6.08	1.41	0.37	13.38	4.02
H4	68	6.33	5.38	11.95	9.77	1.59	0.91	16.34	12.73
H5	83	5.81	5.71	12.23	2.89	2.11	1.46	50.31	41.86
H6	97	2.74	1.75	8.66	0.54	0.7	0.08	46.46	19.1
P4									
Harvest	**Age**	**Leaves**	**STDEV**	**Stems**	**STDEV**	**Roots**	**STDEV**	**Tubers**	**STDEV**
H1	61	15.53	7.05	22.62	9.39	2.71	1.55	27.59	27.76
H2	65	12.07	8.38	9.12	5.25	2.66	0.62	42.27	20.06
H3	72	4.42	2.42	7.93	4.1	1.02	0.76	24.53	12.11
H4	83	3.08	2.18	9.51	5.85	0.76	0.55	32.33	18.72
H5	90	7.72	8.1	16.29	19.02	1.45	0.35	35.67	10.73
H6	97	0.56	0.13	47.35	1.85	0.51	0.66	49.99	2.21
P5									
Harvest	**Age**	**Leaves**	**STDEV**	**Stems**	**STDEV**	**Roots**	**STDEV**	**Tubers**	**STDEV**
H1	74	6	2.4	8.8	4.7	1.5	0.9	38.1	17.8
H2	79	4.2	2.2	8.2	2.6	0.7	0.3	24.3	18.9
H3	83	2.6	2.7	6.5	1.3	1.1	0.7	49.3	54.6
H4	87	4.3	2.4	8.2	2.1	1.6	0.6	75.8	25.8
H5	93	5.1	1.7	15.6	11.3	1.3	1	49.1	30.3
H6	100	2.2	1.9	14.7	2.6	1.6	0.8	76.9	6
P6									
Harvest	**Age**	**Leaves**	**STDEV**	**Stems**	**STDEV**	**Roots**	**STDEV**	**Tubers**	**STDEV**
H1	89	6.21	6.76	14.03	14.9	0.99	0.36	36.66	14.17
H2	90	5.38	4.92	9.02	3.98	1.27	0.61	70.34	24.97
H3	93	6.9	4.96	17.02	7.57	0.69	0.44	48.18	9.43
H4	95	10.89	5.53	17.34	3.99	2.16	0.33	121.68	52.71
H5	97	7.52	8.28	17.08	10.93	1.18	1.47	77.58	68.4
H6	100	3.24	0.45	7.17	0.45	0.23	0.05	40.39	35.06

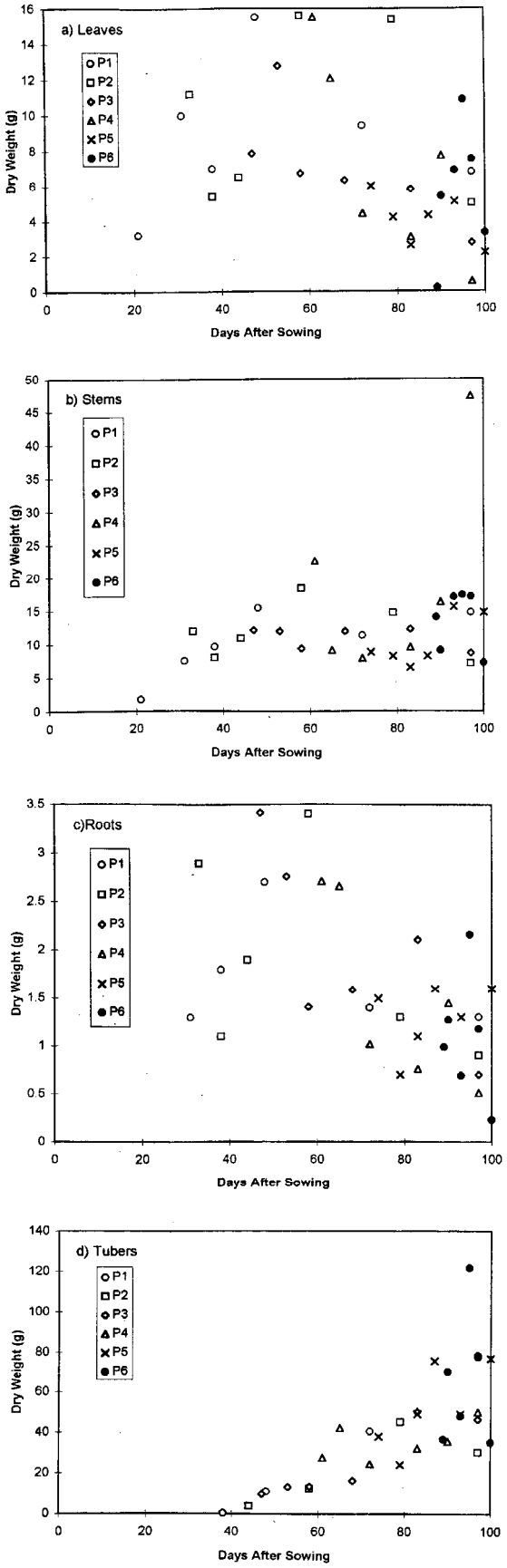

Fig. I.10.4. Dry weights of potato leaves (a), stems (b), roots (c), tubers (d).

Table I.10.7. Dry weight fractions.

P1					
Harvest	**Age**	**Leaves**	**Stems**	**Roots**	**Tubers**
H1	21	0.06	0.02	0.07	–
H2	31	0.09	0.03	0.05	–
H3	38	0.06	0.04	0.07	0.12
H4	48	0.07	0.04	0.08	0.12
H5	72	0.08	0.04	0.07	0.16
H6	97	0.12	0.1	0.09	0.22
P2					
Harvest	**Age**	**Leaves**	**Stems**	**Roots**	**Tubers**
H1	33	0.08	0.04	0.08	–
H2	38	0.05	0.03	0.06	–
H3	44	0.06	0.04	0.06	0.31
H4	58	0.09	0.05	0.08	0.15
H5	79	0.09	0.05	0.06	0.18
H6	97	0.07	0.06	0.06	0.17
P3					
Harvest	**Age**	**Leaves**	**Stems**	**Roots**	**Tubers**
H1	47	0.06	0.05	0.08	0.13
H2	53	0.08	0.03	0.07	0.13
H3	58	0.09	0.04	0.05	0.13
H4	68	0.08	0.04	0.06	0.15
H5	83	0.09	0.05	0.06	0.17
H6	97	0.13	0.13	0.07	0.18
P4					
Harvest	**Age**	**Leaves**	**Stems**	**Roots**	**Tubers**
H1	61	0.08	0.04	0.07	0.15
H2	65	0.07	0.02	0.06	0.16
H3	72	0.09	0.05	0.07	0.18
H4	83	0.08	0.06	0.05	0.19
H5	90	0.17	0.07	0.06	0.16
H6	97	0.25	0.6	0.07	0.2
P5					
Harvest	**Age**	**Leaves**	**Stems**	**Roots**	**Tubers**
H1	74	0.08	0.04	0.05	0.18
H2	79	0.1	0.05	0.06	0.2
H3	83	0.14	0.04	0.07	0.18
H4	87	0.15	0.04	0.06	0.17
H5	93	0.16	0.08	0.08	0.19
H6	100	0.08	0.07	0.08	0.15
P6					
Harvest	**Age**	**Leaves**	**Stems**	**Roots**	**Tubers**
H1	89	0.14	0.06	0.07	0.17
H2	90	0.12	0.04	0.06	0.18
H3	93	0.41	0.07	0.06	0.19
H4	95	0.47	0.08	0.07	0.28
H5	97	0.6	0.13	0.09	0.21
H6	100	0.7	0.17	0.1	0.19

REFERENCES

[I.1] CHO, J.Y., ET AL., Food Crop Science, 4th Edition, Hyangmoon (in Korean) (1986).

[I.2] THIMIJAN, R.W., HEINS, R.D., A review of conversion constants and procedures for photometric, radiometric, and quantum light units of measure, J. Amer. Soc. Hort. Sci. lll, ll4–l2l (1983).

[I.3] YANKOVICH, T.L., KIM, S.B., EMRAS Tritium/C14 Working Group: The Dynamic Perch Lake Mussel Transplantation Scenario Description (Revision 1), AECL Environmental Technologies Branch Memorandum No. ETB-05-99 (Revision 1), 2005 July 27 (2005).

[I.4] KOARASHI, J., AKIYAMA, K., ASANO, T., KOBAYASHI, H., Chemical composition of ^{14}C in airborne release from the Tokai reprocessing plant, Japan, Radiat. Prot. Dosim., 114, 551–555 (2005).

[I.5] KOARASHI, J., KOZAWA, T., YOKOTA, T., ISAKA, K., AKIYAMA, K., ASANO, T., Methods and their performances for collecting tritium, carbon-14 and radioiodine in airborne effluent from Tokai reprocessing plant, JNC TN8410 2004-003 (in Japanese with English abstract) (2004).

[I.6] KOARASHI, J., FUJITA, H., Review of monitoring data (1991–2001) for model-data intercomparison studies on ^{14}C transfer in the environment, JNC TN8450 2004-011 (2005).

[I.7] FUMA, S., INOUE, Y., MIYAMOTO, K., TAKEDA, H., IWAKURA, T., ARAI, K., KASHIDA, Y., ICHIMASA, Y., Environmental background ^{14}C levels in Japan in 1990s, Radioisotopes, 51, 381–391 (in Japanese with English abstract) (2002).

[I.8] KOARASHI, J., AMANO, H., ANDOH, M., IIDA, T., MORIIZUMI, J., Estimation of $^{14}CO_2$ flux at soil-atmosphere interface and distribution of ^{14}C in forest ecosystem, J. Environ. Radioact., 60, 249–261 (2002).

[I.9] OSAKI, M., TANAKA, A., Current photosynthates and storage substances as the respiratory substrates in the rice plant, Nihon Dojou Hiryougaku zasshi (Japanese J. Soil Sci. Plant Nutrition), 50, 540–546 (in Japanese with English abstract) (1979).

[I.10] KONDO, M., National Agricultural Bio-oriented Research Organization, Private communication (2005).

APPENDIX II. MODEL DESCRIPTIONS

II.1. Perch Lake Scenario model descriptions

II.1.1. VNIIEF Model

II.1.1.1. Key model assumptions

- The turnover time for tritiated water in the tissues of aquatic organisms is very rapid.
- Clams, pike and bullheads take in tritium through exchange with water and also through ingestion.
- All water layers are taken into account in calculating concentrations in pike, which migrate throughout the lake.
- Bullhead is a bottom fish so that only deep water is taken into account in calculating concentrations.
- Clams live at the lake bottom but take up detritus formed in all water layers.

The parameter values used in the calculations and further assumptions are based on the work of Murphy [II.1] and Diabate and Strack [II.2].

II.1.1.2. Model description

Table II.1.1 provides a short description of the model. k is the isotopic discrimination factor in OBT formation.

Table II.1.1. VNIIEF model description.

Compartment		Tritium source		Comment
		HTO	OBT	
Bladderwort & hornwort		Surface water	Surface water (k = 0.8)	
Cattails	Above water	Air and sediment water	Sediment and surface water (k = 0.8)	HTO concentration is calculated from $C_{HTO} = 0.75C_{air} + 0.25C_{sediment}$; $C_{air} = 0.9C_{surf}$
	Below water	Sediment water	Sediment water (k = 0.8)	
Algae		Lake water	Lake water (k = 0.5-0.8)	Algae are assumed to access all water layers, which have an effective concentration of $C = 0.5\left(C_{surf} + C_{deep}\right)$
Pike	Head	Essentially lake water	Lake water (k = 0.1-0.5)	Concentration in lake water is calculated as $C = \frac{1}{N}\sum_i 0.5\left(C_{surf} + C_{deep}\right)$, where the summation is over sample points. OBT concentration in the diet is equal to the concentration in lake water.
	Flesh	Lake water and water in diet	Lake water (k = 0.1-0.5) and diet (k = 0.5).	
	Internal organs	Water in diet	Diet (k = 0.5)	
Bullhead	Head	Essentially lake water	Lake water (k = 0.1-0.5)	Concentration in lake water is calculated as $C = \frac{1}{N}\sum_i C_{deep}$ OBT concentration in the diet is equal to concentration in lake water.
	Flesh	Lake water and water in diet	Lake water (k = 0.1-0.5) and diet (k = 0.5).	
	Internal organs	Essentially water in diet	Diet (k = 0.5)	
Clams		Sediment and deep water	Deep water (k = 0.1-0.5) and diet (k = 0.5)	Concentration in lake water and diet are calculated as $C_{water} = \frac{1}{N}\sum_i C_{sediment}$, $C_{diet} = \frac{1}{N}\sum_i \frac{1}{3}\left(C_{surf} + C_{deep} + C_{sediment}\right)$
Sediment		–	Surface water in May	The detritus that makes up sediments is considered to form in May in surface water.

II.1.2. EDF Model

The EDF model for aquatic contamination is a dynamic model that computes concentrations of HTO and OBT in phytoplankton and fish [II.3]. Although freshwater macrophytes, molluscs and sediment are not included in the EDF model, concentrations were calculated for all the compartments covered in the Perch Lake scenario.

II.1.2.1. Concentrations in aquatic plants

The general assumption is that HTO in plants is equal to HTO in the surrounding environment.

For algae, the water concentration to consider is the offshore surface concentration. OBT concentrations were calculated on the assumption that the OBT/HTO ratio is equal to 0.6 in aquatic plants [II.4].

For worts, the water concentration to consider is the near-shore surface concentration. But these data are not available. The July measurements indicate that the ratio "near-shore surface water/offshore surface water" was equal to 0.8. Using this ratio, the near-shore surface water in May was estimated from the offshore surface water in May. OBT was calculated on the assumption that the OBT/HTO ratio equals 0.6 in aquatic plants.

For cattails, the HTO concentration in the below-water parts was assumed to be identical to the concentration in worts. In contrast, the OBT concentration in the below-water parts was assumed to be in isotopic equilibrium with shore sediment water and surface water. The shore sediment water concentrations for a given site were estimated from the measurements made at that site in July and October. HTO concentration in the above-water parts of cattails was assumed to equal the average of the HTO concentrations in air and shore surface water, the latter being calculated in the same way as for worts. Half of the OBT in the above-water parts was assumed to come from the below-water parts with the other half being in isotopic equilibrium with HTO in the above-water parts. None of the OBT calculations for cattails took into account the OBT/HTO ratio of 0.6.

II.1.2.2. Concentrations in animals

HTO in clams was considered to be in isotopic equilibrium with HTO in sediment water, calculated as the average of the near-shore and offshore sediment concentrations at the three sampling sites. The OBT/HTO ratio was set to 0.45 [II.4].

HTO in both bullheads and pike was assumed to be in isotopic equilibrium with the offshore surface water, calculated as the average over the three sampling sites. OBT in fish was assumed to be controlled by the tritium transfer rate between food and fish and by the specific food intake rate (10^{-2} day^{-1}). Moreover, the concentration in food was a function of the concentration in water. Thus, the EDF model is based on a transfer rate from water to fish that is consistent with an apparent OBT/HTO ratio of 0.45 [II.4]. To account for the size difference between bullheads and pike, pike were assumed to be older and to have grown in water with an HTO concentration of 6000 Bq/L in previous years.

II.1.2.3. Concentrations in sediment

OBT in sediment has a very slow turnover rate and is a function of OBT in aquatic biota and OBT in terrestrial organic matter that finds its way into the lake. Since concentrations from

previous years either in the terrestrial or aquatic environment were not available, the following assumptions were made:

- The spatial distribution of sediment OBT is similar to the spatial distribution of lake HTO. Thus concentrations at S2 exceed those at S1, which exceed those at S3.
- OBT concentrations in aquatic biota in previous years could be as high as the upper limit of the 95% confidence interval for water concentration in 2002 (see Section II.1.2.4). This value was assigned to the sediment OBT concentration at S2.
- A fraction of the sediment OBT comes from lake plants and animals growing in 2002. This value was assigned to S1.
- The lowest OBT concentration, the value assigned to S3, was derived by assuming that the sediment is in isotopic equilibrium with organic matter resulting from the decomposition of terrestrial vegetation that finds its way into the lake. The concentration in terrestrial vegetation was calculated from the air concentration near S3 and an OBT/HTO ratio of 0.6.

Hence, the differences in sediment OBT concentrations among sampling sites do not depict actual spatial variations but represent different origins of sediment OBT more or less randomly assigned to each sampling site.

II.1.2.4. 95% confidence intervals

The largest source of uncertainty was the heterogeneity in water concentrations. The 95% confidence interval of a lognormal distribution fitted to the observed water concentrations had upper and lower limits of 1850 and 8745 Bq/L. This interval was used as the uncertainty in the HTO concentrations in all plants and animals with the exception of the above-water parts of cattails, for which the lower limit became the observed atmospheric HTO concentration.

For OBT, a second source of uncertainty is the OBT/HTO ratio, which could vary between 0.4 and 0.9 for plants and between 0.1 and 0.9 for animals. The lower limit of the OBT confidence interval was found by multiplying the lower limit of the confidence interval for water concentrations by the lower value of the OBT/HTO ratio. A similar procedure was used to estimate the upper limit. This is not, in its strictest sense, a 95% confidence interval.

For sediment, the uncertainty range represents the absolute maximum and minimum values corresponding to the different OBT origins: OBT from ‘old organic matter’ in S2, OBT from aquatic biota growing in 2002 in S1, and OBT from terrestrial organic matter in S3.

II.1.3. SRA Model

The calculations for the Perch Lake scenario are based on the assumptions that the tritium flux into the lake is stationary and that the free-water tritium (FWT) and OBT in the plants and animals are in equilibrium with an effective HTO concentration C_{eff}, defined as the average HTO concentration in the lake water or the atmospheric water vapor to which a fish or plant is exposed over its growing period. C_{eff} depends on location and time and, for fish, on the time spent under given living circumstances. At equilibrium, the FWT concentration in a living organism (C_{FW}) is equal to C_{eff}:

$$C_{FW} = C_{eff} = \sum_i F_i \times C_i \qquad \text{(II.1.1)}$$

where:

F_i is the fractional contribution to the effective tritium concentration from the *i*th HTO source, and
C_i is the tritium concentration at equilibrium in the *i*th HTO source.

The OBT concentration is given by:

$$C_{OB} = FC \times C_{FW} \quad \text{(II.1.2)}$$

where:

FC is a discrimination factor for tritium in organic material.

In the absence of experimental data for the organisms considered in the Perch Lake scenario, published values of FC for other animals or plants grown in aquaria or pools were used. The values of F_i and FC used in the calculations are shown in Table II.1.2.

The determining factors for the FWT and OBT levels in algae and worts were assumed to be the near-shore lake water tritium concentration at the sampling time and the tritium discrimination factor in photosynthesis. The HTO concentration in below-water cattails was assumed to be controlled by the near-shore sediment concentrations. For the above-water parts of cattails, the tritium concentration in atmospheric water vapor also played a role. The fractional contribution of the atmospheric HTO was assumed to be 0.3 but was neglected in the present calculation. Thus, the FWT concentration in the above-water cattails was set equal to 0.7 times the near-shore sediment concentration. Since information on the near-shore sediment water concentration was not available for May, the data for July were used instead.

Table II.1.2. Factors determining tritium concentrations in the endpoints of the Perch Lake scenario.

Endpoint	Tritium source	Fractional contribution to effective tritium concentration (F_i)	Averaging time	OBT specific activity relative to effective tritium concentration (FC)
Algae	Near-shore surface water	1.0	Sampling period	0.7
Wort	Near-shore surface water	1.0	Sampling period	0.7
Cattail above water	Near-shore sediment water Atmosphere	0.7 0.3	Sampling period	0.5
Cattail below water	Near-shore sediment water	1.0	Sampling period	0.5
Clam	Lake averaged*	1.0	Sampling period	0.5
Bullhead	Lake averaged* Offshore sediment water	0.5 0.5	Sampling period	0.64 (head), 0.70 (flesh), 0.66(organs)
Pike	Lake averaged*	1.0	Sampling period	0.64 (head), 0.70 (flesh), 0.66(organs)
Sediment	Near-shore sediment water	1.0	Year	0.63

* The lake-average HTO concentration was assumed to be given by the average HTO concentration of the deep and surface waters at Sites S1 and S3 and the sediment water at Site S3.

For each animal species, an effective lake water concentration was estimated from the average tritium concentration in the different parts of the lake weighted by the time the animals spent in each part. For bullheads, lake water and sediment water were assumed to contribute equally to the body FWT, since the fish spends its time near the sediment/water interface. For pike and clams, the lake-averaged HTO concentration was taken as the effective HTO concentration. The tritium discrimination factor FC for OBT was obtained in analogy with published values for other species.

Sediment OBT concentrations at Site S3 were assumed to be equal to 0.63 times the HTO concentration in the near-shore sediment water.

It was rather difficult to determine the confidence level for the model predictions since there are so many sources of uncertainty. The uncertainty estimates reflect solely the standard deviation of the effective tritium concentration estimated for individual samples, based on the observed variation of tritium levels in the lake or sediment water.

II.1.4. BioM Model

The aim of the BioM model is to improve the estimation of long-term tritium doses by re-evaluating the way in which OBT is treated. The model calculates the concentration of buried tritium rather than the tritium traditionally considered to be organically bound. Buried tritium is tritium in exchangeable positions in large molecules that becomes hidden from the effects of washing when the free water of the sample is extracted by freeze-drying or azeotropic distillation. This tritium appears as part of the experimental yield when the sample undergoes a traditional analysis for OBT, but is converted to HTO as soon as it is ingested and so does not contribute to the OBT dose. Improved understanding of the amount of buried tritium that forms in plant and animal species will lead to improved dose estimates from OBT.

II.1.4.1. HTO Concentrations

The HTO concentration in each scenario endpoint was assumed to equal the HTO concentration in the air, water or sediment compartment to which the plant or animal was exposed (Table II.1.3). Bullheads and pike were assumed to move everywhere in the lake.

II.1.4.2. OBT Concentrations

The experimental basis of the BioM model is the observation that freeze-drying or azeotropic distillation of a sample to extract the free water results in a large part of the exchangeable tritium becoming non-exchangeable in OBT analysis [II.5]. The tritium is "buried" inside the biopolymers or in shell water that is separated from bulk water [II.6]. Shell water does not freeze at temperatures of dry ice or liquid nitrogen. Accordingly, the BioM model assumes that OBT measured using traditional methods consists of three components:

$$C_{OBT} = C_{CBT} + C_{OBTex} + C_{SBT}, \quad \text{(II.1.3)}$$

where:

C_{CBT} is carbon bound tritium;
C_{OBTex} is tritium that is nominally exchangeable but buried by freeze drying or azeotropic distillation; and
C_{SBT} is tritium buried in water molecules of the solvation shells.

Table II.1.3. Compartments to which a given endpoint is exposed.

Endpoint	Compartment
Algae	Local offshore surface water
Worts	Arithmetic mean of local offshore sediment and surface water
Submerged cattails	Local sediment water
Emergent cattails	Local sediment water multiplied by 1.1 to account for the difference in vapour pressure between HTO and water vapour
Clams	Arithmetic mean of S1 and S2 offshore sediment water
Bullheads and pike	Offshore surface and sediment water averaged over the 3 sampling sites

C_{CBT} is formed by photosynthetic and enzymatic pathways and is the quantity that determines the long-term radiation dose from tritium. According to Equation (II.1.3), $C_{CBT} \sim (C_{OBT} - C_{OBTex})$, and C_{CBT} can be determined from analytical measurements of C_{OBT} if C_{OBTex} can be estimated. The BioM model provides a way to calculate C_{OBTex}.

The starting point of the calculation is the HTO concentration in the tissues (C_{HTO}, Bq/L) and the proportion of carbohydrates, proteins and DNA in the tissues [II.7]. Then the concentration of buried tritium (C_{OBTex}, Bq/L) is given by:

$$C_{OBTex} = \alpha\, C_{HTO}\, (18/2)\, [\sum_i C_H H_{ex}]/W_{eq} \qquad \text{(II.1.4)}$$

where:

α is the T/H fractionation factor of tritium between water and exchangeable hydrogen positions;
C_H is the hydrogen content (fraction);
H_{ex} is the fraction of exchangeable hydrogens; and
W_{eq} is the water equivalent.

The summation in Equation (II.1.4) is over carbohydrates, proteins and nucleotides. The product $C_H \times H_{ex}$ has a value of 0.019, 0.017 and 0.0057 for carbohydrates [II.8], proteins [II.9] and nucleotides [II.7], respectively. The model does not take into account tritium that accumulates in the hydration shells, which remains with the organic matter following freeze drying, so that the predictions may underestimate C_{OBTex} concentrations by 20 to 40%.

The value of the tritium fractionation factor is uncertain. $\alpha \sim 1.4$ is valid for 1-step exchange reactions and $\alpha \sim 1.4^2 \sim 2$ for 2-step reactions. DNA shows both values. $\alpha \sim 1.4$ is found in the first DNA-hydration shell and $\alpha \sim 2$ in the base pairing H-positions inside DNA [II.10]. Since the dominant type of H/T exchange reaction for aquatic systems is unknown, both values were used in the calculations. For simplicity, all plants were assumed to be made up of carbohydrates only and all animals of proteins only.

The 95% confidence intervals were calculated with 1 degree of freedom by the t-distribution assuming 2% standard deviation of the mean (7% in the case of clams and cattails because they are supplied with HTO from the sediments).

C_{OBTex} makes up a substantial proportion of C_{OBT}. Furthermore, the amount of tritium unaccounted for in the solvation shells (0.25 to 0.75g $g_{H2O}/g_{protein}$ [II.11] and up to $0.3 g_{H2O}/g_{starch}$ [II.8]) and the large primary kinetic isotope effects in enzyme-catalyzed reactions [II.12] suggest strongly that $C_{CBT} < 0.1\ C_{OBT}$ if freeze drying or azeotropic distillation is used to extract the free water from the sample prior to analysing for OBT.

II.1.5. IFIN Model

II.1.5.1. Plants

Based on experimental evidence, HTO concentrations in plants are in equilibrium with local HTO concentrations in water. For the emergent parts of cattails, the role of transpiration and exchange with atmospheric water is also considered. An average HTO concentration for each plant type was determined by averaging over the water column and over the three sampling sites. The concentrations in bottom water given in the scenario description were supplemented with data from Cornett et al. [II.13]. For worts and below-water cattails, the data used in the average were the near-shore concentrations measured in July. These were averaged with the August air concentrations to give an HTO concentration in above-water cattails. The concentration in algae was estimated from the average water concentration at the site where the algae were collected.

OBT in aquatic plants is produced as in terrestrial plants but at a slower rate, which implies that OBT concentrations should be based on average HTO levels in water for the month or so before sampling. In the absence of this information, the OBT concentrations in worts and cattails were found by multiplying the plant HTO concentrations for May by 0.8. OBT concentrations in algae ($C_{o,phpl}$, Bq/kg fw) were calculated using a model for tritium dynamics in the aquatic environment [II.14]:

$$\frac{dC_{o,phpl}}{dt} = 0.4 \cdot \mu \cdot Dryf \cdot C_W - \mu \cdot C_{o,phpl} \qquad \text{(II.1.5)}$$

where μ and Dryf are respectively the growth rate (per day) and dry mass fraction of the algae and C_W is the HTO concentration in water (Bq/L). The growth rate is given by Ray [II.15].

$$\mu = 0.75 * (3 - 0.3 * \log(V_p)) \qquad \text{(II.1.6)}$$

where V_p is the cell volume, which can range from 10 and 10^7 μm^3. Assuming the algae belong to a typical class of the phylum Chlorophyta, Equation (II.1.6) gives a growth rate of 1.8 d^{-1} in full light. A growth rate near 0.5 d^{-1} is assessed for the conditions of the scenario. With this value, and an assumed water equivalent factor of 0.6, the OBT concentration in the algae was found as the steady-state solution to Equation (II.1.5).

II.1.5.2. Animals

Based on experimental evidence, HTO concentrations in animals are in equilibrium with local HTO concentrations in water. A nominal value for the water concentrations to which clams and bullheads were exposed was deduced from an overall assessment of the bottom water and sediment concentrations over time throughout the lake. The HTO concentration in clams and bullheads was assumed equal to this water concentration, with some seasonal variation introduced in the case of bullheads. Similarly, HTO concentrations in pike were set equal to the water concentrations averaged over the water column and over the three sampling sites for each sampling time.

OBT concentrations in aquatic producers (C_{OBT}, Bq/kg fresh weight) are given by:

$$\frac{dC_{OBT}}{dt} = a\, K_1 C_f + b\, K_w C_w(t) - K_{0.5} C_{OBT} \qquad \text{(II.1.7)}$$

where:

a is the assimilation factor for OBT from food;
b is the water to OBT transfer factor;
K_1 is the food uptake rate (kg kg^{-1} d^{-1});
K_w is the water uptake rate (m^3 kg^{-1} d^{-1});
$K_{0.5}$ is the OBT elimination rate (d^{-1});
C_f is the OBT concentration in food of zooplankton (Bq/kg fresh weight); and
C_w is the HTO concentration in water (Bq/m^3).

The constants a and b in Equation (II.1.7) were established using measured specific activity ratios of OBT in the organism of interest and OBT in food or HTO in water (Table II.1.4). Elimination rates were assessed from experimental metabolic data.

Clams are filter feeders, eating phytoplankton and zooplankton but also retaining detritus. OBT in clams is due to OBT in the food they eat but also due to conversion of HTO. Both types of plankton have low OBT halftimes (less than 6 days) so OBT in the food will closely follow the dynamics of HTO in water, but with less variability. The OBT loss rate of clams is in the range of 40-100 days and will reduce the dynamics of OBT in clams. The uncertainty in the predicted OBT concentrations in clams is large because critical information on OBT concentrations is missing.

Bullheads are benthic fish eating mostly zoobenthos, zooplankton, invertebrates and detritus, as well as fish and plants. The exact diet depends on the age of the fish and their environmental conditions. They are abundant in areas with submerged plants. Bullheads have a variable metabolic rate, especially near a mass of 100 g. For the May harvest, when the bullheads had an average mass of 40 g, the OBT half time was estimated to be 20-40 days. In September, when the average mass was 70 g, this increased to 25-50 days. Estimates of OBT concentrations in bullheads are difficult to make because the information needed to assess OBT in sediments is missing. OBT concentrations in viscera may be slightly higher than in flesh but some of the key data needed to make a quantitative assessment were not available.

Pike are pelagic fish that eat other fish. OBT concentrations in viscera may be higher than in flesh.

II.1.5.3. Sediments

A series of papers by Hakanson and Bullion [II.16] on biomass, turnover times and biomass loss rates in freshwater systems suggests that most OBT in sediments comes from benthic algae and macrophytes, and is sensitive to concentrations in bottom water. This information was used to develop nominal estimates of OBT concentrations in sediments.

Table II.1.4. Specific Activity Ratios (SAR) for different organisms.

Organism	SAR (HTO source)	SAR (OBT source)
Zooplankton	0.4	0.6
Molluscs	0.2	0.8
Crustaceans	0.2	0.8
Planktivorous fish	0.2	0.8
Piscivorous fish	0.2	0.8
Terrestrial mammals	0.25	0.75

II.1.5.4. Uncertainty

The key information required to estimate the various endpoints is the HTO water concentration for each sampling time, site and organism. The scenario does not offer enough detail of this kind and this is the main source of uncertainty. An additional difficulty in assessing the confidence interval on OBT concentrations is the fact that the rate at which tritium enters the lake as OBT is not known. The estimated confidence intervals are based on judgment.

II.1.6. Japanet Model

II.1.6.1. Composition

Japanet is composed of the following individuals:

- Kiriko Miyamoto, Yoshikazu Inoue, Hiroshi Takeda, Kazuhide Yamamoto (NIRS);
- Michiko Ichimasa and Yusuke Ichimasa (Ibaraki University);
- Noriyuki Momoshima (Kumamoto University);
- Hiroshi Satake (Toyama University); and
- Masahiro Saito (Kyoto University).

II.1.6.2. Assumptions

(1) No special numerical models or transfer parameters for tritium uptake by plants or animals were used in the calculations.

(2) The HTO concentration in lake water is not homogeneous and varies with location and season.

(3) The concentrations in plants and animals will also vary with time and space.

(4) The tissue free water tritium (TFWT) in plants and clams is equal to the HTO concentration in lake water taken at the time and place the samples were collected.

(5) The TFWT of fish is equal to the HTO in lake water averaged over the whole lake in all seasons.

(6) The non-exchangeable OBT concentration (nOBT) of every plant and animal is 80% of its TFWT concentration.

(7) There is no difference in the nOBT concentration in different parts of the fish.

(8) The nOBT of the sediments is the mean value of the nOBT of plants and animals.

(9) The “95% confidence interval” for a given endpoint is assumed to be ±20% of the HTO concentration in lake water used to predict that endpoint.

(10) Perch Lake is a well-mixed aquatic environment in which the nOBT of living species has reached steady-state.

II.1.7. GE Healthcare Model

II.1.7.1. Basic assumptions

The model is based on 1 kg of fish, as this quantity can be easily amplified to the amount needed for consumption of fish within the critical group. The fish has been divided into two compartments, a fish fast compartment and a fish slow compartment (Figure II.1.1). The fish fast compartment represents the tissue free water inside the fish, whilst the fish slow compartment represents the organic matter of the cells. It is assumed that these two compartments are in equilibrium within the fish. Transfer from the fish fast compartment to the fish slow compartment is anabolism, a constructive metabolic process that synthesizes more complex molecules. Transfer from the fish slow compartment to the fish fast compartment is catabolism, degredative chemical reactions in cells that convert polymer metabolites via monomers. The model is time-dependent and was developed for a marine environment, and had to be modified to treat the Perch Lake scenario, which involves a freshwater ecosystem. Since the model is geared to predicting concentrations in fish rather than aquatic plants, no calculations were carried out for worts or cattails.

II.1.7.2. Concentration of tritium in water

There was no information in the scenario description on the flux of tritium into or out of the lake, which is the starting point of the GE model. Therefore the model was run with nominal concentrations in one inlet and one outlet and the results were tuned so that modeled concentration in the water column matched the measured concentration as given in the scenario.

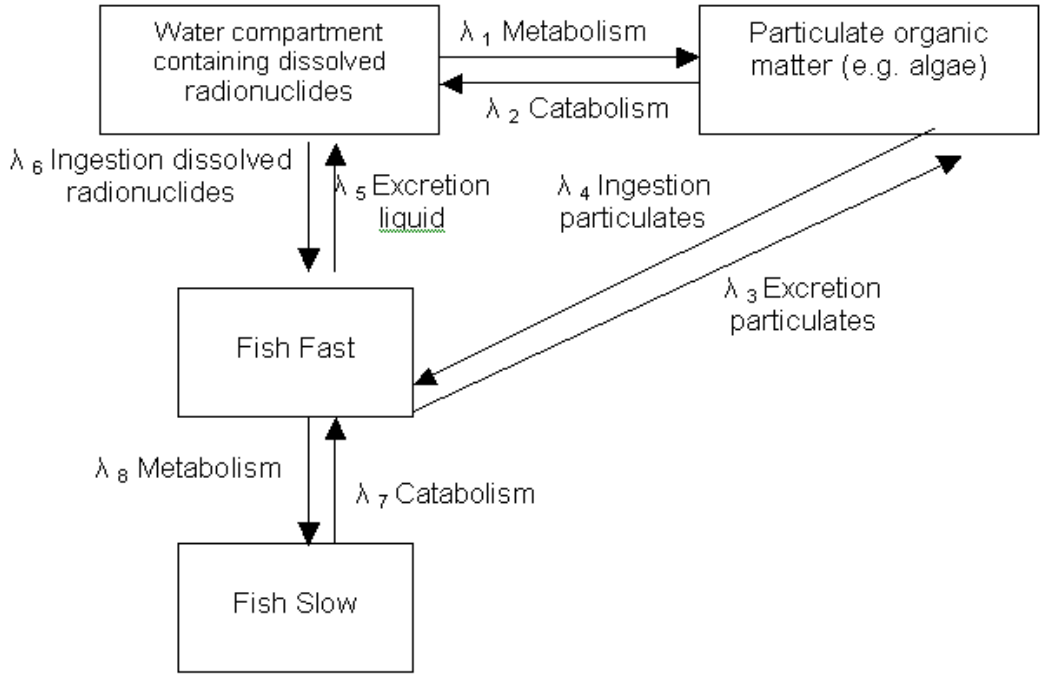

Fig. II.1.1. Dynamic Fish Conceptual Model.

II.1.7.3. Algae

No information was given in the scenario on algal growth rate or turnover rate. Algae were therefore taken to be broadly similar to bacterial particulate organic matter in the GE model, as some green algae are unicellular and reproduce asexually by fission (splitting) or fragmentation. Thus algal growth rate and transfer between the algae and the water column was based on rates of metabolism and catabolism for particulate matter in the GE model, which, in turn, is based on bacterial physiology.

II.1.7.4. Fish and Clams

Clams were taken to be similar to mussels in the GE model, ingesting water and algae (particulate organic matter). Bullheads and pike were taken to be similar to flounder in the GE model.

II.1.7.5. Ingestion

It is assumed that the hydrogen and carbon content in 1kg of fish is the same as the hydrogen and carbon content in the material that 1kg of fish ingests. It has been found that 1kg of fish is made up of 30% carbon, 47% hydrogen and 23% oxygen. Fish (and mussels) were taken to consume 1% of their body weight per day [II.17]. Therefore it was assumed that 1 kg of fish consume 3.65 kg H per year. The ratio of flux/inventory of the donor compartment for tritium was assumed to be the same as for hydrogen.

Tritium has two other routes of ingestion into the fish, as tritiated water from the water compartment that the fish inhabits and as particulate OBT associated with the suspended material in the water compartment. Of the tritium ingested, 20% is ingested via inspiration (as dissolved tritium) and 80% via diet (as particulate tritium) [II.18, II.19].

II.1.7.6. Excretion

All the tritium taken up into the fish is released back into the water from the fish fast compartment via excretion, expiration and death. Excretion is divided into what is excreted in particulate form as faeces and that excreted via expiration. It was assumed that of the hydrogen excreted, 90% is in dissolved form and 10% is particulate matter [II.20].

II.1.7.7. Metabolism rate

Using a cautious approach, it is assumed that 3% of the intake of tritium into the fast compartment (from both the water compartment and particulate suspended material compartment) is incorporated into the organic constituents of the fish in the slow compartment due to growth [II.17. II.21].

II.1.7.8. Catabolism rate

A constant net transfer rate was assumed; therefore there were no transfer losses from one compartment to the next. All that enters the fast compartment is lost at the same rate because the fish is in dynamic equilibrium.

II.1.8. LIETDOS_W Model

The LIETDOS_W model was developed to predict levels of radioactivity in water sediment, fish and aquatic plants in lake ecosystems. LIETDOS_W is a dynamic linear compartment model that is described by first order differential equations with constant or time-dependent coefficients. This model has been developed at the Institute of Physics (Lithuania) and used to evaluate the contamination in the Ignalina NPP cooling pond (Druksiai Lake). In the case of the Perch Lake scenario, an additional submodel was developed for predicting non-exchangeable OBT concentrations. The parameters associated with this new submodel are presented in Table II.1.5.

The prediction of HTO and OBT concentrations in cattails, bladderworts and hornworts was based on measured HTO offshore surface water concentrations at sampling sites S1, S2 and S3 in May. HTO concentrations in all aquatic plants and animals were assumed to be equal to or slightly less than the corresponding water concentration [II.22]. The OBT/HTO ratio varied between 0.66 and 0.82 for worts and cattails and was 0.38 in the case of fish and clams [II.4, II.22]. The modeling of algae and sediments was beyond the capability of the model.

The standard deviation of HTO concentration in lake water was calculated according the data given in the scenario description. In the case of other endpoints, the standard deviation was evaluated according to the data presented in Table II.1.5. The 95% confidence intervals were calculated using lognormal distributions by means of Crystal Ball software.

Table II.1.5. Submodel parameter values.

Endpoint	$HTO_{endpoint}$ / HTO_{water}		OBT / HTO		References
	Mean value	Range	Mean value	Range	
Worts	0.9	0.8–1.0	0.75	0.4–1.0	[II.4, II.22]
Cattail above water	0.75	0.6–0.9	0.66	–	
Cattail below water	0.9	0.8–1.0	0.82	0.5–1.0	
Clam	0.9	0.8–1.0	0.38	0.15–0.6	
Bullhead	0.9	0.8–1.0	0.38	0.15–0.6	
Pike	0.9	0.8–1.0	0.38	0.15–0.6	

II.2. Pickering Scenario model descriptions

II.2.1. LLNL Model

II.2.1.1. Introduction

The stochastic model DCART (Doses from Chronic Atmospheric Releases of Tritium) was used to generate predictions for the Pickering Scenario. DCART was developed as a realistic assessment model to be used in a dose reconstruction for tritium releases from the Lawrence Livermore National Laboratory [II.23]. It is a steady-state, analytical compartment model that calculates uncertainties using parameter distributions and Latin Hypercube Sampling. Compartments include air and air moisture, soil, plant water, plant organic matter, animal water, and animal organic matter.

In the plant, processes include uptake of tritiated water (HTO) from soil water and air moisture and conversion to organically bound tritium (OBT); in the animal, processes include inhalation and skin absorption of air moisture, ingestion of water and food, and the partitioning into HTO and OBT within the animal. For the Pickering Scenario, starting with concentrations of HTO in air (Bq m^{-3}), concentrations of HTO and OBT in vegetables (leafy, fruit and root), fruit, pasture, grain, cow milk, beef, chickens and eggs were calculated; HTO concentrations in soil were also calculated.

II.2.1.2. Key assumptions (unique to the Pickering Scenario)

Four sets of calculations had to be carried out in order to predict the list of items requested in the scenario description. Calculations using air concentrations from 2001 were made to estimate concentrations in the components (e.g., barley, corn, haylage) of the total mixed ration (TMR). Calculations using air concentrations from 2002 were made to estimate the concentrations in various types of fodder, vegetables and fruit. Calculations using air concentrations from 2002 and TMR from 2001 were made to estimate concentrations in milk and calf meat. If the product calculated in 2002 was harvested in July, the mean of the air concentrations from May to July was used; if the product calculated in 2002 was harvested in September, the mean of the air concentrations from May to September was used.

II.2.1.3. Modeling approaches

DCART would normally be used to estimate annual mean concentrations in plant and animal products from annual mean air concentrations. Shorter periods of time, such as those for the Pickering scenario, may also be modeled, as long as the averaging time is long enough for the system to approach equilibrium.

DCART is calibrated so that the ratio of soil moisture concentration to air moisture concentration is a set fraction for a release of HTO. Alternatively, soil water concentrations may be set equal to concentrations in rainfall. DCART was run with both assumptions for the September 2002 predictions and yielded almost identical results in plants and animals in both cases. This is not surprising given that soil water is not an important pathway in DCART and that soil water concentrations differed by less than a factor of two.

The mean concentrations of HTO in plant water of leafy vegetables and pasture are given by the equation:

$$C_{pw} = 1/\gamma \, [R_H \, C_{a\_HTO} / H_a + (1 - R_H) \, C_{sw}] \qquad \text{(II.2.1)}$$

where:

C_{pw} is the concentration of tritium in the plant water (Bq L^{-1} or Bq kg^{-1});
γ is the ratio of vapor pressure between HTO and H_2O (0.909);
R_H is the relative humidity ;
C_{a_HTO} is the concentration of HTO in air (Bq m^{-3});
H_a is the absolute humidity (kg m^{-3}); and
C_{sw} is the concentration of tritium in soil moisture (Bq L^{-1}).

The mean concentrations of HTO in fruits, fruit vegetables and grain are calculated similarly but without accounting for γ or relative humidity. Instead it is assumed that 60% of the HTO in the fruit comes from air moisture and the other 40% comes from soil water. The annual concentration of HTO in a root crop is assumed to equal 95% of the concentration in soil water.

Mixed vegetables were assumed to be equal proportions of beets, cabbage, hot pepper, dill, spinach, onion, and potato.

Concentration of OBT in all plants in Bq L^{-1} water equivalent was assumed to equal the concentration in plant water (as calculated for leafy vegetables and pasture) reduced by a discrimination factor that arises from isotopic effects in OBT formation. Because of this assumption, in DCART all concentrations of OBT in all types of vegetables are the same in Bq L^{-1}, given the same air concentration.

In DCART it has been assumed that the HTO concentration in the animal (in Bq L^{-1}) equals the weighted concentration of tritium obtained from food, water and air (all also in Bq L^{-1}) taken in by the animal. In other words, DCART calculates the Bq L^{-1} HTO in the animal from the concentrations in and fractions of water contributed by plant water, plant organic matter, drinking water, and inhalation and skin-absorption. OBT concentrations in the animal are assumed equal to HTO concentrations.

DCART calculates tritium concentrations in plants and animals in both Bq kg^{-1} fresh weight and Bq L^{-1} water or water equivalent. To convert between the two requires parameters for dry matter content and water equivalent.

Air concentration in Bq m^{-3}, obtained either from measurements at the location of interest or from dispersion modeling, is the primary input to DCART. A value for absolute humidity is needed to convert tritium in air volume to tritium in air moisture, which is the parameter that drives all calculations. All plants and animals are assumed exposed to the same air concentration, regardless of whether this is physically possible.

II.2.1.4. Parameter values used in the Pickering Scenario

— **Air**

The mean air concentrations and standard deviations in Bq m^{-3} that were used for different time periods are shown in Table II.2.1. Distributions are lognormal.

The absolute humidity used for Pickering was 0.012 kg m^{-3} with an uncertainty on a normal distribution of ± 10%. The relative humidity used for Pickering was 73% with a normal distribution ± 10% uncertainty.

Table II.2.1. HTO air concentrations.

Averaging time	Air concentrations in Bq m^{-3}			
	DF8	DF11	F27	P2
2001	1.21 ± 0.944	1.21 ± 0.944		
2002 May–July	1.15 ± 0.344	1.15 ± 0.344	1.77 ± 0.53	
2002 May–September	0.976 ± 0.263	0.976 ± 0.263	1.51 ± 0.403	23.2 ± 6.22

Table II.2.2. Soil water concentrations.

Sampling location	Soil water concentrations in Bq L^{-1}	
	Based on 0.3 x air moisture	Based on rainfall
DF8 and DF11	24.5 ± 9.70	41.5 ± 31.2
F27	37.8 ± 16.2	25.1 ± 15.3
P2	580 ± 238	432 ± 123

Table II.2.3. Animal diets.

Diet (kg dw d^{-1})	Cows – DF8	Cows – DF11	Chickens**/eggs
TMR*	19 ± 0.95	16.4 ± 1.64	
Green beans			0.0135
Feed corn			0.0580
Grass etc.			0.0386
Apples			0.00966
Carrots and potatoes			0.01932
Water	80 ± 8		0.29
Inhalation (m^3 d^{-1})	144 ± 67; left truncated at 74		1 ± 0.6 truncated at 0.3 and 2.0

* TMR is made up of varying amounts of baled hay, corn silage, feed corn, haylage and, for D8 only, barley.

** The uncertainty on the diets for chickens is rectangular with the limits being ± 25% of the best estimate; water ingestion for chickens has a triangular distribution with minimum at 0.15 and maximum at 0.44.

Table II.2.4. Rank correlation coefficient for fodder crops.

HTO in		Parameter	OBT in	
Group 1	Group 2		Group 1	Group 2
0.91	0.92	Air concentration (Bq m^{-3})	0.73	0.73
N/A	N/A	Isotopic discrimination	0.56	0.56
-0.29	-0.30	Absolute humidity	-0.24	-0.24

Table II.2.5. Rank correlation coefficient for dairy and meat cows.

HTO in		Parameter	OBT in	
Milk	Meat		Milk	Meat
0.86	0.87	Natural variability	0.72	0.73
N/A	0.51	Plant OBT to animal OBT	N/A	0.51
0.31	0.32	Drinking water concentration	0.26	0.26
0.28	0.26	Concentration of HTO in TMR	0.23	0.22

Table II.2.6. Rank correlation coefficient for chickens.

Chicken HTO	Parameter	Chicken OBT
0.75	Air concentration (Bq m^{-3})	0.49
N/A	Plant OBT to animal OBT	0.73
0.39	Drinking water (Bq L^{-1})	0.26
-0.29	Drinking water rate (L d^{-1})	-0.20
-0.22	Absolute humidity	-0.15

— **Soil**

A triangular distribution has been applied to the calibrated fraction that relates soil water concentration to concentration in air moisture; the minimum is 0.1, the best estimate 0.3, and the maximum 0.5.

For 2001 calculations, soil was only assumed to have one-third the concentration of air moisture. For 2002, predicted soil concentrations based on 30% air moisture are compared in Table II.2.2 to soil concentrations based on rainfall concentrations. Concentrations are given in Bq L^{-1}, and distributions are lognormal.

— **Plant**

An isotopic discrimination factor for OBT of 0.7 has been chosen. This parameter has an extreme value distribution with a 2.5% confidence limit of 0.49 and a 97.5% confidence limit of 1.18 based on empirical data.

The fractional relationship between concentration of HTO in fruit and grain and concentration in air moisture is described by a triangular distribution (0.5 – 0.6 – 0.7).

— **Animals**

For the calculation of OBT alone, because the transfer of plant OBT to animal OBT occurs preferentially, at least dynamically, the part of the equation that accounts for this transfer has been multiplied by a parameter with value 1 ± 40%; the lower bound is truncated at 0.8. This parameter obviously does nothing to change the best estimate; it only increases the uncertainty about the concentrations of OBT.

A parameter was added to DCART to help account for the natural variability between an average cow and the single individuals sampled for the scenario at farms DF8 and DF11. This parameter has a normal distribution with a value of 1 and an uncertainty of ± 30%.

Ingestion and inhalation parameters are shown in Table II.2.3. Uncertainties have normal distributions unless noted.

To estimate the concentration in TMR, the concentration of the food types making up TMR were calculated for 2001 air concentrations on a Bq kg^{-1} basis for both HTO and OBT. Total HTO or OBT in the daily diet of TMR was calculated by summing the products of the concentration of each foodstuff times the ingestion rate-equivalent for that foodstuff in TMR. Then the Bq kg^{-1} TMR HTO or OBT was calculated by dividing total Bq d^{-1} HTO or OBT by kg TMR d^{-1}. Concentration of TMR in Bq kg^{-1} was then converted to Bq L^{-1}. The TMR from 2001 was input into DCART as animal feed in 2002. The uncertainty on the concentration of TMR was lognormal ± 45%.

The uncertainty on the drinking water concentrations was ± 20% for a normal distribution.

II.2.1.5. Application of the model to the scenario

Air concentrations (Bq m^{-3}) used as input were obtained from the scenario description. The monthly values were averaged, and the standard deviations of the averages were used to estimate uncertainty; this means that the uncertainty about the mean is over-estimated. Concentrations for May to July were weighted averages (four weeks in May, four weeks in June, and two weeks in July).

The average absolute humidity was taken from the Scenario Description (Appendix I.2). Relative humidity was calculated partly using temperatures from Table I.2.2. Rainfall concentrations from Table I.2.9 were averaged to estimate possible concentrations in soil water.

Animal diets were based on the information provided in the Scenario Description (Appenidx I.2). Using the ratios of each type of feed in TMR (from Table I.2.3), a diet of TMR was devised that added up to 19 kg dry weight for Farm DF8 and 16.4 kg dry weight for DF11 (revised upwards from the acknowledged low limit of 8.8 kg). The revised diet for DF11 is reasonable, although it is still less than the diet at DF8: metabolizable calories were estimated at 39 Mcal for DF8 and 20 Mcal for DF11. Concentrations for only the feed grown locally (baled hay, barley, corn silage, feed corn and haylage) were calculated. It was assumed that at each dairy farm the milk cow and the calf ate the same quantity and composition of food, because the concentration in the adult or juvenile would have been nearly the same had the diet for the calf been proportionally smaller; at F27, the chicken and the laying hen ate the same diet. The diet of the chickens was also estimated from Table I.2.4 in the scenario description and the assumption that chickens ate 0.139 kg per day. Drinking water concentrations were taken from Table I.2.8 in the Scenario Description (Appendix I.2).

For this scenario, the values for dry matter and water equivalent given in Tables I.2.5 and I.2.6 of the Scenario Description (Appendix I.2) were averaged between themselves, when appropriate, and with other values from a database. After combining the various values reported, small uncertainties were applied.

II.2.1.6. Sensitivity

Sensitivity analyses were run for various endpoints. In DCART, all types of fodder were modeled as just two groupings based on whether they were derived from foliage or grain:

- Group 1: Alfalfa hay, haylage, baled hay and corn silage; and
- Group 2: Soya meal, barley and feed corn.

The sensitivity of these two categories to various parameters is essentially identical. Parameters having rank correlation coefficients greater than 0.2 are shown in Table II.2.4 for the categories of fodder.

When dairy and meat cows are fed a diet of TMR, the important parameters and their rank correlation coefficients greater than 0.2 from a sensitivity analysis are shown in Table II.2.5.

The two parameters to which the endpoints are most sensitive (Table II.2.5) are those that attempt to account for uncertainty that cannot be quantified easily.

For the various vegetables eaten by the chickens, the sensitive parameters were similar to those above except that, for root crops, the soil concentration parameter had a rank correlation coefficient of 0.58, and the parameter relating concentration in potato to concentration in air moisture had one of 0.22 (Table II.2.6). The parameter for relative humidity had a rank correlation coefficient of 0.22 for grass.

The uncertainty about natural variability was neglected for chickens and eggs because there is much less variability in chickens than in cows. The rank correlation coefficients for chicken and eggs are as similar as those for milk and meat, so only those for chicken are shown in Table II.2.6.

II.2.2. IFIN Model

II.2.2.1. Introduction

- Model name: IFIN_Pick;
- Purpose of the model:IFIN_Pick is an assessment model. It was designed to not underpredict and to overpredict by no more than a factor of 3;
- Type of model: simple, steady-state, analytical;
- Biological/environmental compartments considered: air, precipitation, soil water, plants and animal products;
- Transport processes: HTO transfer from air to precipitation, soil, plants and animal products. OBT formation in plants and transfer to animals. Simplified transfer coefficients are used throughout;
- Endpoints: HTO concentrations in soil, plants and animal products; OBT concentrations in plants and animal products, as required by the scenario.

II.2.2.2. Model formulation and key assumptions

The HTO concentration in soil water is equal to the concentration in rain (60% from the current month and 40% from the previous month) plus 10% of the concentration in air moisture.

The HTO concentration in plant water (C_{pw}) is given by the classic formula [II.24]:

$$C_{pw} = 1.1\,[RH\,C_a + (1\text{-}RH)\,C_s] \quad \text{(II.2.2)}$$

where:

RH is the relative humidity;
C_a is the water vapour HTO concentration; and
C_s is the soil water HTO concentration.

For forage crops, leafy vegetables and TMR, the OBT concentration in the plant combustion water equals the HTO concentration in the plant water averaged over the previous 3 months. The OBT/HTO ratio for fruit and root crops is 0.75 and 0.40 respectively.

86% of TMR is made up of contaminated feed, with 70% coming from the July harvest and 30% from the September harvest.

Animals take in HTO with their drinking water and their food. OBT intake occurs only with food. The cow at DF11 was assumed to have the same diet as the cow at DF8.

HTO concentrations in milk, eggs and meat (C_{an}) were calculated from:

$$C_{an}^{HTO} = FHH*HTO\_intake + FOH*OBT\_intake, \quad \text{(II.2.3)}$$

where:

HTO_intake and OBT_intake are the intake rates of HTO and OBT respectively; and
FHH and FOH are animal-specific transfer factors derived from a metabolic model (see Table II.2.7).

Table II.2.7. Animal transfer factors.

Animal product	FHH	FOH	FHO	FOO
Cow milk	0.01	0.007	0.0003	0.007
Veal meat	0.028	0.02	0.002	0.05
Broiler meat	2.6	2.3	0.2	3.1
Egg	2	1.7	0.13	2.4

Similarly, OBT concentrations in animal products are calculated from:

$$C_{an}^{OBT} = FHO*HTO\_intake + FOO*OBT\_intake\ . \quad \text{(II.2.4)}$$

To convert OBT concentrations in fresh weight to concentrations in combustion water, it was assumed that the dry fraction was 0.13 for milk, 0.28 for veal meat and 0.26 for hens and eggs. The water equivalent was 0.7 for milk, 0.66 for veal meat and 0.8 for egg and hens.

II.2.2.3. Uncertainties

Uncertainties in the model predictions were estimated by expert judgement and are believed to be optimistic.

II.2.3. LIETDOS Model

II.2.3.1. Tritium concentrations in air and soil

LIETDOS is a compartment model for a terrestrial system that has achieved steady state in terms of activity exchange by balancing gains and losses. Taking into account that HTO is present mainly in the aqueous phase of a compartment, the total compartment inventory and the water-phase inventory of tritium are assumed to be the same in soil and in air.

The simultaneous balancing of gains and losses for both soil and air compartments allows the activity inventories of the two compartments to be calculated as follows:

$$S + \lambda_{sa}\, Q_{soil} - \lambda_{air}\, Q_{air} = 0; \quad \text{(II.2.5)}$$

$$\Lambda_{as}\, Q_{air} - \lambda_{soil}\, Q_{soil} = 0, \quad \text{(II.2.6)}$$

where:

S represents the rate of HTO input (i.e., the HTO emission rate) into the air compartment (Bq/d);
Q_{soil} and Q_{air} represent the compartment HTO inventory in soil and air respectively (Bq);
λ_{sa} is the soil to air activity transfer rate constant (d^{-1});
Λ_{as} is the air to soil activity transfer rate constant (d^{-1}); and
λ_{air} and λ_{soil} are the effective activity decrease rate constants in air and soil respectively (d^{-1}).

Using Equation (II.2.6), the long-term average pollutant concentration in air (C_{air}, Bq m^{-3}) can be presented in the following manner:

$$\Lambda_{as}\, h_{air}\, C_{air} - \lambda_{soil}\, h_{soil}\, C_{soil} = 0, \quad \text{(II.2.7)}$$

where:

h_{air} is the atmospheric mixing height (m);
h_{soil} is the soil compartment depth (m);
C_{soil} is the volumetric tritium activity in the soil (Bq/m^3 soil); and
λ_{soil} is the effective activity decrease rate constant in the soil compartment due to evapotranspiration ($\lambda_{evapotrans}$), recharging (λ_{sink}), runoff (λ_{runoff}) and radioactive decay (λ_r) (d^{-1}):

$$\lambda_{soil} = \lambda_{evapotrans} + \lambda_{sink} + \lambda_{runoff} + \lambda_r \quad \text{(II.2.8)}$$

Instead of using the air concentration C_{air}, the activity in precipitation (C_{pr}, Bq/m^3 water) has been used as input to the model. Based on this proposal, the activity balance equation for the soil compartment can be written as:

$$I_{pr} \cdot \phi_{soil} \cdot C_{pr} - \lambda_{soil} \cdot h_{soil} \cdot C_{soil} = 0; \quad \text{(II.2.9)}$$

where:

I_{pr} is the average precipitation rate during the time period of interest (m d^{-1}); and
ϕ_{soil} is the volumetric soil moisture content (m^3 water per m^3 soil).

According to Equations (II.2.7) and (II.2.9):

$$\Lambda_{as} = I_{pr} \cdot \phi_{water} / (h_{air} \cdot \phi_{air}) \quad \text{(II.2.10)}$$

where:

ϕ_{water} is the activity scavenging factor for raindrops passing through air (m^3/m^3); and
ϕ_{air} is the volumetric fraction of water in air (m^3/m^3). ϕ_{air} is given by:

$$\phi_{air} = f_{RH} \cdot e_{sat} \cdot (M_{H2O}/\rho_{H2O}) / (R \cdot T_{air}) \quad \text{(II.2.11)}$$

$$\text{where } e_{sat} = 100 \cdot \exp (11.28\text{-}2319.25/T_{air}) \quad \text{(II.2.12)}$$

$$f_{RH} = 100 \cdot e_{AH} / (M_{H2O} \cdot e_{sat} / (R \cdot T_{air})) \quad \text{(II.2.13)}$$

where:

f_{RH} is the observed relative humidity (%);
e_{sat} is the saturation vapor pressure (Pa);
R is the universal gas constant = 8.31434 (Pa m^3)/(mol K);
T_{air} is the ambient absolute air temperature (K);
M_{H2O} is the molecular weight of water (18.016 g mol^{-1});
ρ_{H2O} is the density of water (10^6 g/m^3); and
e_{AH} is the absolute humidity of the air (g m^{-3}).

The soil to air activity transfer rate constant (λ_{sa}), recharging coefficient (λ_{sink}) and runoff coefficient (λ_{runoff}) can be estimated according to known annual average evapo-transpiration, infiltration to ground water and runoff values $I_{evapotrans}$, $I_{recharge}$, I_{runoff} (m d^{-1}) respectively.

Table II.2.8. Meteorological and soil properties for the PNGS environment.

Parameter	Symbol	Mean value
Air absolute humidity, g m^{-3}	e_{AH}	12
Mean atmospheric mixing height, m	h_{air}	600
Soil compartment depth, m	h_{soil}	2.5
Volumetric moisture content of the soil, L(water)/L(soil)	ϕ_{soil}	0.3
Annual average evapotranspiration, m d^{-1}	$I_{evapotrans}$	0.45
Annual average runoff, m d^{-1}	I_{runoff}	0.13

$$\lambda_{sa} = \frac{I_{evapotrans} \cdot \phi_{water}}{\phi_{soil} \cdot h_{soil}}; \quad \text{(II.2.14)}$$

$$\lambda_{recharge} = \frac{I_{recharge} \cdot \phi_{water}}{\phi_{soil} \cdot h_{soil}}; \quad \text{(II.2.15)}$$

$$\lambda_{runoff} = \frac{I_{runoff} \cdot \phi_{water}}{\phi_{soil} \cdot h_{soil}}. \quad \text{(II.2.16)}$$

The parameter values used in the calculations are presented in Table II.2.8.

Using scenario data, the activity scavenging factor for raindrops passing through air (ϕ_{water}) was determined. The mean value during the time period 2001-2002 was 0.38.

HTO concentrations in the top soil layer for each site and each sampling period were calculated from Equations II.2.5–II.2.16 and the parameter values in Table II.2.8.

II.2.3.2. Tritium concentration in plant products

Equations are applied for leafy vegetable, pasture and hay according to [II.25]. The concentration of tritiated water in the leafy parts of plants ($C_{lv,w}$) is dependent on the tritium concentration in air moisture $C_{air,w}$ and soil water $C_{soil,w}$ according to:

$$C_{lv,w}(HTO) = 1.1 \cdot f_{RH} \cdot C_{air,w}(HTO) + 1.17 \cdot (1 - f_{RH}) \cdot C_{soil,w}(HTO). \quad \text{(II.2.17)}$$

Other food items such as fruit vegetables, fruits, tubers and grain have a higher contribution by soil water and in those cases the HTO concentration was approximated by:

$$C_{other,w}(HTO) = 1.1 \cdot f_{RH} \cdot 0.33 \cdot C_{air,w}(HTO) + 1.17 \cdot (1 - f_{RH} \cdot 0.33) \cdot C_{soil,w}(HTO). \quad \text{(II.2.18)}$$

In our calculations, the concentration of OBT in combustion water, under equilibrium conditions, is related to the concentration of HTO in plant water by a factor 0.8:

$$C_{p,w}(OBT) = 0.8 \cdot C_{p,w}(HTO). \quad \text{(II.2.19)}$$

II.2.3.3. Tritium concentration in animal products

The concentration in animal products (C_{animal}, Bq kg^{-1}) depends on the transfer factor F (day kg^{-1}) and intake activity I (Bq/day):

$$C_{animal} = F \cdot I = F \cdot \Sigma u_i \cdot C_i \quad \text{(II.2.20)}$$

where:

u_i is the intake rate of diet item i (kg day^{-1}); and
C_i is the concentration in that item (Bq kg^{-1}).

In the case of tritium we considered two main chemical forms, HTO and OBT, including metabolic transformations between them. The concentration of HTO or OBT in animal products is:

$$C_{HTO} = F_{HH} \cdot I_{HTO} + F_{OH} \cdot I_{OBT} \qquad \text{(II.2.21)}$$
$$C_{OBT} = F_{HO} \cdot I_{HTO} + F_{OO} \cdot I_{OBT}$$

where:

F_{HH} is the transfer factor from HTO in food to HTO in animal product;
F_{HO} is the transfer factor from HTO in food to OBT in animal product;
F_{OH} is the transfer factor from OBT in food to HTO in animal product; and
F_{OO} is the transfer factor from OBT in food to OBT in animal product.

II.2.4. IRSN Model

II.2.4.1. Introduction

The IRSN Tocatta model simulates the transfer of tritium (and/or carbon-14) within terrestrial ecosystems in response to chronic or accidental releases of HTO (and/or carbon 14) to the atmosphere. It has been developed from bibliographical knowledge and in common with existing models of tritium transfer, in order to come within the conceptual and mathematical frameworks of the SYMBIOSE project[1].

II.2.4.2. Key assumptions

- The model simulates the impacts of HTO releases to the atmosphere. HT and CH_3T releases are not considered;
- The main transfer paths of tritium within the terrestrial ecosystem are the following:
  - Net transfer of atmospheric HTO into the aqueous and organic parts of foliar systems (via diffusion/absorption and net photosynthesis, respectively);
  - Transfer onto soil via dry deposition and precipitation; HTO losses through evapotranspiration and vertical migration into the underlying soil layers (not considered here);
  - Transfer to animals by ingestion of vegetal products, inhalation and skin absorption, translocation and depuration (elimination).

II.2.4.3. Modeling approaches

The conceptual modeling deals with splitting the continental biosphere into elementary components and identifying interactions (or transfer processes) between each component. This approach is based on the global interaction matrix shown in Figure II.2.1.

[1] SYMBIOSE is a modelling and simulation platform for environmental pollutant risk assessment (IRSN, Cadarache, sponsored by Electricité de France).

	ATMOSPHERE	AGRICULTURAL ECOSYSTEM					
		SOIL	VEGETAL		ANIMAL Animal products		
SOURCE	Atmospheric release	Precipitation Dry deposition					
	AIR [HTO]		Absorption	Photosynthesis Translocation		Inhalation & Skin absorption	
		WAT [HTO]					Evaporation Transpiration Migration
			WAT [HTO]				
				O.M. [C14 & OBT]			
			VEGETAL		Ingestion	Ingestion Translocation	
					WAT [HTO]		
						O.M. [C14 & OBT]	
					ANIMAL		Elimination
							∞

Matrix of components (cross) and tranfer processes (vertical). WAT=water; O.M.=organic matter; ∞=all other systems, not considered here (e.g. underlying soil layers)

Fig. II.2.1. Conceptual model of the transfer of atmospheric HTO (and C-14) into the agricultural ecosystem.

In the case of accidental atmospheric releases, the mathematical modeling used for calculating daily inventories and fluxes is based on a system of first order differential equations expressing the conservation of tritium activity for each component:

$$\frac{d\left\{\chi_i [T]_i^{HTO}\right\}}{dt} = \underbrace{\overbrace{\sum_{j\neq i,p} TM_{j,i}^{p}}^{inputs} - \overbrace{\sum_{j\neq i,p} TM_{i,j}^{p}}^{outputs}}_{Transfer\ processes} \qquad \text{(II.2.22)}$$

where:

$[T]_i^{HTO}$ (x,t) is the HTO concentration of component i;

χ_i (x,t) is the density of component i (e.g. plant surface biomass);

$\chi_i [T]_i^{HTO}$ (t) is the HTO inventory of component i; and

$TM_{i,j}^{p}$ (t) is the activity transfer process from component i to component j under process p.

A similar equation is used to estimate the temporal dynamics of non-exchangeable OBT concentration (i.e. $[T]_i^{OBT}$) of each component i considered.

In the case of chronic releases, the analytical solutions are calculated by solving the previous system of differential equations when the temporal derivatives are set to zero.

II.2.4.4. Input data

Tables II.2.9 and II.2.10 list the parameters appearing in the Tocatta model. Table II.2.11 shows the parameter values and distributions used in the calculations.

II.2.4.5. Uncertainties

Uncertainties in the model predictions were determined using Latin Hypercube sampling of the distributions shown in Table II.2.11 in 1000 simulations.

Table II.2.9. Type of input data.

Type of Input	Input data
Radiological	Isotopic discrimination factors HTO dilution factors into plants through soil water HTO drinking water concentration Half-life related to plant growth dilution*
Ecological	Plant growth curves and associated parameters* Sowing, germination and harvest dates*
Physiological	Dry matter fractions Water equivalent factor Water fraction contributed to the diet by inhalation and skin absorption, and by food H metabolism
Trophic chain	Food and water ingestion rates

* Data required in the case of accidental releases only.

Table II.2.10. Parameters.

Symbol	Unit	Description
AIR		
H_a	kg m^{-3}	Absolute humidity
P	mm/month	Monthly precipitation
$[T]_{air}^{HTO}$	Bq m^{-3}	HTO concentration in air
$[T]_{precip}^{HTO}$	Bq L^{-1}	HTO concentration in precipitation
PLANT		
DI_{veg}	–	Isotopic discrimination factor
FD_f	–	HTO dilution factor in leaves by water coming from soil
FD_{veg}	–	HTO dilution factor in whole plant by water coming from soil
FE_{veg}	L kg^{-1} dw	Water equivalent factor
f_{veg}^{H2O}	L kg^{-1} fw	Average water fraction of plants
ANIMAL		
f_{ap}^{H20}	L kg^{-1} fw	Average water fraction of animal products
f_{ap}^{inhabs}	kg kg^{-1}d^{-1}	Water fraction contributed to the diet by inhalation and skin absorption
f_{ap}^{met}	kg kg^{-1}	Water fraction contributed to the diet by metabolism of hydrogen in food
FE_{ap}	L kg^{-1} dw	Water equivalent factor
$R_{water,ap}^{ing}$	L animal^{-1} d^{-1}	Daily water ingestion rate
$R_{i,poa}^{ing}$	kg fw animal^{-1} d^{-1}	Daily food ingestion rate
$[T]_{drink}^{HTO}$	Bq L^{-1}	HTO concentration in drinking water
SOIL		
D	m^{-2} s^{-1}	Diffusion coefficient of tritium into soil
F_{evap}^{HTO}	d^{-1}	Average evaporation rate
F_{transp}^{HTO}	kg m^{-2} d^{-1}	Average plant transpiration rate
f_{soil}^{H20}	L kg^{-1} fw	Water fraction of the sampled soils
H_{sol}	m	Soil layer depth
ρ_b	kg m^{-3}	Bulk density
ρ_v	kg m^{-3}	Saturation vapour mass at soil surface temperature
v_d	m s^{-1}	Dry deposition velocity

Table II.2.11. Parameter values and distributions.

Parameter	Deterministic value	Distribution	Minimum	Maximum	Most likely value
AIR					
H_a , P , $[T]^{HTO}_{precip}$	cf. scenario description				
$[T]^{HTO}_{air}$	cf. scenario description	Uniform	-30%	+30%	
PLANT					
DI_{veg}	0.9	Triangular	0.7	1.1	0.9
FD_f	0.85	Uniform	0.8	0.9	
FD_{veg}	0.9	Uniform	0.85	0.95	
FE_{veg}	cf. scenario description	Uniform	-10%	+10%	
f^{H2O}_{veg}	cf. scenario description				
ANIMAL					
f^{H20}_{ap}	cf. scenario description				
f^{inhabs}_{ap} milk egg beef	0.021 0.036 0.028	Uniform	-10%	+10%	
f^{met}_{ap}	0.3	Uniform	0.2	0.4	
FE_{ap}	cf. scenario description	Uniform	-10%	+10%	
$R^{ing}_{i,poa}$	Total ingestion rates : Cows DF8 : 19 kg dw/d Cows DF11 : 10 kg dw/d Chicken F27 : 0.2 kg dw/d Ratios of feed components: cf. scenario	Uniform	-15%	+15%	
$R^{ing}_{water,ap}$	Cows DF8 : 75 L/d Cows DF11 : 75 L/d Chicken F27 : 0.3 L/d	Uniform	-15%	+15%	
$[T]^{HTO}_{drink}$	DF8 : 18.6 Bq/L DF11 : 21.1 Bq/L F27 : 24.3 Bq/L	Uniform	-10%	+10%	
SOIL					
D	$1x10^{-9}$ m^2/s				
F^{HTO}_{evap}	0.24 d^{-1}	Uniform	0.215	0.265	
F^{HTO}_{transp}	0.8 $L/m^2/d$	Uniform	0.7	0.9	
f^{H20}_{soil}	cf. scenario description				
H_{sol}	0.05 m				
ρ_b	1.08 g/cm^3				
ρ_v	0.015 kg/m^3				
v_d	0.001 m/s	Uniform	0.0005	0.0015	

II.2.5. TUM Model

Analytical procedures such as freeze drying and azeotropic distillation yield "buried" tritium as well as carbon bound tritium. The former amounts to the larger part according to the work of [II.7]. Buried tritium is not relevant to long-term doses because it converts immediately by isotope exchange to HTO during digestion. Here, the Biochem Model calculates the amount of exchangeable tritium, including buried tritium. Carbon bound tritium, which is the tritium fraction that determines long-term dose, is obtained as the difference between OBT obtained experimentally and exchangeable tritium.

II.2.5.1. HTO calculation

The model was driven by tritium concentrations in plants and animals rather than in air. Water inside plants or animals starts from the roots or the intestines and moves towards the leaves or the skin and kidneys. Therefore, it is assumed that the HTO concentration in plants and animals is equal to the mean of the HTO concentration in drinking water (Table II.2.12) and in rainfall (Table II.2.13) averaged over the 2-3 months prior to sampling; where the drinking water concentration was not available in July, the plant and animal concentrations were set equal to the average concentration in rain. Accordingly, the plant and animal HTO concentrations in July were determined to be 47, 30 and 446 Bq L^{-1} at the dairy farms, F27 and P2, respectively; for September, the corresponding values were 24.8, 22.7 and 447 Bq L^{-1}.

II.2.5.2. Buried Tritium

Buried tritium arises by triton-proton exchange during formation of biomolecules. We apply the fractionation factor $\alpha \approx 2$ as found in DNA. In the definition:

$$\alpha = (Bq/H_{ex})_{org}/(Bq/H_{ex})_{aq}\,, \qquad \text{(II.2.23)}$$

Table II.2.12. Measured HTO concentrations in drinking water in 2002 September.

Compartment	DF8	DF11	F27	P2
Drinking water concentration (Bq L^{-1})	18.6	21.1	24.3	Not relevant

Table II.2.13. Measured monthly HTO concentrations in precipitation.

Month	HTO Concentration in Precipitation (Bq L^{-1})		
	DF8	F27	P2
January	not available	not available	3670
February	not available	18	1350
March	not available	24	347
April	24	29	474
May	69	14	525
June	85	61	579
July	9	14	205
Mean April–July	**47**	**30**	**446**
August	49	19	442
September	13	22	452
Mean August–September	31	21	447
Mean of drinking water and precipitatation	**24.8**	**22.7**	

The tritium activity is denoted by Bq and the number of exchangeable hydrogen positions in the molecular unit by H_{ex}. Applying well-known definitions leads to:

$$(Bq/H_{ex}) = (Bq/L)\ WE\ (M/H_{ex}), \quad \text{(II.2.24)}$$

where:

WE is the water equivalent factor (L/kg); and
M is the gram amount of the molecular unit.

With $\alpha = 2$ we obtain:

$$(Bq/L)_{org} = 2 \cdot (Bq/L)_{aq} \cdot (18/2)\ (H_{ex}/M)_{org} / WE_{org}. \quad \text{(II.2.25)}$$

Assuming biomatter with buried hydrogen exists only in carbohydrates (CH_2O; cellulose, glycogen) and proteins, Equation (II.2.25) becomes:

$$(Bq/L)_{org} = 2 \cdot (18/2)(Bq/L)_{aq} \cdot (18/2)\ [(H_{ex}/M)_{CH2O} + (H_{ex}/M)_{protein}]1000 / WE_{org}. \quad \text{(II.2.26)}$$

From the stoichiometry of carbohydrates $(C_6H_{10}O_5)_n$, M=162 and $(H_{ex}/M)_{CH2O} = 3/162 = 0.0185$. Taking account of the stoichiometric mean of 207 unrelated proteins [II.9], $(H_{ex}/M)_{protein} = 0.01676$. Plants are assumed to consist of carbohydrates only. The carbohydrate and protein contents of food are taken from the Nutrient Data Laboratory (www.nal.usda.gov-fnic-foodcomp-search).

II.2.6. FSA Model

The UK Food Standards Agency obtained predictions for the Pickering scenario using the Short-Term Atmospheric Release for H-3 (STAR H-3) model [II.26], which was developed by Intera Information Technologies (now part of Enviros Consulting). The model is implemented in the Amber software package:

(http://www.enviros.com/index.cfm?fuseaction=100&divisionId=6)

STAR H-3 is a dynamic compartment model formulated in terms of a series of coupled first-order differential equations. Rate constants for the transfers between compartments were derived from consideration of the hydrogen inventories of the compartments and the hydrogen fluxes between them. Predictions for the Pickering scenario, which is an equilibrium situation, were obtained from the steady-state solution to the equations.

The model starts with a tritium concentration in air and consists of 6 compartments. These are:

- Atmosphere: The air over an area of agricultural land in which the tritium concentration can be specified as a uniform or time varying concentration.
- Soil in Root Zone: This contains hydrogen in soil water. All tritium in this zone is assumed to be in the form of tritiated water.
- Plant Fast Turnover: This compartment represents the tritiated water and labile organically bound tritium in plant tissues.
- Plant Slow Turnover: This compartment represents the non-labile organically bound tritium within the plant tissues.

— Animal Fast Turnover: The portion of an animal containing tritiated water and labile organically bound tritium.
— Animal Slow Turnover: The non-labile organically bound tritium within the animal.

The model can represent a range of crop and animal types.

The following transfers are represented within the model:

— Transfer from Atmosphere to Soil in Root Zone: This transfer incorporates three components: HTO movement into the soil, water exchange between soil and atmosphere and wet deposition.
— Loss from Soil in Root Zone: Representing losses from the soil via evaporation and by transfer to deeper soil layers.
— Transfer from Soil in Root Zone to Plant Fast: Representing the uptake of water by plants. This process is driven by the net evapotranspiration of the plant.
— Loss from Plant Fast: This process accounts for loss from the plant via evapotranspiration and exchange of tritiated water between plant and atmosphere.
— Transfer from Atmosphere to Plant Fast: Representing the uptake of tritiated water by exchange with the atmosphere.
— Transfer from Plant Fast to Plant Slow: Representing the incorporation of tritiated water and labile organically bound tritium into non-labile forms.
— Transfer from Plant Slow to Plant Fast: The loss of non-labile tritium from plant tissues.
— Transfer from Plant Fast and Slow to Animal Fast: Representing the consumption of crops by animals.
— Transfer from Atmosphere to Animal Fast: This represents the intake by animals of tritium via inhalation.
— Loss from Animal Fast: Representing the losses by excretion.
— Transfer from Animal Fast to Animal Slow: The incorporation of tritiated water or labile organically bound tritium into animal tissues.
— Transfer from Animal Slow to Animal Fast: Representing the loss of non-labile organically bound tritium from animal tissues.

The FSA calculations for the Pickering scenario were reviewed following the meeting of the EMRAS Tritium/C14 Working Group in Cardiff. This revealed that the default value for water content of air appropriate to UK conditions had been used instead of the value specified in the scenario. Use of the scenario specific value for this parameter would have decreased the FSA predicted concentrations by approximately 1/3.

II.2.7. SRA Model

The model calculations were based on the hypothesis that all the compartments are in equilibrium with each other. Soil tritium concentrations were estimated using the formula of Belot and others [II.27] that accounts for the contributions of both wet and dry deposition to the soil water concentration:

$$C_{sw} = \frac{v_d\ C_a\ + F_w}{v_e\ \rho_s\ + I_r}, \qquad \text{(II.2.27)}$$

where:

v_d is the transfer velocity of HTO from air to soil (m s^{-1});
C_a is the tritium concentration in air (Bq m^{-3});
F_w is the average flux density of tritium wet deposition (Bq m^{-2} s^{-1});
v_e is the exchange velocity from soil to air (m s^{-1});
ρ_s is the water concentration in air saturated at the soil surface temperature (L kg^{-1}); and
I_r is the infiltration rate of water through the root zone (m s^{-1}).

For the estimation of the free water tritium (FWT) concentration in plants, the following formula was introduced:

$$C_p = \alpha\left(\frac{C_a + I_W C_{sw} r}{\rho_s + \alpha I_W r}\right) \quad \text{(II.2.28)}$$

where:

C_p is the FWT concentration in the plant (Bq L^{-1});
C_{sw} is the FWT concentration in soil water (Bq L^{-1});
α is the isotope effect factor of HTO;
I_W is the average rainfall intensity (kg m^{-2} s^{-1});
ρ_S is the saturated vapour density of the air in the atmosphere (kg m^{-3}); and
r is the exchange resistance for HTO and H_2O between the plant leaf and the atmosphere. Throughout the present calculations the value of r was assumed to be 67 s m^{-1}.

For all plant samples, including hay and haylage, rapid equilibration of plant FWT with atmospheric tritium vapour was assumed.

Since the water balance data for cows was not given, the daily free water intake was assumed to be 90 L d^{-1}. This value may be higher than the actual one. For tritium metabolism in lactating cows, the experimental results of Kirchmann et al. [II.28, II.29] were referred to. By using a slightly modified version of their data, the ratio of the tritium specific activity in drinking water and the diet to that in milk was derived and is shown in Table II.2.14.

Determination of the confidence interval on the predictions was accomplished with some difficulty. The confidence range of the observed tritium concentrations in the field samples is unknown. The values of the various parameters used in the mathematical formulation depend on a number of other parameters and on the assumed environmental conditions under which the calculation was made. Under such conditions, it was necessary to make a basic assumption about the uncertainty of the driving parameters. Therefore, the standard deviations of the driving parameters were assumed to be 20% of the observed or assumed values.

Table II.2.14. Specific activity ratios.

Tritium source	Samples	Specific activity ratio
HTO	Milk dry matter	0.48
	Milk water	0.91
Tritiated feed	Milk dry matter	0.52
	Milk water	0.09

II.2.8. GE Healthcare Model

The GE Healthcare model is a dynamic compartment model formulated in terms of a series of coupled first-order differential equations. Predictions for the Pickering scenario, which is an equilibrium situation, were obtained from the steady-state solution to the equations. The model is based on 1 kg of plant material, as this quantity can be easily amplified to the amount needed for consumption of crops within the critical group. The model starts with the tritium concentration in air and consists of four compartments representing the atmosphere, soil water, a plant fast compartment and a plant slow compartment. The plant fast compartment represents tissue free water inside the plant whilst the plant slow compartment represents the organic matter of the cells. It is assumed that these two compartments are in equilibrium within the plant. Transfer to animals was not modelled.

The following transfers are represented within the model:

- Transfer from the atmosphere to root zone soil water, including dry and wet deposition
- Loss from soil root zone by evaporation and transfer to deeper soil layers
- Transfer from root zone soil to the plant fast compartment, representing the uptake of water by plants.
- Transfer from the atmosphere to the plant fast compartment, representing the uptake of tritiated water by exchange with the atmosphere.
- Loss from the plant fast compartment, accounting for evapotranspiration and exchange of tritiated water between plant and atmosphere.
- Transfer from the plant fast compartment to the plant slow compartment, representing the incorporation of tritiated water and labile organically bound tritium into non-exchangeable forms.
- Transfer from the plant slow compartment to the plant fast compartment, accounting for the loss of non-exchangeable tritium from plant tissues.

II.3. Pine Tree Scenario model descriptions

II.3.1. NIRS Model

II.3.1.1. Introduction

We developed the Easy Evaluation System for Atmospheric Dispersion for tritium (Tritium-EESAD) code based on the random walk method (RWM). It can deal with hourly changes of weather conditions and tritium release rates, which makes it possible to assess accidental releases. The RWM, which was used in the SPEEDI system [II.30, II.31], expresses transfer of a radioactive cloud by movement of many particles, and estimates the behavior of the plume more effectively than the Gaussian plume model for short-term releases. The Tritium-EESAD code is able to calculate the deposition and the change of chemical form of tritium based on each particle. The process of re-emission from the ground surface soil and infiltration into deeper soil are calculated in each mesh division of the computation domain.

The atmospheric dispersion, deposition and re-emission processes in the tritium-EESAD code were validated using data from BIOMASS (IAEA Biosphere Modeling and Assessment Programme). It was first validated for the endpoints of the Canadian Scenario (Scenario 3 [II.32]) which focused on simulation of the phenomena caused by continuous and long-term tritium release. Tritium-EESAD was secondly validated for the Russian Scenario [II.33], in which additional data of tritium concentrations in atmospheric moisture, snow and soil water samples collected over shorter time intervals were provided by the Scenario developer [II.34].

II.3.1.2. Basic assumptions

- Two heavy water moderated reactors (JRR-2 and JRR-3) and a waste treatment facility (WTF) in JAERI were selected as the sources of tritium (HTO). The Tokai Repressing Plant (TRP) in JNC was neglected, because the contribution to air contamination at the receptors was considered to be small.
- Two locations (receptors) for calculating endpoints (P3 and MS2) were regarded as two different locations whose tritium concentrations were calculated independently.
- The three sources were regarded as three independent release points, and their locations were set up in the mesh coordinates relative to the locations of the two receptors.
- Monthly tritium discharge rates for JRR-2 and JRR-3 were used as inputs. For the WTF, only yearly discharge data were provided and thus monthly tritium discharge rates were calculated by dividing the yearly tritium discharge rates by 12.
- The scale of the mesh coordinates was 100 m by 100 m.

II.3.1.3. Calculation of atmospheric moisture concentration

Monthly mean tritium concentrations in atmospheric moisture were calculated from the arithmetic mean of the tritium activity in a unit volume of the air for the month, and the absolute humidity (the amount of water in a unit volume of air). Tritium activity in a unit volume of air was calculated by Tritium-EESAD as follows:

Atmospheric dispersion and deposition on the ground surface

— *Equations*

Movement of particles is expressed by the sum of movements by wind velocity and diffusion due to air turbulence. The position of a particle at time t+Δt after release, ($x_{t+\Delta t}$, $y_{t+\Delta t}$, $z_{t+\Delta t}$), is expressed by the following equations using particles located at time t after release (x_t, y_t ,z_t):

$$\left.\begin{aligned} x_{t+\Delta t} &= x_t + u_x \Delta t + dx \\ y_{t+\Delta t} &= y_t + u_y \Delta t + dy \\ z_{t+\Delta t} &= z_t + u_z \Delta t + dz \end{aligned}\right\} \quad \text{(II.3.1)}$$

where:

u_x, u_y, u_z is the wind velocity in the x, y, z directions; and
dx, dy, dz is the turbulent displacement in the x, y, z directions.

The turbulent displacements were calculated as a function of uniform random numbers and diffusion coefficients. Each diffusion coefficient was calculated using the Pasquill-Meade equation [II.35, II.36]. The contribution to the concentration at a given location from a particle at that location was calculated by the Kernel Density Estimator (KDE) method [II.37].

The deposition (wet and dry) to the ground surface during the time step Δt was calculated for each particle by the following Equations II.3.2 and II.3.3, where deposition depends on the spatial position of each particle.

$$G_W = \sum_{n=1}^{N} \alpha_n Q_n \left\{ 1 - \exp(-\Lambda \Delta t) \right\} \quad \text{(II.3.2)}$$

where:

G_W is the wet deposition amount in a mesh cell, Bq;
N is the number of particles distributed over the mesh;
α_n is the contribution ratio of particle n;
Q_n is the activity of particle n in the current time step, Bq;
Δt is the time step, s; and
Λ is the washout coefficient, s^{-1} (a function of rain intensity J (mm/h)).

$$G_d = \sum_{n=1}^{N} \alpha_n Q_n \left\{ 1 - \exp(-k v_g \Delta t) \right\} \quad \text{(II.3.3)}$$

where:

G_d is the dry deposition in a mesh cell, Bq;
v_g is the deposition velocity, m/s; and
k is the contribution to deposition in the height, m.

$$k = 2.0 \cdot \left(1 - \frac{h_p}{\Delta z} \right) \Big/ \Delta z \quad \text{(II.3.4)}$$

where:

h_p is the particle height, m; and
Δz is the height contributing to deposition, m.

Values for the washout coefficient and deposition velocity are given in Table II.3.1.

Table II.3.1. Important parameter values.

Variable	Value	Reference
Λ (Washout coefficient)	5.0×10^{-5} $J^{0.8}$ s^{-1}	BIOMASS [II.34]
v_g (Deposition velocity)	0.005 m/s	Field experimental data [II.38, II.39]

— *Meteorological data*

The hourly data on wind direction and wind velocity at a height of 40 m, precipitation intensity, air temperature, dew point and atmospheric stability class supplied by JAERI were used. Except for wind direction and stability class, the meteorological data sets for each month were prepared by averaging the hourly data for each parameter over the month. The stability classes were determined from the maximum frequencies and the wind direction was the monthly mean frequency. The resulting data were processed to fit the input format of Tritium-EESAD.

Infiltration of tritium from surface soil to lower soil layers

— *Equations*

Tritium deposited on the surface soil infiltrates to lower soil layers at a certain rate. The tritium concentration on the surface soil layer at time t after deposition is shown by the following equation:

$$q_{grn}(x,y)(t) = q_{grn}(x,y)(0)\left\{\ 1-\exp\left(-K_{perm}\cdot t\right)\right\} \qquad \text{(II.3.5)}$$

where:

$q_{grn}(x,y)(0)$ is the tritium activity deposited in mesh cell (x, y), Bq;
$q_{grn}(x,y)(t)$ is the tritium activity in mesh cell (x, y) at time t after deposition, Bq; and
K_{perm} is the Infiltration rate, h^{-1},

— *Parameter values*

Regarding K_{perm}, the peak concentration of tritium deposited on the surface soil layer moved downward at a maximum of 2 cm/day (= 0.0833 cm/h) [II.40]. If we assume the surface layer depth is 5 cm and tritium is present homogeneously, an infiltration rate is calculated as 0.0833 (cm/h) / 5(cm) = 1.67% h^{-1}.

Re-emission of tritium from surface soil to the air

— *Equations*

Generally, re-emission from surface soil to the air is driven by the tritium concentration difference between air and soil, and by evaporation caused by solar heating. Modeling evaporation phenomena needs many detailed meteorological data, for example, air temperature and moisture pressure at the soil surface. The re-emission rate from surface soil to the air has been reported from some field experiments. The Tritium-EESAD code considers re-emission only due to differences between the soil and air tritium concentrations:

$$q_{re} = (q_{grn} - q_{air})\ [1 - exp(-re_{HTO}\ t)] \qquad \text{(II.3.6)}$$

where:

q_{re} is the total re-emission in a mesh cell, Bq;
re_{HTO} is the re-emission rate, h^{-1};
q_{grn} is the HTO activity in soil surface, Bq; and
q_{air} is the HTO activity in air at the ground surface, Bq.

Locations where re-emission occurs should become a secondary release source. In Tritium-EESAD, when re-emission occurs, its activity is added to the air concentration only once, but in the next hour, re-emission activity disappears from the air.

— *Parameter values*

Ogram et al. [II.41] reported an re_{HTO} value of about 2% h^{-1} for the first 24 hours after tritium release and about 0.6 for the first 2 weeks. Foerstel [II.42] reported an average value of about 3% h^{-1}, which was not limited to a certain time after release.

II.3.1.4. Rain water

Tritium concentrations in the monthly rain were calculated from the arithmetic mean of the tritium activity wet deposited for the month, and the amount of the monthly rainfall.

II.3.1.5. TFWT and OBT in pine needles

Tritium in pine needles was assumed to originate from the direct uptake of atmospheric moisture through the stomata of the leaves, and also from root uptake of soil water. The tritium concentration in soil water for a given month was calculated from the total amount of tritium deposited on the ground in the month and the mean water content in the surface soil of 5 cm depth. The calculated tritium concentrations in atmospheric moisture and soil water for each month were used to calculate the TFWT in pine needles for the month:

$$PN_{TFWT} = A\ R_a / (R_a + R_b) + B\ R_b / (R_a + R_b) = 0.57\ A + 0.43\ B \quad \text{(II.3.7)}$$

where:

PN_{TFWT} is the TFWT concentration in pine needles, Bq/L;
A is the tritium concentration in air moisture, Bq/L;
B is the tritium concentration in soil water, Bq/L;
R_a is the TFWT in plants/tritium concentration in air moisture observed in steady-state conditions (= 0.8 from literature survey [II.43]); and
R_b is the TFWT in plants/tritium concentration in soil water observed in steady-state condition (= 0.6 from literature survey [II.44]).

The OBT concentration was calculated by Equation II.3.8. The arithmetic mean value of TFWT concentration for the previous six months was used to calculate the OBT concentration at a given time, because OBT is considered to be metabolized slowly in the plant body independent of season.

$$PN_{OBT} = Rc\ PN_{TFWT} \quad \text{(II.3.8)}$$

where:

PN_{OBT} is the OBT concentration in pine needles at time t, Bq/L;
R_c is the concentration ratio of OBT/TFWT in plants observed in steady-state conditions (= 0.8 from literature survey [II.45]); and
PN_{TFWT} is the mean value of TFWT concentration in pine needles over the six months prior to t, Bq/L.

II.3.1.6. OBT in annual rings of a pine tree

The OBT concentration in annual tree rings was considered to be half the mean value of yearly OBT concentration in pine needles, based on the observation by NIRS:

$$PR_{OBT} = PN_{OBT}/2 \quad \text{(II.3.9)}$$

where:

PR_{OBT} is the OBT concentration in annual tree rings, Bq/L; and
PN_{OBT} is the mean annual value of OBT concentration in pine needles, Bq/L.

II.3.1.7. Groundwater

The assumed geological characteristics of the area, including the point G4, are shown in Figure I.3.3 in the Scenario Description (Appendix I.3). The well water at G4 is pumped out from the shallow groundwater layer in the narrow area of a small river basin near a seacoast, where slow vertical infiltration and fast horizontal flow of the groundwater were presumed.

Based on field studies by NIRS [II.46], the volume of storage water in this area is so small that the tritium concentration of the groundwater has a quick time response to tritium input by rainwater. Tritium in the rainwater is considered to mainly come from the nuclear facilities in JAERI, which are located to the northeast of the receptors. The tritium is deposited on the soil surface where it infiltrates the groundwater aquifer, and gradually drains out to the ocean through the river basin.

Monthly rain water at MS2 infiltrates vertically over a distance of 15 m to recharge groundwater at G4. Vertical infiltration of monthly rain water (at a rate of 5.5 m/y) reaches the groundwater aquifer 32 months later:

15 m ÷ 5.5 m/y = 2.7 years = 32 months

Ten percent of the volume of the groundwater aquifer was assumed to run off monthly into the river (Figure II.3.1):

$$T_{Vn} = (T_{Vn-1} - a\, T_{Vn-1}) + T_{Rn}\, x \quad \text{(II.3.10)}$$

where:

T_{Vn} is the tritium concentration in the groundwater layer for the n^{th} month, Bq/L;
T_{Rn} is the tritium concentration in monthly rainwater at MS2 for the n^{th} month, Bq/L;
a is the fraction of water that runs off into the river from the layer at the end of the $(n-1)^{th}$ month (= 0.1); and
x is a turnover rate constant for water in the layer (= rainfall volume/layer volume = 0.17).

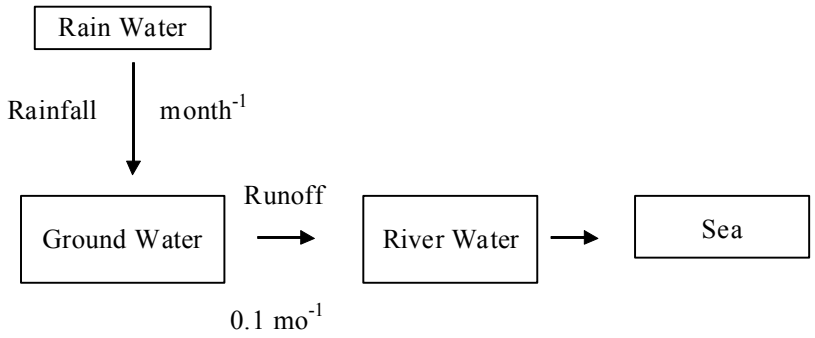

Fig. II.3.1. A model of river runoff in the Tokai area.

II.3.2. SRA Model

II.3.2.1. Atmospheric Diffusion of HTO

The atmospheric diffusion of tritium in the primary plume is described by a Gaussian plume model. The wind blows with equal probability within a given sector. The HTO concentration in the primary plume is calculated by assuming the common frequency of individual atmospheric stability and the corresponding average wind velocity. The interference of neighboring sectors was neglected. The sector-averaged tritium concentration on the ground surface is then approximately given by the following formula [II.47]:

$$\chi(x) = \sum_{S=A}^{F} \sqrt{\frac{2}{\pi}} \frac{F(s)Q}{\sigma_{ZS} U_S (2\pi x/16)} \bullet \exp\left(-\frac{H^2}{2\sigma_{ZS}^2}\right) \qquad \text{(II.3.11)}$$

where:

x is the distance from the release point (m);
$\chi(x)$ is the air tritium concentration at distance x (Bq/m^3);
S is the stability index of the atmosphere;
F(S) is the frequency rate of wind blowing for stability class S;
σ_{ZS} is the vertical dispersion parameter (m);
U_S is the average wind velocity for stability class S (m/s);
Q is the release rate (Bq/s); and
H is the stack height (m).

The secondary emission of HTO after dry deposition of HTO is assumed to take place instantaneously after deposition. The tritium depletion by dry or wet deposition of atmospheric HTO is neglected. The dispersion parameters were calculated using Brigg's formula.

II.3.2.2. Tritium transfer from atmosphere to soil

Atmospheric HTO is deposited to soil and vegetation through two processes. One is the dry deposition process where the atmospheric HTO moisture molecule exchanges with free water molecules in the soil and plant leaves. The other process is the scavenging of atmospheric HTO by rain, snow and frost. The washout of atmospheric HTO by rain is the major cause of

increasing tritium levels in precipitation. Hereafter, solely the washout by rain will be considered as the cause of wet deposition. The washout velocity is estimated by the following equation [II.48]:

$$V_{wash} = \frac{8\Lambda Q}{\pi\ xU} \tag{II.3.12}$$

where:

V_{wash} is the velocity of wet deposition (Bq/(m^2.s));
Λ is the washout constant (s^{-1});
Q is the tritium release rate (Bq/s);
U is the wind velocity (m/s); and
x is the distance to the estimation point from the release point (m).

The value of Λ is related to precipitation intensity, J (mm/a), and a proportionality constant S_{precip} (a / (mm.s)) as:

$$\Lambda = J\,S_{precip}. \tag{II.3.13}$$

Inoue and others determined the value of S_{precip} as 2.6×10^{-8} [II.48]. This value will be used in this report.

The specific concentration of tritium in soil water is estimated as follows. At first, the contribution to the soil HTO from the primary atmospheric HTO by dry deposition is considered. The dry deposition is assumed to occur only during fine or cloudy weather.

Generally, the specific activity of the soil water C_s is described by the following equation.

$$\frac{dC_S}{dt} = -\left(\frac{I_P}{V}\right)C_S + \left(\frac{I_P}{V}\right)C_P + \left(\frac{I_{dry}}{V}\right) \tag{II.3.14}$$

where:

Cs is the specific activity of the soil water (Bq/kg);
C_P is the specific activity of the precipitation (Bq/kg);
I_P is the annual precipitation rate (kg/(y.m^2));
I_{dry} is the tritium flux of dry deposition (Bq/(y.m^2)); and
V is the area density of soil water (kg/m^2).

At equilibrium, C_S is given by:

$$C_S = C_P + \frac{I_{dry}}{I_P} \tag{II.3.15}$$

In the case of HTO release, C_P and I_{dry} are given by:

$$C_P = \left(\sum_S \frac{F(S)}{U_S}\right) \times \left(\frac{8\Lambda Q}{\pi x \bullet I_p}\right) \times (8.64 \times 10^4 \times rainDay) \tag{II.3.16}$$

and:

$$I_{dry} = DryHTO \times C_{air,HTO} \times 8.64 \times 10^4 \times (365 - rainDay) \quad \text{(II.3.17)}$$

respectively, where:

DryHTO is the dry deposition velocity of atmospheric HTO (3×10^{-3} m/s);
$C_{air,HTO}$ is the atmospheric HTO concentration (Bq/m^3); and
rainDay is the number of rainy days per year.

II.3.2.3. Tritium transfer from the atmosphere and soil to the pine trees

If there is no supply of tritium from the soil, the tritium concentration in the plant leaves is described by the following equation of Belot [II.49]:

$$\frac{dC_L}{dt} = \frac{C_a}{\mu r} - \left(\frac{\rho_s}{\alpha\mu r}\right)C_L \quad \text{(II.3.18)}$$

where:

C_L is the tritium concentration in the plant leaves (Bq/kg);
C_a is the atmospheric HTO concentration (Bq/m^3);
ρ_s is the saturation moisture density (kg/m^3);
μ is the leaf water content (kg/m^2);
r is the resistance to moisture exchange between atmosphere and stomata (s/m); and
α is the 1.1 is the ratio of the vapour pressure for water vapour to that of HTO.

Under the circumstance that tritium is supplied from the soil water, an additional term must be added to the above equation:

$$\frac{dC_L}{dt} = \frac{C_a}{\mu r} - \left(\frac{\rho_s}{\alpha\mu r}\right)C_L + \frac{C_{soil} I_W}{\mu} \quad \text{(II.3.19)}$$

where:

C_{soil} is the tritium concentration in the soil water(Bq/kg); and
I_W is the evapotranspiration velocity of the plant leaves ($kg/(m^2.s)$).

At equilibrium, the leaf tritium concentration is given by:

$$C_L = \frac{\alpha r}{\rho_s}\left(\frac{C_a}{r} + C_{soil} I_W\right) \quad \text{(II.3.20)}$$

Let the tritium concentration of the air moisture be C_a^*. By using the relationships $C_a = C_a^* \rho$ and $I_W = \frac{\rho_s - \rho}{r}$, the above equation is reduced to:

$$C_L = \alpha\left(C_a^* f + C_{soil}(1-f)\right) \quad \text{(II.3.21)}$$

where f is the relative humidity of the atmosphere.

II.3.2.4. OBT formation in pine trees

The physiological condition of pine trees is unclear. In the present model, it is assumed that free water tritium in pine trees is converted to OBT only in April through August. The average lifespan of pine tree needles is believably above 2 years. The newly synthesized OBT in the needles is assumed to be retained for two years. The OBT produced in the needles in the growth period is assumed to be transferred to trunks and accumulated as the OBT of the tree rings. The value of the tritium discrimination factor used was 0.73 obtained as an average value from two reference sources [II.50, II.51].

II.3.2.5. Tritium concentration in groundwater

The depth of the G4 well was assumed to be 15 m with some uncertainty. The precipitation containing HTO reaches the aquifer 3 years after deposition. Thus the predicted tritium concentration in the groundwater reflects the tritium concentration of the surface soil water that was recorded about 3 years before. Naturally, convection and diffusion of HTO may take place during migration. The extent of the influence of these phenomena to the tritium level in the well water is unclear at the moment. Therefore, it was assumed that the HTO concentration represents that of surface soil water deposited on the soil surface 2.5–3.5 years before sampling. Furthermore, it was assumed that the contaminated groundwater is diluted by the clean water that is supplied from the surrounding aquifer. Tentatively the dilution factor (DF) was assumed to be 0.3. If there is no dilution (DF=1), the level of groundwater tritium is on the order of that of rain. The choice of the factor DF is a point of debate. Figure II.3.2 shows the effect of varying DF from 0.3 to 1.0.

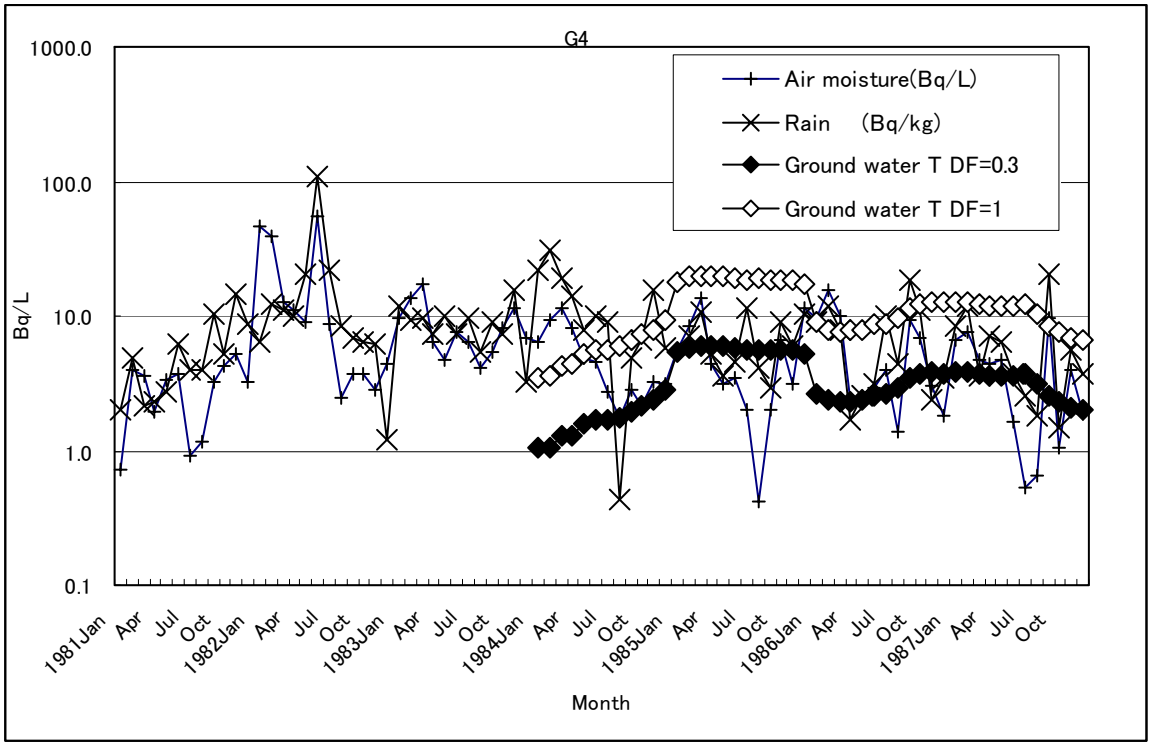

Fig. II.3.2. HTO concentrations in air moisture, rain and groundwater (for two values of the dilution factor DF).

II.3.3. LLNL Model

II.3.3.1. Introduction

DCART (Doses from Chronic Atmospheric Releases of Tritium) [II.52] was developed as a stochastic assessment model to be used in a dose reconstruction for tritium releases from the Lawrence Livermore National Laboratory. It is a steady-state, analytical compartment model that calculates uncertainties using parameter distributions and Latin Hypercube Sampling. DCART accounts for inhalation and ingestion pathways to dose, but for the Pine Tree Scenario, only the compartments for air, air moisture, soil, tissue free-water tritium (TFWT) of pine needles and organically bound tritium (OBT) in pine needles and wood were calculated. Concentrations in rain were also calculated.

To estimate tritium concentrations in pine needles and wood, processes include uptake of HTO from soil water and air moisture and conversion to OBT. For the Pine Tree Scenario, dispersion modeling was used to calculate concentrations of tritiated water (HTO) in air (Bq m^{-3}) from atmospheric releases from specified facilities. From these predicted air concentrations, concentrations in air moisture, TFWT in pine needles, and OBT in pine needles and wood were predicted.

II.3.3.2. Key assumptions

DCART should be used to calculate annual or long-term mean concentrations and dose. Thus, as a more meaningful test of DCART, instead of the monthly predictions that were requested, only predictions for mean annual environmental concentrations of tritium were submitted.

To prepare the input file for the dispersion model, the meteorological data provided by the Japan Nuclear Cycle Development Institute (JNC) and the Japan Atomic Energy Research Institute (JAERI) had to be manipulated into hourly averages (for JNC) with six (instead of ten) stability classes (for both JAERI and JNC data). The conversion from ten stability classes to six was accomplished in Excel® without using macros as follows:

- The Japanese data were sorted first by stability class.
- The column containing stability classes was moved to a separate worksheet so that the "replace" function could be used to replace numbers (1 – 10) with letters (a – j) (i.e., 1 = a; 2 = b; ….10 = j).
- The letters then had to be converted back to numbers of just six stability classes (i.e., a = 1; b = 1 or 2, c = 2; d = 2 or 3; e = 3; f = 3 or 4; g = 4; h = 5; i and j = 6). For Japanese stability classes 2 (b), 4 (d), 6 (f) that had to be broken into two classes, each set of replacement classes (1-2; 3-4; 5-6) was alternated hour by hour and inserted in blocks.
- The revised column was then put back with the rest of the meteorological data and sorted by time.

The meteorological data provided for JAERI and JNC for all years was combined to produce a single wind file for each site to use as input to the dispersion model. Thus one wind file, based on all years of data provided, was used to calculate tritium concentrations in air moisture and pine needles each year for the JAERI releases, and, similarly, another wind file was used to calculate concentrations each year from the JNC releases.

For the preparation of the meteorological files, wind speeds and wind directions for 40 m were used because the JAERI stacks were 40 and 30 m tall. For JNC, 70 m wind speeds and

directions were used because the JNC stack is 90 m tall. No adjustment of wind speed was made to account for the difference between the heights of the measured data and heights of release.

The annual meteorological data provided by JAERI and JNC were sorted for the hours it rained. Rainfall rate was determined from total rainfall divided by the total time it rained in a year, based on whether rain was recorded in 10 minute (JNC) or hourly (JAERI) time-periods. Washout coefficients took into account stack height and distance from stack and were adjusted for the rainfall rate.

Because of the elevated week-long release in June 1982 from stack JRR-3, annual mean air concentrations and concentrations in rain at location P3 were calculated two ways. The first used the total released for 1982, including June. The second assumed a June release that was 10% that observed (and comparable to the releases of the other months). The second assumption was necessary in case the annual wind file for the dispersion model could not account for the semi-acute release. The submitted prediction included the mean and upper confidence limit based on the first assumption and the lower confidence limit based on the second assumption.

The source terms for the rainfall model in DCART and for the other pathways in DCART are slightly different from each other. The monthly source terms for estimating tritium concentrations in rain were weighted based on the duration of rainfall during each month.

II.3.3.3. Modeling approaches (conceptual and mathematical)

CAP88-PC, a model approved by the United States Environmental Protection Agency for regulatory compliance, was used as the dispersion model from which χ/Q was obtained as input for DCART. CAP88-PC is a simple Gaussian model for flat terrain that uses conservative assumptions to increase the probability that air concentrations at a given location will be overestimated. One of the conservative assumptions is that the input wind file should be derived from wind measurements take at 10 m; another is that the roughness length is 0.01 m. With these assumptions, CAP88-PC normally predicts concentrations in air to within a factor of three with a tendency to overestimate rather than underestimate.

In DCART, annual wet deposition of HTO is calculated:

$$\omega = \frac{\Lambda Q \Delta T \exp(-\Lambda x/\mu)}{x \mu \Lambda \theta} \qquad \text{(II.3.22)}$$

where:

ω is the wet deposition (Bq m^{-2} a^{-1});
Λ is the washout coefficient (s^{-1}) (variable, depending on distance from source, stack height, and wind speed during rain);
Q is the release rate (Bq s^{-1});
x is the downwind distance in meters from the source;
u is the mean wind speed (m s^{-1}) for when it rains; sector, release height and year specific data are used when available;
ΔT is the duration of rainfall when plume is present (s a^{-1}); (calculated from fraction of time wind blows into a sector times fraction of time it rains times seconds in a year); and
$\Delta\theta$ is the sector width (radians); 0.393.

The annual mean concentration of HTO in precipitation is calculated:

$$C_{precip} = (\omega / P)(0.001 m^3 / L) \quad \text{(II.3.23)}$$

where:

C_{precip} is the HTO concentration in precipitation (Bq L^{-1}); and
P is the mean annual precipitation (m^3 m^{-2} or m).

Concentrations in air moisture are calculated by dividing the tritium concentration in air volume predicted by the dispersion model by the estimated annual mean absolute humidity.

The annual mean concentrations of HTO in TFWT of pine needles is given by the equation:

$$C_{pw} = 1/\gamma \ [R_H \, C_{a\_HTO} / H_a + (1 - R_H) \, C_{sw}] \quad \text{(II.3.24)}$$

where:

C_{pw} is the concentration of tritium in the plant water (Bq L^{-1} or Bq kg^{-1});
γ is the ratio of vapor pressure between HTO and H_2O (0.909);
R_H is the relative humidity;
C_{a_HTO} is the concentration of HTO in air (Bq m^{-3});
H_a is the absolute humidity (kg m^{-3}); and
C_{sw} is the concentration of tritium in soil moisture (Bq L^{-1}).

Concentration of OBT in needles and tree rings (Bq L^{-1} water equivalent) equals the concentration in TFWT reduced by a discrimination factor that arises from isotopic effects during OBT formation.

Default soil moisture concentrations in DCART are normally set equal to 30% of the tritium concentration in air moisture. However, for this scenario, when air concentrations were obtained from dispersion modeling, the concentration in wet deposition always exceeded 30% of air moisture. Consequently it was felt that soil concentrations would be underestimated if the default ratio were used, and it was assumed that the best estimated soil concentration would equal the concentration of the wet deposition (i.e., the precipitation).

II.3.3.4. Parameter values and associated uncertainties

The parameter values and uncertainties used in the precipitation model are found in Table II-1.1 in the Annex II-1; the parameter values, used in DCART to estimate concentrations in needles and wood, that varied from year to year or location to location are found in Table II-1.2.

Isotopic discrimination for pine needles was 0.7. The distribution was an extreme value distribution with md = 0.067 and scl = 0.014. Isotopic discrimination for tree rings was calculated using a triangular distribution (0.2 – 0.4 – 0.7).

For the Pine Tree Scenario, the concentration in soil water was set equal to the concentration in precipitation. The extremes were then set at best estimate (BE) plus 0.2 and BE minus a multiple of 0.1 that brought the lower limit to about 0.2. Values for the ratio are found in Table II-1.2.

II.3.3.5. Sensitivity

Even though the parameter values to which a model is sensitive are related directly to one particular scenario and endpoint, sensitivity analyses were not carried out for each location and each year because of the similarity between years.

When calculating concentrations in rain, the model was sensitive to the source term and the washout coefficient. When calculating air moisture and TFWT, the parameters to which the model was sensitive were source terms, specifically for JRR2 and JRR3, and χ/Q, for JRR3. When calculating OBT in pine needles and in wood, the model was most sensitive to the isotopic discrimination parameter.

II.3.3.6. Application of the model to the scenario

The stack heights, stack diameters and exit velocities supplied in Table I.3.4 of the Scenario Description (Appendix I.3) were used in the dispersion model. The distances and directions given in Table I.3.5 of the Scenario Description (Appendix I.3) were used in the determination of χ/Q.

All wind speed, wind direction, stability class, and rainfall data provided for all years were used to prepare input files for the dispersion model and for the rain model. In addition, the temperature (both JAERI and JNC) and the relative humidity (JNC) or dewpoint (from JAERI – used to estimate relative humidity) were used to calculate absolute humidity.

Annual source terms were obtained by summing the monthly releases.

The washout coefficients provided were used to determine uncertainty bounds on the best estimates; each distribution was adjusted to include the two values provided.

II.3.3.7. Predictions

Air concentrations were calculated using the χ/Q from the dispersion model, CAP88-PC, and estimated annual release rates. Predicted to observed (P/O) ratios at the three sampling locations for concentrations of tritium in air moisture and precipitation are shown in Table II.3.2 and Table II.3.3, respectively.

All air moisture concentrations are underestimated and the upper confidence limit on the predictions does not include the observations; the mean of all P/O ratios is 0.3. If the results from 1985 (which are noticeably higher) are excluded from the mean, the mean P/O ratio becomes 0.23. These results are surprising given that CAP88-PC, in at least three independent tests, has been shown to predict air concentrations within a factor of 3 and to overestimate air concentrations more than half the time.

Based on the relative success of predictions of tritium concentrations in rainfall (Table II.3.3), the source terms used in the model are probably reasonable. The over-all P/O ratio for concentrations of tritium in rain was 0.57, and just over half of the observations were included within the confidence intervals of the predictions.

Table II.3.2. Predicted to observed ratios in air moisture.

Year	MP-7	P3	MS2
1984	0.16	0.22	0.18
1985	0.43	0.59	0.44
1986	0.21	0.32	0.21
1987	0.25		0.29

Table II.3.3. Predicted to observed ratios in precipitation. Shaded areas indicate when the upper confidence limit was below the observed concentration.

Year	MP-7	P3	MS2
1982		0.63	
1983		0.81	
1984	0.44	0.42	0.39
1985	0.80	0.65	0.45
1986	0.33	0.47	0.57
1987	0.48		0.97

Rather than the use of incorrect source terms, it is likely that the failure to correctly predict air moisture concentrations may be traced to the many errors that could have been introduced during the process by which the ten stability classes were reduced to six while preparing the input wind file for CAP88-PC, but some of the under-prediction may be due to having prepared the input wind file from the 40 and 70 m wind data rather than from 10 m data as recommended by CAP88-PC. The unusually high soil moisture to air moisture ratios (Table II-1.2) that were derived for these calculations are probably symptomatic of the underestimated air concentrations.

Because air moisture concentrations were underestimated, DCART's predictions of TFWT and OBT in pine needles and OBT in tree rings were also underestimated.

II.3.3.8. Conclusions

Predictions from the rain model in DCART were uniformly underestimated, and the reason for this is not known as of this writing. The confidence placed in the parameter values of the rain equation should be reevaluated given that about half of the predicted confidence intervals failed to include the observations.

For whatever reason, the air concentrations calculated from the χ/Q obtained from the dispersion model were unacceptably low, with the result that all initial predictions were also unacceptably low. However, as an exercise, when the observed air moisture concentrations were used as the driving input in DCART, most of DCART's predictions of TFWT in pine needles and OBT in pine needles and tree rings were within a factor of two of the observations.

The observations themselves were not internally consistent, and there were insufficient results to justify reconsidering any of the transfer parameter values in DCART. The degree of confidence in the predictions appears to be justified.

ANNEX II-1. SUPPLEMENTARY TABLES

Table II-1.1. Input data summary to rain model in DCART; distributions are normal unless noted.

Release location	1982	1983	1984	1985	1986	1987
Source term for the rain model in DCART (Bq s^{-1} ±20%)						
JRR- 2	1.22E+04	2.06E+04	2.92E+04	2.26E+04	4.12E+04	3.22E+04
JRR-3	1.19E+05	2.55E+04	9.11E+03	7.81E+03	8.54E+03	2.54E+02
WTF	1.29E+04	2.45E+04	1.69E+04	8.45E+03	5.34E+03	2.31E+03
NFRP	1.43E+05	5.91E+04	2.08E+04	9.85E+04	6.40E+04	9.50E+04
Mean wind speed (m s^{-1} ±5% for the 40 m JAERI towers and ±10% for the other two towers)						
JRR-2; JRR-3	5.27	4.50	4.98	4.83	5.84	4.89
WTF	4.51	3.85	4.26	4.13	4.99	4.18
NFRP	10.4	10.2	9.72	8.02	9.09	8.59
Fraction of time when raining that the wind blows towards MP-7; no uncertainty						
JRR-2	0.232	0.120	0.307	0.211	0.152	0.286
JRR-3	0.290	0.304	0.320	0.295	0.297	0.219
WTF	0.0548	0.101	0.0727	0.0843	0.096	0.043
NFRP	0.0261	0.0410	0.0155	0.0251	0.0472	0.0242
Fraction of time when raining that the wind blows towards P-3; no uncertainty						
JRR-2; JRR-3	0.290	0.304	0.320	0.295	0.297	0.219
WTF	0.0548	0.101	0.0727	0.0843	0.0962	0.0435
NFRP	0.0261	0.0410	0.0155	0.0251	0.0472	0.0242
Fraction of time when raining that the wind blows towards MS-2; no uncertainty						
JRR-2; JRR-3	0.232	0.120	0.307	0.211	0.152	0.286
WTF	0.290	0.304	0.320	0.295	0.297	0.219
NFRP	0.0261	0.0410	0.0155	0.0251	0.0472	0.0242
Frequency of rain - best estimate is mean between frequency at JAERI and frequency at JNC; uncertainty is rectangular with JAERI and JNC values as extremes						
JAERI	0.0713	0.0776	0.0502	0.0866	0.0653	0.0683
JNC	0.0557	0.0631	0.0405	0.0553	0.0560	0.0527
Mean	0.0635	0.0704	0.0453	0.0710	0.0606	0.0605
Annual precipitation (m) is the average of JAERI and JNC with an uncertainty of +/- 25%						
Mean	1.15	1.07	0.611	1.14	1.16	0.980
Washout coefficients (s^{-1}) for all locations; distribution is lognormal with a GSD of about 1.8						
JRR-2; JRR-3	1.14E-04	1.01E-04	9.12E-05	1.01E-04	1.18E-04	1.04E-04
WTF	1.22E-04	1.08E-04	9.77E-05	1.08E-04	1.26E-04	1.12E-04
NFRP	8.49E-05	7.86E-05	7.04E-05	8.29E-05	8.90E-05	7.98E-05

Table II-1.2. Input data for DCART's predicted concentrations in pine needles and wood.

Release location	1982	1983	1984	1985	1986	1987
Source term for DCART (Bq s^{-1} ±20% on a normal distribution)						
JRR-2	1.27E+04	2.00E+04	2.75E+04	2.32E+04	3.65E+04	3.06E+04
JRR-3	9.88E+04	2.67E+04	9.89E+03	1.36E+04	1.22E+04	2.35E+02
WTF	1.18E+04	2.40E+04	1.72E+04	8.24E+03	5.39E+03	2.31E+03
NFRP	1.41E+05	6.07E+04	1.87E+04	8.87E+04	7.02E+04	8.94E+04
Relative humidity; the best estimate is the midpoint of a rectangular distribution with endpoints from JAERI and JNC						
JAERI	0.760	0.764	0.736	0.748	0.782	0.743
JNC	0.812	0.828	0.829	0.861	0.824	0.808
midpoint	0.786	0.796	0.783	0.805	0.803	0.776
Absolute humidity`(kg m^{-3}); the best estimate is the midpoint of a rectangular distribution with endpoints from JAERI and JNC						
JAERI	0.00951	0.00969	0.00929	0.00972	0.00875	0.00960
JNC	0.0102	0.0101	0.00955	0.0108	0.00973	0.0103
midpoint	0.00986	0.00989	0.00942	0.0102	0.00924	0.0100
Ratio of soil moisture/air moisture; uncertainty is triangular: BE + 0.2 or BE – 0.2, 0.3, 0.4, 0.5, or 0.6						
MP-7	-	-	0.82	0.56	0.45	0.94
P3	0.52	0.51	0.45	0.37	0.35	-
MS2	-	-	0.68	0.45	0.31	0.59
χ/Q (s m^{-3} ±30% on a lognormal distribution)						
Release location	**MP-7**	**P3**	**MS2**			
JRR-2	5.03E-07	9.92E-07	5.60E-07			
JRR-3	8.64E-07	9.81E-07	5.32E-07			
WTF	6.08E-07	5.50E-07	9.48E-07			
NFRP	4.52E-08	4.68E-08	5.67E-08			

II.3.4. IFIN Model

II.3.4.1. Method

We adapted the methods used in BIOMASS, considering the specific scenario data. Since the receptor- source positions were given by sector, and since monthly average concentrations were requested, we used the sector average Gaussian model to calculate atmospheric dispersion and wet deposition. The Scenario Description (Appendix I.3) identified 10 atmospheric stability classes whereas it is traditional to specify only 6 (A to F). We established a correspondence by assuming that 1 $\rightarrow$ A, 7 $\rightarrow$ D and 9 $\rightarrow$ F. We used the SCK/MOL scheme to calculate the vertical dispersion parameter, σ_z:

$$\sigma_z = \alpha x^{0.711} \qquad \text{(II.3.25)}$$

where the parameter α depends on stability class with values of 1.31, 1.24, 1.13, 0.99, 0.83, 0.66, 0.50, 0.38, 0.32 and 0.3 for classes 1 to 10 respectively.

For a given receptor in sector i, we added the contributions from the various sources *j*. Using the hourly meteorological data from JAERI, we determined the monthly frequency (f_{ij}) with which the wind blew into the sector encompassing the receptor. For each case where the wind blew from source j to sector i, we calculated the hourly, sector-averaged air concentration, and later the average over all cases. Finally we converted the concentration in air to the concentration in air moisture using the monthly atmospheric humidity.

The average concentration in precipitation was assessed from the total monthly wet deposition and the total precipitation. The scavenging rate considered was $\Lambda = 1 \times 10^{-4} I^{0.8}$ s^{-1}, where I is precipitation intensity in mm/h. The effect of temperature on washout was disregarded.

The HTO concentration in soil water was a superposition of the concentration in precipitation with a small (0.1) contribution from air moisture.

In order to assess the HTO and OBT concentrations in pine needles, we must consider the specific characteristics of evergreen conifers. This is the first time we are faced with such a case. The change in the leaf water concentration depends on the exchange velocity. For evergreen conifers, this is lower than for agricultural crops by a factor 3-5 [II.53, II.54]. However, as we are asked to predict monthly mean concentrations, this slow transfer is irrelevant and we preserve the simple formalism used for crops, as in the BIOMASS study:

$$C_{leaf\_water} = 1.1\,[RH\ C_{air\_moisture} + (1\text{-}RH)\ C_{soil\_water}] \qquad \text{(II.3.26)}$$

As a simplification, the relative humidity RH was set to its annual average value. In order to calculate the OBT concentration in pine needles or wood, we must consider some characteristics of pine trees. The needles found on the trees are of various ages, from new ones formed in the current year to those up to 7 years old; the needle loss rate is 0.33 y^{-1} [II.55]. Old leaves have low photosynthetic activity. In periods of low temperature (<5^o C), the tree is dormant and we have practically no OBT production. Considering the average air temperature and radiation from 1981-1987, we deduce an average net relative photosynthesis rate. This is shown in Table II.3.4 together with information on air temperature, solar radiation and leaf area index.

Table II.3.4. Air temperature, solar radiation, leaf area index and average net relative photosynthesis rate.

Month	Average air temperature (C)	Average radiation (W/m^2)	Average net relative photosynthesis rate	Leaf area index
Jan	2.16	100.93	0.000	6
Feb	3.06	118.75	0.000	6
Mar	5.86	134.72	0.017	6.5
Apr	10.70	171.82	0.067	7
May	15.19	193.58	0.150	7.5
Jun	17.52	167.63	0.167	8
Jul	21.99	173.66	0.167	8
Aug	24.49	188.74	0.167	7.5
Sep	20.98	130.51	0.117	7
Oct	15.83	114.71	0.100	6.5
Nov	9.85	89.55	0.042	6
Dec	5.08	83.64	0.000	6

Table II.3.5. Relative contribution of the monthly OBT concentration to the annual average concentration.

Month	Monthly OBT contribution
May	0.173
Jun	0.192
Jul	0.192
Aug	0.192
Sep	0.135
Oct	0.115

In December, January and February we have no OBT production and no change in leaf OBT concentration. In March and November, the production of OBT is low and influences the average OBT concentration in the needles only marginally. For the rest of the season, the OBT concentration in needles depends on the relative contributions of old and newly-produced OBT. The yearly carbon production in evergreen conifers can be partitioned between needles, fine roots and wood, for a total production of about 2.1 $kgC/(y\ m^2)$ [II.55]. Needle production contributes about 20% of this value. In the summer period (April-October), the daily carbon (and OBT) production rate (0.02 kgC/m^2) is less than the amount of carbon (and OBT) stored in the needles (0.8 kgC/m^2). Little carbon is retained in the needles and much is translocated to roots and trunk.

As a consequence of these considerations, the monthly average OBT concentration in needles in summer is assumed to be given by the arithmetic average of the concentration of old and newly-produced OBT. The concentration of newly-produced OBT is assumed to equal the HTO concentration in needle water apart from an isotopic discrimination factor of 0.6. For example, in August, the OBT concentration (in Bq/L water equivalent) in the needles is

$$OBT_{Aug} = (OBT_{Jul} + 0.6\ HTO_{Aug}) / 2 \quad \text{(II.3.27)}$$

Only the new OBT contributes to the concentration in tree rings, but we must consider the monthly contribution to the annual average, as shown in Table II.3.5.

II.3.4.2. Uncertainties

Using a sector-averaged dispersion model and selecting a specific vertical dispersion parameter induces inherent uncertainties of a factor 3 in the air concentration. This factor is marginally increased for the predicted air moisture concentration (we use yearly averaged relative humidity of 0.7 but it fluctuates between 0.6 and 0.9), but for OBT in needles the uncertainty increases to a factor 5, since our estimate of the contribution of old and new OBT is preliminary. A factor 5 is also assessed for the OBT concentration in tree rings.

The above uncertainties refer to our calculations. In comparing with observations we must consider also potential errors in the data. Usually air moisture and precipitation are collected continuously and the observed monthly mean is a good estimate of the real value. Pine needles can be collected a few times a month, at various hours and under various plume conditions. This affects the average measured HTO concentration in pine needles. If we take the example of December 1983, from 744 hours we have good meteorological records for 712, but in only 48 of those hours did the wind blow from one of the release points to the sampling site P3. About half of those cases occurred during the work day. If only a few samples were taken per month (1-5), the average can be severely biased [II.56]. A “perfect” monthly average must be constructed from at least 2 samples per day (one taken during the night and one during daylight hours) each day in the month. We expect a large spread between modeled and observed HTO concentrations in pine needles. The observed OBT concentrations will be less biased, as OBT is an integral of past HTO concentrations.

II.3.4.3. Results

Predicted HTO concentrations in air moisture, precipitation and pine needles, and OBT concentrations in needles and tree rings are given in Figures II.3.3 and II.3.4 for P3. Predictions for P3 and MS2 are shown in Tables II.3.6 and II.3.7.

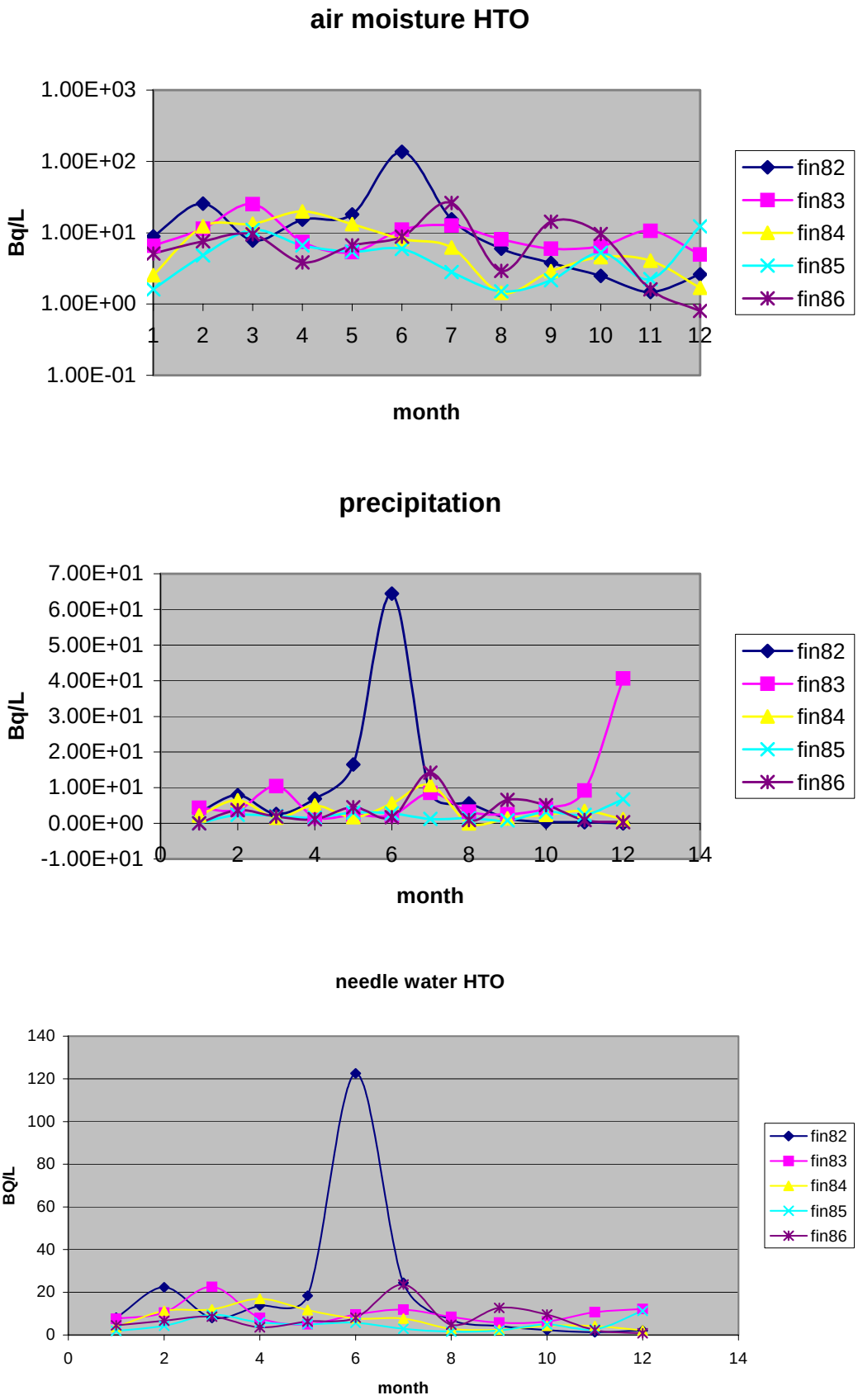

Fig. II.3.3. Predicted HTO concentrations in air moisture, precipitation and pine needles.

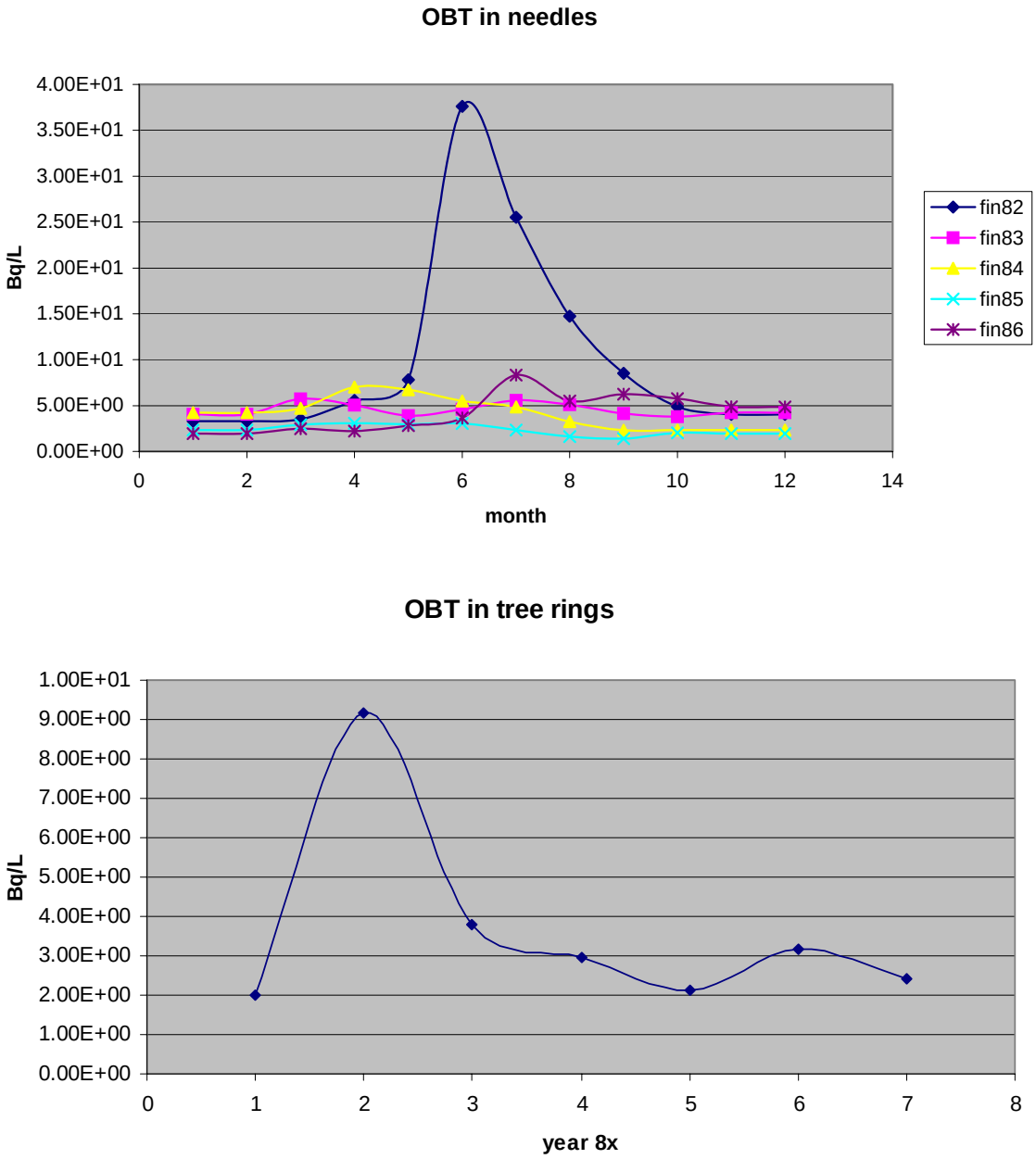

Fig. II.3.4. OBT concentrations in needles and tree rings.

Table II.3.6. Predictions for P3.

Air moisture HTO (Bq/L)													
Year	**Jan**	**Feb**	**Mar**	**Apr**	**May**	**Jun**	**Jul**	**Aug**	**Sep**	**Oct**	**Nov**	**Dec**	**Annual**
1982	8.90E+00	2.56E+01	7.77E+00	1.52E+01	1.80E+01	1.36E+02	1.54E+01	6.00E+00	3.76E+00	2.48E+00	1.48E+00	2.60E+00	2.03E+01
1983	6.56E+00	1.14E+01	2.52E+01	7.41E+00	5.34E+00	1.10E+01	1.26E+01	8.12E+00	5.95E+00	6.45E+00	1.06E+01	4.93E+00	9.63E+00
1984	2.53E+00	1.22E+01	1.33E+01	1.98E+01	1.32E+01	8.13E+00	6.18E+00	1.44E+00	2.88E+00	4.53E+00	4.04E+00	1.69E+00	7.49E+00
1985	1.60E+00	4.80E+00	1.09E+01	6.63E+00	5.45E+00	5.93E+00	2.81E+00	1.50E+00	2.15E+00	5.26E+00	2.23E+00	1.22E+01	5.12E+00
1986	5.08E+00	7.57E+00	9.49E+00	3.82E+00	6.61E+00	8.84E+00	2.62E+01	2.91E+00	1.43E+01	9.58E+00	1.61E+00	7.97E-01	8.07E+00
Precipitation HTO (Bq/L)													
Year	**Jan**	**Feb**	**Mar**	**Apr**	**May**	**Jun**	**Jul**	**Aug**	**Sep**	**Oct**	**Nov**	**Dec**	**Annual**
1982	3.08E+00	7.86E+00	2.61E+00	6.89E+00	1.65E+01	6.44E+01	8.70E+00	5.55E+00	1.39E+00	4.19E-01	3.28E-01	0.00E+00	9.81E+00
1983	4.39E+00	3.76E+00	1.04E+01	1.84E+00	2.36E+00	2.29E+00	8.56E+00	3.32E+00	2.53E+00	4.17E+00	9.17E+00	4.06E+01	7.78E+00
1984	2.22E+00	6.48E+00	1.58E+00	5.05E+00	1.71E+00	5.61E+00	1.08E+01	0.00E+00	1.40E+00	2.38E+00	3.44E+00	1.14E+00	3.48E+00
1985	0.00E+00	2.37E+00	2.10E+00	1.57E+00	3.01E+00	2.79E+00	1.21E+00	1.43E+00	8.18E-01	3.22E+00	2.38E+00	6.76E+00	2.30E+00
1986	0.00E+00	3.70E+00	1.93E+00	1.13E+00	4.50E+00	1.70E+00	1.42E+01	9.53E-01	6.55E+00	5.10E+00	8.84E-01	3.34E-01	3.42E+00
Pine needle HTO (Bq/L)													
Year	**Jan**	**Feb**	**Mar**	**Apr**	**May**	**Jun**	**Jul**	**Aug**	**Sep**	**Oct**	**Nov**	**Dec**	**Annual**
1982	8.06E+00	2.24E+01	7.97E+00	1.38E+01	1.83E+01	1.23E+02	2.44E+01	7.17E+00	4.16E+00	2.29E+00	1.31E+00	2.14E+00	1.95E+01
1983	7.61E+00	1.05E+01	2.26E+01	7.97E+00	4.98E+00	9.60E+00	1.19E+01	8.48E+00	5.74E+00	6.28E+00	1.07E+01	1.22E+01	9.88E+00
1984	3.68E+00	1.12E+01	1.20E+01	1.70E+01	1.17E+01	7.74E+00	7.67E+00	2.94E+00	2.54E+00	4.26E+00	4.20E+00	2.11E+00	7.26E+00
1985	1.86E+00	4.25E+00	9.49E+00	5.93E+00	5.13E+00	5.72E+00	2.92E+00	1.64E+00	2.10E+00	4.89E+00	2.71E+00	1.13E+01	4.83E+00
1986	4.46E+00	6.69E+00	8.55E+00	3.57E+00	6.24E+00	8.12E+00	2.37E+01	4.84E+00	1.27E+01	9.61E+00	2.28E+00	8.41E-01	7.63E+00
Pine needle OBT (Bq/L)													
Year	**Jan**	**Feb**	**Mar**	**Apr**	**May**	**Jun**	**Jul**	**Aug**	**Sep**	**Oct**	**Nov**	**Dec**	**Annual**
1982	3.30E+00	3.30E+00	3.52E+00	5.55E+00	7.81E+00	3.76E+01	2.55E+01	1.47E+01	8.51E+00	4.89E+00	4.05E+00	4.05E+00	1.02E+01
1983	4.05E+00	4.05E+00	5.72E+00	5.05E+00	3.90E+00	4.59E+00	5.57E+00	5.12E+00	4.14E+00	3.80E+00	4.22E+00	4.22E+00	4.53E+00
1984	4.22E+00	4.22E+00	4.70E+00	7.02E+00	6.73E+00	5.49E+00	4.86E+00	3.24E+00	2.32E+00	2.33E+00	2.33E+00	2.33E+00	4.15E+00
1985	2.33E+00	2.33E+00	2.91E+00	3.08E+00	2.95E+00	3.05E+00	2.33E+00	1.61E+00	1.38E+00	2.04E+00	1.93E+00	1.93E+00	2.32E+00
1986	1.93E+00	1.93E+00	2.48E+00	2.22E+00	2.83E+00	3.65E+00	8.33E+00	5.50E+00	6.25E+00	5.77E+00	4.86E+00	4.86E+00	4.22E+00

Table II.3.7. Predictions for MS2.

Air moisture HTO (Bq/L)													
Year	**Jan**	**Feb**	**Mar**	**Apr**	**May**	**Jun**	**Jul**	**Aug**	**Sep**	**Oct**	**Nov**	**Dec**	**Annual**
1982	47.00	40.50	11.30	9.93	7.86	45.30	8.62	2.27	3.47	3.29	2.20	3.33	15.42
1983	9.80	13.80	19.20	6.71	4.01	7.61	6.12	4.17	5.80	7.32	9.51	7.77	8.49
1984	8.09	16.00	13.30	13.00	7.33	5.40	3.00	1.18	2.84	6.20	5.41	3.08	7.07
1985	3.89	6.86	11.60	4.34	3.65	3.81	2.24	0.75	2.20	7.38	3.24	9.72	4.97
1986	8.83	12.10	7.54	2.18	2.27	3.35	4.61	1.41	10.10	5.96	2.87	1.80	5.25
1987	6.99	7.44	3.59	4.86	5.26	2.18	0.64	0.79	11.60	1.08	3.49	1.70	4.13
Precipitation HTO (Bq/L)													
Year	**Jan**	**Feb**	**Mar**	**Apr**	**May**	**Jun**	**Jul**	**Aug**	**Sep**	**Oct**	**Nov**	**Dec**	**Annual**
1982	2.94	4.10	5.51	4.00	6.27	24.40	6.28	2.42	1.43	0.92	1.48	0.88	5.05
1983	3.92	4.76	3.62	1.94	2.99	2.19	3.07	1.65	3.42	2.22	8.90	18.30	4.75
1984	5.20	9.35	7.04	4.06	1.06	4.48	4.36	0.00	1.90	2.36	3.56	1.58	3.75
1985	0.00	1.27	3.58	1.98	2.48	1.92	0.88	1.17	1.01	4.68	1.31	4.84	2.09
1986	2.31	4.16	1.97	0.50	0.59	4.05	7.11	0.53	7.19	3.10	0.34	0.70	2.71
1987	2.81	4.39	0.32	2.63	4.52	0.82	3.67	0.46	4.03	0.31	1.53	1.12	2.22
Pine needle HTO (Bq/L)													
Year	**Jan**	**Feb**	**Mar**	**Apr**	**May**	**Jun**	**Jul**	**Aug**	**Sep**	**Oct**	**Nov**	**Dec**	**Annual**
1982	38.84	33.68	10.66	9.54	8.01	41.44	11.98	3.26	3.42	3.03	2.16	3.06	14.09
1983	8.66	12.51	16.80	6.31	4.03	6.97	5.78	4.13	5.49	6.81	9.47	10.73	8.14
1984	10.37	15.25	13.38	12.27	6.73	5.25	3.87	1.67	2.59	5.68	5.32	3.32	7.14
1985	3.38	5.72	10.12	4.40	3.67	3.79	2.26	0.94	2.13	6.86	3.59	8.82	4.64
1986	8.27	10.78	7.07	2.16	2.00	3.45	5.54	2.39	9.38	6.48	2.87	1.62	5.17
1987	6.19	7.16	3.66	4.39	5.40	2.63	1.25	1.31	10.06	1.58	3.11	1.80	4.05
Pine needle OBT (Bq/L water equivalent)													
Year	**Jan**	**Feb**	**Mar**	**Apr**	**May**	**Jun**	**Jul**	**Aug**	**Sep**	**Oct**	**Nov**	**Dec**	**Annual**
1982	2.94	2.94	3.52	4.39	4.39	13.59	10.09	5.94	3.91	2.79	2.47	2.47	4.95
1983	2.47	2.47	3.82	3.65	2.93	3.38	3.28	2.78	2.90	3.32	3.70	3.70	3.20
1984	3.70	3.70	4.43	5.59	4.65	3.77	2.95	1.93	1.68	2.40	2.51	2.50	3.32
1985	2.50	2.50	3.11	2.77	2.39	2.24	1.74	1.13	1.15	2.46	2.36	2.36	2.23
1986	2.36	2.36	2.67	1.93	1.51	1.71	2.38	1.85	3.50	3.53	3.14	3.14	2.51
1987	3.14	3.14	2.91	2.66	2.82	2.13	1.41	1.07	3.30	2.08	2.01	3.14	2.49
Annual OBT in tree rings (Bq/L water equivalent)													
1981	2.01E+00	**1982**	9.15E+00	**1983**	3.80E+00	**1984**	2.95E+00	**1985**	2.11E+00	**1986**	3.15E+00	**1987**	2.42E+00

II.3.5. EDF Model

II.3.5.1. Atmospheric dispersion

For this exercise, the model ADMS3 was used for atmospheric dispersion. This tool was developed by Cambridge Environmental Research Consultants (http://www.cerc.co.uk). Many companies and regulatory authorities in Europe use this model for impact studies. Nevertheless, this tool has not been used at EDF for nuclear impact studies before now. Here we use the Gaussian plume model of the tool.

As for any other plume model, the meteorological conditions are assumed to be constant in time and space for each hourly time step of the simulations. Moreover, no spatial variations of wind parameters have been modeled, as the region was considered to be flat.

The key parameters are the roughness length (0.5 m), the physical characteristics of the emission sources (height, diameter, emission velocity), and the washout coefficient ($7.3\ 10^{-5}\ s^{-1}$, as suggested in the scenario description). Four different emission sources corresponding to the JRR-2, JRR-3, WTF and NFRP installations were taken into account. The model calculates the effective release height of the plume using its own equations. The output grid resolution is 100 x 100 m.

For the meteorological conditions, we used the JNC data. From these, we calculated hourly-averaged meteorological conditions at 10-m height for input to the model.

The model can perform either short-term simulations, which assume steady-state conditions over one-hour periods, or long-term calculations for impact studies. In this last case, the model outputs mean concentrations or high-order percentiles such as 98 or 99%. For this scenario, monthly concentrations were determined by averaging the hourly predictions for each month of the 7-year study period.

II.3.5.2. Tritium concentration in air moisture and Precipitation

ADMS outputs are air concentration in Bq m^{-3} and ground deposit in Bq $m^{-2}\ s^{-1}$. These quantities were divided by air moisture content and volume of precipitation, respectively, to obtain tritium concentrations in air moisture and precipitation.

Air moisture content was calculated from monthly statistics on air temperature and relative humidity given in the JNC_met_ave_r7.xls Excel file, for the NFRP site. The JNC file was preferred because it contained data on relative humidity whereas the JAERI file contained dew point data.

Monthly precipitation amounts were taken from the JNC dataset.

II.3.5.3. Groundwater concentrations

The outputs of the ADMS3 model were used as inputs to the groundwater calculations, which were performed with ARGUS, an operational tool developed by the EDF Research and Development Division. The aims of the tool are:

— to provide EDF operational sites and engineering units with a crisis assessment and management tool for the treatment of soil and groundwater pollution incidents; and

— to help operators dealing with environmental management of sites to increase their knowledge of the subsoil/groundwater levels through a better integration of groundwater related data.

ARGUS is designed to provide pollutant transport results in the short term in order to answer rapidly questions from local and national authorities about the fate of pollutants in groundwater. Therefore, a conservative approach based on a semi-analytical solution of the transport equations is considered. The model is based on a compartment approach and is able to solve the transport equations in the unsaturated and saturated layers, and also the dispersion of a pollutant source term in rivers.

Due to the lack of knowledge concerning pollutant transport in the unsaturated zone, conservative constant flow parameters are used in this compartment. Adsorption (the reversible partitioning of a solute between the aqueous phase and the surfaces of solids) is described by a linear isotherm, and a constant adsorption distribution coefficient (K_d) is used. As a result, time-dependant concentrations of the pollutant plume can be calculated and plotted.

The aim of this study was to calculate the transfer of HTO deposited on the ground through the unsaturated and saturated layers and finally to evaluate the time-dependent HTO concentration at point G4.

II.3.5.4. Key assumptions

A simplified model of the geological formation around the study area is shown in Figure II.3.5, which is taken from the Scenario Description (Appendi I.3). Since the levels of both ground surface and base rock in the area surrounding JRR-2 and JRR-3 along the inner land line seem about 10 m higher than those along the seaside line, the groundwater may mainly flow eastward in the direction of the sea. Even if the groundwater flows southward from JRR-2 and JRR-3, it might be blocked by an ascending ground surface and base rock about 300 m south of JRR-2, provided that the amount of groundwater is not so plentiful and the mean residence time of groundwater is relatively short, e.g. about half a year.

For this study, a water table starting 300 m south from the JRR-2 and JRR-3 area is considered. The 500 m long calculation area, where a ground deposit source term is taken into account, is presented in Figure II.3.6. The width of the area is set to 200 m, assuming that ground deposit outside this range would not affect the concentration at point G4. Actually, lateral dispersion over a distance of 500 m, which is the maximum distance between an injection point and point G4, would probably not exceed 10 to 20 m.

Compartments corresponding to the unsaturated layer and the water table are considered in this study.

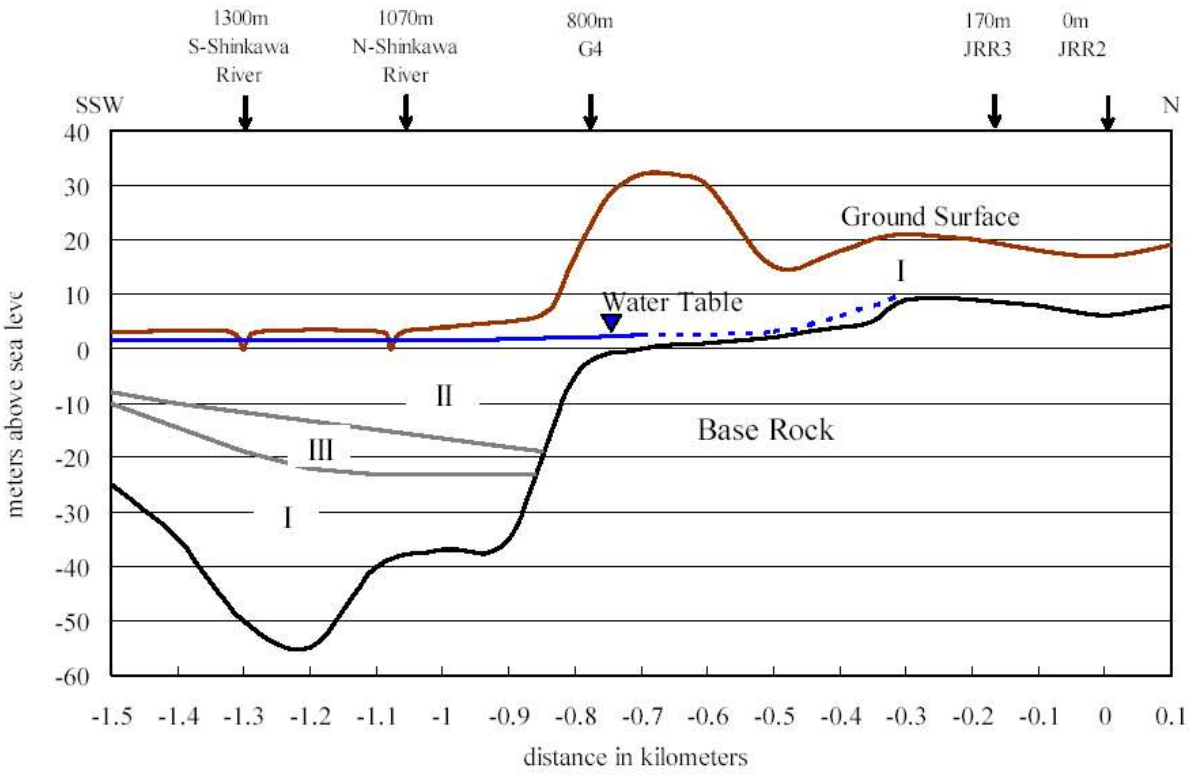

Fig. II.3.5. Simplified geological model along a line connecting the points of northern JRR-2, south south-west G4, and the Shinkawa River. I: Sand/Silt, II: Gravel/Sand, III: Silt/Clay.

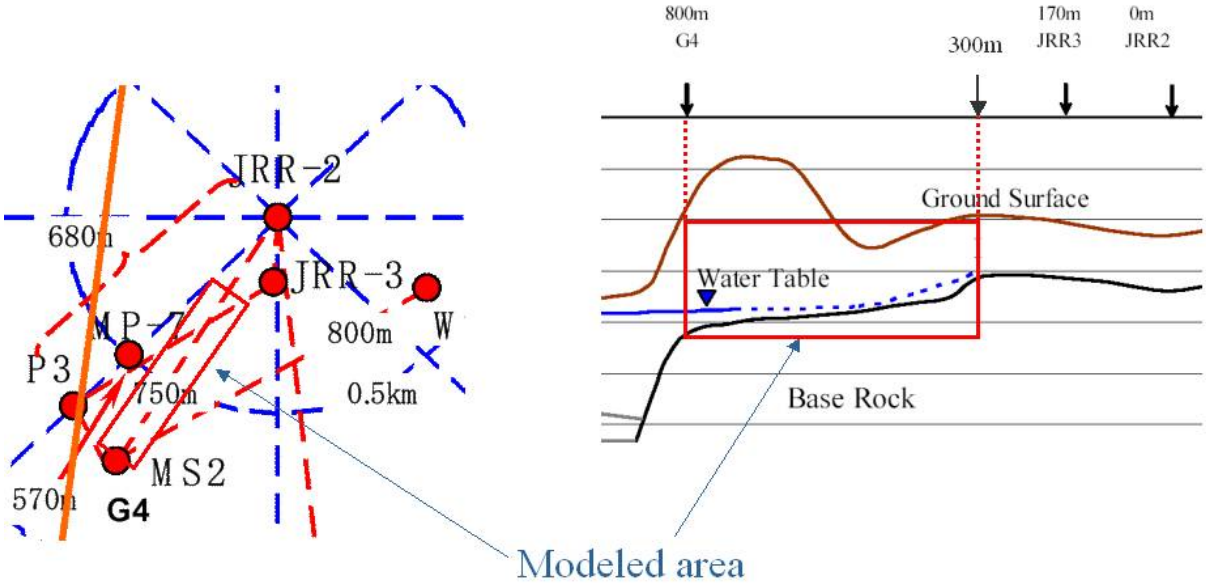

Fig. II.3.6. Description of the modeled area for the concentration calculation.

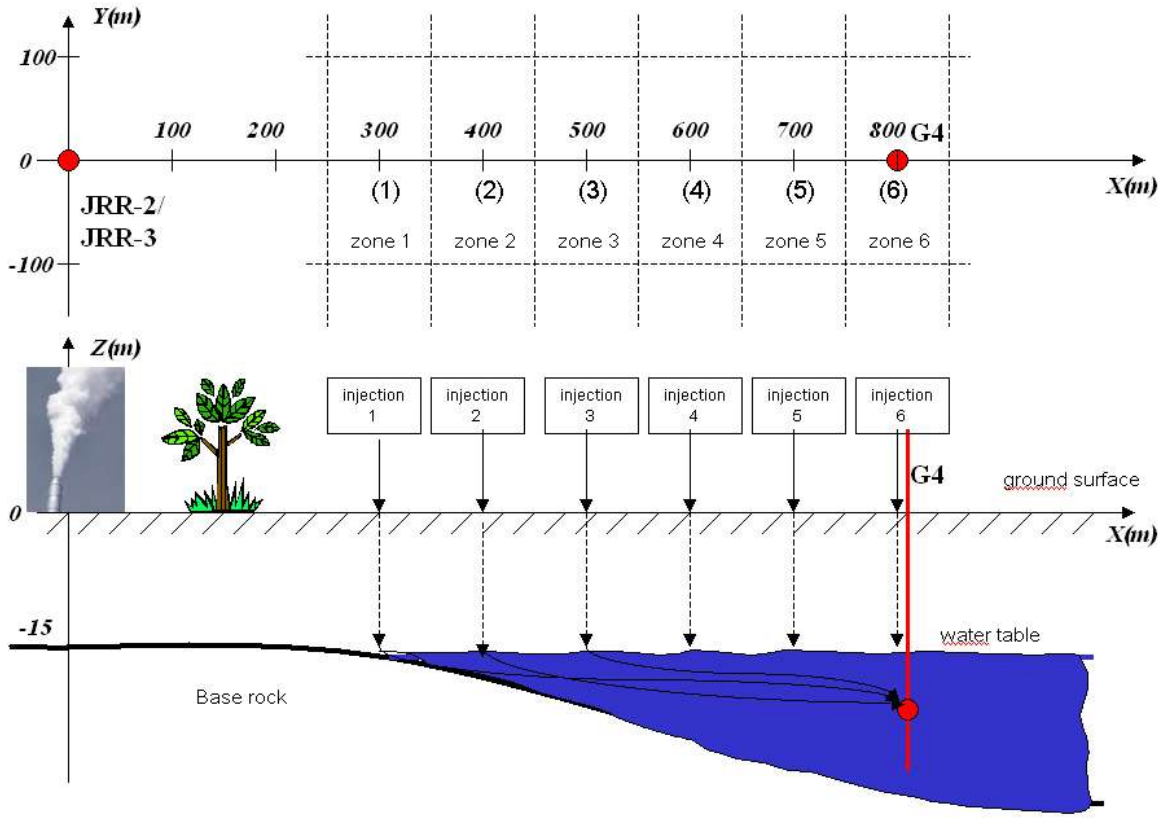

Fig. II.3.7. Schematic illustration of the multipoint injection principle used with the ARGUS software: 6 injection areas are modeled between the JR-R2/JRR-3 tritium discharge source area and point G4 (injection points 1 to 6 are located at the center of each area).

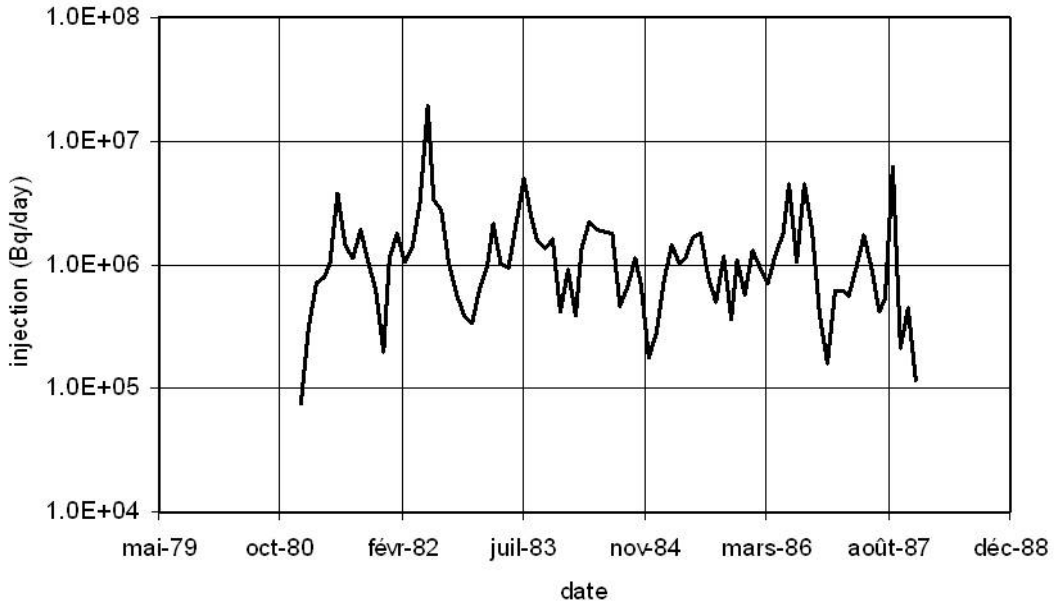

Fig. II.3.8. Injection profile at point 1 (Bq/day).

II.3.5.5. Modeling approaches and application of the model to the scenario

Injection in the soil: In ARGUS, the pollution source is modeled as a single point, time-dependant, multi-pollutant source term. In this study, the atmospheric deposits are distributed over the whole area. The modeled area was therefore divided up into six injection zones. The radioactivity is assumed to be injected at the center point of each zone (see Figure II.3.7 for more details). The source term injected at point 1, which is a result from the atmospheric dispersion simulations, is plotted on Figure II.3.8 for illustrative purposes. Finally, the concentration at point G4 is calculated by summing up the contributions of each of the six injection points.

1-D transfer in the unsaturated layer: The transfer through the unsaturated layer is simulated by solving the following 1-D transport equation:

$$R\theta\frac{\partial C}{\partial t} + V_D\frac{\partial C}{\partial z} - D_L\frac{\partial^2 C}{\partial z^2} + R\theta.\lambda.C = \dot{A}(t).\delta(x)\delta(y)\delta(z) \qquad \text{(II.3.28)}$$

where:

C(t) is the concentration at the interface between the unsaturated layer and the water table;
R is the retardation coefficient;
θ is the mean moisture content;
V_D is the Darcy vertical velocity;
D_L is the dispersion/diffusion coefficient;
λ is the radioactive decay constant; and
A(t) is the injection term.

The dispersion/diffusion coefficient D_L is given by:

$$D_L = \alpha\, V_D + D_0\, \psi\, \theta \qquad \text{(II.3.29)}$$

where the tortuosity is given by $\Psi = \frac{\theta^{10/3}}{\omega^2}$ and α is the dispersion coefficient.

The analytical solution of Equation II.3.28 is given by:

$$C(x,y,h_{ZNS},t) = \frac{1}{\sqrt{\theta\, R}}\int_0^t d\tau\ \frac{e^{-\frac{(V.\frac{(t-\tau)}{\theta R}-h_{ZNS})^2}{4D_L.(t-\tau)/\theta.R}-\lambda.(t-\tau)}}{\sqrt{4\pi.\,D_L.\,(t-\tau)}}\ \dot{A}(\tau).\delta(x)\delta(y) \qquad \text{(II.3.30)}$$

The infiltration rate of water into the unsaturated soil layer was estimated to be about half the annual precipitation of 500~700mm per year. A vertical pore water velocity in the unsaturated soil layer was estimated to be about 5.5 m/y based on an experiment carried out by the JAERI researchers. At G4, the estimated depth from the soil surface to the top of the groundwater aquifer was estimated to be roughly 15~20 m. The mean water content of the top 60 cm of soil was set to 2.84%, the value observed at MS2 in 1986.

The parameter values used for solving Equation II.3.29 are summarized in Table II.3.8. Concerning the dispersivity coefficient, an empirical value equal to 10% of the covered distance is usually considered. In our case, a conservative value of 1 m has been chosen.

The temporal variation of activity at the interface between the unsaturated layer and the water table below injection point 1 is plotted in Figure II.3.9 for illustrative purposes.

2-D transfer in the saturated layer: The output of the unsaturated layer compartment is injected into the saturated layer compartment. In the aquifer, a horizontal, constant flow velocity is considered. The problem can be considered two-dimensional or three-dimensional. In this case, as the depth of the water table is not well known, the 2-D transport equation was selected:

$$\omega R \frac{\partial C}{\partial t} + U.\frac{\partial C}{\partial x} - D_L.\frac{\partial^2 C}{\partial x^2} - D_T.\frac{\partial^2 C}{\partial y^2} + \omega R\lambda.C = \dot{A}(t)\delta(x)\delta(y) \qquad \text{(II.3.31)}$$

where:

U is the Darcy horizontal velocity; and
D_L and D_T are respectively the longitudinal and transverse dispersion/diffusion coefficients.

The 2-D analytical solution is given by an equation similar to that presented above for the 1-D transport equation:

$$C(x,y,t) = \int_0^t d\tau \; \frac{e^{-\frac{\frac{(U.\frac{(t-\tau)}{\omega R} - x)^2}{D_L} + \frac{y}{D_T}}{4(t-\tau)/\omega R} - \lambda.(t-\tau)}}{\sqrt{(64\pi)^2 D_L D_T (t-\tau)^2}} \; \dot{A}(\tau) \qquad \text{(II.3.32)}$$

The parameter values used for simulating transport through the water table are presented in Table II.3.9. According to the scenario description, the mean horizontal flow rate was estimated to be about 0.2 m/day based on Darcy's law applied to the area between a well close to G4 and the point where groundwater flows southward into the Shinkawa River. At this location, the water table is deeper than in the area between JRR-2/JRR-3 and G4. Therefore, a higher value of the groundwater velocity should perhaps have been selected.

An example of the ARGUS interface for the definition of the water table coefficients is shown in Figure II.3.10. The plane concentration at point G4 resulting from injection at point 1 is plotted in Figure II.3.11 and the HTO concentration plume calculated after 2500 days is plotted on Figure II.3.12.

Results at point G4: A plane concentration (Bq/m^2) was obtained as a result of using a 2-D model to calculate tritium transfer in the aquifer. The volumetric concentration (Bq/m^3 or Bq/L) can be estimated by taking into account the thickness of the aquifer at point G4. According to the geological scheme presented in Figure II.3.5, a thickness of 5 m has been adopted.

The concentration at point G4 is obtained by summing the contributions from each of the six injection points. The contributions of injections 1 to 6 and the total concentration at point G4 are plotted in Figure II.3.13. Over the studied period from 1984 to 1987, the concentration at point G4 varied from 10 to 19.5 Bq/L, with the peak occurring in November 1984. With a 7-m thick aquifer, the maximum concentration would have been around 14 Bq/L.

Table II.3.8. Parameter values used for solving the transfer equation for the unsaturated zone.

	Parameter	Value	Comment
UNSATURATED LAYER	Total porosity of surface soil	0.53	
	Water content	28.4 %	mean value
	Vertical pore water velocity in the unsaturated soil layer	5.5 m/y	
	Depth from soil surface to the top of the groundwater aquifer at G4	15 m	conservative value (15-20 m)
	Vertical dispersivity in the unsaturated zone	1 m	empirical

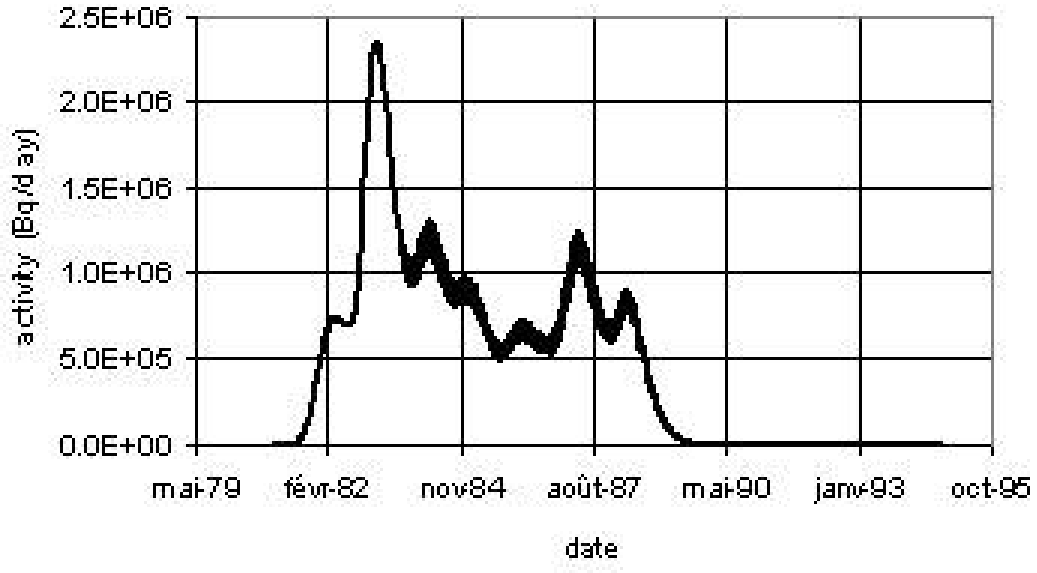

Fig. II.3.9. Time-dependent ^{3}H activity (Bq) at the interface between the unsaturated layer and the water table : contribution of injection at point 1.

Table II.3.9. Parameter values for solving the 2-D saturated layer transport equation.

	Parameter	Value	Comment
WATER TABLE	Hydraulic conductivity	K ~ 6 x 10^{-4} m/s	
	Longitudinal pore water velocity	Ux ~ 0.2 m/d	
	Longitudinal dispersivity	α_X = 10 m	empirical
	Transverse dispersivity	α_X = 1 m	empirical

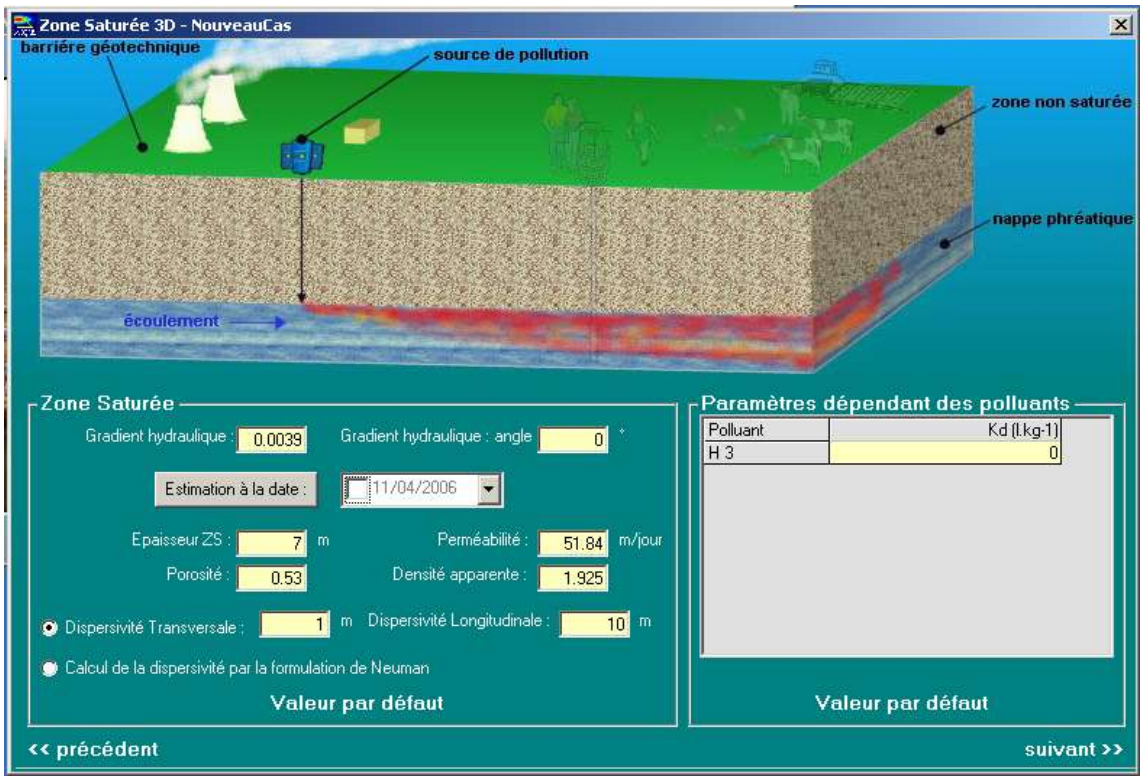

Fig. II.3.10. Example of the ARGUS software interface: definition of the hydrogeological parameters for the water table hydraulic gradient, permeability, porosity and dispersivity.

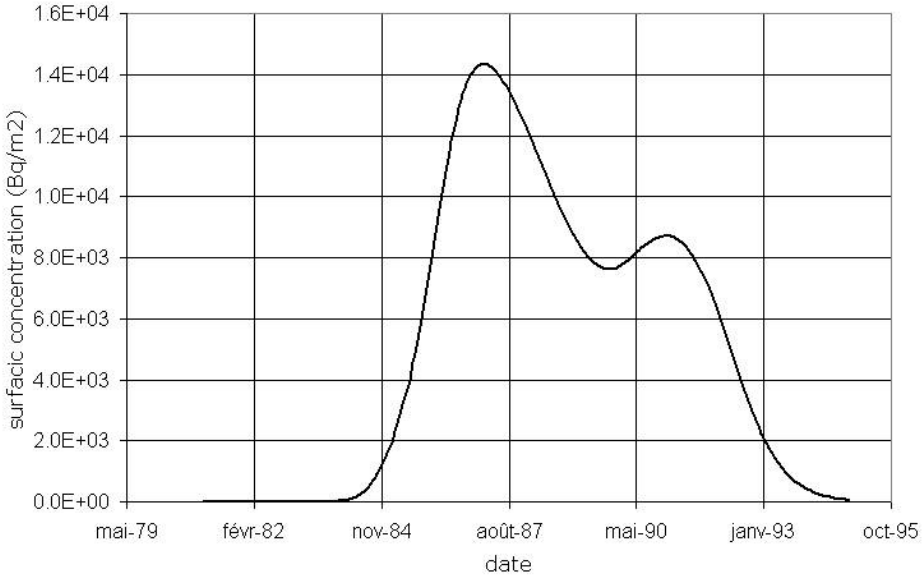

Fig. II.3.11. Time-dependent plane concentration at point G4 resulting from injection at point 1.

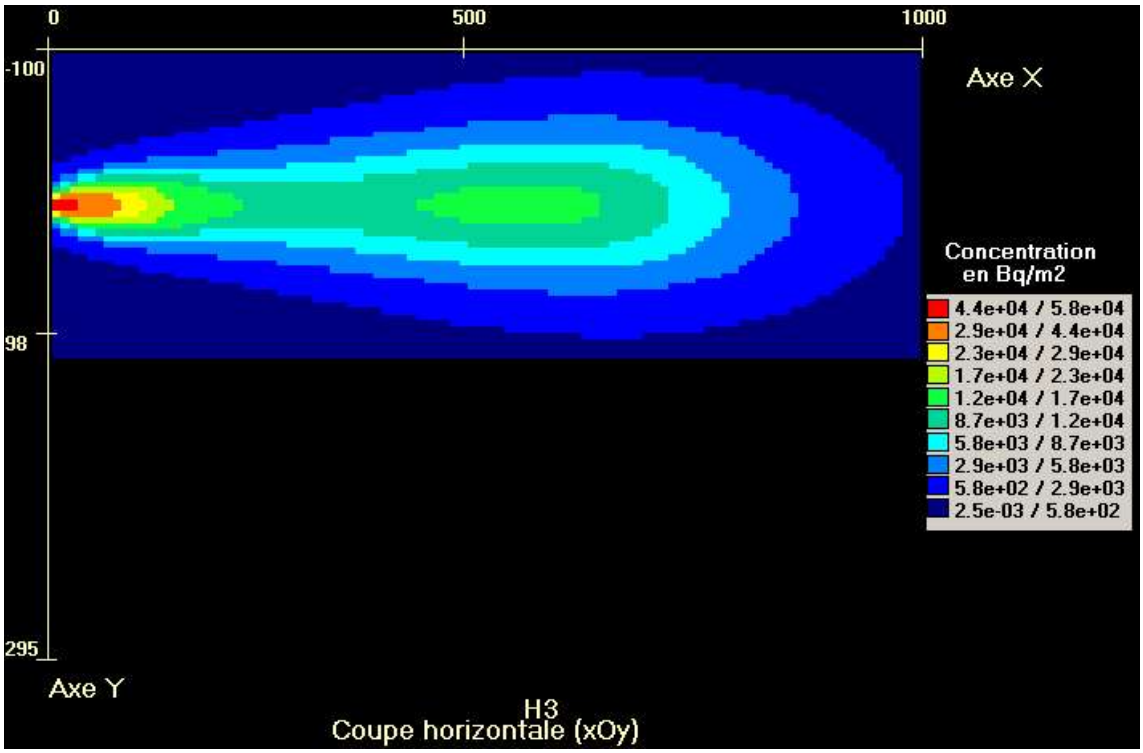

Fig. II.3.12. Plane concentration plume resulting from injection at point 1 (x=0, y=0) after 2500 days (Point G4 is located at x =500 and y=0).

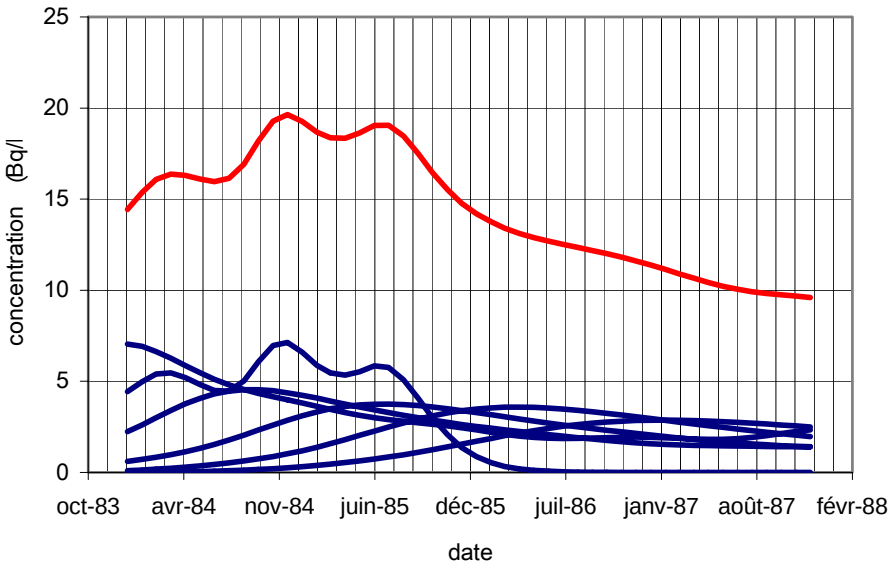

Fig. II.3.13. Time-dependent H-3 concentration at point G4 (Bq/L): sum of the contributions of injection points 1 to 6 obtained for a 5 m thick aquifer (– contribution of injections 1 to 6; – cumulative value).

II.4. Soybean Scenario model descriptions

II.4.1. AECL Model

II.4.1.1. Introduction

The ETMOD (Environmental Tritium MODel) model was developed as a research code but has been used as an assessment tool to predict the consequences of accidental tritium releases to the atmosphere from tritium-handling facilities [II.57, II.58]. It is intended to be realistic. ETMOD is a dynamic, process-oriented type of model that considers the comparments of air, soil, plants and animals. ETMOD covers many transport and exposure pathways including atmospheric dispersion, dry and wet deposition to soil, migration in soil, re-emission from soil, and transfer to vegetation, animals and animal products. It can handle releases of either tritium gas (HT) or tritiated water vapour (HTO) and addresses organically bound tritium (OBT) formation in plants. Final endpoints are ingestion and inhalation (including skin absorption) doses to humans. Intermediate endpoints include tritium concentrations in the various environmental compartments.

II.4.1.2. Key assumptions and modelling approaches

Tritium transfer between air and plants

The exchange of tritium between air and plants is modeled as a diffusion process with the transfer driven by the concentration gradient between air and leaf:

$$\frac{dC_{pw}}{dt} = \frac{V_{ex}}{M_w}(C_a - \gamma\ h\ C_{pw}) \quad , \qquad \text{(II.4.1)}$$

where:

C_{pw} is the HTO concentration per unit mass of plant water (Bq kg^{-1}),
V_{ex} is an exchange velocity (m s^{-1}),
M_w is the mass of plant water per unit ground surface area (kg m^{-2}),
C_a is the HTO concentration in air (Bq m^{-3}),
γ is the ratio of the vapour pressure of HTO to H_2O (0.91), and
h is the saturation humidity at leaf temperature (assumed equal to air temperature) (kg m^{-3}).

Equation II.4.1 describes both deposition to the plant and emission from the plant, depending on the sign of the term in brackets on the right side of the equation. The exchange velocity is calculated using the multiple resistance approach, taking into account the aerodynamic resistance to transfer through the air, the boundary-layer resistance through the laminar sublayer very close to the plant surface, and the stomatal or canopy resistance through the surface of the plant itself. The aerodynamic and boundary-layer resistances are calculated using meteorological data for the current time step. The stomatal resistance is taken from [II.59], which provides values as a function of season and land use. These numbers were modified to account for the values of solar radiation and surface temperature observed at the time of the calculation. The HTO concentrations predicted by Equation II.4.1 are assumed to apply to all aqueous compartments of the plant.

Dry matter production

Gross photosynthesis rates are calculated using the CO_2 consumption model [II.60–II.63] and depend on air temperature, the resistance to CO_2 uptake by the plant and the

photosynthetically active radiation reaching the plant, which in turn depends on leaf area index. The production rate of dry matter is based on net photosynthesis (the difference between gross photosynthesis and respiration), taking into account both growth and maintenance respiration. Plant dry mass is updated using the dry matter produced in the time step. The wet vegetation mass is then calculated from the dry mass and the fractional water content, which is assumed to remain constant as the plant grows. The calculation stops when a pre-specified plant mass or harvest time is reached.

OBT formation

The dry matter produced at a given time is assumed to have a T/H ratio equal to 0.6 times the T/H ratio in the plant water that takes part in the photosynthesis at that time. OBT concentrations following exposure decrease due to dilution with new uncontaminated dry matter. ETMOD does not account for the slow conversion of OBT to HTO in plants due to metabolic processes. OBT concentrations calculated in this way are assumed to apply to all dry matter in the plant.

Translocation

ETMOD can handle four types of crops (pasture, leafy vegetables, root vegetables and grain). In each case, the plant is treated as a single compartment with uniform concentrations throughout. This means that translocation between different parts of the plant must be addressed outside ETMOD. For this scenario, the soybeans were treated as leafy vegetables, and simple conceptual and mathematical models were used to simulate the transfer of tritium between the soybean leaves and the pods. The following assumptions were made:

— The HTO concentration in the pods at the end of the exposure is half the concentration in the leaves. This concentration is reduced through dilution as the plant grows and through losses to the air, with a half time of 2 days.
— Once the leaves and stems are fully grown, all new OBT produced is translocated to the pods. This OBT is distributed in proportion to the stage of development of the plant, with more OBT going to the faster growing of the shells and seeds.
— OBT concentrations in the shells and seeds were calculated by mixing the amount of OBT translocated into the observed dry weight of these compartments at harvest.

II.4.1.3. Parameter values

ETMOD contains a large number of parameters for which values must be specified. These include fixed values for parameters relating to site characteristics, soil properties, plant properties, weather data, dosimetry and the scenario in question. In addition, hourly values of such meteorological parameters as wind speed, air temperature, humidity, cloud cover and precipitation must be entered, together with time-dependent release rates.

II.4.1.4. Model uncertainties

A rigorous uncertainty analysis of ETMOD has not been undertaken. However, the 95% confidence interval is estimated to cover a factor of 10 for HTO concentrations in the plant body and a factor of 4 for OBT concentrations in the pods at harvest, based on results of an uncertainty analysis for UFOTRI, a code similar to ETMOD, for a scenario from BIOMOVS II that was similar to the soybean scenario [II.64]. These estimates reflect the uncertainty due to parameter values only and do not include uncertainties due to model structure. The results

for UFOTRI suggest that the uncertainties are largest for concentrations predicted immediately after exposure and decrease slightly thereafter.

II.4.1.5. Application of ETMOD to the Soybean Scenario

Each simulation began by setting the fresh weights of the plants and their water contents equal to the values observed at the beginning of the exposure (Table II.4.1). The water contents were assumed constant with time as the plant grew. The air concentration in the model was set equal to the average concentration observed in the chamber (Table II.4.1) for one hour and then decreased to zero. It was found that no plant dry matter was produced when the model was run with the air temperature observed in the chamber. Photosynthesis is strongly temperature-dependent and the model in ETMOD assumes that little dry matter is formed for temperatures above 40^{o}C. Accordingly, the temperatures during exposure were arbitrarily set equal to the mean of the temperatures inside and outside the chamber. In all hours after the exposure, the observed temperatures were reduced by 4.2^{o}C, the difference between temperatures in Korea and Canada, to better reflect the Canadian conditions for which ETMOD was developed. The meteorological data supplied with the scenario were filled in so that values for all parameters were available every hour. It was assumed that photosynthetically active radiation equals one-half incoming solar radiation and that the water equivalent factor for soybeans is 0.57. Time steps varied from 0.01 hours for the first 48 hours of each simulation to 0.1 hours for the remainder of the runs.

The leaf area index (LAI) was not calculated in the model but rather was pre-defined at the outset of the run based on information provided in the scenario description.

Predicted plant concentrations were not allowed to drop below the background values that would be expected for a plant growing in an environment with an average air concentration of 0.04 Bq/m^3.

II.4.1.6. Discussion of AECL results

Exchange velocities, fluxes, dry matter production rates and plant masses

Time-dependent ETMOD predictions of exchange velocity, HTO flux from leaf to air, plant mass and dry matter production rate for runs SB1 through SB6 are shown in Tables II.4.2–II.4.7. The exchange velocities fluctuate according to the current meteorological conditions, with most values lying between 2 x 10^{-3} and 8 x 10^{-3} m/s for these daytime conditions. The values decrease by about an order of magnitude toward the end of each run because fall values for the stomatal resistance were used rather than summer values. The HTO flux is directed into the plant at the start of each exposure but reverses as soon as the exposure ends and quickly goes to zero or very small values as the HTO diffuses out of the leaves. The predicted plant mass increases throughout the simulation period for SB1 and SB2, goes through a maximum for SB3 and SB4, and decreases uniformly for SB5 and SB6. In each case, the predicted mass at harvest is substantially smaller than the observed mass, by more than a factor of 3 in the case of SB2. Clearly ETMOD is underestimating the dry matter production rate. The leaf area index does not always increase and decrease in phase with the plant mass since the former is an imposed quantity and the latter is calculated. The assumption that the water content of the plants stays constant with time appears to be good for SB4 and SB5, but in all other cases the observed water contents decreased significantly over the study period.

Table II.4.1. Air concentrations in the chamber and plant water contents and fresh weights.

Experiment	Air concentration (Bq/L)	Plant water content (%)	Initial plant fresh weight (kg/m^2)
SB1	8.42×10^7	82.0	0.96
SB2	1.59×10^8	78.7	1.22
SB3	1.24×10^8	73.3	2.73
SB4	5.71×10^7	68.7	2.02
SB5	9.96×10^7	68.3	4.17
SB6	1.49×10^8	67.5	3.59

Table II.4.2. Time-dependent ETMOD predictions of exchange velocity, HTO flux from leaf to air, plant mass and dry matter production rate for run SB1. The imposed values of leaf area index are also shown.

Time (hours after exposure)	Hour of the day	Exchange velocity ($m\ s^{-1}$)	Flux* ($Bq\ s^{-1}\ m^{-2}$ soil)	Plant mass ($kg\ fw\ m^{-2}$ soil)	LAI	Dry matter production rate ($kg\ CH_2O\ s^{-1}\ m^{-2}$ soil)
-1	10	4.93×10^{-3}	-1.22×10^4	0.961	2.93	2.35×10^{-7}
0.2	11	7.61×10^{-3}	5.24×10^3	0.967	2.93	2.66×10^{-7}
1	12	7.61×10^{-3}	3.03×10^3	0.971	2.93	2.66×10^{-7}
24	11	6.92×10^{-3}	2.12	1.01	3.02	1.67×10^{-7}
120	11	6.95×10^{-3}	0	1.18	3.39	1.91×10^{-7}
336	11	5.97×10^{-3}	0	1.41	4.21	8.99×10^{-8}
936	11	6.21×10^{-3}	0	1.94	6.50	7.60×10^{-8}
1608	11	7.44×10^{-4}	0	2.31	5.70	6.48×10^{-8}
2280	11	6.44×10^{-4}	0	2.37	3.00	5.48×10^{-8}

* From plant to air.

Table II.4.3. Time-dependent ETMOD predictions of exchange velocity, HTO flux from leaf to air, plant mass and dry matter production rate for run SB2. The imposed values of leaf area index are also shown.

Time (hours after exposure)	Hour of the day	Exchange velocity ($m\ s^{-1}$)	Flux* ($Bq\ s^{-1}\ m^{-2}$ soil)	Plant mass ($kg\ fw\ m^{-2}$ soil)	LAI	Dry matter production rate ($kg\ CH_2O\ s^{-1}\ m^{-2}$ soil)
-1	10	5.79×10^{-3}	-2.16×10^4	1.22	3.94	1.47×10^{-7}
0.2	11	2.06×10^{-3}	2.05×10^3	1.22	3.94	1.84×10^{-8}
1	12	2.06×10^{-3}	1.72×10^3	1.22	3.94	1.84×10^{-8}
24	11	2.06×10^{-3}	1.16×10^2	1.23	4.03	1.78×10^{-8}
120	11	6.90×10^{-3}	6.92×10^{-6}	1.29	4.39	1.60×10^{-7}
336	11	6.35×10^{-3}	0	1.46	5.22	1.13×10^{-7}
768	11	5.42×10^{-3}	0	1.72	6.50	4.83×10^{-8}
936	11	6.68×10^{-3}	0	1.82	6.50	1.04×10^{-7}
1368	11	6.81×10^{-4}	0	2.01	5.60	5.44×10^{-8}
1608	11	6.30×10^{-4}	0	2.03	4.60	5.13×10^{-8}
2016	11	6.94×10^{-4}	0	2.05	3.00	5.45×10^{-8}

* From plant to air.

Table II.4.4. Time-dependent ETMOD predictions of exchange velocity, HTO flux from leaf to air, plant mass and dry matter production rate for run SB3. The imposed values of leaf area index are also shown.

Time (hours after exposure)	Hour of the day	Exchange velocity (m s^{-1})	Flux* (Bq s^{-1} m^{-2} soil)	Plant mass (kg fw m^{-2} soil)	LAI	Dry matter production rate (kg CH_2O s^{-1} m^{-2} soil)
-1	10	4.21×10^{-3}	-1.72×10^{4}	2.73	5.49	7.46×10^{-8}
0.2	11	6.78×10^{-3}	7.32×10^{3}	2.73	5.49	8.69×10^{-8}
1	12	6.78×10^{-3}	4.36×10^{3}	2.73	5.49	8.69×10^{-8}
24	11	6.27×10^{-3}	3.20×10^{1}	2.72	5.58	3.85×10^{-8}
120	11	5.68×10^{-3}	4.02×10^{-1}	2.73	5.95	3.75×10^{-8}
336	11	6.13×10^{-3}	1.95×10^{-1}	2.73	6.50	1.86×10^{-8}
768	11	6.66×10^{-3}	2.43×10^{-1}	2.76	6.40	6.31×10^{-8}
936	11	7.44×10^{-4}	3.52×10^{-2}	2.74	5.70	3.94×10^{-8}
1368	11	6.89×10^{-4}	4.02×10^{-2}	2.63	3.90	3.76×10^{-8}
1608	11	6.94×10^{-4}	1.99×10^{-2}	2.57	3.00	3.40×10^{-8}

* From plant to air.

Table II.4.5. Time-dependent ETMOD predictions of exchange velocity, HTO flux from leaf to air, plant mass and dry matter production rate for run SB4. The imposed values of leaf area index are also shown.

Time (hours after exposure)	Hour of the day	Exchange velocity (m s^{-1})	Flux* (Bq s^{-1} m^{-2} soil)	Plant mass (kg fw m^{-2} soil)	LAI	Dry matter production rate (kg CH_2O s^{-1} m^{-2} soil)
-1	10	3.64×10^{-3}	-5.99×10^{3}	2.02	6.41	1.47×10^{-7}
0.2	11	7.39×10^{-3}	2.47×10^{3}	2.02	6.41	1.51×10^{-7}
1	12	7.39×10^{-3}	1.53×10^{3}	2.02	6.41	1.51×10^{-7}
24	11	7.09×10^{-3}	4.26	2.02	6.50	1.21×10^{-7}
120	11	5.42×10^{-3}	0	2.02	6.50	2.58×10^{-8}
336	11	6.62×10^{-3}	0	2.05	6.50	7.11×10^{-8}
768	11	5.22×10^{-4}	0	2.06	5.40	1.47×10^{-8}
936	11	5.36×10^{-4}	0	2.03	4.70	2.19×10^{-8}
1368	11	6.44×10^{-4}	0	1.97	3.00	3.89×10^{-8}

* From plant to air.

Table II.4.6. Time-dependent ETMOD predictions of exchange velocity, HTO flux from leaf to air, plant mass and dry matter production rate for run SB5. The imposed values of leaf area index are also shown.

Time (hours after exposure)	Hour of the day	Exchange velocity (m s^{-1})	Flux* (Bq s^{-1} m^{-2} soil)	Plant mass (kg fw m^{-2} soil)	LAI	Dry matter production rate (kg CH_2O s^{-1} m^{-2} soil)
-1	10	5.48×10^{-3}	-1.39×10^{4}	4.17	6.50	5.51×10^{-8}
0.2	11	7.39×10^{-3}	5.63×10^{4}	4.17	6.50	9.43×10^{-8}
1	12	7.39×10^{-3}	3.40×10^{3}	4.17	6.50	9.43×10^{-8}
24	11	5.61×10^{-3}	9.16	4.16	6.50	2.14×10^{-8}
120	11	6.69×10^{-3}	0	4.11	6.50	1.36×10^{-8}
336	11	7.44×10^{-4}	0	3.97	5.70	-8.50×10^{-8}
768	11	6.89×10^{-4}	0	3.66	3.90	-4.30×10^{-8}
1008	11	6.94×10^{-4}	0	3.52	3.00	-5.18×10^{-8}

* From plant to air.

Table II.4.7. Time-dependent ETMOD predictions of exchange velocity, HTO flux from leaf to air, plant mass and dry matter production rate for run SB6. The imposed values of leaf area index are also shown.

Time (hours after exposure)	Hour of the day	Exchange velocity (m s^{-1})	Flux* (Bq s^{-1} m^{-2} soil)	Plant mass (kg fw m^{-2} soil)	LAI	Dry matter production rate (kg CH_2O s^{-1} m^{-2} soil)
-1	10	7.86×10^{-4}	-2.24×10^{3}	3.59	4.70	6.19×10^{-9}
0.2	11	8.85×10^{-4}	1.37×10^{2}	3.59	4.70	1.64×10^{-8}
1	12	8.85×10^{-4}	1.31×10^{2}	3.59	4.70	1.64×10^{-8}
24	11	6.30×10^{-4}	4.85×10^{1}	3.57	4.60	-1.34×10^{-8}
120	11	6.63×10^{-4}	4.28	3.51	4.20	-6.12×10^{-9}
336	11	6.21×10^{-4}	2.26×10^{-3}	3.38	3.30	-6.84×10^{-9}
432	11	6.94×10^{-4}	3.08×10^{-2}	3.33	3.00	-2.98×10^{-9}

*From plant to air.

HTO concentrations (SB1 and SB4)

Leaves and stems: The predicted HTO concentrations in leaves and stems were higher than the observations immediately after the exposure, by a factor of 4 for SB1 and a factor of 2 for SB4. This suggests that the model overestimates the HTO transfer rate from air to leaves. The degree of overestimation increased through hour 1 for SB1 and through hour 24 for SB4 but decreased thereafter, resulting in predictions that were lower than the observations by 120 hours in each run. This implies that losses of tritium from the leaves occur too rapidly in the model in the period 1-4 days following exposure. Nevertheless, the model performed well over the first 24 hours, the period of high concentration that determines the total amount of OBT formed in the leaves. The large underpredictions beyond 120 hours are believed to arise because ETMOD does not allow for the slow conversion of OBT to HTO.

Shells and seeds: As noted above, the initial HTO concentration in the pods is assumed to be half the concentration in the leaves. This resulted in underpredictions for SB1, where the leaf concentrations were at background levels at the time the pods formed. For SB4, the assumption also resulted in an initial underestimation, by a factor of about 2, which suggests that the HTO taken up during the exposure moves rapidly through all parts of the plant. However, a biological half time of 2 days for the HTO in the pods appears to be too long, since the predictions rose above the observations beginning at 24 hours. The predictions dropped below the observations again at about 500 hours because ETMOD does not allow for the slow conversion of OBT to HTO. The model performed well over the first 24 hours when the concentrations were high.

OBT concentrations

Leaves and stems: ETMOD predictions for OBT concentrations in leaves and stems at harvest agreed well with the observations for exposures that took place before any pods had formed. However, for later exposures, ETMOD assumes that all OBT formed in the leaves is translocated to the pods and sets the leaf concentration to background levels. This assumption was not supported by the observations, which show that some OBT is retained in the leaves even when the exposure occurs at late growth stages, with the result that ETMOD severely underestimated these endpoints.

Shells and seeds: ETMOD's predictions of OBT concentrations in the pods agreed well with the observations for exposures that occurred after the pods had formed (SB3, SB4, SB5 and SB6). In contrast, the model severely underpredicted the concentrations in pods that had not yet started to form at the time of exposure (SB1 and SB2). In this case, the predicted HTO concentrations in the leaves had dropped off to very low values by the time the pods had started to form, so that the dry matter translocated to the pods was essentially uncontaminated with tritium.

II.4.2. Belot Model

II.4.2.1. Model description

To evaluate the accumulation of tritium in the organic matter of plant organs such as fruits, grains, roots or tubers, our preliminary approach is the following. It is assumed for simplification that: (i) the growth rate of the organ is constant during the linear growth phase of the organ and negligible outside this phase; (ii) the organic matter formed in foliar tissues is transported to the growing organ by translocation. At each time, the specific activity of the newly formed organic products (expressed in activity of combustion water) is proportional to the specific activity of leaf water. The final specific activity of the organic matter in the organ at harvest is then proportional to the mean specific activity of leaf water during the whole linear growth phase of the organ in question [II.65]. This is the basis of the following model, which was further refined to take into account the influence of variations in light.

The specific activity of the organic matter of a given storage organ at harvest C_{OBT} is thus calculated by determining a weighted mean activity of leaf water C_{HTO} over the duration T of the linear growth phase of the organ. This is expressed by:

$$C_{OBT} = \frac{\alpha}{T}\int_0^T C_{HTO}(t)g(t)dt \qquad \text{(II.4.2)}$$

where:

α = 0.6 is a dimensionless fractionation ratio defined as the ratio of the specific activities of combustion water and tissue water in equilibrium conditions;

T is the duration of the linear growth phase, which is rather well documented for the most important crops; and

$g(t)$ is a corrective weighting factor that expresses the influence of the diurnal light flux variations on carbon assimilation and therefore concomitant tritium incorporation.

The corrective weighting factor $g(t)$ was introduced in the model equation to take into account the influence of the light flux on the growth rate of the organ at a small time scale. If the growth rate is proportional to the light flux, this dimensionless factor should be equal to the ratio between the light flux at time t and the average light flux over the whole duration of the growth phase (including night). If a light saturation effect is expected, the real light flux should be replaced by the efficacious light flux, which, in a first approximation, can be set equal to the real flux when saturation does not still occur, or to the saturation flux otherwise.

II.4.2.2. Application to the Soybean Scenario

Equation II.4.2 is simplified by assuming, in a first approximation, that the totality of HTO absorbed in the leaves during exposure is flushed out of the leaves in an exponential way within a few hours after exposure and that practically no residual HTO remains in the leaves afterwards. If we suppose moreover that the exchange rate and light flux do not vary substantially during the phases of exposure and early exponential decline, we can integrate Equation II.4.2 and this yields the following much simpler equation:

$$C_{OBT} = C_{HTO}^{air}\ \alpha\ h\ g\ \frac{t_e}{T} \qquad \text{(II.4.3)}$$

where:

C_{HTO}^{air} is the concentration of tritium in air humidity during exposure;

h is the relative humidity of the atmosphere;

g is the corrective factor defined above as the ratio between the light flux during exposure and the mean light flux during the whole growth period;

t_e = 1 h is the duration of exposure;

T = 840 h (35 days) is the mean linear growth duration of the soybean seeds in normal conditions, as estimated from many references in the literature (e.g. [II.66, II.67]).

The simple model above allows to see that, under simplifying assumptions, the normalised concentration of OBT at harvest is directly proportional to the exposure duration and inversely proportional to the duration of the linear growth phase of the organ considered.

II.4.2.3. Discussion of results

The results obtained for the exposures SB4 to SB6 are given in Table II.4.8. The seed's growth period begins between SB3 and SB4, so that the experiments SB1, SB2 and SB3 cannot be treated by the simplified Equation II.4.3. The most important parameter in the model is certainly the seeds linear growth duration T. This parameter does not represent the total duration of the growth phase, which is about 50 days, but the duration of the linear growth phase, which is generally estimated to be about T = 840 h (35 days). The latter value is the statistical mean of a great number of values for many plants in the field, different cultivars and different climatic conditions that may affect growth. The corrective factor g that characterizes the light influence at time of exposure is far from being negligible. This factor is calculated as explained above in Section II.4.2.1, and amounts to 3.11, 2.44 and 2.16 for SB4, SB5 and SB6 respectively.

For leaf exposure within the fruiting period (SB4 to SB6), the predicted concentrations in the seeds at harvest are close to the observed ones within a factor of about two. The somewhat greater difference for SB6 can be explained by the circumstance that exposure was carried out near the end of the linear growth period. Moreover, the simplifying assumptions of the model and the statistical nature of the input data can affect the three results obtained. Nevertheless, for the present scenario, the differences between the observed and predicted values are rather moderate, which comforts the tentative simple model presented above.

Table II.4.8. Results obtained by applying the simplified model to the Soybean Scenario.

Exp.	**Observed** C_{OBT} / C_{HTO}^{air} in pods and seeds at harvest	**Predicted** C_{OBT} / C_{HTO}^{air} in pods and seeds at harvest
SB1	8.63 E-06	*
SB2	2.44 E-05	*
SB3	5.28 E-04	*
SB4	2.61 E-03	1.46 E-03
SB5	1.56 E-03	1.37 E-03
SB6	0.40 E-03	1.24 E-03

*Cannot be estimated by using Equation II.4.3, which assumes a sustained rapid exponential decrease of tritium in leaf water.

For pre-fruiting exposure (SB1 to SB3), the model does not provide any prediction, due to the assumption that the contamination of the seeds is quite negligible in this case. This does not correspond to the reality. In fact, some OBT is observed in the seeds, at a measurable concentration, which is nevertheless much smaller than observed for exposures during the fruiting period. This can be explained by the observation that the real time course of HTO–in–leaves after a short exposure is different from the time course assumed in the model. The elimination of HTO from the leaves is initially very fast as supposed for simplification, but becomes in fact slower and slower as time elapses. After a few days, there still remains in the leaves some amount of HTO that does not vary substantially throughout the growth period of the seeds and induces the accumulation of some OBT in the growing seeds. If we assume that the residual HTO in the leaves over the growth period of the seeds is comprised between 10^{-4} and 10^{-5} of the initial concentration of HTO in leaves, the normalised concentration of OBT in the seeds will be comprised in the same interval of magnitude. This agrees quite well with the observations made in the SB1 to SB3 experiments.

A prediction of OBT in seeds at harvest for pre-fruiting exposures could be obtained if it were possible to predict the real time course of HTO-in-leaves over a long time after exposure. Alternatively, the prediction could be based on the observed curve of HTO retention in soybean leaves or on a curve observed for other plants, assuming that it does not vary substantially with the plant considered. It seems that the form of the retention curve, while being governed in the beginning by the rapid turnover of water in leaves, is governed later on by the backward transport to the leaves, via the xylem path, of some of the HTO initially conveyed to the stem and roots via the phloem path. But, the residual HTO may also be due to a slight contamination of the soil water during the phase of leaf exposure, in spite of the precautions taken to avoid it. It seems that the first hypothesis is most probable, since the same form of HTO retention curve was already observed in much earlier experiments in which potato and vine leaves were exposed to HTO with precautions taken to avoid soil exposure [II.68]. Nevertheless, this needs to be substantiated by further observations, in experiments where the absence of soil contamination would be carefully verified by measuring HTO in soil samples at different times after end of leaf exposure.

II.4.3. FzK Model

II.4.3.1. Introduction

The capabilities of the accident consequence assessment model UFOTRI were extended to consider a wider variety of foodstuffs. In a first step, rice was added to the list of foodstuffs and a generic rice model was developed. This type of model is used to perform the calculations for the soybean scenario. The newly developed model, however, is still not part of the UFOTRI distribution due to a lack of time for intensive testing.

II.4.3.2. Model description

Basis of the modelling are processes that require light such as photosynthesis and photorespiration, and others which are independent on light, such as maintenance respiration and basic metabolism. Light-dependent and light-independent processes are treated in a different way. Light independent transfers were set to constant transfer rates whereas the light dependent transfer rates are described by physically based models. The reason behind this distinction is the lack of quantitative model approaches for the light independent processes, in particular for the basic metabolism.

Photosynthesis is calculated on the basis of net CO_2 assimilation by using an approach presented in [II.60] for wheat. However the approach can be adapted to other crops. This was successfully done in UFOTRI for vegetables, root crops and cereals. The derivation of the required parameter values together with factors taking into account several stress conditions can be found in [II.60] and [II.69]. Parameterisation specific to the new model is discussed below.

With the photosynthesis model it is possible to predict the build up and thus the growth of crops such as the rice plant and soybean. However what has to be adapted is the duration of the growth and the partitioning function. Before flowering, the whole organic matter production will end in either the stem, roots or leaves of the plant. After flowering, more and more material is directed towards the build-up of the seeds. Build up increases until, the linear growing phase starts, where the build up of material is nearly constant. This phase lasts several weeks followed by the drying of the seeds until maturity and harvest. The duration of the three phases can be selected by the user, dependent on the crop. The maximum photosynthesis rate was set to slightly higher values as for wheat.

The OBT incorporation into the edible part of the soybean per hour T_{act} is now directly related to the build up of organic matter and the concentration of tritium in the tissue free water:

$$T_{act} = P_{act} * C_{TWT} * f_g * dis \qquad \text{(II.4.4)}$$

where:

P_{act} is the actual hourly dry matter production rate in g/h;
C_{TWT} is the hourly mean TWT concentration in the crop in Bq/g;
f_g is a function describing the initial partitioning after flowering and before the linear growing phase; and
dis is a parameter taking into account that UFOTRI does only consider the whole plant and not the partitioning into leaves and stem (set to 2).

Table II.4.9. Parameter selection.

Parameter	value
Minimal stomata resistance	2 s/m
Plant water content at maximum	2000 g
Plant organic matter at maximum	500 g
Plant water content at maximum	100 g
Plant organic matter at maximum	600 g
Leaf area index at maximum	5 m^2/m^2
Constant concerning minimal PAR flux	30
Constant concerning water vapour deficit	0.2
Minimal temperature for stomata closure	8 °C
Maximal temperature for stomata closure	45 °C
Optimal temperature for stomata	28 °C
Day of harvest for rice	261
Time interval between anthesis and harvest	90 days
Duration of the first period after anthesis	30 days
Length of linear growing period	30 days
Length of maturity time before harvest	30 days

The function f_g is 1 during the linear growing phase. For the two other periods, f_g can be described as a sinusoidal function normalised to the duration of the phase. The duration of the three phases was assumed to be:

Phase 1: 30 days
Phase 2: 30 days
Phase 3: 30 days

A standard type of crop was applied for all calculations ignoring the variety of weights given in the scenario description. It was assumed that the overall uncertainty hides these variations in particular as the model is robust against these changes. Robustness means that when the crop weight is increased, also the build up of OBT is increased respectively. Only the initial specific HTO concentration in the crop may vary, however, such finesses might be considered in a second run.

II.4.3.3. Parameter values

The parameters used for the soybean scenario are provided in Table II.4.9.

II.4.4. FSA Model

II.4.4.1. Introduction

Short-term discharges warrant special treatment as they may result in greater exposures to the critical group compared to the same activity discharged over a longer period. The reasons for this are two-fold. First, in the case of chronic discharges, these are assumed to be spread over a 360° wind rose over a year according to local weather patterns, whereas an acute release is usually released in a brief period within a small sector. This can result in higher concentrations particularly if the discharge is towards land and not sea. Second, over a short time scale, little weathering or nuclide decay will take place possibly resulting in higher concentrations in harvested crops and livestock. However, over a long time scale, concentrations in crops and livestock would decrease after an acute release.

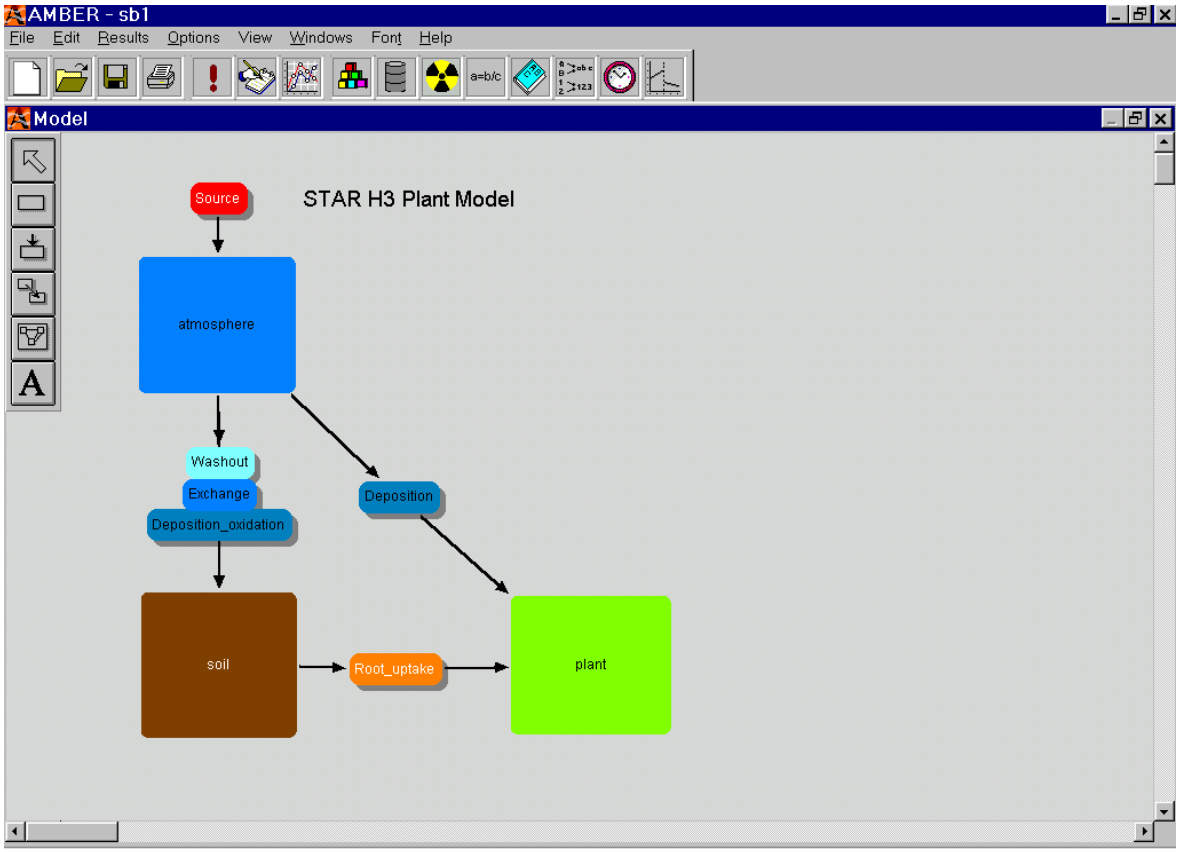

Fig. II.4.1. Basic outline of the compartmental model for STAR-H3.

II.4.4.2. Model approach

The Food Standards Agency has developed the STAR-H3 model to determine the effect that short-term releases of H-3 have on the food chain. With ongoing development, the STAR H-3 model has now been incorporated into the compartmental model 'AMBER', which reproduces and enhances the behaviour of the original STAR-H3 model. These incorporate the methodology developed by Smith [II.70] to take account of the short-term dynamic properties of these nuclides. This also incorporates the results of experimental work undertaken at Imperial College, London. The models include compartments that address losses from the plume through exchange with atmosphere, and through metabolic processes such as respiration. They also include compartments that allow for fixing of activity through photosynthesis in biota, translocation into storage organs in plants, and metabolism into carbohydrates, proteins and lipids in animals.

Figure II.4.1 shows the basic outline of the compartmental model for STAR-H3 used in the soybean analysis.

Model compartments

— **Atmosphere**. This is the concentration of H-3 in air surrounding the plant. This compartment is the source of H-3 for all other compartments. The model inputs for the

compartment are the time integrated H-3 concentration in air, the water content in air and the time over which the concentration persists.

- **Soil.** Soil in the root zone contains water and so hydrogen. Model inputs for this parameter are the bulk soil density and the soil water content. It is important to note that all of the tritium within this compartment is assumed to behave as HTO.
- **Plant (fast turnover)**. The proportion of the plant containing tritiated water. The model inputs for the compartment are the crop density, the areal evaporation rate and water content.
- **Plant (slow turnover)**. The proportion of the plant containing organically bound tritium, OBT. The model inputs for the compartment are the non-labile hydrogen content and mean residence time in the plant.

The two plant compartments need to be separately identified because of the different time constants for hydrogen retention and because OBT in compartment 4 has a higher value per unit intake.

II.4.4.3. Transfer factors

There are 7 transfer factors that relate to the exchange of H-3 between compartments (in Figure II.4.1) in the STAR-H3 plant model. It is a common occurrence that some foodstuffs may not have sufficient data to accurately model uptake. In such situations simple approximations are made concerning the genus of the plant.

- **Atmosphere to soil:** HT movement into soil and rapid oxidation to HTO, exchange of water between soil and atmosphere, wet deposition. For this scenario this transfer was set to zero to reflect the covering of the soil with polythene.
- **Soil to 'out of system':** Losses due to exchange to atmosphere and loss to deep soil below the root zone.
- **Soil to plant 'fast':** Uptake of water by the plant.
- **Plant to 'out of system':** Evapotranspiration and exchange of HTO between plant and atmosphere.
- **Atmosphere to plant 'fast':** HTO exchange, only HTO in the atmosphere
- **Plant 'slow' to Plant 'fast':** Loss of tritium from non-labile or OBT.
- **Plant 'fast' to Plant 'slow':** Rate of conversion of plant tissue water and other labile tritium to the non-labile form.

For all compartments except atmosphere an additional transfer is used to account for radioactive decay.

II.4.5. GE Healthcare

II.4.5.1. Model description

The GE Healthcare model is a dynamic compartment model formulated in terms of a series of coupled first-order differential equations. The model starts with the tritium concentration in air and consists of four compartments representing the atmosphere, soil water, a plant fast compartment and a plant slow compartment. The plant fast compartment represents tissue free water inside the plant whilst the plant slow compartment represents the organic matter of the cells. It is assumed that these two compartments are in equilibrium within the plant.

The following transfers are represented within the model:

- transfer from the atmosphere to root zone soil water, including dry and wet deposition;
- loss from soil root zone by evaporation and transfer to deeper soil layers;
- transfer from root zone soil to the plant fast compartment, representing the uptake of water by plants;
- transfer from the atmosphere to the plant fast compartment, representing the uptake of tritiated water by exchange with the atmosphere;
- loss from the plant fast compartment, accounting for evapotranspiration and exchange of tritiated water between plant and atmosphere;
- transfer from the plant fast compartment to the plant slow compartment, representing the incorporation of tritiated water and labile organically bound tritium into non-exchangeable forms; and
- transfer from the plant slow compartment to the plant fast compartment, accounting for the loss of non-exchangeable tritium from plant tissues.

II.4.5.2. Parameter values

Generic parameter values

The generic parameter values within the model are provided in Table II.4.10.

Scenario specific parameter values

Parameter values specific to each scenario considered are provided in Table II.4.11.

Table II.4.10. Generic parameter values.

Parameter	Value
Volume of the box	1.17325 m^3
Exchange velocity	0.0102 ms^{-1}
Plant fast turnover rate	1 h^{-1}
Residence time	32 days
g hydrogen per g water	1/9
Air turnover	0 during exposure, 1000 at all other times

Table II.4.11. Specific parameter values.

Parameter	SB1	SB2	SB3	SB4	SB5	SB6
Activity concentration in the box (Bq m^{-3})	1.04E+12	1.97E+12	1.52E+12	7.02E+11	1.23E+12	1.83E+12
g water per kg plant [Plant fast water]	712	638.55	697.14	680.44	672.5	590.31
Water content of air (g water per m^3 air)	39.52	29.07	40.23	52.35	35.98	26.7

II.4.6. IFIN-HH Model

II.4.6.1. Model description

An improved version of the tritium module in the EC project RODOS was used, initially developed in our institute in collaboration with FZK-Germany [II.71]. The model has a similar general structure as UFOTRI but the transfer parameters for tritium are derived from plant physiology. The transfer of HTO from air to leaves is modeled with an exchange velocity that includes a canopy resistance. The canopy resistance is modeled using a physiological model depending on canopy photosynthesis rate. The leaf conductance to CO_2 is given by:

$$g_{sc} = g_c + \frac{A_g \cdot (0.9 - \frac{4.7}{A_{m,g}} \cdot \frac{D_s}{D_{\max}})}{C_s - C_{i,vir}} \qquad C_i = f(C_S - \Gamma) + \Gamma \quad f = f_o(1.-D_S / D_{\max}) \tag{II.4.5}$$

where:

C_s and C_i are the CO_2 concentration at leaf surface and leaf interior;
Γ is the CO_2 compensation point;
D_s is the humidity deficit at leaf surfaces;
f_o and D_{max} are parameters describing the effect of humidity deficit on leaf resistance;
g_{sc} is the stomata conductivity for CO_2;
g_c is the cuticle conductivity;
A_n and A_g are the net and gross photosynthetic rate;
A_{min} is the residual cuticle photosynthetic rate;
$A_{m,g}$ is the maximum gross photosynthetic rate; and
Rd is the dark respiration rate.

By integrating over the canopy, the canopy conductance is directly linked to the canopy photosynthesis. For the last quantity we use the submodel from the crop growth model WOFOST with accompanying physiological plant parameters in the database [II.72]. Note that the dry biomass considered is obtained after extraction of maintenance and growth respiration while the canopy resistance uses the initial photosynthetic rate.

The conversion of HTO to OBT is driven by photosynthesis rate, using stoichiometry and an isotopic discrimination rate. We consider the net OBT formation, after maintenance and growth respiration processes. Part of the newly formed OBT is distributed to grain (pod), in accordance with dry matter partition (plant and cultivar specific). The model includes also OBT formation in night, but this is not relevant in the present scenario.

II.4.6.2. Adaptation to the Soybean Scenario

In order to model the biomass dynamics for the present scenario and soybean cultivar, we have constructed a daily weather file, combining scenario data with climatic ones (monthly mean values from Wolsong area in INTERNET were used to generate a daily sequence using free software (wgen.for). An hourly meteorological file was constructed by interpolation from scenario data and further used in the tritium model. We start with an existing tropical cultivar in the database and have slightly adapted the parameters in order to obtain the dynamics of biomass growth as given in the scenario. In our model, the plant growth is modeled in a simplified way but still gives reasonable results. We note that the scenario data have a large

variability of biomass at harvest between experiments, a coefficient of variation of 60 % for seeds and 30 % for total biomass. These can influence the model prediction uncertainty. There are no direct data on leaf area index dynamics. These shortcomings of the input data give some uncertainty in the plant biomass and LAI dynamics. Two plant models were considered, one with minimum biomass and LAI and one with maximum one.

The biomass dynamics from experiment and the two variants of the soybean model are given in Figure II.4.2. Seed mass at harvest was most accurately predicted by model 1 and total biomass by model 2.

Figure II.4.3 gives the model 1 LAI dynamics in comparison with the prediction of plant growth model WOFOST. We note that for SB1, the predictions are lower than the best estimate of LAI. Indeed, from the leaves dry mass and the specific leaf area of soybean (derived from the literature) we deduced a LAI of 3 (at this stage all leaves are green), while model 1 predicted a value of 1.35. Model 2, with increased biomass, gave the right LAI at SB1, but higher LAI later.

Among intermediary model results we present the predictions for the canopy resistance as functions of time and experiment in Figures II.4.4 and II.4.5.

The largest canopy resistance in the light is for the experiment in July 2, in the period of fumigation but also after. The higher resistances in the periods of box experiments can be a result of more factors:

- Increased temperature in the box, as for Aug 9 where we have values of 45-48 °C- definitely depressing photosynthesis and increasing the canopy resistance.
- Under-prediction of solar radiation. A general conversion factor of 5.5 was used to convert luminance to solar radiation. This gives value of solar radiation in the box much lower than that measured (up to a factor 2).

Higher resistance occurs for the first experiment but also for the last (Figure II.4.5) as a result of plant phenology and development. In SB1, the plant was young with few leaves but all green. In SB6, the plant is old with few green leaves.

The results presented partially explain the large difference in the dynamics of HTO concentration of leaf water between experiments, as seen in Figure II.4.6.

OBT concentration in seeds depends on daily OBT production and on the partition to storage organs. No information on the specific Korean cultivar used in the experiments was available and literature values are variable. OBT production is dependant on leaf water HTO concentration and photosynthesis rate.

The growth period is divided into vegetative and reproductive periods. Emergence is considered at development stage 0, flowering at development stage 1 and harvest at development stage 2. The partition to storage organs as in WOFOST database for soybean was initially used.

No data on the translocation to storage organs before flowering was available, but it is known that a part of the new dry matter stored in stems at flowering stage can be potentially translocated to grain (pod) and this fraction is plant dependant (Table II.4.12, [II.73]).

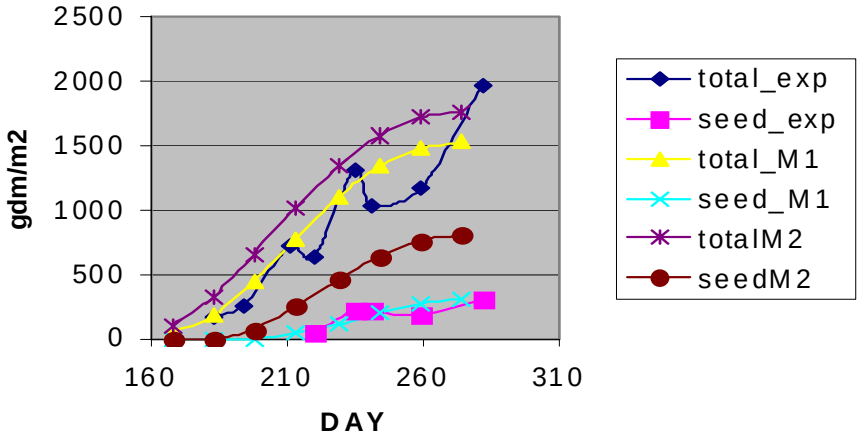

Fig. II.4.2. Biomass dynamics: experiment and models.

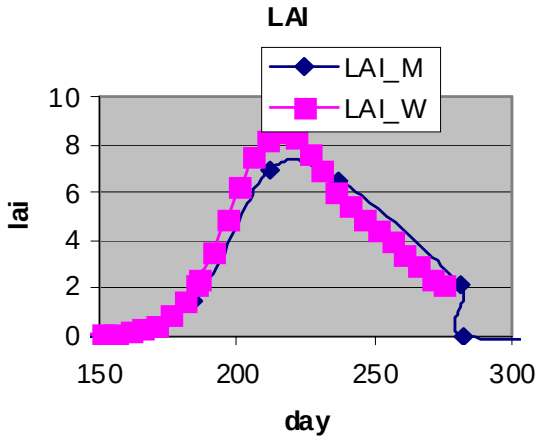

Fig. II.4.3. LAI in tritium model and WOFOST model and RODOS-H result.

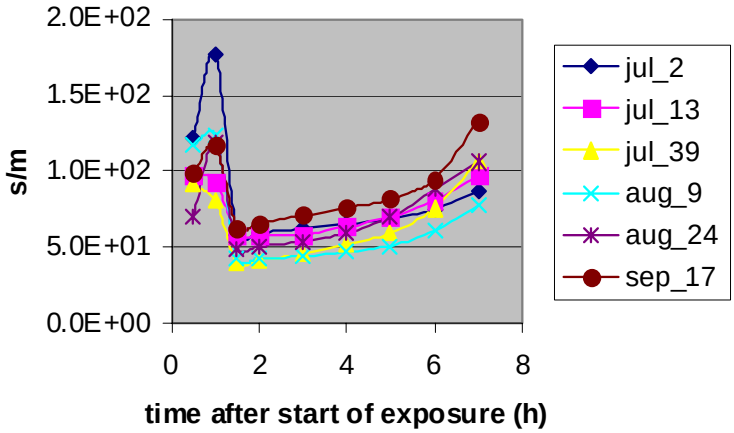

Fig. II.4.4. Canopy resistances in the first 8 hours from the start of the exposure.

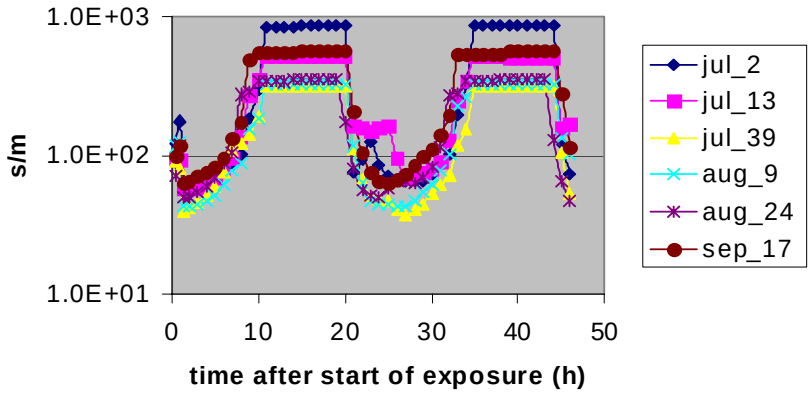

Fig. II.4.5. Canopy resistance for first 46 hours after start experiment

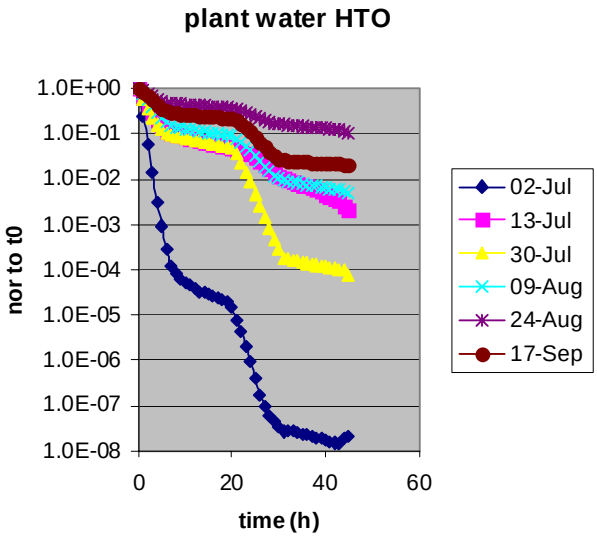

Fig. II.4.6. Leaf water HTO concentrations normalized to end of fumigation.

Table II.4.12. Fraction of stem weight at flowering potentially translocatable to storage.

Plant	Fraction
Soybean	0.18
Wheat	0.4
Faba bean	0.45
Potato	0.3

Table II.4.13. Temperature dependence of maximum photosynthesis rate.

Temperature (°C)	Factor
0	.0001
10	.3
20	.6
25	.8
30	1
35	1
40	.8
50	.001

In absence of information on the Korean cultivar an intermediate situation was considered with low translocation during the flowering stage (fraction of stem weight subject to translocation between 0.05-0.15).

II.4.6.3. Discussion

The model was variable in its predictions of HTO and OBT in relation to the observed values. The HTO concentration in leaves was over-predicted by a factor of 3 to 5 in experiments SB1 and SB4 at the end of exposure, but under-predicted by 40 - 90 times at harvest. OBT in pods was under-predicted by 100 times in SB1, but over-predicted by 10 times in SB6.

A number of sources of uncertainty were analysed:

- Wind speed – unknown anemometer height. This may have a marginal effect on atmospheric resistance and exchange velocity.
- Improper plant LAI and biomass in the model, compared with data used. This could be a potential source of error as the simple growth model used is not appropriate for measured biomass and there is uncertainty in the scenario LAI. This can explain our fast release in SB1, due to under-prediction of leaf biomass and LAI.
- Variability of experimental harvest biomass among experiments. There is a large spread of experimental data and a proper growth trend is therefore difficult to assess. At harvest the total dry biomass is on average 1966 g/m^2, but with a range of 1286-3225. A factor 2 misprediction in the canopy resistance and OBT production from the variability of biomass production between experiments can be expected on this basis.
- Ambiguities in the scenario relating to the large water content in seed at harvest. Based on general agricultural practice, a water content no more than 20 % in seeds at harvest would be expected. However, in the scenario data the water content is close to 60%.
- Difficulties in assessing the proper characteristics of the Korean cultivar, such as translocation from stem to grain, grain filling dynamics, temperature effect on photosynthesis.
- The covering applied to the soil during the exposure may not have been completely effective at preventing a small amount of tritium from depositing to the soil. Root uptake from the soil may then have acted to keep the HTO concentrations in the plant at a relatively high level.

The general over-prediction in HTO at the end of exposure period may result from the unusually high temperature in the exposure chamber. The average temperature for SB1 - SB6 was 40, 33, 39, 47, 40 and 32 °C, respectively. The maximum environmental temperature was only 34 °C. Plants cease photosynthesis at high temperature, the cut-off value depending on plant type and the adaptation to average environmental conditions. We have no idea on the temperature cut-off for the Korean cultivar but literature values are lower than 47°C. Penning de Vries [II.73] gives the values shown in Table II.4.13.

It seems highly probable that in SB4 there is a depression of uptake and photosynthesis while in SB2 and SB6 this is excluded. Both SB1 and SB4 show a low uptake, Cplant/Cair is around 0.125, which implies an uptake rate near 0.33 h^{-1}. Therefore, it appears that plants were under stress in the chamber in SB1 and SB4 and this was not taken into account by most of the modellers.

II.4.7. Japanet Model

II.4.7.1. Japanet members list

NIRS (Kiriko Miyamoto, Yoshikazu Inoue, Hiroshi Takeda, Kazuhide Yamamoto), Ibaraki University (Michiko Ichimasa, Yusuke Ichimasa), Kumamoto University (Noriyuki Momoshima), Toyama University (Hiroshi Satake) and Kyoto University (Masahiro Saito).

II.4.7.2. Assumption for calculation of Soybean Scenario

(1) Model and parameters are mostly based on the observation in Ibaraki University's semi-field release experiments in 1999–2002 of soybeans exposed to deuterium oxide vapor (see Table II.4.14 [II.74, II.75]).
(2) No difference of TFWT in each part of a soybean plant. Errors of TFWT concentration were estimated from 10% variation of the rate constant of HTO loss from plant in the model.
(3) Accumulation rate of non-exchangeable OBT (nOBT) in seeds changes depending on growing stages of soybean plant. Errors of nOBT concentration were estimated from the standard deviations of mean HTO concentration in air vapor during the exposure.
(4) No consideration of soil properties, biomass balance of plant, meteorological and artificial conditions in the glove box and in the field.

II.4.7.3. Ibaraki University model

Belot's equation [II.49] was modified. Uptake of deuterium by the soybean plant is expressed as:

$$Crp = Ca \times Crmax \times [1-\exp(-k_1 t)] \quad \text{(II.4.6)}$$

where:

Crp is the tissue free water deuterium (TFWD) concentration ratio in plant (ppm);
Ca is the deuterium concentration in air moisture around sampling point at time t (ppm);
Crmax is the steady-state concentration ratio (Crp/Ca);
k_1 is the rate constant of D_2O uptake from air (h^{-1}); and
t is the time after the start of exposure (h).

Table II.4.14. Comparison of characteristics of soybean scenario and Ibaraki University's experiment.

Characteristic	Soybean scenario	Ibaraki University's experiment
Tracer	HTO vapor	HDO vapor
Release Time Duration	1 hour	8 hours
Exposure Conditions	20-50°C, 50-90% humidity	20-30°C, 50-90% humidity
TFWT Measurements During Exposure	No	Often to observe a rate constant of D_2O uptake from air
TFWT Measurements Just After Taking Out	3 times	Often to observe a rate constant of D_2O loss from plant
TFWT Measurements Until Harvest	5 times	No
nOBT Measurements After Taking Out	At final yellow bean harvest	Often until final yellow bean harvest including the stage of green bean harvest

Loss of deuterium from the soybean plant is expressed as:

$$Cp = C_0 \times \exp(-k_2 t) \quad \text{(II.4.7)}$$

where:

Cp is the TFWD concentration in plant (ppm);
C_0 is the TFWD concentration in plant at time t=0 (the end of release) (ppm);
k_2 is the rate constant of D_2O loss from plant (h^{-1}); and
t is the time after the end of release (h).

OBD translocation to bean from leaf is expressed as:

$$TLIa = OBD/Ca \quad \text{(11.4.8)}$$

where:

TLIa is the translocation index of OBD to bean (%);
OBD is the OBD concentration in bean at harvest (ppm); and
Ca is the mean D_2O concentration in air moisture at steady state (ppm).

II.4.8. KAERI Model

II.4.8.1. Introduction

Tritium (as HTO) released from nuclear facilities is readily absorbed to plants by photosynthesis, and changes into a constituent tritium of organic compounds by metabolism. The organically bound tritium (OBT) is generally non-exchangeable and remains in tissue of plant after the time of harvesting so that it can be an important contributor to dose [II.76]. To assess potential dose to human from accidental releases, it is necessary to model the behavior of tritium in the environment. To this end a number of dynamic models have been developed and their capabilities have been evaluated and compared through the international studies [II.77–II.79].

In 2003, International Atomic Energy Agency (IAEA) started on a new international joint research programme, EMRAS (Environmental Modeling for Radiation Safety) succeeding BIOMASS programme [II.79]. The EMRAS was organized to test the accuracy of model predictions and to improve existing models and specify their parameters. This paper describes the model prediction for the scenario of tritium absorption by soybean foliage submitted to Tritium-Working-Group of EMRAS (Theme 1, Task 2).

II.4.8.2. Model description

For model prediction, a dynamic compartment model (ECOREA-GH3) that was developed by KAERI (Korea Atomic Energy Research Institute) on the basis of the long-term model of UFOTRI [II.69, II.80] was used. The model was specially designed for evaluating the transfer of tritium into the grain-plant growing in dry-fields such as wheat and soybean after an acute release from a nuclear facility. Figure II.4.7 shows the compartments and transfer pathways of the model. The plant is divided into four compartments: HTO and OBT compartments of plant body (stem + leaves), and HTO and OBT compartments of grain, respectively. The soil is divided into three compartments: layers of 0-5 cm, 5-15 cm and 15-30 cm. There is a reversible tritium exchange between all the plant compartments except the OBT compartment of grain in which all the organically bound tritium is insoluble and remains there after the time of harvesting. Water absorption of plant from soil occurs all via only the body of plant.

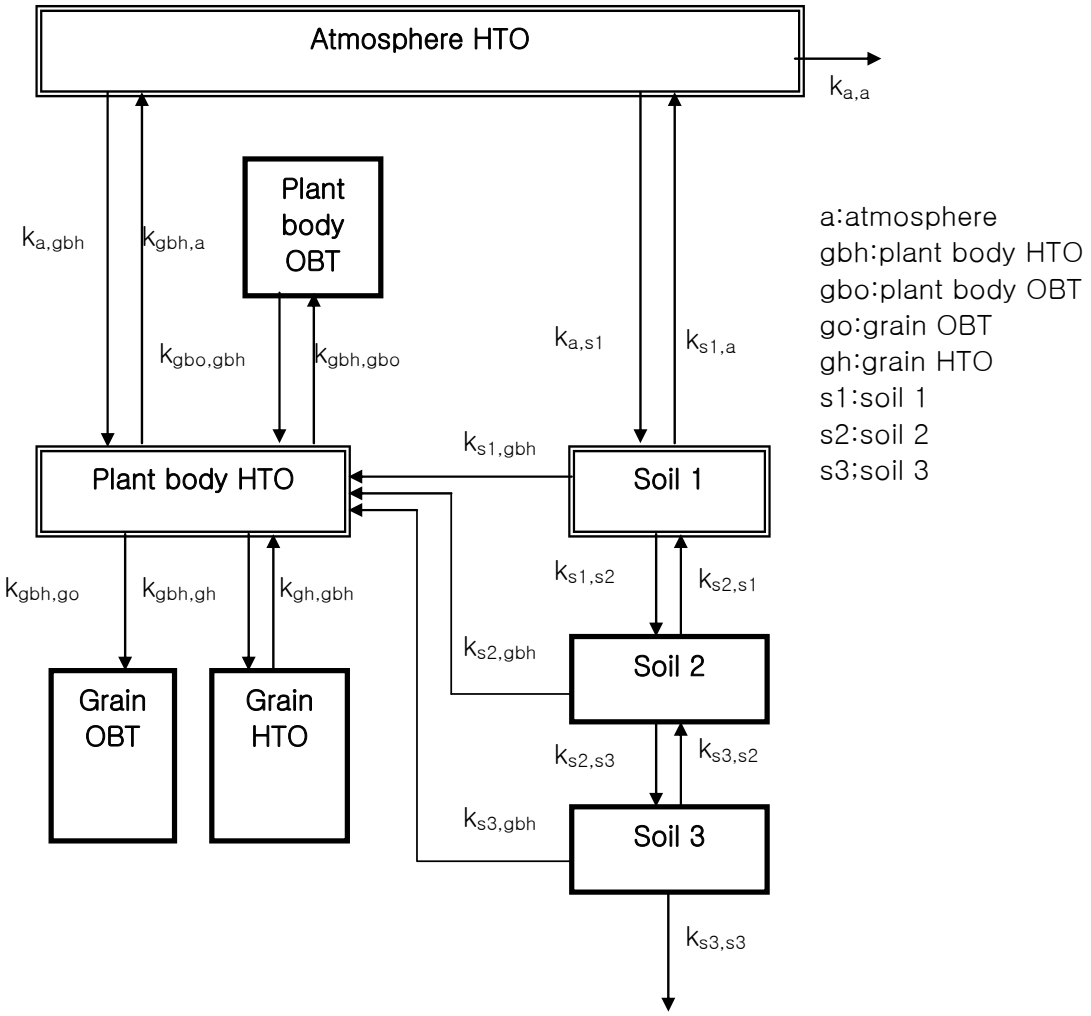

Fig. II.4.7. Compartments and transport pathways for ECOREA-GH3.

The mass transfer between compartments can be generally described as:

$$\frac{dA_i}{dt} = \sum_{k=1}^{m} K_{k,i} A_k - \sum_{i=1}^{n} (K_{i,j} + \lambda) A_i \qquad \text{(II.4.9)}$$

where:

A_i (Bq/m^2) is the activity of compartment i;
$K_{k,i}$ is the transfer rate from compartment k to i; and
λ is the decay constant of tritium (6.44×10^{-6} h^{-1}).

Biomass equation

The hydrogen inventory of plant varies with the growth of biomass, and it subsequently influences the transfer rate between compartments. Figure II.4.8 shows the growth curves of

soybean obtained with the biomass data presented in scenario. All data were fitted to the typical sigmoid growth curve with three parameters.

$$B(t) = \frac{B_1 B_2}{(B_1 - B_2)e^{-B_3 t} + B_2} \quad \text{(II.4.10)}$$

The parameters are summarized in Table II.4.15. The difference of the weight between the dry and fresh biomass at time *t* is assumed to be equivalent to the weight of water of the HTO compartment of plant.

HTO deposited during exposure

During exposure, the amount of HTO deposited onto the soybean plant was calculated using the Belot equation [II.49, II.81]:

$$C_{gbh}{}^{o} = \alpha \times R_{ini} \times C_a{}^{o}(1 - e^{-\tau \Delta t}) \quad \text{(II.4.11)}$$

where:

$C_{gbh}{}^{o}$ is the tritium concentration in body tissue water, Bq/kg;
R_{ini} is the mean relative humidity of air during exposure;
$C_a{}^{o}$ is the mean activity of tritium in air moisture during exposure, Bq/kg;
τ is the time constant until equilibrium which is defined by $\rho_{s,ini}/(\alpha \mu_{ini} \gamma_t)$, h^{-1};
$\rho_{s,ini}$ is the saturated air humidity during exposure, kg/m^3;
μ_{ini} is the water content of plant body at the time of exposure, kg/m^2;
α is the H/T isotope ratio in air and plant (1.1);
γ_t is the total resistance from atmosphere to stomata, h m^{-1}; and
Δt is the exposure time, h.

At equilibrium:

$$C_{gbh}{}^{o} = \alpha \times R_{ini} \times C_a{}^{o} \quad \text{(II.4.12)}$$

On the other hand, there was no tritium deposited onto soil because it was covered with a vinyl paper during the exposure to the plant.

II.4.8.3. Input data

Basic data

In order to calculate the transfer rate between compartments in the model, the following basic input data were used (Table II.4.16). Some of the data came from the UFOTRI [II.80], and others from the experimental condition presented in scenario.

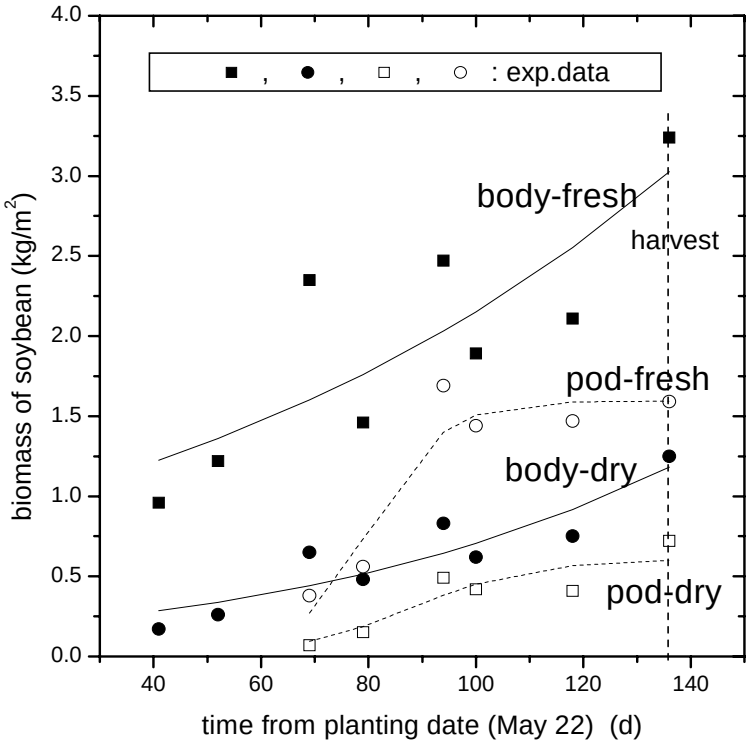

Fig. II.4.8. The growth curve of soybean.

Table II.4.15. Parameter values for the growth curve of soybean.

Parameter / Plant	B1 (kg/m2)	B2 (kg/m2)	B3 (d)
Body (fresh)	1.87E2	0.827	9.6E-3
Body (dry)	7.10	0.147	0.017
Grain (fresh)	1.59	1.72E-5	0.143
Grain (dry)	0.61	2.43E-4	0.089

Table II.4.16. General input data.

Parameter	Value
Mean height of the air mixing layer (H_m)	1000 m
Mean deposition velocity of HTO to soil (V_d)	18.0 m/h
Water humidity of saturated air at 25°C (ρ_s)	0.024 kg/m^3
Mean relative humidity during the growth of soybean (RH_a)	84%
Mean rainfall rate during the growth of soybean (K_{rain})	1.0 kg/(m^2.h)
Thickness of soil layer 1 (d_1)	0.05 m
Thickness of soil layer 2 (d_2)	0.1 m
Thickness of soil layer 3 (d_3)	0.15 m
Mean moisture content in soil (θ)	0.2
Fraction of root uptake of water from soil layer 1 (F_1)	0.2
Fraction of root uptake of water from soil layer 2 (F_2)	0.4
Fraction of root uptake of water from soil layer 3 (F_3)	0.4
Water content of plant body ($\mu(t)$)	B_{body}(fresh)-B_{body}(dry)
Activity ratio between the plant water and the water vapor at equilibrium (R_a)	0.5
Growing period of bean (T_{gg})	1440 h (60 days)
Half-time of tritium loss from plant body OBT (T_{gbo})	240 h (10 days)
Half-time of tritium loss from plant body HTO (T_{gbh})	2 h

Transfer rate

The transfer rates are calculated on the basis of hydrogen inventory and hydrogen exchange between compartments with the assumption of equilibrium. The hydrogen inventory (kg/m^2) of each compartment is calculated by:

$M_a=H_m \times \rho_s \times RH_a \times 11\%$	for atmosphere compartment
$M_{s1}=1000 \times d_1 \times \theta \times 11\%$	for soil 1 compartment
$M_{s2}=1000 \times d_2 \times \theta \times 11\%$	for soil 2 compartment
$M_{s3}=1000 \times d_3 \times \theta \times 11\%$	for soil 3 compartment
$M_{gbh}=(B_{body}(\text{fresh})-B_{body}(\text{dry})) \times 11\%$	for body HTO compartment
$M_{gbo}=B_{body}(\text{dry}) \times 8\%$	for body OBT compartment
$M_{gh}=(B_{grain}(\text{fresh})-B_{grain}(\text{dry})) \times 11\%$	for grain HTO compartment
$M_{go}=B_{grain}(\text{dry}) \times 8\%$	for grain OBT compartment

The hydrogen content in organic part of plant was assumed to be 8%. Transfer rate for the system is summarized in Table II.4.17. The transfer rate of loss of HTO from atmosphere ($K_{a,a}$) was determined with the assumption of the half-time of loss of one hour, but the value of $K_{a,a}$ of 100 was assumed for the time less than 0.1hr in order to consider the effect of ventilation by an external fan just after the exposure. The rate constant of loss of HTO from plant during day-time ($K_{gbh,a}$) was assumed to be inversely proportional to the water content (μ) of the plant, with the reference value of 0.347 that is equivalent to the half-time of loss of one hour when μ is 0.4 kg/m^2. Since the water content of plant varies with the growth of biomass, the rate constant $K_{gbh,a}$ is time-dependent.

II.4.8.4. Results

Modelers were asked to calculate:

(1) TFWT (tissue-free-water-tritium) concentration of the body and pods for the SB1 experiment at the times: 0.2 hr, 1 hr, 24 hrs, 120 hrs, 336 hrs, 936 hrs, 1608 hrs, and 2280 hrs for body (stem and leaves), and 936 hrs, 1608 hrs, and 2280 hrs for pods (shell and seeds);
(2) TFWT concentration of the body and pods for the SB4 experiment at the times: 0.2 hr, 1 hr, 24 hrs, 120 hrs, 336 hrs, 768 hrs, and 1368 hrs for both body (stem and leaves), and pods (shell and seeds);
(3) The non-exchangeable OBT concentration of plant body and shell and seeds at harvest for the six experiments SB1 to SB6;
(4) Estimate the 95% confidence intervals for all the predictions.

The results calculated for the questions (1) to (3) are given in Tables II.4.18 and II.4.19. All calculation results were obtained with the assumption that the HTO exchange between atmosphere and the tissue water of body during exposure was at equilibrium. This means that the initial condition of the body was determined by Equation II.4.12.

Table II.4.17. Transfer rate between compartments.

Transfer rate	from	to	Value in h^{-1}
$K_{a,a}$	Atmosphere	Outside	0.693 for t>0.1 hr, 100.0 for t<0.1hr)
$K_{s3,s3}$	Soil 3	Deep soil	3.42×10^{-4} [II.80]
$K_{gbh,a}$	Body HTO	Atmosphere	$0.139/\mu(t)^*$, 0.347 for μ=0.4 kg/m^2
$K_{a,gbh}$	Atmosphere	Body HTO	$R_a K_{gbh,,a} M_{gbh}/M_a$
$K_{a,s1}$	Atmosphere	Soil 1	$V_d/H_m + K_{rain} / M_a \times 11\%$
$K_{s1,a}$	Soil 1	Atmosphere	$(K_{a,s1}M_a - K_{s3,s3}M_{s3}(1-R_a)/R_a K_{a,gbh} M_a)/M_{s1}$
$K_{s2,s1}$	Soil 2	Soil 1	$K_{s3,s3}M_{s3}/M_{s2}$
$K_{s3,s2}$	Soil 3	Soil 2	$K_{s3,s3}M_{s3}/M_{s3}$
$K_{s1,gbh}$	Soil 1	Body HTO	$(1-R_a)/R_a K_{a,gbh} M_a/M_{s1}F_1$
$K_{s2,gbh}$	Soil 2	Body HTO	$(1-R_a)/R_a K_{,agbh} M_a/M_{s2}F_2$
$K_{s3,gbh}$	Soil 3	Body HTO	$(1-R_a)/R_a K_{a,gbh} M_a/M_{s3}F_3$
$K_{s1,s2}$	Soil 1	Soil 2	$(K_{a,s1}M_a + K_{s2,s1}M_{s2})/M_{s1} - (K_{s1,gbh} + K_{s1,a})$
$K_{s2,s3}$	Soil 2	Soil 3	$(K_{s1,s2}M_{s1} + K_{s3,s2}M_{s2})/M_{s2} - (K_{s2,s1} + K_{s2,gbh})$
$K_{gbo,gbh}$	Body HTO	Body OBT	$0.693/T_{gbo}$
$K_{gbh,gbo}$	Body OBT	Body HTO	$K_{gbo,gbh}M_{gbo}/M_{gbh}$
$K_{gbh,gh}$	Body HTO	Grain HTO	$0.693/T_{gbh}$
$K_{gh,gbh}$	Grain HTO	Body HTO	$K_{gbh,gh}M_{gbh}/M_{gh}$
$K_{gbh,go}$	Body HTO	Grain OBT	$1.386 \times M_{go}/(T_{gg}M_{gbh})$

* $\mu(t)=B_{body}$(fresh)-B_{body}(dry).

Table II.4.18. Calculated TFWT concentration of body and pods with time for SB1 and SB4 experiment.

SB1			SB4		
Time (hrs)	TFWT concentration of body (Bq/mL)	TFWT concentration of pods (Bq/mL)	Time (hrs)	TFWT concentration of body (Bq/mL)	TFWT concentration of pods (Bq/mL)
0.2	72000	–	0.2	23000	3300
1.0	64000	–	1.0	17000	11000
24	2200	–	24	2700	3000
120	8.2	–	120	9.2	9.7
336	4.6	–	336	3.1	3.1
936	1.2	1.2	768	1.1	1.1
1608	0.39	0.39	1368	0.31	0.31
2280	0.14	0.14			

Table II.4.19. Calculated OBT concentration of body and pods at harvest for SB1 to SB6 experiments.

Case	OBT concentration of body at harvest (Bq/mL equivalent water)*	OBT concentration of pods at harvest (Bq/mL equivalent water)*
SB1	0.84	0.07
SB2	3.65	2.38
SB3	9.5	127.7
SB4	7.4	86.0
SB5	48.4	320.7
SB6	450.1	592.8

* One gram of dry matter is equivalent to 0.6 mL of combustion water.

II.4.9. LLNL Model

II.4.9.1. Introduction

Predictions for the Soybean Scenario were the result of manipulating output from the stochastic STAR-H3 model in Excel to account for processes missing in STAR and then using the Crystal Ball software to account for pathways to uncertainty missing in STAR.

II.4.9.2. Model description

Primary modeling was done using STAR-H3, developed by QuantiSci. STAR is a compartmental model with inter-compartment transfer equations governed by user-defined parameters. Rates of transfers between compartments should be controlled by adjusting the parameters and not by altering the transfer rate equations. It's a very conceptually simple time-dependent model that, if run to equilibrium, maintains the T/H ratio from the air in the TFWT and somewhat increases it in the OBT. Although STAR accounts for different uptake and loss-rates of HTO between day and night, it does not account for plant growth or for changes in light-levels after exposure. Time-steps are hourly. STAR may be run either deterministically or stochastically.

There are four compartments (atmosphere, soil, tissue-free-water tritium (TFWT) in plants, and organically bound tritium (OBT) in plants).

HTO is deposited from atmosphere to soil through exchange with units of m^3 / (h kg); I zeroed the deposition velocity in this transfer, so the net deposition to soil was zero. HTO is also deposited via wet deposition, but of course that wasn't a pathway in this scenario.

HTO is deposited from atmosphere to plants:

$$Bq/m^3 \times \text{water content of plant (g } H_2O\text{/kg fw) / water content of air (g/m}^3\text{)} = \text{Bq/kg plant fresh weight (fw)} \quad \text{(II.4.13)}$$

There is a transfer from soil water to TFWT that uses evapotranspiration (g $H_2O/m^2/h$), crop density (kg fw/m^2 crop) and water content of soil (g H_20/kg), but the actual transfer of tritium of course was zero because there was no activity in the soil. The model is insensitive to crop density and evapotranspiration, as least when no transfer of activity occurs.

The transfer between TFWT and OBT in the plant occurs during what is called photosynthesis but is really just exchange based on specific activity coupled with a rate based on residence time:

$$\text{Bq TFWT/kg fw x (g OBH/kg fw / (g } H_2O\text{/kg fw x 1/9) / residence time) = Bq OBT/kg fw} \quad \text{(II.4.14)}$$

Here OBH is organically bound hydrogen and the factor 1/9 is the number of grams hydrogen per gram water.

TFWT is lost from the plant to a losses compartment at a turnover rate of 1 per hour during the daytime and a fraction of the daytime rate (0.06) at night.

OBT is lost to the TFWT compartment via catabolism with a rate based on the inverse of the residence time (contents of the OBT compartment are divided by the residence time of OBH).

The only difference in the way STAR-H3 handles leaves compared with flowers or fruits is by the water and hydrogen contents, or by changes in turnover rates and residence times. Leaves, shells, and beans were therefore modelled separately, although turnover rates and residence times were the same for all (given the uncertainty) (see Table II.4.20).

The parameter values used for the soybean scenario and their distributions are shown in Table II.4.20.

Table II.4.21 shows the water contents used for the parts of the soybean plant to convert predicted concentrations in Bq/kg fresh weight to Bq/L (and to calculate the concentrations in Bq/kg fw in STAR H-3 from air moisture concentrations).

II.4.9.3. Preparation of input

Absolute humidity was calculated for each 5-minute period using the 5-minute observed relative humidity and temperature for each experiment. Then, using the 5-minute calculated absolute humidity and the observed 5-minute air moisture concentrations (Bq/mL), Bq/m^3 for each 5-minute period was calculated. The air concentrations for the 13 time periods of each experiment were averaged for the hourly input to STAR-H3, and the mean absolute humidity was obtained from averaging the calculated 5-minute absolute humidity for the 13 time periods (see Table II.4.22). The uncertainty on the mean absolute humidity was assumed 10% of the value, disregarding the rapid rise and fall of absolute humidity at the start and finish of the experiment. Table II.4.22 also shows the number of hours of each run and the number of runs for the stochastic output. Note that the air concentration for STAR-H3 is deterministic.

Day length was adjusted based on approximate hours of daylight at Seoul for the day of each experiment. Of course, actual day length got shorter before harvest, which was not taken into account.

SB1: sunset at 20:00; sunrise at 5:15; midpoint of experiment: 10:00
SB2: sunset at 20:00; sunrise at 5:15; midpoint of experiment: 10:00
SB3: sunset at 19:45; sunrise at 5:30; midpoint of experiment: 10:15
SB4: sunset at 19:30; sunrise at 5:45; midpoint of experiment: 10:00
SB5: sunset at 19:15; sunrise at 6:00; midpoint of experiment: 9:30
SB6: sunset at 18:45; sunrise at 6:15; midpoint of experiment: 10:00

It was assumed (incorrectly, as it turned out), that unless the shell or bean were growing at the time of exposure, no significant amount of tritium would be transferred. STAR was therefore used to calculate hourly concentrations (with modifications, see below) for only those endpoints shown by the X's in Table II.4.23.

II.4.9.4. Manipulation/adjustment of STAR results in Excel

As mentioned, STAR-H3 basically assumes rapid equilibrium of the final product (mature leaf, mature bean) at the time of exposure. However, in these experiments, growth was occurring. Therefore, a loss was applied to all the hourly output data from STAR-H3 based on estimated growth rates (Table II.4.24) – as the plant doubled in size, the concentrations of tritium were halved. These growth rates were estimated from the KAERI data.

Table II.4.20. Parameter values and distributions varied in STAR-H3.

Name	Units	Best estimate	Distribution	Range
For leaves & stems				
Plant_water	g H_2O/kg fw	869	Normal	± 5.2
Hydrogen_amount	g OBH/kg fw	9.1	Normal	± 0.71
For beans				
Plant_water	g H_2O/kg fw	80	Normal	± 7.4
Hydrogen_amount	g OBH/kg fw	72	Normal	± 2.2
For shells				
Plant_water	g H_2O/kg fw	90.3	Normal	± 10
Hydrogen_amount	g OBH/kg fw	58	Normal	± 5
Parameters for all				
Water_turnover_day	h^{-1}	1	Uniform	0.5 – 2.0
Water_turnover_night	frac. Day value	0.06	Triangular	0.01-0.06-0.1
OBT_Residence_time	d	39	Normal	± 9.3

Table II.4.21. Parameter values to convert Bq/kg fresh weight to Bq/L.

Paramter	leaf	shell	bean	pod
Fresh matter fraction	0.869	0.0903	0.08	0.085
Dry matter fraction	0.131	0.9097	0.92	0.915
Water equivalent	0.6	0.59	0.7	0.65

Table II.4.22. Input to STAR-H3.

Experiment	Air Bq/m3	AH (g m^{-3})	Hours	# Runs
SB1	3.30 E+06	41.4 ± 4.14	2280	1000
SB2	4.46 E+06	29.6 ± 2.96	2016	1000
SB3	4.82 E+06	41.4 ± 4.14	1608	1000
SB4	2.69 E+06	50.5 ± 5.05	1368	1000
SB5	3.68 E+06	37.8 ± 3.78	1008	1000
SB6	3.80 E+06	27.6 ± 2.76	432	1000

Table II.4.23. Parts of the plants that were growing when exposed to tritium.

Experiment	Leaves and stems	Shells	Beans
SB1	X		
SB2	X		
SB3	X	X	
SB4	X	X	X
SB5	X	X	X
SB6	X	X	X

Table II.4.24. Growth rate (doubling) in days of parts of soybean plant.

Plant compartment	Fastest growth	Best estimate	Slowest growth
Leaves and stems	50	55	60
Pods	15 until Sept 2, then ∞	30	45
Shells (after July 12)	40	45	50
Beans (after July 24)	10 to Aug 24, then ∞	30	40

For those parts of the plant not growing when exposed to tritium (not marked with an X in Table II.4.23), it was assumed that the starting concentration in the pod or bean was the same in Bq/L as the concentration in the leaves on the day the pod or bean started to grow (shells were assumed to start growing July 12; beans, July 24). The STAR loss rate from shell or bean was then applied to the new concentration derived from the HTO concentration in leaves. This approach did not account for differences in concentrations between day and night in STAR (which are quite large but never entered into this scenario because all concentrations were measured in daytime[2]). Obviously, there was just a tiny amount of TFWT in the leaves (by these calculations) when shells and beans started to grow.

II.4.9.5. Estimation of uncertainty using Crystal Ball® risk assessment software

Some sources of uncertainty are not accounted for by STAR-H3. To account for one of these additional sources of uncertainty (in the source term) the air concentrations ± one standard deviation and the absolute humidity ± one standard deviation for each scenario (Table II.4.25) were multiplied together in the Crystal Ball® Risk Assessment Software to (re)calculate the air concentrations and calculate the percent associated uncertainty. All distributions were considered normal.

Air concentrations in Bq/m^3 and percent uncertainty (1 standard deviation) predicted by Crystal Ball are shown in Table II.4.26. The median air concentrations predicted by Crystal Ball (Table II.4.26) were within about 5% of the deterministic air concentrations used as input to STAR.

Another source of uncertainty not taken into account by STAR (which assumes the tritium-to-hydrogen (T/H) ratio is maintained throughout the environment) is the empirical reduction in the T/H ratio between air moisture, leaves and fruits and in the T/H ratio between TFWT and OBT. This reduction of T/H ratio was described using triangular distributions (Table II.4.27). The uncertainty on the distribution for pods is quite large because, when the soil is not contaminated, the T/H ratio is often observed to be low in equilibrium conditions.

There's additional uncertainty on when shells and beans start to grow and whether or not they can be exposed directly to the HTO or what the concentration in the plant is at the start of growth. This affects experiments SB1 and SB2. The uncertainty is expressed as the fraction of time on either side of the assumed initiation of growth dates (July 12 for shells and July 24 for beans).

SB1 shell: uniform 0.937 – 1.13
SB1 bean: uniform 0. 82 – 1.2
SB2 shell: uniform $2.2\ 10^{-3}$ – $1.7\ 10^{4}$ (note extreme uncertainty)
SB2 bean: uniform 0.82 – 1.2

[2] The STAR-H3 model output exhibits much higher concentrations at night than during the day. For example, for experiment SB1, the highest concentration from STAR output in any 24 hour period occurs at 5:00, and the lowest occurs at 20:00; the ratio of the highest divided by lowest concentration for each 14 hour period is 8.9! Note that these extreme values occur when the loss rate of the plant changes from day to night and vice versa. The concentration taken as the prediction for this scenario was at 10:00. This value is just 3% higher than the lowest concentration and only 11% of the highest concentration. This behavior is inexplicable, because, although the loss rate from the plant slows at night, the water content must remain about the same so there can be nothing driving an increase in concentration after an acute exposure.

Table II.4.25. Input to Crystal Ball to determine the uncertainty on the initial air moisture concentrations.

Experiment	Mean Air (Bq/L)	Standard deviation	Mean absolute humidity (kg/m3)	Standard deviation
SB1	$8.35\ 10^{7}$	$1.31\ 10^{7}$	0.0414	0.00732
SB2	$1.59\ 10^{8}$	2.3710^{7}	0.0296	0.00336
SB3	$1.23\ 10^{8}$	$2.95\ 10^{7}$	0.0414	0.00370
SB4	$5.61\ 10^{7}$	$1.54\ 10^{7}$	0.0510	0.00874
SB5	$9.91\ 10^{7}$	$2.55\ 10^{7}$	0.0378	0.00805
SB6	$1.48\ 10^{8}$	$5.71\ 10^{7}$	0.0284	0.00712

Table II.4.26. Air concentrations and standard deviations as calculated by Crystal Ball.

Experiment	Median (Bq/m^3)	Standard deviation (Bq/m^3)	Percent uncertainty
SB1	$3.46\ 10^{6}$	$6.11\ 10^{5}$	17.7
SB2	$4.65\ 10^{6}$	$8.79\ 10^{5}$	18.9
SB3	$5.04\ 10^{6}$	$1.32\ 10^{6}$	26.2
SB4	$2.81\ 10^{6}$	$9.36\ 10^{5}$	33.4
SB5	$3.62\ 10^{6}$	$1.26\ 10^{6}$	34.9
SB6	$4.07\ 10^{6}$	$1.95\ 10^{6}$	47.9

Table II.4.27. Triangular distribution of reduction factors between air moisture and TFWT and TFWT and OBT.

Plant compartment	Lower limit	Midpoint	Upper limit
HTO in leaves	0.5	0.75	1.0
HTO in pods	0.2	0.5	0.9
OBT in leaves	0.4	0.6	0.8
OBT in pods	0.1	0.3	0.5

Table II.4.28. P/O ratios for HTO in leaves and pods.

SB1			SB4		
Time in hours	Leaf/stem	Pod	Time in hours	Leaf/stem	Pod
1	17		1	1.8	0.63
24	0.24		24	0.041	0.00039
120	0.010		120	0.0029	0.0047
336	0.025		336	0.0049	0.12
936	0.025	0.132	768	0.0065	0.083
1608	0.014	0.149	1368	0.0043	0.082
2280	0.0042	0.061			

Table II.4.29. P/O ratios for OBT in leaves, shells and beans.

Experiment	Leaves	Shells	Beans
SB1 (2280 h)	0.095	0.00029	0.00011
SB2 (2016 h)	0.059	0.18	0.000052
SB3 (1608 h)	0.12	0.012	0.012
SB4 (1368 h)	0.26	0.011	0.0089
SB5 (1008 h)	0.46	0.039	0.034
SB6 (432 h)	0.52	0.42	0.41

To calculate the effect of these additional sources of uncertainty on the predicted concentrations in parts of the plant, the mean of each STAR (or Excel-massaged STAR) air concentration at time x, with the 2.5 and 97.5% values of the distribution (assumed lognormal) obtained from STAR, was multiplied by 1 ± percent standard deviation for the uncertainty on the air concentration during the experiment (Table II.4.26) times the triangular reduction factor distributions (Table II.4.27) times the ranges on uncertainty on times the growth started. Each distribution was sampled 5000 times. The outcome for each experiment was a new mean with new 2.5% and 97.5% confidence limits.

In nearly all cases, the uncertainty on the results increased after running Crystal Ball.

II.4.9.6. Discussion and explanation of results

The average estimated air moisture concentrations calculated were all within 5% of the observed, so the starting air concentration for each experiment was not a cause of any differences between predictions and observations. Results are presented as predicted-to-observed (average) ratios in Tables II.4.28 and II.4.29.

For leaves and stems, the observed concentrations in SB4 are higher both absolutely (more than a factor of 2, and sometimes much more) and relatively (because the air moisture concentration for SB4 is about two-thirds that of SB1) than those of SB1. Given that the model behaves the same way for SB1 and SB4, the differences in the P/O ratios are due to the differing dynamics of the observations. These variations aside, the dynamics are very different in the model compared with the observations, with over-predictions in the first hour followed by more-or-less increasing under-predictions with time.

Predicted HTO concentrations, particularly towards harvest, are lower than those calculated by STAR alone due to the introduction of growth. For SB1, the HTO concentration in leaves and stems at 2280 hours was one-third that of STAR; for SB4, it was about half that of STAR. Obviously, by introducing growth, the differences between predictions and observations became greater than they would have been had STAR results been used. Furthermore, as pointed out in footnote 2 on page 452, the daily dynamics of STAR do not make sense. Any night time concentration would be significantly higher than the one reported for 10 am and, if chosen, would further decrease the large discrepancy between predictions and observations. Of course, there is no reason to support this action, but then, there seems to be no reason for the large hourly fluctuation in concentrations.

Predicted concentrations of OBT at harvest get closer and closer to the observations as the time between experiment and harvest becomes smaller (Table II.4.29) (concentrations are highest at 432 hours and lowest at 2016 hours). This implies that the residence time in STAR is shorter than in the experiment and that the turnover time for shells and beans is faster than in the experiment; the result is that predictions and observations diverge over time. Furthermore, my model does not account for the fact that, in nature, tritium (or any nuclide) is taken up at a higher rate at certain stages of growth, which is seen in the experimental data in which OBT concentrations in experiments SB4 and SB5 are higher than those in experiment SB6. The P/O ratio for SB2 shells is relatively very high. This is because of the enormous uncertainty applied for when the shells started to grow compared with time of exposure.

Observations fell within uncertainty bounds in just 2/40 cases. In another 5 cases, one of the observations (e.g., for stems or leaves) fell within uncertainty bounds. In 33/40 cases, the observations were outside the uncertainty bounds. The average magnitude of the uncertainty

(disregarding huge uncertainties generated at 24 hours by STAR) was a factor of 41 (value of 97.5% confidence limit (CL) divided by value of the 2.5% CL), with a range of 3.3 (HTO in leaves and stems for SB1) to 486 for OBT in beans for SB1. For those cases where the observation fell within the uncertainty bounds, the magnitude of the uncertainties was less than a factor of 13, so when the model was right, it was confidently right (although probably mostly by chance), because the fewer hours between the experiment and harvest, the better the model did.

II.4.9.7. Calibration of STAR

Based on the results it was considered possible that STAR could be calibrated to resemble the observations (ignoring uncertainty). Only three parameters can be changed – the turnover time of tritium in the plant (day and night) and the residence time of tritium in the plant. Without attempting to change the night/day default water turnover rate in STAR, the other two parameters for HTO and OBT in SB4 leaves and pods were varied. The best results were from:

- For leaves, changing the turnover rate from 1/h to 0.25 per hour and leaving the residence time at 39 days.
- For pods, changing the turnover rate from 1/h to 0.1 per hour and leaving the residence time at 39 days.

This resulted in P/O ratios (Table II.4.30) that may be compared with those from Table II.4.28.

Overall this is much better than the original submission, but the dynamic, even without growth, still is not achieved. Note that these results do not account for any growth or reduction in the T/H ratio between air moisture, TFWT, and OBT.

The calibration had to be done with Experiment SB4 because only it had HTO in pod data for the full time period. The OBT in pods was part of the calibration, although results were not in close agreement for SB4. Similarly (Table II.4.31) new OBT concentrations were calculated for beans using the changed turnover rates that can be compared with Table II.4.29.

Over-predictions for SB1 and SB2 are because STAR had the beans growing at time of exposure, which was not the case. P/O ratios increase from SB4 to SB6 because STAR assumes equal uptake of tritium throughout all stages of development.

By calibrating STAR and ignoring any growth and any reduction in the T/H ratio, the predictions are greatly improved but the dynamic is still unattained. Calibrating STAR also may have reduced the turnover rate below a reasonable value.

Although STAR results could not duplicate the dynamics of the experiment, how well the integrals over time could be predicted was investigated. The estimated observed integrals (hourly sums) for HTO are compared in Table II.4.32 in stems and leaves with the integral of mean predictions, both as submitted and as calibrated.

Table II.4.30. P/O ratios for calibrated STAR for HTO (SB4).

Hours	P/O leaves and stems	P/O pods
1	1.7	0.66
24	3.1	0.48
120	0.02	0.082
336	0.042	1.3
768	0.08	1.9
1368	0.09	4.6

Table II.4.31. P/O ratios for calibrated STAR for OBT.

Experiment	P/O beans
SB1	28
SB2	9.4
SB3	0.65
SB4	0.17
SB5	0.42
SB6	2.7

Table II.4.32. Hourly sums (Bq/mL) over length of experiments for HTO concentrations.

Experiment	Observed integral	Predicted integral	P/O Ratio	STAR calibrated integral	STAR calibrated P/O ratio
SB1 leaves	27300	116000	4.3		
SB1 stems	18000	116000	6.4		
SB4 leaves	82400	55600	0.67	71400	0.87
SB4 stems	13300	55600	4.1	71400	5.4
SB4 shells	276000	55800	0.20	89400	0.33
SB4 beans	274000	55800	0.20	89400	0.33

Except for the high integral for SB4 leaves, the results of leaves and stems are very similar. The model and the calibrated STAR (no growth) model over-predict concentrations in leaves and stems, so, if ingestion is instantaneous in the model, doses will not be under-predicted (if the diet could be composed of soybean leaves!). Note that, although the calibration makes enormous improvement in the P/O ratios at harvest (compare Tables II.4.28 and II.4.30), the change in the integrals from original to calibrated predictions is due primarily to the reduction in T/H ratios (original integral is 75% that calibrated for leaves and 50% that calibrated for shells and beans). This is because the extraordinarily high initial values for the first few hours dominate the entire integral; for SB1 at 2280 hours, the concentration in the soybean leaves that "grew" is 30% that of STAR's (that didn't grow).

II.4.9.8. Conclusions

There are just three parameters in STAR that can be changed in any attempt to calibrate the model output to the observations: the daytime turnover rate, the fraction of the daytime turnover that occurs at night, and the residence time of OBT. For HTO, the turnover rates dominate the dynamics of the predictions, but the residence time does have a small effect on the dynamics. Calibration of the HTO dynamics was attempted in STAR two ways, one described above and one in which the nighttime turnover fraction was set to 1 to simplify the output. Changing the night time turnover fraction to 1 did not noticeably affect the dynamic response at the sampling time of 10 am, but of course it did eliminate that odd fluctuation in

concentration mentioned in footnote 2 on page 452. To calibrate the model to the time-dependent HTO results alone was attempted, because to calibrate single points for OBT at harvest would be, of course, meaningless. Thus, as mentioned above, the dynamics of the STAR predictions are much improved through calibrating the model to a lower turnover time but maintaining the 39 day residence time. The calibration is fairly meaningless, because it does not include lower concentrations due to plant growth or the expected reduction in T/H ratio between compartments.

Apparently, STAR is too simple to account for the changing dynamics of the HTO concentrations. Furthermore, STAR has no way to predict concentrations in pods that are exposed while still flowers; STAR has no mechanism of uptake by the leaf or flower and consequent transport into the fruit. The OBT concentrations cannot be predicted because STAR does not recognize that uptake may be preferential during certain stages of plant growth.

II.4.10. Kyoto University Model

II.4.10.1. TriSoy model

TriSoy (**Tri**tium Behavior in **Soy**bean) is a simple analytical code written in Visual Basic.NET. The calculation is performed through graphical user interface and the result is implicated in an Excel spread sheet. The purpose of the model is to calculate the specific activities of FWT and OBT contained in tissues of a soybean plant that was exposed to atmospheric tritium vapor at various growth stages. The model is applicable to other crop plants by changing basic parameters used in the model.

II.4.10.2. Structure of the model

The scheme of TriSoy is shown schematically in Figure II.4.9.

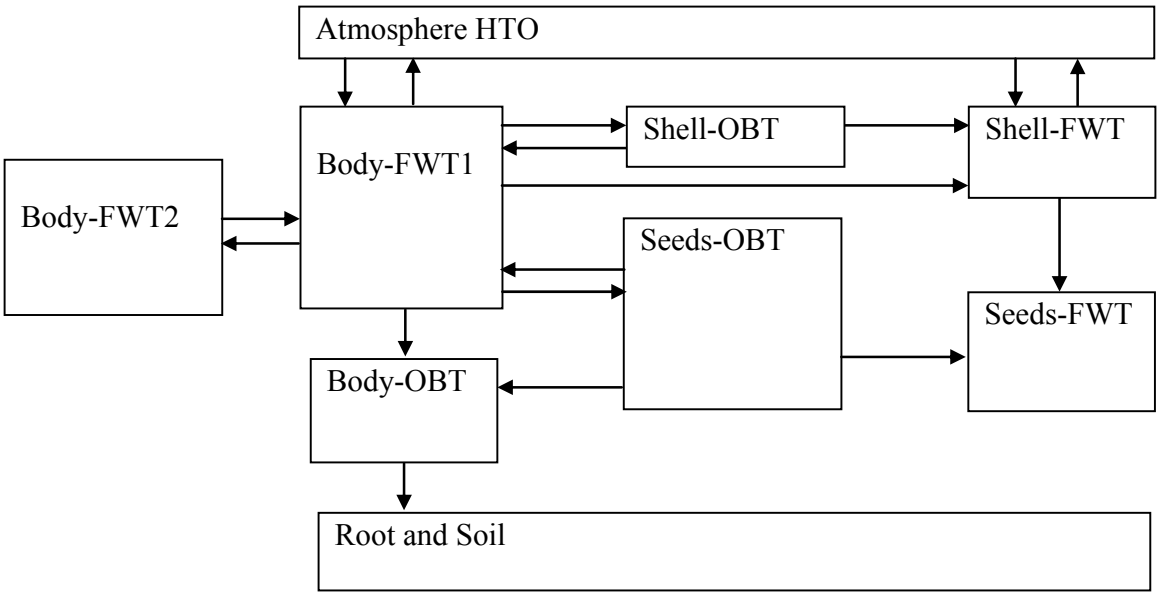

Fig. II.4.9. Schematic of TriSoy model.

The main features of this model are as follows:

(1) The source of tritium is solely the atmospheric HTO vapor.
(2) The atmospheric tritium is taken up by the body, i.e. leaves and stem.
(3) The body FWT could be transferred to the shell FWT compartment.
(4) Carbohydrates are photosynthesized in the leaves and instantaneously translocated to seeds and shell.
(5) A portion of OBT in the plant is converted to FWT by respiration [II.82].

II.4.10.3. Determination of the exchange velocity constant

In this section, the following abbreviations are used:

Λ is the tritium exchange velocity constant;
C_a is the tritium specific concentration in the atmosphere (Bq/Kg);
C_S is the tritium specific concentration in the stomata vapor (Bq/Kg);
C_L is the tritium specific concentration in the leaf vapor (Bq/Kg);
ρ_s is the saturated vapor density of the atmosphere (Kg/m^3);
r is the resistance of water vapor transfer at the leaf surface (/m);
F is the tritium flux on the leaf surface (Bq/m^2.s);
μ is the water content /leaf or canopy area (Kg/m^2);
α is the hydrogen isotope separation factor for tritium : 1.104 at 25℃; and
h_r is the relative humidity of the atmosphere.

Resistance of water vapour transfer at the leaf surface

The process of tritium intake by the plant basically follows the concept of Belot's model [II.49]. The exchange velocity constant λ is given by:

$$\lambda = \frac{\rho_s}{\alpha \mu r} \tag{II.4.15}$$

The value of r was determined by using the relationship between biomass production rate and transpiration rate as follows. The dry mass production velocity (kg/m^2.d) is given by:

$$\frac{dW}{dt} = K_w \frac{E}{\delta} \tag{II.4.16}$$

where:

W is the amount of dry mass (kg/m^2);
K_w is the conversion factor = 0.005 kPa for soybean (Cropsyst Manual) [II.83]; and
δ is the deficit of water vapor pressure (kPa).

The transpiration rate is related to the deficit water vapor concentration (DVC) in the air as:

$$E = \frac{DVC}{r} \quad \text{or} \quad E = \frac{\rho_s - \rho}{r} \tag{II.4.17}$$

where:

ρ_s is the saturated water vapor concentration in the air (kg/m^3);
ρ is the water vapor concentration in the air (kg/m^3); and
r is the the resistance of exchange of HTO and H_2O between the air and the soybean leaf. (d/m)

In principle, by using the above two equations, the value of r can be estimated.

For a representative period of the soybean growth, in the period from July 1 to August 24, the averaged dry mass production rate was 0.0224 $g/(m^2.d)$ and the averaged water vapor deficit was 0.464 kPa or 2.96 $\times 10^{-3}$ kg/m^3. The transpiration rate in this period was then 2.07 $kg/(m^2.d)$.

The value of the resistance r depends on the physiological condition and the meteorological conditions for the plant. As a representative weather condition, the daytime length was assumed to be 13 hours and the night time 11 hours. Then the day-averaged transpiration rate E_{aver} is given by:

$$E_{aver} = \frac{13}{24} \bullet \frac{DVC_{day}}{r_{day}} + \frac{11}{24} \bullet \frac{DVC_{night}}{r_{night}} \tag{II.4.18}$$

Further, it was assumed that in the night time the air vapor is close to saturation and the stomata are closed. Then the second term of the above equation can be neglected. Thus:

$$E_{aver} = \frac{13}{24} \bullet \frac{DVC_{day}}{r_{day}} \quad \text{or} \quad r_{day} = \frac{13}{24} \bullet \frac{DVC_{day}}{E_{aver}} \tag{II.4.19}$$

Again here, using the values of DVC_{day} and E_{aver} for the growth period of soybean, the value of r in daytime is approximated by:

$$r_{day} = \frac{13}{24} \bullet \frac{2.96 \times 10^{-3} (kg/m^3)}{2.07 (kg/m^2.d)} = 7.75 \times 10^{-4} (d/m) \; or \; 66.9 (s/m) \tag{II.4.20}$$

The above argument is based on the plant canopy area.

To consider the resistance in individual leaves, a correction by the leaf area is necessary. Under the assumption that the transpiration velocity is in proportion to the total leaf area, the resistance of individual leaves r_i is given by:

$$r_l = LAI \bullet r_{day} \tag{II.4.21}$$

where:

LAI is the the leaf area index (LAI).

According to Tohachi, for a typical Japanese soybean species, the LAI value is 4.5. If this value is used, the value of the resistance becomes 3.0 s/cm, being close to the value determined by Garland and Cox [II.84] for dwarf French beans.

Table II.4.33. Predicted values of the exchange velocity λ.

Experiment	Date of experiment	Water content of the body (g/m2)	Water vapor density in saturated air (g/m3)	λ(/h)
SB1	2-Jul	788	47.19	2.93
SB2	13-Jul	960	30.63	1.56
SB3	30-Jul	1699	44.28	1.27
SB4	9-Aug	983	80.7	4.02
SB5	24-Aug	1647	41.31	**1.23**
SB6	17-Sep	1361	28.86	**1.04**

Tritium exchange rate velocity constant

Under some situations, the release of tritium to the atmosphere from the plant leaves should be taken into consideration as well. In the present scenario, the plant body FWT quickly equilibrates with the atmospheric HTO vapor. Therefore, the HTO level of the plant water can be at the same level in order throughout the exposure time. In such a case, release of the existing HTO from the plant leaves could not be negligible. Then, the tritium concentration in the leaves at time t or $C_L(t)$ is given by:

$$C_L(t) = C_L(0)\exp(-\frac{\rho_s t}{\alpha\mu r}) + (\alpha h_r C_a)\left(1-\exp(-\frac{\rho_s t}{\alpha\mu r})\right) \quad \text{(II.4.22)}$$

In an extreme case of $C_L(0)=0$ the above equation is reduced to:

$$C_L(t) = (\alpha h_r C_a)\left(1-\exp(-\frac{\rho_s t}{\alpha\mu r})\right) \quad \text{(II.4.23)}$$

The exchange velocity constant λ is given by:

$$\lambda = \frac{\rho_s}{\alpha\mu r} \quad \text{(II.4.24)}$$

Substituting the values of α and r to the above relationship:

$$\lambda = 1.29\times10^3 \bullet \frac{\rho_s}{\mu}(/d) \quad \text{or} \quad \lambda = \frac{63.8\rho_s}{\mu}(/h) \quad \text{(II.4.25)}$$

Some predicted values of λ for the soybean experiment are shown in Table II.4.33. The presented values are those averaged for the exposure time.

Dependence of the exchange rate velocity on solar radiation

During the soybean exposure experiment, the solar radiation flux changed between experiments and time to time. The intensity of solar radiation may influence the photosynthesis of organic compounds in the plant. The λ values for individual time steps were determined by considering the solar radiation flux as follows.

The biomass growth rate is proportional to the effective flux of solar radiation:

$$\frac{dW}{dt} = C_s S_a \quad \text{(II.4.26)}$$

where:

C_s is the light to biomass conversion factor (kg/MJ); and
S_a is the flux of solar radiation (MJ/m^2).

Let λ_0, S_{a0} and h_{r0} to be the values of λ, S_a and h_r averaged for the whole growth period, correspondingly.

By using the Equations II.4.15, II.4.16 and II.4.26, λ is related to λ_0 as:

$$\lambda = \frac{\lambda_0 \delta S_a h_{r0}}{\delta_0 S_{a0} h_r} \quad \text{(II.4.27)}$$

OBT production

Production of OBT was assumed to take place only through photosynthesis. Let the specific activities of FWT and OBT, amount of biomass, FWH concentration of the biomass (w/w) at time t to be F(t), C(t), B(t) and γ, respectively.

From the relationship d(γB(t)) · F(t) = (γB(t))dC(t) the specific activity increase of OBT is described by

$$dC(t)/dt = (F(t)/B(t))(dB(t)/dt) \quad \text{(II.4.28)}$$

Tritium exchange rate at pods

The HTO exchange rates in the pods and the seeds were assumed to be 1/30 and 1/15 of that in the leaves respectively.

Growth rate of biomass

In the present calculation, the information on the growth rate of the biomass at any time is necessary. Therefore, the scenario data were processed by a data processing software S-PLUS to approximate the real growth curve by a logistic growth curve. For instance, the growth curve of the body dry weight B_d(g/m^2) is given by:

$$B_d = 735/(1+3.5\exp(-0.079\times(t-41)) \quad \text{(II.4.29)}$$

where t is the the time elapsed after HTO exposure (d).

Tritium retention after HTO exposure

According to Ichimasa et al. [II.75], after exposed to heavy water vapor the plant body heavy water taken up by exchange process is released slowly with a rate constant that is higher than that for the initial take-up process. This means that there are at least two free water compartments in the plant body. In the present model, two FWT compartments were included. Referring to the result of Cline using French dwarf bean [II.85], the pool size of the second compartment was assumed to be 1.5 % of the whole free water and the retention rate constant 0.00055 d^{-1}.

Under the present scenario, the fraction of FWT converted to OBT was estimated to be less than 1%. The amount of the FWT produced by oxidation of OBT was neglected.

In night, HTO exchange velocity is considerably small compared with that in the daytime. By using the values presented for a heavy water experiment, the value of λ in night was assumed to be 1.1 (h^{-1}).

II.4.10.4. Results and comparison with observed results

The main features of the model prediction are as follows.

- The FWT level after exposure will decay to the BG level within 2 weeks.
- The production rate of OBT is high in growing organs and tissues.
- The translocation rate (TRL) after one-hour exposure is in the order of 10^{-3}.
- In Experiment 6, tritium incorporation into organic material is of minor importance in OBT production since the plant is not growing supposedly.

A considerable discrepancy was seen for the FWT component of the soybean organs after exposure. The predicted FWT concentration in the soybean body at 0.2 hr after exposure was about 4 times larger than the observed value. The same tendency was seen for the results of other modelers. A possible reason of this discrepancy may be due to the tritium exchange velocity that was considerably low compared with that actually found from the laboratory experiment. Seemingly a value of λ around 0.3 (h^{-1}) is necessary to explain the observed FWT concentration. The reason of such low efficiency of HTO exchange is unclear.

In the present model, the pool size of the second FWT compartment was 1.6 % of the first compartment. But the actual contribution from the second compartment was by one order of magnitude less than this as was revealed by the Korean experiment.

Concerning OBT concentration, the model prediction for the pods from 3 to 5 agreed rather well with the experimental result. This fact validates the model for OBT production based on biomass growth kinetics. For the pods 1 and 2, the OBT translocation to the pods from other plant tissues was neglected. However, the experimental result clearly shows that such translocation of OBT should be also taken into consideration.

II.4.11. RFNC-VNIIEF Model

II.4.11.1. Introduction

The model is based upon the data given in the paper by Michiko Ichimasa, et al [II.74].

II.4.11.2. Model description

HTO uptake during exposure

The following equitation was used for modeling of HTO accumulation during the exposure:

$$C_{HTO}(t) = C_{MAX}[1-exp(-K \cdot t)] \quad \text{(II.4.30)}$$

where:

C_{HTO} is HTO concentration in a plant sample at time t;
C_{MAX} is the steady state concentration; and
K is the rate constant.

Table II.4.34 shows C_{MAX} and K of our model.

HTO loss after exposure

HTO loss equation is the following:

$$C_{HTO}(t) = C_0 \cdot exp(-K \cdot t) \quad \text{(II.4.31)}$$

where:

C_{HTO} is HTO concentration in a plant sample at time t;
C_0 is HTO concentration in air moisture; and
K is the exchange rate.

Table II.4.35 shows K of our model.

II.4.11.3. Results

OBT at harvest

OBT concentration was calculated as part of HTO concentration in air moisture. At that the plant growth phase was taken into account.

Table II.4.36 shows the ratio of OBT concentration to HTO concentration.

Table II.4.34. C_{MAX} and K.

Plant part	C_{MAX}, relative units	K, hr^{-1}
Stem	0.534	0.069
Leaves	0.562	2.951
Shell	0.534	0.069
Seeds	0.273	0.23

Table II.4.35. K.

Plant part	K, hr^{-1}
stem	0.347
leaves	1.058
shell	0.139
seeds	0.139

Table II.4.36. Relative OBT concentration to HTO concentration in air moisture.

Experiment	Plant growth phase	Ratio
SB1	The beginning of the growth.	$5 \cdot 10^{-5}$
SB2	growth phase	$1 \cdot 10^{-4}$
SB3	growth phase	$1 \cdot 10^{-4}$
SB4	growth phase	$1 \cdot 10^{-4}$
SB5	growth phase is finished	0.0
SB6	growth phase is finished	0.0

II.4.12. EDF Model

II.4.12.1. Model description

The EDF model used to calculate tritium concentrations in crop was developed for continuous release. It required to be adapted to cover the soybean scenario. The main assumptions made are described here:

- Fluxes of HTO from air to plant leaves were calculated according to Belot's equation [II.49]. A five-minute time step was used; concentrations were assumed to be constant over the time step and equal to the concentration measured at the end of the time step. The value assigned to the exchange rate during the day was 1mm/s, except in SB4 where the value was twice lower to take into account the effect of the high temperature and the low relative humidity on stomatal closure. At night the exchange rate was assumed to be 50 times lower than during the day.
- Background HTO concentration in atmospheric water vapour was calculated from the average monthly tritium concentration in air and meteorological data. The average value was 2.4 10^{-3} Bq/mL.
- OBT formation during each time step is proportional to the growth rate and to the concentration of tritium in the tissue free-water. A discrimination factor of 0.6 is used (ratio between T/H in OBT and T/H in HTO). OBT is calculated with a daily time-step. Linear growth rates on a dry weight basis were derived from the soybean experimental data: 7.5 $g.m^{-2}.day^{-1}$ for shoot and 7.7 $g.m^{-2}.day^{-1}$ for pods. The same growth rates were applied in all experiments.
- OBT conversion to HTO is not considered. Thus, decrease in OBT concentration is only due to dilution by uncontaminated dry matter formed after exposure.

II.4.12.2. Discussion

From the results of this experiment, it seems that OBT conversion to HTO should be included in the model. What was considered at first to be a conservative assumption is shown to under estimate the HTO concentration in the plant free water in the post exposure phase and consequently the OBT concentration in the pods when fruit formation starts after exposure.

II.5. Pig Scenario model descriptions

II.5.1. STAR-H3 (used by LLNL and IFIN-HH)

STAR was the first model used in the UK for assessing tritium and ^{14}C contamination of plants and animals. In the original version [II.26], only cows (beef) were considered for UK conditions, implying that the animal diet consisted of fresh pasture all year. Pasture (and all other plants) is modeled as a two-compartment system: a fast-turnover compartment (water) and a slow-turnover compartment (organic material). Animals are also assumed to have a fast and a slow compartment, the former for HTO and labile organically bound hydrogen and the latter for non-labile organically bound hydrogen. The rate of loss of tritium from the non-labile OBT compartment (catabolism) is an input parameter of the model, as is the rate of excretion from the fast compartment. Both fast and slow compartments represent one kg of "meat" with 70% water. Hydrogen in the fast compartment is presently set at 700/9 g. The amount of non-labile organically bound hydrogen in the slow compartment is fixed at 24 g. All intakes (from drinking and respiration water, as well as from the fast and slow plant compartments) enter the fast animal compartment only. A flowchart of STAR-H3 is shown in Figure II.5.1.

The model was extended [II.86] to sheep, pigs and chickens with the same assumptions but different amounts of feed intake. The intake of food and water for all animals is divided by the "carcass mass" to give the input to the animal fast compartment. All animals are considered to eat pasture. STAR-H3 ignores animal growth and has the same hydrogen content in all animals. Animal hydrogen intake is shown in Table II.5.1.

For all animals, the slow and fast turnover rates are 0.03 d^{-1} and 0.4 d^{-1}, with the exception of the lactating cow, for which the fast turnover rate is 0.5 d^{-1}. In reality, the slow turnover rate varies with animal type. From all this information, the hydrogen contents in the slow and fast compartments and the transfer rates in the model can be assessed (Table II.5.2).

There are some inconsistencies in the model with respect to the assumed hydrogen intake and mass balance.

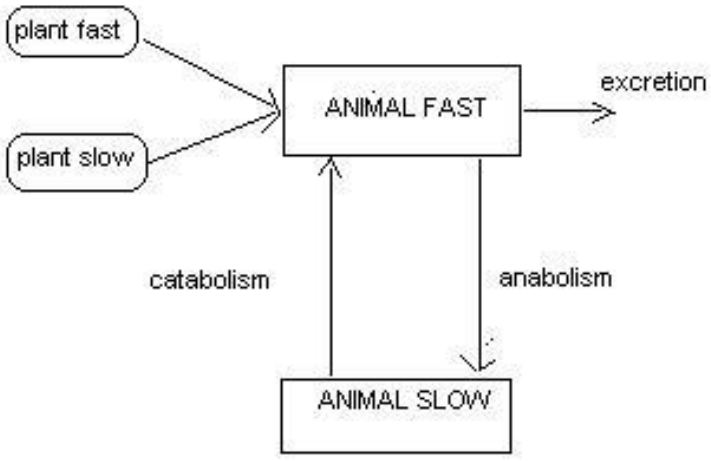

Fig. II.5.1. Flowchart of STAR-H3.

Table II.5.1. Animal hydrogen intake.

Animal	Carcass mass (kg)	Intake (kg fw/d)	Specific intake (kg fw/kg)	Specific intake (gH/kg/d)	Inhalation (m^3/d)	Inhalation (gH/kg/d)
Cow	230	115	0.5	52.44	130	0.50
Sheep	25	7	0.28	29.37	8.64	0.31
Pig	100	30	0.3	31.47	12	0.11
Chicken	2	0.5	0.25	26.22	0.24	0.11

Table II.5.2. Hydrogen contents and transfer rates.

Compartment or Transfer rate	Units	Cattle	Sheep	Pig	Chicken
Slow compartment	gH kg^{-1} meat	22	22	22	22
Slow turnover	d^{-1}	0.03	0.03	0.03	0.03
Fast turnover	d^{-1}	0.5	0.4	0.4	0.4
Growth	-	0	0	0	0
Excretion	d^{-1}	0.492	0.392	0.392	0.392
Intake	gH kg^{-1} d^{-1}	52.4	29.4	31.4	26.2
Fast compartment	gH kg^{-1}	77.8	77.8	77.8	77.8
Anabolism	d^{-1}	0.00849	0.00849	0.00849	0.00849
Catabolism	d^{-1}	0.03	0.03	0.03	0.03

II.5.2. MCT Model (M. Saito, Japan)

II.5.2.1. Introduction

The MCT model was initially developed for humans, particularly Japanese [II.87]. Assuming that humans are a good surrogate for pigs, the model was used with minimal changes since the hydrogen metabolism in the pig is expected to be similar to that of humans. In the MCT model, two OBT compartments and one free water tritium (FWT) compartment are assumed. A schematic diagram of the model is shown in Figure II.5.2.

II.5.2.2. Assumptions and parameter values

The parameter values required by the model are listed in Table II.5.3–II.5.7.

Table II.5.3. Rate constants for hydrogen transfer.

Transfer pathway	Rate constant
Excretion from body water	0.077 d^{-1}
Transfer from body water to fast OBT	0.000270 d^{-1}
Transfer from body water to slow OBT	0.000345 d^{-1}
Transfer from fast OBT to body water	0.022482 d^{-1}
Transfer from slow OBT to body water	0.001443 d^{-1}

Table II.5.4. Body weight and feed intakes.

Days after start of contamination	Body weight (kg)	Feed consumption (kg dm d^{-1})	Water intake (kg d^{-1})
0–21	180	1.86	7
22–46	200	2.06	7
47–79	220	2.31	7
80–84	240	3.01	7
Efficiency of dry matter digestion: 70%			

Table II.5.5. Hydrogen balance.

Compartment	Contribution to total body weight
Body water content of soft tissues	60% of body weight
Dry matter content of soft tissues	30% of body weight

Table II.5.6. Hydrogen content of the sow body.

Compartment	Mass
Free water hydrogen (FWH)	12000 gH
Organically bound hydrogen (OBH)	6000 gH

Table II.5.7. Body composition.

Compartment	Mass
Water content of the sow whole body	108 kg water, or 60% of the body weight including hard tissues
Dry matter of the sow body	72 kg

Fecal excretion

The feed material contains 10% by weight of exchangeable organically bound water. The percent availability of the dry component as nutrient taken up in the GI tract is 70%. The rest of the dry component is excreted as feces.

II.5.2.3. Model structure

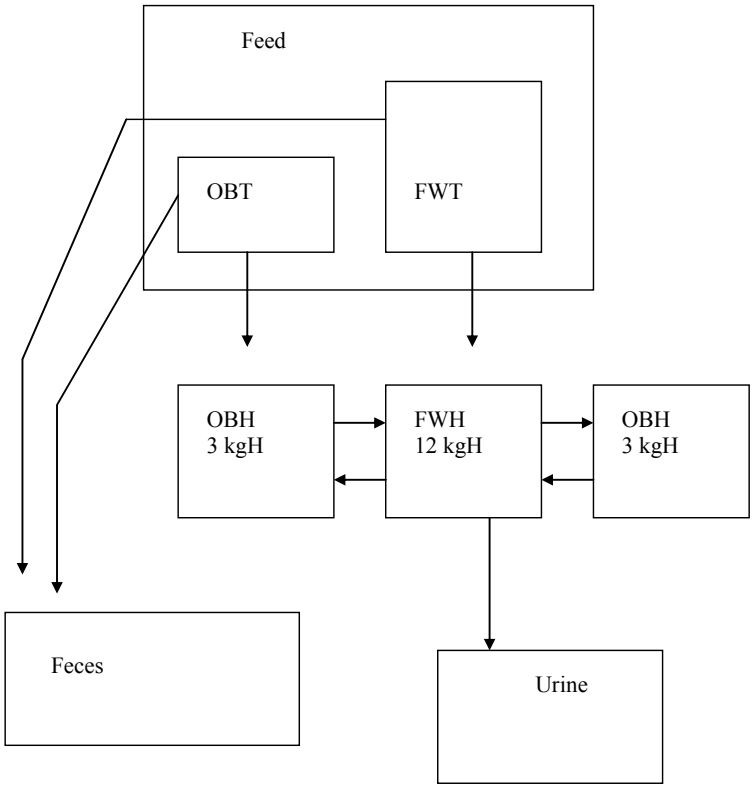

Fig. II.5.2. Schematic diagram of the MCT model.

II.5.3. FSA Model (PRISM)

II.5.3.1. Introduction

- Model Name: Prism 3.0 (H-3/C-14 Model) [II.88–II.93] implemented on the software platform AMBER 5.
- Purpose of Model: Regulatory Assessment; Conservative.
- Type of Model: Dynamic; Numerical; Compartmental.

II.5.3.2. Compartments considered

The animal is assumed to consist of four compartments: GI Tract [GI], body water [BW], labile organics [LO] and non-labile organics [NO] (Figure II.5.3). The use of a single compartment to represent the GI tract is a much simpler approach than is usually taken for other radionuclides. The model also includes an environmental sink compartment [SN]. Losses to this compartment by respiration, evaporation, transpiration and parts of the plant not normally harvested are taken into account.

II.5.3.3. Transport processes considered

PRISM considers transfer to the animal via inhalation and food and water intake, transfer among the various animal compartments, and losses to the sink.

II.5.3.4. Endpoints

The model calculates the concentration in a given compartment by dividing the activity in that compartment (as determined by transfers to and from the compartment) by the mass of the compartment. In the animal model, there is no distinction between concentrations in different animal tissues. OBT and HTO concentrations in urine and faeces cannot be reported directly because it is assumed that all activity from the GI tract and respiration are retained in body water.

II.5.3.5. Key assumptions

- The GI tract is represented by a single compartment since tritium uptake from the tract is complete and rapid.
- Other parts of the system are represented by labile and non-labile compartments rather than by specific organs or tissues.
- Tritium in the aqueous phase of the plant is transferred directly to body water; any loss of water from stored fodder can be neglected.
- Consumed organic plant material enters the GI compartment and is transferred rapidly to the other three animal compartments (body water, labile organics and non-labile organics) according to prescribed partitioning fractions, which are required to sum to 1.0.
- Transfer rates from the body water compartment are expressed in terms of a total loss rate and partitioning fractions f_{BWLO}, f_{BWNO} and f_{BWSN}.
- All tritium taken in with feed is in the form of HTO in contaminated fodder.
- Organ masses (apart from meat, liver and kidney, which are expressed explicitly in the output file) are adapted from ICRP 23 values for Reference Man using the “0.75 Power Rule”.

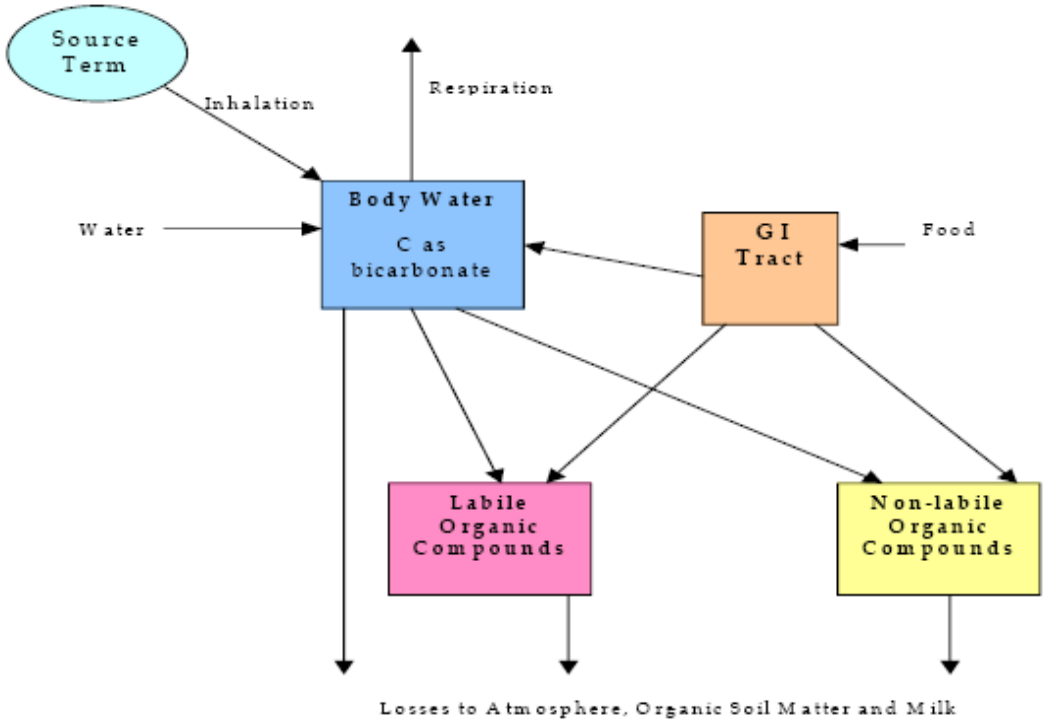

Fig. II.5.3. Scematic diagram of the PRISM model.

— The time of feeding of contaminated fodder is from midnight on the day of contamination to midnight the following day.
— In all cases, the pigs were assumed to have a mass of 20 kg at the start of the run. This avoided the excessively complicated scenario in which the pig first received clean fodder, then contaminated fodder, and then clean fodder again. It also got around the fact that the model does not accept growth scenarios that start before weaning takes place.

II.5.3.6. Temporal and spatial discretization of the model

There is no spatial discretization in PRISM. Where the exposure is via the atmosphere, the user can define the source term as a continuous air concentration, a spike (a discrete, short-term exposure) or a complex exposure (a series of spikes). Where the exposure is via contaminated feed, the daily concentration of activity in fodder can be defined, as well as the duration of the feeding regime. Output is normally reported every three days unless otherwise specified. Experience with the pig scenario suggests that the default interim output times between start and finish should be replaced with the specific times at which results are required.

II.5.3.7. Parameter values

Most parameters were assumed to be uniformly distributed. The maximum and minimum values of the distributions for each parameter, and the best estimates, are shown in Table II.5.8.

Table II.5.8. Attributes of uniform distributions.

Parameter	Units	Best estimate	Range
Fraction transferred from body water to labile organics	–	0.02	0.002–0.1
Fraction transferred from body water to non-labile organics	–	0.01	0.001–0.05
Fraction transferred from body water to sink	–	0.97	0.85–0.99
Fraction transferred from GI tract to labile organics	–	0.14	0.04–0.26
Fraction transferred from GI tract to non-labile organics	–	0.07	0.02–0.13
Transfer rate to body water	d^{-1}	0.13	0.06–0.19
Transfer rate from labile organics to soil organic layer	d^{-1}	0.0011	0.00055–0.0022
Transfer rate from labile organics to sink	d^{-1}	0*	
Transfer rate from non-labile organics to soil organic layer	d^{-1}	7.32×10^{-5}	3.66×10^{-5}–1.46×10^{-4}
Transfer rate from non-labile organics to sink	d^{-1}	0*	
Mass fraction of organic matter	–	0.035	0.0175–0.07
Mass fraction of labile organic compartment	–	0.36	0.1–0.66

*Amended on remodelling to 10 d^{-1}.

II.5.3.8. Uncertainties

The uncertainties in the model predictions were estimated using a probabilistic approach based on sampling the distributions for the various parameters. Concentrations at the 95% level were a factor 7–10 higher than those obtained using best estimate values. Losses to the sink appear to be quite low.

II.5.3.9. Application of the model to the scenario

For the model-data comparison, four feeding regimes were modelled to take into account the different quantities of fodder fed to the sow. In the first instance, the given concentration of activity was scaled to Bq/kg dry weight and input. The growth curve was edited to take into account the final mass of the sow, and the organ masses, at delivery. Additional calculations were carried out to test different combinations of growth curves and activity concentrations in the feed.

The first model intercomparison exercise involved long-term HTO contamination of the feed and water fed to the pig. Since PRISM cannot handle liquid intakes, the contaminated water was replaced in the model with an equivalent amount of contaminated fodder. In the first instance, the given concentration was input and two feeding regimes were set up to model the contaminated and uncontaminated periods. As in the case of the model-data scenario, the growth curve was edited to take into account the final mass of the pig at slaughter. Additional calculations were carried out to test different combinations of growth curves and activity concentrations in the feed.

Some initial runs gave very similar results for both the 110-day and 165-day growth scenarios. Subsequent investigations suggested that this was because the generic growth curve parameters were the same for the two runs, and that the amount of fodder fed in the contamination part of the scenario was also the same (a normal PDF in the range 1.9-2.9 with a best estimate of 2.4 kg d^{-1}). In subsequent model runs, the growth curve was adjusted to take into account the final masses and different rates of growth. The mass of feed was adjusted to take into account the different rates quoted in the scenario.

II.5.4. IFIN-HH Model: MAGENTC (MAmmal GENeric model for Tritium and Carbon transfer)

The MAGENTC model was developed gradually over the last three years as a research tool for the transfer of C-14 and H-3 in mammals, based on energy metabolism. It is the result of an international collaboration led by IFIN-HH with contributions from researchers from the UK and Japan. In its initial form it was used for wild mammals [II.94] and the human dosimetry of tritium [II.95]. A full description will be released soon [II.96].

For adult mammals, the model for the transfer of tritium and ^{14}C in the body is based on the following ideas:

- The most important body organic compartments are the viscera (including the heart), muscle, adipose tissue, blood (plasma and RBC) and the remainder (including the brain). The mass and composition of these organs are well known.
- Tritium in body water equilibrates rapidly and a single body water compartment suffices when modelling tritium.
- The loss rate from organic compartments is similar for intakes of HTO or OBT and can be assessed directly from the energy turnover rate (net maintenance).
- Net maintenance can be considered the sum of the energy needs of basal metabolism and activity, neglecting thermal stress.
- The basal metabolic need is the sum over all organs of the product of the organ specific basal metabolic rate and the organ mass.
- The specific metabolic rate (SMR) for organs in adult mammals varies marginally, except for muscle, compared to the basal state. The basal SMR shows a dependence on the mature mass of the animal.
- Values of SMR have been obtained experimentally for a few mammals only and a zero-order approximation, dependent on mature mass, is normally used.
- There is metabolic conversion of HTO to OBT. The equilibrium value of the OBT/HTO ratio derived from ingested HTO or OBT does not vary across mammals.
- The energy (heat) and accompanying matter lost in transforming the metabolisable input in net requirements is considered a single, fast process.

Under these hypotheses, the model gives reliable predictions with no calibration. A flowchart of the model is given in Figure II.5.4.

For growing mammals, the model needs a clear definition of maintenance energy need, which is difficult to obtain because of the complexity of processes in growing mammals. In a few cases, the experimental data give a reliable definition.

Generic, default parameter values were used in calculations for the blind test of the Pig Scenario. For the model inter-comparison exercises with growing pigs, the model assumes that growth and intake in the various model compartments are driven by the growth rates of each organ (or group of organs) and depend on changes in composition. Experimental data from French researchers [II.97–II.101] have been used to test the model as they permit a good distinction between maintenance and growth needs.

Three distinct pigs were analyzed: a conventional genotype (SL), a lean genotype with low visceral mass (PP), and a fat genotype (MS). These pigs differ in respect to body mass and MEI intake dynamics, as well as in their adipose and visceral tissues (Figures II.5.5 and

II.5.6). Muscle mass differs also (Figure II.5.7). All growth data are extracted from the French papers referenced above. We selected this data partly because they describe the time dependence of muscle and adipose mass. The concentrations in muscle show moderate sensitivity to the SMR in viscera and remainder organs (Figures II.5.8 and II.5.9). Using the same starting body composition and same relationship for body water as a function of body protein for each genotype, and a constant OBT concentration in the diet (1Bq/kg dry matter), we obtained the results in Figure II.5.10. From this figure, we can deduce that genotype is not of peculiar importance for continuous intake and that whole body concentrations overestimate muscle concentrations by a factor that depends on pig obesity.

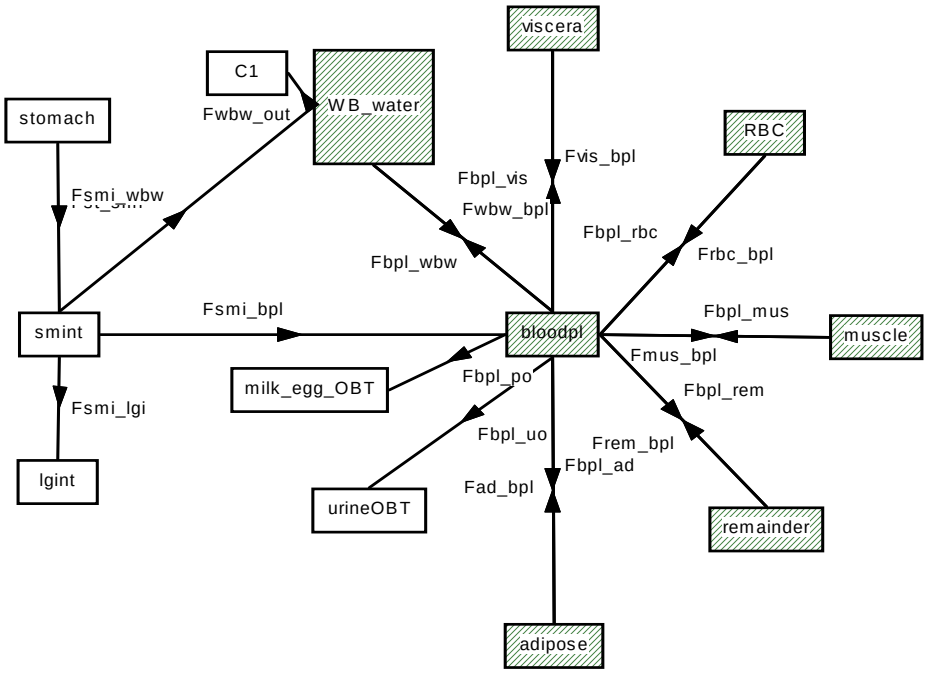

Fig. II.5.4. Flowchart of the MAGENTC model.

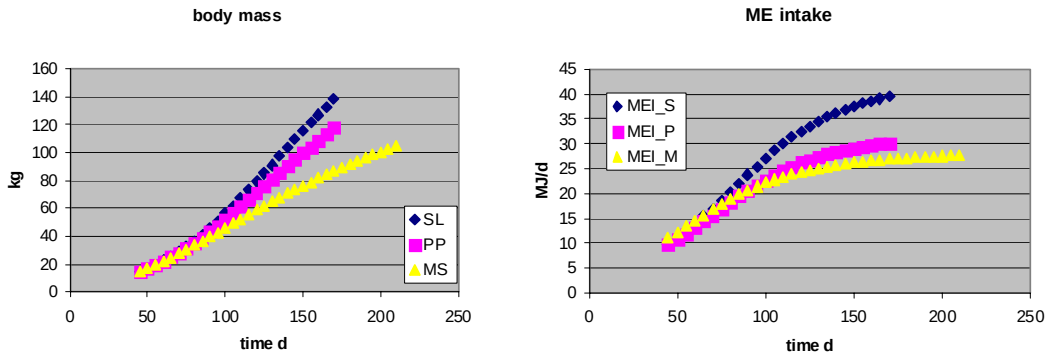

Fig. II.5.5. Dynamics of pig body mass and MEI intake for different pig genotypes.

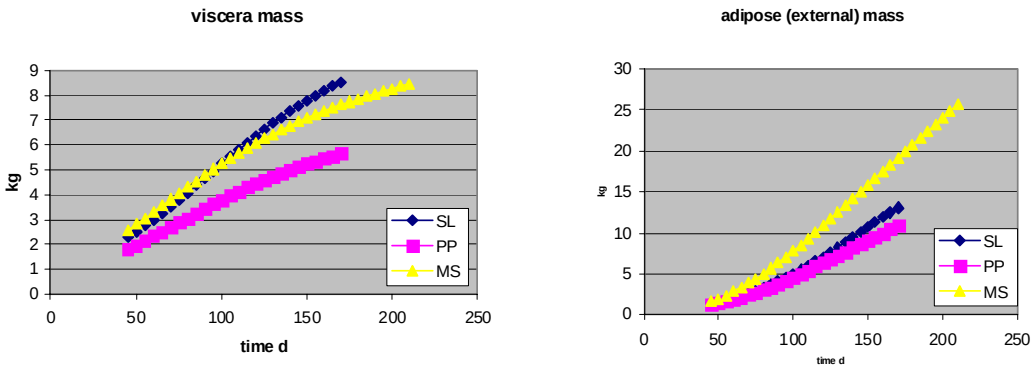

Fig. II.5.6. Dynamics of adipose and viscera mass for different pig genotypes.

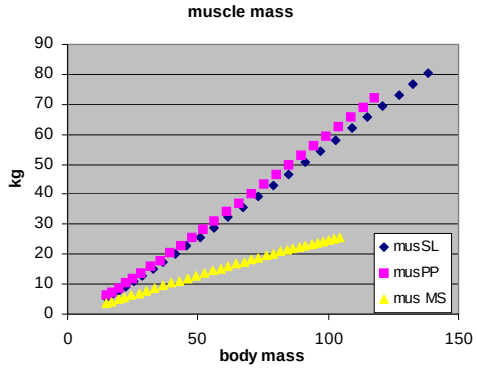

Fig. II.5.7. Muscle mass as a function of body mass for different pig genotypes.

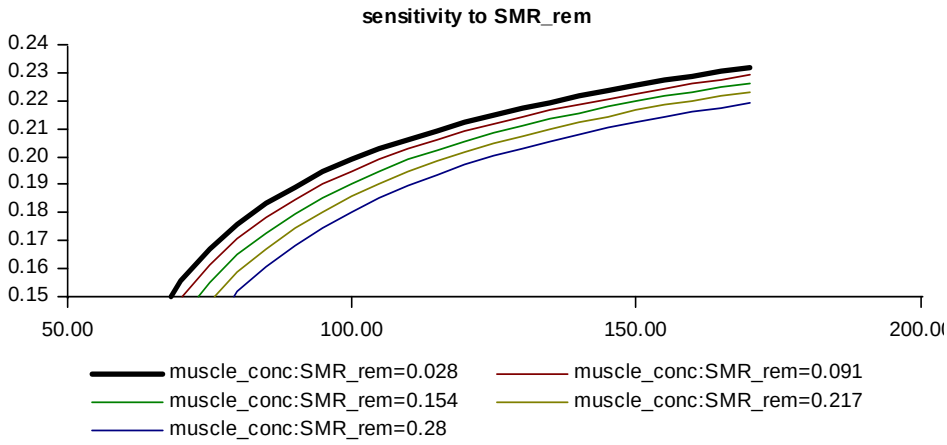

Fig. II.5.8. Sensitivity of muscle concentration to SMR in remainder organs.

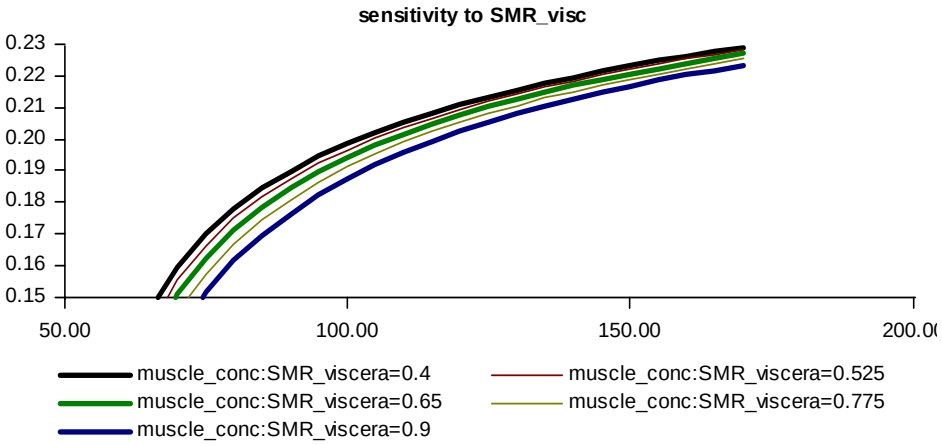

Fig. II.5.9. Sensitivity of muscle concentration to SMR in viscera.

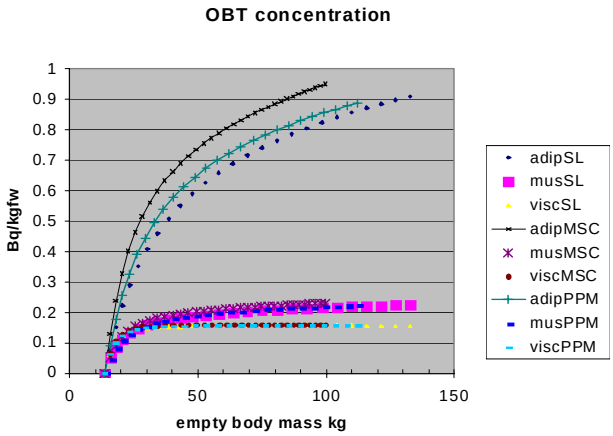

Fig. II.5.10. OBT concentration in muscle, viscera and adipose tissue for three pig genotypes fed 1 Bq/kg dry matter.

II.5.5. EDF Model

II.5.5.1. Model description

The EDF calculations are based on the OURSON model, a dynamic model that evaluates radionuclide concentrations in the aquatic and terrestrial environment resulting from liquid discharges, in order to estimate doses to humans. Consequently, only dose-relevant compartments are included in the model. Milk and meat are the two animal compartments taken into account. Both HTO and OBT are described by single compartment metabolic models.

The pig scenario involves the calculation of tritium concentrations in urine, in faeces and in different body organs. None of these compartments are included in the OURSON model. Therefore it was necessary to make some adaptations.

The HTO concentration in urine was assumed to equal the concentration in body water. The same assumption is used for HTO in cow's milk. Thus the HTO concentration in urine was calculated according to Equation II.5.1. The concentration depends on the HTO activity in the diet, on the turnover of OBT in meat tissue, and on the water intake rate in food and drinking water.

$$\frac{dC_{urine}^{HTO}(t)}{dt} = -\lambda_w C_{urine}^{HTO}(t) + \frac{1}{H_2O_{pig}}\left(HTO_{diet} + k_{ing}.OBT_{pig}(t)\right) \quad \text{(II.5.1)}$$

with:

$$\lambda_w = \frac{\text{water consumption (L/day)}}{H_2O_{pig}(L)}$$

where:

HTO_{diet} is the HTO activity in the diet (drinking water plus food) (Bq/day);
k_{ing} is the OBT turnover rate (d^{-1}) (see Equation II.5.2);
W is the animal dry weight (kg); and
$OBT_{pig}(t)$ is the total OBT in the pig (Bq).

$OBT_{pig}(t)$ was calculated according to the OURSON equation for OBT in meat, where the turnover rate is governed by the relative rate of ingestion of food and the food digestibility:

$$\frac{dA_{meat}^{OBT}(t)}{dt} = -k_{ing} A_{meat}^{OBT}(t) + k_{ing}.\frac{H_{food}}{H_{meat}}.A_{food}^{OBT}(t) \quad \text{(II.5.2)}$$

with:

$$k_{ing} = \frac{I \cdot D}{W}$$

where:

A_{meat}^{OBT} is the OBT specific activity in meat (Bq/g H);
A_{food}^{OBT} is the OBT specific activity in food (Bq/g H);
I is the food intake (kg dry weight d^{-1});
D is the digestibility (unitless);
W is the animal dry weight (kg);
H_{food} is the average food organically bound hydrogen (g/kg dry matter); and
H_{meat} is the average meat organically bound hydrogen (g/kg dry matter).

Urea is another source of tritium in urine. The OBT specific activity in urea was assumed to equal the average OBT specific activity in the pig.

Faeces OBT corresponds to the OBT in the non-digestible fraction of food. It was assumed that the OBT specific activity was identical in the digestible and non-digestible fractions. Faeces HTO was considered to originate from microbial decomposition of the non-digestible food fraction; thus HTO and OBT specific activity in faeces were identical.

To estimate OBT concentrations in the various organs, OBT in the pig was calculated according to Equation II.5.2. It was considered that this value was representative of the muscle compartment. Concentrations in other organs were derived from the concentration in muscle using a correction factor based on the fat and protein contents of each organ, the turnover rate of fats and proteins, and the hydrogen content of fats, proteins and carbohydrates.

The HTO concentration was assumed to be the same in all organs, and was calculated with Equation II.5.1.

II.5.5.2. Parameters

Noblet et al. [II.102] provide digestibility coefficients (for energy) for a pregnant sow for different types of foods (Table II.5.9). However, no value for algal powder was available. The value for alfalfa with a protein content of less than 16% was attributed to algal powder.

Food hydrogen contents and the organically bound hydrogen (OBH) content of pigs were calculated from water equivalent factors [II.103]. The sow dry weight was 90 kg, based on a dry matter content of 50% [II.103].

Human data were used to estimate the OBH content of urea (0.066 g/g [II.104]) and the urea concentration in urine (25 g/L). The same reference was used for the contents of carbohydrates, fats (two types) and proteins in different organs, and the turnover rates of fats and proteins. Calculated turnover rates relative to those in muscle are given in Table II.5.10.

Table II.5.9. Digestibility coefficients and organically bound hydrogen contents of different foods.

Food	Digestibility coefficient	OBH content (% dry matter)
Whole milk powder	0.930	7.43
Whole potato powder	0.925	6.44
Alfalfa powder, proteins<16% (surrogate for algal powder)	0.48	5
Pig		10.04

Table II.5.10. Calculated relative turnover rates in different organs.

Organ	Heart	Lungs	Liver	Jejunum	Ileum	Colon	Kidney	Muscle	Brain	Blood
OBT turn over rate relative to muscle	1	0.80	0.83	0.62	0.62	0.62	0.83	1	0.51	0.80

II.5.6. AECL Model

II.5.6.1. Model description

The AECL calculations were carried out with the animal subroutines of the ETMOD code, an environmental tritium code used for predicting the consequences of accidental tritium releases to the atmosphere from tritium-handling facilities at Chalk River Laboratories and other sites [II.57, II.58, II.105]. ETMOD simulates the behaviour of tritium in the biosphere, covering many transport and exposure pathways including atmospheric dispersion, deposition and migration in soil, re-emission from soil, and transfer to vegetation, animals and animal products. It can handle releases of either tritium gas (HT) or tritiated water vapour (HTO) and addresses organically bound tritium (OBT) formation in plants. As its main endpoint, ETMOD predicts ingestion and inhalation (including skin absorption) doses to humans.

The animal subroutines of ETMOD calculate HTO concentrations in animal products using the HTO taken in by the animal through inhalation and ingestion of water, feed and soil. The dynamics of the HTO concentration in animal body water, C_H, is driven by the concentration gradient between HTO in intake water and in body water, as described by the following equation:

$$dC_H/dt = (H/W_t - C_H)\, W_t/W_b \qquad \text{(II.5.3)}$$

where:

W_t is the total water intake from all sources (L/d);
W_b is the body water content (kg); and
H is the total daily amount of tritium intake (Bq/d), including OBT.

Now $W_b = C_{bwf}\, BM$, where C_{bwf} is the body water fraction and BM is body mass (kg). Also:

$$W_t = W_i + C_{wf1}I_{r1} + (1- C_{wf1})W_mI_{r1} + C_{wf2}I_{r2} + (1- C_{wf2})W_mI_{r2} + 1000R_oI_{inh} + \theta_wI_s \qquad \text{(II.5.4)}$$

where:

C_{wf1} and C_{wf2} are the water fractions in grain and other food types, respectively (unitless);
I_{r1} and I_{r2} are the ingestion rates for grain and other food types (kg/d);
W_m is the metabolic water fraction in dry matter (identical for all food types, unitless);
R_o is the air specific humidity (g/m^3);
I_{inh} is the inhalation rate (m^3/d);
θ_w is the soil water content (L/kg); and
I_s is the soil ingestion rate (kg/d).

In general, H is given by:

$$H = C_wW_i + C_{f1}C_{wf1}I_{r1} + C_1^{OBT}\,(1- C_{wf1})\, W_mI_{r1} + C_{f2}C_{wf2}I_{r2} + C_2^{OBT}\,(1- C_{wf2})\, W_mI_{r2} + 2C_{air}I_{inh} + C_s\theta_wI_s \qquad \text{(II.5.5)}$$

where:

C_w is the HTO concentration in water (Bq/L);
C_{f1} and C_{f2} are the HTO concentrations in grain and other food types, respectively (Bq/kg);
C_1^{OBT} and C_2^{OBT} are the OBT concentrations in grain and other food types, respectively (Bq/kg);

C_{air} is the HTO concentration in air (Bq/m^3). Skin absorption of HTO is assumed equal to inhaled HTO, which is reflected in the multiplier 2 in Equation II.5.5; and
C_s is the HTO concentration in soil (Bq/kg).

OBT is not modeled explicitly in the animal in the current version of ETMOD.

II.5.6.2. Assumptions and model parameterization

Model-data comparison

Total water intake consists of inhaled water vapour, ingestion of water in food, formation of metabolic water following food ingestion, and directly ingested water. The ingestion rate of water (W_i) and of the water in food (W_f) are assumed to be constant throughout the period of the experiment. Two cases are considered:

W_i = 6.0 L/d and W_f = 1.0 L/d; and
W_i = 8.0 L/d and W_f = 1.2 L/d.

Food intake follows the rates prescribed in the scenario description, as shown in Table II.5.11. 60% of the dry matter in the diet is combined with 15% of the food water; the remaining 40% of the dry matter is combined with 85% of the food water. The average food water content equals 70%. One kg of dry weight food yields 0.56 L of metabolic water for all food types.

The soil ingestion rate is 125 g/d with a water content of 30%. The inhalation rate equals 35.9 m^3/d. The air absolute humidity is 12 g/m^3. The pig gains 0.5 kg/d from a weight of 180 kg at the start of the exposure. The body water content is 65%.

Model intercomparison exercise

Total water intake consists of inhaled water vapour, ingestion of water in food, formation of metabolic water following food ingestion, and directly ingested water. The ingestion rate of water (W_i) is assumed to obey the following regression:

$$W_i = 0.3\ BM^{0.71}\ L/d, \qquad \text{(II.5.6)}$$

where BM is body mass in kg.

Table II.5.11. Food intake as a function of time.

Day after start of exposure	Food intake (kg/d dry matter)
1	1.86
22	2.06
47	2.31
80	3.01

Table II.5.12. Food intake as a function of body mass.

Body mass (kg)	Food intake (kg/d dry matter)
20	1
35	1.4
50	1.66
80	1.9
110	2

Food intake corresponds to generic intake rates for slow-growth genotypes, as shown in Table II.5.12. 60% of the dry matter in the diet is combined with 15% of the food water; the remaining 40% of the dry matter is combined with 85% of the food water. The average food water content equals 70%. One kg of dry weight food yields 0.56 L of metabolic water for all food types.

The soil ingestion rate is 125 g/d with a water content of 30%. The inhalation rate (I_r) is scaled by the water ingestion rate:

$$I_r = 4.2\ W_i\ m^3/d \qquad \text{(II.5.7)}$$

The air absolute humidity is 12 g/m^3. The growth of body mass, BM, is approximated by the following regression:

$$BM = a_0 + a_1 t + a_2 t^2 + a_3 t^3 \text{ kg}, \qquad \text{(II.5.8)}$$

where t is time (d) and a_0=21.104, a_1=1.92, a_2= -1.57e-02, a_3= 5.0e-05

The body water content of the pig is W_{bwf} = 65%.

The dynamics of body mass, inhalation rate and food intake are plotted on Figures II.5.11 to II.5.13, respectively.

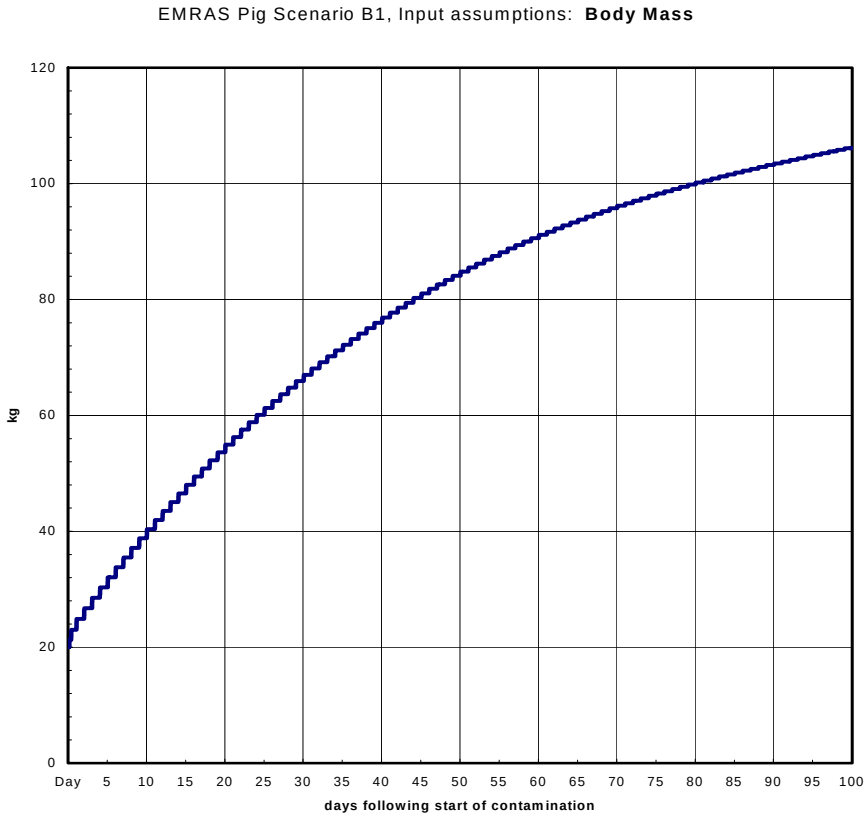

Fig. II.5.11. Dynamics of body mass for the model intercomparison exercise.

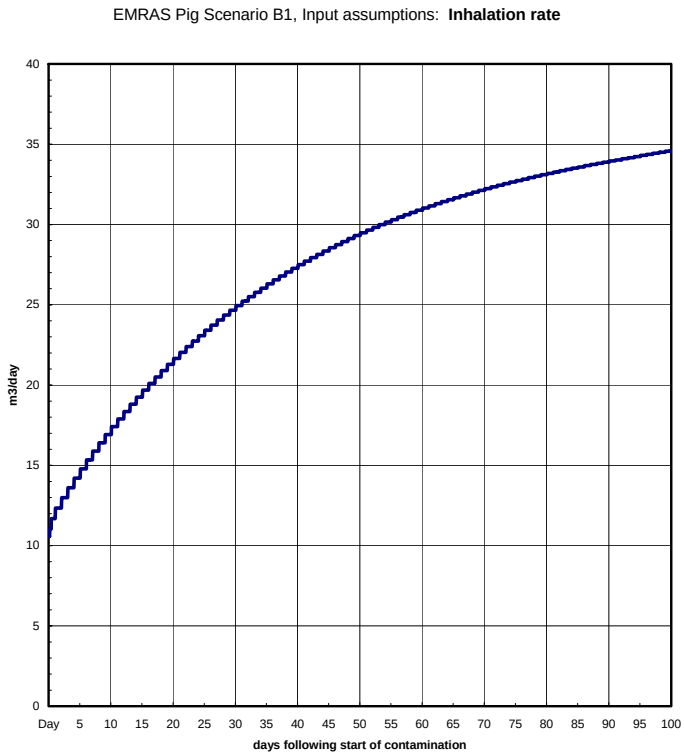

Fig. II.5.12. Dynamics of inhalation rate for the model intercomparison exercise.

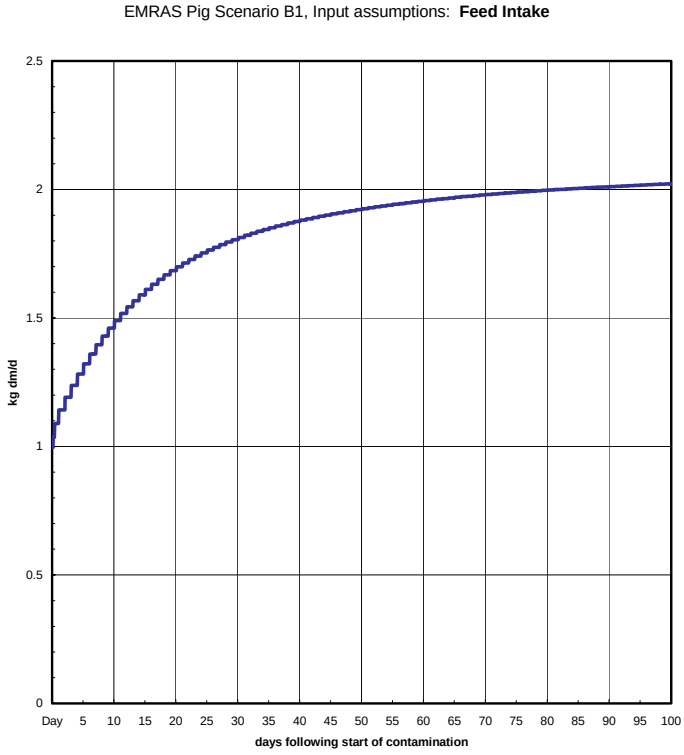

Fig. II.5.13. Dynamics of food dry matter intake for the model intercomparison exercise.

II.6. Mussel Uptake Scenario model descriptions

II.6.1. NIRS Model

A dynamic compartment model with selected transfer coefficients for tritium uptake by aquatic animals (as depicted in Figure II.6.1), was developed by K. Miyamoto of the National Institute of Radiological Sciences (NIRS) in Japan. The NIRS model was run twice (in May and November 2005) for the purposes of this scenario. The November model and calculations included an additional OBT compartment (i.e., mussel OBT-2) that was not present in the May version. The calculations were carried out using the ERMA (Environmental Radionuclide Movement Assessment) system developed by NIRS.

In applying the NIRS model, a number of assumptions were made. For example, based on studies made in Perch Lake [II.106], the HTO concentration in lake water is not expected to be homogeneous, but varies with location and season. Therefore, the triplicate HTO concentration measurements that had been taken in the lake water in the vicinity of each set of cages (i.e., Cages 1 and 2; Cages 3 and 4) were averaged for each sampling time.

It was assumed that the mussels started vigorous filtration of water, suspended materials, plankton and organic matter in the water (for Cages 1 and 2), or of the sediments at the sediment-to-water interface (for Cages 3 and 4), immediately following mussel transplantation into Perch Lake. Visual observation of the transplanted mussels at the start of the experiment confirmed this assumption. In addition, it was assumed that there would be no differences in the filtration activities of the mussels exposed to water only (Cages 1 and 2) and to both water and sediments (Cages 3 and 4); however, it was assumed that a 3-fold higher concentration of sediments was ingested by mussels that had been placed at the sediment-to-water interface, compared to those that had access to the water column only. This assumption was based on the 3-fold advantage in mussel nutrition that has been reported by a fishery in Japan in sea shells of mussels cultivated at the sea bottom compared to those cultivated in cages hanging in the water column.

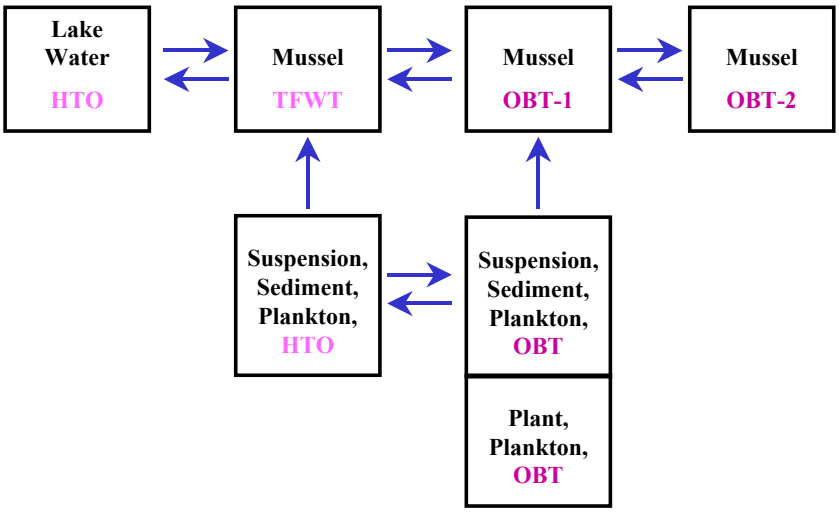

Fig. II.6.1. Conceptual model depicting compartments and the linkages between compartments, as assumed in the NIRS model (Japan).

It was also assumed that the concentration of mussel tissue free-water tritium (TFWT) and non-exchangeable OBT (nOBT) in compartments OBT-1 and OBT-2 increased over time following transplantation. Values for the transfer coefficients were estimated through simulations using the basic model, until the mussel TFWT-to-lake water HTO ratio reached a value of 0.9 and the nOBT-to-lake water HTO ratio reached a value of 0.7, based on the findings of the Perch Lake Scenario.

No consideration was given in the NIRS model to the daily water temperatures and their potential influence on the growth of the mussels during the experiment, to the variation of weight or metabolic activity of individual mussels, or to the order of placement and sampling of the cages. The 95% confidence interval was assumed to be 5% of each endpoint.

II.6.2. SRA Model

The SRA model, which was developed by M. Saito of the Kyoto University Safety Reassurance Academy (SRA) in Japan, is a simple, two-compartment model that includes one TFWT compartment and one OBT compartment. The rate of tritium uptake into each compartment is determined using transfer coefficients, accounting for the difference in specific activity between the environment and the body of the mussel.

The SRA model assumes that the mussels assimilate TFWT from plankton, sediments and surface water, although TFWT uptake from plankton is considered negligible. In addition, mussels are assumed to incorporate OBT from plankton and sediment. Since the fractional uptake of organic hydrogen from individual nutrient sources was unknown, the uptake from plankton was assumed to occur at twice the rate from sediments.

The OBT transfer coefficient, λ, was varied in the range 0.003 to 0.0003 h^{-1}, whereas that of HTO was assumed to fall in the range 0.03 to 0.003 h^{-1}. In the report file, only the results for the case $\lambda_{obt} = 0.001\ h^{-1}$ and $\lambda_{hto} = 0.01\ h^{-1}$ were given.

Key factors determining the uncertainty of the predictions are the rates of tritium uptake from plankton, sediments and lake water. These rates can be varied when the calculations are made. The largest and smallest TFWT and OBT concentrations predicted under the above assumed range of parameter values were taken as the upper and lower limits of the confidence range.

II.6.3. AQUATRIT Model

The AQUATRIT model, which was developed by D. Galeriu of the National Institute for Physics and Nuclear Engineering-Horia Hulubei (IFIN-HH), can be applied for aquatic pathways of tritium [II.14]. The model makes a number of simplifying assumptions. For example, it assumes that both water temperature and HTO concentration are spatially constant, as represented by the mean values taken at a given point in time. The model does not account for any specific attributes of the Barnes mussel but instead makes use of generic knowledge [II.107–II.110]. In addition, although the growth pattern for mussels is unknown, the model assumes growth patterns of quite mature animals.

The OBT concentration in aquatic animals (in Bq/kg fresh weight) is estimated using the following rate equation, where the initial condition (i.e., the initial OBT concentration in mussels) is very important in predicting OBT concentrations in the first few days following mussel transplantation:

$$\frac{dC_{org,x}}{dt} = a_x\, C_{f,x}(t) + b_x\, C_w(t) - K_{0.5,x}\, C_{org,x} \qquad \text{(II.6.1)}$$

where:

$C_{org,x}$ is the OBT concentration in animal x (Bq/kg fresh weight);
$C_{f,x}$ is the OBT concentration in the food of animal x (Bq/kg fresh weight);
C_w is the HTO concentration in water (Bq/L);
a_x is the transfer coefficient from HTO in water to OBT in animal x;
b_x is the transfer coefficient from OBT in food to OBT in animal x; and
$K_{0.5,x}$ is the loss rate of OBT from animal x (d^{-1}).

The tritium concentration in the dietary items consumed by a given species is calculated from:

$$C_f = \sum_{i=1}^{n} C_{prey,i} \cdot P_{prey,i} \frac{\text{Dry}\, f_{pred}}{\text{Dry}\, f_{prey,i}} \qquad \text{(II.6.2)}$$

where:

$C_{prey,i}$ is the OBT concentration in prey species i (Bq/kg fresh weight);
$P_{prey,i}$ is the preference for prey species i;
Dry f_{pred} is the fractional dry weight of the predatory species; and
Dry $f_{prey,i}$ is the fractional dry weight of prey species i.

The parameters a_x and b_x in Equation II.6.1 reflect the metabolic regulation of tritium, as described by:

$$a_x = (1\text{-}SAR_x)\, K_{0.5,x} \qquad \text{(II.6.3)}$$

$$b_x = 0.54 \times 10^{-3}\, SAR_x\, \text{Dry}\, f_x\, K_{05,x} \qquad \text{(II.6.4)}$$

where:

SAR_x is the specific activity ratio when only water HTO is considered in the intake (SAR=0.25); and
$K_{0.5,x}$ is the sum of the relative growth rate and the mass-specific metabolic (respiration) rate, which reflects the tritium loss rate.

The model accounts for the filter-feeding behaviour of mussels, whereby food intake depends upon the water filtration rate and the food concentration in the water. In addition, there is an assimilation factor, which is quite low. Under good environmental conditions (and high food availability), the mussel will grow, and the loss rate, $K_{0.5}$, will correlate with food availability, as well as the tritium concentration in the food (as summarized in Equation II.6.2). Mussels can assimilate material from bacteria, plankton, detritus and dissolved organic matter. For example, the mussels in Cages 1 and 2 did not have access to detritus (sediment) in their food, but were able to consume plankton. The filtered dry matter is expected to be low for plankton, which can result in relatively slow mussel growth. By comparison, mussels in Cages 3 and 4 had access to detritus, and could, therefore, be expected to grow faster, although the average concentration of food was not higher than in Cages 1 and 2.

In the absence of specific information on *Elliptio complanata*, data reported for *Mytilis edulis* was applied in the model to estimate tritium dynamics in the transplanted mussels [II.107–II.110].

Equilibration of mussel HTO with the surrounding water represents a fast process and the estimated HTO values are uncertain by a factor less than 2. However, the OBT concentration depends strongly on factors such as temperature, species and environment (growth rate), resulting in uncertainties of up to a factor 10. These uncertainties can be reduced if mussel growth rates are known.

II.6.4. EDF Model

EDF predictions are based on the OURSON model, a dynamic model that evaluates radionuclide concentrations in the aquatic and terrestrial environment resulting from liquid discharges, in order to estimate doses to humans. Consequently, only dose-relevant compartments are included in the model. In freshwater, the only aquatic animal considered is fish. The fish HTO compartment is assumed to be at equilibrium with the surrounding water:

$$A_{fish}^{HTO} = A_{eau}^{HTO} \tag{II.6.5}$$

where:

A_{fish}^{HTO} is the HTO activity in fish tissue free water (Bq/L); and
A_{eau}^{HTO} is the HTO activity in water (Bq/L).

By comparison, OBT in fish is assumed to be gradually incorporated from plankton OBT, at a rate that is proportional to the feeding rate. Plankton OBT is assumed to be at equilibrium with water HTO. Thus, formation of OBT in fish is described by the following equation:

$$\frac{dA_{fish}^{OBT}(t)}{dt} = -k_{ing} A_{fish}^{OBT}(t) + k_{ing} . DF_{phyto} . \frac{H_{phyto}}{H_{fish}} . A_{eau}^{HTO}(t) \tag{II.6.6}$$

where:

$k_{ing} = \frac{I \cdot D}{W}$ and
A_{fish}^{OBT} is the OBT specific activity in fish (Bq/L combustion water);
k_{ing} is the relative feeding rate (d^{-1});
I is the food intake (kg dry weight d^{-1});
D is the digestibility (unitless);
W is the animal dry weight (kg);
DF_{phyto} is the 'discrimination' factor , ratio between OBT in phytoplankton (Bq/L combustion water) and HTO in water (Bq/L);
H_{phyto} is the average phytoplankton OBH in g/kg dry matter; and
H_{fish} is the average fish OBH in g/kg dry matter.

Adaptation to the Mussel Scenario

First EDF model run (November 2005)

In a first scenario run, the OURSON fish model was directly applied to the mussel. The estimate of k_{ing} was based on a number of considerations. For example, according to the measures of biomass (from Table I.6.5 of Appendix I), there was no visible growth of mussels during the experiment. It was, therefore, assumed that these adult mussels were in the stationary growth phase with a feeding rate corresponding to maintenance metabolism. A value of 3 x 10^{-3} d^{-1} was assigned for this parameter based on the mean value recommended for fish by Sheppard et al. [II.111]. In addition, DF_{phyto} was assumed to be equal to 0.7 (EMRAS Perch lake scenario report), and H_{phyto} and H_{mussel} were assigned the same value of 6% [II.112].

The model was the same for the cages in the water column and those at the sediment-water interface, although the difference in location could have an influence on the filtration rate, which in turn would affect the metabolic requirements of the mussels. In addition, no consideration was given either to the daily water temperatures or their potential influence on mussel metabolism.

Second EDF model run (May 2006)

After the November 2005 Tritium Working Group meeting, an additional compartment was included in the model to address the under-prediction of initial OBT concentrations. This compartment represents the food particles inside the mussel (including food particles on the soft tissue surface, as well as ingested particles). Observations made for *Mytilus edulis*, a marine mussel, showed that food particles could represent as much as 30% of mussel soft tissue weight. This value was assumed to be relevant for Barnes mussels. OBT in this compartment was calculated using Equation II.6.6, with a turn-over rate, k_{ing}, corresponding to the particle filtration rate.

Thus, in the second EDF run, OBT in mussel (Equation II.6.6) was calculated according to the following equation:

$$A_{mussel}^{OBT} = 0.7 \times A_{soft-tissue}^{OBT} + 0.3 \times A_{food-particles}^{OBT} \qquad \text{(II.6.7)}$$

where $A_{soft-tissue}^{OBT}$ and $A_{food-particles}^{OBT}$ were both calculated using Equation II.6.6, with their own k_{ing} values. k_{ing} was set equal to 0.02 d^{-1} when calculating the activity in soft tissue. This value was derived from the metabolic requirement of *Mytilus edulis* [II.113] and seemed more adapted to the scenario than the fish value used in the first model run. Assuming a filtration rate of 38 L/day and a suspended particle concentration in water of 10 mg/L, k_{ing} for food particles was estimated to be 0.33 d^{-1}. The predicted OBT concentrations are shown as a function of time in Figure II.6.2.

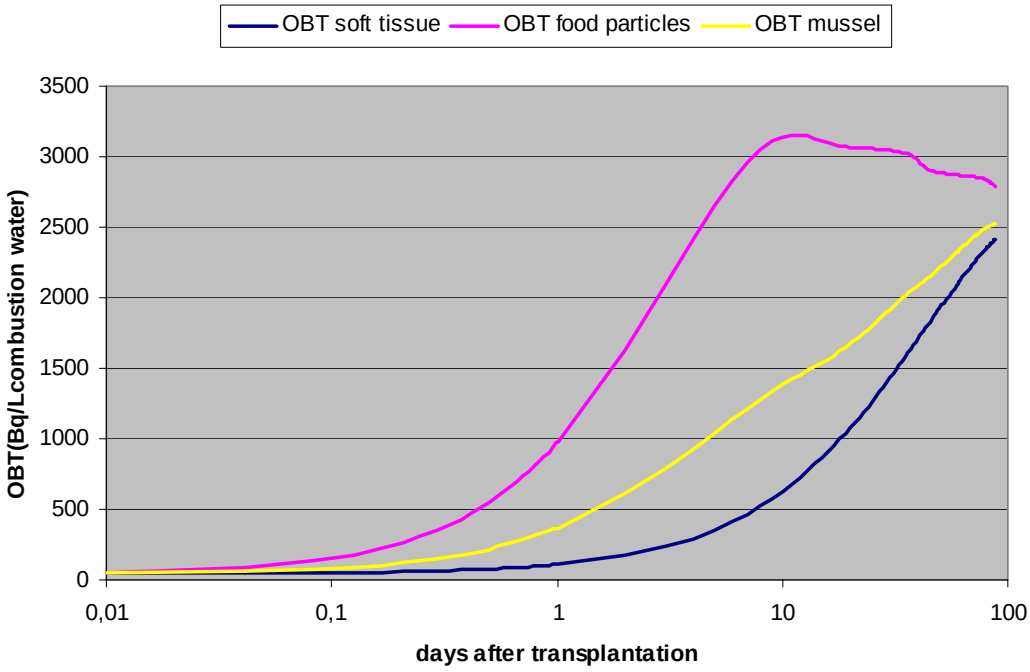

Fig. II.6.2. EDF predictions of OBT in mussels of Cages 1 and 2.

II.6.5. BIOCHEM Model

The BIOCHEM Model was developed by F. Baumgärtner of the Munich Technical University (TUM) in Germany. The basic premise of this model can be summarized by the following equation:

$$OBT = CBT + XBT + YBT \quad \text{(II.6.8)}$$

where:

CBT is carbon-bound tritium (also referred to as non-exchangeable OBT);
YBT means h**y**drate **b**ound **t**ritium (one form of exchangeable OBT); and
XBT is tritium bound to oxygen, nitrogen and sulphur atoms (designated as 'X' atoms), which represents another form of exchangeable OBT.

Basically, the tritium nuclei (or tritons) of YBT and XBT are exchangeable with the hydrogen nuclei of water, but are not transferred to water during the rinsing process of OBT analysis because they are "buried" inside the biopolymers, and thus inaccessible to water during wetting [II.5]. However, in living systems "buried tritium" is exchangeable as biomolecules are formed and undergo biochemical configuration changes. The BIOCHEM model accounts for the differences in exchangeability between exchangeable OBT (i.e., YBT + XBT) and non-exchangeable OBT (CBT) that occur in living systems, so that they can be considered in tritium dose estimation. In doing so, different distribution factors are applied to distinguish between YBT and XBT in model predictions, where α_{YBT} =1.4 and α_{XBT} = 2.0 [II.10]. Such distribution factors have been estimated based on theoretical information and mathematical constants that have been reported by Griffiths et al. [II.114], Saenger [II.11], Klapper [II.9] and Baumgärtner [II.7], as follows:

$$(H_{exch}/M)_{XBT\text{-}DNA} = 1.9 / 331 \quad \text{(II.6.9)}$$

$$(H_{exch}/M)_{YBT} = 20 / 331 \quad \text{(II.6.10)}$$

$$(H_{exch}/M)_{XBT\text{-}protein} = 1.83 / 109 \quad \text{(II.6.11)}$$

where:

H_{exch} represents exchangeable hydrogen (i.e., XBH+YBH);
M is the stoichiometric unit;
XBT-DNA is the XBT bound into DNA; and
XBT-protein is the XBT bound into proteins.

During the combustion process, the tritium in the dry matter (in Bq/kg dry weight) is converted into tritium in combustion water (in Bq/L). This conversion is accounted for using the water equivalent factor, W_{eq} (L/kg dry weight), which differs between different sample types but has a typical value of 0.58 L/kg dry weight.

Estimation of YBT and XBT

The BIOCHEM model provides a numerical estimation of 'buried tritium', YBT and XBT, assuming that living systems consist of proteins, DNA and carbohydrates only, since these represent the main components of any living system and may be relevant in dose calculations. Their overall molecular constitutions are approximately known and the model adopts quantitative relationships between these components. In the mussel uptake scenario calculation, it was assumed that mussels consist of proteins and DNA only, and focus was placed on formation of XBT and YBT.

The model assumes that OBT concentrations in carbohydrates are negligible in mussels (which implies that CBT represents only a small fraction of the total OBT in mussel tissues), although the justification for these assumptions is unclear.

Based on past experimental work to measure OBT concentrations in the DNA of fish sperm [II.10], it was concluded that freeze-drying of the samples might potentially lead to an under-estimation of OBT. YBT is a molecular unit, which is fundamentally volatile either at elevated temperature or at low pressure, and 24-hour freeze drying at -25°C and 10^{-6} mbar is required to separate the hydrates from fish sperm DNA; however, freeze-drying over longer time periods (e.g. 48 or 96 hours) can lead to a loss in YBT. For this reason, for the purposes of the BIOCHEM model, it was important to provide a detailed description of the experimental procedures.

Accordingly, the BIOCHEM model assumes that YBT concentrations in mussel tissues are dependent upon the number of buried hydrates in DNA (YBT_{DNA}), which comprises 10 to 12 water molecules per stoichiometric unit [II.11], as well as the YBT retention fraction, R_{YBT}, which is much less than unity:

$$YBT = YBT_{DNA}\, R_{YBT} \quad \text{(II.6.12)}$$

By comparison, XBT can be found in both DNA and protein. Thus, the maximum amount of buried tritium (or exchangeable OBT) in mussels is estimated according to the following equation:

$$Maximum\ Exchangeable\ OBT = XBT_{DNA} + XBT_{protein} + YBT_{DNA} \cdot R_{YBT} \quad \text{(II.6.13)}$$

In the "non-buried" state, an equilibrium of exchange was assumed to exist between the hydrogen isotopes of water and X-bound hydrogen (i.e., exchangeable hydrogen, XBH) in any organic compartment, i, according to the following equation:

$$\frac{T_i}{XBH_i} = \alpha_{XBT,i} \cdot \frac{T_{aqua}}{XBH_{aqua}} \quad \text{(II.6.14)}$$

where:

T_i is the total tritium concentration in the organic compartments of the mussel (Bq/kg fresh weight);
XBH_i is the amount of X-bound hydrogen in the mussel organic compartments;
$\alpha_{XBT,i}$ is the XBT distribution factor for mussel organic compartment, i, (assumed to equal 2.0);
T_{aqua} is the total tritium concentration in the mussel water compartment (Bq/kg fresh weight); and
XBH_{aqua} is the amount of X-bound hydrogen in mussel water.

Equation I.6.14 is equivalent to:

$$\frac{T_i \cdot M}{XBH_i} = \alpha_{XBT,i} \cdot \frac{M \cdot T_{aqua}}{XBH_{aqua}} = \alpha_{XBT,i} \cdot \frac{M_{oxygen} \cdot T_{aqua}}{M_{(2 \cdot hydrogen)}} = \alpha_{XBT,i} \cdot \frac{18 \cdot T_{aqua}}{2} \quad \text{(II.6.15)}$$

where:

XBH is the number of X-bound hydrogen atoms per atomic mass number of the stoichiometric unit, M;
M_{oxygen} is the molar mass of an oxygen atom (18 g/mol), since there is one oxygen atom per water molecule; and
$M_{(2 \cdot hydrogen)}$ is molar mass of two hydrogen atoms (2 g/mol), since there are two hydrogen atoms per water molecule.

If T_{aqua} is represented by HTO and the contributions of all compartments are summed up, (assuming the nucleotide ratios of different compartments are equal and that CBT is negligible), Equation II.6.15 can be converted to Equation II.6.16, as follows:

$$(XBT + YBT) = \left(\frac{9 \cdot [HTO]}{Weq \cdot \{ \sum_i \alpha_{XBT} \cdot \left(\frac{H_{exch,i}}{M_i} \right) \cdot m_i} \right) + \alpha_{YBT} \cdot \left(\frac{H_{exch,YBT}}{M_{YBT}} \right) \cdot R_{YBT} \cdot \frac{m_{DNA}}{m_{total}} \quad \text{(II.6.16)}$$

where:

(XBT+YBT) is the OBT concentration in mussel tissue (Bq/L);
m_i is the mass of compartment i (kg);
m_{DNA} is the mass of DNA in the mussel tissue (kg); and
m_{total} is the total mass of the mussel tissue (kg).

Despite these findings, however, it is important to note that for other types of samples and tissues (such as plant leaves), such decreases in OBT may not be detectable over several days of freeze-drying.

Dynamics of YBT and XBT Formation

During formation and, to a lesser extent, during metabolic activity of biopolymers, X-bound hydrogen (XBH) atoms and neighbouring water molecules are assumed to rapidly exchange their hydrogen nuclei, at a rate that is influenced by the mass of a given hydrogen isotope [II.115]. Consequently, (YBT+XBT) formation in the transplanted mussels was assumed to proceed spontaneously with the ingress of Perch Lake water into mussel cells. The penetration of HTO into the cells was assumed to occur by diffusion and over a very few days following a linear time scale. Additionally, the BIOCHEM model assumed that the isotope mass effect, which was expected to occur in plankton, would also occur during transfer of HTO into mussel tissue, where:

$$TFWT / [HTO] = 0.99 \quad \text{(II.6.17)}$$

The mussels were near the end of their life span and therefore showed no significant growth in fresh weight between the time of transplantation and mussel harvest. Therefore, no additional OBT increase beyond (YBT+XBT) formation was taken into account in the model and molecular OBT exchange with plankton was considered negligible (although this may not be a realistic assumption).

Sensitivity Analysis and Parameter Definition for the BIOCHEM Model

A sensitivity analysis was carried out to test the potential influence on mussel OBT concentrations of mussel protein and DNA content, the rate of ingress of free-water tritium (FWT) into mussel cells, and the YBT retention factor (Figures II.6.3–II.6.8). The conditions used in the analysis are summarized in Table II.6.1. It was concluded that FWT ingress into mussel cells was complete after 2 days, that mussel tissues consist of 75% protein and 25% DNA, and that the YBT retention factor, R_{YBT}, is 0.2.

Temporal Trends in HTO Relative to Perch Lake Water Temperature

The HTO values in both cages showed fluctuations, even over relatively short time intervals and distances (Table 7.3), as did Perch Lake water temperature (Table I.6.1 in Appendix I). The relationship between mean monthly surface water temperature and time (in months) was summarized as follows for use in the BIOCHEM model (Figure II.6.9):

$$T[^oC] = (meanT_{July} - meanT_{october})_i \, exp(-ln2 \cdot t / \tau) + meanT_{October\text{-}i} \quad \text{(II.6.18)}$$

where:

$T[^oC]$ is the Perch Lake surface water temperature;
$meanT_{July}$ is the mean water temperature in July;
$meanT_{October}$ is the mean water temperature in October;
t is time (d); and
τ is the radiological half-life (d).

Although a similar modelling approach could theoretically be applied to approximate temporal changes in Perch Lake HTO concentrations, very large deviations in HTO were predicted based on measured data. Therefore, arithmetic mean Perch Lake HTO concentrations were used in the model to predict (XBT+YBT) in the mussels, such that mussel OBT fluctuations were proportional to the mean HTO water concentrations.

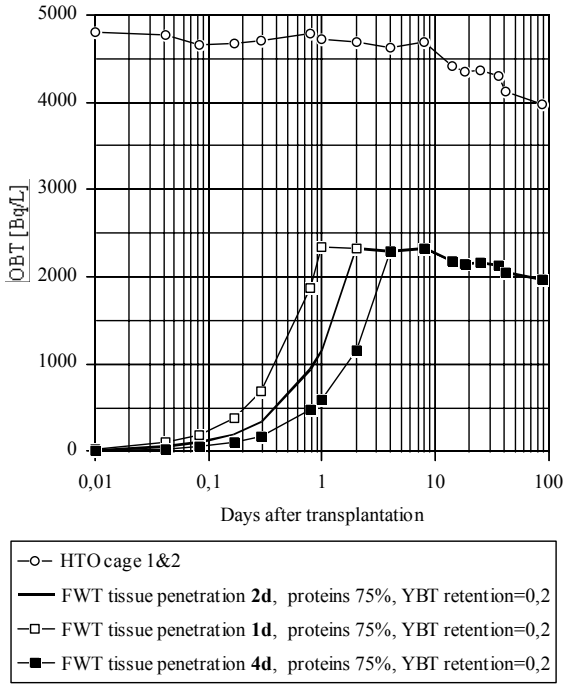

Fig. II.6.3. BIOCHEM model predictions of temporal changes in Cage 1 and 2 mussel tissue OBT concentrations relative to changes in Perch Lake water HTO levels under conditions of varying free-water tritium (FWT) tissue penetration times. Protein levels of 75% and a YBT retention of 0.2 were assumed.

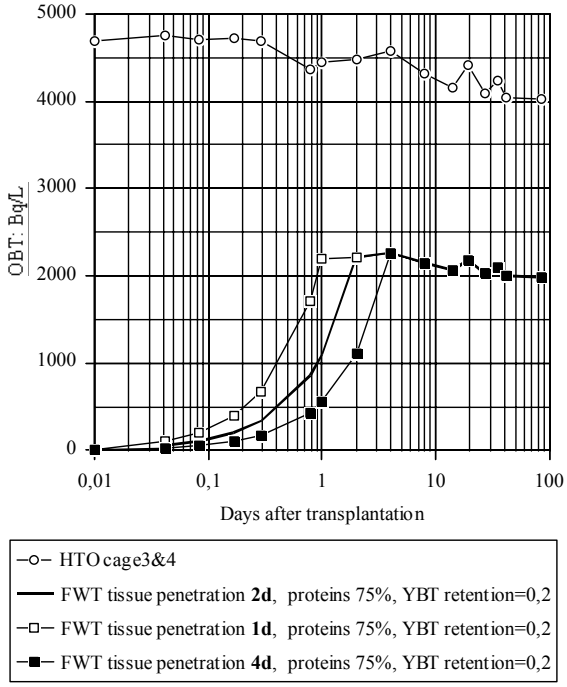

Fig. II.6.4. BIOCHEM model predictions of temporal changes in Cage 3 and 4 mussel tissue OBT concentrations relative to changes in Perch Lake water HTO levels under conditions of varying free-water tritium (FWT) tissue penetration times. Protein levels of 75% and a YBT retention of 0.2 were assumed.

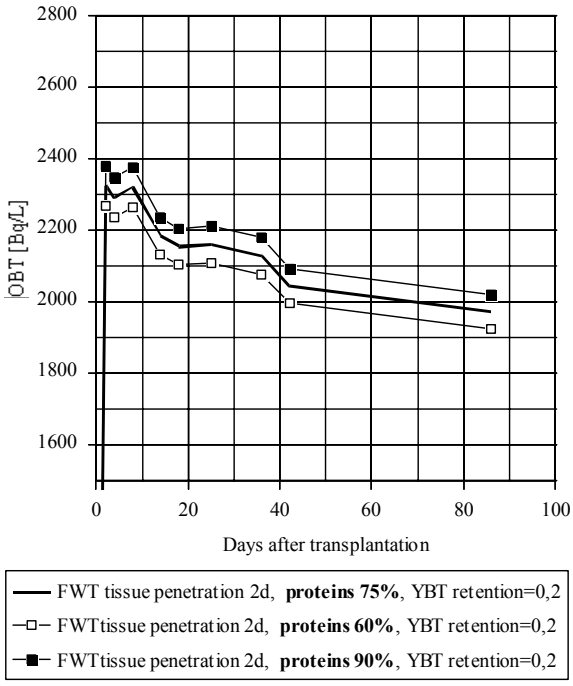

Fig. II.6.5. BIOCHEM model predictions of temporal changes in Cage 1 and 2 mussel tissue OBT concentrations relative to changes in Perch Lake water HTO levels under conditions of varying mussel protein content. Free-water tritium (FWT) tissue penetration times of 2 days and a YBT retention of 0.2 were assumed.

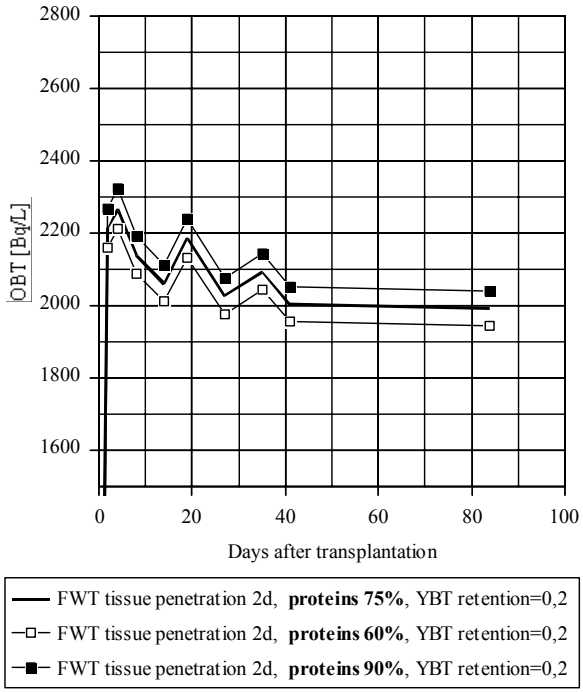

Fig. II.6.6. BIOCHEM model predictions of temporal changes in Cage 3 and 4 mussel tissue OBT concentrations relative to changes in Perch Lake water HTO levels under conditions of varying mussel protein content. Free-water tritium (FWT) tissue penetration times of 2 days and a YBT retention of 0.2 were assumed.

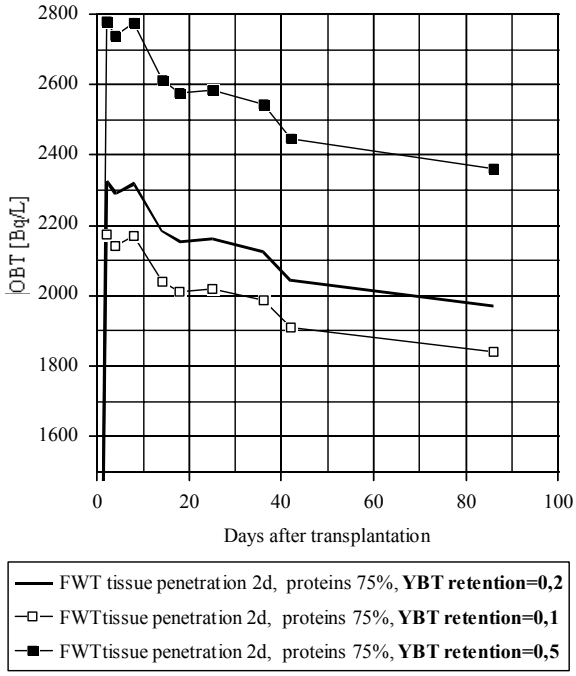

Fig. II.6.7. BIOCHEM model predictions of temporal changes in Cage 1 and 2 mussel tissue OBT concentrations relative to changes in Perch Lake water HTO levels under conditions of varying YBT retention. Free-water tritium (FWT) tissue penetration times of 2 days and a mussel protein content of 75% (with a DNA content of 25%) were assumed.

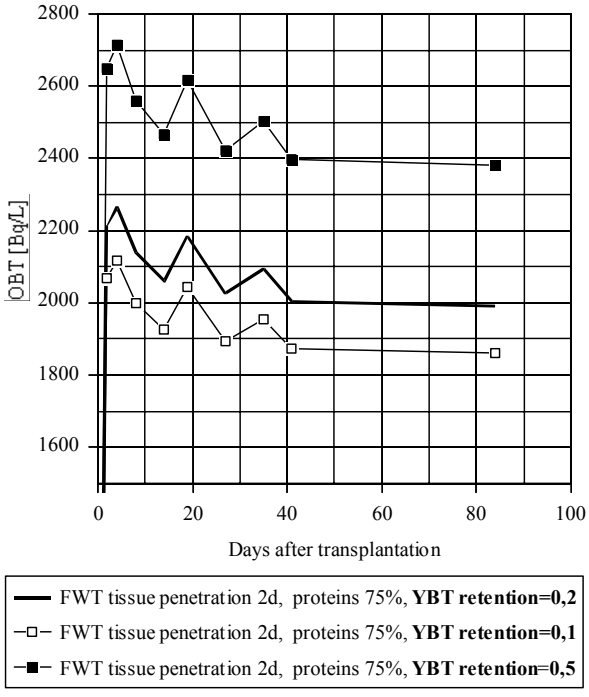

Fig. II.6.8. BIOCHEM model predictions of temporal changes in Cage 3 and 4 mussel tissue OBT concentrations relative to changes in Perch Lake water HTO levels under conditions of varying YBT retention. Free-water tritium (FWT) tissue penetration times of 2 days and a mussel protein content of 75% (with a DNA content of 25%) were assumed.

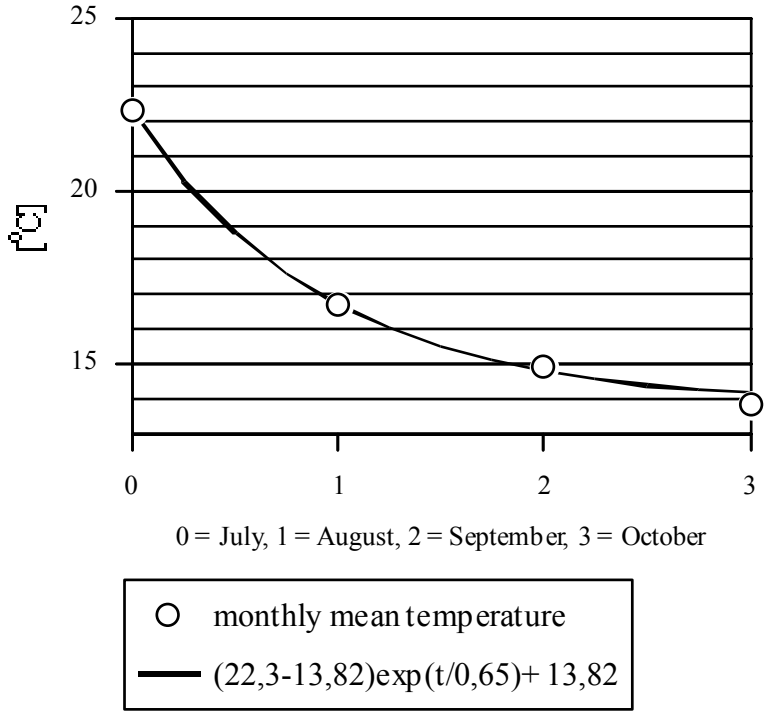

Fig. II.6.9. Approximation of mean monthly Perch Lake water temperature.

Table II.6.1. Summary of BIOCHEM model test conditions for sensitivity analysis to determine the potential influence of mussel percent protein content, mussel percent DNA content, rate of ingress of free-water tritium (FWT) into mussel cells and the YBT retention factor on predicted OBT concentrations in mussel tissue.

Scenario No.	Figure No.	FWT Tissue Ingress (days)	% Protein	% DNA	YBT Retention, R_{YBT}
1. a.	B.3 and B.4	2	75%	25%	0.2
1. b.	B.3 and B.4	1	75%	25%	0.2
1. c.	B.3 and B.4	4	75%	25%	0.2
2. a.	B.5 and B.6	2	75%	25%	0.2
2. b.	B.5 and B.6	2	60%	40%	0.2
2. c.	B.5 and B.6	2	90%	10%	0.2
3. a.	B.7 and B.8	2	75%	25%	0.2
3. b.	B.7 and B.8	2	75%	25%	0.1
3. c.	B.7 and B.8	2	75%	25%	0.5

II.7. Mussel Depuration Scenario model descriptions

II.7.1. BIOCHEM Model

As discussed in Section 8.4, the models used for the depuration scenario (BIOCHEM, EDF, NIRS and AQUATRIT) were the same as those used for the uptake scenario. Detailed descriptions of these models are available in Appendix II.6 of the final report for the uptake scenario. Additional information regarding the BIOCHEM model and its use in the depuration scenario is presented below, as revealed during application of the model to the uptake scenario.

II.7.1.1. Introduction

OBT is traditionally quantified using a methodology that involves rinsing of dry organic matter with tritium-free water prior to combustion to produce an OBT concentration in units of Bq/L combustion water. The BIOCHEM model assumes that when this rinsing process is carried out on dried biological material that is of solid structure, it does not completely eliminate buried tritium (i.e., hydrate-bound tritium, YBT, and tritium bound to "X" atoms (oxygen, nitrogen or sulphur), XBT). The bonds between X atoms and hydrogen or tritium are assumed to form as intra- and inter-molecular H-bonds such as X_i-H/T···X_j. Therefore, in addition to carbon-bound tritium (CBT), the OBT compartment of the BIOCHEM model is defined as:

$$OBT = CBT + XBT + YBT \quad \text{(II.7.1)}$$

Fundamentally, fast proton-triton (H^+/T^+) exchange is assumed to exist between bulk water and XBT and YBT, whereby energetic boundaries, in addition to the spatial structure of the biopolymers, may suppress the H^+/T^+ exchange. Therefore, the calculation of OBT formation and tritium depuration considers:

(1) the energetic boundaries of H^+/T^+ exchange; and
(2) the pathways of XBT and YBT formation.

II.7.1.2. Consideration of energetic boundaries in tritium depuration

The energetic boundaries of H^+/T^+ exchange are derived from the ratios of the tritium distribution in DNA, which is dissolved in HTO with an assumed HTO:YBT:XBT ratio of 1:1.4:1.9 [II.10]. The energy levels ($E_{i/j}$) are calculated according to the Boltzmann distribution law, as follows:

$$N_i = N_j \exp[-\Delta E / (kT)] \quad \text{(II.7.2)}$$

where:

$N_{i/j}$ are the numbers of particles in levels i and j, respectively;
k is the Boltzmann constant;
T is the ambient temperature in degrees Kelvin; and
ΔE (= E_i-E_j) is the difference in energy levels (J).

These parameters are formally represented by differences in temperature, according to (see Figure II.7.1):

$$\Delta E = k \Delta T \quad \text{(II.7.3)}$$

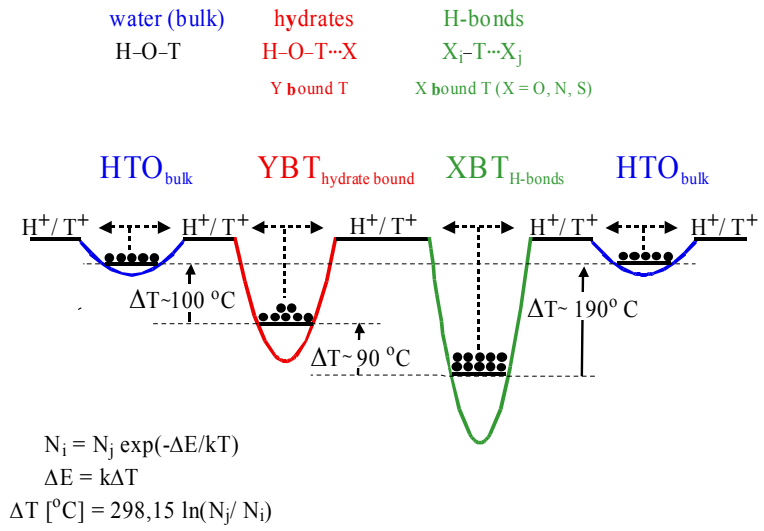

Fig. II.7.1. Energy levels of tritium (T) in DNA.

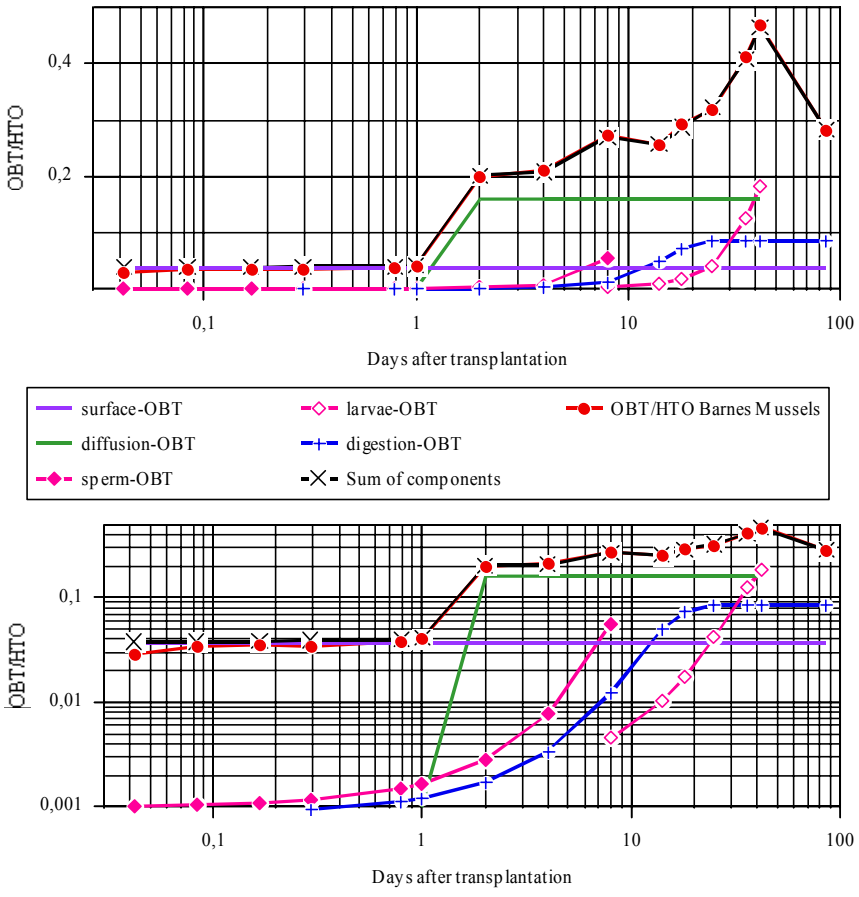

Fig. II.7.2. Comparison of predicted time courses of surface OBT, diffusion OBT, sperm OBT, larvae OBT and digestion OBT with observations for the mussel uptake experiment. The observations are the means of the data from all cages. The ordinate of the lower figure is presented logarithmically to show the detail at small values of the OBT/HTO ratio.

II.7.1.3. Consideration of the pathways of XBT and YBT formation in tritium depuration

Deductions from the use of BIOCHEM in the Mussel Uptake Scenario

The pathways of XBT and YBT formation can be depicted graphically to examine expected temporal changes in the OBT/HTO ratio given by the observed mussel uptake data (Figure II.7.2) to reveal five pathways of OBT formation:

(1) surface OBT, (XBT +YBT),
(2) diffusion OBT, (XBT +YBT),
(3) sperm OBT, (CBT+XBT +YBT),
(4) larvae OBT, (CBT+XBT +YBT),
(5) digestion OBT, (CBT+XBT +YBT)

The pathways of surface OBT and diffusion OBT are expected to be based on non-metabolic growth (i.e., H^+/T^+ exchange), since metabolic OBT formation would not be complete within a time period of a few minutes to hours. The most rapid OBT formation (surface OBT), which is assumed to be complete within 0.1 day, is assigned to XBT and YBT formation near the surface. The next fastest OBT pathway is assumed to be related to diffusion of HTO into the mussel tissue. The initiation of formation of this pool of OBT is expected to begin at the end of the first day and to be complete by the beginning of the second day.

Two additional pathways, possibly corresponding to the formation and release of sperm and larvae by the mussels, are both followed by some OBT loss (Figure II.7.2). The residual OBT can be seen to follow the logistic growth function.

Mussel weight did not increase between the beginning and end of the experiment. As a result, the last type of OBT formation (digestion OBT) is thought to substitute degraded molecules. The resultant newly-formed biopolymers are assumed to contain XBT and YBT from bulk HTO, and C-T labelled amino-acids obtained by the digestion of plankton, which is tritium-labelled during feeding by mussels in Perch Lake.

Depuration is reverse XBT and YBT formation, where re-exchange of exchangeable buried tritium may be restricted because of energetic barriers. Maximum exchangeable OBT values are calculated and shown in Table II.7.1 assuming 25%, 50% and 75% H^+/T^+ exchange. The calculated time dependence of re-exchange of buried exchangeable tritium is the same as that observed in the transplantation studies (Figure II.7.3).

Table II.7.1. Tritium depuration for different pathways in soft tissues of the freshwater Barnes mussel, assuming an HTO concentration in Perch Lake surface waters of 4152 Bq/L.

% Re-exchange from OBT to H_2O	Maximum [Bq/L] OBT loss			
	Surface OBT	Diffusion OBT	Sperm OBT	Digestion OBT
0.25	45	182		52
0.50	89	363	248	113
0.75	134	545		170

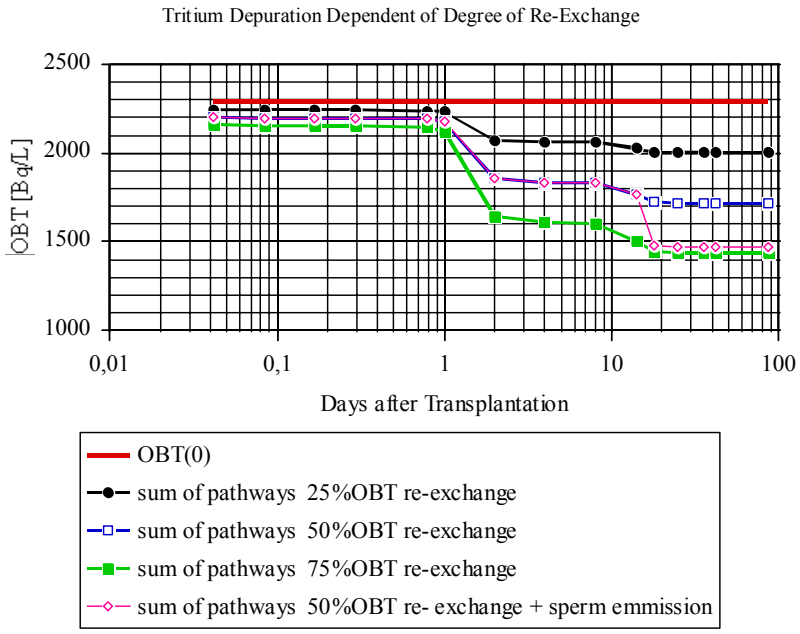

Fig. II.7.3. Estimation of tritium depuration and its dependence on the degree of re-exchange.

Application of BIOCHEM to the Depuration Scenario

With respect to tritium depuration, the BIOCHEM model assumed that H^+/T^+ exchange in surface and diffusion OBT may be as high as 100%. By comparison, the exchange rate for digestion OBT was assumed to be at most 70%, which corresponds to the ratio of physically-based OBT to total OBT on the 86th day of the study. Nothing is known about the ratios of XBT and YBT; however, application of Boltzmann's law and the known tritium distribution in aqueous DNA solution allowed the estimation of the activation energies effective in H^+/T^+ exchange. On this basis, at ambient temperature, the increase of energy needed to transfer tritium from YBT to bulk water was assumed to be approximately 100^{o}C, whereas tritium removal from XBT to bulk water was assumed to occur at 190^{o}C (Figure II.7.1). In addition, irreversible tritium deposition in XBT and YBT was assumed to occur, since at 25^{o}C, only molecular rotations would be effective and very rarely atomic vibrations [II.116]. Rotation with any speed around the HO–T···X axis would not be expected to remove tritium from its position in the hydrate bond, and activation of other rotation axes would require energy to break the hydrate bond. This is thought to support the idea of irreversible tritium deposition in XBT and YBT of living systems, with participation or non-participation of body water in H^+/T^+ exchange. Therefore, because of the unknown local distributions and ratios of XBT and YBT, as well as the possibility of restricted H^+/T^+ exchange, a range of time courses for alternative combinations of H^+/T^+ exchange were calculated (Figure II.7.4). The predictions made assuming 25% H^+/T^+ exchange are given in Table II.7.2.

The implication of sperm OBT for the adult mussels that spent their life times growing in Perch Lake prior to transplantation to Upper Bass Lake is expected to be restricted, as demonstrated when calculating the time course of tritium depuration assuming sperm release (with a 50% H^+/T^+ exchange rate) versus an assumption of no sperm release (Figure II.7.2 and Figure II.7.4). In doing so, it was assumed that the specific activity of the sperm is approximately 0.3 times that of the larvae. On this basis, it was assumed that reproduction by males would not have a significant impact on seasonal mussel OBT predictions.

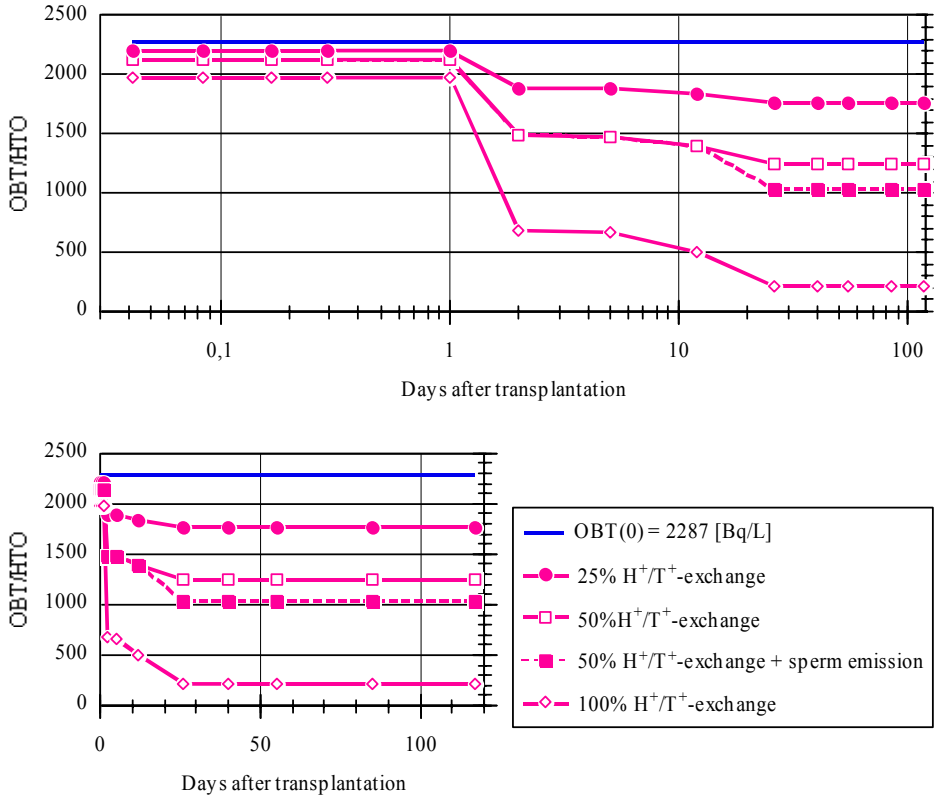

Fig. II.7.4. Tritium depuration as a function of time for alternative assumptions regarding H^+/T^+ exchange. The data are shown with both linear and logarithmic time axes.

Table II.7.2. BIOCHEM model tritium depuration predictions assuming a 25% H+/T+ exchange rate.

Time After Mussel Transplantation	Mussel Tritium Concentration (Bq/L)			
	HTO	Uncertainty	OBT	Uncertainty
0 hours	2,946	589	2,211	442
1 hours	2,503	501	2,211	442
2 hours	2,128	426	2,211	442
4 hours	1,503	309	2,211	442
7 hours	960	192	2,211	442
24 hours	115	23	2,211	442
48 hours	63	13	1,887	377
120 hours	62	12	1,882	376
12 days	62	12	1,840	368
26 days	62	12	1,769	354
40 days	62	12	1,767	353
55 days	62	12	1,767	353
85 days	62	12	1,767	353
117 days	62	12	1,767	353

II.8. Hypothetical Scenario Model Descriptions

II.8.1. German Model (UFOTRI)

II.8.1.1. Introduction

To estimate the spectrum of consequences after accidental releases of tritium from nuclear installations, processes such as dispersion, deposition, re-emission, conversion of tritium gas (HT) into (HTO) and conversion of HTO into organically bound tritium (OBT), must be considered time-dependently. To that purpose, an atmospheric dispersion module has been developed which allows for re-emission after HT/HTO deposition and which considers all relevant transfer processes in the environment (soil, plant and animal) up to approximately 100 hours after the release event (during which time atmospheric transport plays the dominant role). The dispersion module was coupled to a first-order compartment module, which describes dynamically the longer-term behaviour of the two different chemical forms of tritium in the food chains. The physical and mathematical basis of the model, which is called UFOTRI, is described in detail by Raskob [II.69, II.80, II.117].

II.8.1.2. Model description

The present version of UFOTRI is based on the Gaussian trajectory model MUSEMET [II.118]. The importance of the re-emission process necessitates two level modelling of atmospheric dispersion. Primarily, MUSEMET calculates dispersion after a single release event and the subsequent deposition on soil and plants. In a second step, the re-emission of tritium after deposition from soil (evaporation) and plants (transpiration) is taken into account by an area source model specially developed for that purpose and combined with the original model. The area source is simulated by a single source point in the centre of the area, with a given initial widening of the plume [II.119].

All processes which may modify the total balance of the available HT or HTO, such as the conversion of tritium gas into tritiated water (HT into HTO), the transport of tritium into deeper soil layers, the uptake of tritium by the plant root system, and the conversion of HTO into OBT, are taken into account in the atmospheric dispersion module, together with the foodchain pathways such as the production of milk, milk products and beef.

Plant/atmosphere exchange processes

The exchange reaction of the plant with atmospheric tritium takes place via water circulation in the leaves. The mechanisms of the plant/atmosphere exchange are described according to the 'big leaf' approach [II.120, II.121]. There the aerodynamic, boundary layer and stomatal resistances determine the sensible and latent heat fluxes at the earth's surface. At night, when the stomata are closed, the stomatal resistance is replaced by the epidermal resistance, which is a factor of 15 higher than the minimum stomatal resistance. To determine the HTO exchange between the atmosphere and the vegetation, the model of Belot et al. [II.49] has been used in UFOTRI. There the temperature, the inorganic content of plant matter and the transfer resistances determine the uptake of tritium in the vegetation, as well as the loss of tritium from the vegetation. Because vegetation occurs always as a plant population (fields, forests, etc.), an effective stomatal resistance (now the canopy resistance) is calculated by dividing the stomatal resistance of a single plant by the leaf area index, which is the area of all leaves of the vegetation normalised to one square meter. UFOTRI considers four different plant species, namely nutriment plants (leafy vegetables, potatoes and winter wheat) and pasture grass.

Soil/atmosphere exchange processes and transport in soil

The deposition process of HT and HTO to soil is expressed in the form of a deposition velocity. The HT deposition rate depends on the type of soil and on the free pore space in the first soil layer (5 cm). Once deposited, HT is transformed into HTO very quickly as a result of micro-organism activity. Only the transformed part of HT remains in the soil.

The dry deposition rate of HTO to soil is calculated as a function of the soil properties and atmospheric turbulence. It is expressed as the inverse of the atmospheric and soil exchange resistances.

The process of wet deposition of HTO to soil is considered as washout from the whole plume. The washout coefficients depend on the intensity of precipitation. They are very small for HT, i.e. wet deposition of HT is neglected.

The re-emission processes are modelled by coupling the re-emission of HTO to the evaporation of water from soil. Only the water content in the top five centimetres of soil is taken into account. The transport of water between each layer due to matrix forces is considered. Therefore the hydraulic conductivity and the suction tension of the soil are calculated, according to a proposal from Walley and Hussein [II.122].

Plant transpiration is derived by using Monteith's bulk resistance formula for the actual transpiration [II.123]. The uptake of HTO by the plant root system depends on the actual transpiration of the plant, which is compensated by the root uptake.

The evaporation of water vapour from the soil is calculated by applying Monteith's formula together with the remaining radiation reaching the ground surface.

Exchangeable/non-exchangeable tritium

In plants contaminated with HTO, tritium atoms are incorporated into the organic matter of the plant (OBT). A photosynthesis sub-model calculates the hourly build-up of organic material. The photosynthesis rate is based on the amount of CO_2 assimilation within each time step. The specific concentration of the built-up OBT is connected to the actual specific tritium concentration in the water compartment of the plant. The OBT transfer model is only physically based for the hours with solar insolation. During the night, it is assumed that the transfer rate is a quarter of the daily mean.

Cow compartment

In the atmospheric part of UFOTRI, all exchange processes involving the cow that are important for the ingestion pathways via milk, beef and dairy products, are also considered. The transfer rates are in general the same as for the long-term ingestion module of UFOTRI (see below), which were derived on the basis of a constant daily rate, but converted to an hourly value.

Long-term ingestion module of UFOTRI

In this part of the model, the long-term behaviour of tritium in the environment, and the assessment of the long-term doses to the population from the consumption of tritium-contaminated foodstuffs, are described. To that purpose, the model calculates the time-integrated tritium concentrations in vegetables, meat and milk products. To describe the transport processes mathematically, the areas in the environment where tritium may appear are divided into different compartments. The transfer rates, which quantify the transfer

processes, are averaged values valid for longer periods and calculated assuming equilibrium conditions. The exchange processes between the individual compartments are treated by first order differential equations that describe linear dependencies of tritium concentrations or concentration differences [II.124].

II.8.2. Canadian Model (ETMOD)

II.8.2.1. Introduction

- Model Name: ETMOD (Environmental Tritium MODel).
- Model Purpose: ETMOD was developed as a research code but has been used as an assessment tool to predict the consequences of accidental tritium releases to the atmosphere from tritium-handling facilities. It is intended to be realistic.
- Type of Model: ETMOD is a dynamic, process-oriented model.
- Compartments Considered: Air, soil, plants and animals.
- Transport Processes Considered: ETMOD covers many transport and exposure pathways including atmospheric dispersion, dry and wet deposition to soil, migration in soil, re-emission from soil, and transfer to vegetation, animals and animal products. It can handle releases of either tritium gas (HT) or tritiated water vapour (HTO) and addresses organically bound tritium (OBT) formation in plants.
- Endpoints: Final endpoints are ingestion and inhalation (including skin absorption) doses to humans. Intermediate endpoints include tritium concentrations in the various environmental compartments [II.57, II.58].

II.8.2.2. Key assumptions and modelling approaches

Atmospheric dispersion

Air concentrations are calculated using the straight-line Gaussian plume model, with the lateral dispersion parameter given by Briggs' equations [II.125] and the vertical dispersion parameter by the Smith-Hosker approach [II.126, II.127]. Atmospheric stability class is determined by similarity theory. The flux-profile equations are solved iteratively to yield values of the friction velocity and Monin-Obukhov length, which together with the surface roughness length, allow the stability class to be derived from Golder's nomogram [II.128]. A key assumption in ETMOD is that the wind direction remains constant over time. Plume depletion due to deposition of airborne material to the underlying surface is modeled using the source depletion method.

Deposition and behaviour in soil

Dry deposition to soil is modelled through the use of a deposition velocity, values of which are determined at each time in the simulation by the multiple resistance approach. The aerodynamic and boundary-layer resistances are calculated using meteorological data for the current time step. The surface resistance is taken from Wesley [II.59], who provides values as a function of season and land use. The aerodynamic resistance is governed by meteorological conditions alone, but the boundary-layer and surface resistances depend on the contaminant in question (HT or HTO). Wet deposition is also modelled through the use of an effective deposition velocity, which is calculated as the product of a washout ratio (equal to 2×10^4) and the rainfall rate. For both wet and dry deposition, the HTO flux to the soil is determined by multiplying the deposition velocity by the air concentration.

The time-dependent HT concentration in soil is determined as a function of time from Fick's equation modified to allow for the first-order conversion from HT to HTO. The conversion rate depends on the deposition velocity, the effective HT diffusion coefficient in soil and the air-filled volume fraction of the soil. The time-dependent HTO profile in soil is determined by an advection-diffusion equation that considers diffusion, advection by infiltration, loss due to plant uptake and re-emission.

Tritium transfer between air and plants

The exchange of tritium from air to plants (and from plants to air) is modeled as a diffusion process that depends on the exchange velocity and the concentration gradient between air and leaf. The exchange velocity is the same as the deposition velocity used to model dry deposition to soil, except that the surface resistance is representative of plants rather than soil. The exchange velocity is assumed to drop to zero when the stomata are closed so that there is little HTO uptake or loss from the plant at night. In calculating the plant concentration, allowance is also made for transpiration, which is modelled as a mass flow process. The plant fractional water contents are assumed constant with time as the plant grows.

The above model is used for green vegetables, fruit vegetables, cereals and grass. The model for root crops assumes uptake of tritium only from soil water with the transpiration stream.

Air concentrations due to re-emission

Air concentrations from re-emission are calculated by multiplying the plant-to-air emission rate by a dispersion factor. To this end, the area over which the plume is likely to travel is discretized into terrain elements, each of which is treated as a Gaussian point source with an initial lateral dispersion parameter that reflects the crosswind width of the element. The source strength for a given element is assumed to equal the average re-emission rate over the element. The air concentration due to re-emission at a given downwind distance is found by summing the contributions from all upwind elements. The role of soil re-emission in determining air concentrations is neglected.

Dry matter production in plants

Gross photosynthesis rates are calculated using the CO_2 consumption model [II.60–II.63] and depend on air temperature, the resistance to CO_2 uptake by the plant and the photosynthetically active radiation reaching the plant, which in turn depends on leaf area index. The production rate of dry matter is based on net photosynthesis (the difference between gross photosynthesis and respiration), taking into account both growth and maintenance respiration. Plant dry mass is updated using the dry matter produced in the time step. The wet vegetation mass is then calculated from the dry mass and the fractional water content, which is assumed to remain constant as the plant grows. The calculation stops when a pre-specified plant mass or harvest time is reached.

OBT formation in plants

The dry matter produced at a given time is assumed to have a T/H ratio equal to 0.6 times the T/H ratio in the plant water that takes part in the photosynthesis at that time. All dry matter production and OBT formation is assumed to take place in the above-ground part of the plant, even for root crops. ETMOD assumes that dry matter production and OBT formation do not occur at night in the absence of photosynthesis. OBT concentrations following exposure decrease due to dilution with new uncontaminated dry matter. ETMOD does not account for the slow conversion of OBT to HTO in plants due to metabolic processes.

Translocation

ETMOD can handle five types of crops (pasture, leafy vegetables, non-leafy vegetables, root vegetables and grain). In each case, the plant is treated as a single compartment with uniform concentrations throughout. This means that translocation between different parts of the plant must be addressed outside ETMOD.

Concentrations in animals

ETMOD calculates time-dependent HTO concentrations in the aqueous phase of animals using a simple mass balance equation in which the increase or decrease in concentration over a time step is determined by the difference between the amount of HTO taken in and the amount lost. The model assumes that the OBT ingested by animals is converted to HTO, and OBT concentrations are not estimated. All animals are assumed to graze for the 12-hour period from 8 am to 8 pm and to ingest nothing overnight. ETMOD can handle five types of animals (dairy cows, beef cows, chickens, pigs and sheep); the model is the same in each case but parameter values differ from animal to animal. Concentrations in eggs and chickens are assumed to be the same.

Doses

ETMOD calculates the committed effective dose to adults from inhalation, skin absorption and ingestion. The skin absorption dose is conservatively assumed to equal the inhalation dose. The ingestion dose takes into account the ingestion rates of the different components of the diet, and the different dose coefficients for HTO and OBT. Animal OBT does not contribute directly to dose because OBT concentrations are not calculated in animal products.

II.8.2.3. Parameter values

ETMOD contains a large number of parameters for which values must be specified. These include fixed values for parameters relating to site characteristics, soil properties, plant properties, weather data, dosimetry and the scenario in question. In addition, hourly values of such meteorological parameters as wind speed, air temperature, humidity, cloud cover and precipitation must be entered, together with time-dependent release rates.

II.8.2.4. Model uncertainties

A rigorous uncertainty analysis of ETMOD has not been undertaken. However, the uncertainties on the predictions can be deduced from the results of an uncertainty analysis carried out for UFOTRI, a code similar to ETMOD, for a scenario from BIOMOVS II that was similar to the hypothetical scenario [II.64]. The 95% confidence interval varied between a factor 3 and 10 depending on the endpoint. The lower values were obtained for the concentration of OBT in edible plant parts and animal products. The higher values were obtained for HTO concentration in grass and soil. For all endpoints, the uncertainties in the concentrations were largest for predictions made immediately after the exposure, indicating that conditions during the release must be well known if the concentrations are to be predicted accurately. The confidence interval was relatively low (less than a factor 5) for the yearly dose, which depends more on OBT than on HTO concentrations. These estimates reflect the uncertainty due to parameter values only and do not include those due to model structure.

II.8.2.5. Application of ETMOD to the hypothetical scenario

For the most part, ETMOD could be applied directly to the scenario, but it occasionally had trouble addressing some conditions because of the way it is structured. These cases are listed below, together with some of the other key assumptions that affected the predictions:

- The meteorological conditions after the first 6 hours were based on real hourly data collected for a site near Montreal, Canada.
- ETMOD runs on hourly meteorological data so it was difficult to simulate the 15-minute rainfall that occurred during the release in Case 2. In practice, results for this case were obtained by taking the average of the predictions of two separate simulations, one in which rain fell throughout the release and the second in which no rain fell.
- No distinction was made between different types of root crops or fruit crops. The predictions for radishes, turnips, potatoes and carrots were all the same, as were the predictions for beans, peas and tomatoes.
- ETMOD assumes little plant uptake or loss of HTO, and no OBT formation, at night.
- ETMOD cannot handle more than one crop cycle per year. The simulations ended at the latest harvest time for a given crop. At longer times, the concentration in the crop was assumed to decline at the rate predicted just before harvest. The crops were stored and eaten (by animals or humans) throughout the rest of the year, and contributed to the dose in this period, on the assumption that a sufficient amount was available to meet all needs. The exception was green vegetables, which were not stored and did not contribute to the dose past the time of last harvest.
- The cows were assumed to eat grain and grass throughout the year, at the rate specified in the scenario description. These crops were assumed to be contaminated throughout the year at the level described in the previous point.
- Crops eaten by humans between the release and the first harvest were assumed to be uncontaminated and not to contribute to the dose.
- Crops that were already being harvested when the release occurred were ingested by humans and animals as soon as the release ended. Ingestion doses would be much lower if consumption began even a few hours later.
- ETMOD is unable to calculate OBT concentrations in animals. The values given for the animal HTO concentrations are the total tritium concentrations, with all OBT considered as HTO.
- Doses were calculated for adults only since ETMOD is not set up to handle infants.
- Results for the air pathways were obtained by setting the deposition velocities to zero, thereby preventing any contamination of the soil. Doses due to the soil pathways were obtained by subtracting the results for the air pathways from the results for all pathways.
- The time steps in ETMOD varied from 0.1 hour for the first 24 hours of each simulation to 1.0 hour for the remainder of the run.

II.8.2.6. Discussion of AECL results

Case 1 – HTO Release

The predicted tritium concentration in above-ground plants is high immediately after the release as a result of direct uptake of HTO. Most of this tritium is quickly lost to the air once the plume has passed and concentrations drop rapidly at first. The rate of decrease slows at later times as OBT, with its longer biological half-life, begins to dominate the tritium content

of the plant. The concentration in root crops is initially relatively low but builds up gradually to a maximum after about one day before decreasing slowly. This reflects the time variation of the soil concentration, with a lag of a few hours, since root crops in ETMOD draw all their tritium from soil water. Concentrations in animals also show a low initial value followed by an increase to a maximum and a subsequent decline. This pattern reflects the relatively slow build-up of tritium in the animals coupled with the dynamic behaviour of tritium concentrations in their feed.

The adult dose for the HTO release of Case 1 is dominated by inhalation/skin absorption and ingestion of grain and milk. Green vegetables, tomatoes, beef and chicken make a significant contribution to the ingestion dose with other items of the diet less important. Most of the dose comes from the air pathways. HTO is predicted to contribute the largest amount, but this is likely an artefact of ETMOD, which does not track OBT in animals. None of the crops except green vegetables is predicted to impart an HTO dose via the air pathway. This is reasonable for carrots, potatoes, tomatoes and grain. These crops are not harvested for at least 2 weeks after the release, at which point all of the HTO that was originally taken up has been re-emitted to the atmosphere. The zero doses for radishes, peas and beans result from an artefact in ETMOD, which treats all fruit vegetables and all root crops alike. Radishes are modelled as potatoes and peas and beans as tomatoes, which means they are not consumed for at least 2 weeks after the release. This implies that the total dose is underestimated, as is the contribution of fruit and root vegetables to the dose.

Case 1 – HT Release

All concentrations and doses for the HT release are much lower than those for the HTO release because of the relatively small fraction of HT that is converted to HTO. Concentrations in all endpoints start off low, increase to a maximum and then decrease, reflecting the fact that the system is driven by the concentration in soil water, which is the source of HTO for an HT release. Concentrations drop off with time faster for the HT release than for the HTO release because little OBT is formed in the absence of an initial airborne HTO plume. HTO therefore makes up a greater fraction of the total tritium in the various compartments compared to the HTO release and the decay rate is correspondingly higher. Because the HTO source is in the soil, the dose is dominated by the soil pathways, with the various compartments contributing to the total dose in more or less the same proportions as for the HTO release. The total dose from the soil pathways is only about a factor of 3 lower than for an HTO release but the doses from the air pathways are four orders of magnitude lower. HTO is predicted to contribute somewhat more than OBT to the total dose, but this may be an artefact of the way animals are modelled in ETMOD, as noted above.

Case 2 – HTO Release

The air concentrations for Case 2 are relatively high because of the neutral meteorological conditions, leading to initial concentrations for green vegetables, fruit vegetables and cereals that are higher than those for Case 1 by a factor of about 2.5. The initial concentrations for root crops are a factor 13 higher than for Case 1, reflecting the much higher soil water concentrations due to washout in Case 2. The animal concentrations are a factor of 4 higher for Case 2. These ratios tend to decrease over time, although the concentrations in a given compartment show the same general shape with time for both cases. The total dose is a factor 3.3 higher for Case 2 than for Case 1. The increase is only a factor 2.3 for the air pathways but a factor 27 for the soil pathways because of the much higher deposition. The dose from the air pathways remains greater than from the soil pathways, but only by a factor of 2 rather than a

factor of 24 as it was for Case 1. The total dose, and the contribution of radishes, beans and peas to the dose, is probably underestimated for the reasons given above.

Case 3 – HTO Release

Because this case involves a night-time release, there is little initial uptake of HTO by the plants and no OBT formation. The ingestion pathways therefore follow the same pattern as for the HT release of Case 1, with movement through the food chain driven by the HTO concentration in the soil. Accordingly, the initial environmental concentrations are low, rise through a peak and drop off relatively quickly because little of the tritium in the plant is in the form of OBT. Ingestion doses are low and dominated by the soil pathways, but the total dose is the highest of any of the cases due to inhalation, reflecting the high air concentration for these stable conditions.

II.8.3. Japan (Kyoto) Model

The scenario is described rather simply. However, the modeler needs values for many parameters, most of which are unknown to him. Therefore he needs to make assumptions or use analogies from related experimental experience. The main features of the Kyoto model are as follows:

(1) The Gaussian dispersion model was used to calculate tritium concentrations in the primary plume.

(2) In the case of the HT release, conversion to HTO after dry deposition was taken into account. Human dose after HT release is mainly due to HTO re-emitted from the soil.

(3) In the case of the HTO release, tritium exchange between air and soil was assumed to occur quickly and concentrations in the air and soil compartments were assumed to be in equilibrium throughout the release. Depletion and re-emission were assumed to compensate each other. Thus neither of these processes was modelled explicitly and no secondary plume was considered in the model calculations.

(4) The level of free-water tritium in plants reaches equilibrium with the concentration in air moisture by the end of the exposure time.

(5) Leafy vegetables take up tritium through both the air pathway and the soil pathway, while root vegetables access only the soil pathway.

(6) The OBT specific activity in crops was assumed to be 1/1000 of the free-water tritium specific activity at the end of the exposure period. This value was maintained through the harvest period.

(7) The value of the washout coefficient was assumed to be 4.6×10^{-4} s^{-1}.

(8) Human consumption of contaminated animal foods continues until the end of November.

(9) The dose coefficients presented in ICRP Publication 56 [II.129] were used.

II.8.4. Japan (Japanet) Model – EESAD Code and Food Chain Model

II.8.4.1. Introduction

JAPANET used the EESAD code and a food chain model to generate results for the Hypothetical Scenario. The EESAD code, which was developed by the National Institute of Radiological Sciences (NIRS), is a random walk model [II.30] that calculates the spatial distribution of particles released from the source and tracked in a Lagrangian sense through the atmosphere.

The food chain model was developed specially for use in the Hypothetical Scenario. It is a static model whereas the EESAD code is dynamic.

II.8.4.2. Atmospheric dispersion

Atmospheric dispersion model

Particles are advected by the mean wind and diffused by atmospheric turbulence. The position of a given particle at time t+Δt after the release, ($x_{t+\Delta t}$, $y_{t+\Delta t}$, $z_{t+\Delta t}$), is expressed in terms of its position at time t (x_t, y_t, z_t):

$$x_{t+\Delta t} = x_t + u_x \Delta t + dx$$

$$y_{t+\Delta t} = y_t + u_y \Delta t + dy \qquad \text{(II.8.1)}$$

$$z_{t+\Delta t} = z_t + u_z \Delta t + dz$$

where:

u_x, u_y, u_z are the mean wind speed in the x, y and z directions; and
dx, dy, dz are the turbulent displacements:

$$dx = \sqrt{24\ K\ \Delta t}\ (0.5 - R(1)) \qquad \text{(II.8.2)}$$

where:

R(1) is a uniform random number in the domain (0-1); and
K = diffusion factor.

dy and dz are expressed in the same manner using equations similar to Equation II.8.2.

The diffusion factor, K, is calculated from the following equation:

$$K = \frac{1}{2} \cdot \frac{d\sigma^2(r)}{dt} = \frac{1}{2} \frac{dr}{dt} \cdot \frac{d\sigma^2(r)}{dr} = u\sigma(r)\sigma'(r) \qquad \text{(II.8.3)}$$

Table II.8.1. $\theta_{0.1}$ (degrees) for each stability case.

Stability	A	B	C	D	E	F
$\theta_{0.1}$	50	40	30	20	15	10

Table II.8.2. Values of the parameters σ_1, a_1, a_2 and a_3.

Stability	Downwind distance (x)					
	x ≥ 0.2 km				x < 0.2 km	
	σ_1	a_1	a_2	a_3	σ_1	a_1
A	768.1	3.9077	3.898	1.733	165	1.07
B	122.0	1.4132	0.49523	0.12772	83.7	0.894
C	58.1	0.8916	-0.001649	0.0	58.0	0.891
D	31.7	0.7626	-0.095108	0.0	33.0	0.854
E	22.2	0.7117	-0.12697	0.0	24.4	0.854
F	13.8	0.6852	-0.1227	0.0	15.5	0.822

The diffusion coefficients, σ_y and σ_z, are functions of stability and downwind distance and are calculated using the Pasquill-Meade equations [II.35, II.36]:

$$\sigma_y = 0.67775 \cdot \theta_{0.1} \cdot (5 - log_{10} x) \cdot x \tag{II.8.4}$$

where:

x is the downwind distance (km); and
$\theta_{0.1}$ = dispersion angle (degrees) at x = 0.1 km (see Table II.8.1).

$$\sigma_z = \sigma_1 \cdot x^{a_1 + a_2 \ log \ x + a_3 (log \ x)^2} \tag{II.8.5}$$

where:

x is the downwind distance (km); and
σ_1, a_1, a_2, a_3 are the functions of stability and downwind distance (see Table II.8.2)

Air concentrations

Air concentrations are estimated using the Kernel Density Estimator (KDE) method [II.37]. The KDE method assumes that particles diffused by a random walk process spread as a Gaussian distribution about the centre of each particle. The contribution of a particle at position (X, Y, Z) to the concentration χ at (x, y, z) is expressed by Equation II.8.6:

$$\chi(x,y,z) = \frac{q}{(2\pi)^{3/2}\sigma_x\sigma_y\sigma_z} exp\left\{-\frac{1}{2}\frac{(x-X)^2}{\sigma_x^2}\right\} \cdot exp\left\{-\frac{1}{2}\frac{(y-Y)^2}{\sigma_y^2}\right\} \cdot$$

$$\left[exp\left\{-\frac{1}{2}\frac{(z-Z)^2}{\sigma_z^2}\right\} + exp\left\{-\frac{1}{2}\frac{(z+Z-2z_g)^2}{\sigma_z^2}\right\}\right] \tag{II.8.6}$$

where:

z_g is the height of interest (m);
q is the release rate.

Deposition models

Wet deposition

Wet deposition, G_w, onto the ground surface during time step Δt is calculated by the following equation:

$$G_w = \sum_{n=1}^{N} \alpha_n \, Q_n \left\{ 1 - exp \, (-\Lambda \, \Delta t) \right\} \tag{II.8.7}$$

where:

α_n is the contribution ratio of particle n;
Q_n is the activity of particle n in the current time step (Bq);
Δt is the time step (s);
Λ is the washout coefficient, $\Lambda = 5.0 \times 10^{-5} \, J^{0.8}$ (s^{-1}); and
J is the rain intensity (mm/h).

Dry deposition

Dry deposition, G_d, onto the ground surface during time step Δt is calculated by the following equation:

$$G_d = \sum_{m=1}^{M} \alpha_m \, Q_m \left\{ 1 - exp \, (-k \, v_g \, \Delta t) \right\} \tag{II.8.8}$$

where:

α_m is the contribution ratio of particle m;
Q_m is the activity of particle m in the current time step (Bq);
Δ_t is the time step (s); and
v_g is the deposition velocity (m/s).

The parameter k describes the contribution to deposition of a particle at height h_p above the surface:

$$k = 2.0 \cdot \left(1 - \frac{h_p}{\Delta_z} \right) / \Delta_z \tag{II.8.9}$$

where:

h_p is the height of particle (m); and
Δ_z is the layer height contributing to deposition (m).

Infiltration from surface soil to deeper layers

It is assumed that tritium deposited on surface soil infiltrates to deeper layers at an infiltration rate K_{perm}. Infiltration causes the tritium concentration on the surface soil to decrease with time after deposition according to the following equation:

$$q_{grn}(x,y)(t) = q_{grn}(x,y)(0) \left\{ 1 - exp\left(-K_{perm} \cdot t\right) \right\} \quad \text{(II.8.10)}$$

where:

$q_{grn}(x,y)(0)$ is the tritium activity in surface soil immediately after exposure at mesh location (x,y) (Bq/mesh); and

$q_{grn}(x,y)(t)$ is the tritium activity in surface soil at time t (h) after exposure at mesh location (x,y) (Bq/mesh).

Re-emission from surface soil to air

Usually, re-emission (evaporation) from surface soil to air occurs due to the difference in tritium concentration between air and soil. But evaporation is a complex phenomenon that depends on many meteorological parameters (temperature and vapor pressure at the soil surface, etc.). The re-emission rate from surface soil to air has been reported in some field experiments. So EESAD models re-emission very simply based on the measured re-emission rate and the difference between the soil and air concentrations:

$$q_{re} = \left(q_{grn} - q_{air}\right) \cdot \left(1 - e^{re_{HTO} \cdot t}\right) \quad \text{(II.8.11)}$$

where:

q_{re} is the total re-emission (Bq);

re_{HTO} is the re-emission rate (h^{-1});

q_{grn} is the HTO concentration on surface soil (Bq/m^2); and

q_{air} is the HTO concentration in air above the soil (Bq/m^2).

The locations where re-emission occurs become secondary sources of tritium. EESAD handles these sources in the following simple way, since they are difficult to model in detail. Re-emitted tritium activity is added to the air concentration in the hour in which re-emission occurs. But in the next hour, the re-emitted activity is removed from the air.

The calculation of atmospheric dispersion, deposition and re-emission of tritium with the EESAD code was validated for three scenarios from Europe and Canada in the IAEA BIOMASS program [II.34].

II.8.4.3. Food chain pathways and dose estimation

The Japanet model considers doses due to inhalation, skin absorption and ingestion.

Ingestion doses arise from the intake of plant and animal products. The tritium concentration in crops eaten by humans is calculated considering uptake from both air and soil. But it is

assumed that tritium directly deposited on plants is removed before humans eat the plant. The edible parts of root vegetables are washed before eating since they are covered by soil. Fruit vegetables such as apples and tomatoes are also washed before consumption. The edible parts of other fruit vegetables (oranges, bananas, peas) are covered by a skin that is removed before eating. Cereals (grains) have a husk and tritium on the husk will be removed when these crops are processed. Tritium may also be removed from all food products that are processed or cooked.

The tritium concentration in grass and grain eaten by animals is calculated taking into account uptake from the air, root uptake and direct deposition. The tritium concentration on the grass leaves is assumed to be the same as the tritium concentration on the soil surface.

Inhalation and skin absorption

It is assumed that the inhalation dose is caused by breathing tritiated water vapour (HTO); the contribution of HT is not considered.

$$D_{inh} = DCF_{inh} \cdot \left(\frac{2Br_{day} + Br_{night}}{3} \right) \cdot \int C_{air}(t)\ dt \qquad \text{(II.8.12)}$$

where:

D_{inh} is the inhalation dose (Sv);
$C_{air}(t)$ is the air concentration at time t (Bq/m^3);
DCF_{inh} is the dose conversion factor for inhalation (Sv/Bq);
Br_{day} is the daytime breathing rate (m^3/h); and
Br_{night} is the breathing rate when sleeping (m^3/h).

The dose due to skin absorption is also considered. The intake of water by skin absorption is 90 ml/day, which is 0.69 times the water intake by inhalation (130 ml/d) [II.132]. So we assumed the dose due to skin absorption is 0.69 times the inhalation dose:

$$D_{skin} = 0.69\ D_{inh} \qquad \text{(II.8.13)}$$

Ingestion

It is assumed that the ingestion dose is caused by two forms of tritium in food: HTO and organically bound tritium (OBT).

Dose estimation

$$D_{i,ing\_HTO} = DCF_{ing\_HTO} \cdot C_{i,HTO} \cdot W_i \cdot f_{i,water} \cdot N_{i,day} \qquad \text{(II.8.14)}$$

$$D_{i,ing\_OBT} = DCF_{ing\_OBT} \cdot C_{i,OBT} \cdot W_i \cdot (1 - f_{i,water}) \cdot N_{i,day} \qquad \text{(II.8.15)}$$

$$D_{j,ing\_HTO} = DCF_{ing\_HTO} \cdot C_{j,HTO} \cdot W_j \cdot f_{j,water} \cdot N_{j,day} \qquad \text{(II.8.16)}$$

$$D_{j,ing\_OBT} = DCF_{ing\_OBT} \cdot C_{j,OBT} \cdot W_j \cdot (1 - f_{j,water}) \cdot N_{j,day} \qquad \text{(II.8.17)}$$

where:

D_{i,ing_HTO} is the ingestion dose from crop [i] with tritium in the form of HTO (Sv);
D_{i,ing_OBT} is the ingestion dose from crop [i] with tritium in the form of OBT (Sv);
D_{j,ing_HTO} is the ingestion dose from animal product [j] with tritium in the form of HTO (Sv);
D_{j,ing_OBT} is the ingestion dose from animal product [j] with tritium in the form of OBT (Sv);
DCF_{ing_HTO} is the ingestion dose conversion factor for HTO (Sv/Bq);
DCF_{ing_OBT} is the ingestion dose conversion factor for OBT (Sv/Bq);
$C_{i,HTO}$ is the HTO concentration in edible portion of crop [i] due to root uptake from soil (Bq/kg water);
$C_{i,OBT}$ is the OBT concentration in edible portion of crop [i] due to root uptake from soil (Bq/kg dry weight);
$C_{j,HTO}$ is the HTO concentration in animal product [j] (Bq/kg water);
$C_{j,OBT}$ is the OBT concentration in animal product [j] (Bq/kg dry weight);
W_i is the consumption of crop [i] (kg/d);
W_k is the consumption of animal product [j] (kg/d);
$f_{i,water}$ is the water content of crop [i] (-);
$f_{j,water}$ is the water content of animal product [j] (-);
$N_{i,day}$ is the number of days that humans consume crop [i] (d); and
$N_{j,day}$ is the number of days that humans consume animal product [j] (d).

Tritium concentration in food

The tritium concentration in the edible part of crops is given by:

$$C_{i,HTO} = C_{soil} \cdot R_{i,HTO}$$
$$C_{i,HTO} = C_{air} \cdot R_{i,HTO} \quad \text{(II.8.18)}$$

$$C_{i,OBT} = C_{soil} \cdot R_{i,OBT}/(f_H \cdot 9)$$
$$C_{i,OBT} = C_{air} \cdot R_{i,OBT}/(f_H \cdot 9) \quad \text{(II.8.19)}$$

where:

$C_{i,HTO}$ is the HTO concentration in edible part of crop [i] due to root uptake from soil (Bq/L);
$C_{i,OBT}$ is the OBT concentration in edible part of crop [i] due to root uptake from soil (Bq/L);
C_{soil} is the tritium concentration in surface soil water (Bq/L);
C_{air} is the tritium concentration in air moisture (Bq/L);
$R_{i,HTO}$ is the specific activity ratio of HTO in crop to soil water or to air moisture (-);
$R_{i,OBT}$ is the specific activity ratio of OBT in crop to soil water or to air moisture (-); and
f_H is the hydrogen content (-) in OBT form, assumed as 7%.

The tritium concentration in animal products is given by:

$$C_{j,HTO} = C_{soil} \cdot R_{j,HTO}$$
$$C_{j,HTO} = C_{air} \cdot R_{j,HTO} \quad \text{(II.8.20)}$$

$$C_{j,OBT} = C_{soil} \cdot R_{j,OBT}/(f_H \cdot 9)$$

$$C_{j,OBT} = C_{air} \cdot R_{j,OBT}/(f_H \cdot 9) \quad \text{(II.8.21)}$$

where:

$C_{j,HTO}$ is the HTO concentration in animal product [j] due to intake of grass (Bq/L);
$C_{j,OBT}$ is the OBT concentration in animal product [j] due to intake of grass (Bq/L);
C_{soil} is the tritium concentration in surface soil water (Bq/kg water);
C_{air} is the tritium concentration in air moisture (Bq/kg water);
$R_{j,HTO}$ is the specific activity ratio of HTO in animal product [j] to soil water or air moisture (-);
$R_{j,OBT}$ is the specific activity ratio of OBT in animal product [j] to soil water or air moisture (-); and
f_H is the hydrogen content (-) in OBT form, assumed as 7%.

II.8.4.4. Other assumptions

(1) The air concentration after one month is set equal to the calculated concentration due to re-emission.
(2) A mixing height of 800 m is assumed in the calculation of air concentrations. This value is based on our experience with Level 3 PRAs for nuclear power plants. In Japan, the mixing height ranges from about 800 m to about 2000 m. For these calculations, the mixing height was conservatively set to the minimum value.
(3) Ingestion doses to man from the food pathways (via crops or animal products) are calculated for the first harvest only, because doses for subsequent harvests are negligibly small.
(4) The HTO concentrations in air and soil used to calculate OBT concentrations in crops are those in effect immediately after plume passage. But for the calculation of HTO concentration in crops, the geometric mean concentrations between the release and the beginning of harvest are used as representative values.

In calculating HTO or OBT concentrations in foods, use is made of representative values of the specific activity ratios (SARs) of HTO concentration in food to the environmental HTO concentration, or the HTO concentration to the OBT concentration in individual foods, which are estimated from published references.

II.8.5. French Model

II.8.5.1. Introduction

— Model Name: GAZAXI/CERES
— Model Purpose: GAZAXI 2002 and CERES were developed as research codes from a previous plume tritium model GAZAXI. The aim of these codes is to predict the consequences of accidental releases into the atmosphere. CERES is a Gaussian puff

model and GAZAXI 2002 is a Gaussian plume. These models are dedicated to tritium dispersion and take into account processes such as deposition, re-emission, conversion of tritium gas (HT) into tritiated water vapour (HTO), and the conversion of HTO into organically bound tritium (OBT).

The environmental compartments considered are air, soil, plants and animals. The biosphere model also covers transfers in the food chain and exposure pathways including:

— direct transfer from air to vegetation, followed by transfer to animals and animal products;
— dry and wet deposition to soil, followed by migration from soil to plants and from plants to animals and animal products.

CERES and GAZAXI 2002 can handle releases of either tritium gas (HT) or tritiated water vapour (HTO) and address organically bound tritium (OBT) formation in plants.

The final endpoints of the models are ingestion and inhalation (including skin absorption) doses to humans. Intermediate endpoints include tritium concentrations in the various environmental compartments.

II.8.5.2. Key assumptions and modelling approaches

Atmospheric dispersion

Air activities are calculated using the straight-line Gaussian plume model (in GAZAXI) or the Gaussian puff model (in CERES) with horizontal and vertical dispersion parameters given by Doury's equations. Doury's dispersion parameters depend on atmospheric stability and the travel time between the source and observation point of interest. Two classes of stability are considered: normal ($dT/dz < -0.5^{o}C/100$ m) and weak ($dT/dz > -0.5^{o}C/100$ m), where dT/dz is the vertical air temperature gradient.

Key assumptions are as follows:

— the wind direction remains constant over time in GAZAXI 2002 but may vary with time in CERES;
— for HTO releases in the absence of rain, neither plume depletion due to deposition nor re-suspension is modelled on the assumption that these two processes compensate each other;
— for HTO releases during rain, wet depletion is modeled using Chamberlain's equation [II.131];
— for HT releases, the air concentration is calculated taking into account dry deposition whatever the meteorological conditions (rain or no rain).

Deposition and behaviour in soil

Dry deposition to soil is modeled through the use of a deposition velocity that equals 3.10^{-3} m/s for HTO and 3.10^{-4} m/s for HT. Dry deposition depends on the deposition velocity and the time-integrated air concentration.

Wet deposition is modeled using Chamberlain's equation (Equation II.8.22), which gives the average activity of a rain drop falling through the plume. Indeed, atmospheric tritiated water vapor is easily absorbed by the rain drops. For HT, there is no wet deposition.

$$C_{rain} = \beta \, \chi_{vap}^{atm} \left[1 - \exp\ (-\lambda_r h_1 / v_g)\right] \exp\ (-\lambda_r h_2 / v_g) \qquad \text{(II.8.22)}$$

where:

C_{rain} is the average specific activity of the rain drops ($Bq.kg^{-1}_{water}$);
β is the ratio of the water vapor pressure to that of HTO (1.1) (dimensionless);
χ_{vap}^{atm} is the specific activity of water vapor in air (Bq.kg $^{-1}_{vap}$);
v_g is the rain drop velocity, dependent on drop radius (m/s);
λ_r is the exchange constant between atmospheric water vapor and rain drop (s^{-1});
h_1 is the path length of the rain drops in the tritiated plume (m); and
h_2 is the path length of the rain drops under the tritiated plume (m).

Knowing the specific activity of the rain drops, the HTO deposition to soil is calculated using the rain intensity and the rain duration.

The specific activity of the rain drops calculated by Chamberlain's equation depends on:

— rain drop characteristics (radius, velocity);
— the path length of the rain drops in the plume (which allows for the build-up of tritium in the drops), and the path length under the plume (which allows tritium to be lost from the drops).

Key assumptions are:

— dry and wet deposition lead to tritium activity in the soil layer that contains plant roots. Part of the tritium in the soil evaporates to the atmosphere and part is taken up by the roots. The tritium specific activity in the soil water is calculated by integrating dry and wet deposition during plume passage. Dry deposition of HTO to soil is determined by multiplying the deposition velocity by the air concentration;
— HT deposited to the soil is converted to HTO by soil microorganisms;
— in fine weather, half of the deposited HTO (or half of the HTO from HT conversion) is re-emitted to the atmosphere;
— in rainy weather, all deposited HTO (or all HTO from HT conversion) remains in the soil.

Tritium transfer from air to plants

The exchange of tritium from air to plants is modeled as a diffusion process which depends on the air concentration near the leaves and the exchange velocity between air and leaves [II.49]. The exchange velocity is determined by dividing the leaf area index of the plant by the stomatal resistance, which is assumed to be 300 $s.m^{-1}$ during the day when the stomates are open and 3000 $s.m^{-1}$ during the night when stomates are closed.

Two steps are considered: the incorporation step (Equation II.8.23), which leads to HTO incorporation in the leaves when the airborne plume is present; and the transpiration step (Equation II.8.24), which leads to HTO release from plants to the atmosphere after plume passage.

$$\frac{dA_f}{dt} = \frac{\gamma V_c}{m}\left[C_{air} - \frac{C_{water}^{sat}}{\beta} A_f\right] \quad \text{(II.8.23)}$$

$$\frac{dA_f}{dt} = -\frac{\gamma V_c C_{water}^{sat}}{m\ \beta} A_f \quad \text{(II.8.24)}$$

where:

A_f is the specific activity of tritium in leaf water ($Bq.kg_{water}^{-1}$);
γ is the ratio of HTO exchange velocity to that of H_2O ($\gamma = 0.95$) (dimensionless);
V_c is the exchange velocity between air and leaves (m/s);
m is the water mass in leaves per unit soil surface ($kg_{water}.m_{soil}^{-2}$);
C_{air} is the specific activity of tritium in air near the leaves ($Bq.m^{-3}$);
C_{water}^{sat} is the water vapour concentration at saturation ($kg_{water}.m^{-3}$); and
β is the ratio of the vapor pressure for water to that for HTO ($\beta = 1.1$) (dimensionless).

The above model is used for green vegetables, fruit vegetables, cereals and grass. The model for crops assumes uptake of tritium only from soil water with the transpiration stream.

Air concentrations due to re-emission

Air activity concentrations from re-emission are not calculated. Similarly, plume depletion is not taken into account. It is assumed that these two processes compensate each other and that an accurate estimate of the air concentration can be obtained without modelling either process.

OBT formation in plants

The OBT production model is based on a simple approach which considers that:

- all tritium in organic matter is "organically bound tritium";
- whatever the crop, organic matter is continuously produced and depends essentially on climatic factors;
- there is a relationship between the tritium activity in the organic matter and HTO activity in the free water of the plants.

The model calculates an average tritium incorporation rate in organic matter (Equation II.8.25) taking into account the plant yield at harvest, the dry matter formation rate and the time of growth:

$$\tau_{inc} = 0.53\frac{\tau_{ms}^{veg} Y}{86400\ \Delta t_{growth}} \quad \text{(II.8.25)}$$

where:

τ_{inc} is the incorporation rate of tritium into organic matter ($kg_{water}.m^{-2}_{soil}.s^{-1}$);
0.53is the weighting coefficient ($kg_{water}.kg^{-1}_{dry\ plant}$);
τ^{veg}_{ms} is the fractional dry matter content of the plant ($kg_{dry\ plant}.kg^{-1}_{fresh\ plant}$);
Y is the plant yield at harvest ($kg_{fresh\ plant}.m^{-2}_{soil}$);
86400 is the time conversion factor ($s.d^{-1}$); and
Δt_{growth} is the duration of plant growth (d).

The dry matter produced is assumed to have a T/H ratio of 0.95. To calculate the exchangeable fraction, the dry matter is weighted by a factor 0.53, which corresponds to the T/H ratio multiplied by 90 (the molecular weight of five water molecules, the number of water molecules in one cellulose molecule) and divided by 162 (the molecular weight of cellulose $(C_6H_{10}O_5)_n$).

Concentration in animals

The model takes into account animal contamination by plant ingestion, assuming that the animals graze during the accident and consume grass all the time. The grass can be contaminated via the air-plant pathway and the air-soil-plant pathway. In both cases, the model calculates the specific activity in the grass and then evaluates the activity transferred to the organic matter of the animal product. The integrated activity in the animal is calculated by taking into account a transfer factor, the value of which differs from animal to animal. OBT and HTO activities are respectively determined by multiplying the integrated activity in the animal by the fractional dry matter content and the fractional water content. The activity ingested by humans is then calculated taking into account the rates of consumption of the various animal products:

$$CI_{ani} = Ft_{ani}\ A^{ani}_{ing} \qquad \text{(II.8.26)}$$

where:

CI_{ani} is the integrated activity ingested by the animal from both the air-plant-animal pathway and the air-soil-plant-animal pathway ($Bq.d.kg^{-1}_{anifresh}$);
Ft_{ani} is the animal transfer factor (fraction of daily intake that appears in 1 kg of animal product) ($d.kg^{-1}_{anifresh}$); and
A^{ani}_{ing} is the activity ingested by the animal (Bq).

Doses

The model calculates the committed effective doses to adults from inhalation, skin absorption and ingestion. Skin absorption is assumed to be 0.4 times the inhalation dose. The ingestion dose takes into account the ingestion rates of the different components of the diet and the different dose coefficients for HTO and OBT. Animal OBT concentrations are calculated and contribute to the ingestion dose.

II.8.6. Indian Model

II.8.6.1. Introduction

A multi-compartmental ecological model was used for the calculations (Figure II.8.1). A Gaussian plume dispersion model that accounts for wet depletion due to precipitation was used to calculate ground-level tritium concentrations in air. The dispersion parameters σ_y and σ_z were obtained from Hukkoo et al. [II.132]. The model also calculates concentrations in vegetation (from both air and soil pathways), concentrations in animal products and total doses.

II.8.6.2. Tritium activity in plants

An air-to-plant transfer ratio of 0.1 was assumed based on a transpiration model. After the plume passes, the loss of tritium from the plant is driven by transpiration. It is assumed that HTO to OBT conversion takes place throughout at an average conversion rate based on the time-integrated HTO activity in the plant. Wet and dry deposition rates were used to estimate activity in soil. Wet deposition was calculated using a washout coefficient based on the work of Chamberlain [II.133].

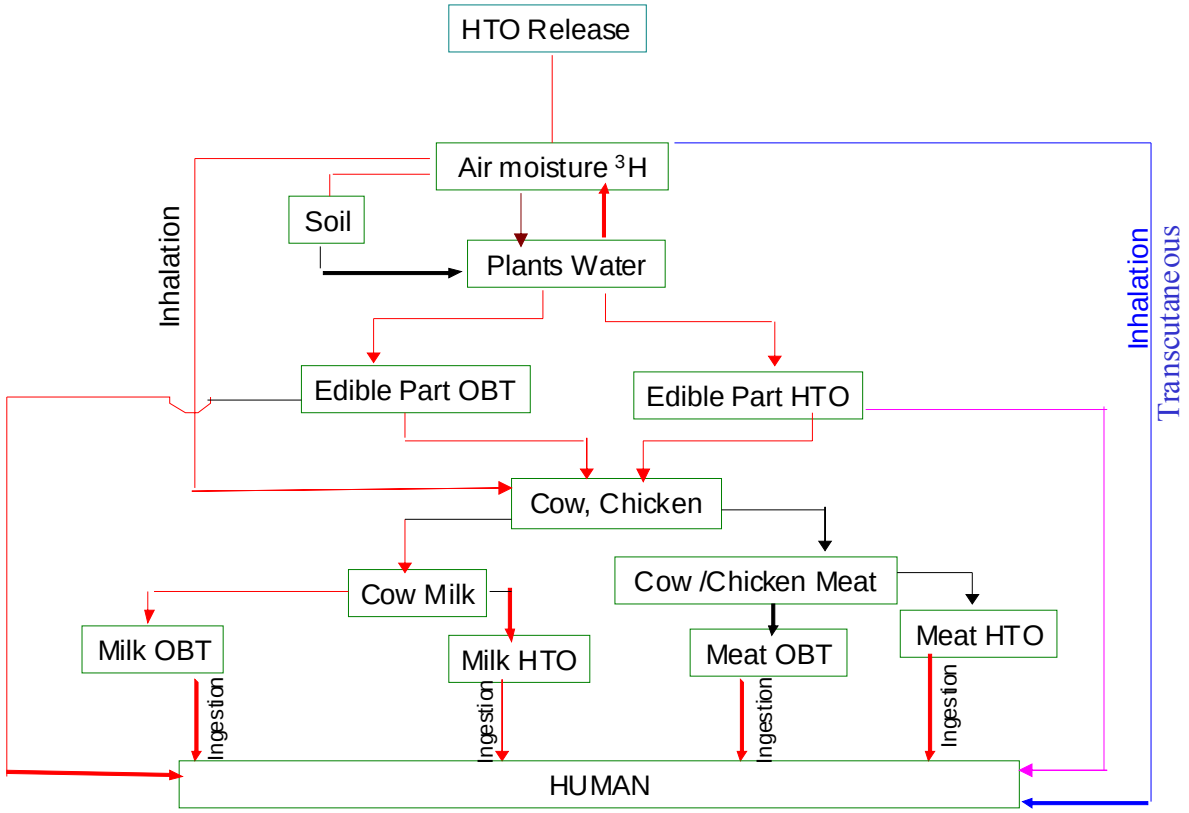

Fig. II.8.1. Description of compartmental model.

II.8.6.3. Tritium activity in animal products

The model assumes that animals become contaminated with HTO through inhalation as well as through ingestion of feed. Transfer coefficients were used to calculate HTO concentrations in milk and meat. Fixed conversion rates were used to calculate the conversion of HTO to OBT in milk and meat. The loss of tritium from the animal was calculated based on biological half-lives.

II.8.6.4. Estimation of intake and total dose

Inhalation, skin absorption and ingestion pathways were considered in evaluating dose. Intake by skin absorption was assumed to equal that by inhalation. Intake of both HTO and OBT from plant and animal products were considered for the ingestion pathway. Dose conversion factors for HTO and OBT were used as specified in ICRP [II.134].

II.8.7. Korean Model

Calculations for the Hypothetical Scenario were carried out using a dynamic compartment model (ECOREA-GH3) developed by KAERI (Korea Atomic Energy Research Institute) on the basis of the long-term model of UFOTRI [II.69, II.80]. The model was specially designed for evaluating the transfer of tritium into grain plants such as wheat and soybeans growing in dry-fields after an acute release from a nuclear facility. In the model, the plant is divided into four compartments: HTO and OBT compartments of the plant body (stem + leaves), and HTO and OBT compartments of the grain. The soil is divided into three layers with depths of 0-5 cm, 5-15 cm and 15-30 cm. There is reversible tritium exchange between all plant compartments except the OBT compartment of grain, in which all organically bound tritium is insoluble and fixed until harvest. The plants take up water from the soil via the body of the plant only.

The mass transfer between compartments can be generally described as:

$$\frac{dA_i}{dt} = \sum_{k=1}^{m} K_{k,i} A_k - \sum_{i=1}^{n} (K_{i,j} + \lambda) A_i \qquad \text{(II.8.27)}$$

where:

A_i (Bq/m^2) is the activity of compartment i;
$K_{k,i}$ is the transfer rate from compartment k to compartment i; and
λ is the decay constant of tritium (6.44×10^{-6} h^{-1}).

Biomass equation

The hydrogen inventory of the plant varies with the growth of biomass, and it subsequently influences the transfer rate between compartments. For these calculations, the plant growth curve was assumed to be sigmoidal with three free parameters, B_1, B_2 and B_3:

$$B(t) = \frac{B_1 B_2}{(B_1 - B_2) e^{-B_3 t} + B_2} \qquad \text{(II.8.28)}$$

The difference in weight between the dry and fresh biomass at time t was assumed to equal the weight of water in the aqueous part of the plant.

HTO deposited during exposure

During exposure, the amount of HTO deposited onto the plant was calculated using Belot's equation [II.49, II.81]:

$$C_{gbh}{}^{o} = \alpha\ R_{ini}\ C_a{}^{o}(1 - e^{-\tau\Delta t}) \qquad \text{(II.8.29)}$$

where:

$C_{gbh}{}^{o}$ is the tritium concentration in body tissue water, Bq/kg;
α is the H/T isotope ratio in air and plant (1.1);
R_{ini} is the mean relative humidity of air during exposure;
$C_a{}^{o}$ is the mean activity of tritium in air moisture during exposure, Bq/kg;
Δt is the exposure time, h; and
τ is the time constant until equilibrium, h^{-1}. τ is defined by:

$$\tau = \rho_{s,ini}/(\alpha\ \mu_{ini}\ \gamma_t) \qquad \text{(II.8.30)}$$

where:

$\rho_{s,ini}$ is the saturated air humidity during exposure, kg/m^3;
μ_{ini} is the water content of plant body at the time of exposure, kg/m^2; and
γ_t is the total resistance from the atmosphere to the stomata, h/m.

At equilibrium, the tritium concentration in the plant body water is given by:

$$C_{gbh}{}^{o} = \alpha \times R_{ini} \times C_a{}^{o} \qquad \text{(II.8.31)}$$

II.8.8. Romanian Model

II.8.8.1. Introduction

- Model Name: FDMH(PC).
- Model Purpose: Research code developed initially as the tritium module in RODOS. A few improvements have been made in the PC version used for these calculations.
- Type of Model: A dynamic, process-oriented model.
- Compartments Considered: Air, soil, plants and animals.
- Transport Processes Considered: Air concentrations and wet deposition must be determined outside FDMH and input to the code. FDMH itself considers deposition to plants and soil, re-emission from plants and soil, and transfer to animals and humans. OBT formation is explicitly considered.
- Endpoints: Final endpoints are ingestion and inhalation (including skin absorption) doses to humans. Intermediate endpoints include HTO and OBT concentrations in the various environmental compartments.

II.8.8.2. Key assumptions and modelling approaches

Atmospheric dispersion was assessed externally using a Gaussian model with SCK/CEN dispersion parameters. Plume depletion was considered explicitly with the same scavenging rate as for wet deposition ($6.0 \times 10^{-5}\ s^{-1}$).

The HTO concentration in plant water (C_{pw}, Bq/kg) is given by the solution of the following equation:

$$M_{wp} dC_{pw} / dt = (v_{exc} \bullet C_a + Tr \bullet C_{sw}) - v_{exc} \bullet \alpha \bullet \rho_{sat}(T_p) \bullet C_{pw} \quad \text{(II.8.32)}$$

where:

C_a is the HTO concentration in air (Bq/m^3);
v_{exc} is the exchange velocity for the canopy (m/s);
Tr is the transpiration rate (kg m^{-2} s^{-1});
C_{sw} is the HTO concentration in soil water (Bq/kg);
$\rho_{sat}(T_p)$ is the saturation vapour pressure at temperature T_p in the stomata;
α is the ratio of HTO and H_2O vapour pressures; and
M_{wp} is the water mass in plant leaves covering 1 m^2 of soil (kg/m^2).

M_{wp} can be estimated from the dry matter fraction of leaves (FD), the leaf area index (LAI) and the specific leaf area (SLA):

$$M_{wp} = (LAI / SLA)\ (1 - FD) \quad \text{(II.8.33)}$$

The exchage velocity is given by the multiple resistance approach:

$$v_{exc} = 1 /(R_a + R_b + R_s) \quad \text{(II.8.34)}$$

where:

R_a is the aerodynamic (turbulent) resistance;
R_b is the boundary layer resistance; and
R_s is the surface resistance (the canopy resistance for deposition to a plant).

The canopy resistance is the stomatal resistance integrated over the depth of the canopy. In our approach it is linked with canopy photosynthesis [II.135].

For each time interval considered, Equation II.8.32 is solved analytically with coefficients that represent mean values for the interval. The solution results in a value for C_{pw} at the end of the interval and a mean value averaged over the interval.

Dry deposition to soil is modelled using the flux from the atmosphere to the upper soil layer, as described by the following equation:

$$M_{ws}\, dC_{sw,1}/dt = v_{exs}\, C_a - v_{exs}\, \alpha\, \rho_{sat}(T_s)\, C_{sw,1} \quad \text{(II.8.35)}$$

where:

$C_{sw,1}$ is the HTO concentration in the upper soil layer (Bq/kg);
$\rho_{sat}(T_s)$ is the saturation vapour pressure at the soil temperature T_s (in FDMH T_s = air temperature);
v_{exs} is the exchange velocity for soil (m/s); and
M_{ws} is the mass of water in the soil layer, which depends on the layer depth z_i and the volumetric water content θ_l

The wet deposition of HTO and the evolution of HTO in the various soil layers is modelled using a simple piston flow approach with a bypass for fast infiltration. This is a crude approach that allows HTO to penetrate the soil too quickly.

The production of OBT in plants is assumed to be proportional to the assimilation (net photosynthesis) rate during daytime and to the basic metabolic rate at night. This leads to the following equations:

P_{OBT} = *fac1*fac2*CO2as_rate*tim*chtomean (daytime)* (II.8.36)

P_{OBT} = *fac1*fac2*ratenight*(LAI/maxlai)*tim*chtomean (night-time)*

where:

P_{OBT} is the OBT produced per m^2 in time period tim;
fac1 is the correction for fractionation and non-exchangeable tritium = 0.6;
fac2 is the conversion from CO_2 to H_2O assimilation rate = 0.41;
CO2as_rate = net CO_2 assimilation rate = gross assimilation rate - respiration rate;
chtomean is the mean concentration of HTO in plant water during time period tim;
ratenight is the maximum night production rate (= 1.2×10^{-3} kg CO_2 m^{-2} h^{-1} for a fully developed plant); and
maxlai is the maximum value of the leaf area index.

The newly formed OBT is stored in the edible part of the crop using the partition fraction derived for the deposition day.

Plant growth is modeled using elements of the WOFOST model; plant parameters are adapted to the region of interest [II.72].

The transfer of tritium from fodder into animal products is described by the equilibrium transfer factor TF and two exponents representing biological excretion rates:

$$C_{m,k} = \sum_{i=H,O} TF_{m,i,k} \sum_{j=1}^{J} \left\{ a_{m,i,k,j} \int_0^{\sigma} I_{m,i}(t) \lambda_{b,m,i,k,j} \bullet \exp\left[-(\lambda_{b,m,i,k,j} + \lambda_r)(T-t) \right] dt \right\} \quad \text{(II.8.37)}$$

where:

$C_{m,k}(T)$ is the activity concentration (Bq kg^{-1}) in animal product m at time T;
$TF_{m,i,k}$ is the transfer factor (d kg^{-1}) for animal product m;
J is the number of biological transfer rates;
$a_{m,i,k,j}$ is the fraction of biological transfer rate j;
$\lambda_{b,m,i,k,j}$ is the biological transfer rate j (d^{-1}) for animal product m; and
$I_{m,i}$ is the feed intake rate (kg/d).

II.8.8.3. Parameters values

The parameter values used to calculate results for the Hypothetical Scenario are the same as those in the RODOS tritium module with the exception of the vegetation period and diet, which were adapted to the scenario. Meteorological data for the first 6 hours were taken from the scenario description, and for subsequent times from archived historical data collected in Karlsruhe.

II.9. Rice Scenario model descriptions

II.9.1. AECL Model

II.9.1.1. Air concentrations

Air concentrations were calculated using a sector-averaged Gaussian plume model. The meteorological data used in the calculations for a given receptor and time period were based on those hours in which the wind direction lay in a 22.5^{o} sector centered on the receptor.

For ST-1, which is only 500 m downwind, separate calculations were carried out for each source and the results added to get the total concentration. For the other receptors, which were further downwind, a single calculation was done assuming the entire release came from a single source with average characteristics of the three sources.

Vertical dispersion was calculated using the Smith-Hosker approach with a surface roughness length of 0.4 m.

Plume rise was calculated using Briggs' equations. The average air temperature for the period in question was used in calculating plume rise under neutral conditions. A temperature 5^{o} warmer was used for unstable conditions, which were assumed to occur during the day. Similarly, a temperature 5^{o} cooler was used for stable conditions, which were assumed to occur at night.

The 100-m meteorological data were used in the calculations. The 100-m wind speeds were reduced by a factor between 0.75 (for near-field receptors) and 0.9 (for far-field receptors) to account for the fact that the plume encounters lower wind speeds as it diffuses down to the ground.

Plume depletion due to dry deposition (with a deposition velocity of 0.003 m/s) was considered in estimating the concentration. Depletion due to wet deposition was not considered.

Reflection from elevated inversions and building wake effects were not taken into account in the calculations.

The concentration of stable carbon in the atmosphere was assumed to increase gradually over the course of the study period from 0.1875 gC/m^3 in 1992 to 0.2015 in 2001. Background concentrations of C-14 were assumed to decrease proportionately from 0.261 in 1992 to 0.243 in 2001.

II.9.1.2. Concentrations in rice

Concentrations in rice were set equal to concentrations in air (on a Bq/gC basis), on the assumption of specific activity equilibrium between plant and air.

II.9.1.3. Uncertainties

An uncertainty analysis was not carried out for this study but uncertainty estimates were made based on results of previous analyses of similar situations. The 2.5% and 97.5% confidence limits (CL) on the predicted seasonal (May – October) air concentrations are shown in Table II.9.1 in terms of the best estimate (BE) predictions.

Table II.9.1. Confidence limits on predicted air concentrations.

Receptor	TRP Alone		TRP + Background	
	2.5% CL	97.5% CL	2.5% CL	97.5% CL
ST-1, R2	BE/7	7•BE	Background	Background + 7•BE
R1	BE/4	4•BE	Background	Background + 4•BE
ST-2	BE/3	3•BE	Background	Background + 3•BE
ST-N, R3	BE/2	2•BE	Background	Background + 2•BE

The uncertainties in air concentrations are high close to the source since the predictions are very sensitive to the value of the vertical dispersion parameter. The uncertainties decrease further downwind.

The uncertainties in the air concentrations due to releases from the TRP alone are much larger than the uncertainties in the total measured concentration, which includes background. For concentrations due to the TRP alone, the upper and lower confidence limits are symmetrical about the best estimate. For the total concentration including background, the lower limit (which equals background) is only slightly smaller than the best estimate. In contrast, the upper limit can be as much as 55% greater than the best estimate.

The uncertainties on the monthly predicted air concentrations are somewhat higher than those shown in Table II.9.1 because the sector-averaged model does not work as well when fewer hours contribute to the average.

The uncertainties in rice concentrations are the same as those in air concentrations since the uncertainty in ^{14}C transfer is much less than the uncertainty in atmospheric dispersion.

II.9.2. EDF Model

II.9.2.1. Atmospheric dispersion

For this exercise, the model ADMS3 was used for atmospheric dispersion. This tool was developed by Cambridge Environmental Research Consultants (CRC) (http://www.cerc.co.uk). Many companies and regulatory authorities in Europe use this model for impact studies. Nevertheless, this tool has not previously been used at EDF for nuclear impact studies. Here we use the Gaussian plume model of the tool.

As for any other plume model, the meteorological conditions were assumed to be constant in time and space for each hourly time step of the simulations. Moreover, no spatial variations of wind parameters were modeled, as the region was considered to be flat.

The key parameters are roughness length (0.5 m) and the physical characteristics of the emission sources (height, diameter and exit velocity). Three different emission sources corresponding to the main, sub-1 and sub-2 stacks were taken into account. The model calculates plume rise and effective release height internally. The output grid resolution is 100 x 100 m. Wet deposition and reemission from soil or paddy fields were not taken into account.

For the meteorological conditions, we used the hourly-averaged meteorological data at 70-m height for the model input. The model can perform either short-term simulations, which represent steady-state conditions for one hour, or long-term calculations (for impact studies, for example). In this last case, the model outputs the mean concentration and higher order

percentiles such as the 98th or 99th. For this study, simulations at an hourly time step were run for each week of the 10 years.

No meteorological data were available for September 1995. Thus, for this month, concentrations were calculated considering a mean transfer coefficient based on the average conditions for the month of September in the other years.

ADMS outputs are air concentrations in Bq m^{-3}. To express the concentration in Bq/gC, the CO_2 air concentration was assumed to be constant over the simulation period and equal to 360 ppm (equivalent to a stable carbon concentration of 0.18 g m^{-3}). Seasonal variations in CO_2 concentrations were not taken into account.

For background ^{14}C concentrations, a linear regression from 1991 to 2000 was fitted to the wine specific activity data given in the Scenario Description (Appendix I.9). Mean background specific activity was then calculated every year from the linear regression. Comparison between observed and calculated values suggests confidence limits of ± 6 Bq/kg C in the estimated background ^{14}C levels. Isotopic discrimination (between air and grape) due to photosynthetic processes was not taken into account.

II.9.2.2. Concentration in rice

The EDF model used to calculate ^{14}C concentrations in crops was developed for continuous releases. It had to be adapted to match to the conditions of the rice scenario, where seasonal variations in ^{14}C emissions were high. A dynamic model was thus developed, based on the OURSON model which addresses the case of crop contamination from soil degassing.

The OURSON model assumes that the incorporation of ^{14}C in the plant results from photosynthetic carbon assimilation, and that remobilisation of plant ^{14}C occurs through respiration. The net photosynthetic carbon assimilation rate, which is photosynthetic assimilation minus respiration, corresponds to the growth rate of the plant.

The other main characteristics of the model are described here:

- Rice is represented by two compartments with their own growth rates: the vegetative part and the ear. A logistic model was fit to the data given in the scenario (Ibaraki province) for both parts of the plant. Values for the parameters of this model are listed in Table II.9.2.
- Contamination of the ear has a double origin: ^{14}C from the air at the time of growth of this organ, and ^{14}C already fixed in the vegetative part and remobilised by respiration. The Osaki and Tanaka [II.136] data presented in Section I.9.6.5 of the Scenario Description (Appendix I.9) was used to calibrate the remobilisation rate to a value of 0.01 day $^{-1}$.
- Isotopic discrimination (between air and rice) due to photosynthesis is not taken into account.

Table II.9.2. Parameters of the logistic growth model.

Parameter	Vegetative part	Ear
Growth rate (day^{-1})	0.116	0.229
Maximum dry biomass (g m^{-2})	935	606

II.9.3. IFIN Model

This scenario is a realistic case of "routine" emissions, where the source intensity varies due to technological problems and the meteorological data are averaged hourly. Note that both pressurized water reactors and boiling water reactors show seasonal variations of ^{14}C emissions [II.137].

II.9.3.1. Atmospheric ^{14}C dispersion

The wind direction given in the meteorological file is interpreted as the direction from which the wind blows. To account for uncertainties in wind direction, a given receptor is assumed to be affected by the airborne plume if it lies within 6^o of the line connecting the source and the receptor. A sector-averaged model is used with 32 sectors. The vertical dispersion parameter, σ_z, is expressed as a function of both downwind distance (x) and stability. As a standard selection we used the SCK/Mol parameterization, but also tested the KJ100 scheme. Both are for elevated emissions (60-100 m) and have the form:

$$\sigma_z = p_z \cdot x^q \qquad \text{(II.9.1)}$$

The values of the coefficients p_z and q are listed in Table II.9.3. The dispersion parameters calculated using the two schemes differed by about 50%.

Plume rise was assessed as recommended in the scenario description, but also with Briggs' formulae, which account for both momentum and buoyancy. The latter gives lower plume rise and higher air concentrations by a factor 2-3. We reported the air concentrations (in Bq/gC) calculated using the SCK/Mol σ_z scheme and the simple plume rise equation (Equation I.9.1) from the scenario (Section I.9.3.1).

For each year, missing data in the original meteorological file were replaced with interpolated values based on data for adjacent hours or days. For 1995, data for the entire month of September was missing and we used an average from 1994 and 1996. This implies large uncertainty.

Table II.9.3. Stability-dependent values of the parameters p_z and q in the vertical dispersion schemes.

Stability class	SCK/Mol		KJ100	
	p_z	q	p_z	q
A	1.32	0.711	0.051	1.317
B	0.95	0.711	0.07	1.151
C	0.7	0.711	0.137	0.985
D	0.52	0.711	0.265	0.818
E	0.382	0.711	0.487	0.652
F	0.311	0.711	0.717	0.486

Uncertainties

The calculated concentrations apply to the SCK/Mol or KJ100 parameterizations, the simple plume rise model (Equation I.9.1) given in the scenario description (Section I.9.3.1) and ignorance of any building or roughness length effect. Both parameterizations for σ_z are appropriate for a stack release near 100 m at a site with moderate to high roughness, but produce a factor of 2 difference in predicted air concentrations. A full uncertainty analysis was not carried out but limited experience and expert judgment was used to estimate a tentative 95% confidence interval with lower and upper limits of factors of 3 and 4 above and below the SCK/Mol values, respectively.

II.9.3.2. Rice growth and ^{14}C transfer

The specific activity approach assumes that full equilibrium is established in all environmental media for a constant ^{14}C activity in the source media. Crops take more than 90% of their ^{14}C from air, which implies that the crop ^{14}C concentration is given by:

$$C_{crop}^{14c} = C_{air}^{c14} \bullet C_{crop}^{c} / C_{air}^{c} \qquad \text{(II.9.2)}$$

where C^c_{crop} and C^c_{air} are the concentrations of stable carbon in crops and air, respectively. In the case of variable air concentration, it is well established that carbon is transferred to crops only in the daylight through photosynthesis.

A crude model for ^{14}C in rice grain was adopted that considered net primary production (NPP) only. Consider the NPP of dry matter dW in a time step dt. The in-growth of ^{14}C in the crop will be:

$$\frac{dC_{crop}^{c14}}{dt} = C_{air}^{c14} \bullet C_{crop}^{c} / C_{air}^{c} \bullet dW / dt \qquad \text{(II.9.3)}$$

The growth of a crop can be split into two major stages, the vegetative and reproductive periods. In the vegetative period, only roots, stem and leaves are growing. In the reproductive stage, grain filling is the main process. The process of flowering (or anthesis) provides a transition between the two periods. At the onset of grain filling, a part of the newly-formed dry matter is partitioned to grain growth but later all new NPP is used for grain filling. Many crops, including rice, have a secondary process: immediately after flowering, a part of the stem dry matter is translocated to the grain. In summary, the uptake of ^{14}C by the rice grain depends on the dynamics of NPP, partitioning to grain and the ^{14}C concentration in air.

The simplest model of the growth of crop dry matter is given by a logistic function:

$$W(t) = \frac{W_{\max}}{1 + b \bullet \exp(-k \bullet t)} \qquad \text{(II.9.4)}$$

where W_{max} is the above-ground dry matter at harvest, k is a growth rate and the parameter b is used to prescribe a specific dry mass at a prescribed time t before harvest. In the Korean model [II.138, II.139], W_{max} and the crop mass at transplanting (W_{min}) are used to set the value for b:

$$b = \frac{W_{\max}}{W_{\min}} - 1 \qquad \text{(II.9.5)}$$

To adopt Korean parameters for all rice crops seems too crude an assumption because they apply to a specific genotype for the weather of a specific year. A better approach is to take into account the influence of genotype and the environment [II.140].

As in many crop growth models [II.141, II.142], we define a parameter DVS describing the development stage of the plant. DVS has a value 0 at emergence, 1 at flowering and 2 at harvest. We assess plant growth in relation to the development stage and not directly to time. Ignoring the effect of daylight, the advance in the development stage depends on the environmental temperature above a plant-specific base temperature, T_{base}. We define the 'degree-day', DD, as the difference between the daily average temperature T_{av} and T_{base}. If $T_{av} < T_{base}$, DD=0. Development stops if T_{av} exceeds a maximum, T_{max}. In between, we use the following values of DD (as in [II.142]):

$$\begin{array}{ll} T_{av} < T_{base} & DD=0 \\ T_{base} < T_{av} < T_{opt} & DD= T_{av} - T_{base} \\ T_{opt} < T_{av} < T_{max} & DD= T_{opt} - (T_{av} - T_{opt}) * (T_{opt} - T_{base}) / (T_{max} - T_{opt}) \\ T_{av} > T_{max} & DD=0 \end{array} \qquad \text{(II.9.6)}$$

Here T_{opt} is the optimal temperature for plant development. The base, optimal and maximum temperatures are genotype-dependent but we used average values in our calculations: T_{base} = 8, T_{opt} = 30, T_{max} = 42^{o} C. In practice we assessed DD daily using hourly temperatures from the meteorological files. A temperature sum, TS, was defined as the sum of DD from a start day until the day of interest.

Flowering is a process with a duration of a few days for most crops. The change from the vegetative period to the reproductive period is assumed to occur when 50% of plants have flowered (DVS = 1). This happens after a genotype-specific value of TS (denoted by TEMFL) is achieved. Harvest comes when TS reaches a higher distinct temperature sum, TFLHA.

Rice transplanting is done once the daily temperature stays above 12^{o} C for at least 3 days [II.142–II.144], at which point DVS has a value between 0.15 and 0.2. We adopted an average value of 0.17 for the present calculations. After transplanting, there is a period of adaptation for a few days before the rice plant starts to re-grow again. Here, we take 5 days as a default value and assume that DVS = 0.17 at this time. We define the temperature sum from restart growth (after transplanting) until flowering as TTRFL=0.83*TEMFL.

We must now establish the values of TTRFL and TFLHA (the temperature sum from transplanting to flowering and flowering to harvest, respectively). From the WFOST database, we can see that TTRFL is 1050-1300 degree days and TFLHA is 580-770 degree days. From the information in the Scenario Description (Appendix I.9), which applies to a rice crop in Tokaimura in 1999, we deduce TTRFL= 980 and TFLHA= 710. For a Yumehitachi cultivar in Mito in 2001 (private communication from Mariko Atarashi-Andoh, JAERI), we deduce TTRFL= 1100 and TFLHA= 624.

For our calculations, we set TTRFL = 1100 and TFLHA = 610 as default values. Next we had to establish the transplanting day. Farmers can choose an early transplanting (to have a second crop on the paddy field) and risk some cold days, or they can be conservative and chose a late transplanting. Practices in Tokaimura were assessed using the 1999 and 2001 data referenced

above. Starting with zero at 1 January and accumulating the temperature sum, we observe that transplanting occurs when TS is between 350 and 420 degree days. We adopted the lower value for our calculations.

At this point we have the following logic of development-stage dynamics:

(1) Find the day with TS = 350 (assuming that TS = 0 on 1 January). This is the transplanting day. Add 5 days for adaptation and restart growth. Define this day as t_0 and begin the simulation of plant growth.
(2) $DVS(t_0) = 0.17$.
(3) For each day after t_0, consider the daily increase of the temperature sum DTS = TS(t)-TS(t-1) and increase the development stage with DTS/TTRFL.
(4) When DVS reaches 1, flowering occurs and future increases in DVS are given by DTS/TFLHA.
(5) When DVS reaches 2, harvest occurs.

The growth of above-ground dry mass W is given by a logistic equation expressed in terms of DVS as:

$$W = Wmax / [1+b*exp(-6.5*DVS)] \quad \text{(II.9.7)}$$

The constant 6.5 in Equation II.9.7 is chosen for convenience to reproduce the time-dependence of the growth curve.

The daily growth of above-ground dry matter, dW/dt, at day iday is given by:

$$dW(iday)/dt = W(iday)*6.5*[1-W(iday)/W_{max}]*[DVS(iday)-DVS(iday-1)] \quad \text{(II.9.8)}$$

The above expression ignores the influence of light on daily dry matter production. This can be introduced later if required. As light will influence both the dry matter production and the transfer of ^{14}C to grain, the influence of light variability will be less important for the concentrations than for the yield itself. To determine the transfer of ^{14}C to grain, we must now define the partition functions that describe the fraction of daily new dry matter that is transferred to the grain, and the fraction of ^{14}C in the stem that is translocated to the grain after flowering. Both processes can be assessed using a single partition function with nonzero values before flowering. Using the database in WOFOST and ORYZA, we set the generic partition function PF = 0 for DVS ≤ 0.8 and PF = 1.0 for DVS ≥ 1.2. Values of PF can be interpolated linearly for DVS between 0.8 and 1.2.

Finally, the ^{14}C transfer to grain is given by:

$$\frac{dC^{c14}_{grain}}{dt} = C^{c14}_{air}(t) \bullet C^{c}_{grain} / C^{c}_{air} \bullet dW / dt \bullet PF(t) \quad \text{(II.9.9)}$$

The above simple growth model and associated ^{14}C transfer to grain considers the influence of ^{14}C concentration in air and the development stage of the rice, which varies from year to year. The ^{14}C concentration in air should consider daylight periods only.

To assess the influence of year-to-year temperature variability, we calculated annual temperature sums each year from 1992 to 2001. 1994 was a cold year but 2000 was hot. The

dates for flowering and harvest varied by about 20 days over this period. These results were obtained considering daylight hours only (hours for which the solar radiation exceeded 0).

The ^{14}C concentration in rice grain depends on management practices and the cultivar in question. We carried out a second round of calculations with a late transplantation date and a different cultivar, characterized by TTRFL= 1000 and TFLHA= 700, and obtained results that differed by as much as a factor 2 from those obtained with our initial assumptions. Based on a mix of experience and expert judgment, and including the uncertainty in the air concentrations, the 2.5th and 97.5th confidence limits on the predicted ^{14}C concentrations in grain lie a factor of 3 below and a factor of 5 above the best estimate predictions, respectively.

Table I.9.6 in the Scenario Description (Appendix I.9) includes some information on ^{14}C utilization at various growth stages. The processes of carbon uptake and translocation in plants are much more complex than are suggested by the simple growth model dealing with dry matter production used here. The gross photosynthetic rate will produce assimilate that is first used for maintenance respiration, with the surplus going to growth, which itself requires respiration. The process of respiration is not uniformly fast, but has both fast and slow components. Of the ^{14}C taken up as a pulse by a plant, 7-17% is respired immediately and 3-13% much later. Experiments with barley and maize [II.145] show that respiration R and the remaining ^{14}C, L, can be described by:

$$R(t) = [k_g(1-Y_g)/(\lambda_1-\lambda_2)]*[(\lambda_2+k_g)\ exp(\lambda_1*t)-(\ \lambda_1+k_g)*exp(\lambda_2*t)]$$

$$L(t) = (1-b-c) + b\ exp(\lambda_1*t) + c\ exp(\lambda_2*t) \qquad \text{(II.9.10)}$$

where:

$\lambda_1 = -0.2\ d^{-1}$;
$\lambda_2 = -2.1\ d^{-1}$;
1-b-c ranges from 0.35-0.44;
b/c ranges from 1.28-0.77;
$k_g = 1.9\ d^{-1}$; and
$Y_g = 0.65$.

Half of the respired carbon has a halftime of 2 d^{-1} and the rest is respired slowly (at a rate of 0.2 d^{-1}). Not all of the ^{14}C taken up a few days before harvest will be respired before harvest. The respiration rate decreases near harvest and the grain mass increases. The net effect of the un-respired ^{14}C can be ignored and the simple model described here will be sufficiently accurate. The uncertainty in the predicted air concentration is larger than that in the model of uptake by grain. Further developments of the model should include the effect of solar irradiance on daily crop growth and associated ^{14}C uptake.

II.9.4. SRA Model

II.9.4.1. Atmospheric diffusion of ^{14}C

The atmospheric diffusion of ^{14}C is described by a Gaussian plume model. The wind blows with equal probability within a given sector. The ^{14}C concentration in the plume is calculated by assuming the common frequency of individual atmospheric stability and the corresponding average wind velocity. The sector-averaged ^{14}C concentration at ground level is then approximately given by the following equation:

$$\chi(x) = \sum_{S=A}^{F} \sqrt{\frac{2}{\pi}} \cdot \frac{F(s) \cdot Q}{\sigma_{ZS} \cdot U_S \cdot (2\pi \cdot x/16)} \cdot \exp\left(-\frac{H^2}{2 \cdot \sigma_{ZS}^2}\right) \qquad \text{(II.9.11)}$$

where:

x is the downwind distance from the release point (m);
χ (x) is the air ^{14}C concentration at distance x (Bq/m^3);
S is the stability index of the atmosphere;
F(S) is the frequency of occurrence of stability class S;
σ_{ZS} is the vertical dispersion parameter (m);
U_S is the average wind velocity for stability class S (m/s);
Q is the release rate (Bq/s); and
H is the stack height (m).

The dispersion parameters were calculated using the formula in "Meteorological Guideline for the Safety Analysis of Nuclear Power Plants" [II.47].

II.9.4.2. Transfer of ^{14}C from the atmosphere to the rice plant

It was simply assumed that the specific activity of ^{14}C in the rice is given by that in air averaged for the growth and maturation period of rice grains between August and September.

II.9.5. UTTY Model

II.9.5.1. Calculation of atmospheric dispersion

C-14 concentrations in air were calculated using the Gaussian plume model:

$$\chi(x,y,z) = \frac{Q}{2\pi \bar{u} \sigma_y \sigma_z} \exp\left[-\frac{1}{2}\left(\frac{y}{\sigma_y}\right)^2\right] \cdot \left\{\exp\left[-\frac{1}{2}\left(\frac{z-h}{\sigma_z}\right)^2\right] + \exp\left[-\frac{1}{2}\left(\frac{z+h}{\sigma_z}\right)^2\right]\right\} \qquad \text{(II.9.12)}$$

where:

χ(x,y,z) is the air concentration (Bq/m^3) at downwind distance x (m), crosswind distance y (m) and height z (m);
Q is the source strength (Bq/s);
h is the effective release height (m);
u is the average wind speed (m/s); and
σ_y andσ_z are the horizontal and vertical dispersion parameters (m)

Table II.9.4. $\theta_{0.1}$ (degrees) for each stability class.

Stability	A	B	C	D	E	F
$\theta_{0.1}$	50	40	30	20	15	10

Table II.9.5. Values of σ_1, a_1, a_2 and a_3 for each stability class.

Stability	0.2km≦x				x <0.2km	
	σ_1	a_1	a_2	a_3	σ_1	a_1
A	768.1	3.9077	3.898	1.733	165	1.07
B	122.0	1.4132	0.49523	0.12772	83.7	0.894
C	58.1	0.8916	-0.001649	0.0	58.0	0.891
D	31.7	0.7626	-0.095108	0.0	33.0	0.854
E	22.2	0.7117	-0.12697	0.0	24.4	0.854
F	13.8	0.6852	-0.1227	0.0	15.5	0.822

Table II.9.6. Plume rise by stability class.

Stability	A	B	C	D	E	F
Plume rise (m)	58.25	31.80	21.25	22.86	23.29	36.34

The dispersion parameters were calculated from the regression formulae in the Japan Safety Review Guide:

$$\sigma_y = 0.67775 \cdot \theta_{0.1} \cdot (5 - \log_{10} x) \cdot x \qquad \text{(II.9.13)}$$

where $\theta_{0.1}$ is the dispersion angle (degrees) at x = 0.1 km (see Table II.9.4)

$$\sigma_z = \sigma_1 \cdot x^{a_1 + a_2 \cdot \log x + a_3 (\log x)^2} \qquad \text{(II.9.14)}$$

where values of the parameters σ_1, a_1, a_2 and a_3 are listed in Table II.9.5.

For the calculation of atmospheric dispersion, we made the following assumptions:

- Plume reflection at the mixing height was neglected. In this scenario, the sampling points were close to the ^{14}C release locations, so that the effect of plume reflection on the air concentration at ground level was negligible except at the control points.
- The value of the vertical dispersion parameter,σ_z, was limited to 1000 m as a maximum value (Japan Safety Review Guide). However this assumption did not affect the results because plume reflection at the mixing height was not considered.
- Concentrations in the plume were not reduced by wet or dry deposition. The major chemical form of ^{14}C is CO_2 gas in the atmosphere, which does not undergo significant deposition. In addition, rain occurs infrequently and for short periods of time at the Tokai site.
- The predicted ^{14}C concentrations in air at the sampling points were sector-averaged.
- The ^{14}C released from the three stacks was all assumed to come from the main stack as a single release point.
- The effective release height was calculated as the physical height of the main stack plus plume rise. Plume rise was assumed equal to 3WD/U, where W is the exit velocity of the stack gases (m/s), D is the internal diameter of the main stack (m), and U is the wind speed (m/s). Plume rise due to buoyancy was not considered. Plume rise was calculated for each stability class, and the values are shown in Table II.9.6.

Air concentrations were calculated for each stability class using Equation II.9.12. These concentrations were multiplied by the frequency of occurrence of each class and summed to give a monthly average concentration. The wind speed used in the calculations was the average speed for each class as determined from the Tokai meteorological data. Finally, the weighted average concentration was multiplied by the wind direction frequency to yield the ^{14}C concentration in air at each sampling point.

II.9.5.2. Calculation of rice concentrations

Model structure

Our model, a dynamic compartment model, was developed using the MOGRA tool (Migration Of GRound Additions). The model, which is shown in Figure II.9.1, consists of the following compartments:

- Two organic compartments (stem-leaf-root and ear);
- One inorganic compartment (the whole plant);
- Two environmental compartments (air and soil).

Compartments and transfer pathways

The definition of each transfer pathway is shown in Figure II.9.2.

The [Plant_inorg] compartment includes the following:

- non-fixed carbon (i.e., inorganic carbon) in the plant;
- organic carbon that exchanges easily with air.

This compartment involves the photosynthates generated by photosynthesis in the leaves that are not yet fixed in the plant. The photosynthates fixed in each part of the plant are considered in the [StemLeaf_org] and [Ear_org] compartments through K_{PL} and K_{PE}.

The [StemLeaf_org] compartment includes the photosynthates fixed in the stem, leaf and root. The amount of carbon (photosynthate) in this compartment that is transferred from the [Plant_inorg] compartment decreases due to translocation to the ear after flowering and due to dark respiration.

The [Ear_org] compartment includes the photosynthates fixed in the ear. The amount of carbon (photosynthate) in this compartment that is transferred from the [Plant_inorg] and/or the [StemLeaf_org] compartment decreases due to dark respiration only.

The K_{PA} pathway represents the transfer of carbon from the [Plant_inorg] compartment to air due to light respiration and/or exchange with air.

The K_{PE} pathway describes the transfer of photosynthates from [Plant_inorg] to [Ear_org] after flowering.

The K_{LE} pathway represents the transfer of photosynthates from [Stemleaf_org] to [Ear_org] due to translocation after flowering. Photosynthates are preferentially transferred to the ear rather than to other plant parts after flowering.

The ratio of K_{PE} to ($K_{PE} + K_{LE}$) is termed the gamma factor, which depends on the growth rate of the ear.

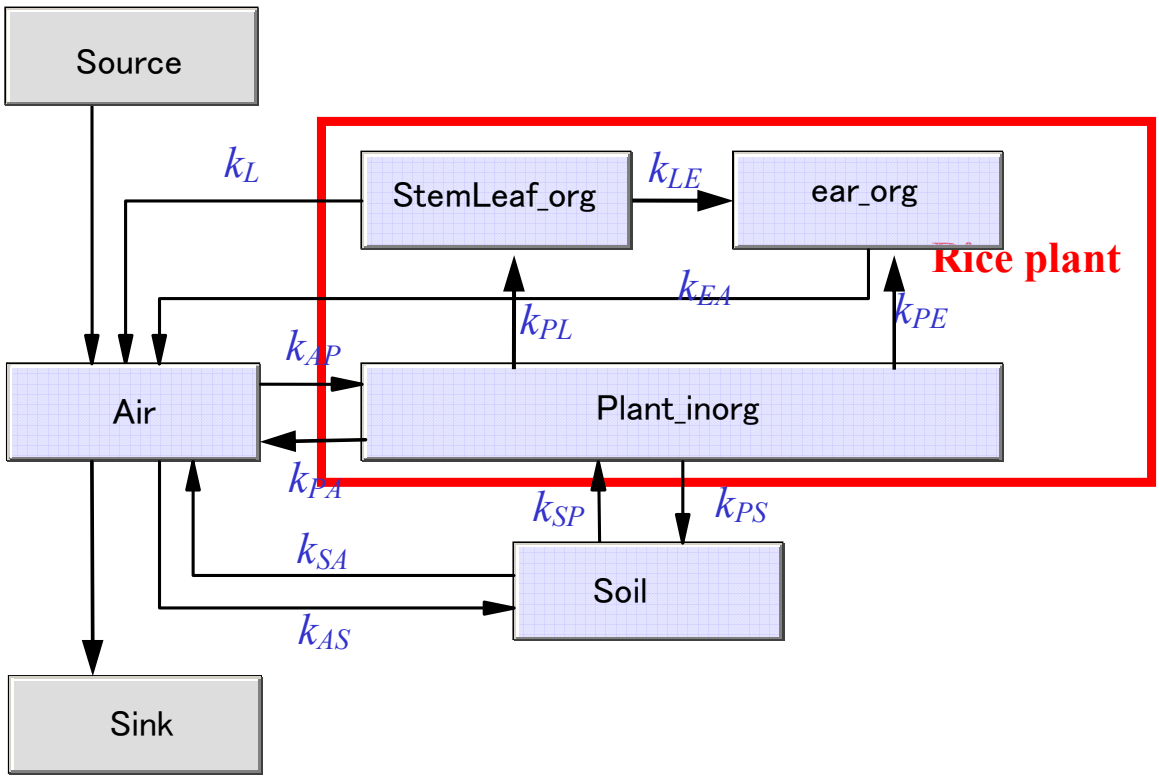

Fig. II.9.1. Rice model of UTTY.

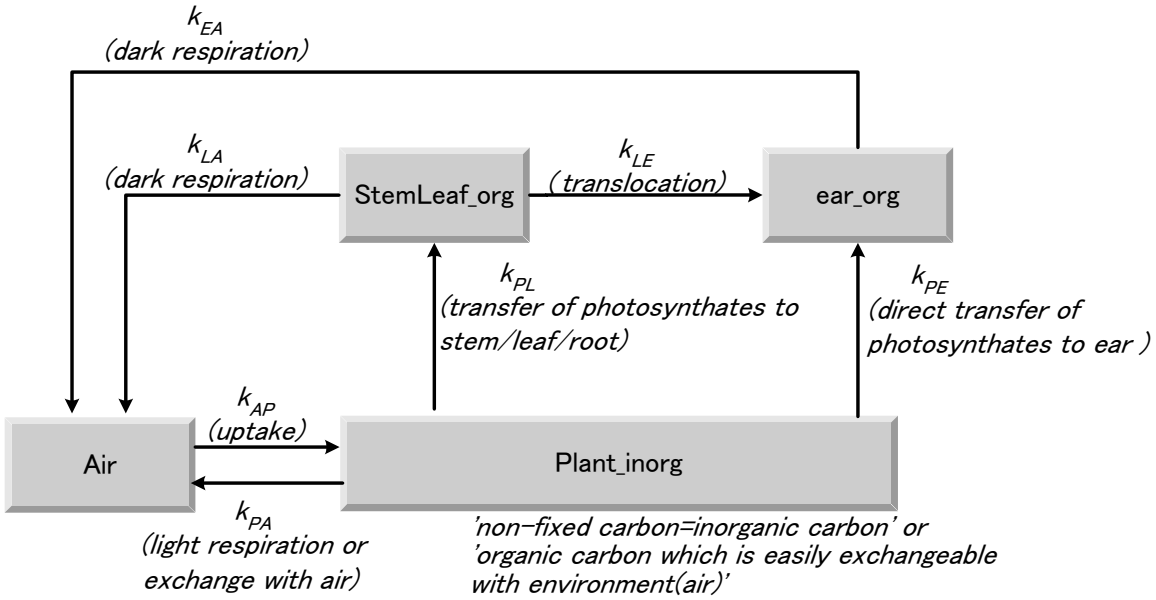

Fig. II.9.2. Definition of each transfer pathway in the UTTY rice model.

Transfer factor equations

Transfer between air and [Plant_inorg] compartments:

$$k_{AP} = R_{air} \cdot \left[\alpha_{ino} \cdot \frac{dW_P}{dt} + \left(1 + \beta_{P\_res}\right) \cdot \alpha_{org} \cdot \frac{d}{dt}\left(W_P - W_E\right) + \left(1 + \beta_{E\_res}\right) \cdot \alpha_{E\_org} \cdot \frac{dW_E}{dt} \right] \Big/ W_A \quad \text{(II.9.15)}$$

where:

R_{air} is the ratio of carbon intake from air to the total intake from air and soil (= 0.999);
α_{ino} is the ratio of inorganic carbon to the total weight of the plant (= 0.02);
α_{org} is the ratio of organic carbon to the total weight of the plant (α_{org} = 0.37 without the ear and 0.41 with the ear);
β_{res} is the ratio of organic carbon used in respiration to the total weight of the plant (β_{P_res}= 0.35 without the ear and 0.15 with the ear);
W_P and W_E are the weights (g) of the total plant and of the ear, respectively. These are functions of their corresponding growth curves;
W_A is the weight of carbon in air (g/m^3); and
$k_{PA} = 0$ (light respiration is not considered).

Transfer between soil and [Plant_inorg] compartments

It is assumed that the concentration in soil quickly comes into equilibrium with the concentration in air. K_{SA} and K_{AS} are set to achieve this assumption. Thus, the equations for K_{SP} and K_{PS} are similar to those for K_{AP} and K_{PA} respectively, but W_A is replaced with W_S (the weight of carbon in soil) and R_{air} is replaced with (1-R_{air}).

Transfer from the [Plant_inorg] compartment to the [StemLeaf_org] compartment:

$$k_{PL} = \left[\left(1 + \beta_{P\_res}\right) \cdot \alpha_{org} \cdot \frac{d}{dt}\left(W_P - W_E\right) + \left(1 + (1-\gamma)\beta_{E\_res}\right) \cdot \alpha_{E\_org} \cdot \frac{dW_E}{dt} \right] \Big/ \left(W_P \cdot \alpha_{ino}\right) \quad \text{(II.9.16)}$$

whereγ is the ratio of transfer from [StemLeaf_org] to [Ear_org] relative to the total transfer to [Ear_org].

Transfer from the [Plant_inorg] compartment to the [Ear_org] compartment:

$$k_{PE} = \gamma \cdot \alpha_{E\_org} \cdot \left(1 + \beta_{E\_res}\right) \cdot \frac{dW_E}{dt} \Big/ \left(W_P \cdot \alpha_{ino}\right) \quad \text{(II.9.17)}$$

Transfer from the [StemLeaf_org] compartment to the [Ear_org] compartment:

$$k_{LE} = \left(1 - \gamma\right) \cdot \alpha_{E\_org} \cdot \left(1 + \beta_{E\_res}\right) \cdot \frac{dW_E}{dt} \Big/ \left\{\left(W_P - W_E\right) \cdot \alpha_{org}\right\} \quad \text{(II.9.18)}$$

In the model, the transfer of photosynthetic products to the ear occurs from both [Plant_inorg] and [StemLeaf_org]. After flowering, the photosynthetic products are directly transferred to the ear rather than to the stem and leaves. The contributions of the two pathways are reflected in the value of the γ factor, which is a function of the ear growth differential curve. The following dependence is obtained by analyzing data on rice ears:

$$\gamma = 1 - \frac{dW(t)}{dW_{\max}} \times 0.7 \qquad \text{(II.9.19)}$$

where $dW(t)$ is the differential increase of ear weight (g) with a maximum value of dW_{max}, which is given by:

$$dW_{\max} = \frac{dW(t = t_{half\_tuber})}{dt} \qquad \text{(II.9.20)}$$

where t_{half_tuber} is the day at which the ear weight becomes half of its maximum weight (day).

Transfer from the [StemLeaf_org] compartment to air (dark respiration of stem and leaves)

$$k_{LA} = \beta_{P\_res} \cdot \alpha_{org} \cdot \frac{d}{dt}(W_P - W_E) \Big/ \{(W_P - W_E) \cdot \alpha_{org}\} \qquad \text{(II.9.21)}$$

Transfer from the [Ear_org] compartment to air (dark respiration of ear)

$$k_{EA} = \beta_{E\_res} \cdot \alpha_{E\_org} \cdot \frac{dW_E}{dt} \Big/ \{\alpha_{E\_org} \cdot W_E\} \qquad \text{(II.9.22)}$$

Other assumptions and conditions

The growth curves of the total plant and the ear were assumed to be sigmoidal:

$$W(t) = W_{harvest} \cdot \frac{10^{K(t - t_{half})}}{1 + 10^{K(t - t_{half})}} \qquad \text{(II.9.23)}$$

where:

$W(t)$ is the total plant (or ear) weight at time t (g dry weight);
$W_{harvest}$ is the total plant (or ear) weight at harvest (g dry weight);
K is the shape parameter of the sigmoidal curve (/day);
t is time (day); and
t_{half} is the day at which the whole plant weight becomes half of its maximum weight (day).

Values for the factors $W_{harvest}$, K and t_{half} are shown in Table II.9.7.

The model was driven by the predicted monthly air concentrations. The rice seedlings before transplanting were assumed to be exposed to background levels of ^{14}C. The plants were exposed to ^{14}C in air for only 20 days in May (a typical planting time is around the first to second week of May in the Tokai area). Transplanting was assumed to occur 10 days after seeding, ear formation at day 100 and harvesting at day 150.

Table II.9.7. Values of $W_{harvest}$, K and t_{half} for the whole plant and the ear.

Plant part	$W_{harvest}$ (g dry weight)	t_{half} (day)	K (d^{-1})
Whole plant	60	80	0.037
Ear	30	120	0.063

II.10. Potato Scenario model descriptions

II.10.1. EDF Model

II.10.1.1. Model description

The OURS0N model used by EDF is a dynamic model primarily developed to evaluate radionuclide concentrations in the aquatic and terrestrial environment resulting from liquid discharges. It assumes that the incorporation of C-14 in plants results from photosynthetic carbon assimilation, and that translocation occurs between the leaves, where photosynthesis takes place, and the storage organs. The net photosynthetic carbon assimilation rate, which is a function of leaf biomass, corresponds to the total growth rate of the plant. Allocation of photosynthates to different parts of the plant depends on the growth stage. For potatoes, two phases are considered: a vegetative stage where shoot growth occurs and a filling stage where tuber growth occurs.

II.10.1.2. Parameter values

- CO_2 air concentration during fumigation: 0.19 g C/m3;
- Daily net photosynthetic rate: 0.0495 g C/g leaf dry matter (variations due to solar radiation were not taken into account);
- Vegetative stage: from planting to 40 days of age;
- Filling stage: from 40 days of age until harvest;
- Translocation to tubers during vegetative stage: 0.10;
- Translocation to tubers during filling stage: 0.50; and
- Fractional carbon content per unit dry biomass (dry) in leaf and tuber: 45%.

II.10.1.3. Results

The predicted ^{14}C concentrations in tubers at final harvest are shown in Figure II.10.1. The predicted ^{14}C concentrations in potato leaves are shown in Figure II.10.2 at each sampling time for each experiment.

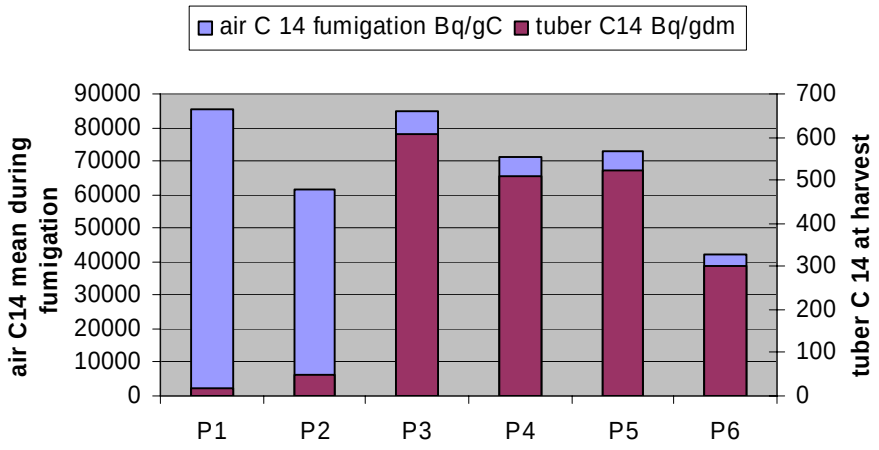

Fig. II.10.1. Observed C-14 concentrations in air during exposure and predicted concentrations in tubers at final harvest.

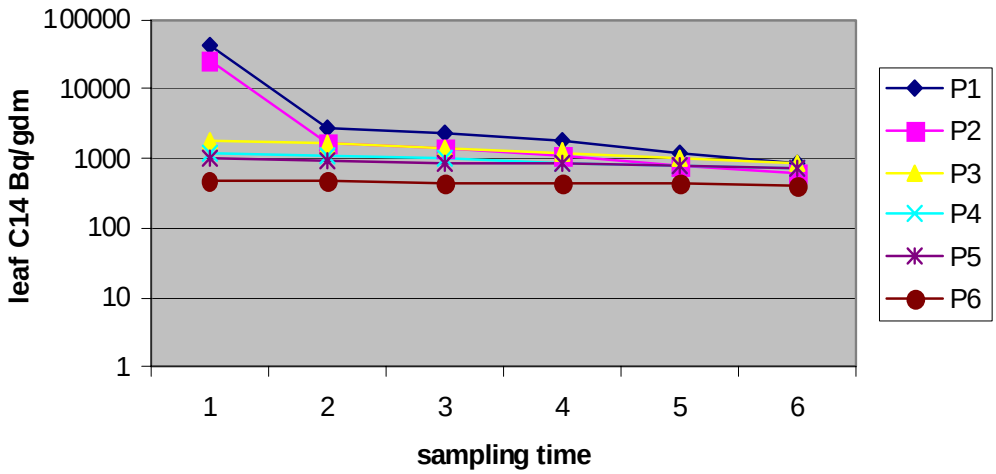

Fig. II.10.2. Predicted C-14 concentrations in potato leaves at each sampling time for each experiment.

II.10.2. FSA Model

II.10.2.1. Introduction

- Model Name: Prism 3.0, Special Radionuclides submodel: H-3 and C-14 [II.88–II.90, II.146–II.148].
- Purpose of Model: Regulatory Assessment; Conservative.
- Type of Model: Dynamic; Numerical; Compartmental.
- Compartments Considered: Biological plant compartments include internal leaf, internal stem, internal grain/fruit, roots, plant water and energy storage. Environmental compartments include soil water, soil organic material and sink. The external parts of the plant are not explicitly represented because all sources are considered to be gaseous. The root store is not considered due to rapid redistribution of H-3 and C-14. Contamination in soil water and soil organic matter is distinguished.
- Transport Processes Considered: Uptake from air; sorption, advective transport and bioturbation in soil; plant uptake from soil and within plant transport via phloem and xylem.
- Endpoints: C-14 concentration in each compartment at the end of the scenario.

II.10.2.2. Key assumption

- Direct uptake from soil to internal plant: a single compartment is used for each soil layer. Sorption is assumed between C-14 in soil water and on soil particles.
- Plant water and stored energy are not represented. For C-14, soil mediated processes are considered less important compared with direct uptake from the atmosphere. The main carbon fluxes are governed by photosynthetic incorporation and respiratory loss.
- It is assumed that any carbon transfers from the plant or soil back to the atmosphere are rapidly lost from the system.

- "Labile" and "non-labile" pools are similar to those in the STAR model.
- The rate of carbon uptake during daylight hours is controlled by photosynthesis.
- Transfers between compartments are calculated using transfer rates or the fraction of activity transferred to each compartment

II.10.2.3. Mathematical formulation

Plant concentrations C_p due to uptake by photosynthesis and by roots are given by:

$$C_p = vd^{co2} C A \quad \text{(II.10.1)}$$

where:

vd^{co2} is the deposition velocity of CO_2;
A is the deposition rate taking place; and
C is the concentration of $^{14}CO_2$ in the atmosphere.

The deposition velocity is given by:

$$vd^{co2} = k G F_{GC} / C_C \quad \text{(II.10.2)}$$

where:

G is the biomass growth rate;
F_{GC} is the fraction of dry matter that is carbon; and
C_c is the concentration of carbon in the atmosphere.

The loss of activity by respiration from the energy store is given by:

$$L = (k-1) G A F_{GC} / M_{ES} \quad \text{(II.10.3)}$$

where M_{ES} is the mass of carbon in the energy store.

The transfer rate from the energy store to the internal leaf is given by:

$$T = G_{IL} A F_{GC} / M_{ES} \quad \text{(II.10.4)}$$

where G_{IL} is the growth rate of the internal leaf. Similar expressions are used to calculate transfers to root, stem and internal grain/fruit.

EquationsII.10.1 to II.10.4 are solved using the AMBER Code.

II.10.2.4. Temporal and spatial discretization of the model

There is no spatial discretization in the model. The user can define the input air concentration as a continuous function, a spike (instantaneous exposure) or a series of spikes (complex exposure). Output is normally reported every three days unless specified otherwise. It is recommended to remove interim output times between the start and finish of the calculations and specify the times at which results are required. No spatial or temporal averaging was used for the potato scenario.

Table II.10.1. Attributes of the distributions of key model parameters.

Parameter	Units	Distribution Type	Range	Best Estimate
Soil surface bioturbation rate	d^{-1}	Lognormal	0.25 - 13	6
Organic degradation rate	d^{-1}	Triangular	5E-05 – 3E-02	4E-03
Adsorption rate	d^{-1}	Log uniform	3.5E-05 - 3.5E-03	3.5E-04
SA_foliage	d^{-1}	Log uniform	15 - 25	20
SA_grain	d-1	Log uniform	1 - 10	5
SA_stem	d-1	Log uniform	1 - 10	5
Fraction of CO_2 recycled during photosynthesis	Unitless	Lognormal	0.04 – 0.3	0.06
Biomass fraction in energy store	Unitless	Log uniform	0.001 – 0.02	0.002
Plant assimilation factor	Unitless	Uniform	0.4 – 0.6	0.5
Dry to fresh weight ratio	Unitless	Triangular	0.05 – 0.3	0.1

II.10.2.5. Input data required

The model requires a number of soil and plant parameters. The growth curve may be adjusted to match information in the model scenario.

II.10.2.6. Parameter values

Most input parameters were distributed and values in each run were determined by sampling in the assigned probability density function (PDF). The attributes of the PDFs for the key model parameters are listed Table II.10.1.

II.10.2.7. Uncertainties

Uncertainties were estimated using a probabilistic approach by sampling in the parameter PDFs. Some C-14 parameters were not sampled. If values are chosen at the 95% level, the predicted concentrations will be conservative by a factor of 7-10 (European Crop Protection Association Dietary Risk Assessment Workshop).

II.10.2.8. Application of the model to the scenario

- The exposure was assumed to be complex in form and modeled as a series of spikes, with different exposures for each experiment.
- The predicted plant biomass at the end of the calculations was scaled to the value observed in the experiments.
- The growth curve for the potatoes was adjusted so that enough growth occurred prior to exposure to ensure some uptake in the leaves for each experiment.

II.10.3. IFIN Models

II.10.3.1. Basic modelling principles

For this scenario, we used the WOFOST crop growth model, which was developed by the Wageningen School in The Netherlands. We ran WOFOST with both default potato parameters and parameters specific to a Scottish cultivar. We also used another model with simpler algorithms for dry matter production and initial inventory. The basic principles used in these models are as follows:

— The specific activity of C-14 transferred to the plant in a given time interval is the same as the average specific activity of the source over that interval.
— Under normal conditions, more than 90% of plant carbon comes from the atmosphere; this was assumed to be the case in the potato experiments.
— In biochemical reactions occurring in the plant, the discrimination factor between C-14 and C-12 is close to 1 (0.96±0.02, [II.149]); consequently, modelling of C-14 transfer is the same as modelling stable carbon transfer.

The processes we considered in implementing the models were as follows:

— Initial incorporation of C-14 in the total plant;
— Loss of C-14 through maintenance and gross respiration;
— Distribution of dry matter to plant parts;
— Further growth dilution and potential translocation.

Each of these processes can be modelled simply or at a process level. We started with the process-oriented model WOFOST, drawing on our previous experience with the tritium module in RODOS (Real Time On-Line Decision Support System for Nuclear Emergencies). In addition, we used a simpler approach to modelling dry matter production.

II.10.3.2. WOFOST Model

Default potato parameters

Genotype has a large influence on plant growth. We first ran WOFOST using default parameter values that reflected a generic cultivar. Growth also depends on climate, but since weather data for 1995 were not available, we used historical data for Cambridge averaged over the 30-year period 1960–1990. This introduced an additional uncertainty into the calculations.

The photosynthesis submodel in WOFOST depends on photosynthetically-active radiation (PAR), leaf area index (LAI), and maximum leaf photosynthesis rate. An example is given in Figure II.10.3. In the experiment, the potatoes were planted extremely late in the year, even for the UK. The normal planting time for England is late April or early May, but in the experiment it was August 4. In these circumstances, WOFOST with default parameter values slightly underestimated the observed biomass dynamics.

The gross canopy photosynthesis rate, A_{gross}, is parameterized in WOFOST as:

$$A_{gross} = A_{max}\, LAI^{1.33}/(K^{1.33} + LAI^{1.33}) \quad \text{(II.10.5)}$$

Here A_{max} is the asymptotic canopy photosynthetic rate, which depends on PAR in the following way:

$$A_{max} = a + b\, PAR - c\, PAR^2 \quad \text{(II.10.6)}$$

The parameter K is given by:

$$K = d + e\, PAR \quad \text{(II.10.7)}$$

The parameters a, b, c, d and e have plant-specific values depending on canopy age and temperature.

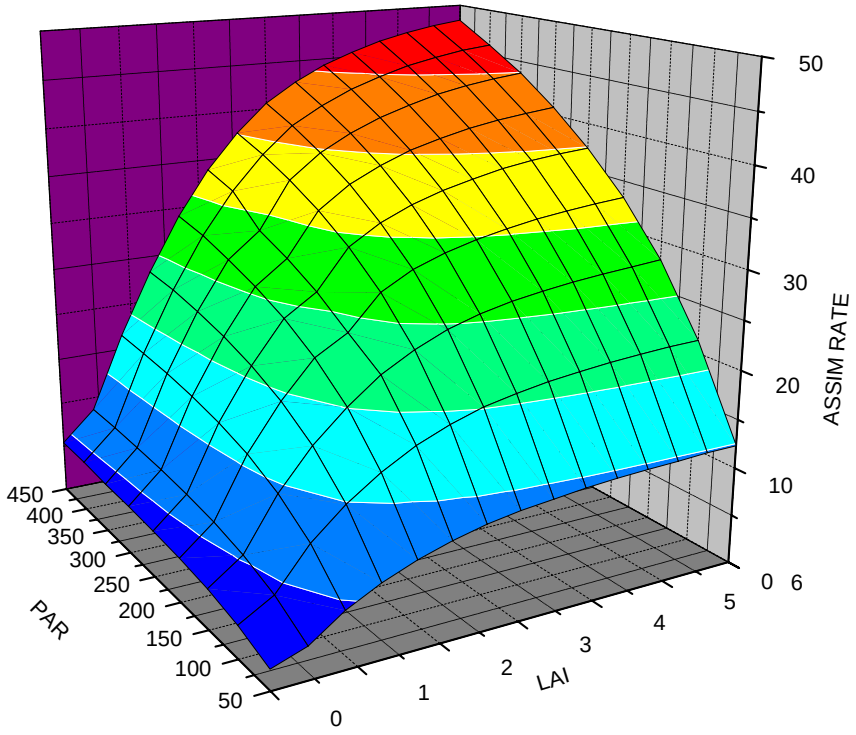

Fig. II.10.3. Dependence of photosynthesis rate on PAR and LAI for potatoes.

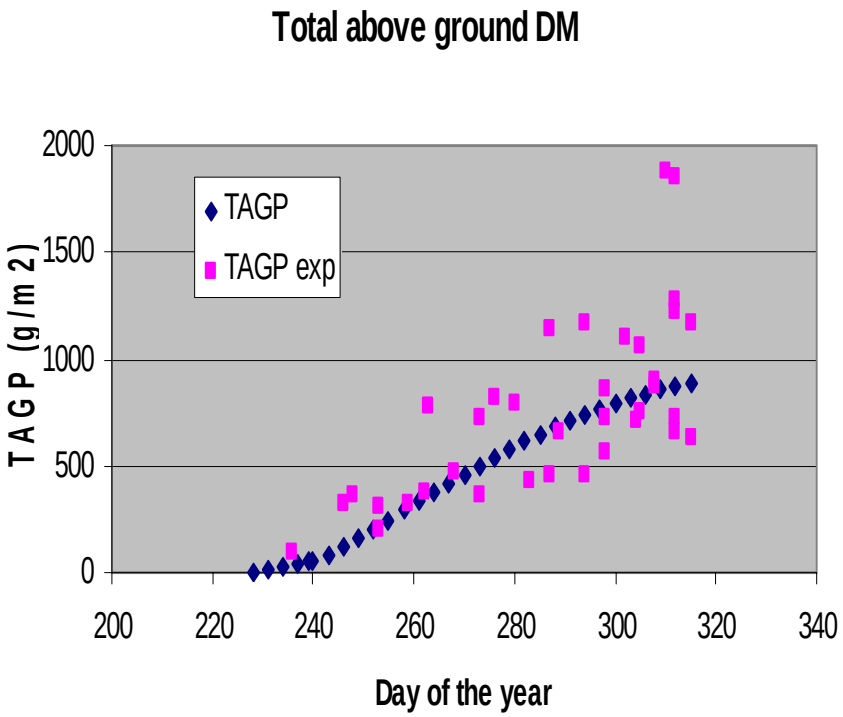

Fig. II.10.4. Comparison between WOFOST predictions and experimental data for total above ground biomass.

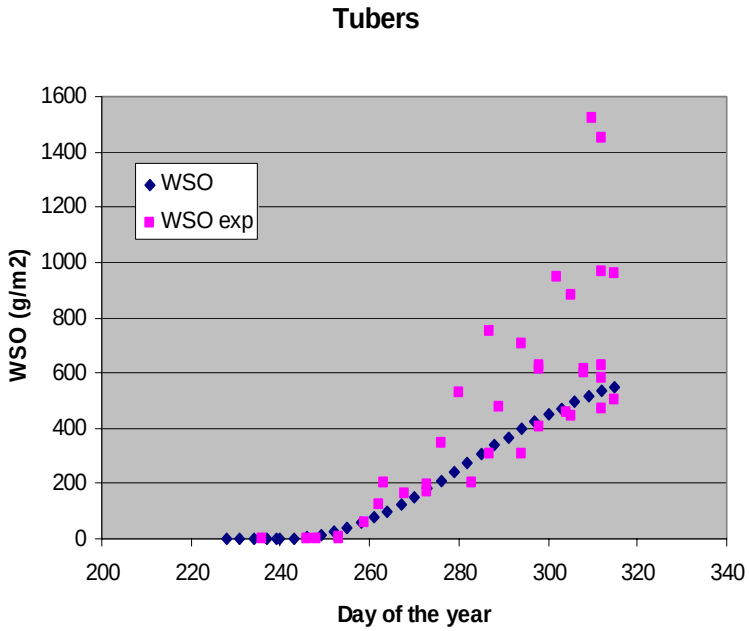

Fig. II.10.5. Comparison between WOFOST predictions and experimental data for tuber biomass.

Table II.10.2. Initial C-14 incorporation per plant.

Exp	Age (d)	Median Temp (C)	Median PAR (W/m^2)	LAI	A_{max}	A_{gross}		Rate of C-14 incorporation ($Bq/m^2/10h$)
						kg/ha/h	g/plant/10 h	
P1	21	25	110	0.3	22.5	3	0.16	6.67
P2	33	23	105	0.5	26	5.5	0.35	12.22
P3	47	21	100	1	30	10.5	0.84	23.33
P4	61	22	80	2.5	30	14	1.12	31.11
P5	74	22	80	1.5	27	11	0.88	24.44
P6	89	18	80	1	15	6	0.48	13.33

WOFOST default predictions and experimental biomass dynamics

WOFOST predictions of potato growth rates are compared with the experimental data in Figures II.10.4 and II.10.5. The model performs well for total above-ground biomass over the entire study period, and for tuber production at the start of the period. However, the growth rate for tubers is underestimated at later times.

Initial C-14 Incorporation

The WOFOST model predicts the photosynthesis rate and C-14 incorporation into plants using the experimental data on PAR, LAI and temperature. Table II.10.2 gives the initial rate of C-14 incorporation into the plants for each experiment.

The C-14 air concentration varied strongly during the exposures, decreasing by a few orders of magnitude in the 10 hours of the experiment. Once the exposure was over and there was no

further transfer of C-14 from air to plant, the plant C-14 concentration decreased due to respiration. Maintenance and growth respiration are not instantaneous processes. They have fast and slow components with rates of about 2 and 0.2 d^{-1}, respectively. WOFOST includes a fully dynamic treatment of incorporation and respiration, which mathematically is represented by an integral convolution. At harvest H1, respiration is not finished. At harvest H2, respiration is finished and we can apply simpler relationships for dry matter production.

Dynamics of incorporation and respiration

At harvest H1, we can approximate the dynamics with a constant air concentration and an average between gross photosynthesis and final dry matter production (Figure II.10.6).

Figure II.10.7 shows the predicted to observed (P/O) ratio for the C-14 concentration in the total plant at harvest H1. The model performs well for plants exposed early in their growth cycle, but overestimates the concentration for plants exposed at later times.

Experimental and model uncertainties are not shown in Figure II.10.7. Experimental uncertainty is at least a factor 2, and model uncertainty is larger still.

Distribution of new dry matter to plant parts

Partition fractions (the fractions of newly-incorporated dry matter that appear in different parts of the plant) depend on the development stage of the plant and the crop genotype. The development stage (DVS) is defined to lie between 0 and 2, with a value of 1 marking the transition from vegetative stage to reproductive stage (the start of tuber formation). There are potato cultivars with early or late tuber formation and this influences the partition fractions to all plant parts. Both default WOFOST partition fractions (Table II.10.3) and data for a Scottish potato genotype [II.150]; Table II.10.4) were used to test the importance of the partition processes on the model results. The predictions for C-14 concentrations in tubers at harvest were better for the Scottish genotype.

II.10.3.3. Simple model

The simple model considers dry matter production only, predicting the dry mass increment ΔW from the following equation [II.150]:

$$\Delta W = LUE\ Flint\ PAR \qquad \text{(II.10.8)}$$

where:

LUE is light use efficiency (g/MJ), an empirical parameter; and
Flint is light interception, which depends on leaf area index (LAI) and the extinction coefficient for photosynthetically-active radiation.

The predictions of the simple model are similar to those of WOFOST (Figure II.10.8). The simple model can be used together with partition fractions and growth dilution to predict C-14 concentrations in the plant. However, only the WOFOST approach can explain sources of uncertainty in the predictions.

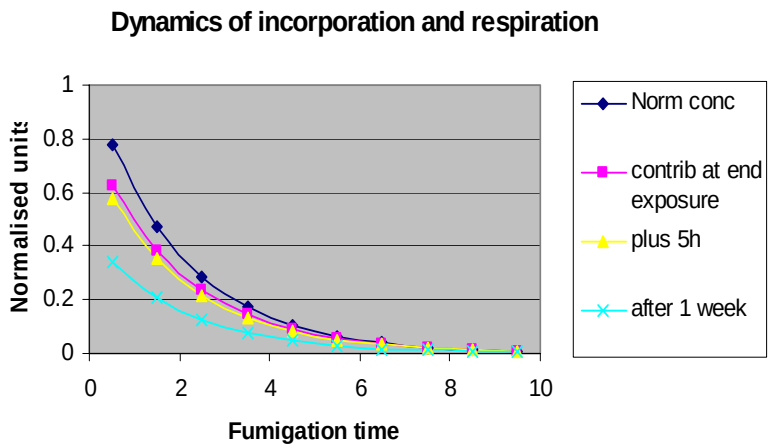

Fig. II.10.6. The dynamics of C-14 incorporation and respiration.

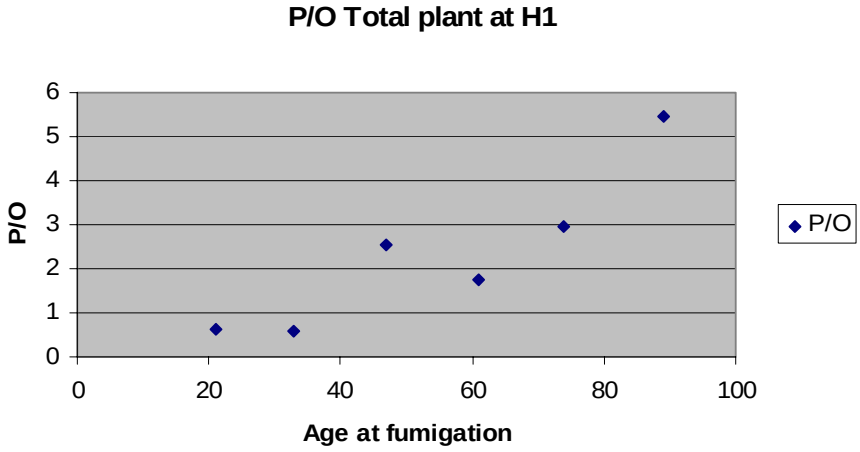

Fig. II.10.7. Predicted to observed ratio of C-14 concentration in the total plant at harvest H1.

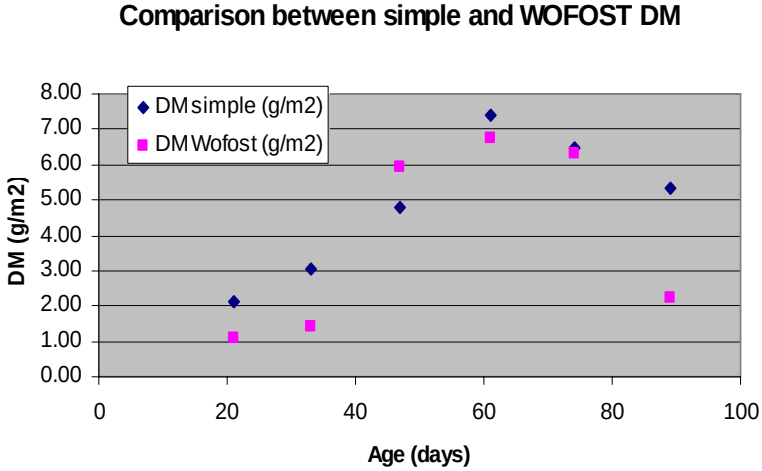

Fig. II.10.8. Comparison between the predictions of WOFOST and the simple model for dry matter (DM) production.

Table II.10.3. Default WOFOST partition fractions.

Exp	Age (d)	DVS	Root fraction	Leaf fraction	Stem fraction	Tuber fraction
P1	21	0.55	0.2	0.64	0.16	0
P2	33	0.87	0.2	0.64	0.16	0
P3	47	1.15	0.1	0.36	0.198	0.342
P4	61	1.37	0	0	0	1
P5	74	1.58	0	0	0	1
P6	89	1.82	0	0	0	1

Table II.10.4. Partition fractions for Scottish cultivar.

Exp	Age (d)	DVS	Root fraction	Leaf fraction	Stem fraction	Tuber fraction
P1	21	0.55	0.2	0.4	0.4	0
P2	33	0.87	0.2	0.24	0.48	0.08
P3	47	1.15	0.1	0.18	0.36	0.36
P4	61	1.37	0	0.05	0.09	0.86
P5	74	1.58	0	0.03	0.05	0.92
P6	89	1.82	0	0.017	0.017	0.966

II.10.4. UTTY Model

II.10.4.1. Model features

Our model, a dynamic compartment model shown in Figure II.10.9, was developed using the MOGRA tool (Migration Of GRound Additions). The model consists of five compartments:

- two organic compartments (stem-leaf-root and tuber);
- one inorganic compartment (whole plant);
- two environmental compartments (air and soil).

Our potato model is almost the same as the rice model used in the Rice Scenario (Section II.9.5 in Appendix II.9). The [ear_org] compartment in the rice model is substituted by the [tuber_org] compartment in the potato model. Differences between the growth rates of potatoes and rice are also considered.

II.10.4.2. Compartments and transfer pathways

The compartments and transfer pathways considered in the UTTY model are shown in Figure II.10.10. The [Plant_inorg] compartment includes the following:

- non-fixed (inorganic) carbon in the plant;
- organic carbon that is readily exchangeable with air.

This compartment considers photosynthesis in the leaves, but the photosynthates generated are not fixed here but rather in the [StemLeaf_org] and [Tube_org] compartments through the transfer parameters K_{PL} and K_{PE}. The [StemLeaf_org] compartment includes the photosynthates fixed in the stem, leaf and root. The amount of photosynthate in this compartment decreases over time because of dark respiration and because most of the photosynthates are directed to the tubers after flowering.

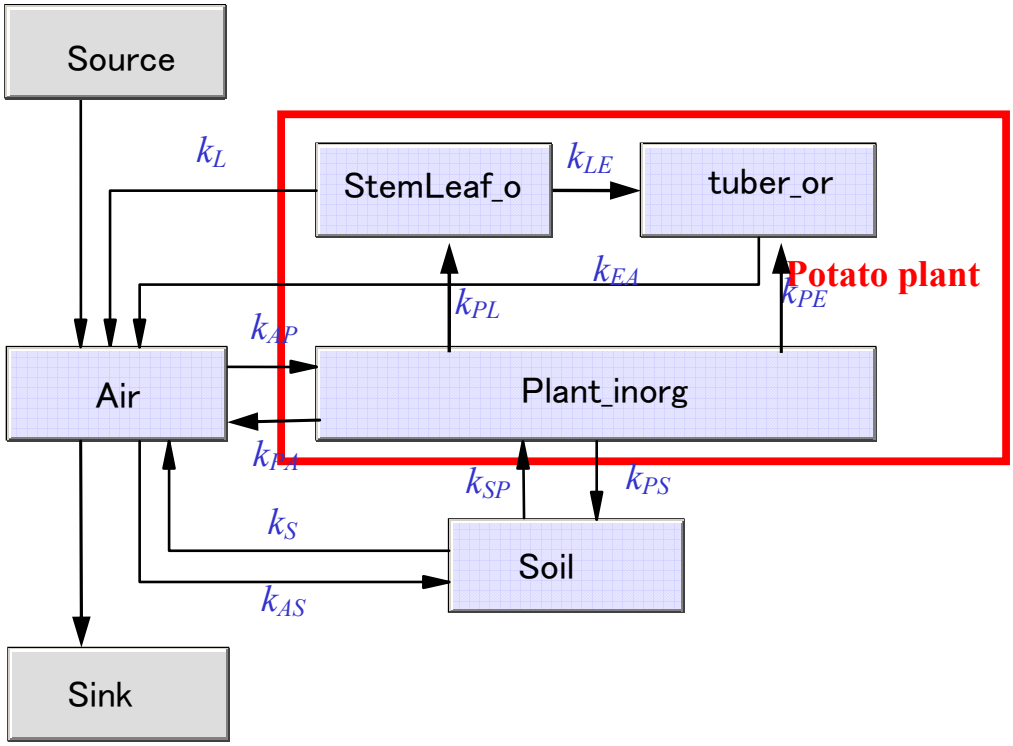

Fig. II.10.9. Potato model of UTTY.

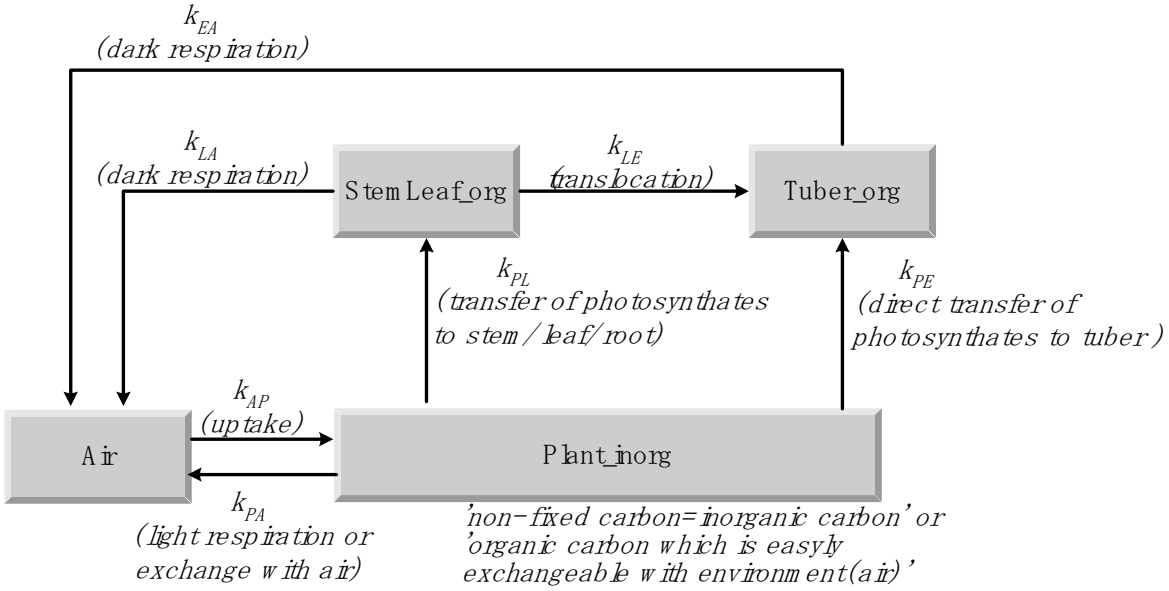

Fig. II.10.10. Compartments and transfer paths in the UTTY potato model.

The [Tuber_org] compartment includes the photosynthates transferred from [Plant_inorg] and/or from [StemLeaf_org] and fixed in the tuber. The amount of photsynthate in this compartment decreases due to dark respiration only.

The [K_{PA}] transfer path represents transfer of carbon from [Plant_inorg] to [Air] due to daylight respiration and/or exchange. The [K_{PE}] transfer path describes the transfer of photosynthates from [Plant_inorg] to [Tuber_inorg] after flowering. Similarly, the [K_{LE}] pathway represents the transfer of photosynthates from [Stemleaf_org] to [Tuber_org] after flowering. Photosynthates are transferred preferentially to the tuber at this stage of plant growth.

The ratio of K_{PE} to (K_{PE} + K_{LE}) depends on the growth rate of the tuber.

II.10.4.3. Transfer factor equations

Air compartment to Plant_inorg compartment: [K_{AP}] is given by the following equation, which is derived in more detail in the Annex II-2:

$$k_{AP} = R_{air} \cdot \left[\alpha_{ino} \cdot \frac{dW_P}{dt} + \left(1 + \beta_{P\_res}\right) \cdot \alpha_{org} \cdot \frac{d}{dt}\left(W_P - W_E\right) + \left(1 + \beta_{E\_res}\right) \cdot \alpha_{E\_org} \cdot \frac{dW_E}{dt} \right] \Big/ W_A \quad \text{(II.10.9)}$$

where:

R_{air} is the ratio of carbon intake from air to total intake from air and soil (= 0.999);
α_{ino} is the ratio of weight of inorganic carbon to total plant weight (= 0.02);
α_{org} is the ratio of weight of organic carbon to the weight of the whole plant without the tuber (α_{org} = 0.37) or to the weight of the tuber (α_{E_org} = 0.40);
β_{res} is the ratio of organic carbon used in respiration to the whole plant without the tuber (β_{P_res} = 0.35) or to the tuber alone (β_{E_res} = 0.15);
W_P, W_E is the total plant and tuber weights (g), which are functions of their respective growth curves; and
W_A is the weight of carbon in air (g/m^3).

The reverse transfer ([Plant_inorg] to [Air]), which represents daylight respiration, is not considered, so that:

$$K_{PA} = 0 \quad \text{(II.10.10)}$$

Soil compartment to Plant_inorg compartment: It is assumed that the concentration in soil quickly equilibrates with the concentration in air. K_{SA} and K_{AS} are set to achieve this assumption. Thus the equations for K_{SP} and K_{PS} are identical to those for K_{AP} and K_{PA} respectively, but with W_A replaced by W_S (weight of carbon in soil) and R_{air} replaced with (1-R_{air}).

Plant_inorg compartment to StemLeaf_org compartment: K_{PL} is given by:

$$k_{PL} = \left[\left(1 + \beta_{P\_res}\right) \cdot \alpha_{org} \cdot \frac{d}{dt}\left(W_P - W_E\right) + \left(1 + (1-\gamma)\beta_{E\_res}\right) \cdot \alpha_{E\_org} \cdot \frac{dW_E}{dt} \right] \Big/ \left(W_P \cdot \alpha_{ino}\right) \quad \text{(II.10.11)}$$

where γ is the ratio of transfer from [StemLeaf_org] to [tuber_org] to the total transfer from all pathways to [tuber_org].

Plant_inorg compartment to tuber_org compartment: K_{PE} is given by:

$$k_{PE} = \gamma \cdot \alpha_{E\_org} \cdot \left(1 + \beta_{E\_res}\right) \cdot \frac{dW_E}{dt} \Big/ \left(W_P \cdot \alpha_{ino}\right) \tag{II.10.12}$$

StemLeaf_org compartment to tuber_org compartment: K_{LE} is given by:

$$k_{LE} = \left(1 - \gamma\right) \cdot \alpha_{E\_org} \cdot \left(1 + \beta_{E\_res}\right) \cdot \frac{dW_E}{dt} \Big/ \left\{\left(W_P - W_E\right) \cdot \alpha_{org}\right\} \tag{II.10.13}$$

In the UTTY model, the transfer of photosynthetic products to the tuber is assumed to occur from both [Plant_inorg] and [StemLeaf_org]. After flowering, the photosynthetic products are directly transferred to the tuber rather than to the stem and the leaves. We recently included the direct path from [Plant_inorg] to [tuber_org] in the model. The relative contributions of the two pathways are determined by the γ factor (Equation II.10.11), which depends on the stage of tuber growth. The following functional relationship was obtained by analysis of the growth curve for rice:

$$\gamma = 1 - \frac{dW(t)}{dW_{\max}} \times 0.7 \tag{II.10.14}$$

where:

$$dW_{\max} = \frac{dW(t = t_{half\_tuber})}{dt} \tag{II.10.15}$$

and

dW(t) is the differential increase in tuber weight (g);
dW_{max} is the maximum differential increase in tuber weight (g);
t_{half_tuberr} is the day at which tuber weight becomes half its maximum value.

StemLeaf_org compartment to Air: This pathway represents dark respiration by the stem and leaves. K_{LA} is given by:

$$k_{LA} = \beta_{P\_res} \cdot \alpha_{org} \cdot \frac{d}{dt}\left(W_P - W_E\right) \Big/ \left\{\left(W_P - W_E\right) \cdot \alpha_{org}\right\} \tag{II.10.16}$$

Tuber_org compartment to Air: K_{EA} describes dark respiration by the tuber and is given by:

$$k_{EA} = \beta_{E\_res} \cdot \alpha_{E\_org} \cdot \frac{dW_E}{dt} \Big/ \left\{\alpha_{E\_org} \cdot W_E\right\} \tag{II.10.17}$$

II.10.4.4. Growth curves

The growth curves for the total plant and for the tuber were both assumed to be sigmoidal (Figure II.10.11):

$$W(t) = W_{harvest} \cdot \frac{10^{K\left(t - t_{half}\right)}}{1 + 10^{K\left(t - t_{half}\right)}} \tag{II.10.18}$$

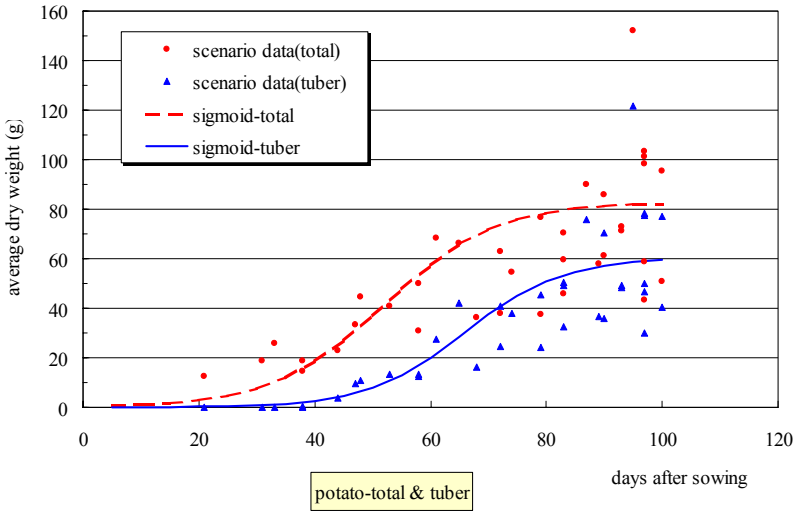

Fig. II.10.11. Observed time-dependent dry weights of the total potato plant and the tuber in the scenario and their sigmoid curves

Table II.10.5. Values of the parameters in the sigmoidal growth curves.

Plant part	**Final dry weight (g) ($W_{harvest}$)**	**t_{half} (d)**	**Shape parameter (d^{-1}) (K)**
Whole plant	83	52	0.04
Tuber	61	66	0.052

where:

$W(t)$ is the total weight of plant (or tuber weight) at time t (g);
$W_{harvest}$ is the total weight of plant (or tuber weight) at harvest (g);
K is the shape parameter of the sigmoid curve (d^{-1});
t = time (d); and
t_{half} is the day at which the whole plant weight becomes half its maximum value.

The factors K and t_{half} were assigned different values for total plant and tuber.

The parameters in Equation II.10.18 were given the values shown in Table II.10.5, based on the experimental data in the Scenario Description (Appendix I.10). It was assumed that the plants were sown on day 0, that the tubers started to grow on day 40 and that the plants were harvested on day 100.

Time-dependent whole plant weights calculated from the sigmoid curves of plant growth are shown in Table II.10.6 for each experiment.

II.10.4.5. Air Concentrations

The UTTY model assumes that the air concentration during exposure is constant over time. A mean concentration for input to the model was obtained by dividing the integrated air concentration by the exposure time (600 min) to give the values in the third column of Table II.10.7 (the [A] concentrations). However, the C-14 amounts in the Plant_inorg

compartment show the effects of the long tail of the exposure (Figure II.10.12). This implies that each part of the potato plant (stem, leaf and tuber) was exposed for more than 10 h. The C-14 amount in the Plant_inorg compartment should quickly become zero (equal to the C-14 concentration in air) after the 10-h exposure; the model should be improved in the future to ensure this. But for the present calculations, the air concentration was adjusted so that the time-integrated C-14 amount in the Plant_inorg compartment became equal to the amount that would have been seen in that compartment during a 10-h exposure to the [A] air concentrations (Figure II.10.12). This resulted in the [B] air concentrations (the last column in Table II.10.7), which were used in the analysis. The ratio of the C-14 amount during the 10-h exposure to the time integrated C-14 amount in the Plant_inorg compartment is different for each experiment because the plant growth rate is different.

Table II.10.6. Time-dependent weights of the whole plant calculated from the sigmoid curves of plant growth for each experiment.

Harvest	P1		P2		P3		P4		P5		P6	
	Day	Weight	Day	Weight	Day	Weight	Day	Weight	Day	Weight	Day	Weight
H1	21	2.93	33	9.01	47	25.30	61	38.03	74	31.51	89	24.31
H2	31	7.54	38	13.69	53	33.05	65	37.36	79	28.21	90	24.09
H3	38	13.69	44	21.13	58	37.15	72	32.98	83	26.22	93	23.57
H4	48	26.69	58	37.15	68	35.79	83	26.22	87	24.82	95	23.31
H5	72	32.98	79	28.21	83	26.22	90	24.09	93	23.57	97	23.11
H6	97	23.11	97	23.11	97	23.11	97	23.11	100	22.89	100	22.89

Table II.10.7. Air concentrations used in the calculations.

Experiment	Integrated air concentration (Bq min/m^3)	Air concentration [A] (Bq/m^3)	Air concentration [B] (Bq/m^3)
P1	9.76×10^6	1.63×10^4	3070
P2	6.98×10^6	1.16×10^4	1877
P3	9.65×10^6	1.61×10^4	1870
P4	8.09×10^6	1.35×10^4	870
P5	8.31×10^6	1.39×10^4	610
P6	4.77×10^6	7.96×10^3	1372
Remark	Table I.10.4 in the Scenario Description (Appendix I.10)	Column 2 divided by 600	Column 3 adjusted (see text and Figure II.10.12)

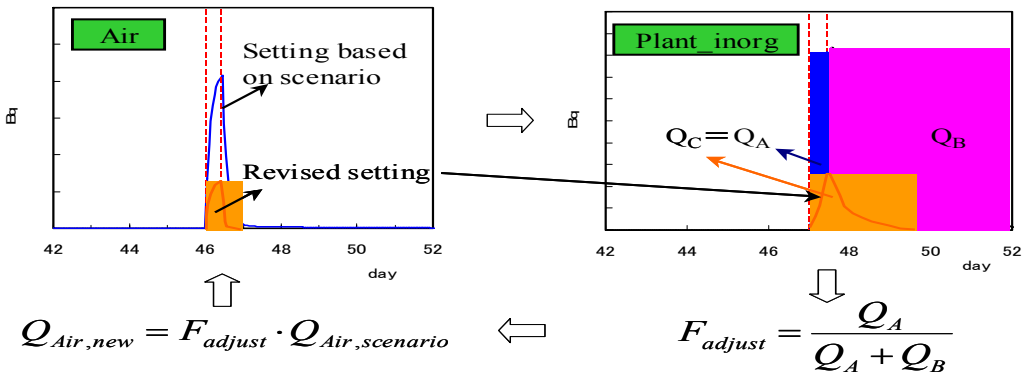

Fig. II.10.12. Adjustment of the amount of carbon in the air compartment.

ANNEX II-2. DERIVATION OF THE EQUATION FOR K_{AP} (TRANSFER FROM AIR TO THE PLANT_INORG COMPARTMENT)

K_{AP} (Equation II.10.9) is determined by all of the increases and decreases of carbon in the plant:

K_{AP} = [increase of inorganic carbon resulting from plant growth]
+ [increase of carbon by photosynthesis]
+ [decrease of carbon by light respiration]
+ [decrease of carbon by dark respiration of stem and leaves]
+ [decrease of carbon by dark respiration of tuber]

$= k_{AP\_ino} + k_{AP\_org} + k_{AP\_res} + k_{AP\_P\_res} + k_{AP\_E\_res}$

where:

$$k_{AP\_ino} = R_{air} \cdot \alpha_{ino} \cdot \frac{dW_P}{dt} \Big/ W_A \tag{II-2.1}$$

$$k_{AP\_org} = R_{air} \cdot \frac{d}{dt}\left\{\left(W_P - W_E\right) \cdot \alpha_{org} + W_E \cdot \alpha_{E\_org}\right\} \Big/ W_A \tag{II-2.2}$$

$$k_{AP\_res} = R_{air} \cdot \beta_{Pl\_res} \cdot \alpha_{ino} \cdot \frac{dW_P}{dt} \Big/ W_A \tag{II-2.3}$$

$$k_{AP\_P\_res} = R_{air} \cdot \beta_{P\_res} \cdot \alpha_{org} \cdot \frac{d\left(W_P - W_E\right)}{dt} \Big/ W_A \tag{II-2.4}$$

$$k_{AP\_E\_res} = R_{air} \cdot \beta_{E\_res} \cdot \alpha_{E\_org} \cdot \frac{dW_E}{dt} \Big/ W_A \tag{II-2.5}$$

Since daylight respiration is not considered in the model:

$$k_{AP\_res} = 0 \tag{II-2.6}$$

K_{AP} is given by the sum of Equations II-2.1 to II-2.6:

$$k_{AP} = R_{air} \cdot \left[\alpha_{ino} \cdot \frac{dW_P}{dt} + \left(1 + \beta_{P\_res}\right) \cdot \alpha_{org} \cdot \frac{d}{dt}\left(W_P - W_E\right) + \left(1 + \beta_{E\_res}\right) \cdot \alpha_{E\_org} \cdot \frac{dW_E}{dt}\right] \Big/ W_A \tag{II-2.7}$$

K_{PL} (Equation II.10.11) and K_{EA} (Equation II-10.17) are obtained in the same manner.

REFERENCES

[II.1] MURPHY, C.E., Tritium transport and cycling in the environment, Health Physics 65, 683–697 (1993).

[II.2] DIABATE, S., STRACK, S., Organically bound tritium, Health Physics 65, 698–712 (1993).

[II.3] CIFFROY, P., SICLET, F., DAMOIS, C., LUCK, N., A dynamic model to assess radiological consequences of tritium routinely released in rivers, Submitted to Journal of Environmental Radioactivity (2006).

[II.4] KIRCHMANN, R., BONOTTO, S., SOMAN, S.D., KRISHNAMOORTHY, T.M., IYENGAR, T.S., MOGHISSI, A.A., Transfer and incorporation of tritium in aquatic organisms, In: "Behaviour of Tritium in the Environment", IAEA-SM-232/96 (1979).

[II.5] BAUMGÄRTNER, F., DONHAERL, W., Non-exchangeable organically bound tritium (OBT): its real nature, Anal. Bioanal. Chem. 379, 204–209 (2004).

[II.6] FALK, M., POOLE, A-G., GOYMOUR, C.G., Infrared study of the state of water in the hydration shell of DNA, Can. J. Chem. 48, 1536–1542 (1970).

[II.7] BAUMGÄRTNER, F., Accumulative tritium transfer from water into biosystems, Proceedings of the 7th International Conference on Tritium Science and Technology, September 2004, Baden-Baden, Germany (2005).

[II.8] DI BARI, M., DERIU, A., ALBANESE, G., CAVATORTA, F., Dynamics of hydrated starch saccharides, Chem. Phys. 292, 333–339 (2003).

[II.9] KLAPPER M.H., The independent distribution of amino acids near neighbour pairs into polypeptides, Biochem. and Biophys. Research Comm. 78, 1018–1024 (1977).

[II.10] BAUMGÄRTNER, F., KIM, M.-A., Tritium/protium fractionation near and inside DNA, J. Radioanal. & Nuclear Chem., 243, 295–298 (2000).

[II.11] SAENGER, W., Structure and dynamics of water surrounding biolmolecules, Ann. Rev. Biophys. Chem. 16, 93–114 (1987).

[II.12] CLELAND, W.W., O'LEARYM M.H., (Editors), Isotope effects on enzyme-catalyzed reactions, Northrop DB, University Park Press (1977).

[II.13] CORNETT, R.J., RISTO, B.A., LEE, D.R., Measuring groundwater transport through lake sediments by advection and diffusion, Water Resources Research 25, 1815–1823 (1989).

[II.14] GALERIU, D.C., HELING, R., MELINTESCU, A., The dynamics of tritium – including OBT – in the aquatic food chain, Proceedings of the 7th International Conference on Tritium Science and Technology, September 2004, Baden-Baden, Germany (2005).

[II.15] RAY, Ecological Modeling 140, 219–234 (2001).

[II.16] HAKANSON, L., BULLION, V., Empirical and dynamical models to predict the cover, biomass and production of macrophytes in lakes, Ecological Modeling 151, 213 (2002).

[II.17] CRAIG, S., HELFRICH, L.A., Understanding fish nutrition, feeds and feeding, Virgnia Co-operative Extension, Publication 420–256 (2002).

[II.18] ROGERS, D.W., Tritium dynamics in juvenile rainbow trout, salmo gairdneri, Health Physics 50, 89–98 (1996).

[II.19] MCCUBBIN, D., LEONARD, K.S., Incorporation of organic tritium by marine organisms and sediment in the Severn Estuary/Bristol Channel, UK (2001).

[II.20] ARAPIS, G., BONOTTO, S., BOSSUS, A., Tritium and technetium uptake and distribution in three marine algae, In: Capuzzo, J.M., Kester, D.R. (Eds.), Oceanic Processes in Marine Pollution, Vol. 1, Biological Processes and Wastes in the Ocean. Krieger, Malabar, FL (1987).

[II.21] HAMBY, D., PALMER, J., Analysis of an internal kinetic model for free and bound tritium. Health Physics (2001).

[II.22] ROMANOV, G.N., Behavior of tritium in the environment and detrimental biological effects, In: The Issue of Science and Technique, ser. Radiation Biology, Vol. 4, 6–31 (In Russian) (1983.).

[II.23] PETERSON, S-R., Historical Doses from Tritiated Water and Tritiated Hydrogen Gas Released to the Atmosphere from Lawrence Livermore National Laboratory (LLNL) Part 1, Description of Tritium Dose Model (DCART) for Chronic Releases from LLNL, Lawrence Livermore National Laboratory, Livermore, CA, UCRL-TR-205083 (2004).
The report is available at http://library.llnl.gov/uhtbin/cgisirsi/0/0/60/55/X.

[II.24] MURPHY, C.E., Jr., The relationship between tritiated water activities in air, vegetation and soil under steady-state conditions, Health Physics, 47, 635–639 (1984).

[II.25] INTER-DISCIPLINARY RESEARCH AND APPLICATIONS BASED ON NUCLEAR AND ATOMIC PHYSICS, A standard guide for dose assessment of routine releases of tritium for any tritium facility, Center of Excellence Report WP3 IDRANAP 31-02/2002 (2002)..

[II.26] SMITH G.M., ROBINSON, P.C., STENHOUSE, M.J., H-3 Foodchain Modelling Following Short Term Release to the Atmosphere, Intera Information Techologies (1995).

[II.27] INTERNATIONAL ATOMIC ENERGY AGENCY, Modelling the environmental transport of tritium in the vicinity of long-term atmospheric and subsurface sources, IAEA-BIOMASS-3, IAEA, Vienna (2003).

[II.28] KIRCHMANN, R., CHARLES, P., VAN BRUWAENE, R., REMY, J., Distribution of tritium in the different organs of calves and pigs after ingestion of various tritiated feeds, Current Topics in Radiation Research, Q 12, 291 (1977).

[II.29] KIRCHMANN, R., REMY, J., CHARLES, P., KOCH, G., Distribution and incorporation of tritium in different organs of ruminants, IAEA-SM-172/81, IAEA, Vienna (1985).

[II.30] CHINO, M., ET AL., Dose evaluation model on complex topography by random walk model using 3 dimension wind speed, AESJ, 26, 526–534 (1984).

[II.31] CHINO, M., ET AL., WSPEEDI (World wide version of SPEEDI); A computer code system for the prediction of radiological impacts on Japanese due to a nuclear accident in foreign countries, JAERI-M, 1334 (1995).

[II.32] INTERNATIONAL ATOMIC ENERGY AGENCY, A test of chronic atmospheric release models using Canadian data, BIOMASS Theme 3, Tritium Working Group Working Document, 3 November 2000, IAEA, Vienna (2000).

[II.33] INTERNATIONAL ATOMIC ENERGY AGENCY, A test of chronic atmospheric release models using Russian data, BIOMASS Theme 3, Tritium Working Group Working Document, 4 November 2000, IAEA, Vienna (2000).

[II.34] YAMAMOTO, K., SAKASHITA, T., MIYAMOTO, K., Development and Validation of an Atmospheric Dispersion Model for Tritium using the IAEA BIOMASS Scenario, Fusion Science and Technology, 48, 500–503 (2005).

[II.35] MAEDE, P.J., The Effects of Meteorological Factors on the Dispersion of Airborne Material, Rassegns Internasionale Elettronica e Nucleare 6 Rassegna Rome 1959, 11, 107–130 (1959).

[II.36] PASQUILL, F., The Estimation of the Dispersion of Windborne Material, Meteorol. Mag. 90, 33–49 (1961).
[II.37] LORIMER, G.S., The Kernel for Air quality modeling (I), Mathematical formulation, Atmos. Environ., 20, 1447–1452 (1986).
[II.38] GARLAND, J.A., COX, L.C., The absorption of tritium gas by English soils, plants and the sea, Water Air Soil Poll., 14, 103–114 (1980).
[II.39] NOGUCHI, H., et al., Tritium behavior observed in the Canadian release study, Fusion Tech., 14, 1287–1292 (1988).
[II.40] SASSCER, D.S., et al., Dynamic model of water movement in soil under various climatological condition, In: "Tritium", Messenger Graphics, Las Vegas, Nevada, 485–495 (1973).
[II.41] OGRAM, G.L., et al., Field studies of the HT behavior in the environment: 2 The interaction with soil, Fusion Tech., 14, 1170–1175 (1988).
[II.42] FORESTEL, H., HT to HTO conversion in the soil and subsequent tritium pathway: Field release data and laboratory experiments, Fusion Tech., 14, 1241–1246 (1988).
[II.43] DIABATE, S., STRACK, S., Organically bound tritium in wheat after short-term exposure to atmospheric tritium under laboratory conditions, J. Environ. Radioactivity, 36, 157–175 (1997).
[II.44] BELOT, Y., Tritium in plants: A review, Radiation Protection Dosimetry, 16, 101–105 (1986).
[II.45] MCFARLANE, J.C., Tritium fractionation in plants. Envirn. Exp. Botany, 16, 9–14 (1976).
[II.46] MIYAMOTO, K., INOUE, Y., IWAKURA, T., TAKEDA, H., FUMA, S., YANAGISAWA, K., ISHII, N., An application of a transfer model to the drainage system of tritium in a river basin in the vicinity of a nuclear site, Fusion Science and Technology, 41, 483–487 (2002).
[II.47] NUCLEAR SAFETY COMMISSION OF JAPAN, Meteorological Guideline for the Safety Analysis of Nuclear Power Plants (Hatudenyougenshiroshisetu no anzenkaisekinikansuru kishoushishin, in Japanese) Taiseishuppansha, Tokyo, p. 398 (2000).
[II.48] INOUE, Y., IWAKURA, T., MIYAMOTO, K., Environmental Aspects of Tritium Released into the Atmosphere in the Vicinity of Nuclear Facilities in Japan, NIRS-M-52, pp. 296–315 (1983).
[II.49] BELOT, Y., GAUTHIER, D., CAMUS, H., CAPUT, C., Prediction of the flux of tritiated water from air to plant leaves, Health Physics, 37, 576–583 (1979).
[II.50] GARLAND, J.A., AMEEN, M., Incorporation of tritium in grain plants, Health Physics, 36, 35–38 (1979).
[II.51] KIM, M.A., BAUMGÄRTNER, F., Equilibrium and non-equilibrium partition of tritium between organics and tissue water of different biological systems, Anal.Radiat. Isot., 45, 351–353 (1994).
[II.52] PETERSON, S-R., Historical Doses from Tritiated Water and Tritiated Hydrogen Gas Released to the Atmosphere from Lawrence Livermore National Laboratory (LLNL) Part 1, Description of Tritium Dose Model (DCART) for Chronic Releases from LLNL, UCRL-TR-205083-REV-1, Livermore, CA (2006). http://library-r.llnl.gov/uhtbin/cgisirsi/i5V55DaK0I/MAIN/230100017/9
[II.53] DORMAN, J.L., SELLERS, P.J., A global climatology of albedo, roughness length and stomatal resistance, J. App. Meteorology 28, 833 (1989).

[II.54] SCHULTZE, E.D., ET AL., Relationships among maximum stomatal conductance, ecosystem surface conductance, carbon assimilation rate, and plant nitrogen nutrition: a global ecology scaling exercise, Annu. Rev. Ecol. Syst 25, 629 (1994).
[II.55] FRIEND, A.D., ET AL., A process-based, terrestrial biosphere model of ecosystem dynamics, Ecological modeling 95, 249 (1997).
[II.56] KIM, C-K., ET AL., Environmental distribution and behaviour of ^{3}H and ^{14}C around Wolsong NPP, Health Physics 78, 693 (2000).
[II.57] RUSSELL, S.B., OGRAM, G.L., ETMOD: A New Environmental Tritium Model, Fusion Technology, Vol. 21, pp. 645–650 (1992).
[II.58] THOMPSON, J.W., KENNEDY, J.A., LINA, J-M., ETMOD Software Quality Assurance Documentation, Volumes 1–3, CFFTP P-9205, Prepared by Atlantic Nuclear Services Limited for CFFTP, 2700 Lakeshore Road West Mississauga, Ontario L5J 1K0 (1992).
[II.59] WESLEY, M.L., Parameterization of Surface Resistances to Gaseous Dry Deposition in Regional-Scale Numerical Models, Atmospheric Environment 23, pp. 1293–1304 (1989).
[II.60] WEIR, A.H., BRAGG, P.L., PORTER, J.R., RAYNER, J.H., A Winter Wheat Crop Simulation Model Without Water or Nutrient Limitations, Journal of Agricultural Science, Vol. 102, pp. 371–382 (1984).
[II.61] SELLERS, P.J., Canopy Reflectance, Photosynthesis and Transpiration, International Journal of Remote Sensing, Vol. 6, No. 8, pp. 1335–1372 (1985).
[II.62] MITCHELL, R.A.C., LAWLOR, D.W., YOUNG, A.T., Dark Respiration of Winter Wheat Crops in Relation to Temperature and Simulated Photosynthesis, Annals of Botany, Vol. 67, pp. 7–16 (1991).
[II.63] PINDER III, J.E., CIRAVOLO, T.G., BOWLING, J.W., The Interrelationships Among Plant Biomass, Plant Surface Area and the Interception of Particulate Deposition by grasses, Health Physics Vol. 55, No. 1, pp.51–58 (1988).
[II.64] GALERIU, D., RASKOB, W., DAVIS, P.A., CHOUHAN, S.L., Uncertainty and sensitivity analysis for the environmental tritium code UFOTRI, Fusion Technology 28, 853–858 (1995).
[II.65] BELOT, Y., Comportement du tritium dans l'environnement In: Le tritium de l'environnement à l'homme, p.63 (eds : Belot, Y., Roy, M. & Métivier, H.) Les Editions de Physique, France (1996).
[II.66] KUMUDINI, S., HUME, D.J., CHU, G., Genetic improvement in short season soybeans: I. Dry matter accumulation, partitioning, and leaf area duration, Crop Sci. 41, 391–398 (2001).
[II.67] PEDERSEN, P., LAUER, J.G., Soybean yield components response to management system and planting date, Agron. J. 96, 1372–1381 (2004).
[II.68] GUENOT, J., BELOT, Y., Assimilation of ^{3}H in photosynthesizing leaves exposed to HTO, Health Physics 47, 849–855 (1984).
[II.69] RASKOB, W., UFOTRI: Description of the New Version of the Tritium Model UFOTRI 4.0, including user guide, Report KfK-5194, Kernforschungszentrum Karlsruhe (1993).
[II.70] SMITH, A.D., Calculation Of Critical Group Doses Resulting From Short-term Aerial Releases Of Radionuclides From Sellafield, BNFL, Risley (1989).
[II.71] GALERIU, D., MELINTESCU, A., TURCANU, C., RASKOB, W., "FDMH – The Tritium Module in RODOS", Workshop on Environmental Behavior and Biological Effects of Tritium, 8–9 May 2000, P.86, Kurri, Kumatori, Osaka, Japan, Ed. M. Saito, S. Kimura, and T. Takahashi ISSN 0287-0852 [KURRI-KR-61] (2000).

[II.72] MELINTESCU, A., GALERIU, D., MARICA, E., "Using WOFOST Crop Model for Data Base Derivation of Tritium and Terrestrial Food Chain Modules in RODOS", P. C1-1241- C1–1246, Radioprotection, Numero special 37, C1, "The Radioecology – Ecotoxicology of Continental and Estuarine Environments ECORAD 2001" (2002).

[II.73] PENNING DE VRIES, F.W.T., JENSEN, D.M., TEN BERGE, H.F.M., BAKEMA, A., Simulation of ecophysiological processes of growth in several annual crops Pudoc Wageningen (1989).

[II.74] ICHIMASA, M., WENG, C., ARA, T., ICHIMASA, Y., Organically bound deuterium in rice and soybean after exposure to heavy water as a substitute for tritiated water, Fusion Science and Technology, 41, 393–398 (2002).

[II.75] ICHIMASA, M., MAEJIMA, T., SEINO, N., ARA, T., TAUCHI, H., ICHIMASA, Y., Organically bound deuterium in soybean exposed to atmospheric D_2O vapor as a substitute for HTO under different growth phase, Proceedings of the International Symposium, Transfer of Radionuclides in Biosphere-Prediction and Assessment, JAERI-Conf. 2003-010, 226–232 (2003).

[II.76] BARRY, P.J., WATKINS, B.M. BELOT, Y., DAVIS, P.A., EDLUND, O., GALERIU, D., RASKOB, W., RUSSELL, S., TOGAWA, O., Intercomparison of model predictions of tritium concentrations in soil and foods following acute airborne HTO exposure, J. of Environmental Radioactivity 42, 191–207 (1999).

[II.77] SWEDISH RADIATION PROTECTION INSTITUTE, BIOMOVS II, Tritium in the Food Chain: Intercomparison of model predictions of contamination in soil, crops, milk and beef after a short exposure to tritiated water vapour in air, Published on behalf of the BIOMOVS II Steering Committee by SSI, Sweden, ISBN 91-972134-7-0 (1996a).

[II.78] SWEDISH RADIATION PROTECTION INSTITUTE, BIOMOVS II, Tritium in the Food Chain: Comparison of predicted and observed behaviour; A: Re-emission from soil and vegetation, B: Formation of organically bound tritium in grain of spring wheat, Published on behalf of the BIOMOVS II Steering Committee by SSI, Sweden, ISBN 91-972958-2-5 (1996b).

[II.79] INTERNATIONAL ATOMIC ENERGY AGENCY, BIOMASS Programme, Version Beta CD-ROM, IAEA, Vienna (2001).

[II.80] RASKOB, W., UFOTRI: Program for assessing the off-site consequences from accidental tritium release, KfK-4605, Kernforschungszentrum Karsruhe (1990).

[II.81] AMANO, H., GARTEN JR., C.T., Uptake of tritium by plants from atmosphere and soil, Environmental International, 17, 23–29 (1991).

[II.82] KIM, M.A., BAUMGÄRTNER, F., Equilibrium and non-equilibrium partition of tritium between organics and tissue water of different biological systems, Appli.Radiat.Isot., 45, 353–360 (1994).

[II.83] STÖCKLE, C.O., DONATELLI, M., NELSON, R., CropSyst, a cropping systems simulation model, Europ. J. Agronomy, 18, 289–307 (2003).

[II.84] GARLAND, J.A., COX, L.C., Uptake of tritiated water vapor by bean leaves, Water, Air, and Soil Pollution, 17, 207–212 (1982).

[II.85] CLINE, J.F., Absorption and metabolism of tritium oxide and tritium gas by bean plants, Plant Physiol., 28, 717–723 (1953).

[II.86] WATKINS, B.M., ROBINSON, P.C., SMITH, G.M., Update of models for assessing short-term atmospheric releases of C-14 and tritium in the light of new information and experimental data, Quantisci – MAFF-5044-1 (1998).

[II.87] SAITO, M., A modified three-compartment model for tritium metabolism in man, Radiation Protection Dosimetry 42, 17 (1992).

[II.88] MAUL, P., THORNE, M.C., WATSON, C., WALKE, R., Prism food chain modelling software, Version 3.0 Technical Guide, Quintessa Report QRS-3004A-2 (2006).
[II.89] WATSON, C., ROBINSON, P., The Prism food chain modelling Software, Version 3.0 User Guide, Quintessa Report QRS-3004A-3 (2006).
[II.90] WALKE, R., THORNE, M.C., WATSON, C., The Prism food chain modelling software, Version 3.0 Testing and Verification Report, Quntessa Report QRS-2004A-4 (2006).
[II.91] OULD-DADA, Z., A demonstration of SPADE and AMBER, Notes from the European Crop Protection Association meeting "Dietary Risk Assessment Workshop", Brussels (2005).
[II.92] XU, X.G., CHAO, T.C., BOZKURT, A., VIP-Man: An image-based whole-body adult male model constructed from colour photographs of the Visible Human Project for multi-particle Monte Carlo calculations (for Reference Man organ masses), Health Physics 78, 476–486 (2000).
[II.93] WALKE, R., THORNE, M.C., Adaptation of Prism H3 to partition excretion, Quntessa Report QRS3004B (2007).
[II.94] GALERIU, D., BERESFORD, N.A., MELINTESCU, A., CROUT, N.M.J., TAKEDA, H., ^{14}C and tritium dynamics in wild mammals: a metabolic model, Radioprotection, Suppl. 1, Vol 40, 351–357 (2005a).
[II.95] GALERIU, D., TAKEDA, H., MELINTESCU, A., TRIVEDI, A., Energy metabolism and human dosimetry of tritium, Fusion Science and Technology, Vol 48, 795–798 (2005b).
[II.96] GALERIU, D., MELINTESCU, A., BERESFORD, N.A., TAKEDA, H., CROUT, N.M.J., The dynamic transfer of ^{3}H and ^{14}C in mammals – a proposed generic model. Radiation and Environmental Biophysics. DOI: 10.1007/s00411-008-0193-9 (2008).
[II.97] VAN MILGEN, J., NOBLET, J., Energy partitioning in growing pigs: The use of a multivariate model as an alternative for the factorial analysis, J. Anim. Sci. 77, 2154–2162 (1999).
[II.98] VAN MILGEN, J., NOBLET, J., Partitioning of energy intake to heat, protein and fat in growing pigs, J. Anim. Sci. 81(E. Suppl. 2), E86–E93 (2003).
[II.99] VAN MILGEN, J., NOBLET, J., VALANCOGNE, A., DUBOIS, S., DOURMAD, J.Y., InraPorc : un modèle pour analyser les performances et évaluer les stratégies alimentaires chez le porc en croissance, Journées de la Recherche Porcine en France 37, 291–298 (2005).
[II.100] VAN MILGEN, J., NOBLET, J., Modelling energy expenditure in pigs, In: Modelling nutrient utilisation in farm animals, Ed J.P. McNamara, CAB International (2000).
[II.101] QUINIOU, N., NOBLET, J., Prediction of tissular body composition from protein and lipid deposition in growing pigs, J. Anim. Sci. 73, 1567–1575 (1995).
[II.102] NOBLET, J., BONTEMS, V., TRAN, G., Estimation de la valeur énergétique des aliments pour le porc., INRA Prod. Anim., 16(3), 197–210 (2003).
[II.103] PETERSON, S.R., DAVIS, P.A., Tritium doses from chronic atmospheric releases: a new approach proposed for regulatory compliance, Health Physics 82, 213–225 (2002).
[II.104] RICHARDSON, R.B., DUNFORD, D.W., A biochemical-based model for the dosimetry of dietary organically bound tritium, Part 2: Dosimetric evaluation, Health Physics 85, 539–552 (2003).
[II.105] CHOUHAN, S.L., Addendum computer program abstract and theory manual for ETMOD 2, AECL Report RC-2901, Vol. 2, Revision 0, 123p (2004).

[II.106] KIM, S-B., WORKMAN, W.G.J., DAVIS, P.A., YANKOVICH, T., Tritium concentrations in the Perch Lake ecosystem, AECL document CRD-03700-ENA-003. Chalk River Laboratories, Chalk River, Ontario (2004).
[II.107] REN, J.S., ROSS, A.H., HAYDEN, B.J., Comparison of assimilation efficiency on diets of nine phytoplankton species of the greenshell mussel Perna canaliculus, J. of Shellfish Res. (2006).
[II.108] SUKHOTIN, A.A., PORTNER, H.-O., Age-dependence of metabolism in mussels Mytilus edulis (L.) from the White Sea, Journal of Experimental Marine Biology and Ecology 257[1], 53–72 (2001).
[II.109] WONG, W.H., LEVINTON, J.S., Culture of the blue mussel Mytilus edulis (Linnaeus, 1758) fed both phytoplankton and zooplankton: a microcosm experiment, Aquaculture Research, 35(10), 965–969 (2004).
[II.110] ZOTIN, A.A., OZERNYUK, N.D., Age-Related Changes in Oxygen Consumption in the Edible Mussel Mytilus edulis from the White Sea. Biology Bulletin of the Russian Academy of Sciences, 31(5), 465–468 (2004).
[II.111] SHEPPARD, S.C., CIFFROY, P., SICLET, F., DAMOIS, C., SHEPPARD, M.I., STEPHENSON, M., Conceptual approaches for the development of dynamic specific activity models of ^{14}C transfer from surface water to humans, Journal of Environmental Radioactivity, 87(1), 32–51 (2006).
[II.112] JORGENSEN, S.E., Handbook of Environmental Data and Ecological Parameters, Pergamon Press, Oxford (1979).
[II.113] TREMBLAY, R., MYRAND, B., SEVIGNY, J.M., GUDERLEY, H., Bioenergetic and genetic parameters in relation to susceptibility of blue mussels, Mytilus edulis (L) to summer mortality, J. Exp. Mar. Biol. Ecol., 221, 27–58 (1998).
[II.114] GRIFFITHS, A.J.F., MILLER, J.H., SUZUKI, D.T., LEWONTIN, R.C., GELBART, W.M., An Introduction to Genetic Analysis, 5th ed. W.H. Freeman and Comp, New York. p. 308 (1993).
[II.115] EIGEN, M., Protonenübertragung, Säure-Base-Katalyse und enzymatische Hydrolyse, Teil I, Elementarvorgänge, Angewandte Chemie 75, 489–508 (1963).
[II.116] ATKINS, P.W., Physical Chemistry, 6th Edition, W.H. Freeman and Company, New York (1997).
[II.117] RASKOB, W., Modelling of the Tritium Behaviour in the Environment, In: Proceedings of the 4th Topical Meeting on Tritium Technology in Fission, Fusion, and Isotopic Applications. Albuquerque, 29.9.91–4.10.91, Fusion Technology, 21, 2, 636–645 (1992).
[II.118] STRAKA, J., GEISS., H., VOGT, K.J., Diffusion of Waste Air Puffs and Plumes under Changing Weather Conditions, Contr. Atm. Phys., Vol. 54, 207–221 (1981).
[II.119] TURNER, D.B., Workbook of Atmospheric Dispersion Estimates, Public Health Service Publication No. 999-AP-26 (1970).
[II.120] JARVIS, P.G., The Interpretation of the Variation in Leaf Water Potential and Stomatal Conductance Found in Canopies in the Field, Phil. Trans. R. Soc. London, Vol. B 273, 593–610 (1976).
[II.121] DEARDORFF, J.W., Efficient Prediction of Ground Surface Temperature and Moisture, with Inclusion of Layer of Vegetation, Journal of Geophysical Research, Vol. 93, No. 4, 1889–1903 (1978).
[II.122] WALLEY, W.J., HUSSEIN, D.E.D., A Development and Testing of a General Purpose Soil-Moisture-Plant Model, Hydrological Sciences Journal, Vol. 27, Nr. 1, 1–17 (1982).
[II.123] BRUTSAERT, W.H., Evaporation into the Atmosphere, D. Reidel Publishing Company, Dordrecht (1982).

[II.124] SHAW, P.V., HAYWOOD, S.M., A Dynamic Model for Predicting the Movement of Tritium in the Environment, Radiation Protection Dosimetry, Vol. 16, No. 1–2, 59–62 (1986).
[II.125] BRIGGS, G.A., Diffusion estimation for small emissions, 1973 Annual Report ATDL-106, Environmental Research Laboratories Air Resources Atmospheric turbulence and Diffusion Laboratory, National Oceanic and Atmospheric Administration (1974).
[II.126] SMITH, F.B., A scheme for estimating the vertical dispersion of a plume from a source near ground level, Proceedings of the Third Meeting of the Expert Panel on Air Pollution Modelling, NATO Committee on the Challenges of Modern Society, Report No. 14, Brussels (1972).
[II.127] HOSKER, R.P., JR., Estimates of dry deposition and plume depletion over forests and grassland, In: Physical Behaviour of Radioactive Contaminants in the Atmosphere, IAEA-SM-181/19, 291–309 (1974).
[II.128] GOLDER, D., Relations among stability parameters in the surface layer, Boundary Layer Meteorology 3, 47 (1972).
[II.129] INTERNATIONAL COMMISSION ON RADIOLOGICAL PROTECTION, Age-dependent doses to members of the public from intake of radionuclides, Part 1, ICRP Publication 56, Elsevier (1990).
[II.130] MEADE, P.J., The effects of meteorological factors on the dispersion of airborne material, Rassegna Internasionale Elettronica e Nucleare 6, 107–130 (1959).
[II.131] CHAMBERLAIN, A.C., EGGLETON, E.J., Washout of tritiated water vapour by rain, Air Water Pollution 8, 135–149 (1964).
[II.132] HUKKOO, R.K., BAPAT, V.N., SHIRVAIKAR, V.V., Manual of dose evaluation from atmospheric releases, Bhabha Atomic Research Centre Report BARC-1412 (1988).
[II.133] CHAMBERLAIN, A.C., Aspects of travel and deposition of aerosol and vapor clouds, UKEA Report HP/R-1261 (1953).
[II.134] INTERNATIONAL COMMISSION ON RADIOLOGICAL PROTECTION, Annals of ICRP, Individual monitoring for internal dose exposure of workers, ICRP Publication 78, Elsevier (1997).
[II.135] MELINTESCU, A., GALERIU, D., A versatile model for tritium transfer from atmosphere to plant and soil", Radioprotection Suppl 1, Vol. 40, S437-442 (2005).
[II.136] OSAKI, M., TANAKA, A., Current photosynthates and storage substances as the respiratory substrates in the rice plant, Nihon Dojou Hiryougaku zasshi (Japanese J. Soil Sci. Plant Nutrition), 50, 540–546 (in Japanese with English abstract) (1979).
[II.137] AQUILONIUS, K., HALLBERG, B., Process-oriented dose assessment model for ^{14}C due to releases during normal operation of a nuclear power plant, J. Environ. Radioact. (2005).
[II.138] CHOI, Y.H., LIM, K.M., YU, D., PARK, H.K., CHOI, Y.G., LEE, C.M., Tissue free water tritium and organically bound tritium in the rice plant acutely exposed to atmosphere HTO vapor under semi-outdoor conditions, J. Environ. Radioact., 58, 67–85 (2002).
[II.139] KEUM, D-K., HAN-SOO LEE, HEUI-JU CHOI, HEE-SEOK KANG, KWANG-MUK LIM, YOUNG-HO CHOI, A dynamic compartment model for assessing the transfer of radionuclide deposited onto flooded rice, J. Environ. Radioact., 76, 349–367 (2004).
[II.140] YU, QIANG, JIANDONG LIU, YONGQIANG ZHANG, JUN LI, Simulation of rice biomass accumulation by an extended logistic model including influence of meteorological factors, Int. J. Biometeorol., 46, 185–191 (2002).

[II.141] WOFOST, User's guide for the WOFOST 7.1 crop growth simulation model and WOFOST Control Center 1.5 Technical Document 52 DLO, Vinand Staring Centre, Wageningen, 1998
[II.142] ORYZA, www.icasa.net/oryza. (2000).
[II.143] BOUMAN, B.A.M., KROPFF, M.J., TUONG, T.P., WOPEREIS, M.C.S., TEN BERGE, H.F.M., VAN LAAR, H.H., ORYZA2000: modeling lowland rice. Los Baños (Philippines): International Rice Research Institute, and Wageningen: Wageningen University and Research Centre, 235 pp + CD-ROM (ISBN 971-22-0171-6) (2001).
[II.144] BOUMAN, B.A.M., TUONG, T.P., KROPFF, M.J., VAN LAAR, H.H., The model ORYZA2000 to simulate growth and development of lowland rice, In: Eds F. Ghassemi, D. White and S. Cuddy (2001).
[II.145] THORNLEY, J., JOHNSON, I., Plant and crop Modelling, Clarendon Press Oxford (1990).
[II.146] Notes from Course on Probabilistic Modelling of Exposures for Risk Assessment – UK IGHRC (2005).
[II.147] OULD-DADA, Z., SPADE Training, Food Standards Agency (2002).
[II.148] OULD-DADA, Z., A Demonstration of SPADE and AMBER, MAFF (1999).
[II.149] SHEPPARD, S.C., SHEPPARD, M.I., SICLET, F., Parameterization of a dynamic specific activity model of ^{14}C transfer from surface water to humans, Journal of Environmental Radioactivity 87, 15–31 (2006).
[II.150] KOOMAN, P.L., SPITTERS, C.J.T., Coherent set of models to simulate potato growth, In: Modelling and parameterization of the soil-plant-atmosphere system, A comparison of potato growth models, P. Kabat et al (eds.), Wageningen Press, 253–274 (1995).

APPENDIX III. MODEL PERFORMANCE AS A FUNCTION OF AIR CONCENTRATION AVERAGING TIME

Most participants in the Pickering scenario overestimated OBT concentrations in most plant and animal products by a factor ranging from 2–5. The overpredictions were attributed to a number of factors, including a conservative bias in the model for HTO concentration in plants and the use of high values for the isotopic discrimination factor. Another possible explanation is investigated here, namely that the air concentrations used to drive the models were not the most appropriate.

The air concentrations given in the scenario description for sampling site P2 were based on measurements of the monthly average concentrations from an active air sampler, which were considered reliable. However, at the other sampling locations (DF8, DF11 and F27), air concentrations were available only as annual averages from passive diffusion samplers. These observations showed some unexpected features. Concentrations at DF8 and DF11 differed by 60% despite the fact that these two farms are located close together. Similarly, the observed concentration at F27, which is closer to PNGS than either of the dairy farms and experiences comparable meteorology, was lower than the concentration at DF8 or DF11. Finally, a comparison carried out by the utility showed that the concentrations measured by a number of passive samplers at the same location differed by a factor of 2 on average.

For these reasons, the observed air concentrations at DF8, DF11 and F27 were deemed untrustworthy and were replaced with the predictions of a sector-averaged atmospheric dispersion model that produced concentrations in good agreement with the observations at P2 and the dairy farms. The model was used to predict annual average concentrations because, at the time, annual average meteorological data were all that were available. The monthly concentrations at DF8, DF11 and F27 were deduced from the observed monthly variation at P2. The uncertainties in these concentrations, which were the concentrations given in the Scenario Description (Appendix I.2), were therefore high. The values averaged over the two months prior to the September sampling period are shown in Table III.1. This averaging time was chosen to reflect the mean conditions under which the OBT observed in September was formed, given that OBT has a biological half-life of a few weeks in plants and animals.

The opportunity to construct more accurate air concentrations arose when monthly meteorological data became available shortly after work on the scenario was finalized. The atmospheric dispersion model was used with these data to generate monthly average air concentrations for DF8, DF11 and F27. The predictions for DF8 and DF11 were found to be 20% lower than the concentrations initially supplied to the modellers, and 35% lower at F27 (Table III.1). These reductions resulted in improved model performance at all sampling sites, but still left a large gap between predictions and observations.

Table III.1. Air concentrations (Bq m^{-3}) averaged over the period 2002 July 18 – September 17. All values include a background of 0.19 Bq m^{-3}.

Source of air concentrations	DF8 and DF11	F27
Values provided in the scenario description	0.84	1.30
Values calculated from monthly meteorological data	0.68	0.84
Values calculated from monthly meteorological data (daylight hours only)	0.29	0.26

Model performance was investigated for one further averaging time. HTO transfer between air and plant, and OBT formation, occur more rapidly during the day than at night, suggesting that daylight air concentrations may be more relevant in determining plant tritium concentrations than 24 hour concentrations. Accordingly, the dispersion model was used to calculate daylight air concentrations over the period July 18 to September 17. These were found to be a factor 2–3 lower than the 24 hour averages (Table III.1) because of the prevalence of unstable conditions during the day and stable conditions at night. Since plant concentrations are directly proportional to air concentrations, OBT predictions for daylight conditions were found by multiplying the initial result for each model by the ratio of the daylight air concentration to the concentration provided in the scenario description. The results are shown in Figures III.1 and III.2 (for OBT concentrations in forage crops at DF8 and DF11 combined) and Figures III.3 and III.4 (for OBT concentrations in fruit and fruit vegetables at F27). In each case, the figure showing the original results for each model is repeated from the main text, followed by the results obtained for daylight air concentrations. The use of daylight concentrations dramatically improves the performance of the models, with essentially all of the predictions agreeing with observations when uncertainties are taken into account.

The predicted OBT concentrations in animal products corresponding to daylight air concentrations could not be found using the simple scaling applied above to plants since animal concentrations are not directly proportional to air concentrations: drinking water provides an additional, independent intake route. To estimate the animal concentrations without re-running all the models, the LLNL model was used to determine the ratio of the OBT concentration calculated from daylight air concentrations to the OBT concentration determined from the concentrations given in the scenario description. This ratio was then applied to all model results (Figures III.5–III.8). As was the case for plants, the use of daylight air concentrations brings the predictions into much better agreement with the observations, although some variability is observed from model to model, and the concentration in eggs is still overestimated by all models except TUM.

Not all models produced better results when they were driven by daylight air concentrations. A model developed by AECL, which was run specifically to investigate the effects of averaging time on model predictions, achieved more accurate results using the 24 hour concentrations (Table III.2). The AECL model is similar to the LLNL model but is designed to be realistic rather than conservative. It produces lower concentrations for most scenario endpoints than the models in the study, and the use of daylight air concentrations resulted in predictions that were lower than the observations by a factor of 2. Thus conclusions regarding the best averaging time for the air concentrations appear to be model dependent and more work is required to determine whether the 24 hour or daylight averaging period is most appropriate. This question is directly related to the amount of OBT that is formed at night. If most OBT is produced during the day, the models should be run with daylight air concentrations. If significant amounts of OBT are produced at night, the 24 hour concentrations would be more appropriate.

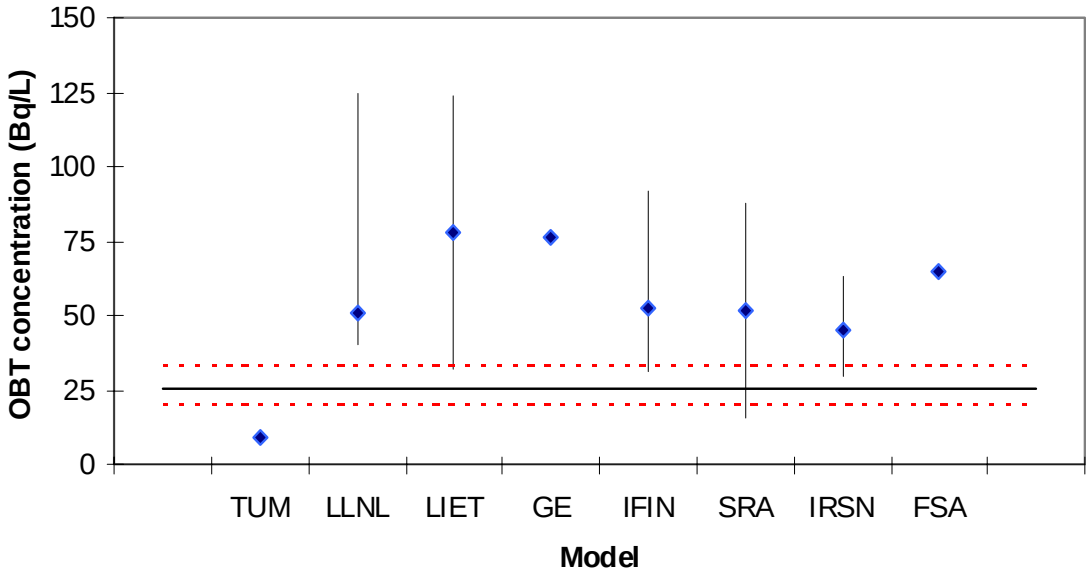

Fig. III.1. OBT concentrations in forage crops for the September sampling period at DF8 and DF11 combined, predicted using the air concentrations given in the Scenario Description (Appendix I.2). The model predictions are shown as solid diamonds with the vertical lines representing 95% confidence intervals as estimated by the modelers. The solid horizontal line is the observation with the 95% confidence interval indicated by the dashed lines.

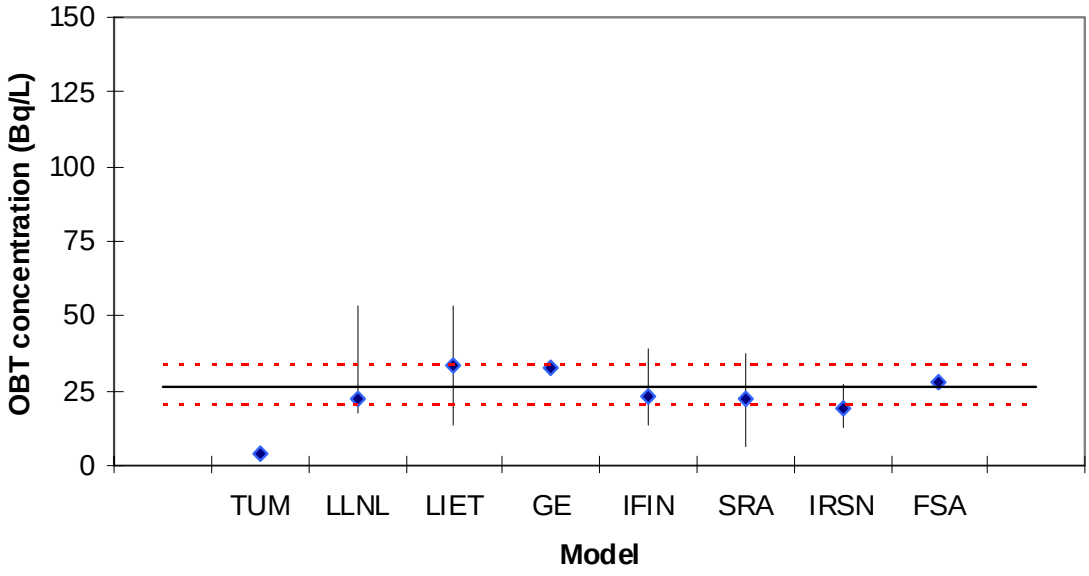

Fig. III.2. As in Figure III.1 but predictions were obtained using air concentrations calculated from monthly meteorological data (daylight hours only).

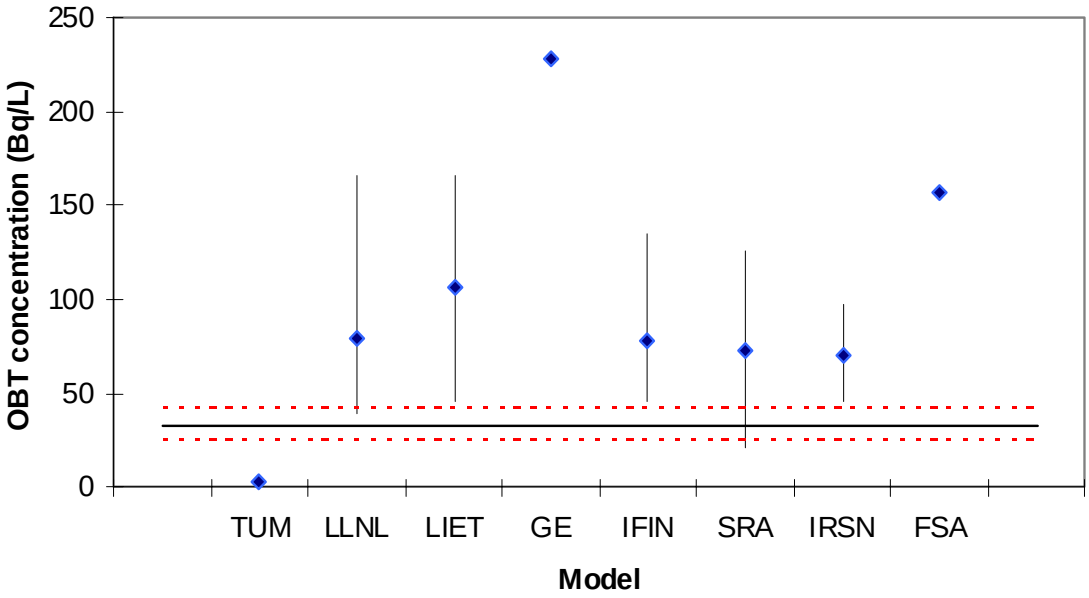

Fig. III.3. OBT concentrations in fruit and fruit vegetables for the September sampling period at F27, predicted using the air concentrations given in the Scenario Description (Appendix I.2).

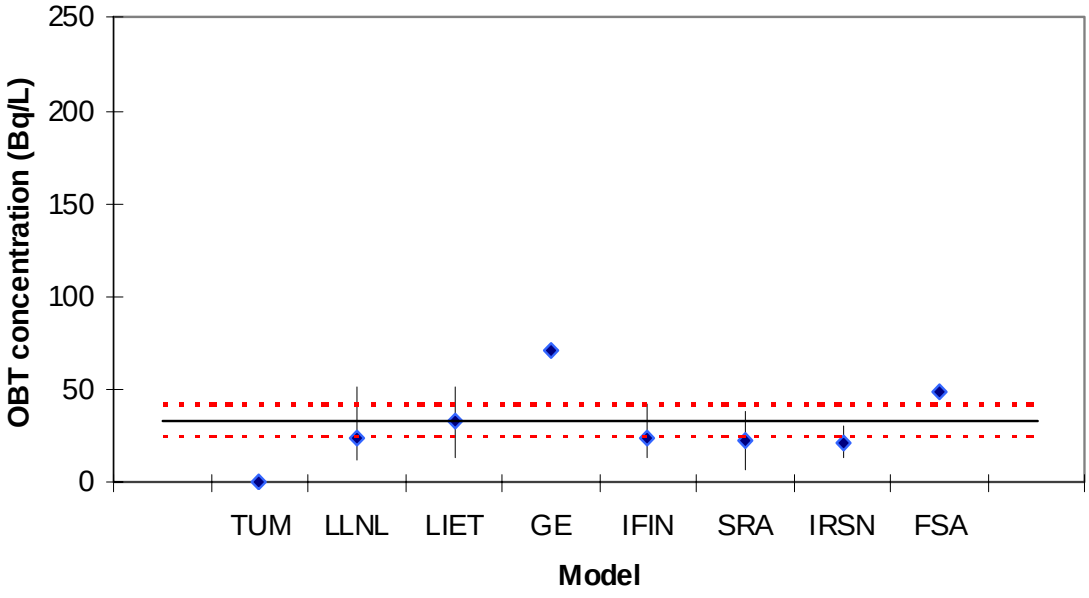

Fig. III.4. As in Figure III.3 but predictions were obtained using air concentrations calculated from monthly meteorological data (daylight hours only).

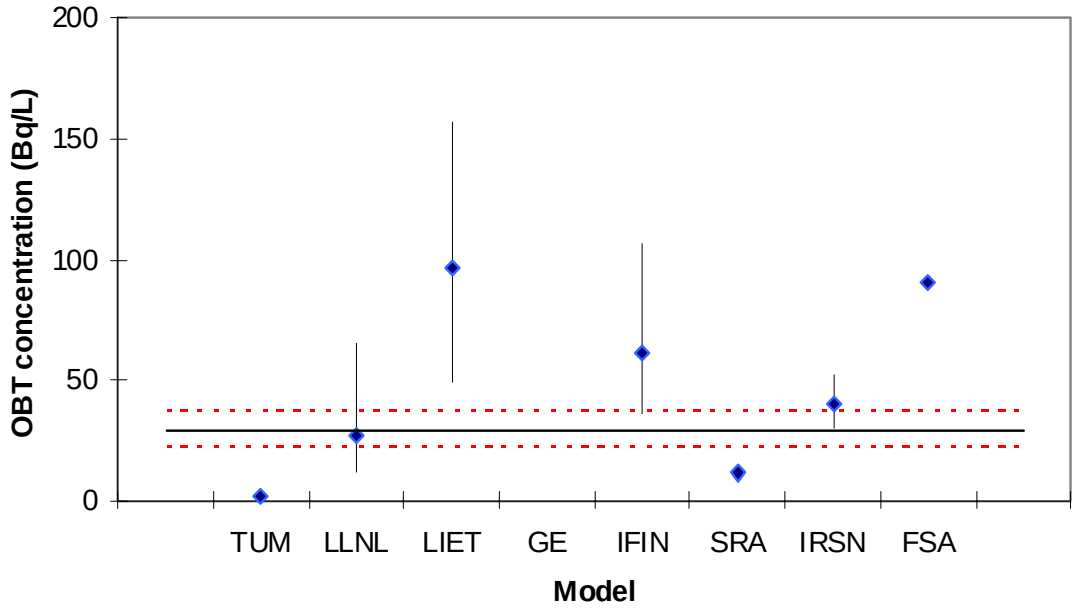

Fig. III.5. Average OBT concentrations in calf flesh and heart at DF8 in September, predicted using the air concentrations given in the Scenario Description (Appendix I.2).

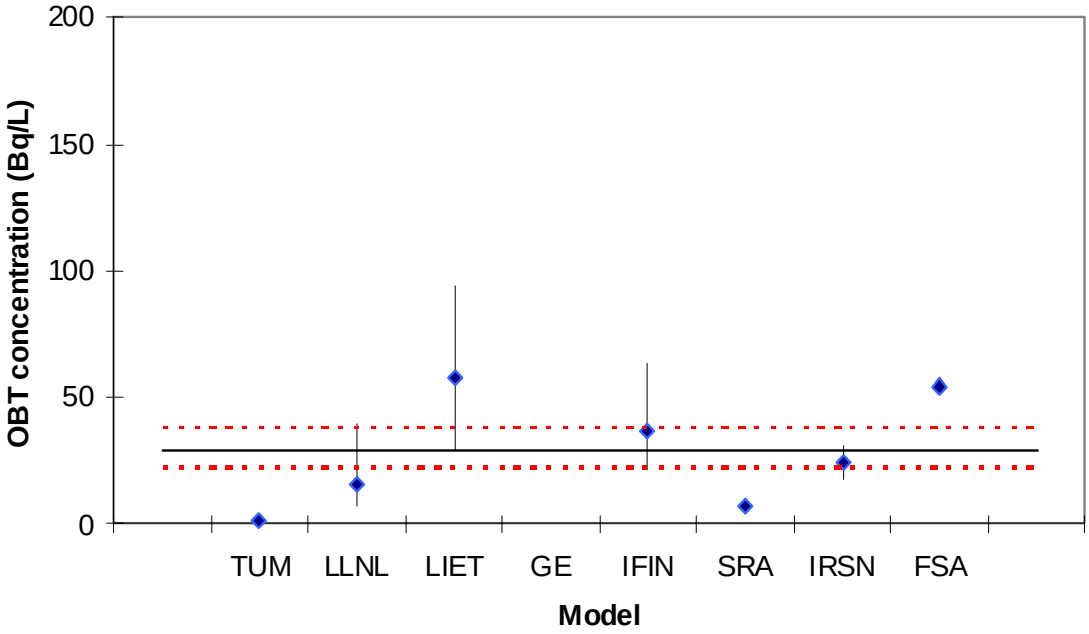

Fig. III.6. As in Figure III.5 but predictions were obtained using air concentrations calculated from monthly meteorological data (daylight hours only.)

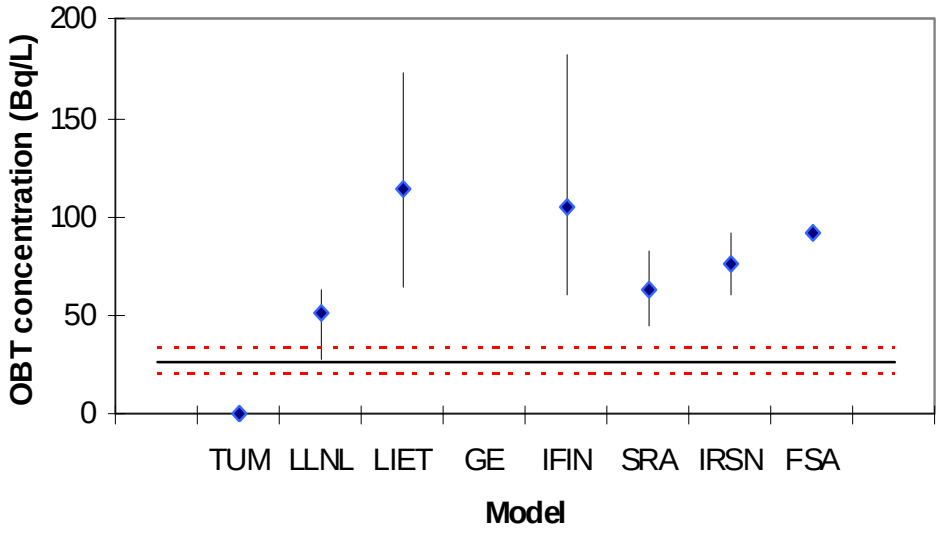

Fig. III.7. Average OBT concentration in eggs at F27 in September, predicted using the air concentrations given in the Scenario Description (Appendix I.2).

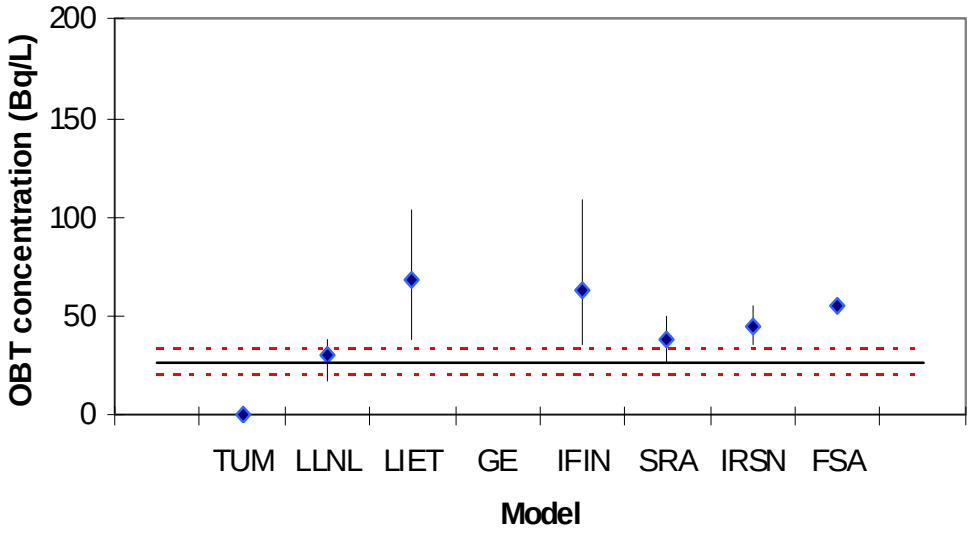

Fig. III.8. As in Figure III.7 but predicted using air concentrations calculated from monthly meteorological data (daylight hours only).

Table III.2. Predicted to observed ratios using the AECL model averaged over all sampling sites and sampling times.

Endpoint	Averaging Time	
	24 hours	Daylight hours
Plant OBT	1.18	0.40
Animal HTO	0.95	0.32
Animal OBT	1.10	0.37

APPENDIX IV. PREDICTED TOTAL DOSES FOR THE HTO RELEASE FOR THE HYPOTHETICAL SCENARIO

Table IV.1. Total doses for the HTO release (mSv) – Case 1.

Model	Downwind distance (km)			
	1	3	10	30
Germany	7.41×10^{-1}	1.25×10^{-1}	4.15×10^{-2}	6.24×10^{-3}
Canada	6.39×10^{-1}	8.56×10^{-2}	1.27×10^{-2}	3.39×10^{-3}
Korea	9.10×10^{-1}	1.10×10^{-1}	1.23×10^{-2}	1.93×10^{-3}
India	4.39×10^{-1}	1.60×10^{-2}	4.92×10^{-3}	1.83×10^{-3}
Japan	6.45×10^{-1}	1.83×10^{-1}	6.24×10^{-2}	2.35×10^{-2}
Japanet	5.56×10^{-1}	8.69×10^{-2}	1.07×10^{-2}	9.28×10^{-4}
Romania	7.40×10^{-1}	1.44×10^{-1}	2.70×10^{-2}	1.60×10^{-2}
France	9.69	1.36	1.66×10^{-1}	2.78×10^{-2}

Table IV.2. Total doses for the HTO release (mSv) – Case 2.

Model	Downwind distance (km)			
	1	3	10	30
Germany	3.03×10^{1}	5.61	4.91×10^{-1}	3.08×10^{-2}
Canada	2.15	2.83×10^{-1}	4.84×10^{-2}	5.20×10^{-3}
Korea	3.50	6.97×10^{-1}	1.36×10^{-1}	3.65×10^{-2}
India	2.86	2.64×10^{-1}	2.64×10^{-3}	2.08×10^{-5}
Japan	1.01×10^{1}	2.85	9.73×10^{-1}	3.67×10^{-1}
Japanet	3.91×10^{1}	4.95	8.52×10^{-2}	6.92×10^{-3}
Romania	2.55	8.50×10^{-1}	8.10×10^{-2}	1.60×10^{-3}
France	3.90 × 101	8.68	1.59	3.24×10^{-1}

Table IV.3. Total doses for the HTO release (mSv) – Case 3.

Model	Downwind distance (km)			
	1	3	10	30
Germany	1.79×10^{1}	7.99	1.34	2.00×10^{-1}
Canada	2.65	6.79×10^{-1}	1.47×10^{-1}	3.23×10^{-2}
Korea	1.79×10^{1}	8.63	2.45	9.99×10^{-1}
India	2.70×10^{1}	1.09×10^{1}	2.61	7.01×10^{-1}
Japan -K	8.35×10^{1}	2.37×10^{1}	8.07	3.04
Japanet	3.88×10^{1}	1.13×10^{1}	1.05	1.33×10^{-1}
Romania	2.84	9.10×10^{-1}	1.90×10^{-1}	7.70×10^{-2}
France	1.47×10^{1}	9.29	2.08	3.97×10^{-1}

APPENDIX V. DETAILS OF DOSE PREDICTIONS FOR THE HTO RELEASES FOR THE HYPOTHETICAL SCENARIO

Table V.1. Details of predicted doses at 1 km - Case 1, HTO release.

Case 1	*Canada*				
	Dose via air pathway (mSv)		Dose via soil pathway (mSv)		Total dose (mSv)
	HTO	OBT	HTO	OBT	
Inhalation	1.00E-01	5.00E-03			1.05E-01
Skin absorption	1.00E-01	5.00E-03			1.05E-01
Salad vegetables	3.79E-02	3.89E-03	2.30E-03	0	4.41E-02
Radish and turnip	0	1.24E-03	2.68E-06	2.96E-05	1.27E-03
Potatoes	0	8.25E-03	1.79E-05	1.97E-04	8.46E-03
Carrots	0	2.06E-03	4.46E-06	4.93E-05	2.11E-03
String beans	0	5.96E-03	6.83E-06	8.50E-05	6.05E-03
Peas	0	5.96E-03	6.83E-06	8.50E-05	6.05E-03
Tomatoes	0	1.19E-02	1.37E-05	1.70E-04	1.21E-02
Cereals	0	1.18E-01	1.98E-05	8.28E-03	1.26E-01
Beef	3.43E-02		5.60E-04		3.49E-02
Milk	1.71E-01		2.80E-03		1.74E-01
Chicken and eggs	1.31E-02		9.04E-04		1.40E-02
Total doses	2.56E-01	1.57E-01	6.64E-03	8.90E-03	6.39E-01

Case 1	*India*				
	Dose via air pathway (mSv)		Dose via soil pathway (mSv)		Total dose (mSv)
	HTO	OBT	HTO	OBT	
Inhalation	4.97E-02	0	0	0	4.97E-02
Skin absorption	4.97E-02	0	0	0	4.97E-02
Salad vegetables	1.30E-02	1.39E-02	4.23E-06	1.35E-05	2.69E-02
Radish and turnip	2.61E-03	1.95E-03	1.08E-06	4.60E-06	4.57E-03
Potatoes	0	1.47E-01	1.13E-06	1.47E-05	1.47E-01
Carrots	1.84E-18	9.75E-03	6.69E-7	4.28E-06	9.75E-03
String beans	4.08E-03	4.35E-03	1.33E-06	5.66E-06	8.44E-03
Peas	4.08E-03	4.35E-03	1.33E-06	8.49E-06	8.43E-03
Tomatoes	0	2.25E-02	6.74E-7	8.75E-06	2.26E-02
Cereals	0	8.50E-02	1.28E-06	1.67E-05	8.50E-02
Beef	6.27E-04	4.33E-04	0	0	1.06E-03
Milk	6.33E-03	1.97E-02	0	0	2.60E-02
Chicken and eggs	1.06E-04	2.20E-05	0	0	1.28E-04
Total doses	1.30E-01	3.09E-01	1.17E-05	7.67E-05	4.39E-01

Case 1	*Korea*				
	Dose via air pathway (mSv)		Dose via soil pathway (mSv)		Total dose (mSv)
	HTO	OBT	HTO	OBT	
Inhalation	7.62E-02				7.62E-02
Skin absorption	4.78E-02				4.78E-02
Salad vegetables			1.51E-01	1.28E-02	1.64E-01
Radish and turnip			1.94E-02	7.48E-03	2.69E-02
Potatoes			1.90E-02	4.87E-02	6.77E-02
Carrots			1.56E-02	9.94E-03	2.55E-02
String beans			2.81E-02	1.48E-02	4.29E-02
Peas			2.97E-02	1.48E-02	4.45E-02
Tomatoes			1.45E-02	6.20E-03	2.07E-02
Cereals			8.84E-03	3.81E-01	3.90E-01
Beef					2.45E-03
Milk					8.50E-04
Chicken and eggs					0
Total doses	0	0	2.86E-01	4.96E-01	9.09E-01

Totals in columns "dose via air pathway" and "dose via soil pathway" do not include inhalation and skin absorption doses.

Table V.1 (Continued).

Case 1	*France*				
	Dose via air pathway (mSv)		Dose via soil pathway (mSv)		Total dose (mSv)
	HTO	OBT	HTO	OBT	
Inhalation	0	0	0	0	5.16E-01
Skin absorption	0	0	0	0	2.06E-01
Salad vegetables	1.09E-01	1.17E-02	7.02E-02	7.55E-03	1.99E-01
Radish and turnip	0	1.58E-02	1.17E-02	7.26E-03	3.48E-02
Potatoes	0	2.37E-01	1.66E-01	1.09E-01	5.12E-01
Carrots	0	2.11E-02	2.06E-02	9.67E-03	5.13E-02
String beans	3.42E-02	1.41E-02	2.20E-02	9.07E-03	7.94E-02
Peas	3.42E-02	1.41E-02	2.20E-02	9.07E-03	7.94E-02
Tomatoes	8.58E-02	6.77E-03	5.52E-02	4.35E-03	1.52E-01
Cereals	0	4.59E+00	1.40E-01	1.67E+00	6.40E+00
Beef	4.72E-01	9.73E-02	3.09E-01	6.36E-02	9.42E-01
Milk	2.56E-01	5.26E-02	1.67E-01	3.43E-02	5.09E-01
Chicken and eggs	8.41E-04	1.73E-04	5.97E-04	1.23E-04	1.73E-03
Total doses	9.92E-01	5.06E+00	9.84E-01	1.92E+00	9.69E+00

Case 1	*Japanet*				
	Dose via air pathway (mSv)		Dose via soil pathway (mSv)		Total dose (mSv)
	HTO	OBT	HTO	OBT	
Inhalation					1.89E-02
Skin absorption					1.31E-02
Salad vegetables	1.99E-05	4.69E-03	2.40E-06	5.67E-04	5.28E-03
Radish and turnip	3.65E-06	2.51E-03	1.07E-06	7.26E-04	3.24E-03
Potatoes	0	5.27E-02	0	1.53E-02	6.80E-02
Carrots	3.33E-07	5.02E-03	9.76E-08	1.45E-03	6.48E-03
String beans	4.67E-06	4.23E-03	2.51E-06	2.27E-03	6.50E-03
Peas	3.11E-06	2.82E-03	1.67E-06	1.51E-03	4.33E-03
Tomatoes	2.82E-08	4.06E-03	1.52E-08	2.18E-03	6.24E-03
Cereals	1.81E-08	2.50E-01	9.72E-09	1.34E-01	3.84E-01
Beef	1.16E-06	1.89E-02	1.40E-07	2.29E-03	2.12E-02
Milk	7.39E-06	1.49E-02	8.93E-07	1.80E-03	1.67E-02
Chicken and eggs	6.01E-10	2.03E-03	3.23E-10	1.31E-09	2.03E-03
Total doses	4.02E-05	3.62E-01	8.81E-06	1.62E-01	5.56E-01

Case 1	*Romania*				
	Dose via air pathway (mSv)		Dose via soil pathway (mSv)		Total dose (mSv)
	HTO	OBT	HTO	OBT	
Inhalation	1.00E-01				1.00E-01
Skin absorption					
Salad vegetables	2.24E-02	2.21E-02			4.45E-02
Radish and turnip	1.50E-05	6.30E-02			6.30E-02
Potatoes	1.30E-04	1.50E-01			1.50E-01
Carrots	1.60E-04	2.40E-03			2.60E-03
String beans					
Peas					
Tomatoes					
Cereals	1.50E-04	2.44E-01			2.44E-01
Beef	7.20E-03	2.28E-02			3.00E-02
Milk	6.10E-02	3.50E-02			9.60E-02
Chicken and eggs	5.00E-03	7.70E-03			1.30E-02
Total doses	9.61E-02	5.47E-01			7.43E-01

Table V.1 (Continued).

Case 1	*Germany*				
	Dose via air pathway (mSv)		**Dose via soil pathway (mSv)**		**Total dose (mSv)**
	HTO	**OBT**	**HTO**	**OBT**	
Inhalation	1.19E-02	0	1.20E-03	0	1.31E-02
Skin absorption	7.44E-03	0	8.90E-04	0	8.33E-03
Salad vegetables	6.93E-03	2.03E-03	2.05E-03	3.75E-04	1.14E-02
Radish and turnip	0	0	0	0	0
Potatoes	2.16E-04	4.19E-02	7.02E-04	8.25E-03	5.11E-02
Carrots	0	0	0	0	0
String beans	0	0	0	0	0
Peas	0	0	0	0	0
Tomatoes	0	0	0	0	0
Cereals	2.61E-04	5.32E-01	8.14E-04	7.56E-02	6.09E-01
Beef	3.35E-03	5.48E-63	2.35E-03	1.54E-03	1.27E-02
Milk	1.49E-02	7.76E-03	1.05E-02	2.49E-03	3.57E-02
Chicken and eggs	0	0	0	0	0
Total doses	2.57E-02	5.84E-01	1.64E-02	8.83E-02	7.41E-01

Case 1	*Japan K*				
	Dose via air pathway (mSv)		**Dose via soil pathway (mSv)**		**Total dose (mSv)**
	HTO	**OBT**	**HTO**	**OBT**	
Inhalation	2.90E-02	0	0	0	2.90E-02
Skin absorption	1.45E-02	0	0	0	1.45E-02
Salad vegetables	1.34E-01	1.87E-04	1.34E-01	1.87E-04	2.68E-01
Radish and turnip	0	0	7.04E-05	1.91E-07	7.06E-05
Potatoes	0	0	0	1.53E-05	1.53E-05
Carrots	0	0	8.36E-07	5.11E-07	1.35E-06
String beans	4.21E-02	2.25E-04	4.21E-02	2.25E-04	8.46E-02
Peas	4.21E-02	2.25E-04	4.21E-02	2.25E-04	8.46E-02
Tomatoes	4.85E-06	2.13E-04	4.85E-06	2.13E-04	4.35E-04
Cereals	3.10E-06	7.85E-02	3.10E-06	7.85E-02	1.57E-01
Beef	6.24E-03	8.66E-05	2.19E-04	4.94E-06	6.55E-03
Milk	2.58E-02	1.78E-04	1.42E-03	4.94E-06	2.74E-02
Chicken and eggs	6.91E-05	5.32E-07	0	0	6.96E-05
Total doses	2.50E-01	7.96E-02	2.20E-01	7.94E-02	6.72E-01

Table V.2. Details of predicted doses at 1 km - Case 2, HTO release.

Case 2	*Canada*				
	Dose via air pathway (mSv)		**Dose via soil pathway (mSv)**		**Total dose (mSv)**
	HTO	**OBT**	**HTO**	**OBT**	
Inhalation	2.91E-01		7.30E-02		3.64E-01
Skin absorption	2.91E-01		7.30E-02		3.64E-01
Salad vegetables	1.01E-01	7.12E-03	6.50E-02	4.70E-04	1.74E-01
Radish and turnip	0	2.31E-03	1.08E-04	1.05E-03	3.47E-03
Potatoes	0	1.54E-02	7.21E-04	7.03E-03	2.32E-02
Carrots	0	3.84E-03	1.80E-04	1.76E-03	5.78E-03
String beans	0	1.02E-02	2.53E-04	3.65E-03	1.41E-02
Peas	0	1.02E-02	2.53E-04	3.65E-03	1.41E-02
Tomatoes	0	2.05E-02	5.05E-04	7.30E-03	2.83E-02
Cereals	0	1.51E-01	7.37E-04	3.02E-01	4.54E-01
Beef	8.78E-02		2.18E-02		1.10E-01
Milk	4.38E-01		1.07E-01		5.45E-01
Chicken and eggs	1.97E-02		3.08E-02		5.05E-02
Total doses	6.47E-01	2.21E-01	2.27E-01	3.27E-01	2.15E+00
Case 2	***India***				
	Dose via air pathway (mSv)		**Dose via soil pathway (mSv)**		**Total dose (mSv)**
	HTO	**OBT**	**HTO**	**OBT**	
Inhalation	3.83E-01	0	0	0	3.83E-01
Skin absorption	3.83E-01	0	0	0	3.83E-01
Salad vegetables	7.81E-02	8.34E-02	9.78E-05	3.13E-04	1.62E-01
Radish and turnip	1.57E-02	1.17E-02	2.49E-05	1.07E-04	2.75E-02
Potatoes	0	8.81E-01	2.62E-05	3.40E-04	8.82E-01
Carrots	1.11E-17	5.86E-02	1.55E-05	9.91E-05	5.87E-02
String beans	2.45E-02	2.62E-02	3.07E-05	1.31E-04	5.08E-02
Peas	2.45E-02	2.62E-02	3.07E-05	1.96E-04	5.09E-02
Tomatoes	0	1.35E-01	1.56E-05	2.02E-04	1.36E-01
Cereals	0	5.11E-01	2.97E-05	3.86E-04	5.11E-01
Beef	4.83E-03	3.34E-03	0	0	8.18E-03
Milk	4.88E-02	1.52E-01	0	0	2.01E-01
Chicken and eggs	8.19E-04	1.70E-04	0	0	9.89E-04
Total doses	9.64E-01	1.89E+00	1.71E-04	1.77E-03	2.86E+00
Case 2	***Korea***				
	Dose via air pathway (mSv)		**Dose via soil pathway (mSv)**		**Total dose (mSv)**
	HTO	**OBT**	**HTO**	**OBT**	
Inhalation	4.07E-01				4.07E-01
Skin absorption	2.55E-01				2.55E-01
Salad vegetables			5.41E-01	5.07E-02	5.92E-01
Radish and turnip			5.10E-02	2.91E-02	8.01E-02
Potatoes			6.30E-02	1.93E-01	2.56E-01
Carrots			5.20E-02	3.71E-02	8.91E-02
String beans			7.28E-02	5.66E-02	1.29E-01
Peas			7.48E-02	5.66E-02	1.31E-01
Tomatoes			4.85E-02	2.45E-02	7.30E-02
Cereals			2.93E-02	1.45E+00	1.48E+00
Beef					9.56E-03
Milk					3.32E-03
Chicken and eggs					0
Total doses	0	0	9.32E-01	1.90E+00	3.50E+00

Table V.2. (Continued).

Case 2	*France*				
	Dose via air pathway (mSv)		Dose via soil pathway (mSv)		Total dose (mSv)
	HTO	OBT	HTO	OBT	
Inhalation	0	0	0	0	9.38E-01
Skin absorption	0	0	0	0	3.75E-01
Salad vegetables	3.25E-01	3.49E-02	5.04E-01	5.42E-02	9.18E-01
Radish and turnip	0	4.19E-02	8.43E-02	5.21E-02	1.78E-01
Potatoes	0	7.05E-01	1.19E+00	7.81E-01	2.68E+00
Carrots	0	5.59E-02	1.48E-01	6.95E-02	2.73E-01
String beans	1.02E-01	4.20E-02	1.58E-01	6.51E-02	3.67E-01
Peas	1.02E-01	4.20E-02	1.58E-01	6.51E-02	3.67E-01
Tomatoes	2.92E-01	2.30E-02	3.96E-01	3.13E-02	7.42E-01
Cereals	0	1.35E+01	1.02E+00	1.21E+01	2.67E+01
Beef	1.15E+00	2.37E-01	1.93E+00	3.97E-01	3.71E+00
Milk	6.23E-01	1.28E-01	1.04E+00	2.14E-01	2.01E+00
Chicken and eggs	2.48E-03	5.11E-04	4.25E-03	8.75E-04	8.12E-03
Total doses	2.60E+00	1.49E+01	6.63E+00	1.38E+01	3.92E+01

Case 2	*Japanet*				
	Dose via air pathway (mSv)		Dose via soil pathway (mSv)		Total dose (mSv)
	HTO	OBT	HTO	OBT	
Inhalation					2.70E-01
Skin absorption					1.90E-01
Salad vegetables	1.46E-03	3.45E-01	1.77E-04	4.17E-02	3.88E-01
Radish and turnip	2.69E-04	1.85E-01	7.88E-05	5.35E-02	2.39E-01
Potatoes	0	3.88E+00	0	1.12E+00	5.00E+00
Carrots	2.45E-05	3.70E-01	7.18E-06	1.07E-01	4.77E-01
String beans	3.44E-04	3.11E-01	1.85E-04	1.67E-01	4.79E-01
Peas	2.29E-04	2.07E-01	1.23E-04	1.11E-01	3.18E-01
Tomatoes	2.08E-06	2.99E-01	1.12E-06	1.60E-01	4.59E-01
Cereals	1.33E-06	1.84E+01	7.15E-07	8.89E+00	2.73E+01
Beef	8.56E-05	1.39E+00	1.03E-05	1.68E-01	1.56E+00
Milk	5.44E-04	1.10E+00	6.57E-05	1.32E-01	1.23E+00
Chicken and eggs	4.42E-08	1.49E-01	2.38E-08	1.31E-09	1.49E-01
Total doses	2.96E-03	2.66E+01	6.49E-04	1.10E+01	3.80E+01

Case 2	*Romania*				
	Dose via air pathway (mSv)		Dose via soil pathway (mSv)		Total dose (mSv)
	HTO	OBT	HTO	OBT	
Inhalation	1.80E-01				1.80E-01
Skin absorption					
Salad vegetables	6.78E-02	4.72E-01			5.40E-01
Radish and turnip	1.54E-03	2.43E-01			2.44E-01
Potatoes	1.40E-02	4.51E-01			4.65E-01
Carrots					0
String beans					0
Peas					0
Tomatoes	1.60E-02	2.40E-01			2.56E-01
Cereals	1.55E-02	3.36E-01			3.51E-01
Beef	3.49E-02	5.33E-02			8.82E-02
Milk	3.16E-01	9.37E-02			4.09E-01
Chicken and eggs	8.01E-03	1.06E-02			1.86E-02
Total doses	4.73E-01	1.90E+00			2.55E+00

Table V.2. (Continued).

Case 2	*Germany*				
	Dose via air pathway (mSv)		**Dose via soil pathway (mSv)**		**Total dose (mSv)**
	HTO	**OBT**	**HTO**	**OBT**	
Inhalation	4.34E-01	0	1.40E-02	0	4.48E-01
Skin absorption	2.71E-01	0	9.00E-03	0	2.80E-01
Salad vegetables	4.79E-01	1.01E-01	2.31E-01	3.39E-02	8.45E-01
Radish and turnip					
Potatoes	6.98E-03	1.69E+00	1.77E-01	4.86E-01	2.36E+00
Carrots					
String beans					
Peas					
Tomatoes					
Cereals	8.27E-03	1.63E+01	2.13E-01	6.58E+00	2.33E+01
Beef	1.23E-01	1.83E-01	3.07E-01	1.43E-01	7.55E-01
Milk	5.47E-01	2.62E-01	1.37E+00	2.51E-01	2.43E+00
Chicken and eggs		0			
Total doses	1.16E+00	1.85E+01	2.30E+00	7.49E+00	3.03E+01

Case 2	*Japan K*				
	Dose via air pathway (mSv)		**Dose via soil pathway (mSv)**		**Total dose (mSv)**
	HTO	**OBT**	**HTO**	**OBT**	
Inhalation	5.76E-01	0	0	0	5.76E-01
Skin absorption	2.88E-01	0	0	0	2.88E-01
Salad vegetables	2.07E+00	2.88E-03	2.07E+00	2.88E-03	4.14E+00
Radish and turnip	0	0	1.40E-03	3.80E-06	1.40E-03
Potatoes	0	0	0	3.04E-04	3.04E-04
Carrots	0	0	1.66E-05	1.01E-05	2.67E-05
String beans	6.45E-01	3.47E-03	6.45E-01	3.47E-03	1.30E+00
Peas	6.45E-01	3.47E-03	6.45E-01	3.47E-03	1.30E+00
Tomatoes	7.45E-05	3.27E-03	7.45E-05	3.27E-03	6.69E-03
Cereals	4.78E-05	1.21E+00	4.78E-05	1.21E+00	2.41E+00
Beef	9.51E-02	1.32E-03	7.05E-03	9.79E-05	1.04E-01
Milk	3.93E-01	2.72E-03	2.92E-02	2.02E-04	4.25E-01
Chicken and eggs	1.37E-03	1.05E-05	0	0	1.38E-03
Total doses	3.85E+00	1.23E+00	3.40E+00	1.22E+00	9.98E+00

Table V.3. Details of predicted doses at 1 km - Case 3, HTO release.

Case 3	*Canada*				
	Dose via air pathway (mSv)		Dose via soil pathway (mSv)		Total dose (mSv)
	HTO	OBT	HTO	OBT	
Inhalation	1.15E+00		4.50E-02		1.20E+00
Skin absorption	1.15E+00		4.50E-02		1.20E+00
Salad vegetables	1.74E-07	9.70E-09	2.03E-02	4.16E-04	2.07E-02
Radish and turnip	0	3.08E-09	2.79E-05	4.12E-04	4.40E-04
Potatoes	0	2.06E-08	1.86E-04	2.74E-03	2.93E-03
Carrots	0	5.15E-09	4.64E-05	6.86E-04	7.32E-04
String beans	0	1.30E-08	6.35E-05	1.58E-03	1.64E-03
Peas	0	1.30E-08	6.35E-05	1.58E-03	1.64E-03
Tomatoes	0	2.60E-08	1.27E-04	3.16E-03	3.29E-03
Cereals	0	6.88E-08	1.23E-04	9.83E-02	9.84E-02
Beef	8.28E-03		8.32E-03		1.66E-02
Milk	4.08E-02		4.14E-02		8.22E-02
Chicken and eggs	2.00E-02		1.03E-02		3.03E-02
Total doses	6.91E-02	1.59E-07	8.10E-02	1.09E-01	2.65E+00

Case 3	*India*				
	Dose via air pathway (mSv)		Dose via soil pathway (mSv)		Total dose (mSv)
	HTO	OBT	HTO	OBT	
Inhalation	8.68E-01	0	0	0	8.68E-01
Skin absorption	8.68E-01	0	0	0	8.68E-01
Salad vegetables	9.88E-01	1.05E+00	2.46E-04	7.88E-04	2.04E+00
Radish and turnip	1.98E-01	1.48E-01	6.27E-08	2.68E-07	3.46E-01
Potatoes	0	1.11E+01	6.59E-08	8.56E-07	1.11E+01
Carrots	1.40E-16	7.41E-01	3.89E-08	2.49E-07	7.41E-01
String beans	3.10E-01	3.31E-01	7.71E-08	3.29E-07	6.40E-01
Peas	3.10E-01	3.31E-01	7.71E-08	4.94E-07	6.40E-01
Tomatoes	0	1.71E+00	3.92E-08	5.09E-07	1.71E+00
Cereals	0	6.46E+00	7.47E-08	9.70E-07	6.46E+00
Beef	3.65E-02	2.52E-02	0	0	6.17E-02
Milk	3.68E-01	1.15E+00	0	0	1.51E+00
Chicken and eggs	6.18E-03	1.28E-03	0	0	7.46E-03
Total doses	2.22E+00	2.31E+01	6.82E-07	4.46E-06	2.70E+01

Case 3	*Korea*				
	Dose via air pathway (mSv)		Dose via soil pathway (mSv)		Total dose (mSv)
	HTO	OBT	HTO	OBT	
Inhalation	1.92E+00				1.92E+00
Skin absorption	1.21E+00				1.21E+00
Salad vegetables			2.49E+00	1.89E-01	2.68E+00
Radish and turnip			4.95E-01	1.15E-01	6.10E-01
Potatoes			4.68E-01	6.55E-01	1.12E+00
Carrots			3.91E-01	1.39E-01	5.30E-01
String beans			7.41E-01	2.31E-01	9.72E-01
Peas			7.41E-01	2.07E-01	9.48E-01
Tomatoes			3.68E-01	7.28E-02	4.41E-01
Cereals			2.25E-01	7.15E+00	7.38E+00
Beef					3.35E-02
Milk					1.16E-02
Chicken and eggs					0
Total doses	0	0	5.92E+00	8.76E+00	1.79E+01

Table V.3 (Continued).

Case 3	*France*				
	Dose via air pathway (mSv)		**Dose via soil pathway (mSv)**		**Total dose (mSv)**
	HTO	**OBT**	**HTO**	**OBT**	
Inhalation					5.13E-01
Skin absorption					2.05E-01
Salad vegetables	2.00E-01	2.15E-02	6.98E-02	7.51E-03	2.99E-01
Radish and turnip	0	2.89E-02	1.17E-02	7.22E-03	4.78E-02
Potatoes	0	4.34E-01	1.65E-01	1.08E-01	7.07E-01
Carrots	0	3.86E-02	2.04E-02	9.62E-03	6.86E-02
String beans	6.26E-02	2.58E-02	2.19E-02	9.02E-03	1.19E-01
Peas	6.26E-02	2.58E-02	2.19E-02	9.02E-03	1.19E-01
Tomatoes	1.57E-01	1.24E-02	5.49E-02	4.33E-03	2.29E-01
Cereals	0	8.40E+00	1.40E-01	1.66E+00	1.02E+01
Beef	8.65E-01	1.78E-01	3.07E-01	6.32E-02	1.41E+00
Milk	4.68E-01	9.64E-02	1.66E-01	3.42E-02	7.64E-01
Chicken and eggs	1.54E-03	3.17E-04	5.94E-04	1.22E-04	2.57E-03
Total doses	1.82E+00	9.26E+00	9.79E-01	1.91E+00	1.47E+01

Case 3	*Japanet*				
	Dose via air pathway (mSv)		**Dose via soil pathway (mSv)**		**Total dose (mSv)**
	HTO	**OBT**	**HTO**	**OBT**	
Inhalation					2.11E+00
Skin absorption					1.46E+00
Salad vegetables	1.31E-06	3.09E-01	1.17E-04	2.75E-02	3.36E-01
Radish and turnip	2.40E-07	1.65E-01	5.20E-05	3.53E-02	2.01E-01
Potatoes	0	3.47E+00	0	7.41E-01	4.21E+00
Carrots	2.19E-08	3.31E-01	4.74E-06	7.06E-02	4.01E-01
String beans	3.07E-07	2.78E-01	1.22E-04	1.10E-01	3.89E-01
Peas	2.05E-07	1.85E-01	8.13E-05	7.35E-02	2.59E-01
Tomatoes	1.86E-09	2.67E-01	7.37E-07	1.06E-01	3.73E-01
Cereals	1.19E-09	1.65E+01	4.72E-07	6.53E+00	2.30E+01
Beef	7.65E-05	1.25E+00	6.83E-06	1.11E-01	1.36E+00
Milk	4.86E-04	9.79E-01	4.34E-05	8.74E-02	1.07E+00
Chicken and eggs	3.96E-08	1.34E-01	1.57E-08	1.31E-09	1.34E-01
Total doses	5.65E-04	2.38E+01	4.28E-04	7.89E+00	3.53E+01

Case 3	*Romania*				
	Dose via air pathway (mSv)		**Dose via soil pathway (mSv)**		**Total dose (mSv)**
	HTO	**OBT**	**HTO**	**OBT**	
Inhalation					3.40E-01
Skin absorption					
Salad vegetables	6.72E-02	8.09E-02			1.48E-01
Radish and turnip	9.66E-05	1.80E-01			1.80E-01
Potatoes	8.82E-04	4.09E-01			4.09E-01
Carrots					0
String beans					0
Peas					0
Tomatoes	1.01E-03	1.46E-02			1.56E-02
Cereals	9.90E-04	8.78E-01			8.79E-01
Beef	5.26E-02	1.18E-01			1.70E-01
Milk	4.59E-01	1.94E-01			6.53E-01
Chicken and eggs	1.81E-02	2.76E-02			4.56E-02
Total doses	6.00E-01	1.90E+00	0	0	2.84E+00

Table V.3 (Continued).

Case 3	*Germany*				
	Dose via air pathway (mSv)		**Dose via soil pathway (mSv)**		**Total dose (mSv)**
	HTO	**OBT**	**HTO**	**OBT**	
Inhalation	1.51E+00	0	3.00E-02	0	1.54E+00
Skin absorption	9.41E-01	0	2.00E-02	0	9.61E-01
Salad vegetables	1.56E-01	2.62E-02	1.25E-01	2.40E-02	3.31E-01
Radish and turnip					0
Potatoes	9.36E-04	5.88E-01	8.50E-02	4.03E-01	1.08E+00
Carrots					0
String beans					0
Peas					0
Tomatoes					0
Cereals	1.31E-03	7.70E+00	1.02E-01	4.42E+00	1.22E+01
Beef	1.27E-01	7.99E-02	1.25E-01	8.43E-02	4.16E-01
Milk	5.68E-01	1.30E-01	5.57E-01	1.36E-01	1.39E+00
Chicken and eggs					0
Total doses	8.53E-01	8.52E+00	9.94E-01	5.07E+00	1.79E+01

Case 3	*Japan K*				
	Dose via air pathway (mSv)		**Dose via soil pathway (mSv)**		**Total dose (mSv)**
	HTO	**OBT**	**HTO**	**OBT**	
Inhalation	2.83E+00	0	0	0	2.83E+00
Skin absorption	1.42E+00	0	0	0	1.42E+00
Salad vegetables	1.76E+01	2.45E-02	1.76E+01	2.45E-02	3.51E+01
Radish and turnip	0	0	6.86E-03	1.87E-05	6.88E-03
Potatoes	0	0	0	1.49E-03	1.49E-03
Carrots	0	0	8.14E-05	4.97E-05	1.31E-04
String beans	5.50E+00	2.95E-02	5.50E+00	2.95E-02	1.11E+01
Peas	5.50E+00	2.95E-02	5.50E+00	2.95E-02	1.11E+01
Tomatoes	6.35E-04	2.78E-02	6.35E-04	2.78E-02	5.69E-02
Cereals	4.07E-04	1.03E+01	4.07E-04	1.03E+01	2.05E+01
Beef	9.51E-02	1.14E-02	7.05E-03	4.89E-04	1.14E-01
Milk	3.93E-01	2.36E-02	2.92E-02	1.01E-03	4.47E-01
Chicken and eggs	1.37E-03	5.18E-05	0	0	1.42E-03
Total doses	2.91E+01	1.04E+01	2.86E+01	1.04E+01	8.27E+01

APPENDIX VI. DETAILS OF DOSE PREDICTIONS FOR THE HT RELEASES FOR THE HYPOTHETICAL SCENARIO

Table VI.1. Details of predicted doses at 1 km - Case 1, HT release.

Case 1	*Canada*				
	Dose via air pathway (mSv)		**Dose via soil pathway (mSv)**		**Total dose**
	HTO	**OBT**	**HTO**	**OBT**	**(mSv)**
Inhalation	1.17E-05		1.17E-03		1.18E-03
Skin absorption	8.05E-10		1.17E-03		1.17E-03
Salad vegetables	3.05E-10	3.14E-11	7.57E-04	1.02E-05	7.67E-04
Radish and turnip	0	9.99E-12	1.14E-06	1.31E-05	1.42E-05
Potatoes	0	6.67E-11	7.57E-06	8.71E-05	9.47E-05
Carrots	0	1.66E-11	1.89E-06	2.18E-05	2.37E-05
String beans	0	4.80E-11	2.78E-06	4.76E-05	5.04E-05
Peas	0	4.80E-11	2.78E-06	4.76E-05	5.04E-05
Tomatoes	0	9.60E-11	5.55E-06	9.54E-05	1.01E-04
Cereals	0	9.50E-10	8.15E-06	3.31E-03	3.32E-03
Beef	2.77E-10		2.95E-04		2.95E-04
Milk	1.38E-09		1.46E-03		1.46E-03
Chicken and eggs	1.06E-10		3.42E-04		3.42E-04
Total doses	1.17E-05	1.27E-09	5.22E-03	3.63E-03	8.87E-03
Case 1	***France***				
	Dose via air pathway (mSv)		**Dose via soil pathway (mSv)**		**Total dose**
	HTO	**OBT**	**HTO**	**OBT**	**(mSv)**
Inhalation	0	0	0	0	5.16E-05
Skin absorption	0	0	0	0	0
Salad vegetables	0	0	6.98E-03	7.51E-04	7.73E-03
Radish and turnip	0	0	1.17E-03	7.22E-04	1.89E-03
Potatoes	0	0	1.65E-02	1.08E-02	2.73E-02
Carrots	0	0	2.04E-03	9.62E-04	3.01E-03
String beans	0	0	2.19E-03	9.02E-04	3.09E-03
Peas	0	0	2.19E-03	9.02E-04	3.09E-03
Tomatoes	0	0	5.49E-03	4.33E-04	5.92E-03
Cereals	0	0	1.40E-02	1.66E-01	1.80E-01
Beef	0	0	3.09E-02	6.36E-03	3.72E-02
Milk	0	0	1.67E-02	3.43E-03	2.01E-02
Chicken and eggs	0	0	5.61E-42	1.40E-42	7.01E-42
Total doses	0	0	9.81E-02	1.91E-01	2.90E-01
Case 1	***Germany***				
	Dose via air pathway (mSv)		**Dose via soil pathway (mSv)**		**Total dose**
	HTO	**OBT**	**HTO**	**OBT**	**(mSv)**
Inhalation	5.79E-05				5.79E-05
Skin absorption	3.63E-05				3.63E-05
Salad vegetables	1.82E-04	3.11E-05			2.13E-04
Radish and turnip					0
Potatoes	7.96E-05	5.56E-04			6.36E-04
Carrots					0
String beans					0
Peas					0
Tomatoes					0
Cereals	9.25E-05	5.84E-03			5.93E-03
Beef	2.28E-04	1.09E-04			3.37E-04
Milk	1.02E-03	1.90E-04			1.21E-03
Chicken and eggs					0
Total doses	1.60E-03	6.73E-03	0	0	8.42E-03

Table VI.1. (Continued).

Case 1	*Japan K*				
	Dose via air pathway (mSv)		Dose via soil pathway (mSv)		Total dose (mSv)
	HTO	OBT	HTO	OBT	
Inhalation	1.49E-04	0	0	0	1.49E-04
Skin absorption	7.44E-05	0	0	0	7.44E-05
Salad vegetables	6.75E-04	9.45E-07	6.75E-04	9.45E-07	1.35E-03
Radish and turnip	0	0	2.91E-06	7.92E-09	2.92E-06
Potatoes	0	0	0	6.34E-07	6.34E-07
Carrots	0	0	3.46E-08	2.11E-08	5.57E-08
String beans	2.12E-04	1.14E-06	2.12E-04	1.14E-06	4.26E-04
Peas	2.12E-04	1.14E-06	2.12E-04	1.14E-06	4.26E-04
Tomatoes	2.45E-08	1.07E-06	2.45E-08	1.07E-06	2.19E-06
Cereals	1.56E-08	3.94E-04	1.56E-08	3.94E-04	7.88E-04
Beef	3.13E-05	4.35E-07	1.79E-06	2.48E-08	3.35E-05
Milk	1.29E-04	8.96E-07	7.39E-06	5.11E-08	1.37E-04
Chicken and eggs	3.47E-06	2.67E-09	0	0	3.47E-06
Total doses	1.26E-03	4.00E-04	1.11E-03	3.99E-04	3.40E-03

Table VI.2. Details of predicted doses at 1 km - Case 2, HT release.

Case 2	*France*				
	Dose via air pathway (mSv)		**Dose via soil pathway (mSv)**		**Total dose (mSv)**
	HTO	**OBT**	**HTO**	**OBT**	
Inhalation	0	0	0	0	9.38E-05
Skin absorption	0	0	0	0	0
Salad vegetables	0	0	2.45E-02	2.64E-03	2.72E-02
Radish and turnip	0	0	4.11E-03	2.54E-03	6.64E-03
Potatoes	0	0	5.79E-02	3.80E-02	9.60E-02
Carrots	0	0	7.19E-03	3.38E-03	1.06E-02
String beans	0	0	7.69E-03	3.17E-03	1.09E-02
Peas	0	0	7.69E-03	3.17E-03	1.09E-02
Tomatoes	0	0	1.93E-02	1.52E-03	2.08E-02
Cereals	0	0	4.99E-02	5.94E-01	6.44E-01
Beef	0	0	9.62E-02	1.98E-02	1.16E-01
Milk	0	0	5.20E-02	1.07E-02	6.27E-02
Chicken and eggs	0	0	1.82E-41	4.20E-42	2.24E-41
Total doses	0	0	3.27E-01	6.79E-01	1.01E+00
Case 2	***Germany***				
	Dose via air pathway (mSv)		**Dose via soil pathway (mSv)**		**Total dose (mSv)**
	HTO	**OBT**	**HTO**	**OBT**	
Inhalation	9.77E-04				9.77E-04
Skin absorption	6.13E-04				6.13E-04
Salad vegetables	1.38E-02	2.31E-03			1.61E-02
Radish and turnip					0
Potatoes	7.34E-03	3.34E-02			4.07E-02
Carrots					0
String beans					0
Peas					0
Tomatoes					0
Cereals	1.56E-03	6.39E-02			6.55E-02
Beef	1.06E-02	5.62E-03			1.62E-02
Milk	9.75E-02	1.96E-02			1.17E-01
Chicken and eggs					0
Total doses	1.31E-01	1.25E-01	0	0	2.57E-01
Case 2	***Japan K***				
	Dose via air pathway (mSv)		**Dose via soil pathway (mSv)**		**Total dose (mSv)**
	HTO	**OBT**	**HTO**	**OBT**	
Inhalation	1.07E-03	0	0	0	1.07E-03
Skin absorption	5.33E-04	0	0	0	5.33E-04
Salad vegetables	3.61E-03	5.05E-06	3.61E-03	5.05E-06	7.23E-03
Radish and turnip	0	0	2.44E-06	6.64E-09	2.45E-06
Potatoes	0	0	0	5.31E-07	5.31E-07
Carrots	0	0	2.90E-08	1.77E-08	4.67E-08
String beans	1.13E-03	6.05E-06	1.13E-03	6.05E-06	2.27E-03
Peas	1.13E-03	6.05E-06	1.13E-03	6.05E-06	2.27E-03
Tomatoes	1.31E-07	5.70E-06	1.31E-07	5.70E-06	1.17E-05
Cereals	8.35E-08	2.11E-03	8.35E-08	2.11E-03	4.22E-03
Beef	1.66E-04	2.31E-06	1.23E-05	1.10E-07	1.81E-04
Milk	6.87E-04	4.75E-06	5.09E-05	3.52E-07	7.43E-04
Chicken and eggs	2.40E-06	1.85E-08	0	0	2.42E-06
Total doses	6.73E-03	2.14E-03	5.94E-03	2.13E-03	1.85E-02

Table VI.3. Details of predicted doses at 1 km - Case 3, HT release.

Case 3	*France*				
	Dose via air pathway (mSv)		**Dose via soil pathway (mSv)**		**Total dose (mSv)**
	HTO	**OBT**	**HTO**	**OBT**	
Inhalation	0	0	0	0	5.13E-05
Skin absorption	0	0	0	0	0
Salad vegetables	0	0	5.89E-04	6.33E-05	6.52E-04
Radish and turnip	0	0	9.85E-05	6.09E-05	1.59E-04
Potatoes	0	0	1.39E-03	9.13E-04	2.30E-03
Carrots	0	0	1.72E-04	8.11E-05	2.54E-04
String beans	0	0	1.85E-04	7.61E-05	2.61E-04
Peas	0	0	1.85E-04	7.61E-05	2.61E-04
Tomatoes	0	0	4.63E-04	3.65E-05	4.99E-04
Cereals	0	0	1.18E-03	1.40E-02	1.52E-02
Beef	0	0	3.07E-02	6.32E-03	3.70E-02
Milk	0	0	1.66E-02	3.42E-03	2.00E-02
Chicken and eggs	0	0	5.61E-42	1.40E-42	7.01E-42
Total doses	0	0	5.16E-02	2.51E-02	7.66E-02
Case 3	***Germany***				
	Dose via air pathway (mSv)		**Dose via soil pathway (mSv)**		**Total dose (mSv)**
	HTO	**OBT**	**HTO**	**OBT**	
Inhalation	1.98E-03				1.98E-03
Skin absorption	1.24E-03				1.24E-03
Salad vegetables	4.71E-02	8.98E-03			5.61E-02
Radish and turnip					0
Potatoes	2.62E-02	1.16E-01			1.42E-01
Carrots					0
String beans					0
Peas					0
Tomatoes					0
Cereals	5.82E-03	2.36E-01			2.42E-01
Beef	3.17E-02	2.09E-02			5.26E-02
Milk	2.91E-01	6.93E-02			3.60E-01
Chicken and eggs					0
Total doses	4.02E-01	4.51E-01	0	0	8.56E-01
Case 3	***Japan K***				
	Dose via air pathway (mSv)		**Dose via soil pathway (mSv)**		**Total dose (mSv)**
	HTO	**OBT**	**HTO**	**OBT**	
Inhalation	1.14E-02	0	0	0	1.14E-02
Skin absorption	5.71E-03	0	0	0	5.71E-03
Salad vegetables	6.90E-02	9.65E-05	6.90E-02	9.65E-05	1.38E-01
Radish and turnip	0	0	2.70E-05	7.34E-08	2.71E-05
Potatoes	0	0	0	5.87E-06	5.87E-06
Carrots	0	0	3.20E-07	1.96E-07	5.16E-07
String beans	2.17E-02	1.16E-04	2.17E-02	1.16E-04	4.36E-02
Peas	2.17E-02	1.16E-04	2.17E-02	1.16E-04	4.36E-02
Tomatoes	2.50E-06	1.10E-04	2.50E-06	1.10E-04	2.25E-04
Cereals	1.60E-06	4.04E-02	1.60E-06	4.04E-02	8.08E-02
Beef	9.51E-02	4.50E-05	7.05E-03	1.93E-06	1.02E-01
Milk	3.93E-01	9.28E-05	2.92E-02	3.97E-06	4.22E-01
Chicken and eggs	1.00E-03	2.04E-06	0	0	1.00E-03
Total doses	6.02E-01	4.10E-02	1.49E-01	4.09E-02	8.49E-01

ADDITIONAL PUBLICATIONS USED IN THE PREPARATION OF THIS REPORT

BOOGAARD, H.L., VAN DIEPEN, C.A., ROETTER, R.P., CABRERA, J.M.C.A., VAN LAAR, H.H., User's guide for WOFOST 7.1 crop growth simulation model and WOFOST Control Center 1.5, Technical Document 52, International Rice Research Institute, Wageningen (1998).

GALERIU, D., RASKOB, W., MELINTESCU, A., TURCANU, C., Documentation of the tritium food chain and dose module FDMH in RODOS pv4.0, RODOS WG3, TN99-56 (1999).

GALERIU, D., RASKOB, W., MELINTESCU, A., HTO deposition in RODOS, RODOS WG3, TN99 (1999).

GALERIU, D., RASKOB, W., MELINTESCU, A., TURCANU, C., FDMH – the tritium module in RODOS, Proceedings of the RODOS Workshop "The European Decision Support System for Off Site Management of Nuclear Emergency", 20–24 Sept. 1999, Rhodes (1999).

GALERIU, D., RASKOB, W., MELINTESCU, A., TURCANU, C., Model description of the tritium food chain and dose module FDMH in RODOS pv4.0, RODOS WG3-TN99-54 (1999).

GALERIU, D., TURCANU, C., MELINTESCU, A., User guide for the tritium food chain and dose module FDMH of RODOS – PV4.OF_02. RODOS Version 4 Handbook, Volume 1 (http://www.rodos.fzk.de/RodosHomePage/RodosHomePage/Documents/handbook_v1.html).

JACOBS, C.M.J., Direct impact of atmospheric CO_2 enrichment on regional transpiration, PhD Thesis, Agricultural University, Wageningen (1994).

KABAT, P., MARSHALL, B., VAN DEN BROEK, B.J., Comparison of simulation results and evaluation of parameterization schemes, In: Modelling and parameterization of the soil-plant-atmosphere system, A comparison of potato growth models, P. Kabat et al (eds.), Wageningen Press, 439–501 (1995).

KARVONEN, T. KLEEMOLA, J., CROPWATN: Prediction of water and nitrogen limited potato production, In: Modelling and parameterization of the soil-plant-atmosphere system, A comparison of potato growth models, P. Kabat et al (eds.), Wageningen Press, 335–369 (1995).

RASKOB, W., BARRY, P., Importance and variability in processes relevant to environmental tritium dose assessment models, J. Environ. Radioact., Vol. 136, 237–251 (1997).

RITCHIE, J.T., GRIFFIN, T.S., JOHNSON, B.S., SUBSTOR: Functional model of potato growth, development and yield, In: Modelling and parameterization of the soil-plant-atmosphere system, A comparison of potato growth models, P. Kabat et al (eds.), Wageningen Press 401–435 (1995).

SHARMA, K.D., SEN, D.N., Dry matter production in four Solanaceous species, Photosynthetica 3 (3), 276–278 (1969).

SPITTERS, C.J.T., SCHAPENDONK, H.C.M., Evaluation of breedind strategies for drought tolerance in potato by means of crop growth simulation, Plant and soil, 123, 193–203 (1990).

VAN DER ZAAG, D.E., Cartoful si cultivarea lui in Olanda, Institutul Consultativ Olandez al cartofului, Ministerul Agriculturii si Pescuitului, den Haag, Olanda (1992) (in Romanian).

LIST OF PARTICIPANTS

Aign, J.	Technische Universität München, Germany
Amano, H.	Japan Atomic Energy Research Institute, Japan
Arapis, G.	Agricultural University of Athens, Greece
Atanassov, D.	National Institute of Meteorology and Hydrology, Bulgaria
Atarashi-Andoh, M.	Japan Atomic Energy Research Institute, Japan
Balonov, M.[a]	International Atomic Energy Agency
Barbeau, C.	Université Laval, Canada
Barraclough, I.[b]	Enviros Consulting Limited, United Kingdom
Baumgärtner, F.	Technische Universität München, Germany
Belot, Y.	Consultant, France
Benovich, I.	Ontario Power Generation, Canada
Berkovskyy, V.[a]	International Atomic Energy Agency
Boyer, C.	Commissariat á l'Energie Atomique, France
Brennwald, M.	National Cooperative for the Disposal of Radioactive Waste, Switzerland
Choi, Y.	Korea Atomic Energy Research Institute, Republic of Korea
Conney, S.	Food Standards Agency, United Kingdom
Cutts, D.	Food Standards Agency, United Kingdom
Davis, P.[c]	Atomic Energy of Canada Limited, Canada
Dovlete, C.	Consultant, France
Filistovic, V.	Institute of Physics, Lithuania
Galeriu, D.	Institute of Physics and Nuclear Engineering "Horia Hulubei", Romania
Golubev, A.	Russian Federal Nuclear Centre, Russian Federation
Golubeva, V.	Russian Federal Nuclear Centre, Russian Federation
Guetat, P.	Commissariat á l'Energie Atomique, France
Gulden, W.	European Fusion Development Agreement, Germany
Inoue, Y.	National Institute of Radiological Sciences, Japan
Ioannides, K.	The University of Ioannina, Greece
Jackson, D.[b]	Enviros Consulting Limited, United Kingdom
James, J.	Bhabha Atomic Research Centre, India

[a] Scientific Secretary.
[b] Technical Secretary.
[c] Working Group Leader.

Kakiuchi, H.	National Institute of Radiological Sciences, Japan
Kennedy, P.	Food Standards Agency, United Kingdom
Koarashi, J.	Japan Atomic Energy Agency, Japan
Kozar Lagar, J.	Jozef Stefan Institute, Slovenia
LeDizès-Maurel, S.	Institut de Radioprotection et de Sûreté Nucléaire, France
Lee, C.	Korea Atomic Energy Research Institute, Republic of Korea
Lee, H.	Korea Atomic Energy Research Institute, Republic of Korea
Marks, P.	Amersham Plc, United Kingdom
Masuda, T.	Institute for Environmental Sciences, Japan
Mavrin, S.	Russian Federal Nuclear Centre, Russian Federation
Melintescu, A.	Institute of Physics and Nuclear Engineering, “Horia Hulubei”, Romania
Miyamoto, K.	National Institute of Radiological Sciences, Japan
Momoshima, N.	Kumamoto University, Japan
Montfort, M.	Commissariat á l’Energie Atomique, France
Nedveckaite, T.	Institute of Physics, Lithuania
Patryl, L.	Commissariat á l’Energie Atomique, France
Peterson, S-R.	Lawrence Livermore National Laboratory, United States of America
Raskob, W.	Institut für Kern und Energietechnik, Germany
Ravi, P.	Bhabha Atomic Research Centre, India
Saito, M.	Kyoto University Safety Reassurance Academy, Japan
Siclet, F.	Electricité de France, France
Smith, K.[b]	Enviros Consulting Limited., United Kingdom
Suolanen, V.	Technical Research Centre of Finland, Finland
Tagami, K.	National Institute of Radiological Sciences, Japan
Takeda, H.	National Institute of Radiological Sciences, Japan
Venter, A.[b]	Enviros Consulting Limited, United Kingdom
Vichot, L.	Commissariat á l’Energie Atomique, France
Wierczinski, B.	Technische Universität München, Germany
Yamamoto, K.	Yfirst Inc., Japan
Yankovich, T.	Atomic Energy of Canada Limited, Canada

[b] Technical Secretary.

EMRAS Combined Meetings

1–5 September 2003 (78 participants, from 24 countries)
8–11 November 2004 (84 participants, from 24 countries)
21–25 November 2005 (106 participants, from 31 countries)
6–10 November 2006 (101 participants, from 32 countries)
5–9 November 2007 (99 participants, from 30 countries)

Interim Working Group Meetings, Theme 1, Working Group 2

California, USA: 19–22 April 2004; Baden-Baden, Germany: 13–17 September 2004; Cardiff, Wales, UK: 12/13–15 April 2005; Chatou Cedex, France: 7–9 June 2006; Bucharest, Romania: 30 May – 1 June 2007

BACK TO CONTENTS